橋梁の構造健全度モニタリングに関する国際ワークショップ／橋梁振動コロキウム'03論文集

Proceedings of the International Workshop on Structural Health Monitoring of Bridges / Colloquium on Bridge Vibration '03

September 1-2, 2003
Kitami Institute of Technology

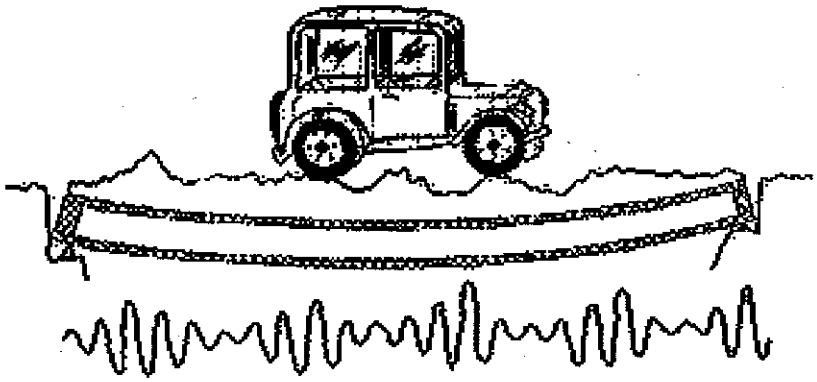

2003年9月1日（月）～2日（火）
北見工業大学

土木学会構造工学委員会
橋梁振動モニタリングとその標準化研究小委員会

Task Committee on Monitoring of Bridge Vibration and its Standardization
Committee of Structural Engineering
Japan Society of Civil Engineers

Preface

Task Committee of Japan Society of Civil Engineers (JSCE) on " Monitoring of bridge vibration and its standardization" is working on ISO standard drafting (ISO18649 Evaluation of results from dynamic tests and investigations on bridges) and developing new technologies of bridge vibration monitoring. Up to now, five domestic Colloquiums on Bridge Vibration were held in 1987, 1989, 1995, 1997 and 2001 in Kanazawa and Tokyo, Japan.

The International Workshop on Structural Health Monitoring of Bridges/ Colloquium on Bridge Vibration'03 will explore the subjects about the structural health monitoring, bridge vibration monitoring and maintenance management of bridges among the international and domestic experts. This Workshop/ Colloquium includes eight keynote lectures by the eminent international researchers and 44 papers from international and domestic contributors.

I hope this Workshop/ Colloquium can contribute to the future development of this field and provide the opportunity of the exchange of information, opinions and friendship among the participants.

I would like to express my sincere appreciation to keynote speakers, all the contributors to the proceedings, participants, international advisory committee members and the members of the task committee of JSCE on " Monitoring of bridge vibration and its standardization". I would like to also express my sincere appreciation to Prof. T. Oshima and other members of Kitami Institute of Technology, the chief secretariat of this Workshop/ Colloquium Dr. T. Obata and JSCE secretariat Mr. T. Hashimoto for realizing this Workshop/ Colloquium. Furthermore, I would like to appreciate the financial supports from Japan Society of Civil Engineers, Kitami City Government and Kitami Institute of Technology for this Workshop/ Colloquium.

September 2003

A. Nakajima
Chairman
Task Committee on Monitoring of Bridge Vibration and its Standardization/
Committee of Structural Engineering/
Japan Society of Civil Engineers

Organizing committee

Chairman :
Akinori Nakajima, Utsunomiya University, Japan

Co-chairman:
Toshiyuki Oshima, Kitami Institute of Technology, Japan
Yasuo Kajikawa, Kanazawa University, Japan

Organizing committee members:
Kenichi Maeda, Tokyo Metropolitan University, Japan
Takashi Obata, Hokkaido University, Japan
Masato Abe, University of Tokyo, Japan
Hiroki Yamaguchi, Saitama University, Japan
Toshiro Hayashikawa, Hokkaido University, Japan
Shuichi Mikami, Kitami Institute of Technology, Japan
Zhishen Wu, Ibaragi University, Japan

International Advisory Committee

Yozo Fujino, University of Tokyo, Japan
Koh Chan Ghee, The National University of Singapore, Singapore
Bojidar Yanev, New York City, U.S.A.
Aftab A. Mufti, University of Manitoba, Canada
John J. Lesko, Virginia Polytechnic Institute and State University, U.S.A.
Jean-Paul Lebet, Ecole Polytechnique Federale De Lausanne, Switzerland
A. Emin Aktan, Drexel University, U.S.A.

Secretariat

Takashi Obata, Hokkaido University, Japan
Akimitsu Tanaka, Chuo Fukken Consultants, Co. Ltd., Japan
Saiji Fudaka, Kanazawa University, Japan

土木学会　構造工学委員会
橋梁振動モニタリングとその標準化小委員会名簿

The member of
Task Committee on Monitoring of Bridge Vibration and its Standardization
Committee of Structural Engineering
Japan Society of Civil Engineers

委員長	中島　章典	宇都宮大学大学院工学研究科
幹事長	小幡　卓司	北海道大学大学院工学研究科
幹　事	阿部　雅人	東京大学大学院工学研究科
〃	田中　玲光	中央復建コンサルタンツ（株）
〃	田中　信治	中部復建（株）
〃	深田　宰史	金沢大学大学院自然科学研究科
委　員	青地　知也	（株）開発工営社
〃	上半　文昭	（財）鉄道総合技術研究所
〃	烏野　清	九州共立大学工学部土木工学科
〃	大木　太	オリエンタル建設（株）
〃	大島　俊之	北見工業大学工学部土木開発工学科
〃	岡林　隆敏	長崎大学工学部社会開発工学科
〃	小塩　達也	名古屋大学大学院工学研究科
〃	梶川　康男	金沢大学大学院自然科学研究科
〃	勝浦　啓	三菱重工業（株）
〃	加藤　雅史	九州東海大学工学部都市工学科
〃	河田　直樹	（株）エース
〃	川谷　充郎	神戸大学工学部建設学科
〃	北村　幸嗣	日立造船（株）
〃	許　斌	茨城大学工学部都市システム工学科
〃	児玉　洋	（株）ドーコン
〃	小林　義和	（株）ニチゾウテック
〃	佐々木伸幸	菱明技研（株）
〃	佐藤　恒明	木更津工業高等専門学校環境都市工学科
〃	枡本　正信	（株）フジエンジニアリング
〃	津村　直宜	ＪＦＥエンジニアリング（株）
〃	林川　俊郎	北海道大学大学院工学研究科
〃	本田　秀行	金沢工業大学土木工学科
〃	前田　研一	東京都立大学大学院工学研究科
〃	松本　信之	（財）鉄道総合技術研究所
〃	松本　泰尚	埼玉大学工学部建設工学科
〃	三ツ木幸子	（株）綜合技術コンサルタント
〃	柳澤　則文	川田工業（株）
〃	山口　宏樹	埼玉大学工学部建設工学科
〃	山田　靖則	高田機工（株）
〃	横川　英彰	オイレス工業（株）

CONTENTS

KEYNOTE SPEECHES

Limitations in the Structural Identification of Long-Span Bridges ····· 1
F.N. Catbas, S.K.Ciloglu, K. Grimmelsman, Q. Pan, M. Pervizpour and A.E. Aktan

Monitoring the Condition of Bridges in New York City ····· 17
Bojidar Yanev

Structural Parameter Identification: A Divide –and-Conquer Approach ····· 27
Chan-Ghee Koh

Vibration-based Monitoring of Infrastructures - R& D of Sensors and Analysis at the University of Tokyo ····· 37
Yozo Fujino and Masato Abe

Structural Health Monitoring of Innovative Bridge Decks ····· 55
Aftab A. Mufti

Preserving the Health of the US Bridge Infrastructure:
The Role of New Technologies in the Federal Bridge Program ····· 63
Raymond McCormick, Edgar Small, and Glenn Washer

Safety Assessment and Health Monitoring of Suspension Bridge Cables ····· 77
Harukazu Ohashi, J. A. Barbas and R.Q. Haight

Progress of Research and Applications in Structural Health Monitoring of Bridges in Korea ····· 89
Hyun-Moo Koh, Jinkyo F. Choo, Chul-Young Kim, Sung-Kon Kim and Chan-Min Park

SUBMITTED PAPERS (English)

Health Monitoring 1

Interpretation of Bridge Test Data to Determine Dynamic Load Allowance
and its Influence on Bridge Design and Evaluation ····· 101
Baider Bakht , A. A. Mufti, Alan Clayton, W. Saltzberg and Chad Klowak

Vibration-based damage detection on a steel free bridge deck ····· 109
Zhengjie Zhou, Leon D. Wegner and Bruce F. Sparling

Sensors Based Bridge Monitoring System ····· 117
Jeong-Hwan Jang, Sung-Pil Chang, Sung-Kon Kim and Wan-Jong Kim

Health monitoring using FBG sensors for structural members ····· 121
Hiro-Yuki Nakazawa and Seishi Yamada

Evaluation of the Atmospheric Environment for corrosion of Steel Members of Civil Structures ····· 127
Tomoyuki Yamazaki, T. Oshima and S. Mikami

Dynamic Response

Nonlinear Behavior of Cable-Stayed Bridge Tower Under Level II Earthquake Ground Motion ····· 133
Shehata E. Abdel Raheem and Toshiro Hayashikawa

Hardening Effect of Lead-Rubber Bearings on Nonlinear Seismic Behaviour

of Highway Viaducts with Piers of Unequal Heights 141
Daniel Ruiz Julian and Toshiro Hayashikawa

Development of Cable Exciting System for Evaluating Modal Damping of Stay Cables 149
Nam-Sik Kim, Woon Jeong, Ju-Won Seo and Sang-Sup Ahn

A Large Deflection and Inelastic Analysis of Steel Elements at Elevated Temperature by Simulation 157
Jerry Chi Kin Iu and S.L, Chan

Vibration Analysis of the Second Saikai Bridge -A Concrete Filled Tubular (CFT) Arch Bridge- 165
Qingxiong Wu, Mitsuhiro Yoshimura, Kazuo Takahashi, Shozo Nakamura, Hiroyuki Fujita and Kazuyoshi Furukawa

Health Monitoring 2

On Remaining Asset Values and Maintenance Necessity Level (MNL) of Bridges 173
Makoto Sato, Shuichi Mikami, Ikue Tamba, Kenji Ikeda and Toshiyuki Oshima

Performance Measures for Bridge Management 181
Hitoshi Furuta, Takahiro Kameda and Dan M. Frangopol

Comparative Study of Vibration-Based Structural Damage Identification Methods 187
Sherif Beskhyroun, Toshiyuki Oshima, Shuichi Mikami and Tomoyuki Yamazaki

Optimal Sensor Locations for Long-term Structural Health Monitoring 195
Soobong Shin, Soon-Jung Kwon and Young-Hwan Park

Vibration Based Damage Identification for a Three Span Continuous
Steel Free Deck Bridge Located in Canada 203
Jag L. Humar, A. Bagchi and H. Xu

Health Monitoring 3

Study on Damage Identification of Bridge Structures based on Sound Monitoring Data 211
Takashi Obata, Yasuhiro Asaka, Yasunori Miyamori, Toshiro Hayashikawa, and Koichi Sato

A Consideration of Bridge Vibration Measurement by using Digital Video Processing with PC Camera 217
Yasunori Miyamori, Takashi Obata, Kazunori Adachi, Toshiro Hayashikawa, Koichi Sato

The Telemetry System based on Data Communication Technology
for Remote Monitoring of Bridge Construction 223
Takatoshi Okabayashi and Toshihiro Okumatsu

Static Method for In Situ Estimating Tension in Hanger Cable 231
Sang-Sup Ahn, In-Hwan Bae and Nam Sik Kim

System Identification in Time Domain for Structural Damage Assessment
Using L_1-Regularization and Time Windowing Technique 237
Hae Sung Lee and Seung-Keun Park

Bridge-Vehicle Problem

Dynamic Response Analysis of Rationalized Monorail Bridges under Moving Trains 243
Takumi Kamizono, Chang Hun Lee, Takeshi Kanbara, Chul Woo Kim, Mitsuo Kawatani and Nobuo Nishimura

Dynamic Response Analysis of Elevated Railway Bridges
due to Shinkansen Trains and Influence of Train Models 249
Mitsuo Kawatani, Xingwen He, Ryo Sobukawa and Seiji Nishiyama

FE Model Update of Seohae Bridge ····· 257
Jah-Geol Yoon , Sung-Pil Chang and Young-In Baek

End-Cross Beam Reinforcement as a Countermeasure against Traffic-Induced Vibration of Six-Span Continuous Steel Two-Girder Bridge ····· 261
Chul-Woo Kim, Mitsuo Kawatani and Naoki Kawada

Bridge Weigh-in-Motion System using Reaction Force Method ····· 269
Kentaro Yamada and Tatsuya Ojio

On ISO Draft DIS 18649 for Bridge Vibration Measurement and Its Evaluation ····· 277
Toshiyuki Oshima, Akinori Nakajima and Jun Tsunabuchi

SUBMITTED PAPERS (Japanese)

Bridge Vibration 1

Vibration Serviceability of Pedestrian Slab Bridges Developed using GFRP Pultrusion Members ····· 283
Ken-ichi Maeda, Hitoshi Nakamura, Nobuhiko Kitayama, Koshiro Hayashi and Yasuo Kajikawa
ＧＦＲＰ引き抜き成型材を用いた歩行者用床版橋と振動使用性
前田 研一，中村 一史，北山 暢彦，林 耕四郎，梶川 康男

The Vibration Serviceability of Nielsen System Lohse Girder Bridge with Long Period of Road Surface Roughness ····· 289
Saiji Fukada, Yasuo Kajikawa, Yotaro Kitamura, Masahiko Harada and Hideki Shimizu
長周期の路面凹凸を有したニールセンローゼ橋の振動使用性
深田 宰史，梶川 康男，北村 洋太郎，原田 政彦，清水 英樹

A Fundamental Study on Traffic Load Monitoring System using Genetic Algorithm on Highway Bridges ····· 297
Masahiro Yoneda and Katsuya Edamoto
遺伝的アルゴリズムを適用した橋梁交通荷重の推定法
米田 昌弘，枝元 勝哉

Bridge Weigh-in-Motion using Lower Flange Strain of Main Deck ····· 305
Hiroshi Katsuura, Takuya Arakawa, Nobuo Amano and Seiichi Noda
主桁下フランジ応力を用いた車両重量計測について
勝浦 啓，荒川 卓哉，天野 信雄，野田 整一

Theoretical Analysis of Low Frequency Noise Radiated by Traffic-induced Vibration of Bridge ····· 311
Mitsuo Kawatani, Naoki Kawada, Masakazu Tona and Chul-Woo Kim
道路橋の交通振動により放射される低周波音の理論解析
川谷 充郎，河田 直樹，十名 正和，金 哲佑

The Influence of the Traffic Vibration upon Highway Bridge due to Running Vehicles with the Difference Suspension ····· 319
Yasuo Kajikawa, Saiji Fukada, Takahiko Hayashishita, Kentaro Yamada and Tatsuya Ojio
サスペンション構造の違いによる高架橋振動への影響
梶川 康男，深田 宰史，林下 貴彦，山田 健太郎，小塩 達也

Bridge Vibration 2

Numerical Simulation for the Traffic control at the Corroded Truss Bridge ····· 328
Tsuneaki Sato, Yutaka Miyamoto and Naoki Ikura and Nobuhiro Onizuka

鋼トラス橋通行管理のためのシミュレーション
佐藤 恒明，宮本 裕，伊倉 直樹，鬼塚 信弘

Discontinuous Deformation Analysis on Base Subsidence and Failure Behavior of Old Stone Bridge ····· 331
Akira Aikawa
老朽化した石橋基礎の沈下と破壊挙動に関する不連続体変形法解析
相川 明

Study on Structural Property of Covered Timber Highway Bridge by Vibration Measurement ····· 337
Masafumi Kato and Syoichi Yamashita
屋根付き木造トラス道路橋の振動測定による構造特性の検討
加藤 雅史，山下 昇一

A study of Vibration Characteristics of Hybrid Stress Ribbon Deck Bridge ····· 343
Futoshi Ooki, Taku Yoshikawa, Meguru Tsunomoto and Yasuo Kajikawa
端部分離型上路式 PC 吊床版橋の振動特性の検討
大木 太，吉川 卓，角本 周，梶川 康男

Vibration Characteristics of 8 Spans Prestressed Concrete Rigid Frame Bridge with Joint Less ····· 351
Yasuo Kajikawa, Saiji Fukada and Satoshi Udagawa
ヒンジ部分を連続化した 8 径間 PC ラーメン橋の振動特性
梶川 康男，深田 宰史，宇田川 敏

The Evaluation of the Vibration Characteristics and Aerodynamic Stabilities of a Bridge with Fewer Girders ····· 357
Jun Murakoshi, Koichiro Fumoto, Kenichiro Ashizuka, Renji Kiyota and Masao Miyazaki
鋼少数主桁橋の耐風安定性と振動特性に関する実験的検討
村越 潤，麓 興一郎，芦塚 憲一郎，清田 錬次，宮崎 正男

Monitoring, Control and Damage Identification

Development of Handy System to Measure Vibration-Induced Displacement ····· 363
Satoshi Yamada, Kentaro Yamada and Tatsuya Ojio
振動による変位とその頻度を計測する簡易な計測器の開発と適用試験
山田 聡，小塩 達也，山田 健太郎

Examples of Remote Measurement System by General Telephone Network ····· 369
Naofumi Inaba and Hideo Mutsukado
一般電話回線を用いた遠隔データ収集システムの実施事例
稲葉 尚文，陸門 英男

Vibration and Noise Reduction of Expansion Joint by the Response Control Damper ····· 373
Hiroshi Koyama, Taichi Sanpei, Hiroki Inada, Katuo Nakamachi and Tetsuji Arai
制振ダンパによる伸縮装置の振動、騒音低減
小山 博，三瓶 太一，稲田 大輝，中町 華都雄，新井 哲治

Vibration Characteristic of a Lightening Pole on an Elevated Highway Bridge
and Effect of TMD for Mitigating Vibration ····· 379
Tomohiko Ishibashi and Toshiyuki Kitada
高架橋上に設置された照明柱の振動計測および制振装置の同構造物への適用
石橋 知彦，北田 俊行

Fundamental Study on Development of Management Map for Potential Damage
to Portal Marker Columns and Lighting Poles on Highway Bridges ····· 385
Hideo Isha, Toshiyuki Kitada, Yoshihiro Yamaguchi and Ken Tokumasu
道路橋付属構造物の損傷可能性管理マップに関する基礎的研究
井舎 英生，北田 俊行，山口 良弘，徳増 健

Experimental Study on Vibration Characteristics of Portal Marker Columns
and Lighting Poles with Damages on Highway Bridges ····· 393
Hideo Isha, Toshiyuki Kitada and Kenichi Tani
道路橋付属構造物の損傷と振動特性に関する実験的研究
井舎 英生，北田 俊行，谷 憲一

KEYNOTE SPEECHES

Limitations in the Structural Identification of Long-Span Bridges

F. N. Catbas, S. K. Ciloglu, K. Grimmelsman, Q. Pan, M. Pervizpour and A. E. Aktan

Drexel University Intelligent Infrastructure and Transportation Safety Institute
3001 Market Street, One Drexel Plaza, Philadelphia, PA 19104

The writers discuss an in-depth analysis of the limits in St-Id of large structures, including the mitigation of human errors and the control of uncertainty due to the complexity of large structures and their loading environment. After globally and locally calibrating a 25,218 DOF 3D FE model of a major bridge, the average error between the model and experimental frequencies is determined to be 2.3 % for the frequencies of the first 15 modes. The confidence in the simulated local characteristics such as the stresses and distortions is judged to be around 50-75%, based on local calibration results. It is important to note that inherent assumption in ambient monitoring data analysis is that the structure remains stationary, observable and reasonably linear during the course of the monitoring. The data collected during a large number of intermittent time windows over several weeks included periods of different levels of traffic-induced vibration, various wind environments and temperature ranges. Averaging such data represents an effective composite of various inputs and the corresponding structural states and behaviors throughout the course of the monitoring, therefore in effect smearing all non-linearity and non-stationarity and effectively linearizing the structure.

Key words: Long span bridges, structural identification, finite element modeling and calibration, ambient vibration test, controlled load test.

1. Introduction

The origins of systems science trace back to "cybernetics" and "operations research", two scientific endeavors initiated in biological and mathematical sciences nearly 50-years ago[1]. Systems modeling, identification, optimization and control are concepts that have found extensive applications in electrical and industrial engineering. System identification and its adaptation to mechanical and structural systems, i.e. structural-identification (St-Id), are concepts introduced to the engineering mechanics and civil engineering disciplines several decades ago by Hart and Yao[2] and Liu and Yao[3]. Since then, many researchers have explored the St-Id concept. However, St-Id applications are not yet common in civil engineering practice. Since the powerful experimental and analytical tools needed for meaningful applications of St-Id are now available mainly following the advances in computers and information technology, this concept should now find routine applications in the civil engineering practice[4].

St-Id involves analytical conceptualization, modeling, designing experiments for measuring and quantifying structural behavior and the phenomena affecting it[5,6]. The outcome of St-Id is an analytical model that simulates the mechanical characteristics of a structure and its behavior under various load effects with an established level of confidence. This paper focuses on linear and deterministic finite element modeling at various levels of resolution since physics-based analytical models that represent a structure at some local detail offer greater promise for addressing practical problems in civil engineering practice than more abstract or more complex (i.e. nonlinear) models. In addition, it is possible to reduce a linear, deterministic 3D FE model at a local resolution to a more practical one with fewer "critical" coordinates, or transform this into a nonlinear one. The authors note that 3D FE modeling is becoming a common tool in the design and evaluation of many major structures by the consulting industry.

It is the authors' belief that proper applications of St-Id hold the key for reliable condition assessment of civil infrastructure systems. The current transportation infrastructure inventories, such as the National Bridge Inventory, contain subjective data on condition. St-Id offers promise for an objective, quantitative evaluation of the mechanical characteristics of a constructed system. Engineers may not recognize the lack of reliability of predictions based on an idealized analytical representation of a structure, often constructed from drawings without actual observations and inspections. The writers' experience based on applications of St-Id on actual buildings and bridges of various sizes and conditions revealed that structural characteristics, responses, load effects and capacities predicted by idealized analytical models commonly used in design have discrepancies and errors compared to actual measurements exceeding 10 times (1000 percent).

Even in the case of a simple beam test in the laboratory, errors in the predicted global mechanical characteristics such as frequency, displacement and rotational flexibility may exceed 25%, errors in the predicted local responses such as strains and curvatures may exceed 100% and errors in the predicted load or deformation capacity may exceed 200%. Eliminating blatant human errors and those errors due to a lack of complete conceptualization, the analyst still faces significant ***uncertainty*** due to the necessity of idealizations related to dimensions, supports, local geometry, materials and mechanics (both kinetics and especially kinematics). St-Id permits blatant human errors to be mitigated, and bounds and controls, or reduces the ***uncertainty due to the complexities of reality***.

The objective of this paper is to discuss recent research focused on a closer understanding of the reliability in St-Id applications for large and complex constructed structures in general (kilometer scale), and for long-span bridges in particular. The writers have studied a long-span bridge for five years, and constructed an analytical model to simulate both the global and the local responses of this structure. The writers instrumented the bridge extensively, with a density, duration and bandwidth uncommon in past examples of instrumentation of a constructed system. The study permitted an in-depth analysis of the limits in St-Id of large structures, including the mitigation of human errors and the control of uncertainty due to the complexity of large structures and their loading environment. Following the field studies, the writers have developed a phenomenological physical model in the laboratory and are currently conducting systematic studies of the limits of reliability in observation, measurement and conceptualization of complex structural systems. These studies provide insight on the limits in a linear and deterministic representation by a detailed FE modeling of a large and complex structural system.

2. St-Id of Long-Span Bridges

Long span bridges represent a special, critical class of construction in terms of their value and the impact of their performance on the economic well-being of major metropolitan areas. Each long-span bridge offers unique challenges in their individual design and construction. Motivations for the St-Id of a long-span bridge and a field-calibrated FE modeling for simulating such a structure may include:

(a) An objective documentation of the as-is mechanical characteristics and condition as a benchmark through its lifespan;

(b) Prediction of performance and vulnerability to hazards such as earthquakes and/or extreme winds;

(c) Inspections, rating and permits;

(d) Structural modification due to any changes in operational conditions and loads;

(e) Establish the impacts of damage due to aging, deterioration, accidents, etc. on structural reliability;

(f) Designing retrofit and/or hardening the structure to improve its structural reliability;

(g) Health monitoring for asset management;

Several researchers have conducted studies for determining the structural dynamic properties under ambient conditions due to wind and traffic induced loads and for calibrating analytical models using the dynamic properties. Mazurek and Dewolf[7], Agbabian[8], Nigbor[9] used calibrated models for baseline for health monitoring. Chang[10] developed the finite element model of a long-span bridge in Hong Kong and compared the results of the ambient vibration tests conducted at different times. Brownjohn and Xia employed software based automated model calibration methods to calibrate a model for the Safti Link Bridge[11]. A comprehensive literature survey on modal calibration is available in Mottershead and Friswell[12] and Natke[13].

Presently, a number of major long-span bridges such as the Storebaelt Bridge in Denmark, the Lantau Crossings in Hong Kong[14], the Akashi Strait Bridge in Japan[15], and the Commodore Barry Bridge in the U.S.[16] are modeled and instrumented for continuous monitoring for seismic, wind and general health monitoring purposes. Their global dynamic properties identified by ambient vibration monitoring as well as additional experimental approaches. These applications provide an excellent opportunity for evaluating the state-of-the-practice, pointing to major research needs to eliminate the barriers that limit the application of various experimental and analytical technologies for structural identification of long span bridges. It is possible to tabulate the major research needs in reliable structural identification of long span bridges with respect to the sources of uncertainties and difficulties as shown in Table 1.(Table 1 is attached in Appendix)

3. The Commodore Barry Bridge

The Commodore John Barry Bridge (CBB) (Fig.1) spans the Delaware River between Chester, Pennsylvania and Bridgeport, New Jersey. The bridge has five traffic lanes, serving more than six million vehicles annually, a significant percentage of which is heavy truck traffic. It opened to traffic in 1974 with a main span length of 501m and a total bridge length of 4.24km. The focus of discussion here is the principal long-span through-truss system shown in Figure 1.

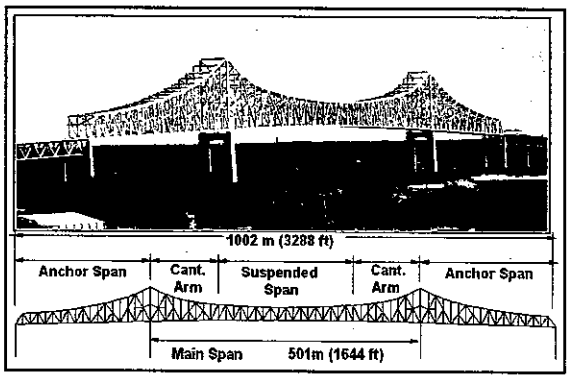

Figure 1: Commodore Barry Bridge

The sub-structures of the through-truss consist of four reinforced concrete piers shown in the photo in Figure 1. The two principal trusses of the through-truss are spaced 22.10m apart. Each truss has 73 panel points spaced at 13.93m intervals. The top and bottom chords of the trusses are constructed from welded box sections. A combination of welded box and H-sections are used for the vertical and diagonal truss members.

Lateral "wind" bracing includes horizontal plane K-bracing at the top and bottom chord levels, and by lateral

portal and sway frames located at various panel points throughout the structure. The suspended span of the bridge connects to the cantilever arms via vertical truss hangers, which are pinned at their upper and lower extremities. Truss members with axial and rotational releases transition the top and bottom chords between the suspended span and the adjacent cantilever arms. The floor system of the bridge consists of a 20.32cm thick lightweight reinforced concrete deck that is composite with steel beams laterally spaced at 2.10m. The steel (stringer) beams are continuous over the floor beams in either four span or five span increments.

4. Integration of Experiment, Analysis and Information

St-Id of large structural systems requires the integration of: (1) Structural conceptualization, (2) Analytical (geometric-FE) modeling, (3) Designing and executing various experiments, (4) Data processing and identifying modal and other characteristics, (5) Model calibration and validation, (6) Simulation and interpretation, (7) Decisions and heuristics[5,6].

Conceptualizing a large and complex kilometer-scale structure that would incorporate several structural sub-systems of different hierarchy, such as the main trusses, the horizontal wind-bracing, the floor system, etc., followed by the foundations and sub-structures, bearings and a multitude of movement systems is a major challenge. Structural engineering expertise, many visits to the bridge for close-range inspections and photogrammetry, followed by a virtual 3D CAD reconstruction are essential elements for conceptualizing so that an analytical model may be constructed. Two issues need to be resolved before a final decision regarding analytical modeling:

(a) Principal reason(s) for needing a field-calibrated model. In many applications that are in the realm of research, constructing a field-calibrated analytical model represents the culmination of the effort. However, it is really a proper utilization of a field-calibrated model for simulations and reaching decisions based on the insight gained from the simulations that should govern the attributes of the analytical model.

(b) The most significant source(s) of uncertainty related to the actual structure and whether/how these may be represented by various types and resolutions of analytical modeling?

Analytical modeling should be governed by the above issues in terms of form and resolution. Civil engineers have been engaged in numerical simulation for decades, and there are many examples of knowledge driven methods, such as Fuzzy Logic and Probabilistic Reasoning, and data driven methods, such as Artificial Neural Networks and Evolutionary Computing approaches, both independently and in hybrid forms, in various fields of civil engineering. For example, there have been recent efforts for "agent-based" modeling of synthetic infrastructure systems by taking advantage of supercomputers [17,18].

However, the solution of most civil and structural engineering problems require predicting physical quantities such as load effects, responses and capacity at the local level under a variety of external or intrinsic loads. This requires physics-based models such as those that are macroscopic-level (smeared), element-level or microscopic-level where predicted quantities may be related to local stresses, strains and deformations in the actual structure. Recent advances in personal computers and general-purpose finite element modeling and analysis software make 3D mixed element-and-microscopic-level modeling by using a variety of finite elements feasible. Therefore, this paper focuses on 3D FE modeling at an element level, where at least one analytical element simulates each structural element. In addition, the sub-structures (piers and foundations) are modeled by a smeared approach, and the RC deck is represented by shell finite elements, discussed further in the following.

The second question concerns whether the analytical model would do justice to the uncertainty prevailing in real life. Even with extensive effort for conceptualizing a structure and measurements, uncertainty may be due to a lack of observability, and many mechanisms causing extensive variability in local material and connection properties, discontinuity, nonlinearity and non-stationary loads, responses and behaviors. If the uncertainty in real life does not permit simulating the structure and its loading with a linear, stationary and deterministic representation, there may not be merit for a 3D FE modeling. The writers were interested in investigating whether it is ***possible and meaningful*** to characterize a long span bridge in terms of a field-calibrated 3D FE model such that the movements, deformations, forces and stresses caused by live loads at the critical regions may be reliably estimated (for example within a confidence interval of 75%).

Experimental technologies may be classified into four classes based on how various specializations developed in the realm of research and practice (Table 2). Dynamic testing of major bridges are often necessitated by a lack of other test techniques providing a direct measurement of the global dynamic properties of a structure-foundation-soil system within a set of coordinates distributed throughout a structure and without the need for any external measurement reference frame. In the case of evaluation of seismic vulnerability and seismic retrofit design, dynamic testing again becomes a necessity. Depending on the required data, other experimental techniques such as controlled load testing may be applied to characterize the as-is mechanical characteristics and conditions of a bridge. The important requirement is an optimum integration of various experiments so that data sets complement each other in terms of duration, bandwidth and density of measurements and do justice to the nature and level of uncertainty prevailing in the structure and its loading environment.

Table 2: Technologies for St-Id

Experimental Technologies			
Geometry Monitoring: *Photogrammetry, GPS Laser*	Controlled Load Testing and Field Measurements	Local NDE and Material Characterization	Continous Monitoring: *Real time, multi-mode image and data*
Analytical Technologies			
CAD, Reverse CAD, Conceptualization	Analytical Modeling: *FE, Statistical, Probabilistic*	Linear FE Analysis: *Static, dynamic, moving load*	Non-linear FE Analysis, Stochastic analysis, Systems Optimization, Decision Analysis
Information Technologies			
Wide Area, Multi-mode Sensing, Data Acquisition Communication, Computing and Control in Real-Time	Data Quality Assessment, Data Processing, Multi-Variable Correlation Analysis, Patterning	Transformation Data to Information, Data Management, Interpretation, Archival, Security, Mining	Transforming Information to Knowledge, Visualization, Interpretation and Decision making

Information technologies cover the entire spectrum of efforts related to the acquisition, processing and interpretation of data. This includes sensing, data acquisition, pre-processing, communication and control, transmission and synchronization, quality testing, post-processing, analysis, display and visualization, database archival and management, and, interpretation for decision-making. It is not possible to separate and investigate sensing, data acquisition, communication, signal/data processing and other information management steps that are required for systems-identification and health monitoring from the reality of actual infrastructure. A flow-chart of an integrated, intelligent information system has been developed by the writers for a real-time systems-identification application to a long-span bridge and discussed in a recent publication by the writers[19].

5. Finite Element Modeling of the CBB

The criteria considered in developing the analytical model of the through truss of the CBB, shown in Figure 2 is summarized as follows:

a) *At least one analytical element represented each real structural element:* The structural elements of the bridge were modeled using a mix of shell and beam elements. In-plane and out-of-plane deformations of the deck slab were simulated by discretizing the slab into 2.13m x 3.05m mesh of rectangular shell elements with six degrees of freedom at each node, with 2966 shell elements. 3D beam elements represented the upper chords, lower chords, verticals, diagonals, floor beams, out-of-plane truss members, bracing, and roadway stringers. The piers were modeled with 3D frame elements in a smeared manner for computational efficiency. The total number of frame elements utilized in the model was 6,047.

b) *Model geometry should accurately represent the actual geometry:* The overall geometry of the bridge was discretized at joints such that the model could represent the local 3D aspects of the bridge geometry. The total number of degrees of freedom in the 3D FE model was 25,218 corresponding to 6,047 joints.

c) Boundary and continuity conditions: The bearings at the extremities of the through truss were modeled by rollers in the preliminary model. For the fixed bearings at the tower connections, longitudinal translations were restrained as consistent with the design. Roller and fixed bearings were represented with beam elements with released or restrained degrees of freedom between the piers and the through truss chords. Moment releases were defined at the top and bottom of the hanger since there are pins that allow rotation in the plane of the main truss. The axial, moment releases at the lower chord between the cantilevered arms and suspended span were simulated. Zero force members between suspended span and cantilever arms were simulated. Wind linkage mechanisms were simulated using appropriate releases. Discontinuities of the stringers and releases in the deck system from intermediate expansion joints and expansion dams were modeled. Rigid links and constraints were used to simulate the actual 3D geometry within all connections.

d) *Stiffness and deformation kinematics:* The cross sectional properties of the truss members were defined based on the design documents. Torsional properties of the truss members were calculated and incorporated in the FE model. The local axis orientation of each member was checked in the model for conformance with the actual orientation of the members on the bridge.

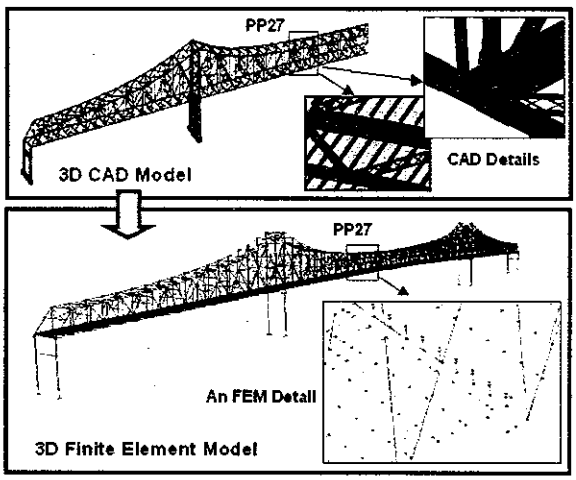

Figure 2: 3D CAD and FE Model of the Bridge

Before calibration, any human errors in input have to be eliminated by quality assurance and control measures developed for large-scale models since analyses may be carried out and global equilibrium may be maintained with such models even with the presence of many errors at the local level. Quality assurance and control requires a very systematic procedure for a rapid, accurate and thorough diagnosis of all the probable human errors in the model in addition to checking and verifying equilibrium for many free bodies. Such a systematic inspection methodology was implemented to review the FE models of Commodore Barry Bridge, by taking advantage of three tools: a) Graphical user interface, b) Structural response interface, and, c) Numerical pattern searching by spreadsheet manipulations. All the three tools were integrated to achieve the most effective review of the FE models. Naturally, the rigor and training of the model developer, as well as the patience and thoroughness of the inspector remain as the most important factors in the assurance process. These tools help visualize various direct (within the input data arrays) or consequent (in the resulting structural system) patterns inherent in the data as a result of the physics of the structure, due to symmetry, anti-symmetry and geometric continuity, as a means of identifying input errors and validating the accuracy of the output. It is important to note that many errors in element properties and connectivity that may not be apparent from a review of the output of the diagnostic analyses were indeed discovered by such a scrutiny of the patterns in the input data.

6. Experiments for Calibration of the FE Model of the CBB

6.1 Ambient Vibration Testing of Long Span Bridges

Ambient vibration testing has been applied by many researchers: on the Golden Gate and San Francisco Oakland Bay Bridges by Carder[20], again on Golden Gate by Abdel-Ghaffar and Scanlan[21], on the Deer Isle Bridge by Kumarasena[22], on the Quincy Bayview Bridge by Wilson and Gravelle[23], on the Fatih Sultan Mehmet suspension bridge over Bosphorus by Brownjohn[24], the

Alamillo cable stayed bridge in Spain by Casas[25], on a welded steel plate girder bridge by Farrar and James[26], on the Vasco Da Gama Bridge in Portugal by Cunha[27], on the Tsing Ma Bridge by Xu[28], on the Hakucho Suspension Bridge in Japan by Fujino and his colleagues[29,30], on the Kap Shui Mun Bridge in Hong Kong by Zhang[31].

6.2 Design of the Ambient Vibration Test

The design and execution of the ambient vibration tests for long span bridges requires a careful analysis of issues related to observability and measurability, nonlinearity and non-stationarity. Many of the tools and technologies developed for modal analysis of mechanical systems and validated in the laboratory may require modification for successful ambient monitoring of large structures. The ambient vibration test of the Commodore Barry Bridge was designed as summarized in the following:

a) ***Preliminary information on the dynamic characteristics of the bridge:*** The ambient vibration measurements should capture the frequency band of interest modal frequencies and shapes of the structure so that the number of modes that are identified from the test are sufficient to capture the global behavior for global calibration. For large structures such as CBB, the first fundamental frequency is often under 1 Hz, and several closely coupled modes should be expected. Preliminary analyses indicated the first lateral mode at 0.20 Hz and the first bending mode at 0.31 Hz. The lowest frequency is especially important for selecting the sensors and data acquisition system.

b) ***Instrumentation plan:*** The sensor locations, distribution and orientations are based on FE analysis results. Of the several test grid options, if the sensors are not roved, either the full bridge can be tested or one half of the bridge can be tested with a denser sensor grid. It is possible to rove the sensors while keeping a few stationary, which help to splice the data sets. This option is labor intensive, required installing and dismantling the test grids, and laying and routing cables to different locations and the data may not be as reliable as data from a stationary set of sensors. Collecting data simultaneously ensures that the ambient temperature, wind and traffic conditions are the same for all the sensor channels during the acquisition of the data. Therefore, one-half of the through truss was instrumented with 45 stationary sensors as shown in Figure 3. Access and safety requirements naturally dictated the sensor locations.

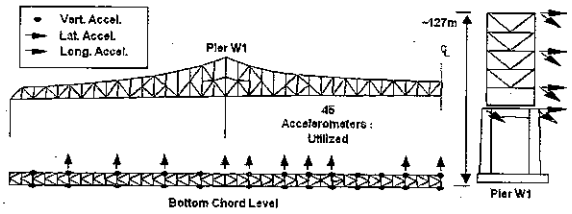

Figure 3: Ambient Vibration Test Grid

c) ***Data acquisition strategies:*** The large set of sensors that are used necessitated especially powerful data acquisition hardware. The Agilent Technologies VXI system with three 16 channel E1432A boards was used for data acquisition. This system is capable of simultaneously measuring up to 48 channels. The system has a 90dB typical dynamic range, and on board DSP's for filtering. The E1432A board, which has a dedicated 16 bit ADC per channel for continuous data acquisition, can be used for frequency analysis up to 23 kHz. HP DAC Express was used for data acquisition software. Firewire (IEEE-1394) communication protocol was used on the PC running DAC Express, controlling the VXI system and storing the data.

d) ***Sensor requirements:*** 32 PCB Model 393C ICP and 13 PCB Capacitive accelerometers were installed by using industrial magnets. The ICP type 393C accelerometers have a nominal sensitivity of 1000 mV/g, and a specified frequency range of 0.025 Hz to 800 Hz, and the amplitude range is +/- 2.5 g with a resolution of 0.0001 g. The capacitive sensors also have a nominal capacity of 1000mV/g within a frequency range of DC to 100 Hz. The amplitude range is +/- 3 g with a resolution of 30 μg. Two ICP signal conditioners and a capacity signal conditioner were used with the accelerometers.

e) ***Cabling requirements:*** Co-axial cables transmit the signals from the PCB 393C accelerometers. For the capacitive accelerometers, 4 pair shielded CAT5 cables were used. The expected signal amplitudes and spectra, and the cable characteristics were evaluated for possible signal loss due to cable length and it was determined that this was not an issue for the frequency band of interest. Very recently, wireless sensors/data acquisition systems are becoming available. Although there are laboratory and field studies on smaller bridges using wireless sensors/data acquisition systems, there is a great need to understand the limitations such as distance, interference and loss of data synchronization on long span bridges.

6.3 Conducting the Field Test

The main inputs during the data collection are induced by wind, traffic and temperature. Since these inputs cannot be controlled, it is important to have an on-line monitoring scheme to make necessary adjustments to the voltage level for the optimal dynamic range and to detect any problems with sensors or cables. For each sensor channel, time and frequency response plots are defined using HP DAC Express software. Time domain data is important for monitoring signal characteristics such as the magnitude of the signals, the level of DC off-set, overloads etc. This allowed real time monitoring and quality control of the data both in time and frequency domains. Since the frequency band of interest is below 4 Hz from the preliminary analysis, data sampling rate is defined as 40 Hz and data sets were collected for 307 sec. windows before saving and backup. Each of the 45 channels collected 12288 data points. DC signal coupling avoided the need for high-pass filters. Sample data presented in Figure 4a indicates acceleration levels within 2% of g.

6.4 Data Analysis

The input(s) that excite the structure during ambient monitoring are assumed to have Gaussian white noise characteristics. Therefore, the Random Decrement (RD) technique is applicable for transforming the measured random time series into free decay responses. Free decay responses contain information only on the structure and

not on the random inputs[32]. The random response of a structure at the time t0+t is a superposition of:

(a) Response due to the initial displacements at t_0,

(b) Response from initial velocity at time t_0, and,

(c) Random part due to the load applied to the structure between t_0 and $t_0 + t$.

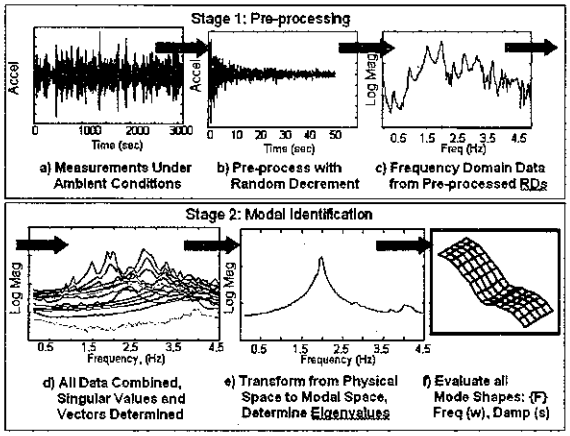

Figure 4: System Identification using Ambient Vibration Data

By taking averages of time segments of equal duration, that start every time the response exhibits an initial displacement the random part due to random load will eventually average out and become negligible. Furthermore, since the sign of the initial velocity should vary randomly with time, the resulting initial velocity will also be zero[33]. In this manner, the only part left in the averaged response data will be the free decay response from the initial displacement. Figure 4 illustrates the data processing steps.

Based on research by Asmussen[33], a zero crossing greater than 1.5 times the standard deviation of the signal may be an acceptable trigger realizing that the trigger levels depend on the nature of the signal. One of the difficulties in testing the bridge was that the vibration amplitudes of the modes within the 0-0.9 Hz range were much lower than the higher mode amplitudes easily excited by traffic. Selection of a trigger at a level higher than low amplitude vibration modes creates signals that are shadowed by the residuals of the higher modes. On the other hand, if lower triggering levels are selected to include the amplitude range of the lightly excited lower frequency modes, the generated time domain responses may not correspond to good exponential decay functions. When the triggering levels are higher, whether the RD averaging retains any output from lower modes requires careful evaluation. Sub-sampling the data and utilizing windows where mainly the lower modes are excited due to wind should enhance the RD process for this problem; however, a thorough sensitivity study is essential before an optimum processing of this type of signals obtained from long span bridges. Clearly, data acquisition or ambient monitoring for long durations, while also recording the environmental conditions and traffic, and covering a variety of input conditions, is important. This is the key to success to modal identification of long-span bridges from ambient vibration data, discussed further in the following.

After completing the first stage (pre-processing stage), a pseudo multiple input-multiple output data set is obtained. The time records appear as impulse response functions, as shown in Figure 4b. An impulse response function is an exponential decay function that incorporates combinations of structural vibration periods within the time window. The time window should be long enough to capture periodicities of the modes through the critical bandwidth as well as decay to zero. The windowing should eliminate noise but not response data at the tail end of a window. As shown in Figure 4, frequency spectra of the data are generated by taking Fast Fourier Transforms (FFT) of the individual data sets.

There are many algorithms that may be used to process impulse response functions and extract modal characteristics. At this stage, the data sets that consist of FFTs of the individual datasets are combined using a spatial domain algorithm to determine the dynamic properties. ***The spatial domain algorithm*** (SDA) is particularly effective in the case of large number of experimental degrees of freedom[34,35]. Therefore SDA is very suitable as in the case of Commodore Barry Bridge test where a large number of sensors are used in conjunction with transforming the data to a multiple input-multiple output format. Using SDA, first the modal vectors are identified by using singular value decomposition of the combined data set. The left singular vectors are close approximations of the modal vectors. Each modal vector is then used to decompose (spatially filter) the data into a single degree of freedom system by taking advantage of modal orthogonality. The single degree of freedom system corresponds to the modal vector that is used to decompose the data set. The single degree of freedom system is then analyzed to obtain the eigenvector of the particular mode of interest. Figure 5 illustrates how the first two modes are extracted after being filtered along with the experimental and analytical mode shapes.

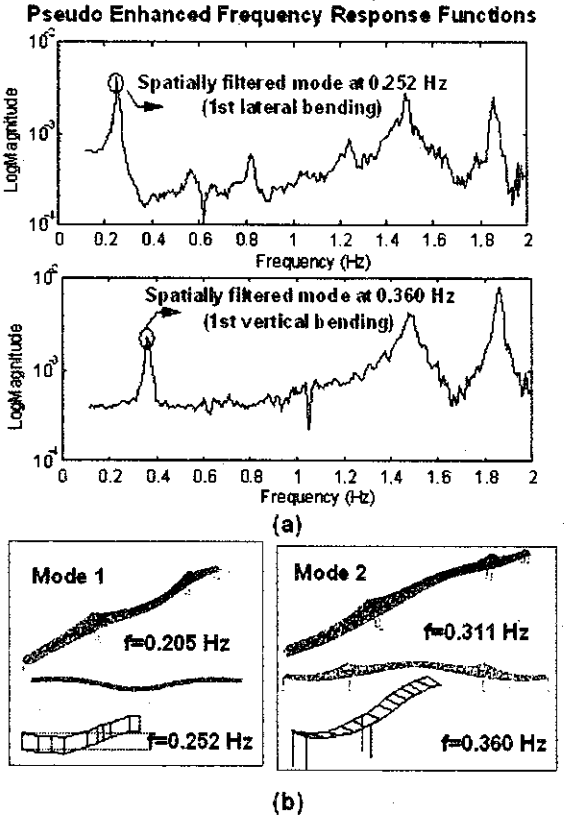

Figure 5: Modal Identification and Correlation Examples

6.5 Experimental Modes and Their Correlation with Nominal Model Results

A minimum number of modes covering the critical bandwidth of interest is required if the ambient vibration monitoring is to lead to reliable St-Id. Establishing the bandwidth and modal density within the bandwidth is needed before the test is conducted and data analyzed. Although it is possible to determine the frequency band of interest visually from a spectral analysis of data obtained at various cut-offs, it is very important to quantitatively determine the frequency band and the number of modes that are to be determined.

The writers investigated the convergence of the Uniform Load Surface, using an index defined as Load Dependent Modal Convergence[35]. Using this method, the modal flexibility based deflection profiles are evaluated. Assume m modes are identified from a modal analysis; m different modal flexibility matrices can be obtained, each time adding one higher mode to the flexibility matrix. As a result, m different deflected shapes are obtained for 1, 2...m modes included in the flexibility matrix. The sum of the squares of the differences of deflection values at each degree of freedom can be determined when a new mode is added to the flexibility matrix. Figure 6 shows the convergence of the modal flexibility and it is seen that modal truncation effects decrease considerably for 15 modes for the analytical study shown in this figure.

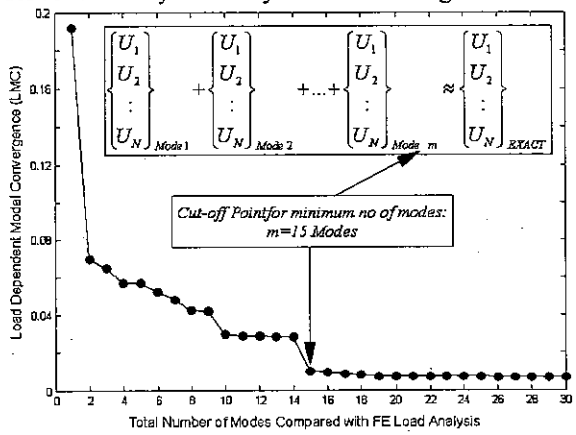

Figure 6: Identification of minimum number of modes

After the global frequencies were identified from the analysis of the Commodore Barry Bridge data, the first fifteen modes were extracted. It should be noted that these modes were operational modes excited by wind and traffic during the execution of the test. Such inputs may not excite every vibration mode that may be indicated by a FE model. In the ideal case for small-scale structures, a wide band force input such as vertical impact or lateral forced-excitation tests cause the structure to vibrate in a wide spectrum of frequencies, and may excite all measurable modes within a given bandwidth. However, because of the size of the Commodore Barry Bridge, it is extremely difficult to provide dynamic input sufficient to excite all the global modes. As a result, the test is conducted under varying environmental and traffic conditions unlike stationary laboratory conditions. The non-stationarity of the structural behavior coupled with random ambient vibration is a major challenge, which requires experience and skill making modal analysis more of an art than a well-defined procedure.

The experimental (measured) frequencies were correlated with the simulated frequencies obtained by an eigenvalue value analysis of the nominal through truss model. This correlation was performed in order to observe the degree of success of the nominal model in predicting and simulating the dynamic response of the bridge. The nominal model is based on the nominal values for the material and geometric properties, as well as the idealized movement and floor system. A closer study of the first five experimentally measured modes and frequencies revealed that the first, third and fifth modes are typical lateral vibration modes with frequency values of 0.252, 0.581 and 0.666 Hz, respectively. The second mode is a vertical bending mode with a frequency value of 0.360 Hz, and the fifth mode is a combination of vertical bending and torsion modes with a frequency value of 0.666 Hz. For these modes, the nominal model yields much lower simulated frequencies in comparison to the experimental ones. More specifically, for the first and second modes, the measured frequencies are 0.205 and 0.311 Hz, which are approximately 19% and 15% lower than their experimental counterparts (Fig.5). In particular, the frequency error becomes more definite for the third mode and above, reaching its maximum value of 46% for the third mode. In general, the average frequency error of the first five modes is found to be 28%.

Without any additional effort, the preliminary correlation indicated the following two conclusions. Firstly, a relatively high level of discrepancy existed between the experimental and analytical results in terms of simulation of global structural dynamic behavior such that the nominal model should be improved and calibrated to better simulate the measured responses. Secondly, the case that measured frequencies were higher than analytically generated ones, implied that the bridge was stiffer than its analytical representation by the nominal model.

6.6 Parameter Sensitivity Studies

Parameter sensitivity studies were carried out to examine the impact of the variation of parameters upon the dynamic properties of the bridge, and thus to determine the most critical parameters for the global calibration of the through truss model shown in Figure 2. Parameter sensitivity based model updating can be conducted using an automated procedure[11], or manually by analyzing the sensitivity of parameters and ensuring their impact on structural response not only mathematically but also physically[6]. In this paper, the writers define the parameters that are associated with high uncertainty and also impact the structural behavior.

The actual physical parameters were determined to be: sectional properties of rigid links, elasticity modulus of deck concrete, elasticity modulus of pier concrete, the variations in boundary conditions, and, the force releases and kinematics of the movement systems. In conducting the sensitivity studies, these parameters were varied and the changes in modal order and frequencies were investigated for the first 15 modes.

The analyses show explicitly that the modal properties (frequency, order and existence of modes) are highly sensitive to elasticity modulus of pier concrete, and thus to any variation in the stiffness of piers. For instance,

variation in the elasticity modulus causes a switch in the order of some modes.

Table 3: Summary of the Parameters for the three Analytical Models of the Through Truss

PARAMETER	NOMINAL MODEL	ONLY GLOBALLY CALIBRATED	GLOBALLY AND LOCALLY CALIBRATED
MATERIAL PROPERTIES			
Concrete, Elasticity Modulus			
Deck (GPa)	24.82	24.82	24.82
Pier (GPa)	24.82	24.82	24.82
Steel, Elasticity Modulus (GPa)	200.00	200.00	200.00
STRUCTURAL PROPERTIES			
Pier Stiffness	Fully Flexible	Fully Rigid	(0.50-0.75)L Flexible
Movement System			
at Piers (W1,E1)	Fix Bearing	Fully Restrained	Fully Restrained
at Piers (W2,E2)	Exp Bearing	Fully Restrained	Fully Restrained
at Suspended Span (PP27,PP45)			
Hangers	Moment Release	Fully Restrained	Fully Restrained
Low and Upp Chord Memb	Axial and Moment Releases	Fully Restrained	Fully Restrained
Wind Linkage	Moment Releases	Fully Restrained	Fully Restrained
Floor System			
Deck	Body Constraint	Body Constraint	Body Constraint
Stringer	Body Constraint	Body Constraint	Body Constraint
Floorbeam	Fixed or Expansion Shoes	Fixed or Expansion Shoes	Body Constraints

The variation of modal properties with respect to boundary conditions and movement systems shown in Figure 7 indicate that rotational degrees of freedom have a slight impact on modal properties; however, as far as the translational DOFs are concerned, the variations in modal properties are very obvious. Similar to the effect of pier stiffness, they also result in remarkable changes in modal shapes, frequencies and orders as well as their existences. A summary of the parameter study is given in Table 3.

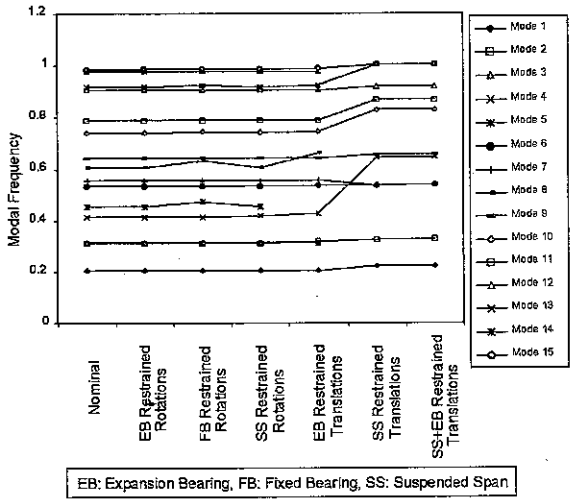

Figure 7: Modes vs. Boundary Conditions and Movement System

6.7 Initial Global Calibration

A correlation of measured frequencies with simulated ones obtained with different models during calibration is given in Table 4 and Figure 8 in terms of the first two modes. The first model "1.0LPRI+NMS", in essence, is the nominal model itself with its idealized movement systems and fully flexible pier lengths, and the second model "1.0LPRI+RMS" is the stiffest nominal model that can be created without any change in the piers' stiffnesses. However, even for the second model the analytically generated frequencies are observed to be lower than their experimental counterparts, implying that the structure in reality is still stiffer. This observation illustrated the availability of additional mechanisms of rigidity contributed by the piers. As a result, the models "0.5LPRI" and "0.0LPRI" were created, where the piers' stiffnesses were increased by decreasing their flexible lengths.

Table 4: Initial Global Calibration

			Mode 1 (Hz)	Mode 2 (Hz)
Experimental	Modal Analysis		***0.252***	***0.360***
Analytical (FE Model)	1.0LPRI	NMS	0.205	0.312
		RMS	0.223	0.330
	0.5LPRI	NMS	0.215	0.313
		RMS	0.234	0.346
	0.0LPRI	NMS	0.230	0.313
		RMS	***0.248***	***0.359***
	PRE	NMS	0.279	0.314
		RMS	0.282	0.364

aLPRI: "a" percent of length of pier is included as flexible, "1-a" percent as rigid, retaining the bearing
PRE: Piers are totally excluded along with with bearing
NMS: Nominal Movement System (at Piers and Suspended Span)
RMS: Restrained Movement System

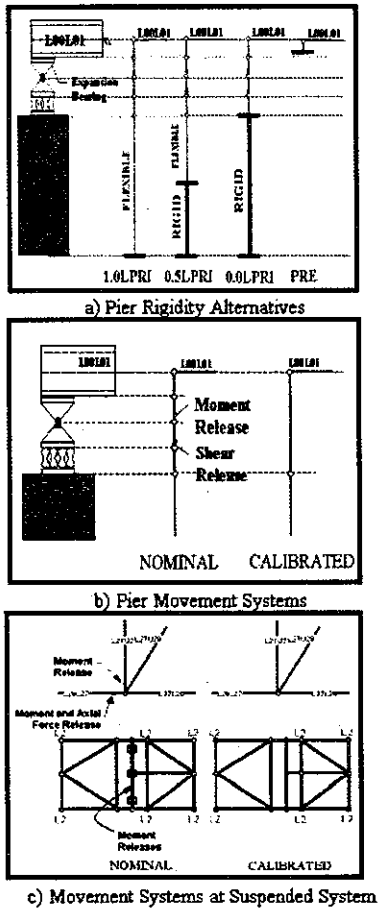

Figure 8: FEM Details for boundary and continuity conditions

Among all the models tested, the best correlation between the measured and simulated frequencies was obtained with the model "0.0LPRI+RMS". In other words, the model where the piers are assumed entirely rigid and

the movement systems of the bridge are fully restrained, yielded the closest results to the experiment in consideration of the frequencies of the first two modes. A more comprehensive correlation between this model and the experiment is given in Table 5. As seen in this table, the model exhibits an excellent correlation in terms of all the modal properties of the first five modes, including the frequencies, shapes and order. It should be noted that as global and local calibration progresses, correlation for the first 15 modes are prepared and evaluated. This model is referred to as "Only Globally Calibrated" model of the through truss here, since the model was calibrated without a verification of its validity and acceptability in simulating the local structural responses measured with the controlled load tests.

Table 5: Correlation for the Initial Global Calibration

Mode (1)	Experimental Freq. (Hz) (2)	Analytical Freq. (Hz) (3)	Percent Error (4)	Mode Type (5)
1	0.252	0.248	1.59%	First Global Lateral
2	0.360	0.359	0.28%	First Global Bending
3	0.581	0.581	0.00%	Second Lateral
4	0.602	0.61	-1.33%	First Torsion, Bending
5	0.679	0.657	1.35%	Lateral Bending and Torsion

6.8. Controlled Load Test for Local Calibration

6.8.1 Controlled Load Tests

To permit local calibration of the FE models, the writers performed controlled load tests on the through truss spans using two 49 tons cranes while recording strains at 38 critical locations. The first scenario consisted of a crawl speed test using a single crane. The crane was driven across the bridge at a crawl speed (8 to 16 km/h) as the structural responses at the instrumented locations were continuously captured (Fig.9). The second scenario was a static load test during which single and double cranes were positioned at various pre-determined locations along the bridge in 18 configurations on the main truss.

6.8.2 Local Calibration with Controlled Load Test Results

Figure 10 shows the instrumented sensor cluster locations of the through truss for the purpose of local calibration and Figure 11 presents sample data from the crawl speed and static load tests. As illustrated in Figure 10, sensor clusters are in the vicinity of panel points 27 and 36 (hanger and mid-span), and the sensors located at positive and negative moment regions of these sections were used to measure the incremental local strains (and estimate the incremental stresses) developing at these regions during the controlled load tests. The local calibration was performed by comparing and correlating these experimental results with the corresponding analytical responses obtained from the FE model.

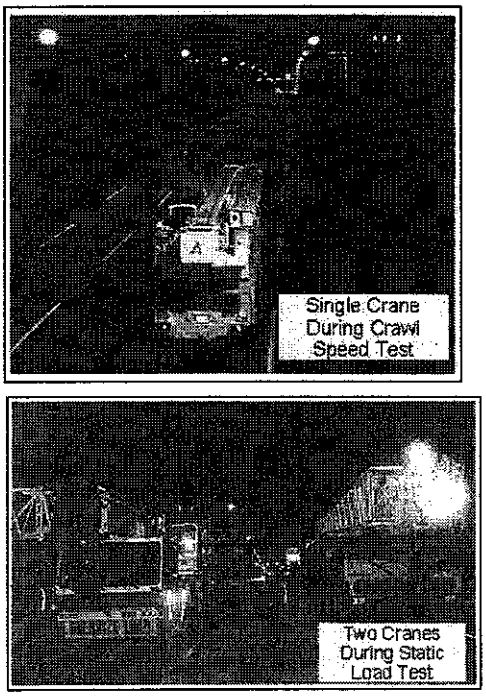

Figure 9: Load Test at the Commodore Barry Bridge

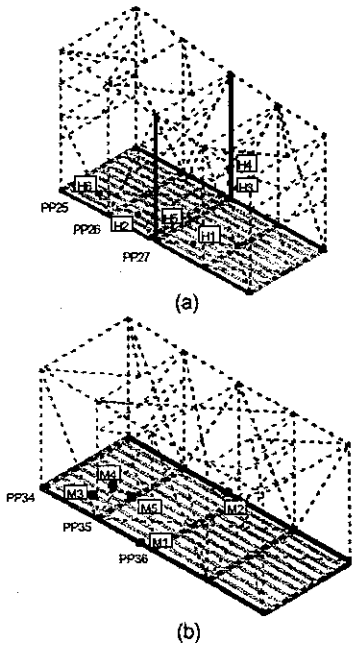

Figure 10: Sensor cluster locations near a)Panel point 27, b)Panel point 36

The results of local calibration of the through truss model are summarized in Table 6. A comparative study of "Experimental" and "Nominal" columns clearly shows that the nominal model performs poorly in simulating the local stresses obtained during the experiment. For example, the data from the experiment for the section H1 indicates that the bottom flange stresses (sensors L1 and L4) are 44.47 MPa and 41.44 MPa, whereas the bottom flange stress from the nominal model is found as 68.12 MPa for the same section and load configuration. This indicates that the stresses produced by the nominal model

overestimate the actual measured stresses for almost all sections.

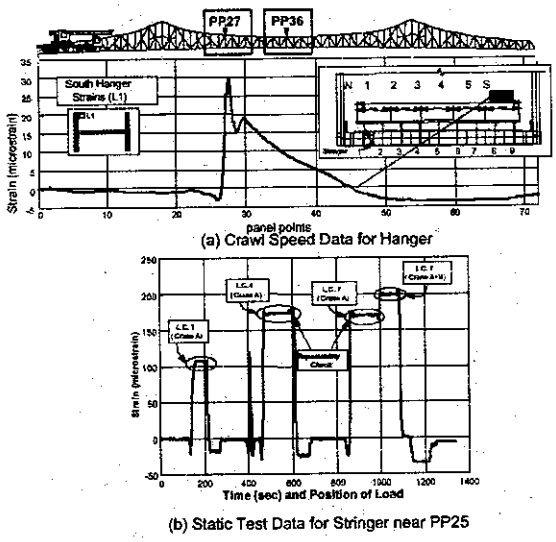

(a) Crawl Speed Data for Hanger

(b) Static Test Data for Stringer near PP25

Figure 11: Sample data from the load test

A comparison of "Nominal" and "Only Globally Calibrated" reveals that except for the section M1, the only globally calibrated model does not yield any better results than the nominal model in simulating the local responses, whereas it has been shown in initial global calibration that this model produced an excellent correlation in simulating the modal properties in global sense. From a mathematical point of view, the order of error averaging the stress measurements of 21-sensors at 7-instrumented sections between the experiment and analysis is around 55% in the case of nominal model, it is reduced to only a slightly lower value of 48 % for the "Only Globally Calibrated" model. The margin of error in the correlation of analytical and experimental results was significant enough to warrant a further calibration of the only globally calibrated model to better simulate the stresses measured during the truck load test.

Table 6: Local Calibration of the Through Truss

Sensor Location	Sensor ID	Load Case	Experimental MPa	Nominal MPa	Only Globally Calibrated MPa	Glob & Local Calibrated MPa
Around the Hanger (PP27)						
H1	L1	H9	44.47	68.12	68.01	46.54
	L4		41.44			
	L2		-0.90	3.31	3.59	1.45
	L3		2.96			
H2	L1	H8	40.20	59.92	59.43	45.71
	L2		-4.00	3.10	3.03	1.59
H6	L1	H7	39.78	55.99	56.19	43.85
	L2		1.03	3.24	2.96	1.31
H5 (U27L27)	L1	H9	8.62	11.51	11.79	11.72
	L2		8.41	11.51	10.62	10.69
	L3		5.38	6.83	5.72	5.72
	L4		5.79	6.83	6.89	6.76
Around the Mid-span (PP36)						
M3	L1	M7	40.20	57.36	57.30	46.82
	L2		38.68			
	L3		1.79	2.96	2.96	2.83
	L4		2.28			
M4	L1	M7	30.96	44.20	44.13	37.23
	L2		0.34	0.00	0.00	0.48
M1	STW	M7	4.27	6.76	5.17	3.10
	SOW		4.00	6.76	5.17	2.90

6.8.3 Final Global and Local Calibration and Model Updating

A series of analyses with alternative models, created by modifying the critical structural systems of the only globally calibrated model indicated that when a fully composite floor system (FCFS) was assumed this yielded highly favorable solutions in approximating the local stresses. In order to achieve this calibration, the floor system was modeled in a way to account for the relative movements due to the expansion or fixed shoes between the floor beams and stringers, a fully composite floor system assumes a perfectly rigid body behavior between the deck, stringer and floor beam. As shown in Figure 12, this was achieved by either eliminating the releases of the rigid links, or simply introducing body constraints between the corresponding nodes of deck, stringer and floor beam.

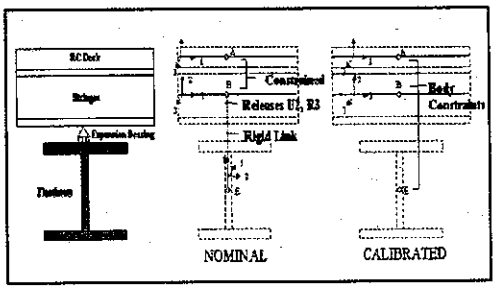

a) Floor System

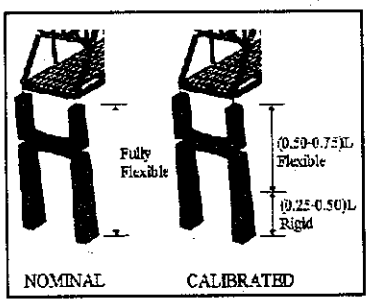

b) Stiffness of Piers

Figure 12: Globally and Locally (final) Calibrated Model of the Through Truss

The analytically simulated stresses obtained with the analytical model where perfect composite action is simulated between the deck and stringer beams by body constraints (Fig.12) are listed in the last column of Table 6. The simulated stresses correlated better with the measured ones such that the order of error obtained by averaging the difference between the measurements of 21-sensors at 7-instrumented sections and their simulated counterparts is reduced to 24 % with this model, from a value of 48 % in the only globally calibrated model. This level of correlation for the local calibration was the best that could be achieved given the manual approach to correlation as opposed to in the context of an automated optimization problem.

Given the high level of uncertainty governing the local structural responses, it was deduced that the model was adequately calibrated to the point that it could properly simulate the measured responses in both the global and local senses, and so it was considered to be the final calibrated model of the through truss. A summary of comparison of the three analytical models (nominal, only globally calibrated, and both the globally and locally calibrated) of the through truss is given in Table 3, in terms of modified parameters and structural properties in the models, as well as numerical results of the global and local calibration. A further discussion of the final correlations between frequencies and mode shapes is in the following.

7. Discussion of the FE Model Calibration Results

The evaluation of the calibrated finite element model is carried out is first to evaluate the level of match between the measurements and the model globally and locally. Then, whether the calibrated model may serve for interpreting the current condition is discussed.

The model was examined in terms of its success in simulating the modal properties first. An eigenvalue analysis of the model was performed with different flexible lengths of the piers (a = 1.0, 0.75 and 0.5) while the movement systems were assumed as fully restrained (RMS), as in the case of only globally calibrated model. The results of this study indicate that the model exhibits good performance if the flexible portion of the piers are taken as between 50-75 % (a = 0.5-0.75) of their total length, as shown in Figure 12. By assuming that the flexible length was equal to 62.5 % (a = 0.625) of the total length, the first fifteen modes between this the model and the experiment show a very good correlation as shown in Figure 13 and Table 7.

Table 7: Frequency Correlation Globally and Locally (Final) Calibrated Model

Mode (1)	Experimental Freq. (2)	Analytical Freq. (Hz) (3)	Percent Error (4)	Mode Type (5)
1	0.252	0.25	0.79%	First Global Lateral
2	0.36	0.365	-1.39%	First Global Bending
3	0.581	0.579	0.34%	Second Lateral
4	0.602	0.606	-0.66%	First Torsion, Bending
5	0.666	0.679	-1.95%	Lateral Bending and Torsion
6	0.716	0.693	3.21%	Torsion of the Midspan
7	0.88	0.867	1.48%	In-phase Bending of Mid-span and the Anchor spans
8	0.97	0.966	0.41%	Lateral Bending and Torsion
9	1.037	1.037	0.00%	Double curvature bending of mid-span and out-of-phase bending of anchor spans
10	1.232	1.145	7.06%	Out-of-phase lateral bending mid-span and lateral-torsional bending of anchor spans
11	1.311	1.15	12.28%	Lateral-torsional bending of mid-span and anchor spans
12	1.428	1.328	7.00%	Triple curvature lateral bending of mid-span, in-phase lateral bending of anchor
13	1.487	1.417	4.71%	Triple curvature vertical bending of the mid-span and in-phase bending of lateral
14	1.605	1.571	2.12%	Out-of-phase lateral bending and torsion of cantilever arms and mid-span
15	1.859	1.874	-0.81%	Quadruple curvature vertical bending of the mid-span and out-of-phase bending of lateral spans

Table 7 indicates the average percentage error between the model and the measurements is around 2.3 %, showing a very good correlation except in the case of mode 11, where the discrepancy is higher than 10 %. However, despite the fact that this model mathematically yields the best correlation, it is misleading to claim that the piers in reality have rigid and flexible components exactly as modeled. In general, there will be a variety of and different levels of uncertainties governing both the experiment and the analysis. Therefore, the ratio a = 0.625 should be considered only as a value which compensates the uncertainties given the operating conditions, the execution of the experiment and data processing, and the many assumptions and idealizations made in the analysis of this particular FE model. The writers have shown that the non-stationarity or time-variant nature of CBB in terms of both the inputs and the responses are significant[36], depending on the stationarity of sustained high wind speed and direction, and of the average ambient temperature. In the course of five years of monitoring the bridge, occasional weather fronts caused very large temperature drops within a matter of several hours. The corresponding bridge stresses and movements were as if the structure experienced major shocks. Significant shifts in intrinsic forces and movements indicated that significant changes in the force and deformation states of the bridge were induced due to such temperature shocks.

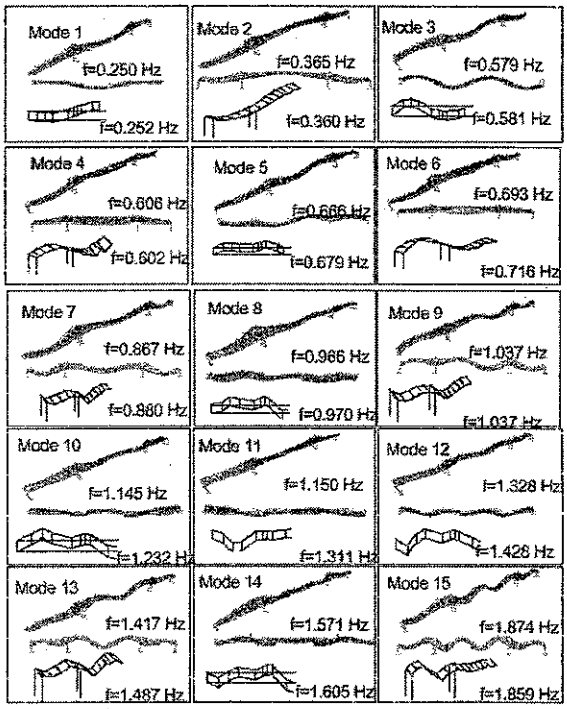

Figure 13: Modal Vectors from the Final Calibrated Model and the Ambient Test

After a sufficiently close correlation was obtained between the measured and simulated global dynamic properties, the strains at the critical elements obtained during the controlled load test were used for local calibration of the floor system element and connection stiffnesses. When a fully-composite behavior of the deck and the stringers, and full continuity between the stringers and the deck were simulated, the root-mean-square (RMS) of the error between measured and simulated strains at 20 measurement locations were reduced from 55% to 24%. After globally and locally calibrating the model, the average error between the model and experimental frequencies is determined to be 2.3 % for the first 15 modes. Hence, this model is considered to provide acceptable simulations of the bridge in relation to the measurements taken from the bridge. ***The confidence in simulated global characteristics such as frequency, mass, stiffness, flexibility, deflections, etc. is judged to be around 75-90% while the confidence in the simulated local characteristics such as the stresses and distortions is judged to be around 50-75%. Naturally, these confidences would remain valid only as long as the structural conditions, ambient conditions and the operating inputs correspond to those during the duration of the experiments.***

8. Conclusions

The writers have demonstrated that a mixed microscopic-structural element level 3D FE modeling of a kilometers-long structure and its St-Id by integrating various experimental techniques is possible. It is now possible to estimate the deformations, forces and stresses caused by live loads at the critical regions of the cantilever through-truss structure of the long-span bridge with reasonable confidence. The writers are currently using the model for health monitoring of the bridge, to interpret the long-term implications of measured load inputs and responses of the bridge. In addition, the model is serving for interpretation of the measured responses in the course of a recent retrofit of the four hangers of the bridge. The writers will discuss these experiences in future papers.

The reliability in the global attributes such as boundary and continuity conditions that may be identified and simulated by means of field-calibrated models using only dynamic test results (globally calibrated models) may appear to be high (as much as 90%). However, this reliability may often be misleading for the level of confidence that one can get for a local stress fields that the dynamic tests are unable to reveal. This is especially true for long span bridges because the resolutions of the dynamic test grids are often quite sparse due to the large size of the structures. It may be possible to improve the resolution by means of multiple overlapping test grids by roving sensors. However issues such as non-stationarity in the loading environment as well as the behaviors of a bridge complicate the modal identification effort and the reliability of data obtained by means of roving sensors should be carefully investigated. Controlled load tests conducted within a shorter duration are very useful and in fact essential for checking the validity of an identified analytical model. The writers show that the reliability of only a globally calibrated model may not be satisfactory and local calibration (adjusting local behavior mechanisms and associated parameters) mitigated the large discrepancy between the strain measurements and the model responses.

An important implication from the FE model calibration studies relates to the apparent fixity at the movement mechanisms including the sliding bearings supporting the ends of the cantilever trusses at the outer piers. The inherent assumption in ambient monitoring data analysis is that the structure remains stationary, observable and reasonably linear during the course of the monitoring. The data collected during a large number of intermittent time windows over several weeks included periods of different levels of traffic-induced vibration, various wind environments and temperature ranges. Averaging such data represents an effective composite of various inputs and the corresponding structural states and behaviors throughout the course of the monitoring, therefore in effect smearing all non-linearity and non-stationarity and effectively linearizing the structure. Hence, although many of the movement mechanisms are measured to intermittently experience slippages, the effective stiffness of the bridge averaged over a period of several weeks corresponded to the frozen condition of the movement systems. The findings also indicate the need for long term monitoring to track not only seasonal but also those changes in structural state that may take place within just a few hours.

An important conclusion relates to increasing use of 3D FE modeling and analysis in the design and evaluation of major constructed systems. It is shown that even when a 3D FE model of a large structure is constructed in the realm of research, the scale of such models provide a high probability for human errors. Many "blatant" errors may be mitigated by careful checking and by diagnostic analyses, however, many others that may significantly influence local responses may not be apparent with cursory evaluations. It follows that there is a need for systematic error checking by techniques that are not common in modeling smaller structural systems. A related issue with large structural systems is the increasing types and number of mechanisms of uncertainty that affect the behaviors of a structure, its analytical modeling and the St-Id process. As a structural system becomes larger, one may approach the limits in its representation by a linear, deterministic and stationary analytical model for most applications. How to systematically deal with uncertainty in making decisions for management of large constructed systems, and how to model and analyze large systems (such as infrastructures with engineered, natural and human sub-systems) so that simulations lead to decisions accomplishing prudent and optimum use of resources is an issue that can only be researched by studying actual large systems in real-life.

9. Acknowledgments

This research has been funded by the Federal Highway Administration (FHWA) and the Delaware River Port Authority (DRPA) of New Jersey and Pennsylvania. The writers would like to acknowledge the support of our sponsors and partners: Messers. Dan Faust, Robert Box, Robert Bistline, Pat McCullough and Dr. Alex Rong of DRPA.as well as Drs. Steve Chase, Hamid Ghasemi and Harold Bosch of FHWA. We are also grateful to many colleagues, research associates, graduate and undergraduate students for their participation and invaluable support in the research reported in this paper.

10. Appendix

Table 1: Sources of Uncertainty in Reliable System Identification

Source of Uncertainty	Mechanisms and Methods	Critical Parameters and Considerations
Structural	Boundary and Continuity Conditions Connectivity Material Prop. Aging, Deterioration, Damage Failure Modes	Lack of ideal boundaries (e.g. at piers, supports) Seasonal changes Lack of perfect connections (e.g. at movement systems, locations of member and sub-system releases, hinges etc.) Variation in material properties due to construction, variation due to aging, deterioration and damage Functioning of critical mechanisms due aging Deterioration, damage, defects Unexpected, unpredictable failure modes
Analytical	FE Modeling (Geometric Modeling)	Access to and overview of legacy documentation Model creation Visualization, conceptualization Error mitigation and quality control Completeness and reality checks Parameter sensitivity study Model calibration, quality control, validation, interpretation
Loading	Ambient Sources Operational Conditions	Random input due to wind, temperature and traffic Non-stationarity of ambient sources Human decisions, actions for traffic Operational conditions and changes
Experimental and Field Implementation	Sensing Data Acquisition (DAQ) Test Design Data Acquisition Regimes	Type of sensor and type of output Sensor performance; environmental and economic constraints Sensor cabling, wireless sensor communication Sensor-measurand mismatch Sensor calibration and verification DAQ architecture, hardware, peripherals and software DAQ speed, resolution, accuracy Signal conditioning, Analog-to-Digital Conversion Networking, communication and control Data quality control issues Number and location of sensors, sensor installation, access Sensor roving and data splicing Sampling, quantization, range adjustment DSP errors such as leakage, aliasing; detection of errors Data acquisition duration, storage Automated or manual data collection, trigger levels Personnel, equipment, cost issues
Data Post-Processing	Parameter Estimation (Modal Modeling)	Digital signal processing e.g. averaging, windowing strategies Optimum no of averages, averaging technique Time, Frequency or Spatial domain algorithms, other methods such as Wavelet, HHT etc. Non-linearity, non-stationarity Input assumptions Identification of global characteristics vs. distinct events Reliability and verification of dynamic properties Modal expansion possibilities Reliable identification of a minimum number of modes with sufficient spatial resolution Data presentation, interpreting data for decision making

11. References

1) Blanchard, B.S., and Fabrycky, *Systems Engineering and Analysis,* W.J., Prentice Hall, 3rd Edition, 1998
2) Hart, G.C., and Yao, J.T.P. (1977)., System Identification in Structural Dynamics, *J of Engineering Mechanics,* Division ASCE, Vol. 103 (EM6), pp.1089-1104, 1977
3) Liu, S.C., and Yao, J.T.P., Structural identification concept, *J. of Structural Engineering,* Division ASCE, Vol. 104 (ST12), pp.1845-1858, 1978
4) Aktan, A.E., and Yao, J.T.P., On structural identification of constructed facilities, *Proc., Structures Congress XIV,* S.K. Ghosh and J. Mohammadi, eds, ASCE Press, New York, N.Y., Vol. 2, pp.651-658, 1996
5) Aktan A.E., Farhey D. N., Helmicki, A.J., Brown, D.L., Hunt, V.J., Lee, K.L., and Levi, A., Structural identification for condition assessment: experimental arts, *J. of Structural Engineering,* ASCE, 123(12), pp.1674-1684, 1997
6) Aktan A.E., Catbas F. N., Turer A., Zhang Z.F, Structural identification: Analytical aspects, *J. of Structural Engineering,* ASCE, 124(7), pp.817-829, 1998
7) Mazurek, D.F. and Dewolf, J.T., Experimental Study of Bridge Monitoring Technique, *J. of Structural Engineering,* ASCE, Vol. 116, No.9, pp.2532-2549, 1990
8) Agbabian, M.S., Masri, S.F., Miller, R.K. and Caugher, T.K., System Identificatin Approach to Detection of Structural Changes, *J. of Engineering Mechanics,* ASCE, Vol. 117, pp.370-390, 1991
9) Nigbor, R.L., Abdel-Ghaffar, A. and Masri, S.F., Dynamic Monitoring of Suspension Bridges, *Proc. Int. Workshop of Technologies for Hong Kong's Infrastr.*, Commecial Press, Hong Kong, pp.325-336, 1991
10) Chang, C.C., Chang, T.Y.P., Zhang, Q.W., Ambient Vibration of Long Span Cable-Stayed Bridge, *J. of Bridge Engineering,* Vol. 6, No.1, pp.46-53, 2001
11) Brownjohn, J. M.W. and Xia, P. Q., Dynamic Assessment of Curved Cable-Stayed Bridge by Modal Updating, *J of Structural Engineering,* ASCE, Vol. 126, No.2, pp.252-260, 2000
12) Mottershead, J.E. and Friswell, M.I., Model Updating in Structural Dynamics: A Survey, *J. of Sound and Vibration,* Vol.167(2), pp.347-375,1993
13) Natke, H.G., Cottin, N. and Prells, U., Problems and related counter-measures in mathematical model improvement: A Survey, *Struct. Safety and Reliability,* G.I. Schueller, M. Shinozuka and J.T.P. Yao, eds. Balkema, Rotterdam, pp.821-827, 1994
14) Wong, K.Y, Lau, C.K. and Flint, A.R, Planning and Implementation of the Structural Health Monitoring System for Cable Supported Bridges in Hong Kong, Nondestructive Evaluation of Highways, Utilities and Pipelines IV, A.E. Aktan and S.R. Gosselin, eds, *Proc. Of SPIE* Vol. 3995, pp.266-275, 2000
15) Kashima, S. Yanaka, Y., Suzuki, S. and Mori, K., Monitoring the Akashi Kaikyo Bridge: First Experiences, *Structural Engineering International,* SIE Vol. 11, No. 2, pp.120-123
16) Catbas, F.N., Pervizpour, M., Grimmelsman, K.A. and Aktan, A.E.,The Health Monitoring Paradigm for Infrastructure Systems, *Proc. Workshop on Structural Health Monitoring and Diagnostics of Bridge Infrastructure,* University of California, San Diego, La Jolla, CA, March 7-8. 2003
17) Bush, B., Gordon, R., Holland, J., Roach J., and Thompson, D., *The SOFIA Project for Interdependent Infrastructure Modeling, Simulation, and Analysis,* LA-UR-99-3412, Los Alamos National Laboratory, 1999
18) Nagel, K., Beckman, J., and Barret, C., *TRANSIMS for Urban Planning,* Report LA-UR 98-4389, Los Alamos National Laboratory. 1999
19) Aktan A.E., Catbas F. N., Grimmelsman, K.A., Pervizpour, M., *A Model Health Monitoring Guide For Major Bridges*, Report Submitted to FWHA, DOT/FHWA Solicitation: DTFH61-01-Q-00072, September 2002.
20) Carder, D.S., Observed Vibrations of Bridges, *Bulletin of the Seismological Society of Americ*a, 29(4), pp.267-303 1937
21) Abdel-Ghaffar, A.M. and Scanlan, R.H., Ambient Vibration Studies of Golden Gate Bridge: Suspended Structure, *J. of Engineering Mechanics, ASCE,* 111(4), pp.463-482, 1985
22) Kumarasena, T., Scanlan, R.H. and Morris, G.R., Deer Isle Bridge: Field and Computed Vibrations, *J. of Structural Engineering*, ASCE, Vol. 115, pp.2313-2328, 1989
23) Wilson, J.C. and Gravelle, W., Modeling of a cable-stayed bridge for dynamic analysis, *Earthquake Eng. and Structural Dynamics.,* Vol.20, pp.707-721, 1991
24) Brownjohn, J.M.W., Dumanoglu, A.A., and Severn, R.T. (1992). "Ambient Vibration Survey of the Fatih Sultan Mehmet (Second Bosporus) Suspension Bridge", *Earthquake Eng. and Structural Dynamics*, Vol. 21, pp.907-924, 1992
25) Casas, J.R.,Full Scale Dynamic Testing of the Alamillo Cable-Stayed Bridge in Sevilla, *Earthquake Eng. and Structural Dynamics*, Vol. 24, pp.35-51., 1995
26) Farrar, C.R., and James, G.H., System Identification from Ambient Vibration Measurements on a Bridge, *J. of Sound and Vibration*, 205(1), pp.1-18, 1997
27) Cunha, A., Caetano, E. and Delgado, R., Dynamic Tests on Large Cable-Stayed Bridge, *J of Bridge Engineering*, ASCE, Vol. 6, No. 1, pp.54-62, 2001
28) Xu, Y.L., Ko, J.M. and Zhang, W.S., Vibration Studies of Tsing Ma Suspension Bridge, *J. of Bridge Engineering*, ASCE, Vol. 2, No. 4. pp.149-156. 1997
29) Fujino, Y. and Abe, M., Vibration-based Structural Health Monitoring of Civil Infrastructures, *Structural Health Monitoring Workshop*, Organized by ISIS-Canada, A. Mufti edt., Winnipeg, Canada pp.45-55, 2002
30) Abe, M., Fujino, Y., Yanagihara, M. and Sato, M., Monitoring of Hakucho Suspension Bridge by Ambient Vibration Measurement, Nondestructive Evaluation of Highways, Utilities and Pipelines IV, A. E. Aktan and S.R. Gosselin, eds, *Proceedings of SPIE,* Vol. 3995, pp.237-244, 2000
31) Zhang, Q.W., Chang, T.Y.P. and Chang, C.C., Finite Element Model Updating for the Kap Shui Mun Cable-Stayed Bridge, *J. of Bridge Eng*, ASCE, Vol. 6, No. 4, pp.285-293, 2001

32) Cole, H.A., On-the-line Analysis of Random Vibrations, *AIAA* Paper No.68-288, 1968
33) Asmussen, J.C., Modal Analysis Based on the Random Decrement Technique, *Ph.D. Thesis*, Dept. of Building Technology and Structural Engineering, Aalborg University, 1997
34) Catbas, F.N., Aktan, A.E., Brown, D.L., Parameter Estimation for Multiple Input Multiple Output Analysis of Large Structures, *J. of Eng. Mechanics*, ASCE, 2002 (submitted for re-review, 2003)
35) Catbas, F.N., Lenett, M., Brown, D.L., Doebling, S.W. and Farrar,C.R., Turer, A., Modal Analysis of Multi-Reference Impact Test Data for Steel Stringer Bridges, *Proc. 15th International Modal Analysis Conf.*, Orlando, Florida, 1997, p.381-391, 1997
36) Catbas, F.N. and Aktan, A.E., Condition and Damage Assessment: Issues and Some Promising Indices, *J. of Structural Engineering,* ASCE, Vol. 128, No. 8, pp.1026-1036, 2002

Monitoring the Condition of Bridges in New York City

B. Yanev, Eng.Sc.D., P.E.
Department of Transportation, New York City

The New York City Department of Transportation is responsible for 755 of the more than 2200 bridges in the Metropolitan area. The average age of these structures approaches 80 years and their condition has varied over the years from new to potentially hazardous. Annual rehabilitation expenditures have exceeded 600 ml. USD in capital and expense funds. The Bridge Inspection & Bridge Management Unit of the Department must ensure the safety of the traveling public while traffic is maintained at maximum level and available funds are invested in the most appropriate projects. The advanced state of structural deterioration observed on the onset of the program (1988), the high transportation demands and the sophisticated nature of some of the bridges (including the Brooklyn, Manhattan, Williamsburg and Queensboro across East River) occasionally called for the use of a wide variety of structural monitoring techniques. Along with traditional visual inspection, strain gauges, accelerometers, acoustic emission, x-ray diffraction, surveying, interferometry, magnetic flux, corrosion potential measurement, etc. were occasionally used. Some lessons learned in the process are briefly described. The need for reliable cost/benefit analysis of non-invasive monitoring techniques as part of bridge life-cycle management is stressed.

Key words: benefit, bridge, condition, inspection, management, monitoring

1. Non-Destructive Testing (NDT) for Bridge Condition Evaluation

In June 2001 The Federal Highway Administration published a report[1] on the reliability of visual inspection for highway bridges. The report concluded that visual inspections are still the prevalent non-destructive method, that they are not particularly reliable and that condition ratings, training and inspection procedures could all use some improvement. Non-destructive methods of condition assessment are recommended as one possible source of such improvement. In recent years these methods have developed so rapidly that it is difficult to keep up. A brief and partial review of the background may be helpful.

The theory of NDT applications to material quality control was addressed for instance in [2]. The following general NDT categories were identified in [3]: visual, radiological, ultrasonic, magnetic, electrical, penetrant flaw detection, acoustic emission and others. Non-destructive techniques are specifically applied to structural evaluation (NDE) in [4]. Evaluation is divided into primary, secondary and tertiary, depending on whether the sought parameters are related to the primary function of the structure, a fault that might lead to a failure thereof or directly measure a failure parameter.

The American Society for Non-Destructive Testing (ASNDT) has produced a large number of important publications. ASTM[5] and CRC Press[6] specify a number of non-destructive methods. The application of NDE to bridge monitoring has been greatly stimulated by the work of the Nondestructive Evaluation Validation Center at FHWA. A number of Strategic Highway Research Projects (SHRP) have developed and assessed NDT&E techniques. One of many examples is the FHWA Demonstration Project No. 84 "Corrosion Detection Equipment". In 1986 FHWA sponsored a training program for Nondestructive Testing of Steel Bridges, conducted by the Stone & Webster Engineering Co. The National Science Foundation (NSF) sponsored an international workshop on NDE[7] in 1988. FHWA Conferences on NDT are organized biennially since 1994, jointly with AISC, ACI, ASNDT, the New York, New Jersey, Texas and California DOT[8]. In 2002 The NDE Validation Center at FHWA organized a workshop summarizing comprehensively the current state of the art.

Most texts group the latest developments and applications of non-destructive techniques into several general categories. These include strain gauging, corrosion surveying by half-cell potential, magnetic particle evaluation of welds, ultrasonic evaluation of steel, acoustic emission and other methods for evaluation of fatigue crack propagation, infrared

thermography for concrete decks, nuclear measuring of water/cement ratio in fresh concrete, impact-echo thickness and flaw evaluation, fiber optic sensors for concrete, radar survey for roadway surfaces, dynamic characteristic method, long range remote monitoring using electronic clinometers, ultrasonic testing, etc. Pile and foundation testing are gaining interest. An experimental highway in Minnesota was instrumented for continuing monitoring of the wearing surface and roadway under live loads. The State of Virginia Transportation Council reported results of acoustic monitoring of steel bridge members in 1997 [9].

Typical for the current stage of development is the globalization of the NDT&E expertise. A number of world-class bridges, including the Akashi-Kaikyo, have been instrumented and are continually monitored in Japan. An early presentation by the BMC Corporation of Chiba City, among many others, showed the considerable interest on structural health monitoring. The Organization for Economic Cooperation and Development (OECD) has a record of Road Transport Research activities promoting bridge management. In September, 1994 OECD sponsored a Workshop A6 "Management of Existing Bridges". Discussed were a number of relevant topics. Significant contributions to the same subject were due to the participants from Denmark and Switzerland. Extreme caution was recommended in applying such methods. Independent means of result verification were highly recommended.

The International Society of Optical Engineering (SPIE) is a very active source of information on all NDE technological developments, maintaining a highly accessible website and regularly organizing conferences. Of particular interest was the SPIE – NSF conference in Irvine, CA., March, 2001, where articles, such as [10] discussed both the possibilities and the limitations of the new techniques.

Non-destructive testing is prominent among the topics at the biennial International Conferences on Bridge Management at the University of Surrey and the Conferences on Structural Faults & Repair organized by the University of Edinburgh, as well as at the events regularly organized by the International Association for Bridge and Structural Engineering (IABSE).

The Technical University of Braunschweig, Germany is conducting research on life-cycle structural assessment via monitoring[11]. The Bauhaus University in Weimar, Germany organizes biennial international conferences on the subject[12].

Strongly emphasized on both sides of the Atlantic is the need to investigate & evaluate the condition of embedded or encased high strength tendons and rods, addressed in NCHRP report 10-30(3)[13]. FHWA organized a study tour of European post-tensioned bridges in October, 1999. Urgency is growing after the collapse of a 5 year old prestressed concrete pedestrian bridge in Concord, North Carolina on May 21, 2000, due to tendon corrosion. Acoustic monitoring of the helical strand suspension cables at Pont de Tancarville prior to their replacement was reported by M. Virlogeux[14]. R. Maybaurl reported acoustic monitoring by Soundprint at the Bronx-Whitestone bridge (TRB 1999). NCHRP project 10-57[15] emphasizes the need for reliable non-destructive testing of suspension bridge parallel wire cables. 1 ml. USD was appropriated by the US Senate in 2003 towards the development of such a capability on the East River suspension bridges in New York City.

2. New York City

In 2002 New York City Department of Transportation (NYC DOT) was responsible for 755 of the more than 2200 bridges in the Metropolitan area. Their average age approaches 80 years and condition ranges from new to poor. Since the Bureau (Division) of Bridges was re-established at the Department in 1988, a major rehabilitation and maintenance program has developed. Annual expenditures have exceeded USD 600 ml. in capital and expense funds. A Bridge Inspection & Bridge Management Unit was founded by the author in 1990 as part of the Bureau. The bridge management task could be defined as follows: to ensure the safety of the traveling public, while maintaining traffic capability at maximum level and directing the available funds to the most appropriate projects.

Bridge inspections had to satisfy all Federal and State requirements, while addressing the following combination of transient and permanent conditions:

Advanced state of structural deterioration. 80% of the bridges were rated below 5 on the 7 (new) to 1 (failed) New York State bridge condition rating scale and 35% - less than 3 (not functioning as designed). 20 bridges were fully or partially closed and a large number were posted for reduced live load. Since 1980, the number of potentially hazardous conditions escalated at the compounded annual rate of 30%, peaking at 3000 in 1996.

High transportation demands. More than 4 million passengers use the City bridges daily and over 1 million - the 4 East River crossings.

Complex and unique structures, approaching 100 years of age. Included are the Brooklyn (1883), Manhattan (1908), Williamsburg (1903) and Queensboro (1908), as well as 24 moveable bridges of the same construction period, some enjoying a landmark status.

The Bridge Division of New York City DOT regularly hosts presentations by NDT experts, such as

ISMES (Italy), Smartec (Switzerland), Osmos (Germany), Fugro (UK), FG Detection Technics (the Netherlands), Vaisala (Finland), InterSpect, Proto and Soundprint (Canada), Margan (Israel), Physical Acoustics (New Jersey), Wiss & Janney & Elstner Assoc., Strain Monitoring Systems (Georgia), Sika – Cypro, the Sowthwest Research Institute, the Edison Welding Institute, C-Probe Technologies and many other local and foreign companies. Along with traditional visual inspection, strain gauges, accelerometers, acoustic emission, x-ray diffraction, surveying, interferometry, magnetic flux, corrosion potential measurement, etc. were occasionally used. Some of the successes, disappointments, future hopes and questions raised by these attempts are briefly described.

3. Enhanced Methods of Observation

Enhanced methods of observation, such as dye-penetrant testing and thickness-meters have long been common practice, however bridge inspectors are reluctant to use this excessively sensitive or cumbersome equipment. Steel thickness meters, for instance, are largely underused despite the importance of the information they provide, primarily because of their need for repeated calibration and the unrealistic demand for surface preparation. Dye penetrant testing is extremely helpful in determining the size of fatigue cracks, but only after they have been localized or at least suspected.

4. Surveying

With the advent of laser equipment, geodesic surveying has gained high accuracy and excellent field performance. Laser beam distance gauges have greatly facilitated and improved the essential (and previously deficient) bridge inspection task of measuring clearances. Using such equipment to monitor changes in the bridge geometry can be extremely useful. Essential is the appropriate choice of monitored locations and frequency of sightings, as well as adequate record keeping (including ambient temperature, etc.). Typical applications include long-term monitoring of moveable bridges for indications of approach settlement and temperature effects. The East River bridges have been surveyed as part of their extensive rehabilitation projects. A 10mm (4 in) leaning of the Williamsburg Bridge, Manhattan side, main tower (Fig. 1) towards the main span was noted during such an operation. A leaning of a side span tower on the same bridge, was continually monitored. In both cases, demonstrating that the movement was arrested became essential to the scope of rehabilitation work under design.

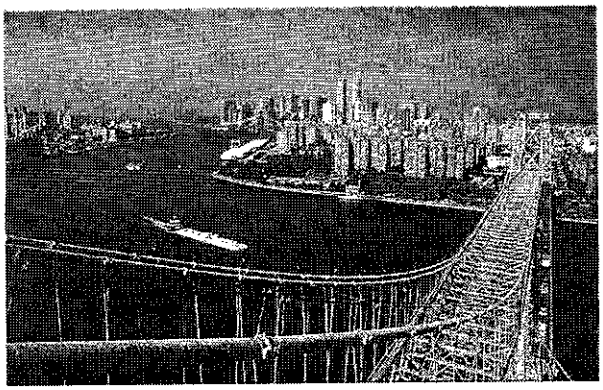

Fig. 1 Williamsburg, Manhattan and Brooklyn bridges

5. Load-Deflection Tests

On a number of occasions bridges have been subjected to calibrated loadings, for instance with hydraulic jacks and the response has been measured with extensometers and strain-gages. This was done repeatedly during the replacement of the bearings and other work on the reconstruction of the Long Island Expressway. Load-cells are used during the replacements of suspenders on suspension bridges.

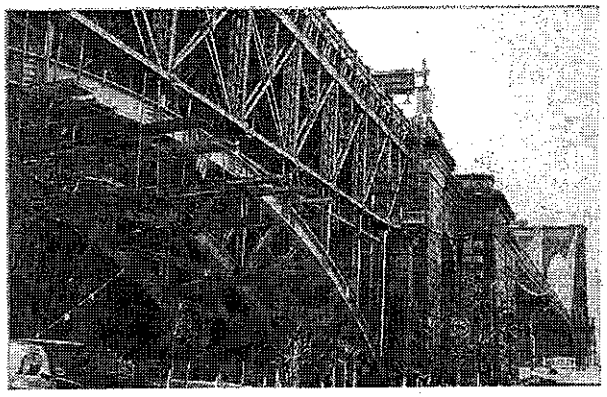

Fig. 2 Franklin Square truss, Brooklyn bridge

An unique demand on the Brooklyn Bridge Franklin Square approach span (Fig. 2) exceeded the capabilities of traditional surveying. This landmark approach consists of a seven-truss system with eye-bar bottom chords dating back to 1883. During the mid-1990s overstress was suspected in the eye-bars and their pinned connections. Laboratory tests showed the material to perform beyond design specification requirements, but did not resolve all concerns. New arches (Fig. 2) were built to support the structure under traffic. Weekly monitoring was required for approximately 2 years until the load was picked up by the new structure. No reliable stationary reference

point could be established for surveying. Instead, piano wires were stretched across the span and kept tight with counterweights. Concurrently, Bridge Diagnostics, Inc. of Colorado, used strain gauge transducers to evaluate the live load response of the eye-bars, while Proto Manufacturing, Ltd. of Canada applied X-ray diffraction to evaluate the total load. Both produced realistic results.

6. Strain Gauges

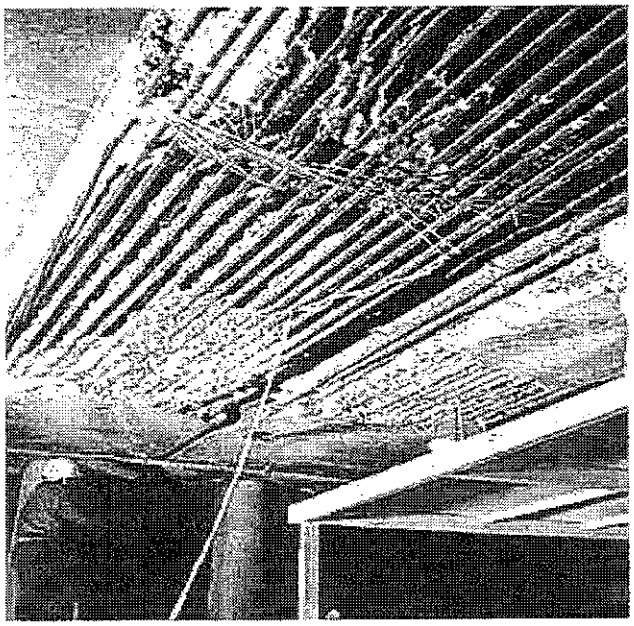

Fig. 3 Strain gauges under the F.D.R. driveway

In a functioning structure, strain gauges mainly determine the response to transient loads, such as those due to traffic and temperature variation. At the F. D. Roosevelt Drive in Manhattan the steel reinforcement of the primary concrete members, supporting three lanes of traffic, was exposed over more than 75% of the span (perpendicular to traffic) due to spalling (Fig. 3). In a controlled load test, the Columbia University Strength of Materials Laboratory installed strain-gauges on the exposed re-bars and the bridge was test-loaded with vehicles of known weight. Concurrently, deflections were monitored by extensometers. A minimal response (200 psi) was measured, suggesting that: a) the exposed steel reinforcement still functioned jointly with the rest of the structure and b) the structural rigidity was considerably underestimated by traditional stiffness analysis. As a result, traffic of limited weight was allowed on the structure for the several years preceding rehabilitation.

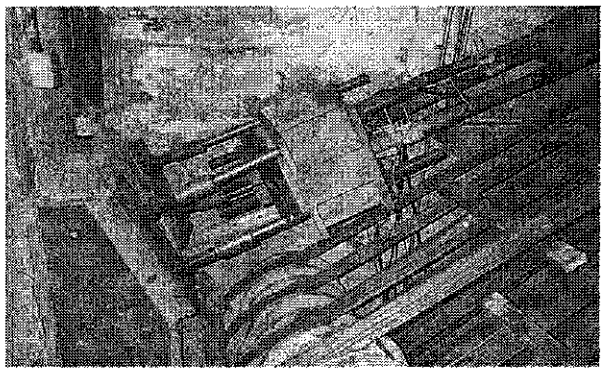

Fig. 4 Re-anchored strand on Manhattan bridge

In exceptional cases strain-gauging may yield data on the structural response to the total load. Such opportunities arose on both the Manhattan and Williamsburg bridges across the East River during the re-anchoring of suspension cable strands. In these instances the new anchorage rods were strain-gauged and the load was monitored during the load-transfer operation (Fig. 4).

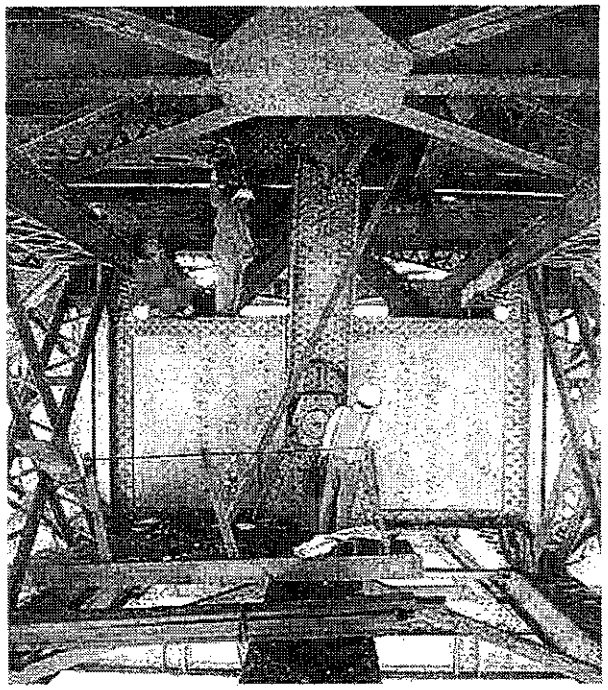

Fig. 5 "Frozen" linkage at Williamsburg bridge

A side-span tower on the Williamsburg bridge (Fig. 5) was instrumented with strain-gauges in the fall of 1994 in order to monitor its behavior during temperature fluctuations after it was found to have lost have of its support. Results demonstrating the failure of the articulated connections between the tower and

the primary span structure it supports were reported by N. Dini in 1996[8].

Laboratory and field testing were combined in the evaluation of the new orthotropic deck on the Williamsburg bridge. A 20 m (60 ft) deck panel was tested at the ATLSS Center, Lehigh University. The findings were compared to field results obtained by strain gauges on the bridge deck and the floor beam cut-out radius (Fig. 6) was modified.

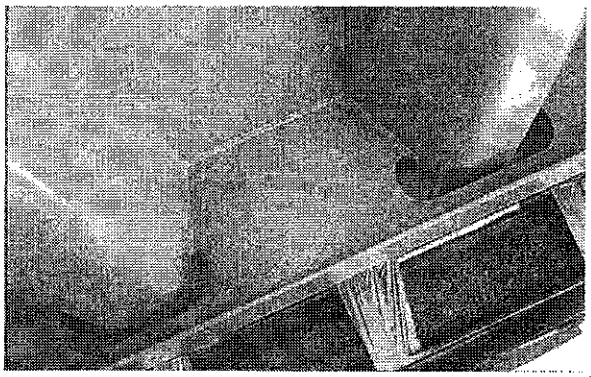

Fig. 6 Orthotropic deck, Williamsburg bridge

Strain-gauges, once again of the traditional electric resistance type, were used to assess the effectiveness of a new lateral stiffening system at the Manhattan bridge (Fig. 7). Sonic Force of Burlingame, California successfully demonstrated an acoustic gauge on the same bridge.

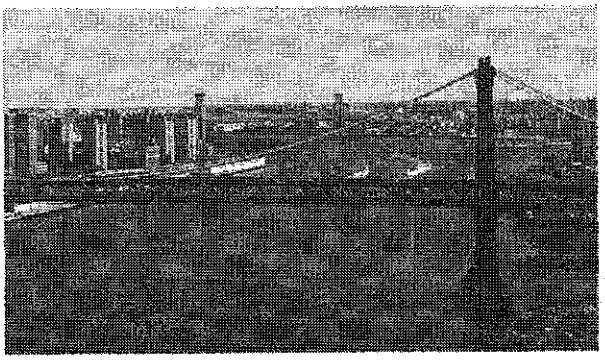

Fig. 7 Manhattan and Williamsburg bridges

7. Displacement Gauges

Strain Monitoring Systems of Norcross, Georgia offers a 6 in (152 mm)-base aluminum gauge, easy to attach and to monitor by connecting to an electronic reader. It provides two readings – one of the extreme measurement to date, another – of the current one. Since the output is averaged over the gauge length, the gauge might be considered as a "displacement" one. Bridge Inspections are using it to monitor very wide cracks in the concrete monoliths of the Manhattan Bridge anchorages (Fig. 8). The objective is to determine whether the cracks are active and, thereby - if remedial measures are required.

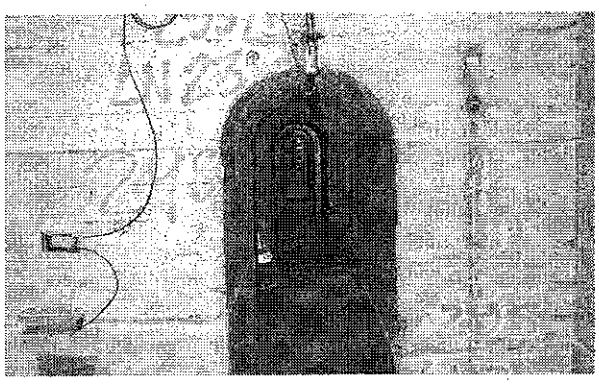

Fig. 8 Monitoring of cracks in the Manhattan bridge anchorage

8. X - Ray Diffraction

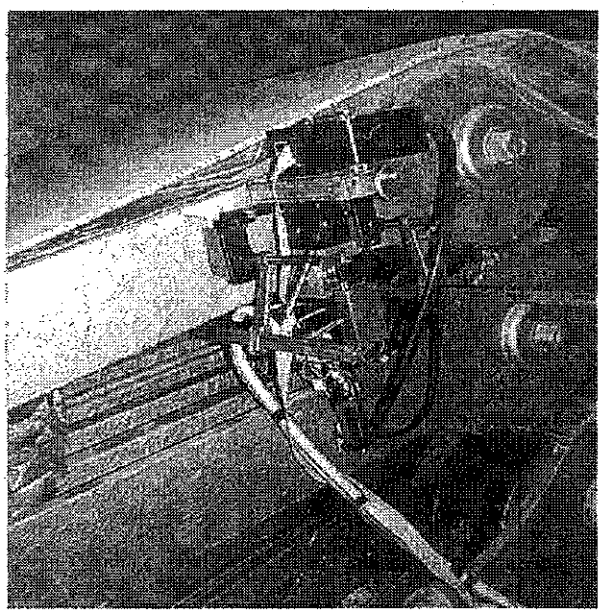

Fig. 9 X-Ray diffraction measurement at the Williamsburg bridge anchorage

X-ray diffraction is typically used to determine residual stresses in steel. When the stress distribution across the section of a structural member is relatively uniform or well known, this method can estimate the total stress in a loaded structure. Proto Manufacturing Ltd., Canada, showed good results in a test at the Williamsburg bridge anchorage eye-bars (Fig. 9) and on the Brooklyn bridge Franklin Square truss (Fig. 2). Jointly with the Port Authority of New York & New

Jersey, they reported on stress measurement in post-tensioning tendons at the La Guardia Airport runways[16].

The method could verify if stresses, designed to be uniform, have re-distributed. In that case, comparing surface stress readings is meaningful even if the average stress in the members remains uncertain. A reliable calibration of a stress-free sample, comparable to the "in situ" tested material, is highly desirable, but not always possible. A good understanding of the elastic and plastic stress-strain relationships in steel, comprehensively described in[17] is indispensable.

9. Acoustic Emission (AE)

The application of acoustic emission for the detection of fatigue or corrosion-fatigue cracks in steel bridge members has been under development for over a decade[9]. Physical Acoustics of New Jersey, USA and DNL Technologies of Canada have tested their equipment on City bridges. In the early 90's NYC DOT Bridge Inspections purchased DNL AE equipment, which essentially scans for signals in the 300 kHz range under ambient excitations. The main purpose was to determine whether repairs of cracked components, such as bolted sandwich plates or drilled holes at crack tips (Fig. 10), are effective in arresting the crack propagation.

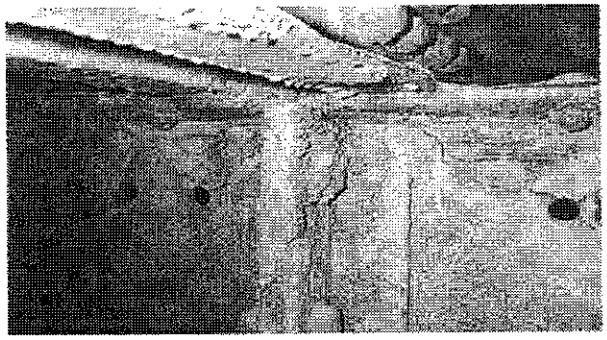

Fig. 10 Cracks in stringers, Manhattan bridge

NYC DOT has not been able to detect previously unknown cracks by AE. Once crack locations are known, AE can monitor their activity. One major difficulty in this method's application is the inability of vehicular traffic to generate a meaningful response from the structure. It is recommended to combine acoustic emission with other instrumentation, for instance, strain-gauges.

The lower frequency sound waves generated by wire breaks are commonly monitored on suspension and stay cables, as well as in pre-stressing strands. Results obtained by Soundprint at the Bronx-Whitestone Bridge (Fig. 11), owned by the New York Metropolitan Transit Authority were reported by R. Mayrbaurl of Weidlinger Assoc. at the TRB Annual Conference in 1999.

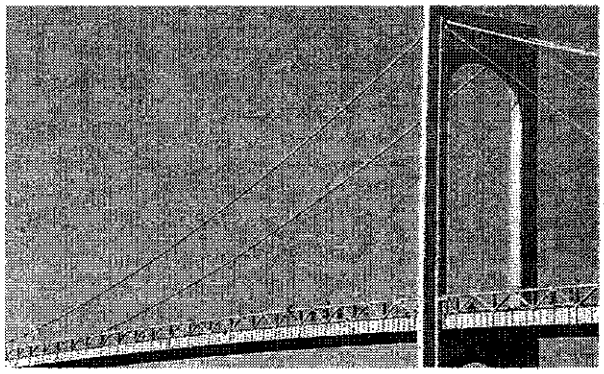

Fig. 11 Whitestone bridge

10. Ultrasonic Testing

During the mid-1980's the method was considered for the inspection of nickel alloy steel pins (approx. diam. 40 mm, length 2000 mm) with exposed face sections on the New York State owned Gowanus Expressway in Brooklyn (Fig. 12).

Fig. 12 Gowanus expressway

The main reservation was that the obtained signals may suggest irregularities without an ability to distinguish between crack initiation and surface roughness of the type shown on Fig. 13. California Department of Transportation reported improving results by self-compensating techniques.

The method was successfully used at the Williamsburg bridge in the late-1990's for evaluating the condition of original nickel alloy steel pins (Fig. 5) as part of the structural rehabilitation. Sonograms of test pins were calibrated by visual inspection. The results were found satisfactory.

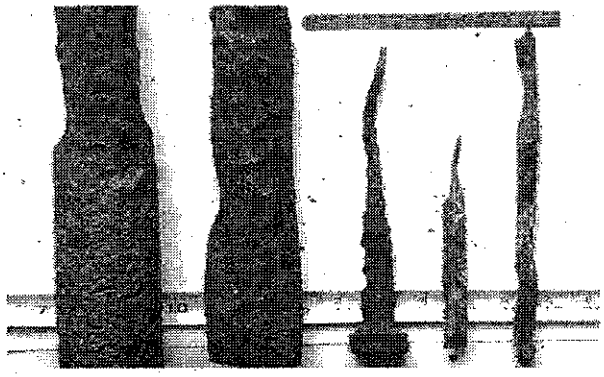

Fig. 13. Typical corrosion in steel components

The numerous nickel alloy pins and eye-bars on Queensboro Bridge (Fig. 14) must be tested under heavy traffic and with a limited budget. The process must be rapid enough to allow for the testing of a statistically significant sample. Field demonstrations suggest that phased-array transducers, such as those used by Edison Welding Institute of Columbus, OH., could scan faster and with higher probability of detection.

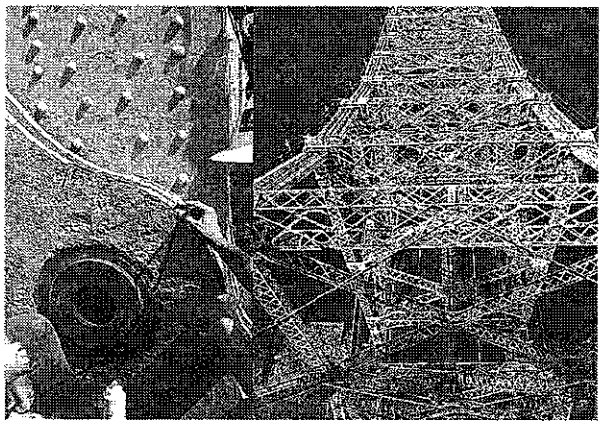

Fig. 14 Acoustic testing of eye-bars at Queensboro bridge

11. Corrosion Detector

A corrosion detector, such as the one developed at the ATLSS Center, Lehigh University by Dr. R. Granata, can be installed at a structural sight. Testing the DC current resistance in the detector indicates its own rate of corrosion. An estimate can be made of the ambient corrosion accordingly. During the rehabilitation of the Williamsburg bridge main cables (Fig. 15), one experimental device was implanted among the high strength cable wires with conductors protruding through at a cable band. The wires were mishandled and no meaningful results were measured, however the potential for monitoring the corrosion rate in the inaccessible suspension bridge cables became a higher priority.

The need for such a capability was further emphasized by the NCHRP project 10-57[15] on the evaluation of suspension bridge cables' condition and strength (pending publication in 2003). The United States Senate appropriated 1 ml. USD for research in this field to be pursued at the suspension bridges of New York City by the Federal Highway Administration.

Fig. 15 Cable inspection on Williamsburg bridge

12. Half-Cell Potential

Potential readings have been used to assess the corrosion of deck reinforcing bars on several bridges prior to their demolition. This demonstrated that the method, when adequately applied can yield accurate results. Currently similar techniques are used to evaluate the effect of a deck water-proofing membrane. One reservation in applying this method is that corrosion in re-bars embedded in concrete decks is usually localized in certain areas, while other areas remain free of it. This highly non-uniform condition is difficult to evaluate. The erratic nature of the results can cast (sometimes unduly) doubt on the procedure.

13. Dynamic Signature

The "in situ" stiffness of a structural member can be compared to its design value by measuring the member's significant natural frequencies and comparing them to theoretical values or to earlier measurements. Deterioration of the stiffness is expected to show an effect on the natural frequencies. The method has had some success in components with particularly pronounced lowest vibration modes and well defined support conditions, such as the vertical suspenders of the George Washington bridge (Fig. 16), which were investigated by the Port Authority of New York & New Jersey and Columbia University in the 1980's.

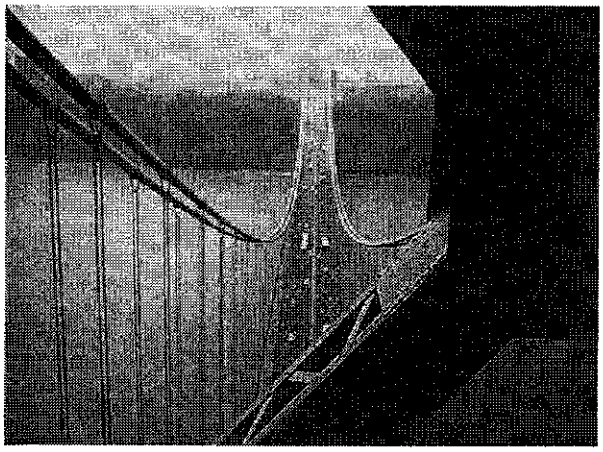

Fig. 16 George Washington bridge

Traditionally, analysis was the only source of obtaining bridge natural frequencies, essential in determining structural dynamic behaviour. In recent work by the Lamont-Doherty Laboratory, Columbia University, at the Tappan Zee, Queensboro (Fig. 14) and Macomb's Dam bridges, natural frequencies were obtained under ambient loads by a number of transducers located on the structures and synchronized by satellite. A review of the analytical models in the light of the field measurements typically follows. It is noted that standard structural modeling for computerized analysis has tended to underestimate the stiffness of these large truss structures. One possible explanation is that a number of rotation and translation release devices in the investigated structures act rigidly under the small traffic-induced excitations.

14. Magnetic Particle Flux

This test was applied with considerable benefits at a City bridge over railroad tracks. The steel primary structure had been newly re-painted. State inspectors subsequently noted impact damage to one of the main bridge girders. The impacted area had been covered by the new paint and could not be inspected for cracks by the routine dye-penetrant test. It was, therefore recommended to remove the paint by sand-blasting. This would have been extremely costly, due to the railroad presence and in view of the new paint, which would have had to be restored. Dr. S. Chase of FHWA recommended a magnetic particle test, currently under review at the Fairbank Center. The field test was conducted as part of the evaluation process for this procedure. No cracks were found in the steel. NYS DOT accepted the findings.

15. Ultraviolet Rays for Detection of Alkali-Silica Gel in Concrete

In the procedure adopted at Columbia University, the concrete specimen is treated with a 5% uranil acetate solution. The alkali-silica gel exhibits a yellow pigmentation under ultraviolet light. The method is not quantitative, but has effectively confirmed that alkali-silica reaction is widespread in concrete bridges.

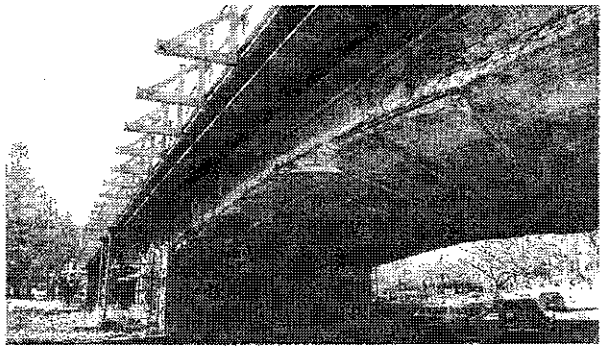

Fig. 17 Bridge afflicted by alkali-silica reaction.

16. Global Positioning Systems (GPS)

Global positioning systems can monitor the response of large structures, such as suspension bridges, to dynamic loads. Such a capability is in demand, because the very precise laser beam surveying technology has distance limitations, while GPS were not considered sufficiently accurate, particularly in the vertical direction. In a recent presentation at NYC DOT Bridges, however GPI and Ashtech Precision Products undertook to demonstrate highly improved precision, quoting on material presented in [18) 19)]. If effective, this GPS-based capability should be very useful during bridge rehabilitations, under high winds, extreme live, other loads. Direct applications to the East River bridges in New York City can be easily envisioned.

17. Method of Application

The method of selecting NDT&E for practical applications is of interest. NYC DOT Bridge Management Unit regularly invites specialized companies for presentations and, as in many of the above cases, field demonstrations. The intent is to introduce the bridge managers to the commercially available capabilities. NDT&E is most frequently required to help in determining:

- dead load acting on an existing structure;
- live load the structure can safely carry;
- scope and sequence of structural rehabilitation.

NDT&E monitoring can be included in the bridge rehabilitation scope of work, as for instance on the East River and moveable bridges. The consultants of record on major projects routinely recommend NDT&E use, however the City as owner has also sought such applications directly. Vibration monitoring under ambient excitations is standard during rehabilitation of all large and essential bridges as part of their seismic design.

In all NDT&E applications, analysis must precede field application. Field data is systematically wasted, unless it fits into a pre-determined coherent structural evaluation plan. Concurrent monitoring of different structural responses, such as strain and acoustic emission, strain and displacement, acceleration and velocity, is becoming standard procedure.

Since the safety of the public is the governing consideration, the appropriateness of a NDE monitoring technique is selected primarily according to its ability to ensure that safety. The extended use of surveying, for instance, would be questioned in the case of a deteriorating brick masonry arch, because a collapse can follow after relatively small displacements. NDT has occasionally indicated no significant structural distress, but existing codes and safety considerations have overruled in favor of emergency repairs. The approval of a given method by ASTM, ASCE and AASHTO is essential. The HITEC group in Washington DC conducts evaluations of NDT&E methods which greatly facilitate their use.

The economic effect of the described NDT&E applications is hard to quantify because the most significant benefits are expressed in terms of the elusive user costs. Successful NDT&E can lead to either maintaining a bridge in operation, thus benefiting the traveling public and the local economy to an unspecified degree, or to avoiding potentially fatal accidents by closing unsafe structures (another incalculable cost). Direct benefits to the bridge owner, however are also becoming quantifiable. As a result, structural health monitoring becomes a viable bridge management tool.

18. Towards Structural Health Monitoring

As bridge management efforts nationwide gradually improve bridge conditions, the emphasis is shifting from hazard mitigation and remedial work to life-cycle planning. The objective is to reduce bridge-related life-cycle costs at all stages of engineering work as follows:

a) design, by eliminating components requiring labor-intensive or complex maintenance;
b) construction, by improving quality;
c) inspection, by more accurate structural evaluation;
d) maintenance, by improving service and extending the bridge useful life;
e) management, by accurate needs assessment, strategy selection and implementation.

This trend is aptly illustrated by the comparison between typical annual bridge-related expenditures in New York City and the alternative, recommended in[20] [million USD/annum].

Annual Expenditure:	Typical	Recommended
Full Rehabilitation	500 – 600	150 – 300
Component Rehab.	20 – 40	20 – 40
Prevent. Maintenance	20	92
Hazard Mitigation	25	8 – 10
Total	565 – 685	270 - 342

NDT&E can contribute to all of the above and, as a result, is incorporated in current bridge management considerations. The non-destructive testing cases in New York City reported herein were primarily motivated by the need to determine and quantify the loss of structural integrity. In contrast, at new and rehabilitated structures monitoring can enhance maintenance. The added costs of a health monitoring system must be compared to the benefits they provide in protecting the considerable construction and user costs. The 25 movable bridges in New York City, for instance, will require USD 900 million for rehabilitation over a period of less than 20 years. The rehabilitation cost for the East River bridges over 20 years is currently estimated at USD 2.5 billion. Such investments generate an interest in monitoring techniques not intended to expose structural malfunctions, but to prevent their occurrence. A weigh-in-motion instrumentation system has been developed in Japan[21]. Preventing oversized vehicles from causing impact damage to structures is investigated by NYC DOT and State agencies. "On-line" data acquisition systems, capable of continued remote monitoring of bridge and environment condition indicators, are becoming part of modern bridge design. Structural performance under seismic and wind induced excitations has already been monitored for several decades, however new capabilities have greatly improved the quality, variety of the collected data at continually dropping costs. At important new bridges, such as the Akashi-Kaikyo[22] in Japan, Tsing Ma in Hong Kong and Woodrow Wilson in Washington, D.C., monitoring systems are being designed along with the original structure with the intent to assist maintenance and extend the structural useful life. On the East River bridges in New York, in order to facilitate anti-icing without use of salt, a weather monitoring system is proposed. FHWA has modified its earlier position and approves Federal funding for the project.

Publications, such as[23], suggest that the NDT&E industry is extremely flexible, with expanding capabilities and customized applications. The SAMCO network on Monitoring, Assessment and Control of Structures is advancing the process by compiling the growing variety of methods, techniques and research topics into an accessible database on the Internet. Due to the rapid advances of NDT technologies, abundant solutions, as in the famous words of A. Einstein, are looking for problems. Structural problems, however are best avoided rather than corrected. A design alternative does not become competitive merely because the structural response can be monitored. With the proliferation of NDT information (ranging from simple advertisements to detailed technical reports), engineers face a new responsibility: to conduct comprehensive cost/benefit evaluations of all life-cycle bridge management options with consideration of available non-destructive health monitoring techniques.

Acknowledgement

This article describes work conducted at the Bridge Division, New York City Department of Transportation. The views expressed are those of the author and do not reflect the position of any agency or organization.

References

1) M. Moore et al., Reliability of Visual Inspections for Highway Bridges, Report FHWA – RD01-020, June 2001.
2) B. Hull, & J. Vernon, Non-Destructive Testing, Macmillan Education, London, 1988.
3) R. Halmshaw, Non-destructive Testing, Edward Arnold, London, 1987.
4) R. A. Collacott, Structural Integrity Monitoring, Chapman and Hall, London/New York, 1985.
5) J. Bush, and G. Y. Baladi, Nondestructive Testing of Pavements and Backcalculation of Moduli, editors, ASTM 89-38726.
6) Handbook on Nondestructive Testing of Concrete, editors V. M. Malhorta, and N. J. Carino, CRC Press 1991.
7) Nondestructive Evaluation for Performance of Civil Structures, editors: M. S. Agbabian and S. F. Masri, USC, Los Angeles, CA 1998.
8) Structural Material Technology, NDT Conference, Technomic Publishing Co., Inc. Lancaster, Pennsylvania. Editors: R. J. Scancella and M. E. Callahan, 1994; P. E. Hartbower and P. J. Stolarski, 1996; R. Madlock, 1998; S. Alampalli, 2000, 2002.
9) M. Lozev, G. Clemena, J. Duke, Jr., M. Sison, Jr., and M. Horne. Acoustic Emission Monitoring of Steel Bridge Members, Report No. FHWA/VTRC 97-R13, 1997.
10) E. Aktan et al., "Monitoring and Managing the Health of Infrastructure Systems", Proceedings, NSF/ SPIE Conference on Highway Transportation Infrastructure, Irvine, CA., 3/2001.
11) U. Peil et al., Life-Cycle Assessment of Structures via Innovative Monitoring, SFB 477, Technical University Carolo- Wilhelmina, Braunscheig, Germany, 2000.
12) P. Schwesinger and F. H. Wittmann (editors), Present and Future of Health Monitoring, Aedificatio Publishers, Freiburg, 2000.
13) M. Burdekin, et al., Non-Destructive Methods for Field Inspection of Embedded or Encased High Strength Steel Rods and Cables. CAPCIS Ltd., NCHRP 10-30(3), Univ. of Manchester, UK, 1991.
14) M. Virlogeux, Replacement of the Suspension System on the Tancarville Bridge, pp. 113-120, Paper No. 99-0604, TRR No. 1654, TRB, NRC, National Academy Press, 1999.
15) R. Mayrbaurl and S. Camo, Structural Safety Evaluation Guidelines for Suspension Bridge Parallel Wire Cables, NCHRP Project 10-57, TRB, National Research Council, Washington, 2003.
16) M. G. Carfagno, F. S. Noorai, M. Brauss, J. Pineault, X-Ray Diffraction Measurement of Stresses in Post-Tensioning Tendons, pp. 201-206, in Extending the Lifespan of Structures, IABSE Symposium, San Francisco, ETH Honggerberg, CH-8093 Zurich, 1995.
17) C. Noyan, and J. B. Cohen, Residual Stress, Springer-Verlag 1987.
18) E. Harrison Teague et al., Carrier Differential GPS for Real-Time Control of Large Flexible Structures, ION-GPS96, Kansas City, Mi., 9/1996.
19) G. W. Roberts et al., The Use of Kinematic GPS and Triaxial Accelerometers to Monitor the Deflections of Large Bridges, the 10th FIG International Symposium on Deformation Measurements, pp. 268-275, Orange, Ca., 3/2001.
20) R. Vaicaitis, et al., Preventive Maintenance Management System for New York City Bridges. Technical Report No. 98-1, The Center of Infrastructure Studies, Department of Civil Engineering and Engineering Mechanics, Columbia University, New York, 1999.
21) K. Yamada et al., Bridge Monitoring and Weigh-in-Motion Systems in Japan, Workshop on Structural Monitoring of Bridges, Monash University, 9/2002.
22) S. Sumitro, Current and Future Trends in Long Span Bridge Health Monitoring System in Japan, Proceedings, NSF/ SPIE Conference on Highway Transportation Infrastructure, Irvine, CA., 3/2001.
23) Bridge Design Issues, TRR No. 1688, TRB, NRC, Washington, 1999.

Structural Parameter Identification: A Divide-and-Conquer Approach

C. G. Koh

Ph.D. (U.C. Berkeley), Associate Professor
Department of Civil Engineering, National University of Singapore, Singapore 117576

By determining structural parameters such as stiffness values, the state of structural health can be quantified and monitored. This process, based on numerical analysis of input and output signals, is known as "system identification" and provides a non-destructive evaluation method of engineering structures that deteriorate or suffer damage. While considerable progress has been made in the subject area, a major challenge is the robust convergence of parameter identification. Classical methods of system identification often fail when dealing with real systems that are large in terms of number of degrees of freedom and number of unknowns. This study adopts a soft computing method of using genetic algorithm to tackle the otherwise ill-condition problem associated with large systems. To reduce the computational time associated with the combinatorial explosion problem and improve identification accuracy, an elegant divide-and-conquer approach by means of substructuring is presented. Three different strategies of substructural identification are formulated, i.e. in time domain, frequency domain and static domain. Numerical examples of fairly large systems are presented.

Key Words: System identification, substructural approach, genetic algorithm

1. Introduction

For civil engineering structures such as bridges, towers and buildings, regular inspection and maintenance measures are necessary to detect and take action against weakening of structures due to deterioration and damage (arising from natural or man-made actions). This may be called structural health monitoring, i.e. to monitor the "health" state of the structures concerned, and preferably should be carried out in non-destructive and quantifiable ways. Vibration-based inspection is one such method of structural health monitoring, by determining structural parameters based on the numerical analysis of measured input and output (I/O) signals. One advantage is that non-accessible structural members can be monitored too. This approach of structural health monitoring has become an increasingly viable option due to rapid advances in hardware technology in terms of computation and instrumentation capabilities. The main hurdle is the lack of a robust and accurate computational strategy to identify parameters, in view of limited number of sensors and inevitable noise in reality.

Many studies on structural identification have adopted classical methods such as extended Kalman filter, instrumental variable and maximum likelihood methods; see References 1-3 for literature review on classical methods. These methods are typically gradient-based and they perform point-to-point search. They may converge falsely to local optimal point rather than the global optimal point, depending considerably on the initial guess. On the other extreme, exploration methods such as random search may be used to increase the chance of global convergence but are obviously very time consuming for large systems due to the huge number of possibilities. A soft computing approach of genetic algorithm (GA) is adopted in the study as the "search engine", which has the virtues of both exploration and exploitation methods. Both binary and real-value versions of GA are employed in the study.

2. Time-Domain Substructural Identification

To address the numerical difficulty associated with identification of large structural problems, Koh et al.[4] presented a substructural identification method in time domain making use of extended Kalman filter. The substructuring approach essentially divides the system into smaller and more manageable systems. Better identification accuracy and efficiency are hence achieved as compared to identifying the complete system. Subsequent research works adopting similar strategies to tackle large structural assessment problems include References 5-10.

Consider a multi-DOF lumped mass system (Fig. 1). The equations of motion for the complete system are

$$\begin{bmatrix} \mathbf{M}_{FF} & \mathbf{M}_{Ff} & & & & \\ \mathbf{M}_{fF} & \mathbf{M}_{ff} & \mathbf{M}_{fr} & & & \\ & \mathbf{M}_{rf} & \mathbf{M}_{rr} & \mathbf{M}_{rg} & & \\ & & \mathbf{M}_{gr} & \mathbf{M}_{gg} & \mathbf{M}_{gG} & \\ & & & \mathbf{M}_{Gg} & \mathbf{M}_{GG} & \end{bmatrix} \begin{Bmatrix} \ddot{\mathbf{u}}_F \\ \ddot{\mathbf{u}}_f \\ \ddot{\mathbf{u}}_r \\ \ddot{\mathbf{u}}_g \\ \ddot{\mathbf{u}}_G \end{Bmatrix}$$
$$+ \begin{bmatrix} \mathbf{C}_{FF} & \mathbf{C}_{Ff} & & & & \\ \mathbf{C}_{fF} & \mathbf{C}_{ff} & \mathbf{C}_{fr} & & & \\ & \mathbf{C}_{rf} & \mathbf{C}_{rr} & \mathbf{C}_{rg} & & \\ & & \mathbf{C}_{gr} & \mathbf{C}_{gg} & \mathbf{C}_{gG} & \\ & & & \mathbf{C}_{Gg} & \mathbf{C}_{GG} & \end{bmatrix} \begin{Bmatrix} \dot{\mathbf{u}}_F \\ \dot{\mathbf{u}}_f \\ \dot{\mathbf{u}}_r \\ \dot{\mathbf{u}}_g \\ \dot{\mathbf{u}}_G \end{Bmatrix}$$
$$+ \begin{bmatrix} \mathbf{K}_{FF} & \mathbf{K}_{Ff} & & & & \\ \mathbf{K}_{fF} & \mathbf{K}_{ff} & \mathbf{K}_{fr} & & & \\ & \mathbf{K}_{rf} & \mathbf{K}_{rr} & \mathbf{K}_{rg} & & \\ & & \mathbf{K}_{gr} & \mathbf{K}_{gg} & \mathbf{K}_{gG} & \\ & & & \mathbf{K}_{Gg} & \mathbf{K}_{GG} & \end{bmatrix} \begin{Bmatrix} \mathbf{u}_F \\ \mathbf{u}_f \\ \mathbf{u}_r \\ \mathbf{u}_g \\ \mathbf{u}_G \end{Bmatrix} = \begin{Bmatrix} \mathbf{P}_F \\ \mathbf{P}_f \\ \mathbf{P}_r \\ \mathbf{P}_g \\ \mathbf{P}_G \end{Bmatrix} \quad (1)$$

where subscript r denotes internal DOFs of the substructure system as in Fig. 1, and subscripts f and g denote the

interface DOFs of the substructure concerned with the remaining structures on the two sides denoted as F and G, respectively. For conciseness, let subscript j denote all interface DOFs (i.e. f and g). The equations of motion for the substructure considered are extracted as

$$\begin{bmatrix}\mathbf{M}_{rj} & \mathbf{M}_{rr}\end{bmatrix}\begin{Bmatrix}\ddot{\mathbf{u}}_j(t)\\ \ddot{\mathbf{u}}_r(t)\end{Bmatrix}+\begin{bmatrix}\mathbf{C}_{rj} & \mathbf{C}_{rr}\end{bmatrix}\begin{Bmatrix}\dot{\mathbf{u}}_j(t)\\ \dot{\mathbf{u}}_r(t)\end{Bmatrix}$$
$$+\begin{bmatrix}\mathbf{K}_{rj} & \mathbf{K}_{rr}\end{bmatrix}\begin{Bmatrix}\mathbf{u}_j(t)\\ \mathbf{u}_r(t)\end{Bmatrix}=\mathbf{P}_r(t) \qquad (2)$$

leading to

$$\begin{aligned}&\mathbf{M}_{rr}\ddot{\mathbf{u}}_r(t)+\mathbf{C}_{rr}\dot{\mathbf{u}}_r(t)+\mathbf{K}_{rr}\mathbf{u}_r(t)\\&=\mathbf{P}_r(t)-\mathbf{M}_{rj}\ddot{\mathbf{u}}_j(t)-\mathbf{C}_{rj}\dot{\mathbf{u}}_j(t)-\mathbf{K}_{rj}\mathbf{u}_j(t)\end{aligned} \qquad (3)$$

In an earlier substructural formulation by the author[4], accelerations, velocities and displacements at the interface DOFs are all required. For dynamic response, it is easier to measure acceleration than velocity and displacement. To this end, the displacements for internal DOFs are split into quasi-static displacements (denoted by superscript s) and "relative" displacements (superscript *):

$$\mathbf{u}_r(t)=\mathbf{u}_r^s(t)+\mathbf{u}_r^*(t) \qquad (4)$$

where

$$\mathbf{u}_r^s=\mathbf{r}\,\mathbf{u}_j \qquad (5)$$

$$\mathbf{r}=-\mathbf{K}_{rr}^{-1}\mathbf{K}_{rj} \qquad (6)$$

Since damping force is usually small compared to inertia force and elastic force in typical civil structures, the velocity-dependent part in the interface motion forces is neglected. Hence, Eq. (3) becomes

$$\begin{aligned}&\mathbf{M}_{rr}\ddot{\mathbf{u}}_r^*(t)+\mathbf{C}_{rr}\dot{\mathbf{u}}_r^*(t)+\mathbf{K}_{rr}\mathbf{u}_r^*(t)\\&=\mathbf{P}_r(t)-(\mathbf{M}_{rj}+\mathbf{M}_{rr}\mathbf{r})\ddot{\mathbf{u}}_j(t)\end{aligned} \qquad (7)$$

The right-hand side without $\mathbf{P}_r$ term may be referred to as interface motion forces. Note that only accelerations at interface DOFs are required to compute the interface motion forces. The forward analysis as required in the GA approach involves solving the above equations of motion subjected to the excitation and interface motion forces. The fitness function is defined in terms of the measured components of the relative accelerations.

There are two versions of substructural identification method -- one without overlap members and the other with overlap members[3-4]. The first version yields better numerical accuracy while the second version requires less measurement points as illustrated in of Figs. 2(a) and (b), respectively, where S_i denotes substructure i. Only the results for the substructural method with overlap are presented here due to space constraint. In general, identification results get better with increasing number of available response measurements. In the above substructural approach, only measurements within the substructure of concern and at interface ends are used when identifying the substructure parameters. Given a limited number of sensors, the identification results can be improved greatly if the measurement program allows shift of measurement sensors according to the substructure under investigation. If this is not feasible, an alternative is to make use of as many response measurements as possible by progressively expanding the domain of substructural identification.

A variation of substructural identification is hence proposed, called the progressive structural identification method. As illustrated in Fig. 2(c), the main difference is that the substructure expands progressively while keeping the number of unknowns manageable at each stage. The top substructure is selected as the first substructure (S_1) for identification. After its unknown parameters are identified, an expanded substructure is considered, i.e. S_2 which includes S_1. The identified parameters of S_1 are now taken as known, and the measurements in substructure S_1 are used again in the fitness evaluation while identifying the next substructure S_2. This procedure continues until the complete or required part of the structure is identified. An important feature of the progressive structural identification method is that it takes advantage of increasing availability of response measurements but without increasing the number of unknowns as the substructure expands. The cost incurred is the increase in computational time for solving progressively larger systems, but this shortcoming can be offset by faster convergence at each stage.

A fairly large system of 50 DOFs with 50 unknown stiffness parameters is investigated. The input force is random excitation by means of Gaussian white noise. The exact parameter values of the 50-DOF system are that all masses are 300 kg except for m_1 which is 600 kg, and all stiffness coefficients are 700 kN/m. Damping effect is taken into account by adopting Reyleigh damping. The damping ratios for the first two modes are both 0.05 and also taken as unknown. For every ten levels, three random forces are applied at the respective 3rd, 6th and 9th nodes, and four acceleration measurements are taken at the respective 3rd, 5th, 8th and 10th nodes.

The effects of I/O noise are accounted for by numerically contaminating time signals of excitations and responses. The noise level is defined as the ratio of standard deviation of the zero-mean white Gaussian noise to the root-mean-square value of the uncontaminated signals. 5% I/O noise level is used. Substructural identification without overlap generally requires more measurements than substructural identification with overlap. Thus, only the version with overlap is used here by considering 10 substructures: S_1=[45-50), S_2=[40-46), S_3=[35- 41), S_4=[30-36), ... S_{10}=[0- 6). Square bracket indicates that acceleration measurement at interface node 5 is required (as input). Parenthesis indicates that acceleration measurement at node 10 is optional and, if available (as in this case), is treated as output. For the progressive structural identification method, the identification is carried out in ten stages: S_1=[45-50), S_2=[40-50), S_3=[35,50), ... S_{10}=[0,50).

The GA software adopted here is GENESIS[11], which uses binary encoding of chromosomes as opposed to real-value encoding. The GA search is carried out in a range from a half to twice of the exact value with 6-bit resolution within the chosen range. The resolution of each parameter is therefore $1/2^6\times(2\text{-}0.5)$ = 2.3% of the corresponding exact value. The GA parameters used are crossover rate of 0.6 and mutation rate of 0.01. Population size of 50 is sufficient. The results obtained by the complete structural identification, substructural identification and progressive structural identification methods are compared in Fig. 3, in terms of the ratio of identified stiffness to exact value. The plot range is set as the parameter search range (i.e. 0.5 to 2). It can be seen that there is significant improvement in the accuracy of identified parameters by the substructural identification and progressive structural identification methods. Moreover, considerable saving in computational

time is achieved mainly due to smaller system size for identification. On the same computer, the saving in computational time is 43% for substructural identification and 37% for and progressive structural identification methods as compared to complete structural identification. More details can be found in Reference 12.

3. Frequency-Domain Substructural Identification

In practice, it may not be practical or cost-effective to measure interface DOFs. To address this issue, a frequency-domain method of substructural identification is formulated. Consider part of the structure called substructure B, separated from the remaining parts A and C of the structure at interface points a and b as shown in Fig. 4. The system is excited at the e-th DOF by a sinusoidal force which can be mathematically represented in complex harmonic form as $F_E \exp(i\omega t)$, where ω is the excitation frequency. The formulation for substructural identification is based on the concept of receptance, which is a (complex) transfer function relating displacement at one point to excitation acting at another point, defined as follows

$$H(j,e:\omega) = [X_j \exp(i\omega t)] \,/\, [F_E \exp(i\omega t)] \tag{8}$$

where $X_j \exp(i\omega t)$ is the harmonic displacement at the j-th DOF. The dynamic equations for the whole structure in the frequency domain are given by

$$\left(-\omega^2 \mathbf{M} + \mathrm{i}\,\omega \mathbf{C} + \mathbf{K}\right) \mathbf{X} \exp(i\omega t) = \mathbf{F} \exp(i\omega t) \tag{9}$$

Now consider substructure B to be identified. First, the excitation force F_E is assumed to act within the domain of the substructure. Substructure B is thus in equilibrium under the applied force F_E and interface forces F_{Ia} and F_{Ib} (subscript I denoting interface). The displacements at two selected points, called "base points" p and q within the substructure, can be represented by using the substructure receptance (where * denotes substructure) as follows

$$\begin{Bmatrix} X_p \\ X_q \end{Bmatrix} = \begin{Bmatrix} H^*(p,k) \\ H^*(q,k) \end{Bmatrix} F_E + \begin{bmatrix} H^*(p,a) & H^*(p,b) \\ H^*(q,a) & H^*(q,b) \end{bmatrix} \begin{Bmatrix} F_{Ia} \\ F_{Ib} \end{Bmatrix} \tag{10}$$

where ω is omitted in the receptance notations for brevity from here onwards. The above equations can be written more concisely as

$$\mathbf{X} = \mathbf{H}_{\mathbf{E}}^* \mathbf{F}_{\mathbf{E}} + \mathbf{H}_{\mathbf{I}}^* \mathbf{F}_{\mathbf{I}} \tag{11}$$

The unknown interface force vector $\{F\}_I$ can be computed given measured responses at the base points p and q. The substructure stiffness matrix is to be identified for the purpose of model updating or other reasons. The objective is to determine unknown stiffness parameters of the substructure such that the interface forces generated by the above procedure correctly predict (within acceptable error) displacement at other points called the "check points". In principle, one check point is sufficient for the identification procedure. Consider a check point r (different than p and q) within the substructure. The displacement X_r can be back-analyzed using the computed interface forces as

$$X_r = H^*(r,k) F_E + H^*(r,a) F_{Ia} + H^*(r,b) F_{Ib} \tag{12}$$

The objective function can thus be posed as the minimization of the difference between the predicted response and the measured response for X_r. The identification procedure thus requires displacement measurements at a minimum of three points, i.e. X_p and X_q at the base points used to compute the interface forces, and X_r at the check point used in back analysis procedure. An advantage is that the substructure can be identified in a standalone manner, i.e. without the knowledge of the remainder of the structure. This not only facilitates identification of only the required part(s) of the structure but also makes the substructural identification more accurate since no error propagation takes place between substructures. Furthermore, if the excitation force is applied outside the domain of the substructure, the terms involving F_k in the above equations simply vanish as a special case. Hence, the procedure is still applicable even when the external force is applied outside the substructure of concern. As a matter of fact, no measurement of external force (input) is required in such a case, and the method becomes a powerful output-only identification method.

The computational procedure is illustrated in Fig. 5. With initial guess of stiffness parameters which presumably are incorrect, the substructure receptance matrix and hence the estimated response at the check point would be wrong. The substructural identification problem is thus reduced to an optimization problem of minimizing the difference between the estimated response and measured response at the check point. The required optimization task is carried out by means of the GA approach, and a general purpose package in Matlab[12] is used. The real-value GA approach is adopted here. The search range of stiffness values is ±70% of the exact value. Damping ratio is treated as unknown with search range ±100% of the exact value.

Consider a 200-DOF lumped mass system. The exact value of each mass is 1000 kg. To test the proposed method on stiffer structures with higher system frequencies, relatively high stiffness value of 5×10^5 kN/m is used for all levels. A substructure of 20 DOFs is to be identified, from level 90 to level 109 inclusive. Excitation force is applied outside the substructure at level 85; force measurement is thus not required. Displacement measurements are taken at the base-points: levels 95 and 102. Damping ratio of 2% is assumed for all modes required and is treated as unknown as well in the identification.

To improve accuracy, two check points are used, viz. levels 97 and 107, in the GA fitness function evaluation. To account for the effects of noise, the signal is artificially polluted in the numerical study as follows. A random noise is added to the displacement signal, conforming to uniform probability distribution with zero mean and range equal to 10% of the range of unpolluted signal. With 20 substructure stiffness values to be identified, it is necessary to use a larger population size. The GA population size used is 200 with 100 crossover operations. It is beneficial to average several sets of identification results for problems involving many unknowns. Two sets of excitation frequencies are thus considered: (a) 120, 130, 140 and 150 rad/s, and (b) 140, 150, 160 and 170 rad/s. For each set of frequencies, the displacements obtained at the four frequencies are used in the GA fitness function. The identified results for both sets are then averaged. As shown in Fig. 6, the mean error of identified stiffness parameters is only 4.5% and the maximum error 10%. The results are good in view of the large system size and incomplete and noisy measurements. Further details can be obtained from Reference 13.

4. Static Substructural Identification

Most studies on system identifications are carried out based on dynamic responses. In an attempt to carry out

structural identification based on only static response, Sanayei applied static forces instead to a set of DOFs and measured displacements on another set[14]. It was found by Jenkins et al. that the use of static responses for damage detection may be better in terms of local sensitivity than using dynamic response.[15] Chou used static responses together with GA to detect structural damage, and unmeasured displacements were encoded in the chromosomes (unknown parameter set).[16] Furthermore, unlike in the dynamic approach, no mass or damping parameters are needed in the process. Lastly, the amount of computational time is reduced substantially since only static equation is involved. Nevertheless, when the structure is large in terms of DOFs and unknowns, long computational time and numerical difficulty in convergence would still pose a hindrance, which calls for the need of substructuring as proposed below. The static equations may be obtained from Eq. (2) by neglecting the inertia and damping terms:

$$\begin{bmatrix}\mathbf{K}_{rj} & \mathbf{K}_{rr}\end{bmatrix}\begin{Bmatrix}\mathbf{u}_j \\ \mathbf{u}_r\end{Bmatrix} = \begin{Bmatrix}\mathbf{P}_j \\ \mathbf{P}_r\end{Bmatrix} \tag{13}$$

Hence

$$\mathbf{K}_{rr}\mathbf{u}_r = \hat{\mathbf{P}}_r \tag{14}$$

where

$$\hat{\mathbf{P}}_r = \mathbf{P}_r - \mathbf{K}_{rj}\mathbf{u}_j \tag{15}$$

When the complete structure is divided into substructures, the displacements at the interfaces must be known, be them measured or imposed. Strategically dividing the structure and placing the sensors can achieve a good balance between the required number of sensors and identification accuracy. Some DOFs are measured (denoted by subscript m) while others are unmeasured (subscript n). Accordingly, Eq. (14) can be written as

$$\begin{bmatrix}\mathbf{K}_{nn} & \mathbf{K}_{nm} \\ \mathbf{K}_{mn} & \mathbf{K}_{mm}\end{bmatrix}\begin{Bmatrix}\mathbf{u}_{rn}^* \\ \mathbf{u}_{rm}^*\end{Bmatrix} = \begin{Bmatrix}\mathbf{p}_{rn} \\ \mathbf{p}_{rm}\end{Bmatrix} \tag{16}$$

Note that the displacement vector $\mathbf{u}_r$ is only an estimate during the GA search and is herein represented by an asterisk to distinguish it from the measured displacement vector (without *). Accordingly, $\mathbf{u}_{rn}^*$ is a vector of displacements for the non-measured DOFs provided by GA within the chromosome. On the other hand, $\mathbf{u}_{rm}^*$ represents a vector of estimated displacements for the measured DOFs by using the second row of Eq. (16) based on given GA-estimate of $\mathbf{u}_{rn}^*$. The error between the estimated and measured values at the measured DOFs is to be minimized by including it in the fitness function.

For updating in the GA iterations, a scaling factor r is defined as the ratio of the Euclidean norm of the measured displacement $\mathbf{u}_{rm}$ to that of the estimated $\mathbf{u}_{rm}^*$ as follows

$$r = \frac{\|\mathbf{u}_{rm}\|}{\|\mathbf{u}_{rm}^*\|} \tag{17}$$

where $\|.\|$ denotes the Euclidean norm. The full estimated displacement vector $\mathbf{u}_r^*$ is then updated by

$$\mathbf{u}_r^* = r\begin{Bmatrix}\mathbf{u}_{rn}^* \\ \mathbf{u}_{rm}^*\end{Bmatrix} \tag{18}$$

The fitness of each chromosome is computed as the inverse of the sum of two kinds of errors, i.e. the output error and equilibrium error as follows.

$$(\text{Fitness})^{-1} = \varepsilon_{\text{output}} + \varepsilon_{\text{equilibrium}} = \frac{\|\mathbf{u}_{rm}^* - \mathbf{u}_{rm}\|}{\|\mathbf{u}_{rm}\|} + (\hat{\mathbf{P}}_r - \mathbf{K}_{rr}\mathbf{u}_r^*) \tag{19}$$

The first error term is defined as the difference between the estimated responses $\mathbf{u}_{rm}^*$ and the measured responses $\mathbf{u}_{rm}$. The second error term is the residual in satisfying the equilibrium equation, where $\mathbf{K}_{rr}$ is computed based on the identified parameters. A flow chart for the computational procedure is shown in Fig. 7. For better accuracy, two or more load cases are used, and the total fitness will include errors from all load cases.

A plane truss structure system is considered as shown in Fig. 8(a). There are a total of 23 truss members with exact axial stiffness of 400 kN/m. The objective is to identify the axial stiffness values of all members in the substructure as shown in Fig. 8(b). Three load cases are considered for the procedure as illustrated in Fig. 9. Vertical displacements at all internal nodes are assumed to be available as response, while both horizontal and vertical displacements at interface nodes are required as input. A population of 50 is used, and each individual substructure will undergo 100 generations of GA computation. The lower bound of the search range is half its exact value while the upper bound is twice its exact value. A mutation level of 0.1 is used and crossover rate is 0.6. The identification results are presented in Table 1 and the mean error is only 3.4%. The identification is repeated with an introduction of 5% random noise in all measured displacements. The mean error expectedly increases to about 8.1% due to measurement inaccuracy. These results show that the proposed static approach of system identification is feasible with several advantages.

5. Conclusions

By determining structural parameters, system identification provides a quantifiable method of structural health monitoring. Traditional ways of analysing the entire system do not necessarily work and the non-traditional approach of GA is adopted. Three substructural identification strategies are presented to make the system identification task efficient. The methods can be applied to large and complex problems with many unknown parameters, by simply dividing the problem into smaller problems of manageable size. Numerical examples presented include a large structure of 200 DOFs, which is the largest system reported in the literature thus far to the authors' knowledge.

6. References

1) Natke, H. G. "Recent trends in system identification." *Proceedings of the European Conference on Structural Dynamics*, EURODYN ' 90, Kratzig W. B. et al. eds, Bochum, F.R. Germany, pp. 283-289, 1990.
2) Ghanem R., and Shinozuka M. "Structural-system identification.1. Theory." *J. Engrg. Mech., ASCE,* 121(2), pp. 225-264, 1995.
3) Koh C. G. and See L. M. "Techniques in the identification and uncertainty estimation of

parameters", Chapter 5 in *Structural Dynamic Systems Computational Techniques and Optimization: Computational Techniques*, Gordon and Breach Science Publishers, Netherlands, 1999.
4) Koh C. G., See L. M., and Balendra T. "Estimation of structural parameters in time domain: A substructure approach." *Earthquake Engrg. Struct. Dyn.*, 20, pp. 787-801, 1991.
5) Koh C. G., See L. M., and Balendra T. "Determination of storey stiffness of three-dimensional frame buildings." *Engrg. Struct.*, 17(3), pp. 179-186, 1995.
6) Koh C. G., See L. M., and Balendra T. "Damage detection of buildings – numerical and experimental studies." *J. Struct. Engrg., ASCE,* 121(8), pp. 1155-1160, 1995.
7) Oreta W. C., and Tanabe T. A. "Element identification of member properties of framed structures." *J. Struct. Engrg., ASCE,* 120(7), pp. 1961-1976, 1994.
8) Yun C. B., and Lee H. J. "Substructural identification for damage estimation of structures." *Struct. Saf.*, 19(1), pp. 121-140, 1997.
9) Herrmann T. and Pradlwarter H. J. "Two-step identification approach for damped finite element models." *J. Engrg. Mech., ASCE,* 124(6), pp. 639-647, 1998.
10) Yun C. B., and Bahng E. Y. "Substructural identification using neural networks." *Comput. Struct.*, 77(1), pp. 41-52, 2000. Grefenstette, J. J. GENESIS and OOGA. Two genetic algorithm systems. Melrose, Massachusetts, 1991.
11) Houk, C. R., Joines, J. A. and Kay, M. G. *A Genetic Algorithm for Function Optimization: A Matlab Implementation*, NCSU-IE Technical Report 95-09, North Carolina State University, Raleigh, North Carolina, 1994.
12) Koh, C. G., Hong B. and Liaw, C.Y. "Substructural and progressive structural identification methods." *Engrg. Struct.*, 25(12), pp. 1551-1563, 2003
13) Koh, C. G. and Shankar, K. "Stiffness identification by a substructural approach in Frequency domain", *Int. J. Struct. Stability and Dynamics,* 3(2), pp. 267-281, 2003.
14) Sanayei, M. and Onipede, O. (1991). "Damage assessment of structures using static test data", *AIAA Journal,* 29(7), 1174-1179, 1991.
15) Jenkins, C. H., Kjerengtroen, L. and Oestensen, H. (1997). "Sensitivity of parameter changes in structural damage detection.", *Shock Vib,* 10(4), pp.135-42, 1997.
16) Chou, J. H. and Ghaboussi, J. (2001). "Genetic algorithm in structural damage detection", *Computers and Structures,* 79, pp. 1335-1353, 2001.

7 Acknowledgement

The author thanks Dr K. Shankar, Dr B. Hong and Mr S. C. Mak, for their contributions. Financial supports by the National University of Singapore and the DSO National Laboratories to support the research are gratefully acknowledged. The invitation and financial support by the JSCE Task Committee for the author to deliver this keynote are greatly appreciated.

Table 1. Identification results for truss structure by static substructural approach

	With 0% noise		With 5% noise	
Axial stiffness	Est. Value (kN/m)	Error (%)	Est. Value (kN/m)	Error (%)
K_8	430.59	7.60	438.54	9.59
K_9	405.81	1.41	461.53	15.34
K_{10}	390.75	-2.35	433.27	8.27
K_{11}	421.41	5.31	415.98	3.96
K_{12}	401.99	0.46	392.22	-1.98
K_{13}	433.05	8.22	420.93	5.19
K_{14}	389.13	-2.76	440.88	10.18
K_{15}	419.80	4.91	439.43	9.81
K_{16}	432.06	7.97	448.74	12.14
Mean absolute error	3.42%		8.06%	

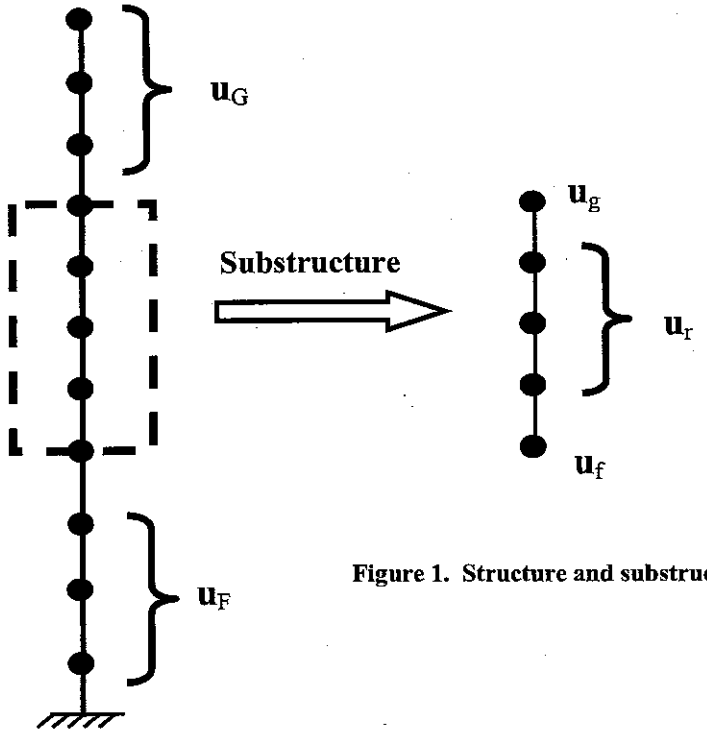

Figure 1. Structure and substructure

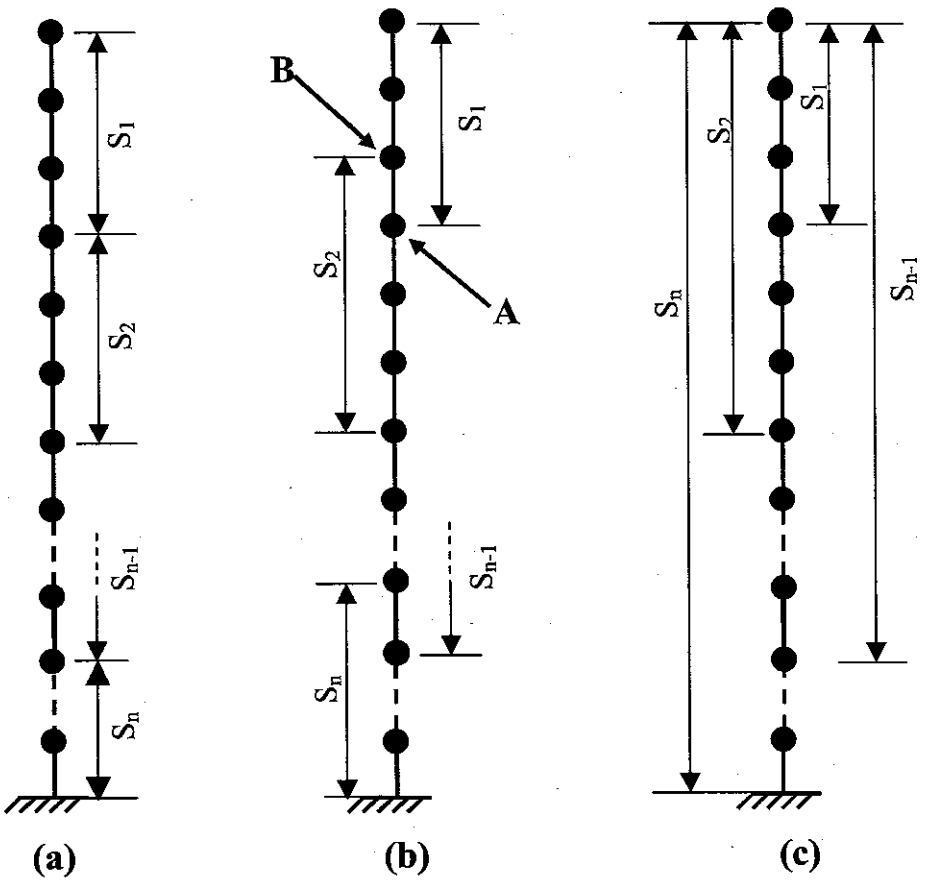

Figure 2. (a) Substructural identification without Overlap;
(b) Substructural identification with Overlap; (c) Progressive identification

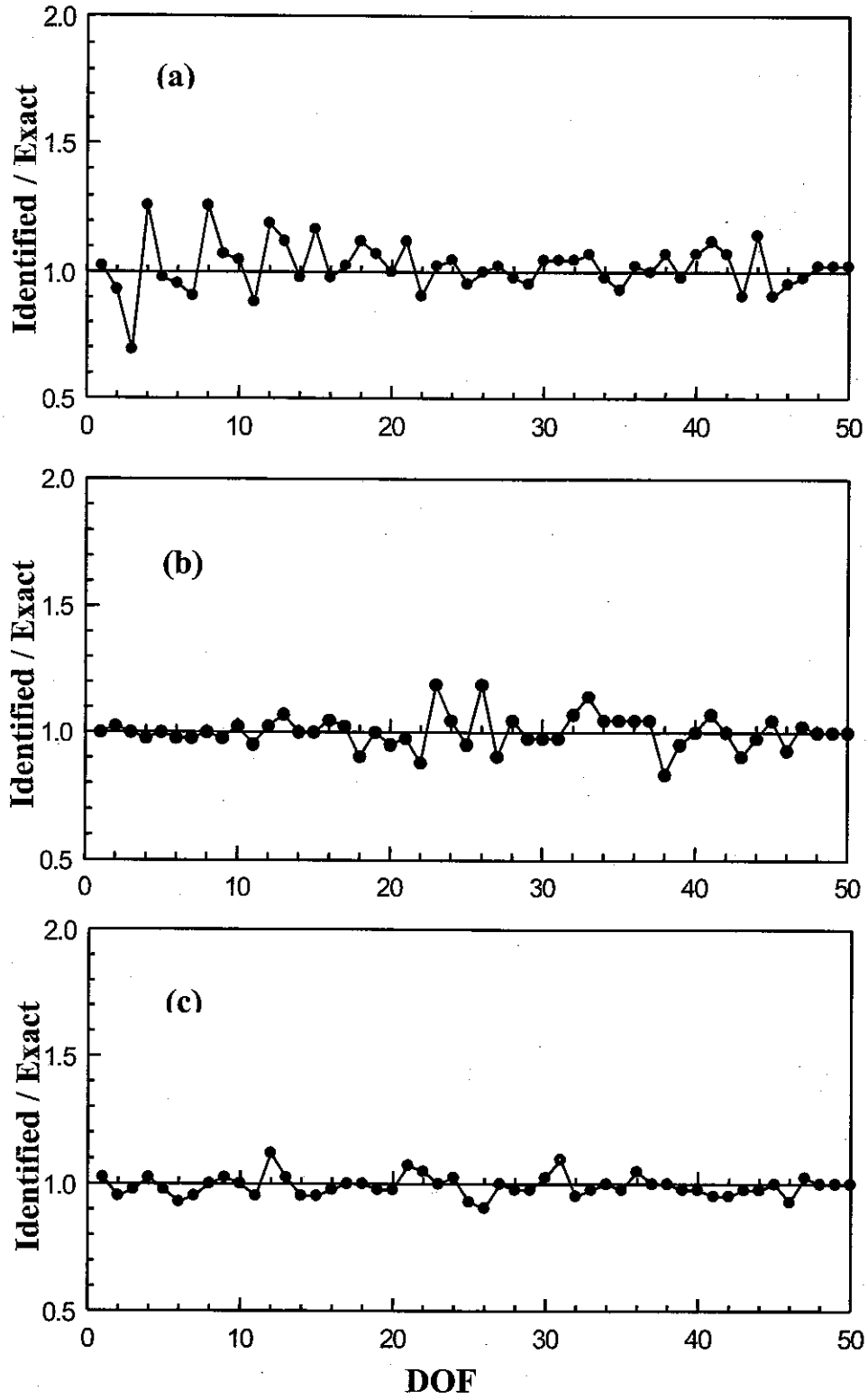

Figure 3. Ratio of identified stiffness to exact value for 50-DOF system: (a) Complete structure (b) Substructural method (c) Progressive method

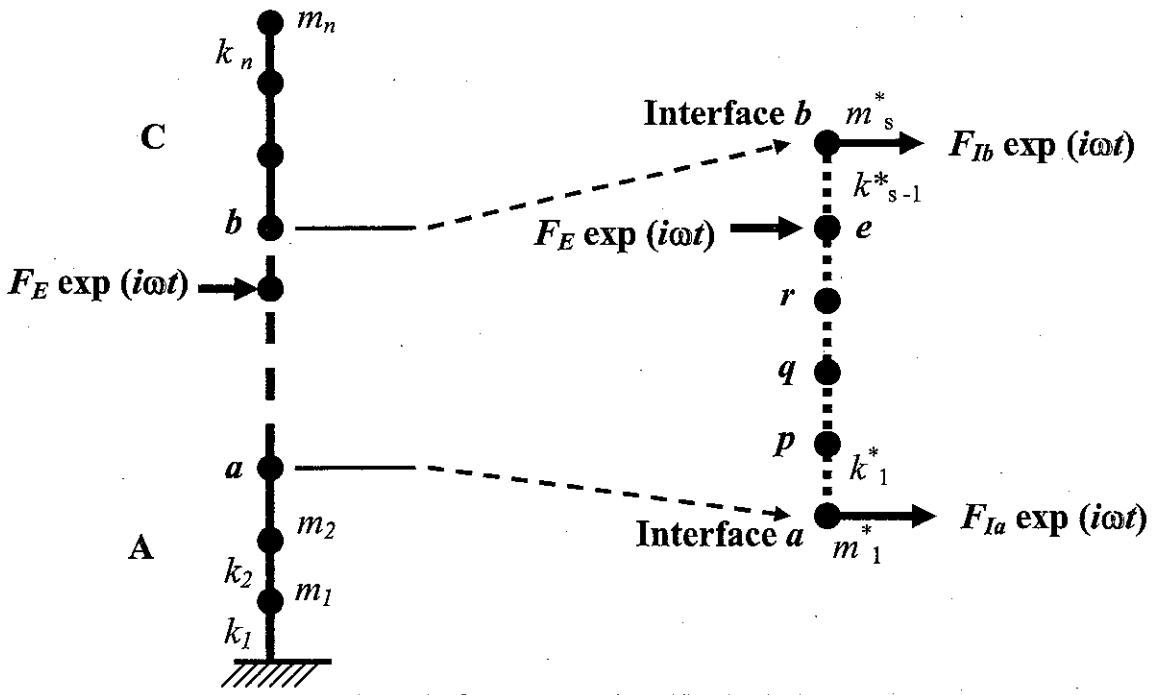

Figure 4. Substructural identification in frequency domain

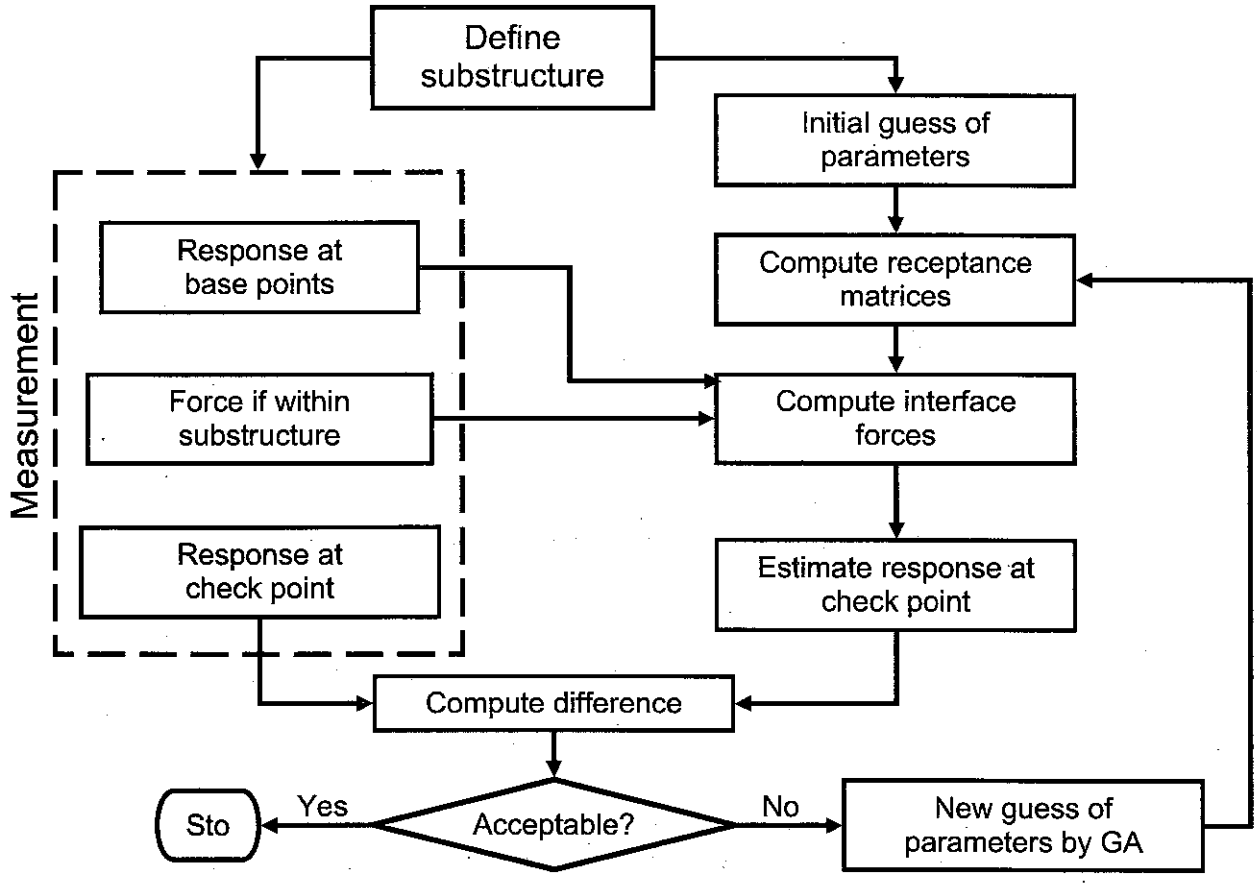

Figure 5. Substructural identification procedure in frequency domain

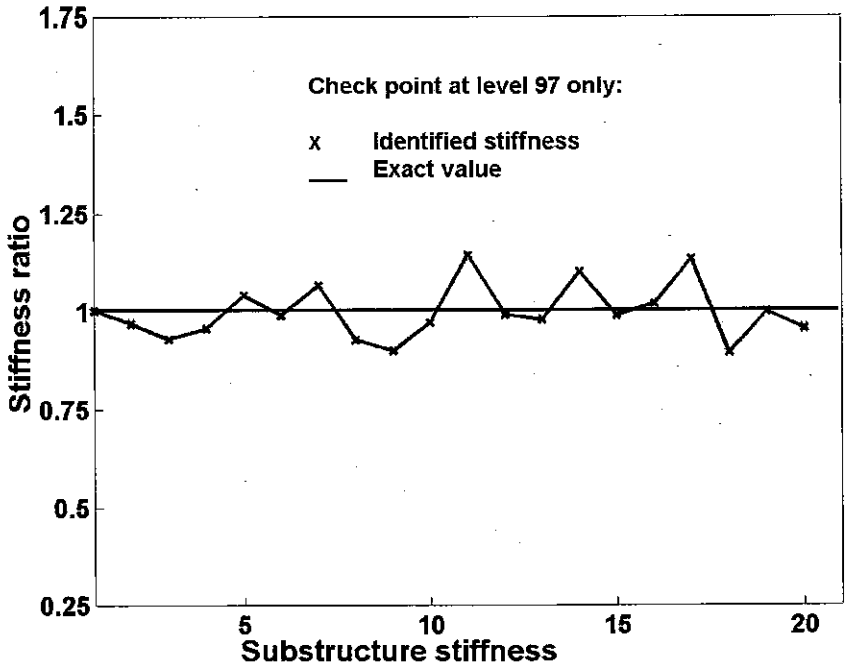

Figure 6. Stiffness identification for 20-DOF substructure of 200-DOF system

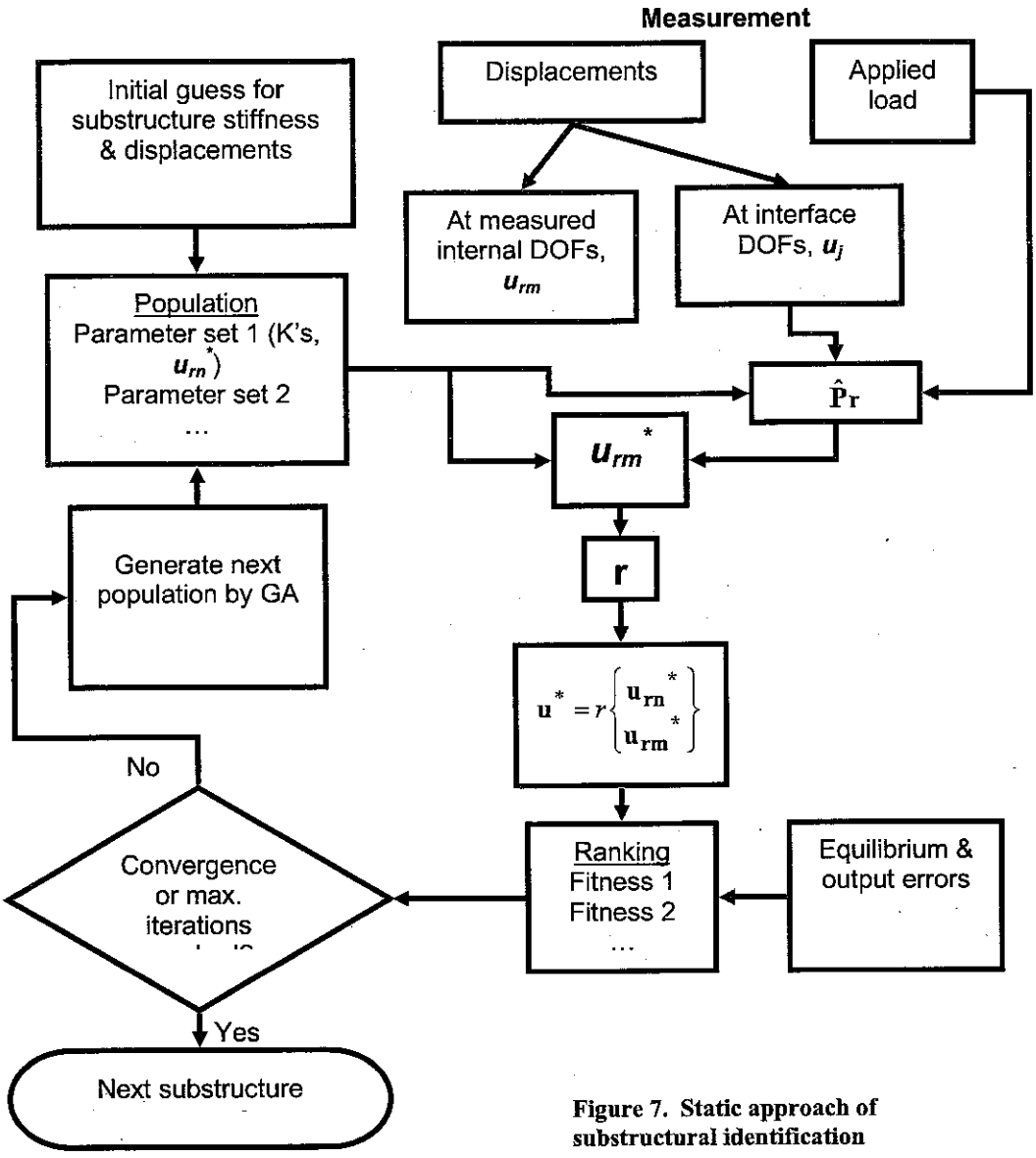

Figure 7. Static approach of substructural identification

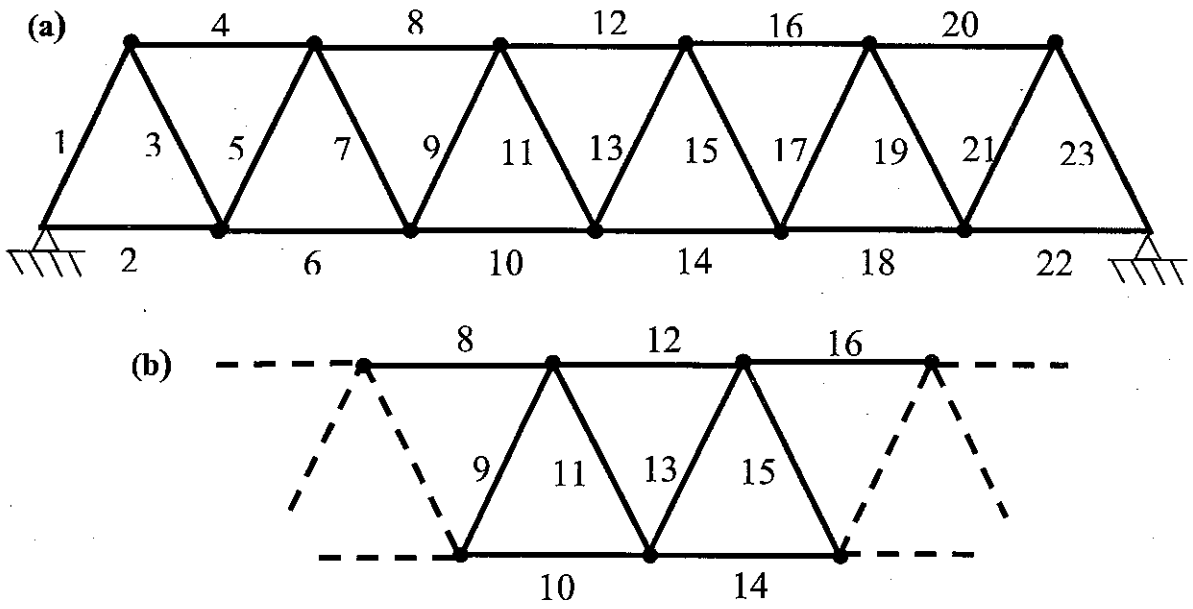

Figure 8. A plane truss: (a) complete structure; (b) substructure

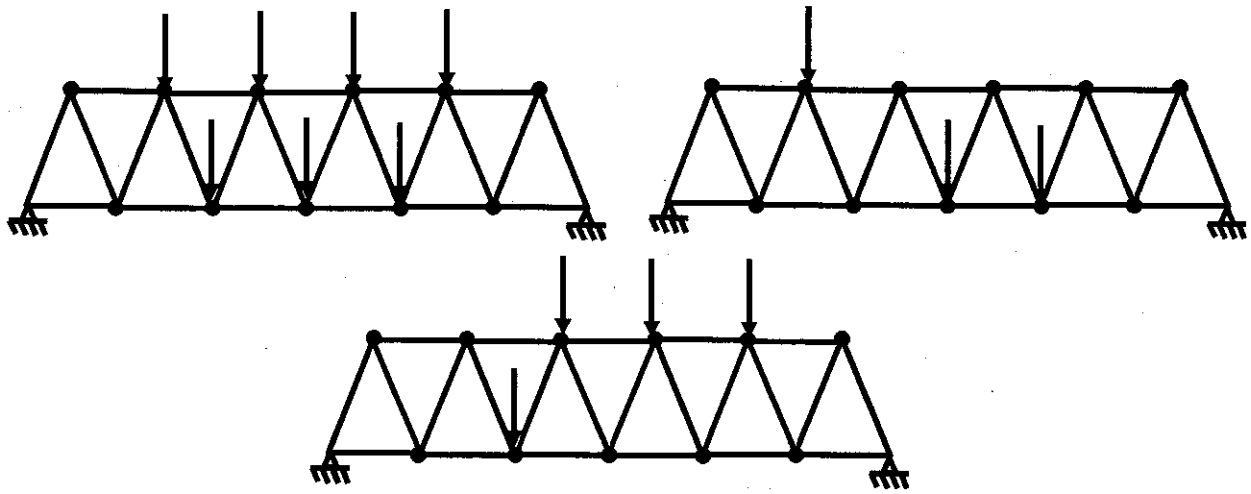

Figure 9. Three load cases for truss identification

Vibration-based Monitoring of Infrastructures
—R& D of sensors and analysis at the University of Tokyo—

Yozo FUJINO and Masato ABE

Dept. of Civil Engineering, University of Tokyo, Tokyo, 113-8656 Japan
fujino@bridge.t.u-tokyo.ac.jp masato@bridge.t.u-tokyo.ac.jp

This paper firstly presents an overview of civil infrastructures and their problems in Japan, and discusses characteristic features of structural health monitoring for civil infrastructures. The focus of the discussion is placed on bridges in the transportation system. In the second place, research and development of health monitoring systems at the Bridge and Structure Laboratory of the University of Tokyo is presented. Ambient vibration based approaches for Laser Doppler Vibrometer(LDV) and long-span suspension bridges show possible wide applications in this field. In both cases, although the excitation is unknown, densely distributed and accurate measurement is shown to provide valuable information on the status of structures. Especially, a LDV based approach can provide information on damage and loading to the structure with practically applicable system configuration. Toward easy and inexpensive monitoring, development of a compact remote intelligent sensing system, RIMS and simple monitoring system of road surface condition, VIMS is also described.

1. INTRODUCTION

Civil infrastructures include various units and systems such as buildings, transportation systems, communication systems, power generation and distribution systems, and water supply/drainage systems. Significant investment expenditures and long time periods are necessary for a society to build up its infrastructure systems; indeed, any advanced society has already put enormous effort toward this goal. The continued performance of these infrastructure units and systems is vital to our human and economic activities. Even a short-term malfunction affects the society tremendously.

The built environment supported by infrastructures is an asset if they are well maintained and properly operated. However, if they are degraded by improper maintenance, they can be, sooner or later, a big debt to the society. To prevent this, it is absolutely necessary to develop maintenance technology that involves inspection, monitoring, repair, rebuilding and even financial planning. Structural health monitoring is one of the important components in the maintenance technology for civil infrastructures.

This paper primarily presents an overview of civil infrastructures and their problems in Japan, and discusses characteristic features of structural health monitoring for civil infrastructures. The focus is placed on bridges in the transportation system. Additionally, recent research related to structural health monitoring conducted at Bridge & Structure Laboratory, Department of Civil Engineering, University of Tokyo (to which the authors belong) is described.

2. INFRASTRUCTURE DEVELOPMENTS IN JAPAN

In Japan, construction of modern infrastructures started in Meiji Era (~1868). Investment in railway development was considered a high priority in those days. The present railway network was practically established in 1940's.

Construction of roads was rather slow before the 1940's. Rapid growth of the Japanese economy started in the 1960's and intensive investment in road construction followed to meet expansion of industrial activities.

The first bullet train railway line and the first highway were started in the middle of 1960's. Construction of the bullet railway network has not yet been finished, but the total length of the railway system is saturated and even decreasing somewhat; consequently, new construction of railway bridges is rare. Many railway infrastructures are rather old and need elaborate maintenance.

Development of the highway network system is still actively on-going at present. However, the amount of new road bridge construction has also been decreasing in recent years. Road bridges constructed in the 1970's will be more than 50 years old in 20 years. Further, the number of the aged bridges is will constitute half of all road bridges by the year 2020. A similar situation can be also observed in buildings in Japan.

Although Japan is considered to be active in new construction of infrastructures, maintenance is becoming increasingly important.

3. PROBLEMS OF EXISTING STRUCTURES

Infrastructures constructed in the rapid growth period (1960 to 1980) are enormous, but they are not considered to be of the highest quality because of the construction boom during that time. In concrete structures, for example, sand taken from the sea was often used without adequate washing, so chemical degradation is rapidly progressing in such concrete structures. It is reported that tendons in many pre-stressed concrete bridges are rusted because water leaked into the tendon tubes due to incomplete grouting.

In 2000, a number of un-reinforced concrete blocks fell from tunnel linings for a bullet train railway that were constructed around 1970. Fortunately, the concrete blocks did not hit any train cars. After these incidents, the concrete linings in old railway tunnels, as well as road tunnels, were extensively investigated by the "hitting-by-hammer" method. Thousands of potentially dangerous cracks were indeed found in the lining of many tunnels.

In an elevated viaduct of the Tokyo Metropolitan Expressway, a relatively new traffic sign pole fell down and hit a motorcar beneath the bridge. The cause of this accident was improper welding.

These accidents clearly highlight the importance of inspection and maintenance of civil infrastructures. Inspection rules for railway and roads were revised after these accidents; more frequent and detailed inspection was specified. The public had tended to think that civil structures are permanent maintenance-free fixtures, but has now realized that this is not the case.

Regarding the road bridges, the traffic volume in major highways is as large as 15,000 vehicles per lane and the ratio of heavy trucks in the traffic is also high (as high as 30%). On some of the bullet train routes, trains run quite frequently. The high intensity and high frequency loading generated by this high traffic volume creates many problems in bridges: the most typical problem is fatigue damage in concrete slabs and steel welded girders.

Fig. 1 shows the cost of maintenance of the highway as a function of the service period. It shows that the maintenance and repair cost increases sharply when the service period exceeds 15 to 20 years. The average age of bridges in Japan will soon become 40 or even 50 years soon, so the necessity of frequent and detailed inspection and maintenance/repair is also expected to increase significantly in the near future. However, because of the tight budget in Japan, expenditures for maintenance-related activities are not expected to increase in proportion to the need. Consequently, more efficient and economical inspection and maintenance strategies are required.

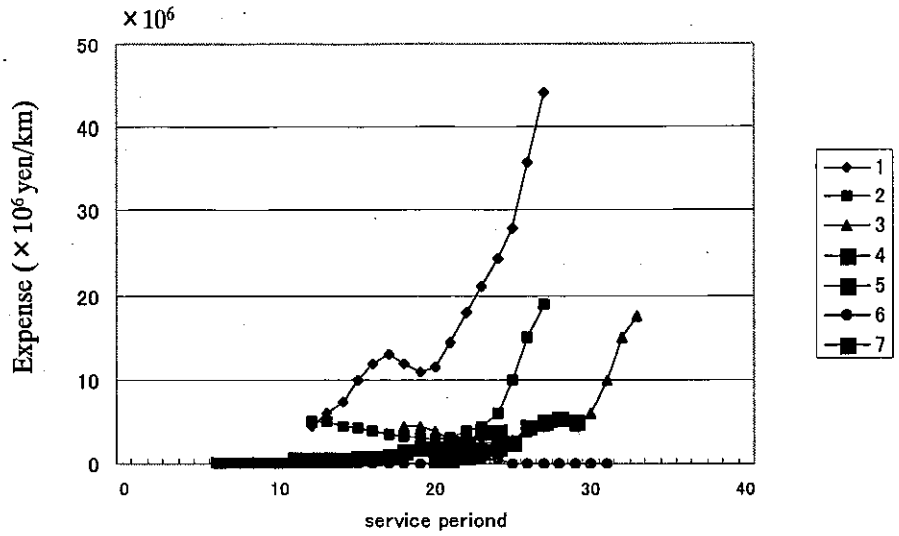

Figure 1. Expenditure for maintenance and repair in high way bridges (routes 1 to 7)

4. CHARACTERISTIC FEATURES IN MONITORING AND INSPECTION OF CIVIL INFRASTRUCTURES

Inspecting, monitoring and maintenance are systematic in the field of aircrafts, ships and so forth. Those for civil infrastructures are different from these other in many ways;

1) Infrastructures are in general very much distributed and spatial, and areas to be inspected are quite huge.
2) Inspection must be made onsite, where the site conditions are often inconvenient, dangerous or somewhat hostile. For example, investigation of concrete lining in tunnels is a very tiring work. Especially in the case of road tunnels, inspection must be conducted while traffic is in service. Inspection of fatigue cracks inside box girders is also rather unpleasant.
3) Some of the components to be inspected are difficult or even dangerous to access. Elevated bridges require inspection work at a high elevation and complete inspection needs expensive temporary walkway. Soil slopes need to be monitored, especially during heavy rainfall, but they are inaccessible at those times monitoring is most needed.
4) Components to be inspected are often embedded within the structure or otherwise not immediately visible. Typical examples are re-bars and pre-stressed tendons inside concrete and underground utility lines.
5) Infrastructure is not made by mass production: each infrastructure is different from the others and is exposed to different environment.

So far, inspection of civil infrastructures is basically made by human beings. It is extremely labor-intensive. Inspectors are often exposed to dangerous conditions and/or uncomfortable working environments. Considering that the volume of inspection work will be significantly increased in the near future, inspection by human beings must be replaced with automated instruments and inspection efficiency and accuracy must be improved.

Inspection of civil infrastructures is considered by some to be an old fashioned, low-tech and unpleasant subject. Recent development of sensors and information technology, however, may completely modernize the content of the work and may increase the efficiency of the work dramatically. For example, the human-based "hit-by-hammer" method to find cracks in the dust-covered lining of tunnels has been considered the only reliable method. Recently, a method using the infrared rays and an image analysis method using digital video camera were being developed; these methods can reduce the labor and the time considerably.

Many civil infrastructures are spatially distributed and the area and points to be inspected/monitored

is huge. Certainly, sensors that measure spatial information rather than a point are to be developed. Accuracy of the sensors is important, but often simplicity, durability and robustness are more important than accuracy since they are exposed to severe and hostile environments.

To detect damage from the sensor signal is also another important subject. The signals from the sensors in civil infrastructures are in many cases contaminated by ambient noise due to traffic and other environmental effects. To efficiently remove noise from ambient signals and to obtain useful information requires not only data processing techniques, but also knowledge of traditional disciplines of civil engineering such as mechanics, dynamics, soil mechanics, material technology and so forth.

Structural Health Monitoring (SHM) for civil infrastructures is an extremely important research area to keep our advanced society functional and requires a balanced combination of new sensor/computer technology and civil engineering technology. In this sense, SHM attracts young promising engineers and researchers.

The Bridge and Structure Laboratory at the University of Tokyo has made recent attempts to contribute to the development and establishment of SHM. Some research activities at the Laboratory related to SHM are given hereafter.

5. LASER DOPPLER VIBROMETRY USING AMBIENT VIBRATION

Development of reliable health monitoring and inspection technology is essential to maintain existing civil infrastructures. Monitoring of civil structures has several difficulties in addition to those that arises in structural health monitoring of other structures due to (1) their scale; and (2) ambient environmental effects [1]. The scale makes measurement of the entire structure extremely difficult and costly, which inherently requires dangerous labor work at considerable height, and reduces quality and density of measurement. Ambient environmental effects induced by various causes such as traffic, wind, temperatures, etc., are difficult to estimate or measure reliably, which makes identification of structural parameters extremely difficult. Because of these difficulties, current inspection works of civil structures tends to be labor extensive, and rely on subjective judgment of experienced specialists. Figure 2 shows the example of typical inspection procedure of tunnel linings using hammer echo. The sound excited by hammer impact is subjectively judged by skilled experts to evaluate damage or defects in concrete.

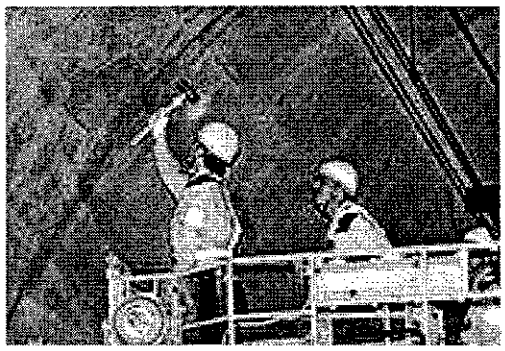

Figure 2. Hammer echo inspection at a highway tunnel.

In order to rationalize and automate the subjective judgment method and eliminate the dangerous inspection works in tunnels or bridges, applicability of remote measurement by Laser Doppler Vibrometer (LDV) has been studied extensively at the University of Tokyo.

The Laser Doppler Vibrometer basically uses the Doppler principle to measure velocity at a point where its coherent laser beam is directed to. The reflected laser light is compared with the incident light in an interferometer to give the Doppler-shifted wavelength. This shifted wavelength provides information of surface velocity in the direction of the incident laser beam. For the LDV used in this experiment, two

deflecting mirrors are provided to enable the light beam to be directed at any desired point. Providing non-contact measurement, the LDV is capable to detect a velocity of magnitude of 0.5μm/s at a distance of maximum 30m. Detailed characteristics of the LDV can be found in [2].

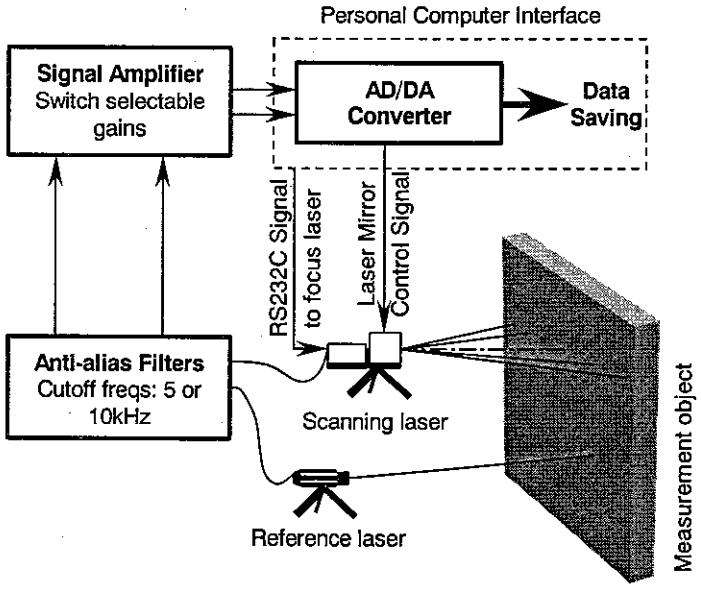

Figure 3. Data Acquisition System and the LDV

There are two laser sources to be used to measure the structural vibration response in this research. One is to measure a fixed point on the measured surface to provide global information, *i.e.,* to synchronize other measurements; the other is directed by the two deflecting mirrors to measure the response spatially. The first one will be called the *reference laser* and the second the *scanning laser* hereafter. A mesh of measured points should be defined first and then, under control of a computer, vibration responses of these pre-defined points will be measured point by point.

The data acquisition system is illustrated in Figure 3, in which a personal computer acts as a central processing unit, receiving measured response signals and sending control signals to rotate the deflecting mirrors and to focus the scanning laser at different distances while the laser beam is scanning over the object surface. The measurement process is automatic, and requires the least command from an operator.

Most modal of modal identification methods for ambient vibration use a spectral analysis technique. In this technique, a structural motion is measured by a series of sensors. The structure's natural frequencies are estimated from peaks in the power-spectral density function of the measurement records, while the modal damping ratios are estimated using the half-power bandwidth method. The cross-power spectra between a designated reference measurement and other measurements will contain information of the structure's mode shapes. Although the drawbacks of this technique have been detailed in [3] and [4], it is still widely used in ambient vibration because of its simplicity. Recent development in ambient vibration is applications of Eigensystem Realization Algorithm (ERA) [5] [6], Auto Regressive Moving Average Vector (ARMAV) [7], Autoregressive Modeling (AR) [8], covariance matrix [9], and Eigenspace Algorithm [10]. These techniques are either applied for simultaneous data, (*i.e,*. data acquired at all points at the same time) or not suitable for a personal computer due to its intensive computation. For modal parameter identification using the LDV, there are limited numbers of response measurements that can be recorded at the same time because of the availability of laser sources. Among the aforementioned techniques, the ERA is the most general multi-input-multi-output (MIMO) technique that can be developed and applied to the LDV measurement if a data synchronization technique can be formulated.

Introduced in this paper is the modal analysis identification technique using the ERA that is developed for the LDV in ambient vibration measurement. A mathematical model is presented in the

first part and an experiment of a steel plate was carried out in a laboratory environment to verify the mathematical model. The steel plate was tested under ambient excitation that might result from ground waves caused by traffic on a nearby street. Identification of the plate's modal parameters is successful by the ERA. A mass was then attached to the plate to verify a change in its modal parameters as a result of the change in its mass property. This finding will provide background for a structural health monitoring program using the LDV to measure ambient vibration and to use identified modal parameters to monitor the performance of a structure.

6. A Brief Review on ERA

A viscously damped system with N DOF can be modeled in the following equation:

$$[M]\{\ddot{x}(t)\}+[C]\{\dot{x}(t)\}+[K]\{x(t)\}=[F]\{u(t)\} \tag{1}$$

where $[M]$, $[C]$, $[K]$ are the $N\times N$ mass matrix, damping matrix, and stiffness matrix, respectively; $\{\ddot{x}(t)\}$, $\{\dot{x}(t)\}$, $\{x(t)\}$ are the $N\times 1$ acceleration vector, velocity vector, and displacement vector, respectively; $[F]$ is a matrix of input coefficients and $\{u(t)\}$ is the input vector at q locations.

The above system is equivalent to the continuous state-space model:

$$\begin{aligned}\{\dot{y}(t)\}&=[A']\{y(t)\}+[B']\{u(t)\}\\ \{x(t)\}&=[R]\{y(t)\}\end{aligned} \tag{2}$$

where $\{y(t)\}=\begin{Bmatrix}\{x(t)\}\\ \{\dot{x}(t)\}\end{Bmatrix}$, $[A']=\begin{bmatrix}[0] & [I]\\ -[M]^{-1}[K] & -[M]^{-1}[C]\end{bmatrix}$ and $[B']=\begin{bmatrix}[0]\\ [M]^{-1}[F]\end{bmatrix}$

By considering $\{x(t)\}$ as the impulse responses at p measured locations and arranging them into the generalized Hankel matrix, Juang and Pappa [11] have shown that the state transition matrix $[A]=e^{[A']\Delta t}$ can be "realized". By eigenvalue decomposition of matrix $[A]$, modal parameters of the system can be extracted. Full details of this method can be found in [11] or [12].

The above procedure is called the Eigensystem Realization Algorithm (ERA). The algorithm requires the synchronous impulse response measurements at p locations. What follows are a technique to synthesize the impulse responses from ambient vibration measurement and to synchronize those responses from asynchronous measurement using the LDVs.

7. Impulse Response Synthesis from Ambient Vibration Measurement

Farrar and James [3] has pointed out that if the unknown excitation is a white-noise random process, the cross-correlation function between two response measurements will have the same form as the impulse response of the structure.

Detailed formulation of these two parameters can be found in [3]. If all p locations are measured at the same time, the factor that represents the phase and magnitude difference can be cancelled out in the ERA. However, measurement by the LDV does not possess this characteristic. It, therefore, requires a synchronization process before inputting these free responses to the ERA.

Furthermore, to minimize the effect of noise in the laser measurements, many finite time history measurements will be performed (at every point) and then the cross-correlation function described above is averaged out in the frequency domain (cross-spectrum). The averaged cross-correlation function will then be recovered by the Inverse Fourier Transform of its corresponding averaged spectrum. As a matter of fact, the finite time history does not guarantee the energy flowing into the system to be the same during each period of measurement.

Denoting $x_{R0}(t_0)$ the base reference laser measurement, $x_{S0}(t_0)$ the simultaneous scanning laser measurement at a specific scanning point. Again denoting $x_{Ri}(t_j)$ the reference laser measurement while the scanning laser at point i starting time t_j, $x_{Si}(t_j)$ the scanning laser at point i starting time t_j.

Let a hypothetical frequency response function $H_{x_{R0}x_{Rij}}(f)$ be defined, as in Bendat and Piersol [1], by:

$$H_{x_{R0}x_{Rij}}(f) = \frac{F[x_{Ri}(t_j)]}{F[x_{R0}(t_0)]} \tag{3}$$

where $F[\bullet]$ denotes finite Fourier Transform of $(\bullet)$

If the excitation is a stationary and ergodic process, this relation will also be applied for the scanning laser measurement, *i.e.,*

$$H_{x_{S0}x_{Sij}}(f) = H_{x_{R0}x_{Rij}}(f) = \frac{F[x_{Si}(t_j)]}{F[x_{S0}(t_0)]} \tag{4}$$

For simplicity, the parameter t is dropped. Combining equations (4) and (5) and multiplying it by the complex conjugate of equation (4), the following relationship can be obtained:

$$\frac{F^*[x_{Rij}]\,F[x_{Rij}]}{F^*[x_{R0}]\,F[x_{R0}]} = \frac{F^*[x_{Rij}]\,F[x_{Sij}]}{F^*[x_{R0}]\,F[x_{S0}]} \tag{5}$$

Arranging the above equation leads to:

$$F^*[x_{Rij}]F[x_{Sij}] = \frac{F^*[x_{Rij}]}{F^*[x_{R0}]}\frac{F[x_{Rij}]}{F[x_{R0}]}F^*[x_{R0}]F[x_{S0}] \tag{6}$$

The *cross-spectrum* and *auto-spectrum* between two records are defined by Bendat and Piersol [1] as:

$$\begin{aligned} G_{xy}(f) &= F^*(x)F(y) \\ P_x(f) &= F^*(x)F(x) \end{aligned} \tag{7}$$

Therefore, equation (6) can simply be written as:

$$G_{x_{Rij}x_{Sij}} = \frac{P_{x_{Rij}}}{P_{x_{R0}}}G_{x_{R0}x_{S0}} \tag{8}$$

The meaning of equation (8) is that the cross-spectrum of the subsequent measurements will differ from the base measurement by a factor of $\frac{P_{x_{Rij}}}{P_{x_{R0}}}$. Therefore, for a noise reduction scheme by averaging in the frequency domain, any cross-spectrum that is not the base spectrum should be divided by this factor to convert it to the base spectrum. It can be seen that this factor is calculated by the auto-spectrum only; it hence does not eliminate the effect of correlated noise at the reference laser measurement. It is, therefore, necessary to set up the reference laser measurement that will have the largest signal-to-noise ratio. More details of the technique can be found in [13].

By inverse Fourier Transform of the averaged cross-spectrum, the averaged cross-correlation function can be estimated and subsequently entered to the ERA. Details of this modal analysis identification process can be summarized in Figure 4. Since the averaging process is carried out in the frequency domain, windowing should be applied to minimize the effect of leakage. The Hanning window is chosen for this type of signal in the following examples.

8. Application Examples of LDV

The proposed measurement method has been applied to damage detection in concrete specimens, steel bolted joints, and measurement of vibration of existing bridge slabs under service traffic condition.

In damage detection of concrete structures, as shown in Figure 2, the hammer-echo inspection method is widely used. The principle of this method is to excite vibration on the surface of the structure and, then, to judge the soundness by listening to the sound excited by the surface vibration. Hence, precise and dense measurement of surface vibration by LDV has the potential to replace this work.

Figure 5 shows the measurement results by LDV on damaged and undamaged portions of concrete specimens by hammering. Damage is modeled by a void behind the concrete surface, which is shown in Figure 6. Vibration with higher frequencies is observed to be prominent at the damaged part.

Vibration modes of this concrete specimen are also identified using the proposed method. To simulate ambient vibration sources in actual measurement such as traffic noise, the specimen is excited by arbitrary

Figure 4. Determination of modal parameters from ambient vibration measurement

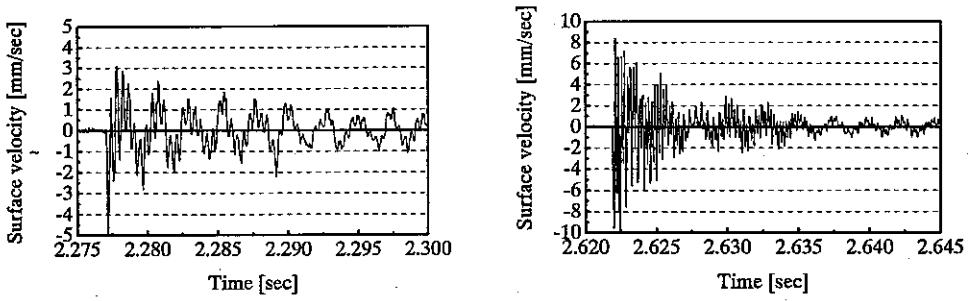

(a) Undamaged part. (b) Damaged part.

Figure 5. Comparison of LDV measurement at damaged/undamaged parts.

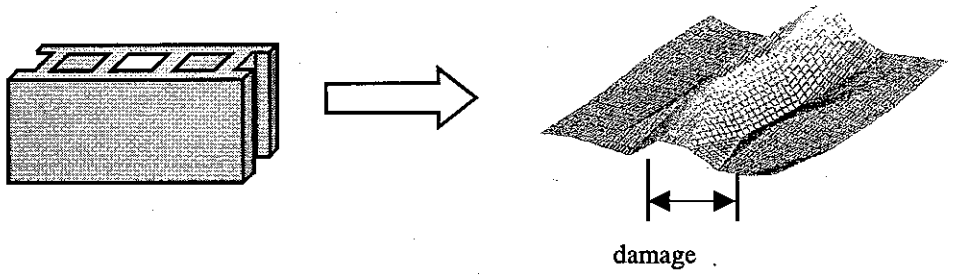

Figure 6. Comparison of LDV measurement at damaged/undamaged parts.

sound generated by sound speaker. The right half Figure of Figure 6 shows the identified mode shape at the high frequency component observed in Figure 5. Clearly, the vibration contains modal amplitude locally magnified at the place of damage. Therefore, damage in this concrete specimen can be identified by observing associated vibration modes [14].

Figure 7 shows a model for steel joint loaded by a weight. Measurement and control of torque in bolts is critical for the safety of the system especially when the joint is designed as friction connection. The vibration mode whose node is at the location of connection plate is of particular interest, because induced strain by that mode is the highest. Figure 8 shows the identified mode shape of that mode. No significant difference is observed for the magnitude of the mode shape by loosening the bolts, while phase in mode shape, or equivalently, imaginary part of the mode shape shows significant change. Figure 9 shows this relationship. The horizontal axis expresses the amount of the torque loosened and the vertical axis shows the summation of phase lag at the connection plate. Good correlation is observed. This phenomenon is most likely due to the infinitesimal sliding induced by vibration [15].

The proposed system has been applied to field measurement of a bridge. Figure 10 shows the objective structure that is the slab of an elevated highway bridge. A panel of the slab is measured by the proposed system. Figure 11 shows the identified mode shape for the slab panel. Identified natural frequencies are found to be in agreement with the theoretical prediction, which verifies the validity of the proposed method [16].

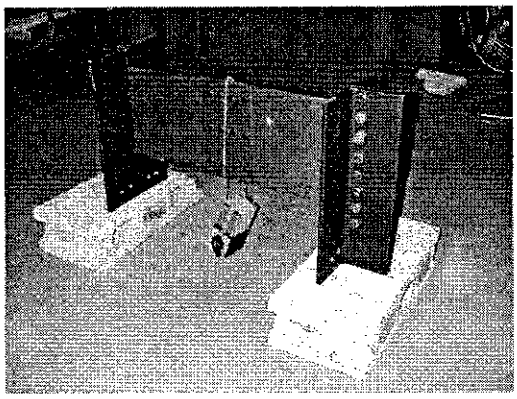

Figure 7. Steel joint model.

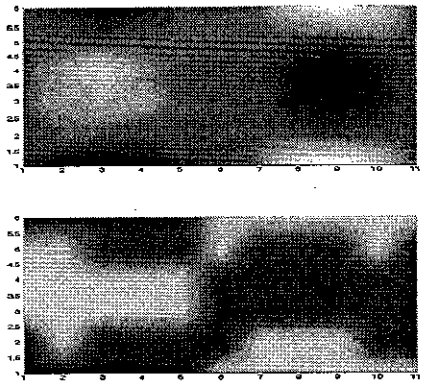

Figure 8. Identified mode shape (magnitude and phase).

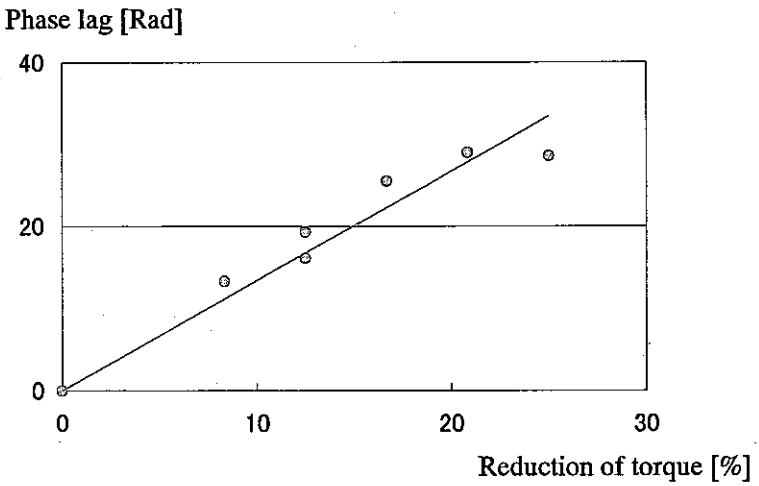

Figure 9. Phase lag in mode and loosened torque.

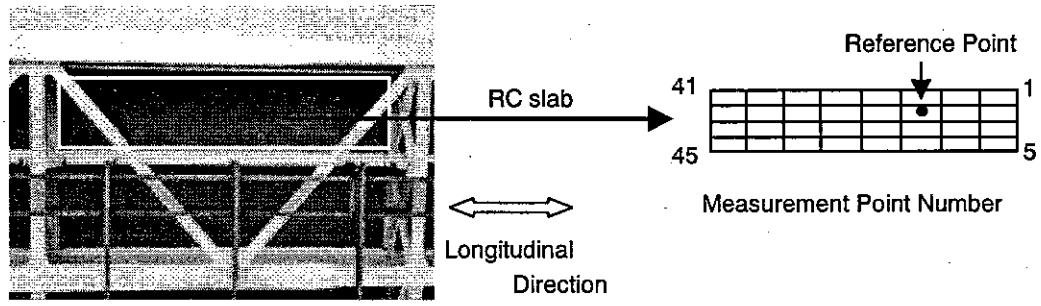

Figure 10. Objective concrete slab and measurement points

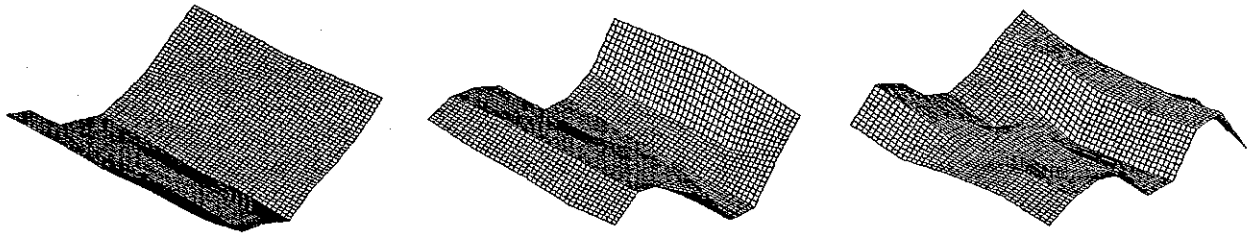

(a) 1st mode (43.2Hz) (b) 2nd mode (97.3Hz) (c) 3rd mode (187Hz)

Figure 11. Identified mode shapes for the slab panel

9. Impact Force Identification by LDV

Accurate identification of forces in a structure subject to operational excitations is an important issue for design, control and health monitoring of the system.

Assuming modal expansion, orthogonality and proportional damping, the equation of motion of a system can be decomposed into a series of modal equations in frequency domain using matrix notation as

$$[A]\{X(\omega)\} = \{B(\omega)\} \tag{9}$$

$$[A] = \begin{bmatrix} j\omega[\hat{\Phi}] & \{0\} \\ [K] - \omega^2 I + \omega[C] & -[\Phi]^T\{\delta\} \end{bmatrix}_{(2+p)\times(p+1)} \tag{10}$$

$$\{X(\omega)\} = \left\{\{Q(\omega)\}^T \quad F(\omega)\right\}^T_{(p+1)\times 1} \tag{11}$$

$$\{B(\omega)\} = \left\{\{\dot{U}(\omega)\}^T \quad \{0\}\right\}^T_{(p+2)\times 1} \tag{12}$$

$$K = diag\left[\omega_1^2 \quad \omega_2^2 \quad \ldots \quad \omega_p^2\right] \tag{13}$$

$$C = diag\left[2\xi_1\omega_1 \quad 2\xi_2\omega_2 \quad \ldots \quad 2\xi_p\omega_p\right] \tag{14}$$

where Q, U and F denote Fourier transforms of modal amplitude, global displacement and impact force magnitude respectively. j denotes the imaginary unit and the superscript T refers to matrix transpose. ξ_i, and ω_i represent modal damping ratio and modal frequency of i-th mode, respectively. p denotes the number of lower modes used in modal expansion. $\hat{\Phi}$ is the mode shape matrix at the measuring points. δ denotes a location vector and can be defined as

$$\{\delta\} = \{0 \quad 0 \quad \ldots \quad 1 \quad \ldots \quad 0\}^T \tag{15}$$

That is, all the positions on the plate are set to be zero except the real location of the impact. It is important to note that the problem set as in equation (10) is over-determined and can be solved in the least-squares sense employing the pseudo-inverse technique, *i.e.*,

$$\{X(\omega)\} = [A]^+\{B(\omega)\} \tag{16}$$

$$[A]^+ \equiv \left([A]^T[A]\right)^{-1}[A]^T \tag{17}$$

This identification algorithm is implemented with the LDV measurement system and applied to the problem of impact force identification on a clamped-free steel plate. First, modal parameters are obtained at ambient sound excitation condition. Mode shapes of the identified modes are given in Figure 12. These experimentally obtained modal parameters are directly applied to the above algorithm to identify impact force. The comparisons between experimental and identified results are shown in Figures 13 and 14 [17]. Both time history and location of impact are successfully identified with high accuracy.

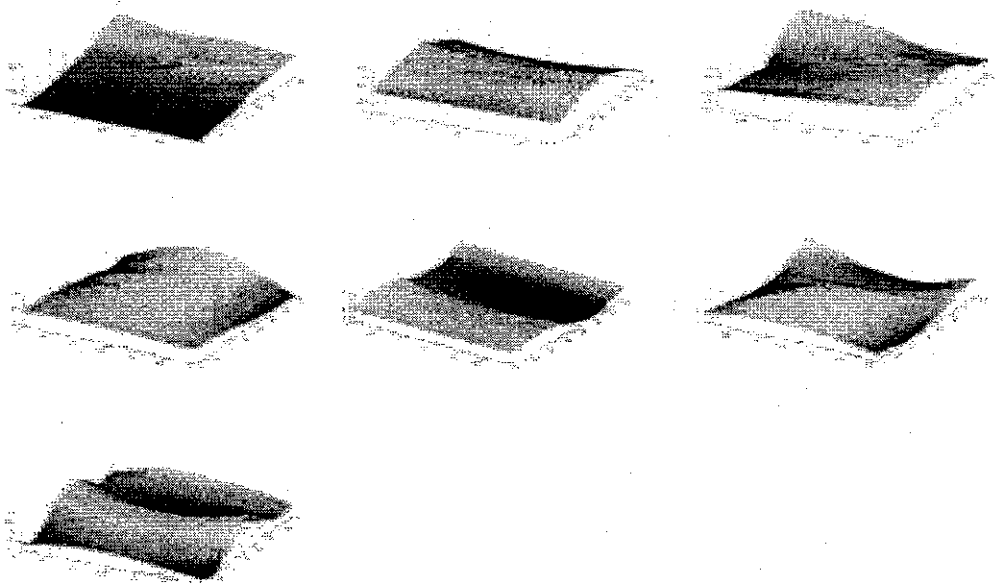

Figure 12. Identified mode shapes for the plate

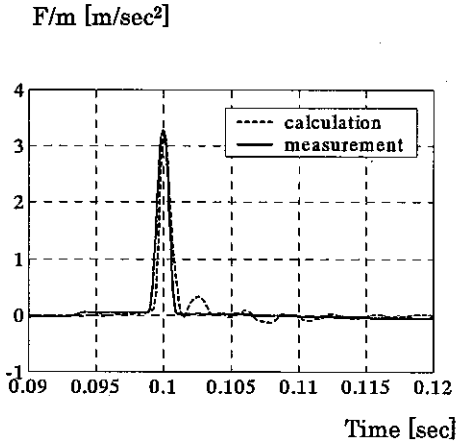

Figure 13. Identified force time history

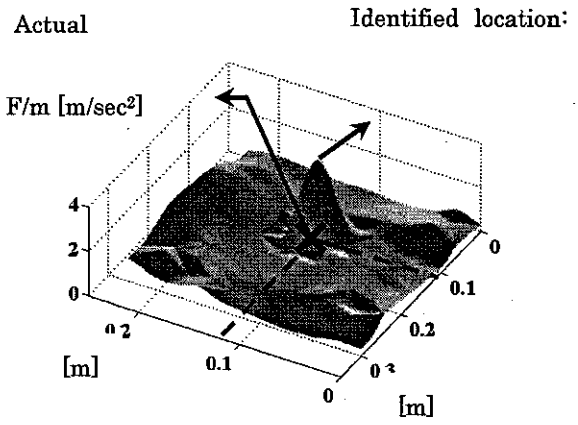

Figure 14. Identified force distribution

10. AMBIENT VIBRATION BASED MONITORING OF A LONG SPAN SUSPENSIO BRIDGE

The ambient vibration based monitoring technique developed for LDV has also been applied to monitoring the long-span suspension bridge shown in Figure 15. The bridge has been monitored by a densely-distributed ambient vibration measurement system with 19 measurement points. Details of the measurement installations can be found in [18].

In this case, because all 19 measurements are simultaneous, the synchronization method developed for LDV is not necessary, and random decrement method is employed to obtain impulse responses. By application of the ERA method, modal parameters up to 19 vibration modes are successfully identified. Especially, modal natural frequencies are found to be in good agreement with

the results of the forced vibration test and finite element prediction.

Based these modal properties that are found to be amplitude dependent, aerodynamic stiffness and damping for various amplitude levels are obtained as can be seen Figure 16 and 17 [19]. The difference of mass normalized stiffness and damping from the values at amplitude of 0.55cm/sec^2 are presented. Because amplitude and wind velocity are in good correlation, aerodynamic damping predicted by the wind tunnel results are also presented. It can be seen that it is feasible to track changes in stiffness and damping using identification through ambient vibration measurements.

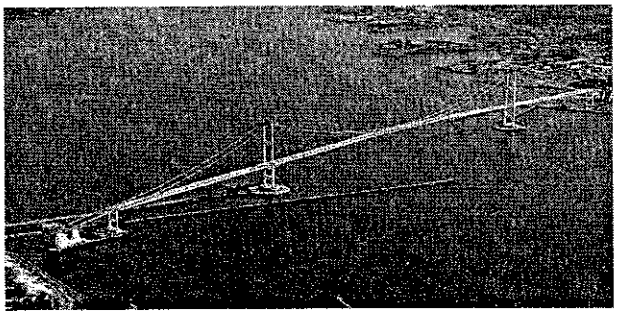

Figure 15. Hakucho Bridge

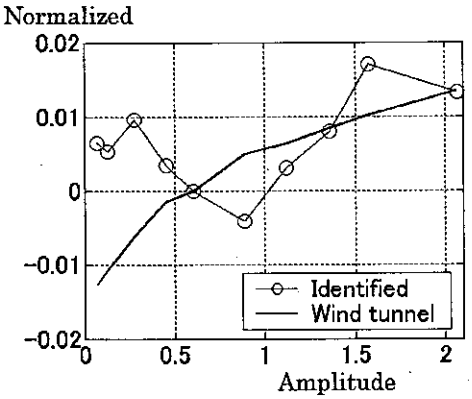

Figure 16. Identified aerodynamic stiffness

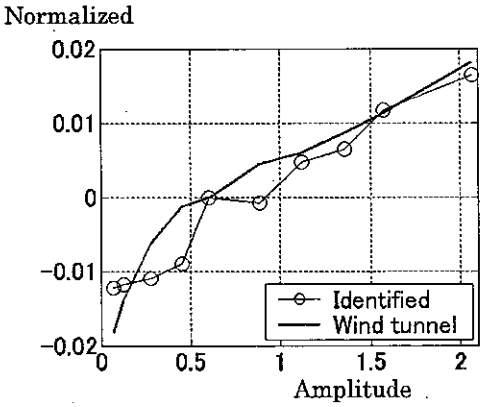

Figure 17. Identified aerodynamic damping

11. REMOTE INTELLIGENT MONITORING SYSTEM(RIMS)

In recent years, MEMS(micro electro-mechanical systems), micro controllers and network technology have made a remarkable development. Indeed, micro-controllers which have high data processing capability as well as control capability are readily available nowadays. Combining such advanced MEMS sensors and micro-controllers, we can make inexpensive, compact and intelligent sensing systems without using expensive data logger and A/D transform interface. Monitoring system consists of sensor, communication and processing parts. Installing huge number of sensors to infrastructures can be made possible by MEMS, but this means that enormous amount data has to be handled. This data explosion can be avoided by making sensors intelligent and the data communication wireless. This remote intelligent monitoring system is expected to drastically reduce the monitoring cost. An inexpensive, compact and wireless intelligent sensing system, called *Remote Intelligent Monitoring System*(RIMS) using these technologies is developed.

Concept and Design of RIMS

The concept of development of the RIMS is as follows(Fig. 18);

1) develop an intelligent, compact and inexpensive sensor as a small package, so that data processing can be made, and
2) install a function to the sensor which enables to send the processed information to the PCs or PDAs in a wireless manner, so that the data collection is easy.

In this study, measuring acceleration of bridges and their attachments such as traffic poles and light poles is chosen as an example problem.

RIMS consists of accelerometers, micro-controller and communication part(Fig. 19). Each component was carefully selected to meet the requirements. A MEMS accelerometer that the voltage is output for acceleration magnitude was chosen. As a controller, small processor such as PIC, control processor and standard micro-processor were compared and control processor, namely H8 processor(Renesas co. Ltd. Hitachi-Mitsubishi)was employed. For communication, ethernet was adopted because of its versatile capability, i.e., wide bandwidth and stability.

Hardware(Fig. 20) and Software

3-axis Piezo-resistance-type accelerometer MA-3(Microstone ltd.) with H8/4069F processor is realized for the acceleration measurement. H8 processor is relatively inexpensive and high-speed computing(20 MHz). A/D transformer in H8 is used to make the system simple. A 2MB buffer memory is connected through external D-RAM interface. Using this, measured data is stored temporarily and its processing can be made possible in the sensor. By doing this, measured data can be checked and only small-sized processed information can be sent.

Ethernet is employed and large scalability is achieved and wireless sending of processed data can be realized. As the ethernet controller, RTL-8019AS (Realtek Corp.) was used. This controller is compatible to NE2000 and has been widely used.

The software in RIMS was developed as a firmware and installed in the ROM inside the H8 processor. RIMS performs as a web server and can be operated independently from clients' side. The C language was used. TCP/IP and http which are the standard communication tools in the internet were used in the communication part. Using these, high operational performance by PC/PDA and cost reduction for the development of GUI(graphical user interface) were achieved.

In this study, accelerometer measurement in light poles is assigned to the task of RIMS. Light poles in the bridge girder are subjected to wind and excitation due to the traffic-induced vibration of the girder and their fatigue failure. Indeed, one light pole in the urban elevated expressway was failed due to fatigue and the frequent inspection of a huge number of the light poles and traffic signal poles is becoming necessary.

In the RIMS, the time history record measured by the accelerometer is continuously transformed from analog data to digital data and is stored in the ring buffer on the RAM. The level crossings of the measured acceleration time history are counted and transformed as histogram of the crossing of levels; the histogram data is only sent to PC/PDA.

The software of RIMS consists of 3 parts, namely, acceleration measurement part, HTTP manager, and 'servelet functions.' Acceleration measurement part converts the signal from accelerometer to digital data continuously, and written into the ring buffer, and the indices such as the histogram for a certain interval period. HTTP manager is a web server which manages TCP/IP state changes, and accepts minimum command set of http(GET method only). Next, it creates http response by calling suitable 'servelet functions'. The 'servelet functions' are the parts that make HTML documents show via http. Documents created here are for initialization, for parameter setting, display indexes, and display time history. Due to the separation of HTTP manager from 'servelets,' adding new functions to the RIMS is very easy.

The prototype RIMS consists of MEMS, micro-controller and ethernet. The MEMS accelerometer adopted is about 200$US and the micro-controller is about 20$US, while the Ethernet is about 10$US. D-RAM(2MB) in the controller is 4 $US. The circuit board is 120$US. The overall cost is around 350$US including the sensor box. The cost can be more reduced, especially if less expensive MEMS acceleration sensor can be used.

Prototype and its field testing

A prototype of the RIMS was made(Fig. 21) and its accuracy in the acceleration measurement was verified in the shaking table test. A field testing was done at the light pole in the girder of the Tokyo Rainbow Bridge(Fig. 22). In this testing, installation to existing structure and data acquisition were verified. The installation took less than 1 hour by 2 persons, and this is much less than that of other existing monitoring systems. Collecting the processed data from the RIMS was succeeded by using wireless LAN adaptor inside the RIMS package and wireless LAN card inserted to notebook PC. The communication was stable within 50m distance from RIMS to PC/PDA.

Fig.23 shows a time history of acceleration recorded in the RIMS and Fig.24 shows histograms of acceleration level crossing) for 18 hours. One can understand the histograms change depending on the time, High level crossing became lower in midnight, suggesting that the vibration of this light pole is mainly induced by the traffic.

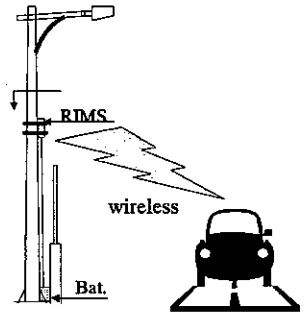

Fig. 18 Concept of RIMS

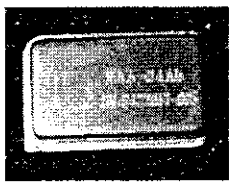

MEMS accelerometer
A/D conversion

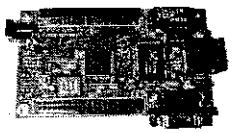

Micro-controller

Pc or PDA

Fig. 19 Components in RIMS

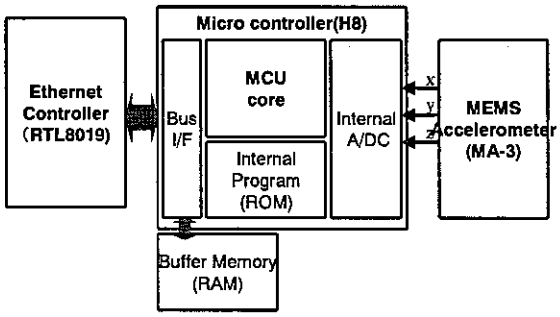

Fig. 20 System in RIMS

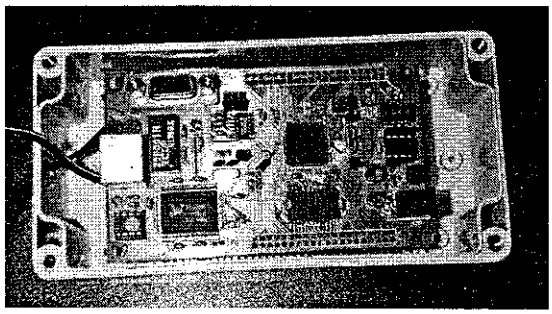

Fig. 21 RIMS package box(30cm x 6cm x 8cm in size)

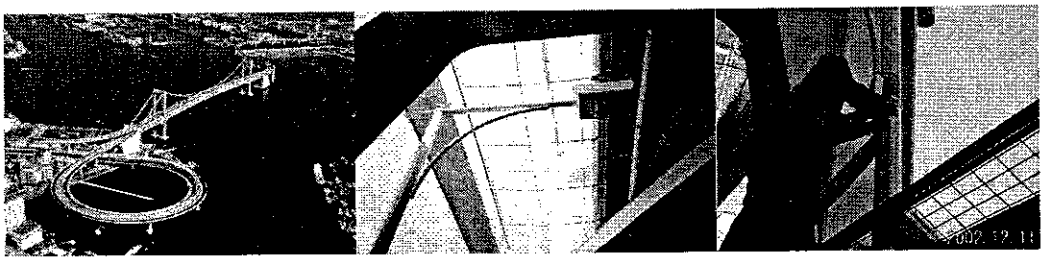

Fig. 22 Rainbow bridge, light pole and installation of RIMS to light pole

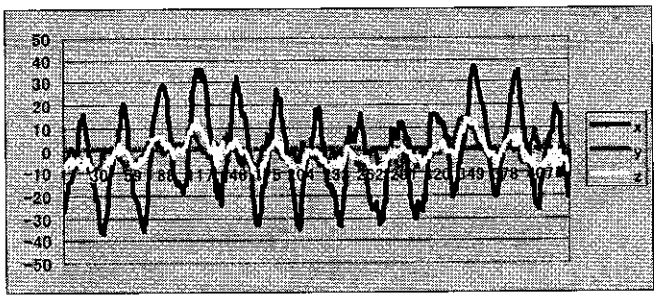

Fig. 23 Sample time history of acceleration of light pole, measured by RIMS

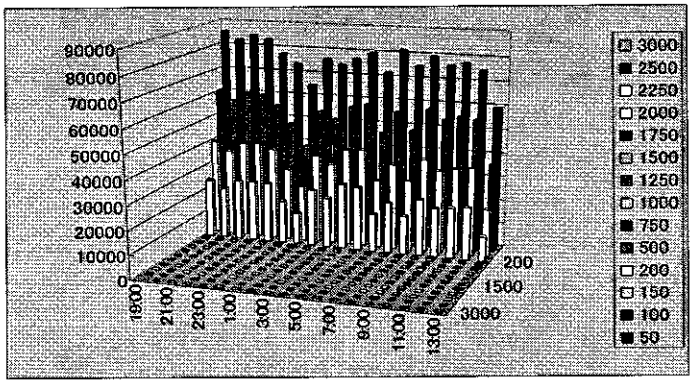

Fig. 24 Histograms of level crossing numbers of acceleration in light pole(measured by RIMS)

12. VEHICLE INTELLIGENT MONITORING SYSTEM

Monitoring the condition of road surface is an extremely important issue in highway network management because of the enormous volume of road stock and because of its continuous degradation under the passage of a large number of heavy vehicles. In the case of elevated highway, monitoring of viaducts, bridges and expansion joints are to be of concern in monitoring. Regarding the road surface, profiler system has been developed to measure the various components of road conditions such as smoothness of the surface and indeed it has been used in the road maintenance. However, measurement of the road surface by the profiler requires significant time and cost.

In the highway system, inspection vehicles are widely used to visually monitor the highway condition in general at least once per day. Making the inspection vehicle more intelligent by installing some instruments such as accelerometer, GPS, microphone and PC may be one possibility to achieve easy and inexpensive monitoring and a prototype is developed, namely *Vehicle Intelligent Monitoring System* (VIMS).

Acceleration of the vehicle may be related to the road surface condition and sound by microphones is placed in order to capture the expansion joint condition. GPS is used to relate the time-history of these measurements to the location in the road system. One accelerometer is placed at the front floor and microphones are placed near the rear tire (Fig. 25).

The vehicle was driven in a highway route owned by the Tokyo Metropolitan Expressway for two times. The speed was maintained at 40km/h as much as possible. Note that that route of the highway is all of viaduct type, i.e., elevated highway. It is confirmed that GPS can very accurately identify the location from the time history measurement; amazingly the error is much less than 0.1%. Fig. 26 shows an example of acceleration time history. Large accelerations are when the vehicle crossed the expansion joints. RMS of the acceleration during the road portion excluding those from the expansion are compared with the road surface index measured by a road profiler as shown in Fig. 27. One can observe high repeatability of RMS acceleration by the VIMS measurement and high correlation between the road surface index(by a profiler) and the RMS acceleration by VIMS. Actually the correlation is 0.8.

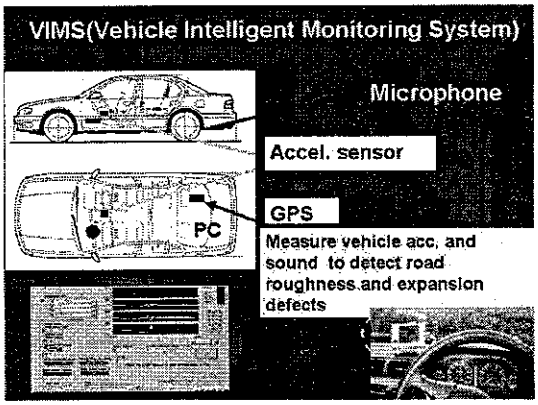

Fig 25. VIMS

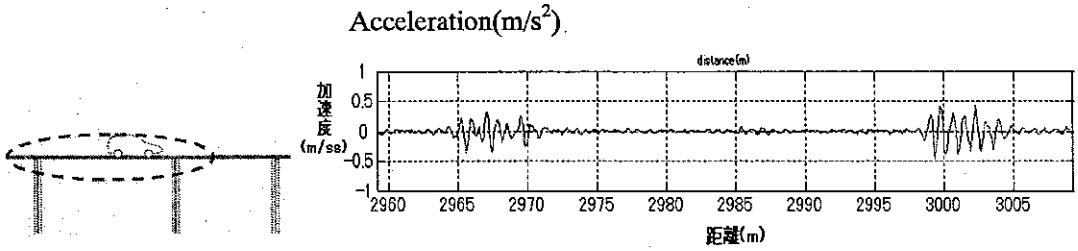

Fig 26. An example of acceleration time-history

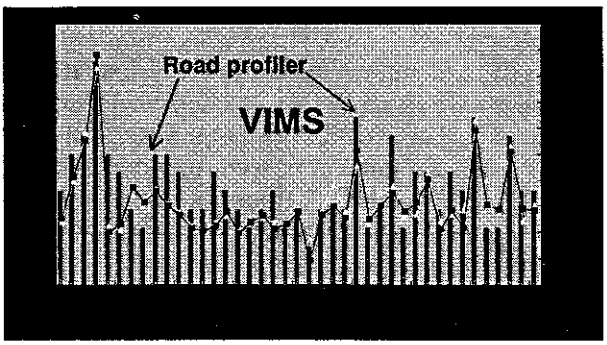

Fig. 27 RMS acc by VIMS and comparison to the index by profiler

SUMMARY

Research and development of health monitoring systems at the Bridge and Structure Laboratory of the University of Tokyo is presented.

Ambient vibration based approaches for LDV and long-span suspension bridges show possible wide applications in this field. In both cases, although the excitation is unknown, densely distributed and accurate measurement is shown to provide valuable information on the status of structures. Especially, a LDV based approach can provide information on damage and loading to the structure with practically applicable system conFiguration.

Toward easy and inexpensive monitoring, development of a compact remote intelligent sensing system, RIMS and simple monitoring system of road surface condition, VIMS is also described.

REFERENCES

1. Abé, M. 1998. "Structural monitoring using vibration measurement – current practice and future -," *Artificial Intelligence in Structural Engineering*, Ian Smith, ed, Lecture Notes in Artificial Intelligence 1454, Springer, pp.1-18.
2. Kaito K, Abe M., Fujono Y., and Yoda H. 2000. "Detection of Structural Damage by Ambient Vibration Measurement using Laser Doppler Vibrometer", *Non-Destructive Testing in Civil Engineering 2000*, Uomoto (ed.), Tokyo.
3. Farrar C.R., and James III, G.H. 1997. "System Identification From Ambient Vibration Measurement on A Bridge", *Journal of Sound and Vibration*, Vol.205, No.1, pp. 1-18.
4. Bendat J.S., and Piersol A.G. 1993. *Engineering Applications of Correlation and Spectral Analysis*, 2nd ed., John Wiley & Sons, Inc.
5. Dyke S.J., and Johnson E.A. 2000. "Monitoring of a Benchmark Structure for Damage Identification", *Proceedings of the Engineering Mechanical Specialty Conference*, Austin, Texas.
6. Farrar C.R., Cornwell P.J., Doebling S.W., and Prime M.B. 2000. *Structural Health Monitoring Studies of the Alamosa Canyon and I-40 Bridges*, Los Alamos National Laboratory.
7. Garibaldi L., Giorcelli E., and Piombo B.A.D. 1998. "ARMAV Techniques for Traffic Excited Bridges", *Journal of Vibration and Acoustics*, Vol.120, pp713-718.
8. Kadakal U., and Yuzugullu O. 1996. "A comparative study on the identification methods for the autoregressive modeling from the ambient vibration records", *Soil Dynamics and Earthquake Engineering*, Vol.15, pp. 45-49;
9. Lardies J., 1997. "Modal Parameter Identification From Output-Only Measurements", *Mechanics Research Communications*, Vol.24, No.5, pp. 521-528;
10. Quek S.T, Wang W, and Koh C.G. 1999. "System Identification of Linear MDOF Structures Under Ambient Excitation", *Earthquake Engineering and Structural Dynamics*, Vol.28, pp61-77;
11. Juang J.N., and Pappa R.S. 1985. "An Eigensystem Realization Algorithm For Modal Parameter Identification And Model Reduction", *Journal of Guidance, Control, and Dynamics*, Vol. 8, No. 5., pp. 620-627.
12. Maia N.M.M, and Silva J.M.M (ed) 1997. *Theoretical and Experimental Modal Analysis*, Research Studies Press Ltd.
13. Vu Manh H. 2001. *Application of Laser Doppler Vibrometer in Structural Health Monitoring*, Master Thesis, Department of Civil Engineering, The University of Tokyo.
14. Abe, M., Fujino, Y. and Kaito K., 2001. "Damage detection of civil concrete structures by laser Doppler vibrometry", *The 19th International Modal Analysis Conference*, Kissimmee, Florida.
15. Murata, H. 2001. *Structural damage detection by Laser Doppler Vibrometer*, Bachelor Thesis, Department of Civil Engineering, The University of Tokyo, (in Japanese)
16. Kaito, K., Abe, M., and Fujino, Y. 2000. "Identification of Vibration Mode Shapes for a Bridge Deck under Ambient Vibration", *International Workshop on The Present and Future in Health Monitoring*, Bauhaus-University Weimar, Germany.
17. Chajworawitkul, S., Abe, M. and Fujino, Y. 2001. "Identification of impact force using Laser Doppler Vibrometer", *The 56th Annual Meeting of the Japan Society of Civil Engineers*.

18. Abe, M., Fujino, Y., Kajimura, T., Yanagihara, M. and Sato, M. 1999. "Monitoring of a long span suspension bridge by ambient vibration measurement", *The Second International Conference on Structural Health Monitoring*, Stanford University, California, pp.400-407.
19. Abe, M., Fujino, Y. and Nagayama, T. 2001. "Identification of non-porportionally damped system using ambient vibration measurement and its application to a suspension bridge", *Proceedings of the Japan Society of Civil Engineers*, 2002.
20 Aoki,S., Fujino, Y. and Abe,M,2003." Intelligent bridge maintenance system using MEMS and network technology",*Proc. SPIE conference*, 2003 San Diego, USA
21 Kono, H. Abe, M and Fujino, Y. 2003 "Development of Vehicle Intelligent Monitoring System(VIMS)", *Proc. of Annual Tech..Meeting of JSCE*, 2002

(Received July 31, 2003)

Structural health monitoring of innovative bridge decks

*Dr. Aftab A. Mufti, Professor, Department of Civil Engineering, University of Manitoba, Winnipeg, Manitoba, Canada and President, ISIS Canada

For more than a century, important civil engineering structures such as dams, bridges, high-rise buildings, and marine platforms have contained iron or steel, sometimes as the dominant structural material and sometimes as reinforcement for concrete or wood[1]. The useful lives of such structures have often been severely limited by the corrosion of this ferrous component. The need to delay the onset of corrosion has resulted in structures that are heavier than they otherwise need to be. Much thought has been given in recent years to constructing structures that are lighter, stronger and non-corrosive. For these innovative structures to be accepted by the engineering community, monitoring is mandatory. This paper highlights some of the innovative structures developed and monitored by ISIS Canada.

Key Words: bridge decks, fibre reinforced polymers, monitoring, steel-free

1. Introduction

For infrastructure owners, one of the greatest values of ISIS Canada research lies in its practical application. New opportunities for applying ISIS Canada technology are increasing as evidenced by the growing number of field demonstration projects underway. The projects range from a new concrete steel-free bridge deck for the Salmon River Bridge in Nova Scotia, to the strengthening of a nuclear containment structure in Quebec, to the testing of timber piles for use in an Inuvik housing project in the cold, northern region of Canada.

Of thirty-six projects that are being field assessed, those that deal with the Steel Free/FRP Reinforced Bridge decks are described in the following paper.

2. Salmon River Highway Bridge, Nova Scotia[2]

The first steel-free deck-slab in Canada was cast on the Salmon River Bridge, part of the Trans Canada 104 Highway near Kemptown, Nova Scotia. Construction of the bridge, which consists of two, 31-m spans, includes a steel-free deck over one span and a conventional steel reinforced deck over the other. Internal arching in the slabs helps transfer the loads to the girders. Although the cost of the steel-free side was six percent more than the steel-reinforced side, the overall design tends to be less expensive than conventional decks. This is because steel-free decks do not suffer from corrosion, so traditional maintenance costs are greatly reduced. This concept has won six national and international awards including the prestigious NOVA award from the Construction Innovation Forum (CIF) of the United States.

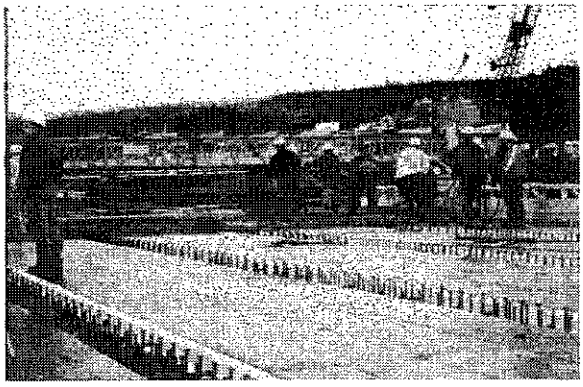

Fig. 1 Casting of the steel-free deck

The deck contains no rebar (refer to Figure 1). Instead, longitudinal beams or girders support it. The load is transferred from the deck to the supporting girders in the same way that an arch transfers loads to supporting columns. Although steel straps are applied to tie the girders together, because they are not embedded in the concrete, they can be easily monitored and inexpensively replaced.

The Structural Health Monitoring (SHM) of the steel-free bridge deck was conducted by installing sensors, as shown in Figure 2. SHM indicates that the load sharing of the Salmon River Highway Bridge is similar to conventional decks, as shown in Figure 3.

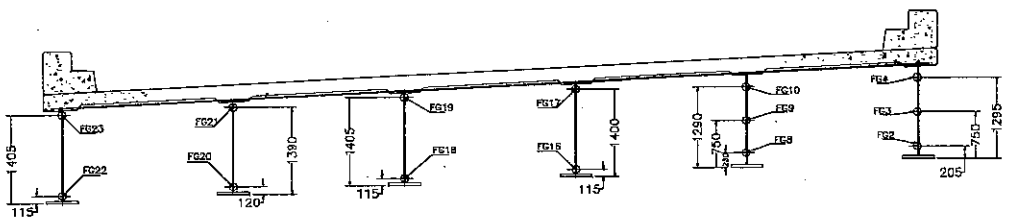

Fig. 2 Sensor locations

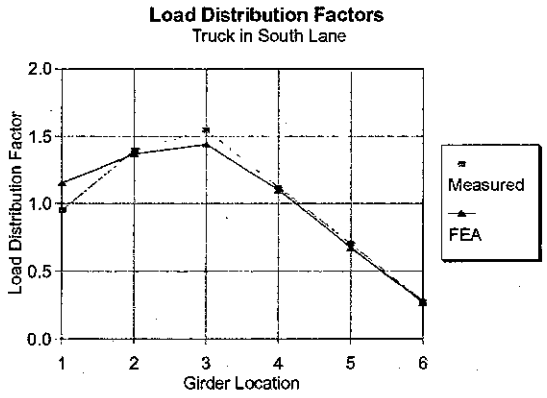

Fig. 3 Load sharing of the Salmon River Highway Bridge

With no steel inside the concrete, no unnecessary weight is added, meaning thinner deck designs. The steel straps are welded to the top flanges of the girders thereby resisting any lateral movement. The Salmon River steel-free bridge deck has withstood a number of Canadian winters, and it appears to be defying the conventional approach to building steel-reinforced bridge decks. There are six steel free bridge decks across Canada.

3. Crowchild Trail Bridge, Calgary, Alberta [3]

The original Crowchild Trail Bridge in Calgary, Alberta was a two-lane, three-span prestressed concrete box-girder bridge. The bridge was found to be under-strength as a result of deterioration over 20 years and increased traffic loads. Therefore, the bridge superstructure was replaced in June 1997.

The new superstructure is the first continuous span steel-free bridge deck in the world. The removal of internal steel reinforcement is made possible by providing lateral restraint to the supporting steel girders through evenly spaced transverse steel straps placed across the tops of the adjacent girders. Glass fibre reinforcements are used at the regions of interior supports and overhanging cantilevers. Prefabricated glass fibre reinforcing grid, NEFMAC, is used for the reinforcement of side barriers.

A total of 103 strain gauges, two fibre optic strain sensors, and five thermisters were used in the monitoring program.

The first tests (1997) consisted of a static truckload test, an ambient vibration test, an effect of temperature test, and dynamic measurements under passing trucks. The second tests (1998) consisted of static and dynamic truckload tests and an ambient vibration test.

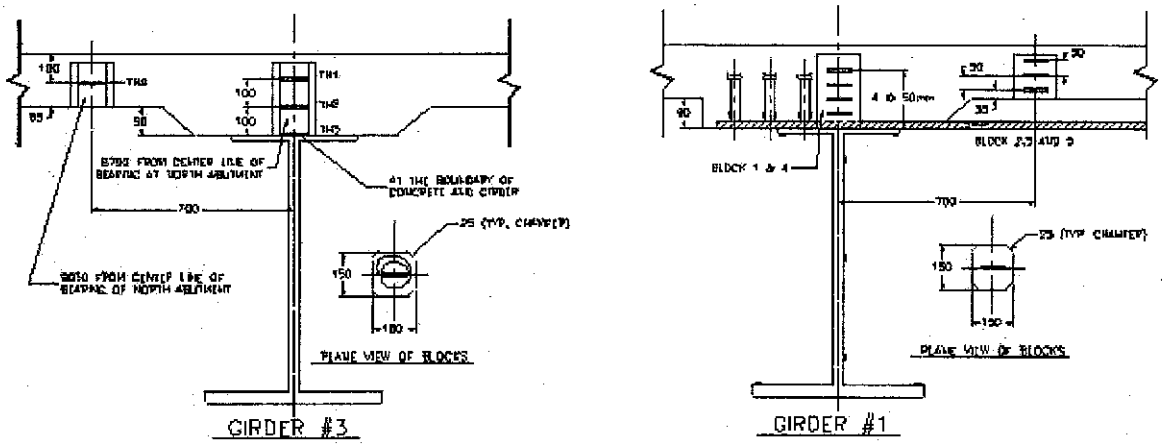

Fig. 4 Embedded strain gauges

To monitor strain distribution in the transverse direction of the bridge deck, 17 embedded strain gauges were installed in a total of five precast blocks – three in the positive moment region and two in the negative moment region. Figure 4 shows the location of the embedded strain gauges

Eighteen gauges monitored the performance of the steel straps. Six strain gauges were used to monitor strains in end shear studs of the strap. Thirty-four strain gauges were used to monitor steel girders. The webs of all five girders were instrumented with three gauges at both positive and negative moment regions to monitor load sharing among the girders and moment distributions along the girders. Four gauges were also installed on the flanges to measure any warping of the girders. The response of one cross frame was monitored by four strain gauges. At the barriers, two strain gauges were installed on a NEFMAC and two on a stainless steel stud. Six gauges at the overhanging cantilevers and 14 gauges at the pier monitored glass fibre reinforcement.

To evaluate the use of FOS technology, two commercially available sensors were installed on the glass fibre reinforcement at the same section as the electrical strain gauges. The sensors were Fabry-Perot type and non-compensated for temperature. To measure deflections of the bridge under heavy traffic load, a testing program was organized by the City of Calgary before the bridge was open to traffic. Two trucks, each loaded nominally to 355 kN, were used to produce nine different load cases [6].

Temperature profiles were recorded with the thermisters and strain measurements were taken using the strain indicator and the manual switching box. As the test took several hours, it was necessary to account for the thermal effects. The results provided preliminary information such as load sharing among the girders,

location of the neutral axis, and moment distribution between mid-span and support. Similar information was later obtained from the results of the dynamic measurements. Measured strains were all less than 80 με in the girders, and less than 40 με in the steel straps. Concrete strains were insignificant.

3.1 Thermal effect

Temperature effects produce the most significant strains in the bridge. To evaluate the performance of the two FOS, strains caused by temperature change are plotted in Figure 5. As the sensors were not temperature-compensating gauges, they measured the total strain caused by both free expansion and restrained thermal deformation. The constraint strains for only 13° C increase in air temperature are comparable with strain measured during static test using truck load, as shown in Figure 6.

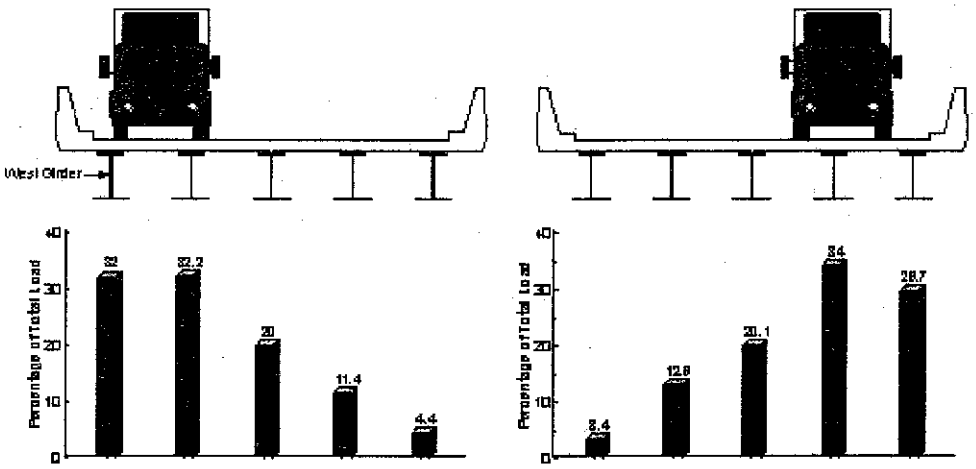

Fig. 5 Load sharing among girders based on dynamic strain measurements 1997

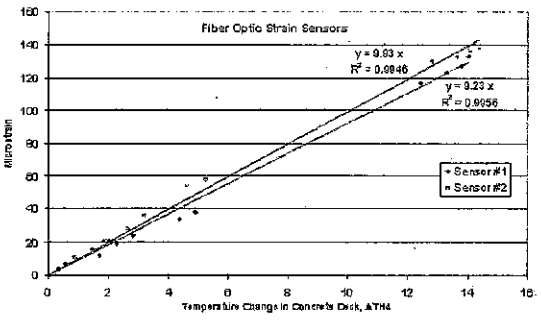

Fig. 6 Effect of temperature change on fibre optic strain sensors

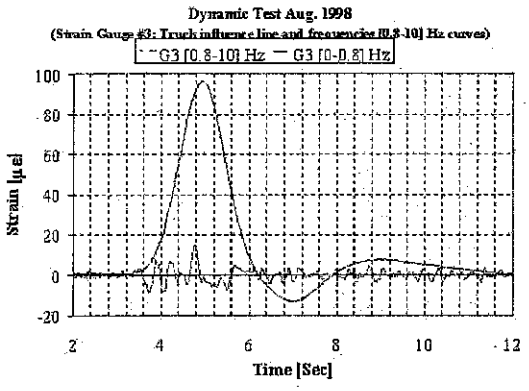

Fig. 7 Response of a strain gauge to the truck in 1998 test

3.2 Dynamic measurements under passing heavy vehicles

The response of the bridge to car traffic was insignificant. For passing trucks a 10 s window of data at a scan rate of 1000 readings/s was gathered. Information such as type of truck, number of axles, and passing lane was recorded by videotape. Electronic low pass filters in the data acquisition unit were set at 10kHz. Figure 7 shows the response of one strain gauge to a passing truck.

Figure 8 illustrates the load sharing among girders based on the measured strains. It illustrates the vibratory and non-vibratory portions of the response of a strain gauge to the truck. The non-vibratory portion was almost identical to the response in the static test. It can be seen that the vibration of the bridge is quite small in magnitude, resulting in a dynamic amplification factor of less than 1.15.

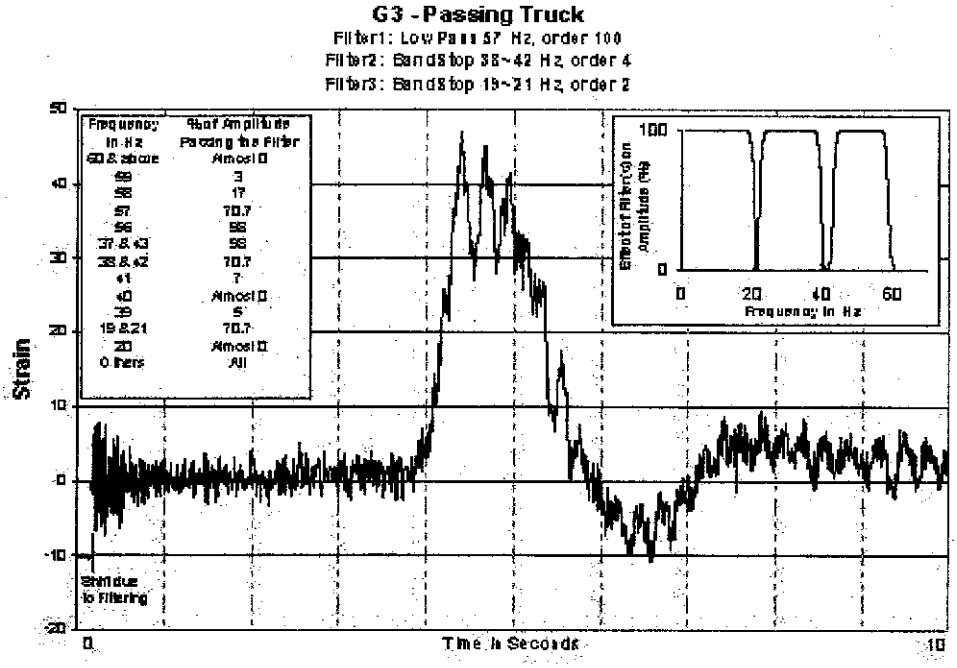

Fig. 8 Dynamic measurement on gauge 3 of girder number 1 and effects of digital filtration

4. Taylor Bridge, Headingley, Manitoba[4]

A significant international research breakthrough was achieved on October 8, 1998, when Manitoba's Department of Highways and Transportation opened the award winning Taylor Bridge in Headingley.

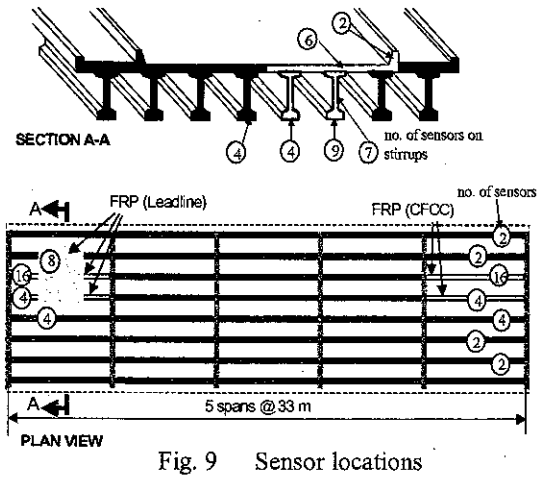

Fig. 9 Sensor locations

Shown in Figure 9, the two-lane, 165.1-metre-long structure has four out of 40 precast girders reinforced with carbon fibre reinforced polymer (FRP) stirrups. These girders are prestressed with carbon FRP cables and bars. Glass FRP reinforces portions of the barrier walls. As a demonstration project, it is vital that the new materials be tested under the same conditions as conventional steel reinforcement – thus only a portion of the bridge is designed using FRP.

Two types of carbon FRP reinforcement were used in the Taylor Bridge. Carbon fibre composite cables produced by Tokyo Rope, Japan, were used to pretension two girders while the other two girders were pretensioned using indented leadline bars produced by Mitsubishi Chemical Corporation, Japan. Two of the four girders were reinforced for shear using carbon FRP stirrups and leadline bars in a rectangular cross section. The other two beams were reinforced for shear, using epoxy coated steel rebars.

The deck slab was reinforced by indented leadline bars similar to the reinforcement used for prestressing. Glass FRP reinforcement produced by Marshall Industries Composites Inc. was used to reinforce a portion of the Jersey-type barrier wall. Double-headed stainless steel tension bars were used for the connection between the barrier wall and the deck slab.

The bridge has a fibre optic structural sensing system that will allow engineers to compare the long-term behaviour of the two materials. This remote monitoring is the key to acquiring data on FRP that will ultimately help it gain widespread acceptance through national and international codes of practice

5. Joffre Bridge[5]

The Joffre Bridge, located over the St-François River in Sherbrooke, Quebec, Canada, built in 1950, showed signs of deterioration of the concrete deck slab and girders primarily due to reinforcement corrosion. The City of Sherbrooke and the Ministry of Transport of Quebec reconstructed a significant part of the bridge deck, sidewalk and traffic barrier using carbon and glass FRP reinforcements, and monitored the performance not only to answer the safety concerns, but also to generate valuable data for the research and development of FRP technology for reinforced concrete structures.

The selected CFRP reinforcement used to reinforce the concrete deck slab is manufactured by Autocon Composites Inc. in Ontario, Canada, and is commercially known as NEFMAC C19-R2 grid. The CFRP reinforcement was in the form of a rectangular cross-section 100 mm x 200 mm grid with a constant thickness of 19 mm. The grids were manufactured with longitudinal spacing of 200 mm and transverse spacing

of 100 mm. The GFRP rebars used as reinforcement for the concrete sidewalk and traffic barrier are produced by Marshall Industries Composites Inc. and commercially known as GFRO C-BAR. The lightweight of the FRP reinforcements was very convenient for easy handling and placement during construction.

The bridge was extensively instrumented with several different types of gauges. A total of 180 critical locations were identified and instruments (fibre optic sensors, vibrating wire strain gauges, and electrical strain gauges) were installed at those locations in the concrete deck slab and on the steel girders.

A number of CFRP reinforcement grids were integrated with fibre optic sensors during the manufacturing process, as shown in Figure 10. Gauges were installed on the steel girders and embedded strain gauges were placed inside the concrete to measure the strain inside the concrete to provide information about the hidden structural damage in the concrete deck slab.

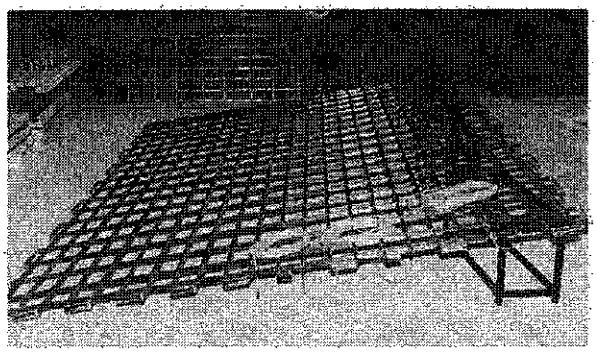

Fig. 10 CFRP grid with integrated Fabry-Perot fibre optic sensors

The bridge was opened to traffic on December 5, 1997. The dynamic responses of different components of the bridge are being regularly recorded using computer aided data logging systems. The interim results indicate confidence in the use of FRP reinforced concrete structures and the use of state-of-the-art instrumentation for continuous long-term structural performance monitoring. Figure 11 shows typical data recorded by fibre optic sensors installed on a CFRP grid reinforcement under normal traffic load. The variation of recorded strain with time and temperature clearly indicates that it is possible to obtain meaningful and consistent results from fibre optic sensors and that temperature is the most prominent factor influencing the strain variation in the bridge deck.

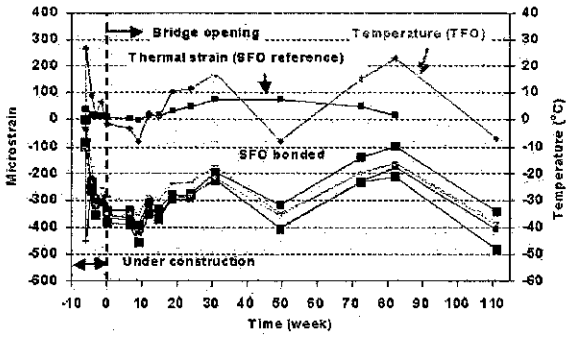

Fig. 11 Data recorded by fibre optic sensors installed on CFRP grid

In November 1998, one year after the opening of the bridge to traffic, field dynamic and static tests, using calibrated heavy trucks (Figure 12), were conducted on the bridge to evaluate the stress level in the FRP reinforcement, concrete deck, and steel girders. Figure 13 shows the results of strains recorded using FOS at the middle of the web of steel girders due to movement of the trucks. The data clearly show that during a 35 s duration, a large strain event (e.g. a truck) followed by two similar strain events (e.g. two consecutive trucks) took place on the bridge.

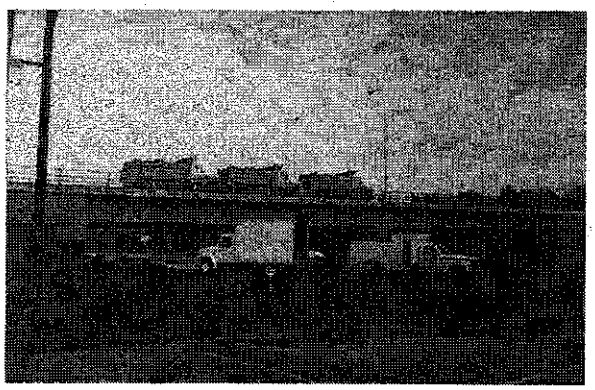

Fig. 12 Trucks being positioned for static calibrated load testing

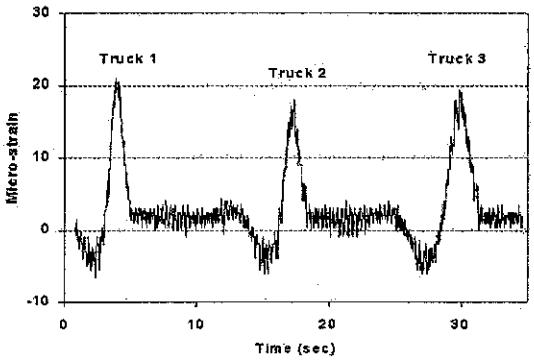

Fig. 13 Strain responses from dynamic load tests of Joffre Bridge

6. Hall's Harbour Wharf, Hall's Harbour, NS[6]

Hall's Harbour Wharf in Nova Scotia is a 96-year-old combination wharf/breakwater, shown in Figure 14(a). It is the world's first marine structure with fibre optic sensors embedded in a steel-free concrete deck for remote monitoring. It is designed to last 80 years – three times longer than traditional construction methods. This design received the "Award of Excellence" from the Canadian Consulting Engineer Association.

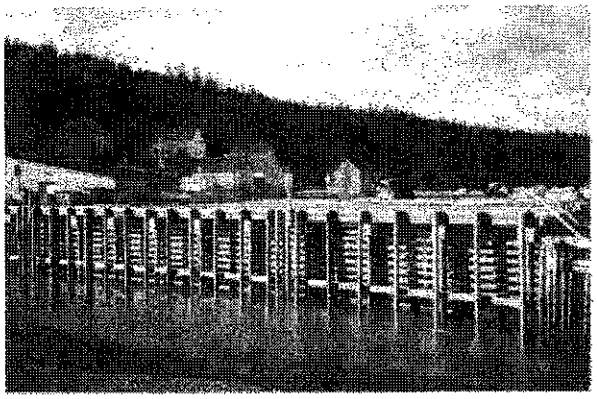

(a)

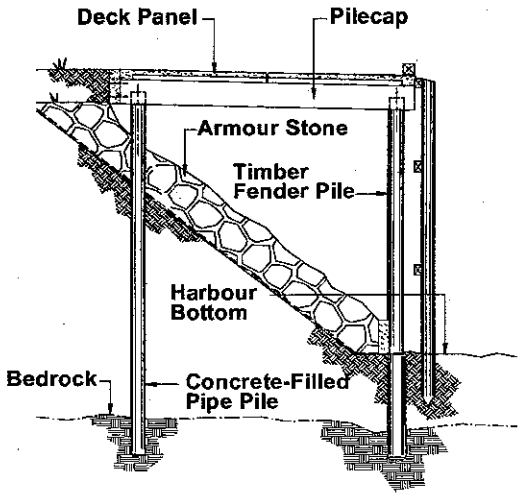

(b)

Fig. 14 Hall's Harbour Wharf

The new wharf consists of piles supporting concrete beams and deck elements above an armour stone and timber crib breakwater. The concrete beams are designed with a hybrid reinforcement scheme of steel and glass FRP rods. The outer durable layer of FRP protects the inner core of steel reinforcement, which was included for code considerations. The deck consists of precast steel-free concrete bridge deck panels modified to meet the durability needs of this structure. Refer to Figures 14, 15 and 16. The design is based on draft versions of both the Canadian Highway Bridge Design Code and the American Concrete Institute Code.

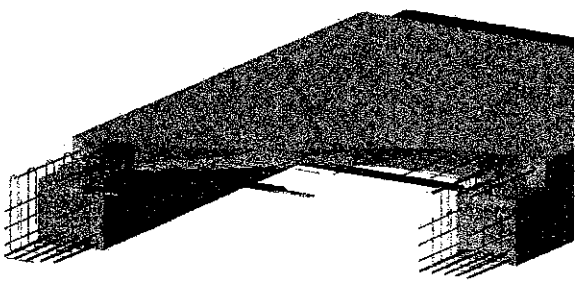

Fig. 15 3D view of deck and beam details

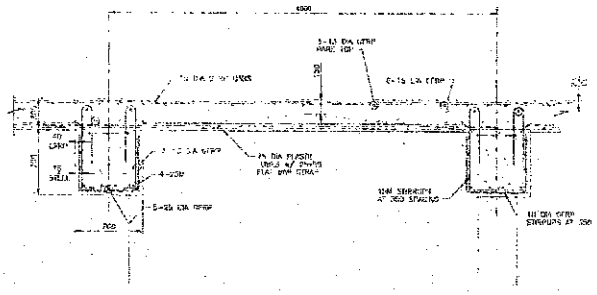

Fig. 16(a) Cross section and sensor locations

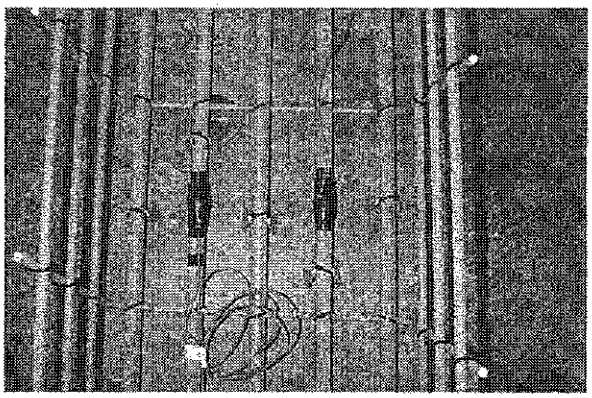

Fig. 16(b) Installed sensors

It is anticipated that rehabilitation of marine structures using FRPs will become standard practice through time, with the inner core of steel reinforcement considered unnecessary.

7. Red River Bridge, Winnipeg, Manitoba[7]

The combination of a typical steel free bridge deck and a FRP reinforced bridge deck have led to the design of a very economical and non-corrosive hybrid bridge deck that is currently being constructed. Use of the external steel strap allows for the substantial reduction in the use of CFRP and GFRP as reinforcements. GFRP reinforcement is used in the internal panels to reduce crack widths and CFRP reinforcement is used in the cantilever sections of the deck to satisfy moment design requirements. The cross-sectional area for the steel straps and percentage of FRP reinforcement were both optimized in the design of the bridge deck. The span containing the new hybrid bridge deck is planned to contain a significant number of sensors and structural health monitoring scheme to monitor the deck and verify that design theories are correct. Figure 17 is an elevation view of the 10 span Red River Bridge prior to construction of the deck and Figures 18 and 19 illustrate the FRP reinforcing details and structural health monitoring schemes.

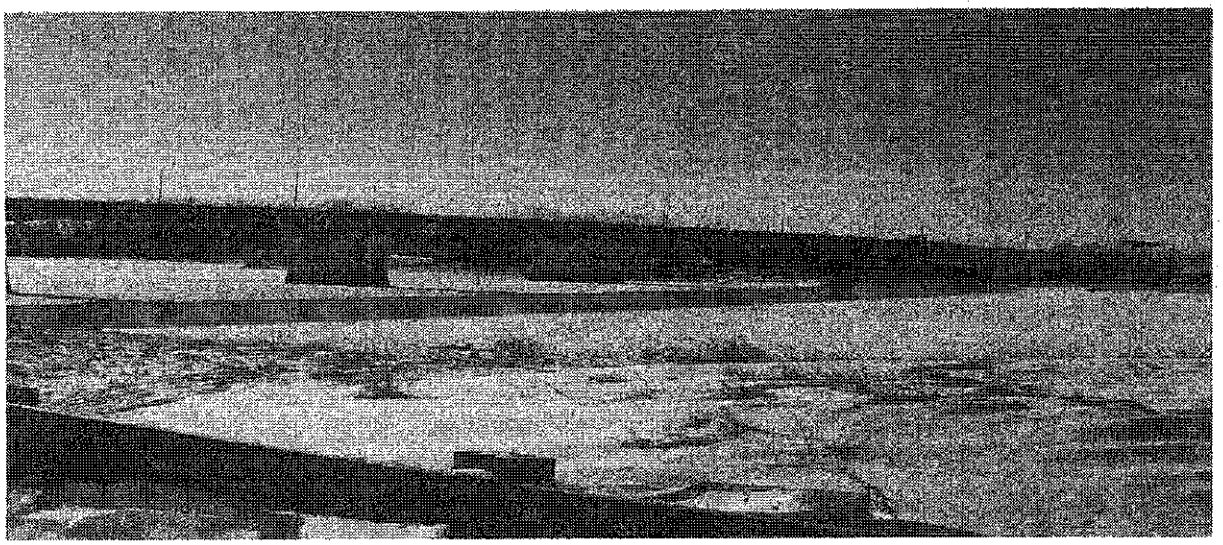

Fig. 17 Red River Ten Span Bridge

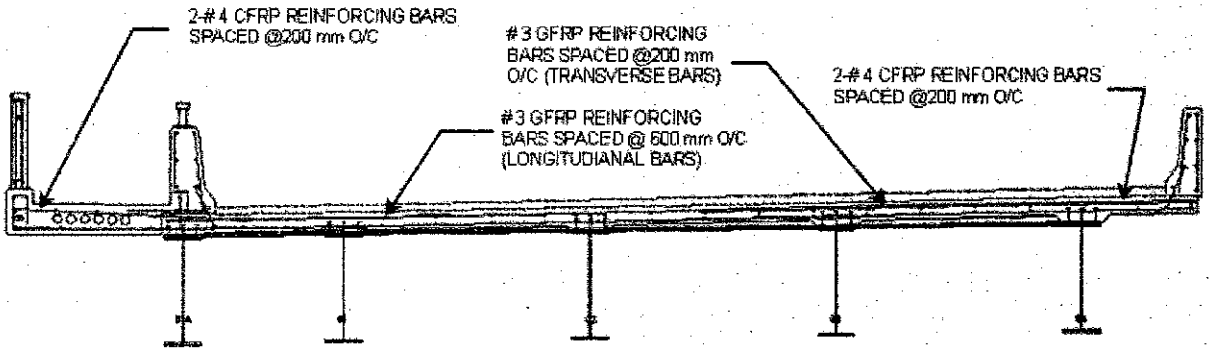

Fig. 18 FRP Reinforcing Detail for Span 10 of the Red River Bridge

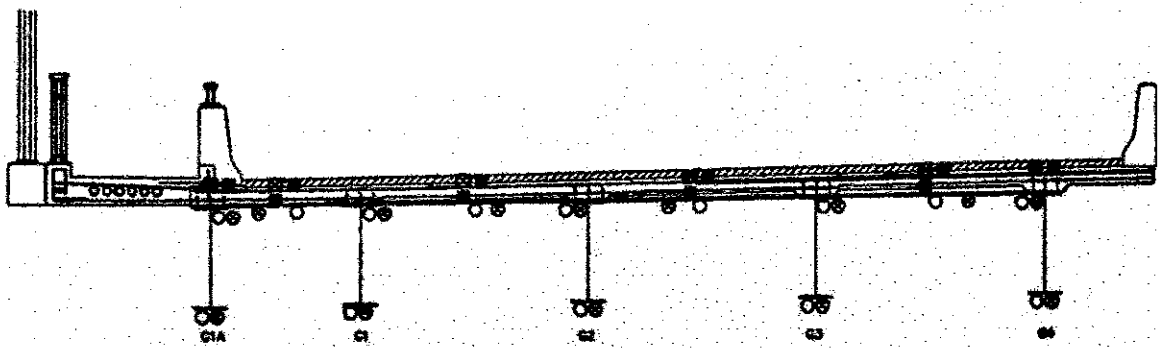

- WELDABLE STRAIN GAUGE TO STEEL STRAP OR GIRDER
- FIBRE OPTIC STRAIN GAUGE TO STEEL STRAP OR GIRDER
- FIBRE OPTIC STRAIN GAUGE IN SLAB TO FRP
- RESISTANCE STRAIN GUAGE IN SLAB TO FRP

Fig. 19 Structural Health Monitoring Scheme for Span 10 of the Red River Bridge

Acknowledgments

The financial assistance of NCE, ISIS Canada and NSERC is gratefully acknowledged. Also, Assistance of Ms. Nancy Fehr, Executive Assistant to the President of ISIS Canada for typing, formatting and editing the paper is gratefully acknowledged.

References

1) ISIS Canada, *Strategic Plan 2nd Funding Cycle*, ISIS Canada Room 227 Eng. Bldg., University of Manitoba, Winnipeg, MB, Canada, R3T 5V6, 2000.
2) Newhook, J.P., and Mufti, A.A. A reinforcing steel free concrete bridge deck for the Salmon River Bridge, *Concrete International*, Vol. 18(6), pp. 30-34, 2000.
3) Afhami, S., and Cheng, J.J.R. Field instrumentation and monitoring of Crowchild Trail Bridge in Calgary, Alberta, *Project Report,* University of Alberta, 1999.
4) Shehata, E., and Rizkalla, S.H. Intelligent sensing for innovative bridges, *Journal of Intelligent Materials and Structures,* Vol. 10, pp. 304-313, 2000.
5) Benmokrane, B, et al., Application of fibre optic sensors for structural health monitoring of bridges and other structures, *Research Report*, University of Sherbrooke, 2000.
6) Newhook, J.P, Bakht, B., Tadros, G., and Mufti, A.A. Design and construction of a concrete marine structure using innovative technologies, *ACMBS-III Conference Proceeding,* Ottawa, pp. 777-784, 2000.
7) Mufti, A.A, Tadros, G. and Bakht, B. Design calculations for steel free deck for Red River Bridge, *Technical Report,* submitted to Earth Tech Consultants, Winnipeg, Manitoba, Canada, 2003.

Preserving the Health of the US Bridge Infrastructure: The Role of New Technologies in the Federal Bridge Program

Raymond McCormick, P.E.
U.S. Federal Highway Administration
Office of Bridge Technology, HIBT-30
Washington, DC
(202) 366-4675
Raymond.McCormick@fhwa.dot.gov

Dr. Edgar Small
The Catholic University of America
Dept. of Civil Engineering
Washington, DC
(202) 319-4381
small@cua.edu

Dr. Glenn Washer, P.E.
U.S. Federal Highway Administration
Office of Infrastructure R&D, HRDI-10
McLean, VA
(202) 493-3082
glenn.washer@fhwa.dot.gov

Abstract

The United States bridge program in partnership with the States has ensured safety and functionality of the sizeable U.S. bridge population since the early 1970's. Billions of U.S. dollars have been spent on major rehabilitation and replacement activity. As the inventory continues to age, rehabilitation and replacement needs continue to escalate and preservation of the inventory becomes increasingly important. New technologies, policies, and procedures are required for management, measurement, inspection, and assessment of in-service structures in order to enhance the program to ensure continuing safety and health of the inventory, and to enable effective use of bridge funds.

An overview of the U.S. bridge program is presented. Current decision approaches are either based on the component level or on more detailed element-level models employed in bridge management systems (BMS's). Both approaches are based upon visual observation and visual condition assessment. Predominant causes of deficiencies in the network will be discussed and the need for new technologies to assist in identification of condition and safety related deficiencies will be identified. New technologies for non-destructive testing and evaluation examined by the Federal Highway Administration are discussed including coherent laser systems, bridge deck inspection systems and bridge monitoring systems. A discussion of future directions will be presented.

Overview of the Federal Bridge Program

Through the late 1960's, the civil engineering community in the United States was focused on the design and construction of the Interstate highway system. Maintenance and preservation were performed reactively and bridge management systems were basically non-existent. There were no national-level requirements for the inspection of bridges. It was widely perceived that the bridge network was safe and that the existing practices were sufficient to ensure safety. Public confidence was shattered, however, with the collapse of the Silver Bridge (Figure 1). Shortly before 5:00 pm on December 15, 1967, the structure collapsed resulting in 46 fatalities.

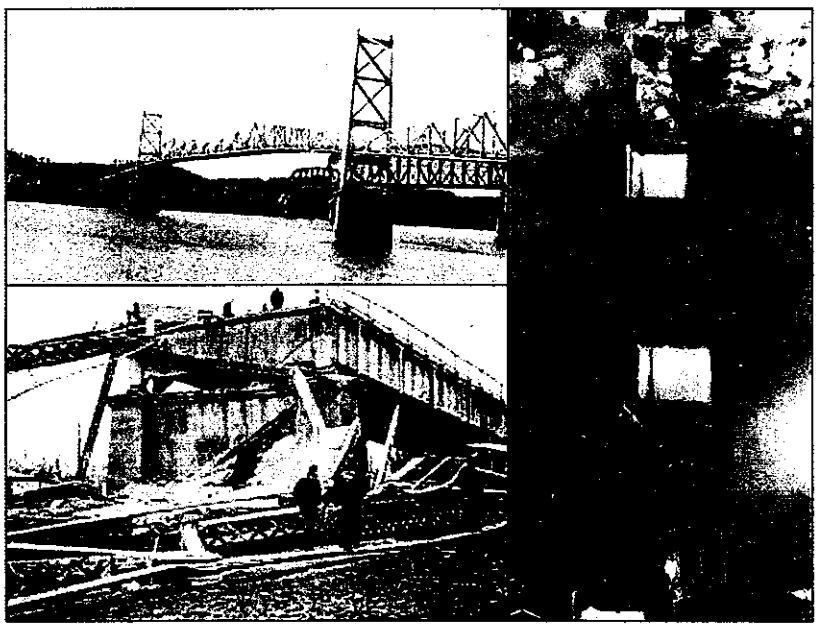

Figure 1: Pictures of the Silver Bridge Before and After the Collapse

Following this collapse, and other less notable failures, national attention focused on the safety of the bridge inventory. The U.S. Congress initiated hearings and investigations were performed to identify the cause of the collapse. It was determined that the Silver Bridge collapse resulted from stress-corrosion, which initiated a sudden fracture of an eye-bar within the suspension chain. A national-level bridge inspection program was initiated to ensure that bridges received periodic inspections and provide safety to the public.

The U.S. Congress directed the Secretary of Transportation to develop and implement the National Bridge Inspection Standards (NBIS). The NBIS, developed by the FHWA in cooperation with the American Association of State Highway Officials (AASHO), was enacted as part of the Federal-Aid Highway Act passed on April 27, 1971. This landmark act established, for the first time in U.S. history, uniform, national standards for bridge inspection and safety evaluation and funding to assist States in replacing deficient bridges. As a result of the legislation:

- All States were required to perform periodic inspection of bridges located on Federal-aid highway systems with lengths in excess of 6.1 m (20 ft).
- Minimum bridge inspection data collection requirements were established
- Qualifications for bridge inspection personnel were defined,
- Training programs for bridge inspectors were developed and implemented
- The Special Bridge Replacement Program (SBRP) to provide funding for the replacement of bridges located on the Federal-aid system was established.

Over time, the NBIS requirements have been refined, additional inspection requirements have been added, and funding programs have been updated. The requirement to inventory and inspect bridges on Federal-aid highways was extended to all bridges in excess of 6.1 m located on all public roads. Data collection requirements were enhanced. Training programs continued to be developed and expanded as more knowledge became available through research. Funding programs were expanded to permit the use of federal funds for replacement and rehabilitation of both federal-aid and non-federal-aid system bridges.

As a result of the NBIS, structures receive periodic safety inspections; however, unforeseen events periodically necessitated expansion of the program and highlighted the need for continued enhancement. On June 28, 1983, a section of the Mianus River Bridge catastrophically failed due to corrosion-induced expansion of a pin and hanger detail. This structure carried Interstate 95, the primary highway on the Atlantic seaboard that provides connectivity between Florida and Maine near Greenwich, CT. This failure (Figure 2) resulted in several fatalities and disrupted commerce in the Northeastern U.S. for several months. Research on fatigue of steel connections was accelerated and additional, fracture critical detail inspection and training programs implemented.

Figure 2: Collapse of the Mianus River Bridge Carrying I-95 in Connecticut

On April 5th, 1987, disaster struck again with the collapse of a bridge carrying the New York State Thruway (Interstate 90) across the Schoharie River (Figure 3). There were several fatalities as the result of the failure of the center pier due to scour. With rising water levels due to localized flooding, the soil around the pier was simply washed away. This was followed by the subsequent loss of bearing capacity for the foundation of the pier. Then On April 1, 1989 the Hatchie River Bridge in Tennessee failed due to scour. These failures indicated a serious problem, given that a significant proportion of the 600,000 bridges on public roads cross over waterways. The FHWA acted quickly by mandating scour assessments and periodic underwater inspection of all structures susceptible to scour. Scour research and prevention is continuing.

Figure 3: Collapse of the Schoharie Creek Bridge Carrying I-90 Near Albany, NY

Along with the NBIS, the Special Bridge Replacement Program (SPRP) was created by the Federal-Aid Highway Act to help states fund the replacement of bridges. This provided funding to Federal-Aid highway bridges only. It provided $816.5 million for the design and construction of 1,578 bridges. In 1978 the Surface Transportation Assistance Act replaced the SBRP with the Highway Bridge Replacement and Rehabilitation Program (HBRRP). This provided funding for both Federal-Aid and non-Federal-Aid highway bridges. It also expanded the program to include both bridge rehabilitation and replacement.

Today, all bridges in excess of 6.1 m located on public roads are inspected to ensure safety. "Best-practices" for routine, fracture critical and underwater inspections have been defined and published. Qualifications of inspection personnel have been established, and training programs implemented to ensure completeness of engineering reviews and consistency of inspection condition assessments. Funding programs have been established and expanded in an attempt to address expanding bridge work needs and to provide funding for retrofit against natural hazards (scour, earthquakes), and extreme events (allisions, fracture). The U.S. Congress, U.S. DOT and State DOT's have created a system to keep the growing number of deteriorating bridges as safe as possible.

Bridge Management and Bridge Inspection

Decisions made through the NBIS program are based on the information collected during the periodic inspections. The NBIS requires bridges to be inspected, at a minimum, once

every two years. Inspections are performed by the bridge owners (States, cities, municipalities, etc.) with oversight by the State DOT's. Information is collected on the bridge composition and conditions and reported to the FHWA where the data is maintained in the National Bridge Inventory (NBI) database. Inventory information includes location and description fields, geometric data, functional descriptions and design characteristics. This information permits classification of structures according to serviceability and essentiality for public use.

Condition information is collected for the primary components of the structure. The following information is collected:

- The bridge deck, including the wearing surface
- The superstructure, including all primary load carrying members and connections
- The substructure, considering the abutments and all piers
- Culverts, recorded only for culvert bridges
- Channel/channel protective systems, for all structures crossing waterways

Bridge inspectors utilize a ten (10) point system, where code 9 indicates excellent, as-new condition and code 0 indicates a failed condition. Inspectors assess the ratings in a visual fashion based on engineering expertise and experience. Extensive training for inspectors is available to assist the bridge owners in ensuring consistency in the assignment of condition ratings. References on bridge inspection, such as the Recording and Coding Guide for the Structure Inventory and Appraisal of the Nations' Bridges and the Bridge Inspectors Reference Manual 2002 are available to guide the inspectors in the assignment of condition ratings.

Following collection of the inventory information and condition ratings, appraisal ratings are calculated to assess the adequacy of the structure to provide the required service. Appraisal ratings are quantified for:

- Structural evaluations (load carrying capacities),
- Deck geometry (indicating constrictions which affect safety),
- Underclearances, and
- Waterway adequacy (the ability of the opening to handle the flow-rates).

Condition ratings and appraisal ratings are utilized to assess the deficiency status of the structure. Deficient bridges may result from structural or functional characteristics. Structural deficiencies result from poor condition ratings or from low load ratings. Functional obsolescence results from inadequate appraisal ratings or from low design-load capacities. Inadequate waterway adequacy can be a contributing factor for either structural deficiencies or functional obsolescence.

To guide the assessment of federal fund eligibility, a performance measure considering multiple variables is developed. This performance measure, termed as the "sufficiency rating," considers the following variables:

- Structural Adequacy and Safety (55%) – By condition ratings
- Serviceability and Functional Obsolescence (30%) – Assessed using the appraisal ratings and the service characteristics of the structure
- Essentiality for Public Use (15%) –Detour lengths, traffic, defense
- Special Reductions (-13%) – Based on redundancy and safety features

The sufficiency rating is calculated using a point deduction approach. A structure receives a 'score' of 100 when no deficiencies exist and a 'score' of 0 when it is totally inadequate for all considerations in the formula. The sufficiency rating is "a method of evaluating highway bridge data by calculating four separate factors to obtain a numeric value which is indicative of," whether the structure should remain in service. The sufficiency ratings form the basis for the prioritization on a National-level and, when combined with other variables, is also a factor in the determination of fund eligibility and allocation.

The data collected through the bridge inspection process, including the calculated fields and the performance measures as described, provides the basis for bridge management under the NBIS. While the inspection information and the calculated performance measures have been effective for national-level prioritization and apportionment of funds there is a need for more detailed data to support bridge management system approaches. As a result more detailed element-level models have been developed. These models defined the structure in greater detail. Consider the structure shown in Figure 4. Under the NBI definition, subjective ratings are assigned to the primary components: the deck, superstructure and substructure. In an element-level model, inspections assess the varying condition states quantitatively defined for elements based on deterioration. Elements include bearings, joints, girders, abutments, etc. Element-level inspection models enable the use of bridge management systems for determination of optimal preservation actions, prediction of future condition given budgetary restrictions, and assessment of network and project-level needs. The data, when compared to the existing NBI component-level approach, provides a significant amount of additional detail and the basis for making more rational maintenance, rehabilitation, and replacement decisions.

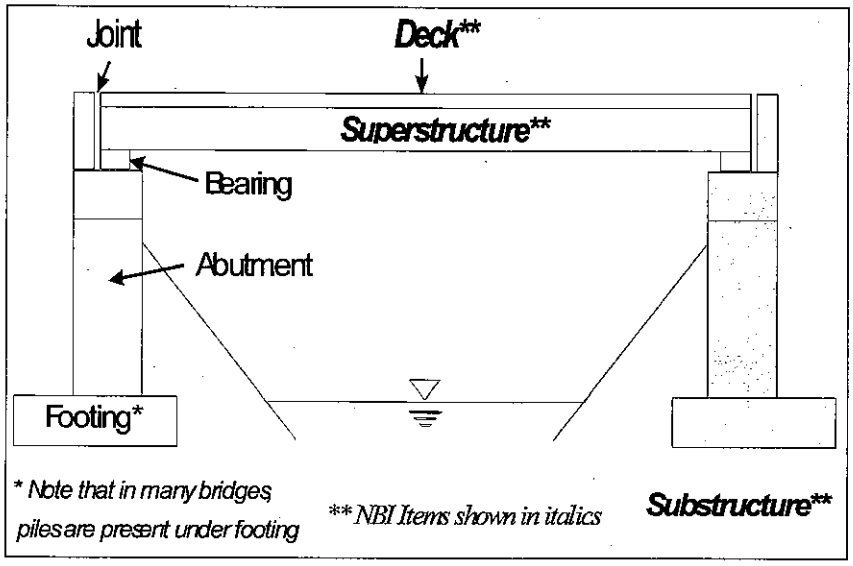

Figure 4: Sample Structure Composition Using NBI and Element-Level Descriptors

The FHWA NDE Program

The condition information collected in both the National Bridge Inventory (NBI) and through element-level inspections is typically based on visual assessments. The NBI component based inspection is subjectively assigned whereas the element-level ratings are determined using quantitative measures of visually identified deficiencies, such as rusting of beams or spalling on concrete columns. Unfortunately some problems are impossible to see by the human eye and to more accurately assess the health of structures; the FHWA has initiated research into quantitative approaches to non-destructively collect more detailed information on both structural conditions and health.

Several techniques for quantitative, subjective Non Destructive Evaluation (NDE) techniques for bridges have been developed. Ultrasonic eddy current, magnetic particle, liquid penetrant, bridge acoustic emission monitoring, laser, ground-penetrating radar, radiography, and active thermographic crack detection are examples of techniques either being developed or already in use. Brief descriptions of each type follows and details on selected technologies described in subsequent paragraphs:

- Ultrasonic inspections send sonic waves into the material to detect subsurface defects.
- Eddy current testing uses small probes to create magnetic fields that interact with the material under test, revealing surface defects through impedance changes measured in the probe.
- Magnetic Particle testing consists of inducing a magnetic field in the surface of a steel specimen, and using iron particles to identify cracks that cause distortions in the field and attract the particles.
- Liquid penetrant utilizes a liquid chemical sprayed onto the material to wet the surface and penetrate surface-breaking defects. When the surface is cleaned,

liquid entrapped in the defect emerges through capillary action, and the application of a second chemical of contrasting color makes defects visible to the inspector.

- Bridge acoustic emission monitoring detects acoustic waves emitted by cracks as they grow. The technology can be used to track the rate of growth of fatigue cracks, determine if corrective measures are working, and monitor structural integrity of welds and connection points.
- Laser distance measurement technologies can track the deformation of the materials and structures under loading.
- Ground-penetrating radar penetrates dielectric materials such as concrete with high-frequency electromagnetic waves. Reflections caused by subsurface features such as reinforcing steel, voids and delaminations can be analyzed to identify deterioration.
- Radiography uses x-rays to penetrate a material and create images showing internal features, including defects such as voids and cracks.
- Active thermography detects changes in the thermal conductivity of a material caused by cracks or subsurface defects that impede heat flow through the material.

Laser Measurement Technologies

Through the FHWA NDE research program, numerous applications have been explored using laser-based distance measurements. A scanning laser system was developed which is capable of measuring distances with sub-millimeter accuracy over a range of 30 meters. The mechanized scanning head enables the laser to be scanned over +/- 200° on one axis and +/- 60° on a second axis. Two angles and the distance measurement are combined to locate a point being measured in three-dimensional space. Targets are not required. Applications for this measurement technology include measuring bridge deflections under calibrated load to evaluate the structural behavior, measuring out-of-plane distortions in girder webs and flanges, and measuring as-built construction of large structures such as abutments.

As an example, the system was investigated for measurement of out-of-plane web distortions in a curved-girder bridge. Figure 5 illustrates laser collected deformation data on a 1 x 6 meter section of a curved girder web under loading. Figure 5A indicates the out-of-plane distortion of a web without vertical stiffeners. Figure 5B indicates the out-of-plane distortions for a web with vertical stiffeners as indicated in the figure.

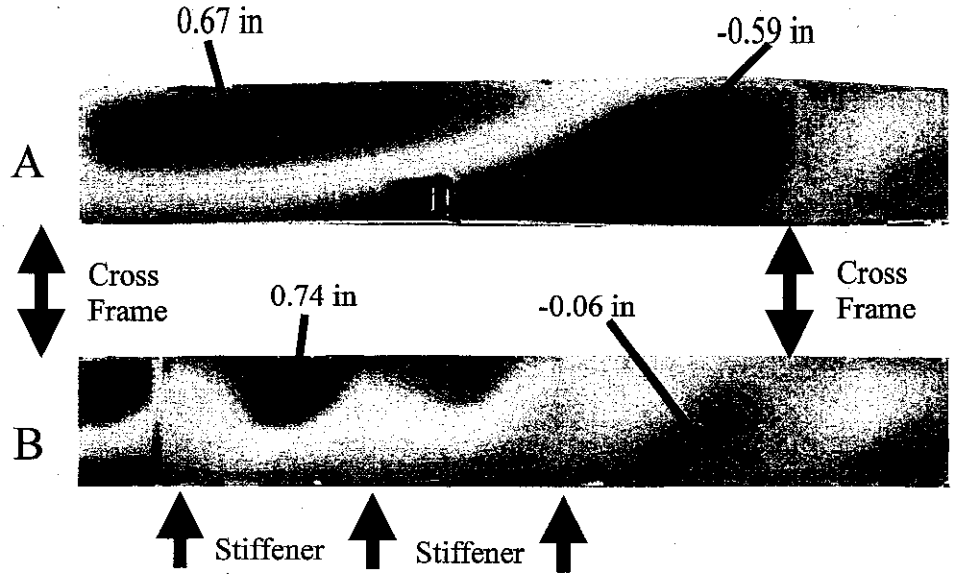

Figure 5: Example of Laser Measurement Results for Out of Plane Bending

Bridge Deck Inspection with Ground Penetrating Radar

The service life of a deck is typically much shorter than the substructure and superstructure of a bridge. Bridge decks deteriorate due to corrosion of reinforcing steel and the resulting delamination and spalling that can make a deck structurally deficient. The ability to detect this deterioration in its early stages is critical in directing repairs to the most at-risk bridges and will help optimize use of limited funds. To address this need, the FHWA has developed ground penetrating radar (GPR) systems for the detection and imaging of subsurface defects in bridge decks.

In 1998, a system constructed by Lawrence Livermore National Laboratories (LLNL) was delivered to the FHWA for testing. The system, known as the HERMES (High Speed Electromagnetic Roadway Measurement and Evaluation System) consisted of a towable array of 64 GPR transceivers that operated at normal highway speeds. The goal of the HERMES project was to develop a GPR system that can reliably detect, quantify and image delaminations in bridge decks at highway speeds. HERMES, together with a smaller system used for research of the technology, has been utilized to collect images of the type shown in Figure 6. The figure depicts a section of bridge deck approximately 0.8 x 3 meters in dimension imaged by a recently developed prototype GPR antenna. Figure 6A is the GPR image of the bridge deck surface. Notable in this image is a concrete patch in the deck shown as a bright, circular feature in the lower right of the figure. Figure 6B is an image at the depth of the top reinforcing bar (rebar) mesh. Reinforcing Steel bars are clearly evident as bright lines in the image, except for an area

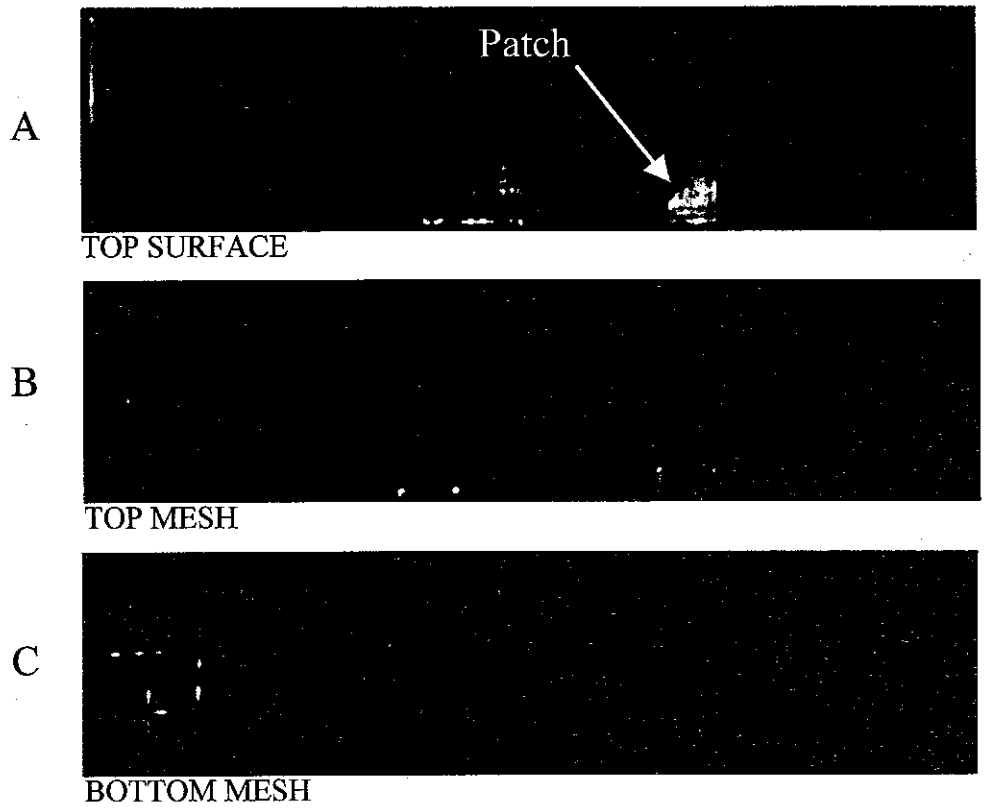

Figure 6. GPR images of a delamination in a concrete bridge deck

of the figure where delaminated concrete is indicated by higher amplitude reflection between rebar locations and a loss for contrast for the rebar itself. Figure 6C is the image of the bottom rebar elevation indicating rebar imaged in the area of the figure outside the delaminated area, and a loss of the rebar image in the area where there is a delamination.

Bridge Monitoring Systems

FHWA has been involved in the development of various instruments for the health monitoring of civil infrastructure. These systems are generally dedicated, remote data-acquisitions systems that collect information on the behavior of a structure over time. Data is logged in system memory and downloaded periodically for evaluation. The systems are built on a flexible platform that can be customized for the particular application. The systems are designed to be inexpensive, rugged, battery-operated and install quickly in the field.

Several systems have been constructed for various applications. One example is the long-term monitoring of a cellular abutment and a wing-wall. For this application, transducers were constructed that could monitor the displacement of the wing-wall relative to the abutment using a unique eddy-current sensor, shown in Figure 7. The sensor was designed at the FHWA Laboratories, and is intended to provide a stable

measurement of displacement over long periods of time with minimal power consumption. The system of sensors measures the relative movement and tilt of the wing-wall, and has been in place for 31 months. Data is periodically downloaded for analysis.

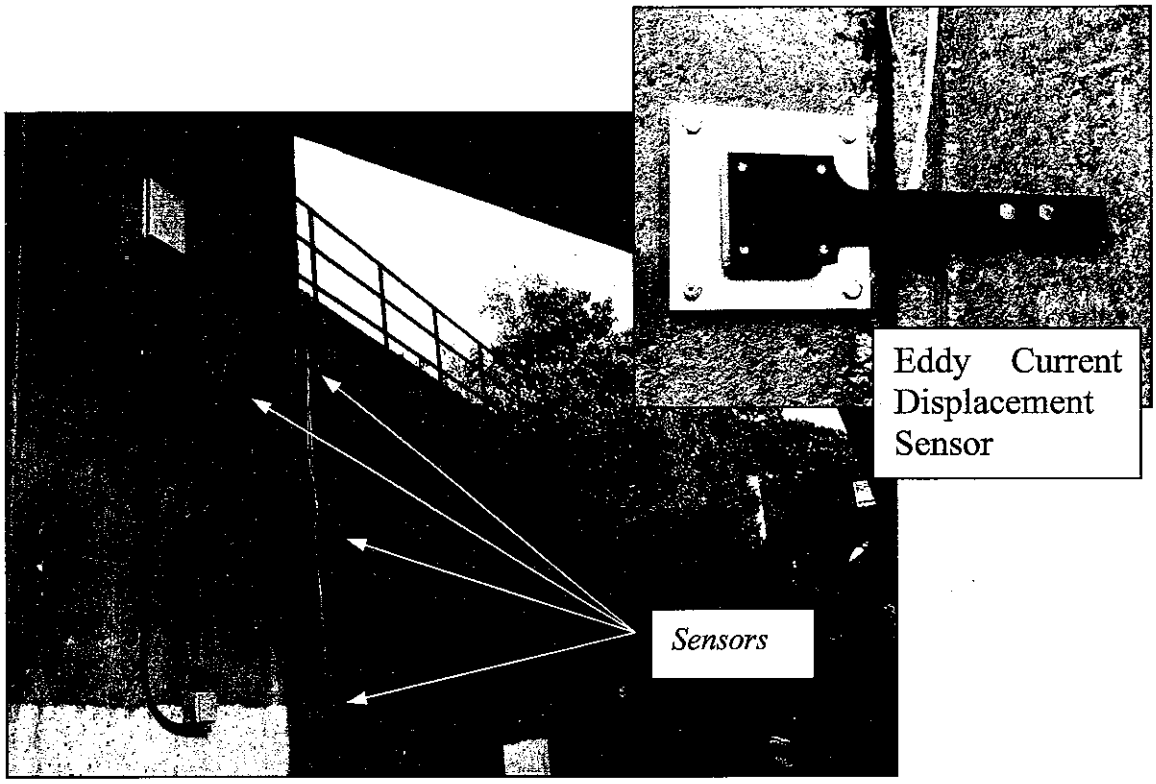

Figure 6. Eddy current displacement sensor in-place on cellular abutment and wing-wall. Data is collected on-site by a battery operated data acquisition system.

Preparing for the Future: The Next Generation

As can be seen, a significant amount of work has been performed to ensure the safety of the bridge population. Inspection processes have been developed and enhanced over the last several decades. Routine inspections are performed on a 2-year cycle for the majority of bridges on public roads in excess of 6.1 meters in total length. Special inspections (fracture critical, underwater) are performed where required for individual structures susceptible to fatigue or scour. Information is collected and maintained at the State and Federal levels and utilized for bridge safety assurance.

The information collected through the NBIS program has historically been utilized for system-level decision making. Such as when utilizing this component-level inspection data for bridge-level decision making. To add more detail, element-level models were developed. These models permit system-level optimization and bridge-level project programming; however, limitations are still present even with this more detailed

information as the inspection data is visually based. New approaches are required to proactively identify damage within a structure, even when the damage is not evident to the naked eye. The FHWA research and development program in Non-Destructive Testing and Evaluation has been designed to develop tools and techniques to collect more detailed information on damage with less effort and less impact to the highway user.

Conclusion

Several new NDE techniques under development by the FHWA were described in this paper including: laser measurement techniques, ground penetrating radar applications, and bridge monitoring systems. These and other techniques hold significant promise in identifying damage and deterioration at the early stages of initiation, where costs of intervention are lower and actions more effective in extending the life of the structure. These technologies promise to collect more detailed information with less effort.

The FHWA continually updates its policies, regulations, and procedures to keep up with changing needs and improvements in technology as well as the States needs. For instance, the regulations for the National Bridge Inspection Standards are currently being updated for the first time in almost twenty years. The new regulations will provide clarifications over the existing regulations and will strengthen the requirements for bridge inspector qualifications and bridge inspection procedures. In addition through reauthorization of the current surface transportation legislation the FHWA is seeking increased flexibility in the use of Highway Bridge Programs funds by the States so that they can more effectively use the funds to manage their aging bridge populations.

The U.S. Department of Transportation, through its latest legislative proposal for reauthorization of the Surface Transportation Program is seeking to improve technologies, which can be used to extend the service life of existing bridges as well as to allow for the design of bridges, which have a service life in excess of 100 years with minimal maintenance required. These are exciting and challenging times for the U.S. in terms of managing its aging infrastructure. The FHWA will continue to be a leader in innovation and technology with the goal of improving the condition of the nations bridges.

References:

Commonly Recognized (CoRe) Structural Elements, AASHTO, Washington, DC, 1998.

Cooper, J.D., McCormick, R.J. and Small, E.P., *Balancing Bridge Management And System Preservation Needs Against The Need To Replace And Rehabilitate Deficient Bridges*, Proc. First International Conference on Bridge Maintenance, Safety and Management, Barcelona, Spain, July 2002.

McCormick, R. and Small, E. P. *Federally Assisted Bridge Programs in the United States: Past, Present and Future*, 16th US-Japan Workshop on Bridge Engineering.

O'Connor, D. S. and Hyman, W.A., "Bridge Management Systems", Summary of FHWA Demonstration Project 71, Report # FHWA-DP-71-01, Office of Engineering, Bridge Division, Federal Highway Administration, U.S. Department of Transportation, Washington, DC. 1991.

US Department of Transportation, *National Bridge Inventory Information System Documentation*, Bridge Division, Office of Engineering R&D, Federal Highway Administration, 1992.

U.S. Department of Transportation, "Recording and Coding Guide for the Structure Inventory and Appraisal of the Nation's Bridges," Report No. FHWA-PD-96-001, Office of Engineering, Bridge Division, Federal Highway Administration, U.S. Department of Transportation, Washington, DC. 1995.

Washer, Glenn, *Nondestructive Evaluation Technologies for Highway Bridges*, to be published in *Public Roads*, January 2004.

Safety Assessment and Health Monitoring of Suspension Bridge Cables

Dr. Harukazu Ohashi*, Jamey A. Barbas**, Roger Q. Haight***

*Senior Structural Engineer, Parsons, 100 Broadway, New York, NY 10005 USA
**Senior Project Manager, Parsons, 100 Broadway, New York, NY 10005 USA
*** Project Engineer, Parsons, 100 Broadway, New York, NY 10005 USA

This paper reviews major rehabilitation work in suspension bridges to identify problems in long-term maintenance. Recent development of new rehabilitation technologies enables us to extend the useful life of existing structures rather than recommend total replacement. In this regard, assessment of cable safety is of utmost importance. First, cable critical conditions, corrosion and hydrogen assisted stress corrosion cracking, and properties of corroded and pre-cracked wires are shown. Methods of evaluating strength and projecting longevity of cables by use of fracture mechanics are described. Finally, an acoustic monitoring technique used for detecting wire breaks in service is presented as a useful tool for risk management.

Key Words: Suspension Bridge, Cable, Safety Assessment, Stress Corrosion/ Hydrogen Embrittlement, Longevity, Fracture Mechanics, Acoustic Monitoring

1. Introduction

It is crucial to rehabilitate the major components of many old suspension bridges in the U.S. After several decades of service, much longer than the original design life, these bridges are not only a vital link in major road networks but also often stand as national landmarks in the surrounding environment. Therefore, in many cases, demolition and replacement of these bridges is not a viable option, and revitalization of these bridges has ensued. Many engineering efforts have been devoted to extend their useful life and increase the traffic capacity as well. As a result, new technologies in reinforcement, replacement, and addition of new components have been developed.

In assessing deteriorated suspension bridges that carry ever-increasing traffic, the main cables, the primary load-carrying members, are of prime importance. The evaluation of main cable safety includes evaluation of the strength and projecting the remaining useful life. Engineers are faced with how to interpret the condition of the aging main cables containing corroded and cracked wires.

In this paper, recent rehabilitation work is reviewed in major suspension bridges around the world. Then, attention is focused on assessment of main cable safety by describing the corrosion and stress-corrosion or hydrogen embrittlement cracking. A methodology for evaluating longevity of cables with corroded and pre-existing cracks is presented. Then the safety of the main cables is assessed. Finally, an acoustic monitoring technique is presented as a useful means to detect wire breakage for ensuring bridge safety.

2. Overview of Rehabilitation in Major Suspension Bridges

There are currently approximately 46 suspension bridges spanning over 700 feet (214m) in the U.S.[1] The majority of cables on these bridges are made of parallel wire strand cables, and approximately 12 are composed of helical strand cables. One bridge with helical strand cables, the U.S. Grant Bridge (Portsmouth Bridge) built in 1927, was demolished in 2001 due to severe cable deterioration, despite two recabling operations.

After several decades of service these bridges have experienced years of environmental fluctuations in temperature and humidity, industrial particulate and vapor emissions, changing traffic demands, and general degradation. In order to satisfy often competing demands, engineers are expected to provide optimal solutions that balance both economic priorities with historic and environmental preservation.

Table 1 classifies some of the reasons necessitating bridge rehabilitation. Reasons include increased demands, decrease of capacities, or both. Increasing traffic volume and live load intensity are major trends.

Table 1. Changes in Demand and Capacity

Changes in Time	Major Causes
Increasing Demands	▪ Increased traffic volume ▪ Installation of walkway/bikeway ▪ Increased live load intensity ▪ Increased seismic demand
Decreasing Loading Capacities	▪ Section area loss due to corrosion, stress corrosion cracking, fatigue ▪ Strength reductions

Decreasing of capacity results from reduction of section, primarily due to atmospheric corrosion. In some cases, structures need to be strengthened after new requirements or findings are made known, such as seismic demands. Increasing demands and decreasing capacity both lead to re-evaluation of the structural loading capacity.

Table 2 shows some major rehabilitation work performed around the world. The most frequent type of rehabilitation is replacing the decks, suspenders, and re-wrapping main cables. Most of this work results directly or indirectly from corrosion. The original concrete decks have, in many cases, been replaced by orthotropic steel decks. These new decks reduce dead load by approximately 30%, allowing some margin for accommodating extra lanes and increasing live loads. These orthotropic steel decks, having already been in service for 20-30 years, exhibit fatigue problems. Another consideration worth noting is that rehabilitation of major components may result in re-verification of the aerodynamic stability, as it changes configurations, dead load, and stiffness.

A number of new technologies have been developed: replacement of main cables, addition of secondary cables, and replacement of suspended structures. In the Tagus River Bridge[2], addition of extra traffic lanes and new railroad tracks were facilitated by installing secondary parallel wire cables above the original cables, 33 years after its opening in 1966. The helical wire strand cables of the Tancarville Bridge[3] over the Seine in 1959 were replaced. The entire suspended structure and the suspenders of the Lions Gate Bridge[4] in British Columbia, Canada, were replaced in segments each night while allowing daytime traffic. The Tamar Bridge[5] in the United Kingdom added extra traffic lanes outboard of the trusses by installing new stay cables, both of which extended and tied beneath the mid-portion of the main span suspended structure. Development of these new cutting-edge technologies for life extension will enhance utilization of existing structures suffering from heavy deterioration and/or over capacity.

Table 2. Rehabilitations in Suspension Bridges

Bridge Name (span in m)	Year Built	Major Rehabilitation
Wheeling*	1860	Re-decking to open grating
Brooklyn (486m)	1883	Suspender replacement, re-decking, cables rehab.
Manhattan (448m)	1909	Torsional strengthening suspended structure
Williamsburg (488m)	1903	Orthotropic re-decking, towers/ suspended structure strengthening, pedestrian/bikeway installation, suspender replacement, cables rehab.
Ben. Franklyn (533m)	1926	Orthotropic re-decking
Tancarville* (608m)	1959	Main cable replacement
G.Washington (1067m)	1931	Orthotropic re-decking
Waldo-Hancock* (244m)	1931	Suspender replacement
Golden Gate (1280m)	1937	Orthotropic re-decking, Suspender replacement
Lions Gate* (472m)	1938	Suspended structure and suspender replacement
Tagus River (1013m)	1966	Addition of lanes and railroad tracks, installation of secondary cables and suspenders
Throgs Neck (549m)	1961	Orthotropic re- decking
Deer Isle* (329m)	1939	Wind fairing installation, precast concrete re-decking
Tamar (335m)	1961	Installation of new cantilevered lanes, installation of stay cables

* Helical strand cables

3. Cable Condition

3.1 Atmospheric Corrosion of Galvanized Wires

It is known that the galvanized steel wires used for most suspension bridge main cables exhibit pitting, a localized attack confined to a relatively small area. Because a localized area is acting as an anode, the resultant pits are deep. Pitting not only reduces section area but also, more importantly, it is a stress riser.

It is customary to classify cable corrosion in four stages as shown in Table 3. Wires exhibiting Stage-I and –II corrosion do not exhibit significant strength reduction, but when corrosion develops to Stage-III, cracking may be observed and the strength and ductility decrease.

Table 3. Corrosion Stages in Steel Wires

Stage-I	Wire surfaces have a shiny, metallic appearance, though some signs of white zinc corrosion product may be visible in spots.
Stage-II	Wire surfaces dull as the zinc corrodes. The wires eventually are covered with white corrosion product. However, there is no ferrous corrosion under the white corrosion product.
Stage-III	Signs of ferrous rust are visible on wire surfaces. The zinc coating is almost completely consumed. Random wire cracking is possible during this stage.
Stage-IV	Ferrous rust stains or displaces most of the white corrosion product on wires. Wire surfaces become very rough and pitted. Wire cracking is anticipated at this stage of deterioration

A preliminary condition of the main cables can be ascertained from the exterior paint condition on the wrapping, because paint cracking/peeling and rust stains are both signs of deterioration inside. The most reliable and accurate method is wedged inspection in which a number of wedges are driven radially into a cable to open the interior, and then the corrosion stage and wire breaks are visually inspected. Photo 1 shows a wedging operation for a parallel wire cable. Wedging into helical wire strand cables is more difficult, as wedges can only penetrate at interstices between strands as shown in Photo 2.

In this case, only first layer wires of the strands are visible, and interior wires in strands are only visible from windows resulting from first layer wire breaks.

Non-destructive testing such as using magnetic flux leakage methods and magnetstrictive methods have been used in limited applications for suspenders, and future development of this method for reliable quantitative evaluation is highly promising as a quick and economical tool.

Photo 3 shows Stage-IV corrosion wire in a parallel wire cable. Photo 4 shows Stage-IV corrosion in a helical strand cable exhibiting severe ferrous corrosion localized in a contact surface between strands, where the elliptical shape indicates the helix trajectory of the overlaying wire.

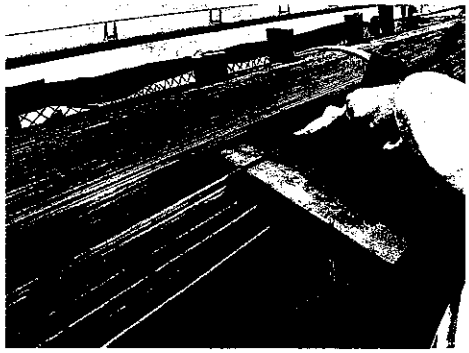

Photo 1. Wedge Inspection (Parallel Wire Cable)

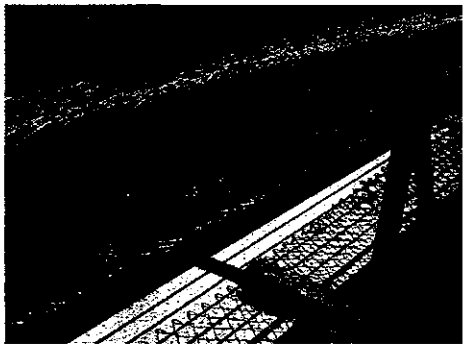

Photo 2. Wedge Inspection (Helical Wire Cable)

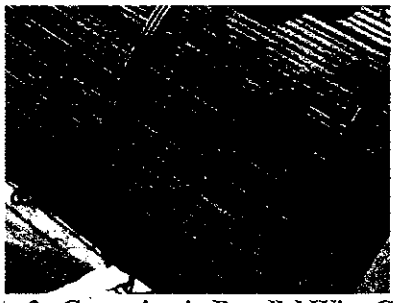

Photo 3. Corrosion in Parallel Wire Cable

Photo 4. Corrosion in Helical Wire Strand

3.2 Stress-Corrosion Cracking

Stress-corrosion cracking (SCC)[6] is known as intergranular or transgranular cracking of a metal by the combined action of a static tensile stress and a specific environment, and the crack growth is sometimes very rapid. It is barely detectable from the surface, and then penetrates inward to destroy the integrity of the metal, resulting in a decrease of the load-carrying area and causing extreme stress concentrations. Stress-corrosion cracking has been observed in cable wires in suspension bridges.

As a similar phenomenon, hydrogen-embrittlement (HE), is also known as a cause of cracking in high strength steel wires. It is explained by atomic hydrogen entrapped in steel that weakens molecular bonding, and microcracks develop when tensile stress is applied. Hydrogen may be supplied during the wire's manufacturing process such as acid pickling, and also as a result of an electro-chemical corrosion process. Although the scientific definition of both phenomena differs, it is not always easy to identify the exact cause of cracking in actual cable wires. The combined effect of corrosion and tensile stress is common to both SCC and HE.

Photos 5 and 6 are typical fracture surfaces found on in-service cable wires, displaying an inclined slip plane initiated from localized pitted corrosion.

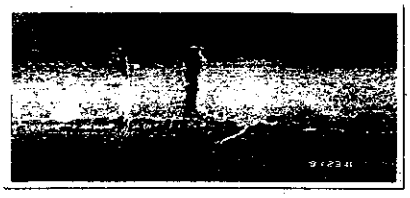

Photo 5. In-situ Wire Fracture in Longitudinal Section

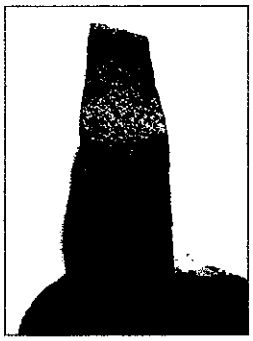

Photo 6. In-Situ Wire Fracture Surface

A fractographic examination by Scanning Electron Microscope (SEM) of an in-service fracture surface shown in Photo 7 exhibits transgranular cracking.

Photo 7. Transgranular Crack

Photo 8 shows a typical fracture surface morphology obtained by SEM. The top photo shows a feather-like morphology exhibited by the fracture surface in the pre-existing crack zone, as is characteristic of progressive transgranular hydrogen –assisted or stress corrosion cracking. The final fracture zone shown in the bottom photo exhibits micro-void coalescence, as is characteristic of ductile overload fracture. It is also interesting to note secondary cracks found in the fracture surface as shown in Photo 9.

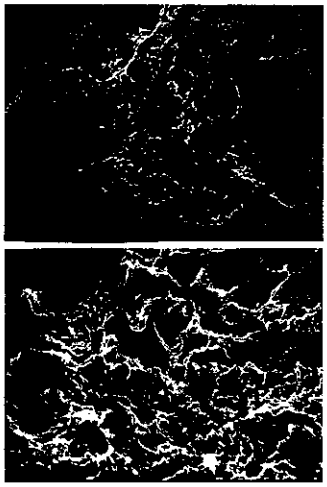

Photo 8. Morphology Top: Feather-like Bottom: Micro void coalescence

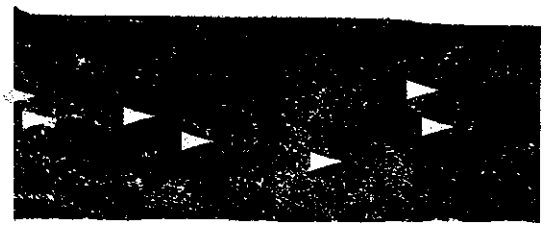

Photo 9. Secondary Cracks in Fracture Surface

Stress-corrosion cracking was reported in suspension bridge cables at Mt. Hope and Ambassador[7] (heat treated wires), Ben Franklin, Bear Mountain, Mid-Hudson[8] , U.S. Grant[9] (demolished after 74 yrs. in service), Tancarville[3] (main cables replaced after 41 yrs. in service) and Waldo-Hancock bridges.

3.3 Physical Properties of Corroded Wires with Pre-existing Cracks

Wire samples were taken from broken wires for testing tensile strength, elongation, fatigue, chemical composition, and fracture morphology from in-service as well as strength test fractures. Tensile test data were normalized by nominal wire diameter after galvanization. Figure 1 shows tensile strength vs. elongation for Stage-IV wires. Wires can be classified whether elongation at failure is less than or equal to 0.6% or greater than 0.6%. Wires are defined as brittle when elongations are less than or equal to 0.6%, and ductile wires are those with elongations greater than 0.6%.

Noting that 0.7% elongation is used as a strain at proof load, brittle wires are those that do not reach the proof load elongation. When the data are plotted for brittle and ductile wires only, brittle wire data had more scatter with a higher coefficient of variance of 11%, whereas that of ductile wires is 6%.

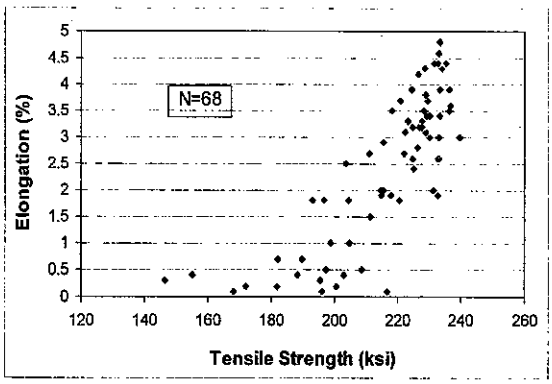

Figure 1. Tensile Strength vs. Elongation (Stage-IV Wires)

The scattering of data is due to the existence of micro cracks. The minimum strength is 143ksi (987MPa) and the maximum is 236ksi (1,629MPa), whereas the original wire tensile strength is specified as 220ksi (1,519MPa) minimum. The coefficient of variance of new wires used in modern suspension bridges is less than 2%.

Figure 2 shows the tensile strengths that relate to pre-existing crack depth, indicating significant reduction in strength with increasing crack depth, for samples taken from in-service broken wires, all rated as Stage-IV. This figure also implies that crack depth less than 5% of wire diameter (0.25mm deep) did not result in strength reduction. It is considered that a crack depth greater than 45% of diameter is a threshold condition of fracture. It was also confirmed by Service et al.[10] It is noteworthy that all these cracks were found in fracture surfaces after the tensile tests were performed, and were not visible during inspection. This is the most crucial limitation of visual inspection. Therefore, classification of corrosion stage is not sufficient for strength evaluation.

The distributions of tensile strengths of specimens taken from the same wire are compared in Figure 3. It is shown that reductions in tensile strength along the wire suggest fractures occurred at pre-existing micro-cracks. This was confirmed by examining the fracture surface after the test.

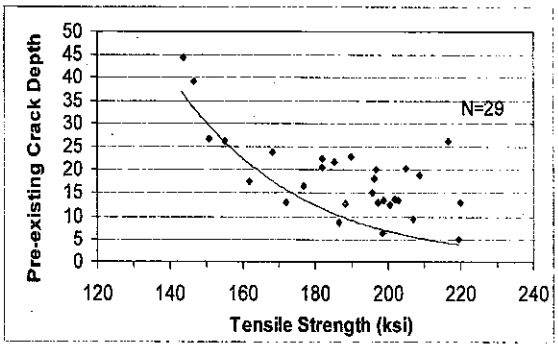

Figure 2. Tensile Strength vs. Pre-existing Crack (Crack depth/diameter in %)

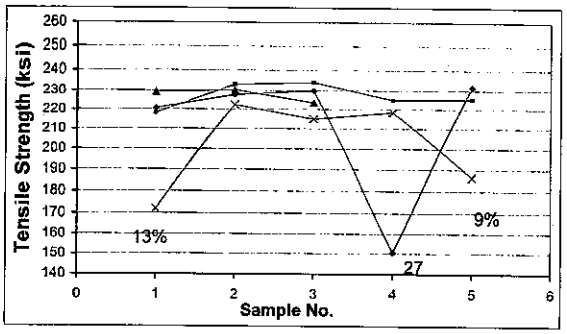

Figure 3. Tensile Strength Distribution (% in chart indicates crack depth/diameter)

Fatigue testing was performed at stress amplitudes of 10-18ksi (69-124MPa), and only 4 samples out of 15 samples tested fractured below 2-million cycles. Fatigue test results for wire samples taken from already broken wires (all were rated as Stage-IV wires) showed that wires were strong (exceeding 2-million cycles at 18 ksi stress range) when there was no pre-existing crack, but wires broke at much lower stress cycles when there was a pre-existing micro crack. The depth of pre-existing cracks ranged from 8% to 38% of the wire diameter. Photo 10 shows a fracture surface with pre-existing crack, fatigue crack, and final fracture surface.

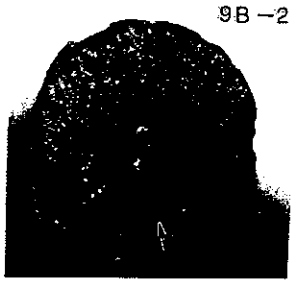

Photo 10. Fracture Surface after Fatigue Test indicating Initial crack, fatigue crack and final fracture

4. Evaluation of Cables Safety Factor

Conventionally, safety of main cables is expressed by using a safety factor, an index used for indicating the safety level against failure defined as tensile strength divided by tensile forces. The safety factor in design ranges from 2 to 4, and the design safety factors tend to decrease for modern suspension bridges. When evaluating cable safety of existing bridges, however, it is important to consider other factors that bridges have experienced.

4.1 Limit States

(1) Strength Limit State

Cable safety is demonstrated by the strength limit state in which a safety margin is taken for the tensile strength so that the most plausible maximum tensile stress in cable is not exceeded. This is a simplified format in that the secondary bending stresses at saddles, cable bands and strand shoes are considered implicitly in the safety margin. Since a new wire normally exhibits elongation exceeding 4% at fracture, the strength limit state may not guarantee the serviceability condition. Current specification for galvanized steel wires for suspension cables (1,570 MPa tensile strength) requires a minimum proof stress (0.2% offset stress) as 1,180MPa. The ratio of proof stress to tensile strength is 75% to 85%. Assuming that the secondary stress is approximately 20% of tensile stress, this indicates that a safety factor of 2.0 against tensile strength means that cables are subject to a stress level of 70 to 80% of the proof stress.

(2) Serviceability Limit State

Since main cables of suspension bridges are their primary non-redundant component, other limit states such as excessive vertical deflections and angular bending at expansion joints (due to elongation in cables resulting from the sectional loss etc.), may control. The towers and stiffening girders may be overstressed by additional bending resulting from increasing deflections due to cable elongation.

(3) Stress-Corrosion/Hydrogen Embrittlement

Stress-corrosion and hydrogen embrittlement cracking may become another limit state for deteriorated cables. Stress-corrosion cracking becomes a major concern for cables that are in Stage-III or worse. It is known that unless sustained stresses (tensile stresses) in the cables are substantially lowered and/or the surrounding environment is improved, stress corrosion continues to initiate and propagate. Since dead load stresses in cables are typically around 70-85% of total stress, reduction of sustained stress is practically only feasible by reducing dead load (replacing the deck with a lighter one, for example).

(4) Fatigue

Normally fatigue would not become a problem in suspension bridge cables as the stress ranges due to live loads are 5-10% of the allowable stress, and far below the endurance limit. However, when wires are in a stage with pre-cracking and/or heavy corrosion, then application of repetitive stress due to live loads may enhance the crack propagation leading to wire fracture[11].

4.2 Strength Evaluation of Cables

Methods of strength evaluation for deteriorated suspension bridge cables have been proposed by many authors for parallel wire cables. These studies primarily focus on how accurately to evaluate cable strength from limited inspection data and limited tested strength data. Wires constituting cables of aging suspension bridges of more than 50 years in service range from 1,100 for the Wheeling Bridge to 52,948 for the George Washington Bridge. Inspection difficulties lie in determining the amount and the quality on inspection (usually driven by cost and traffic impact), inaccessibility and inability to such location as saddles, and in validity of extracted samples for testing. Even more difficulty exists in helical wire strand cables in which interior wires cannot normally be visually inspected.

In evaluating existing bridge cables that contain corroded and broken wires, it is important to consider

that broken wires regain their ability carry tension after an effective clamping length due to frictional clamping by cable bands. Confinement by wrapping wires' radial pressure also contributes somewhat to the clamping effect.

4.2.1 Strength Models

(1) Ductile Wire Model[1]

The ductile wire model assumes that all unbroken wires in the cable section possess full ductility, so that they ultimately fail simultaneously. This assumption is not valid for cables composed of wires with different elongation properties since brittle wires break before ductile wires reach their peak strength.

(2) Ductile-Brittle Wire Model

The ductile-brittle wire model assumes that wires with elongations less than 0.6% are assumed to break after yielding, and they are therefore discounted in the number of effective wires used for computing overall cable strength. However, it may become conservative to discount the contribution of wires with elongation less than 0.6% until these wires fracture, since the strain level under service load conditions is approximately 0.3% in typical cable sections, and it is higher in locations such as strand shoes and saddles.

(3) Refined Ductile-Brittle Wire Model

The refined ductile-brittle wire model considers the strength contribution of wires with less than 0.6% elongation up to the elongation. Minimum cable strength will be found at each strain (elongation) by summing up the strength of wires before they break.

(4) Monte-Carlo Simulation

Effects of random distribution of wires in cables with different properties can be analyzed by using Monte-Carlo simulation[12]. It assigns randomly different stress-strain curves to each wire, and the cable strength is computed by summing up wire strengths at incremental strains. The minimum strength is the theoretical cable strength.

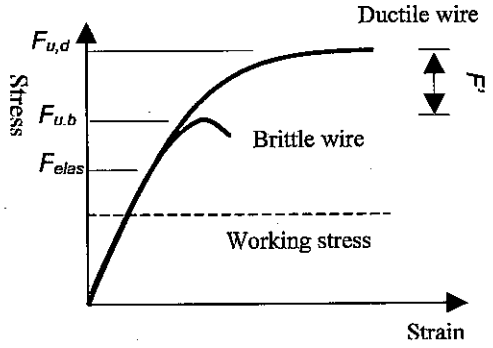

Figure 6. Schematic Stress-Strain Curve for Ductile and Brittle Wires

4.2.2 Effective Clamping Length

Even if a wire breaks at one location, tension carried by adjacent wires gradually transfers back to the broken wire by development of friction after a certain length away from the broken location. This is called effective clamping length, and usually friction is developed primarily by cable band clamping forces. Retraction measurement, cutting a wire and measuring the gap, L' at the broken ends, is used to calculate the effective clamping length, L_{eff}.

$$L_{eff} = \frac{a \cdot L'}{p} E$$

a: section area of wire, L': retraction, p: tension in wire, and E: Young's modulus of wire

Clamping length is less than the cable band spacing as long as cable bands restrain slippage. Practically speaking, it is important to maintain cable band bolts at their prescribed tension so that the cable bands hold all cable wires/strands against slippage.

A number of retraction measurements were performed for parallel wire cables. Computed effective clamping length for the Bear Mountain Bridge (1924) was 6.9m, which is approximately the cable band spacing.

For helical wire strand cables, it is expected that effects of helical winding and interlocking would develop additional friction resulting in shorter effective clamping length than parallel wire cables. Observation of in-situ wire fractures in the second layer revealed, however, that while there is high variability in the data, these retractions in the second layer correspond largely to effective clamping lengths past the first cable band on each side of a wire fracture.

Several wires were cut and measured the retractions. It is interesting to note that the initial retraction of these wires results in average effective clamping length of 1.17m (46 inches) when compared to in-situ natural fractures that result in effective clamping lengths averaging 3.66m (144inches). The in-service breaks were measured from both first- and second-layer wires, while the induced retractions were all from wires cut from the outer layer of strands. Monitoring of the cut wires is on-going to determine the relaxation rate of these induced retractions.

Table 4. Effective Clamping Length for In-Service Cracks vs. Cut Wires

Type of Wire Break	Average Clamping Length, as Measured by Retraction	Standard Deviation
In-Service Cracks	3.66m (8 samples) (10-lay length)	3.56m
Cut Wires	1.17m (7 samples) (3-lay length)	0.71m

4.2.3 Helical Wire Strand Cables

Unlike parallel wire strands, the strength of helical wire strands depends on the wire composition and lay, so it is difficult to make a precise strength model. The interior wires carry higher axial stresses. The strength reduction due to lay is approximately 10-

12%. This strength reduction is also included in cable strength evaluations mentioned above.

Axial and bending stresses of a strand made of 37 wires with 18 wires at the exterior, 12 wires at the second layer, and 6 wires at the third layer and 1 core wire, are expressed below.

$$T = (1 + 6\cos(\beta_1) + 12\cos(\beta_2) + 18\cos(\beta_3)) \cdot s_{t0}$$

$$s_{bi} = \frac{E \cdot \sin(\beta_i)^2}{n}$$

β: lay angle, s_t: tensile stress, s_b: bending stress
i: layer number (0 is core wire, 1 is third layer wires, 2 is second layer wires, and 3 is exterior wires)

Figure 5 shows load-wirebreak curves for three helical strands, approximately 60 inches long, taken from the site. All of the specimens' exterior wires are rated Stage-IV corrosion. Generally, wire breaks were not clustered in one location but dispersed at a few locations along the specimens. However the lowest strength strand showed that wires broke in a clustered area. When load reduced at approximately 10 exterior wire breaks, the test was aborted. After the tensile tests, the specimens were dismantled layer by layer to investigate the interior conditions. Test broken wires exhibited pre-existing cracks with their depths ranging from 5% to 25% of the wire diameter. It was found that 3rd layer and core wires were Stage-II to III condition, the remaining tensile strengths were 224ksi (1,546MPa) to 242ksi (1,671MPa), and the elongations were 6% to 7%, indicating no degradation in those wires.

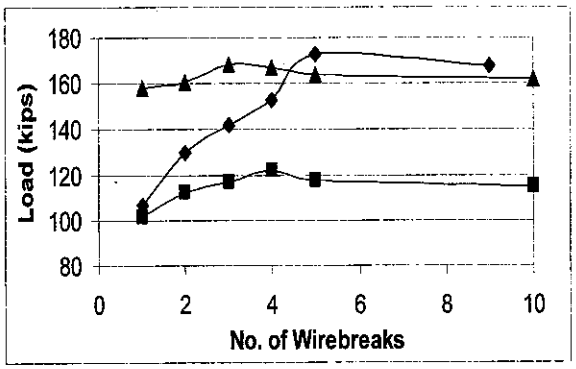

Figure 5. Load-Wirebreak Curves for 37-wire Helical Strand Specimens (Approx. 60" long Samples taken after 71 years in service)

The fracture mechanism of helical strands made of corroded/pre-cracked wires is complex. The relieved tensions carried originally by broken wires are transferred primarily within the strand, but if wire breaks in a strand are extensive, these tensions may be transferred to the remaining strands. Tension relieved by multiple wire breaks may cause the strand to slip at cable bands.

4.3 Projection of Long-term Safety

In already deteriorated cables, the safety factor decreases with time as section area loss progresses. In some situations, projecting future safety factor deterioration is of interest for scheduling a rehabilitation program. Conceptual models have been developed for predicting the remaining life of cables: "Historical Maintenance Model", "No Maintenance Model" and "Special Maintenance Model", but they are not yet practical since parameters in the models are not available in most cases. However, two major factors govern the process: the amount of sulfur and chloride in the environment, and the effectiveness of the cable protection system. Figure 6 shows future predictions of broken wires for safety evaluation. Three curves indicate three plausible situations in the future: (1) wire breaks cease due to improvements; (2) wire breaks linearly progress; or (3) wire breaks accelerate.

If past inspection records are available in order to correlate with the present condition, and if future external conditions (including maintenance) are assumed, the longevity of the cables can be estimated by using a fracture mechanics approach. Pre-existing cracks in wires develop with time and result in strength reduction according to the mechanism shown in Figure 7.

The crack propagation rate under a corrosive environment is given by the following equations, and the remaining life defined by the time from an incipient crack developing to fracture can be computed by integrating the equation. This latter approach is difficult to apply in practice, since reliable information for assessing the long-term environmental condition and its effects on galvanized steel wires is normally not readily available.

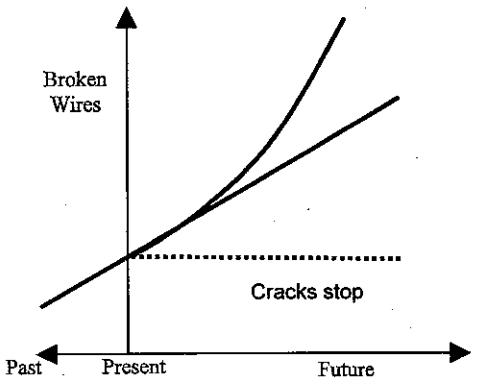

Figure 6. Schematic Future Prediction Models

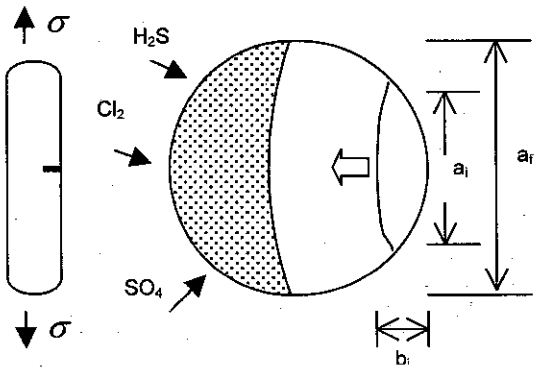

Figure 7. Crack Propagation Model

$$\frac{db}{dt} = f(K_I, Environment)$$

$$\int dt = t_0 + \int_{b_0}^{b_f} \frac{db}{f(K_I, Environment)}$$

$$K_I = \sigma\sqrt{\pi b_i} F_I(a_i / b_i, b_i / r)$$

t: time to fracture, t_0: induction period, K_I: stress intensity factor for a round bar containing a semi-elliptical surface crack under uniform tension[13] (Mode-I), σ : tensile stress due to sustained load, and F_I: shape factor as a function of crack aspect ratio

4.4 Safety Evaluation – A Case Study

A 70–year old suspension bridge main cable was taken as a case study for safety evaluation. Each cable is composed of 37 helical wire strands, and each strand is made of 37 wires with 18 exterior wires, 12 wires in the 2nd layer, 6 wires in the third layer, and one core wire. Except for the center core wire, wires are helically wound with lay angle of 5-15 degrees.

4.4.1 Cable In-Depth Inspection

The outer two circumferential rings of strands in the hexagonal arrangement generally exhibit Stage-IV corrosion, with the inner core of seven strands generally exhibiting Stage-III to Stage-IV corrosion, or occasionally Stage-II corrosion. While the degree of Stage-IV corrosion varied according to the location of the strand in the cross section, it also varied circumferentially on individual strands. Strands comprising the outer ring of the cross section generally showed less corrosion on the surface of the circumference where red lead paste had presumably protected the strand wires from corrosion. Away from the circumferential surface however, these same strands showed white corrosion product, zinc oxide, with various degrees of brown ferrous rust spotting and pitting. Strands in the outer two circumferential rings generally exhibited more ferrous corrosion in the lower half of the cable cross section. All Stage-IV strands exhibited some degree of localized pitting and wire section loss.

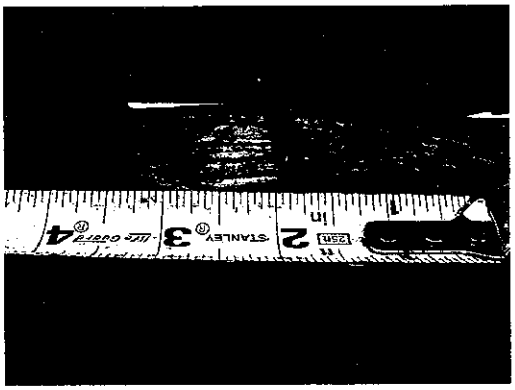

Photo 11. Multiple Wirebreaks in 2nd Layer (Exposed 3rd Layer Wires Remain Galvanized)

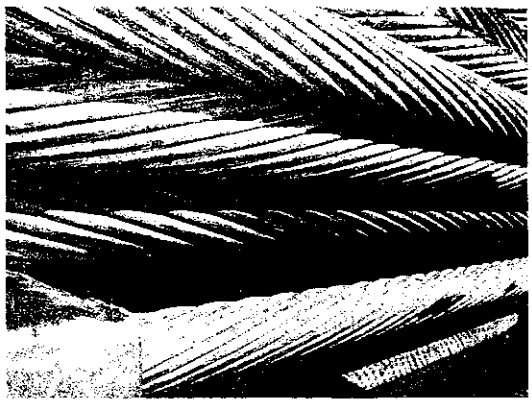

Photo 12. Contrast of Stage-II in Exterior Strands and Stage-IV in Interior Strands (Orange Color is Red Lead Paste)

The pattern of moderate to severe Stage-IV ferrous corrosion with pitting at the locations where strands are in contact with each other is typical for every strand throughout the cross section. The corrosion and pitting with section loss is more severe where strands are in contact in the horizontal plane, where corrodant accumulation was often observed. At these locations moisture is more likely to be retained and further aggravate corrosion. Each first layer wire in helical strands contacts adjacent strands in the horizontal plane, two times per lay length. The location of wire fractures correspond to clock positions at, or very near, contact points between strands.

4.4.2 Evaluation of Cable Strength

For Stage-III corrosion, where the protective zinc galvanizing layer has largely corroded to at least the zinc oxide stage, it was assumed that the zinc layer is effectively depleted, and the cross section of the wire is reduced in a corresponding manner (98% of its original area) to 215ksi (1,484 MPa). Stage-II wires were assumed to retain full original specified strength at 220ksi (1,519 MPa). Wire samples taken from broken wires in service are tested and the results are summarized in Table 5. The tensile strength performance after 61 years in service was not degraded from the original specified strength; however, the next 10-year period showed significant and accelerated deterioration.

Table 5. Tensile Strength Properties of Stage-IV Wires (ksi)

	Original (Spec.)	After 61 yrs.	Present (After 71 yrs.)	
			Ductile	Brittle
Samples		4	55	13
Min.	220	207	182	147
Max.		215	240	217
Average		211	223	187
SD		4	13	21
Ave.– 2SD		204	197	145

SD: Standard Deviation, Ductile: Wires exhibiting elongation greater than 0.6%, Brittle: Wires exhibiting elongation less than or equal to 0.6%.

Second and third layer strand wires lay in a helical pattern, while the central wires were assumed to behave essentially as parallel wires. Lay length for the outer wires was measured at the site and is approximately 15 inches (381mm). Due to the helical nature of the strands, the effective strength as a strand was reduced by approximately 12% to account for the tensile component of force in the direction of the cable.

Although no wires under tensile load were cut to compute wire retraction, a few gaps in in-situ wire fractures in the second layer were noted where first layer wire fractures afforded a window of observation while holding the second layer wires in place. While there is variability in the data for the few opportunities to observe in-situ retractions, these retractions in the second layer correspond generally to Effective Clamping Lengths past the first cable band on each side of a wire fracture. Since the Effective Clamping Length is assumed to be approximately the length between cable bands, a broken wire does not regain its load-bearing ability until past the adjacent cable band. Thus, each length of cable between cable bands is analogous to a link in a chain, and the worst safety factor computed for any cable length between bands is the governing safety factor. In a similar fashion, each first layer wire in the helical strand touches first layer wires in adjacent strands several times in its lay length, and many times between cable bands. It is these locations where first layer wires are in contact that corrosion is severe and Stage-IV pitting corrosion is observed. Therefore, the lowest breaking strength in a particular wire along its length between cable bands will be the governing wire strength.

The range of safety factors in the near future for these panel points assumes that the current Stage-III wires deteriorate to Stage-IV ductile wires, current Stage-IV ductile wires deteriorate to Stage-IV brittle wires, and current Stage-IV brittle wires deteriorate to fractured wires. This deterioration is assumed because inspection showed that ferrous corrosion, very often accompanied by moderate to severe pitting, already exists at nearly every location where strands contact each other. The nature of the in-situ fractures observed in the laboratory tests as well as the presence of micro cracks in the specimens is strong evidence that microscopic cracking is likely to be prevalent in areas where ferrous corrosion and pitting already exist, characterized by the Stage-IV brittle condition. This would lead to future brittle fractures. This was confirmed by the many tensile tests and fatigue tests that showed wire fractures at locations of pre-existing cracks.

4.4.3 Projection of Long Term Safety

In the near- to mid-future, it is anticipated that the controlling safety factor reduces to a critical level, and the safety factor erosion would occur as wire deterioration advances and the current stage IV-brittle wires break. In order to project the critical level of safety, inspection data taken at the same location in a 10-year period were used. The number of broken wires increased from 13 to 87, and the number of pitted wires increased from 480 to 552.

Assuming that newly found wire breaks resulted from the development of pre-existing cracks (with initial depth at 5% of the wire diameter) to 50% of the wire diameter in a 10-year period (at which point the wire breaks), the following equations correlate degradation in the next 10 years if the environmental effect is considered to be similar for the next 10 years. This assumption would not be valid if the cables' exposed condition showed advanced degradation due to lack of maintenance, or improvement due to a stepped-up maintenance program rehabilitation. Using fracture mechanics equations as an example, two powers of n, years to fracture, are used, 1 and 3. The crack aspect ratio, b/a was assumed as 0.4. Figure 8 shows the wirebreaks with time for different values of n. In this calculation, tensile stress in wires was changed as fracture increased with time.

$$T = C\sum_{0.1r}^{1.0r} \frac{\Delta b}{(\sigma\sqrt{\pi b_i}F_I)^n}$$

$$T_i = C\sum_{0.1r_i}^{1.0r} \frac{\Delta b}{(\sigma_{i+1}\sqrt{\pi b_i}F_I(b_i/a_i, b_i/r))^n}$$

The estimated times for wirebreak varied significantly between two powers, and further study is required to increase the accuracy. Further study would include investigating the degree of decay in the wire coating with time, and slope of stress intensity factor, threshold stress intensity factor, K_{ISCC}, and threshold fatigue stress range. In addition, effort should be expended to ensure the reliability of inspection/rating data.

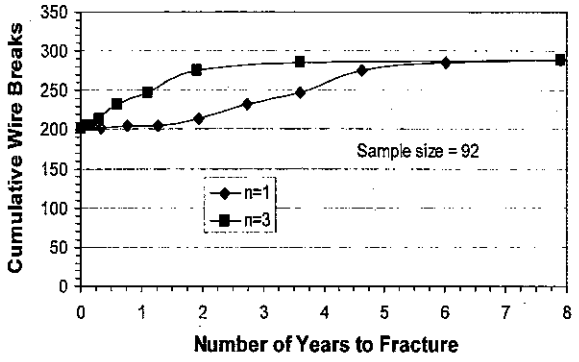

Figure 8. Projection of Wirebreaks

5. Acoustic Monitoring for Detecting Wire Breakage

Several aging suspension bridges in the U.S. have already exhibited a number of wire breaks in their main cables. In such a situation, it is important to maintain the cables in a condition that alleviates further deterioration, but at the same time, it is also prudent to provide a monitoring system to detect abnormalities and continuous information that provides another perspective on the aging cables.

Acoustic monitoring detects the release of strain energy associated with a wirebreak. An array of sensors that can detect energy release is installed along the main cable. The energy release from a wire break causes high frequency vibrations, and the sensors contain a piezoelectric device that creates a voltage from the vibration. The voltage is sent to a data acquisition system for analysis. By analyzing the signal, various characteristics can be determined about specific acoustic events. These characteristics have been used to establish criteria to identify wire breaks amidst the typical ongoing ambient noise. The data are filtered for noise and the final results show the locations and occurrence of wire breaks as real time information.

Up to today, a number of bridges have used this technique: Bear Mountain[14], Bronx-Whitestone, George Washington and Waldo-Hancock bridges. In the Bear Mountain Bridge in February 2001, an array of acoustic sensors (Photo 13 and Figure 9) were installed at the backstay cables and anchorage chambers to catch acoustic emission waves from wire breaks. Figure 10 shows acoustic emissions identified as wire breaks at three locations of the backstay cable.

Photo 13. Acoustic Sensor Installed at cable band

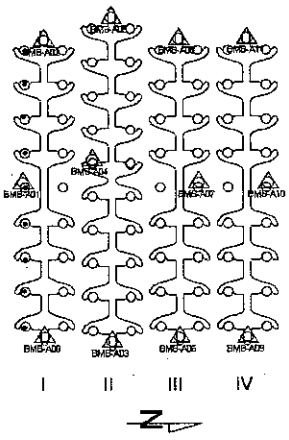

Figure 9. Acoustic Sensor Installed at Anchorage Strand Shoes

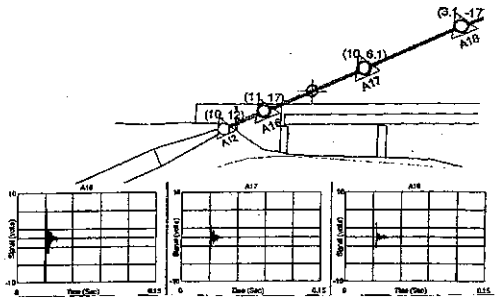

Figure 10. Indications of Wire Breakage

6. Conclusions

Many aging suspension bridges are nearing the time when rehabilitating their major components is required. New technologies have been developed to extend the life of these bridges. For this purpose, safety assessment of main cables, the critical non-redundant members of suspension bridges, are always essential. The characteristics of cables, which are composed of thousands of wires, make accurate assessment extremely difficult. Cross sections vary, some cables comprise parallel wires while others comprise shop-fabricated helical strands that make visual inspection of their interior wires impossible. Cable coatings and other protective measures vary as well, and the expense of maintaining and inspecting cables and keeping meticulous records of field observations, while of utmost importance, often seems to be a nearly insurmountable task. This paper has introduced concepts for safety evaluation of cables using practical examples. In addition, acoustic emission is shown as a useful method to monitor wire breakage to prevent progressive failure.

References

1) Roger Q. Haight et al: Cable Safety Factors For Four Suspension Bridges, Journal of Bridge Engineering, American Society of Civil Engineers, November 1997
2) The Suspension Bridge Over the River Tagus: renovation in motion 1996/1999
3) Michel Virlogeux: Replacement of the Suspension of the Tancarville Bridge
4) John Clenance, Seth Condell: Lions Gate Bridge Suspended Structure Replacement, 3rd International Suspension Bridge Operators' Conference, Kobe, 2002
5) Richard J. Fish: Tamar Bridge Strengthening & Widening – A Case Study, 2nd Suspension Bridge Operators' Conference, West Point, New York, 2000
6) V. J. Colangelo, F. A. Heiser, Analysis of Metallurgical Failures, Second Edition, John Wiley & Sons
7) R.E. Pollard: Stress-Corrosion of Bridge-Cable Wire, A.I.M.E. Symposium on Stress-Corrosion Cracking, Philadelphia, 1994

8) Peter Sluszka: Inspection and Rehabilitation of Suspension Bridge Cables
9) Theodore Hopwood II, James H. Havens: Corrosion of Cable Suspension Bridges, Research Report UKTRP-84-14, May 1984
10) Thomas H. Service, Ronald M. Latanision, Ockert J. Van Der Schijff, Carolina Molina, Ronald Mayrbaurl, Todorka Paskova: Strength Degradation, Cracking and Corrosion of Galvanized High-Strength Suspension Bridge Cable Wire, The 3rd International Suspension Bridge Operators' Conference, Kobe, May 2002
11) Yoshio Sasaki, Akira Kiuchi, Tohru Shinke, Tadahiro Minato, Ken-ichi Sugii: Fatigue Resistance Analysis of Corroded Wire, Kobe Steel Technical Report, Vol. 38, No.1, 1998
12) Gongkang Fu et al: Strength of Parallel Wire Cables for Suspension Bridges, 8th ASCE Conference on Probabilistic Mechanics and Structural Reliability, 2000
13) Y. Murakami: Stress Intensity Factors Handbook, Volume 2, Pergamon Press
14) William M. Moreau, Jamey A. Barbas: The Rehabilitation, Survey and Monitoring of the Bear Mountain Bridge, The 3rd International Suspension Bridge Operators' Conference, Kobe, May 2002
15) Robert Nickerson: Safety Appraisal of Suspension Bridge Main Cables, NCHRP Web Document 20, Project 20-01/Task 100

(Received July 31, 2003)

Progress of Research and Applications in Structural Health Monitoring of Bridges in Korea

Hyun-Moo Koh* Jinkyo F. Choo** Chul-Young Kim*** Sung-Kon Kim**** Chan-Min Park*****

* Professor, Dept. of Civil Eng., Seoul National University, Seoul, Korea
** Ph.D. Candidate, Dept. of Civil Eng., Seoul National University, Seoul, Korea
*** Professor, Dept. of Civil Eng., Myongji University, Yongin, Kyunggido, Korea
**** Professor, Dept. of Civil Eng., Seoul National University of Technology, Seoul, Korea
***** Ph.D., Senior Eng., Highway and Transportation Technology Institute, Hwasung, Kyunggido, Korea

Korea has seen active development and applications of structural health monitoring systems in the early of 1990s, especially focusing on bridge structures, since they constitute the most vulnerable part of civil transportation structures directly related to public safety. The very first application began by installing health monitoring systems in existing bridges in order to collect field data for design verification and, subsequently, to monitor long-term performance of bridges in the scope of systematic inspection and management programs. Recently, modern and integrated monitoring systems have been introduced since the design stage in newly built long-span bridges. Three main stages can be distinguished in the evolution of bridge monitoring system in Korea according to its developing stage and functionality. This paper outlines the progresses and applications of monitoring systems in Korea for both existing and newly built bridges and describes their aims and characteristics. A brief summary on dynamic field testing of seismically isolated bridges is also presented.

Key Words: structural health monitoring, bridge management system, integrated monitoring system, dynamic field test

1. Introduction

1.1 Beginning of Bridge Monitoring in Korea

In the early of 1990's Korea has seen active development and applications of structural health monitoring. Such activation could be explained partly by the deterioration of infrastructure systems built for the most part during the industrialization boom of 1970's, which often resulted in a lack of quality, and partly by the increasing recognition of potential devastating disruption of infrastructure systems due to natural hazards, i.e. typhoons and earthquakes. At the time, attention has been first focused on bridges since they constitute the very vulnerable part of civil structures affecting directly public transportation, which by extent is closely related to public safety.

During the last 3 decades following the boom of 1970's, the volume of road bridges in Korea saw a rapid increase, as shown in Fig. 1, beginning with 9,332 bridges for a total length of 268 km in 1970 to reach 20,219 bridges developing a total length of 1,685 km in 2002. The total developed length of the bridges built after 1970 multiplied by 5, while the stock only doubled, and recent erection of the Gwangan bridge, a 900 m long suspension bridge and, the Seohae bridge, a 990 m long cable-stayed bridge, spoke for the remarkable progresses and the trend to build long-span bridges in Korea. According to the construction of these new long-span bridges, interest began to grow because of their impact in the economy and road network.

In addition, the disastrous collapse in 1994 of the Sungsu bridge crossing the Han River in Seoul, only 25 years after its opening to traffic in 1979, emphasized the necessity to establish management system for bridges not only to avoid human loss but also reduce economical costs. This accident combined with the fact that a large number of bridges built before 1970 still remain in operation today led the governmental authorities to issue more stringent requirements on bridge management and operational programs, including systematic visual inspection, instrumentation, load capacity tests and field measurements for

design and construction verification, and long-term performance monitoring and assessment.

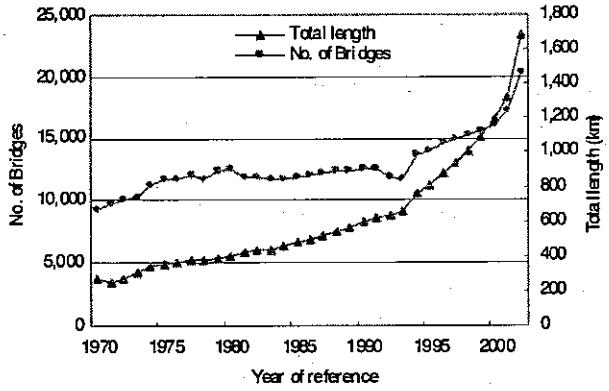

Fig. 1 Evolution of the road bridge stock in Korea[16)]

Fig. 2 summarizes the maintenance investment and health level of bridges since 1995 in Korea. "C level" stands for operational health level under normal condition. Until the mid of 1990's, focus was concentrated on the construction of bridges much more than on their maintenance. However, after the occurrence of large disasters, understanding of the importance of bridge management became a reality and maintenance began to be systematically applied to bridges. The maintenance cost decreased monotonically since 1995, which can be explained by the adoption of an organized management system that made it possible to invest rationally the costs within the budget limits and prevent large catastrophes. Another effect of this systematization of management is the remarkable improvement of the bridge's health even in a short term.

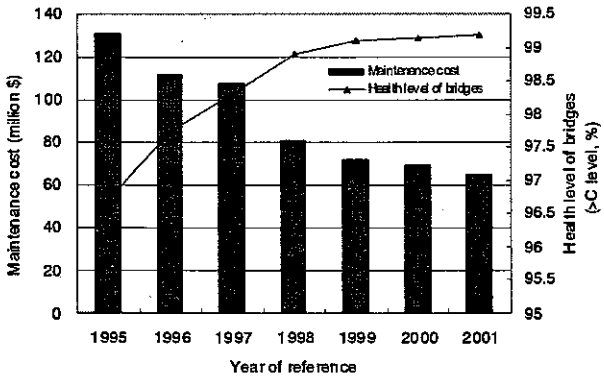

Fig. 2 Records of bridges' maintenance and health level in Korea[13)]

As shown in Fig. 3, Korea remains still far behind advanced countries, with only 8% of the construction cost invested for the rehabilitation and maintenance facilities, which represents only 14% of the investment in Italy (57.2%). Efforts should thus be done to increase such investment so as to improve the durability and functionality of facilities.

1.2 Evolution of Bridge Monitoring in Korea

In order to deploy a successful monitoring system, requirements are: proper instrumentation, reliable signal processing and knowledgeable information processing. Three main stages or generations can be distinguished in the evolution of bridge monitoring system in Korea according to its developing stage and functionality.

System corresponding to the first generation is characterized by a stand-alone field system consisting of sensors, field hardware and online signal transmission to a computer on field. In the second generation, this stand-alone evolved to an overall bridge management integrated system involving two kinds of integrations: operational integration where multiple stand-alone systems operate together and, functional integration where bridge monitoring system operates with different systems such as bridge management system or vehicle monitoring system[11)]. The third generation, also called future system, will provide advanced innovative functions like sensor fusion, reliable massive signal transmission, automated surveillance, adaptive signal processing, etc. Many research efforts toward the third generation system are actually led to develop and enhance the performance of the current system by introducing new sensing techniques, power generation from bridge vibration, web-based operating system or wireless signal transmission.

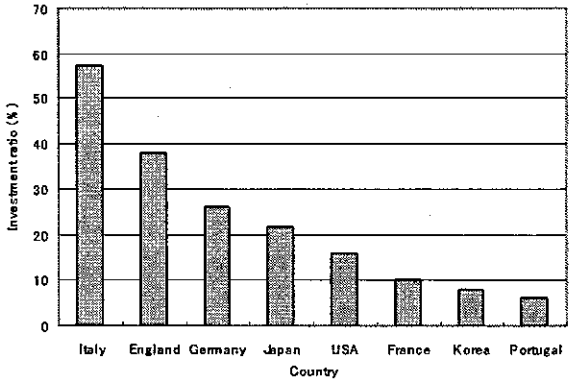

Fig. 3 Investment ratio for maintenance and rehabilitation of facilities per country[17)]

2. Bridge Management System

2.1 Bridge Management System in Korea

Total bridge management system (BMS) attempts to include inspection, evaluation, estimation and rehabilitation of bridges in a systemized organization, which integrates structural health monitoring systems installed in bridges. BMS is an information-oriented system, which aims the global supervision of all the information gathered in every bridge so as to help the supervisor deciding the requirements for the current and future management and rehabilitation of bridges using optimal methods. To perform a scientific and rational management and rehabilitation of bridges, the Korean Ministry of Construction and Transportation (MOCT) developed such system in 1995, which is actually operating for the road bridge network.

The development of BMS in Korea began in the late of 1980, a little bit later than USA and nearly simultaneously with Japan and Europe. However, facing a series of trial-and-errors, the Korea Institute of Construction Technology (KICT) started concretely the development of the Korean BMS (KOBMS) for ordinary road bridges in 1995[13].

The hardware of KOBMS is constituted by regional networks and, high-performance and high-capacity computers to manage efficiently the huge volume of data. Such network, being built in 1996, operates interactively by linking the KICT, road facilities of the MOCT, 5 regional offices, 1 R&D office, and 18 road management offices.

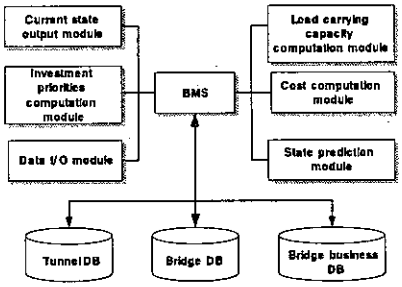

Fig. 4 Composition of the KOBMS

The software of the KOBMS is composed by a database (DB) recording archives related to bridges, a program computing the investment priorities, a rehabilitation and retrofit techniques DB, a tunnel DB, a program outputting the current state of bridges, a decision-making system performing the essential functions of the BMS, etc (Fig. 4). The BMS DB stores and compiles about 230 items per bridge, such as parameters of bridges, crossings, structures, bridge inspection, load carrying capacity, etc.

The investment priorities, as a basic function of the BMS, stand for the process by which one decides the bridge to be considered at first for the budget established annually in order to perform management and rehabilitation of the bridges. The external appearance, safety, functionality and serviceability of the bridge are considered in the investment priorities algorithm.

64 basic rehabilitation and retrofit techniques for bridge have been arranged in the KOBMS database after examination of the most utilized techniques. And, 120 types of damage that may occur in bridge have been defined and correspondence between each of these damage types and basic techniques has been established. The DB is thus able to select automatically rehabilitation and retrofit technique appropriate to the damage that has been occurred.

Based on the KOBMS DB, a report on the current state of the bridges is published annually and, provides statistics of the basic parameters of the bridges and their current state according to their classification, i.e. expressway, highway, metropolitan, provincial and county roads.

The decision-making system for rehabilitation and management of bridges aims the selection of measures to take to improve the performance of each bridge with maximum profit according to the limitation of personal and material resources. As a result, future state of the bridge could be predicted, maintenance measures and corresponding costs could be computed, and appropriate countermeasures for each bridge could be computed for an optimal cost-effectiveness of the investment for the whole bridge stock.

2.2 Results and prospects of the KOBMS

The introduction of BMS made it possible to manage efficiently the huge volume of bridge data. These data stored and processed in various forms, are exploited effectively in management and maintenance tasks. Moreover, systematization of state evaluation and records management of rehabilitation and retrofit for each bridge as well as for the whole bridge stock has been realized. The state of bridges has seen significant improvement while large reduction of the budget invested for their management, being rationally shared, has been obtained.

On the other hand, even if the KOBMS selects optimal maintenance measures for the whole bridge stock, it does not mean optimal measures for individual bridges. Therefore, developing a project level BMS that reflects the characteristics and conditions of each individual bridge should be performed. An expert system considering the severity and range of damage occurring in bridges should also be introduced.

3. Health Monitoring Systems for Existing Bridges

Health monitoring systems in Korea at the very beginning were installed in existing bridges in order to collect field data by full scale load capacity tests for design verification and, subsequently, evaluate the health of the structure. Immediately after the collapse of the Sungsu bridge, this first generation of monitoring systems has been applied in existing bridges of which two representative examples, the Namhae and Jindo bridges, are described hereafter.

3.1 The Namhae bridge

The Namhae bridge (Fig. 5), the first suspension bridge built in Korea, opened to traffic in 1973. It is three-span suspension bridge (128 m + 404 m + 128 m). The main cables are made of parallel wires and the stiffening system consists of a welded steel box with an orthotropic steel deck.

At the time of its design, the load carrying capacity prescribed in the code was quite smaller than the current one. A long period of service along with excessive vehicle weights resulted in defects such as fatigue cracks at welding and corrosion of steel members. Resulting from the safety evaluation performed in 1993[15], short-term strengthening and rehabilitation have been carried out and a long-term maintenance and health monitoring project has been scheduled to extend service life and prevent further loss of load carrying capacity.

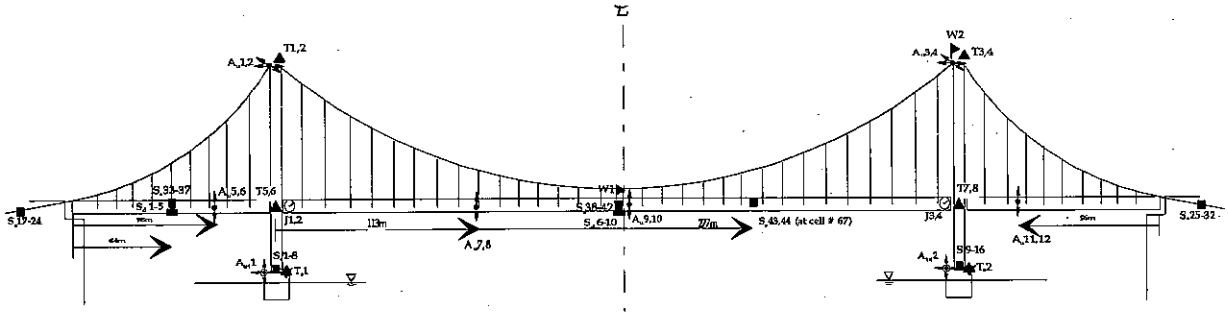

Fig. 6 Location of sensors in the Namhae bridge

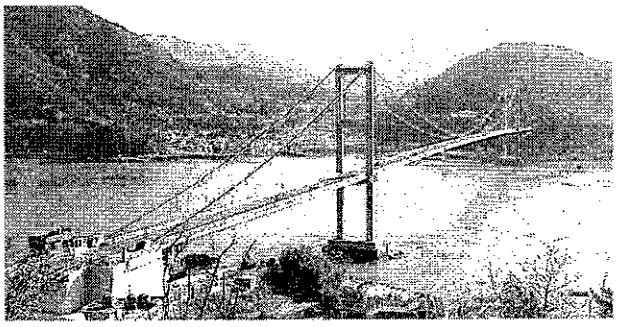

Fig. 5 The Namhae bridge

Table 1. Sensors installed in the Namhae bridge

Sensor		Q'ty	Characteristics
Static	Tiltmeter	10	Electrolytic biaxial
	Strain gage	44	Vibrating wire
	Data logger	2	Modem
Dynamic	Accelerometer	12	Force balanced*
	Strain gage	10	Electric resistance
	Accelerometer	2	Force balanced**
	Jointmeter	4	LVDT
	Anemometer	2	3D-propeller
	DAQ system	2	GPS system

* Uni-axial, ** Tri-axial

According to the project, the initial status of the bridge prior to logging the long-term behavior by health monitoring system has been evaluated by geometric survey, static loading test[3] and ambient vibration test[7]. After evaluation of the initial status, the health monitoring system has been installed in the bridge. Fig. 6 illustrates the location of the sensors and their specifications are listed in Table 1.

Measured modal parameters being frequently used to evaluate the current status of bridge structures, an ambient vibration test (AVT) was carried out in 1999, avoiding high cost and traffic control that occur when using artificial vibration exciter. The whole acquisition of measured vibration data on the bridge took almost 2 weeks. A few natural frequencies were found by simple impact test, and the monitoring system was also used to evaluate the effect of thermal variation on the change of the fundamental frequencies during 9 months[8].

Impact test appeared to be adaptable if only lower bending modes were of interest and traffic-induced vibration was found to be utilizable for this type of bridge. In addition, it was shown that when dynamic properties obtained from measured data were used to assess damage, variation of factors such as temperature should be considered.

3.2 The Jindo bridge

The Jindo bridge (Fig. 7), a three-span (70 m + 344 m + 70 m) semi-harp type cable-stayed bridge completed in May 1984, is another example of health monitoring system installed in existing bridge.

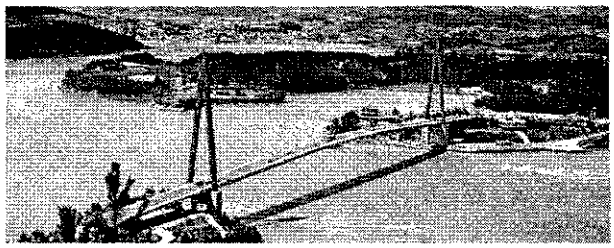

Fig. 7 The Jindo bridge

Table 2. Sensors installed in the Jindo bridge

Sensor	Q'ty	Location
Tiltmeter	6	Pylon
Accelerometer	20	Steel girder, pylon
Strain gage	49	PC slab, steel girder
Laser disp. Sensor	1	PY1, mid span
Joint meter	2	P39, P42
Cable tension	24	Stay cable
Anemometer	2	PY1 top, mid span
Thermocouple	14	Girder, pylon, air, cable
Seismometer	2	PY1, PY2 base
BWIM sensor	6	Asphalt pavement

An AVT for the Jindo bridge was carried out in 1998. Mode shapes as well as natural frequencies were found to give a more precise description of the current bridge state. During the AVT, the acquisition was carried out without traffic restriction, and the dynamic properties were computed from these ambient vibrations under normal traffic. With 6 accelerometers, a couple of weeks were needed to acquire all the vibration data[8].

Similarly to the Namhae bridge, though the traffic-induced vibration was used, very smooth and reasonable spectrums that contain negligible noise were obtained. Finally, 26 natural frequencies and corresponding 16 mode shapes were found by AVT. No significant noise was found on the mode shapes, allowing conclusion that traffic-induced vibration could be used

for this type of bridge since the mass of traffic is relatively small compared with that of the structure and the traffic could excite the structure with enough energy in the frequency band of interest. Such results are believed to provide a precious reference for future monitoring.

4. Health Monitoring Systems for New Bridges

Unlike the first generation, the second generation of health monitoring systems exploits modern technologies in order to monitor long-term performance and durability of the bridges in the scope of systematic inspection and maintenance programs. This second generation of health monitoring system has been applied to newly built bridges since their design stage as illustrated through representative examples.

More recently, efforts tending to increase and upgrade the monitoring efficiency and performance of the second generation, that is sensor based bridge monitoring systems (SBBMS), have also been introduced effectively in newly built bridges.

4.1 Integrated health monitoring systems

The majority of the long-span bridges newly built in Korea are equipped with modern monitoring systems. Unlike earlier applications of health monitoring systems installed in existing bridges, where conventional sensors, loggers and transmission methods were used and individual systems served each bridge independently, recent systems adopted in new bridges employ modern technologies from sensing to processing, i.e. many sensors and data acquisition systems that measure the behavior of the bridge during its construction become part of the long-term health monitoring system. Specifically, monitoring systems installed in highway bridges are integrated into a total BMS including the inspection, evaluation, estimation and rehabilitation.

An attempt to integrate health monitoring systems of several bridges together has been achieved to reduce the total cost and increase significantly the management efficiency management. This integrated system includes BMS as well for inspection, estimation and rehabilitation. The integrated system for the Seohae, Youngjong and Banghwa bridges may be cited as the best example of the current monitoring and BMS's trend. The data collected at each bridge is processed exclusively at each field station for real-time monitoring and alarming the sudden abnormal behavior. But data that is useful for long-term evaluation of bridge condition, as well as periodical inspection data, can be transmitted through high-speed internet line to the management center located far from the site (Fig. 9). Once data are collected at the center, integrated BMS (Fig. 10) handles them to classify, store and retrieve.

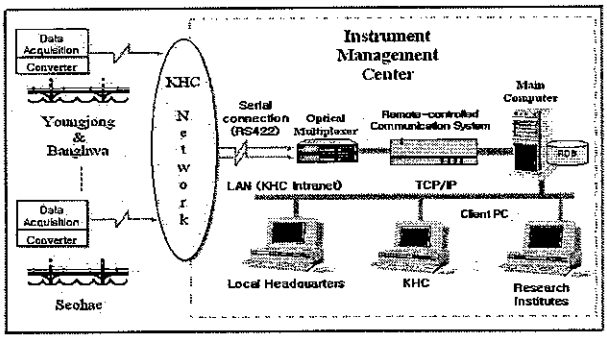

Fig. 9 Integrated Operating System

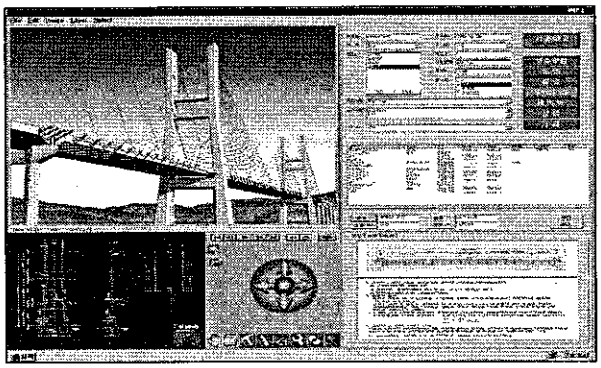

Fig. 10 Functional Integration with BMS

This integrated BMS is able to itemize bridge maintenance details, not only physical information but also knowledge. And, based on the inspection results, it may manage status assessment, rating, repair and strengthening history.

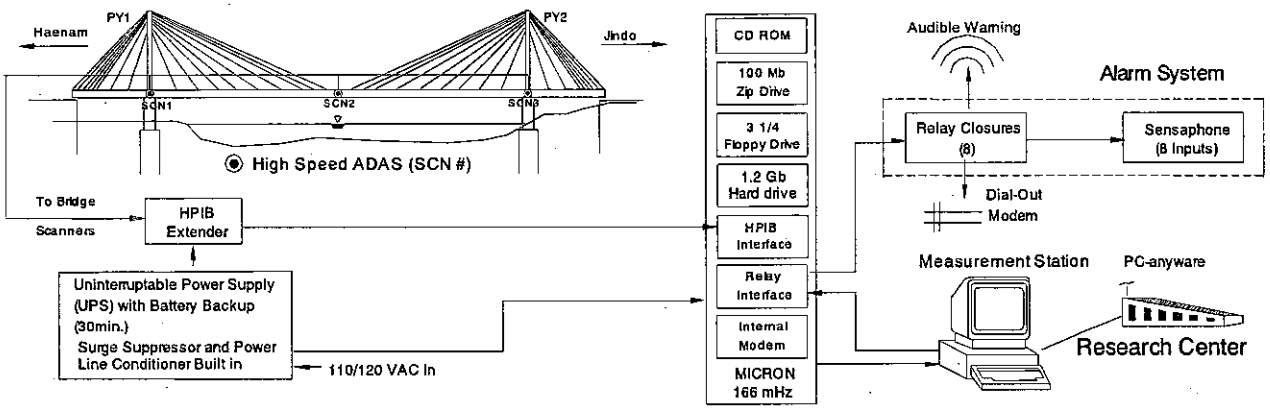

Fig. 8 Conceptual diagram of the health monitoring system installed in the Jindo bridge

4.2 The Seohae bridge

As the longest cable-stayed bridge in Korea, the Seohae bridge (Fig. 11) has been constructed in 2000 to link Pyongtaek and Dangjin by crossing the Asan bay. The bridge has a total length of 990 m with five spans (60 m + 200 m + 470 m + 200 m + 60 m) of stiffened steel girders with precast slab. The main cable-stayed span (470 m) and the two side spans are connected at the tower locations.

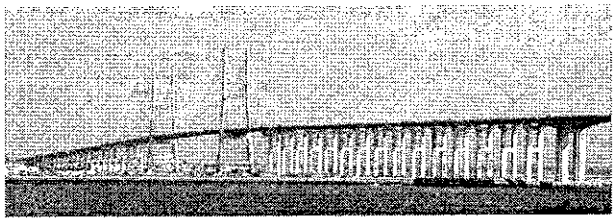

Fig. 11 The Seohae bridge

More than 10 types of sensors for a total of 180 units are actually installed in the principal parts of the cable-stayed bridge, PSM and FCM bridges of the Seohae bridge (Table 3, Fig. 12). The signals collected by these sensors are transmitted in real time to the main server via optical or wireless data logger. The cable-stayed bridge itself has a total of 111 sensors, which collect data every 10 minutes in case of static measurement and, compute representative values (maximum, minimum, average) from the 100 data recorded every second in case of dynamic measurement. The actual behavior of the cable-stayed bridge has been analyzed by means of measured data gathered during 2 years after its completion[12].

Table 3. Sensors installed in the Seohae bridge

Sign	Sensor	Q'ty
◑	Anemometer	2
●	Cable tension force (accel.)	12 @ 2
▲	Accelerometer (deck)	6
△	Accelerometer (tower)	4
▮	Tiltmeter	6
▬	Thermometer	14
⊡	Static strain gage	12
▣	Dynamic strain gage	82
⬍	Laser disp. sensor	4
▶◀	Jointmeter	10
◆	Field control box	4
■	Accelerometer for earthquake	2

On the basis of these 2 years' data, the following observations have been obtained. The variation of vertical displacement in the stiffening girder ranged from -320 to 30 mm, which satisfies the allowable design limit and, its daily variation due to thermal and live loads averages 119.3 mm with a maximum of 216 mm, which represents only 25 % of the design limits. As illustrated in Fig. 13 depicting the monthly variation of stress range in the stiffening girder, the range of the stress in the stiffening girder due to live loads showed good correlation with the actual traffic volume monitored during these 2 years and, as it represents only 5 to 12 % of the design stress, it appeared that the stress margin of the member is still considerable. According to such observation, it can be affirmed that designing long-span cable-stayed bridges based on the ordinary highway bridge design specifications may result in excessively conservative structures. Measurement data obtained through systematic health monitoring may thus constitute a very precious material that may be utilized in the future to draw out design specifications adapted to long-span bridges. Resulting from the analysis of data, the deformations of the bridge deck and tower due to thermal variations are also shown to correspond accurately with theoretical estimations (Fig. 14). An essential parameter in the management of cable-stayed bridges is the cable tensioning. Data showed that the tensioning force ranged within 95 to 104 % of the initial value, attesting for the stability of the bridge.

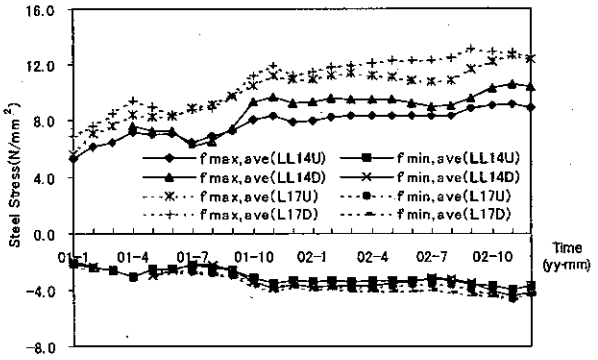

Fig. 13 Monthly variation of stress range in the lower stiffening girder flange of the Seohae bridge

A synthesis of all these results makes it possible to conclude that the actual behavior of the Seohae bridge is healthy. However, much more data are required to analyze correctly the behavior of the bridge subjected to long-term actions such as creep and thermal effect and to manage more efficient maintenance. To reach such goal, the monitoring system operates continuously so as to provide reliable database.

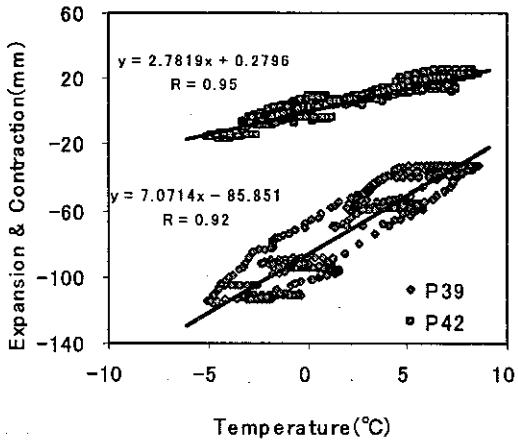

Fig. 14 Comparison between measured and theoretical thermal deformations at the extremities of the Seohae bridge

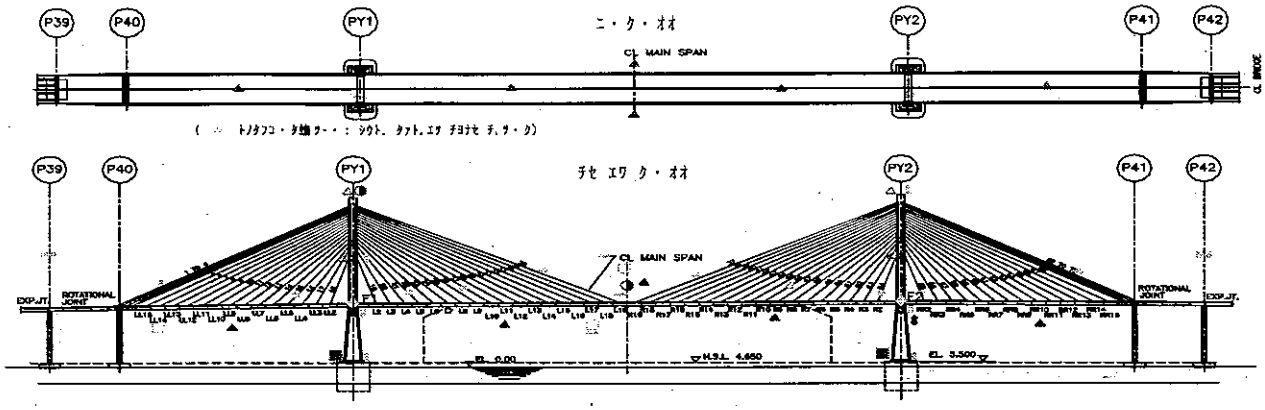

Fig. 12 Location of sensors in the Seohae bridge

4.3 The Youngjong bridge

The Youngjong bridge (Fig. 15) is a self-anchored suspension bridge (125 m + 300 m + 125 m) with a double-deck warren truss girder carrying both railway and roadway. A total of 380 sensors, listed in Table 4, were planned to be installed at locations shown in Fig. 16.

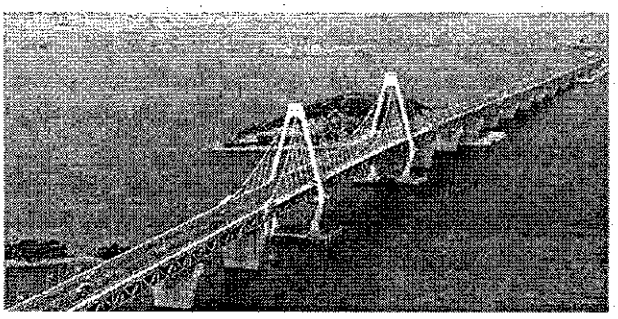

Fig. 15 The Youngjong bridge

Vibration tests were performed after the pavement, using two vibrators (Fig. 17) to investigate the vibration characteristics of the bridge. The two vibrators generated flexural and torsional vibrations of the bridge. The measured dynamic properties, such as natural frequencies, vibration modes, and damping ratios were compared with design values.

Table 4. Sensors installed in the Youngjong bridge

Sign	Sensor	Q'ty	Location
●	Thermometer	33	Cable, member, tower
==	Static strain gauge	122	Anchor, deck cross-section, link shoe
▬	Dyn. strain gauge	175	Deck cross section, etc.
◆	2D tiltmeter	10	Tower inclination
■	1D accelerometer	12	Cable
◘	2D accelerometer	14	Tower top, deck
□	3D accelerometer	3	Tower foundation
○	Anemometer	4	
×	Laser disp. sensor	3	
⬟	Potentiometer	4	Expansion joint
SL	Static data logger	2	
DL	Dyn. data logger	2	

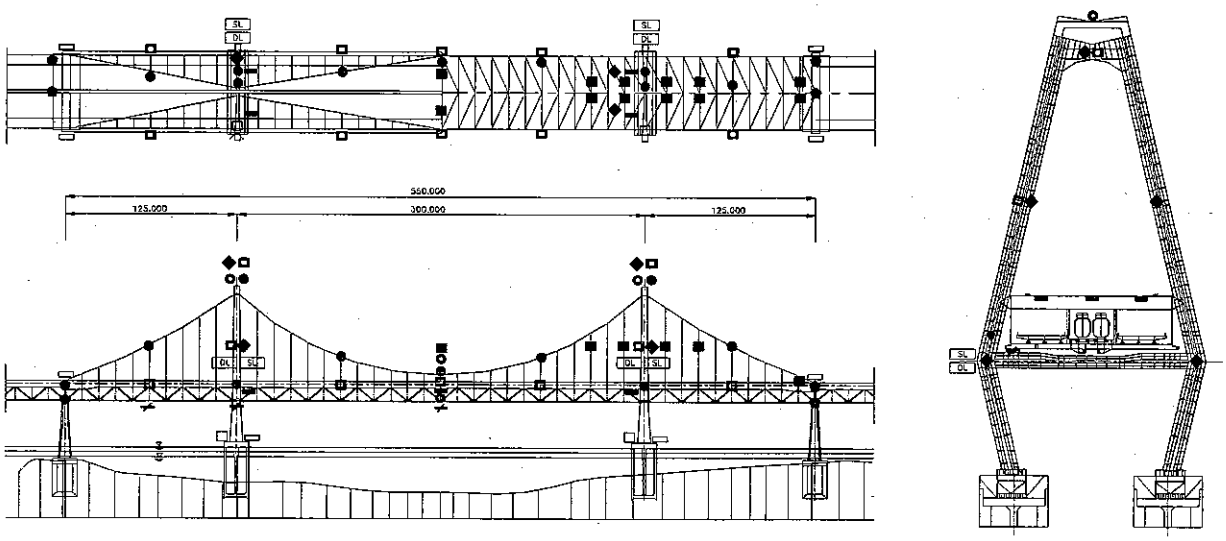

Fig. 16 Location of sensors in the Youngjong bridge

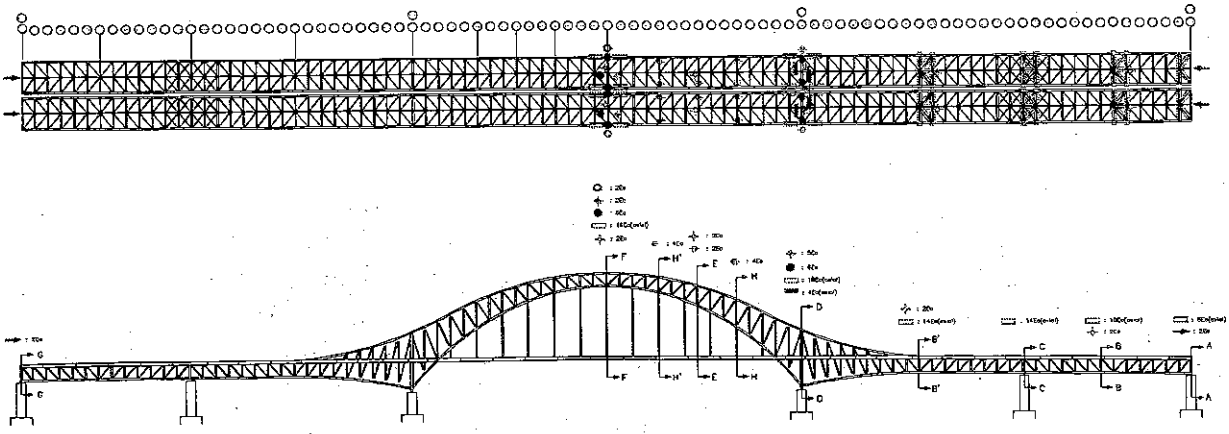

Fig. 19 Location of sensors in the Banghwa bridge

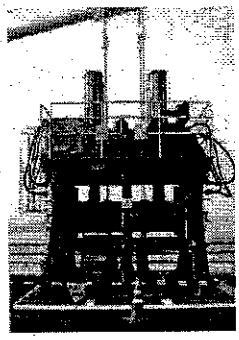

Fig. 17 Vibrator installed on the Youngjong bridge

Table 5. Sensors installed in the Banghwa bridge

Sign	Sensor	Q'ty
●	Thermometer	12
==	Static strain gage	82
▬	Dynamic Strain Gage	4
⊕	2-D Accelerometer	8
⊟	1-D Tiltmeter	10
⋕	2-D Tiltmeter	7
➔	Longitudinal Disp. Transducer	4
○	Anemometer	2

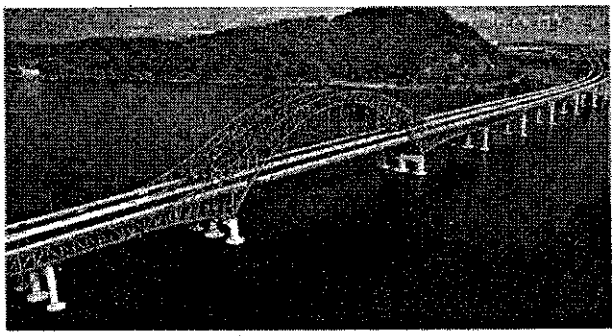

Fig. 18 The Banghwa bridge

4.4 The Banghwa bridge

The Banghwa bridge (Fig. 18), opened to the public in 2000, is an important bridge crossing the Han River and leading to the Incheon International Airport Expressway. Even though it spans 2,559 m to cross the river, the main bridge is a balanced arch-truss of 540 m. The monitoring system of the bridge includes the sensors listed in Table 5 and installed at the locations shown in Fig. 19. This system is managed together with the system of the Youngjong bridge by the same authority.

4.5 The Gwangan bridge

Recently, sensor based bridge monitoring systems (SBBMS)[5] have been proposed and effectively applied on newly built bridges to increase the monitoring efficiency and performance of the second generation by exploiting new sensor technologies. One of such applications is the health monitoring system for the Gwangan bridge.

The Gwangan bridge (Fig. 20), the central part of Gwangan principal road, is located in front of Gwangan town beach and is the longest suspension bridge in Korea with its 900m overall length. It is an earth-anchored suspension bridge with a double-deck warren truss girder carrying roadways. The pylon is a steel tower where the main cable is sustained with its stiffening girder at 105 m height.

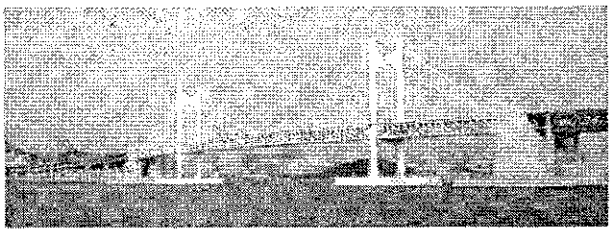

Fig. 20 The Gwangan bridge

The health monitoring hardware system for the management of the Gwangan bridge has been designed to perform real time monitoring of the bridge structural behavior. Composed by dynamic monitoring instruments like laser displacement sensor, anemometer, accelerometer, and by static sensors such as tilt meter, thermometer, and joint meter, the monitoring system processes signals, analyzes data and stores the data acquired from the sensors in the Monitoring Center. Fig. 21 illustrates the location of the measurement instrumental devices and their specifications are listed in Table 6.

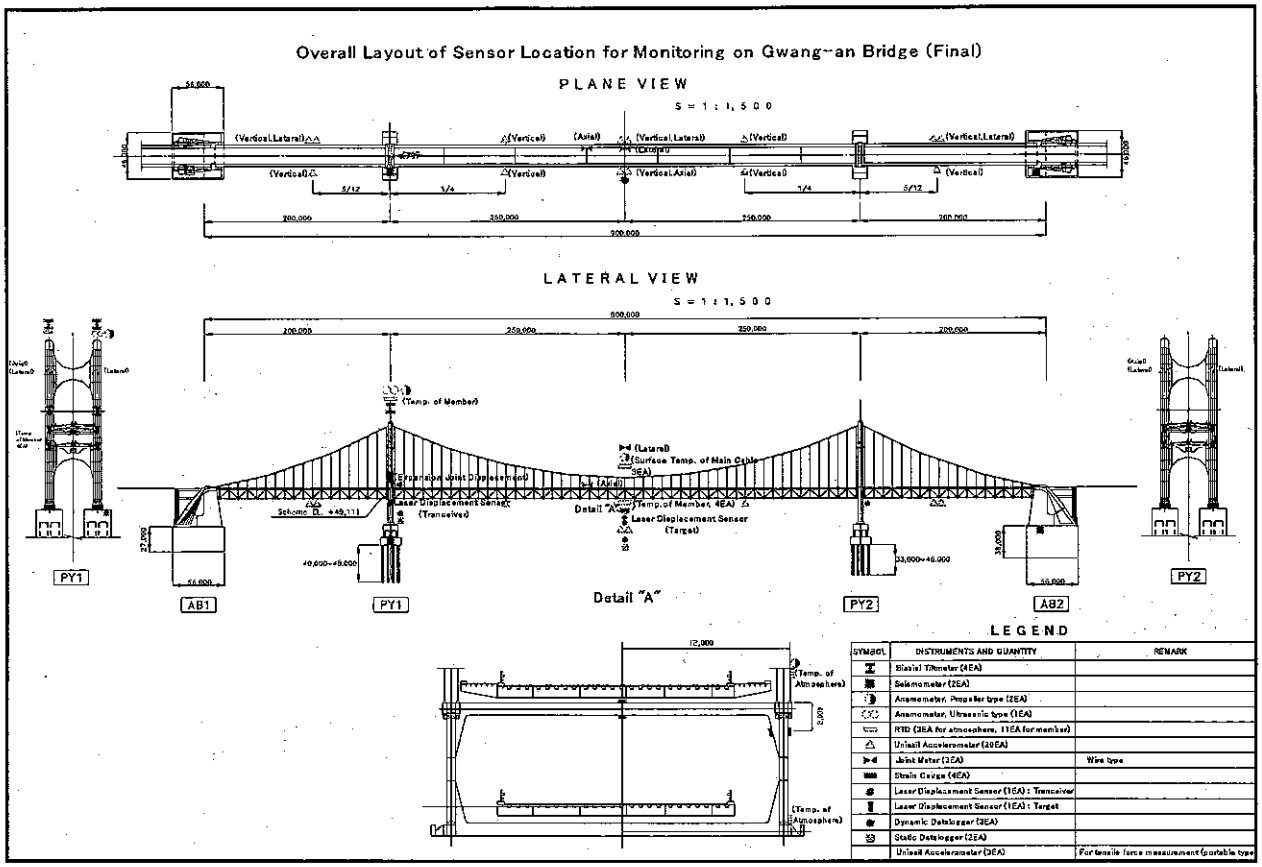

Fig. 21 Location of sensors in the Gwangan bridge

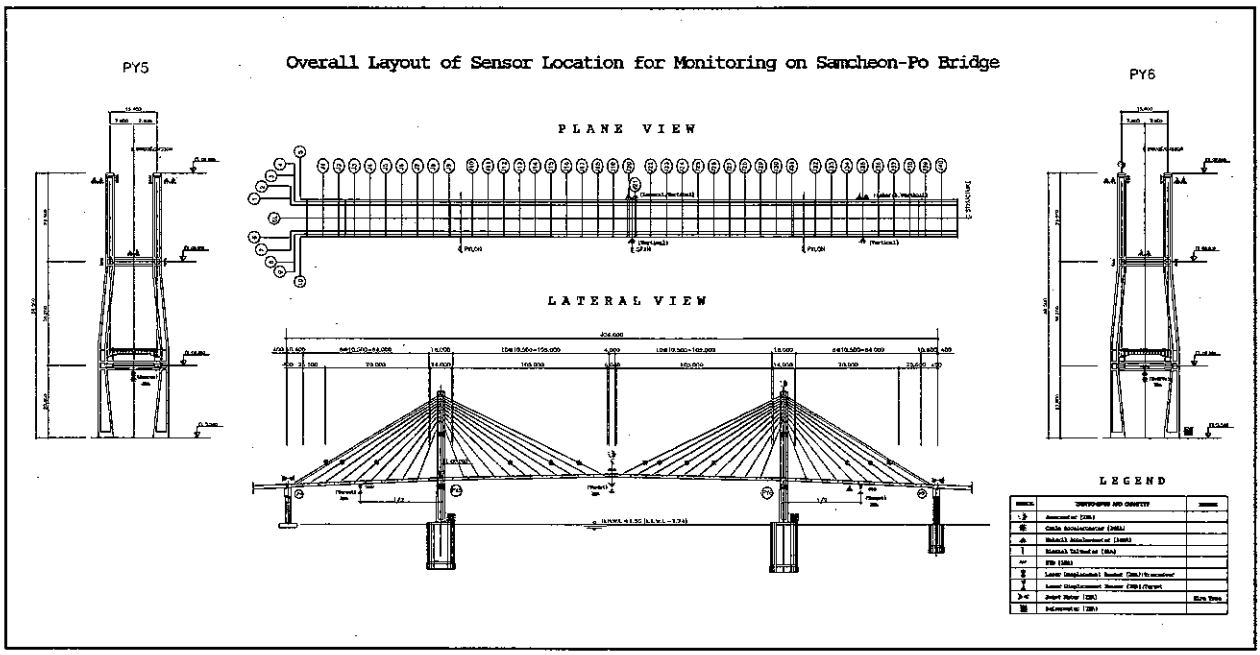

Fig. 23 Location of sensors in the Samcheonpo bridge

4.6 The Samcheonpo bridge

The Samcheonpo bridge (Fig. 22), located in the Hallyeo maritime national park and opened to the public in April 2003, has been constructed to connect Sacheon city and Changsun island. It is a 436 m long three-span (103 m + 230 m + 103 m) cable-stayed bridge with composite girder.

The health monitoring hardware system for the management of the Samcheonpo bridge is similar to the Gwangan bridge. Fig. 23 depicts the location of the measurement instrumental devices and their specifications are listed in Table 7.

Table 6. Sensors installed in the Gwangan bridge

Sign	Sensor	Q'ty	Location
◑	Anemometer	3**	PY1, mid-span
□	Thermometer	14*	Truss, PY1, cable, air
■	Seismometer	2**	PY1, AB2
●	Laser disp. sensor	1**	Mid-span
I	Tiltmeter	4*	PY1
▶◀	Jointmeter	3*	Exp. joint, shoe
—	Strain gauge	4**	Truss,
△	Accelerometer	20**	PY1, PY2, truss

* Static, ** Dynamic

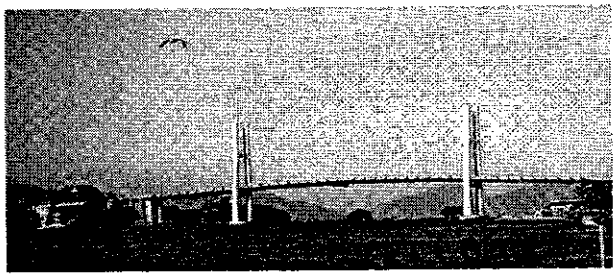

Fig. 22 The Samcheonpo bridge

5. Ongoing Researches and Future Systems

Ongoing research efforts are led to improve monitoring system performances in various domains: innovated sensor system using fiber optics, exclusively bridge monitoring-oriented compact data acquisition system, web-based signal processing, etc. Since sensor systems deal with the raw data obtained from the real bridge structure at the first stage of processing, sensor technology arises as critical for enhancing performance of the system. For the future system purposes, numerous researches applied new innovative sensory devices and new sensing technologies in order to meet them.

Table 7. Sensors installed in the Samcheonpo bridge

Sign	Sensor	Q'ty	Location
◑	Anemometer	2**	PY5, PY6
—	Thermometer	5*	Girder, PY5, PY6
■	Seismometer	2**	PY5, PY6
I	Laser disp. sensor	3**	Side-span, mid-span
I	Tiltmeter	8*	PY5, PY6
▶◀	Jointmeter	2*	P4 exp., P7 exp.
●	Cable tension (accelerometer)	26**	Cables
▲	Accelerometer	18**	PY5, PY6, girder

* Static, ** Dynamic

Due to a number of potential advantages compared to other sensors including immunity to electromagnetic interference, ability of multiplexing, ability to sense a variety of physical parameters, and ease of installation via embedding or surface mounting, optic fibers with laser have emerged with strong potential to support the future system.

Recently, fiber optics application effort has been performed (Fig. 24) to a concrete beam retrofitted by composite patches to detect peel-out effect by monitoring strain differences between main beam and retrofitting materials. Results revealed the possibilities of optical fiber sensor to detect strain differences in retrofitted structures.

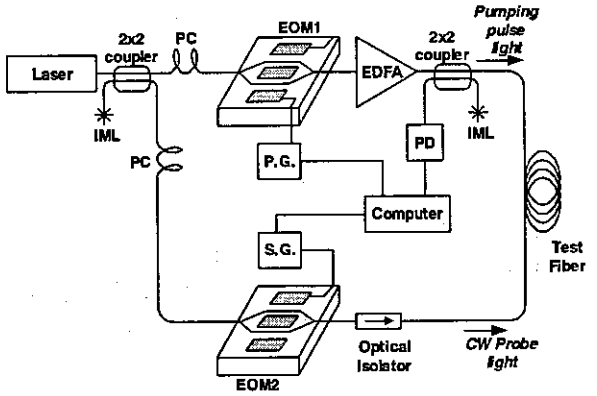

Fig. 24 Bragg Grating FO

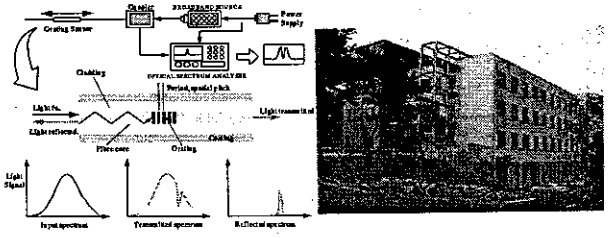

Figure 25. BOTDA

Temperature distribution on large structure can be measured by embedded fiber optic sensors[14]. A fiber optic BOTDA (Brillouin Optical Time Domain Analysis) sensor system has been mounted in a building during its construction for a feasibility study (Fig. 25). This sensor network system was able to measure accurately the temperature changes normally up to 4 degree through one day.

6. Dynamic Field Testing of Seismically Isolated Bridges

The dynamic field test of seismically isolated bridge will be performed for the first time in Korea. The objectives of the test may be seen in the scope of health monitoring of existing bridges mentioned in chapter 3, to acquire the dynamic properties of the tested bridge, evaluate its current health condition, and verify the proposed seismic isolation design of bridge.

Design criteria of seismic isolators based on lifecycle cost (LCC)-effectiveness have been proposed considering the characteristics of low to moderate seismic region like Korea. Ensuring the reliability of such designed isolators via experimental verification, the aim is to propose a new design concept for seismically isolated bridges adapted to the seismic characteristics of Korea and different from the one used in regions representing strong seismic activities.

The bridges selected for the test are the West Busan IC bridge (Fig. 26), scheduled to be demolished in 2003, and the Namhan River bridge (Fig. 27), which is now out of service and reserved as a bypass for emergency .

The West Busan IC bridge is a 3-span (17.5 m + 35 m + 17.5 m) continuous plate girder bridge with a 6 m high rahmen substructure. Built in 1981, the bridge being non-seismically designed, the bearings of the bridge should be replaced by seismic isolators for the test. Two types of seismic isolators, a lead-rubber type bearing (LRB, Fig. 28) and a friction type pot-bearing (FPB, Fig. 29), optimally designed according to the LCC concept have been manufactured. The tests will be performed with both types of isolators installed consecutively in the bridges.

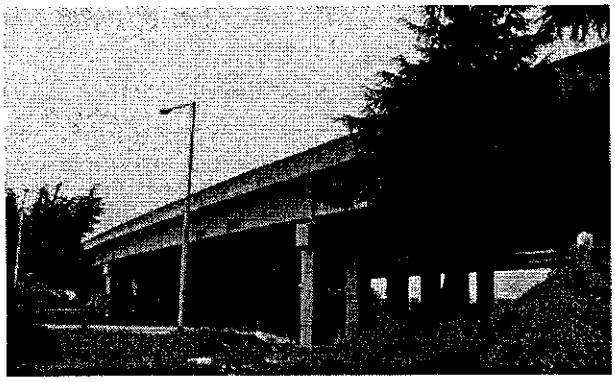

Fig. 26 The West Busan IC bridge

Completed in 1971, the Namhan River bridge is a 18-span PSC I bridge with 5 girders and averaging a total length of 540 m (6 × 3 @ 30 m). The span length being 30 m long, it shows a maximum of 3 continuous spans. The T-shape piers are divided for a part on ground and for the other part in the riverbed, and their heights range from 8 to 11 m. Similarly to the West Busan IC bridge, the bearings of the bridge will be replaced by seismic isolators for the test.

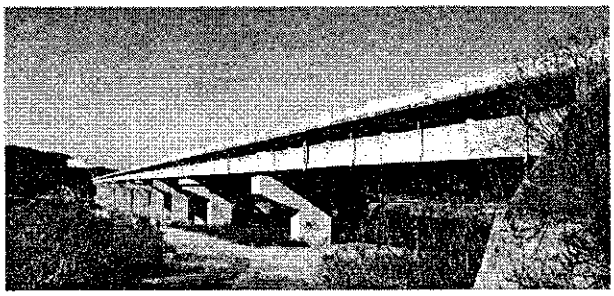

Fig. 27 The Namhan River bridge

The dynamic test to be performed is a quick-release test, which proceeds by first imposing initial displacement in the longitudinal direction to the bridge's superstructure using hydraulic jacks and, after quick release of the jacks, authorizing free vibration of the bridge equipped with seismic isolators. The quick release devices have been manufactured with a capacity decided according to the tested bridges (Fig. 30). According to the imposed initial displacement, both low and high level tests will be achieved for both types of seismic isolators.

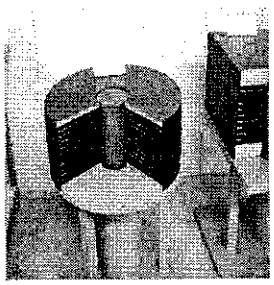

Fig. 28 LRB

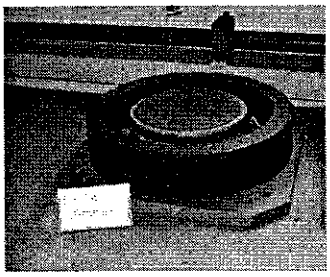

Fig. 29 FPB

Low level test is to evaluate and verify the dynamic properties corresponding to the elastic behavior of the bridge. The piers behave elastically and initial displacement is imposed to the isolator to reach its yield displacement. High level test is to evaluate and verify the nonlinear properties of the isolator. Therefore, the initial displacement is imposed so as to provoke nonlinear behavior of the isolator. Such displacement depends on the capacity of the quick release devices, the restoring of the bridge, and field conditions. At this stage, the imposed initial displacement has been preliminary decided to 2/3 of the isolator's design displacement.

Processing of experimental data will be achieved by system identification (SI) techniques in order to evaluate the dynamic properties of the seismic isolator. Thereafter, reliability of the numerical model used for the LCC concept design will be evaluated. The evaluation of dynamic properties of the bridge model will be performed using the experimental data measured during the quick release tests, and the measurements of the isolators' response under ambient vibration. Numerical simulations using three-dimensional FEM modeling of bridges (Fig. 31) have been now almost completed before the actual field testing. Future testing results will be used to verify the adequacy of the proposed LCC design concept for isolators in low to moderate seismic areas. In addition, monitoring of experimental results is also believed to provide us dynamic properties of the tested bridges and enable us to evaluate their current health condition.

Fig. 30 Quick release device

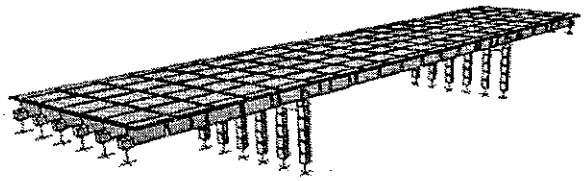

Fig. 31 Three-dimensional model of the West Busan IC bridge

7. Conclusions

The progress of research and applications in structural health monitoring of bridges in Korea have been addressed by following its developing stages through representative examples in Korea that have been adopted in existing and newly built bridges. The importance of health monitoring for bridge structures has been explained in the light of disastrous events that may occur during their lifetime and the efficiency of systematic health monitoring system on the budget invested for management, and the enhanced health level and durability of the bridges.

Although health monitoring system itself plays an important role to study real behavior of structures in real environment and to reduce uncertainties in further design process, it has been being combined with other innovative technologies to give overall estimation of bridge condition and to make proper management decision and, finally, to lengthen the service life of structures. Current researches are focusing on implementing decision algorithm for repair and strengthening method, priority and budgeting as well as to improve hardware performance of health monitoring system.

References

1) Chang, S.P. and Kim, S., Monitoring system of a suspension bridge, *Proc. intern. seminar on new technologies for bridge management, Seoul*, 1996
2) Chang, S.P. et al., Modal parameters for a cable-stayed bridge using ambient vibration, *The 1st workshop on the current state of control and health-monitoring technologies, Korea*, June 2000
3) Hyundai Institute of Construction Technology, Geometry evaluation and monitoring system of the Namhae suspension bridge, 1996
4) Hyundai Institute of Construction Technology, Jindo bridge safety evaluation report, 1998
5) Jang, J.H., Kim, S.K. and Kim, W.J., Sensors based bridge monitoring system, *Int. workshop on structural health monitoring, Colloquium on bridge vibration '03, Kitami*, 1-2 September 2003
6) Jung, D.S. et al., Estimation of dynamic characteristics of Namhae suspension bridge using ambient vibration test, *J. of the Korean Soc. of Civil Eng.*, Vol. 22, pp. 1501-1514, November 2002
7) Kim, C.Y. et al., Monitoring system and ambient vibration test of the Namhae suspension bridge, *Conf. proc. SPIE, California*, 3995(A-36), pp. 324-332, March 2000
8) Kim, C.Y. et al., Ambient vibration tests on two cable-supported bridges in Korea, *Report of IABSE conf., Seoul*, pp. 268-269, 2001
9) Koh, H.M. et al., Progress of application and R&D for seismic isolation and passive energy dissipation for civil and industrial structures in Korea, *7th int. seminar on seismic isolation, passive energy dissipation and active control of vibrations of structures, Assisi*, 2-5 October 2001
10) Koh, H.M. et al., Application and R&D of active, semi-active and hybrid vibration control techniques for civil structures in Korea, *7th int. seminar on seismic isolation, passive energy dissipation and active control of vibrations of structures, Assisi*, 2-5 October 2001
11) Koh, H.M. et al., Development and application of health monitoring system for bridges in Korea, *Proc. of 1st int. conf. on bridge maintenance, safety and management, Barcelona*, 14-17 July 2002
12) Korea Highway Co., Development of management system for Seohae bridge summary, 2000
13) Korea Institute of Construction Technology, Current status of bridge management system, *Workshop on maintenance system of public facilities*, June 1996
14) Kwon, B. et al., Temperature distribution on a building construction measured by FO BOTDA sensor. *Proc. US-Korea workshop on smart infra-structural systems, Busan*, 2002
15) Ministry of Construction and Transportation, and Korea Institute of Construction Technology, Namhae Grand bridge safety evaluation report, 1993
16) Ministry of Construction and Transportation, Records of the current status of bridges, 2002
17) Ministry of Communication and Transportation, Final report on bridge management system and management in 2002, 2003

(Received July 31, 2003)

SUBMITTED PAPERS
(English)

SUBMITTED PAPERS

(English)

Interpretation of bridge test data to determine dynamic load allowance and its influence on bridge design and evaluation

Baidar Bakht*, Aftab A. Mufti**, Alan Clayton***, Walter Saltzberg****, Chad Klowak*****

*Dr. of Eng., JMBT Structures Research Inc., Toronto, Canada M1V 3G1
**Dr. of Eng., President, ISIS Canada, Winnipeg, Canada R3T 2N2
***M. of Eng., Professor, Dept. of Civil Engineering, University of Manitoba, Canada R3T 2N2
****B. of Eng., Associate Professor, Dept. of Civil Engineering, University of Manitoba, Canada R3T 2N2
*****B. of Eng., Masters Student, Dept. of Civil Engineering, University of Manitoba, Canada R3T 2N2

Impact factor, or dynamic load allowance (DLA), has been an essential component of bridge design and evaluation for a long time. With the help of test data on a highway bridge in the Canadian province of Manitoba, it is demonstrated that the DLA, not given to direct measurement, is an interpreted entity. It is also shown that not all the interpreted values of DLA are relevant to bridge design and evaluation. The interpretation of the test data has confirmed that the value of DLA drops with increase in the vehicle weight. Since the values of DLA are always determined under vehicles carrying no more than the legally-permissible loads, a question is raised in the paper about the validity of these values for the much heavier design and evaluation loads corresponding to the ultimate limit state. It is recognized that the dynamic magnification of load effects above their static values takes place at an 'intermediate' strain rate, under which the strengths of most materials are at least 25 % higher than the strengths determined at 'low' strain rates, or in 'static' tests. Although a case can be made for dropping the DLA altogether from both bridge design and evaluation, it is recommended that as a first measure, the DLA should be reduced by 50 % for the evaluation of the load carrying capacities of existing bridges.

Key Words: bridge design, bridge evaluation, dynamic load allowance, impact factor, strain rate

1. Introduction

The term 'dynamic load allowance' (DLA) was first introduced in the Ontario Highway Bridge Design Code (1979) to replace the familiar 'impact factor,' which has been an important part of bridge design and evaluation for a long time. Some design codes specify the DLA explicitly (e.g. CHBDC 2000, and AASHTO 1996). Others embed it in the live loading (e.g. BS 5400 1982). The DLA is usually denoted as I; its values specified by the Canadian Highway Bridge Design Code (CHBDC 2000) depend upon the number of axles of the 5-axle design truck and are as follows.

a) 0.50 for deck joints
b) 0.40 for one axle
c) 0.30 for any two axles, or for the first three axles of the design truck
d) 0.25 for three or more axles, except as noted in (c) above.

In the AASHTO LRFD Bridge Design Specifications (1996), the DLA for deck joints for all limit states is 0.75, the DLA for all other bridge components depends upon the limit state under consideration: for the fatigue and fracture limit state, the DLA is 0.15, whereas that for all other limit states it is 0.33.

There is a widely-held belief that DLA is a measurable entity. For example, O'Connor and Shaw in their recent textbook on bridge loads (2000) have a section entitled *Measured Impact Values*; in this section, the authors have cited several experimental studies, including their own, in which the 'measured' value of I is reported to be as high as 1.0. For a given response – say deflection – I is related to the 'static' and 'dynamic' values of the response as follows.

$$\delta_{dyn} = \delta_{stat}(1 + I) \qquad [1]$$

where δ_{dyn} is the maximum response under the vehicle travelling at normal speed and δ_{stat} is the corresponding maximum response under the vehicle travelling at crawling speed. Notwithstanding the apparent logic and

simplicity of the above equation, different researchers have used different methods for extracting the value of I from observed bridge responses. From the technical literature dealing with dynamic testing of highway bridges, Bakht and Pinjarkar (1989) collected eight different definitions of I; they used these definitions for calculating I from one set of observed deflection data from a bridge test (Biggs and Suer 1956), and obtained eight different values of I ranging between 0.2 and 0.5.

The dynamic load allowance is not given to direct measurement; it is an interpreted entity. As will be shown later in this paper with the help of actual dynamic bridge test data, not all the interpreted values of I obtained from a dynamic bridge test are relevant to bridge design and evaluation.

In his handbook of vehicle-road interaction, Cebon (1999) has defined DLA through the following simple equation.

$$\textit{Dynamic design load} = (1+\text{DLA}) \times \textit{Static design load} \quad [2]$$

While the above equation is useful in understanding the significance of DLA, it sheds little light on the interpretation of test data to obtain DLA or I.

Cebon (1999) has also noted that the value of DLA can be effectively reduced by either or both: (a) avoiding surface roughness (of both the bridge and approach roads), and (b) replacing leaf-spring suspension systems of trucks with air-spring suspension systems.

It is argued in this paper that especially for bridge evaluation, the DLA can be safely reduced substantially, if not dropped altogether.

2. Test Bridge and Vehicle

The Taylor Bridge, located on Provincial Road No. 334 over the Assiniboine River in the Province of Manitoba, comprises five simply supported spans, each 33 m long. Each span has eight prestressed concrete girders at a spacing of 1.8 m. Two girders of this bridge in Span No. 1 are pre-tensioned with tendons made of carbon fibre reinforced polymer (CFRP); one of these girders also incorporates CFRP stirrups. A photograph of the Taylor Bridge is presented in Fig. 1.

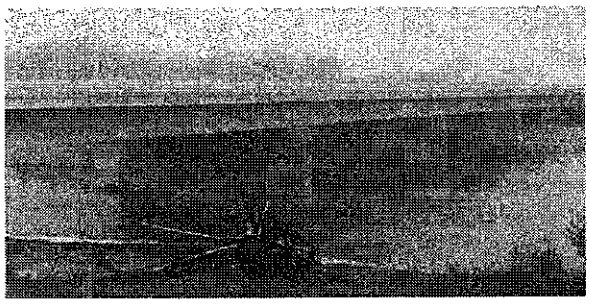

Fig. 1 The Taylor Bridge

The girders of Span No. 1 of the Taylor Bridge have been installed with a large number of embedded strain- and temperature-measuring sensors (Rizkalla et al. 1998). The internal sensors were recently complemented with electrical resistance strain gauges applied to the underside of all girders in Span No. 1. The purpose of all the instrumentation on the Taylor Bridge is to monitor its performance on a continual basis; the data from these sensors, as well as visual images of the bridge, can be seen in real time on the ISIS Canada website: www.isiscanada.com (through the 'Remote Monitoring' icon).

The cross-section of the Taylor Bridge is shown in Fig. 2, in which it can be seen that the bridge has two sidewalks, each separated from the vehicle lanes by a concrete barrier.

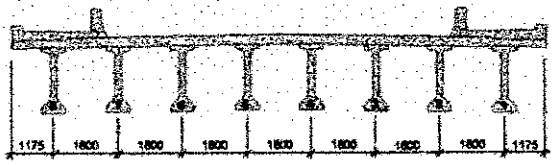

Fig. 2 Cross-section of the Taylor Bridge

In order to calibrate its sensors, the Taylor Bridge was tested on 18th October 2002 under a control 5-axle vehicle of known axle weights (Fig. 3). The field calibration included both 'static' and 'dynamic' tests; the latter conducted with the help the vehicle at two different weight levels, and traversing the bridge in three different transverse positions at speeds of 40 and 5 km/h, respectively. For the calibration test, the permanent sensors on the bridge were complemented with deflection transducers (Fig. 4), which measured mid-span deflections of all girders in Span No. 1.

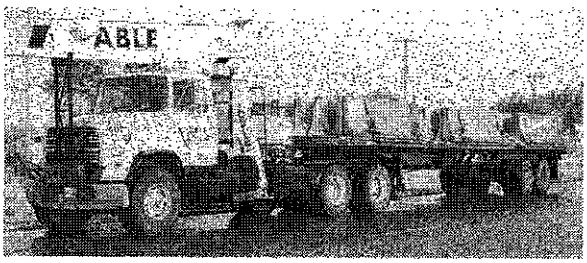

Fig. 3 Loaded test vehicle

The centre-to-centre spacing of the axles, starting from the front axle, was 4.90, 1.55, 7.85 and 2.35 m, respectively. The front axle of the empty truck weighed 4,360 kg, and the front and rear 2-axle tandems weighed 9,410 and 8,320 kg, respectively. The corresponding weights for the loaded vehicle, seen in Fig. 3, were 7,440, 19,410 and 19,410 kg, respectively. The gross weight of the empty vehicle was 22,090 kg, and that of the loaded vehicle 46,260 kg.

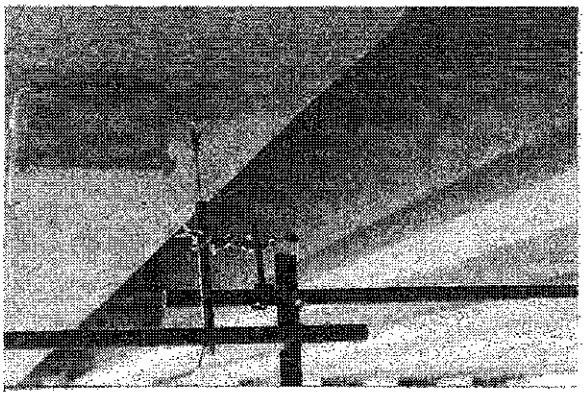

Fig. 4 A deflection transducer attached to a girder

3. Static Test

The static tests were also conducted with the test vehicle in three different transverse positions. In one transverse position, the vehicle travelled in the middle of the roadway, and in the other two positions, the vehicle was placed as close to the closer barrier wall as possible. For the static tests, the vehicle in each transverse position was stopped at ten longitudinal positions and data recorded. The maximum observed deflections at the mid-span of the girders corresponding to the loaded vehicle placed in an eccentric position are plotted in Fig. 5.

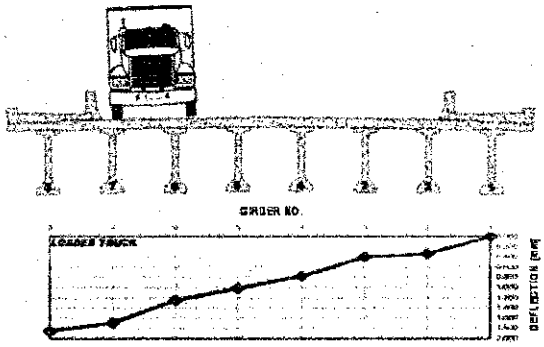

Fig. 5 Observed 'static' girder deflections at mid-span

For the same 'static' loading case, for which the girder deflections are plotted in Fig. 5, the strains at the underside of the girders at the mid-span are plotted in Fig. 6.

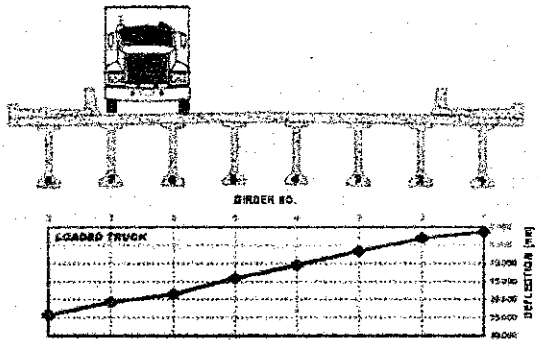

Fig. 6 Observed bottom flange strains at mid-span

It can be seen in Figs. 5 and 6 that under the vehicle placed eccentrically, the external girder close to the vehicle has the largest deflection and strain, whereas the girder farthest from the vehicle has nearly zero values for both deflection and strain. As discussed later, this observation has a significant influence on the use of the interpreted values of I in bridge design and evaluation.

4. DLA from Dynamic Test Data

As noted earlier, the dynamic tests were conducted with the vehicle travelling in the same three transverse positions as those for the static tests. Two examples of observed dynamic deflections plotted against time are presented in Fig. 7, which corresponds to the same eccentric transverse vehicle position as shown in both Figs. 5 and 6.

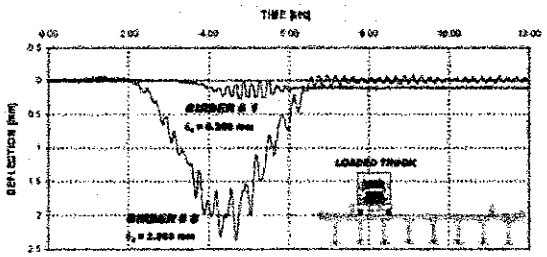

Fig. 7 Mid-span deflections of two girders plotted against time

One deflection-time plot of Fig. 7 corresponds to Girder No. 8, which is loaded most heavily, and the other to the most-lightly loaded Girder No. 1.

4.1 Calculation of I

The static and dynamic time-deflection curves from a bridge test by Biggs and Suer (1956) are reproduced to scale in Fig. 8, it being noted that the 'Static' curve corresponds to a vehicle travelling at crawling speed. A curve obtained by smoothening the dynamic curve is also shown in Fig. 8 as the 'Mean' curve. The curves of this figure were used by Bakht and Pinjarkar (1989) to calculate DLA from the eight available definitions of I. The main reason for the different answers was that, as shown in Fig. 8, the static and mean curves were not identical. While the exact reason for this discrepancy is not known, it is suspected that the forces generated by restraint at the bearings of the girders might be responsible for this unexpected behaviour (Bakht and Pinjarkar 1989).

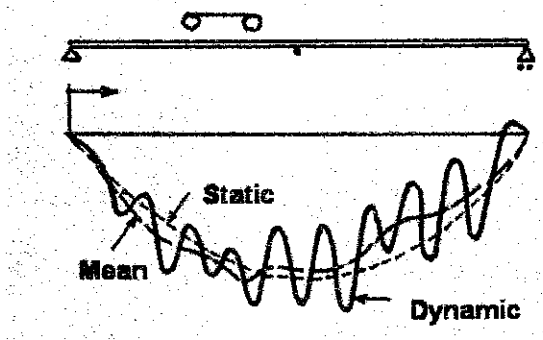

Fig. 8 Deflection-time curves from Biggs and Suer (1956)

As discussed in the following, the 'static' and 'mean' curves were identical for the Taylor Bridge, thus removing a major difficulty in the interpretation of I from the test data.

The girders of the instrumented span of the Taylor Bridge were installed at their undersides with electrical resistance strain gauges, placed near the girder bearings. It was found that under test loads, the longitudinal strains of the bottom flanges of all girders (Fig. 9) near their bearings were tensile and small in magnitude. This observation, which is contrary to the observation of Bakht and Jaeger (1992) for a steel plate girder bridge, confirms that the bearing restraint forces in the bridge under consideration were negligible.

Fig. 9 Underside of the Taylor Bridge

The deflections of Girder No. 8 from Fig. 7 are re-plotted in Fig. 10, by filtering the dynamic response. This latter curve is similar to the 'Mean' curve in Fig. 8. It can be seen in Fig. 10 that under the truck travelling at nearly 40 km/h, the maximum filtered, i.e. mean, deflection of Girder No. 8 is nearly 2.0 mm.

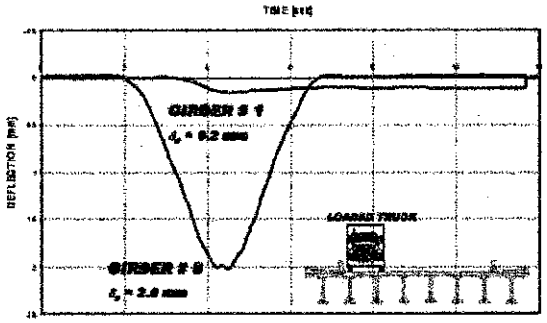

Fig. 10 Deflections of Girder No. 8 under vehicle travelling at 40 km/h

Dynamic and filtered deflections of the same Girder No. 8 are plotted in Fig. 11 when the vehicle was travelling at nearly 5 km/h. Not surprisingly, the dynamic magnification of deflections is very small in this case. It can be seen in Fig. 11 that the maximum filtered deflection in Girder No. 8 under the vehicle travelling at a very slow speed is also nearly 2.0 mm. For the Taylor Bridge, continuous measurements under a crawling vehicle were not taken during the test. However, the two examples presented in Figs. 10 and 11 seem to indicate that the girder deflections under a crawling vehicle would not be significantly different from the filtered deflections under the vehicle travelling at normal speeds.

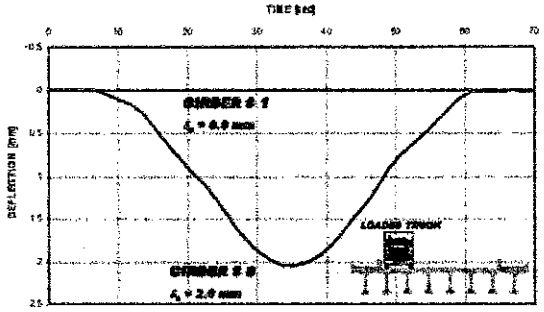

Fig. 11 Deflections of Girder No. 8 under vehicle travelling at 5 km/h

The procedure for calculating I from dynamic data is explained in the following with the help of the deflection-time curves presented in Fig. 7. For Girder No. 8: δ_{dyn} = 2.353 mm, and δ_{stat}, found by filtering the dynamic data, = 1.980 mm. From Eq. [1], I is found to be 0.19.

For the load case under consideration, the value of δ_{stat} for Girder No. 1 is very small, being 0.003 mm. Using this value of the filtered strain, I is found to be 87.3, clearly unrealistic. If the value of δ_{stat} is zero – as was found in several cases – the value of I would be infinity. In bridge design and evaluation, the DLA has relevance for only the most-heavily loaded girder. Dynamic amplification of load effects of girders, which attract very little loads, might be of academic significance, but has no application in the design or

evaluation of a bridge. It is suspected that the very large values of I reported by O'Connor and Shaw (2000) are for bridge components not carrying the maximum static loads.

Using the procedure explained above, the values of I were calculated from the observed dynamic deflection data. Table 1 lists the calculated values of I for the most-heavily loaded girder for each load case, calculated from measured deflections.

Table 1 Values of I for most-heavily loaded girders, calculated from deflections

Vehicle speed	Vehicle empty/ loaded	Transverse position of vehicle		
		Eccentric 1	Eccentric 2	Central
40 km/h	Empty	0.52	?	0.25
	Loaded	0.19	0.06	0.19
5 km/h	Empty	0.13	0.05	0.17
	Loaded	0.11	0.01	0.01

Values of I for the most-heavily loaded girders calculated from observed bottom flange strains are listed in Table 2. A comparison of Tables 1 and 2 will readily show that while the corresponding values of I obtained from deflections and strains are slightly different from each other, the trends are similar.

It is emphasized that the values of I in Tables 1 and 2 are noted to discuss certain trends, and not to imply that these values could be used in either design or evaluation. As noted by Cebon (1999), the DLA changes with the suspension system of the truck. If another set of tests were conducted by changing the suspension system of the vehicle, the interpreted values of I would be different.

Table 2 Values of I for most-heavily loaded girders, calculated from strains at bottom of girders

Vehicle speed	Vehicle empty/ loaded	Transverse position of vehicle		
		Eccentric 1	Eccentric 2	Central
40 km/h	Empty	0.46	0.30	0.32
	Loaded	0.21	0.23	0.20
5 km/h	Empty	0.12	0.14	0.18
	Loaded	0.03	0.07	0.06

4.2 Discussion of results

It cannot be over-emphasized that the values of I calculated from the results of a particular dynamic test are valid only for the specific test vehicle and road surface conditions prevalent at the time of the test. Any change in either will lead to a different set of interpreted values of I.

Notwithstanding the above disclaimer, the values of I listed in Tables 1 and 2 are useful in understanding the influence of two important factors on the values of the DLA, these being the weight of vehicle and its speed of travel.

From Tables 1 and 2, it can be seen that the value of I decreases with increase in the weight of the vehicle. This trend, confirmed by several researchers (e.g. Billing 1982; Cantieni 1981), is not surprising. Experienced operators of truck weighing stations can tell by the bouncing of a vehicle whether it is empty or loaded. An empty vehicle bounces so much that sometimes its wheels leave ground. A heavily-loaded vehicle, on the other hand, does not bounce visibly. It can be seen in Tables 1 and 2 that by nearly doubling the gross weight of the vehicle, the value of I is reduced by nearly 24 percent.

All dynamic tests on bridges are conducted with vehicles carrying not more than the legally-permissible loads. The factored design truck for the Ultimate Limit State (ULS), on the other hand, is much heavier than the legal loads. For example, the CL-W Truck of the CHBDC (2000) is based on legal loads. For the main ULS load combination, the load of this truck is multiplied by a load factor of 1.70. Thus it can be seen that the factored CL-W Truck is at least 70 % heavier than the corresponding truck carrying the maximum legal load. We should ask ourselves the question: Is the value of I obtained under trucks carrying the maximum legal loads valid for 70 % heavier trucks? Clearly the answer is that it is not. It is suggested that different DLAs should be specified for different limit states.

For example, the current values of DLA specified in the CHBDC (2000) can be retained for the Serviceability and Fatigue Limit States, but should be reduced for the ULS, especially for evaluating the load carrying capacities of existing bridges. As noted earlier, AASHTO (1996) specifies a higher value of I for the ULS; this specification is contrary to the observed trend.

Tables 1 and 2 confirm that when a vehicle travels at a very slow speed, the value of I drops significantly. It is reassuring to note the CHBDC (2000) has already taken advantage of this phenomenon by requiring that for evaluation under permit vehicles, the DLA should be multiplied by the following factors, which depend upon the speed of the vehicle.

a) 0.30 for vehicle speed of 10 km/h or less
b) 0.50 for vehicle speeds between 10 and 25 km/h
c) 0.75 for vehicle speeds between 25 and 40 km/h
d) 1.00 for vehicle speeds greater than 40 km/h

5. Effect of strain rate on strength

It is well known that the strength of a structural component increases with decrease in the load duration, or with increase in the strain rate. Most ASTM-type tests for material strengths are conducted at a low strain rate of 10^{-6}/second, which for all practical purposes can be regarded as 'static' (Banthia, 1987). Malvar and Ross (1998), in reviewing the effect of strain rate on concrete strength, have concluded that at high strain rates, corresponding to blast loading and lying between $10\ s^{-1}$ and $1000\ s^{-1}$, the compressive strength of

concrete is up to 100 % higher than the static strength. Similarly the tensile strength of steel reinforcement at a high strain rate is up to 50 % higher than the static strength. Nadeau and Bennett (1982) discuss the effect of load duration on the strength of timber, and provide a probabilistic basis for including the effect of load duration in structural design. From the test data presented by Madsen (1992), it can be seen that the effect of the duration of load is most pronounced on the strength of wood components.

A scrutiny of response-time curves, such as those in Figs. 7, 10 and 11, will readily show that the dynamic increment of the 'static' response takes place over a very short duration of time. For example, a close up of the strain-time curve for Girder No. 8 corresponding to an eccentric vehicle running at about 40 km/h, is presented in Fig. 12.

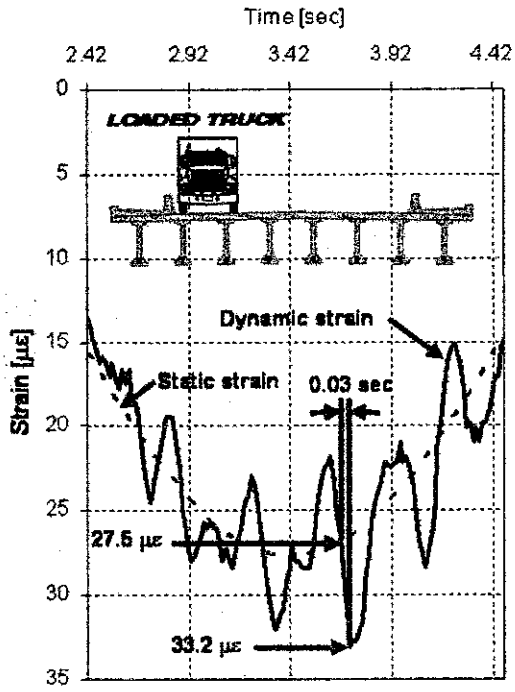

Fig. 12 close up of a strain-time curve

As can be seen in Fig. 12, the peak 'static' tensile strain in the most heavily-load girder is 27.5 με, whereas the corresponding peak dynamic strain is 33.2 με. The time interval between these two strains is 0.03 seconds. The rate of change of strain from peak static to peak dynamic values=$(33.2–27.5)\times10^{-6}/0.03 = 1.9\times10^{-4}$ s^{-1}. Banthia (1987) has provided a chart in which the ratios of dynamic to static strengths of concrete in tension, flexure and compression are plotted against the strain rate. By referring to this chart, one can readily conclude that a strain rate of 1.9×10^{-4} s^{-1}, which corresponds to a single lightly-loaded vehicle, does not lead to a significant increase above the static strength. However, when we examine the dynamic increment in the context of the ULS loading, the strain rate is no longer low. For example, we consider the realistic example of a prestressed concrete girder in the textbook by Collins and Mitchell (1997), in which they have shown that the maximum compressive strain in concrete in a prestressed concrete girder immediately after the transfer of the prestress is 0.401×10^{-3}. For simplicity, it is assumed that the ULS will be reached for the girder when the peak static tensile strain in concrete becomes equal to 0.401×10^{-3}. It is further assumed that the DLA at the ULS is the same as that calculated above under the lightly-loaded vehicle, clearly a conservative assumption.

It can be readily calculated that the corresponding peak values of the static and dynamic strains at the ULS would be 0.401×10^{-3} and 0.484×10^{-3}, respectively. Since the time duration between the peak values of the static and dynamic strains is not likely to be affected by the truck weights, the strain rate corresponding to the ULS is $=(0.484–0.401)\times10^{-3}/0.03 = 0.0027$. This strain rate, lying between low (i.e. static) and high (i.e. blast) strain rates, can be regarded as an intermediate strain rate. Referring to the chart provided by Banthia (1987), and reproduced by Banthia et al. (1994), one can conclude that at intermediate strain rates, the flexural strength of plain concrete is likely to be at least 35 % higher than the static strength.

A quantitative investigation of the effect of intermediate strain rate on the strength of various building materials used in bridges is beyond the expertise of the authors. It can nevertheless be concluded that at intermediate strain rates, a gain of at least 25 % in the static strength of all these building materials provides a conservative estimate.

6. A Case for Reducing DLA in Bridge Evaluation

Since the live load capacity of longitudinal components of most bridges are governed by more than three axles of the CHBDC Design or Evaluation Trucks, the operative value of DLA in the load carrying capacity of a bridge is likely to be 0.25. As noted above, the intermediate strain rate associated with the dynamic increment of the static load effects can increase the static strength of most materials by at least 25 %. Accordingly, a case can be made for dropping the DLA in the evaluation of bridges. However, in order to remain conservative and be accepted by the engineering community, it is proposed that as a first measure, the DLA used in the evaluation of main longitudinal bridge components should be reduced by 50 %; this reduction will clearly make available a 12.5 % extra live load capacity in bridges. Such a relatively small increase in the live load capacity, having little economic premium in new bridges, is highly significant in existing bridges. It can be appreciated that even a small additional live load carrying capacity can lead to the removal of weight or speed restrictions in some bridges.

It is noted that in the above recommendation, advantage has not been taken of the fact that the DLA for the US loading is likely to be smaller than the DLA values interpreted from field tests.

7. Removal of DLA from Design and Evaluation

Further investigation, undertaken with the help of experts in material behaviour, is most likely to confirm that the DLA can be safely eliminated from both evaluation and design of highway bridges.

The removal of the DLA from both bridge design and evaluation is likely to give credence to a case for increasing loads on closely-spaced axle groups in commercial vehicles, which are usually governed by consideration of bridge strength; this outcome will be welcomed by the transportation industry. Any extra live load capacity of bridges should also be welcomed by the owners of bridges, i.e. mainly governmental bodies. However, they are likely to resist the dropping of the DLA for the same reason that the transportation industry would want to welcome it.

8. Conclusions

It has been shown that the dynamic load allowance (DLA) is not an entity given to direct measurements; it is an interpreted measure of dynamic increment of load effects. It has also been shown that not all the interpreted values of DLA are relevant to bridge design and evaluation.

With the help of one set of dynamic field test data, it has been confirmed that the DLA reduces with increase in vehicle weight. The DLA also becomes small when the vehicle travels at a very slow speed.

The main thrust of the paper lies in recognizing the fact that the dynamic magnification of 'static' load effects in bridges takes place over a very small time interval, during which the strain rate is much higher than the 'low' strain rate at which the 'static' strengths of materials are determined. It is argued that the increase in the material strength due to the 'intermediate' strain rate associated with the dynamic increment of bridge load effects is at least 25 %. By taking advantage of such an increase in strength, a case can be made for dropping DLA from both bridge design and evaluation. Notwithstanding the above argument, it is proposed that as a first measure, the DLA should be reduced by 50 % for only bridge evaluation.

9. Acknowledgements

The bridge test described in the paper was carried out under the auspices of the Bridges and Structures Office of Transportation and Government Services of Manitoba. The bridge instrumentation was installed and monitored by ISIS Canada. The involvement of both these organizations in the test is gratefully acknowledged. It is also gratefully acknowledged that the data during the Taylor bridge test was collected and manipulated by Liting Han.

References

1) AASHTO. American Association of State Highway and Transportation Officials, Standard Specifications for Highway Bridges, Washington, D.C., USA, 1996.
2) Bakht, B. and Pinjarkar, S.G. Dynamic testing of highway bridges – a review. Transportation Research Record 1223, Transportation Research Board, Washington, D.C., USA, pp. 93-100, 1989.
3) Bakht, B. and Jaeger, L.G. Observed behaviour of a new medium span slab-on-girder bridge, Journal of the Institution of Engineers (India), Vol. 70, January, pp. 164-170, 1992.
4) Banthia, N. Impact resistance of concrete, Ph.D. thesis, the University of British Columbia, Canada, 1987.
5) Banthia, N.P., Mindess, S. and Bentur, A. Impact behaviour of concrete beams, Materials and Structures, 20, pp. 293-302, 1987.
6) Biggs, J.M. and Suer, H.S. Vibration measurements on simple-span bridges, Highway Research Board Bulletin 124, Highway Research Board, Washington, D.C., 1956.
7) Billing, J.R. Dynamic loading and testing of bridges in Ontario, Proceedings, International Conference on Short and Medium Span Bridges, Toronto, Canada, Vol. I, pp. 125-139, 1982.
8) BS 5400. Design of composite bridges, British Standards Institution, London, 1979.
9) Cantieni, R. Dynamic tests on bridges. Section Concrete Structures Report, Swiss Federal Laboratories for Materials and Testing Research, Dübendorf, Switzerland, 1981.
10) Cebon, D. Handbook of vehicle-road interaction, Swets & Zeitlinger Publishers, the Netherlands, 1999.
11) CHBDC. Canadian Highway Bridge Design Code, CAN/CSA. S6-00, CSA International, Toronto, Canada, 2000.
12) Collins, M.P. and Mitchell, D. Prestressed concrete structures, Response Publications, Canada, p. 197, 1997.
13) Madsen, B. Structural Behavior of Timber, Timber Engineering Ltd., North Vancouver, BC, Canada. 1992.
14) Malvar, L. and Ross, C.A. Review of strain rate effects in tension, ACI Materials Journal, November-December, 1999.
15) Nadeau, J.S. and Bennett, R. An explanation for the rate-of-loading and duration-of-load effects in wood in terms of fracture mechanics, Journal of Materials Science, 17, pp. 2831-2840, 1982.
16) O'Connor, C. and Shaw, P.A. Bridge Loads. Spon Press, London. 2000.
17) OHBDC. Ontario Bridge Design Code, Ministry of Transportation of Ontario. Downsview, Ontario, Canada. 1979.
18) Rizkalla, S.H. et al. Design and construction of a highway bridge with GFRP. Concrete International. (1998).

Vibration-based damage detection on a steel free bridge deck

Zhengjie Zhou*, Leon D. Wegner**, Bruce F. Sparling**

* M.Sc., Doctoral Candidate, Dept. of Civil and Geological Eng., University of Saskatchewan, Saskatoon, Canada, S7N 5A9
** Ph.D., Associate Professor, Dept. of Civil and Geological Eng., University of Saskatchewan, Saskatoon, Canada, S7N 5A9

The dynamic properties of a half-scale two-girder steel-free slab-on-girder bridge deck were measured using accelerometers and strain gauges as several states of small scale damage were induced. Applying four different vibration-based damage detection techniques reported in the literature, each relying primarily upon changes to measured mode shapes, it was found that the damage could be reliably detected and located longitudinally using as few as five measurement points equally spaced along the supporting girders, provided the damage was not located too near a simple support. Only the first mode of vibration was required. The most reliable technique was able to determine the longitudinal location of damage with a minimum accuracy of half the spacing between sensors. The accuracy of locating damage was influenced by the proximity of damage to the nearest sensor and spacing of sensors.

Key Words: damage detection, steel-free bridge deck, dynamic properties

1. Introduction

The primary goal of structural health monitoring (SHM) is to ascertain the condition or "health" of a structure. This may be achieved to varying degrees by using any of numerous techniques, including detailed visual inspections, local non-destructive evaluation (NDE) techniques such as ultrasonic or radiographic methods, and global methods that use changes in the overall response of a structure as indicators of damage. Several NDE and global methods are theoretically capable of detecting damage at early stages when mitigation measures may be less extensive and less costly. Global methods have the added advantage of generally being less labour intensive since they are capable of assessing the condition of an entire structure at once. They may also be set up for remote monitoring. However, global techniques have been relatively limited in their ability to locate and quantify the extent of damage unless applied to very simple structures.

One set of global SHM techniques receiving increasing attention in recent years are vibration-based damage detection (VBDD) methods that rely on changes to the dynamic characteristics of a structure (i.e. its natural frequencies, mode shapes, and damping properties) as indicators of damage. The underlying principle for the application of VBDD methods is relatively straightforward: damage will modify a structure's global dynamic characteristics, and since these characteristics are readily quantifiable and can be related directly to specific physical properties, any measurable changes over time may be used to detect, locate and possibly quantify damage at an early stage before visible signs of distress are apparent. While conceptually simple, considerable research is still required before VBDD methods can be reliably applied to complex structures such as bridges. Perhaps the greatest challenge in using these methods lies in the need to characterize the dynamic properties, particularly mode shapes, using sensors of finite precision and subject to unwanted noise installed at a relatively small number of locations, with sufficient accuracy to detect and locate damage. The ability of VBDD techniques to meet this challenge has yet to be fully explored.

An earlier numerical modelling investigation[1] found that small scale damage on a two-girder simple-span steel-free bridge deck could be detected and located both longitudinally and transversely with reasonable accuracy using mode shapes characterized by as few as five measurement points equally spaced along the supporting girders using one particular VBDD method. That study verified the theoretical feasibility of applying VBDD methods to a bridge superstructure. In an attempt to determine whether similar results could be achieved on a physical system, an experimental study was undertaken to investigate the ability of four specific VBDD techniques reported in the technical literature to detect and locate small scale damage on a steel-free bridge deck using a relatively small number of

strain gauges and accelerometers. This paper describes the results of this study.

2. Experimental Program

The investigation was performed using a half-scale laboratory model of a 2-girder simple-span slab-on-girder steel-free bridge deck similar to that modelled in the numerical study cited above.[1] Details of the system are shown in Fig. 1. The steel-free fibre-reinforced concrete (FRC) slab was supported on two structural WT sections spaced at 1.5 m and spanning 6.0 m. They were made composite with the deck by means of shear studs. The use of WT sections created a relatively flexible system. The FRC deck slab was 75 mm thick at the centre and tapered transversely to 113 mm thick at the girders. Girders were tied together using steel straps spaced at 500 mm to provide the lateral restraint required for the development of internal arching forces.

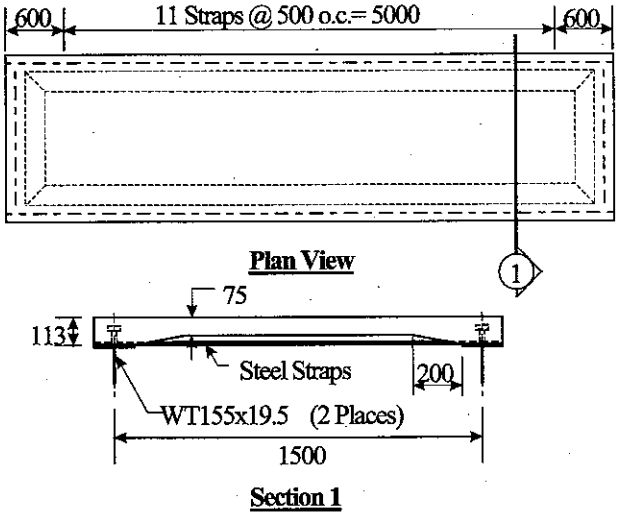

Figure 1. The slab-on-girder bridge deck used for the study. (Dimensions in mm)

The experimental procedure consisted of measuring the initial (undamaged) dynamic properties of the system, and then alternately inducing a new damage state and measuring the properties again at the new state of damage. The baseline signature for a particular damage state was taken to be that measured for the previous state of damage.

Damage was induced by removing small square blocks of concrete, 100 x 100 mm in plan and 25 mm deep, from the surface of the deck, as shown in Fig. 2. This was done at the nine damage locations indicated in Fig. 3.

The model was excited by means of a hydraulic shaker mounted on the surface of the deck slab. The device consisted of a hydraulic cylinder mounted vertically in the centre of a steel frame, with a 22 kg weight mounted on the bottom end of the cylinder. The signal for the shaker was generated using LabView™ 5.1 software implemented on a PC.

To identify the natural frequencies of the system, it was typically first subjected to a white noise random excitation signal to excite as many modes as possible. Fig. 4 shows a typical response spectrum acquired by an accelerometer mounted on the bridge deck in its undamaged state when subjected to white noise. Natural frequencies for the first three modes were identified at 7.36, 18.8, and 25.3 Hz, respectively. When possible, the

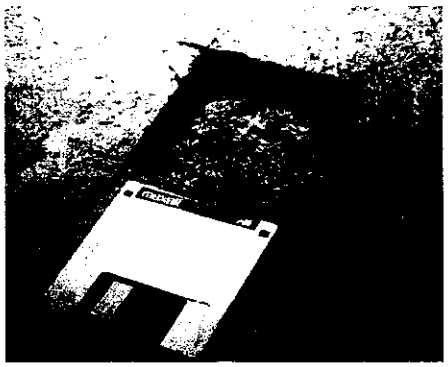

Figure 2. Damage induced on the surface of the deck.

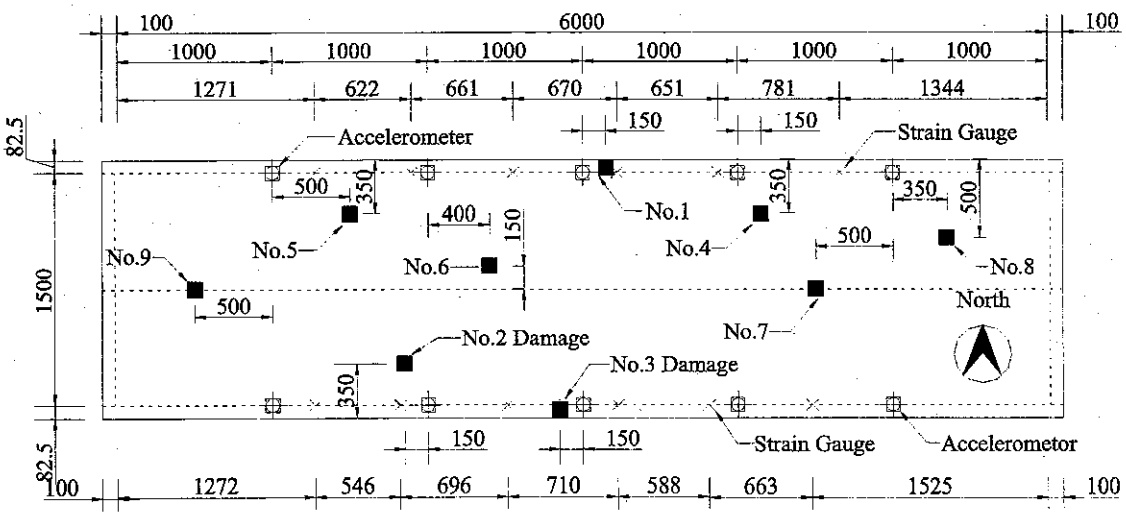

Figure 3. Schematic plan of deck showing locations of damage and sensors (Dimensions in mm).

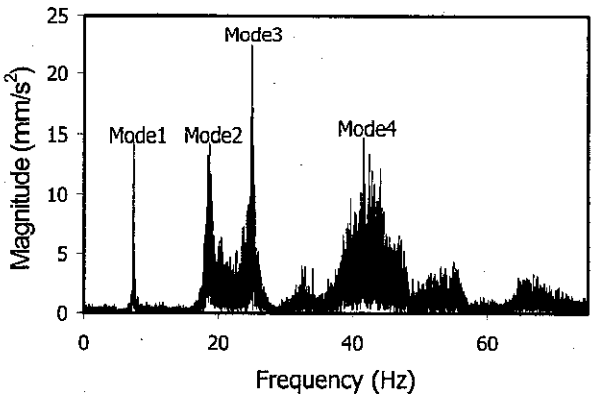

Figure 4. Accelerometer response spectrum acquired when bridge deck was in an undamaged condition.

response of the system to ambient environmental excitation in the laboratory was measured to more accurately identify natural frequencies. The smaller amplitude ambient excitation typically produced slightly higher natural frequencies, as is expected from a non-linear system. After natural frequencies had been identified, a sinusoidal excitation signal was applied at each of the natural frequencies in sequence to accurately measure the corresponding mode shapes. For the work described in this paper, only the first mode was used.

Measurements were made using five accelerometers, each configured for a maximum range of ±0.5g and precision of 0.00025g. These were mounted on the deck slab above each girder and evenly spaced longitudinally, as shown in Fig. 3. Separate tests were performed with the accelerometers first installed along one girder and then along the other. Prior to each test, the accelerometers were calibrated relative to each other by mounting them in a stack and subjecting them to a sinusoidal signal. Displacements at each accelerometer location were obtained by double integration of the measured accelerations, using a high pass filter to eliminate any baseline drift in the signal.

In addition to the accelerometers, 120 ohm conventional electronic strain gauges were bonded to the girder webs in vertically aligned groups of three to measure curvature at six locations along each girder. These locations are also shown in Fig. 3. The strain profile through the cross section at each location was obtained by fitting a line through the three individual strain signals at each location for each point in time.

Data was acquired using a 12-bit data acquisition system (National Instruments SCXI 1001, LabView™ 5.1). For identification of the natural frequencies using the white noise excitation, data was acquired at 150 samples per second for an interval of 220 seconds. For mode shape measurement using a sinusoidal excitation, data was acquired at 300 samples per second for 21 seconds.

For application of the damage detection techniques discussed in the following section, it was necessary to define either the displacement mode shape or the curvature profile along each girder associated with the fundamental mode. When accelerometer data was used, displacements determined by double integration of measured accelerations were known at the five measurement points and at girder supports. Prior to applying the techniques, a cubic polynomial was fit to the measured data, and displacement values at 59 points along the fit curves were extracted and used to define the mode shapes between the supports. Thus mode shape vectors had a dimension of 59. These mode shapes were unit mass normalized prior to applying the damage detection techniques. When strain gauge data were used, measured curvatures at the six locations along each girder were used directly.

3. Damage Detection Techniques

As mentioned above, four different damage detection techniques were applied to the measured data. These techniques are summarized in this section. Further details may be found in the cited references.

3.1 Mode shape curvature method[2)]

It is well known that the curvature of a beam is directly proportional to the inverse of its flexural stiffness. Thus, a reduction of stiffness associated with damage will, in turn, lead to an increase in curvature. Pandey et al.[2)] demonstrated that absolute change in mode shape curvature can be a good indicator of damage for beam structures. If the displacement mode shapes are known at discrete points, the curvature values may be computed using the central difference equation for second derivative,

$$\nu''_{ji} = \frac{\psi_{(j+1)i} - 2\psi_{(j)i} + \psi_{(j-1)i}}{h^2}, \qquad (1)$$

where h is the average distance between measurement points, ν''_{ji} is the curvature at point j corresponding to the i^{th} mode, and ψ_{ji} is the displacement at point j corresponding to the i^{th} mode. This computation is not required if the curvatures are measured directly, as they were for the current study when the strain gauge data were used. For multiple modes, the sum of the absolute differences in curvature is used to indicate the damage.

3.2 Change in flexibility method[3)]

The flexibility matrix, $[F]$, of a structure in undamaged and damaged states can be easily and accurately estimated from a few of the lower vibration modes as follows:

$$[F] \approx \sum_{i=1}^{n} \frac{1}{\omega_i^2} \{\phi_i\}\{\phi_i\}^T \quad \text{and} \qquad (2)$$

$$[F]^* \approx \sum_{i=1}^{n} \frac{1}{\omega_i^{*2}} \{\phi_i\}^* \{\phi_i\}^{*T} \quad , \tag{3}$$

where ω_i is the i^{th} modal frequency, ϕ_i is the i^{th} unit-mass-normalized mode shape, n is the number of measured modes, and the asterisks signify properties of the damaged structure. From the pre- and post-damage flexibility matrices, a measure of the change in flexibility caused by damage can be obtained from the difference between the respective matrices, i.e.

$$[\Delta F] = [F] - [F]^* \ , \tag{4}$$

where $[\Delta F]$ is the change in flexibility matrix. For the j^{th} column of this matrix, let $\bar{\delta}_j$ be the absolute maximum value of the elements in that column. Hence,

$$\bar{\delta}_j = \max\left|\delta_{ij}\right|, \quad i = 1...m, \tag{5}$$

where δ_{ij} are elements of $[\Delta F]$, m is the number of points at which the mode shape is defined (59 in this case), and $\bar{\delta}_j$ is taken to be a measure of the flexibility change at each point j. The column of the flexibility matrix corresponding to the largest $\bar{\delta}_j$ is indicative of the location where the change in physical properties (i.e. damage) is located.

3.3 Damage index method[4]

For a structure that can be represented as a beam, a damage index, β, based on changes of curvature of the i^{th} mode at location j is defined as

$$\beta_{ji} = \frac{\left(\int_a^b \left[\psi_i^{*"}(x)\right]^2 dx + \int_0^L \left[\psi_i^{*"}(x)\right]^2 dx \right)}{\left(\int_a^b \left[\psi_i^{"}(x)\right]^2 dx + \int_0^L \left[\psi_i^{"}(x)\right]^2 dx \right)} \times \frac{\int_0^L \left[\psi_i^{"}(x)\right]^2 dx}{\int_0^L \left[\psi_i^{*"}(x)\right]^2 dx}$$

$$= \frac{NUM_{ji}}{DEN_{ji}} \ , \tag{6}$$

where $\psi_i^{"}(x)$ and $\psi_i^{*"}(x)$ are the second derivatives of the i^{th} mode shape corresponding to the undamaged and damaged structures, respectively, L is the length of the beam, and a and b are the limits of a segment of the beam where damage is being evaluated. To account for all available modes a single indicator for each location is formed:

$$\beta_j = \frac{\sum_i NUM_{ji}}{\sum_i DEN_{ji}} . \tag{7}$$

A normal distribution is fit to the damage indices, and the ratio Z_j is calculated as the difference between an individual damage index (β_j) and the mean (μ), divided by the standard deviation (σ):

$$Z_j = (\beta_j - \mu)/\sigma \ . \tag{8}$$

Values of β_j falling two or more standard deviations from the mean (i.e. $Z_j \geq 2$) are indicative of a possible damage location.

3.4 Change in uniform flexibility curvature method[5]

The i^{th} column of the flexibility matrix $[F]$ calculated by Eq. (2) corresponds to the deflected shape assumed by the structure when a unit load is applied at the i^{th} degree of freedom. The sum of all columns of the flexibility matrix therefore represents the deflected shape if a unit load is applied at each degree of freedom simultaneously. This shape is referred to as the uniform load flexibility.

Zhang and Aktan[5] indicated that the change in curvature of the uniform load flexibility surface could be used to determine the location of damage. Elements of the curvature vector $\{F''\}$ corresponding to the uniform load flexibility surface, can be obtained with a central difference operator,

$$F_j^{"} = \frac{F_{(i+1)} - 2F_{(j)} + F_{(j-1)}}{h^2} , \tag{9}$$

in which F_j is the displacement of the uniform load flexibility surface at location j, and h is the average distance between measurement locations.

The absolute curvature change at location j is evaluated as

$$\Delta F_j^{"} = \left| F_j^{*"} - F_j^{"} \right| , \tag{10}$$

where the asterisk indicates the damaged state. The largest value of $\Delta F_j^{"}$ is indicative of the location of damage.

3.5 Method to determine transverse damage location

The above methods are particularly applicable to determining the longitudinal location of damage on a bridge deck. A method for estimating the transverse location of damage was proposed by Zhou et al.[1] It uses the results of the change of flexibility method (Section 3.2) applied to each of the girders of a two-girder bridge deck.

Let Δ_s be the difference between the damaged and undamaged unit-mass-normalized mode shapes at the point of maximum change of flexibility for the girder with the smaller difference, and let Δ_l be that difference for the girder with the larger difference. Then the transverse distance, z_d, from the girder with the larger difference to the location of damage may be

estimated by

$$z_d = \frac{\Delta_s}{|\Delta_s|} \cdot \sqrt{\frac{|\Delta_s|}{\Delta_l}} \cdot \frac{S_g}{2}, \qquad (11)$$

where S_g is the girder spacing.

4. Results and Discussion

4.1 Use of strain gauge data to locate damage

The mode shape curvature method was applied to the strain gauge data since strain gauges were configured to measure curvature directly. Although it would have been possible to process the strain gauge data to retrieve displacements so that other methods could be applied, this process would result a lower degree of accuracy than was possible using accelerometer data. Only determination of the longitudinal location of damage was attempted using strain gauge data.

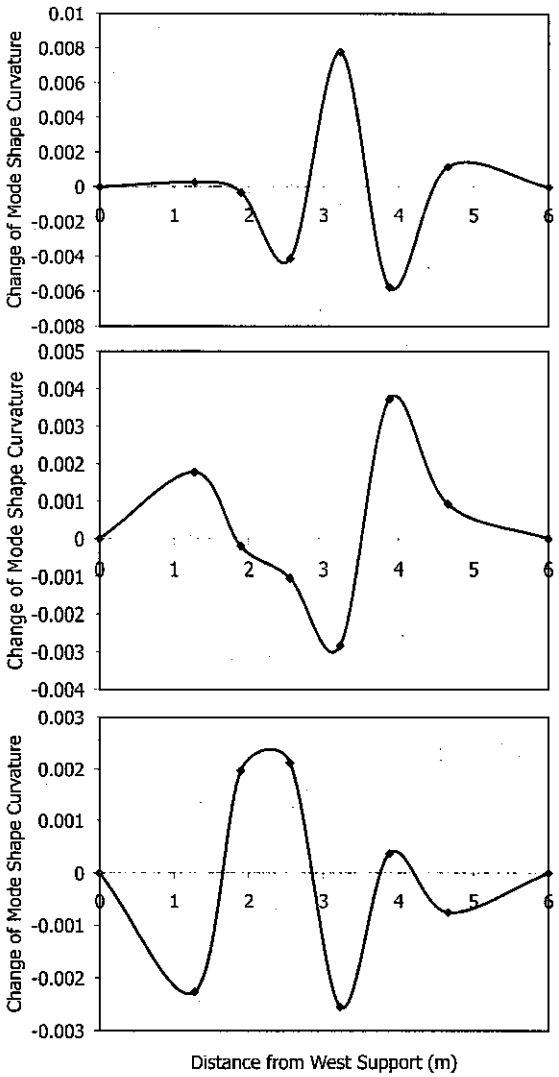

Figure 5. Change in curvature measured along one girder calculated from strain gauge data for damage cases 1 (top), 4 (middle), and 6 (bottom).

Fig. 5 shows representative plots of change in curvature, ν''_j, associated with the introduction of new damage states. It should be recalled that the baseline curvature for each state of damage was that associated with the previous state of damage. The highest upward peaks in these plots indicate the predicted longitudinal location of damage. While the complexity of the curves appears to increase somewhat with an increasing number of damage states, no ambiguity is apparent with respect to identifying the highest upward peak.

Predicted and actual damage locations for all damage states are listed in Table 1. The error listed in the table is the absolute difference between predicted and actual locations. Good agreement between predicted and actual damage locations was achieved for the first seven damage states. The maximum absolute error observed was 0.25 m, and corresponded to the third damage state, which was located the greatest distance longitudinally from the nearest gauge point. This corresponds to a relative error of approximately 35% of the spacing between instrumented points at that location.

The proximity of damage to a measurement point was found to significantly influence the accuracy with which the damage could be located. When absolute error is plotted relative to the longitudinal distance to the nearest gauge, as shown in Fig. 6, a high correlation (R = 0.963) is apparent if the seventh damage state is omitted. The location of the seventh damage state—transversely mid-way between girders and longitudinally near the first measurement point relative to a support—is thought

Table 1. Comparison of predicted and actual longitudinal damage locations using strain gauge data.
(in m from west support)

Damage Case	*1*	*2*	*3*	*4*	*5*	*6*	*7*	*8*	*9*
Predicted	3.22	1.82	3.10	4.00	1.35	2.30	4.67	F*	F
Actual	3.15	1.85	2.85	4.15	1.50	2.40	4.50	5.35	0.50
Error (m)	0.07	-0.03	0.25	-0.15	-0.15	-0.10	0.17	—	—

* F = failure to locate damage

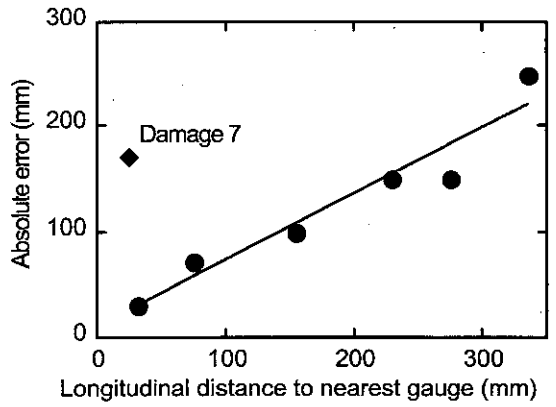

Figure 6. Absolute error in location of damage as a function of longitudinal distance to nearest strain gauge group.

to have influenced its predicted accuracy. Although the error in locating this damage state did not follow the trend of Fig. 6, it was still located with relative accuracy. It appears that the error in locating damage is a function of both proximity to nearest measurement point and proximity to a support.

Damage states 8 and 9 could not be located by studying the changes in mode shape curvature calculated using the strain gauge measurements. The location of these damage states between a support and first measurement point along a girder is believed to have contributed to this lack of success. In addition, these damage states were located a greater distance from measurement points than other damage states, and in regions where absolute curvature values were small.

4.2 Use of accelerometer data to locate damage

(1) Longitudinal damage location

All four techniques described in Section 3 were applied to the accelerometer data to evaluate their abilities to locate damage. Fig. 7 shows plots of the damage locating parameters for each of the four methods corresponding to the fifth damage state. Again, the highest upward peaks in these plots indicate the predicted longitudinal location of damage. These plots are typical of those obtained using the four techniques.

Table 2 summarizes the longitudinal locations of all damage states as predicted by the four methods investigated, along with the actual locations and absolute errors in predictions. When damage was successfully detected and located, the maximum absolute error in the predicted location by all methods was 0.6 m, or 60% of sensor spacing. The lowest maximum error was achieved by the change in flexibility method—0.5 m or half the

Table 2. Comparison of predicted and actual longitudinal damage locations using accelerometer data.
(in m from west support)

Damage Case:	*1*	*2*	*3*	*4*	*5*	*6*	*7*	*8*	*9*
Actual	3.15	1.85	2.85	4.15	1.50	2.40	4.50	5.35	0.50
Meth. 1†	3.0	2.0	3.0	4.0	2.0	3.0	4.0	F*	F
Error	-0.15	0.15	0.15	-0.15	0.5	0.6	-0.5	—	—
Meth. 2	3.0	2.0	2.8	3.7	2.0	2.9	4.1	F	F
Error	-0.15	0.15	-0.05	-0.45	0.5	0.5	-0.4	—	—
Meth. 3	3.0	2.0	3.0	4.0	2.0	3.0	4.0	F	F
Error	-0.15	0.15	0.15	-0.15	0.5	0.6	-0.5	—	—
Meth. 4	3.0	2.0	F	4.0	F	F	4.0	F	F
Error	-0.15	0.15	—	-0.15	—	—	-0.5	—	—

* F = failure to locate damage

† Meth. 1 = Mode shape curvature method
Meth. 2 = Change in flexibility method
Meth. 3 = Damage index method
Meth. 4 = Change in uniform flexibility curvature method

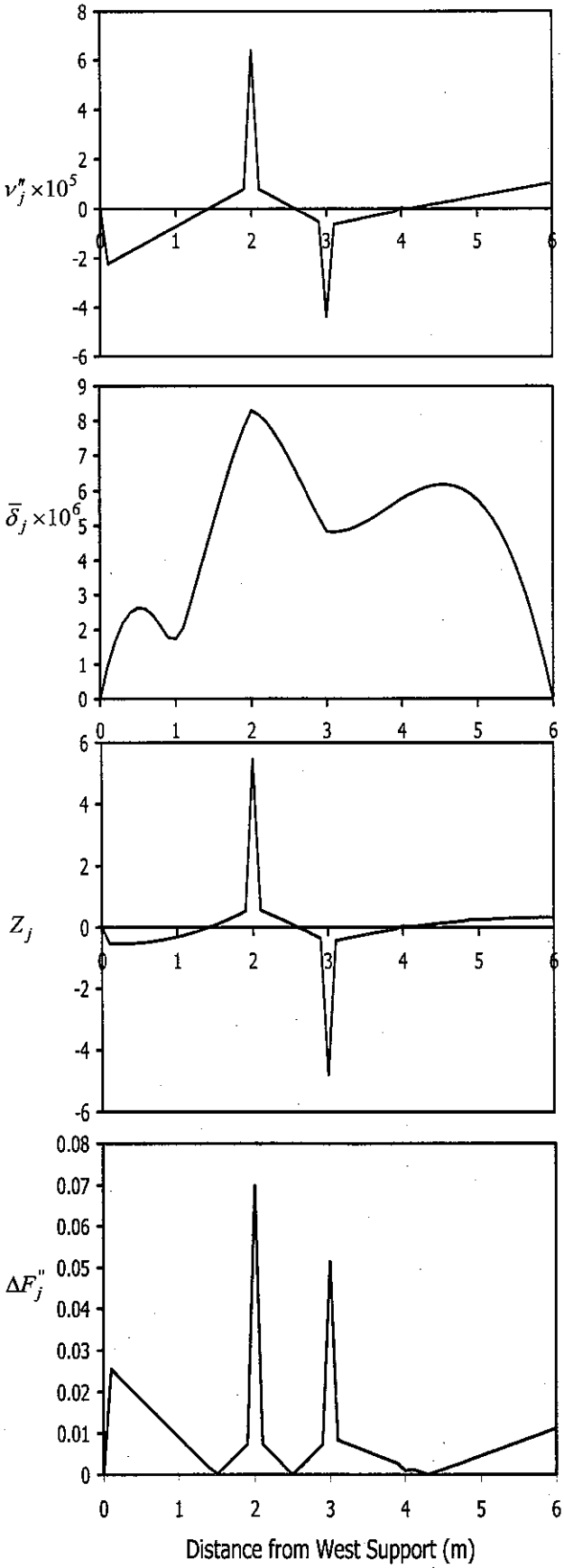

Figure 7. Damage indicator parameters along one girder for damage state 5 as calculated by mode shape curvature (top), change in flexibility (2nd from top), damage index (3rd), and change in uniform flexibility curvature (bottom) methods.

spacing between sensors.

The mode shape curvature and damage index methods produced identical results, with a maximum error of 60% of spacing between sensors. These two methods both use changes in the mode shape curvatures as damage indicators. The change in uniform flexibility curvature method proved to be the least reliable, being unable to determine the location of several damage states due to ambiguity associated with the existence of more than one large upward peak in the change in absolute curvature.

Damage states 8 and 9, which were located between a support and the first sensor, could not be reliably located by any of the methods used. This is in agreement with one of the results of the earlier numerical study[1], which concluded that damage between the first sensor location and support could not be located.

Of note is the fact that all methods typically predicted damage to be located exactly at a sensor location. The change in flexibility method was the only one that predicted damage locations not at a sensor location, although most predicted locations were near a sensor. This underlines the importance of sensor configuration. If there is reason to expect greater susceptibility to damage at a particular location, it may be beneficial to reduce the spacing between sensors near that point to improve the accuracy of locating damage.

Although there is not much apparent difference between the performance of the first three methods, the change in flexibility method appears to the most robust and reliable. Not only did this method have the lowest maximum error (50% of sensor spacing), it was also the only method able to detect the existence of damage state 8 to be near the first sensor or between the support and the first sensor, although it was not able to determine the location accurately.

These experimental results are in general agreement with the findings of the earlier numerical study[1], which concluded that small scale damage could be located longitudinally with an accuracy of at least half the spacing of sensors, and that damage between the support and first sensor could not be reliably located.

(2) Transverse damage location

Table 3 summarizes the predicted transverse damage locations determined using Eq. (11), and compares these to the actual transverse locations. The performance of the proposed method is not consistent. A maximum error in predicted location of 42% of girder spacing was achieved. This is much poorer than the performance of this method using numerical results[1], in which the transverse location of damage was found within 10% of girder spacing. The inaccuracies associated with characterizing the fundamental mode shape using experimental measurements do not permit the same level of accuracy to be achieved. Further work is required to develop a more reliable method to determine the transverse location of damage.

Table 3. Comparison of predicted and actual transverse damage locations. (mm from nearest girder)

Damage Case:	*1*	*2*	*3*	*4*	*5*	*6*	*7*	*8*	*9*
Actual	-33	267	-33	267	267	600	750	417	750
Predicted	F*	F	-670	830	780	870	620	460	F
Err. (mm)	—	—	-637	563	513	270	-130	43	—
Err. ($\%S_g$)†	—	—	-42	38	34	18	-8.7	2.9	—

* F = failure to locate damage

† S_g = girder spacing

5. Conclusions

It has been demonstrated experimentally using measurements on a half-scale model of a two-girder steel-free bridge deck that small scale damage to the deck can be detected and located longitudinally using vibration-based damage detection methods, provided the damage is not located too near a simple support nor too distant transversely from an instrumented girder. This was achieved using only the first mode of vibration and a relatively small number of measurement points (as few as five) along each girder.

The degree of accuracy with which damage was located was strongly influenced by the configuration of instrumentation—i.e. the spacing between sensors and the location of damage relative to sensors. When the fundamental mode shape was determined using five evenly spaced accelerometers along each girder, the longitudinal location of damage was determined with an accuracy of approximately one half the spacing between accelerometers. The change in flexibility method produced the highest level of accuracy among the methods investigated.

When strain gauges were used, configured to measure curvature of the girders at six locations along each girder, the longitudinal location of damage was determined with an accuracy of approximately 35% of the spacing between instrumented locations. This was achieved using the mode shape curvature method, which relies upon the absolute changes to the curvature of a girder associated with the introduction of damage. Although the accuracy appears to be better when strain gauges were used, higher amplitudes of vibration were required to obtain strain gauge signals with sufficiently high signal to noise ratios. The required amplitudes may not be feasible in field applications.

This study confirmed results of an earlier numerical study, in which the location of damage could not be determined if it was located between the support and the first measurement point. Reduced spacing near supports may be required for reliable assessment of damage in this region. The use of higher modes may also improve the accuracy with which damage may be located, both near supports and in other areas. Higher modes are also more sensitive to damage. However, the measurement of

higher modes requires a larger number of measurement points, and the accuracy with which higher mode shapes can be measured is much lower than that of the fundamental mode because of smaller amplitudes. It may be more efficient to strategically position measurement points rather than use sufficient instrumentation to measure higher modes.

The transverse location of damage could be determined with an accuracy of approximately 40% of girder spacing using the proposed method. Additional work is required to develop a more reliable transverse location method.

While the results of this study are promising for the application of vibration-based damage detection techniques to bridge superstructures, it is recognized that their application to field structures will involve a number of additional challenges. However, this study demonstrates the experimental feasibility of applying vibration-based damage detection techniques to a real structure.

Acknowledgements

The financial support of the ISIS Canada Network of Centres of Excellence for this work is gratefully acknowledged. The contributions of Mr. D. Pavier, Mr. A. Duffy, and Mr. D. Bitner to the experimental aspects of this work are also gratefully acknowledged.

References

1) Zhou, Z., Wegner, L.D. and Sparling, B.F., Assessing damage to a bridge deck using measured dynamic characteristics — influence of the number of measurement points, *Proceedings of the Sixth International Conference on Short and Medium Span Bridges,* Vol. I, pp.65-72, 2002.
2) Pandey, A.K., Biswas, M., and Samman, M.M., Damage detection from changes in curvature mode shapes, *Journal of Sound and Vibration.* 145(2), pp.321-332, 1991.
3) Pandey, A.K. and Biswas, M., Damage detection in structures using changes in flexibility, *Journal of Sound and Vibration.* 169(1), pp.3-17, 1994.
4) Stubbs, N. and Kim, Y.I., Field verification of a non-destructive damage localization and severity estimation algorithm, *Proceedings of the 13th International Modal Analysis Conference,* pp.210-218, 1995.
5) Zhang, Z. and Aktan, A.E., The damage indices for constructed facilities, *Proceedings of the 13th International Modal Analysis Conference,* pp.1520-1529, 1995.

(Received July 31, 2003)

Sensors Based Bridge Monitoring System

Jeong-Hwan Jang*, Sung-Pil Chang**, Sung-Kon Kim***, Wan-Jong Kim****

*Dr. of Eng., Manager, Dept. of Structural Eng., Ejtech Co., LTD., Boondang-Gu, Seongnam, Kyungki-Do, 463-800, Korea
** Dr. of Eng., Professor, Dept. of Civil Eng., Seoul National University, Kwanak-Gu, Seoul, 151-742, Korea
*** Dr. of Eng., Professor, Dept. of Structural Eng., Seoul National University of Technology, Nown-Gu, Seoul, 139-743, Korea
**** M. of Eng., President, Ejtech Co., LTD., Boondang-Gu, Seongnam, Kyungki-Do, 463-800, Korea

Sensors based bridge monitoring system (SBBMS) is designed to perform real-time monitoring and to store the performance history of in-service bridges. In general, visual inspections play a major role in maintenance of in-service bridges; however, they are not adequate to document the behavior of a bridge. Therefore, visual inspections and sensor based monitoring systems complement each other. Sensor based bridge monitoring systems consist of hardware and software systems. The hardware system contains the sensors and data-loggers to measure the behavior of a structure, the communicational equipment to transmit the measured data from the site to the monitoring center, and the computers to arrange and analyze the data. The software system controls data-loggers, arranges and analyzes the measured data, makes real-time display, stores the performance history.

Key Words: bridge monitoring, behavior history, hardware system, software

1. Introduction

The bridge can be considered as an organism. The construction of a bridge means the birth of life. The life grows old as time goes by, which means the performance of a bridge goes decreased. The bridge should be repaired/reinforced to sustain lifespan of a bridge expected on the design stage, as human being takes medication for disease treatment to lengthen his/her life. Surely the bridge cannot be treated precisely as human being. So the bridge should be repaired/reinforced in consideration with economics. If it proves to bring too much cost for renovation and improvement, the bridge should be closed. However, like that we can lengthen our lives by taking well-timed medication on disease with minimum cost to do so, the lifespan of a bridge can be extended with minimum cost by taking well-timed repair and reinforcement, which results in guarantee of safety and serviceability. This means literally effectiveness increase on maintenance cost over the bridge. However, good method to take assessment of bridge performance has not been established so far, which resulted from deactivated research and development for bridge performance assessment method, caused by insufficiently accumulated research materials for bridge maintenance, which includes visual inspection and performance history.

We can classify the methods for data generation of bridge maintenance into the following ones; visual inspection and measurement. Generally maintenance work over the bridge is usually performed only by visual inspection; however, it is impossible for us to acquire the behavior of a bridge. It is considered that we can determine the state of the bridge more precisely with behavioral information and data collected from visual inspection.

Bridge monitoring system is complicated but organized process, consisting of items needed to be measured set up by bridge structural engineers, hardware configuration performed by bridge structural engineers and electrical engineers, and software configuration performed by software programmers. It is considered that such *measurement system (sensors based monitoring system)* provides more objective and systematic information on bridge maintenance, in addition to the data from visual inspection.

2. Sensors Based Monitoring System

The monitoring system consists of hardware system and software system; the former performs measurement and data acquisition over the behavior of a bridge by remote sensing, and the latter performs data arrangement and storage, analysis and

display in customized form. The purposes of sensors based monitoring system are as follows;

a. Provides behavioral information on the bridge to take assessment of the bridge.

b. Provides necessary information for obtaining serviceability and safety during service stage of a bridge.

c. Provides necessary information for design, construction, and maintenance over the bridge similar to objective structures.

2.1 Hardware System

The hardware system contains the sensors and data-loggers to measure the response of the bridge, the communicational equipment to transmit the measured data from the site to monitoring center, and the computers to arrange, store, and analyze the data.

Sensors

In order to determine the state of the bridge utilizing monitoring system, such information as traffic capacity loaded over the bridge, temperature, and wind direction and velocity should be measured, as well as behavioral information collected from the bridge. In general, there are vertical displacement, strain, inclination, displacement through expansion joint, and natural frequency in the behavioral information. Measurement sensors should be appropriate for measurement items and purposes with customized type.

When we measure vertical displacement of a bridge, especially time-dependant displacement, rather than the one by live load, it is economically proper to use static displacement transducer for more accurate measurement. In order to get some information on dynamic vertical displacement of bridge; however, dynamic laser displacement sensor should be used. We have to decide whether we use dynamic laser displacement sensor or not, considering span length of objective bridge and displacement by live load, since measurement range and resolution differs in proportion to the distance between the transceiver and target in using dynamic laser displacement sensor. Strain gages are usually used for stress measurement in the structures. When we measure time-dependant stress distribution, it is proper to use vibration wire type strain gages, but electric resistance type strain transducers should be used for stress variation exerted by live load. Recently fiber optic strain gages have been developed which have some sort of advantage over the conventional sensors, but they are still not proper to be applied to field measurement for their weak figures. It is considered that fiber optic sensors are the best items, which can replace the conventional sensors, on condition that fiber optic sensors are produced in commercial quantity if feasibility problems over field measurement can be overcome.

Data-logger

The data-logger, equipment for data acquisition and transmission, can be classified into static data-logger and dynamic data-logger according to scanning rate. A static data-logger acquires the data from the linked channels - one sensor may have one channel or more - through mechanical relay type device, while a dynamic data-logger acquires the data through electronic relay type device. Static data-logger is cheaper and has more availability to expand the channels than dynamic data-logger. However, dynamic data-logger should be used for dynamic response from a loaded structure. Thus the choice between static data-logger and dynamic is made by what kind of structural response the user wants to obtain, not by which type of data-logger has more advantage of each other.

Communicational Method and Equipment

The method to transmit the acquired data to remote place should be decided whether it is done by wired or wireless communication. The latter is adequate for small volume of data acquired from the site, and the former has the advantage that a lot of data can be steadily transmitted rather than wireless communication. This advantage generally makes the structural engineers inclined to use the "wire" method for bridge monitoring system. In case of taking up the wired method, communicational equipment is installed in consideration of the amount of data and the distance to transmit.

With static data-logger, RS-232 serial communication method is usually taken up for small volume of data transmission, while Ethernet TCP/IP communication method is usually taken up for large volume of data transmission for dynamic data-logger. Such method is flexible to choose; even though it is the circumstance that we have to use dynamic data-logger, RS-232 serial communication can be used if the amount of data is small enough to convey with the method.

In case that the distance to transmit the data is close enough, the data can be sent as electric signal (almost in raw format), however, it must be converted into optical signal if the distance is quite far.

The method for sending raw electric signal as acquired is economical but no good for a long distance data transmission, and has such disadvantage as the longer the distance gets, the more noise will interrupt during the data transmission. The method for sending optical signal converted from raw electric signal is relatively expensive but appropriate for a long distance transmission, and has the advantage of lower interference with noise during data transmission. Thus the system must be constructed in relevant combination with the data transmitting section for electric signal and optical signal, simultaneously considering the economic and technical factor. Figure 1 shows a general diagram for monitoring hardware system.

Computer

The computer system is needed to take arrangement of measured data. It is needed for data arrangement, analysis, and storage. The data acquired is stored up for database construction. Figure 1 shows a general diagram of bridge monitoring hardware system.

The steps to design the sensor based monitoring hardware system are as follows;

a. Set up measurement items and quantity of sensors - when the items to be measured for an objective structure are fixed, quantity of sensors will be decide according to its measurement type, static or dynamic.

b. Set up quantity of data-loggers - quantity of data-loggers will be fixed in consideration of that of sensors and installation points. Since it is expected the too much noise might interrupt along the way of data transmission, the data-loggers should be installed adjacent to the sensors as close as possible. For decision on quantity of data-loggers, technical and economical point should be considered simultaneously, recognizing data-logger is usually a high-priced equipment.

c. Decide how to communicate - the way of communication should be decided considering quantity of acquired data and distance to transmit.

d. Decide the type of computer (server and personal computer) - the size and quantity of server computer will be set, considering the amount of data needed to be processed, and the computer system for generally industrial purpose will be also decided to make checkup for the state of measurement.

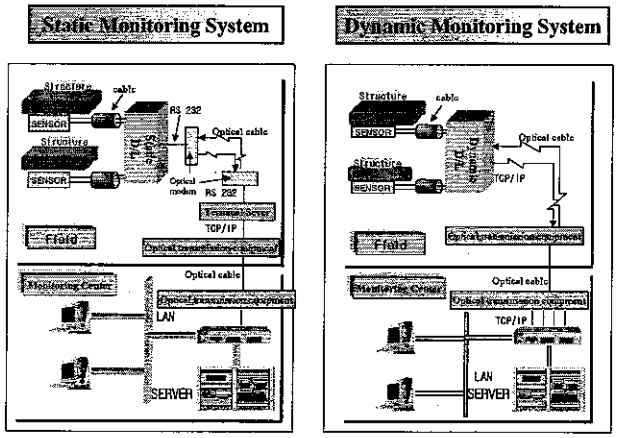

Fig.1 A general diagram for monitoring hardware system

2.2 Software System

Once the structural engineers transfer the final goal for monitoring system set up under the cooperation of end-users to computer programmer, he/she construct the monitoring software. The monitoring software should have the following function;

A. *Data-logger control* - with this function it must be able to control such values as sampling rate and gage factor and monitor the network. Figure 2 shows us how the software can monitor the network.

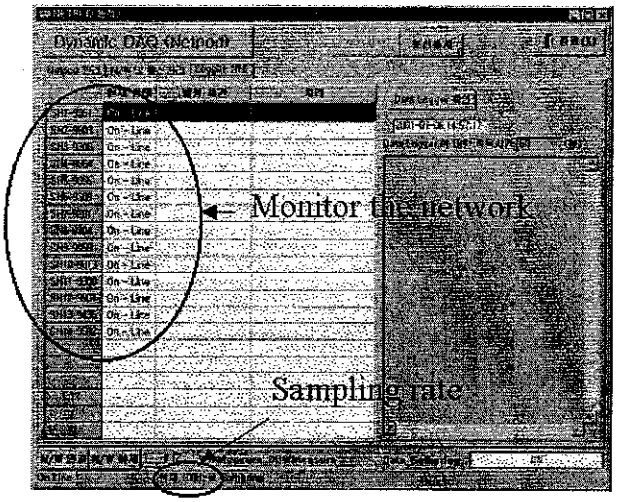

Fig.2 Display of network monitor with software

B. *Signal processing* - the monitoring software must have the function of converting electric signals into engineering signals. It must be programmed that the user is always available for the database in which gage factors and offset values are stored up for converting electric signals into engineering signals. In cable-stayed bridge, the tensions of cables are very important measurement. The software calculates the tensions of cables automatically using accelerations of cables.

The software must be programmed that it excludes doubtful signals that might be triggered with abnormality of sensors and data-logger in building up the database of the behavioral information of a bridge. Additionally, the warning alarm function must be included in the program to generate alarms in the case of emergency such as typhoon and earthquake. Figure 3 shows us how the gage factor and offset value are allocated in the database. Figure 4 shows us how to calculate the tension of a cable.

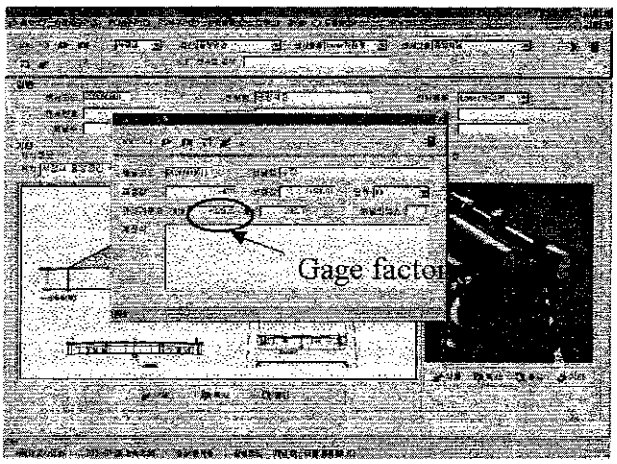

Fig.3 Display of gage factor and offset value of a sensor

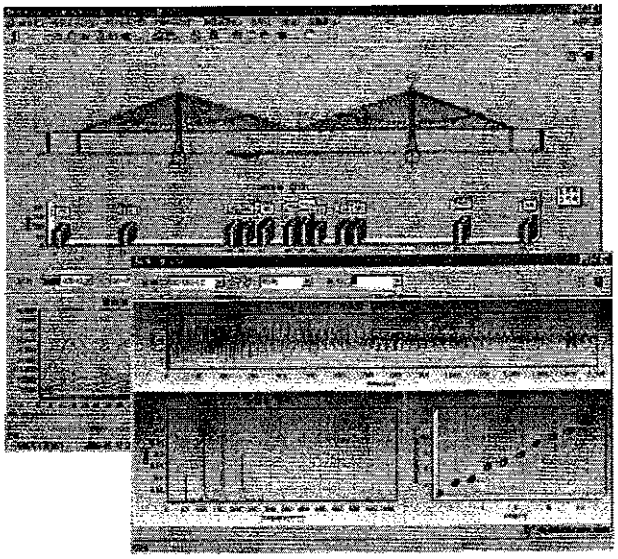

Fig. 4 Automatic calculation of the tension of a cable

C. *Data storage* - one of the most basic goals for sensors based monitoring system is to provide practical information with the designers, structural engineers, and the maintenance personnel by systematically constructing database built up with structural behavior information. The software stores statistics -average, max, min - of a measured data every ten minutes. The average shows us the behavioral information of a bridge under the temperature. The max. and min. shows us the behavioral information of a bridge under live loads
Sometimes structural engineers need raw data to research the behavior of a structure. Thus, it is recommended that a regular portion of a data acquired should be recorded as raw format.

D. *Data display* - data display is basically made through GUI Interface. The software must be programmed in a way that it displays real-time data and the user can refer to statistical data for a period they want to fix. In addition to the function mentioned above, monitoring software might have such function as correlation computation and summary report for measurement by user's request. Figure 4 shows the real-time displays and database of the behavioral information. Figure 5 shows the correlation of each item to be measured.

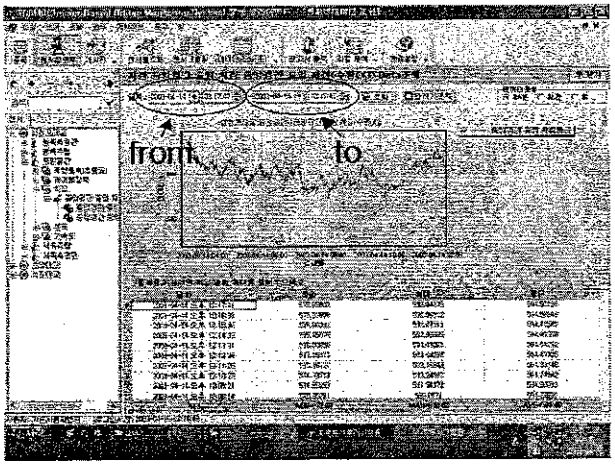

Fig.4 Display of real-time data and database

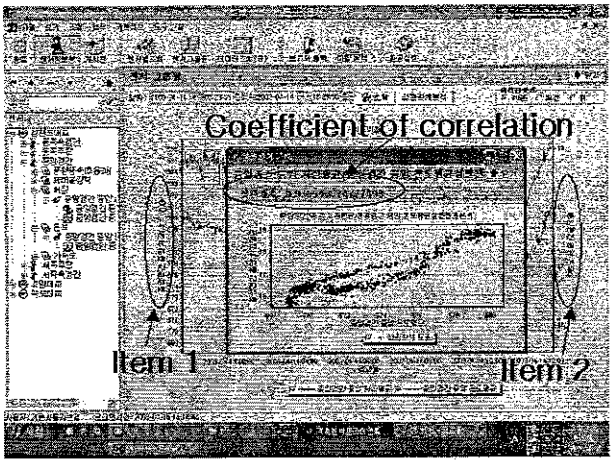

Fig.5 Correlation of measurement items

3. Summary

Sensors based bridge monitoring system is designed to make real-time monitoring and store up the performance history of in-service bridges. The monitoring system consists of hardware system and software system. The hardware system contains the sensors and data-loggers to measure the behavior of a structure, the communicational equipment to transmit measured data from the site to monitoring center, and the computer to arrange and analyze the data. The software system should have the functions such as data-logger control, signal processing, data storage, and data display. Finally, Structural engineers to select monitoring items, electric engineers to build hardware system and programmers to make software system should work together for sensors based bridge monitoring system.

Health monitoring using FBG sensors for structural members

Hiro-Yuki Nakazawa* **and** **Seishi Yamada****

* Dr. of Eng., JRPS Research Fellow, Dept of Arch. and Civil Eng., Toyohashi Univ. of Tech., Toyohashi 441-8580
** Dr. of Eng., Assoc. Prof., Dept of Arch. and Civil Eng., Toyohashi Univ. of Tech., Toyohashi 441-8580

In the present paper, thin-walled pultruded glass fiber reinforced polymer (FRP) structural member has been used and structural health using fiber Bragg grating sensor (FBG) embedded into the pultruded FRP has been discussed. In the case of the longitudinal tensile tests of members, the strain response has been recognized to be approximately the same as the conventional strain gauge, and optical power spectra have been measured in detail. In the case of the transverse direction tensile tests of joints have been performed, and an alternative new method for the installation of FBG sensor by using grass-fiber multi axial netting polymer layers has been proposed.

Key Words: FBG sensor, waveshape measurement, pultruded FRP, multi-axial

1. Introduction

The Japanese Specifications for Highway Bridges has recently been revised and the bridge design life has been redefined as 100 years. But, the actual life-cycles of the structural elements of bridges are much shorter, so it is necessary to develop a maintenance strategy for this kinds of sustainable infrastructures.

Fiber reinforced polymer (FRP) composite materials have potentialities of long-lived structural member, and are applied to the constructions of brides, space frames and buildings[1-4]. The FRP materials have many advantages, such as light weight, high specific strength, high corrosion resistance, long life, automated fabrication and rapid installation. Especially, pultruded FRP members, which consist of continuous fibers aligned in the pultrusion direction sandwiched between layers of continuous strand mat, are very suitable for this kind of the construction because of enhancement of the mass productivities due to the improvement of processing and manufacturing techniques. In addition, it is very attractive to reduce the environmental burden that carbon dioxide emissions in the fabrication process are much smaller than that in other fabrication process such as hand-layup and spray up. A great number of works on the FRP materials have been published in literature but limited information exists on the pultruded ones. Our previous papers in the FRP composites have dealt with the deflection behavior[5], the axially compressed buckling[6] and the connection collapse[7].

For realization of long-lived structure, not only applying the long-lived structural members but also monitoring the structural health will be surely needed. Fiber optic sensors are expected as new sensing device which replace conventional strain gauge. Fiber Bragg grating (FBG) sensor is one of the most exciting developments in the area of fiber optic sensing, and applying to civil engineering structure such as steel and concrete bridges has been tried[8].

In this paper, the strain output detail of fiber optic sensors embedded in pultruded FRP has been indicated, and the failure behavior of the structural FRP members has been discussed. In this study, two kinds of experiments have been performed to consider the application of FBG sensors to pultruded FRP members. In the case of the longitudinal tensile tests of members, the strain response has been recognized to be approximately the same as the conventional strain gauges, and optical power spectra have been measured in detail. In the case fo the transverse direction tensile tests of joints, an alternative new method for the installation of FBG sensor by using grass-fiber multi axial netting polymer layers has been proposed.

2. FRP material

A pultruded glass FRP plate is of the thickness t = 5.5mm, and cut from the flange of a 100mm×100mm box section. The pultruded section consists of two continuous fiber layers (28.3 vol%), three continuous strand mats (10.2 vol%) and two surfacing veils as shown in Fig.1. In the present study, the longitudinal x-direction is defined to be parallel to the continuous fiber. The mechanical properties identified through the tensile and bending tests for the strip elements (the identification technique is mentioned in Ref.5) are listed in Table 1. As shown in the table the transverse elastic coefficients are approximately half of those in the x-direction.

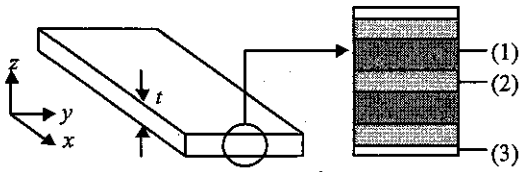

	thickness
(1) Continuous fiber	1.725 mm
(2) Continuous strand mat	0.65 mm
(3) Surfacing veil	0.05 mm
total (t)	5.50 mm

Fig. 1 Cross section

Table 1 Mechanical properties

Young's modulus for tension	E_x (GPa)	22.1
	E_y (GPa)	11.5
Young's modulus for bending	E_{bx} (GPa)	14.7
	E_{by} (GPa)	7.62
Poisson's ratio	ν_x	0.260
	ν_y	0.135
Tensile strength	σ_t (MPa)	347

3. Fiber optic sensing system

The fiber optic sensors in this study were of fiber Bragg grating (FBG). The FBG sensor consists of the clad and the core in which the simple intrinsic elements called Bragg diffraction grating are photo-imprinted. The sensor length is 10mm and the grating pitch Λ is 500nm. The strain response arises due to the elongation of the sensor which corresponds to fractional change in grating pitch. Generally, the shift in Bragg wavelength with strain can be expressed using[9)]

$$\Delta\lambda_B = 2n\Lambda\left\{1-\left(\frac{n^2}{2}\right)[P_{12}-\nu(P_{11}+P_{12})]\right\}\varepsilon \qquad (1)$$

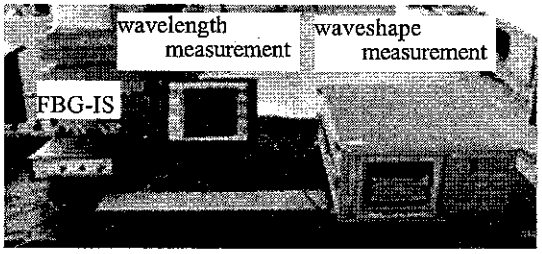

Photo 1 Measurement system

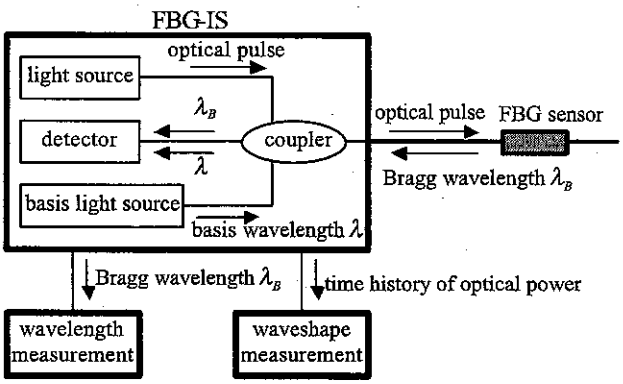

Fig. 2 Diagram of measurement system

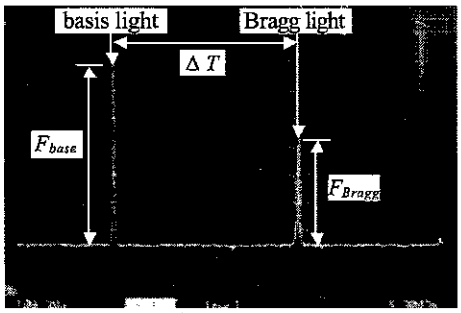

(a) $\varepsilon = 0\mu$

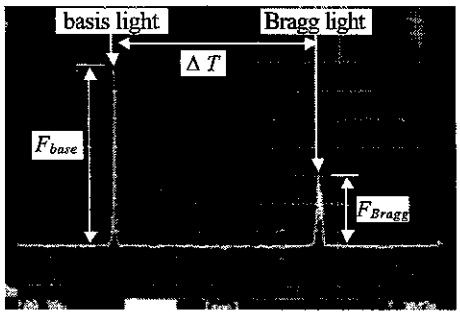

(b) $\varepsilon = 2000\mu$

Photo 2 Time history of optical power

where $\Delta\lambda_B$ is the shift in Bragg wavelength with strain, n is the effective index of the core, P_{ij} coefficients are Pockel's coefficients of the stress-optic tensor, ν is Poisson's ratio. In the present measurement the applied strain e is given by

$$\varepsilon[\mu] = 833[\mu/\text{nm}] \times \Delta\lambda_B\,[\text{nm}] \qquad (2)$$

Also the dependence of the Bragg wavelength on temperature arises due to both the dependence of the index of refraction of the glass and the thermal expansion

of the glass; the calibration factor in the present sensors is 0.010nm/ °C .

Figure 2 shows the schematic diagram of the strain measurement system: the main equipment consists of the input of light with a broadband spectrum and the wavelength detection system of the narrowband component reflected by the FBG. It is associated with the wavelength monitor and the waveshape measurement monitor as shown in Photo 1. Photo 2 is an example of waveshape measurements. As the basis light is invariable at all times, the time difference (ΔT in Photo 2) between the peak time of the basis light and that of the Bragg light is directly related to the wavelength measurements.

4. Longitudinal tensile tests of members

Figure 3 shows the schematic set up of the specimens for longitudinal tensile tests of members. A groove having a depth of 0.5mm was chiseled in the pultruded FRP member, and the FBG sensor was embedded into the groove using epoxy regin. This specimen collapsed completely at 367MPa in tensile stress which correspond to 1.8% strain. This ultimate strength is approximately equal to the result of material test as listed in Table 1, and the embedding effect of the FBG sensors on load carrying capacity does not occur.

Figure 4 shows the relationship between the strain ε_{gauge} measured by strain gauge and the strain ε_{FBG} calculated by equation (2). In this figure, it was demonstrated that the FBG sensor was measured with sufficient accuracy with in 18000 μ strain.

Figure 5 indicates the results of wavelength measurements: the value of the horizontal axis is the Bragg wavelength λ_B . All the results are roughly linear in not only loading but also unloading stages. But, in the second loading stage, the bifurcations of the Bragg wavelength occurred at a point of around 6000 μ strain, and the bifurcation load decreases as the cumulative repetition tensile load increases. This bifurcation behavior is shown to be related to the change of the waveshape which is defined as the shape of the equivalent optical power spectra shown in Fig.6. Here, the vertical axis F_{op} is normalized by the optical power of the basis light. The optical power decreases as the load increases, and the shape have two peaks after reaching at a critical load. The critical load is recognized to be approximately the same as the bifurcation load in Fig.5. It would be considered that when the optical power spectrum has two peaks the FBG becomes two different FBGs due to the occurrences of small transverse cracks[10] inside the FRP member.

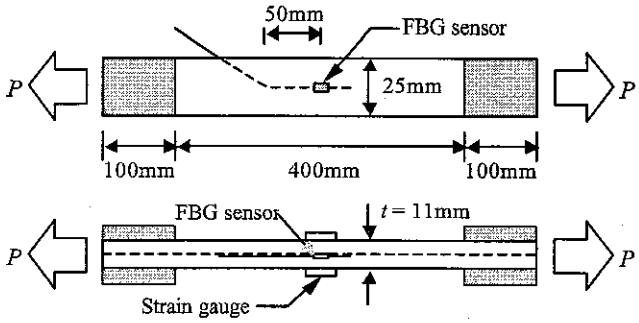

Fig. 3 Set up of specimens for longitudinal tensile tests

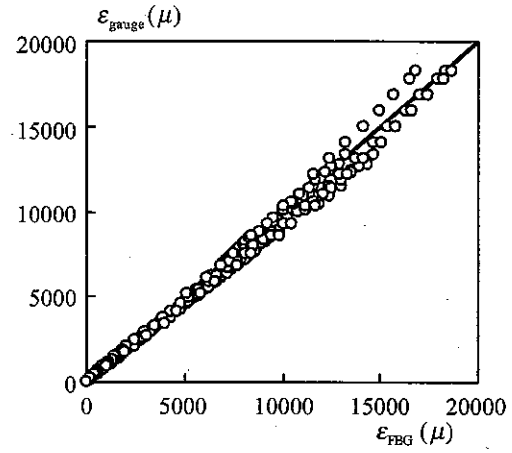

Fig. 4 The accuracy of strain obtained FBG sensor

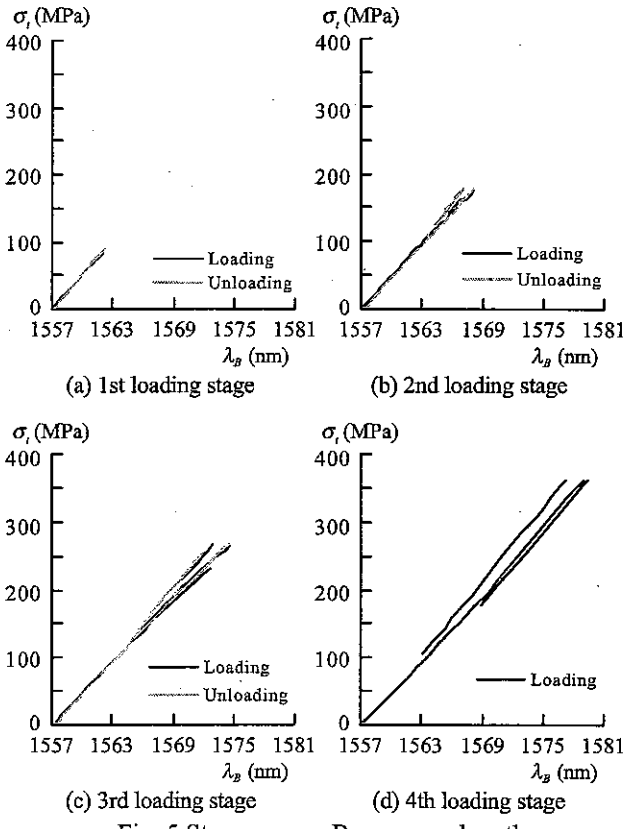

Fig. 5 Stress versus Bragg wavelength

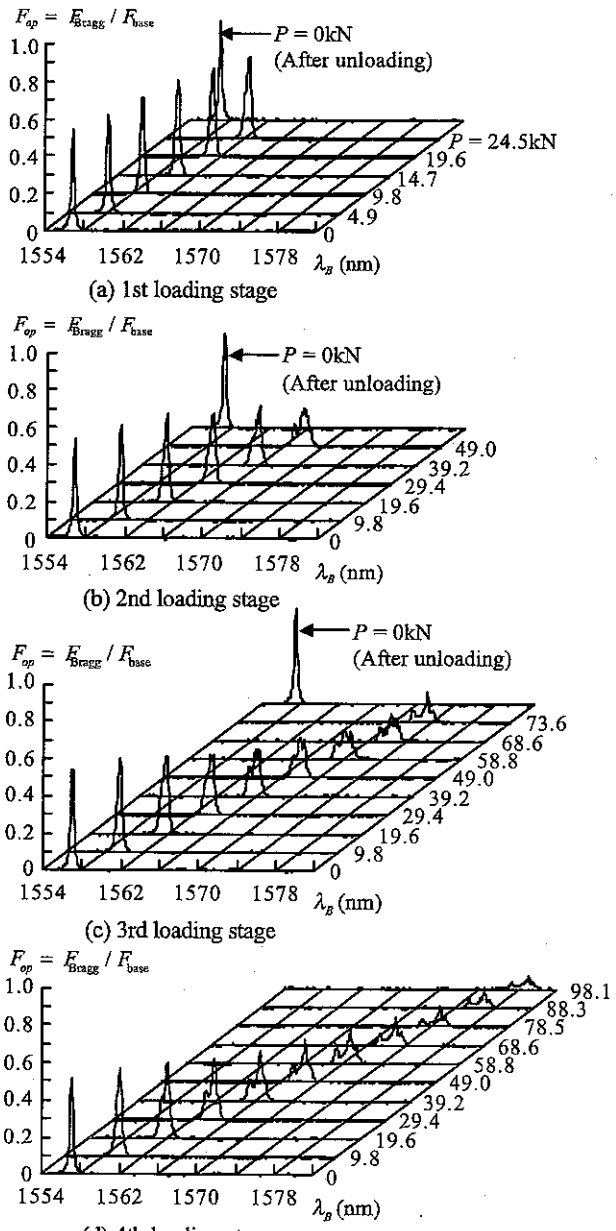

Fig. 6 Variations of optical power spectra

5. Transverse tensile tests of joints

Figure 7 shows the schematic setup of the joint test. The transverse y-direction of the specimens was subjected to tensile loading via a 98kN oil-pressure test machine. The non-structural member was connected to the FRP structural member with three M10 bolts, and the fastened torque level in this study was adopted to be 25N· m. The FBG sensor was embedded beside the center bolt hole as shown in Fig.7.

Normally the transverse y-direction strength of the pultruded FRP member is very small. For that case it would be useful to reinforce the y-direction strength of the FRP member by using the multi-axial layers as shown in Fig.8. In the figure the FBG sensor was embedded during the hand-lay-up of the second multi-axial layer.

Photo 3 shows the appearance of the FRP members beside the holes after non-structural member failure. In the present study, repeated tensile loading was performed, that is, the FRP member in the first and the second loading stage was the same, and only the non-structural member was changed after the first loading stage. In Photo 3(a), no damages in the FRP members in the first loading stage were observed visually. But, in the second loading stage the damages occurred due to the bearing of bolts as referred in Photo 3(b). However, since the maximum load of the first loading stage is 15% larger than that of the second loading stage, it is difficult to comment whether new damages related to the loading repetition occur or not.

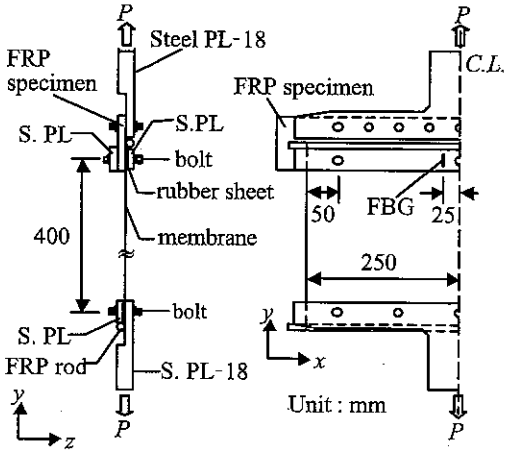

Fig.7 Set up of specimen

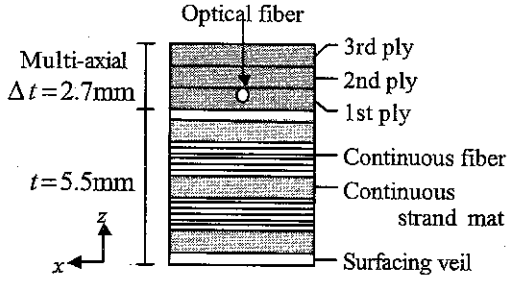

Fig. 8 Cross section of the FRP member with multi-axial covering layer

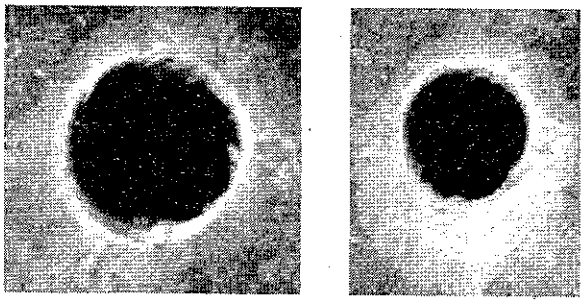

(a) After 1st loading (b) After 2nd loading

Photo 3 Appearance of the FRP members beside the holes after non-structural member failure

Table 2 Results of strain measurements for no-loading stage

		initial state	after embedding	after laminating	after drilling	after fastening bolt
original data	λ_B (nm)	1557.272	1557.255	1557.257	1557.347	1557.647
	strain ε	0	-15 μ	-13 μ	63 μ	312 μ
	temp.°C	[17.4]	[15.9]	[16.6]	[16.6]	[17.5]
revision for temperature	λ_B (nm)	1557.272	1557.270	1557.265	1557.355	1557.646
	strain ε	0	-2 μ	-6 μ	69 μ	312 μ
	temp.°C	[17.4]	[17.4]	[17.4]	[17.4]	[17.4]

Table 2 lists the measurement data of FBG sensors at various pre-loading stages. In sensor embedding process and multi-axial laminating process, negligibly small strain was observed; and relatively large strain, which would be related to the freedom of the hardening shrinkage beside the bolt hole, was obtained after drilling. But considering that the fracture elongation of FRP is over 18000 μ strains, these strains are negligible in practice.

Figure 9 shows the tensile load versus the Bragg wavelength plots. Around 300 μ strains occurred due to the effects of the fastening of bolts. In the initial loading stages the curves are approximately vertical because the friction force between the lapping surfaces would occur. After the alienation the curves have the lower slope and then bifurcate. When the optical power spectrum in the first loading stage has two peaks as shown in Fig.10, the value of ε_{FBG} is of around 1500 μ strain. This result means that the locally large stress-concentration beside the bolt hole occurs. The critical load in the first loading stage is smaller than that in second loading stage; the reason would be of the accumulation of the transverse cracks under the loading repetition. It would be possible to use these behaviors in order to estimate the structural health of the joints.

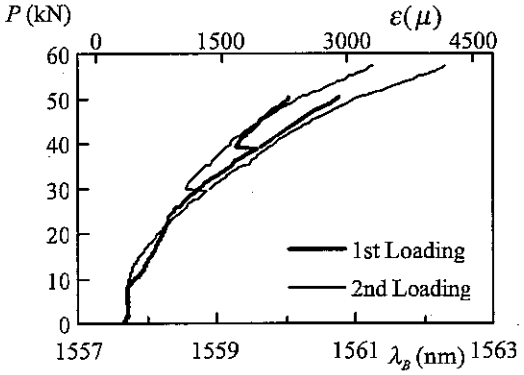

Fig. 9 Load versus Bragg wavelength

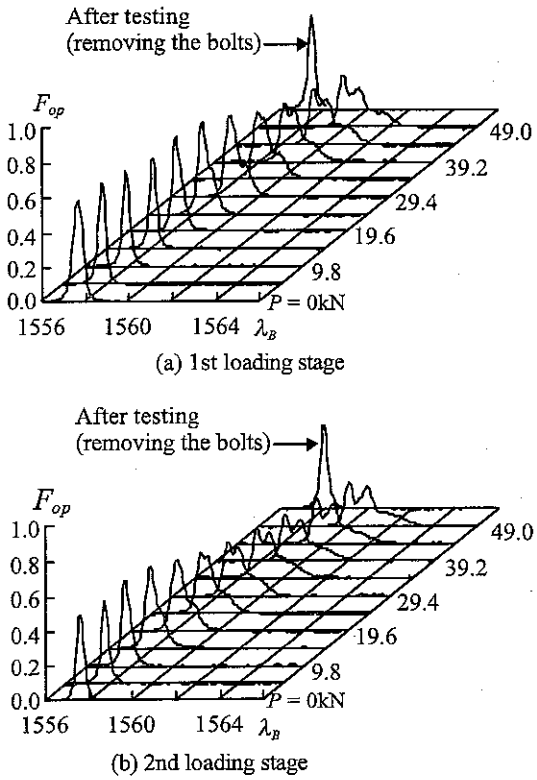

Fig. 10 Variations of optical power spectra

6. Conclusions

This present paper dealt with the fiber optic sensing for the members and the joints of the pultruded FRP structures. The fiber optic sensors in this study were of fiber Bragg grating (FBG). The strain output detail of the FBG sensors embedded into the pultruded FRP members has been measured with in 18000 μ strain, and the strain response has been recognized to be approximately the same as the conventional strain gauge. In the second loading stage, the bifurcations of the Bragg wavelength occurred at a point of around 6000 μ strain, and the bifurcation load decreases as the cumulative repetition tensile load increases. Then the optical power, which obtained waveshape measurements, decreased rapidly, its shape had two peaks because of the FBG sensor became two different FBG sensors due to the occurrences of small transverse cracks inside the pultruded FRP member.

On the other hand, the fiber optic sensing for the joints of the pultruded FRP has been performed, and an alternative new method for the installation of FBG sensor by using grass-fiber multi axial netting polymer

layers has been proposed. The bifurcation of the Bragg wavelength occurred at a point of around 1500 μ strain; this value was smaller than that in tensile test of the pultruded FRP member. Therefore, in the case of health monitoring of FRP structure, it is more important to evalute properly the structural health of the joints. It is believed that the present paper should contribute to the important task of health monitoring not just for the FRP structures but, when extended, for wider classes of buildings and civil engineering structures.

Acknowledgements

This paper was supported by a grant-in-aid for scientific research No.11049, Reserch Fellowships of the Japan Society for the Promotion of Science for Young Scientists. Also this study is the part of The 21st Century COE Program, Ecological Engineering for Homeostatic Human Activities.

References

1) Burgoyne, C.J. : Advanced composites in civil engineering in Europe, IABSE, pp.267-273, 1999.
2) Keller, T : Overview of fibre-reinforced polymers in bridge construction, Structural Engineering International, IABSE, pp.66-70, 2002.
3) Keller, T. and Castro, J.: Structural applications of advanced composite materials for bridges and buildings, *CD-ROM Proc., IASS Symp., Nagoya,* TP197, 2001.
4) Sugizaki, K.: Development of space frame and monocoque roof with CFRP for large-span structures, *CD-ROM Proc., IASS Symp., Nagoya*, TP158, 2001.
5) Yamada S., and Komiya I., Elastic Deflection Behavior of a Box-Shaped Pultruded Composite Member and its Collapse, *Fiber Composites in Infrastructure, ICCI'96*, pp.699-707, 1996.
6) Yamada, S., Nakazawa, H.Y. and Komiya, I., Buckling and collapse of pultruded fiber reinforced polymer member under Compression, *APCS Symp., SEOUL*, Vol.2, pp.961-968, 2000.
7) Yamada S., Nakazawa H., Fukatsu N., and Komiya I., Experiments on the Connection Collapse of Pultruded Fiber Reinforced Polymeric Composites, *CD-ROM Proc. IASS Symp.*, TP071, 2001.
8) Schultz, W.L., Conte, J.P and Udd, E., Long gage fiber optic Bragg grating strain sensors to monitor civil structures, *Smart Structures and Materials 2001, Proc. SPIE* Vol.4330, pp.56-65, 2001.
9) Kersey, A.D., et al., Progress Towards the Development of Practical Fiber Bragg Grating Instrumentation Systems, *SPIE*, Vol.2829, 1996.
10) Satori,K. Fukuchi, K. Kurosawa, Y. Hongo, A. and Takeda, N., Polyimide-coat small-diameter optical fiber sensors for embedding in composite laminate structure, *Smart Structures and Materials 2001, Proc. SPIE* Vol.4328, pp.285-294, 2001.

(Received July 31, 2003)

Evaluation of the Atmospheric Environment for Corrosion of Steel Members of Civil Structures

Tomoyuki Yamazaki *, Toshiyuki Oshima **, Shuichi Mikami ***

* Research Associate, Dept. of Civil Eng., Kitami Institute Technology, 165, Koencho, Kitami, Hokkaido 090-8507
** Dr. of Eng., Professor, Dept. of Civil Eng., Kitami Institute Technology, 165, Koencho, Kitami, Hokkaido 090-8507
*** Dr. (Eng.), Associate Professor, Dept. of Civil Eng., Kitami Institute Technology, 165, Koencho, Kitami, Hokkaido 090-8507

Knowledge of corrosion conditions or environment of the steel materials is crucial for performing maintenance management of civil engineering structures. Accurate measurement of the relation of the installation environment of a steel structure and corrosion can yield an effective evaluation because deterioration prediction of a structure or maintenance repair can be done. Experiments in this study include exposure experiments for sensors in interior rooms and outdoors. This paper reports results for measured corrosion environments under paint.

Key Words : ACM sensor, atmosphere corrosion, maintenance management

1. Introduction

It is crucial to know corrosion conditions or the corrosion environment of a steel structural member for performing maintenance management of civil engineering structures. Quantitative measurement of the environment (urban, rural, mountainous, river, seashore, etc.) of a structure's location can clarify the relation between steel-material corrosion and that environment. Moreover, predicting paint degradation for preventing steel-materials corrosion serves as reference data to determine the repainting period of steel materials. Especially for bridges, this factor influences changes in corrosion or paint degradation with the installation direction of a bridge and bridge parts of a form. Quantitative measurement of the degree to which the environment (urban, rural, mountainous, river, seashore, etc.) influences steel-member corrosion can facilitate effective damage prediction for structures and a standard of maintenance. Moreover, prediction of damage to the paint that prevents steel-member corrosion will become reference data for scheduling of steel member repainting. Structural components and their orientation with respect to the member surface are considered to be influential factors on corrosion and paint damage on the bridge.

This study uses the recently developed Atmospheric Corrosion Monitor (ACM) type corrosion sensor. It is intended to quantitatively evaluate the relation between structural degradation and the corrosive environment, and differences in corrosive environments for each bridge part.

In this experiment, exposure experiments were conducted in the following environmental conditions to obtain fundamental ACM sensor data: 1) indoor (laboratory), 2) outdoor (inland environment), 3) an artificial corrosion acceleration environment, and 4) a lakeside (waterside environment) of a brackish lake. These environments were evaluated using an ACM sensor and a painted sensor. Those results are reported.

2. Experiment Outline

2.1 Experimental device

(1) ACM corrosion type sensor[1)]

The constitution of an ACM sensor (Fig. 1, Photo 1) used a carbon steel board (64 × 64 mm) with thickness of 0.8 mm as the basal plate with painted on insulating paste (30 ~ 35 μm in thickness) to this basal plate. Furthermore, lamination printing of the electric conduction paste (Ag, 30 ~ 40 μm thick) was carried out on the pattern of insulated paste to maintain insulation with this basal plate. This conductive paste serves as the cathode of the sensor; the pattern exposure part of the carbon steel basal plate serves as the anode. Moreover, copper foil (5 × 5 mm) is adhered to the electric conduction paste for use as a lead-wire terminal. Ultrasonic washing and a nitrogen atmosphere in the working area prevent oxidization of a basal plate or electric conduction paste during the ACM sensor manufacturing process.

The principle of ACM sensor exposure is the atmosphere the

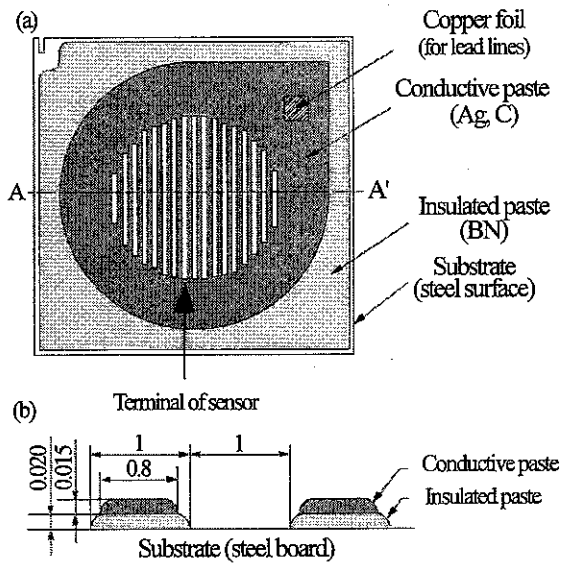

Fig. 1 Outline figure of ACM sensor

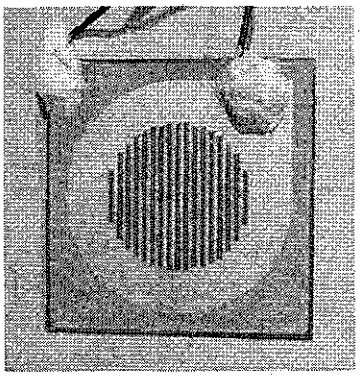

Photo 1. ACM sensor

terminal of two different-species metal (Fe-Ag). Connecting these metals with a film of water will engender an oxidation reaction and corrosion current will occur. Moreover, corrosion current can be measured not only in the inside of solution, but in the inside of the atmosphere and an indoor environment because the water film is produced in comparatively high humidity conditions among both metals with this sensor. We measured this corrosion current and monitored the corrosion environment.

Regarding sensor characteristics, the measurement range of the sensor output is 1 nA ~ 13 mA; the decomposition ability is 1 nA in 1 nA ~ 10 μA, and 1 μA in 10 μA ~ 13 mA. In measurements using this sensor, current larger than 10 nA(s) is inferred to be a significant signal of corrosion. The atmospheric environment is judged at three periods: a rainy period (Rain), a dew-condensation period (Dew), and a dry period (Dry) by this corrosion current. We consider wet-time = Rain + Dew; this wet-time serves as an evaluation of the corrosion environment.

Moreover, it is possible to update and exchange sensors to measure prolonged corrosion information even though the typical sensor lifetime is several months: the sensors are mass-produced and reproducible.

(2) ACM data recorder

This data recorder can measure 16-track ACM sensors and 8-track temperature and humidity sensors simultaneously. This recording device has an automatic meter that can record a minimum measurement interval of 10 min. The recorder can use a compact flash memory card; a battery and an exchangeable power supply can serve as a power supply. This recorder measures only ACM sensors data; it can measure very feeble current to the nano-ampere scale.

Data measurable from these ACM sensors and the recorder system are corrosion current, environmental temperature, and humidity. The total time of the wet condition in which steel materials corrode from this measurement data can be judged. The quantity of adhered airborne salt can be inferred from corrosion current and environmental humidity[1].

2.2 Experiment conditions

(1)The sensor situation during measurement

The basal plate of an ACM sensor is made of corrosive carbon steel material. For this reason, after adhering the basal plate of a sensor on the plastic sheet and plate so that a basal plate and a steel member might not be contacted directly, it was installed in the object part. Moreover, compared to a normal ACM sensor, the same paint as the steel girder of a bridge was applied to the ACM sensor. It was measured in the same environment.

(2) Environmental conditions

Environmental conditions exposed sensors in the following four conditions.

1) Indoor exposure in the laboratory (Indoor environment)
2) A position about 20 cm over the ground with outdoor exposure outside the laboratory (Inland environment)
3) Direct fog-like sea water is blown upon a sensor. Then it is placed into a sealed container for about two days. It is taken from a container and is dried for about two days indoors. After measurement, the cycle repeats. (Accelerating environment)
4) A waterside environment with steel sheet pilings constructed to the civil engineering structure by a lake side. It is an inferior environment (Waterside environment of a brackish lake)

Table 1 Environmental conditions

Environmental conditions	Paint conditions	Sensor number
1) Indoor (inside)	normal	ACM1-1
	paint	ACM1-2
2) Inland (outside)	normal	ACM2-1
	paint	ACM2-2
3)Accelerating (sealed box)	normal	ACM3-1
	paint	ACM3-2
4) Waterside (lake side)	normal	ACM4-1 (0.3 m)
	normal	ACM4-2 (1.5 m)
	normal	ACM4-3 (2.0 m)

Automatic measurement is done at 10 min intervals in the above conditions. Moreover, temperature and humidity for every environmental condition are measured simultaneously. The sensor was installed so that the sensor terminal side might become level to the ground on the conditions of 1), 2) and 3); it was perpendicularly installed in 4). Table 1 shows environmental conditions and each sensor number.

3. Measurement Result

Herein, we report the result with the data, measured 10/2001 ~ 12/2001.

1) Indoor environment (inside of a laboratory, measurement starting date: 9/27/2001)

Corrosion current was not generated in ACM1-1 (normal) after two months. As expected, current was not generated in ACM1-2 (with paint), probably because the highest relative humidity was also 60% and the average was lower than 50% in the laboratory. Rust discolored the sensor surface (Photo 2).

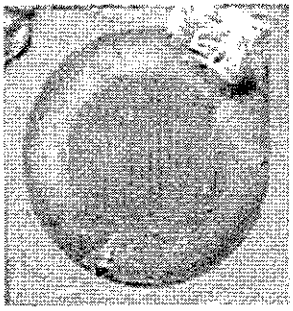

(12/7/2001 Photograph)
Photo 2. Sensor ACM1-1

2) Inland environment (outside of a laboratory, measurement starting date: 9/27/2001)

Examples of data measured in sensor number ACM2-1 is shown in Figs. 2 and 3. The vertical axis of this graph shows corrosion current and the horizontal axis shows measurement time. Moreover, temperature and humidity data which were measured in the same environment for reference are also shown. Measured values of corrosion current are shown on a logarithmic because their range is large. Shown are measured data of Fig. 2 on 10/27 to 10/30 and data of Fig. 3 on 11/28 to 12/2. Corrosion current was not generated in painted sensor ACM2-2 in this environment, but the sensor ACM2-1 of paint generated no corrosion current.

The weather of 10/27 to 10/30 was fine with some rain. That data is shown in Fig. 2. Section ① shows extremely larger data before and after that period because it is during the rainy term (Rain). Section ② is larger than 10 nA, so it is inferred to be a dew-condensation term (Dew). Because section ③ is lower than 10 nAs, it is considered to be the dry term (Dry). Moreover, by this data, the rate for which it gets wet-time (= Dew + Rain) accounts is considered to be a term during which corrosion occurs.

Next, the weather of the 11/28 to 12/2 was fine and with snow.

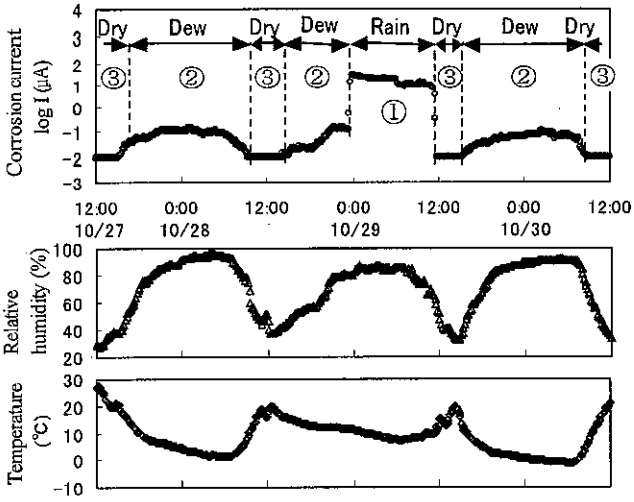

Fig. 2 Data of Sensor ACM2-1 (1)
(10/27/2001~10/30/2001)

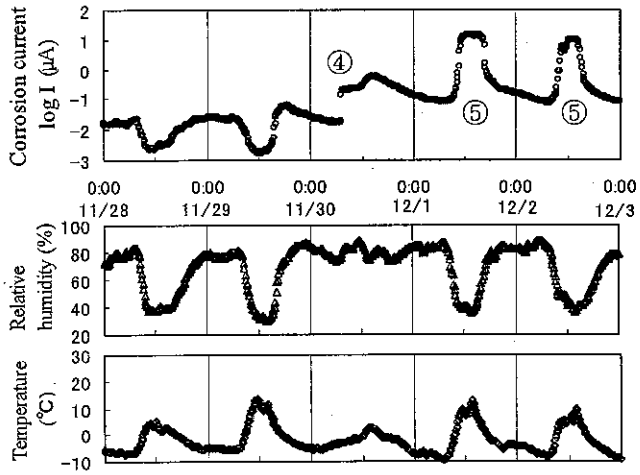

Fig. 3 Data of Sensor ACM2-1 (2)
(11/28/2001~12/2/2001)

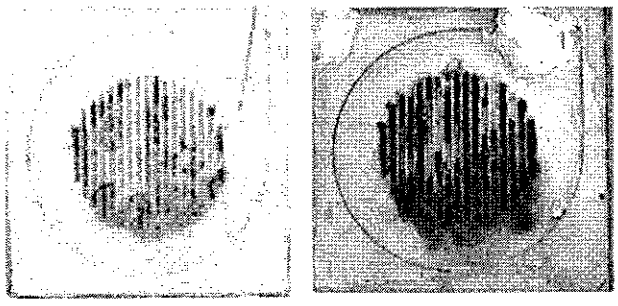

(10/15/2001) (11/16/2001)
Photo 3. Sensor ACM2-1

That measured data is shown in Fig. 3. Data on 11/28 and 11/29 show it to be a dew-condensation term during the night, whereas daytime can be judged as a dry term with fine weather. Next, corrosion current becomes large abruptly in section ④ when rain or the snow fell. However, although corrosion current became low abruptly as shown in Fig. 2 after the rain finished, a sudden change was not shown in this section. Snow lies on the sensor surface and is considered to have continued passing corrosion current because we had installed the sensor horizontally. Furthermore, by data at 12:00 on 12/1 and 12/2 in

section ⑤, corrosion current was extremely large, humidity is as low as about 40%, and temperature show the highest temperature of the day. Snow thaws during fine days between the terminal dew periods. It is inferred that corrosion current occured then. Sensor ACM2-1, shown in photographs on 10/15 and 11/16, is shown in Photo 3. Photo 3 shows the rust generated among 30% of the sensor terminal parts on 10/15. The rust will be generated among all terminal parts on 11/16.

3) Accelerating environment (inside of the sealed box, measurement starting date: 9/27/2001)

Sensor ACM3-1 (accelerating environment, normal) measured data is shown in Fig. 4; that data is for the period between 10/1/2001 to 10/6/2001. During this term, after seawater exposure at 17:00 on 10/1, it was put into the sealed box, and it was taken from the sealed box to 13:00 on 10/4, and is made to dry in the laboratory. Data of ACM3-1 show that high corrosion current occurred after exposure to seawater; high current continues to occur after that. Although the current became slightly lower after dryness, generated corrosion current continued. After that, this current was larger than 10nA. Since the salt of sea water adhered to the sensor terminal, this is considered for promoting oxidation reaction also in slight humidity.

Moreover, corrosion current was not generated even though sensor ACM3-2 (paint) was put in the accelerating environment for over two months.

4) Field environment (lakeside, measurement starting date: 10/27/2001)

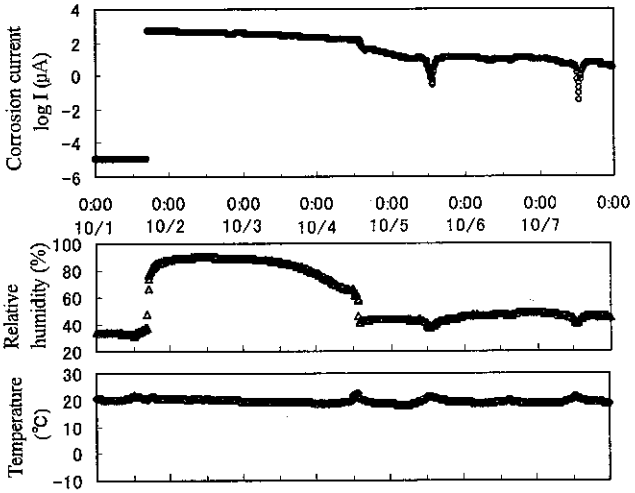

Fig. 4 Data of Sensor ACM3-1
(10/1/2001 ~ 10/6/2001)

Figure 5 shows the measurement situation in the waterside environment (lakeside) of the civil engineering structure is shown in Photo 4. Although the installation position of the sensor was installed at a height of about 0.3 m (ACM4-1), 1.5 m (ACM4-2), and 2.0 m (ACM4-3) from the lake water surface, as shown in Fig. 5, the height from the water surface was not fixed by the water level. The sensor is installed perpendicularly to the water surface. Moreover, temperature and the humidity sensors are installed in 1.0 m upper part from ACM4-3.

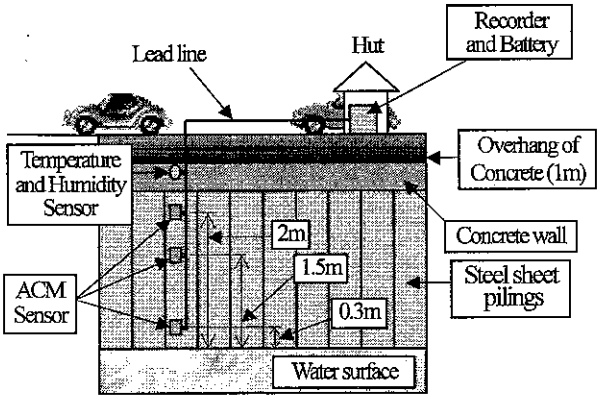

Fig. 5 Sensor installed position in waterside environment

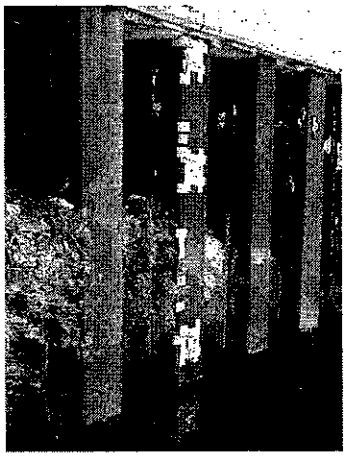

Photo 4.
Photograph of the waterside environment

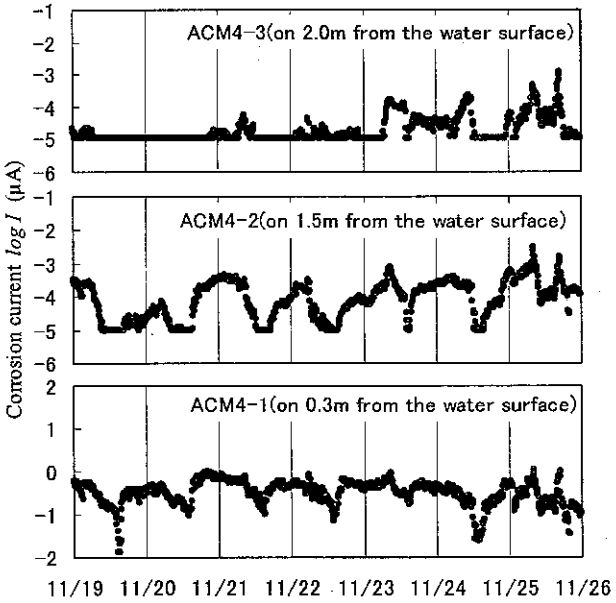

Fig.6 Data of sensor measured in waterside environment
(11/19/2001~11/26/2001)

Data measured from 11/19/2001 to 11/26 are shown in Fig. 6. As a tendency of field environment data, corrosion current occurred early from the sensor near the water surface; that current is also high. Moreover, when high corrosion current occurred in sensor ACM4-1 near the water surface, it did not occur in another sensor ACM4-2 and 4-3. Sensor ACM4-1it is considered to be easily influenced by water

of the lake because it is installed in the position near the water surface. For example, the water driven upward by wind pressure. It is inferred that water evaporation, submersion in the lake, etc., generated the current.

Moreover, although corrosion current of ACM4-1 and ACM 4-2 showed similar tendencies, ACM4-3 had lower measured values. Some weather interruption occurred because the concrete overhang (about 1 m) is in the upper part of steel sheet pilings with installed sensors, as shown in Fig. 5. A photograph of the field sensor was taken on 1/15/2002 (Photo.5). The photograph shows ACM4-1 is the terminal part whole region, ACM4-2, about 1/3 of terminal part, and ACM4-3 where the terminal part is rusty. The entire terminal surface was discolored.

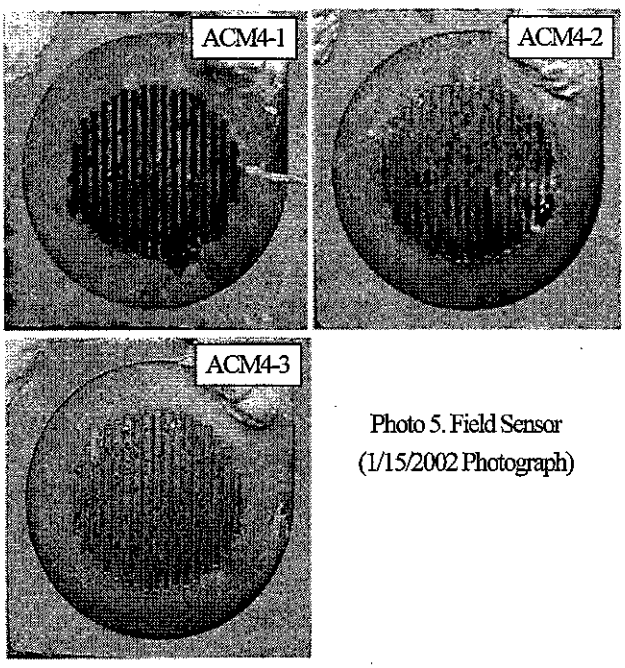

Photo 5. Field Sensor
(1/15/2002 Photograph)

4. Estimation of Airborne-Salt Adhesion

Here, estimation of the amount of airborne-salt adhesion is explained. It is estimated using the calibrating curve. The calibrating curve is made from the test using an ACM sensor. First, salt water of known concentration is applied to an ACM sensor; then the sensor is put in a location which can regulate humidity. The humidity is changed and corrosion current is measured. A calibrating curve, which shows the relation of salt concentration and relative humidity, can be made.

The calibrating curve used here uses the calibrating curve indicated in 1). Data measured by the calibrating curve and this experiment are shown in Fig.7. The vertical axis of the graph shows corrosion current; the horizontal axis shows relative humidity and the calibrating curve of each salt concentration (1.0E+1 ~ 1.0E-3 mg/cm^2) is plotted. Measurement data shown here is data of the ACM sensor arranged horizontally, Δ is measured inland and ○ is data measured by the lake-side. Moreover, it is used measured in the fine weather when estimating the amount of salt adhesion.

Data (Δ , 9/10) of inland is estimated to be 1.0E-4 mg/cm^2 from the measurement result of a figure lower than the calibrating curve of 1.0E-3 mg/cm^2; it is thought that salt has hardly adhered. Moreover, because data (○, 10/9) of the lake side is close to the calibrating curve of 1.0E-3 mg/cm^2, the amount of salt adhesion is estimated to be 1.0E-3 mg/cm^2.

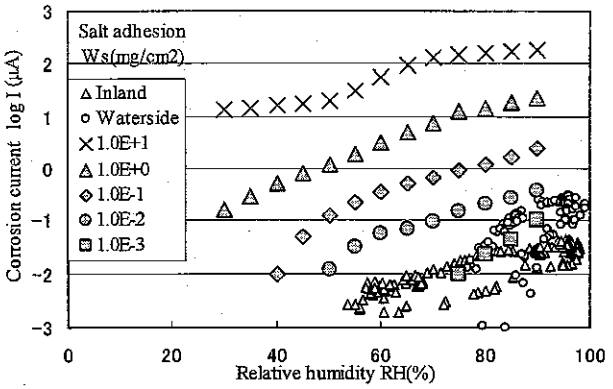

Fig. 7 Calibrating curve airborne-salt adhesion

5. Conclusions

The atmospheric environment can be distinguished using corrosion current measured by the ACM sensor in the rain term, the dew-condensation term, and a dryness term. The corrosion by dew condensation of a high humidity term can also be discriminated clearly.

1) Evaluation of the corrosion environment is possible from estimation of the wet-time.

2) The ACM sensor has a thin shape and is lightweight; therefore a sensor could be installed in each part of a structure to evaluate the environment of each structural component.

3) The salt adhesion amount is estimated from corrosion current and relative humidity; evaluation of damage from salt water is possible as corrosion environment.

It is thought of because the measurement period of this experiment was short by the painted ACM sensor that corrosion current has not occurred. If the crack and delamination of paint arise by degradation of paint, it will be thought that moisture adheres to the ACM sensor surface and current arises. And evaluation of paint degradation will be enabled from the result.

Moreover, in this experiment, it is measuring by the sensor of perpendicular installation and horizontally installation. Since measurement environment is different, it cannot compare simply. Corrosion current generating of horizontally installation is earlier than perpendicular installation. There were also many amounts of generating of current. In order to examine this result further, these sensors will be measured in the same environment.

Acknowledges

The authors wish to thank Mr. Satoshi Yasue of Docon Co., Ltd., Mr. Tomiji Abe of Hokkaido Regional Development Bureau and Mr. Satoshi Kyoya of Aomori City Office for their assistance in this study.

References

1) Motoda, O., Suzuki, Y., Shinohara, T., et al.: ACM Type Corrosion Sensor to Evaluate Corrosivity of Marine Atmosphere, "Zairyo-to-Kankyo", Vol.43, pp. 550-556, 1994
2) Motoda, O., Suzuki, Y., Shinohara, T., et al.: Corrosive Factors of A Marine Atmosphere Analyzed by ACM Sensor for 1 year, "Zairyo-to-Kankyo", Vol.44, pp. 218-225, 1995
3) Motoda, O., Suzuki, Y., Shinohara, T., Tsujikawa, S.: Corrosivity of Indoor Atmosphere for a Prefabricated House, "Zairyo-to-Kankyo", Vol.47, pp. 651-660, 1998
4) Yamazaki, T., Oshima, T., Mikami, S., Yasue, S.: Evaluation Atmosphere Environment for Corrosion of Steel Member of Civil Structure, Proc. Hokkaido Chapter of JSCE, No.58, pp. 26-28, 2002

Nonlinear Behavior of Cable-Stayed Bridge Tower under Level II Earthquake Ground Motion

Shehata E. Abdel Raheem[*] and Toshiro Hayashikawa[**]

[*]Graduate Student, Graduate School of Eng., Hokkaido University, Nishi 8 Kita 13 Kita-ku, Sapporo 060-8628
[**]Assoc. Professor, Graduate School of Eng., Hokkaido University, Nishi 8 Kita 13 Kita-ku, Sapporo 060-8628

The dynamic analysis of cable-stayed bridges in seismically active regions is potentially important to highway facilities design. A quite general nonlinear dynamic analysis is developed for a realistic prediction of cable-stayed bridge tower seismic performance. One of the most important decisions in carrying out proper analysis is to select a design earthquake that adequately represents the ground motion expected at certain site and in particular the motion that would drive the bridge structure to its critical response, resulting in the highest damage potential. So an extensive series of seismic response analyses using a wide range of recorded and simulated ground motions are carried out. The ductility and base shear demands due to near-fault and long duration ground motions are compared. The stipulation of code standard input excitation limitations and the present calculated demands are discussed.
Keywords: Steel tower, cable-stayed bridge, seismic response, near-fault ground motion

1. Introduction

In recent decades, long span bridges such as cable-stayed bridges have gained much popularity due to their aesthetic appearance, technically innovative, structurally sound, efficient utilization of structural materials, increase of the horizontal navigation clearances and the economic trade off of span length cost of deep water foundation. As a result, the trend today for cable-stayed bridges is to use more shallow or slender stiffening girders combined with increasing span length. This structural synthesis provides a valuable environment for the nonlinear behavior due to material nonlinearities and geometrical nonlinearities of the relatively large deflection of the structure on the stresses and forces [1, 2]. After the January 17, 1995, Hyogoken Nanbu earthquake, the ductility design and dynamic analysis have been reconsidered in Japan [3 - 5]. The necessity has arisen to develop more efficient analysis procedures that can lead to a through understanding and a realistic prediction of the precise three-dimensional nonlinear dynamic response of bridge structural systems to improve the bridges seismic performance and to provide damage control and post-earthquake functionality.

Because of the unsatisfactory performance of highway bridges in the 1995 Hyogoken Nanbu earthquake [6 - 8], the Japanese Design Specifications of Highway Bridges were revised in 1996 and near-fault ground motions developed in the Kobe earthquake were included in the 1996 Japanese design codes. The recent earthquake damage to bridges located within a few kilometers from a fault rupture clearly indicated the importance to consider the near-fault ground motion effect. The intensity of acceleration was very high and was characterized by single pulse with large acceleration and long predominant period, as well as the strong intensity. The directivity of the near-field ground motion is important in seismic design. The pulses with large intensity are generally different in a direction parallel or perpendicular to the fault plane and depend on the amount and distribution of slip developed on the fault rupture. This is important in considering the bilateral directional excitation effect. Moreover, under seismic excitations of relatively long durations, a structure undergoes several cycles during the forced vibration part of the response; therefore, its response depends more on the amount of energy dissipation particularly in the inelastic range.

The dynamic analysis of long span bridges such, as cable-stayed bridges in seismically active regions is potentially important to highway facilities design. A quite general nonlinear dynamic analysis methodology and a mathematical model are developed to estimate dynamic characteristics and for a realistic prediction of the seismic response of cable-stayed bridge tower. To simulate the tower earthquake response, a three-dimensional finite element model is established for the tower based on design drawings. Free vibration of three-dimensional framework structures is analyzed by using the consistent mass matrix based on the finite element approach. One of the most important decisions in carrying out proper is to select a design earthquake that adequately represents the ground motion expected at a certain site and in particular the motion that would drive the bridge structure to its critical response, resulting in the highest damage potential. So an extensive series of seismic response analyses using a wide range of peak ground accelerations, frequency contents and energy or duration for the records, vertical ground motion, near-fault and long duration ground motions that are potentially important to bridge facilities design are carried out. The bridge structure is designed based on the current Japanese Specification for Highway Bridges. The ductility and base shear demands due to the near-fault and the long duration earthquake

ground motions are compared and conclusions are drawn. The stipulation of code standard input excitation limitations and the calculated demands are discussed.

2. Tower Finite Element Model

In the past two decades, construction of long-span cable-supported bridges has been very active in the world especially in Japan. Long-span bridges that attract engineers and offer many exciting technical problems will continue to be constructed. Since long-span bridges are flexible and low-damped, hence they are prone to vibrate under dynamic loading. Cable-stayed bridges exhibit nonlinear behavior under either static or dynamic loads; the nonlinearities can be attributed to change in cable geometry due to sagging effects, interaction between axial forces and bending moments in the towers and the deck and changes of bridge geometry due to its deflections. The steel tower of a three span continuous cable-stayed bridge located in Hokkaido, Japan is considered, in which the length of main span and two-side spans are equal to 284 and 115m, respectively. **Fig. 1** shows a schematic representation of bridge elevation, the tower is H-shaped steel structures as illustrated in **Fig. 2**. The tower consists of two steel legs and horizontal connected beam. The cross section of each leg has a hollow rectangular shaped with an interior stiffener and the cross-section size changes over the tower height. The geometrical properties of the tower legs and horizontal beam (strut) are summarized in **Table 1**. Since the cable-stayed bridges are not structurally homogeneous, it is concluded [9, 10] that the tower, deck and cable-stays affect the structural response in a wide range of vibration modes. The tower seismic response problem may be approximately analyzed separately from the bridge structures, as long as restraint at the top of the tower provided by the cables is accounted for properly. The steel tower is taken out of the cable-stayed bridge and modeled as three-dimensional frame structure. A fiber flexural element is developed for the steel tower characterization and that element incorporates both geometric and material nonlinearities. The stress-strain relationship of the beam element is modeled as bilinear stress strain constitutive relation with unaxial yield criterion and kinematic hardening flow rule. The yield stress and the modulus of elasticity are equal to 355 MPa (SM490Y) and 200GPa, respectively; the strain hardening in the plastic region is equal to 0.01. Inelasticity of the fiber flexure element is accounted for by the division of the cross section into a number of fiber zones with uniaxial plasticity defining the normal stress-strain relationship for each zone, the element stress resultants are determined by integration of the fiber zone stresses over the element cross section.

The nonlinear behavior of cable elements is idealized by using the equivalent modulus approach in which each cable is replaced by a truss element with equivalent modulus of elasticity E_{eq} that is given by Ernst [11] as:

$$E_{eq} = E / \{1 + EA\,(wL)^2 / 12T^3\} \qquad (2)$$

where E is the material modulus of elasticity, L is the horizontal projected length of the cable, w is the weight per unit length, A is the cross sectional area and T is the pretension force. It can be noticed that the cable-stays nonlinearity originates with an increase in the loading followed by a decrease in the cable sag, as a consequence the apparent axial stiffness increases. The inclined cable is represented by an equivalent straight cable element with relative axial deformation (Δl), the stiffness matrix of the cable element **K** has the value equal to $E_{eq}A/l$ for $\Delta l > 0$, and the cable stiffness vanishes and no element force exist when shortening occurs, i.e. $\Delta l < 0$.

This cable-stayed bridge has nine cables in each tower side. The stiffening girder dead load is considered to be equivalent to the vertical component of the cables pretension force. A scheme of Rayleigh's damping is used to form damping matrix as a combination of mass and stiffness matrices, which effectively captures the tower

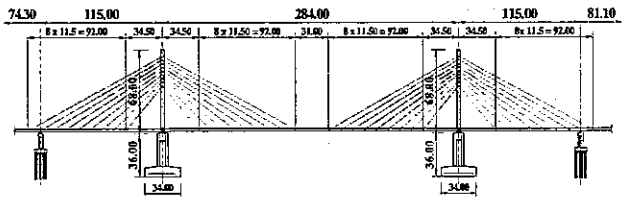

Fig. 1 General view of cable-stayed bridge (m)

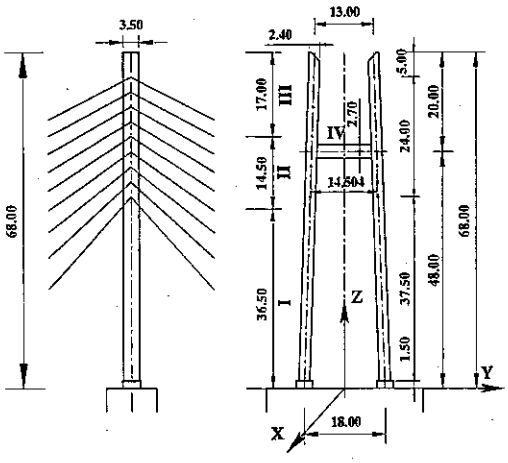

(a) Tower geometry (m)

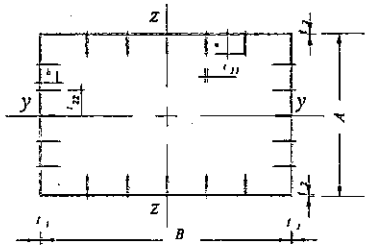

(b) Cross section

Fig. 2 Steel tower of cable-stayed bridge

Table 1 Cross section dimensions of tower parts (cm)

Tower parts	Outer dimension				Stiffener dimension			
	A	B	t_1	t_2	a	b	t_{11}	t_{22}
I	240	350	2.2	3.2	25	22	3.6	3.0
II	240	350	2.2	3.2	22	20	3.2	2.8
III	240	350	2.2	2.8	20	20	2.8	2.2
IV	270	350	2.2	2.6	31	22	3.5	2.4

structures damping and is computationally efficient. The damping ratio corresponding to the frequencies of the in-plane and out-plane vibration modes is set to 2%. Using standard expressions [12], the mass (α) and stiffness (β) proportional constants are 0.0836 sec^{-1} and 0.0041 sec, respectively; the damping coefficients for vibration modes can be computed.

3. Input Earthquake Ground Motions

The Hyogoken Nanbu Earthquake of January 17, 1995 caused severe damage to buildings, highway bridges, railways and so on. This event is the first instance in which engineering structures that were designed for the highest seismic forces in the world have been subjected to such destructive ground motions. Following the 1995 Hyogoken Nanbu earthquake, Japan Society of Civil Engineers issued "Proposal on Earthquake Resistance for Civil Engineering Structures". According to the proposal, two types of earthquake ground motions should be taken into account in earthquake resistant structures design. One is Level I motion of moderate intensity, which is likely to experienced by the structures once or twice during their life time and the other is Level II motion of extreme intensity rarely experienced during the life time. One of the most important decisions in carrying out proper is to select a design earthquake that adequately represents the ground motion expected at a particular site and in particular the motion that would drive the bridge structure to its critical response, resulting in the highest damage potential. A wide range of peak ground accelerations, frequency contents and energy or duration for the records, and near source ground motion are potentially important to bridge facilities design.

A suite of recorded and simulated standard ground motion records are used for the nonlinear time history analysis: Three near-fault ground motion records [13] obtained during the 1995 Hyogoken Nanbu earthquake (M7.2) and the 1994 Northridge Earthquake (M_w = 6.7), including three-components acceleration time histories recorded at JMA, JR Takatori and Sylmar-Converter STA. The near-field region of an earthquake is considered to be the region within several kilometers of the extension to the ground surface of the fault rupture plane. Even for moderate magnitude earthquakes, near-fault ground accelerations, velocities and displacements can be quite high especially toward the propagation direction of fault rupture. One or two distinctive large pulses with relatively long period characterize near-fault ground motions. Such large pulses are generated by forward rupture directivity effects in the fault-normal component, which are caused by the coherent summation of ground motions from extended fault planes.

Furthermore, two long duration ground motion records [13] obtained during the Hachinohe record of the 1968 Tokachi-oki Earthquake (M_w = 8.2, M7.9), and the Ofunato record of the 1978 Miyagi-oki earthquake (M_w = 7.6, M7.4) that caused by a rupture of a portion of the plate boundary of the sub-ducting Pacific plate in the region east off northeastern Honshu. Together with the standard ground motions [4, 5] Level II introduced through Japan Highway Specification 1996 for different types of soil condition (Type I, II and III), to reflect a more realistic ground motion. Level II ground motions occur at a very short distance with a magnitude of about 7-7.2. The calculated responses for different records are compared. The characterizations of ground motions for improved analysis are shown in **Figs. 3** and **4**, and their values are given in **Table 2**, where a_{max} is the maximum

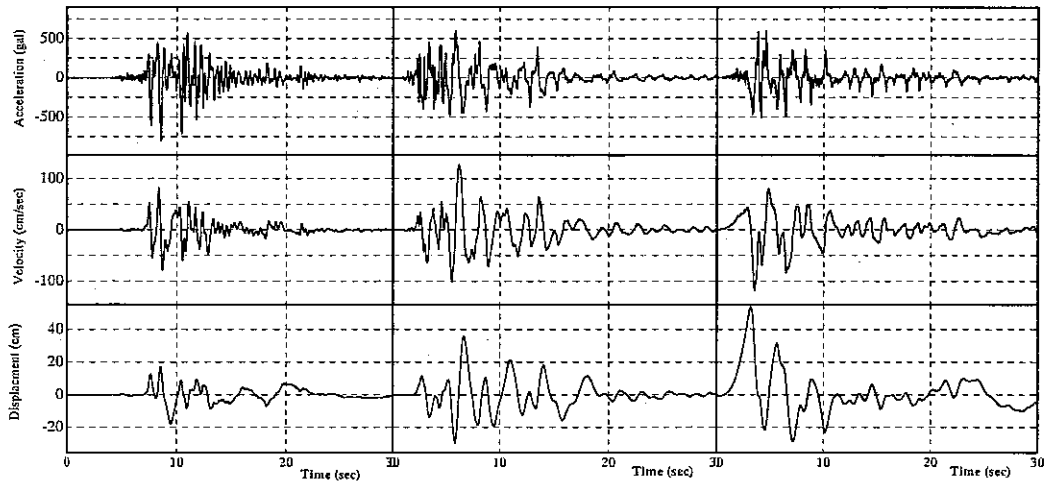

(a) JMA Observatory (N-S) (b) JR Takatori Observatory (N-S) (c) Sylmar Converter STA (N-S)

Fig. 3 Horizontal near fault ground motions in the 1994 Northridge and the 1995 Hyogoken Nanbu Earthquakes

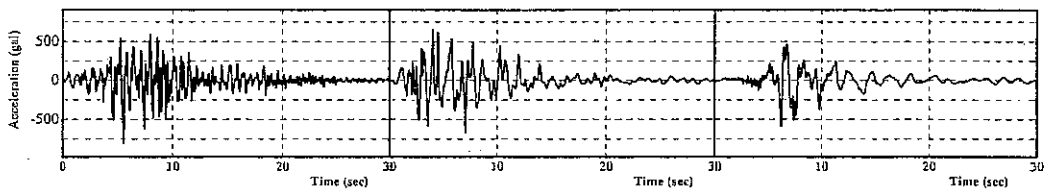

(a) Type I (Rock soil, T-I) (b) Type II (Stiff soil, T-II) (c) Type III (Soft soil, T-III)

Fig. 4 Standard ground motions Level II introduced through Japan Highway Specification 1996

acceleration, v_{max} and d_{max} are the maximum velocity and displacement obtained by integrating accelerogram using trapezoidal rule. Predominant period is taken as period corresponding to maximum value of Fourier amplitude spectra. The ground displacement consists of two main long period cycles, the first cycle being the largest and the subsequent ones decaying. These long period pulses are also distinguishable in the ground velocity history, where the amplitude of the positive pulses is larger than the amplitude of the negative pulses.

The peak ground acceleration is the parameter most often associated with severity of ground motion. However, it has generally come to be recognized that this is a poor parameter for evaluating the damage potential. Since, large recorded peak acceleration may be associated with a short duration impulse of high frequency (acceleration spike) or with a long duration impulse of low frequency (acceleration pulse). In the first case, most of the impulse is absorbed by the structure inertia with little deformation. However, a more moderate acceleration in the second case can result in a significant structure deformation. Since near-fault impulse type ground motion results in a sudden burst of energy into the structure, which must be dissipated immediately and is characterized by a single un-directional large yield excursion.

4. Natural Vibration Analysis

According to a number of full scale tests conducted for cables-stayed bridges and results of previous investigations, it is well known that the natural frequencies and natural mode shapes can be predicted with acceptable accuracy by means of linear elastic analyses that assume appropriate mass and stiffness distributions [14]. The dynamic characteristics of the tower structure are considered on the assumption of fixed boundary conditions at its base. The natural vibration analysis is carried out for the previous described steel tower modal. The eigen values (natural periods) of the tower with the description of mode shapes for the first eight modes and corresponding effective modal mass and the damping coefficient obtained from the analysis are listed in **Table 3**. Depending on the relative amplitude of the mode shapes, these modes can be classified into the following three groups: the lateral dominant modes (right angle bridge axis, H and longitudinal bridge axis, L); the torsional dominate modes, T, and the vertical dominate modes, V. The first significant mode with a relatively large mass participation is the lowest vibration mode with 2.07 sec period, which essentially involves transverse vibration of the entire tower structure (right angle bridge axis). The second significant mode (0.93 sec) is the longitudinal vibration mode (bridge axis direction) with effective mass of about 30%.

5. Nonlinear Dynamic Response

Nonlinear structural response analyses, including the use of time history inputs are required to meet the goals of performance-based design. It is well known that different ground motion time histories, which match the same response spectrum, produce variations in the response of a structure subjected to nonlinear time history analysis. Specially, when the input time history is a near-fault pulse, this effect is accentuated to the point where small modifications of a near-fault time history that have no significant effect on the response spectrum can have a major effect on the response of a structure subjected to nonlinear time history analysis. This demonstrates that the current standard of practice does not provide a reliable basis for providing near-field ground motion time histories that are specified solely on the basis of a design response spectrum. To identify damaging characteristics of near-fault ground motions, nonlinear dynamic structural analyses using large set of ground motion time histories and potentially vulnerable bridges are developed, where the nonlinear time history response adequately represents the demand for a high rate of energy absorption presented by near-fault pulses. This is especially true for high ground motion levels that drive structures into the nonlinear range, invalidating the linear elastic assumption on which the elastic response spectrum is based. Nonlinear dynamic behavior of the cable-stayed bridge tower under a suite of ground motions representing near-fault and long duration ground motions at both rock and soil sites is presented, and compared to the response under artificial standard magnitude 7 - 7.2 earthquake Level II specified at Japanese highway bridge specification.

Table 2 Input ground motions characterization

Ground Motion		a_{max} (g)	v_{max} (cm/sec)	d_{max} (cm)	Period (sec)
Kobe, JMA	E-W	0.5985	74.32	19.95	0.7032
	N-S	0.8213	81.26	17.68	0.6884
	U-D	0.3428	38.29	10.29	1.011
Northridge, Sylmar	E-W	0.8972	102.22	44.71	1.575
	N-S	0.6125	117.45	53.43	0.8623
	U-D	0.5862	34.60	25.20	0.7728
Miyagi-oki, Ofunato	E-W	0.2267	14.1	5.1	0.3023
	N-S	0.2109	12.80	2.2	0.5285
	U-D	0.0776	4.90	0.9	0.2668
Tokachi-oki, Hachinohe	E-W	0.2104	40.5	20.6	1.146
	N-S	0.3181	35.7	11.9	2.731
	U-D	0.138	11.40	9.0	0.2471

Table 3 Summary of tower principal vibration modes

Mode order	Period (sec)	Effective mass as a fraction of total mass	Viscous damping percent	Mode type
1	2.0723	33.195	2.00	H_1
2	0.9335	30.330	2.00	L_1
3	0.7726	0.000	2.18	T_1
4	0.5235	0.034	2.81	V_1
5	0.3751	1.735	3.68	L_2
6	0.3625	0.080	3.79	H_2
7	0.3296	0.000	4.12	T_2
8	0.1559	34.079	8.35	V_2
Sum	--	99.423	--	--

H: transverse vibration (in-plane), T: torsional vibration
L: longitudinal vibration (out-plane), V: vertical vibration

5.1 Acceleration and displacement response

It is noticeable that the results of nonlinear dynamic response vary significantly for different earthquakes for the same structure. The acceleration response for the JMA, JR Takatori and the Sylmar records show higher acceleration response than the Ofunato and Hachinohe records along the time history. The acceleration responses in the right angle bridge axis of the near-fault records (JMA, JR Takatori and Sylmar) show more than gravity acceleration (g) and are dominated by the long period first vibration mode, while that in the bridge axis is dominated by the second natural mode. Moreover, the acceleration response is significantly affected by the tower lateral stiffness in both direction (natural frequency) and the input excitation predominant period. The response of the JMA record in bridge axis direction shows more than twice gravity acceleration (2g) and higher response than that of JR Takatori and Sylmar records. It is interesting to see that JR Takatori and Sylmar records show similar acceleration responses along the time history with higher amplification of input excitation in the high frequency bridge axis direction as can be illustrated in **Fig. 5**.

The displacement responses of the tower structure for the JMA, JR Takatori and the Sylmar records display much larger displacement in the right angle bridge axis flexible direction. This effect in JR Takatori and Sylmar responses is characterized by three cycles of large displacement amplitude related to the large pulse in the input ground motion, decaying rapidly after the peak excursions due to the large plastic deformation caused by the high intensity. The phenomenon of large ductility demand for JR Takatori and the Sylmar records could be attributed to the large acceleration pulses in the these ground motions. Unfavorable residual deformation in the tower response due to JR Takatori earthquake is attained.

The JMA and long duration records (Ofunato and Hachinohe) show elastic behavior; as a result the response is characterized and dominated by tower free vibration. But when the long duration records are scaled three times of the original ground motion amplitude, the response of scaled Ofunato record still has elastic behavior and the displacement response amplitude of the tower top seems to increase fairly linearly with the amplitude of the applied excitation; while the response of scaled Hachinohe record shows inelastic behavior and accumulation of inelastic deformation increase as the duration of the ground motion is increased, as a result the hysteretic characteristics affect ductility demand and residual deformation, moreover the displacement response amplitude increase nonlinearly as can be shown in **Figs. 6** and **7**. From the curvature time history at tower base, it can be understood one direction yield phenomena due to acceleration pulse in the JR Takatori record, the accumulation of inelastic deformation within 30-50sec range for long duration scaled Hachinohe motion.

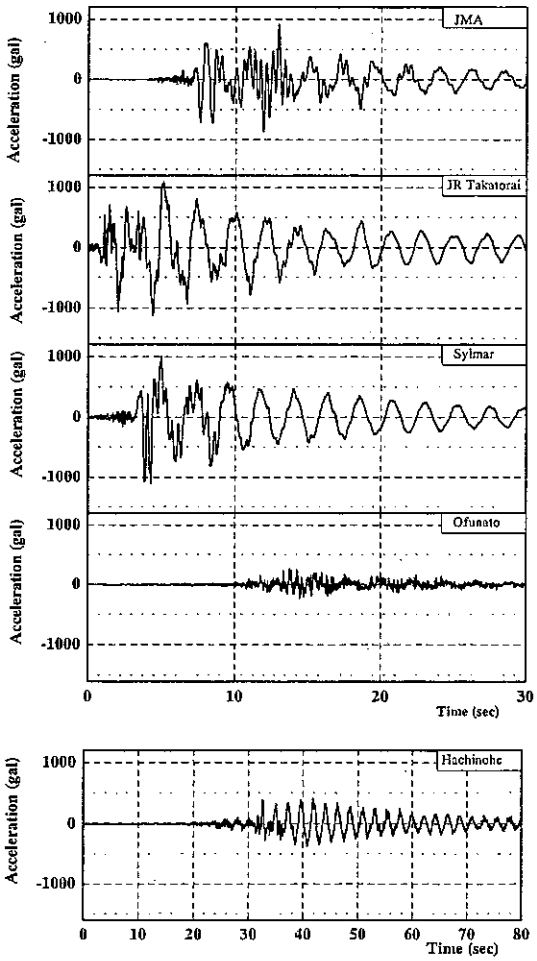

(a) Right angle bridge axis direction

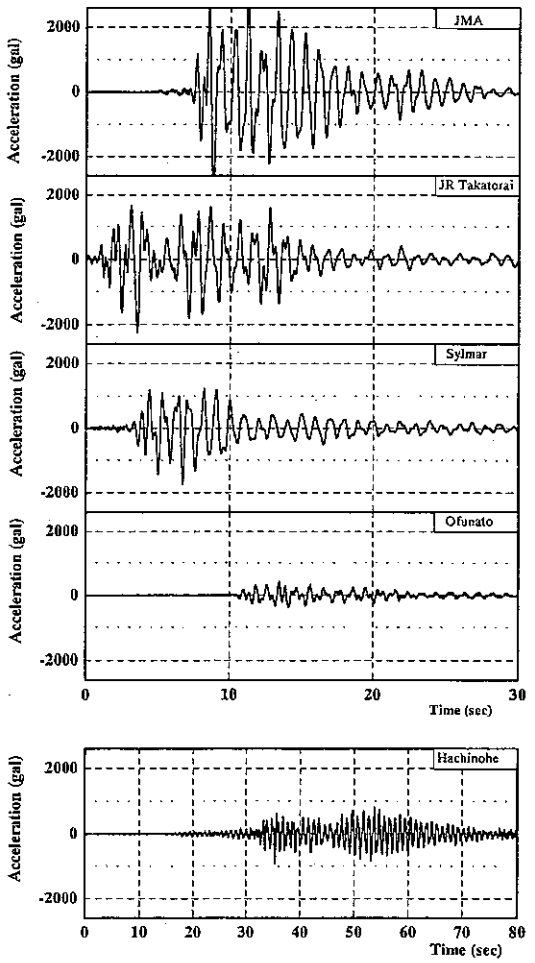

(b) Bridge axis direction

Fig. 5 Acceleration time history at tower top

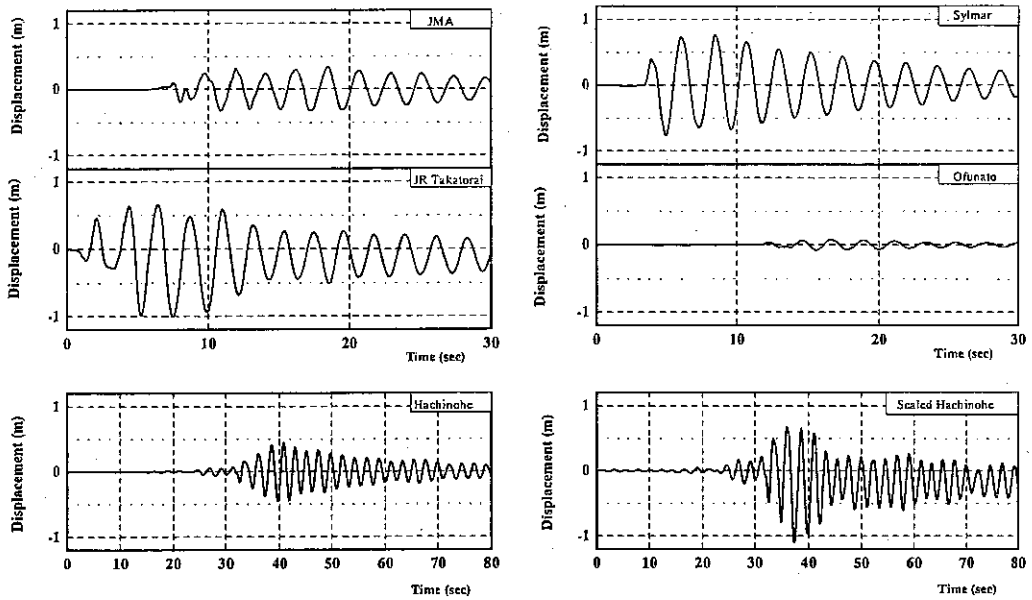

Fig. 6 Displacement time history at tower top

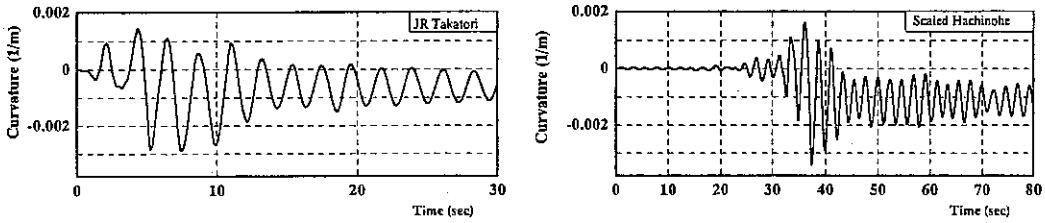

Fig. 7 Curvature time history at tower base

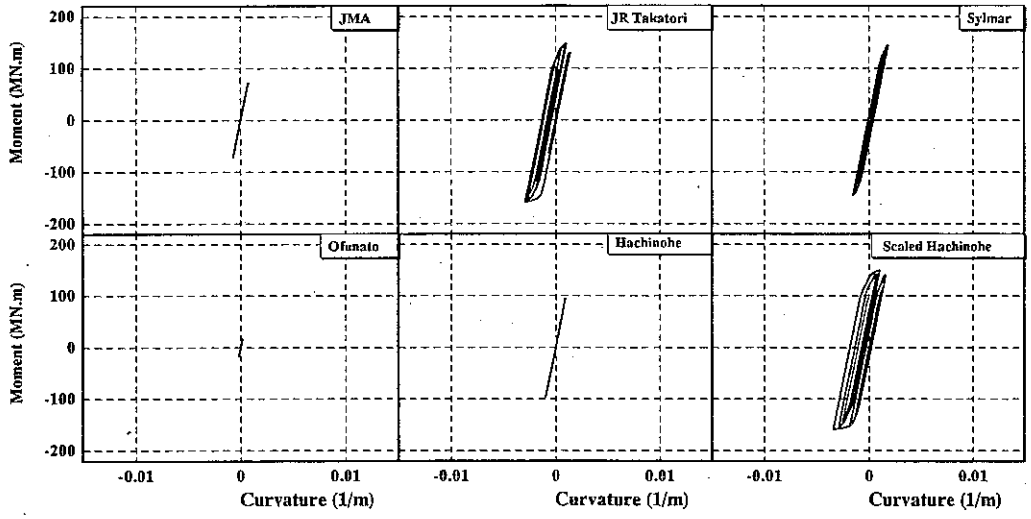

Fig. 8 Moment & curvature relationship at tower base

5.2 Strength demands

The nonlinear time history response adequately represents the demand for a high rate of energy absorption presented by near-fault pulses. This is especially true for high ground motion levels that drive structures into the nonlinear range, invalidating the linear elastic analysis. For the long duration records, the required strength level is much less than that required in near-fault records. For the bridge axis direction that characterized by high strength, the flexural strength is significant low compared to that in the right angle bridge axis direction. The JR Takatori presents the highest flexural and curvature ductility demands among the input excitations as shown in **Fig. 8**. Form the moment curvature relation for JR Takatori record; it can clarify the effect of the near-fault acceleration pulse on the tower structural response that tends to be characterized by progressive

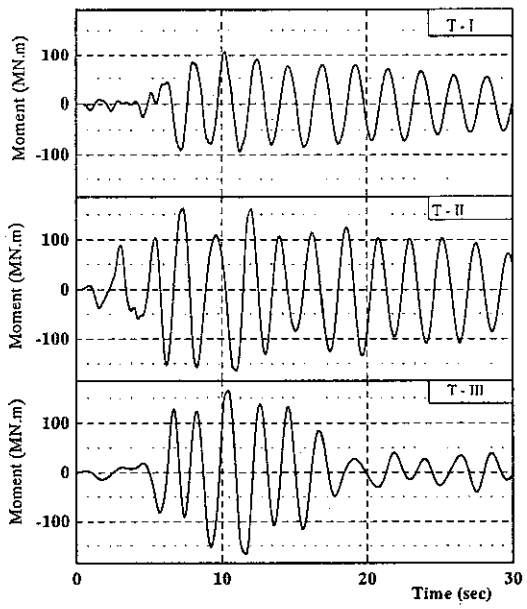

(a) Right angle bridge axis direction

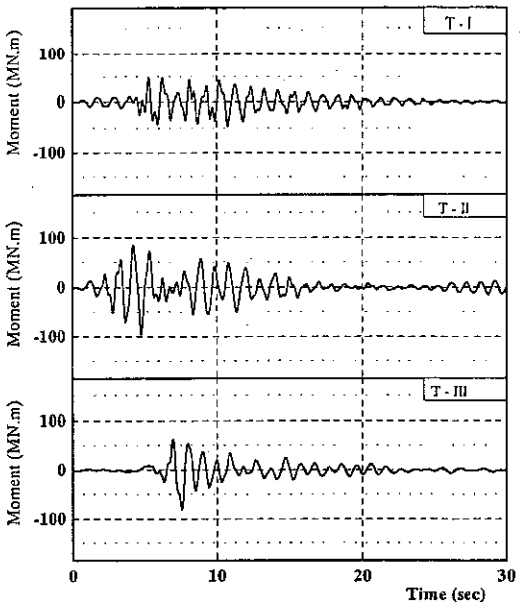

(b) Bridge axis direction

Fig. 9 Moment time history at tower base for standard ground motions

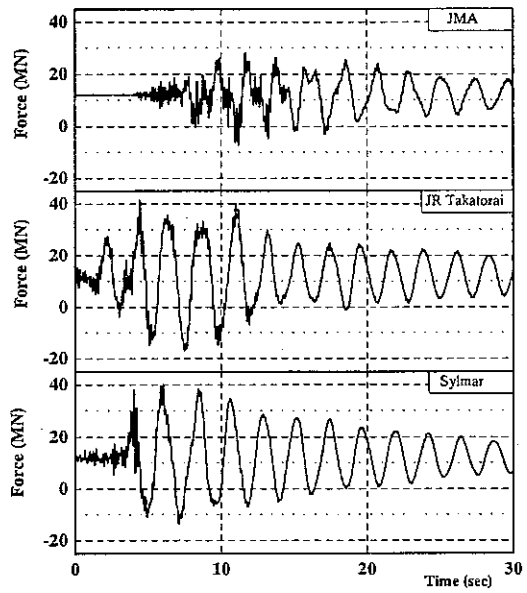

(a) Near fault ground motions

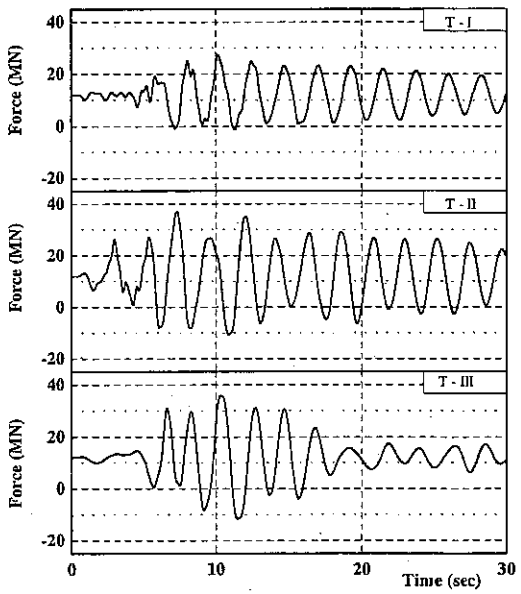

(b) Standard ground motions

Fig. 10 Vertical force time history at tower base

yielding in one direction. The asymmetric accumulation of inelastic deformation in one direction becomes increasingly important as the ground motion duration is increased. Since the hysteretic characteristics of yielding elements have a pronounced influence on the ductility demand and residual deformation, the effect of input excitation duration on the inelastic deformation accumulation can be obviously seen in the scaled Hachinohe record response as illustrated in **Fig. 8**.

For the standard ground motions Level II response, which introduced through Japan Highway Specification 1996 for different types of soil condition (rock, stiff and soft), the shear and flexural strength demands are slight different compared to that of three component JR Takatori record, which can be attributed to the slight horizontal excitation bi-directional effect and slight coupling of tower vibration modes. These demands are higher for soft soil condition ground motion compared to rock and stiff soil condition ground motion. The standard ground motions are significantly underestimated the axial strength demand, which may be attributed to the significant

bi-directional and vertical ground motion effects on tower axial force response as illustrated in **Figs. 9** and **10.** The vertical reaction force response of three components input excitation is characterized by high frequency spike override long duration pulse response that may be attributed to the effect of the U-D motion of the input ground motion. It can be concluded, that the main effect of the vertical motion is the axial forces generation, which are uncoupled to that due to lateral forces and have a lower vibration period.

6. Conclusions

The seismic analysis and design of long-span bridges such as cable-stayed bridges in seismically active regions are potentially important to highway facilities design. The numerical analysis of a structure subjected to a strong earthquake is a challenging task, due to the highly nonlinear nature of the phenomena involved in the response, both at the material and at the structural level. In this study, the effects of earthquake ground motions and structural characteristics on the response and performance of cable-stayed bridge tower are studied using nonlinear analysis tools for seismic structural analysis. A quite general nonlinear dynamic analysis methodology and a mathematical model are developed to estimate seismic response characteristics and for a realistic prediction of the seismic response of cable-stayed bridges tower. An extensive series of seismic response analyses using a wide range of peak ground accelerations, frequency contents and energy or duration for the records, vertical ground motion, near-fault and long duration ground motions that are potentially important to bridge facilities design are carried out. The following conclusions can drawn out:

The acceleration response is significantly affected by the tower lateral stiffness in both directions, the large ductility demand attained for JR Takatori and Sylmar records could be attributed to the large acceleration pulse in these ground motions. The duration of ground motion almost has no effect on the tower elastic response, while this effect become significant in inelastic behavior, the hysteretic characteristics affect ductility demand and residual deformation, moreover the displacement response amplitude increase nonlinearly as could be seen in the response of scaled Hachinohe record. The JR Takatori presents the highest shear, flexural and curvature ductility demands among the input excitations. The shear and flexural strength demands for standard ground motions are slight different compared to that of three component JR Takatori record, these demands are higher for soft soil condition ground motion compared to rock and stiff soil condition ground motions, while the standard ground motions are significantly underestimated the axial strength demand.

References

[1] Ali, H. M. and Abdel-Ghaffar, A. M.: Modeling the nonlinear seismic behavior of cable-stayed bridges with passive control bearings, *Computers & Structures,* Vol. 54, No. 3, pp. 461-492, 1995.

[2] Hayashikawa, T. and Abdel Raheem, S. E.: Nonlinear dynamic behavior of steel tower of cable-stayed bridges with passive energy dissipation system, *Journal of Structural Engineering,* JSCE, Vol. 48A, pp. 863-874, 2002.

[3] Committee of Earthquake Engineering, *The 1995 Hyogoken-Nanbu Earthquake, Investigation into Damage to Civil Engineering Structures,* Japan Society of Civil Engineers, June, 1996.

[4] Japan Road Association, *Specification for Highway Bridges - Part V Seismic Design*, Chapter 1-8, 1996.

[5] Japan Road Association, *Reference for Highway Bridge Design, Specification for Highway Bridges-Part IV Substructures*, Chapter 7-9, 1996.

[6] Watanabe, E., Sugiura, K., Nagata, K. and Kitane, Y.: Performance and damages to steel structures during 1995 Hyogoken-Nanbu earthquake, *Engineering Structures,* Vol. 20, Nos. 4-6, pp. 282-290, 1998.

[7] Kawashima, K.: Seismic performance of RC bridge piers in Japan: an evaluation after the 1995 Hyogo-ken Nanbu earthquake, *Progress in Structural Engineering and Materials*, Vol. 2, No. 1,pp. 82-91, 2000.

[8] Kawashima, K.: Seismic design and retrofit of bridges, *Proceedings of 12th. World Conference on Earthquake Engineering,* Auckland, New Zealand, Paper No. 2828, 2000.

[9] Ernst, J. H.: Der E-modul von seilen unter berucksichtigung des durchhanges, *Der Bauingenieur,* Berlin, Vol. 40, No. 2, 52-55, 1965 (in German).

[10] Fleming, J. F. and Egeseli, E. A.: Dynamic behavior of a cable-stayed bridge, *Earthquake Engineering and Structural Dynamics,* Vol. 8, pp. 1-16, 1980.

[11] Abdel-Ghaffar, A. and Scanlan, R. H. Ambient vibration studies of golden gate bridge. II: pier-tower structure, *Journal of Engineering Mechanics,* ASCE, Vol. 114, pp. 483-499, 1985.

[12] Clough, R. W. and Penzien, J.: *Dynamics of Structures*, McGraw-Hill, Inc., New York, Second edition, 1993.

[13] Elgamal, A., Ashford, S. and Kramer, S. Eds: 1st PEER workshop on characterization of special source effects, Workshop Report, UCSD, July 20-21, 1998, *Pacific Center for Earthquake Engineering Research,* UC, Berkeley, 1999.

[14] Wilson, J. C. and Liu, T.: Ambient vibration measurements on a cable-stayed bridge, *Earthquake Engineering and Structural Dynamics,* Vol. 20, pp. 723-747, 1991.

(Received July 31, 2003)

Hardening Effect of Lead-Rubber Bearings on Nonlinear Seismic Behaviour of Highway Viaducts with Piers of Unequal Heights

Daniel RUIZ JULIAN * and Toshiro HAYASHIKAWA **

* Grad. Student, Grad. School of Eng., Hokkaido University, Nishi 8 Kita 13 Kita-ku, Sapporo 060-8628, Japan
** Dr. of Eng., Assoc. Prof., Grad. School of Eng., Hokkaido University, Nishi 8 Kita 13 Kita-ku, Sapporo 060-8628, Japan

The effect of nonuniform distribution of masses and stiffnesses along highway viaducts with piers of unequal heights may result in complicated seismic behaviour. The installation of isolation lead-rubber bearings is generally positive since their inherent flexibility can be used to reduce, distribute and direct the seismic forces to the different piers. However, the hardening experienced by lead-rubber bearings at high strain levels significantly influences the overall seismic behaviour. The equilibrium of balanced pier ductility is broken, plastic ductility is found in cases in which without hardening, the demands are expected to be under elastic range, and significant variations of deck displacement response are observed.

Keywords: *Nonlinear seismic response, highway viaduct, lead-rubber bearings, pier height, hardening*

1. Introduction

Base isolation is considered an effective technique for improving the seismic performance of highway viaducts. The basic principle of seismic base isolation consists in decoupling the structure from the destructive effects of great earthquake ground motions. This is achieved by increasing the fundamental natural period of the bridge beyond the energy-containing periods of earthquakes, and by the additional damping provided to dissipate the seismic energy[1].

Bridges are ideal candidates for the application of base isolation technology in new design and for retrofitting of existing structures, due to the facility of installation, inspection and maintenance of isolation devices. In addition, one of the differences between conventional and base isolation design is that in isolated bridges the distribution of lateral loads is a function of the force-deformation characteristics of the isolation bearings. Consequently, seismic loads can be distributed to all substructure units. Moreover, it may be possible to direct forces to specified piers by changing the characteristics of the base isolation bearings, indicating the substructure units to have minimal seismic forces. For all of these reasons, a large number of base isolation systems have been developed and implemented in bridge during the last decades[2].

Lead-rubber bearings are one of the most commonly used base isolation systems, and they are proved to be effective in reducing the seismic response of bridges[3), 4]. However, the adoption of lead-rubber isolation bearings may create certain disadvantages due to the increased flexibility introduced at bearing level. Excessively large deck displacements in the event of large earthquakes may result in collision between adjancent decks or deck and abutments. On the other hand, the necessary adoption of large expansion joints may lead to maintenance, traveling, vibration and noise problems[5].

Experimental dynamic tests for identifying the mechanical characteristics of lead-rubber bearings have shown that these bearings exhibit significant hardening behaviour beyond certain strain levels[6)-8]. This hardening phenomenon, attributed to material properties of the rubber and originated mainly due to geometric causes, sensibly modifies the response of the bearings at large shear strains. Subsequently, it is expected that the overall seismic bridge response could be affected in case of large earthquakes.

The advantage of base isolation of distributing the seismic lateral forces among the substructures in a way that benefits the global design is sensibly complicated in the case of irregular bridges. Due to the nonuniform distribution of masses and stiffnesses along highway viaducts with piers of unequal heights, one or more piers will attract significantly more lateral inertia force from the superstructure. Therefore, it would be expected that hardening of lead-rubber bearings could have a more important effect on bridges with different pier heights than in regular structures.

In this study, in order to improve the seismic performance of highway viaducts with piers of unequal heights, the hardening effect of lead-rubber bearings at high strain levels has been considered to evaluate its influence on the overall behaviour of seismically isolated viaducts subjected to great earthquake ground motions. For this purpose, the bilinear analytical force-deformation

model of the bearing supports is substituted by a trilinear element, introduced to accurately represent the influence of hardening at high bearing deformation levels. The influence of unbalanced distribution of seismic loads due to hardening in the seismic response of isolated bridges in the event of large earthquakes is investigated.

2. Analytical model of highway viaduct

In the study of seismic behaviour of viaducts with piers of unequal heights, it is not possible to consider a large number of bridge models including a wide range of variation in pier heights due to the limitations of numerical simulation. Therefore, two representative models, shown in **Fig. 1**, are selected having common geometry with the exception of the substructure. In Model 1 the irregularity of the bridge is introduced by increasing gradually the pier heights, while Model 2 represents a case of bridge with great contrast of height between adjacent piers.

2.1 Deck superstructure and piers

The deck of the highway viaduct consists of three-span continuous segments. The overall length of 120 m is divided in equal spans of 40 m, with a mass of 1.5×10^4 kg/m. The superstructure is modeled using linear elastic elements with properties based on the composite action between the reinforced concrete deck-slab and the steel girders. The deck weight is supported on four hollow box section steel piers of unequal heights. The bridge piers have been designed according to the seismic design code in Japan[5], and modeled using fiber elements. The pier cross-section changes due to the differences in pier height, with properties summarized in **Table 1**.

2.2 Lead-rubber bearing supports

Both models of highway viaducts are isolated with lead-rubber bearings (LRB) installed at top of the steel piers. Two different analytical models for the bearings are presented in **Fig. 2** and used for nonlinear dynamic analysis. LRB bearings are generally represented with bilinear force-displacement hysteretic loop[9], but trilinear analytical model is adopted when hardening effect at high strain levels is considered. The pre-yield stiffness K_1 corresponds to the stiffness of the lead plug, K_2 is the stiffness of the rubber, F_1 is the yield force of the lead plug, and K_3 and F_2 represent the hardening parameters effect. The pre-yield to post-yield stiffness ratio is 10.0, while the yield force, F_1, has been considered a parameter of study related to the size of the lead plug.

Properties of the LRB bearings are selected depending on the pier height and the differences in dead load supported from the superstructure. The aim is to attract the appropriate proportion of nonseismic and seismic loads according to the resistance capacity of each substructure, ensuring fully elastic behaviour and a near equal distribution of ductility demands over all piers.

By varying the size of the lead plug or equivalently modifying the ratio of bearing yield force to the superstructure weight (F_1/W), from 2.5% (case a) to 20% (case h) by intervals of 2.5%, 8 different lead-rubber bearings have been considered.

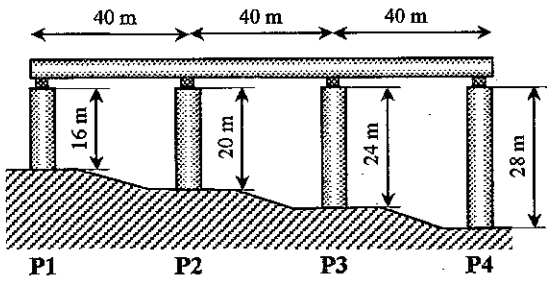

(a) Model 1

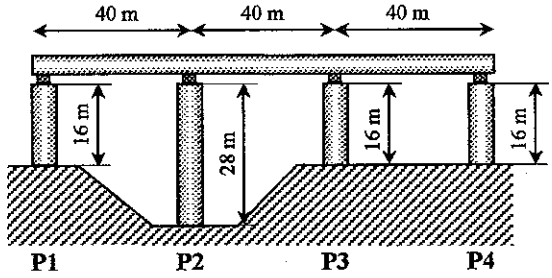

(b) Model 2

Fig. 1 Models of highway viaducts

Table 1 Characteristics of bridge piers cross sections

		A (m^2)	I (m^4)	M_y (MNm)
Model 1	P1	0.4300	0.33146	70.81
	P2	0.4500	0.37988	77.63
	P3	0.4700	0.43279	84.76
	P4	0.4700	0.43279	84.76
Model 2	P1	0.4300	0.33146	70.81
	P2	0.4900	0.49041	92.20
	P3	0.4500	0.37988	77.63
	P4	0.4300	0.33146	70.81

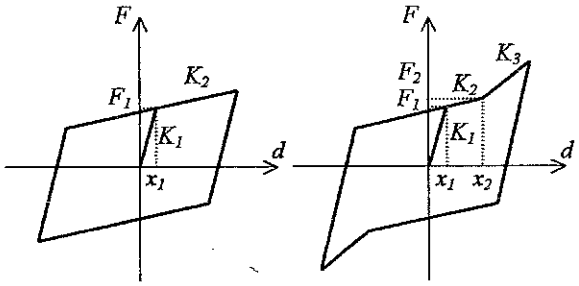

(a) Bilinear model (b) Trilinear model

Fig. 2 Analytical models of lead-rubber bearings

Hardening parameters for the trilinear model are selected according to experimental values[6), 7)] to assure good agreement between experimental and analytical results, ensuring an effective prediction for the bearing seismic response.

Design parameters of the isolation bearings for the two models of highway viaducts are summarized in **Table 2**.

Table 2 Design parameters of lead-rubber bearings

Model	Pier	Case	K_1 (MN/m)	K_2 (MN/m)	F_1 (MN)	K_3 (MN/m)	F_2 (MN)
Model 1	P1	a	64.7	6.47	0.392	27.0	1.323
		b	64.7	6.47	0.637	27.0	1.544
		c	64.7	6.47	0.882	27.0	1.764
		d	64.7	6.47	1.127	27.0	1.985
		e	64.7	6.47	1.372	27.0	2.205
		f	64.7	6.47	1.617	27.0	2.426
		g	64.7	6.47	1.862	27.0	2.646
		h	64.7	6.47	2.107	27.0	2.867
	P2	a	70.9	7.09	0.294	28.3	1.328
		b	70.9	7.09	0.539	28.3	1.549
		c	70.9	7.09	0.784	28.3	1.769
		d	70.9	7.09	1.029	28.3	1.990
		e	70.9	7.09	1.274	28.3	2.210
		f	70.9	7.09	1.519	28.3	2.431
		g	70.9	7.09	1.764	28.3	2.651
		h	70.9	7.09	2.009	28.3	2.872
	P3	a	64.3	6.43	0.196	25.6	1.141
		b	64.3	6.43	0.441	25.6	1.361
		c	64.3	6.43	0.686	25.6	1.582
		d	64.3	6.43	0.931	25.6	1.802
		e	64.3	6.43	1.176	25.6	2.023
		f	64.3	6.43	1.421	25.6	2.243
		g	64.3	6.43	1.666	25.6	2.464
		h	64.3	6.43	1.911	25.6	2.684
	P4	a	52.9	5.29	0.098	22.1	0.882
		b	52.9	5.29	0.343	22.1	1.102
		c	52.9	5.29	0.588	22.1	1.323
		d	52.9	5.29	0.833	22.1	1.543
		e	52.9	5.29	1.078	22.1	1.764
		f	52.9	5.29	1.323	22.1	1.984
		g	52.9	5.29	1.568	22.1	2.205
		h	52.9	5.29	1.813	22.1	2.425
Model 2	P1	a	55.9	5.59	0.196	23.3	1.058
		b	55.9	5.59	0.441	23.3	1.279
		c	55.9	5.59	0.686	23.3	1.499
		d	55.9	5.59	0.931	23.3	1.720
		e	55.9	5.59	1.176	23.3	1.940
		f	55.9	5.59	1.421	23.3	2.161
		g	55.9	5.59	1.666	23.3	2.381
		h	55.9	5.59	1.911	23.3	2.602
	P2	a	60.0	6.00	0.294	24.5	1.147
		b	60.0	6.00	0.539	24.5	1.367
		c	60.0	6.00	0.784	24.5	1.588
		d	60.0	6.00	1.029	24.5	1.808
		e	60.0	6.00	1.274	24.5	2.029
		f	60.0	6.00	1.519	24.5	2.249
		g	60.0	6.00	1.764	24.5	2.470
		h	60.0	6.00	2.009	24.5	2.690
	P3	a	67.9	6.79	0.245	27.4	1.103
		b	67.9	6.79	0.490	27.4	1.323
		c	67.9	6.79	0.735	27.4	1.544
		d	67.9	6.79	0.980	27.4	1.764
		e	67.9	6.79	1.225	27.4	1.985
		f	67.9	6.79	1.470	27.4	2.205
		g	67.9	6.79	1.715	27.4	2.426
		h	67.9	6.79	1.960	27.4	2.646
	P4	a	55.9	5.59	0.196	23.3	1.058
		b	55.9	5.59	0.441	23.3	1.279
		c	55.9	5.59	0.686	23.3	1.499
		d	55.9	5.59	0.931	23.3	1.720
		e	55.9	5.59	1.176	23.3	1.940
		f	55.9	5.59	1.421	23.3	2.161
		g	55.9	5.59	1.666	23.3	2.381
		h	55.9	5.59	1.911	23.3	2.602

3. Method of analysis

The analysis on the bridge models is conducted using an analytical method based on the elasto-plastic finite displacement dynamic response analysis. The tangent stiffness matrix, considering both geometric and material nonlinearities, is adopted in this study, being the cross sectional properties of the nonlinear elements prescribed by using fiber elements. The stress-strain relationship of the beam-column element is modeled as a bilinear type. The yield stress is 235.4 MPa, the elastic modulus is 200 GPa and the strain hardening in plastic area is 0.01. The implicit time integration Newmark scheme is formulated and used to directly calculate the responses, while the Newton-Raphson iteration method is used to achieve the acceptable accuracy in the response calculations. The damping of the structure is supposed a Rayleigh's type, with a damping coefficient of the first two natural modes of the structure of 2%.

4. Input earthquake ground motions

To evaluate the effect of hardening of lead-rubber bearings on the seismic performance of the multi-span continuous bridges, the nonlinear models are subjected to the action of two different input earthquake ground motions: Standard Earthquake Wave (SEW)-Ground Type I and Ground Type II, horizontal component accelerations, represented in **Fig. 3**. These accelerograms, provided by the Japan Road Association[5], are modified from direct-inland-strike type earthquake records from the 1995 Hyogoken-Nanbu earthquake, and they have been selected according to their destructive energy content and the suitability of ground Types I and II for base isolation design. These input earthquakes have been suitably scaled in acceleration, multiplied by using factors (a) to clearly appreciate the effects of hardening at high bearing strain levels.

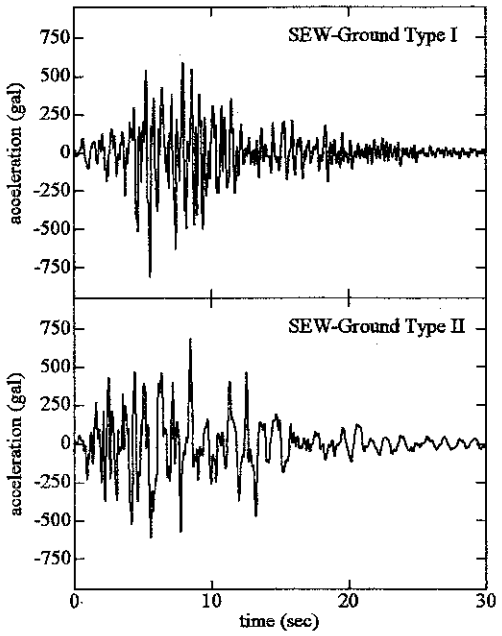

Fig. 3 Input earthquake ground motions

5. Numerical results

5.1 Natural vibration analysis

The fundamental natural period of the viaducts is calculated by using the effective stiffness[10] of the LRB isolation bearings. According to recommendations of Specifications of Highway Bridges[5], the pre-yield to post-yield stiffness ratio (K_1/K_2) of the bearings is pre-selected to obtain a moderate period shift. Design properties of isolation bearing devices are selected to obtain periods slightly larger than twice the natural period of the bridge when no isolation bearing is applied, 0.60 seconds and 0.55 seconds for Model 1 and Model 2, respectively.

For the two viaduct models, the fundamental natural period corresponds to the modal vibration in the longitudinal direction of the bridge, and it is observed to be significantly influenced by characteristics of the isolation bearings. Depending on the yield force level of the lead plug and the rubber stiffness, the fundamental natural period varies in the intervals 0.94~1.40 seconds and 0.78~1.31 seconds, for Model 1 and Model 2, respectively. Low values of period indicate that the size of the lead plug is excesivelly large and the viaduct is not able to shift its fundamental natural period into ranges that exceed those of the input ground motion. On the other hand, the moderate period shift, obtained for the other values, allows for reflecting a major portion of the earthquake energy, limiting the increased displacements experienced by the bridge deck during strong earthquake ground motions.

5.2 Nonlinear dynamic response

Nonlinear analyses of the highway viaduct models, designed either accounting for hardening or neglecting it, have been carried out under the same input earthquake ground motion histories: SEW-Ground Type I (a=3.0), and SEW-Ground Type II (a=1.0).

For a more comprehensive comparison of nonlinear response of the isolated bridges, calculated results are presented firstly at bearing support level where hardening takes place, and secondly at piers and deck superstructure to evaluate the effect of hardening on important structural elements of the highway viaducts.

(1) Maximum response of bearing supports

The effect of hardening on the maximum bearing responses is shown in **Fig. 4**. The envelopes of peak shear forces and displacements for LRB bearings indicate that hardening generally tends to simultaneously increase the maximum forces acting on the isolation bearings reducing the peak bearing deformation. Quantification for these variations depends on the bearings as well as on the earthquake ground motion characteristics.

It is clear that hardening effect is pronounced for flexible LRB bearings with small yield force ratio. This is due to the high deformation experienced for these bearings in which the lead plug yields at low levels of force, and consequently, the geometric effect leads to significative hardening behaviour.

The peak bearing responses show great differences among the two seismic input waves. The effect of hardening is small in case of SEW-Ground Type I, and it has been necessary to amplify the original input accelerations by a factor a=3.0 to clearly appreciate the hardening behaviour of the LRB bearings. This is because peak accelerations of the earthquake ground motion corresponds to low periods (0.73 seconds) which are out of the range of the natural periods of the viaducts.

It is also observed in this figure the difference in seismic force distribution among the bearing supports of each pier. Seismic forces are gradually reduced as the pier height is increased. This fact results firstly from the natural tendency of superstructure inertia forces to be attracted by the stiffer substructure elements, like short piers. Secondly, it has been enhanced by selection of different properties of the LRB bearings with the aim of protecting the tall piers, specially vulnerable to seismic loading due to the significant amplification of bending moment response at the pier bottoms with the increase of pier height.

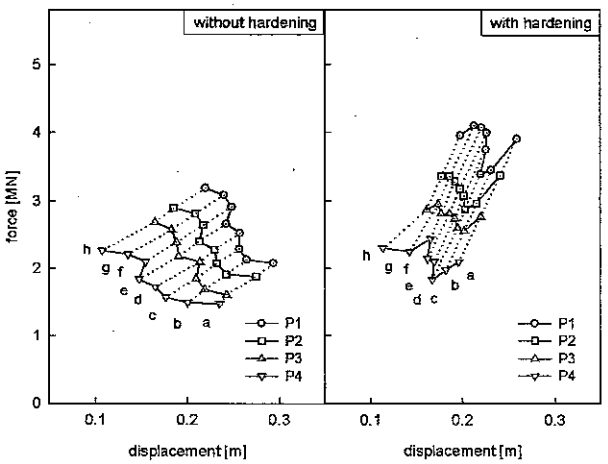

(a) Model 1 under SEW-Ground Type I (a=3.0)

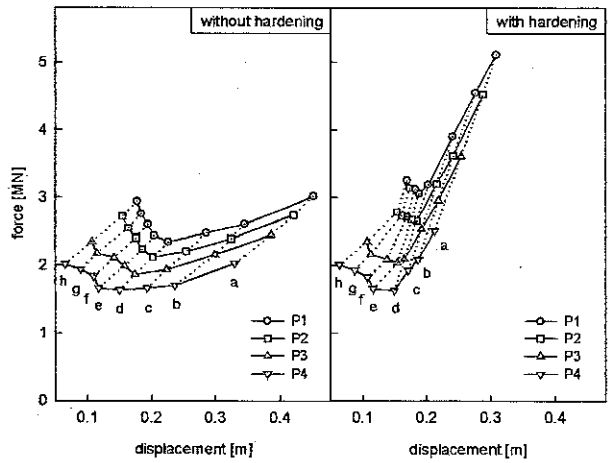

(b) Model 1 under SEW-Ground Type II (a=1.0)

Fig. 4 Envelopes of maximum bearing responses

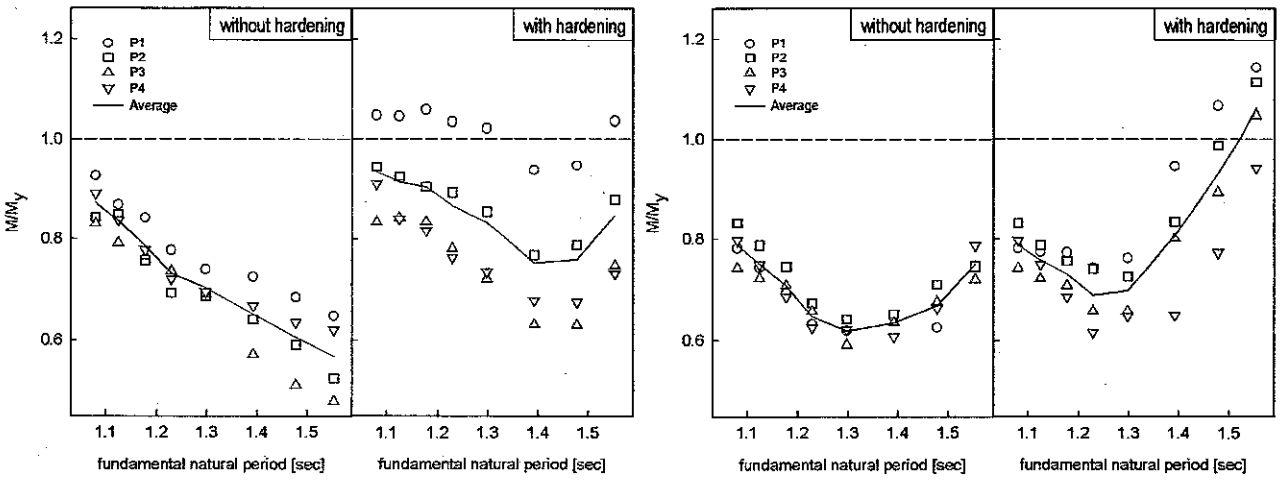

(a) Model 1 under SEW-Ground Type I (a=3.0)

(b) Model 1 under SEW-Ground Type II (a=1.0)

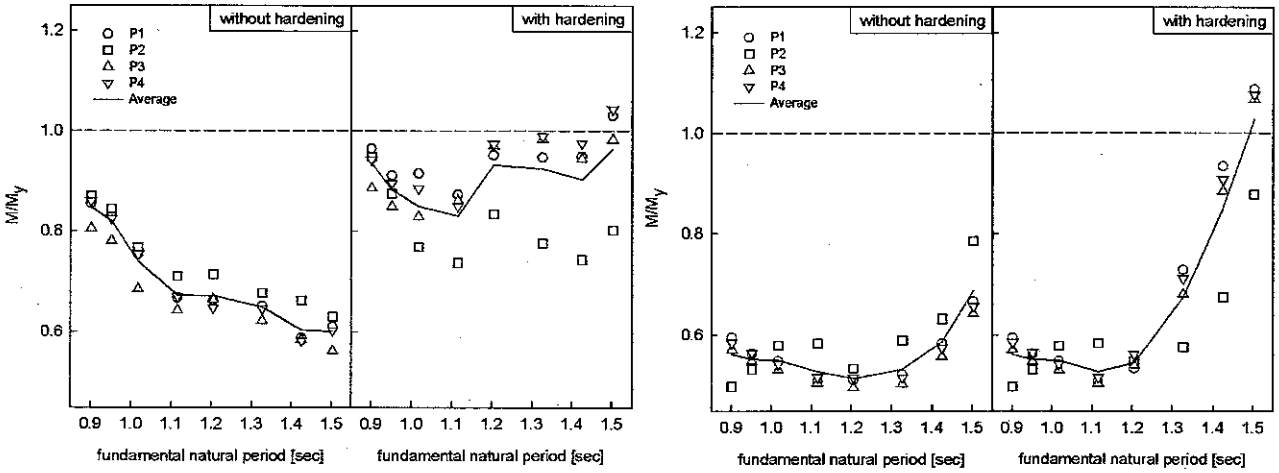

(c) Model 2 under SEW-Ground Type I (a=3.0)

(d) Model 2 under SEW-Ground Type II (a=1.0)

Fig. 5 Ratio of absolute maximum bending moment response at base of piers

(2) Maximum response of piers

It is well-known that bending moment at the base of bridge piers is considered to be a good measure of seismic structural damage. Therefore, the values of the ratio of absolute maximum bending moment to the yield moment at pier bottoms (M/M_y), varying with the viaduct fundamental period, are presented in **Fig. 5**

Calculated results indicate, as expected, that pier ductility demands are increased with hardening as a consequence of increase of reaction forces acting on bearings. It is also observed a noticiable trend to amplify the maximum bending moment at the piers with the natural period of the viaduct because the effect of hardening is larger in case of flexible bearings.

An important remarkable point is that the base isolation feature of reducing the forces acting on the substructure with the increase of the isolation period could be inverted when hardening effect is considered. Moreover, in several cases plastic ductility of piers is found in cases in which without hardening, the demands are expected to be under elastic range. Thus, indicating that an excessive period shift could have a considerable effect on the increase of seismic structural response due to hardening.

One of the differences between conventional and base isolation design is that in isolated bridges the distribution of lateral loads is a function of the force-deformation characteristics of the isolation bearings. Both the size of the lead plug and the plan size and height of the bearings can be used to control the distribution of the seismic forces. Therefore, in the original design strategy, when hardening is not considered, the loads are distributed reasonably uniformly to all substructures. It can be observed that the ductility demands in all piers remain fully elastic and approach a constant, since the bearings are sized such that the force transmitted into the piers at maximum displacement would not exceed the moment capacity of the piers.

This balance is relatively complicated to obtain in case of these types of irregular bridges because, due to the nonuniform distribution of masses and stiffnesses along highway viaducts with piers of unequal heights, one or more piers will attract significantly more lateral inertia force from the superstructure.

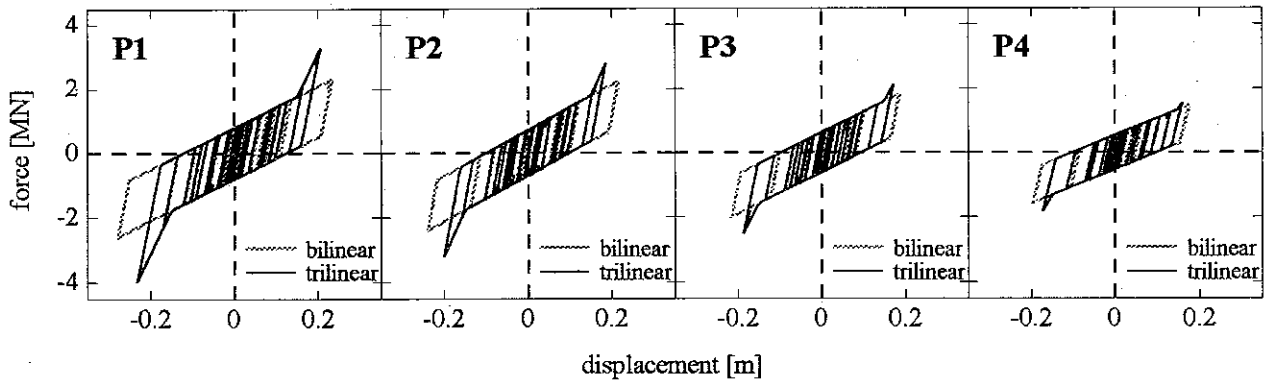

(a) Model 1 (case c) under SEW-Ground Type II (a=1.0)

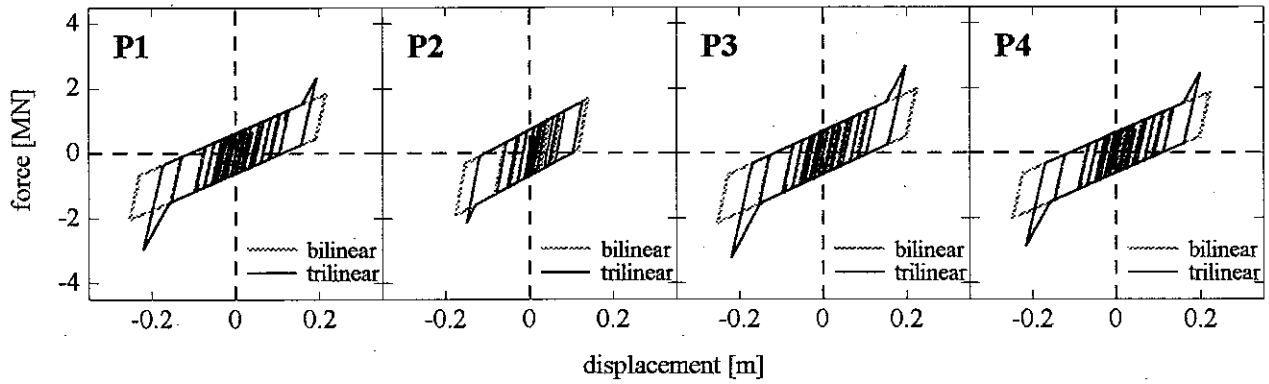

(b) Model 2 (case c) under SEW-Ground Type II (a=1.0)

Fig. 6 Hysteresis loops of LRB bearings

If hardening is considered, the equilibrium of balanced pier ductility is broken. Maximum differences of M/M_y ratio among piers are over 50% in several cases, while for models designed neglecting the hardening effect the maximum differences are less than 10%. In case of Model 1, it is observed that moment ratio is higher than average values for P2 and specially for P1, the shortest piers. For Model 2, the most remarkable fact is that maximum bending moment of P2, the tallest pier, presents lower values than the average. To obtain a coherent explanation for this fact, hysteresis loops of LRB bearings for the four piers are represented in **Fig. 6**.

It is clearly observed that hardening produces a force redistribution, and higher forces are resisted at short piers and lower forces concentrates on tall piers. LRB bearings of tall piers do not attract as much force as the other bearings since most of the deck displacement is absorbed by the pier. Consequently, bearings of short piers are subjected to large deformations resulting in significative large reactions forces due to hardening.

Ignoring the hardening effect, maximum response of tall piers is overestimated. On the other hand, it is noted that short piers are in a critical situation for what concerns the ductility demand. The short piers do in fact take up more shear forces than expected, being possible that the ductility of the short piers increases beyond their capacity.

(3) Maximum response of deck

Deck displacement is an important response factor related to the possibility of damage due to collision between deck and abutments, and crucial from the design point of view of expansion joints at the abutment level in continuous bridges.

Fig. 7 compares the effect of hardening of LRB bearings on the maximum deck displacements. In this figure, the absolute maximum deck displacements are presented as the contribution of movement of the pier tops plus the shear deformation of the isolation bearing supports.

The maximum deck displacement response is expected to follow a similar trend of reduction as the experienced by maximum bearing deformations when hardening is considered in the bearing analytical model. However, considerable differences in seismic response, depending on the input ground motions, are observed.

It is seen that the effect of hardening on deck displacements, in case of SEW-Ground Type I (a=3.0), is small. Maximum deck displacements with hardening are slightly higher than those without hardening because, even the bearing deformation is considerably reduced, the contribution to total deck displacements by pier top displacements is larger. Thus suggesting that in case of neglecting hardening, a significant underestimation of deck displacement is obtained.

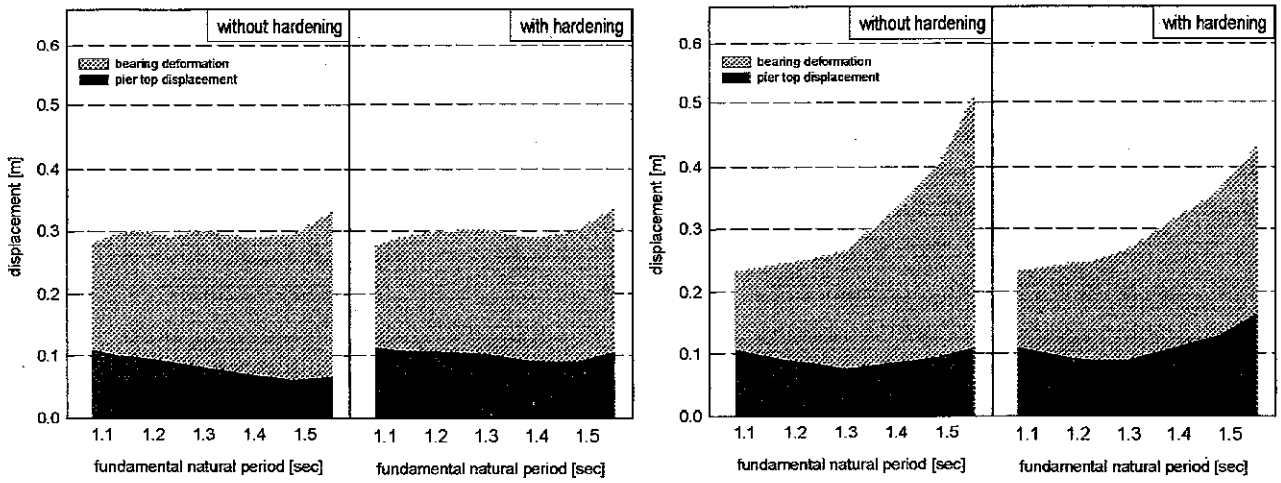

(a) Model 1 under SEW-Ground Type I (a=3.0)

(b) Model 1 under SEW-Ground Type II (a=1.0)

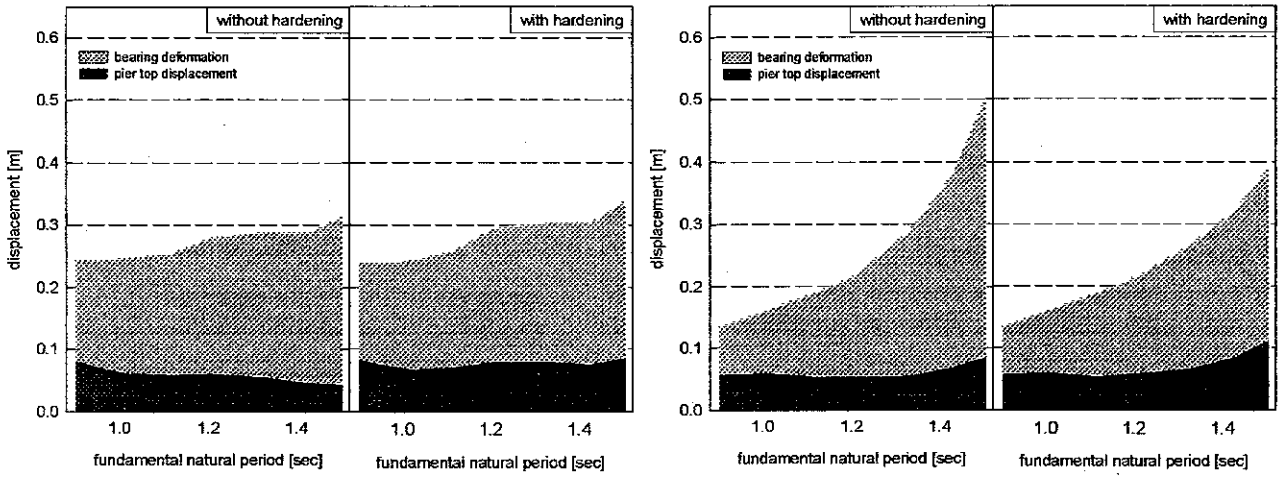

(c) Model 2 under SEW-Ground Type I (a=3.0)

(d) Model 2 under SEW-Ground Type II (a=1.0)

Fig. 7 Absolute maximum displacement response of deck superstructure

For SEW-Ground Type II, the LRB bearings are subjected to larger deformations as a result of the particular nature of this motion. Therefore, the reduction in bearing deformation is more significative than in case of SEW-Ground Type I. Ignoring the effect of hardening, the maximum deck displacements are overestimated because, even hardening increases the displacements at piers, significant reduction in terms of peak bearing deformation results in smaller maximum total deck displacement.

Consequently, it is observed that deck displacements may have both possibilities of increasing or decreasing depending on the counterbalance between contributions of top pier displacements and bearing deformation to the total deck displacement response.

Both viaduct models analyzed in this study are bridge with tall piers. Although these bridges may attract smaller spectral accelerations due to their long fundamental periods, displacement at the piers location and deck superstructure are very large. Therefore, the decision on the adoption of base isolation techniques to this type of structures should be carefully analyzed. Application of partial base-isolation, with limited period shift, could be considered a satisfactory alternative in order to obtain reduced maximum deck displacement response.

6. Conclusions

The hardening effect of lead-rubber bearings on the overall seismic response of highway viaducts with piers of unequal heights is examined in this study through nonlinear finite element seismic response analysis.

Comparison of calculated results, presented for two different bridge models, indicate that neglecting the effects of hardening, the base isolation feature of reducing the forces acting on the substructure with the increase of the isolation period could be inverted. Plastic ductility of piers is found in cases in which without hardening, the demands are expected to be under elastic range. Thus, indicating that an excessive period shift could have a considerable effect on the increase of seismic structural response due to hardening.

In addition, hardening produces a force redistribution, and higher forces are resisted at short piers and lower forces concentrates on tall piers. The equilibrium of balanced pier ductility, significantly unstable in case of highway viaducts with piers of unequal heights, is broken. Ignoring the hardening effect, maximum bending moment response of tall piers is overestimated and, on the other hand, the short piers do in fact take up more shear forces than expected, being possible that the ductility of the short piers increases beyond their capacity.

Considerable differences in peak deck displacement response, depending on the input ground motions, are observed. Maximum deck displacements may have both possibilities of increasing or decreasing depending on the counterbalance between contributions of top pier displacements and bearing deformation to the total deck displacement response.

The hardening effect is obviously of special relevance from the point of view of analytical modeling. The most important implication is that the bilinear model assumption is not acceptable in case of extreme earthquakes. The adoption of more accurate force-deformation models for lead-rubber bearings is required, being the trilinear analytical model very efficient to represent the hardening behaviour without excessive computational cost.

The above considerations indicate that, under large earthquakes, special attention should be paid to hardening of lead-rubber bearings, since their effects can significantly modify the overall structural seismic response of highway viaducts with piers of unequal heights. In addition, the same research methodology can be extended to bridges supported on different types of elastomeric bearings, laminated rubber and high damping rubber bearings, expected to experience similar hardening behaviour.

References

1) Kelly, J. M., Aseismic base isolation: review and bibliography, *Soil Dynamics and Earthquake Engineering*, **5** (4), pp.202-216, 1986.
2) Savage, I., Eddy, J. C. and Orsolini, G. I., Seismic analysis and base isolation retrofit design of a steel truss vertical lift bridge, *Computers and Structures*, **72**, pp.317-327, 1999.
3) Turkington, D. H., Carr, A. J.,Cooke, N. and Moss, P. J., Seismic design of bridges on lead-rubber bearings, *Journal of Structural Engineering*, ASCE, **115**, pp.3000-3016, 1989.
4) Tan, R. Y. and Huang, M. C., System identification of a bridge with lead-rubber bearings, *Computers and Structures*, **74**, pp.267-280, 2000.
5) Japan Road Association, *Specifications for highway bridges-Part V Seismic Design*, Maruzen, Tokyo, 1996.
6) Morishita, N., Maeno, H., Mori, N. and Ouchi, H., Experiments and application of seismic characteristics of isolation bearings in urban highway viaducts, *Bridge and Foundations*, **3**, pp.39-46, 2002 (in Japanese).
7) Highway Innovative Technology Evaluation Center, Evaluation findings for Dynamic Isolation Systems, Inc. elastomeric bearing. Report #40369. Web-site of Civil Engineering Research Foundation. Available from: http://www.cerf.org/about/reports/40369.htm
8) Adachi, Y. and Unjoh, S., Seismic response characteristics of seismically isolated bridge considering hardening effect of seismic isolator where non-linear response occur at both seismic isolator and bridge column, *Journal of Structural Engineering*, **47**, pp.905-916, 2001 (in Japanese).
9) Fragiacomo, M., Rajgelj, S. and Cimadom, F., Design of bilinear hysteretic isolation systems, *Earthquake Engineering and Structural Dynamics*, **32**, pp.1333-1352, 2003.
10) Hwang, J. S. and Chiou, J. M., An equivalent linear model of lead-rubber seismic isolation bearings, *Engineering Structures*, **18** (7), pp.528-536, 1996.

(Received July 31, 2003)

Development of Cable Exciting System for Evaluating Modal Damping of Stay Cables

Nam-Sik Kim*, Woon Jeong**, Ju-Won Seo**, Sang-Sup Ahn***

* Dr. of Eng., Hyundai Inst. of Construction Tech., Hyundai Construction Corporation, Yongin 449-710 Korea
** M. of Eng., Hyundai Inst. of Construction Tech., Hyundai Construction Corporation, Yongin 449-710 Korea
*** Dr. of Eng., Highway & Transportation Tech. Inst., Korea Highway Corporation, Hwaseong 445-812 Korea

One of the effective alternatives to suppress hazardous vibration of stay cables is to employ cable dampers. In order to design the cable damper optimally, it is necessary to exactly estimate the dynamic characteristics of the existing cables. To estimate more reliable dynamic properties of stay cables, precise excitations inducing forced vibration are mandatory. Hence, in this study, a cable exciting system(exciter) controlled digitally is developed. Design formula for exciter is also derived by the solution of equation of motion of a cable-exciter system. The performance of the cable exciter is verified by the sine sweeping test and resonance test for the cable model in a laboratory. Also from those tests, the precise dynamic properties of the cable model are obtained. Thus, it is ascertained that structural damping of stay cables is proportional to the amplitude of cable vibration.

Key Words: stay cable, cable exciting system, modal damping, resonance test

1. Introduction

As a critical member of cable-stayed bridges, stay cables play an important role of supporting the entire structure. The inherently low damping of stay cables makes it sensitive to various vibrations induced from some sources such as traffic, wind and rain-wind vibrations. To solve these hazardous vibration problems, various measures have been developed. One of the effective ways is to install the dampers[1),2)] near to the anchorage of stay cables. Optimal design for cable dampers needs the precise estimation of dynamic properties of cables. Moreover, in order to verify the performance of the installed dampers, sophisticated dynamic tests of cables are mandatory. Dynamic tests require the excitation of structures such as by ambient condition, moving vehicle or man-power. By those previous excitation methods[1),3)], however, it is often that satisfying response signal enough to estimate the precise results could not be obtained. Furthermore, large structures are hardly excited by the previous excitation methods.

Therefore, in this study, a cable exciting system is developed to acquire dynamic properties of stay cables. Design formula for exciter is also derived from the solution of equation of motion of a cable-exciter system. Using the design formula, unbalanced mass required or eccentricity of mass is easily determined depending on the location of exciter and the required amplitude of cable. Also those capabilities of exciter, inducing the modal excitations resonant with cable frequencies, make it possible to obtain the fine response signal and reliable dynamic properties of stay cables.

To verify the design formula and the performance of cable exciting system, some tests such as sine sweeping test and resonance test are carried out for the cable model in a laboratory. Test results show that the cable exciter can precisely excite the cable model to obtain the required amplitude and vibration mode. And the dynamic properties of the cable model are acquired satisfactorily.

Dynamic properties of the cable model, amplitude and modal damping, are estimated using the test results. Especially, cable damping of the fundamental mode is investigated varying with the amplitude of cable vibration.

2. Design of Cable Exciting System

2.1 design formula for cable exciter

A mathematical model of a cable-exciter system, as shown in Fig.1, is described based on the following assumptions.

i) The sag of cable is small enough to be neglected.
ii) The static profile of cable is represented by a parabolic equation.
iii) The dynamic tension of cable is neglected.
iv) The flexural rigidity of cable is ignored.
v) The unbalanced mass of cable exciter is so small as to be negligible, comparing with the entire cable mass.

In Fig.2, when the unbalanced exciting masses rotate in the opposite direction against each other and the exciter is installed at y-axis of exciter in parallel to the cable chord, exciting forces are

exerted only in perpendicular to the cable chord and all the chord-wise component of exciting forces are vanished.

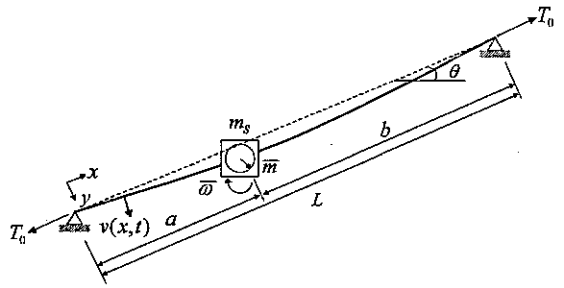

Fig.1 Cable-exciter system

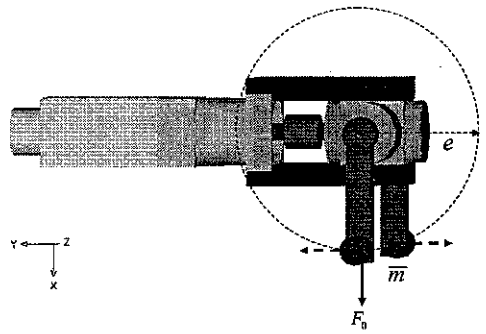

Fig.2 Cable exciting mechanism

Thus, magnitude of exciting force, F_o, can be represented as follows:

$$F_o = \overline{m}\, e\, \overline{\omega}^2 \tag{1}$$

From the above assumptions and the harmonic exciting force with magnitude given by Equation (1), the equation of motion of a cable-exciter system can be written as the following partial differential equation:

$$\begin{aligned} &-T_o \frac{\partial^2 v(x,t)}{\partial x^2} + \frac{w}{g}\frac{\partial^2 v(x,t)}{\partial t^2} + c\frac{\partial v(x,t)}{\partial t} \\ &= \left(-m_s \frac{\partial^2 v(x,t)}{\partial t^2} + \overline{m} e \overline{\omega}^2 \sin \overline{\omega} t \right) \delta(x-a) \end{aligned} \tag{2}$$

in which a is the distance from cable anchorage to exciter, T_o is the initial tension of cable, w is the cable mass per unit length, c is the equivalent viscous damping coefficient of cable per unit length, m_s is the entire mass of the exciter including the unbalanced exciting masses, $\overline{m}$ is the mass of the unbalanced exciting pendulums, e is the eccentricity of the unbalanced exciting masses, ϖ is the exciting frequency of the exciter, and $\delta()$ is the Dirac delta function.

It can be assumed that the transverse displacement $v(x,t)$ of the cable is represented by the infinite series of a linear combination with free vibration modes and generalized coordinates as follows:

$$v(x,t) = \sum_{i=1}^{\infty} v_i(t)\phi_i(x) \tag{3}$$

According to the assumptions i) and v), free vibration modes of cable can be represented by the sine function as follows:

$$\phi_i(x) = \sin i\pi \frac{x}{L} \tag{4}$$

When applying the Galerkin method using Equations (3) and (4), the equation of motion of a cable-exciter system can be rewritten as an uncoupled form by

$$\begin{aligned} &\ddot{v}_i(t) + 2\xi_i \omega_i \dot{v}_i(t) + \omega_i^2 v_i(t) \\ &= \frac{\overline{m}\, e}{M_i}\overline{\omega}^2 \sin(\overline{\omega}\, t)\sin(i\pi\alpha) \end{aligned} \tag{5}$$

where $\alpha(=a/L)$ is the distance ratio of exciter,

$M_i = Lm/2 + m_s \sin^2(i\pi\alpha)$

$\xi_i = Lc/(4\omega_i M_i)$

$\omega_i^2 = i^2\pi^2 T_o/(2LM_i)$.

The steady-state response at resonant condition can be obtained by using the solution of Equation (5) and applying $\varpi=\omega_i$ to the solution. Therefore, the response on cable amplitude is given by

$$v(x,t) = \sum_{i=1}^{\infty} \frac{\overline{m} e \sin(i\pi\alpha)}{2\xi_i M_i} \sin(\overline{\omega}\, t - \theta_v) \sin i\pi \frac{x}{L} \tag{6}$$

where

$$\theta_v = \arctan\left(\frac{2\omega_i \overline{\omega} \xi_i}{\omega_i^2 - \overline{\omega}^2} \right) \tag{7}$$

For the 1st mode vibration(i=1), maximum amplitude at cable center can be obtained by using Equation (6) as follows:

$$v_{\max,0.5L} = \frac{\overline{m} e \sin(\pi\alpha)}{2\xi_1 M_1} \tag{8}$$

In this study, Equation (8) is used as a preliminary design formula for a cable-exciter system. That is, according to the assumed damping ratio of cable and the installation location of exciter, unbalanced mass or eccentricity of the exciter can be determined, based on amplitude intended at cable center. A resonant frequency of the exciter is determined by the sine sweeping test because natural frequencies on the cable-exciter system can not be calculated accurately, even though using a sophisticated mathematical model.

2.2 cable exciting system

The cable exciting system developed in this study consists of both hardware and software. The hardware as shown in Fig.3 has the component parts of AC servomotor, decelerator, coupler, gearbox and outer frame for fixing.

As shown in Fig.4, the software has a function which can control the servo driver with the computer added DAQ card, and also supports the sine sweeping test and the resonance test by controlling the rotating frequency of the servo motor in the fixed frequency domain. Dimensions and specifications of the cable exciting system are summarized in Table 1.

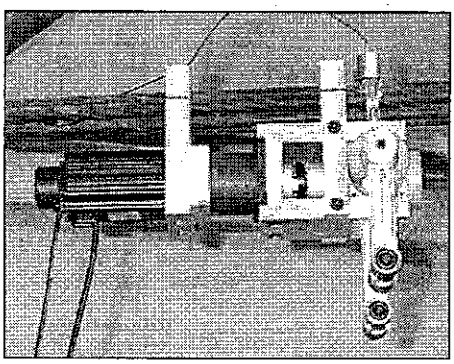

Fig.3 Prototype of exciter

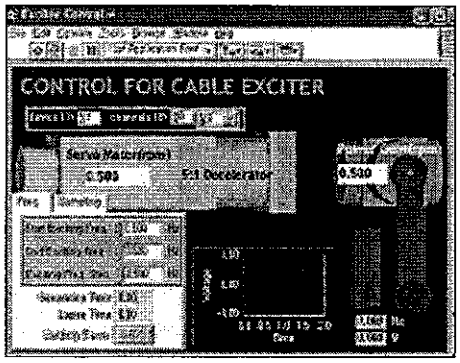

Fig.4 Control program for exciter

Table 1 Dimensions and specifications of cable exciting system

Items		Characteristics
Frequency	Exciting frequency range	0~10Hz
	Resonant frequency range of exciter	250~350Hz
Exciting Force	Exciting direction	Perpendicular to the cable chord
	Exciting force control	Mass control by rotating pendulum
	Exciting torque range	0~1.63kN·cm
Control	Local	Digital Loader
	PC	Control Program

3. Performance Tests of Cable Exciting System

3.1 cable model

The cable model[3] shown in Fig.5 consists of 7 strands of which each is 7-wire strand coated by PVC. The inclined angle θ of cable model is about 8.37° and the hydraulic jack installed at the lower anchorage introduces the initial tension of cable model. More detailed properties of the cable model are presented in Table 2.

In Fig.6, the sag effect of the cable model with different initial tensions, ranged from 100kN to 600kN, is verified by comparing it with the existing stay cables of cable-stayed bridge such as Jindo bridge[2] and Seohae bridge[1] located in Korea. As shown in Equation (9), non-dimensional parameter λ^2 introduced by Irvine[4] means a ratio of catenary stiffness to elastic stiffness of the cable.

$$\lambda^2 = (Lw\cos\theta)^2(EA/T_o^3) \tag{9}$$

The cable model has the reasonable sag effect compared with the existing stay cables in range of λ^2 of 0.0~1.0, except for initial cable tension of 100kN.

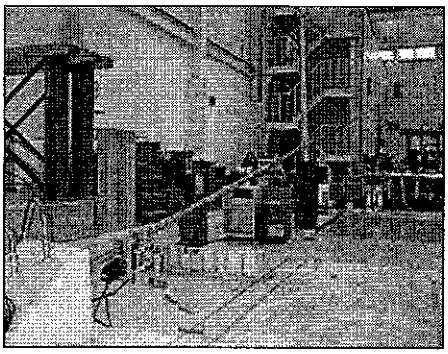

(a) test setup

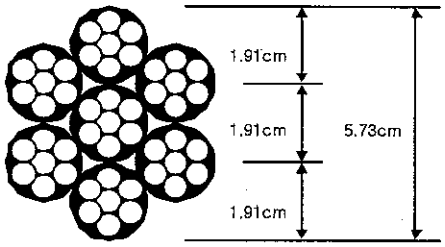

(b) cross section

Fig.5 Cable model

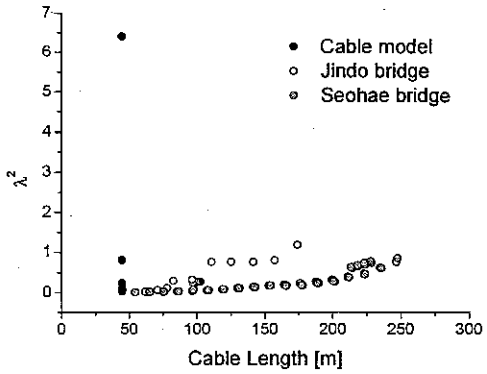

Fig.6 λ^2 comparison of cable model with existing stay cables

Table 2 Cable properties

L (m)	w (kN/m)	E (kN/m^2)	EA (kN)	EI (kN·m^2)
44.7	0.08986	1.89×10^8	3.79×10^5	77.36

3.2 performance of cable exciter

For the assumed damping ratios of cable model, maximum amplitudes at cable center are calculated by Equation (8) with varying the installation location of exciter for different mass ratios and are plotted in Fig.7. In general, assumed damping ratio is 0.15% for the 1st mode and is a reasonable value for the existing

stay cables. From this figure, the appropriate installation location depending on the specified mass ratios can be determined or conversely the required amplitude response obtained.

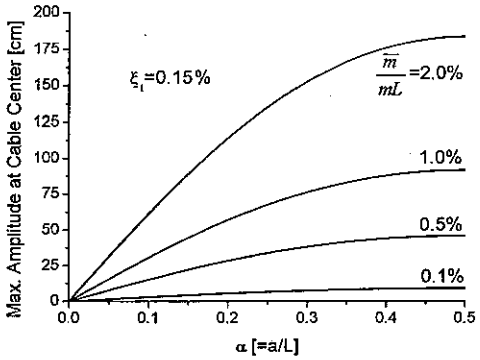

Fig.7 Maximum amplitude at cable center varying with exciter location(assumed damping ratio; ξ_1=0.15%)

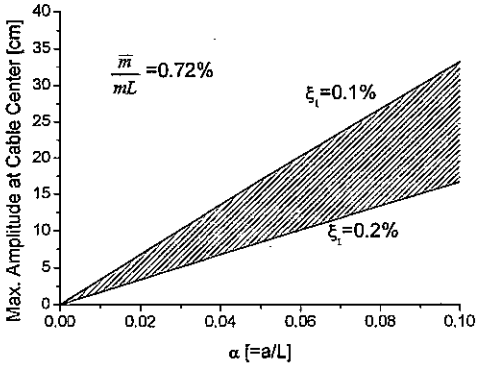

Fig.8 Maximum amplitude at cable center varying with exciter location(assumed damping ratios; ξ_1=0.1~0.2%)

In this study, the installation location of exciter is determined as 3%(α=0.03) and also the mass ratio is determined to be 0.72% corresponding to the unbalanced exciting mass of 3kg. From these parameters obtained, maximum amplitudes at cable center are calculated again varying with damping ratios of 0.1 to 0.2% because of its uncertainty, and is plotted in Fig.8. From the figure, it can be convinced that maximum amplitudes at cable center are within 5 to 10cm.

3.3 performance tests

(1) sine sweeping test : To acquire exactly resonant frequencies of the cable-exciter system, it is needed to perform the sine sweeping test, which drives continuously the exciter in the pre-determined frequency range. Frequency range can be determined by referring ω_j of the system as given in Equation (5) and is presented in Table 3. The resolution of varying frequencies is defined as 0.01Hz. Acceleration responses are simultaneously measured at two points, both 0.03L (exciter installation point) and 0.3L.

The acceleration responses and their power spectra are shown in Fig.9 and Fig.10, respectively, for cable tension of 600kN. From these figures, resonant frequencies of the cable-exciter system can be obtained. Fig.9 shows the controlled exciting frequencies and the amplified acceleration responses on the cable model. In Fig.10, a sharp peak at resonant frequency is observed.

All the resonant frequencies with various cable tensions are summarized in Table 4.

Table 3 Exciting frequency range in sine sweeping test

Tension (kN)	100	200	300	400	500	600
Exciting Freq. Range(Hz)	0.5~1.5	1.0~2.5	1.5~2.5	1.5~3.0	2.0~3.5	2.0~4.0

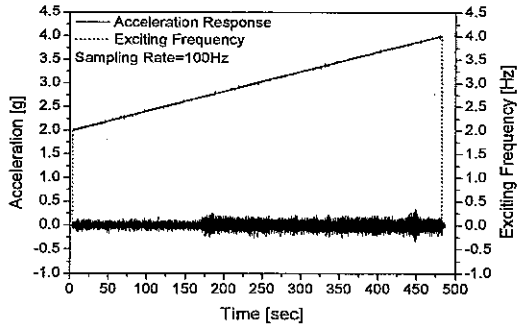

(a) at exciter (0.03L)

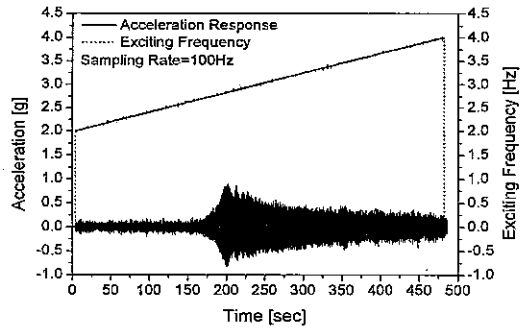

(b) at 0.3L

Fig.9 Acceleration responses from sine sweeping test with cable tension of 600kN

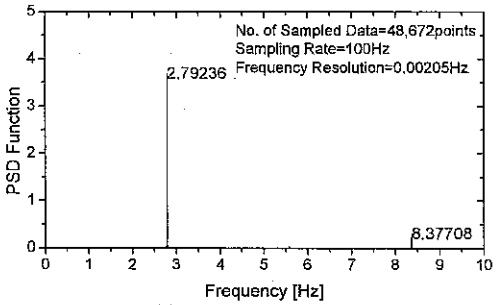

(a) at exciter (0.03L)

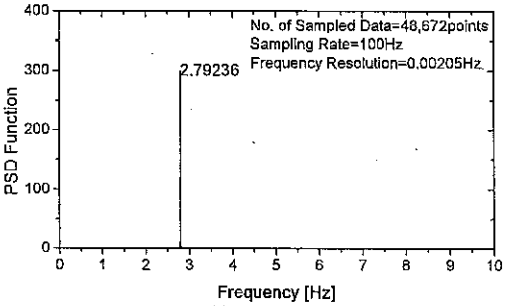

(b) at 0.3L

Fig.10 Power spectra from sine sweeping test with cable tension of 600kN

From the results of sine weeping test, cable excitation effects on the exciting frequencies are investigated as shown in Fig.11. Inertance function $I(\varpi/\omega_1)$, defined as a ratio of peak acceleration response to maximum exciting force, can be expressed as

$$I(\varpi/\omega_1) = \ddot{v}_{j,0.3L}/\overline{me}\varpi^2 \quad (10)$$

where ω_1 is the resonant frequency obtained from sine sweeping test and $\ddot{v}_{i,0.3L}$ is the cable acceleration response at $0.3L$ according to each positive peak j.

At higher cable tension and lower cable damping, cable response can be easily amplified under a constant excitation force. From Fig.11, it is observed that excitation on the cable model with the lower sag-to-span ratio is more efficient to obtain dynamic properties.

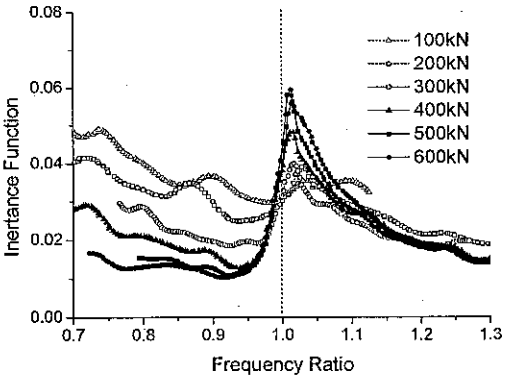

Fig.11 Cable excitation effect on varying frequency ratio

Table 4 Resonant frequencies obtained from sine sweeping test

Tension (kN)	100	200	300	400	500	600
Resonant Frequency(Hz)	1.328	1.648	1.968	2.261	2.536	2.792

(2) resonance test : In order to obtain the maximum amplitude of the cable model, the exciter is consecutively controlled to sustain the resonant frequencies acquired from sine sweeping test, as shown in Table 4. The cable motion excited is then in the state of resonance. However, due to the inherent damping of the cable itself, the resonant amplitude keeps constant after some minutes. Then the operation of cable exciter is manually stopped and the acceleration responses corresponding to free vibration are measured. Acceleration responses and their power spectra on cable tension of 600kN are plotted in Fig.12 and Fig.13, respectively.

In Fig.13(a), a peak at higher mode frequency of 8.4Hz is obtained and also observed in Fig.10(a). However there are no higher mode frequencies in Fig.10(b) and Fig.13(b). When considering the measuring points and ratio(about 3) of 8.4Hz to resonant frequency, it can be presumed that the second peak corresponds to the 3rd mode(anti-symmetric mode) of the cable-exciter system. Although the cable is excited in accordance with the 1st mode, the acceleration response measured near to cable exciter could be contaminated by the 3rd mode component. However, the unexpected excitation can be avoided by using the response measured at $0.3L$.

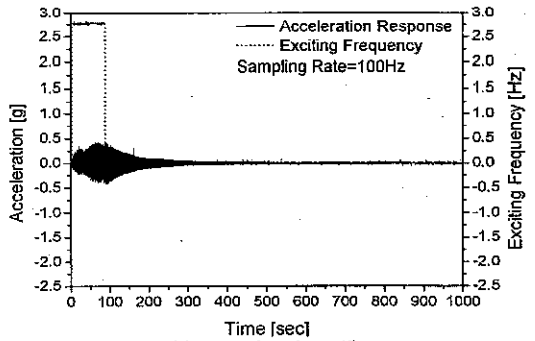

(a) at exciter ($0.03L$)

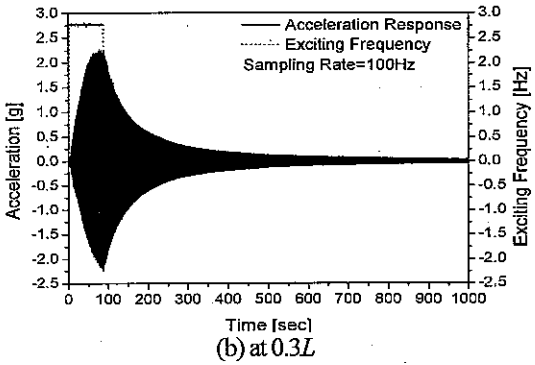

(b) at $0.3L$

Fig.12 Acceleration responses from resonance test with cable tension of 600kN

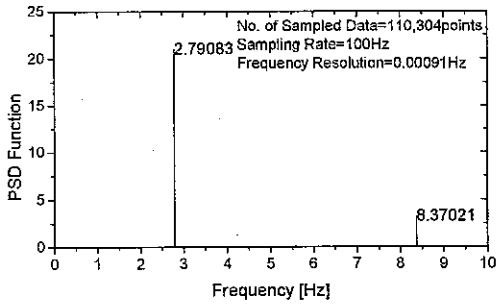

(a) at exciter ($0.03L$)

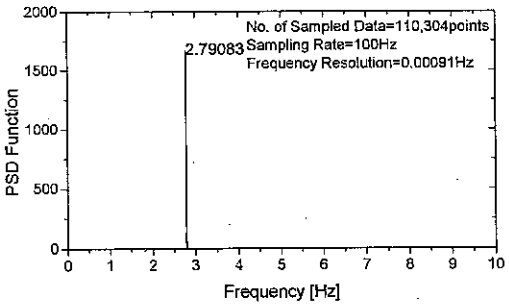

(b) at $0.3L$

Fig.13 Power spectra from resonance test with cable tension of 600kN

4. Estimation of Modal Properties

4.1 maximum amplitude

Cable amplitude can be easily estimated from the measured acceleration response, which has a single vibration mode. Two

methods, pseudo-displacement and direct time integration of acceleration response, are mainly used. Cable amplitude at $0.3L$, estimated by two methods, is converted to maximum amplitude at cable center, assuming the shape function of cable motion to be a sinusoidal. In Table 5, the estimated cable amplitudes are compared with one predicted by Equation (8).

Maximum amplitude predicted by Equation (8) has only a constant value corresponding to the assumed damping ratio, nevertheless varying with cable tension. From Table 5, it can be inferred that damping ratio of the cable model may be varied with initial tension or amplitude of the cable as major parameters.

Table 5 Maximum cable amplitude estimated at cable center

Tension (kN)	$v_{max,0.5L}$ (cm)		
	Pseudo-displacement	Direct time integration	Eq. (8)
100	5.56	4.71	6.79
200	5.81	5.58	
300	7.42	6.86	
400	6.30	6.09	
500	7.05	7.03	
600	8.90	8.59	

4.2 modal damping

From free vibration part of cable responses, damping ratios of the cable model are estimated. A logarithmic damping ratio of cable can be calculated approximately by using the following equation[5].

$$\xi_{logarithmic} \doteq \frac{v_j - v_{j+k}}{2k\pi\, v_{j+k}} \tag{11}$$

where v_j is the amplitude at the jth peak and k is the number of response peaks used to estimate the logarithmic damping ratio.

Using Equation (11), the logarithmic damping ratios of the cable model are calculated with $k = 100$. It is shown in Fig.14 that the logarithmic damping ratio decreases as the amplitude v_j decreases. This shows strongly hysteretic damping characteristics of the cable model. As shown in Fig.14, cable damping ratio depends on the initial cable tension and the amplitude of cable.

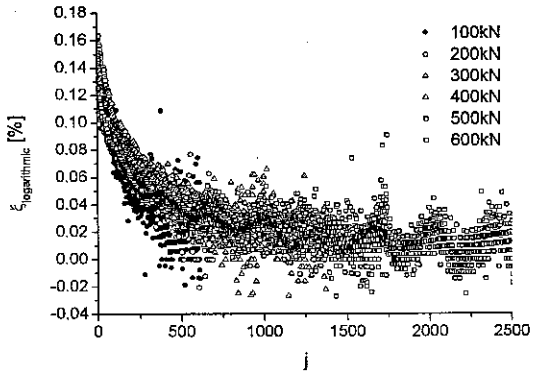

Fig.14 Estimated damping ratios according to j with k=100

Also, the estimation of cable damping ratio for stay cables could be simply calculated as a practical formula[6] written by

$$\xi_{practical}[\%] = 0.24 - 6\times10^{-4}\times L \tag{12}$$

where L is the cable length with a unit of meter. From Equation (12), the damping ratio of cable model is calculated as 0.21%.

In Table 6, $\xi_{logarithmic}$ estimated from Equation (11) is compared with both ξ_1 reversibly calculated from Equation (8) with the amplitudes estimated by two methods in Table 5 and $\xi_{practical}$ estimated from Equation (12). From the results, it can be understood that as the cable tension is increased so the estimated damping ratios are almost converged. To examine these facts, the estimated damping ratios versus the cable tension are compared with the sag-to-span ratio[4] in Fig.15. Therefore, when the sag-to-span-ratio of stay cables is negligible, the damping ratios estimated from three methods are nearly identical.

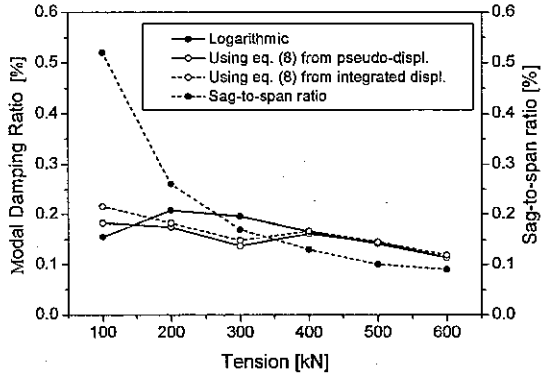

Fig.15 Comparison of estimated damping ratios and sag-to-span ratios

In Table 6, the logarithmic damping ratios $\xi_{logarithmic}$ are estimated using cable amplitude in the same range of 11.9mm(v_j) to 1.5mm(v_{j+k}) at $0.3L$. Consequently, the damping ratios are obtained with different k.

Table 6 Estimated damping ratios

Tension (kN)	$\xi_{logarithmic}$ (%)	ξ_1 by Equation (8), (%)		$\xi_{practical}$ (%)
		Pseudo-displacement	Direct time integration	
100	0.157(k=713)	0.183	0.216	0.21
200	0.208(k=507)	0.175	0.183	
300	0.195(k=581)	0.137	0.148	
400	0.169(k=663)	0.162	0.167	
500	0.148(k=750)	0.144	0.145	
600	0.118(k=950)	0.114	0.119	

* Estimated in range of 11.9mm to 1.5mm at $0.3L$

The damping ratios estimated from the above three methods, except for cable tension of 100kN, are generally decreased as the cable tension is increased. The damping of cable itself is constituted of both the frictional damping between cable wires and the material damping. Generally, the increase of cable tension decreases the frictional damping and also increases the cable potential energy by initial tension. Thus, the damping ratio of cable itself is decreased because of these phenomena, which

are verified in former studies of Raoof[7] and Yamaguchi[8]. Consequently, the damping ratios estimated from Equation (8), which neglects the effect of the cable sag, could be as reliable as the sag-to-span ratio is small.

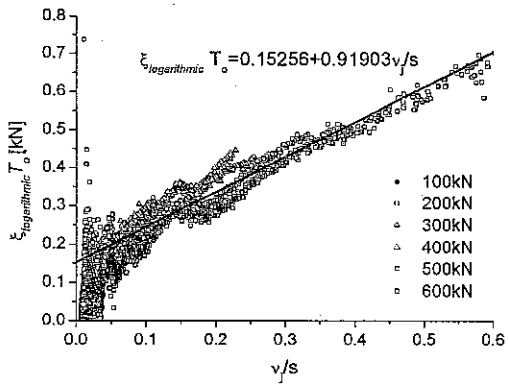

Fig.16 $\xi_{logarithmic}T_o$ according to v_j/s with k=100

The linear dependency on $\xi_{logarithmic}T_o$ according to v_j/s can be examined and all the results, except for cable tension of 100kN, are nearly coincided as shown in Fig.16. Here, the amount of cable sag[9], s, equals to $wL^2/8T_o$, which means the vertical deflection of stay cables due to self-weight. From the above figure, an empirical formula regressed could be derived depending on both initial cable tension and cable maximum amplitude as follows:

$$\xi_{empirical}[\%] = \frac{15.256}{T_o} + \frac{594.796}{wL^2} v_{\max,0.5L} \qquad (13)$$

where units for force and length are kilo-Newton and meter, respectively. According to Equation (13), it is shown that cable damping ratios would be varied depending on amplitude of stay cables. In case of cable vibration with large amplitude-to-sag-ratio(v_j/s), cable damping ratios could be linearly proportional to the amplitudes of cable.

5. Conclusions

In this study, the cable exciting system, which could excite the existing stay cables such as cable-stayed bridges, is developed with deriving the design formula from a mathematical model, and the performance tests on the cable model are carried out in a laboratory. From test results, it is verified that the cable model could be resonated at the fundamental vibration mode.

Cable amplitude can be easily estimated from the measured acceleration response, which has a single vibration mode. Two methods, pseudo-displacement and direct time integration of acceleration response, are mainly used for estimating cable amplitudes. Consequently, using the estimated amplitudes, the damping ratios predicted from the design formula, which neglects the effect of the cable sag, could be as reliable as the sag-to-span ratio is small.

Based on the correlation between $\xi_{logarithmic}T_o$ and to v_j/s, an empirical formula regressed could be derived depending on both initial cable tension and cable maximum amplitude. It is shown that cable damping ratios would be varied depending on amplitude of stay cables. In case of cable vibration with large amplitude-to-sag- ratio, the damping ratios could be linearly proportional to the amplitudes of cables.

Hereafter, this system would be applied to the existing cable-stayed bridges, and further developed in effective point of view.

References

1) Ahn, S.-S. and Lee, I.-K., "Study on Devices for Suppressing Vibration of Bridges", Report No. HRC 00-30, Korea Highway Corporation, 2000.

2) Seo, J.-W., Kim, N.-S., Ha, D.-H. and Suh, J.-I., "Development of Cable Damper with High Damping Rubber Bearing for Cable-stayed Bridge", *Fifth European Conference on Structural Dynamics, EURODYN2002*, pp.217-221, Munich, September 2002.

3) Kim, N.-S., Jeong, W., "Evaluation of Tension Force of Stay Cables Using Vibration Method", *Trans. of the Korean Society for Noise and Vibration Engrg.*, Vol. 12, No.12, pp.956-963, 2002.

4) Irvine, M., *Cable Structures*, Dover Publications Inc., New York, 1981.

5) Clough, R.W. and Penzien, J., *Dynamics of Structures*, McGraw-Hill Co., Singapore. 1993.

6) Fuzier, J. and Stubler, J., "Wind Vibrations and Damping Systems for Stay Cables", *Long-span and high-rise structure, IABSE Symposium*, Kobe, Japan, pp.205-210, 1998.

7) Raoof, M. and Huang, Y.P., "Upper-Bound Prediction of Cable Damping under Cyclic Bending", *Journal of Engineering Mechanics*, Vol. 117, No. 12, pp.2729-2747, 1991.

8) Yamaguchi, H. and Adhikari, R., "Energy-Based Evaluation of Modal Damping Treatment", *Journal of Sound and Vibration*, Vol. 181, No. 1, pp.71-83, 1995.

9) Gimsing, N. J., *Cable Supported Bridges*, John Wiley & Sons, Norwich., 1983.

(Received July 31, 2003)

A large deflection and inelastic analysis of steel elements at elevated temperature by simulation

C.K.J. Iu and S.L. Chan*

* Department of Civil and Structural Engineering, The Hong Kong polytechnic University

This paper presents an accurate and reliable nonlinear inelastic formulation to predict structural behaviour at elevated temperature. A fire analysis including large displacement effect for elasto-plastic frame structures is presented. This finite element formulation of beam-column element is based on the plastic hinge approach. The Newton-Raphson method with this thermal-time dependent effect was employed for the solution of the nonlinear governing equations to allow the prediction of large deformation in thermal history. Total formulation is employed in this nonlinear solution procedure for the convenience of incorporating the thermal effects. Creep deformation effect is implicitly included in these relationships. The effects of uniform or non-uniform temperature distribution are also considered. Several numerical verifications are also presented in this study. This fire analysis is efficient to predict the nonlinear inelastic response of steel structures, especially for steel bridge. Therefore, this analysis is a costless and quick assessment technique for steel bridge under fire.

Keywords: fire analysis; large deflection effect; inelastic material behaviour

1. Introduction

When a steel frame is heated, the steel member deteriorates rapidly and exhibits geometric nonlinearity due to change of geometry, resulting in a necessity to utilize such nonlinear solution techniques to obtain the instability structural behaviour under fire. Most of the fire analyses utilize Newton-Raphson method to predict large deflection effects.

In continental Europe, Schleich et al. [11] simulated the effect of thermal-time dependence using an incremental Newton-Raphson iterative procedure at each thermal load step. The advantage of such formulation is to save the computational effort. Franssen [6] presented a fire analysis which considers non-uniform temperature distribution, material yielding and geometric nonlinearity. He has developed a user-friendly computer program SAFIR using a fine grid of elements over each cross section [7].

In UK, Saab and Nethercot [10] presented the nonlinear structural behaviour of two-dimensional frame under fire using finite element method. Their basic formulation of nonlinear solution at normal temperature was mainly based on the research work from El-Zanaty and Murray [4] on which Najjar and Burgess [8] were further based to incorporate three-dimensional behaviour of steel members, including warping effect.

Wang and Moore [12] developed a package of analytical finite element method to predict the response of

structure under fire. Second-order geometrical nonlinearity, residual stress and initial deflection are included. The material nonlinear effect is modeled by plastic zone method used by numerous previous researchers.

In this paper, the fire study is mainly based on the nonlinear inelastic finite element program, GMNAF [2], to incorporate the thermal effects for steel structures. The present fire analysis includes both uniform and non-uniform temperature distribution over the member section. An incremental-iterative solution procedures based on the Newton-Raphson method is employed to model the effect of thermal-time dependence. The proposed formulation is derived in an updated Lagrangian local system, which allows large deformation effect. Elasto-plastic material nonlinear basing on plastic hinge method is simulated. And the material properties at elevated temperature are according to ECCS [5].

2. Thermal strain and curvature in fire analysis

Based on experimental observations, the total strain of steel at elevated temperatures can be subdivided into thermal strain, instantaneous stress related strain and creep strain as,

$$\varepsilon_t = \varepsilon_{th} + \varepsilon_\sigma \tag{1}$$

in which ε_t is total deformation strain. ε_σ is instantaneous stress related strain and ε_{th} is thermal strain in which consists of both thermal axial strain and curvature. The thermal axial strain $\varepsilon_{th,a}$ is given by,

$$\varepsilon_{th,a} = \alpha\Delta T = \alpha({}_{t+1}T - {}_tT) \tag{2}$$

in which α is the coefficient of thermal expansion. It is taken as a constant of $14\times10^{-6}/^0C$ in the present fire analysis. ${}_{t+1}T$ and ${}_tT$ are respectively the temperature at current $(t+1)$th and last tth thermal configuration. The thermal bowing effect is simulated by thermal curvature ϕ_{th} given by,

$$\phi_{th} = \frac{\varepsilon_t - \varepsilon_b}{D} = \frac{\alpha\beta_{t+1}T}{D} \tag{3}$$

where ε_t and ε_b are the thermal strains at the extreme top and bottom fibers, respectively. D is the depth of member section. β is the ratio of the temperature difference between the top and bottom surface of the member.

3. Basic formulation of the proposed fire analysis

The incremental internal strain energy should be based on the Castigliano's first theorem in term of stress and strain components as,

$$\delta U = \sigma\delta\varepsilon_t \tag{4}$$

Only the thermal strain due to non-uniform temperature distribution across the major axis is only considered.

$$\varepsilon_{th} = \varepsilon_{th,a} - y\phi_{th} = \alpha\Delta T - y\frac{\alpha\beta T}{D} \tag{5}$$

In a nonlinear analysis using the finite element formulation, it is customary to use the Green's strain tensor to express the strain-displacement relation as,

$$\varepsilon_t = \frac{\partial u}{\partial x} + \frac{1}{2}\left(\frac{\partial v}{\partial x}\right)^2 + \frac{1}{2}\left(\frac{\partial w}{\partial x}\right)^2 - y\frac{\partial^2 v}{\partial x^2} - z\frac{\partial^2 w}{\partial x^2} \tag{6}$$

The stress-related strain ε_σ is expressed from the total strain extracting from the thermal strain as compressive strain. By back substitution into eqn (4) and integration of incremental strain, the incremental internal strain energy is obtained as eqn (7).

$$U = \int_\varepsilon \delta U = E\int_l\int_A\int_\varepsilon (\varepsilon - \varepsilon_{th})d\varepsilon dA dx \tag{7}$$

The range of strain ε is from 0 to ε_t at a particular temperature-stress-strain relationship for updated

Lagrangian formulation in which it regards the last current configuration as an undeformed configuration as zero strain.

And the external work done V is equal to the external applied force multiplied by the corresponding displacement as follows:

$$V = \{d_k\}^T \{f_k\} \tag{8}$$

in which $\{d_k\}$ and $\{f_k\}$ are respectively the vector of the corresponding displacement and external applied force at k degree of freedom.

The total potential energy of fire analysis is equal to the sum of eqn (7) and eqn (8) as.

$$\Pi = U - V$$

$$\Pi = \frac{EA}{2}\int_l \left(\frac{du}{dx}\right)^2 dx + \frac{P}{2}\int_l \left[\left(\frac{dv}{dx}\right)^2 + \left(\frac{dw}{dx}\right)^2\right] dx + \int_l \left[\frac{EI_z}{2}\left(\frac{d^2v}{dx^2}\right)^2 + \frac{EI_y}{2}\left(\frac{d^2w}{dx^2}\right)^2\right] dx - EA\alpha\Delta T\int_l \left(\frac{du}{dx}\right) dx - \alpha\Delta T\frac{EA}{2}\int_l \left[\left(\frac{dv}{dx}\right)^2 + \left(\frac{dw}{dx}\right)^2\right] dx - \{d_k\}^T\{f_k\} \tag{9}$$

After substitution of cubic shape function into total potential energy function as eqn (9), the secant stiffness equation is expressed as,

$$\frac{\partial U}{\partial d_k} = [K_s]\{d_k\} \tag{10}$$

On the other hand, the tangent stiffness matrix can be obtained by taking a second variation of the total potential energy in eqn (9) as,

$$\frac{\partial^2 \Pi}{\partial d_j \partial d_k} = [K_T] = [K_L] + [K_G] + [K_{th}] \tag{11}$$

in which $[K_L]$ and $[K_G]$ are the linear and geometric tangent stiffness.

4. Plastic hinge in stiffness formulation

The material nonlinear effect in the proposed fire analysis is simulated through the plastic hinge approach, as it has a high convergent rate and simplicity in stiffness formulation. This plastic hinge method is an extension of the previous works by Yau and Chan [13] and Chan and Chui [3]. Their spring stiffness formulation is modified to be suitable to the present analysis. This spring stiffness formulation can model the load redistribution effect after yielding.

Using total moment-rotation relationship and after condensation of the rotations of beam, then substitution back into the elastic beam-column formulation in term of the rotations of connection, we have,

$$\begin{Bmatrix} M_{c1} \\ M_{c2} \end{Bmatrix} = \frac{1}{|K|}\begin{bmatrix} K_{11} & K_{12} \\ K_{21} & K_{22} \end{bmatrix}\begin{bmatrix} S_1(K_{22}+S_2) & -S_2K_{21} \\ -S_1K_{12} & S_2(K_{11}+S_1) \end{bmatrix}\begin{Bmatrix} \theta_{c1} \\ \theta_{c2} \end{Bmatrix} \tag{12}$$

in which $|K| = \begin{vmatrix} K_{11}+S_1 & K_{12} \\ K_{21} & K_{22}+S_2 \end{vmatrix} = (K_{11}+S_1)(K_{22}+S_2) - K_{12}K_{21}$

When the moment M_{c1} at the first node of an element exceeds the plastic moment capacity M_p of the section and the member is elastic at the second node, the spring stiffness at this yielded node is then reduced as eqn (13) so that the additional moment over the plastic capacity can be redistributed to the elastic spring of another node. For this case, $M_{c1} = M_p$ and $S_2 \to \infty$, the spring stiffness about first yielded node is given as,

$$S_1 = \frac{K_{11}M_p}{K_{11}\theta_1 + K_{12}\theta_2 - M_p} \tag{13}$$

Similarly, the spring stiffness of the second node for the first yielded moment can be expressed as eqn (14) with elastic moment at the first node. For this case, the similar conditions are $M_{c2} = M_p$ and $S_1 \to \infty$ similarly.

$$S_2 = \frac{K_{22} M_p}{K_{21}\theta_1 + K_{22}\theta_2 - M_p} \qquad (14)$$

When two nodes of the element are also yielded, the additional moments over the plastic moment capacity redistributed to other members through the equilibrium equation of the whole structure. And the moments about the yielded nodes of the element are assigned to be plastic moment capacity, M_p.

5. Illustration of solution for fire conditions

The adapted nonlinear solution procedure incorporating allowance for the effects of thermal expansion and thermal bowing is illustrated in Fig. 3 and Fig. 4 for both unrestrained and restrained cases, respectively. The restraining effect is important in fire analysis, while the additional thermal forces can be developed in the restrained case so as to cause the geometric nonlinear effects at elevated temperature.

In the case of simply supported beam, thermal axial strains and thermal curvature are added as compressive mechanical strains during non-uniform heating. The unbalanced forces at unrestrained support degrees-of-freedom are obtained due to thermal expansion and rotation. These unbalanced forces at the support degrees-of-freedom cause the incremental displacements according to equilibrium equation. It is summarized in the Fig. 1.

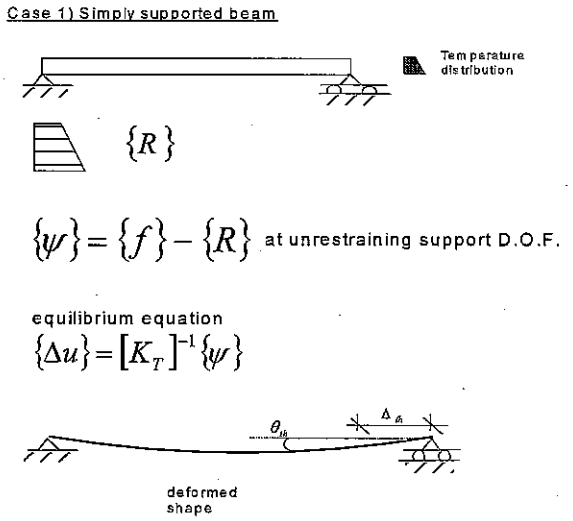

Fig 1: Thermal effects in simply supported beam

Second case of fixed ended beam, the axial expansion and rotation is not permitted at the restrained support. The member reactions at the restrained support degrees-of-freedom are similarly induced due to thermal axial force and moment, when member reactions at the corresponding degree-of-freedoms do not balance. Therefore, these member reactions convert into member forces, which weaken the tangent stiffness of the beam and cause the second order bowing effect. Consequently, the larger deformations except at the supports are resulted in. It is also demonstrated and summarized on Fig. 2.

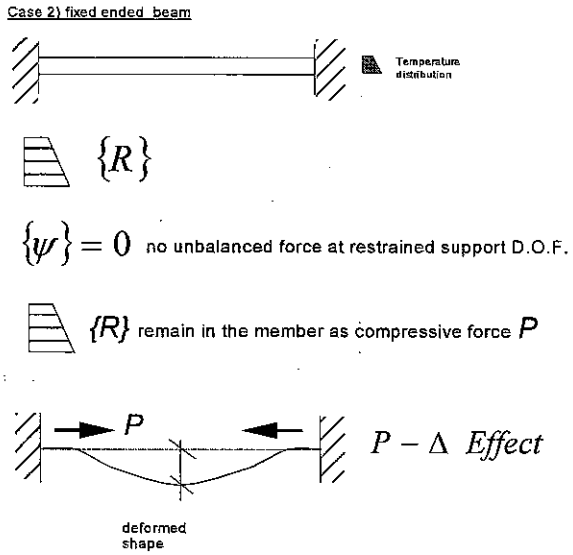

Fig 2: Thermal effects in fixed ended beam

6. Numerical verification

For verification of the present fire analysis, the nonlinear finite element program, GMNAF [3], is modified to incorporate the thermal effect for different structures. Both uniform and non-uniform temperature distribution over the member section are also considered in this fire analysis. Thus the verifications of different cases are carried out in this section.

6.1. Theoretical examples

The proposed fire analysis is compared with the theoretical hand calculations based on simple elasticity theory, so all these numerical simulations exclude material nonlinearity. There are four simulated members used in this theoretical verification including a cantilever beam, two simply supported beams subjected to uniform and non-uniform heating. And the elastic modulus is 210kN/mm ^{2} and section properties is according to IPE80. These examples selected is exclusive material and geometric nonlinearity. They are all consistent with the theory and shown on the corresponding Figs. 3, 4 & 5.

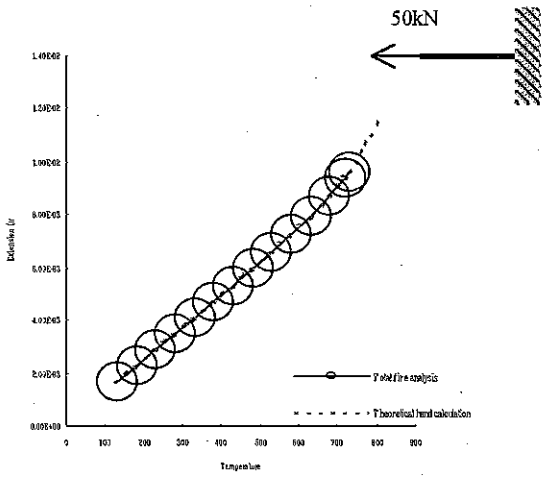

Fig. 3: Tip extension between theory and fire analysis

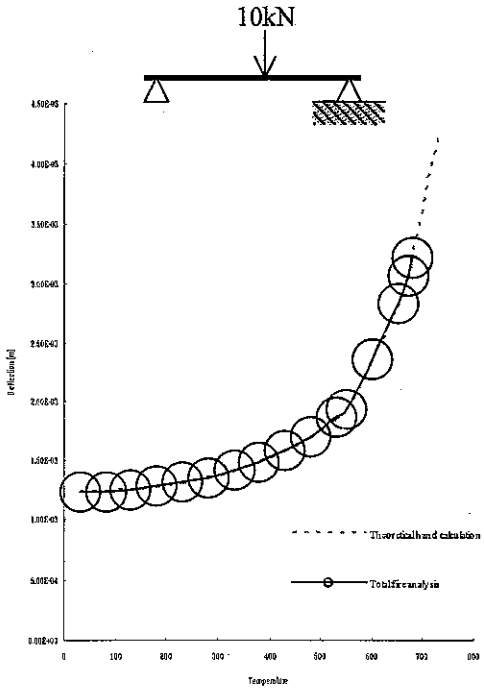

Fig. 4: Mid-span deflection between theory and fire analysis under uniform temperature distribution

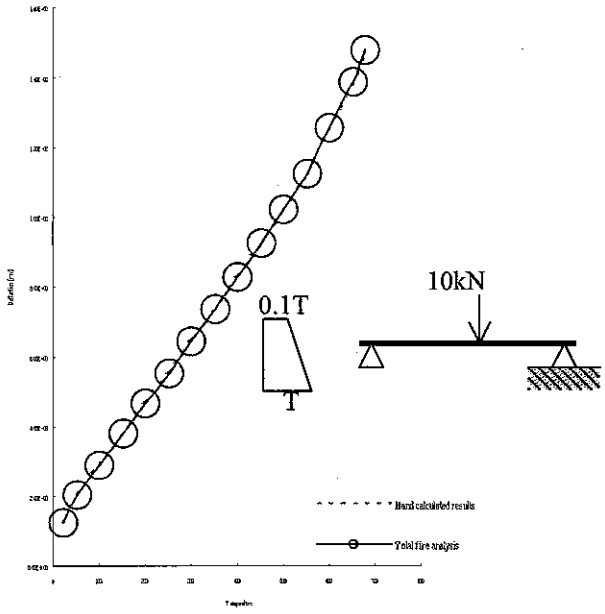

Fig. 5: Mid-span deflection between theory and fire analysis under non-uniform temperature distribution

6.2. Axially unrestrained steel column tests

A number of steel columns were comprehensively tested by Aasen (1985) [1]. The same reference numbers for the columns as those used by Aasen have also been adopted in this paper. However, the axially unrestrained steel columns are only considered for verification of second order effect in this fire analysis. The numerical results of these column tests conducted by Poh and Bennetts (1995) [9] are also included in this verification. All the steel columns are discretized into 20 elements in this fire study.

All of these input data and the average measured temperatures along the half-length of each column over the test period are according to reference [1]. The temperatures are assumed to be uniform over the cross section. The temperature-stress-strain relationships for steel material recommended by ECCS were used for this numerical analysis.

The selected columns No. 2, 5, 6 & 14 are compared with the test results and numerical results of [9]. The lateral deflections are all in good agreement with both test and numerical results, which are shown on Figs. 6 to 9.

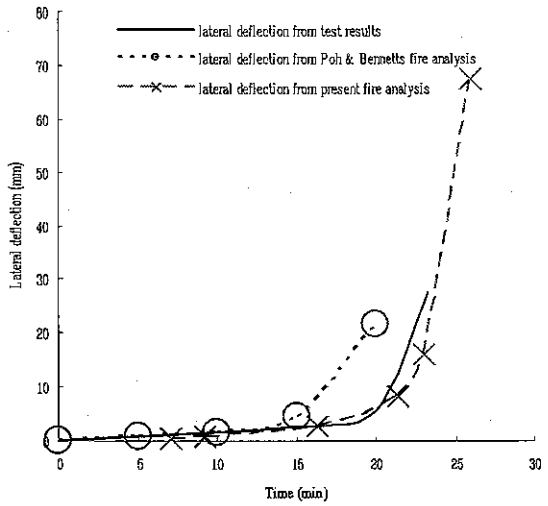

Fig: 6 Lateral deflection at mid-span for column No. 2

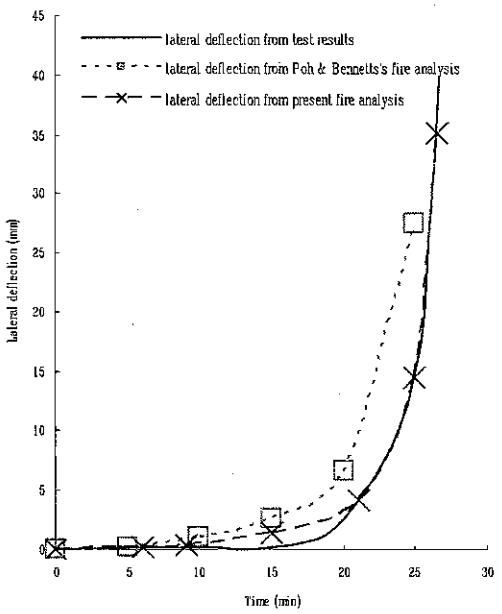

Fig. 7 Mid-span deflection for column No. 5

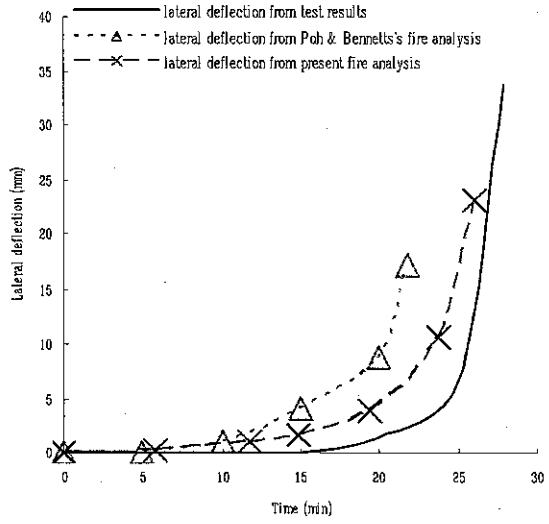

Fig. 8 Mid-span deflection for column No. 6

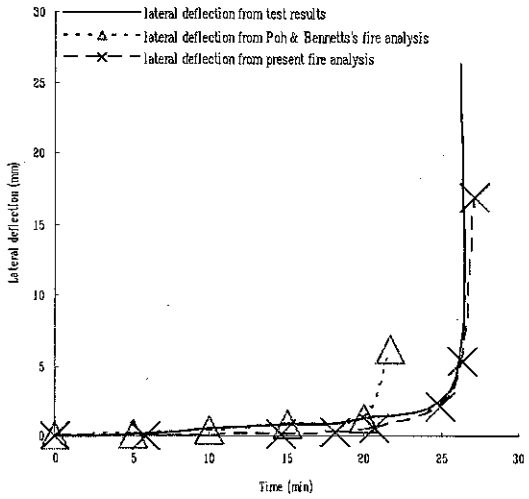

Fig. 9 Mid-span deflection for column No. 14

7. Conclusions

The proposed fire analysis based on the second-order inelastic analysis at ambient conditions extends to study the structural behaviour of steel members at elevated temperature. The increment-iterative Newton-Raphson method is utilized to simulate the geometric nonlinearity basing on total formulation in which the thermal-time dependence is based. And the material yielding is modeled by the plastic hinges at both ends of an element with the elasto-plastic spring stiffness. The loading redistributing effect is included in this spring stiffness, when one node of the member is yielded.

From the numerical examples, the proposed fire analysis is successfully verified to include thermal effects, such as material deterioration, thermal expansion and bowing, under fire conditions of both uniform and non-uniform temperature distribution. From the experimental examples, geometric nonlinear effect is also accurately incorporated in this fire numerical simulation. Since the thermal effects and second-order inelastic behaviour is successfully incorporated, this analysis therefore efficiently models these different structural behaviour of steel bridge under fire due to traffic accident.

On the basis of plastic hinge method, this fire analysis has a good convergent rate and requires less computational time so as to suit to the use in the practical fire design for steel bridge structure. In addition, this analysis is costless and reliable to assess the structural health of steel bridge at fire condition against the thermal history.

References

[1]. *Aasen, B. (1985), "An experimental study on steel column behaviour at elevated temperatures", Research report, Division of steel structures, University of Trondheim, Norwegian institute of technology, Norway.*

[2]. *Chan, S.L. GMNAF (1993), "Geometric and material nonlinear analysis of frames, program manual".*

[3]. *Chan, S.L. and Chui, P.P.T. (1997), "A generalized design-based elastoplastic analysis of steel frames by section assemblage concept", Engineering structures, Vol. 19(8), pp 628-636.*

[4]. *EI-Zanaty, M.H. and Murray, D.W. (1983), "Nonlinear finite element analysis of steel frames", Journal of structural division, ASCE, Vol. 109(ST2), pp.353-368.*

[5]. *ECCS (1985) European recommendations for the fire safety of steel structures: Technical committee 3 – Fire safety of steel structures.*

[6]. *Franssen, J.M. (1987), "Etude du comportement au feu des structures mixtes acier-beton (CEFICOSS), A study of the behaviour of composite steel-concrete structures in fire", These de Doctorat, Universite de Liege, Belgique.*

[7]. *Franssen, J.M., Kodur, V.K.R. and Mason, J. (2000), "User's manual for SAFIR: a computer program for analysis of structures submitted to fire", Internal Report SPEC/2000_03, 2000, University of Liege, Ponts et Charpentes, Belgium.*

[8]. *Najjar, S.R. and Burgess, I.W. (1996), "A nonlinear analysis for three-dimensional steel frames in fire conditions", Engineering structures, Vol.18(1), pp 77-89.*

[9]. *Poh, K.W. and Bennetts, I.D. (1995), "Behaviour of steel columns at elevated temperature", Journal of structural division, ASCE(ST4), Vol. 121, pp.676-684.*

[10]. *Saab, H.A. and Nethercot, D.A. (1991), "Modelling steel frame behaviour under fire conditions", Engineering structures, Vol. 13, pp 371-382.*

[11]. *Schleich, J.B., Dotreppe, J.C. and Franssen, J.M. (1986), "Numerical simulations of fire resistance tests on steel and composite structural elements or frames", Fire safety science: Proceedings of the first international symposium, pp 311-323.*

[12]. *Wang, Y.C. and Moore, D.B. (1995), "Steel frames in fire: analysis", Engineering structures, Vol. 17, No. 6, pp.462-472.*

[13]. *Yau, C.Y. and Chan, S.L. (1994), "Inelastic and stability analysis of flexibly connected steel frames by spring-in-series model", Journal of structural division, ASCE, Vol. 120(ST10), pp.2803-2819.*

Vibration Analysis of the Second Saikai Bridge

-A Concrete Filled Tubular (CFT) Arch Bridge-

Qingxiong Wu*, Mitsuhiro Yoshimura**, Kazuo Takahashi***, Shozo Nakamura****,
Hiroyuki Fujita***** and Kazuyoshi Furukawa******

* Ph.D., Res. Assoc., Dept. of Civil Eng., Nagasaki University, 1-14, Bunkyo-machi, Nagasaki 852-8521
** M. Eng., Nagasaki Shipyard&Machinery Works, Mitsubishi Heavy Industries, LTD., 180, Koyagi-cho, Nagasaki 850-8610
*** Dr. of Eng., Prof., Dept. of Civil Eng, Nagasaki University, 1-14, Bunkyo-machi, Nagasaki 852-8521
**** Dr. of Eng., Assoc. Prof., Dept. of Civil Eng, Nagasaki University, 1-14, Bunkyo-machi, Nagasaki 852-8521
***** Bachelor, Graduate School of Science and Technology, Nagasaki University, 1-14, Bunkyo-machi, Nagasaki 852-8521
****** Bachelor, Civil Engineering Information Office, Public Works Department, Nagasaki Prefectural Government, 2-13, Edo-machi, Nagasaki 850-8570

Concrete-filled steel tubular (CFT) arch bridges have been rapidly developing in China since 1990. Research has focused on the static behavior, thermal stress and erection technique, however, and there has been very little research of natural vibrations and dynamic responses of these bridges. Japan's first CFT arch bridge, the Second Saikai Bridge, is now under construction in Nagasaki Prefecture. This paper describes the natural vibrations and dynamic responses of this bridge that are produced by a moving vehicle and pedestrians, and compares them to those of CFT arch bridges in China. The Second Saikai Bridge has a footbridge that is rare. This paper describes the interaction between the main bridge and the footbridge and the dynamic response characteristics of this footbridge.

Key Words: Concrete filled steel tube, arch bridge, footbridge, dynamic response analysis, Second Saikai Bridge

1. Introduction

In arch bridges, it may be practical to use concrete filled steel tubes (CFT) for the arch ribs in which the compression axial force is predominant. The infilled concrete delays local buckling of the steel tube, and the steel tube reinforces the concrete against tension, bending moment, and shear force. The tube also serves as a formwork for the concrete during construction of the bridge, thus saving a major construction cost[1),2)]. Moreover, the composite structural action between the infilled concrete and the steel tube improves the member's load-carrying capacity. As a result of these advantages, CFT construction for bridges has become widespread in recent decades[3),4)]. More than one hundred CFT arch bridges have been constructed since 1990[5), 6), 7)] in China, and a CFT arch bridge with the span length of over 400m is now being constructed[8)]. The Second Saikai Bridge, the first CFT arch bridge in Japan, is under construction in Nagasaki Prefecture.

Research into CFT arch bridges has focused on the static behavior, thermal stress and erection technique[7)]. However, there has been very little research into vibrations and seismic responses of CFT arch bridges. The dynamic properties of CFT arch bridges have not been examined in detail. Therefore, it is necessary to evaluate the characteristics of the natural vibration, the dynamic response under traffic loading and the nonlinear seismic response of the actual Second Saikai Bridge. This paper focuses on the in-plane vibrations and discusses the properties of the natural vibration and the traffic-induced vibration. The nonlinear seismic analysis of this bridge will be discussed in a separate paper[9)].

This bridge has a footbridge under the girder. The footbridge allows pedestrians to cross the Second Saikai Bridge and visit a nearby public park. There is no other example in Japan of a highway bridge with such a structure suspended under the girder so it is necessary to understand the dynamic response characteristics of the footbridge. In particular, the response levels

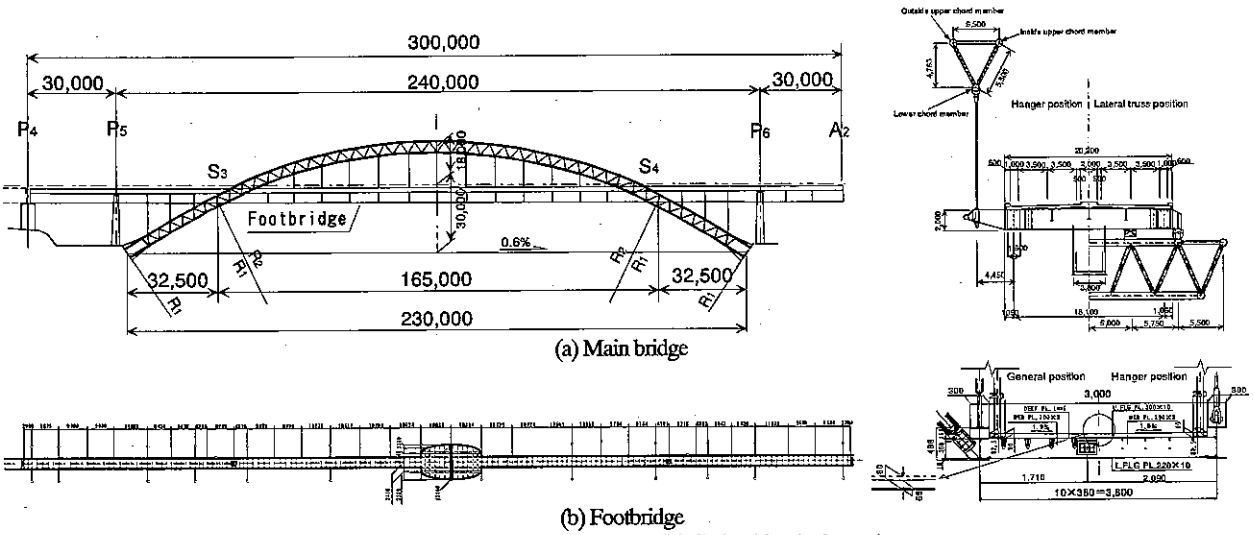

(a) Main bridge

(b) Footbridge

Figure 1 General view of the Second Saikai Bridge (unit: mm)

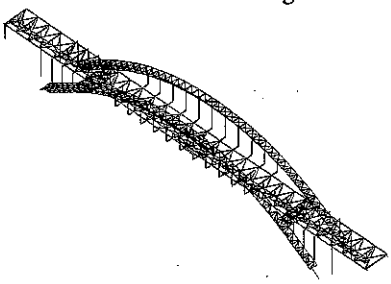

Figure 2 Integrated bridge model

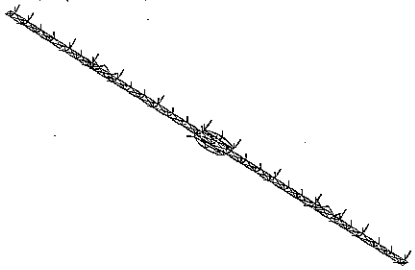

Figure 3 Separate footbridge model

of the footbridge when a vehicle passes over the girder or when a pedestrian walks on the footbridge must be understood.

In this paper, the in-plane natural vibration properties of the bridge and the footbridge are examined, and the influence of the footbridge structure on the natural vibration of the bridge is discussed first. A response analysis induced by a moving vehicle is carried out, and the response characteristics of the bridge and the footbridge are clarified. The natural vibrations and responses are compared to those of CFT arch bridges that have been constructed in China. Finally, the response induced by a pedestrian walking on the footbridge is evaluated.

2. A Brief Description of the Second Saikai Bridge

The Second Saikai Bridge (tentative name) is a highway bridge on the Nishisonogi Region Expressway. The bridge crosses the Harioseto channel, connecting the Sasebo urban area and the Nagasaki urban area. The bridge is scheduled to be completed in 2003. As shown in Figure 1(a), the main span is 240m in length and the side spans are 30m in length. The bridge is 20.2m in width. The landscape of the site, the need to harmonize the design with that of the present Saikai Bridge (a deck type steel arch bridge with a span of 216m, completed in 1955) and the need to reduce the bridge's construction costs together lead the selection of the half-though braced-rib CFT arch bridge design for the main span. The bridge has two parallel arch ribs, each of which has a triangular cross-section consisting of three steel tubes. High fluidity concrete fills the three steel tubes. The three steel tubes have an outer diameter of 812.8mm and a thickness that differs depending upon the position of the arch rib. The deck system consists of I-beams arranged longitudinally, upon which a concrete slab is placed.

There is a footbridge under the bridge that allows pedestrians to cross the Second Saikai Bridge and visit the public park. This footbridge is 293.225m long and 3m wide. The footbridge itself has a girder made of two H-beam steel plates. This girder hangs by strand rope and steel tube from the lateral beams of the bridge. A general view of the footbridge is shown in Figure 1(b). The center of the footbridge has been widened to allow visitors to enjoy the view from the Second Saikai Bridge.

3. Analytical Model

3.1 Integrated bridge model

Figure 2 shows a model of the integrated bridge. This model takes into account the rigidity and mass of the footbridge. The arch rib, stiffening girder, lateral bracing, and pier are all modeled using three-dimensional beam elements based on actual cross-sectional properties. The column and hanger are modeled using three-dimensional truss elements. The lump mass matrix is adopted for this analysis.

On the footbridge, the girder and lateral beams of the footbridge are modeled using three-dimensional beam elements. The strand ropes and steel tubes are modeled using three-dimensional truss elements. The girder of the footbridge takes into account the stiffness of the floor system of footbridge.

Regarding boundary conditions, the springing position of the arch rib and the pier bases are fixed in all degrees of freedom. The earthquake shear force distribution rubber bearings are installed in the joints between the stiffening girder and the piers (P_4, P_5 and P_6), the joints between the stiffening girder and abutment A_2, and the joints between the stiffening girder and the lateral beams (S_3 and S_4). The model uses linear springs to simulate these bearings. The points linking the suspension members of the footbridge and the stiffening girder of the bridge have the same longitudinal, vertical and out-of-plane displacements as the stiffness girder of the main bridge. The vertical displacements in the origin points and the end points of the footbridge are restrained, as are the out-of-plane displacements in the lateral bracing of the footbridge.

3.2 Separate footbridge model

In order to examine the influence of the footbridge on the natural vibrations of the bridge, the original bridge model and a separate footbridge model are used in addition to the integrated bridge model.

In the original model of the bridge, the rigidities of the footbridge are not taken into account, and the masses of the footbridge are included with those of the girder. This original bridge model is adopted for the nonlinear seismic analysis of the main bridge.

The separate footbridge model is shown in Figure 3. In this model, only the footbridge's structure is considered. Regarding the boundary condition of the footbridge model, the points that link the hangers of the footbridge and the stiffening girder of the bridge are fixed in the longitudinal, vertical and out-of-plane degrees of freedom.

4. Natural Vibration Characteristics

The natural vibration analysis is carried out using the integrated bridge model, and the natural vibration characteristics are examined. In this paper, the natural vibrations of the bridge except for the local oscillation of the footbridge are called the *'natural vibrations of the main bridge'*, and the local natural vibrations of the footbridge are called the *'natural vibrations of the footbridge'*.

4.1 Natural vibration characteristics of main bridge

The natural frequencies and modal shapes of the in-plane natural vibrations of the main bridge are shown in Table 1.

The first in-plane natural vibration, which has a frequency of 0.472Hz, corresponds to the floating mode, as it does with cable-stayed bridges. This is due to the rubber bearings installed in the longitudinal direction of the bridge that distribute earthquake shear forces. The second in-plane natural vibration has a frequency of 0.639 Hz, which corresponds to the unique antisymmetric mode of arch bridges.

Furthermore, there are in-plane natural vibration modes in which the vibrations of the side spans are predominant. They have natural frequencies of 2.553Hz (the 13th mode) and 2.644Hz (the 15th mode).

Table 1 In-plane natural vibrations of the main bridge

No.	Freq.(Hz)	Modal shape
1	0.472	
2	0.639	
3	0.929	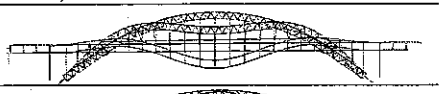
4	1.474	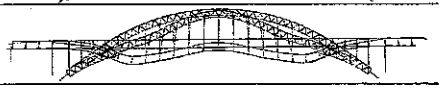
5	1.509	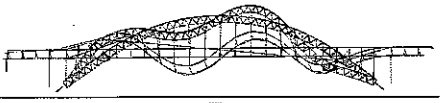
6	1.948	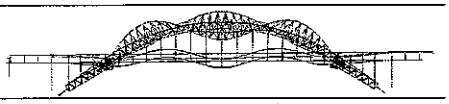
7	2.025	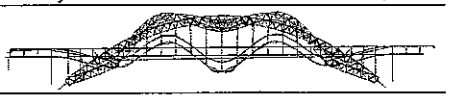
12	2.512	
13	2.553	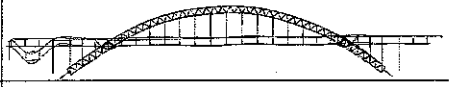
14	2.631	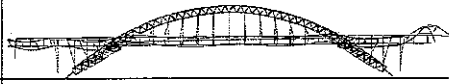
15	2.644	
18	2.856	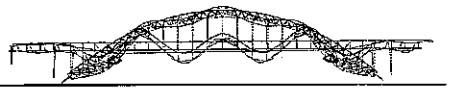
19	2.909	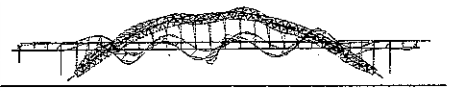
20	2.979	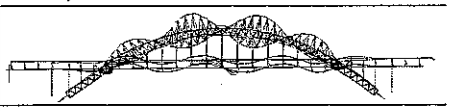
24	3.285	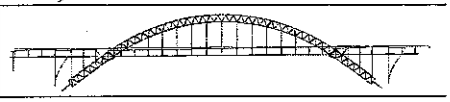

4.2 Natural vibration characteristics of footbridge

Table 2(a) shows in-plane natural vibrations of the footbridge using the integrated bridge model. The lowest in-plane natural frequency of the footbridge natural vibration is 2.276Hz, which is much higher than the lowest in-plane natural frequency of the natural vibration of the main bridge.

4.3 Influence of natural vibrations of footbridge on natural vibrations of main bridge

The weight of the footbridge on the Second Saikai Bridge is 8% of the steel weight of the integrated bridge. Therefore, in the model of the integrated bridge, the original bridge and the

Table 2 In-plane natural vibrations of the footbridge

(a) Integrated bridge model			(b) Separate footbridge model		
No.	Freq. (Hz)	Modal shape	No.	Freq. (Hz)	Modal shape
8	2.276		1	2.276	
9	2.285		2	2.285	
10	2.367		3	2.367	
11	2.383		4	2.383	
16	2.716		5	2.716	
17	2.733		6	2.733	
21	3.017		7	3.017	
22	3.147		8	3.147	

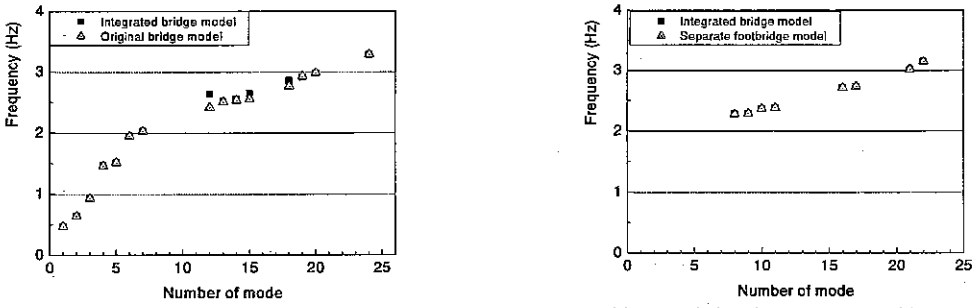

(a) Natural vibrations of the main bridge (b) Natural vibrations of the footbridge

Figure 4 In-plane natural frequencies

Table 3 Natural frequencies of CFT arch bridges and steel arch bridge

Bridge name	Span (m)	Type	Natural frequencies of in-plane modes (Hz)			
			1st antisymmetric	1st symmetric	2nd antisymmetric	2nd symmetric
Second Saikai Bridge	230	CFT	0.639	0.929	1.509	1.474
Jianghan Wuqiao Bridge [10]	240	CFT	0.724	1.229	1.878	2.041
Saikai Bridge [11]	216	Steel	1.153	1.507	2.805	2.306

footbridge are treated as a monolithic structure. However, the original bridge is used for the seismic analysis of the main bridge[9] and the separate footbridge model is used for the natural vibration analysis of the footbridge itself. In other words, it is assumed that the effect of the rigidity of the footbridge on the vibration of the main bridge is negligible. The influence of the natural vibrations of the footbridge on the natural vibrations of the integrated bridge is considered using the integrated bridge, original bridge, and independent footbridge models in order to analyze the validity of the assumption.

The in-plane natural frequencies of the main bridge vibrations using the integrated bridge model and the original bridge model are plotted in Figure 4(a). There are some differences in the natural modes near the natural frequency of 2.5Hz-2.8Hz, though the results using the original bridge model coincide with those using the whole bridge model. The vertical displacements in the origin points and the end points of the footbridge in the integrated bridge model are restrained, but these boundary conditions are not applied to the original bridge model. In other words, the differences in the natural frequencies are due to the different boundary conditions. The natural frequency of the original bridge model is about 8% lower than that of the integrated bridge model. Therefore, the influence of the natural vibrations of the footbridge on the natural vibration of the main bridge is small.

Figure 4(b) and Table 2 show the natural vibrations of the footbridge for the integrated bridge model and for the separate footbridge model. The natural frequencies of the separate footbridge model agree well with those for the integrated bridge model. Therefore, the effect of the rigidity of the footbridge on the vibration of the main bridge is negligible. Moreover, the natural vibrations of the footbridge can be evaluated using the separate footbridge model.

However, when a moving vehicle passes by the girder of the main bridge, the dynamic analysis of the footbridge must use the integrated bridge model.

4.4 Comparison of CFT arch bridges and steel arch bridges

The Jianghan Wuqiao Bridge (240m, CFT, China)[10] and the Saikai Bridge (216m, steel, Japan)[11], which have almost the same span length as the Second Saikai Bridge, are used to compare the natural vibration properties of CFT arch bridges with those of steel arch bridges. The in-plane natural frequencies of those three bridges are summarized in Table 3. It is known that the in-plane natural frequencies of CFT arch bridges are lower than those of the steel arch bridge.

5. Response Characteristics Under a Moving Vehicle

In this section, the vibrations of the Second Saikai Bridge under traffic loading are examined using the bridge–vehicle–road surface model[12]. The vehicle in the present analysis is a single-degree-of-freedom system that has a mass of 250 kN, a frequency of 3Hz and a damping constant of 0.03. The power spectral density of the road surface roughness is determined using Ref. 12). The response of the bridge under a moving vehicle is obtained using the Runge–Kutta method.

5.1 Response characteristics of girder

Figure 5 shows the maximum accelerations of the girder and arch rib when a vehicle passes by the girder of the main bridge at a speed of 80km/h. The vertical axis corresponds to the maximum acceleration and the horizontal axis corresponds to the coordinate in the longitudinal direction.

The maximum acceleration of the girder of the main span is observed at the point between pier P_6 and pier P_5, whose maximum acceleration is about 35gal.

There is an investigation for the response level of a CFT arch bridge built in China[13]. The Shitanxi Bridge is a half-through CFT arch with a span length of 136m. The bridge has two parallel arch ribs, each of which has a rectangular cross-section consisting of four steel tubes. The response level of this bridge under the vehicle loading is investigated in 2000. The maximum acceleration of the girder in the Shitanxi Bridge is about 50-100gal.

Comparing the maximum acceleration of the Second Saikai Bridge with that of the Shitanxi Bridge, the vibration level in the girder of the main span of the Second Saikai Bridge under traffic loading is smaller than that of the Shitanxi Bridge.

The maximum acceleration in the arch rib of the Second Saikai Bridge is about 33gal as shown in Figure 5(b), while that of the Shitanxi Bridge is about 50-80gal[13]. Therefore, the vibration level in the arch rib of the Second Saikai Bridge is smaller than that of the Shitanxi Bridge.

However, a vibration with a maximum acceleration of 70gal is generated in the side spans, which have a span length of 30m. Time histories of displacement and acceleration at the center point (N1004) of the side span are shown in Figure 6. When a vehicle passes by the center point of the side span (t=0.59 sec), the displacement and acceleration of the center point N1004 of

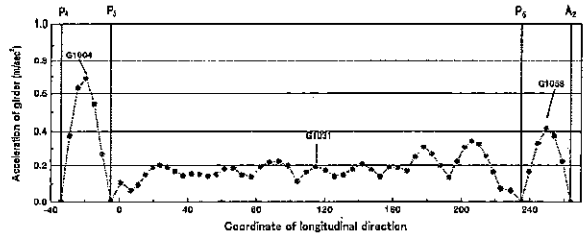

(a) Girder

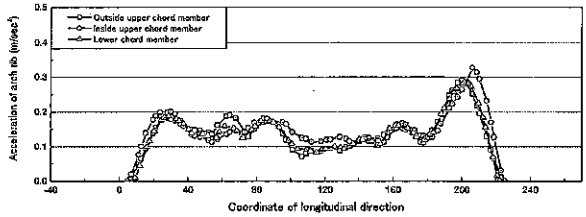

(b) Arch rib

Figure 5 Maximum accelerations under moving vehicle

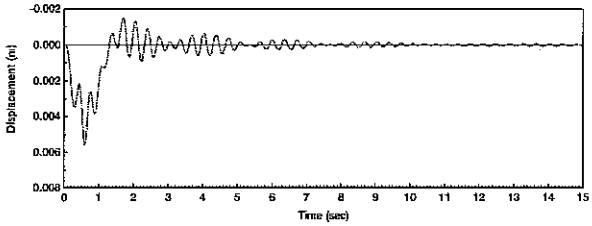

(a) Displacement

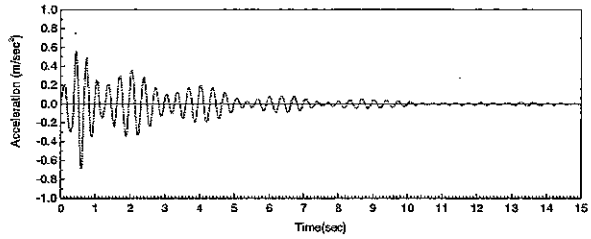

(b) Acceleration

Figure 6 Time histories at the center point of side span (N1004)

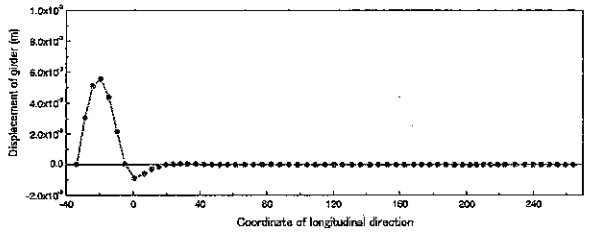

Figure 7 Displacement of the girder at t=0.59sec

the side span is largest. The displacement of the girder at t=0.59sec is shown in Figure 7. The girder in the main span generates small displacements even if the displacement of the side span is predominant. In other words, the vibration of the side span is local, and an in-plane natural vibration in which the vibration of the side span with natural frequency of 2.553Hz is predominant (the 13th mode in Table 1) is induced. The dynamic response of the side span between pier P_6 and abutment A_2 is large, since an in-plane natural vibration mode with a natural frequency of 2.644Hz (the 15th mode in Table 1) is induced. In other words, the response of the side span is large due to the correspondence of the in-plane natural frequency of the side spans and the natural frequency of the vehicle.

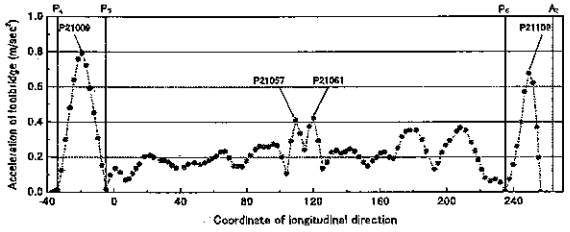

Figure 8 Maximum accelerations of footbridge under moving vehicle

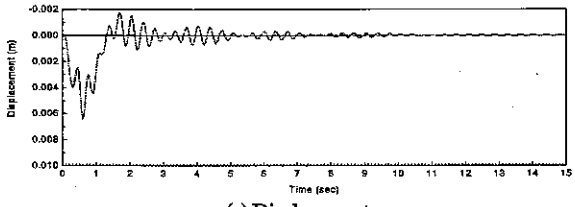

(a) Displacement

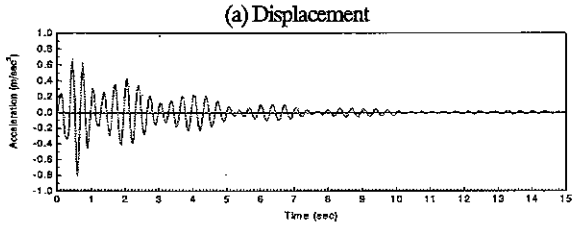

(b) Acceleration

Figure 9 Time histories of point (P21009) in the footbridge

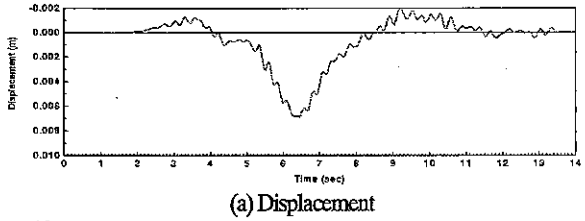

(a) Displacement

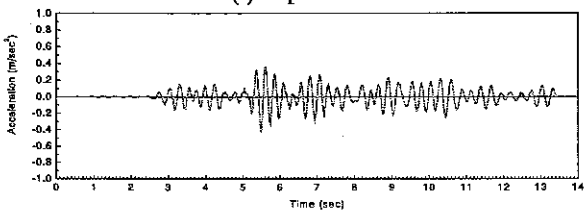

(b) Acceleration

Figure 10 Time histories of point P21057 in the footbridge

5.2 Response characteristics of footbridge

Figure 8 shows the maximum accelerations of the footbridge when a vehicle passes by the girder of the main bridge at a speed of 80km/h. Figure 9 shows the time histories for center point P21009 of the side span. The maximum acceleration of the main span is about 40gal and that of side spans is about 80gal, which are the same values as those of the girder of the main bridge.

However, unlike the girder of the main bridge, the maximum accelerations of points P21057 and P21061 at the center position of the footbridge are large. This is because the footbridge is wider at the center.

5.3 Response level

The ergonomic evaluation method developed by Kobori and Kajikawa[14] is used to appraise the vibration sensibility of the traffic-induced vibration on the Second Saikai Bridge. The vibration stimulation S(cm/sec) is calculated using the effective value of the maximum velocity V_{max} (cm/sec). It is described by the following equation.

Table 4 Category and lower limit of VG for pedestrian

No.	Content of category	VG
1	Slightly perceptible	0.32
2	Definitely perceptible	0.61
3	Lightly hard to walk	1.12
4	Extremely hard to walk	1.48

$$S = V_{\max} / \sqrt{2} \quad . \tag{1}$$

The vibration greatness level VGL(dB) is shown as described by the following equation.

$$VGL = 20\log_{10}(S / S_0) \quad (S_0 = 1.4\times10^{-2} \text{ cm/sec}). \tag{2}$$

The vibration greatness VG can then be obtained from the following equation.

$$\log_{10} VG = 0.05(VGL - 40) \text{ when } VGL \le 40dB \ ,$$
$$\log_{10} VG = 0.03(VGL - 40) \text{ when } VGL > 40dB \ . \tag{3}$$

The relationship between the category and the lower limit of the VG for pedestrians is shown in Table 4.

Regarding the main span, both the maximum velocity of the girder and that of the footbridge are about 0.020m/sec, which is equal to VG=1.00. From the viewpoint of vibration sensation, its VG is in the category of '*definitely perceptible*', and the vibration of the main span under traffic loading is small.

In the side spans, the maximum velocity of the girder of the main bridge and that of the footbridge are about 0.033m/sec and 0.036m/sec, which are equal to VG=1.37 and VG=1.43, respectively. These VG are in the category of '*lightly hard to walk*'. Therefore, the examination should take into account the vibration dampers in the side spans.

6. Response Characteristics Under Pedestrian Traffic

The lowest natural frequency of the footbridge is 2.276Hz. This is close to 2.0 steps/sec, which is the pace of an adult walking down a street[15]. There is some apprehension about the resonance induced by a pedestrian walking on the footbridge when the predominant frequency of the footbridge is near the pace of the pedestrian. Therefore, the dynamic response characteristics of the footbridge induced by pedestrian traffic are examined.

6.1 Analysis of vibrations induced by pedestrian

The following walking load, which takes into account the dead load of a pedestrian[15),16)], is used to examine the dynamic response characteristics that are induced by a pedestrian walking on the footbridge.

$$F(t) = W(1 + \alpha \cos \omega t) \ , \tag{5}$$

where W is the weight of the pedestrian (set to 0.588kN (60kgf) in this paper), $\omega = 2\pi f$ is the circular frequency of the pace, α is the ratio of the impulsive force according to the pace as described in Ref. 15).

The modal analysis method is used for dynamic response analysis and the Runge-Kutta method is used for numerical integration. The natural modes to the frequency of 4.28Hz are

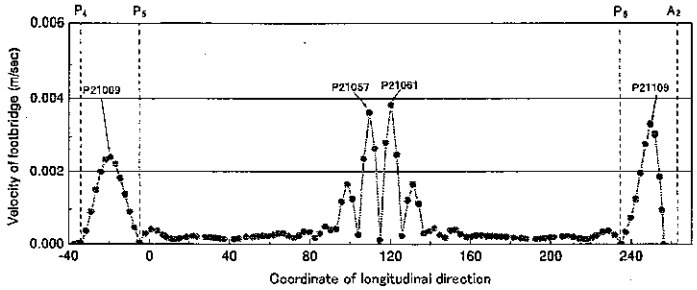

Figure 11 Maximum velocity of the footbridge in the pace of 2.55steps/sec

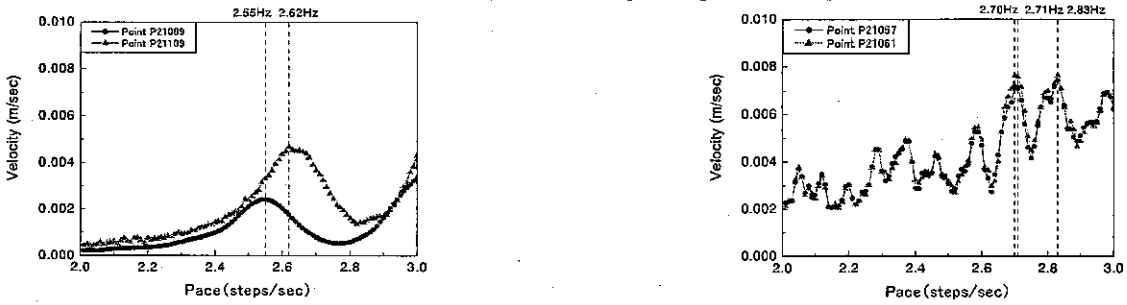

(a) Center point of side spans (b) Wide part

Figure 12 Relationship between the velocity and the pace of pedestrian

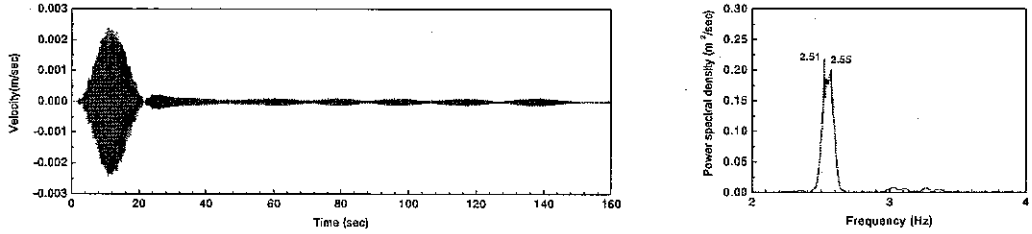

Figure 13 Time history of velocity and power spectrum of P21009 in the pace of 2.55steps/sec

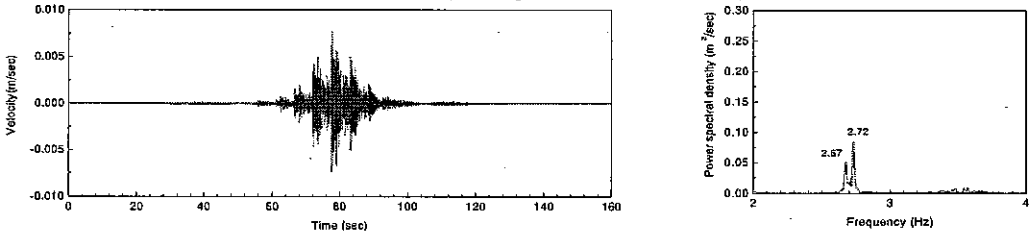

Figure 14 Time history of velocity and power spectrum of P21061 in the pace of 2.70steps/sec

adopted, and the damping constant of each mode is set to 0.02. The initial condition is that the footbridge is stationary before the pedestrian begins walking on it.

6.2 Response characteristics of footbridge

The maximum velocities of the footbridge at the pace of 2.55 steps/sec are shown in Figure 11. Among all the points shown, the largest velocities are generated at center point P21009 of the side span between pier P_4 and pier P_5, at center point P21109 of the side span between pier P_6 and abutment A_2, and at points P21057 and P21061 in the wide part of the main span.

The relationship between the pace of a walking pedestrian and the velocity at those four points is shown in Figure 12.

Regarding point P21009, shown in Figure 12(a), the peak of maximum velocity appears near 2.55steps/sec. Figure 13 shows the time history of the velocity and the power spectrum at this pace. The power spectrum indicates that the frequencies of 2.51Hz and 2.55Hz are predominant. 2.51Hz corresponds to the natural frequency of the 12th vibration mode of the main bridge (see Table 1), and 2.55Hz corresponds to the natural frequency of the 13th vibration mode of the main bridge (see Table 1) and the frequency of the pedestrian's pace. In other words, a pace of 2.55 steps/sec induces vibrations at the frequencies of the 12th and 13th modes of the main bridge.

The peaks of the maximum velocities of points P21057 and P21061 in the main span appear near 2.70steps/sec, 2.71steps/sec and 2.83steps/sec, as shown in Figure 12(b). In the response spectrum shown in Figure 14, the frequencies of 2.72Hz and 2.67Hz are predominant. The frequency of 2.72Hz corresponds to the natural frequency of the 16th mode of the footbridge (see Table 2), and the frequency of 2.67Hz corresponds to that of the pedestrian's pace. So vibrations at the frequencies of the 16th mode of the footbridge are induced at a pace of 2.70steps/sec.

Regarding the response level induced by a pedestrian walking on the footbridge, the maximum velocity of the footbridge induced by a walking pedestrian is less than 0.008m/sec (*VG*=0.39), which is in the category of *'Slightly perceptible'*. Therefore, the responses induced by a pedestrian walking on the footbridge are small.

7. Conclusions

This paper examined the natural vibrations, vehicle-induced vibrations and pedestrian-induced vibrations of the Second Saikai Bridge, which is the first CFT arch bridge in Japan. The main findings are as follows:

(1) The floating mode and the unique antisymmetric mode of the arch bridge are the first two in-plane vibrations of the main bridge, and the first natural frequency of the footbridge is higher than the lower frequencies of the main bridge.

(2) The influence of the rigidity of the footbridge on the main bridge is small. The independent footbridge model can be used to evaluate the natural vibrations of the footbridge, since the natural frequencies the footbridge are separate from those of the main bridge.

(3) The vehicle-induced responses of the main span are small, while the responses in the side spans are larger than those of the main span. The maximum acceleration of the side span is about 80gal.

(4) The dynamic response induced by a pedestrian walking on the footbridge increases when the predominant frequencies of the footbridge are close to the pace of the pedestrian. However, the response level of the footbridge is small.

Acknowledgements

The authors wish to express their gratitude to Nagasaki Prefectural Government and Chodai Co. Ltd. for providing the materials used in this study.

References

1) Roeder, C.W., Cameron, B. and Brown, C.B., Composite action in concrete filled tubes, *Journal of Structural Engineering*, ASCE, Vol.125, No.5, pp.477-484, 1999
2) Varma, A.H., Ricles, J.M., Sause, R., and Lu, L.W., Experimental behavior of high strength square concrete-filled steel tube beam-columns, *Journal of Structural Engineering*, ASCE, Vol.128, No.3, pp.309-318, 2002
3) Clawson, W.C., Bridge Applications of Composite Construction in the U.S., *Structural Engineering in the 21st Century, Proceedings of the 1999 Structures Congress*, pp.544-547, 1999.4
4) Nakamura, S., New structural forms for steel/concrete composite bridges, *Structural Engineering International* 1, *Journal of the International Association for Bridge and Structural Engineering (IABSE)*, pp.45-50, 2000
5) Zhen, Z., Chen, B. and Wu, Q., Recent development of CFST arch bridge in China, *Proceeding of 6th ASCCS Conference*, pp.205-212, 2000.3
6) Liu, Y., Chen, B. and Hikosaka, H., Recent developments in concrete-filled tubular arch bridge and horizontal swing erection method in China, *Bridge and Foundation Engineering*, Vol.33, No.2, pp.41-44, 1999.2 (in Japanese)
7) Wu, Q., Chen, B., Takahashi, K. and Nakamura, S., Construction and technical subjects of concrete filled steel tubular arch bridges in China, *Bridge and Foundation Engineering*, Vol.35, No.10, pp.40-45, 2001.10 (in Japanese)
8) Peng, D., Wu, Q., Takahashi, K., and Nakamura, S., Recent construction and development of long-span bridges in China, *Bridge and Foundation Engineering*, Vol.37, No.2, pp.43-49, 2003.2 (in Japanese)
9) Wu, Q., Yoshimura, M., Takahashi, K., Nakamura, S., Fujita, H. and Furukawa, K., Vibration and Nonlinear Seismic Analysis of the Second Saikai Bridge-Concrete Filled Tubular (CFT) Arch Bridge-, *Proceedings of the 5th Japan-German Joint Symposium*, Osaka, Japan, 2003.9 (in press)
10) Wu, Q., Takahashi, K., Matsuzaka, H., Chen, B., and Nakamura, S., Study on natural vibrations and nonlinear seismic response of CFT arch bridge constructed in China, *Journal of Constructional Steel*, Vol.11, 2003.11 (in press, in Japanese)
11) Wu, Q., Takahashi, K., Kobayashi, H. and Nakamura, S., Natural vibration properties and nonlinear seismic responses of the Saikai Bridge, *Journal of Constructional Steel*, Vol.11, 2003.11 (in press, in Japanese)
12) Okabayashi, T., Mean square response analysis of highway bridges under a single moving vehicle, *Journal of Structural Mechanics and Earthquake Engineering*, JSCE, No.286, pp.15-27, 1979.6 (in Japanese)
13) Okatani, M., Chen, B., Wu, Q. and Okabayashi, T., Dynamic behavior of a concrete filled steel tubular arch bridge under traffic road, *Proceedings of Annual Conference of the Japan Society of Civil Engineers*, Vol.56, Part 1, pp.288-289, 2001.9 (in Japanese)
14) Kobori, T. and Kajikawa, Y., Ergonomic evaluation methods for bridge vibrations, *Journal of Structural Mechanics and Earthquake Engineering*, JSCE, No.230, pp.23-31, 1974.10 (in Japanese)
15) Yoneda, M., Dynamic response characteristics of the stress ribbon pedestrian bridges due to a walking human and a simplified method for evaluating maximum amplitude of this type of bridges, *Journal of Structural Engineering*, Vol.47A, pp.351-362, 2001.3 (in Japanese)
16) Yoneda, M., Relationships between numerical dynamic responses using various human walking force models and full scale measurements of single span pedestrian bridges, *Journal of Structural Engineering*, Vol.46A, pp.439-448, 2000.3 (in Japanese)

(Received July 31, 2003)

ON REMAINING ASSET VALUES AND MAINTENANCE NECESSITY LEVEL (MNL) OF BRIDGES

Makoto SATO [*], **Shuichi MIKAMI** [**], **Ikue TAMBA** [***], **Kenji IKEDA** [****], **and Toshiyuki OSHIMA** [*****]

*Docon Co., Ltd., 1-5-4-1 Atsubetsu-chuo, Atsubetsu, Sapporo, Hokkaido, 0048585, Japan
**Dr. of Eng., Associate Professor, Dept. of Civil Eng., Kitami Institute of Technology
165 Koencho, Kitami, Hokkaido, 0908507, Japan
***Dr. of Eng., Docon Co., Ltd., 1-5-4-1 Atsubetsu-chuo, Atsubetsu, Sapporo, Hokkaido, 0048585, Japan
****Civil Engineering Research Institute of Hokkaido,
1-3-1-34 Hiragishi, Toyohiraku, Sapporo, Hokkaido, 0628602, Japan
*****Dr. of Eng., Professor, Dept. of Civil Eng., Kitami Institute of Technology
165 Koencho, Kitami, Hokkaido, 0908507, Japan

Bridge maintenance costs extremely. Therefore bridge managers are required to use limited budget effectively and plan cost-efficient long-term strategies. This study intends to show an evaluation method for bridges using the Bridge Health Index (BHI) and examines how to use evaluation results for management of bridges. This study analyzes national highway bridges in Hokkaido, Japan, by applying two quantitative diagnostic methods. These are the BHI and the Bridge Integrity Evaluation (BIE), which have already been developed and reported previously by other authors. Moreover, the Maintenance Necessity Level (MNL) is also proposed. It supports decision-making for repair or reinforcement of bridges. The MNL is evaluated synthetically in consideration of the integrity evaluation of the bridges and the social value and the traffic of the route.

Key words: *Quantification Method, Bridge Integrity Evaluation, Bridge Health Index, Bridge Maintenance*

1. INTRODUCTION

Though many researchers have studied Bridge Management System (BMS), this attempt has not been standardized yet in Japan. Therefore, immediate development of a uniform BMS is necessary.

This paper describes Bridge Integrity Evaluation (BIE), which the authors have studied to establish an improved BMS. This BIE models recommendations of skillful engineers; these recommendations are obtained through comprehensive evaluation that is based on damage inspections of the bridge members (using quantification theory). This paper also reports an investigation of the estimation method to determine unit cost and a Bridge Health Index (BHI) analysis of national highway bridges in Hokkaido, Japan. The BHI is calculated using a database of bridge inspections and the unit cost of bridge members. The unit cost of bridge members is determined based on their real construction costs. Results of the BHI and BIE are compared and discussed. In this study, the priority of bridge repair, indicated by the Maintenance Necessity Level (MNL), is examined using the BHI and BIE results.

2. THE QUANTIFICATION METHOD

Quantification theory can determine the integrity of a bridge according to the overall judgment of engineers based on their inspections of bridge members. Using a questionnaire sent to bridge diagnosis experts, judgment examples were collected from expert bridge engineers. These produce a quantitative judgment model. This

questionnaire elicited evaluations of bridges from ten experts concerning 480 bridges (240 steel bridges and 240 concrete bridges). Inspection items in this research were extracted from the Ministry of Construction's bridge inspection points (proposed), which are shown in Table 1. External decisions for this questionnaire are shown in Table 2. These can evaluate the overall health of each bridge.

3. BRIDGE INTEGRITY EVALUATION (BIE)

Fig. 1 shows the weight factor for the first axis computed from quantification theory. This weight factor shows the importance of the member to the expert when performing integrity evaluation. Diagnosis of the inspected bridges is done using this weight factor in BIE.

In this paper, the Hokkaido Development Bureau used BIE from 1988 to 1999 for national highway bridges in Hokkaido using inspection results from 2238 inspected bridges. Analysis results are summed and shown in Table 3. These results can indicate the condition of these bridges overall and thereby create an integrity-ranking table for the bridges.

4. METHODOLOGY OF THE BHI

The California Department of Transportation (Caltrans) developed the California Bridge Health Index, which is a bridge condition assessment based on the economic worth and physical condition of a bridge. The BHI is an integrity rating showing bridges' asset value.

4.1 The Asset Value of a Bridge

The asset value of a bridge can be represented by the construction expense of the bridge. This study adopts the construction expense of a bridge as its asset value. Table 4 shows nine principal members that are selected for bridge construction expense computation. The unit cost of each member is set. The unit cost is unified to current prices to reflect price fluctuation. On a practical level, the bridge construction expense requires circumstantial calculation of the bridge material cost. However, the calculation needs to be simplified because it will accelerate as the number of bridges increases. Fig. 2 shows the relationship between span and unit cost using the main girders on a continuous steel bridge as an example. The unit cost is determined on the basis of the actual cost of some sample bridge types: simple steel bridges, continuous concrete bridges, etc. A linear equation approximates the relationship between span and unit cost. Changes in unit

Table 1: Inspection item for BIE

Super structure	Girder 1(Corrosion)
	Girder 2(Crack)
	Girder 3(Other)
	Secondary member
	Slab 1 (Delamination)
	Slab 2 (Crack)
	Slab 3 (Other)
Sub structure	Pier, Abutment
	Basement
Other	Shoe
	Handrail
	Coping
	Pavement
	Expansion joint

Table 2: External decision

OK	Good
VI	Needs minor repair
III	Needs major repair
II	Reconstruction / Replacement

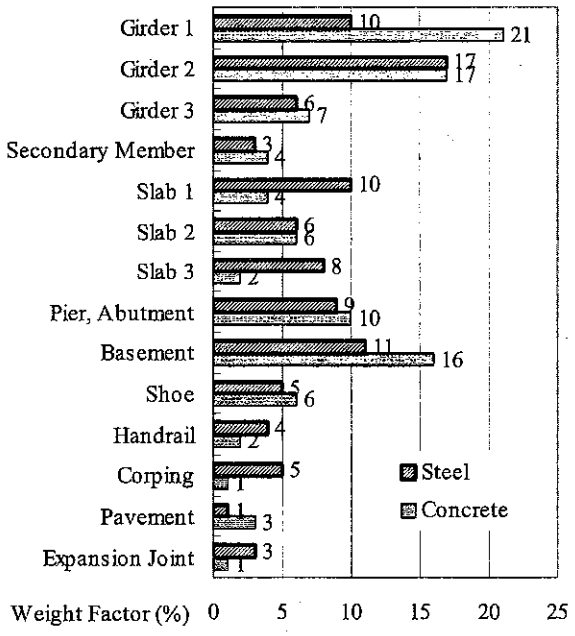

Fig. 1 Item weight factor

Table 3: Bridge Integrity Evaluation (BIE) results

BIE	Number (%)
OK	904 (40)
IV	830 (37)
III	431 (19)
II	73 (3)
Total	2238 (100)

cost are formulated within the application coverage of the span in each kind of girder types. Also, unit costs of the nine principal members shown in Table 4 are determined. Therefore, the construction expense of the bridges is calculated using these unit costs. It is then inferred to be the asset value of each bridge.

Table 4: Inspection item for BHI

Super structure	Girder
	Slab
Sub structure	Pier, Abutment
	Basement
Other	Shoe
	Handrail
	Coping
	Pavement
	Expansion joint

4.2 Definition of the BHI

The BHI is defined as:

$$BHI = \frac{Present\ Price\ as\ Asset}{Initial\ Construction\ Cost} \times 100 \quad (1)$$

The initial construction cost is the asset value of a bridge at the time of construction. It is converts into the required cost for reconstruction at present costs. It is taken from the construction expense of the bridge that is mentioned in 4.1.

The price as an asset at any time is determined by the deterioration of the asset; deterioration is based on the condition of the bridge members, which is obtained from bridge inspection data. According to the deterioration factor for rank shown in Table 5, it is assumed that the asset value (initially, construction cost) of each member declines.

5. ANALYTICAL RESULTS

The 2238 bridges used for the analysis are all national highway bridges located in Hokkaido, Japan.

5.1 The BHI

The distribution of analytical results of the BHI (Fig. 3) shows the state of maintenance on the bridges. The BHI is classified into eight categories (horizontal axis). The evaluation results for BHI for the bridges in each classification are expressed with the number of bridges. About 60% of the bridges show more than 80 on the BHI, meaning that the state of maintenance on the bridges is

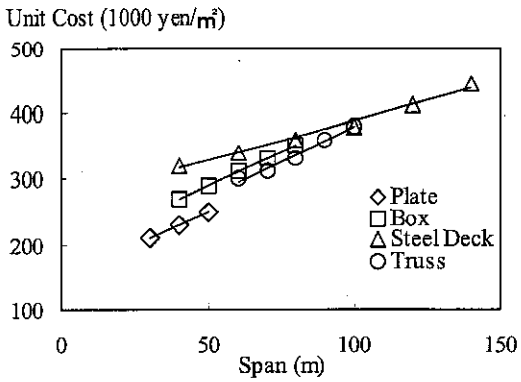

Fig. 2 Relationship between span and unit cost (Continuous steel bridge)

thought to be good. A BHI of 80 is the standard value of a sound bridge in the state of California (according to Caltrans). Fig. 4 shows the relationship between BHI and bridge age. The figure shows that the BHI decreases as the bridge age increases.

5.2 Weight factor

The analytical results of the BHI yielded weight factors of respective bridge members. Bridge member weight factors were divided into the categories of steel and concrete girders; they are shown in Fig. 5. The weight represents the economic worth of the bridge members; it differs from the weight determined using physical importance of the bridge members (Fig. 1).

Table 5: Deterioration factor for rank

Inspection Rank for Member	Factor
II	0.75
III	0.50
IV	0.25
OK(V)	0.00

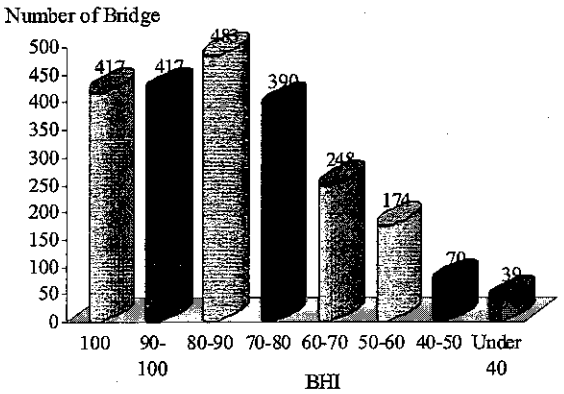

Fig. 3 Results of BHI

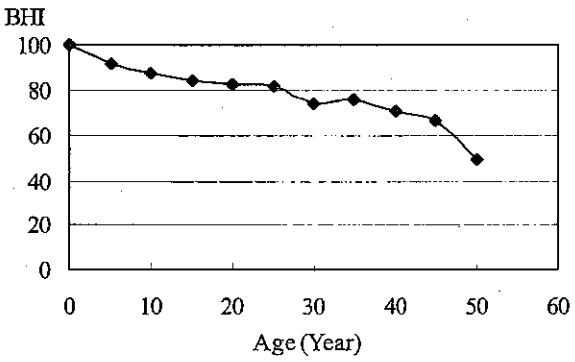

Fig. 4 Relationship between BHI and age

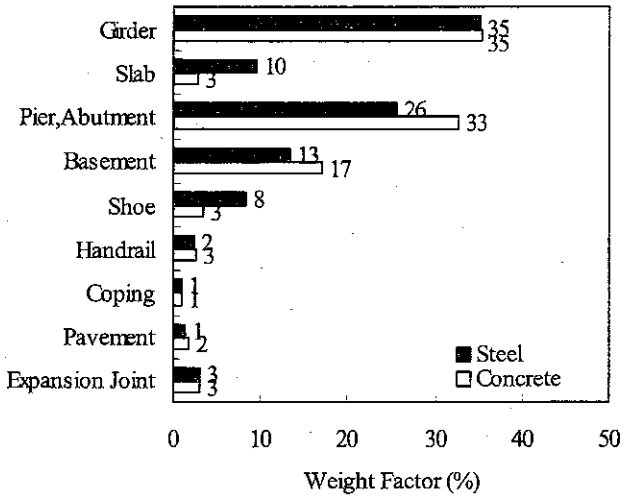

Fig. 5 Weight factors of members

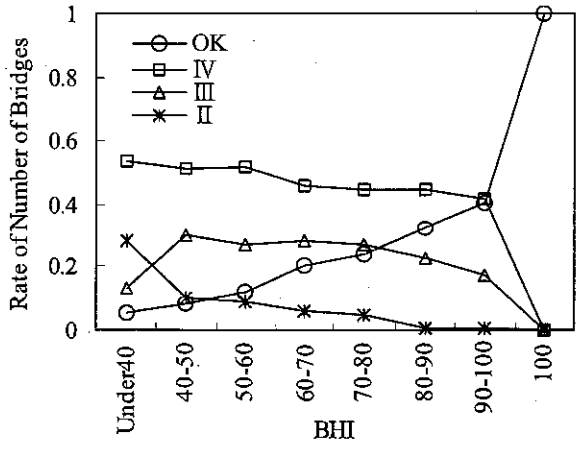

Fig. 6 Comparison of BHI and BIE

6. COMPARISON OF BHI AND BIE

The result of the BHI evaluation is compared with the BIE, and it is shown in Fig.6. The evaluation results, when using the quantification theory (Table 2), for the bridges in each of the eight BHI classifications are expressed with the rate of the number of bridges.

7. REPAIR OR REINFORCEMENT PRIORITY

This chapter proposes the Maintenance Necessity Level (MNL), a technique for determining socially preferential repair or reinforcement according to bridge importance. The priority for repair or reinforcement the existing bridge is not specified clearly at present. However, when determining the priority of repair or reinforcement, it is necessary to consider the importance of routes and the area. In addition, accountability based on a quantitative judgment standard is required at planning or enforcement of the project. A target bridge for preferential repair or reinforcement is a bridge that garners a high MNL score.

The MNL is calculated as

$$MNL = (1+\alpha)(1+\beta)\left\{\frac{Sto - St}{Sto} + a\frac{Fto - Ft}{Fto}\right\} \qquad (2)$$

where

α: route importance
β: bridge importance
St: current BIE or BHI
Sto: initial value of BIE or BHI
Ft: current Bridge Function Evaluation
Fto: initial value of Bridge Function Evaluation
a: correction coefficient

In this paper, the MNL is calculated using the following equation, which yields the expected Bridge Function Evaluation (Ft).

$$MNL = (1+\alpha)(1+\beta)\left\{\frac{Sto - St}{Sto}\right\} \qquad (3)$$

8. ROUTE IMPORTANCE α

Route importance α is evaluated for national highway 45 routes of Hokkaido, Japan. However, if one route is considered as one section, the accuracy of this evaluation is declining. Therefore, the route is divided by each branch office (jurisdictional area) to comprise 86 routes for evaluation. Table 6 shows those details. This study uses route evaluation data which indicate safety and improvement in convenience of life, and local activation support that Mie Prefecture[4] created. At this time, weights attached to respective items are between 10 and 2 points.

Table 6: Route in Hokkaido

Subprefectural Office Name	The number of national highways	National highway number
Ishikari Sorachi	14	5, 12, 36, 230, 231, 233, 234, 239, 274, 275, 337, 451, 452, 453
Oshima Hiyama	9	5, 37, 227, 228, 229, 230, 227, 278, 279
Shiribeshi	6	5, 229, 230, 276, 337, 390
Kamikawa	9	38, 39, 40, 237, 239, 273, 275, 333, 452
Iburi Hidaka	8	36, 37, 230, 234, 235, 274, 276, 453
Kushiro Nemuro	12	38, 44, 240, 241, 243, 244, 272, 274, 334, 335, 391, 392
Tokachi	9	38, 235, 236, 237, 241, 242, 273, 274, 336
Abashiri	11	39, 238, 239, 240, 242, 243, 244, 273, 333, 334, 391
Rumoi	5	40, 231, 232, 233, 239
Souya	3	40, 238, 275
Total	86	-

The system computes evaluation points of a route with an addition-of-points system. Route importance α is $1/100^{th}$ of these evaluation points.

Data for route evaluation value in Mie Prefecture are shown in Table 7. These data are values of route evaluation that are adopted for Mie Prefecture. It is necessary to change to the proper value for evaluation in Hokkaido. Therefore, the weight was calculated using Analytic Hierarchy Process (AHP) to determine the route evaluation value in Hokkaido.

This AHP is one decision-making method; it is a method that attaches a status based on a layered structure. It can be compared with ordering according to priority. The layered structure is based on a policy objective, a valuation basis, and alternatives. Therefore, AHP has garnered interest as an evaluation method for road enterprises in recent years.

Analytical results by AHP are shown in Figs. 7–9. Fig. 7 shows that the weight in Hokkaido for attention to network maintenance of a trunk road (A1) is high compared to that in Mie Prefecture. In addition, the weight of a multi-level crossing with a road or a railroad (C2) and maintenance of the trunk road for sightseeing (B2) are high by Fig. 8. In contrast, Fig. 8 shows that items for a dam (D1), a defense installation (D4), etc., are lower than for Mie Prefecture. The tendency of weight was similar: the values were smaller than Mie Prefecture in Fig. 9. Items regarding activation of the city area and improvement in life convenience within the prefecture are low. Fig. 10 shows an example of results regarding weights for route importance in Hokkaido.

Table 7: Evaluation Value of Route

Evaluation Item		Points
Ⅰ. Trunk Access Road		
A. Trunk Road		
A1	Maintenance of trunk road	9
B. Shortening of Access to Highway		
B1	Access route to highway	10
B2	Access strengthening route to highway	7
C. Shortening of Access to Airport		
C1	Access route to airport	10
C2	Access strengthening route to airport	7
Ⅱ. Local Industrial Transportation Road		
A. Route for Safety		
A1	The first emergency transportation road	7
A2	The second emergency transportation road	5
A3	The third emergency transportation road	3
A4	Emergency route for disaster measure	4
A5	Route for snow removal	4
A6	Rainfall regulation section	2
B. Measures for Traffic Congestion		
B1	Route of the third measures for traffic congestion	8
B2	Route of measures for traffic congestion	5
B3	Useful road for overpass other road or railroad	5
C. Useful Road for Local Industry		
C1	Physical distribution route (Access road to important port)	4
C2	Maintenance of Trunk for sightseeing (Access road to resort)	4
C3	Residence	4
C4	Company	4
D. For Project		
D1	Large-project dam	6
D2	Construction section of broad area agricultural road	5
D3	Required for progress of public enterprise	5
D4	Defense institution	5
Ⅲ. Revival Road for Local Life		
A. Improvement in Convenience of Sphere of Life		
A1	Connection road of central city and public office (town, village)	6
A2	Substitutive road for connection to central city and public office	3
A3	Connection road with neighboring towns and villages	4
A4	Route for the wide area cooperation in a sphere of life	4
A5	Maintenance of a beltway network in central city	4
A6	Connection route of neighboring towns and villages	3
B. Support of Local Life		
B1	Medical route	4
B2	Connection route to each public office and each branch office	2
B3	Bus line	2
B4	School zone	2
C. Activation of City Area		
C1	Street before station	5
C2	Main street	4
C3	Requires underground project for electric wiring	4
C4	Frame route supporting activation of city area	4

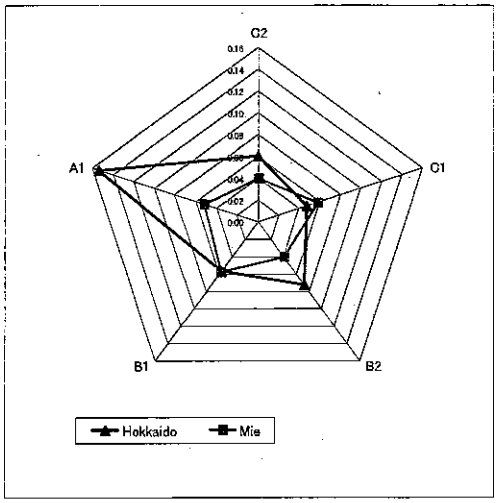

Fig. 7 Weight factor (Trunk Access Road)

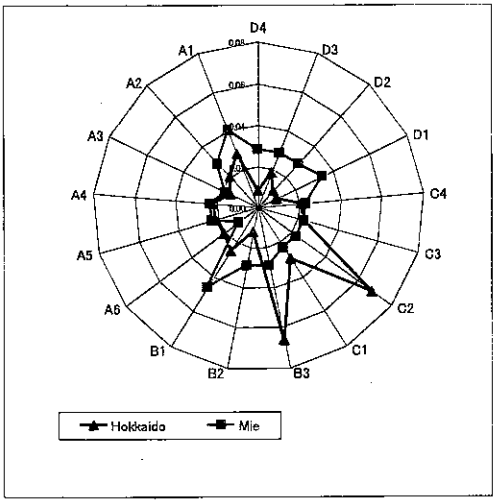

Fig. 8 Weight factor (Local Industrial Transportation Road)

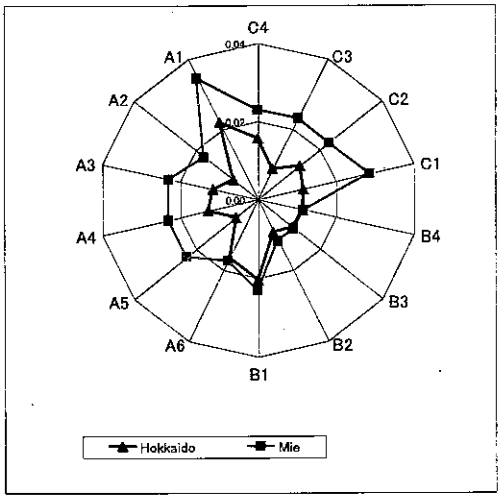

Fig. 9 Weight factor (Revival Road for Local Life)

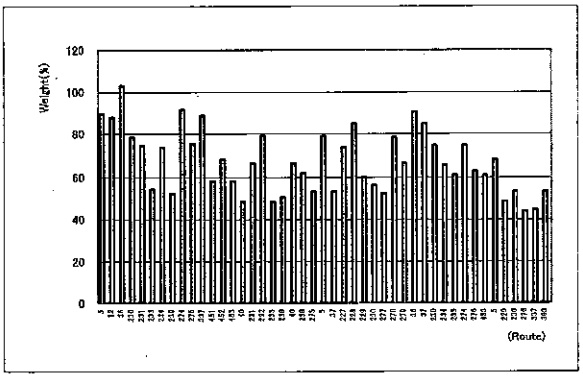

Fig. 10: Route importance (with AHP)

9. BRIDGE IMPORTANCE β

Bridge importance is calculated based on the route traffic volume[5]. The running cost C (Total transit cost, Total travel costs) for each vehicle type, e.g., car, bus, truck, is calculated referring to the cost-benefit analysis manual[6] of the Ministry of Land Infrastructure and Transport Road Bureau Road Investor Relations site. It is divided into sections. The unit section present value *Pv* (average current value per kilometer) computes the total of the present values of each branch office (jurisdiction region) by having broken it by the sum total of investigation section extension. Carrying out division of the present value of each traffic observation section by unit section present value defines the importance of a bridge β (Table 8). This method distinguishes those sections of each branch office where important traffic is distributed; it yields evaluation of important routes.

Table 8: Bridge Importance β

section name	Run cost	section extension	current value	β
section A	C_1	L_1	$C_1/L_1=P_1$	$P_1/Pv=\beta_1$
section B	C_2	L_2	$C_2/L_2=P_2$	$P_2/Pv=\beta_2$
section C	C_3	L_3	$C_3/L_3=P_3$	$P_3/Pv=\beta_3$
⋮	⋮	⋮	⋮	⋮
section N	Cn	Ln	Cn/Ln=Pn	$Pn/Pv=\beta n$
	ΣCn	ΣLn	ΣCn/ΣLn=Pv	

10. CALCULATION METHOD FOR *St* AND *Ft*

10.1 Bridge Integrity Evaluation *St*

This study gives *St* by two types values upon evaluation: BIE, based on the deterioration of each member; and BHI, using the bridge asset value.

10.2 Bridge Function Evaluation *Ft*

Function evaluations of bridges are a quantitative evaluation method for "vehicle running comfort", "structural stability", "environmental stability", and so on.

11. ANALYTICAL RESULTS OF MAINTENANCE NECESSITY LEVEL

The MNL is computed using coefficients (α, β, *St*, *Ft*) for inspection data of existing bridges in Hokkaido, Japan. Table 9 shows some examples of results.

11.1 Maintenance Necessity Level

(1) Maintenance Necessity Level and BIE

This section explains the MNL using the BIE. The priority of repair and reinforcement by the BIE or the BHI is determined based only on the integrity (damage) of the bridge. The MNL suggests a plan for repairing and reinforcing of the bridges by addressing the importance of bridges and routes in the area. Table 9 shows a comparison

of Bridge B, located on national route a, and Bridge C located on national route b. Bridge B is rank III and Bridge C is rank II for BIE results. Therefore, repair and reinforcement Bridge C is suggested for an earlier timer than Bridge B when considered only on damage of members, even the MNL result for Bridge B is higher than for Bridge C. This indicates the higher route importance of Bridge B and its greater value to users. Bridge Y is located on the same route as Bridge B and has a good condition; its MNL is 0. Therefore Bridge Y shows no need for repair or reinforcement.

(2) Maintenance Necessity Level and BHI

This section explains MNL using BHI. The weight factor in BIE indicates the physical importance of each member to the overall integrity of the bridge. On the other hand, the weight factor in the BHI represents the economic worth of bridge members. The weight factor is large for bridge members with expensive construction cost. This results from evaluating the condition of each member from a cost perspective.

Table 9 shows a comparison of Bridges D and E, which are located on national route c. Both bridges have rank III for the BIE result. However, Bridge D is 59.2 and Bridge E is 75.9 for the BHI result; Bridge D is lower than Bridge C in terms of bridge asset value. Bridge D has a higher ranking in MNL evaluation.

Therefore, this technique can select the bridge that has a high priority socially as using the inspection data of the bridges. Also, it can be determined which bridge is planned at early timing as repair candidate.

11.2 Result of a MNL computation for the bridge in Hokkaido

The MNL for every development construction department was calculated based on bridge inspection data for bridges in Hokkaido. Bridge MNLs are computed using BIE and BHI. Then, they are classified into separate MNL levels for the newest bridge inspection data (1903 bridges). Those are shown in Table 10.

Regarding BIE in Table 10, the four branch offices for "Kushiro and Nemuro", "Ishikari and Sorachi", "Tokachi", and "Oshima and Hiyama" have bridges with MNL of the highest level (over 9): "Kushiro and Nemuro" have a bridge, "Ishikari and Sorachi" have 2 bridges, "Tokachi" has 4 bridges, and "Oshima and Hiyama" have 2 bridges.

Table 9: Maintenance Necessity Level (MNL)

Route name	Bridge name	Inspection year	Route Importance α	Bridge Importance β	BIE	BHI	MNL(BIE)	MNL(BHI)
a	A	2001	0.80	4.56	II	28.4	7.51	7.16
a	B	1994	0.80	4.56	III	27.3	5.00	7.28
b	C	1994	0.49	1.31	II	31.5	2.58	2.36
c	D	1995	0.65	2.11	III	59.2	2.57	2.09
c	E	1998	0.65	2.11	III	75.9	2.57	1.24
a	F	1995	0.80	1.55	III	27.1	2.30	3.35
:	:	:	:	:	:	:	:	:
:	:	:	:	:	:	:	:	:
b	W	2001	0.65	0.17	IV	96.1	0.48	0.08
e	X	1996	0.36	0.12	IV	82.7	0.38	0.26
a	Y	1999	0.80	4.56	OK	100.0	0.00	0.00
e	Z	2000	0.33	0.17	OK	100.0	0.00	0.00

Table 10: Maintenance Necessity Level (MNL) in Hokkaido

	Kamikawa		Kushiro Nemuro		Ishikari Sorachi		Iburi Hidaka		Shiribeshi		Tokachi		Souya		Oshima Hiyama		Abashiri		Rumoi		
MLN	(BIE)	(BHI)	(BIE)	(BHI)	(BIE)	(BHI)	(BIE)	(BHI)	(BIE)	(BHI)	(BIE)	(BHI)	(BIE)	(BHI)	(BIE)	(BHI)	(BIE)	(BHI)	(BIE)	(BHI)	
9～			1	2	2	2					4	3			2	2					high
8～9	1		1																		
7～8				1												1	1	1			
6～7															1						
5～6	1		2	1	3	3	1	1		2		1			1	4			1	1	
4～5	2	2	1	1	4	5					1										
3～4	6	4	2	5	6	1	7	6	1	2	6	2			6	1	1	1		1	
2～3	17	15	12	10	18	12	14	25	7	6	13	22	1		14	13	5	5	7	9	
1～2	43	43	28	21	65	53	57	35	34	31	59	47	9	16	68	53	44	30	19	22	
0～1	57	102	68	115	111	191	51	101	62	93	83	138	21	18	68	132	93	149	20	31	
0	77	38	104	63	79	21	49	11	53	23	81	34	14	11	61	15	102	60	50	33	Low
Total (Number of Bridge)	204		219		288		179		157		247		45		221		246		97		

Maintenance Necessity Level

Judgment of bridges that should be repaired immediately is clearer because of computing ranking based on the MNL.

The MNL results by BIE and BHI re-compared. They appear to differ in the low level of MNL. These are levels 0 and level 0−1. The evaluation technique strongly affects the results: bridges with MNL=0 are 670 bridges in BIE and 309 bridges in BHI.

12. CONCLUSIONS

This research described a method of quantitative evaluation with the present value of a bridge. It also explained a method to determine the priority of repair or reinforcement of a bridge and the degree of required repair. The following summarizes that description.

1) Priority in consideration of the importance of a bridge in a route or area was calculated using the route importance α and the bridge importance β.
2) Importance as a structure and priority in consideration of asset value were calculated using the two-degree evaluation method *St* of health, BIE, and BHI.
3) Ranking attachment of high priority for repair and reinforcement was calculable for a concrete numerical social value that incorporates various kinds of importance into consideration in evaluation of bridge health and damage state.
4) Future study will address the route importance α and the bridge importance β in reference to evaluation examples actually performed in various regions. This may establish a better regional standard for evaluation.
5) Bridge Function evaluation *Ft* will be completed in the future to include the MNL degree level of repair required. Consequently, we can obtain a support method with a more practical repair and reinforcement plan.

ACKNOWLEDGMENT

The authors are grateful for useful advice from Dr. Takahashi, an associate professor at the Dept. of Civil Eng., Kitami Institute of Technology, and Mr. Yasue, a general Manager at the Dept. of Structure., Docon Co., Ltd.; also, for data arrangement, the authors had cooperation from Mr. Hasegawa, a graduate student of Kitami Institute of Technology.

REFERENCES

1) The Public Works Research Institute, the Ministry of Construction: The bridge inspection manual (proposal), the Public Works Research Institute data, No. 2651, 1988.
2) H. Mori, T. Oshima, S. Mikami, S. Amano, and M. Inoue, "Evaluation Method in Maintenance Inspection of a Bridge by means of Computer Graphics and Quantification Theory," Journal of JSCE, No.501/I-29, pp. 113–121, 1994.10.
3) T. Oshima, S. Mikami, I. Tamba, S. Sasaki, and K. Ikeda, "Asset Evaluation of Each Bridge Member and Analysis of Bridge Health Index (BHI)," No.703/I-59, pp. 53− 65, 2002.4.
4) Mie Prefecture: a road maintenance 10-year maintenance program, Japan Society of Civil Engineers, Vol.84, pp. 12–15, 1999.8.
5) The Hokkaido Development Bureau road plan division Heisei 11 fiscal year Situation investigation 2001.1 of national road traffic (road traffic census)
6) The Ministry of Land, Infrastructure and Transportation, Road Bureau, The Cost-Benefit Analysis Manual (proposal), Road IR (Investor Relations) Site
7) Hideo Nakamura (ed.) and road investment evaluation study group work "Social Economy Evaluation of Road Investment," Toyokeizai Inc., 1997.
8) T. Oshima, S. Mikami, T. Yamazaki, and I. Tamba, "Investigation of Total Evaluation Method on Bridge Integrity and Analysis of its Effective Constituents," Journal of JSCE, No.501/I-29, pp. 201–217, 2001.4.

(Received July 31, 2003)

Performance Measures for Bridge Management

Hitoshi Furuta*, Takahiro Kameda**, Dan M. Frangopol***

* Dr. of Eng., Professor, Dept. of Informatics, Kansai University, Takatsuki, Osaka 569-1095
** Gradutae Student, Graduate School of Informatics, Kansai University, Takatsuki, Osaka 569-1095
*** Ph. D, Professor, Dept. of Civil Eng., University of Colorado at Boulder, Co 80309-0428,USA

In order to develop a rational maintenance program, it is necessary to predict the performance of existing structures. So far many measures have been proposed to evaluate the performance of existing structures, most of which are based upon the structural condition regarding its damage or deterioration. Then, it is important and inevitable to bridge the condition rating and safety evaluation. In this paper, an attempt is made to develop a method for evaluating the safety and reliability of existing structures with damage or deterioration. Furthermore, the relationships among the minimization of LCC, the optimal extension of structural service life, and the target safety level are discussed by using the multi-objective genetic algorithm.

Key Words: Life-cycle cost, maintenance, performance measure, safety level, structural service life

1. Introduction

Recently, the importance of structural maintenance has been widely recognized. In order to establish a rational maintenance program, it is necessary to predict the performance of existing structures. So far many measures have been proposed to evaluate the performance of existing structures, most of which are based upon the structural condition regarding its damage or deterioration. Then, it is important and inevitable to bridge the condition rating and safety evaluation.

In this paper, an attempt is made to develop a method for evaluating the safety and reliability of existing structures with damage or deterioration. Rating of structrural condition regarding damage or deterioration is intriduced into te safety evaluation through the linguistic expressions such as very slight, slight, moderate, severe, and very severe, which are defines in terms of fuzzy sets.

On the otrher hand, it is also necessary to develop a cost-effective decision-support system for the maintenance of existing structures. Life-Cycle Cost (LCC) is a useful concept in reducing the overall cost and achieving an appropriate allocation of resources (Frangopol and Furuta, 2001).

In general, Life-Cycle Cost optimization is to minimize the expected total cost which includes the initial cost involving design and construction, routine or preventive maintenance cost, inspection, repair and failure cost. Then, the optimal strategy obtained by LCC optimization can be different according to the prescribed safety level and required service life. In this paper, an attempt is made to discuss the relationships among the minimization of LCC, the optimal extension of structural service life, and the target safety level by using the multi-objective Genetic Algorithm (GA). Namely, the following three objective functions are employed:

1) LCC is minimized.
2) Service life is maximized.
3) Target safety level is maximized.

By introducing the multi-objective GA, it is possible to obtain several available solutions that have different structural life spans, safety levels and LCC values.

2. Reliability Evaluation of Damaged Structures

According to Yao (Yao and Furuta, 1986), damage measurement can be generally classified into three types; numerical measurement, monetary measurement, and

verbal measurement, the most desirable apparently being the numerical measurement.

However, it is difficult, because of technical and financial constraints concerning the particular properties of civil engineering structures, to establish a useful numerical measurement for practical use.

The information sources available for damage assessment include design specifications or drawings, visual inspections, field testing, laboratory testing, and structural analysis. However, not all the available information can generally be used due to cost constraints. Actual daily maintenance work is carried out on the basis of the intuition and engineering judgment of experienced inspectors. This judgment may possibly be derived from subjective feelings and insufficient vague data obtained from limited inquiries.

An attempt is made here to apply the fuzzy sets so as to introduce the subjective assessment of engineers into the system reliability analysis of damaged structures. The damage state is evaluated by a verbal measurement such as "very severe", "severe", "moderate", "slight", and "very slight". The verbal evaluations correspond to the condition evaluation like damage 4, 3, 2, 1, and 0, respectively, and are represented by reduction factors that can be defined by fuzzy sets.

Suppose that damage does not affect the load S but does affect the resistance R. Then, the safety margin Z can be written as

$$Z = \phi R - S \tag{1}$$

where ϕ is a reduction factor defined by a fuzzy set. Then, the reliability index β can be calculated as

$$\beta = (\phi \mu_R - \mu_S)/(\sqrt{\phi^2 \sigma^2_R + \sigma^2_S}) \tag{2}$$

where μ and σ are the mean value and standard deviation, respectively. Then, the failure probability P_f is obtained as

$$P_f = \Phi(-\beta) \tag{3}$$

where Φ is the normal distribution function.

It should be noted that Eqs. 2 and 3 are obtained as fuzzy quantities so that usual arithmetic operations can be no longer used for these calculations. Here, a calculating method called "extension principle" is employed for the implementation of Eqs. 2 and 3.

When the structure under consideration is expressed as serial and parallel systems, the structure function can be used to calculate the system reliability. However, in order to calculate the system reliability of such redundant structures as rigid frames, it is necessary to consider the correlation between every failure mechanisms. In this analysis, the PNET method proposed by Ang et al. (Ang and Ma, 1981) is employed to obtain the system failure probability. While the PNET method is useful for calculating the system reliability of any type of structure, it requires to find out all the possible failure mechanisms. As the number of failure mechanisms increases, this becomes more difficult. To overcome this problem, a technique proposed by Ishikawa et al. (Shiraishi and Furuta, 1987) is used here, which can provide a sufficient number of dominant failure mechanisms.

The calculating procedure of the PNET method is as follows:

Step 1: The first representative failure mechanism is determined as the mechanism possessing the greatest failure probability or the least reliability index.

Step 2: The next step is to find out the second representative failure mechanism. Similarly, the second failure mechanism can be determined by minimizing β.

Step 3: Step 2 is repeated until P_{fm} being the failure probability of the m-th representative mechanism is sufficiently small.

Step 4: Finally, the system failure probability P_f is obtained as

$$P_f = \Sigma \quad P_{fm} = \Sigma \quad \Phi(-\beta) \tag{4}$$

To illustrate the proposed method, consider an example of the portal frame whose statistical data are given in Table 1. Three damage patterns are considered, in which the upper portion or lower portion of columns and the center of beam are damaged.

Table 1 Statistical Data of Portal Frame

	Mean value	C. O. V.
$M_{pj}(j=1,\cdots,8)$	40.0 N cm	0.2
H	0.5 N	0.2
P	1.0 N	0.2

For this example, ϕ = (0.75, 0.50, 1.00) is employed as a reduction factor, in which 0.75, 0.50 and 1.00 mean the central value, lower value and upper value, respectively. In this simple example, the number of total failure mechanisms is eight, as shown in Figure 1. For each failure mechanism, reliability indices are obtained as shown in Table 2, and the failure probability of each mechanism can be calculated corresponding to

the reliability indices obtained. Using these values of β, the first representative failure mechanism is found as Mechanism 1, because it has the least reliability index. Next, the second representative mechanism is chosen as the mechanism having the smallest value of β among the failure mechanisms whose coefficients of correlation to the first failure mechanism are less than the critical correlation coefficient. Mechanism 8 is chosen as the second one, because its value of β is the smallest. Similarly, Mechanism 5 is chosen as the third representative mechanism. However, Mechanism 5 is not considered in the calculation of system failure probability, because its value is comparatively small. Finally, the system failure probability is obtained as

$$P_f = P_f^1 + P_f^8 \tag{5}$$

Table 2 Reliability Indices for Eight Mechanisms

	β_L	β_M	β_S	$(\beta_S + 2\beta_M)/3$
Z1	3.88	2.34	0.29	1.66
Z2	3.88	2.76	1.36	2.29
Z3	3.88	3.15	2.29	2.86
Z4	5.83	5.83	5.83	5.83
Z5	5.83	5.52	5.13	5.39
Z6	5.83	5.20	4.34	4.91
Z7	3.97	2.90	1.49	2.43
Z8	3.97	3.40	2.76	3.19

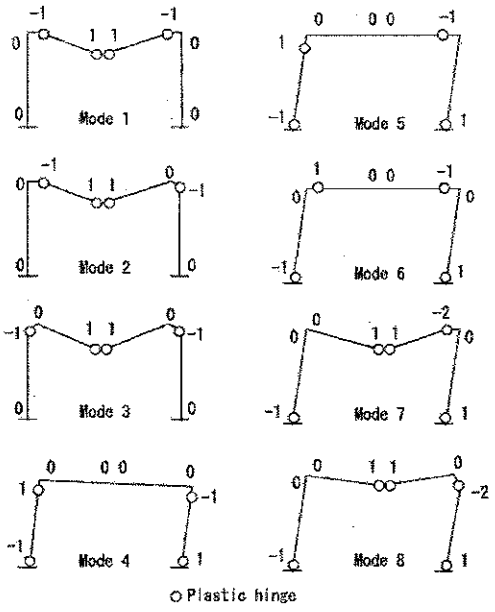

Figure 1 Representative Failure Mechanisms

3. Relationship among LCC, Safety Level and Service Life

3.1 Multi-Objective Genetic Algorithm

Multi-objective optimization problem has several objective functions, in which Pareto solutions are obtained as a set of solutions. Since GA pursues the optimal solution by random and multiple-points searches, it is suitable to obtain the Pareto solutions. The Multi-Objective Genetic Algorithm (MOGA) is performed according to the following procedures (Goldberg, 1989):

Step 1: Generation of initial populations.
Step 2: Crossover. Two-points crossover is employed here.
Step 3: Mutation.
Step 4: Evaluation of fitness function.
Step 5: Selection.

The process is depicted as shown in Figure 2.

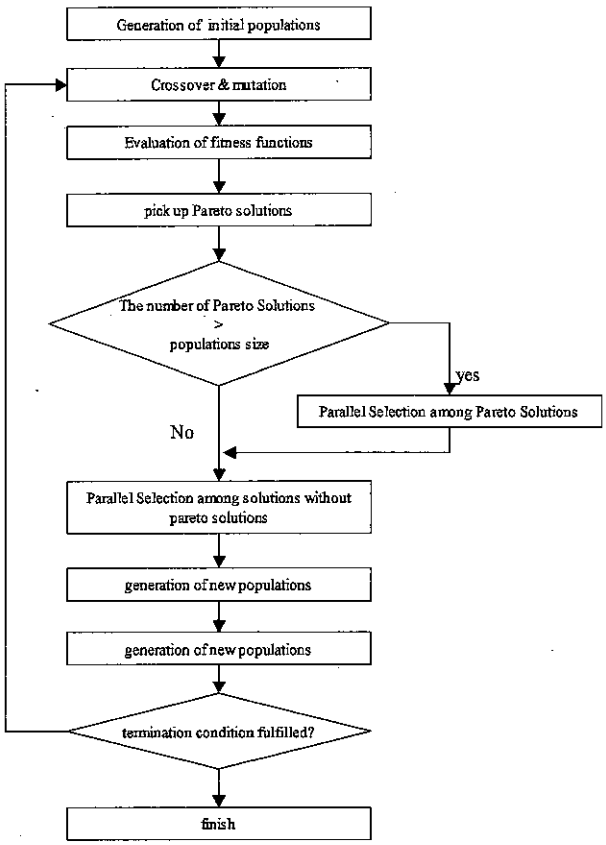

Figure 2 Process of Multi-Objective Genetic Algorithm

3.2 Maintenance of Bridge Structures

Figure 3 shows a deterioration curve of bridge structures, in which D_{pr} is the decreasing rate of structural capacity (structural capacity is often expressed as "durability" or "safety level") defined by

$$D_{pr} = (R_{max} - R_{min})/(S_{life} - D_{year}) \tag{6}$$

where R_{max}, R_{min}, S_{life}, and D_{year} mean maximum durability (safety), allowable minimum durability, service life, and year starting deterioration, respectively.

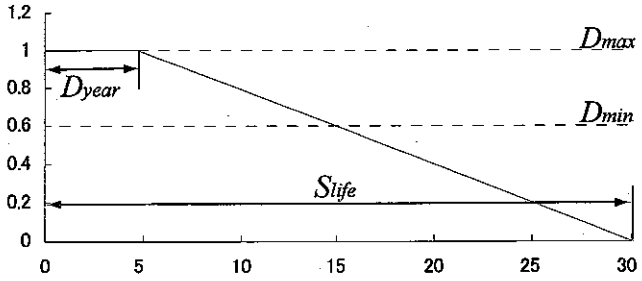

Figure 3 Deterioration of Bridge Structures

Table 3 presents the cost and effect of representative repair methods. The repair cost is a part of Life-Cycle Cost (LCC), whereas User Cost (UC) is defined as the loss for passengers due to the repair works and included in LCC. (Table 4)

Table 3 Repair Methods

No.	Method	Cost (1,000yen)	Average effect
1	Surface painting I	1,640	Delays D_{pr} decrease for 7 years
2	Surface painting II)	4,100	Delays D_{pr} decrease for 10 years
3	Section restoring	22,140	Restores D_{pr} to 1.0, and then allows it to deteriorate along the initial deterioration curve
4	Desalting (Re-alkalization)	7,380	Allow D_{pr} to deteriorate along the initial deterioration curve.
5	Cathodic protection	8,200	Delays D_{pr} decrease for 40 years
6	Section restoring with surface covering	26,240	Restore D_{pr} to 1.0, delays IP decrease for 10 years, and then allows IP to deteriorate along the initial deterioration curve

Table 4 User Cost (1,000yen)

Bridge No.	UC
1	5,000
2	10,000
3	15,000
4	20,000
5	25,000

3.3 Application of Multi-Objective Genetic Algorithm to Maintenance Problem

In the calculation of GA, the coding is very important to obtain a good solution. In this study, chromosome is defined by the combination of repair methods and repair intervals as shown in Figure 4.

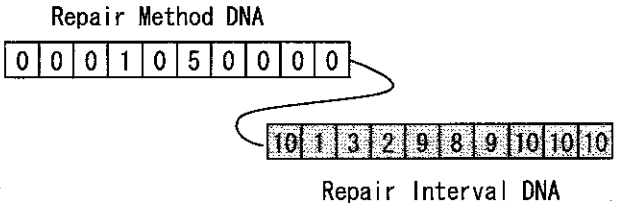

Figure 4 DNA Structure

The service life is calculated as the summation of repair intervals.

Then, the optimal maintenance problem is expressed in the following as a form of multi-objective optimization:

Objective function 1 : $C_{total}=\Sigma LCC_i \rightarrow min$

LCC_i : LCC for Bridge i

Objective function 2 : $Y_{total}=\Sigma Y_i \rightarrow max$

Constraints : $Y_i > 30$

Y_i : Service life of Bridge i

Objective function 3 : $P_{total}=\Sigma P_i \rightarrow max$

Constraints : $P_i > 0.6$

P_i : Durability of Bridge i

The above objective functions have trade-off relations to each other. Namely, the maximization of durability or maximization of service life cannot be realized without increasing the cost. On the other hand, the minimization of LCC can be possible unless the service life does not decrease nor the durability level gets down.

Figure 5 shows the change of durability, in which an optimal repair plan is implemented for a bridge.

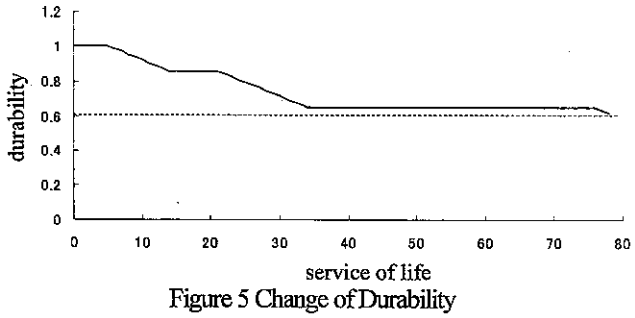

Figure 5 Change of Durability

For a bridge, the relationships among the three objective functions are examined through the multi-objective optimization process. GA parameters are given in Table 5. Figures 6

through 8 show the change of each objective function; LCC, service life and durability (safety) level.

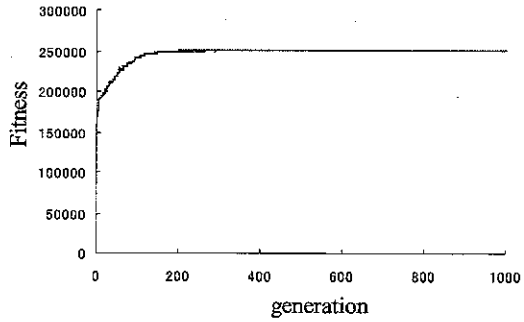

Figure 6 Change of LCC

Figure 6, 7 and 8 show the changes of average LCC, average service life and average durability level, respectively. From Figure 7 and Figure 8, it is observed that the average values of service life and durability level converge at earlier steps, whereas the average value of LCC gradually converges to the optimal solution. It seems that the MOGA converges after 200 generations.

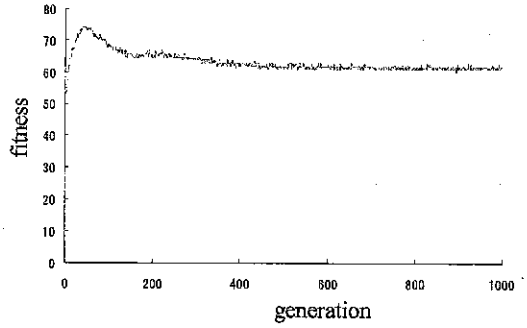

Figure 7 Change of Durability Level

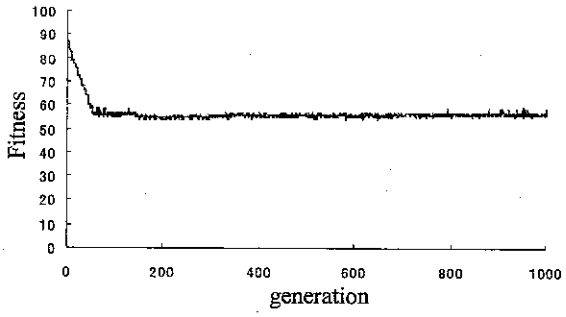

Figure 8 Change of Service Life

Table 5 GA Parameters

GA Parameter	Value
Gene length	20
Population	500
Generation	1000
Crossover rate	0.6
Mutation rate	0.1

Finally, 244 Pareto solutions are obtained, however only repair 1, repair 2 and repair 5 listed in Table 3 are selected, which cannot reinforce but prevent the deteriorating. The 244 Pareto solutions can be classified into 13 patterns. Table 6 presents the maximum service life obtained for 13 patterns. It is noted that the maximum service life is calculated assuming 0.6 for the allowable durability level. Consequently, it is said that all repair plans have 30 through 120 years service life and satisfy the requirement of durability lever that is 0.6. Table 7 shows the relation between LCC and allowable durability level where the service life is fixed to be 100 years. Figures 9 through 11 depict the changes of durability for repair plan 1, repair plan 2 and repair plan 3, respectively.

Table 6 Maintenance Plans

LCC(yen)	Service life
1,640,000	37
3,280,000	44
4,920,000	51
6,560,000	58
8,200,000	70
9,840,000	77
11,480,000	84
13,120,000	91
14,760,000	98
15,580,000	94
16,400,000	110
18,040,000	117
20,500,000	120

Table 7 Solutions with Maximum Service Life

Solution	LCC(yen)	Service life (year)	Durability
1	20,500,000	100	0.92
2	18,040,000	100	0.872
3	16,400,000	100	0.76

Table 8 Solutions with Maximum Safety

Solution	LCC(yen)	Service life (year)	Durability
1	20,500,000	95	1.0
2	16,400,000	85	1.0

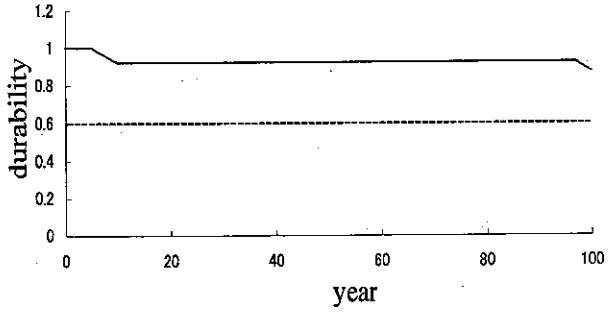

Figure 9 Durability by Rpair Plan 1

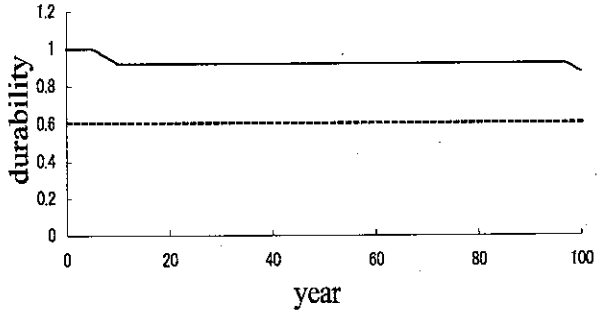

Figure 10 Safety by Repair Plan 2

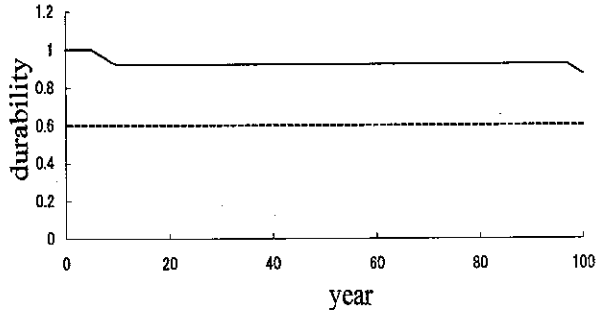

Figure 11 Safety by Repair Plan 3

Table 8 presents the relationship between LCC and service life where the allowable service life is maximized under the fixed value of durability.

4. Conclusions

In this paper, an attempt was made to develop a method for evaluating the performance of existing structures with damage in a quantitative manner, using fuzzy sets. When a structure is damaged, its dominant failure mechanisms may change, because the grade, location and cause of damage can greatly affect the system reliability of the structure. However, it is hardly estimated accurately due to technical and financial constraints, and it may be better to accept a vague or ambiguous evaluation as a practical and meaningful basis for the reliability assessment of the damaged structure. For this reason, fuzzy sets are useful because they can represent the verbal expression of experienced engineers in a clear and informative manner.

It was also attempted to discuss the relationships among the minimization of LCC, the optimal extension of structural service life, and the target safety level by using the multi-objective genetic algorithm. As expected, it was confirmed that LCC, service life and allowable durability level have trade-off relations to each other. In order to grasp the relation and find a practical maintenance plan, the multi-objective genetic algorithm is quite useful. Further study is necessary to apply the proposed method for practical use.

References

1) Frangopol, D. M., and Furuta, H. (2001) *Life-Cycle Cost Analysis and Design of Civil Infrastructure Systems*, ASCE, Reston, Virginia.

2) Yao, J.T.P. and Furuta, H. (1986) "Probabilistic Treatment of Fuzzy Events in Civil Engineering", *Journal of Probabilistic Mechanics*, Vol. 1(1), pp.58-64.

3) Goldberg, D. E., (1989) *Genetic Algorithms in Search, Optimization and Machine Learning*, Addison Wesley Publishing Company, Inc.

4) Ang, A. and Ma, H. (1981), "On the Reliability of Structural Systems", *Proc. of ICOSSAR-3, Trondheim, Norway*, pp.295-314.

5) Shiraishi, N. and Furuta, H. (1987), "Reliability Analysis of Damaged Structures", *Proc. of ICASP-5, Vancouver, Canada*, Vol. 1, pp.190-197.

(Received July 31, 2003)

Comparative study of vibration-based structural damage identification methods

Sherif Beskhyroun*, Toshiyuki Oshima**, Shuichi Mikami*** and Tomoyuki Yamazaki****

*Doctoral Student, Dept. of Civil Eng., Kitami Institute of Technology, (165 Koen-cho, Kitami, 090-8507)
**Professor, Dept. of Civil Eng., Kitami Institute of Technology, (165 Koen-cho, Kitami, 090-8507)
***Assoc. Professor, Dept. of Civil Eng., Kitami Institute of Technology, (165 Koen-cho, Kitami, 090-8507)
****Research Assoc., Dept. of Civil Eng., Kitami Institute of Technology, (165 Koen-cho, Kitami, 090-8507)

This paper provides an overview of methods to detect, locate, and characterize damage in structural and mechanical systems by examining changes in measured vibration response. The basic idea behind this technology is that modal parameters (notably frequencies, mode shapes, and modal damping) are functions of the physical properties of the structure (mass, damping, and stiffness). Therefore, changes in the physical properties will cause detectable changes in the modal properties. The paper compares the applicability and accuracy of four different damage identification methods to detect and locate different damage types. Some improvement has been introduced to these methods in order to increase the accuracy of localizing the damage position.

Key Words: *vibration characteristics, damage detection, modal properties*

1. Introduction

The basic idea of vibration based damage detection is that modal parameters (frequencies, mode shapes, and modal damping) are a function of the physical properties of the structure (mass, damping, stiffness, and boundary conditions). Therefore, changes in physical properties of the structure, such as its stiffness or flexibility, will cause changes in the modal properties[1), 2)]. Vibration-based structural damage detection and evaluation can be categorized into the following four levels: (I) detecting the existence of damage, (II) finding the location of damage, (III) estimating the extent of damage, and (IV) predicting the remaining load carrying capacity and fatigue life[3)]. In this paper, only levels (I), (II) and (III) are concerned.

Different damage detection methods, based on the changes in frequency and modal shape, are applied in this paper. Structural damage is determined by using different vibration characteristics. Strain energy distribution of each mode, curvature change of modal shape and change of flexibility matrix are used in different damage detection methods. Those methods are explained in more details in chapter 4. Four different damage identification methods are applied and compared using experimental and numerical data extracted from simple steel beam after releasing some supporting bolts. Two multi-layer piezoelectric actuators are used for local excitation and acceleration of structural member is measured and analyzed to find the changes of modal parameters as an effect of structural damage. Finite element model of the real beam is used to produce different types and positions of damage. Effectiveness in detecting different damage types, localizing the damage and measuring the damage increase is compared for the different damage detection methods. Modification in applying these methods is introduced to improve the accuracy of localizing the damage position.

2. Measurements by two actuators system

2.1 Experimental equipments

In this research a simple steel beam supported by four bolts in both sides has been examined before and after releasing some bolts as shown in Fig. 1. The multi-layer piezoelectric actuator is used for local excitation. The main advantage of using piezoelectric actuators is that it produces vibration with different frequencies ranging from 0 to 400 Hz that is effective in measuring higher modes. Main characteristics of equipment used in this experiment are shown in Table 1. Oshima et al.[4)] have measured and evaluated the location of released bolts by using one excitation actuator system. In this paper we use two actuators excitation system, which has more advantages than one actuator system. Larger amplitude of vibration and more complicated vibration modes will be produced by using multiple actuators in excitation system.

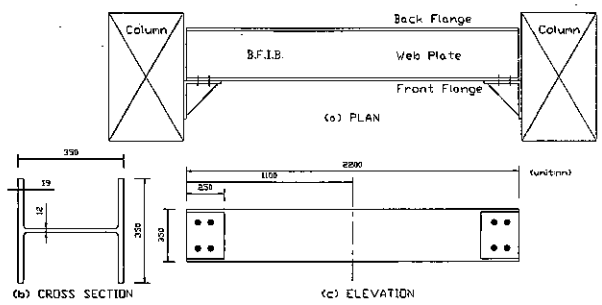

Fig. 1 Beam dimensions

Table 1 Equipment characteristics

Piezoelectric actuator	
Dimensions (W×T×H)	10×10×20(mm)
Min. and Max freq.	0~982Hz
Displacement (100V)	12.3 μm
Max Force	3500N
Wave function generator	
Min. and Max freq.	0.01 μHz~15MHz
Max. Output Volt	20Vp-p/OPEN, ±10V/OPEN
Power source	
Max. Power	150V

2.2 Measurement of mode shapes and resonant frequencies for undamaged and damaged structure.

The main objective in this section is to determine different mode shapes and resonant frequencies for the beam before and after each case of damage. The measured mode shapes and frequencies before and after each case of damage will be compared using different damage identification methods in order to detect and localize small types of damage. Two cases of damage are introduced to the left support of the beam. Case 0 represents the undamaged beam, Case 1 represents one bolt released, the upper right bolt from the left support, and Case 2 after releasing two bolts, the upper right and the lower right bolts as shown in Fig. 2.

Two piezoelectric actuators having the same waveform were used for excitation. Nine accelerometers and one reference accelerometer were used to measure the beam response. Position of actuators and accelerometers is shown in Fig. 3. Cross power spectrum for the measured acceleration between one reference channel and different measuring points are calculated. Mode shapes were determined from amplitude and phase information contained in CPS of the various accelerometer readings relative to the reference accelerometer. Resonant frequencies and mode shapes are measured for the undamaged beam as well as for each case of damage and these data will be used in the different damage identification methods.

3. Numerical model

The finite element model of the actual beam is created using Structural Analysis Program, SAP2000. The model is benchmarked against the measured frequencies of the actual beam[1), 5)]. Case 1 of damage is simulated by removing the springs in all directions X, Y, and Z at 4 nodes and Case 2 is simulated similarly by removing springs at 8 nodes. Mode shapes and frequencies given by the numerical model before and after each case of damage will be compared using the same damage identification methods in order to compare the results of the damage detection methods for both experimental and numerical data. The numerical model is used to introduce more damage cases, crack type, in order to compare the results of the different damage identification methods when they are applied to different damage types (crack and bolt release) moreover to examine the effect of used modes and the effect of accelerometer position relative to damage position.

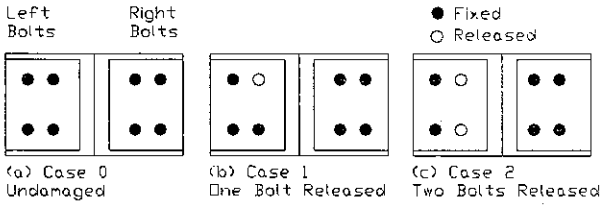

Fig. 2 Damage cases

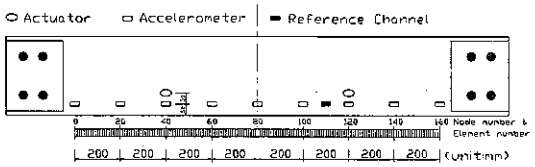

Fig. 3 Actuators and accelerometers positions

4. Damage detection methods.

In this section a brief summary of each method will be summarized. For a more detailed summary the reader is referred to the cited references.

4.1 Damage index method

This method [1), 2), 6)] is used to detect and locate damage in structures using mode shapes before and after damage. For a structure that can be represented as a beam, a damage index β is developed based on the change in strain energy stored in the structure when it deforms in its particular mode shape. For location j on the beam this change in the i^{th} mode strain energy is related to the change in curvature of the mode at location j. The damage index for this location and this mode, β_{ij}, is defined as

$$\beta_{ij} = \frac{\left(\int_a^b [\psi_i^{*''}(x)]^2 dx + \int_0^L [\psi_i^{*''}(x)]^2 dx\right)\int_0^L [\psi_i''(x)]^2 dx}{\left(\int_a^b [\psi_i''(x)]^2 dx + \int_0^L [\psi_i''(x)]^2 dx\right)\int_0^L [\psi_i^{*''}(x)]^2 dx} \quad (1)$$

where $\psi''(x)$ $\psi^{*''}(x)$ are the second derivative of i^{th} mode shape corresponding to the undamaged and damaged structure, respectively. L is beam length and a, b are the limits for element j. When more than one mode is used, damage index is defined as the sum of damage

indices from each mode as follows

$$\beta_j = \sum_{i=1}^{n} \beta_{ij} \tag{2}$$

where n is the number of modes. Assuming that the collection of the damage indices, β_j, represents a sample population of a normally distributed random variable, a normalized damage localization indicator is obtained as follows

$$Z_j = \frac{\beta_j - \overline{\beta_j}}{\sigma_j} \tag{3}$$

where $\overline{\beta_j}$ and σ_j represent the mean and standard deviation of the damage indices, respectively. A statistical decision making procedure is employed to determine if the normalized damage index, Z_j, is associated with a damage location. Values of two standard deviations from the mean are assumed to be associated with damage locations.

4.2 Mode shape curvature method

In formulating the eigenvalue problem, i.e. Eq. (4), structural damage only affects the stiffness matrix and not the mass matrix[1),2),7)]. For the undamaged condition the eigenvalue problem is given as

$$([K] - \lambda_i[M])\{x_i\} = \{0\} \tag{4}$$

where [K] = the stiffness matrix, λ_i = the i^{th} eigenvalue, [M] = the mass matrix, and $\{x_i\}$ = the i^{th} displacement eigenvector.
Similarly, the eigenvalue problem for the damaged condition is

$$([K^*] - \lambda_i^*[M])\{x_i^*\} = \{0\} \tag{5}$$

where the asterisks signify properties of the damaged structure. Eigenvectors for the damaged and undamaged structure are the basis for damage detection. For a beam cross section subjected to a bending moment M(x), the curvature at location x, $v''(x)$, is given by

$$v''(x) = M(x) / EI \tag{6}$$

where E = the modulus of elasticity and I = the moment of inertia of the section. From Eq. (6), it is shown that the curvature of the beam is proportional to the inverse of the stiffness for a given moment. Therefore for the same moment applied to the structure before and after damage, any reduction in the stiffness of the structure associated with damage will increase the curvature. Furthermore, the amount of change in the mode shape curvature is proportional to the level of damage. Higher level of damage, which means larger reduction in stiffness, will lead to larger change in curvature. Maximum difference in mode shape curvature before and after damage indicates the position of damage.

4.3 Change in flexibility method

Flexibility matrix, [F], of a structure may be expressed in terms of modal parameters as follows[1),2),8)]

$$[F] \approx [\Phi][\Omega]^{-1}[\Phi]^T \approx \sum_{i=1}^{n} \frac{1}{\omega_i^2} \{\phi_i\}\{\phi_i\}^T \tag{7}$$

where $\{\phi_i\}$ = the i^{th} mass-normalized mode shape, [Φ] = the mode shape matrix= $[\phi_1, \phi_2 \ldots \phi_n]$, (ω_i) = the i^{th} modal frequency, [Ω] = the modal stiffness matrix = diag. (ω_i^2), and n = the number of measured or calculated modes.
Similarly, for the damaged structure

$$[F^*] \approx [\Phi^*][\Omega^*]^{-1}[\Phi^*]^T \approx \sum_{i=1}^{n} \frac{1}{(\omega_i^*)^2} \{\phi_i^*\}\{\phi_i^*\}^T \tag{8}$$

where the asterisks signify properties of the damaged structure. Flexibility of a point k may be interpreted as a measure of the energy in a structure due to a unit load at node k. Hence, variation of flexibility coefficients in the neighborhood of a node k may reveal damage localized in its vicinity[9)]. Therefore the change in flexibility caused by the damage can be obtained as follows

$$[\Delta F] = [F] - [F^*] \tag{9}$$

where ΔF represents the change in flexibility matrix. Now, for each column of matrix ΔF let δ_j be the absolute maximum value of the elements in the j^{th} column. Hence,

$$\delta_j = \max|\delta_{ij}|, \; i = 1,\ldots n \tag{10}$$

where δ_{ij} are elements of matrix ΔF and n is the number of degrees of freedom. The degree of freedom corresponding to the maximum value of δ_j indicates the position of damage.

4.4 Change in uniform load surface curvature method

In this method certain aspects of the mode shape curvature method and change in flexibility method are combined[1),2),10)]. In this method the change in curvature is obtained from the uniform flexibility shape instead of the mode shapes. Recall that the flexibility matrices, before and after damage, can be expressed in terms of modal parameters as:

$$[F] \approx [\Phi][\Omega]^{-1}[\Phi]^T \approx \sum_{i=1}^{n} \frac{1}{\omega_i^2} \{\phi_i\}\{\phi_i\}^T \tag{11}$$

and

$$[F^*] \approx [\Phi^*][\Omega^*]^{-1}[\Phi^*]^T \approx \sum_{i=1}^{n} \frac{1}{(\omega_i^*)^2} \{\phi_i^*\}\{\phi_i^*\}^T \tag{12}$$

where the asterisks designate the damaged structure. The coefficients of the i^{th} column in the flexibility matrix represent the deflected shape assumed by the structure with a unit load applied at the i^{th} degree of freedom. Change in curvature of the uniform load flexibility is used to determine the location of damage. The uniform load flexibility represents the deflected shape assumed by the structure when all degrees of freedom are loaded with a unit load. Thus, the uniform

load flexibility corresponds to the sum of the unit load flexibilities. In terms of the unit load flexibilities, the curvature change is evaluated as follows

$$\{\Delta\} = \sum_{i=1}^{n} \left| \{F_i^{*n}\} - \{F_i^{n}\} \right| \tag{13}$$

where $\{\Delta\}$ and n represent the absolute curvature change and the number of degrees of freedom, respectively. The degree of freedom corresponding to the maximum value of $\{\Delta\}$ indicates the position of damage.

5. Application of different damage identification methods to experimental and numerical data for released bolt damage case.

5. 1 Damage identification methods applied to experimental data

Different mode shapes of the beam are measured at nine points as was explained in section 2.2. Interpolation between the measured points using cubic polynomial has been made to approximate mode shape amplitudes between sensors. This interpolation introduces artificial degrees of freedom into the experimental data[1]. By using this technique, the beam was divided into 160 nodes starting from the first left accelerometer as shown in Fig.3. Fig. 4 shows the results from different damage identification methods when they are applied to experimental data for case 1 of damage. In Fig. 4-a, damage index exceeds the value of two at elements 40 and 120, which indicates the occurrence of damage. Position 40 is close to the damage position but position 120 is false position. For the change in mode shape curvature method the maximum change occurs at nodes 100 and 120 as shown in Fig. 4-b. The same remarks are obtained for change in flexibility method and change in flexibility shape curvature method as shown in Figs. 4-c and 4-d, respectively. From the previous results, the following remarks are concluded that all methods indicated the existence of damage from the first case of damage, the indicated positions of damage are similar for most of methods but no method could determine the position of damage accurately. These results will be verified using the numerical data extracted from the finite element model.

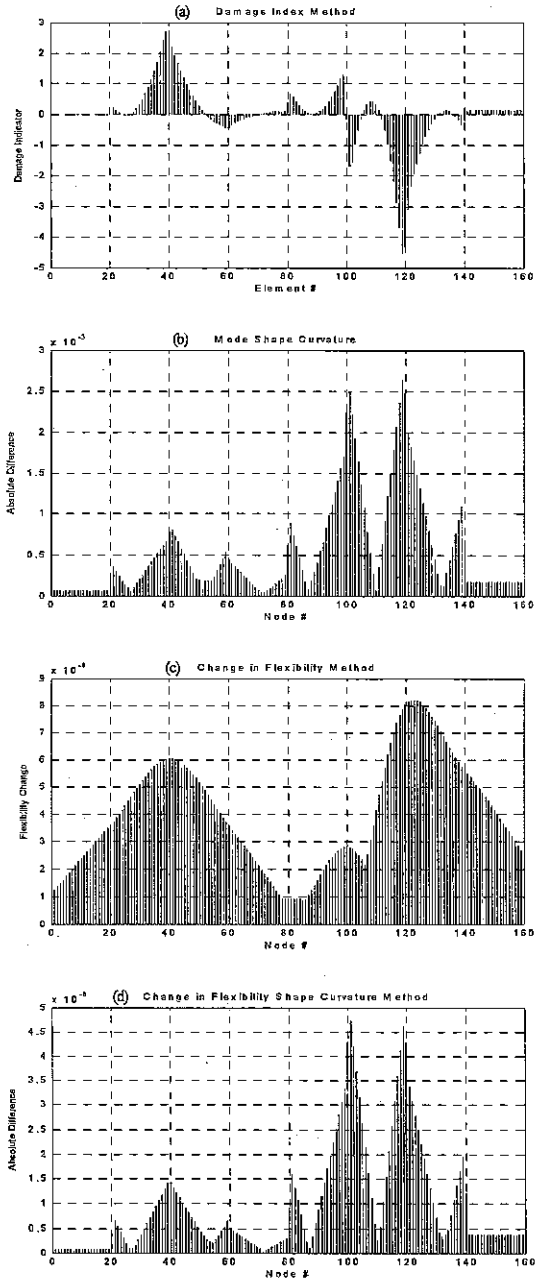

Fig. 4 Damage detection methods applied to experimental data for damage Case 1.

5.2 Damage identification methods applied to numerical data

Similar to experimental data, mode shapes were measured along nine points on the front flange, and then interpolation between the measured points using cubic polynomial has been made to approximate mode shape amplitude between the measured points. Therefore the beam is also divided into 160 nodes as shown in Fig. 3. Damage detection methods were applied to the numerical data after introducing two cases of bolt release simulating the actual cases of damage. Damage index method indicated damage at element 20, which is very close to the actual position of damage, for both cases of damage. All other methods could detect the occurrence of damage but the position of damage could be determined close to the actual position only by change in flexibility method and change in flexibility shape curvature method for case 2. It is therefore very difficult to determine the position of the released bolt accurately because no response can be measured at the fixed ends of the beam.

5.3 Damage position as indicated by different methods

Table 2 summarizes the position of damage as indicated by different damage methods for experimental and numerical data for both cases of damage. It is observed that the numerical results are consistent with the experimental results and damage position is determined more accurately for the numerical data. Therefore, the finite element model can be used to produce different damage types, positions and sizes of damage and hence the results of different damage identification methods for each type of damage are obtained.

Table 2 Damage position as indicated by different damage methods*)

Damage method	Dam. position (Exp. data)		Dam. position (Num. data)	
	Case 1	Case 2	Case 1	Case 2
Damage index	40, 120	40, 100, 120	20	20
Mode shape curavature	100, 120	100, 120	40, 120	40, 120
Change in flexibility	40, 120	40, 120	120	0, 40
Uniform load surface curvature	100, 120	100, 120	20, 120	20

*) Number in table indicates node number or element number.

These results can be used to estimate the type and position of damage from the results of the actual structure. Damage index method has shown the best results in detecting and localizing the damage from the first case of damage and for both experimental and numerical data for the bolt release case.

6. Application of different damage identification methods to numerical data for crack damage case.

In this chapter, different damage detection methods will be applied to numerical data after making one crack in order to compare the results of the different methods when they are applied to different types of damage. The position of the same crack will be changed to three different positions to examine the change of the most sensitive modes with the change of damage location. At the end of this chapter mode shapes will be measured on another line far from the crack position to determine the effect of the position of accelerometers to the accuracy of the results.

6.1 The effect of used modes in different damage identification methods

In this section, the numerical model is used to compare the effect of chosen modes that can be used in damage identification methods. One crack, 3 mm in width and 50 mm in length, is made as shown in Fig. 5. The position of the same crack is changed as indicated by crack 1 at point 20, crack 2 at point 50 and crack 3 at point 90 as shown in Fig. 5 in order to examine the change of the effective modes with the position of damage.

For the different damage identification methods, we used one mode only (from mode 1 to mode 9), then we used the first three modes together and finally we used the nine modes together. Tables 3, 4 and 5 show the measured position of damage by the different methods using different mode shapes for crack 1, crack 2 and crack 3, respectively. By comparing the results of the three tables the following remarks can be concluded:

1- For damage index method: the sensitive modes are changed with the change of crack position. Using the first three modes gave good results for the three different crack positions and using all modes gave very accurate results.
2- For change in mode curvature method: the sensitive modes are changed with the change of crack position. Using the first three modes gave better results than using all modes.
3- For change in flexibility method: it was observed that at mode 4 the results are always accurate even with the change of the crack position and the same remark can be observed for mode 5 with less accuracy. Using the first three modes gave the same results as using all modes.
4- For change in flexibility shape curvature method: it was observed that modes 4 and 5 are always the most sensitive for the three different crack positions. Using the first three modes gave the same results as using all modes.

6.2 The effect of position of measured modes relative to the damage position.

Table 6 shows the measured position of damage by the different damage detection methods when mode shapes are measured along position B as shown in Fig. 5. Position B lies 250 mm from the crack tip and position A lies exactly on the crack tip. By comparing the

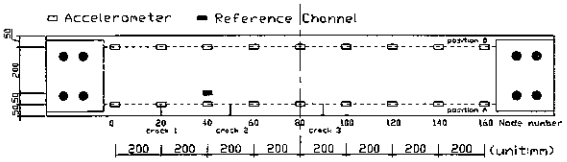

Fig. 5 Crack and accelerometers position

Table 3 Measured position of damage for crack 1 (at node 20)

	Dam. Ind.	Mod. Curv.	Ch. Flex.	Flex. Curv.
Mode 1	20, 40	20	25	20
Mode 2	40	20	25	20
Mode 3	40, 60	40	40	40
Mode 4	20, 40	20	20	20
Mode 5	20	20, 40	20	20
Mode 6	20	20, 40	20	20, 40
Mode 7	20	20, 40	20	20, 40
Mode 8	20	20, 80, 120	20	20, 40
Mode 9	20	20, 80, 120	20	20, 40
Mode 1,2,3	20	20	25	20
All modes	20	20	20	20

Table 4 Measured position of damage for crack 2 (at node 50)

	Dam. Ind.	Mod. Curv.	Ch. Flex.	Flex. Curv.
Mode 1	40, 60	60	60	60
Mode 2	60	60	60	60
Mode 3	60, 80	60	60	60
Mode 4	40	20, 40	50	20, 40
Mode 5	20, 40	40	40	40
Mode 6	20, 40, 60	60	130	60
Mode 7	40, 60	40, 60	30, 70, 130	40, 60
Mode 8	40, 60	40, 60, 80	30, 70	40, 60
Mode 9	40, 60	40, 60, 80	40, 70	40, 60
Mode 1,2,3	60	60	60	60
All modes	40, 60	40, 60, 80	60	60

Table 5 Measured position of damage for crack 3 (at node 90)

	Dam. Ind.	Mod. Curv.	Ch. Flex.	Flex. Curv.
Mode 1	80, 120	80, 120	80, 120	80, 120
Mode 2	100, 120	100, 120	100, 120	100, 120
Mode 3	100, 120	100, 120	90	100, 120
Mode 4	100, 120	100	97	100
Mode 5	100	100	100	100
Mode 6	80, 120	80	30	40, 80, 100
Mode 7	80	80	120	80
Mode 8	100, 120	40, 80, 120	20, 90, 120	100, 120
Mode 9	100, 120	40, 80, 120	90, 120	100, 120
Mode 1,2,3	100, 120	100, 120	80, 120	120
All modes	100	40, 80, 120	80, 120	120

Table 6 Measured position of damage for crack 2 (at node 50) and accelerometers are positioned at line B

	Dam. Ind.	Mod. Curv.	Ch. Flex.	Flex. Curv.
Mode 1	60	20, 60	60	20, 60
Mode 2	60	20, 60	65	20, 60
Mode 3	20, 60	20, 60	60	20, 60
Mode 4	40	40	50, 110	40
Mode 5	20, 40	40	40, 110	40
Mode 6	60, 80	60, 80, 120	30, 70, 130	60, 80, 120
Mode 7	60, 80	60, 80, 120	40, 130	60, 80
Mode 8	60, 80, 100	40, 80, 120	30, 70, 130	40, 60, 80
Mode 9	60, 80, 100	40, 80, 120	70, 130	40, 60, 80
Mode 1,2,3	60	20, 60	70	20, 60
All modes	60, 80, 100	40, 80, 120	70	20, 60

results of tables 4 and 6 it can be shown that the accuracy of determining the position of damage is affected and the number of false position of damage increased in all methods.

6.3 Evaluating damage increase

In this section, crack size at node 20 is increased from 3 * 50 mm to 3 * 75 mm. Fig. 6 shows the results of different damage identification methods when they are applied to the two crack sizes. It was observed that the damage measure decreased after increasing the crack length for damage index method and change in mode shape curvature method as shown in Figs. 6-a and 6-b, respectively. For change in flexibility method and change in flexibility shape curvature method, the measure of damage increased with the increase in crack length as shown in Figs. 6-c and 6-d, respectively. Therefore change in flexibility method and change in flexibility shape curvature method have shown better results in measuring the damage increase than damage index method and change in mode shape curvature method.

6.4 Detection of multiple damage position

The same cracks at nodes 20 and 90 as described in section 6.1 were used together in order to compare the results of different damage identification methods to detect multiple damage positions. Results from the different methods are shown in Fig. 7. In Fig. 7-a, damage index method indicated the damage at elements 20 and 100. In Fig. 7-b, change in mode curvature method showed poor result in indicating the damage position. Both change in flexibility method and change in flexibility shape curvature method determined the position at node 20 only but they did not indicate the damage at node 90 as shown in Figs. 7-c and 7-d, respectively.

7. Improving the accuracy of localizing the damage position

When more than one mode is used in damage detection methods, the damage measure is summed over the different modes for each individual element (or node) as explained in chapter 4. In this section another technique will be used. Each damage detection method will be applied using only one mode and then the maximum change among different elements (or nodes) and among different modes will be used as a limit. The damage measures less than this limit will be omitted and the damage measures equal this limit will be added together for each element (or node) over different modes. By using this technique, false damage position can be omitted effectively. Fig. 8 shows the results of damage detection methods when they are applied to detect crack at position 50 when the mode shapes are measured at line B and Fig. 9 shows the results after applying the new technique. By comparing Fig. 8 to Fig. 9, it can be shown that the position of damage is determined more accurately using the new technique in damage index, mode curvature and change in flexibility methods. Table 7 summarizes the results of different methods after applying the new technique. Comparing the results in this table with the results in tables 3,4,5 and 6, when all modes are used, it is shown that results are improved specially in damage index and mode shape curvature methods. Damage index method has shown the best results among the different methods in localizing the damage position.

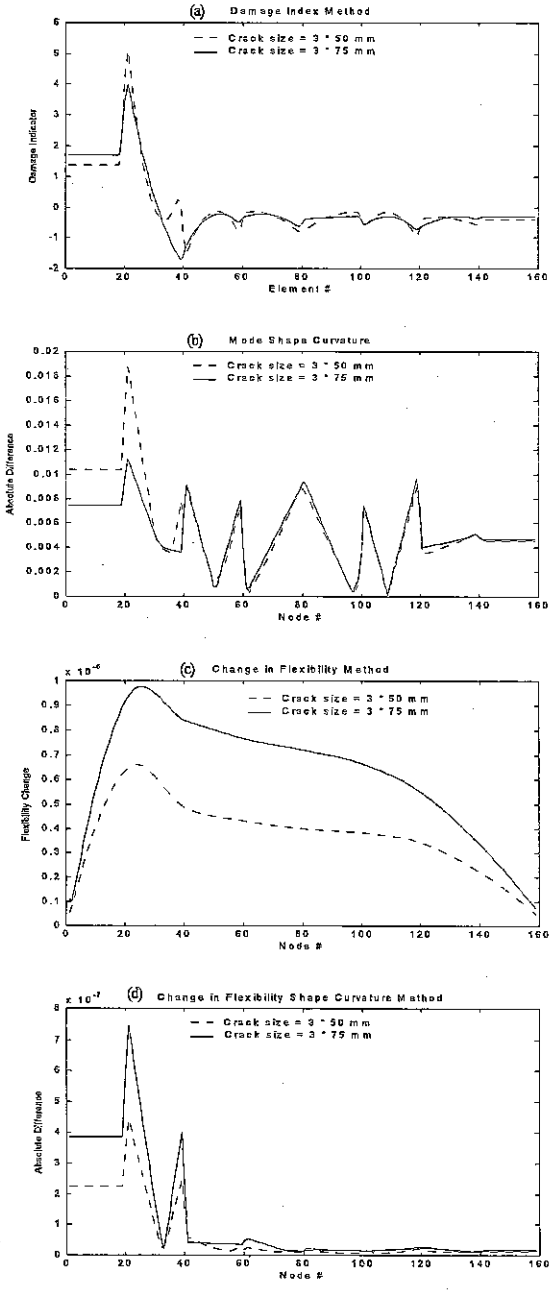

Fig. 6 Damage detection methods applied to numerical data for damage at node 20 for different crack size.

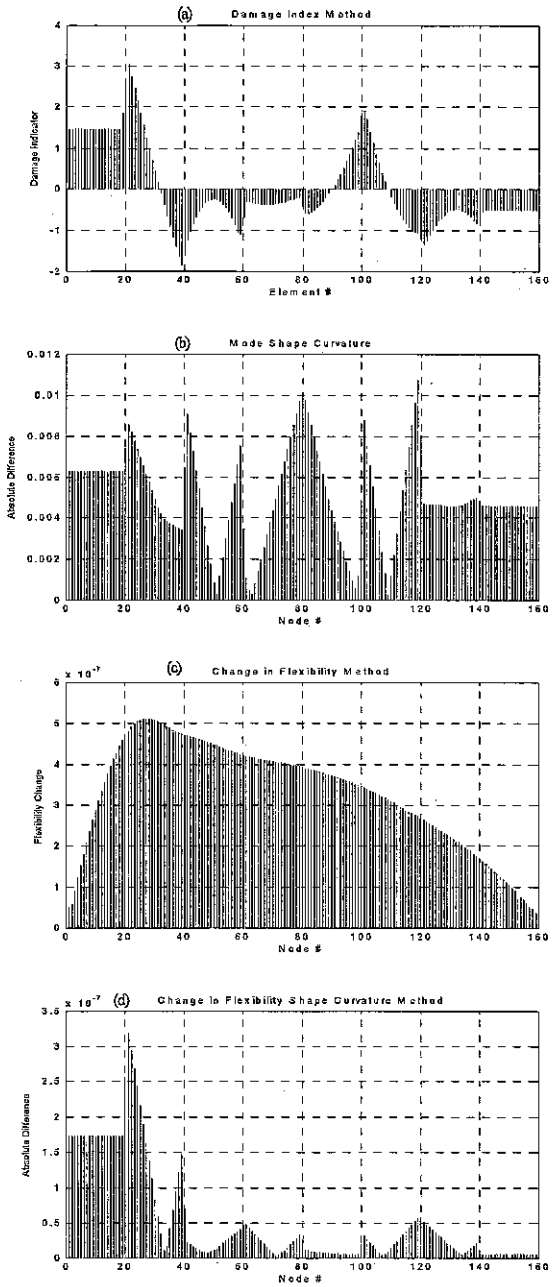

Fig. 7 Damage detection methods applied to numerical data for damage at nodes 20 and 90.

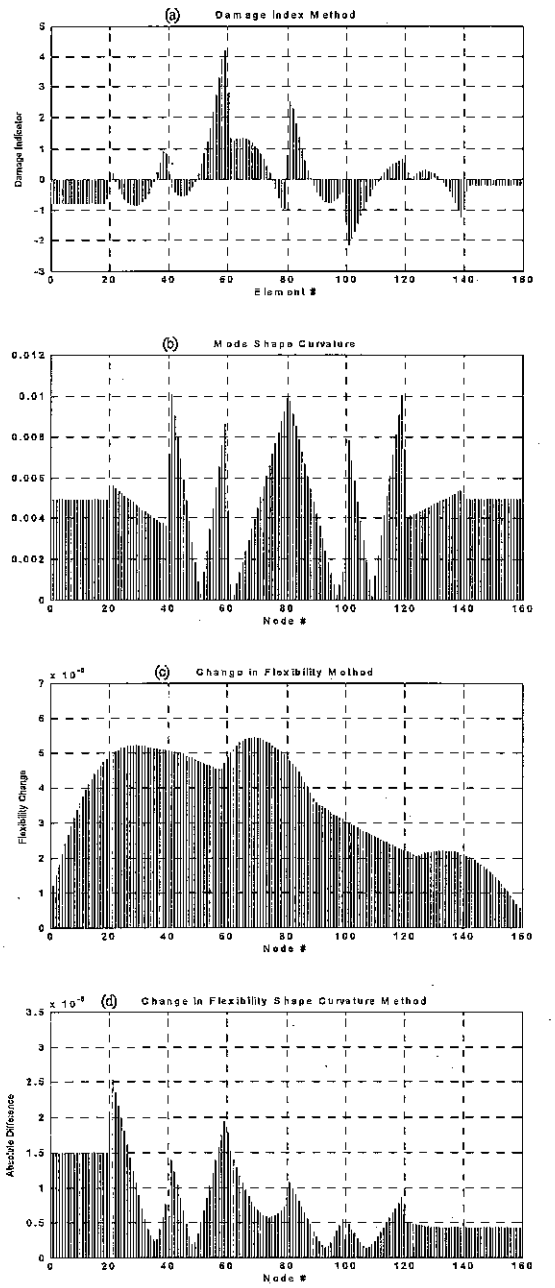

Fig. 8 Damage detection methods applied to numerical data for damage at node 50 and mode shapes are measured along Line B.

Table 7 Damage position as indicated by different damage methods for cracks at nodes 20, 50 and 90*)

	Cr. at 20	Cr. at 90	Cr. at 50	
			Posit. A	Posit. B
Dam. Ind.	20	100	40	60
Mod. Curv.	20	120	42	42
Ch. Flex.	25	120	62	65
Flex. Sh. Curv.	20	120	60	21

*) Number in table indicates node number or element number.

8. Concluding remarks

(1) All damage detection methods can detect the existence of damage for both types of damage introduced in this research but those methods are more sensitive in localizing the damage position for crack type of damage than in case of released bolts.

(2) The sensitive modes that should be used with each method are changed with the change of damage type, damage position and the used method. Damage index method has shown the best results when the first few modes or all measured modes are used. In change flexibility method and change in flexibility shape curvature method, the same sensitive modes remained the same even after changing the position of crack to three different positions.

(3) The accuracy of localizing the damage position is reduced in all methods when the position of measured modes is moved farther from the crack position.

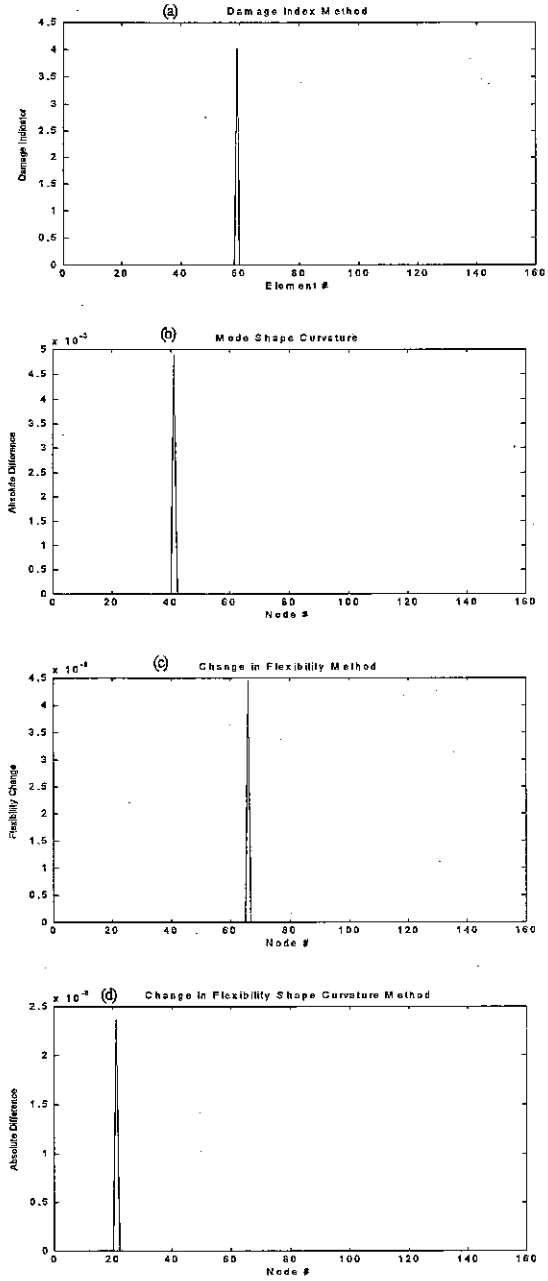

Fig. 9 Modified damage detection methods applied to numerical data for damage at node 50 and mode shapes are measured along Line B.

(4) Damage index method has shown the best results among the different methods in detecting and localizing the damage. This method has shown the best results in detecting multiple damage positions.

(5) Change in flexibility method and change in flexibility shape curvature method have shown better results in measuring the damage increase than damage index method and change in mode shape curvature methods.

(6) The accuracy of localizing the damage position is improved in damage index, mode curvature and change in flexibility methods after applying the new technique explained in chapter 7.

Acknowledgement

This research is supported by the Grant-in-Aids for Scientific Research, Ministry of Education. The authors wish to thank for this support.

References

1) Farrar C. R. and D. A. Jauregui, *Damage Detection Algorithms Applied to Experimental and Numerical Model Data from the I-40 Bridge*, Los Alamos National Laboratory Report, LA-12979-MS, 1996.

2) Farrar C. R. and D. A. Jauregui, Comparative study of damage identification algorithms applied to a bridge: I. Experiment, *Smart Mater. Struct.* 7 pp.704-719, 1998.

3) Ton-Lo Wang and Zhouhong Zong, *Improvement of Evaluation Method for Existing Highway Bridge*, Florida International University, Report No. FL/DOT/RMC/6672-818, March 2002.

4) Oshima T. et al., Study on damage evaluation of joint in steel member by using local vibration excitation, *Journal of Applied Mechanics*, Vol.5, pp.837-846, 2002.

5) Farrar, C. R. and D. A. Jauregui, Comparative study of damage identification algorithms applied to a bridge: II. Numerical study, *Smart Mater. Struct.* 7 pp.704-719, 1998.

6) Stubbs N., J. T. Kim, and C. R. Farrar, Field Verification of a Nondestructive Damage Localization and Sensitivity Estimator Algorithm, *Proceedings of the 13th International Modal Analysis Conference*, pp. 210-218, 1995.

7) Pandey A. K., Biswas M. and Samman M. M., Damage detection from changes in curvature mode shapes, *J. Sound Vib.* 145 pp.321-332, 1991.

8) Pandey A. K., Biswas M., Damage detection in structures using changes in flexibility, *J. Sound Vib.* 169 pp.3-17, 1994.

9) Raghavendrachar M. and Aktan A. E., Flexibility by multireference impact testing for bridge diagnostics, *Structural Engineering*, Vol. 118, No.8, pp.2186-2203, 1990.

10) Zhang Z. and Aktan A. E., The damage indices for the constructed facilities, *Proc. 13th Int. Modal Analysis Conf.* Vol 2, pp.1520-1529, 1995.

(Received: July 31, 2003)

Optimal Sensor Locations for Long-term Structural Health Monitoring

Soobong Shin*, Soon-Jung Kwon**, Young-Hwan Park***

* Ph.D., Assistant Professor, Dept. of Civil Eng., Inha University, 253 Yonghyun-dong, Nam-ku, Incheon 402-751, Korea
** M.S., Graduate Student, Dept. of Civil Eng., Inha University, 253 Yonghyun-dong, Nam-ku, Incheon 402-751, Korea
*** Ph.D., Research Fellow, Civil Eng., Div., KICT, 2311 Taehwa-dong, Ilsan-ku, Koyang-si, Kyonggi-do 411-712, Korea

The paper presents a methodology to determine optimal accelerometer locations for long-term structural health monitoring where structural condition is assessed by modal system identification. A Fisher information matrix in terms of mode shape sensitivity is formulated with respect to structural parameters by the maximum likelihood approach. A scheme of effective independence distribution vector has been applied to determine optimal accelerometer locations. To reflect the role of critical members for the structural safety, a way of implementing importance weight in selecting sensor locations is proposed. Simulation studies have been carried out on a multi-girder multi-span bridge to examine the proposed algorithm.

Key Words: optimal accelerometer locations, long-term monitoring, system identification

1. Introduction

Sensor layout is one of the important tasks to provide useful information for a long-term structural health monitoring system. Various types of sensors are installed for different purposes. Some sensors are for checking environmental conditions such as wind velocity or temperature fluctuation and others are for catching any change in structural behaviors. Strain gages may be the most economical and widely applied type of sensors for checking local change in a structure while accelerometers for global behavior of the structure. Although diverse types of sensors are applied in actual applications, however, the main focus of any sensor is to provide information useful for guaranteeing the structural safety as efficient and economical as possible.

Structural condition assessment methods using these measured response data can be categorized into model-based and non-model-based ones. Non-model-based methods usually define condition indices using raw time-history response data or transformed frequency response data[1]. One of the advantages of this approach is the simplicity and applicability without a complicated process of defining a mathematical model for the structure. Sensors for checking local change may be more fit to this category. However, one vivid disadvantage of these methods is the fact that a local sensor can provide information of only limited surrounding region and can be less influenced by distant events. On the other hand, model-based methods usually define mathematical models by identifying structural parameters using measured response data[2]. System identification (SI) method is a typical example of the model-based methods. Sensors for global behaviors may be more fit to this category with almost opposite advantages and disadvantages to those of the local sensors.

The current study is to develop a scheme of determining optimal accelerometer locations (OAL). Accelerometers have been widely applied for long-term structural health monitoring, and the obtained acceleration data can provide useful information on the global behavior of a structure. To locate accelerometers for long-term monitoring of structural behaviors, the number and locations are generally fixed in the design stage of a monitoring system. This situation is a little different from the case of load-carrying tests for achieving modal data of a structure where locations of accelerometers can be moved during series of tests with a fixed reference location. Selection of accelerometer locations has usually been determined based on structural analysis, structural symmetry, conventional choice, or engineers' experience rather than a systematic procedure. Especially when the number of accelerometers and the number of possible observation points are limited, the use of an effective OAL scheme is desirable.

Various methods for determining optimal sensor locations (OSL) have been introduced[3-8]. It is generally known that OSL can be determined by maximizing characteristic properties of Fisher information matrix (FIM), which may yield a possible minimum covariance of the estimation error[8-9]. Penny et al. evaluated some OSL methods and observed that it is better to combine Guyan reduction scheme with a scheme of effective independence distribution vector (EIDV) defined by mode shapes[8]. Sensitivity analyses in OSL problems were studied for applying SI schemes[10-11]. Fadale et al. proposed that estimation of structural parameters can be improved by locating sensors at the locations of maximum sensitivity[12].

The paper proposes an OAL algorithm based on the maximum likelihood (ML) approach by Fadale et al.[12]. Through mathematical manipulations with assumptions on measurement noise and by applying the Cramer-Rao inequality, a FIM is obtained as the inverse of the lower bound of the estimation error. Each column of the obtained FIM is a vector of mode shape sensitivity with respect to each unknown structural parameter. Minimization of the ML functional introduces the minimization of the output error of mode shapes through assumptions on measurement noise. The applied SI scheme estimates structural parameters by minimizing a least squared objective function defined by the output error in mode shapes and an additional regularization function[2]. Rank deficiency in the computed FIM may occur due to the linear dependence in the vectors of computed mode shape sensitivities. The paper applies a truncated singular value decomposition scheme to overcome the rank deficiency problem with a pre-defined tolerance for the singular values.

Simulation studies on a two-span multi-girder bridge model have been carried out to examine the proposed OAL algorithm. To examine and evaluate the properness of the proposed OAL scheme for modal SI applications, the estimated parameters using measured acceleration data at the locations by the proposed OAL algorithm are compared with those by a customary choice and also with those by a FIM of mode shape themselves as proposed by Penny et al.[8]. For the simulation studies, it has been assumed that the number of available accelerometers is pre-defined and all the accelerometers have equal noise sensitivity.

To consider the importance of critical members for the structural safety in selecting OAL, a way of implementing importance weight is proposed in the paper. For the current context of the study, the importance weight is defined based on the sum of static strain energies obtained by locating a vertical unit load on every node in a bridge model. In addition to the selection of critical members based on the strain energy, weighting on the presumed critical members around the supports are also simulated through the simulation studies.

2. OAL Algorithm for Long-Term Monitoring

The undamped linear governing modal equation can be written as follows.

$$\mathbf{K}(\mathbf{x}) = \lambda_i \mathbf{M} \phi_i(\mathbf{x}) \tag{1}$$

where λ_i = the i-th eigenvalue, $\mathbf{x}(N_p \times 1)$ = unknown structural parameters, $\mathbf{K}(N \times N)$, $\mathbf{M}(N \times N)$ = stiffness and mass matrix, $\phi_i(N \times 1)$ = modal displacement vector of mode i, N_p = number of unknown parameters, and N = number of degrees of freedom (DOF), respectively. In Eq.(1), it is assumed that stiffness is the only unknown structural parameter and mass is the *a priori* information.

In a large scale civil structure, responses can be measured at only limited DOF in the analytical model. The modal displacement vector ϕ_i can be decomposed into measured and unmeasured DOF by

$$\phi_i(\mathbf{x}) = \left\{ \tilde{\phi}_i^T(\mathbf{x}) \quad \bar{\phi}_i^T(\mathbf{x}) \right\}^T \tag{2}$$

where $\tilde{\phi}_i(N_m \times 1)$, $\bar{\phi}_i(N_u \times 1)$ = parts of modal displacement vector corresponding to measured and unmeasured DOF's and N_m, N_u = number of measured and unmeasured DOF, respectively.

The best estimates of structural parameters $\mathbf{x}$ by a modal system identification (SI) scheme can be obtained by maximizing the likelihood of the computed mode shapes relative to the measured ones. In other words, unknown parameters are reliably estimated by maximizing the probability density function of measurements defined by

$$f(\tilde{\Phi}_m \mid \mathbf{x}) = \left[(2\pi)^{N_m \times nmm} \prod_{i=1}^{nmm} \mathrm{Det}(\mathbf{S}_i) \right]^{-1/2} \times \exp\left[-\frac{1}{2} \sum_{i=1}^{nmm} \left(\tilde{\phi}_i(\mathbf{x}) - \tilde{\phi}_{mi} \right)^T \mathbf{S}_i^{-1} \left(\tilde{\phi}_i(\mathbf{x}) - \tilde{\phi}_{mi} \right) \right] \tag{3}$$

where $\tilde{\Phi}_m(N_m \times nmm)$ = measured modal displacement matrix defined by Eq.(4), nmm = number of measured modes, $\tilde{\phi}_{mi}(N_m \times 1)$ = measured modal displacement vector of mode i, and $\mathbf{S}_i(N_m \times N_m)$ = the covariance matrix of the measurements of the i-th mode, respectively.

$$\tilde{\Phi}_m = \begin{bmatrix} \vdots & & \vdots \\ \tilde{\phi}_{m1} & \cdots & \tilde{\phi}_{m,nmm} \\ \vdots & & \vdots \end{bmatrix} \tag{4}$$

By assuming that the experimental noise distribution is independent of the estimated structural parameters $\mathbf{x}$ and the variance of the measurement σ_n^2 is equal at all the measuring DOF's, the following least squared minimization problem of

Eq.(5) can be formulated by applying logarithm to the likelihood function of Eq.(3).

$$\text{Minimize } L(\mathbf{x}) = \sigma_n^{-2} \sum_{i=1}^{nmm} \left(\tilde{\phi}_i(\mathbf{x}) - \tilde{\phi}_{mi}\right)^T \left(\tilde{\phi}_i(\mathbf{x}) - \tilde{\phi}_{mi}\right) \quad (5)$$

The above equation is an output error estimator by the error between measured and computed mode shapes at the measured DOF. In order to solve the least-squared minimization problem, the identifiability criterion of $N_m \times nmm \geq N_p$ must be satisfied. If the condition is not satisfied, the system of equations will be under-determined so that multiple solutions may be possible if additional constraints are not provided.

By applying the Cramer-Rao inequality to Eq.(5), the inverse of a Fisher information matrix (FIM) $\mathbf{F}(N_p \times N_p)$ of Eq.(6) can be obtained as a lower bound of the estimation error.

$$\mathbf{F}(\tilde{\Phi}_m, \mathbf{x}) = \sum_{i=1}^{nmm} \left[\Theta_i^T \Theta_i\right] \quad (6)$$

where $\Theta_i(N_m \times N_p)$ = sensitivity matrix for mode i each column of which is the mode shape sensitivity with respect to each unknown parameter defined by Eq.(7).

$$\left(\Theta_i\right)_j = \frac{\partial \tilde{\phi}_i}{\partial x_j} \quad i = 1, 2, \ldots, nmm \quad j = 1, 2, \ldots, N_p \quad (7)$$

The mode shape sensitivity can be computed directly by solving Eq.(7) when only distinct eigen-values are considered. For a case of multiple eigen-values, a similar direct computation is also proposed by Lee and Jung[13].

$$\begin{bmatrix} \mathbf{K} - \lambda_i \mathbf{M} & -\mathbf{M}\phi_i \\ -\phi_i^T \mathbf{M} & \mathbf{0} \end{bmatrix} \begin{Bmatrix} \partial \phi_i / \partial x_j \\ \partial \lambda_i / \partial x_j \end{Bmatrix} = \begin{Bmatrix} -\mathbf{G}_j \\ 0.5\, \phi_i^T \mathbf{M} \end{Bmatrix} \phi_i \quad (8)$$

where x_j = the j-th structural parameter, and $\mathbf{G}_j(N \times N) = \partial \mathbf{K}(\mathbf{x}) / \partial x_j$ = the j-th kernel matrix composed of constant coefficients.

Because $\mathbf{M}$ is assumed as known and $\mathbf{K}$ and ϕ_i can be considered as given with estimated values of parameters $\mathbf{x}$ at an iteration step during the estimation process, the mode shape sensitivity can be expressed by

$$\left(\Theta_i\right)_j = \frac{\partial \tilde{\phi}_i}{\partial x_j} = \mathbf{D}_j^{(i)} \tilde{\phi}_i \quad (9)$$

where $\mathbf{D}_j^{(i)}(N_m \times N_m)$ = a constant coefficient matrix as a function of $(\lambda_i, \mathbf{x}, \phi_i, \mathbf{K}(\mathbf{x}), \mathbf{M}, \mathbf{G}_j)$.

Therefore, depending on the computed $\mathbf{G}_j$, the linear independence of the column vectors in Θ_i may not be guaranteed so that rank deficiency problem can occur. For a critical case that $\mathbf{G}$ is constant for all the members, $rank(\Theta_i) = 1$ can be possibly obtained.

To resolve the rank deficiency problem involved in Θ_i, the singular value decomposition scheme has been applied. The modal displacement matrix Θ_i can be decomposed with singular values as

$$\Theta_i = \mathbf{U}_i \mathbf{W}_i \mathbf{V}_i^T \quad (10)$$

where $\mathbf{U}_i(N_m \times N_p)$, $\mathbf{W}_i(N_p \times N_p)$, $\mathbf{V}_i(N_p \times N_p)$ = column orthogonal matrix, diagonal matrix defined by Eq.(11), and row orthogonal matrix of mode i, respectively, where $\mathbf{U}^T\mathbf{U} = \mathbf{V}^T\mathbf{V} = \mathbf{I}(N_p \times N_p)$. The diagonal matrix $\mathbf{W}_i$ is defined with singular values at the diagonal terms as

$$\mathbf{W}_i = \left[diag\left(\omega_j^{(i)}\right)\right] \quad j = 1, \ldots, N_p \quad (11)$$

where $\omega_j^{(i)}$ = positive or zero singular value of Θ_i with $\omega_1 \geq \omega_2 \geq \ldots \geq \omega_{Np} \geq 0$.

The inverse of Θ_i can be defined by Eq.(12) with a diagonal matrix of the inverse of each singular value.

$$\Theta_i^{-1} = \mathbf{V}_i \left[diag\left(\frac{1}{s_j^{(i)}}\right)\right] \mathbf{U}_i^T \quad j = 1, \ldots, N_p \quad (12)$$

The matrix Θ_i is singular if the condition number is infinite, and it is ill-conditioned if the condition number is too large where the condition number is defined as the ratio of the largest of the s_j's to the smallest of the s_j's.

In our approach of determining OAL, only limited number of DOF's are usually needed. Therefore, we may deal with the terms with relatively large singular values to determine OAL and the result may not be so much influenced by truncating the terms with singular values less than a pre-defined tolerance.

To determine OAL, we have modified the scheme of effective independence distribution vector (EIDV) proposed by Penny et al.[8]. The original idea of EIDV by Penny et al. was to determine OSL with the information of mode shapes. Since the current approach is to determine OAL based on the computed mode shape sensitivities rather than the mode shapes, the EIDV $\mathbf{e}_d$ is computed as the sum of $\mathbf{e}_{di}$ from all the participating modes as Eq.(13). In the computed EIDV, we can eliminate terms with relatively small values one-by-one which contribute less to the modal behavior. Instead of using EIDV, some alternative schemes of selecting sensor locations are also introduced using the computed matrices[8].

$$\mathbf{E}_i = \Theta_i \left[\Theta_i^T \Theta_i\right]^{-1} \Theta_i^T \;, \quad \mathbf{e}_{di} = diag\left[\mathbf{E}_i\right] \;, \mathbf{e}_d = \sum_{i=1}^{nmm} \mathbf{e}_{di} \quad (13)$$

where $\mathbf{E}_i(N_m \times N_m)$, $\mathbf{e}_{di}(N_m \times 1)$ = idempotent matrix and the EIDV of mode i, respectively. A typical characteristic of an idempotent matrix is that its rank is the same as the sum of the diagonal terms of the matrix. If $rank(\Theta_i)$ is full, $\mathbf{E}_i = \mathbf{I}$ so that $rank(\mathbf{E}_i) = N_p$ will be satisfied.

3. Modal SI Scheme

A modal SI algorithm modified from the algorithm proposed by Jang et al.[2] has been applied to investigate the effectiveness of the proposed OAL algorithm. The applied SI algorithm has demonstrated its usefulness in identifying structural parameters even with noisy and sparse measured data. As a similar process to the maximum likelihood approach, a constrained optimization problem of Eq.(14) is formulated to solve for an optimal stiffness parameter vector $\mathbf{x}$.

$$\underset{\mathbf{x}\in\Re^{N_p}}{\text{Minimize}} \quad J(\mathbf{x}) = J_o(\mathbf{x}) + J_r(\mathbf{x}) = \frac{1}{2}\sum_{i=1}^{nm} \| \mathbf{e}_i(\mathbf{x}) \|^2 + \frac{\beta}{2} \| \Delta\mathbf{K}(\mathbf{x}) \|_F^2 \qquad (14)$$

$$\text{subject to} \quad \mathbf{x}_{lo} \le \mathbf{x} \le \mathbf{x}_{up}$$

where $\mathbf{x}_{lo}$, $\mathbf{x}_{up}(N_p \times 1)$ = lower and upper bounds of the parameter vector $\mathbf{x}$ and β = regularization factor.

The primary error vector $\mathbf{e}(\mathbf{x})(N_m \times 1)$ of Eq.(15) is defined by the error in the equality condition.

$$\mathbf{e}_i(\mathbf{x}) = \left[\lambda_i \mathbf{B} \breve{\mathbf{K}}_i^{-1}(\mathbf{x}) \tilde{\mathbf{M}} - \tilde{\mathbf{I}} \right] \tilde{\phi}_{mi} \qquad (15)$$

where $\mathbf{B}(N_m \times N)$ = a Boolean matrix to indicate the measured DOF's among the full modal displacement vector ϕ_i, $\tilde{\mathbf{I}}(N_m \times N_m)$ = identity matrix with the size of measured DOF's, and $\tilde{\mathbf{M}}(N \times N_m)$ = part of mass matrix corresponding to the measured DOF's, respectively. The pseudo-stiffness matrix in Eq.(15) is defined by

$$\breve{\mathbf{K}}_i(\mathbf{x}) = \mathbf{K}(\mathbf{x}) - \lambda_i \left[\tilde{\mathbf{O}} \quad \bar{\mathbf{M}} \right] \qquad (16)$$

where $\tilde{\mathbf{O}}$ = part of zero matrix corresponding to the measured DOF's and $\bar{\mathbf{M}}$ = part of mass matrix corresponding to the unmeasured DOF's.

A regularization term of a Frobenius norm of Eq.(17) is added to alleviate the inherent ill-posed properties of such an inverse problem during optimization process[14].

$$\| \Delta\mathbf{K}(\mathbf{x}) \|_F^2 = \| \mathbf{K}(\mathbf{x}) - \mathbf{K}(\mathbf{x}_o) \|_F^2 \qquad (17)$$

where $\mathbf{x}_o$ = the baseline value of structural parameters.

4. Weight on Critical Members

If accelerometers are placed at locations only with the considerations on modal behavior but if damage possibility is high around supports, damage may not be easily identified by a modal SI using data measured at the locations determined by a usual OAL scheme. Since modal energy around the supports is relatively low and accelerometer locations by the selected OAL may be usually around the middle of the span, it may be highly difficult to identify damage correctly without considering special weight on the critical members.

There may be various methods for implementing importance weight on critical members for structural safety. Long time visual inspection data on damage or deterioration pattern depending on structural type may be one of the useful information. In the current context of the paper, however, we simply determine the importance weight based on the sum of static strain energies obtained by locating a vertical unit load on every node in a model.

The relative strain energy of members connected to node k is defined by d_k as

$$d_k = \frac{U_k}{Max(U_i)} \quad i = 1, \ldots, N \qquad (18)$$

where U_k = sum of computed maximum strain energy of each member connected to node k and N = number of DOF in a discretized analytical model. In the computation of d_k, we may eliminate the immeasurable DOF's such as rotational DOF's.

By assuming that the value of relative strain energy at each DOF may indicate the level of damage possibility, a weighting matrix $\Omega(N_m \times N_m)$ can be defined by Eq.(19) and multiplied to the idempotent matrix to construct a modified one as Eq.(20).

$$\Omega = [diag(d_k)] \qquad (19)$$

$$\mathbf{E}^* = \Omega^T \mathbf{E} \Omega \qquad (20)$$

The modified idempotent matrix $\mathbf{E}^*(N_m \times N_m)$ is applied to Eq.(13) and can be used to determine OAL with the consideration on damage possibility.

In addition to the critical members based on the strain energy, some locations may be also selected from engineering experience. For example, structural members around internal supports may be strong candidates for long-term monitoring for damage possibility. A similar procedure as implementing an importance weight based on strain energy can be applied for those members, too. However, the way of implementing importance weight should be revised in the future with more field inspection data on damage pattern.

5. Simulation Study

For the simulation study, a two-span three-girder structure of Fig.1 has been utilized to examine the proposed OAL algorithm. The material and sectional properties of all the members are assigned as equal for the study. It has been assumed that the number of accelerometer locations is pre-defined by six and the lowest four modes can be measured. The measurable DOF are limited to the vertical direction without measuring horizontal and rotational DOF's at each joint. The lowest four modes are shown in Fig.2. For the parameter estimation, members are grouped by three groups of girder members and one group with all cross beams.

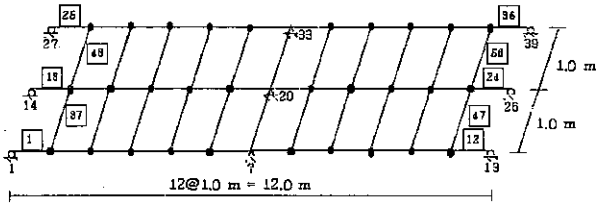

Fig.1 A two-span three-girder grid structure

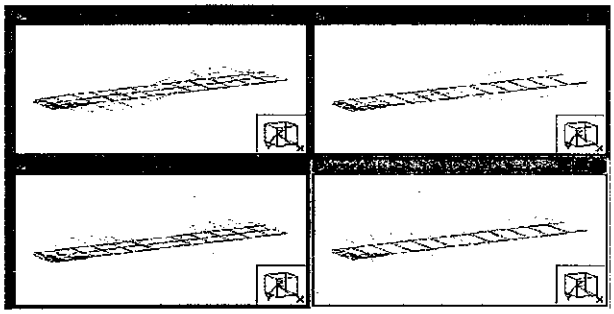

Fig.2 Computed mode-shapes for the lowest four modes

Fig.3 shows the selected six DOF by the proposed OAL method. The first four DOF are on the exterior joints at the middle of each span as expected and the next two joints are selected axi-symmetric due to the influence of the 2nd and 4th torsional mode shapes. The 5th and 6th choices can be switched by the opposite two joints adjacent to the 2nd and 3rd selections without losing any generality. The locations may also be selected by a conventional manner from the observation of the computed four mode-shapes of Fig.2 with some hesitation in selecting the 5th and 6th locations.

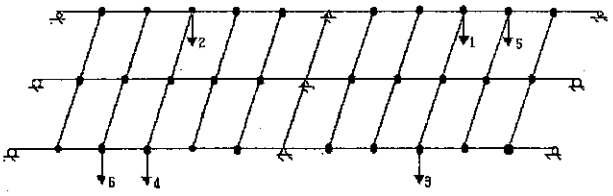

Fig.3 Sensor locations by the proposed OAL method

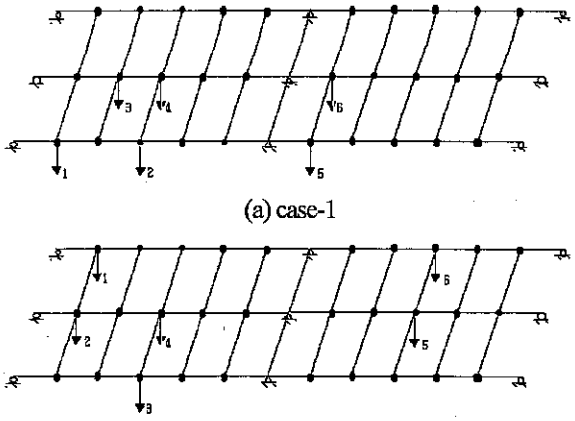

(a) case-1

(b) case-2

Fig.4 Two possible sets of sensor locations

To check the properness of the selected OAL in Fig.3, two other possible sets of sensor locations shown in Fig.4 are also selected for comparison. The SI scheme proposed by Jang et al. has been applied for the investigation[2]. The estimated parameters by the SI method are compared in Fig.5(a) and 5(b). For each measurement case, 30 different measured responses were simulated with different random noise in measurement and thus resulted in 30 different estimated parameters. The vertical axis is a non-dimensional value with respect to the baseline value so that 1.0 indicates no change from the baseline value. The spots within a dot-circle are from the proposed OAL. From the figures we can observe that the estimated values by the proposed OAL are more correct and gather near-by.

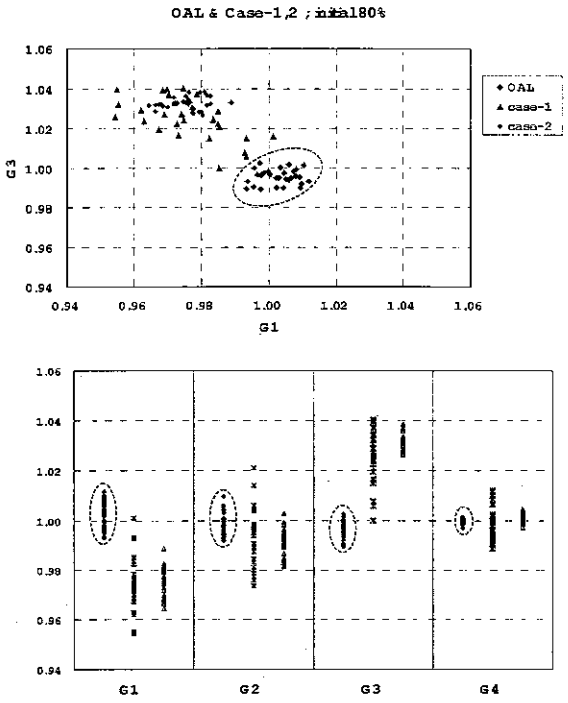

(a)

(b)

Fig.5 Estimated stiffness parameters of each member group using different sensor location cases

The OAL vary depending on the number of measurable modes and the number of accelerometers. Fig.6 shows the selected OAL when $nmm = 1$ and $N_m = 8$ while Fig.7 is for the case of $nmm = 2$ and $N_m = 8$. In each case, the identifiability criterion of $N_m \times nmm \geq N_p$=4 is satisfied. Change of the 7th and 8th location with the increase of measurable modes can be easily understood with the computed mode shapes of Fig.2. However, it may not so easy to figure out that the locations still stay on the middle girder without the help of the OAL algorithm for a better SI result. Fig.8 is for the case of $nmm = 4$ and $N_m = 8$.

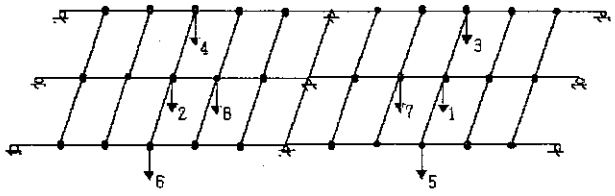

Fig.6 OAL for 1 mode – 8 accelerometer

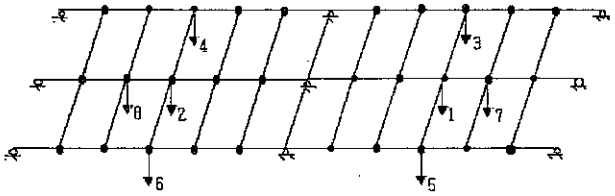

Fig.7 OAL for 2 mode – 8 accelerometer

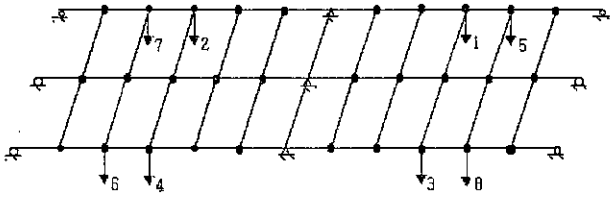

Fig.8 OAL for 4 mode – 8 accelerometer

To examine the implementation of importance weight, a simulation study is carried out by setting a member connected to a middle support as a critical one as shown in Fig.9.

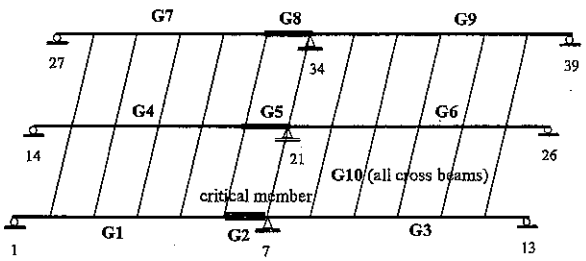

Fig.9 Group definition for implementing importance weight

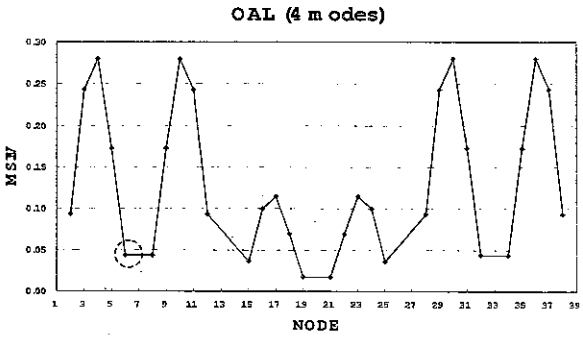

Fig.10 Selected general OAL with 4 modes

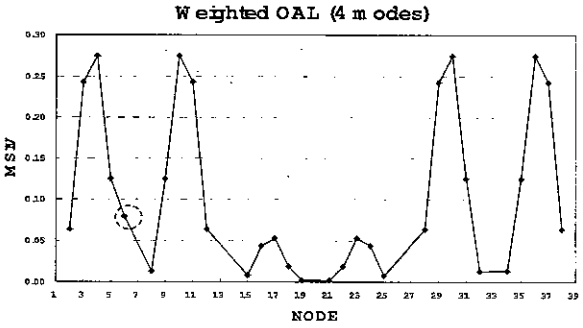

Fig.11 Selected weighted OAL with 4 modes

Fig.10 shows the selected OAL based on the proposed algorithm, while Fig.11 is the case of OAL with the consideration of weight on the critical member. However, from both figures, vertical DOF of node 6 is still far from being selected even though the possibility increases a little bit in the weighted case of Fig.11.

Fig.12 shows the estimated parameters when 40% reduction in the flexural stiffness was simulation. The OAL was determined for the case of $nmm = 4$ and $N_m = 6$ from Fig.10 and Fig.11. Even if vertical mode at node 6 was not measured in this case, it can be observed from the figure that a relative low parameter value at member 6 can still indicate the possibility of damage.

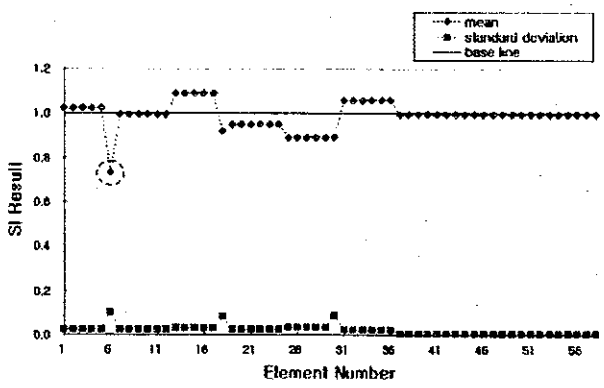

Fig.12 Estimated parameters with OAL of Fig. 10 and 11

To exaggerate the case of implementing the critical member, node 6 is included as the 1st choice as shown in Fig.13. The estimated parameters for the case of Fig.13 are drawn in Fig.14. From the figure, it can be easily observed that damage at member 6 is more vivid when it is compared with Fig.12.

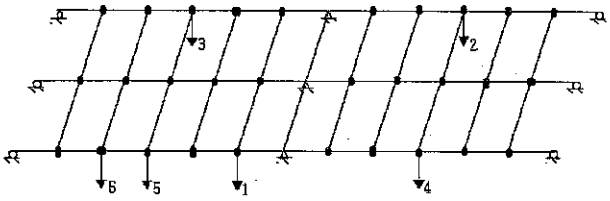

Fig.13 OAL when node 6 is included

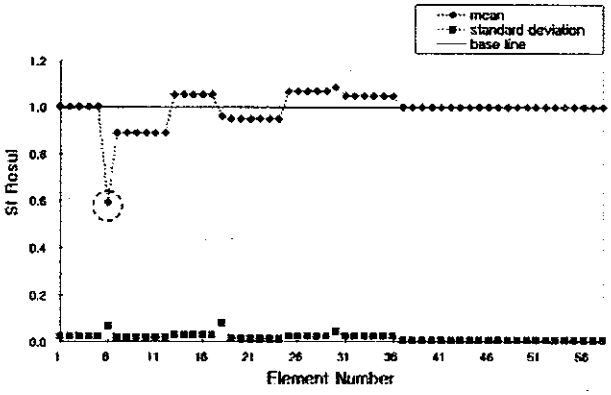

Fig.14 Estimated parameters with OAL of Fig. 13

6. Conclusion

A methodology to determine optimal accelerometer locations (OAL) for a modal SI is proposed based on a maximum likelihood (ML) approach. The method is mathematically developed using a Fisher information matrix (FIM) each column of which consists of mode shape sensitivity with respect to unknown structural parameter. A modified scheme of effective independence distribution vector (EIDV) is proposed to determine OAL. To overcome the rank deficiency problem in the computed sensitivity matrix, a truncated singular value decomposition scheme is also proposed. To consider importance weight of critical members for the structural safety, a way of implementing importance weight is proposed by using a weight matrix computed from static strain energy.

Simulation studies on a two-span multi-girder grid structure have been carried out and demonstrated the usefulness of using the proposed OAL scheme in modal SI applications. Implementation of importance weight on critical members is not so satisfactory when it is only based on the computed static strain energy. A more reliable method reflecting actual inspection data may be needed in the future.

References

1) Hwang, S. H., *Temperature Effect on Structural Health Monitoring of Cable Supported Bridges*, M.S. Thesis, Seoul National University, Korea, February, 2003.

2) Jang, J. H., Yeo, I. H., Shin, S., and Chang, S. P., Experimental investigation of system-Identification-based damage assessment on structures, *ASCE, Journal of Structural Engineering*, 128(5), May, pp.673-682, 2002.

3) Lim, K. B., Method for optimal actuator and sensor placement for large flexible structures, *Journal of Sound and Vibration*, 15(1), pp.49-57, 1992.

4) Jung, J. N., and Pappa, R. S, An eigensytem realization algorithm for modal parameter identification and model reduction, *Journal of Guidance, Control, and Dynamics*, 8(1), pp.620-627, 1984.

5) Tongco, E. and Meldrum, D., Optimal sensor placement for large flexible space structures, *Journal of Sound and Vibration*, 19(4), pp.961-963, 1996.

6) Kammer, D. C., Optimal sensor placement for modal identification using system-realization methods, *Journal of Sound and Vibration*, 19(3), pp.729-731, 1995.

7) Poston, W. L. and Tolson, R. H., Maximizing the determinant of the information matrix with the effective independence method, *Journal of Guidance, Control, and Dynamics*, 15(6), pp.1513-1515, 1992.

8) Penny, J. E. T., Friswell, M. I., and Garvey, S. D., Automatic choice of measurement locations for dynamic testing, *AIAA Journal*, 32(2), pp.407-414, 1994.

9) Mehra R. K. and Lainiotis D. E., *System Identification – Advances and Case Studies*, Academic Press, New York, 1976.

10) Udwadia F. E., Methodology for optimum sensor locations for parameter identification in dynamic systems, *ASCE, Journal of Engineering Mechanics*, 120(2), pp.368-390, 1994.

11) Kirkegaard, P. H. and Brincker, R., On the optimal location of sensor for parametric identification of linear structural systems, *Mechanical Systems and Signal Processing*, 8(6), pp.639-647, 1993.

12) Fadale, T. D., Nenarokomov A. V., and Emery, A. F., Two approaches to optimal sensor locations, *Journal of Heat Transfer*, 117, pp.373-379, 1995.

13) Lee, I.-W. and Jung, G.-H., An efficient algebraic method for the computation of natural frequency and mode shape sensitivities – part I. distinct natural frequencies; part II. multiple natural frequencies, *Computers & Structures*, 62(3), pp.429-443, 1997.

14) Yeo, I., Shin, S., Lee, H. S., and Chang, S. P., Statistical damage assessment of framed structures from static responses, *ASCE, J. of Eng. Mech.*, 126(4), pp.414-421, 2000.

Vibration based damage identification for a three span continuous steel free deck bridge located in Canada

J.L. Humar*, A. Bagchi**, H. Xu***

* Professor, **Post-Doctoral Fellow, ***Graduate Student
Department of Civil & Environmental Eng., Carleton University, Ottawa, Ontario, Canada, K1S 5B6

Vibration based damage identification techniques are based on the fact that damage in a structure causes changes in its dynamic characteristics, such as, frequencies and mode shapes. The paper presents a study of the application of this technique in the identification of the location and severity of potential damage in a three-span continuous bridge with steel-free deck, constructed under the technical advice of Intelligent Sensing for Innovative Structures, a Canadian center of excellence. Computer simulation is used to study the identification of a number of different damage patterns, and the effects of measurement errors and incomplete mode shapes on the quality of results are evaluated. The effectiveness of some selected damage identification techniques is studied, at the same time the potential difficulties are identified and areas of further research are suggested.

Key Words: vibration based damage identification, structural health monitoring, steel-free deck, computer simulation

1. Introduction

Structural health monitoring (SHM) is an essential part of the maintenance of large civil engineering structures. A comparatively recent development in SHM of civil engineering structures is the application of vibration based damage detection. Vibration characteristics, such as, frequencies and mode shapes are global properties that change when the structure suffers damage. It should therefore be possible to determine the location and severity of the damage based on the differences in the vibration characteristics of a healthy and a damaged structure. Vibration based assessment offers several advantages, one of which is that the location of damage need not be known *a-priori*. The sensors required to measure the vibration characteristics need not be located in the vicinity of the damage, and a limited number of sensors can, at times, provide sufficient information to locate the damage and assess its severity. Vibration measurements can also be carried out remotely, permitting the development of an early warning system and efficient management of maintenance schedules. However, in practice, the VBDI techniques have a number of problems including, but not limited to, effect of measurement errors, availability of only incomplete mode shapes, mode truncation, non-unique nature of the solutions, and environmental factors. These difficulties are particularly severe for civil engineering structures.

This paper discusses the application of vibration based structural damage identification (VBDI) techniques in health monitoring of the Crowchild Bridge, a three-span continuous bridge with steel-free deck, constructed under the technical advice of Intelligent Sensing for Innovative Structures (ISIS), a Canadian center of excellence. The bridge is located in Calgary, Alberta. Innovative techniques and materials have been used in the construction of this bridge. Sensors for measuring strain and temperature have been installed in the structure to facilitate remote monitoring of the structural health. The expectation is that the data collected from the sensors will be helpful in evaluating the extent and location of any damage in the structure.

Computer simulation is used here to study the identification of a number of potential damage patterns in the bridge and to evaluate the effects of measurement errors and incomplete mode shapes on the quality of results. A finite element model of the bridge is developed and this analytical model is updated and correlated with available vibration test data on the undamaged structure. The damage in an element is simulated by reducing its stiffness by a specified ratio. A revised finite element model is then constructed and used to obtain the analytical mode shapes and frequencies of the damaged structure. These analytical mode shapes are then reduced in size based on a selected practical placement of sensors to simulate the availability of only incomplete mode shapes. The incomplete mode shapes are expanded to the full size using a modal expansion technique. Random errors are introduced in the incomplete modes to simulate the noise in measured quantities. The effectiveness of selected VBDI techniques is

studied; at the same time the potential difficulties are identified and possible areas of further research are suggested.

2. Details of the Crowchild Bridge

The Crowchild Bridge in Calgary is a two-lane traffic overpass with three continuous spans. The details of the bridge superstructure are shown in Figures 1 and 2. The superstructure is said to be the first continuous-span steel-free bridge deck in the world. It is composed of five longitudinal steel girders (900 mm deep), a polypropylene fiber reinforced concrete slab deck and prefabricated glass fiber reinforced concrete barriers. There are four evenly spaced cross-frames in each span, and steel girder diaphragms at the supports to hold the main girders in place. The main girders are also connected by evenly spaced steel straps placed across the top of the girders to provide lateral restraint to them. The girders and straps are connected to the deck slab by stainless steel stubs. The deck is 9030 mm wide and does not contain any internal steel reinforcement. The slab thickness is 275 mm along the girders and 185 mm elsewhere. There are five longitudinal girders spaced at 2 m.

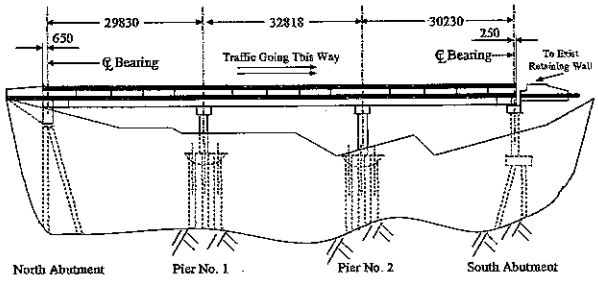

Figure 1: Crowchild Bridge - west elevation

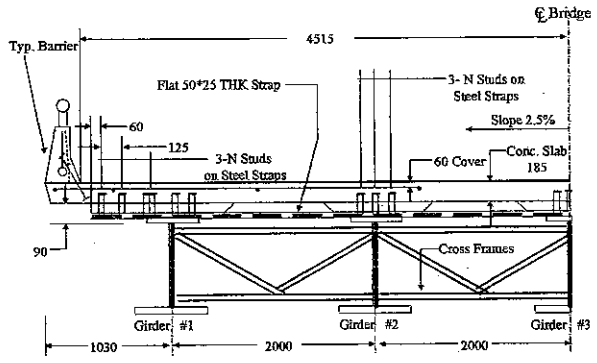

Figure 2: Cross section of the Crowchild Bridge

A monitoring program for the bridge has been developed by ISIS Canada. Sets of static and ambient vibrations tests have been conducted by the University of British Columbia in 1997[1], and the University of Alberta in 1998-99[2].

3. Vibration based damage identification techniques

A number of techniques for vibration based damage identification are available in the literature[3-5]. They include: (a) methods based on frequency changes, (b) methods based on mode shape changes, (c) mode shape curvature method, (d) methods based on change in flexibility matrix, (e) methods based on changes in uniform flexibility shape curvature, (f) strain energy based damage index method, (g) method based on modal residual vector, (h) matrix update methods, and (i) neural network methods. Here, the strain energy based damage index method, and matrix update methods are used because of their relative advantages.

3.1 Method based on modal strain energy

This method as originally developed by Stubbs *et al*[6] is applicable to beam type structures and is based on the comparison of modal strain energy before and after damage. The method can be extended to a structure of a general type. For the healthy structure the modal strain energy of member j in mode i is given by

$$S_{ij} = \boldsymbol{\phi}_i^T \mathbf{k}_j \boldsymbol{\phi}_i \tag{1}$$

The total strain energy of the structure deforming in its mode i is obtained from

$$S_i = \sum_j \boldsymbol{\phi}_i^T \mathbf{k}_j \boldsymbol{\phi}_i = \boldsymbol{\phi}_i^T \mathbf{K} \boldsymbol{\phi}_i \tag{2}$$

where $\mathbf{k}_j$ is the stiffness matrix of member j and $\mathbf{K}$ is the stiffness matrix of the structure. Similar expressions can be written for the damaged structure. In deriving S_i^d the global stiffness matrix of the damaged structure $\mathbf{K}^d$ is taken as being approximately equal to $\mathbf{K}$. The fractional strain energy expressions as given in Eq. (3) can be used to define a damage index.

$$f_{ij} = \frac{\boldsymbol{\phi}_i^T \mathbf{k}_j \boldsymbol{\phi}_i}{\boldsymbol{\phi}_i^T \mathbf{K} \boldsymbol{\phi}_i} \quad \text{and} \quad f_{ij}^d = \frac{\boldsymbol{\phi}_i^{dT} \mathbf{k}_j \boldsymbol{\phi}_i^d}{\boldsymbol{\phi}_i^{dT} \mathbf{K} \boldsymbol{\phi}_i^d} \tag{3}$$

The ratio of the fractional strain energy expressions given in Eq. 3 is defined as the damage index for the jth element in mode i. With the information available from the nm measured modes the damage index is defined as follows

$$\gamma_j = \sum_{i=1}^{nm} f_{ij}^d \Big/ \sum_{i=1}^{nm} f_{ij} \tag{4}$$

Elements for which γ_j is relatively large are likely to have been damaged. This provides the location of damage. Numerical problems may arise in the evaluation of Eq. 4 when the denominator is very small in magnitude, which may be the case when the strain energy contributed by the jth member in the modes being considered is very small. In such a case Eq. 4 is modified as follows

$$\gamma_j = (1+\textstyle\sum_{i=1}^{nm} f_{ij}^d)/(1+\sum_{i=1}^{nm} f_{ij}) \tag{5}$$

3.2 Matrix update methods

The matrix update methods constitute the largest class of methods developed for the identification of damage from

measured vibration properties. The methods are based on the determination of perturbations in the property matrices, such as δK, that will satisfy the eigenvalue equation given by

$$K\phi_i = \lambda_i M\phi_i \tag{6}$$

where **K** is the stiffness matrix, ϕ_i is the *i*th mass-orthonormal mode shape, λ_i is the associated eigenvalue (squared frequency), and **M** is the mass matrix. Damage in the structure may change both the stiffness and the mass matrices, altering the frequencies as well as the mode shapes. The eigenvalue equation for the damaged structure is given by

$$\begin{aligned}&(\mathbf{K}+\delta\mathbf{K})(\phi_i+\delta\phi_i)\\&=(\lambda_i+\delta\lambda_i)(\mathbf{M}+\delta\mathbf{M})(\phi_i+\delta\phi_i)\end{aligned} \tag{7}$$

Assuming that damage does not alter the mass matrix and using Eq. 6, we get:

$$K\delta\phi_i + \delta K\phi_{di} = \lambda_i M\delta\phi_i + \delta\lambda_i M\phi_{di} \tag{8}$$

where $\phi_{di} = \phi_i + \delta\phi_i$ is the *i*th mode shape of the damaged structure. Premultiplying both sides of Eq. 8 by ϕ_{di}^T and using the transpose of Eq. 6 we get:

$$\frac{\phi_{di}^T \delta K \phi_{di}}{\phi_i^T M \phi_{di}} = \delta\lambda_i \tag{9}$$

Perturbation matrix $\delta\mathbf{K}$ can be expressed as

$$\delta K = \sum_j k_j \beta_j \tag{10}$$

where β_j is the damage factor for element *j*. Using Eq. 9, Eq. 10 can be expressed as

$$\delta\lambda_i = \frac{-\sum_{j=1}^{ne} \phi_{di}^T \mathbf{k}_j \phi_{di} \beta_j}{\phi_{di}^T \mathbf{M} \phi_{di}} \tag{11}$$

or

$$D\beta = -\delta\lambda \tag{12}$$

where *ne* is the number of elements and **D** is an *m* by *ne* matrix whose elements are given by

$$d_{ij} = \phi_{di}^T k_j \phi_{di} \Big/ \phi_{di}^T M \phi_{di} \tag{13}$$

β is the *ne*-vector of the unknown changes in element stiffness matrices, and $\delta\lambda$ is the *m*-vector of measured eigenvalue changes.

Solution of Eq. 12 provides both the location and severity of the damage. In general the number of unknown parameters in that equation is significantly greater than the number of measured frequencies and mode shapes, the problem is therefore under-determined and has an infinite number of probable solutions. A unique solution can be obtained through the minimization of an objective function subject to some specified constraints. The matrix update methods can thus be classified on the basis of the objective function selected and the constraints used.

Many different objective functions may be used. They include the norm of the estimated solution, rank of the perturbation matrix δK, norm of the modal residual and others. The constraints may include satisfaction of the eigenvalue equation, and preservation of the sparsity and connectivity of the property matrices. Because of the many different ways in which the objective function and constraints can be defined and the different numerical techniques that can be used in the solution of the resulting optimization problem, a large number of methods have been developed. Here we present only one such method where we choose to minimize the quadratic norm of the stiffness changes given by

$$J = \beta^T \beta \tag{14}$$

with the constraint that Eq. 12 must be satisfied. The optimization technique can be used in the correlation of a finite element model of the structure so that the analytical frequencies and mode shapes calculated from such a model are close to their values obtained from modal tests on the healthy structure. For a damaged structure the following additional constraint must be satisfied.

$$0 \le \beta_j \le 1 \tag{15}$$

The problem now becomes a nonlinear optimization problem; it can be solved by using any one of the several algorithms available for the solution of constrained quadratic nonlinear optimization problems, for example, those in the computer software MATLAB[7]. The optimization routine used in the present work is based on a sequential quadratic programming (SQP) method. The SQP methods represent state-of-the-art in nonlinear programming. Gill *et al*[8] provide an overview of the SQP methods.

When a system involves a large number of elements, the optimization process would require a long time to complete. In addition many times when incomplete mode shapes are used and random noise exists in the measured data, the optimization process fails to converge to a stable solution. The process could be accelerated by excluding from consideration those elements that are not likely to have been damaged, and formulating the problem in terms of a smaller set of potentially damaged elements (reduced system). A damage localization algorithm such as the strain energy based damage index method can be used for identifying the potentially damaged elements that should be included in the reduced system.

4. Finite element modeling

The bridge structure is modeled with a MATLAB based finite element program (M-FEM) developed at Carleton University. The element library in M-FEM includes the plate-shell and three dimensional beam elements. The plate and shell element is formed using the DKT plate element[9] and the plane stress element with drilling degrees of freedom[10]. Program M-FEM also incorporates the VBDI techniques discussed earlier.

An analytical model of the Crowchild bridge is constructed using three dimensional beam elements for the piers, girders, diaphragms and the cross frames including the steel straps, and shell elements for the deck and side barriers. The deck elements are connected to the girder elements by rigid beam elements. The piers are assumed to be fixed at their base, while roller and pin supports are assumed to exist at the north and south abutments, respectively. The FE model contains 351 elements, 247 nodes and 1399 active degrees of freedom. The density of steel and concrete is assumed to be 76 and 24 kN/m^3, respectively. The concrete compressive strength is taken as 35 MPa. The modulus of elasticity for concrete is assumed to be 30 GPa for the deck and 27 GPa for the barrier and pier; for steel it is assumed to be 200 GPa.

Figure 3: The finite element model of Crowchild Bridge

Initially, the concrete is assumed to be un-cracked. The model that is based on this assumption is updated and correlated with the data obtained from vibration test conducted in 1997 by the University of British Columbia[1], and is used as the base model for the undamaged structure as of 1997. This model will be referred to as CC-97 model and is shown in Fig. 3. The model correlation is carried out by using an optimization process defined by Eqs. 14 and 12. The natural frequencies of the undamaged structure derived from model CC-97 are given in Table 1 while the mode shapes are shown in Fig. 4.

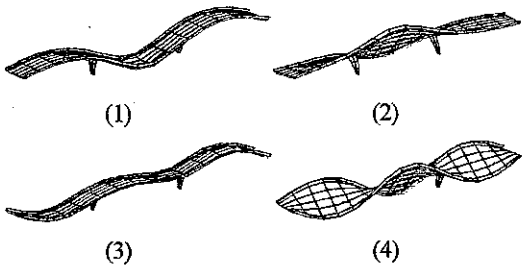

Figure 4: The mode shapes for CC-97 model

Field test conducted by the University of Alberta team in 1998-99[2] revealed that the frequencies of the bridge reduced slightly due to some cracking of concrete. To consider the effect of cracking the stiffness of the concrete elements is reduced, and the model is correlated with the 1999 test results. The stiffness of deck elements is assumed to be 90% of un-cracked stiffness in the positive moment region, and 70% in the negative moment region. The stiffness of the barrier is assumed to be 80% in the positive moment region and 70% in the negative moment region. The pier stiffness is reduced by 10%. The correlated base model will be referred to as CC-99. Its mode shapes are similar to those of CC-97 (as shown in Fig. 4). The frequencies of the undamaged structure are shown in Table 1.

Table 1: Natural frequencies of the bridge models

Bridge model	Mode	Frequency		
		Measured	Uncorrelated	Correlated
CC-97	1	2.78	2.89	2.78
	2	3.13	3.41	3.13
	3	3.76	3.44	3.72
	4	4.05	3.89	4.03
CC-99	1	2.60	2.72	2.60
	2	2.90	3.21	2.90
	3	3.63	3.21	3.63
	4	3.85	3.62	3.85
CC-03	1	–	2.48	–
	2	–	2.87	–
	3	–	2.88	–
	4	–	3.20	–

Another model is constructed by accounting for additional cracking in concrete to a level that could be expected in 2003 or a few years hence. The stiffness of deck elements is assumed to be 70% of the un-cracked stiffness in the positive moment region, and 40% in the negative moment region. The stiffness of the barrier is assumed to be 60% in the positive moment region and 30% in the negative moment region. The pier stiffness is reduced by 20%. No field test results are available for correlation of this model, and the uncorrelated analytical model is used as the base model for undamaged structure. This model would be called CC-03. The mode shapes of the model are shown in Fig. 5, and the frequencies are listed in Table 1.

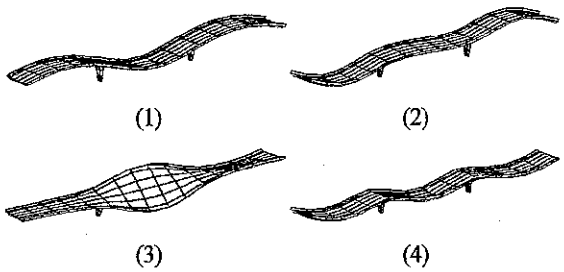

Figure 5: The mode shapes for CC-03 model

5. Computer simulation of damage

The effectiveness of the vibration based damage identification techniques considered here has been studied through detection of simulated damage in the bridge models. The damage is assumed to be concentrated in the area identified in Fig. 6. The following scenarios are considered for CC-97 model.

Damage case D1: The longitudinal girders (corresponding to element numbers 174, 177, 180, 183, and 186 in the finite element model) suffer 70% damage.

Damage case D2: The deck slab along the affected patch as shown in Fig. 6 has been damaged by 70%. The element numbers corresponding to the affected part of the deck slab are 53 through 58.

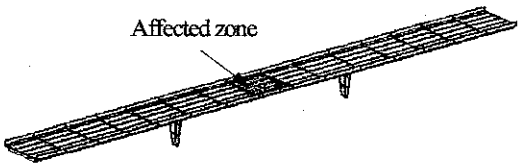

Figure 6: Damage area for computer simulation

For CC-99 and CC-03 models, only Scenario D1 is considered. The damage in a particular element is simulated by reducing its stiffness by the specified ratio. The frequencies and mode shapes of the structure with simulated damage are obtained from a modal analysis. The changes in frequencies for different models are shown in Figs. 7 through 9.

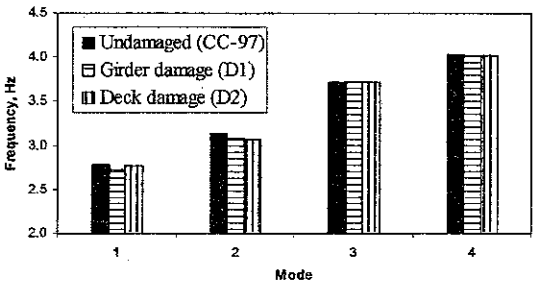

Figure 7: Frequencies of the undamaged and damaged structures for CC-97 model

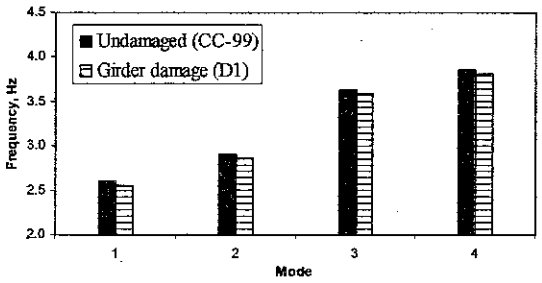

Figure 8: Frequencies of the undamaged and damaged structures for CC-99 model

The frequencies and the mode shapes of the damaged structure could be used in the damage detection techniques to identify the location and severity of damage. In practice, such frequencies and mode shapes are obtained from modal tests. The experimental frequencies and mode shapes are often corrupted by random noise. Another factor to be considered is that the finite element model usually contains a large number of degrees of freedom, but in the field only a limited number of sensors could be deployed. In addition measurement of rotational degrees of freedom is not practical. Thus only a few translation degrees of freedom are measured, and the experimental mode shapes are far from complete. This implies that either the incomplete mode shapes need to be expanded to the full size of the finite element model, or the finite element model condensed to the measured degrees of freedom. A number of techniques are available for achieving these.

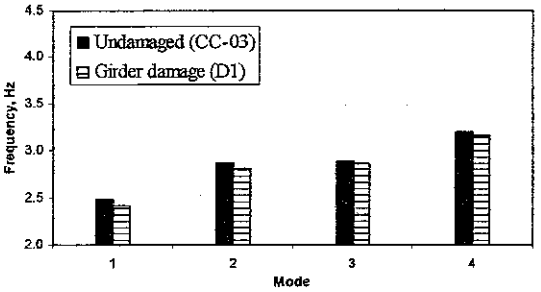

Figure 9: Frequencies of the undamaged and damaged structures for CC-03 model.

In the present study, incomplete mode shapes are constructed by selecting those elements of the analytical damaged mode shapes that correspond to a set of degrees of freedom along which measurements would be probably be made during a field test. The incomplete mode shapes are corrupted by adding a small amount of random error to simulate the noise in measurement; they are then expanded using a method proposed by O'Callahan *et al*[11] to obtain a complete set of mode shapes for the damaged structure. In this study, two cases of incomplete mode shapes are considered; in one case it is assumed that all three translation degrees of freedom at every node have been measured (M1), and in the other case only the vertical displacements at all nodes are assumed to have been measured (M2). Two cases of random noise in measurement are considered. In one case the eigenvalues and mode shapes of the damaged structure are assumed to have been corrupted by 0.5% and 1% random noise, respectively (E1), and in the other case the errors are assumed to be 1% and 2%, respectively (E2).

6. Results and discussion

In this section, selected results are presented to show the applicability of the VBDI techniques to a complex structure like the Crowchild Bridge. The modified damage index (Eq. 5) is used for damage localization, and the matrix update method, represented either Eq. 12 by itself, or a combination of Eqs. 12, 14 and 15 is used for estimating the severity of damage.

Figure 10 through 18 show the damage identification results for CC-97 model with damage case D1. It is observed from Fig. 10 that the damage index identifies the damage locations correctly when complete and noise free mode shapes of the damaged structure are used. Figures 11 and 12 show the severity of damage as expressed by damage factors (β in Eq. 12) evaluated using the matrix update methods. Estimates of β obtained from Eq. 12 by taking the pseudo inverse of **D**

provide rough estimates of the severity of damage and are shown in Fig. 11. It should be observed that in this case β can take negative values The results obtained from the optimization of the objective function in Eq. 14 with the constraints defined by Eqs. 12 and 15 give a very good measure of the damage extent, as seen from Fig. 12.

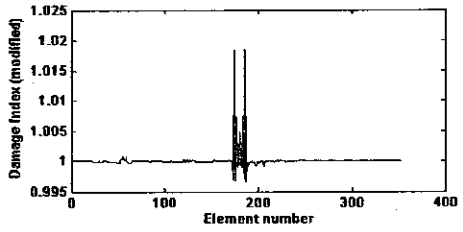

Figure 10: Damage index for damage case D1, with complete modes and no noise (CC-97 model)

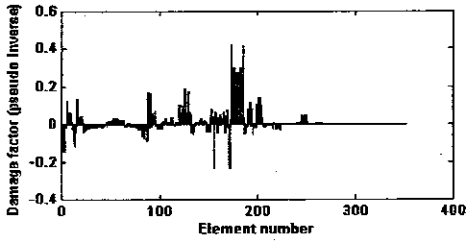

Figure 11: Damage factors by matrix update method (CC-97: damage case D1, complete modes and no noise)

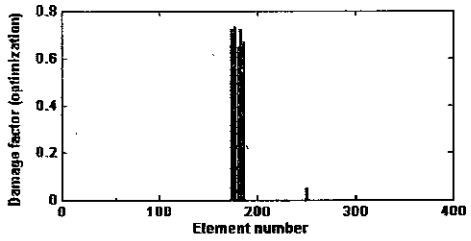

Figure 12: Damage factors by matrix update method (CC-97: damage case D1, complete modes and no noise).

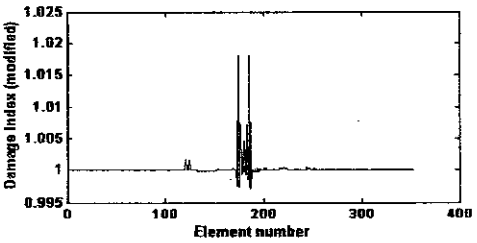

Figure 13: Damage index for damage case D1, with incomplete modes M1 and no noise (CC-97)

As mentioned earlier, the optimization process could be very slow for a large system, such as the one considered here. A reduced system constructed using only the potentially damaged elements, as determined using the damage index method, is also considered. In order to identify the elements with potential damage an average value is obtained for the damage index considering all of the elements. This average provides a threshold value. Elements having a damage index that is higher than the threshold are considered to be elements with potential damage. In the present case, based on the data presented in Fig. 10, only 27 elements out of 351 are identified as having been potentially damaged when error free and complete mode shapes are used. Damage factors obtained by solving the optimization problem for the reduced system are almost identical to those presented in Fig. 12.

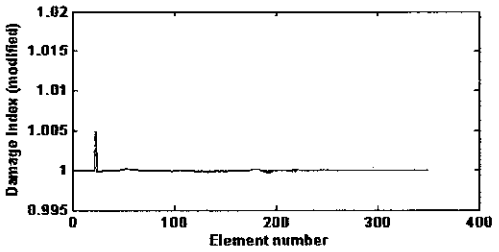

Figure 14: Damage index for damage case D1, with incomplete modes M2 and no noise (CC-97).

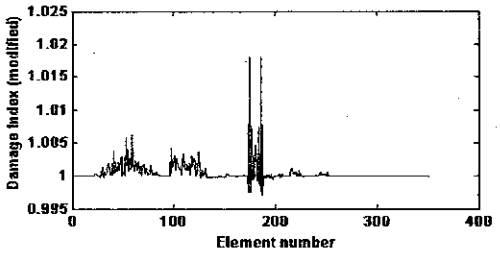

Figure 15: Damage index for damage case D1, with incomplete modes M1 and noise case E1 (CC-97).

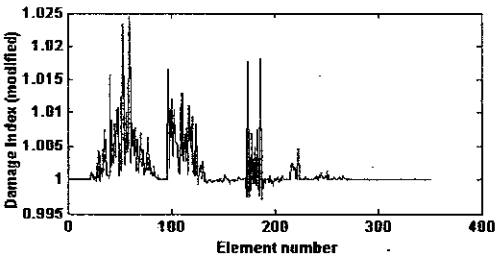

Figure 16: Damage index for damage case D1, with incomplete modes M1 and noise level E2 (CC-97).

Figures 13 through 18 show the effect of using various combinations of incomplete mode shapes and random measurement errors or noise on damage detection. Figure 13 shows the damage indices obtained when incomplete mode shapes, in which all of the translational degrees of freedom are measured (M1), are used and there are no measurement errors. It is observed that in this case the damage identification algorithms perform reasonably well and the damage index

gives accurate indication of damage locations. Figure 14 shows the results for case M2, where fewer sensors are used and only the z-direction (vertical) displacements, one at each node, are measured. The strain energy based method fails to provide useful information about damage locations in this case.

Figure 15 presents the damage indices obtained when incomplete mode shapes (M1) having a small amount of noise (E1) are used. The results indicate the presence of some spurious damage locations although the actual locations of damage are quite clearly identified. When the level of noise is increased (case E2), the locations of actual damage are overshadowed by the spurious locations (Fig. 16).

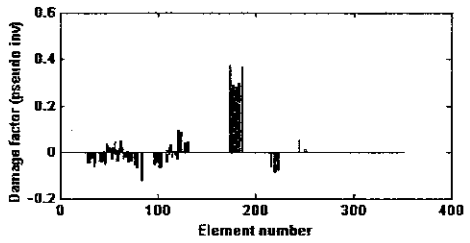

Figure 17: Damage factors by matrix update method of the reduced system (CC-97: D1-M1-E1)

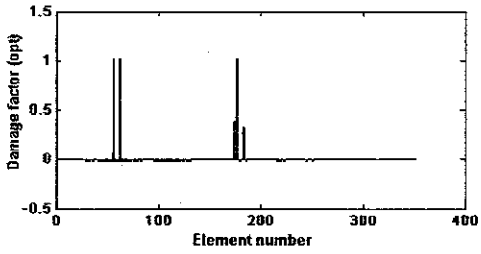

Figure 18: Damage factors by matrix update method of the reduced system (CC-97: D1-M1-E1).

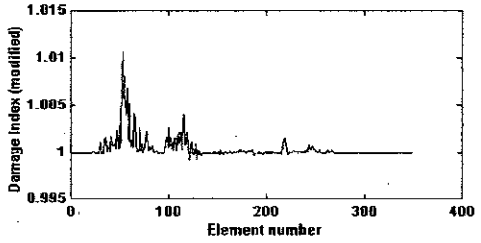

Figure 19: Damage index for damage case D2, with incomplete modes M1 and noise case E1 (CC-97).

Figures 17 and 18 show the performance of the matrix update method when incomplete mode shapes M1 having noise at level E1 are used. The pseudo inverse solution of the reduced system provides a useful estimate of damage location and severity, although the estimates of damage are lower than expected. The optimization process for the full system does not converge, and the solution for the reduced system (Fig. 18) picks up spurious damage due to the effect of measurement noise. When these results are used in conjunction with the damage index estimates as shown in Fig. 15, the damage estimates for spurious locations can be ignored. However, the estimates of severity even for the sites of real damage are not accurate.

Figures 19 and 20 show the damage indices and damage factors, respectively for damage case D2 of CC-97 model with noisy (E1) and incomplete mode shapes (M1). Determination of the location and the extent of damage are affected both by the measurement errors and incomplete modes. However, the quality of the results is not very bad. The general area of damage is identified correctly, while the severity of damage is slightly over estimated for some elements.

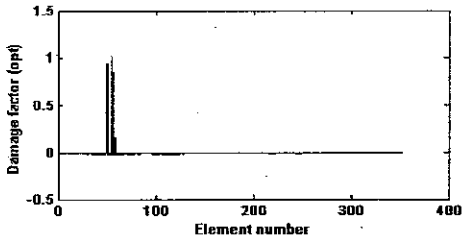

Figure 20: Damage factors by matrix update of the reduced system (CC-97: D2-M1-E1).

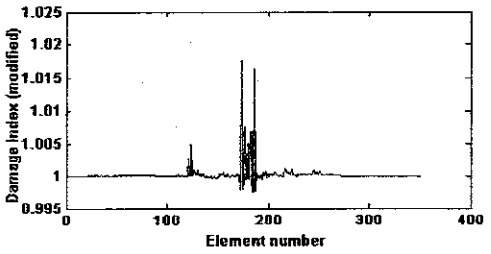

Figure 21: Strain energy based damage index for CC-99 model (D1-M1-E1).

Figs. 21 and 22 show the results of damage identification for CC-99 model with damage case D1, incomplete modes M1, and noise level E1. It is observed that the damage index method identifies the damage location quite effectively, but the estimates of the damage extent by matrix update method on a reduced system are not very good. However, when Figs. 21 and 22 are considered together, it is still possible to get some useful clues about the severity and location of the damage.

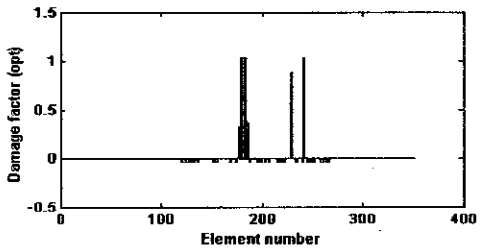

Figure 22: Damage factors obtained by matrix update method with the reduced system (CC-99: D1-M1-E1)

The analysis for CC-03 model with damage case D1, incomplete modes M1, and noise level E1, has been carried out. The results are not presented here for lack of space. They show that it is possible to identify the locations of damage quite well,

but the estimates of damage extent are not very good. However, as in the case of model for CC-99 (Figs. 21 and 22), in this case too it is possible to get some idea about the damaged area and the severity of damage.

7. Summary and conclusions

Vibration based damage identification is a useful tool for structural health monitoring. In the past its success has been demonstrated by applications in the damage detection of simple structures. However, its application to real life and complex civil engineering structures is still beset with considerable challenge. The first challenge manifests itself in creating a realistic mathematical model of the structure. This is because structural properties, such as the effective moment of inertia and modulus of elasticity, are quite uncertain and variable, especially in structures built from reinforced concrete where concrete cracking and quality of concrete may have a marked influence on the physical properties. Most modeling attempts, including those used in the present study, use arbitrary estimates of the effective moments of inertia, based on engineering judgment. Correlation of a model which must be based on such choices often requires unrealistic adjustments in the element stiffnesses, even when the differences between the analytical and experimental frequencies are small. In the present case, such adjustments could be kept within reasonable bounds only after the selection of the physical properties was fine tuned by a process of trial and error.

Other challenges include the practical limitation on the degrees of freedom along which modal measurements can be made, the number of modes that can be measured and the measurement errors that are inevitably present in field tests. As shown here all of these have profound impact on the success of damage identification. In the present study, in order for the methods to succeed, measurements were required along all of the translational degrees of freedom

Of the many VBDI techniques available only two are used here because of for their relative merit in comparison to others. The results obtained form these methods show that in spite of all of the problems, VBDI methods may be successful in identifying at least the location of damage in a civil engineering structure, such as the Crowchild Bridge. It is generally not possible to detect damages of small magnitudes through VBDI techniques since the changes in modal properties due to small degree of damage are not appreciable. Also, if the modal strain energy contribution of an element is very small, even a large degree of damage in it could not be detected by the VBDI techniques. Finally, it should be noted that computer simulation studies can not quite predict the effect of environmental factors, such as temperature changes, changes in boundary conditions, and nonlinearities caused by the opening and closing of cracks and slip in bolted joints. These are potential areas of further research.

The present study has shown that the use of a refined finite element model presents a number of problems in the application of VBDI technique. One reason for this is the fact that it is impractical to measure the modal displacements at the large number of degrees of freedom included in a detailed model. The VBDI technique may be more successful when used with a simpler model, for example, a beam model that may be used in conjunction with only the longitudinal flexural modes, or a grillage model that may work with both flexural and torsional modes.

Acknowledgement

The work has been supported by Intelligent Sensing for Innovative Structures (ISIS) Canada.

References

1) Ventura, C.E., Onur, T., and Tsai, R.C., Dynamic characteristics of the Crowchild Trail Bridge, *Can J of Civil Eng.*, Vol.27, pp.1046-1056, 2000.
2) Roger Cheng, J.J., and Afhami, S., Field Instrumentation and Monitoring of Crowchild Bridge in Calgary, Alberta, *University of Alberta Report for ISIS Canada*, Nov. 1999.
3) Doebling, S.W., Farrar, C.R., Prime, M.B., and Shevitz, D.W. Damage identification and health monitoring of structural and mechanical systems from changes in their vibration characteristics: A literature review. *Los Alamos National Laboratory*, Los Alamos, New Mexico, Report No. LA 13070-MS, 1996.
4) Farrar, C.R, Baker, W.E., Bell, T.M., Cone, K.M., Darling, T.W., Duffey, T.A., Eklund, A., and Migliori, A. Dynamic characterization and damage detection in the I-40 bridge over the Rio Grande. *Los Alamos National Laboratory*, Los Alamos, New Mexico, Report No. LA 12767-MS, 1994.
5) Humar, J.L., Bagchi, A., and Xu, H., Challenges in vibration based structural health monitoring, Accepted in *First International Structural Health Monitoring II-1'2003 Conference*, Toyko, Japan, Nov.13-15, 2003.
6) Stubbs, N., Kim, J. -T., and Farrar, C.R. Field verification of a non-destructive damage localization and severity estimation algorithm. *13th International Modal Analysis Conference*, 210-218, 1995.
7) MATLAB, *User Guide*, Mathworks Inc., Natick, MA, 1999.
8) Gill, P.E., Murray, and W., Wright, M.H. Practical optimization. Academic Press, London, 1981.
9) Batoz, J. L., An explicit formulation for an efficient triangular plate bending element, *Int. J of Numerical Methods in Engineering*, vol.18, pp.1077-1089, 1982.
10) Allman D. J., A compatible triangular element including vertex rotations for plane elasticity analysis, *Computers & Structures*, vol.19, no.1-2, pp.1-8, 1984.
11) O'Callahan, J., Avitabile, P., Riemer, R., System equivalent reduction expansion process (SEREP). *7th International Modal Analysis Conference*, Las Vegas, Nevada, 29-37, 1989.

(Received July 31, 2003)

Study on Damage Identification of Bridge Structures based on Sound Monitoring data

Takashi Obata*, Yasuhiro Asaka**, Yasunori Miyamori***, Toshiro Hayashikawa**** and Koichi Sato*****

* Dr. of Eng., Res. Assoc., Grad. School of Eng., Hokkaido University,
Division of Structural and Geotechnical Eng., Nishi 8 Kita13 Kita-ku, Sapporo 060-8628, Japan
** Grad. School Student, Grad. School of Eng., Hokkaido University, Division of Structural and Geotechnical Eng.
*** Dr. of Eng., Res. Assoc., Grad. School of Eng, Kyusyu University,
Dept. of Civil and Structural Eng., 6-10-1 Hakozaki, Higashi-ku, Fukuoka 812-8581, Japan
**** Dr. of Eng., Assoc. Prof., Grad. School of Eng., Hokkaido University, Division of Structural and Geotechnical Eng.
***** Dr. of Eng., Professor, Grad. School of Eng., Hokkaido University, Division of Structural and Geotechnical Eng.

Recent years, long-lived active use of infrastructures has become a very important problem in all over the world as well as Japan. The damage identification of infrastructures based on monitoring data is the effective technique for the maintenance and rehabilitation of bridges, tunnels and so on. The purpose of this study is to propose a sound monitoring system for bridge structures and investigate damage identification method by using sound monitoring data. In the sound monitoring system, it is possible to take the 8 channels of sound data at the same time and record directly in PC for digital sound. The system is constructed by using digital audio interface and dynamic microphone sensors. The damage identification method in this study is fractal dimension analyses performed for sound spectrogram on damaged and non-damaged data, and is investigated of alteration of fractal dimension. From results, the possibility of application for identifying bridge damage is discussed.

Key Words: sound monitoring system, damage identification, sound spectrogram, fractal dimension

1. Introduction

In Japan, the too many infrastructures were constructed for preparation and spread the transportation network from 50's to 70's. The most of infrastructures in Japan are middle-aged structures, also the bridges that more than 50 years active serviced are increase drastically in 2004 and these kind bridges will be over 50,000 in 2021. The developmental spending or investment for preparation of infrastructures such as construction of new transportation network is very difficult in Japan from the problem of economic condition and environmental impact. Therefore it has become a very important subject to aim at the life extension improvements of infrastructures by performing the maintenance and rehabilitation of those infrastructures efficiently and promptly[1].

For the life extension of structures, it is necessary to search for the early stage damages by using some methods of health monitoring and damage identification[2),3)]. The general inspection method of damage identification is eye-estimation by specialists of maintenance. In the near future, the serious problems that are the shortage of professional engineers on maintenance occur because the long-serviced bridges rapidly increase. The satisfaction for social demand of maintenance engineers is difficult due to financial condition and the long term to train technicians. From reason, it is necessary to establish the convenient and useful health monitoring system of bridges that easily operate from measurement to judgment without special knowledge. As one of the effective method of health monitoring, the technique of measuring vibration and sound data has good applicability for identifying damage of structures[2 ~ 12)]. In recent years, measurement of vibration and sound data can be easily carried out as compared with that of displacement and so on. The vibration or sound monitoring is also carried out by development of information technology. High precision monitoring results such as resonant frequencies, vibration mode shape, damping ratios and others are obtained by applying information technology. Based on the above back-ground, authors are investigate the rational sound monitoring system, and the change of vibration characteristics of higher frequency components from local damage by using analytical methods in time domain and frequency domain[9~12)].

The purposes of this study are to make up the multi-sensor sound monitoring system and to investigate the damage identification method by using sound data.

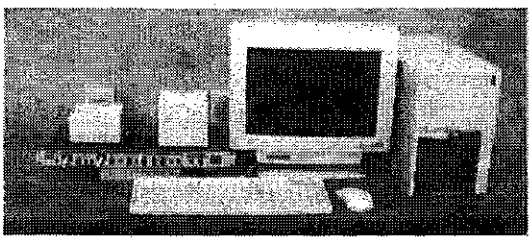

Picture.1 Sound Monitoring System

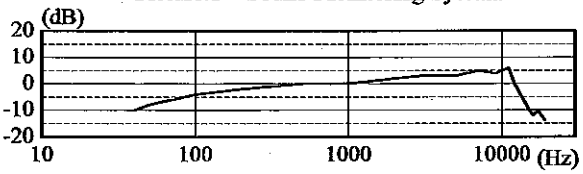

Figure.1 Gain for input frequencies

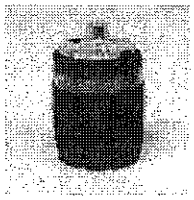

Picture.2 Microphone

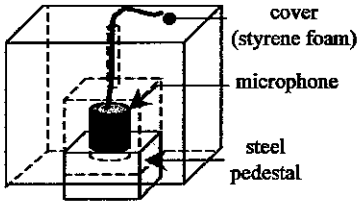

Figure.2 structure of sensor

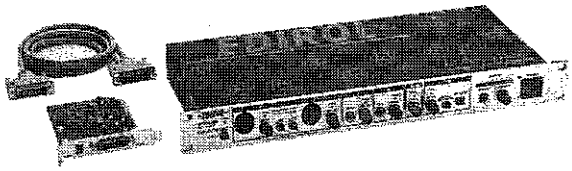

Picture.3 Roland Digital Audio Interface (DA-2496)

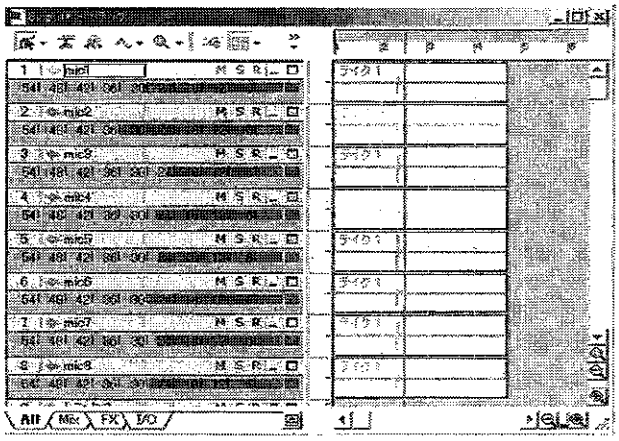

Figure.3 Operation screen in measuring sound data

The sound monitoring system in this study is composed of dynamic microphone sensor, digital audio interface and personal computer. This system is able to measure the 8 channel's sound from each sensor and also to record in PC directly at the same time. The damage identification method in this study is fractal dimension analyses performed for sound spectrogram on damaged and non-damaged data. And the several damaged case and condition of alteration of fractal dimension on experimental structural model are compared. Therefore, the applicability of sound monitoring system and damage identification method on infrastructures from both experimental and analytical results in this study are discussed.

2. Sound Monitoring System

The sound monitoring system consists of Digital Audio Interface, 8 dynamic microphones sensors and a personal computer as shown in Picture 1. The microphone used in this study is multi-purpose single directionality type. The size of microphone is 30mm × ϕ 20mm, and the sensitivity gain is –58dB±2dB in sound pressure level. The Picture 2 is the microphone used in this study and the relationship of gain and input frequencies is shown in Figure 1. The sensor is composed of microphone, the cover of styrene foam for noise canceling from the outside of structure and the steel pedestal of 40mm×40mm×30mm as shown in Figure 2. The microphone is embedded in steel pedestal, and covered by styrene foam nose canceller unit. Digital audio interface makes the core of this sound monitoring system. In this study, Roland DA2496[13] of Picture 3 is adopted for audio interface. This interface is realized easily high performance digital recording and playback of sound data. DA2496 has independent 8 channels Input /Output sound ports, it is able to measure 8 different sound data individually. The format of analog-digital translation is supported 24-bit and the frequency of sampling rate is 22.05-96kHz. The installation with a computer is slotting the card for PCI bus and extending to 16Ch is also possible by using one more PCI card. For the application software for measurement and recording, SONAR 2.0 is used in this study. Although this software of originally purpose is for sound mixing, music manufacture and editing. The reason to use the software is easy to take out the all performance of digital audio interface such as analog-digital translation format, sampling frequency, the number of sensors and others. The operation screen on computer at the time of measuring sound data is shown in Figure 3.

3. Experiments and Analytical Procedure

3.1 Sound Monitoring Experiments

The sound monitoring experiments are performed for checking the system performance and damage identification test of structural model in this study.

At first the system performance tests for sensor and noise receptivity are checked by using the 1000mm span length of simple steel beam model. Actually, in order to examine the performance of sensor's cover, two covers made of normal and porous styrene foam are prepared. And to confirm the sensoring of sound data by using steel platform, two kinds of steel pedestal that have microphone embedded depth of 5mm and 15mm are investigated. In measuring sound data, the sensor is fixed to steel beam model with epoxy adhesive. The excitation

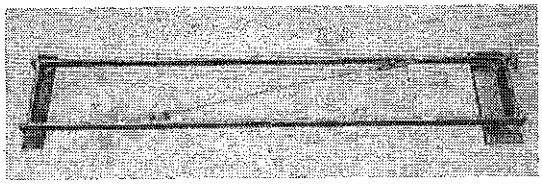

Figure.4 Steel bridge model

Table.1 Properties of specimen

Member	$l \times h \times b$ (mm)
Main girder	Flat bar 2500×65×22
End strut	Flat bar 400×65×22
Lateral bracing	Flat bar 1120×21×4
Gusset plate	Flat bar 263×9×69

of beam model for sound response is occurred by hammering, inputting constant frequency sound data and sweep sound that have frequencies increasing from 0Hz to 1000Hz per second. The digital recording specifications are 16bit format and sampling rate of 44.1kHz as used.

As for the examination of applicability for damage identification, the experiments are performed on a steel bridge structural model with bolt-jointed lateral bracing and main girder shown in Figure 4. Table 1 is the specifications of the structural model. The hypothetical damages in this study are given by changing the restriction of main girder and lateral bracing, in other words, by adjusting the torque of 4 high-tension bolts that connect main girder and lateral bracing. As for the restriction of high-tension bolts, the torque of 9.8kNm is added in the non-damaged condition. In hinge connection, after releasing the restriction of bolt, the torque is added as stiff as possible by hand. Finally the open cases indicate the condition in which the restriction of bolt is perfectly released. The measurement points of sound data are set up to 7 points shown in Figure 5 and sound monitoring data are obtained from these points at the same time. Hammering and sweep sound inputting are used as the excitations of the model.

3.2 Analytical Procedure

The analyses are performed by using sound spectrogram and fractal dimensions. The sound spectrogram is time-dependent frequency analysis. In this study, the windowed discrete-time Fourier transform of sound monitoring data is calculated. On the specifications of this analyses, the number of data length for which Fourier transform is performed is set to 1024 samples (approximately 0.023 seconds) and the time interval in which the sections overlap is set to 512 samples (approximately 0.011 seconds). The Kaiser Window is applied for the widow function. The amplitude of spectrum is expressed with the degree of color map of RGB. When the spectrum is the maximum, the color is 255 of red (R). The minimum case in which

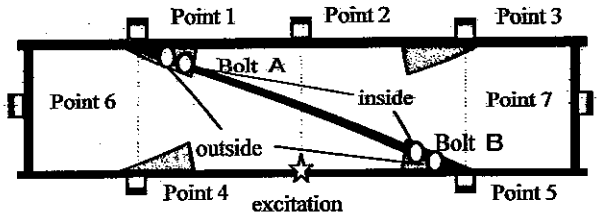

Figure.5 Measurement point on bridge model

Table.2 Damage condition of the specimen

Level	Damage condition	Bolt A		Bolt B	
		A-out	A-in	B-in	B-out
1	Non damage	●	●	●	●
2	Small	●	○	○	●
3	↓	●	—	—	●
4	↓	○	○	○	○
5	Large	○	—	—	○

●stiff connection ○hinge —open

the spectrum is almost 0 is expressed with 255 of blue (B)[15].

In this study, the fractal dimensions of sound spectrogram are calculated as the damage level identification parameters. The image of sound spectrogram expresses the 3 dimensional information of sound characteristics such as time domain, frequency domain and spectrum amplitude. The well-known application method of fractal, 1/f noise is 2 dimensional fractal dimensions in frequency domain of power spectrum. 1/f noise is often used for research on the sound characteristics of musical instrument and so on.

In this study, 3 dimensional extension of 1/f noise are attempted by using fractal dimension from sound spectrogram, and the influence of damage is estimated from the alteration of fractal dimension in comparison with non-damaged and damaged data.

The box counting method is adopted in the calculation of fractal dimension. This method has high applicability to image data such as photograph and so on. The calculation of fractal dimension in this method, at first the image is subdivided into the squares, and the number of squares that cover the significant image data is counted. In changing the size of squares into various sizes, the number of counted squares and a length of square are plotted in logarithm scale and the gradient of approximate line of plotted data is obtained as fractal dimension. If the image X is covered by square of the number of $N(d)$ that size is $d \times d$ and both relation are in proportion, the following equation is obtained.

$$N(d) = \mu \cdot d^{-k_0} \quad \cdots\cdots\cdots (1)$$

And the equation (1) is expressed in logarithm scale as equation (2).

$$\log N(d) = -k_0 \log d + \log \mu \quad \cdots\cdots (2)$$

Therefore, the relation of log $N(d)$ and log d becomes equation (3).

$$y = -k_0 x + \log \mu \quad \cdots\cdots\cdots (3)$$

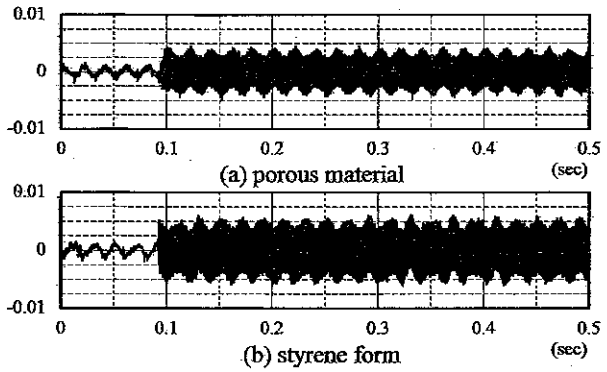

Figure.6 Comparison of cover (2000Hz)

Equation (3) is expressed in linear relation, and the line of gradient k_0 is obtained. This k_0 is given as fractal dimension of image X.

4. Results and Discussions

The sound monitoring system performance tests are done for the microphone sensoring and noise receptivity.

For the noise cut off performance of the sensor cover, the material of normal and porous styrene foam are compared. The results in case that the 2000Hz frequency sound is emitted by the speaker from the 100mm distance are shown in Figure 6. The porous material cover is more excellent than normal styrene foam in the performance to shut off air propagation sound noise from Figure 6. The maximum input level of normal styrene foam is –42dB and that of porous material is –48dB, and approximately -22dB of maximum level in the case without covering the microphone sensor. When the sound pressure level is decrease in 20dB, the maximum input become 1/10 times in intensity of sound data. The porous styrene foam cover is more effective for noise receptivity from these results and porous material is used in this study for sensor cover.

The examination of microphone embedded depths both 5mm and 15mm in the steel platform is performed. The experimental results are shown in Figure 7. The case of 5mm of embedded depth is little smaller sound input level than the other case, the 5mm case is able to measured clearly significant signal in the all frequencies range. As for the reason of this tendency, the non-significant sound signal is taken from the surface of wall of embedded hole and the side of microphone. This non-significant signal will be chance the noise component and decreases the S/N characteristic of sensor system. And the 15mm depth platform has possibility of

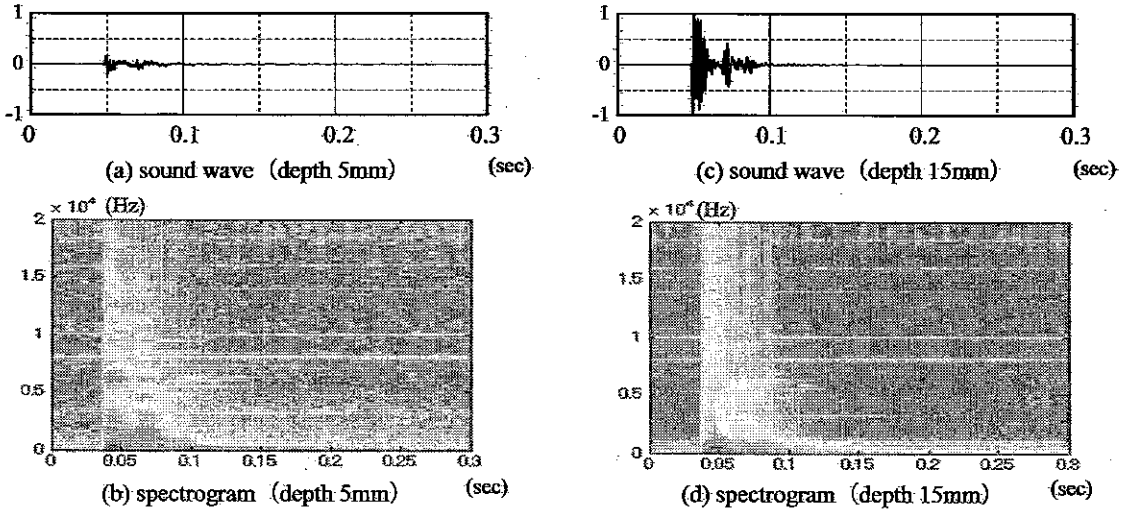

Figure.7 Comparison of steel pedestals (sound by hammering)

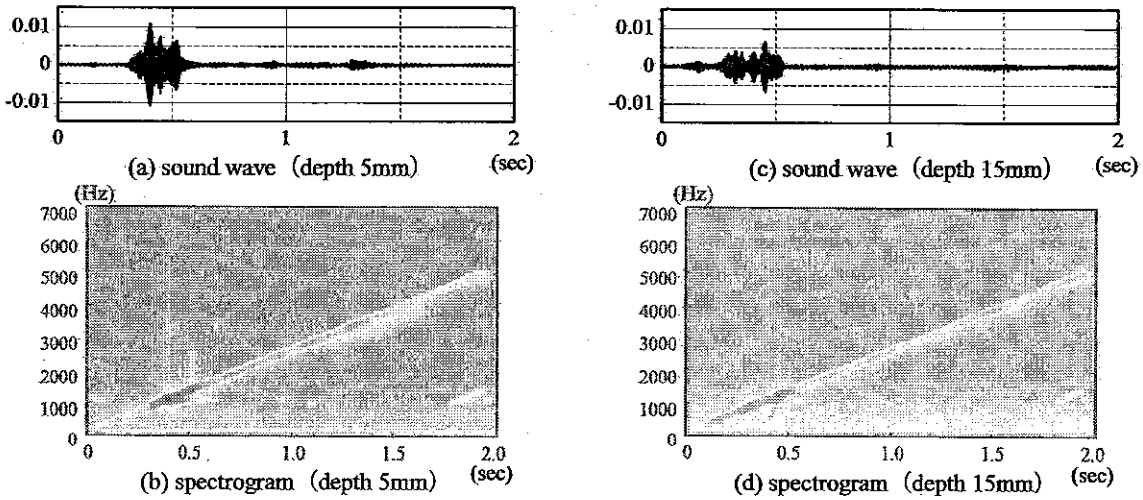

Figure.8 Comparison of steel pedestals (sweep sound)

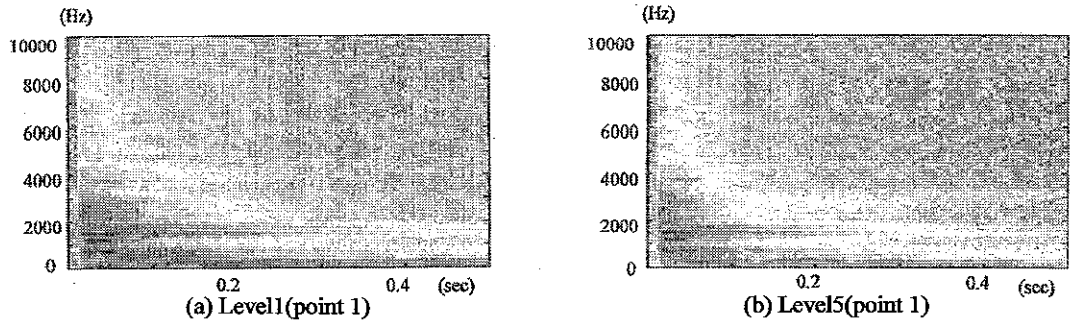

(a) Level1(point 1) (b) Level5(point 1)

Figure.9 Sound spectrogram (sound by hammering)

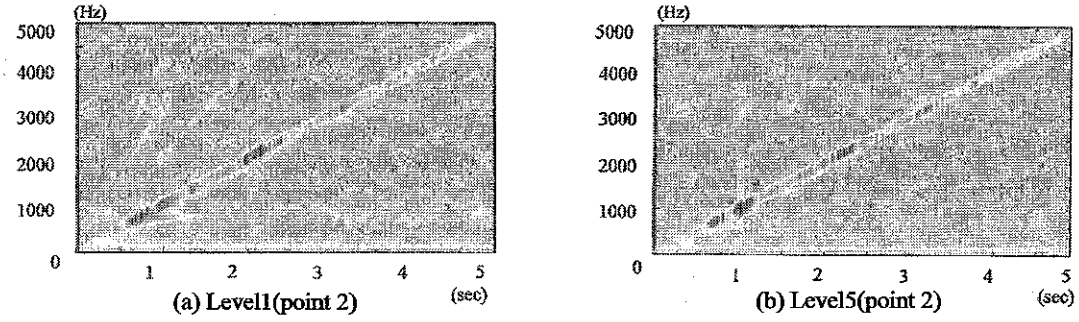

(a) Level1(point 2) (b) Level5(point 2)

Figure.10 Sound spectrogram (sweep sound)

jumping or colliding of microphone due to the impact of hammering excitation. Figure.8 is the results of inputting sweep sound excitation. The gain of monitoring data is little change due to input frequencies, the main factor of this tendency is given from microphone gain characteristic. In the case of using 5mm depth of platform, the sound data also can be measured very clearly. From the above results, the steel pedestal that embedded depth is 5mm are adopted in this study. It is presumed that the sound monitoring system has a possibility to catch the change of the sound characteristic due to damage level in steel structure.

The investigation of damage identification on steel bridge structural model is actually performed. The 5 hypothetical damage conditions in Table.2 are given on the structural model, and the sound data is measured in each damage condition from 7 points.

The sound spectrograms are calculated to grasp the frequency characteristic in non-damaged and damaged conditions. Figure 9 is the analytical results of sound spectrogram at point 1 by hammering excitation. There are some difference occurring between level1 and level5. The response continuance time is short with increase of damage level especially in the over 1800Hz frequencies. This phenomenon means that both sound response and damping characteristics change by effect of the hypothetical damage. Figure 10 shows the analytical results of sweep sound excitation case measured at point 2. When two conditions of non-damaged and damaged in Figure 10 are compared, significant signal level of non-damaged condition (a) is lager than level5 of damaged case (b). This phenomenon will occur by increase of damping due to damage increasing. The Frequencies characteristic of damaged case quite change

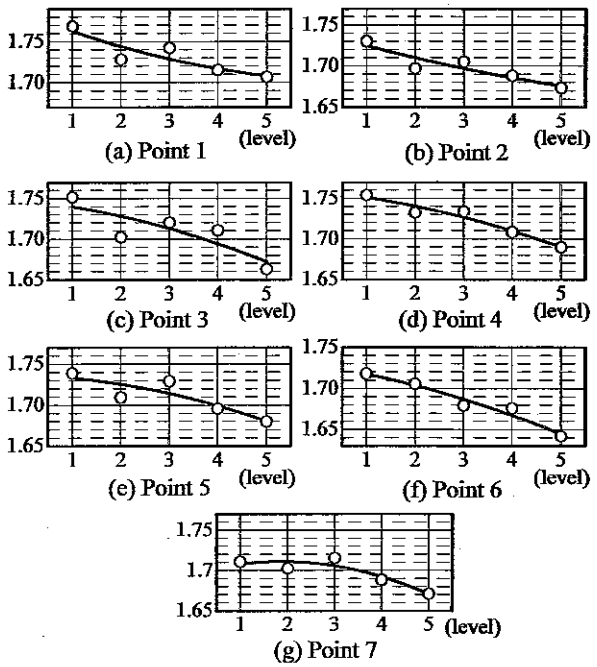

Figure.11 Fractal dimension and damage level

in approximately 1000Hz. The response besides 1000Hz occurred in non-damage condition, but damaged condition is not excitation other frequencies component. From results, sound spectrogram is able to judge the qualitative change in the sound characteristic of structures easily and visually.

The fractal dimension analyses are carried out to the spectrogram of sound monitoring data excited by hammering. The relation between the fractal dimension and damage level is shown in Figure.11. The results in Figure.11 have the tendency of decrease the fractal dimensions with increase of damage in every

measurement point. The qualitative characteristics of sound response in both time and frequency domain on sound spectrogram are simplified due to increasing of damage. This thing means that the self-similarity in spectrogram image increase and the fractal dimensions decrease. Therefore, it is considered that the fractal dimensions are expressing the quantitative level of damage from sound monitoring data.

The damage identification method in this study has possibility to provide the quantitative analysis for steel bridge structures.

5. Conclusions

The purpose of this study is to propose a sound monitoring system for bridge structures and investigate damage identification method by using sound monitoring data. In the sound monitoring system, it is possible to take the 8 channels of sound data at the same time and record directly in PC for digital sound. The system is constructed by using digital audio interface and dynamic microphone sensors. The damage identification method in this study is fractal dimension analyses performed for sound spectrogram on damaged and non-damaged data, and alteration of fractal dimension is investigated.

The major conclusions obtained in this study are summarized as follows: The usual microphone is used as sensor in the sound monitoring system of this study. The porous styrene foam cover is more effective for noise receptivity from results, porous material is used in this study for sensor cover. In the case of using 5mm embedded depths of platform, the sound data can be measured very clearly. From the above results, the steel pedestal that embedded depth is 5mm are adopted in this study.

In experiment using a steel specimen of bridge model, the applicability as damage identification method is examined. The sound spectrogram is able to judge easily and visually the qualitative change in the sound characteristic of structures. It is considered that the fractal dimensions are expressing the quantitative level of damage from sound monitoring data. The damage identification method in this study has possibility to provide the quantitative analysis for steel bridge structures.

6. Reference

1) Kazuhiro Nishikawa : Life Time and Maintenance of Highway Bridges, Journal of Structural Mechanics and Earthquake Engineering, No.501/I-29, pp.1-10, 1994.(In Japanese)
2) JSCE : Guidelines for Bridge Vibration Monitoring, JSCE,2000.(In Japanese)
3) Ippei Kondo and Takuji Hamamoto : Damage Detection of Multi-storey Buildings using Random Response Data from Shaking Table Tests, Journal of Structural and Construction Engineering (Transactions of AIJ), No.473, pp67-74, 1995.(In Japanese)
4) Masafumi Kato, Yasushi Takagi and Shizuo Simada:Vibrational Characteristics of a PC Frame Bridge under The Failure Process, Proceedings of The Japan Society of Civil Engineers, No.341, pp.113-118, 1984.(In Japanese)
5) Kato, M. and Shimada, S. : Vibration of PC Bridge during Failure Process, Journal of Structural Engineering, ASCE, Vol.112, No7, pp1692-1703, 1986.
6) Tomoyuki Yamazaki, Tosiyuki Ohshima, Kohki Ohnishi and Shuichi Mikami:Study on Damage Evaluation of Joint in Steel Member by using Local Vibration Excitation, Journal of Applied Mechanics, JSCE, Vol. 5, pp.837-846, 2002. (In Japanese)
7) Masato Abe, Yozo Fujino, Tomonori Nagayama and Hong Vu-Manh : A non-iterative approach in vibration-based damage detection for a damped mechanical, Journal of Applied Mechanics, JSCE, Vol. 5, pp.855-862, 2002.(In Japanese)
8) Akira Nishimura, Manabu Fujii, Ayaho Miyamoto and Taiichi Kagayama:Sensitivity of mechanical behavior of bridges for their damage assessment, Journal of Structural Mechanics and Earthquake Engineering, No.380/I-7 , pp.355-526 , 1987.(In Japanese)
9) Takashi Obata, Kouhei Ueda, Toshiro Hayashikawa and Koichi Sato:Consideration of Applicability for Damage Identification Steel Bridges by using of Sound data, JSSC Journal of Constructional Steel,Vol.8, pp.611-616, 2000. (In Japanese)
10) Takashi Obata, Kouhei Ueda, Toshiro Hayashikawa and Koichi Sato:Consideration on Damage Identification of Steel Bridge Structures based on 1/f noise analyses, Proceedings of Hokkaido Chapter of the JSCE, Vol57, pp.104-107, 2001. (In Japanese)
11) Takashi Obata, Kouhei Ueda, Toshiro Hayashikawa and Koichi Sato:Study on Damage Identification of Steel Bridge Structures based on Characteristic of 1/f noise, JSSC Journal of Constructional Steel, Vol.9, pp.569-574, 2001. (In Japanese)
12) Takashi Obata, Kouhei Ueda, Yasunori Miyamori, Toshiro Hayashikawa and Koichi Sato : Fundamental Study on Applicability of Sound Monitoring for Damage Identification on Steel Bridges, Journal of Applied Mechanics, JSCE, Vol. 5, pp.827-836, 2002.(In Japanese)
13) ROLAND HOMEPAGE, Products information, http://www.roland.co.jp/products/index.html
14) Sadaoki Furui : Digital Processing of sound, Tokai University Press, 1985.(In Japanese)
15) The Math Works Inc. : MATLAB Signal Processing Toolbox User's Guide, The Math Works Inc., 1999.

(Received July 31, 2003)

A consideration of bridge vibration measurement by using digital video processing with PC camera

Yasunori Miyamori*, Takashi Obata**, Kazunori Adachi***, Toshiro Hayashikawa****, Koichi Sato*****

* Dr. of Eng., Res. Assoc., Dept. of Civil Eng., Kyushu Univ., 6-10-1 Hakozaki, Higashi-ku, Fukuoka 812-8581
** Dr. of Eng., Res. Assoc., Div. of Structural and Geotechnical Eng., Hokkaido Univ., Kita 13 Nishi 8, Kita-ku, Sapporo 060-8628
***Ms. of Eng., Chubu Regional Bureau, Ministry of Land, Infrastructure and Transport, 2 Tsukiji-cho, Minato-ku, Nagoya 455-0045
**** Dr. of Eng., Assoc. Prof., Div. of Struct. and Geotech. Eng., Hokkaido Univ., Kita 13 Nishi 8, Kita-ku, Sapporo 060-8628
***** Dr. of Eng., Prof., Div. of Struct. and Geotech. Eng., Hokkaido Univ., Kita 13 Nishi 8, Kita-ku, Sapporo 060-8628

Vibration measurement is important task to identify structural characteristics for bridge managements. Many new sensors for vibration monitoring based on innovative information processing technologies are proposed recently. In this study, low-cost mobile vibration displacement measuring system is developed by using household PC camera. And vibration-measuring experiments are performed to clarify applicability of the system.
A PC camera records movies of vibrated target. Displacement time history of the target is obtained by digital image processing. Field experiments are performed on free damped vibration of a pedestrian bridge. From experimental results, displacement wave and predominant vibration frequency of bridge is obtained almost correctly and applicability of this measuring system is verified for bridge vibration monitoring.

Key Words: Bridge vibration measurement, Digital Video Processing, CCD Camera

1. Introduction

Structural maintenance and rehabilitation to aging bridges has attracted attention in infrastructure management. Proper maintenance and rehabilitation extend service life and preserve safety and service ability of structures. These bridge managements are performed based on structural condition of bridges. The general inspection method of damage identification of bridge structures is eye-estimation by maintenance specialists. And special-purpose systems are used for quantitative measurement such as vibration monitoring. Under these conditions, rapidly increase of long serviced bridges cause large serious problems, which are the shortage of professional engineers and maintenance cost. Therefore, it is necessary to establish a convenient and inexpensive structural monitoring system for structural characteristics investigation.

In the performance assessments of bridges, dynamic characteristics of structures are important measuring item. Vibration of structure is gauged as acceleration, velocity, displacement and so on. Dynamic displacement of structure is most dominant in low frequency range such as fundamental natural frequency of bridges. And displacement is easy to comprehension vibration shapes. Many conventional displacement sensors have been developed at present. These sensors are divided into contact type and non-contact type. Contact type sensors need reference point near measurement point, and this requirement often prevents gauging deflection at center of the span of bridge girders. Non-contact type sensors with image sensor such as CCD (Charge Coupled Device) need no reference point. However, optical sensing systems with image sensor are generally very expensive and they have difficulty to ordinary use. Recent development of semiconductor technology improves the sensor capability and reduces the cost of device. And recent high performance PC processors stimulate development of data processing software. These innovations make digital image processing popular and inexpensive. Therefore, there is a possibility to establish inexpensive dynamic measurement system with adequate ability for bridge vibration monitoring. And these monitoring systems will contribute to efficient infrastructure managements.

The digital image processing for infrastructure management have been applied to static phenomena such as detecting cracks

on pavements and concrete piers[1),2)]. Measurements of static deflection of beam or bridge are performed in references 3 and 4. For application in dynamic measurement, Isha et al.[5)] measured vibration of portal marker columns and lightning poles on highway viaducts. And there are few precedents for vibration measurements of bridge girder using these kinds of monitoring system.

In this study, low-cost mobile vibration displacement measuring system is developed[6)]. And measuring experiments on bridge vibration are performed to clarify applicability of the system. This vibration displacement measuring system is fabricated by using a household PC camera with a fieldscope. Vibration measuring experiments are performed on free damped vibrated pedestrian bridge. A target is set on bridge surface at a center of the span. A PC camera captures images of vibrated target from top of abutment. A notebook PC receives captured images and saves as a digital video movie. An image-processing program calculates time history displacement immediately after recording. In the image processing procedure, dynamic displacement is obtained from movement of the target comparing each video frame. In these experiments, acceleration sensors are also fitted on bridge to compare the results of displacement measuring system. Therefore the purpose of this study is to show the performance and applicability of this measuring system by comparing calculated displacement data and acceleration data. And the possibility of structural identification using this measuring system is discussed from these experimental results.

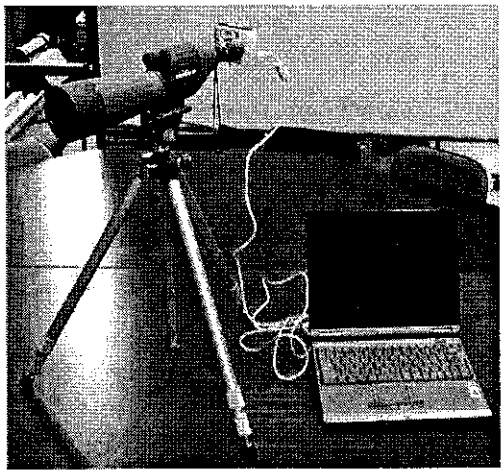

Photo 1. The Displacement Measuring System

Table 1. PC Camera Specifications

Intel Pocket PC camera (CS 630)	
Image Sensor	CCD (640x480)
Lens	50 Deg., F=2.8
Frame rate	30 fps (Maximum)
Interface	USB 1.1
Dimension	W 107mm, H 70mm, D 35mm

Table 2. Fieldscope Specifications

Kenko PRO FIELD 70	
Zoom	20 – 50x
Angle of view	1.6 – 0.9 Deg.
Object lens diameter	70mm
Weight	980g
Length	380mm

2. Displacement measuring system and data processing procedures

2.1 Non-contact displacement measuring system

The displacement measuring system developed in this study is composed of a household PC camera with a fieldscope, a notebook PC and a 20mm square target on bridge. Photo 1 shows the appearance of the displacement measuring system. PC camera, which is often called 'Web cam' or 'USB Camera', are popularly used for personal videophone via Internet. This PC camera with CCD sensor has USB interface to connect PC. A fieldscope, which has zoom lens, is attached to the camera for magnifying captured image. The magnification of fieldscope is fixed to 50x. The specifications of PC camera and fieldscope are summarized in Table 1 and Table 2. Total cost of the system is less than 40,000 yen and total weight is less than 1.5kg without notebook PC. Therefore inexpensiveness and mobility are mainly advantages of this system and its cost will reduce by using simple telephoto lens instead of fieldscope.

The resolution of this measuring system is influenced by frame rate and frame size. Frame rate is number of capture images at one second and this is equivalent to sampling frequency. Frame size is the pixel size of captured image. It is equivalent to bit resolution of A/D board. Data transfer size between PC and camera is estimated by multiplying frame rate by frame size. There is an unavoidable trade off between frame size and frame rate in consideration of USB data transfer speed. In this study, the frame size is decided to 160x120 pixels to keep maximum frame rate of 30 fps.

2.2 Image processing Procedure

The movie of vibrated target taken by PC camera is saved as an AVI format file to hard disk in computer. After recording movie, the image-processing program divides the movie into picture frames based on frame rate. The dynamic displacement of the target is taken from difference of target position between each picture frames. The image processing procedures are performed in following steps and Fig. 1 (a)-(c) are processed images at each step[7),8)].

(1) Color space transformation

The original color space of image taken by PC camera is RGB color system. RGB color system consists of luminance of red, green and blue to express natural color. Because image processing in this study is performed based on monotone luminance of pixels, RGB color image is transformed to monochrome color image. The following equation is used for

color space transformation in each pixel.

$$Y=0.299R+0.587G+0.144B \cdots\cdots (1)$$

where Y is equivalent luminance value of original RGB image. R, G and B are luminance value of each color components of red, green and blue. Fig. 1(a) shows a gray level transformed image.

(2) Image segmentation

Image segmentation is a task to segment monochrome image into a high luminance target and low luminance background. Bilevel luminance thresholding is a basic method to set a mid-gray threshold to segment the target from the background. Threshold level is set to 0.8 of a full luminance in consideration of pretests. Binary image which is shown in Fig 1(b) is taken by image segmentation. Binary image is defined as discrete image function $F(j,k)$ with two values of 1 or 0. When luminance of a pixel is more than threshold, value of image function $F(j,k)$ is one. When a luminance is less than threshold, value of image function is zero. The segmented area is labeled to operate the area as a meaningful assembly of pixels.

(3) The centroid of image

The centroid called center of the gravity, which is shown as a white point in Fig 1(c), is one of typical parameters of object position. For a discrete image function $F(j,k)$, the center of the gravity in XY plane is shown in Equation 2 and Equation 3.

$$\bar{x}=\frac{\sum_{j=1}^{J}\sum_{k=1}^{K} jF(j,k)}{\sum_{j=1}^{J}\sum_{k=1}^{K} F(j,k)} \cdots\cdots\cdots (2)$$

$$\bar{y}=\frac{\sum_{j=1}^{J}\sum_{k=1}^{K} kF(j,k)}{\sum_{j=1}^{J}\sum_{k=1}^{K} F(j,k)} \cdots\cdots\cdots (3)$$

where J is x-direction length and K is y-direction length of image. In this study, $\bar{y}$ is regarded as vertical displacement of target. The location of the target is expressed in the center of the target and dynamic displacement is relative difference of the center of the target between each picture frame.

2.3 Displacement calculation from acceleration

In this study, acceleration is also measured by acceleration sensors to compare the displacement recorded by PC camera. The time-history displacement is calculated based on the linear acceleration method. Velocity and displacement in each time step is calculated by following equations.

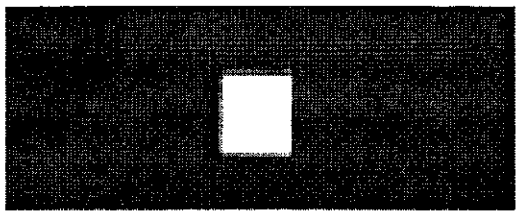

Fig. 1 (a) Monochrome Image

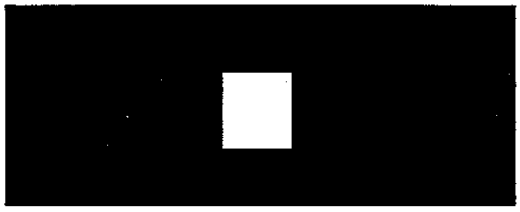

Fig. 1 (b) Binary Image

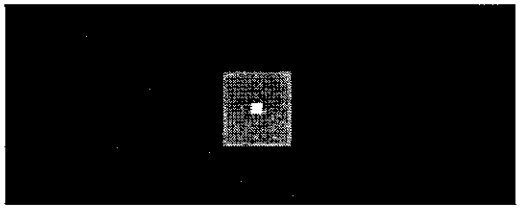

Fig. 1(c) Center of The Gravity

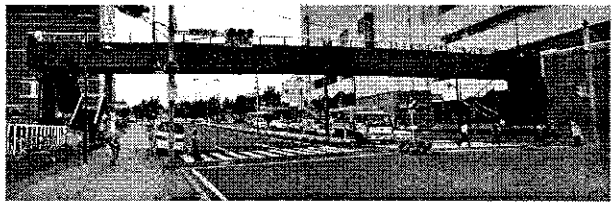

Photo 2. Pedestrian bridge

$$\dot{u}(t+\Delta t)=\dot{u}(t)+\frac{1}{2}\left[\ddot{u}(t+\Delta t)+\ddot{u}(t)\right]\Delta t \cdots (4)$$

$$u(t+\Delta t)=u(t)+\frac{1}{2}\left[\dot{u}(t+\Delta t)+\dot{u}(t)\right]\Delta t \cdots (5)$$

where u is response displacement and Δt is time step.

Experimental acceleration data has unavoidably noise and non-zero mean value. Displacement or velocity data integrated from acceleration are often not calculated correctly because of these errors. The moving average method with a quadratic polynomial weight function is used for error canceling and a residual linear trend is also removed from computed data.

3. Vibration measurement experiments

In field experiments, the dynamic deflection of pedestrian bridge shown in Photo 2 is measured. The span length is 35.6m and width is 3.0m.

The location of instruments is shown in Fig. 2. PC camera and notebook PC are positioned on the abutment heading for the target at the center of the span. The distance between the camera and target is 17.8 m. Acceleration sensors are set up at 1/6~5/6 points of the span. The input acceleration data are acquired to

another PC via dynamic strain amplifiers and A/D conversion board. The sampling frequency of the A/D board is 1000Hz. The response displacement calculated from acceleration data at the center of the span by linear acceleration method. Data from other 4 sensors are used for verifying the first vibration mode shapes.

The experiments are performed in 2 excitation cases. In the first case, one person repeats jumping on the bridge to oscillate the first vibration mode. PC camera and acceleration sensor measures the free damped vibration after forced excitation. In the second case, one person jumps only once on the center of the span. Camera and accelerometers start recording data at the same time. The excitation force of the second case is comparatively small and amplitude of response displacement is expected to be considerably small. The performance of the system for small amplitude vibration is tested in this excitation case.

Fig. 3 shows the response displacement of the bridge measured by the proposed displacement measuring system. Fig. 4 is the calculated displacement by using the linear acceleration method and Fig. 5 is original acceleration data. In these figures, (a) are time-history waves and (b) are these Fourier spectrums.

Amplitude value of displacement and wavelength are almost same in Fig. 3(a) and Fig. 4(a). The displacement measuring system has passable capability from result of time-history displacement. The waveform in Fig 3(a) has a little roughness due to insufficiency space resolution. In image processing steps, pixel size of the target is 11px square at the first frame. The space resolution is 1.82mm/px considering the real target size that is 20mm square. In Fig. 3(a), displacement varies less than 1.82mm intervals however. As shown in Fig.6, luminance of pixel at target edge is intermediate between white and black. The value at this pixel is classified as white or black according to threshold in bilevel luminance thresholding. And the number of pixels in target area changes at each frame. Therefore, calculating the centroid of a target, which is thought as a kind of averaging method, improves space resolution in appearance.

In frequency domain, the peak frequency of the 1st vibration mode is 2.14Hz in both Fig. 3(b) and Fig. 4(b). The computed

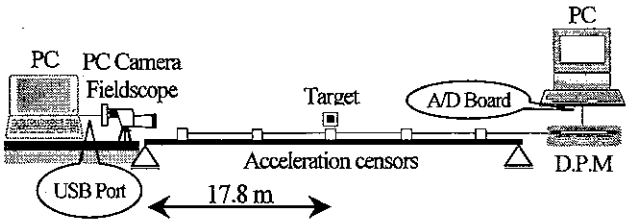

Fig. 2 Experimental system

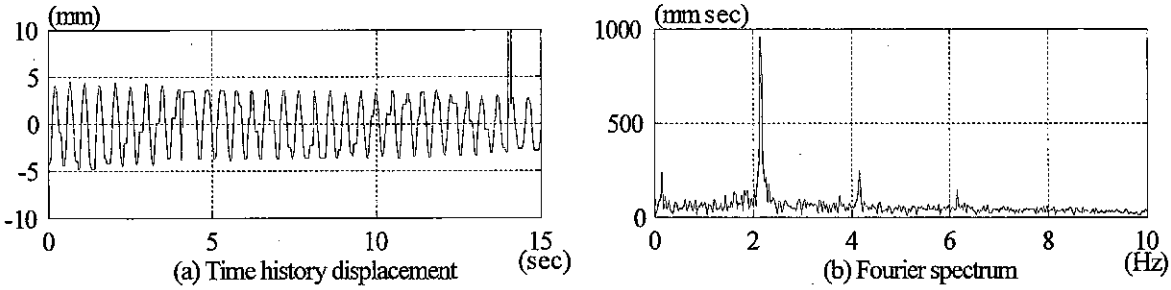

Fig. 3 Measured displacement by image processing (1st case)

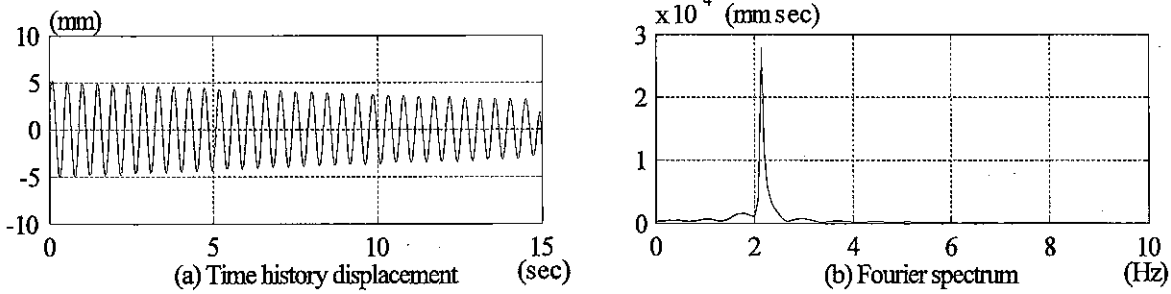

Fig. 4 Calculated displacement from acceleration (1st case)

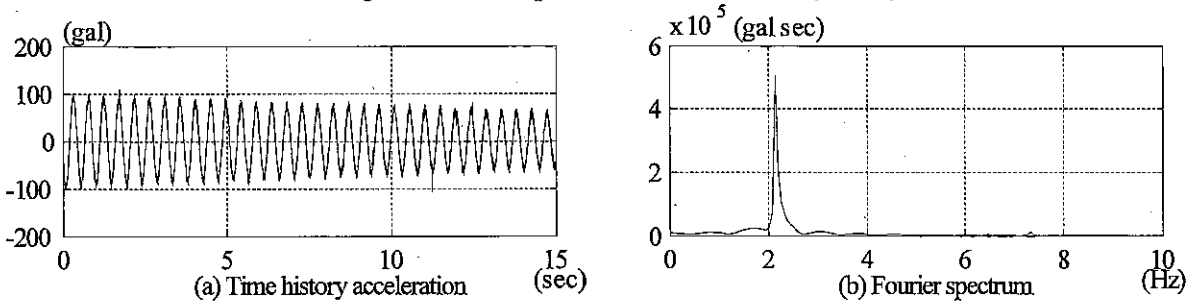

Fig. 5 Measured acceleration (1st case)

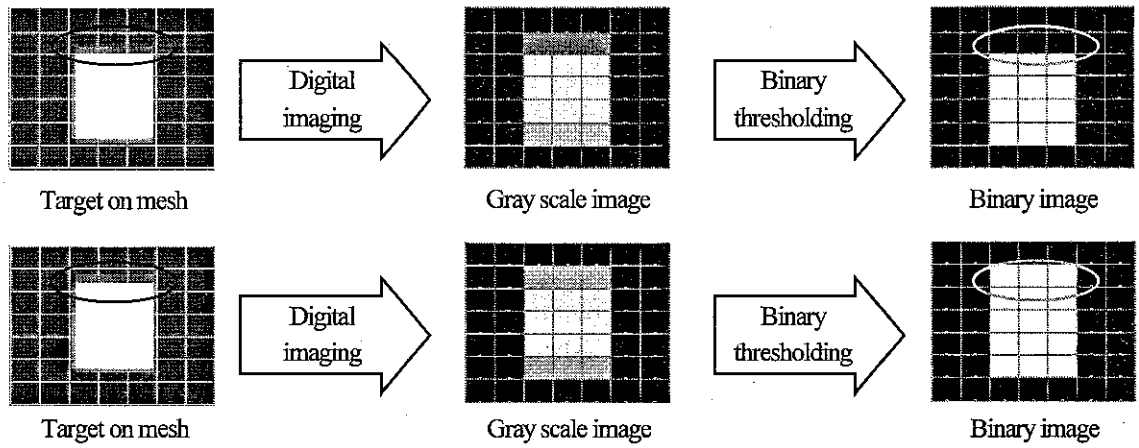

Fig. 6 Difference of target area in binary image

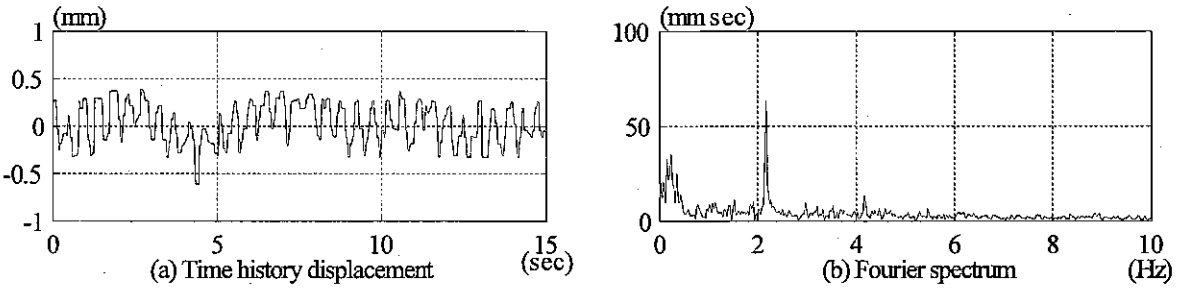

Fig. 7 Measured displacement by image processing (2nd case)

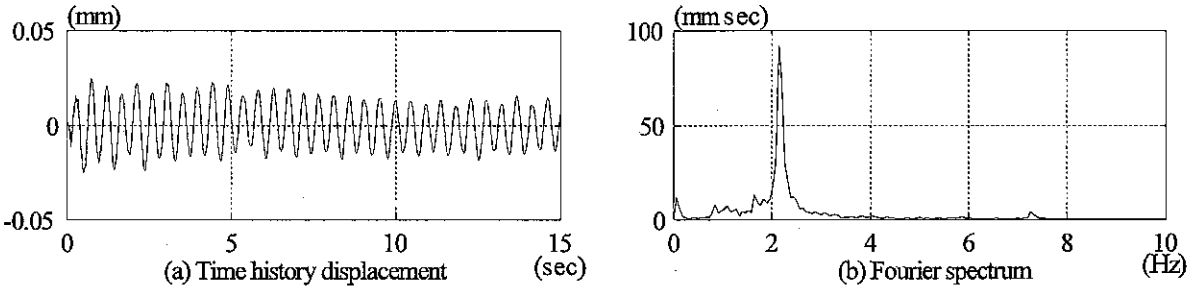

Fig. 8 Calculated displacement from acceleration (2nd case)

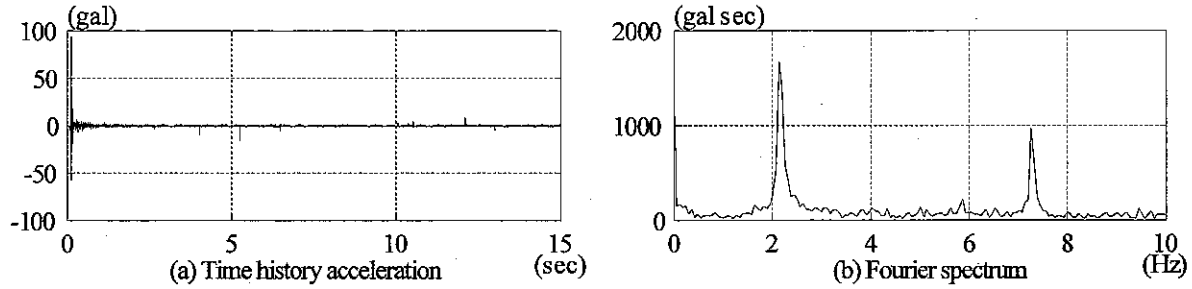

Fig. 9 Measured acceleration (2nd case)

displacement from digital video movie has sufficiently precision in this frequency range. Moreover in Fig. 3(b), another peak appears at 4.16Hz, which is almost twice of the first predominant frequency. It is thought that this peak is due to varying the number of target pixel shown in Fig. 6. This varying target area frequently occurs in both end of up and down vibration. Considering rapidly improvement of image sensors and development of high-speed interface, increasing frame size will solve roughness of time-history wave and false peak of spectrum. Therefore, the displacement measuring system has ability to measure the bridge vibration in predominant vibration mode.

Figs. 7-9 are results in second experimental case. The excitation force is impulsive and bridge is vibrated with small amplitude. Response acceleration shown in Fig. 9 is damped immediately after excitation, and higher frequency components predominate. For calculated displacement from acceleration data shown in Fig. 8, amplitude of displacement wave is

considerably small and the 1st vibration mode predominates at 2.14Hz. The different results are shown in Fig. 7. The amplitude of image-processed displacement is more than 10 times as large as displacement in Fig. 8(a). The maximum amplitude displacement 0.6mm is almost 1/3 of the space resolution of 1.82mm/px. Therefore it seems that this displacement measuring system has less preciseness for small amplitude vibration such as this excitation case. However in Fig. 7(b), the 1st vibration mode clearly appears at 2.17Hz. Little movement of the center of target is correctly found in frequency domain by these image processing. From these results in the second case, predominate vibration frequency is evaluated though precision of the measurement system declines for small amplitude vibration. Therefore this non-contact displacement measuring system has possibility to estimate predominant frequency for microtremor measurement.

4. Conclusions

Low-cost mobile non-contact displace measuring system is developed for bridge vibration measurement. The measuring system is composed of household PC camera, fieldscope and notebook PC. The PC camera records vibration of target on bridge as a digital video movie. Image processing program computes dynamic displacement of target from changing position of target.

Field experiments are performed on pedestrian bridge in two excitation cases. In the first case, the measuring system records free damped vibration. In the second case, the system measures small amplitude vibration. The main results of the present study are summarized as follows:

1) In the first experimental case, vibration amplitude and predominant frequency are almost exactly measured by proposed measuring system. Calculating the center of the gravity as target position increases a resolution of measured displacement.
2) Roughness of waveform and false peak of spectrum are caused because of small frame size of captured image and it will be easily improved by increasing frame size considering recent development of image sensors.
3) The amplitude of small vibration is not computed exactly in second excitation case. However, predominant frequency is identified almost exactly. Therefore this measuring system has applicability to microtremor measurement for identification of structural characteristics.

It is expected that structural monitoring will be more important task in infrastructure management in the near future. Optical vibration measurement and analysis has many applications and possibility as one of low-cost solutions. The non-contact displacement measuring system using ordinary instruments and basic image processing techniques applied in this study has large possibility for bridge vibration measurement and determining structural properties.

References

1) Toshihiko Fukuhara, Keiji Terada, Makoto Nagao, Atsushi Kasahara and Shigeki Ichihashi, Automatic Pavement-Distress-Survey System, *Journal of Transportation Engineering*, Vol. 116, No. 3, pp. 280-286, 1990.
2) Yoshimasa Nakata, Masanobu Sugimoto, *The traveling method of crack investigation using the High Definition Video System camera*, Proceedings of colloquium on bridge vibration '01, pp. 201-204, 2001. *(in Japanese)*
3) David V. Jauregui, Kenneth R. white, Clinton B. Woodward and Kenneth R. Leitch, *Noncontact Photogrammetric Measurement of Vertical Bridge Deflection*, Journal of Bridge Engineering, Vol. 8, No. 4, pp.212-222, 2003.
4) Gongkang Fu and Adil G. Moosa, *An Optical Approach to Structural Displacement Measurement and Its Application*, Journal of Engineering Mechanics, Vol. 128, No. 5, pp. 511-520, 2002.
5) H. Isha, T. Kitada, T. Yamaguchi, K. Miyawaki, Y. Otoguro and J. Toki, *Fundamental study about early detecting portal marker columns and lighting poles on highway bridges*, Proceedings of colloquium on bridge vibration '01, pp. 239-244, 2001. *(in Japanese)*
6) K. Adachi, Y. Miyamori, T. Obata, T. Hayashikawa and K. Sato, *A consideration on applicability of CCD camera for household use to non- contact displacement measuring system*, Proceedings of annual conference of the Japan society of civil engineers, Vol. 57, pp.1143-1144, 2002.
7) Pratt, William K., *Digital Image Processing*, J. Wiley, New York, 1991.
8) The MathWorks, Inc., *Image Processing Toolbox User's Guide*, The MathWorks, Inc., 2001.

(Received July 31, 2003)

The telemetry system based on data communication technology for remote monitoring of bridge construction

Takatoshi OKABAYASHI* , Toshihiro OKUMATSU **

* Dr. of Eng., Professor, Dept. of Civil Eng., Nagasaki University, 1-14 Bunkyo-machi, Nagasaki 852-8521
* *M. Eng., Research Associate, Dept. of Civil Eng., Nagasaki University, 1-14 Bunkyo-machi, Nagasaki 852-8521

As progress of the digital communication technology, structural behavior at remote location can be monitored automatically in real time. This paper describes the data communication methods for monitoring of highway brides. The communication methods are the wireless LAN system, the ISDN public telephone line and the mobile communication service. The static data such as strains and loads, the vibration data and the image data are treated. As practical remote monitoring cases, the remote monitoring by the wireless LAN, the remote monitoring by the ISDN, the remote monitoring by the mobile communication, the remote monitoring by Internet camera, and remote monitoring on cellular phone display screen are introduced in this paper.

Key Words: remote monitoring, data communication, wireless LAN, mobile communication, Internet camera, cellular phone

1. Introduction

Many highway bridges, constructed in Japan after World War II, have been becoming old for use. These bridges should be maintained and prolonged their lives under the circumstance of domestic situations. Comprehensive strategy will be required for management of infrastructures[1]. Developing effective structural maintenances such as evaluating structural condition, detecting damages, and repairing are present subjects to be treated. To achieve health monitoring of existing infrastructures, developing (1) sensing technologies[2], (2) data processing technologies for detecting structural damages[3),4)], and (3) data transmission for remote monitoring are important.

The authors have developed the remote monitoring system [5),6)]with digital communication technologies, and then applied to site monitoring on bridges. To monitor many decentralized highway bridges at times, low cost and portable monitoring system would be effective for actual use. By developing the featured monitoring system, an innovation in measurement of static or dynamic behaviors of bridges would be brought. Benefit from following reasons of (1) development of PC technologies (processing speed, low cost, portable style), (2) spread of digital communication technologies (IT, TCP/IP), (3) spread of mobile communication tool (wireless radio, cellular phone, combination with PC), and (4) progress of hardware and software for measurement (A/D board, LabVIEW[7]), an effective remote monitoring system for health monitoring can be established.

In this paper, the authors described bridge remote monitoring focused on data transmission, based on past researches and developments. The introduced monitoring cases using respective data transmission technologies are as follows. Fig.1 shows the abstract of bridge remote monitoring.

1) Remote monitoring with wireless LAN[6)]
2) Remote monitoring with public digital phone line[6)]
3) Remote monitoring with mobile communication devices[5)]
4) Remote image monitoring[6)]
5) Remote monitoring on cellular phone display screen[8)]

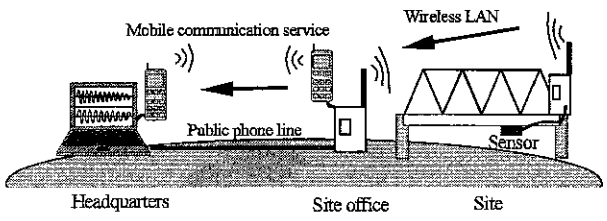

Fig.1 Bridge remote monitoring system

2. System configuration for remote monitoring of measurement data

Remote monitoring system consists of three parts, which are the sensing part, data transmitting part, and data-processing part. Innovations in technologies have been progressing in all of these parts. Fig.2 shows the diagram of flow of the remote monitoring system.

2. 1 Sensing devices

Conventional sensing devices such as strain gauge, displacement meter, and accelerometer have been used for measurement of structural dynamic or static change. With rapid progress of sensing devices, new types of sensing devices using fiber optic, carbon fiber or some other materials, have been developed. These types of devices are reasonable for structural health monitoring and its maintenance. There are some examples for evaluating existing aging structures.

2.2 Data processing

In observing structural characteristics of vibration such as natural frequency, damping constant, and vibration mode, by ambient vibration of the structure, high accurate structural identification is indispensable. Development of theory of mode analysis helps us in estimating vibration characteristics. On the other hand, progress of computer hardware and interface for A/D converter makes the total measurement system cost effective and portable.

With these kinds of progresses, sensed data of structure such as strain, displacement, and acceleration, are processed in high speed, and realize real-time structural health monitoring.

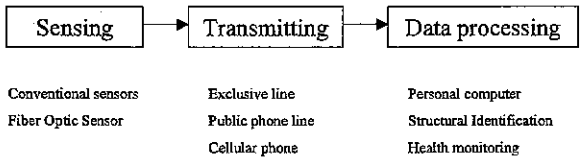

Fig.2 Flow of the remote monitoring

2.3 Data transmitting

In order to monitor the condition of structures at a distant place, we have to establish a connection for data transmission between the site and monitoring place. Although some remote monitoring of structure or unmanned construction[9] were executed before, exclusive data transmitting line, its initial cost for the installation is not small, had been mainly used for data transmission. More convenient and less expensive data transmission method should be introduced to these kinds of fields. Public phone line is conventional media for sending data. Data transmitting speed and its capacity using digital communication and mobile wireless communication of public phone have been developing rapidly by progress of our lifestyle. By using these public services, an innovation on remote monitoring of infrastructures will be brought.

3. Application of remote monitoring system for bridge management

3.1 Bridge remote monitoring with wireless LAN

(1) Bridge outline

Sashiki Bridge[10] is a 3-span consecutive extra dosed prestressed concrete bridge, constructed in Ashikita district, located in South Kumamoto, with a length of 225m, and a center span of 105m. Ashikita District is famous for producing large amounts of citrus fruits. Ashikita district aims at developing farming in this area and stability of its business by improving the distribution and transportation. In this district, the wide-area agricultural roads are now developing.

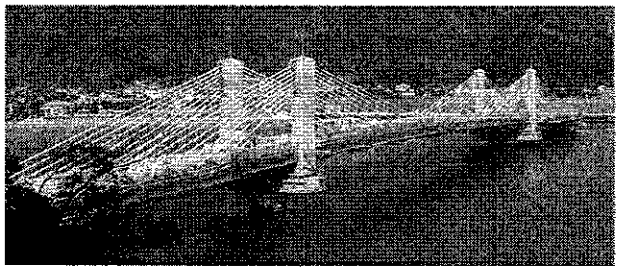

Photo.1 Sashiki Bridge

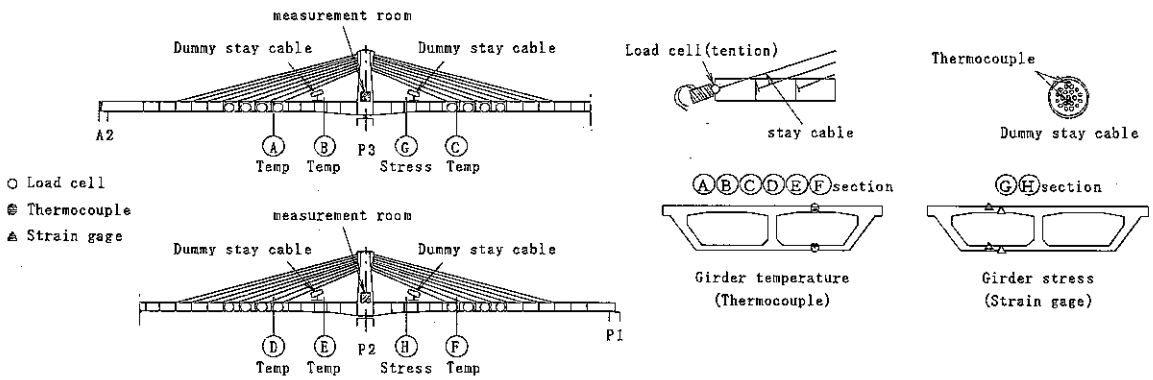

Fig.3 Measurement device layout

Table 1 Measurement items

Structural member	Measurement item	Measuring device	Purpose
Main girder	Temperature	Thermocouple	To ascertain deflection quantity caused by temperature change. To correct the actual measurement value to the design code temperature value.
	Stress	Strain gage	To confirm that variations in stress during the course of time are as designed by measuring concrete stress.
Stay cable	Tension	Load cell	To put on a PC tendon of the cables, and measure the initial tension and its variations during the course of time
	Temperature	Thermocouple	To ascertain the variations in tension during the course of time. To correct the actual measurement value to the design code temperature value.

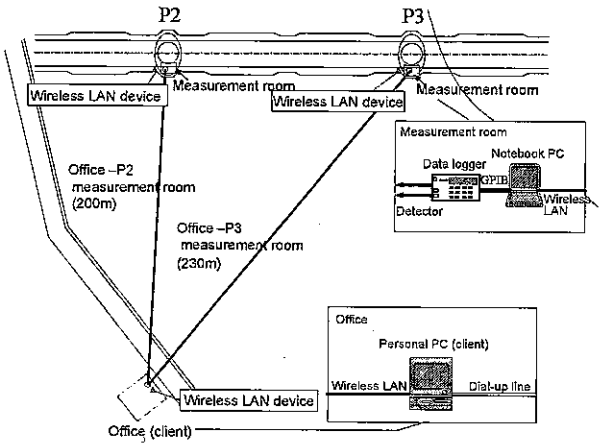

Fig.4 Remote monitoring system with wireless LAN

The outline of Sashiki Bridge is described below. Its general viewing is shown in Photo.1.

Type of bridge : 3-span continuous extra dosed pre-stressed concrete bridge

Bridge length (span) : 225.000m (60.750m + 105.000m + 57.513m)

Width : 2.000m + 7.250m ~ 2.000m + 10.250m

(2) Measurement items

The main construction management items of this bridge are camber management of the main girder and strain management of stay cables. Measurements were conducted under construction in order to precisely ascertain variations in the main girder and stay cables under construction during the course of time. Stress measurements were also obtained in order to ascertain the validity of the design condition. The measuring device layout and the main measurement items of this bridge are shown in Fig.3 and Table 1 respectively.

(3) Remote monitoring system with wireless LAN

The measurement rooms were set up at the P2 bridge support and P3 bridge support respectively for measurement under construction. In the individual rooms, the data loggers are permanently installed. The measurement data of temperature or diagonal member tension are automatically measured, and they are saved in the built-in memory of the data loggers temporarily. In order to manage the actual measurement data, which are obtained from the individual measurement rooms, at the site office approximately 200m away from the measurement rooms,

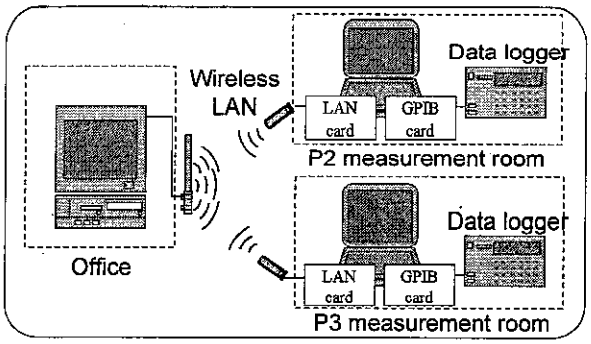

Fig.5 Configuration of remote monitoring system

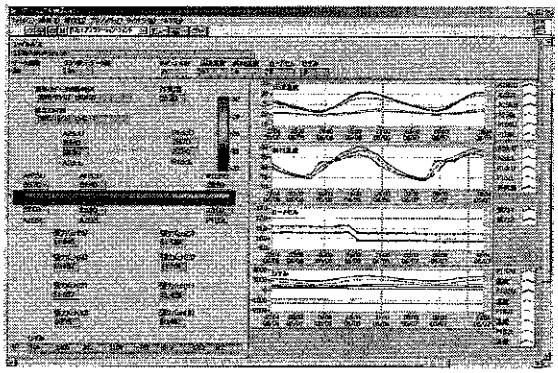

Fig.6 Monitoring screen created with LabVIEW

we connected the measurement rooms and the site office with wireless LAN bridge to constitute the construction site LAN. The wireless LAN bridge is the network for wireless communications using radio waves. Compared with the metal cable of telephone line and wired communications system through optical cable, it is only required to install radio antennas for wiring; communications LAN in the site can be constructed at a lower cost. Fig.4 shows the schematic diagram of remote monitoring system with wireless LAN for this bridge. Wireless LAN device BR-200 made by ICOM was used for this bridge. A non-directional antenna was installed in the site office, while a directional antenna was installed in each measurement room. A wireless LAN unit is different in data transmission distances by a combination of antennas to be used, and the maximum communications distance between directional antennas is approximately 2 kilometers.

(4) Remote monitoring

Fig.5 shows the system configuration of the remote monitoring. The data loggers and laptop PC with LAN card and GPIB card were installed in the measurement rooms set up at the P2 and P3 bridge support. The data loggers measured the data automatically every two hours. Actual measurements of temperatures of the main girder, concrete deflection quantity, temperatures of the dummy diagonal member, and the diagonal tension are minutely saved in the built-in memory. The data loggers are connected to the laptop PCs with GPIB and that enables to operate from the laptop PCs; HTTP is booted on the laptop PCs. Using GPIB enables each GPIB address to be assigned to each device; therefore, multi-channel measurement

device can be controlled simultaneously. Using the browser, the desktop PC of the site office (client-side) can operate the laptop PCs of the measurement rooms (the server side) by remote control. When URL is specified, the screen created with LabVIEW[7], a programming tool, as shown in Fig.6, is displayed. When a permanent file name is specified and executed, the laptop PCs of the construction site start to read the accumulated data from the data loggers. Later on, the measurement data are saved in a text file. The current temperature and deflection quantity, and variations for the past 48 hours are displayed on the browser. The saved data can be freely treated, by sharing the file via LAN.

3.2 Bridge remote monitoring with ISDN-line

(1) Bridge outline

Ootsurokawa Bridge, constructed in Fukui prefecture, is a part of the Tsuruga line of the Kinki Highway line. The bridge, as shown in Photo 2, has a continuous two-girder composite bridge with PRC deck, and mean-length of each center span of approximately 50m. Construction procedure-design for composite girder was made methodically. Girder pre-stress toward bridge axis was going to be installed with jacking operation so that tension stress would not be generated with influence of static load, creep, shrinkage, or thermal stress. Remote monitoring of normal force was conducted to ascertain the effect of introduction of pre-stress. Fig.7 shows the measurement items on the main girder and lateral beam. Each measurements start at intervals right after the completion of concrete placement to the slab. We installed the remote monitoring system to the measurements for long term monitoring. This system can monitor the obtained data from anywhere.

(2) Remote monitoring system with ISDN-line

Measurement items are stresses on studs at slab, main girder, and vertical stiffener around P4 and P5 support. The remote monitoring system, as shown in Fig.8, consists of sensor, data logger, and GPIB-connected laptop PC at site and Desktop PC at office. The two PCs are connected with ISDN-public phone line via dial-up looters. Data acquisition is automated with interval timer, and the data are being sent to laptop PC via GPIB. We used LabVIEW for data acquisition. This system enables data browsing with a browser, and data receiving with FTP at a distance from the site, e.g.: headquarters.

(3) Remote monitoring

Using the system constituted, we actually performed remote monitoring and data transfer from headquarters. The monitoring screen, as shown in Fig.9, is displayed on the browser. By adding a LabVIEW's function of HTTP server, we can browse the HTML formatted data screen on PC display from anywhere. The figures show the obtained data at each sensing point. By using network camera at site, not only these data, but also live picture images can be seen at a distant point. We introduce about the image monitoring at chapter 3.4.

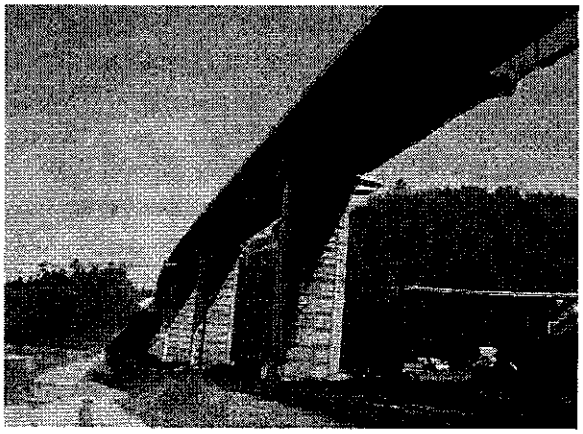

Photo 2 Ootsurokawa Bridge

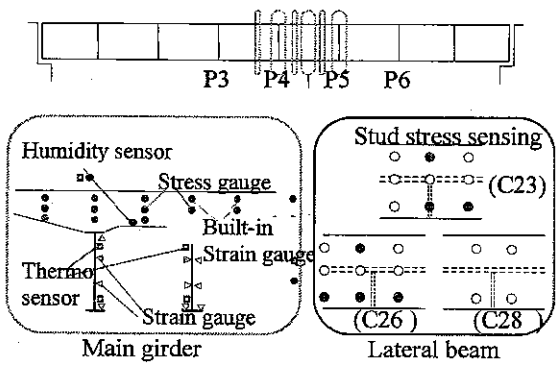

Fig.7 Measurement items

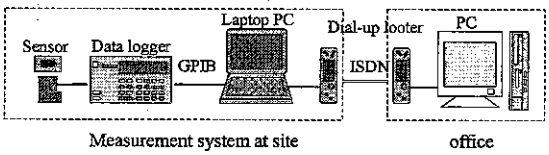

Fig.8 Remote monitoring system

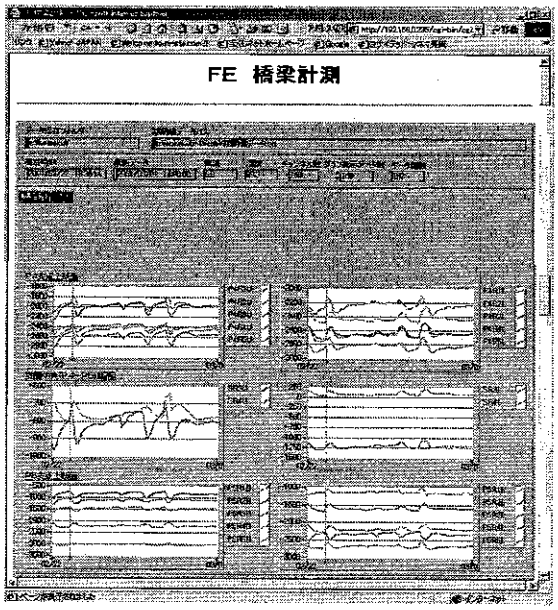

Fig.9 Monitoring screen on browser

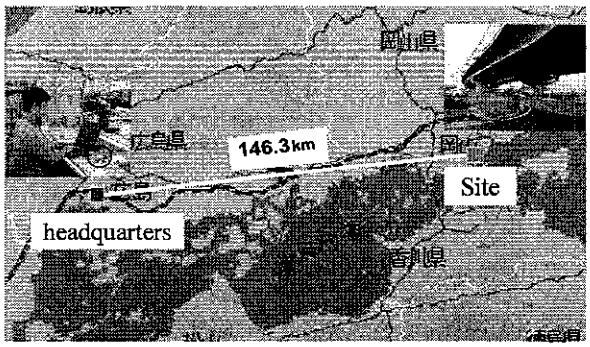

Fig.10 Location of the site and monitoring office

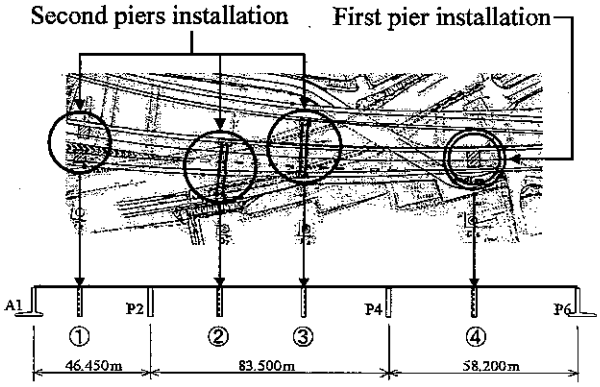

Fig.11 Schematic of plan of construction

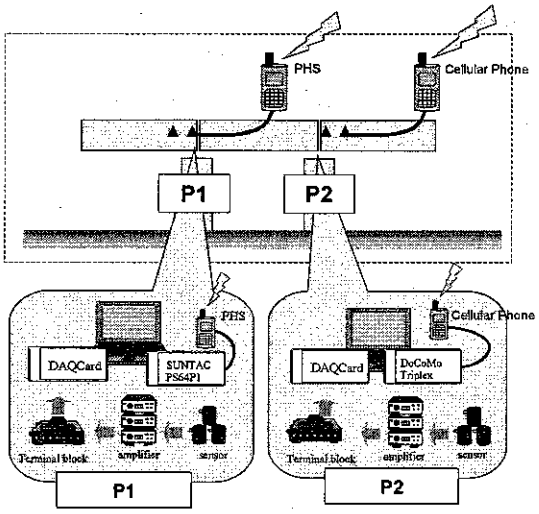

Fig.12 Monitoring system

3.3 Bridge remote monitoring with mobile communication devices

(1) Abstract of remote monitoring

Next issue is bridge vibration monitoring about 150km away from the site with mobile communication devices such as cellular phone and PHS. Fig.10 shows the distance between the site and headquarters, monitoring place. This remote monitoring was conducted to ascertain the change of bridge vibration on behalf of retrofit to existing bridge piers. The retrofit was to lower bridge vibration, which was caused by moving vehicles, by additional temporary bridge piers between existing piers.

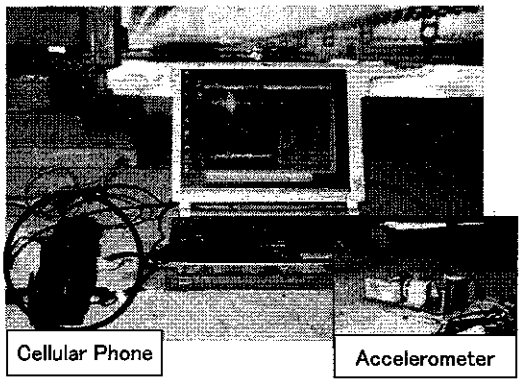

Photo 3 Configuration of the monitoring system

Photo 4 Monitoring at office

Total additional bridge piers of four were installed. Fig.11 shows the schematic plan of the construction. Pier No.4 was installed at first and pier No.1, 2, and 3 were installed at next construction. By measuring the acceleration at pier No. 1 and 2, before and after the each construction, we could see the effect of the retrofit. Fig.12 shows the monitoring system placed on the bridge pier.

(2) Monitoring system

Three-dimensional of lateral, a right angle to bridge axis, and vertical acceleration at pier P1 and P2 were measured by each six accelerometers. Photo 3 shows the configuration of the monitoring system to the bridge. By placing each monitoring system and sending data by cellular phone and PHS, we could see them on the PC display at headquarters (Photo 4), about 150km away from the site.

3.4 Image remote monitoring

(1) Abstract of remote monitoring

Site image monitoring is also important as well as data monitoring when we implement bridge management. Images of the site help us to know actual conditions of the structures or monitoring devices. Data sizes of images are generally big so that we should care about the data transferring speed under actual condition of use. At first, we introduced an Internet live camera system on the market for testing and comparing. Then, we developed a remote image monitoring system and

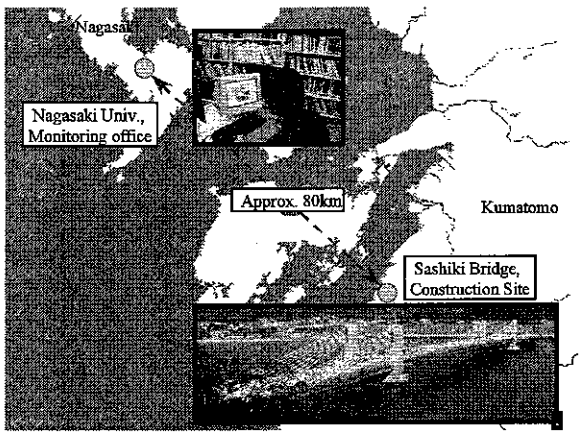

Fig.13 Location of the site and monitoring office

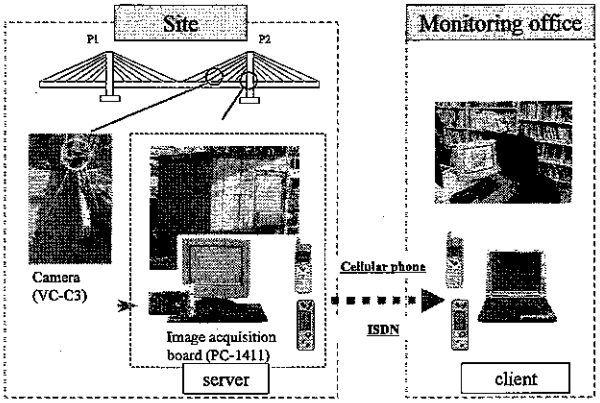

Fig.14 Image remote monitoring system

introduced to a bridge under construction. The object bridge for image monitoring is Sasiki Bridge, introduced in chapter 3, about 80km away from Nagasaki University, monitoring office. Fig.13 shows the location of the site and Nagasaki University.

(2) System configuration

To monitor the site image from office, we used VC-C3, a remote- controllable small camera, and VB-100, a camera server, and PCI-1411, a video capture-board. For transmitting data from the site to monitoring office, we used ISDN-line, Cellular phone, and PHS. LabVIEW were installed to the PCs at both side of the site office and monitoring office. Also, a developed program for transmitting data with IMAQ[11] vision, an additional tool of LabVIEW, was installed. By using IMAQ vision and PCI-1411, image data are expressed with digital data and treated directly so that time consuming data processing would be reduced.

The configuration of the communications method between the site measurement rooms and the office is the same as that described in Chapter 3.1. Fig.14 shows the schematic diagram of image monitoring system. The measurement rooms were set up at the P2 bridge support and P3 bridge support respectively for measurement under construction. We connected the measurement rooms and the site office with wireless LAN bridge to constitute the construction site LAN. A non-directional antenna for a wireless LAN device was installed in the site office,

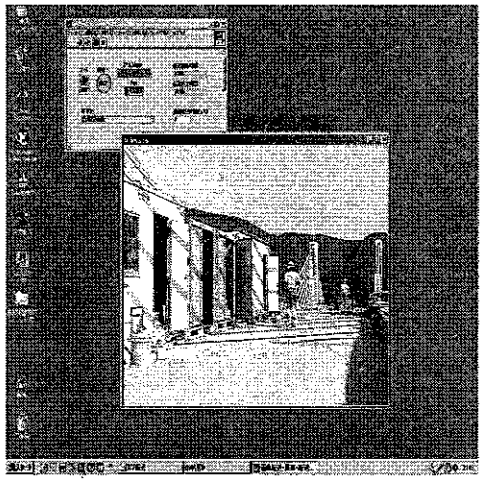

Fig.15 Monitoring screen by browser

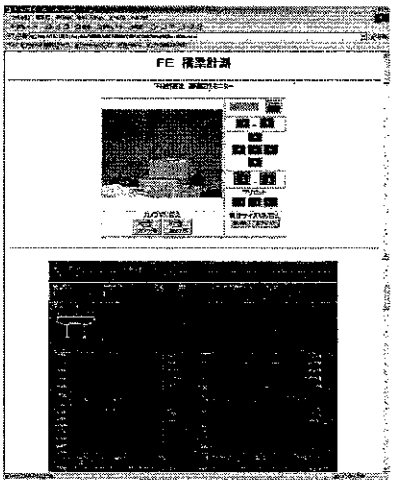

Fig.16 Camera control by browser with data monitoring

Table 2 Image transmitting rate (as of year 2000)

Device	Data transferring rate (f/s)	
VB-100 (camera server)	Spec.value	Test result
PHS 32kbps	0.48	0.27
Cellular phone	0.16	0.05
ISDN 64kbps	1.04	0.73
ISDN 128kbps	2.08	1.18
PCI-1411 (LabView)	Spec.value	Test result
PHS 32kbps	0.048	0.032
Cellular phone	0.016	0.003
ISDN 64kbps	0.1	0.04
ISDN 128kbps	0.21	0.1

Applied image size for transferring :320 × 240

while a directional antenna was installed in each measurement room.

In order to connect from Nagasaki University to the site intranet at first, we connected dial-up rooters to the PCs of Nagasaki University and site office respectively, for communications between them on LAN via dial-up connections using ISDN line. Fig.15 shows the monitoring screen by browser on a PC at Nagasaki University. Furthermore, by adding a function of operation of camera, as shown in Fig.16,

we realize to control the site camera from the same browser of data monitoring screen. Table 2 shows the result of image transmitting rate by using VB-100 and PCI-1411.

4. Remote bridge vibration monitoring on the Cellular phone display[8)]

4.1 Monitoring system

For the purpose of structuring health monitoring system or effective bridge management system, we focus on browsing function of cellular phone. In this chapter, we introduce a developed bridge vibration monitoring system on cellular phone display and a case conducted at an existing cable-stayed bridge. This system would be effective especially for hazardous areas where emergency situation will be predicted. This system is based on descript monitoring system as before, but additional function for database and displaying data on the cellular phone are newly adopted. For data transmitting, PHS was used from the site PC to the office PC, which also serves database of measurement data. Then, the obtained data are transformed into LabVIEW data. The office PC is connected to an Internet provider with a phone line and that makes the PC as Web server. This realizes data monitoring with cellular phone. Fig.17 shows schematic network diagram of cellular phone data monitoring using general phone line.

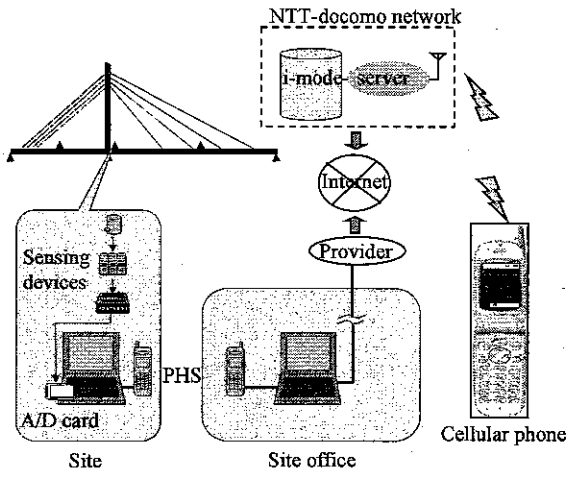

Fig.17 Cellular phone data monitoring system

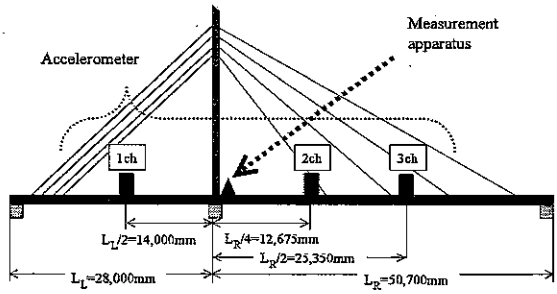

Fig.18 Urakami pedestrian overpass and layout of apparatus

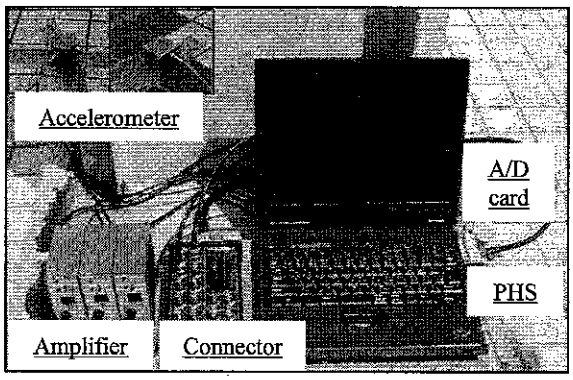

Photo 4 Measurement apparatus

4-2. Abstract of vibration measurement

A vibration-monitoring test was conducted at Urakami pedestrian overpass, an existing cable-stayed bridge made of steel, at Nagasaki city. The bridge has total span of 80m with two spans. As shown in Fig.18, accelerometers were installed in the point of half-length of the left span, half-length and quarter-length of the right span of the bridge. Accelerations in vertical direction of bridge slab were measured with 100Hz of data sampling rate. The measurement system, which consists of

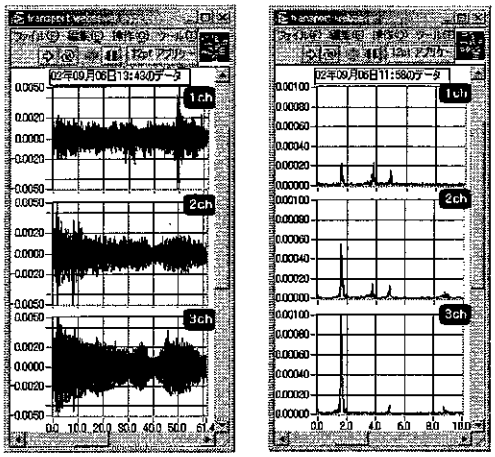

a) Acceleration b) power spectrum density

Fig.19 Measurement result images on the Web server

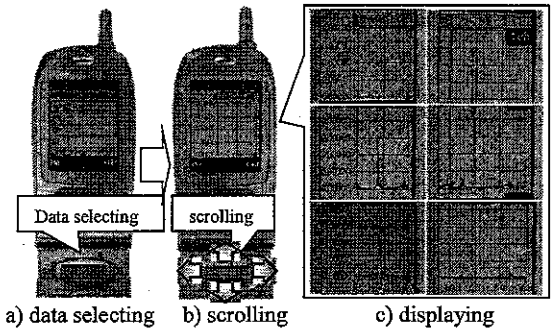

a) data selecting b) scrolling c) displaying

Fig.20 Measurement result images on cellular phone

apparatus and data transmitting devices installed on the bridge are shown in Photo 4. The obtained data in the site measurement system are regularly sent to the Web server, described above, with PHS at intervals. Then the sent data such as acceleration and power spectrum curve can be seen on the cellular phone display by connecting at will. A cellular phone of SONY- made SO503i was applied to the system.

4-3. Result of the monitoring test

Fig.19 shows a series of measurement result on the Web server. Fig.19 a) shows acceleration and Fig.19 b) shows power spectrum density of the acceleration. These two types of data are separately archived in the database so that we can easily find them. Fig.20 shows the procedure for displaying the requested data in the power spectrum density. When connected to the Web server from a cellular phone, menu title will be shown on the cellular phone display as shown in Fig.20 a). By selecting recorded data with cursor, requested image of data are displayed as shown in Fig.20 b). As the pictures are saved in larger scale than the display so that detail of the data can be seen, we installed image-scrolling function to the browser. Fig.20 c) shows the scrolled images. As a result of these developments, data browsing will be more effective in health monitoring not only in just browsing data but also in analytical aspect of phenomenon.

5. Conclusion

The remote monitoring system classified with data transmitting methods and its applications to the bridge management are introduced in this paper. For the construction management or measurement of structural static and dynamic behavior, it is important to use optimal and cost-effective data transmission media according to the data characteristics. We adopted the remote monitoring control system with wireless LAN, ISDN-phone line, and/or mobile communication services. As a result of the test at the bridge construction or measurement sites, the remote monitoring system were verified to be useful and effective. From the viewpoint of data transmission, in the near future, the technologies of the remote monitoring of highway bridges are established by the benefit of high speed and big capacity communication services, which are continuously upgraded. Then, we developed and tested a site image monitoring on Cellular phone display. By seeing the cellular phone display, we can easily obtain the site information and it would be effective especially for monitoring hazardous areas where emergency situation will be predicted. Although the remote monitoring systems are almost established, we have a subject to be sold, that is power supply to the measurement system. Introduction of a solar cell will be one of the measures. If the problem is being solved, the remote monitoring system can work as robot system.

References

1) Aktan, A. E., Grimmelsman, K. A.,The role of NDE in bridge health monitoring, *Nondestructive Evaluation of Bridges and Highways 3, Proc. of SPIE,* pp.2-15, 1999
2) Ohshima, T., *Guideline of Bridge Vibration Monitoring, Series of Structural Engng.No.10,*.JSCE, 2000
3) Okabayashi, T., Yamamori, K., Tamaru, Y., Yoshimura, T : Estimation of dynamic characteristics for structures by the mobile vibration measurement system, *Journal of Structural Mechanics and Earthquake Engineering,* Vol.591/I-43, pp.327-337, 1998.
4) Okabayashi, T., Yamamori, K., Sanuki, Y., Tamura, T : Estimation of dynamic characteristics for structures with closely spaced eigenvalues, *Journal of Structural Mechanics and Earthquake Engineering,* Vol.633/I-49, pp.93-102, 1999.
5) Kawamura, S., Okabayashi, T., Takagi, S. : Development of remote measurement system for bridge vibration by mobile communication, *Journal of Structural Engineering,* Vol.46A, pp.539-546, 2000
6) Okabayashi, T., Yoshimura, T., Kawamura, S., Hosokawa, M : The telemetry system based on Internet technology with wireless LAN for execution management of bridge construction. *Journal of Structural Engineering,* Vol.47A, pp.285-292, 2001
7) *LabVIEW User Manual,* National Instruments, 1998
8) Okabayashi, T., Itonaga, Y., Koba, T., Okumatsu, T.: Development of the remote-vibration monitoring system with cellular phone using Internet function, *Journal of Structural Engineering,* Vol.49A, pp.299-307, 2003
9) Kita, S., Aokage, H., Sakou,S., Okano., M., Okumatsu, T.,Development of Tele-earthwork system, *Journal of Fujita Technical Research Institute,* Vol.31, pp73-78,1995
10) Imada, K., Matsuda, H., Nagahisa, N., Yoshimura, T.: Design and Construction of the Sashiki-Bridge. *Proc. of 9th Symposium on Development in Prestressed Concrete,* pp.609-614, 1999
11) *Internet Developers Toolkit for G Reference Manual,* National Instruments, 1998

(Received July 31, 2003)

Static Method for In Situ Estimating Tension in Hanger Cable

Sang-Sup Ahn*, In-Hwan Bae**, Nam Sik Kim***

* Ph.D., Project Leader, Highway & Transportation Tech. Inst., Korea Highway Co., Dongtan, Hwaseong 445-812 Korea
** Ph.D., Director, New Airport HIWAY Co. Ltd., Seo-gu, Incheon 404-160 Korea
** Ph.D., Chief Researcher, Hyundai Inst. Of Const. Tech., Goosung, Yongin 449-912 Korea

Hanger cables of suspension bridges have complicated boundary conditions and large flexural rigidity compared to its length being inadequate to the application of vibration method. Therefore, the totally different method is required and the static method, proposed in this paper, may be one of alternatives. Suggested method utilizes the load-deflection relation of hanger cable in transverse direction. To accomplish these, theoretical formula is derived considering the flexural rigidity and boundary conditions of hanger cables and measuring devices are manufactured. To set the boundary conditions of real hanger cable consistent with the theory, additional two devices (constraint devices) are simultaneously used with main measuring device. Proposed static method with devices is implemented to measure the hanger cable tension of Yong Jong Bridge, connecting Incheon with the new airport, Korea.

Key Words: Measurement, Tension, Hanger, Suspension bridge

1. Introduction

Estimation of cable tension is frequently required to verify the design tension and to obtain the intended profile of bridge in erection stage. Furthermore, its monitoring is mandatory to accomplish the proper maintenance of bridge in service state.

Various estimation methods are used to obtain the cable tension in erection stage or in service stage. For example, by post tensioning jack, by surveying the shape of cable, by load cell installed at the anchorage or by strain gauge fixed on the strand of cable. However regardless of their simple theoretical basis, their applicability and accuracy are somewhat doubtable.

On the other hand, vibration method[1)] is often adopted to estimate the cable tension on site. This is simple and economical method. Vibration method uses the dynamic signal measured from oscillation by excitations such as by man, by exciter, by vehicle or by wind. When natural frequencies are obtained from dynamic signal using FFT, cable tension can be estimated by appropriate theoretical formula. This method has been broadly applicated to estimate stay cable tension of cable-stayed bridges or hanger tension of suspension bridges. Vibration method can be successfully applied when the considered cable is excited with ease and has the simple support condition. Furthermore, the more modes of natural frequencies we obtain, the more accurate tension we can expect.

However, when those conditions are not met, vibration method gives poor results or can not be totally applicable. Actually, for short cables or cables having complicated support conditions, vibration method can not be hardly applicable because of lack of obtained signals or limitation of theoretical formula.

As one of the alternatives to the vibration method, static method can be considered. Bati et al.[2)] estimated the tension of tie rod used by the reinforcement member of building by applying static method. They measured lateral deflections and bending moments at three points on the tensioned tie rod for various lateral loads. Load-deflections relations are plotted from measured quantities and tension can be estimated using appropriate theoretical formula. To apply their method, required measurements are deflections, bending moments which are calculated by using strains at the lower and upper surface of tie rod and tension increments which are measured by load cell installed at the end of tie rod. These make their method hard to apply in situ although their method gives good results. Furthermore, measurement of tension increment is impossible at the cable of bridge in service.

This paper presents the static method to estimate the hanger cable tension with a minimum of measurement.

Measuring devices was fabricated and used to estimate the tension of hanger cable in Yong Jong suspension bridge. Applicability and accuracy of proposed method are described.

2. Theoretical bases

When the lateral force is applied to the middle point on one portion of hanger cable, exerted forces are shown in Fig. 1. Hanger cable is free from the self weight, so the initial equilibrium state (C^0) can be modeled by the taut cable having flexural rigidity. At each end of considered portion, flexural rigidity of cable can be represented by rotational spring when cable bents by external load.

Under these conditions, static equilibrium equation of hanger cable subjected to external load is as follows.

$$\frac{\partial^4 w(x)}{\partial x^4} - \alpha^2 \frac{\partial^2 w(x)}{\partial x^2} = \frac{P}{EI}\delta(x-l) \tag{1}$$

where $w(x)$ is lateral deflection at x located from support A, $\alpha^2 = (H+h)/EI$, H is horizontal component of initial tension of hanger cable, h is additional tension by external load, EI is flexural rigidity of cable, P is external load, l is the half length of measuring portion and $\delta(\cdot)$ is Dirac Delta function. Horizontal component of initial tension is equal to the initial tension because the hanger cable is horizontal before acting external load.

Eq. (1) contains discontinuous function, Dirac Delta function. The solution of Eq. (1) can be obtained by Laplace transformation, so as to be single solution for entire length of cable. Following boundary conditions must be satisfied.

$$w(0) = 0, \qquad w'(0) = -\theta_0, \tag{2}$$

$$w''(0) = -\frac{M_0}{EI}, \qquad w'''(0) = -\frac{V_0}{EI} - \alpha^2\theta_0 \tag{3}$$

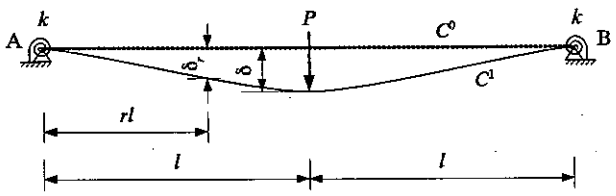

(a)

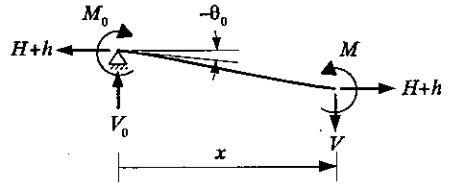

(b)

Fig. 1 Hanger cable with constraint at both ends ((a) Modeling of test section, (b) Forces acting on small segment)

Then, the solution of Eq. (1) is

$$w(x) = -f_1(x)\theta_0 - f_2(x)\frac{M_0}{EI} - f_3(x)\frac{V_0}{EI} + f_3(x-l)U(x-l)\frac{P}{EI} \tag{4}$$

where

$$f_1(x) = \frac{1}{\alpha}\sinh\alpha x \tag{5}$$

$$f_2(x) = \frac{1}{\alpha^2}(\cosh\alpha x - 1) \tag{6}$$

$$f_3(x) = \frac{1}{\alpha^3}(\sinh\alpha x - \alpha x) \tag{7}$$

Other boundary conditions at the support B are considered to obtain $P-\delta$ relation. That is,

$$w(2l) = 0, \quad w'(2l) = \theta_0, \quad w''(2l) = -\frac{k\theta_0}{EI} \tag{8}$$

where k is rotational spring constant at the support produced by the constraint device.

Finally, we can obtain following $P-\delta$ relation.

$$\frac{Pl^2}{EI} = \frac{\delta}{l}\frac{2\xi^3(\xi + \kappa\tanh\xi)}{2\kappa(\operatorname{sech}\xi - 1) + \xi(\xi + (\kappa-1)\tanh\xi)} \tag{9}$$

where $\xi = \alpha l$ and $\kappa = kl/EI$.

According to Eq. (9), $P-\delta$ relation seems to be linear. However, α contains h which is dependant on lateral deflection, so that $P-\delta$ relation is no more linear. If lateral displacement of cable is so small as to be ignored, we could obtain linear $P-\delta$ relation.

In order to obtain practical formula, Eq. (9) is approximated. For general structural cables, $\xi \square 1$[3], so that following approximations are possible with minor errors.

$$\tanh\xi \approx 1 \tag{10}$$

$$\operatorname{sech}\xi \approx 0 \tag{11}$$

When considering Eqs. (10) and (11), Eq. (9) can be rewritten as following simple form after some manipulations.

$$\frac{P}{\delta} = \frac{EI}{l^3}\frac{2\xi^3(\xi+\kappa)}{\xi^2 + \xi(\kappa-1) - 2\kappa} \tag{12}$$

The additional tension, h, when applying lateral load might be ignored because the hanger cable is not perfectly constrained to axial direction and lateral deflection by applied load is so small. Thus, the slope of load-deflection relation obtained from in situ experiment

is same as $P-\delta$ relation in Eq. (12). We can obtain ξ by the use of Eq. (12). And using $H = EI(\xi/l)^2 - h$, tension of hanger cable, H, can be estimated finally. Also, ξ can be directly calculated by using Eq. (9) without much effort, because the behavior of function in Eq. (9) is definite and simple.

To apply the proposed method, flexural rigidity of hanger cable and rotational spring constant at the supports must be known. These parameters can be estimated by several experiments in situ and theoretical values.

3. Measuring device

3.1 Components of device

Measuring device is fixed between two hanger cables as shown in Fig. 2 and designed to act lateral force on the cable when we turn the grip. Other devices are constraint devices, and they are installed at lower and upper location of measuring device. Constraint devices are intended to simulate the mathematical model used in this paper and maintain the same constraint condition at both ends of test section.

Measuring device is equipped with load cell and LVDT in order to measure the lateral deflection and applied load as shown in Fig. 3. Signals from load cell and LVDT are stored on notebook computer in real time in situ. Load cell shown in Fig. 4 has the maximum capacity of 200kN. LVDT used in experiment can measure the deflection from minimum 0.01mm to maximum 5cm.

Measuring device is in compression when acting lateral force. Therefore, precise manufacturing is required to avoid any eccentricity or buckling.

3.2 Method of measurements

The theoretical equation reveals good results for longer distance between two constraint devices. However, it is often that limitations in installation distance exist because of the free length of the hanger cable or for the purpose of the easy treatment of constraint device. Lower constraint device is usually installed at 5cm above from collar of hanger and is at a right angle to the cable as shown in Fig. 2. Upper constraint device is installed at the maximum height without subsidiary equipments. Usually the distance between two constraint devices is appropriate to be 120cm. Rod of constraint device is threaded at both ends. When installing the constraint devices on the cable, devices are moderately fixed by bolts, so as not to slip down on the cable. Over-tightening the bolts leads to induce the additional tension on the cable. Under-tightening the constraint devices will give rise to slip down or obtain the unstable initial deflection or lateral force.

Measuring device is fixed on the middle point between two constraint devices in parallel and also tightened by the turn grip.

After installing the devices on the cable, calibrations are followed in the measurement software installed on the notebook computer. It is convenient that LVDT is set to zero on the dial to identify the introduced deflection in real time.

From theoretical point of view, there is no need to do calibration. However, calibration helps us to obtain the reliable and consistent signal.

After calibration, lateral force and deflection are recorded on notebook computer by turning the grip on measuring device.

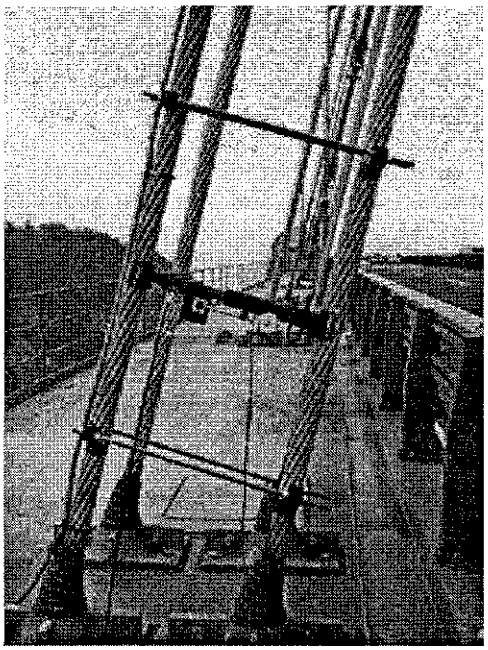

Fig. 2 Installation of devices on the cable (NTS 37)

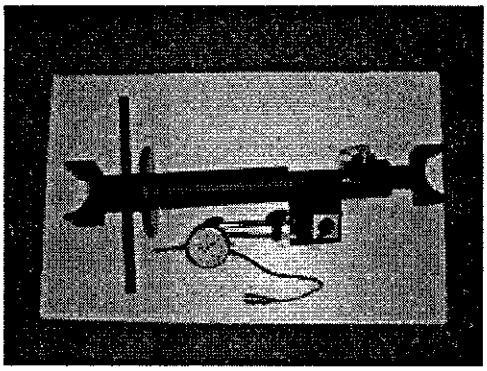

Fig. 3 Measuring device

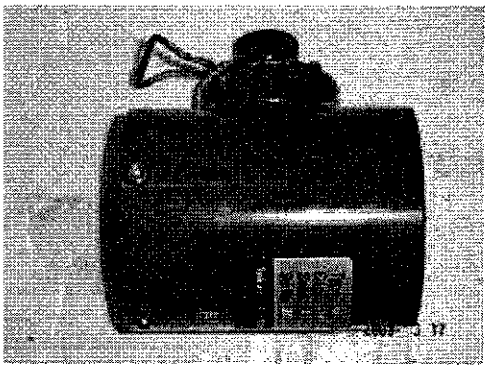

Fig. 4 Load cell

It is adequate that the sampling rate is in the range of 5Hz ~ 15Hz. When sampling rate is high, we obtain enormous data to analysis and useless data which is recorded in intermediate between forcing.

Continuous turning the grip is ideal. However, it is not easy in situ. Pitch of thread on measuring device is about 1mm. If sampling rate is 10Hz, it is adequate to turn the grip one rotation per 10 seconds. According to experience in situ, maximum lateral force by two men was approximately 1.5ton. Over-forcing to obtain large lateral deflection leads to unstable turning the grip and to get inaccurate signal. Generally lateral force in the range of 1~ 1.5ton is enough and adequate. Then, lateral deflection is in the range of 2.5~ 3.5mm in case of distance between two constraint devices of 120cm.

Signals of deflection less than 1mm are eliminated because they contain unstable data caused by the deformation of protection rubber attached on the grip of devices and the settling of devices on the cable. Lateral deflection-force relation is plotted by remained signals.

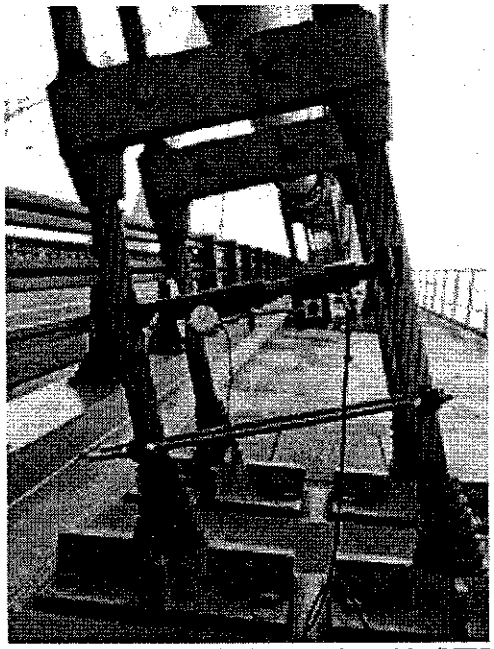

Fig. 5 Installation of devices on the cable (NTS24)

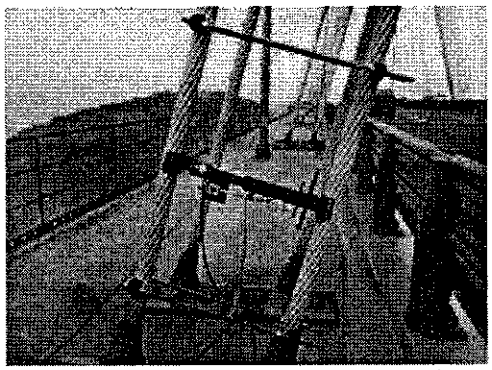

Fig. 6 Installation of devices on the cable (NTS25)

4. In Situ tension measurement

4.1 Hanger cables

Proposed static method with devices is implemented to measure the hanger cable tension of Yong Jong Bridge, connecting Incheon with the new airport, Korea.

Selected hanger cables are NTS24, NTS25 and NTS37. NTS24 and NTS25 are the first and the second hanger cable, respectively, from center hanger cable of center span as shown in Figs. 5 and 6. These cables are impossible to estimate tension by vibration method. On the other hand, NTS37 is longer than NTS24 or NTS25 and tension may be estimated by vibration method.

The free length of NTS24 is so short that the possible maximum length was 67cm as shown in Fig. 5. Also upper constraint device was not installed because we expected the same constraint effect as socket of hanger clamp instead of upper constraint device. While the distance between two constraint devices of NTS25 and NTS37 was 120cm.

4.2 Measured results

For each hanger cable, the measured force- deflection ($P-\Delta$) relations are plotted in Figs. from 7 to 9. In the figures, continuous lines are plotted by continuous lateral loading. On the other hand, discontinuous portion is caused by the stopping the loading.

Sampling rate of NTS24 and NTS25 was 5Hz and that of NTS37 was 500Hz. As shown in Fig. 9, high sampling rate generates many signals and makes the high deviation among continuous signals during stopping loading. Also, the slopes of continuous line have high variance compared to two measured results. The measured results of NTS24 and NTS25 show comparably consistent in the slope of continuous lines. However, in all cases, exerted force decreases during stopping loading. Therefore, it is important that the lateral load should be applied slowly and continuously if possible.

Magnitude of required lateral force is closely related to the distance between two constraint devices and the tension of hanger cable. Because the magnitude of design tension of hanger cables does not have much variation, the distance between two constraint devices may be main parameter for magnitude of required lateral force. As mentioned above, the distance between two constraint devices of NTS24 is 67cm which is half of other two cables. Thus more lateral force is required in order to displace the cable to similar magnitude. This is shown in Fig. 7. Additional lateral force of about 500kgf is required for same deflection as other two cables. However, because over-forcing to obtain enough deflection generates poor signal, it prefers to limit the lateral force rather than to obtain enough deflection. According to measurement experience in situ and measured signals, lateral force in the range of 1~ 1.5tonf is adequate for precise results.

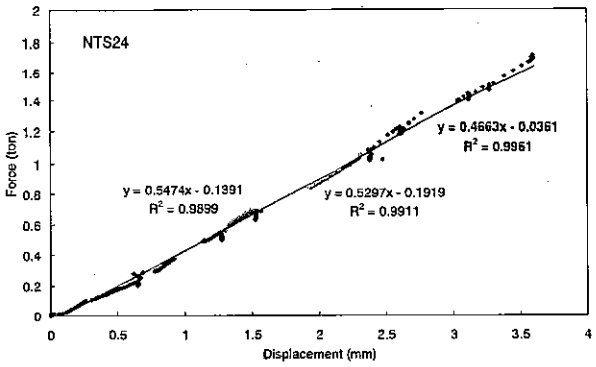

Fig. 7 Measured $P-\Delta$ curve (NTS24)

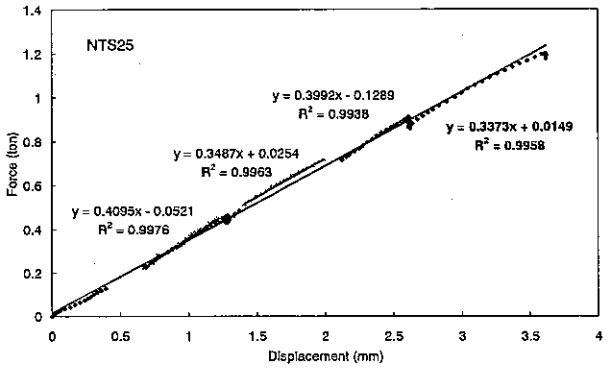

Fig. 8 Measured $P-\Delta$ curve (NTS25)

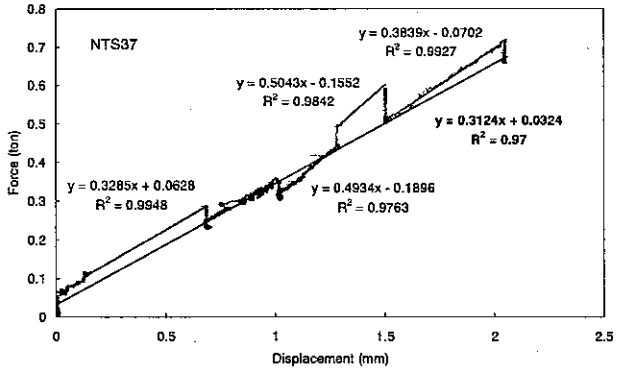

Fig. 9 Measured $P-\Delta$ curve (NTS37)

4.3 Tension estimation

For each cable, slope of $P-\Delta$ relation and parameters described in section 2 are shown in Table 1.

Estimation procedures of tension proposed in this paper is simple. However some considerations are required. The deflection measured in situ is twice of deflection in section 2 because the measured deflection in situ is relative deflection between two hanger cables.

Therefore, the slope of $P-\Delta$, S_Δ, measured in situ is as follows from Eq. (9).

$$S_\Delta = \frac{EI}{l^3}\frac{2\xi^3(\xi+\kappa\tanh\xi)}{\kappa(\operatorname{sech}\xi-1)+\xi[\xi+(\kappa-1)\tanh\xi]} \tag{13}$$

Rotational constraint, κ, at both ends is contained in Eq. (13) for calculating ξ. According to the analysis of experiment results, when $\kappa=0$, ξ is non-trivial. This is rational because the constraint devices do not fix the cable rigidly, but they constrain the lateral deflection at their installed point.

Eq. (13) is complicated in form. However it is slowly varying continuous function for ξ. Therefore, when we use the numerical solution technique, Eq. (13) is preferred rather than practical formula, Eq. (12).

After solving Eq. (13) for ξ, the tension of hanger cable is calculated by following equation.

$$H = EI(\xi/l)^2 \tag{14}$$

Using these equations, the procedures for estimating the hanger cable tension are shown in Table 1.

The slope of $P-\Delta$ relation in Table 1 is obtained by averaging the slope of continuous lines except for the discontinuous portion and deflection less than 1mm.

The flexural rigidities of NTS25 and NTS37 are averaged values obtained by vibration method. However that of NTS24 is assumed by considering the tendency of variation of flexural rigidity according to the length of cable.

The hanger cable tension estimated by this paper's method is compared with vibration method in Table 2. Although the number of measured cables was restricted, results show that the hanger cable tension by static method is closer to design tension than that by vibration method.

Table 1 Tension estimation parameters

ID	Slope of $P-\Delta$ curve (S_Δ, tonf/mm)	Measurement length($2l$,cm)	EI (tonf/m^2)	κ	ξ	Tension (tonf)
NTS24	0.5386	67	3	0	1.78	84.6
NTS25	0.3858	120	15.89	0	1.37	83.2
NTS37	0.3839	120	15.89	0	1.37	82.3

Table 2 Comparison of tension by various methods (Unit : tonf)

ID	Design tension	Vibration method		Static method (This paper)
		Ambient vibration	Forced vibration	
NTS24	81.870	-	79.4	84.6
NTS25	81.624	-	86.2	83.2
NTS37	83.023	80.5	95.2	82.3

Table 3 Measuring procedures

Procedures	Contents		Remark
Installation	Lower constraint device	Installed at about 5cm above from hanger cable collar	Moderate tightening so as not to rattle on the cable
	Upper constraint device	Installed at 120cm above from the lower constraint device	
	Measuring device	Half location between lower and upper constraint devices	Fixing to what extent not easy to rotate the turn grip
Exertion	Rate of exertion	One rotation of turn grip per about 10 seconds	Continuous exertion is preferred
	Maximum lateral force	1~1.5 tonf, which is identified on recording	Over-exertion can give signal of poor quality
Measuring and analyzing	Sampling rate of signal	5~15Hz	-
	Slope of $P-\Delta$ curve	Average slope of continuous lines	-

5. Conclusions

This paper proposes the static method to estimate the hanger cable tension in situ. To accomplish this purpose, measurement device was manufactured and an experiment in situ was performed. Also, the theoretical formula was derived.

The procedures and the method for in situ test using manufactured device are summarized in Table 3.

From the field test, we can conclude that the boundary conditions by the constraint devices coincides well with the theoretical ones and the proposed static method can estimate the hanger cable tension more precisely regardless of the cable length or flexural rigidity.

Although there are some minor problems to resolve such as the determination of flexural rigidity of cable, the distance between two constraint devices, etc., proposed method and manufactured device show feasibility and applicability of static method for estimation of cable tension.

To stabilize the method and to find out how to obtain more reliable and consistent results, further experiment in situ is under way.

References

1) Zui, H., Shinke, T., and Namita, Y., Practical Formulas for Estimation of Cable Tension by Vibration Method, *Journal of Structural Engineering*, Vol. 122, No. 6, pp.651-656, 1996.
2) Bati, S. B. and Tonietti, U., Experimental Methods for Estimating In Situ Tensile Force in Tie-Rods, *Journal of Engineering Mechanics*, Vol. 127, No. 12, pp.1275-1283, 2001.
3) Fürst, A. and Marti, P., Bending of Stay Cables, *Structural Engineering International*, Vol. 1, pp.42-46, 2001.

(Received July 31, 2003)

System Identification in Time Domain for Structural Damage Assessment Using L_1-Regularization and Time Windowing Technique

Hae Sung Lee*, Seung-keun Park **

*Professor, School of Civil, Urban and Geosystem Eng., Seoul National University, Seoul, Korea 151-742
** Graduate Student, School of Civil, Urban and Geosystem Eng., Seoul National University, Seoul, Korea 151-742

This paper presents a system identification (SI) scheme in time domain using measured acceleration data. The error function is defined as the time integral of the least square errors between the measured acceleration and the calculated acceleration by a mathematical model. Damping parameters as well as stiffness properties of a structure are considered as system parameters. The structural damping is modeled by the Rayleigh damping. A new regularization function defined by the L_1-norm of the first derivative of system parameters with respect to time is proposed to alleviate the ill-posed characteristics of inverse problems and to accommodate discontinuities of system parameters in time. The time window concept is proposed to trace variation of system parameters in time.

Key Words: System Identification, Regularization, Time Window

1. Introduction

Immediate safety assessment structures after an earthquake is extremely important in evaluating serviceability and functionality of social infrastructures. Nowadays, not only ground acceleration but also acceleration of important social infrastructures is monitored during earthquakes. It would be very helpful for quick restoration of social activities if structural damage caused by an earthquake is accessed with the measured acceleration during an earthquake in real time or near real time.

Various damage assessment schemes based on system identification (SI) have been extensively investigated for social infrastructures during the last few decades[1),2),3),4)]. The modal analysis approaches[2),3)] have been widely adopted to detect structural damage using measured acceleration of structures. The modal analysis approaches, however, suffer from drawbacks caused by insensitiveness of modal data to changes of structural properties.

To overcome the drawbacks of the modal analysis approaches, this paper presents a system identification scheme in time domain using measured acceleration data. The error function is defined as the time integral of the least square errors between the measured acceleration and the calculated acceleration by a mathematical model. The structural damping is modeled by the Rayleigh damping. A regularization technique[1),4),5)] is employed to overcome the ill-posedness of inverse problems. A regularization function defined by the L_1-norm of first time derivatives of stiffness parameters is proposed to accommodate abrupt changes of system parameters in time. The L_1-truncated singular value decomposition (TSVD)[5)] is adopted to optimize the error function with the L_1-regularization function. To trace the variation of stiffness parameters in time, a time windowing technique is introduced. In the time windowing technique, SI is performed sequentially within a finite time interval, which is called a time window. The time window advances forward at each time step to identify changes of system parameters in time. The validity and accuracy of the proposed method are demonstrated through two numerical simulation study.

2. Parameter Estimation Scheme In Time Domain

The discretized equation of motion of a structure

subjected to ground acceleration a_g caused by an earthquake is expressed as follows.

$$\mathbf{Ma}+\mathbf{C}(\mathbf{x}_c)\mathbf{v}+\mathbf{K}(\mathbf{x}_s)\mathbf{u}=-\mathbf{Ma}_g \tag{1}$$

where **M**, **C** and **K** represent the mass, damping and stiffness matrix of the structure, respectively, and **a**, **v** and **u** are the relative acceleration, velocity and displacement of the structure to ground motion, respectively. The damping parameters and the stiffness parameters of the structure are denoted by $\mathbf{x}_c$ and $\mathbf{x}_s$ in (1), respectively. Newmark β-method is used to integrate the equation of motion. Since the operational vibrations of a structure are negligible compared to those induced by an earthquake, the initial condition of (1) is set to zero.

In case ground acceleration as well as accelerations of a given structure at some discrete observation points are measured, the unknown system parameters of a structure including stiffness and damping properties are identified through minimizing least squared errors between computed and measured acceleration. In case the system parameters are invariant in time, the parameter estimation procedure is represented by the following optimization problem[4].

$$\underset{\mathbf{x}}{\text{Min}}\ \Pi_E(t)=\frac{1}{2}\int_0^t \left\|\tilde{\mathbf{a}}(\mathbf{x})-\bar{\mathbf{a}}\right\|_2^2 dt \ \text{ subject to } \mathbf{R}(\mathbf{x})\le 0 \tag{2}$$

where $\tilde{\mathbf{a}}$, $\bar{\mathbf{a}}$, **x** and **R** are the calculated acceleration and the measured acceleration at observation points relative to ground acceleration, system parameter vector and constraint vector, respectively, with $\|\cdot\|_2$ representing the 2-norm of a vector. Linear constraints are used to set physically significant upper and lower bounds of the system parameters. The minimization problem defined in (2) is a constrained nonlinear optimization problem because the acceleration vector $\tilde{\mathbf{a}}$ is a nonlinear implicit function of the system parameters.

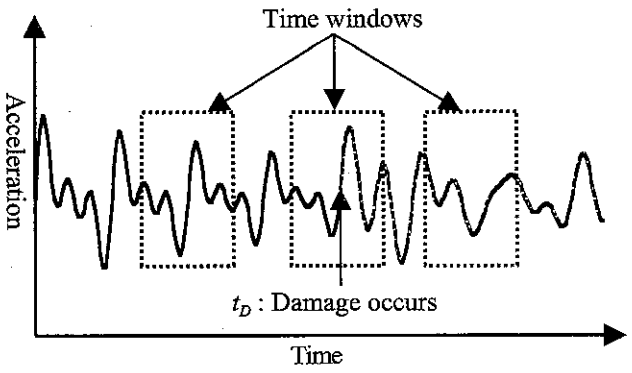

Fig. 1 Time window concept

In case the system parameters vary with time, the time window technique is proposed. Fig.1 illustrates the time window concept. In this technique the minimization problem for the estimation of the system parameters is defined in a finite time interval, which is referred to as a time window.

$$\begin{aligned}&\underset{\mathbf{x}}{\text{Min}}\ \Pi_E(t)=\frac{1}{2}\int_t^{t+d_w}\left\|\tilde{\mathbf{a}}(\mathbf{x}(t))-\bar{\mathbf{a}}\right\|_2^2 dt\\ &\text{subject to } \mathbf{R}(\mathbf{x}(t))\le 0\end{aligned} \tag{3}$$

Here, t and d_w is the initial time and the window size of a given time window. It is assumed that system parameters are constant in a time window, and that system parameters estimated by (3) represent the system parameters at time t. As the time window advances forward sequentially in time, the variations of system parameters in time are identified.

3. L_1-Regularization Scheme

The parameter estimation defined by the minimization problems is a type of ill-posed inverse problems. Ill-posed problems suffer from three instabilities: non-existence of solution, non-uniqueness of solution and discontinuity of solution[5] when measured data are polluted by noise. Because of the instabilities, the optimization problem given in (2) and (3) may yield meaningless solutions or diverge in optimization process. Attempts have been made to overcome instabilities of inverse problems merely by imposing upper and lower limits on the system parameters. However, it has been demonstrated by several researchers that the constraints on the system parameters are not sufficient to guarantee physically meaningful and numerically stable solutions of inverse problems[5].

The regularization technique proposed by Tikhonov is widely employed to overcome the ill-posedness of inverse problems. In the Tikhonov regularization technique, a positive definite regularization function is added to the original optimization problem.

$$\begin{aligned}&\underset{\mathbf{x}}{\text{Min}}\ \Pi(t)=\Pi_E(t)+\lambda\Pi_R(t)\\ &\text{subject to } \mathbf{R}(\mathbf{x})\le 0\end{aligned} \tag{4}$$

where Π_R and λ are a regularization function and a regularization factor, respectively. Various regularization functions are used for different types of inverse problems. Kang et al[4] proposed the following regularization function defined by the L_2-norm for the SI in

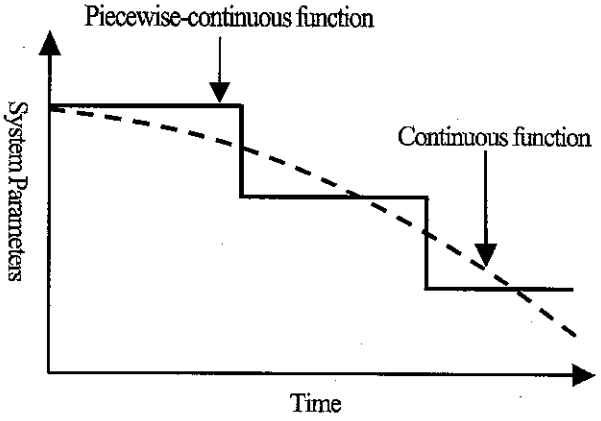

Fig. 2 Continuous and piecewise-continuous functions

time domain.

$$\Pi_R(t) = \frac{1}{2}\int_0^t \left\| \frac{d\mathbf{x}}{dt} \right\|_2^2 dt \tag{5}$$

The regularization function defined in (5) is able to represent continuously varying system parameters in time. Since, however, the system parameters may vary abruptly (Fig.2) with time during earthquakes due to damage, a regularization function that can accommodate piecewise continuous functions in time is required to access damage that occurs during an earthquake. To represent discontinuity of system parameters in time, this paper proposes an L_1-regularization function of the first derivative of system parameters with respect to time.

$$\Pi_R(t) = \frac{1}{2}\int_t^{t+d_w} \left\| \frac{d\mathbf{x}}{dt} \right\|_1 dt \tag{6}$$

where $\|\cdot\|_1$ representing the 1-norm of a vector.

Since the error function is nonlinear with respect to stiffness parameters, a Newton-type optimization algorithm, which requires gradient information of an objective function, is usually employed in SI. As the L_1-regularization function is non-differentiable, the objective function in the Tikhonov regularization scheme defined in (4) contains a non-differentiable function, and thus a Newton-type optimization algorithm cannot be applied. To avoid this difficulty, this paper employs the L_1-TSVD to impose the L_1-regularization function in the optimization of the error function[5),6)]. In the proposed method, the incremental solution of the error function is obtained by solving the quadratic subproblems without the constraints. The noise-polluted solution components are truncated from the incremental solution. Finally, the regularization function is imposed to restore the truncated solution components and the constraints. The above procedure is defined as follows.

$$\begin{aligned} &\underset{\mathbf{x}}{\text{Min}}\,\Pi_R(t) = \frac{1}{2}\int_t^{t+d_w} \left\| \frac{d\mathbf{x}}{dt} \right\|_1 dt \\ &\text{subject to } \mathbf{R}(\mathbf{x}) \le 0 \text{ and} \\ &\underset{\mathbf{x}}{\text{Min}}\,\Pi_E(t) = \frac{1}{2}\int_t^{t+d_w} \left\| \tilde{\mathbf{a}}(\mathbf{x}) - \bar{\mathbf{a}} \right\|_2^2 dt \end{aligned} \tag{7}$$

The error function and the regularization function are easily discretized in time domain using simple numerical methods. The truncated solution of the minimization problem of the error function is obtained by the truncated singular value decomposition, while the simplex method is employed to solve the minimization problem of the L_1-regularization function with constraints. Detailed solution procedures are presented in Ref. 5 and 6.

4. Damping Model

It is a difficult task to model damping properties of real structures. In fact, existing damping models cannot describe actual damping characteristics exactly, and are approximations of real damping phenomena to some extents[7]. Since the damping has an important effect on dynamic responses of a structure, the damping properties should be considered properly in the parameter estimation scheme. In most of previous studies on the parameter estimation, the damping properties of a structure are assumed as known properties, and only stiffness properties are identified. However, the damping properties are not known a priori and should be included in system parameters in the SI.

Among various classical damping models, the modal damping and the Rayleigh damping are the most frequently adopted model. In the modal damping, a damping matrix is constructed by using generalized modal masses and mode shapes. In Rayleigh damping, a damping matrix is defined as a linear combination of the mass matrix and stiffness matrix as follows.

$$\mathbf{C} = a_0\mathbf{M} + a_1\mathbf{K} \tag{8}$$

The damping coefficients of the Rayleigh damping can be determined when any two modal damping ratios and the corresponding modal frequencies are specified.

In case the modal damping is employed in the parameter estimation, the number of the system parameters associated with the damping is equal to that of the total number of DOFs, which increases the total

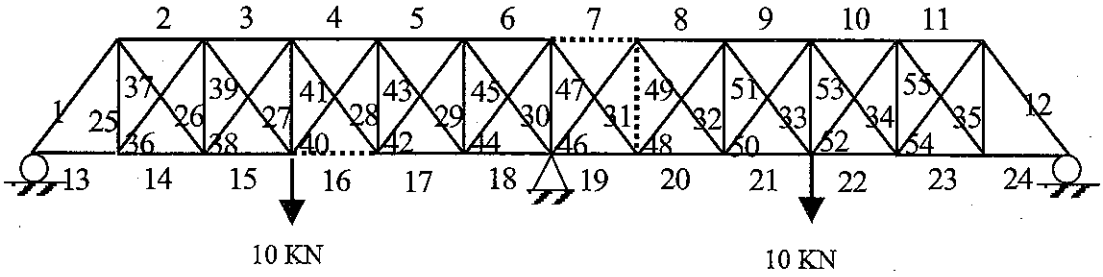

Fig.3 2-span continuous truss

number of unknowns in the optimization problem given in (8). Since neither modal damping nor Rayleigh damping can describe actual damping exactly, and the modal damping requires more unknowns than the Rayleigh damping in the parameter estimation, this study employs the Rayleigh damping for the SI. The Rayleigh damping yields a linear fit to the exact damping of a structure. To approximate actual damping of a structure more accurately, Caughey damping, which is the general form of the rayleigh damping[7], may be adopted.

$$\mathbf{C} = \mathbf{M}\sum_{i=0}^{J-1} a_i(\mathbf{M}^{-1}\mathbf{K})^i, \quad J \le ndof \tag{9}$$

where *ndof* is the total number of degrees of freedom of the given structure. For J=2, the Caughey damping becomes identical to the Rayleigh damping.

5. Examples

Two numerical simulation studies are presented to illustrate validity of the L_1-regularization function and the time window technique.

5.1 two-span continuous truss

The validity of the proposed L_1-regularization function is examined through a simulation study with a two-span continuous truss shown in Fig. 3. Typical material properties of steel (Young's modulus = 210 GPa, Specific mass = 7.85Kg/m^3) are used for all members. The cross sectional areas of top, bottom, vertical and diagonal members are 112.5 cm^2, 93.6 cm^2, 62.5 cm^2 and 75.0 cm^2, respectively. The natural frequencies of the truss range from 6.6 Hz to 114.7 Hz. Damage of the truss is simulated with 40%, 50% and 34 % reductions in the sectional areas of member 7, 16 and 31, respectively. The damaged members are depicted by dotted lines in Fig. 7. It is assumed that the stiffness and the damping properties of the truss do not vary during the measurement. Accelerations of the truss are measured from a free vibration induced by a sudden release of applied loads of 10 KN shown in Fig. 7. The measurement errors are simulated by adding 8% random noise generated from a uniform probability function to accelerations calculated by the finite element model. The observation points are located at 12 bottom nodes of the truss. Both x- and y- direction accelerations are measured in the time period from 0 sec to 0.2 sec with the interval of 1/200 sec. The modal damping ratios used in the calculation of measured accelerations are shown in Fig. 6.

In case either the regularization scheme or damping estimation is not included in the SI, the optimization procedure does not converge or converges to meaningless solutions. Therefore, only the results with the regularization scheme and damping estimation are presented here. Fig.4 and Fig.5 show the variation of the identified stiffness properties of damaged member 7 and undamaged member 46 by the L_1- and L_2-regularization function, respectively. Although rather large measurement noise of 8% is presented, both regularization functions are able to identify the severity of damage of the damaged member accurately, and yield no significant differences in identified results. Estimated stiffness properties of the other damaged members are similar to those of damaged member 6, which are not presented in this paper. For a undamaged member, however, the L_1-regularization function yields much faster convergence rate in time than the L_2-regularization function. Since the parameter estimation is performed in finite time interval in the time window technique, the identification results of all system parameters should converge within a given time window. Therefore, fast convergent characteristic of the L_1-regularization function is extremely important in the time window technique. Fig. 6 shows the exact modal damping ratios used for the calculation of measured accelerations together with identified modal damping ratios by the Rayleigh damping. The initial modal damping ratios calculated by the assumed Rayleigh damping coefficients are also drawn in the same

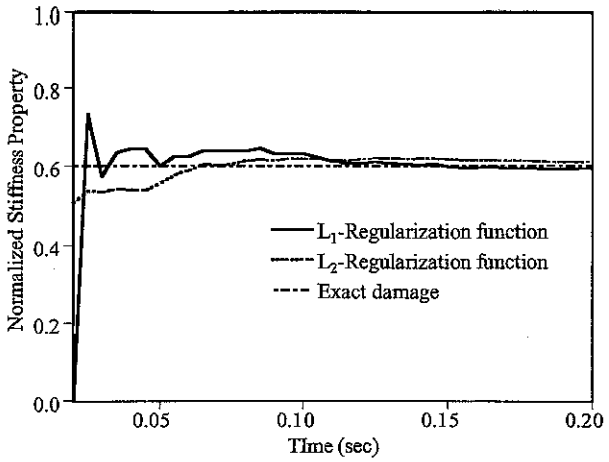

Fig.4 Variation of stiffness property of member 7

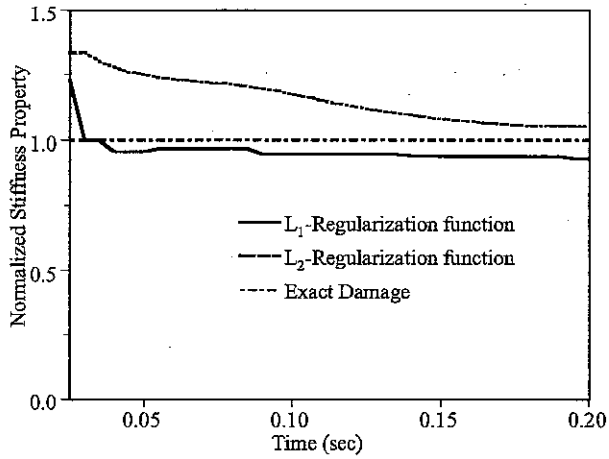

Fig.5 Variation of stiffness property of member 46

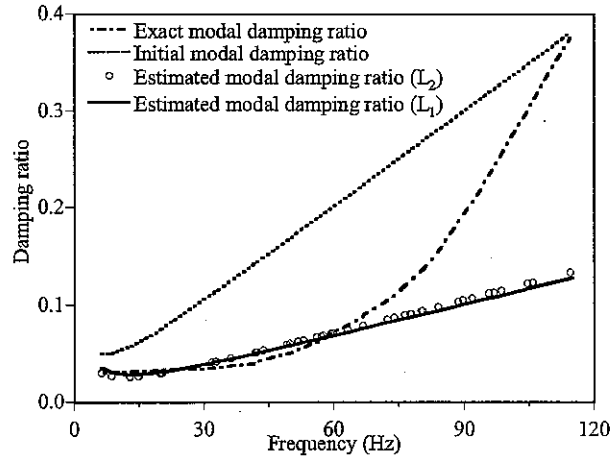

Fig.6 Estimated damping ratio

figure. Both regularization functions yield almost identical results for the damping ratios, and well approximate the real modal damping. The identified stiffness properties of all members at the final time step are shown in Fig. 7. Since stiffness properties of the damaged members reduce prominently compared with the oscillation magnitudes of the other members, the damaged members are clearly assured by both regularization functions. Since the L_1- and the L_2-regularization function specify different continuity conditions in time domain only, identified results at the final time by the two regularization schemes are very similar to each other.

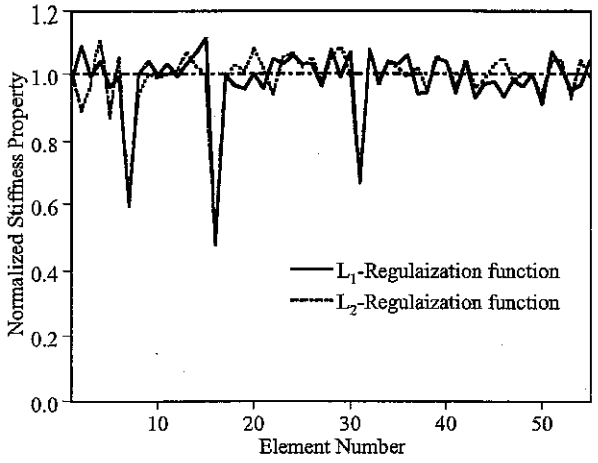

Fig.7 Estimated stiffness properties at the final time step

5.2 SDOF system

Fundamental investigations on the time window technique are performed in this example through a SDOF system. Since it is difficult to apply a regularization scheme in a SDOF system, a regularization function is not applied to the error function. Fig. 8 shows the SDOF system used in this example. The initial stiffness of spring, the mass and the damping ratio of the SDOF system are 297.88 N/m, 10.24 Kg and 3 %, respectively. A free vibration of the system is introduced by sudden release of an applied load of 100 N. Damage of the spring occurs at time 5 sec and the stiffness of the spring reduces by 50%. The acceleration of the system is measured for 20 sec at the sampling rate of 40/sec. Noise in measurement is not considered, and the stiffness of the spring is the only system parameter in this example.

Fig.9 shows the estimated stiffness of the spring with time window size of 0.25 sec and 1.0 sec. The time window size of 0.25 sec yields severely oscillatory results after damage, which are suppressed by the longer time window size of 1.0 sec. At the current stage of

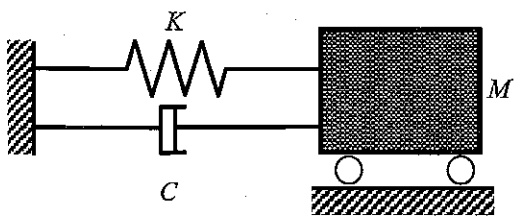

Fig. 8 SDOF system

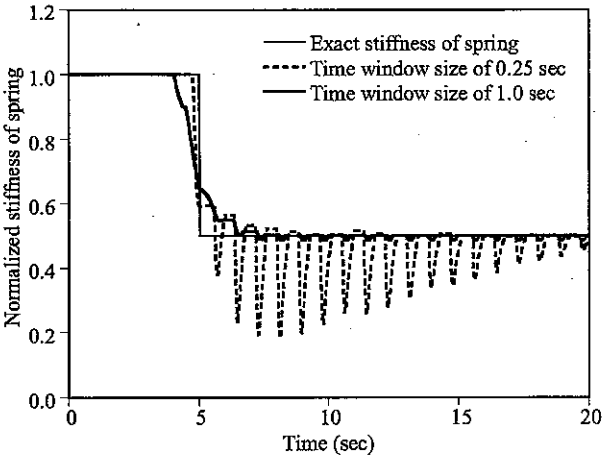

Fig.9 Estimated spring stiffness by time window

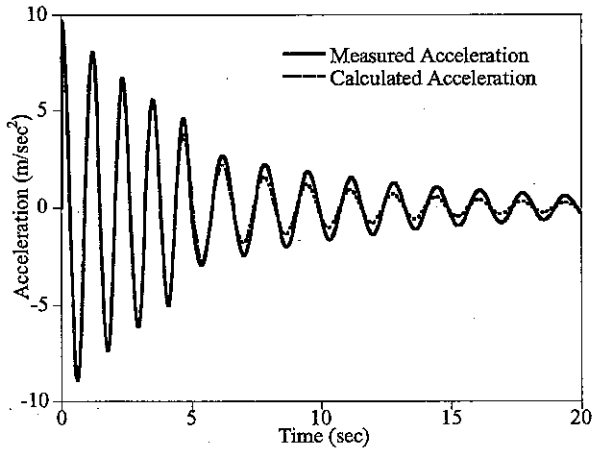

Fig.10 Measured and calculated acceleration

research, it is believed that the oscillations are caused by inaccurate estimation of the acceleration at the time of damage that acts as noise in the initial condition. In case that a longer time window is used, the effect of noise in the initial condition is smeared out by larger amount of measured data included in the window. Therefore, the regularization scheme proposed in this paper can suppress the oscillations of identified results after damage if properly applied. Fig. 10 shows accelerations calculated by the estimated stiffness. The accelerations after damage are underestimated.

6. Conclusion

The L_1-regularization function and the time window technique are proposed for SI in time domain using measured acceleration data is proposed. The system parameters include the damping parameters as well as the stiffness parameters of a structure. The Rayleigh damping is used to estimate the damping characteristics of a structure. The least square errors of the difference between calculated acceleration and measured acceleration is adopted as an error function. The regularization technique is employed to alleviate the ill-posedness of the inverse problem in SI. The L_1-TSVD is utilized to optimize a non-differential object function.

The L_1-regularization function exhibits very compromising characteristic of fast convergence, which is very crucial in the time window technique. Although the time window technique has not been fully developed yet, the example presented in this paper shows capabilities of the time window technique for the identification of damage caused by earthquakes.

References

1) Yeo, I. H., Shin, S. B., Lee, H. S. and Chang, S. P., Statistical damage assessment of framed structures from static responses, *Journal of Engineering Mechanics*, ASCE, Vol. 126, No. 4, pp. 414-421, 2000
2) Shi, Z.Y., Law, S.S. and Zhang, L.M., Damage localization by directly using incomplete mode shapes, *Journal of Engineering Mechanics*, ASCE, Vol. 126, No. 6, pp. 656-660, 2000
3) Vestouni, F. and Capecchi, D., Damage detection in beam structures based on frequency measurements, Journal of Engineering Mechanics, ASCE, Vol. 126, No. 7, pp. 761-768, 2000
4) Kang, J.S., Yeo, I.H. and Lee, H.S., Structural damage detection algorithm from measured acceleration, *Proceeding of KEERC-MAE Joint Seminar on Risk Mitigation for Regions of Moderate Seismicity*, pp. 79-86, 2001
5) Hansen, P.C., *Rank-deficient and discrete ill-posed problems : Numerical aspects of linear inversion*, SIAM, Philadelphia, 1998
6) Hansen, P. C., and Mosegaard, K. Piecewise polynomial solutions without a priori break points, *Numerical Linear Algebra with Applications*, Vol. 3, 513-524, 1996
7) Chopra, A.K., *Dynamics of Structures (theory and applications to earthquake engineering*, Prentice Hall, 1995.

(Received July 31, 2003)

Dynamic Response Analysis of Rationalized Monorail Bridges under Moving Trains

Takumi Kamizono*, Chang Hun Lee**, Takeshi Kanbara***, Chul Woo Kim****,
Mitsuo Kawatani*****, Nobuo Nishimura******

*Graduate School of Science and Technology, Kobe University, 1-1 Rokkodai, Nada, Kobe 657-8501, Japan
**M. of Eng., Graduate School of Engineering, Osaka University, 2-1 Yamadaoka, Suita, Osaka 565-0871, Japan
*** Graduate School of Engineering, Osaka University, 2-1 Yamadaoka, Suita, Osaka 565-0871, Japan
****Ph.D., Dept. of Civil Eng., Kobe University, 1-1 Rokkodai, Nada, Kobe 657-8501, Japan
*****Dr. of Eng., Prof., Dept. of Civil Eng., Kobe University, 1-1 Rokkodai, Nada, Kobe 657-8501, Japan
******Dr. of Eng., Prof., Dept. of Civil Eng., Osaka University, 2-1 Yamadaoka, Suita, Osaka 565-0871, Japan

Modern bridges require design strategy to make bridges more cost-efficiency. The efficiency-based design strategy also influences to the design of a bridge system for monorail has been expected to get good marks on decreasing the total steel weight and numbers of secondary members. However, the less weight and members than existing monorail bridge system will make the bridge easily vibrated. In this study, the analytical procedure is introduced to derive equations of motion for train-monorail structure interaction system based on Lagrange's formulation. The dynamic behavior of monorail bridges is calculated to investigate the difference of dynamic features between conventional and advanced rationalized monorail bridges by using the developed analytical method.

Key Words: Rationalized monorail bridge, traffic-induced vibration, dynamic response analysis, 15DOF of train model

1. Introduction

In the last two decades, there have been significant needs of new transportation systems due to traffic problems in major cities of Japan. Consequently, the challenge to adopt the new transportation system like a monorail has been broader range in recent years. A modern bridge design requires not only strength but also cost-efficiency, and the situation stimulate structural engineers bring about a concept of rationalized design strategy even in the monorail structure.[1] New types of rationalized steel bridges for monorails thus have been developed. The rationalized bridge equipped less lateral members than the conventional bridge to enhance the work regard to fabrication, erection, maintenance, etc. The RC tramway is also adopted as one of advanced concepts to enhance breaking performance of trains. The simplified lateral bracing system of the rationalized monorail bridge can make the bridge easily vibrated especially in lateral direction, and it can give rise to a problem related to the vibration serviceability or riding comfort of the monorail trains. This study thus derives equations of motion for a train-monorail structure interaction system based on the Lagrange's formulation.[2),3)] A train is idealized as a dynamic system with 15-degree-of-freedom (15DOF). The simultaneous differential equations of motions for the interaction system are solved by Newmark's β method as a direct integration method. Dynamic behaviors of monorail bridges are calculated to investigate the difference of dynamic features between conventional and rationalized monorail bridges by using the developed analytical method.

2. Dynamic Equations of Train-Monorail Structure Interaction System

2.1 Three-dimensional train modal

Figure 1 shows the idealized train model as a dynamic system with 15-degree-of-freedom (15DOF). In **Fig.1** m indicates the mass; K, the stiffness constant; C, the damping constant; z, y and θ indicate the vertical, lateral and rotational displacements, respectively.

2.2 Dynamic equations of monorail structure-train interaction system

Dynamic equations for a train system are derived by using Lagrange equation of motion, as shown in Eq.(1).[2),3)] Lagrange

equation of motion has been one of the most popular methods to formulate a dynamic system, which provides a method of great power and versatility for the formulation of equation of motion for any dynamic system.

$$\frac{\partial}{\partial t}\left(\frac{\partial T}{\partial \dot{a}_i}\right)-\frac{\partial T}{\partial a_i}+\frac{\partial U_e}{\partial a_i}+\frac{\partial U_d}{\partial \dot{a}_i}=0 \qquad (1)$$

where, T is kinetic energy, U_e is potential energy by elastic motion and U_d means dissipation energy by damping, and a_i generalized coordinates or unknown variables of the system. The equations of kinetic energy and potential energy including strain energy and dissipation energy by viscous damping of a train system are expressed in a set of generalized coordinates as follows.

$$T=\frac{1}{2}\left[\sum_{v=1}^{nv}\left\{m_{v11}\dot{Z}_{v11}{}^2+m_{v11}\dot{Y}_{v11}{}^2+I_{xv11}\dot{\theta}_{xv11}{}^2+I_{yv11}\dot{\theta}_{yv11}{}^2+I_{zv11}\dot{\theta}_{zv11}{}^2+\sum_{i=1}^{2}\left(m_{v2i}\dot{Z}_{v2i}{}^2+m_{v2i}\dot{Y}_{v2i}{}^2+I_{xv2i}\dot{\theta}_{xv2i}{}^2+I_{yv2i}\dot{\theta}_{yv2i}{}^2+I_{zv2i}\dot{\theta}_{zv2i}{}^2\right)\right\}\right] \qquad (2)$$

$$U_e=\frac{1}{2}\sum_{v=1}^{nv}\left[\sum_{i=1}^{2}\sum_{j=1}^{2}\sum_{n=1}^{2}\left\{k_{w1jn}R_{w1jn}{}^2\delta_{1j}+k_{w2jn}R_{w2jn}{}^2+k_{w3jn}R_{w3jn}{}^2+k_{w4jn}R_{w4jn}{}^2\delta_{1j}\right\}+\sum_{i=1}^{2}k_{w5i1}R_{w5i1}{}^2\right] \qquad (3)$$

$$U_d=\frac{1}{2}\sum_{v=1}^{nv}\left[\sum_{i=1}^{2}\sum_{j=1}^{2}\sum_{n=1}^{2}\left\{c_{w1jn}\dot{R}_{w1jn}{}^2\delta_{1j}+c_{w2jn}\dot{R}_{w2jn}{}^2+c_{w3jn}\dot{R}_{w3jn}{}^2+c_{w4jn}\dot{R}_{w4jn}{}^2\delta_{1j}\right\}+\sum_{i=1}^{2}c_{w5i1}\dot{R}_{w5i1}{}^2\right] \qquad (4)$$

In Eqs.(2), (3) and (4), nv means the numbers of trains, I is the mass moment of inertia, and R_{vimjn} denotes the relative displacement at springs (or dampers). The relative displacement can be described as shown in Eq.(5) to Eq.(9), and δ_{ij} is Kronecker's delta. Other notations used in Eqs.(2), (3) and (4) are as shown in **Table 1**.

$$R_{w1jn} = Z_{v1l}-Z_{w2i}+(-1)^n\theta_{vd1}l_{vy2}-(-1)^n\theta_{vx2i}l_{vy2}-(-1)^j\theta_{vy1l}l_{vxi} \qquad (5)$$

$$R_{w2jn} = Z_{v2i}-(-1)^j\theta_{vy2i}l_{vx3}+(-1)^n\theta_{vx2i}l_{vy4}-V_{0jn} \qquad (6)$$

$$R_{w3jn} = Y_{2i}-V_{0jn}+(-1)^j\theta_{vz2i}l_{vx4} \qquad (7)$$

$$R_{w4jn} = Y_{2i}-V_{0jn}+\theta_{vz2i}l_{vz3} \qquad (8)$$

$$R_{w5jn} = Y_{v1l}-Y_{v2i}-\theta_{vd1}l_{vz1}+(-1)^j\theta_{vz1l}l_{vxi} \qquad (9)$$

where, V_{0imjn} denotes the relative displacement of the bridge and road surface roughness at the contact point of wheels.

The equation of the forced vibration for a bridge is obtained as the following Eq. (10).

$$\boldsymbol{M}_b\ddot{\boldsymbol{w}}_b+\boldsymbol{C}_b\dot{\boldsymbol{w}}_b+\boldsymbol{K}_b\boldsymbol{w}_b=\boldsymbol{f}_b \qquad (10)$$

where M_b, C_b and K_b denote mass, damping and stiffness matrices of the bridge system, respectively. f_b is an external force vector which trains give to a bridge. w_b indicates displacement vector of bridge in the original coordinates. The displacement vector can be defined as,

$$\boldsymbol{w}_b=\sum_i\boldsymbol{\phi}_i\boldsymbol{q}_i=\boldsymbol{\Phi}\cdot\boldsymbol{q} \qquad (11)$$

where, Φ denotes mode vector, and q is generalized displacement vector.

The simplified matrix form of monorail structure - train interaction system can be expressed as follows.

$$\begin{bmatrix}\mathbf{M}_b & 0\\ Symm. & \mathbf{M}_v\end{bmatrix}\begin{Bmatrix}\ddot{q}\\ \ddot{\Delta}\end{Bmatrix}+\begin{bmatrix}\mathbf{C}_b^{*} & \mathbf{C}_{bv}\\ Symm. & \mathbf{C}_v\end{bmatrix}\begin{Bmatrix}\dot{q}\\ \dot{\Delta}\end{Bmatrix}+\begin{bmatrix}\mathbf{K}_b^{*} & \mathbf{K}_{bv}\\ Symm. & \mathbf{K}_v\end{bmatrix}\begin{Bmatrix}q\\ \Delta\end{Bmatrix}=\begin{Bmatrix}\mathbf{f}_b\\ \mathbf{f}_v\end{Bmatrix} \qquad (12)$$

where, M_b, M_v, C_b^*, C_v and C_{bv} indicate the mass and damping matrixes of monorail structure, train, structure-train interaction system. and K_b^*, K_v and K_{bv} indicate the stiffness matrixes of monorail structure, train, structure-train interaction system.

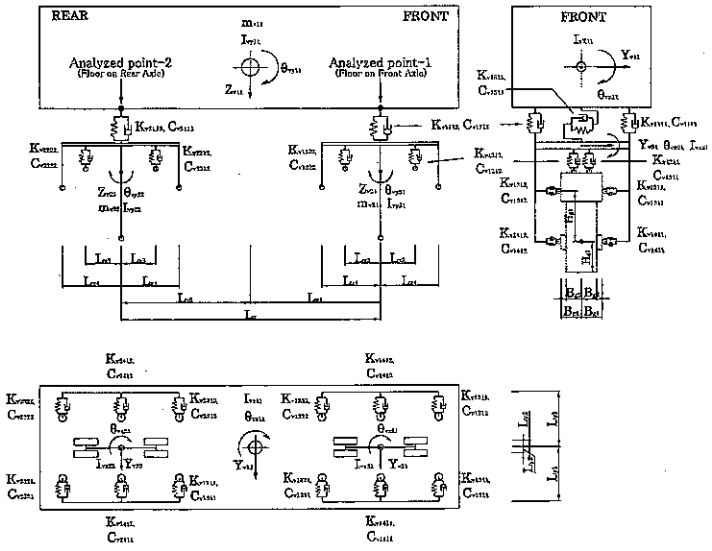

Fig. 1 Idealized monorail train with 15DOF

Table 1 Notations of train model

Descriptions	Nomenclatures
Mass of body	m_{v11}
Mass of suspension system	m_{v21},m_{v22}
Spring constant of air suspension(Vertical)	k_{v1111},k_{v1112},k_{v2111},k_{v2112}
Spring constant of tire	k_{v1211},k_{v1212},k_{v1221},k_{v1222} k_{v2211},k_{v2212},k_{v2221},k_{v2222}
Spring constant of guide wheel	k_{v1311},k_{v1312},k_{v1321},k_{v1322} k_{v2311},k_{v2312},k_{v2321},k_{v2322}
Spring constant of safe wheel	k_{v1411},k_{v1412},k_{v2411},k_{v2412}
Spring constant of air suspension(Horizonal)	k_{v1511},k_{v2511}
Damping constant of damper(Vertical)	C_{v1111},C_{v1112},C_{v2111},C_{v2112}
Damping constant of tire	C_{v1211},C_{v1212},C_{v1221},C_{v1222} C_{v2211},C_{v2212},C_{v2221},C_{v2222}
Damping constant of guide wheel	C_{v1311},C_{v1312},C_{v1321},C_{v1322} C_{v2311},C_{v2312},C_{v2321},C_{v2322}
Damping constant of safe wheel	C_{v1411},C_{v1412},C_{v2411},C_{v2412}
Damping constant of damper(Horizonal)	C_{v1511},C_{v2511}
Vertical and horizonal displacement of body	z11,y11
Vertical displacement of front and rear suspension system	z21,z22
Horizonal displacement of front and rear suspension syste	y21,y22
Rolling, pitching and yawing of body	θ x11, θ y11, θ z11
Rolling of front and rear suspension system	θ x21, θ x22
Pitching of front and rear suspension system	θ y21, θ y22
Yawing of front and rear suspension system	θ z21, θ z22

3. Dynamic Response Analysis

3.1 Analytical method

Guyan reduction is used for the sake of the effectiveness. The Newmark-β method is adopted to solve the simultaneous differential equations of the system. The time interval is taken as shorter than 1/5~1/6 of the natural frequency of the highest mode. A value of 0.25 is adopted as β to obtain the stable and accurate solutions. The solutions can be obtained within the error of 0.001.

3.2 Surface roughness

The tramway, steering-guideway and stabilizing-guideway roughness profiles used in the numerical analysis are artificially generated based on the power spectral density (PSD) function as shown in Eq. (13).[4] As a PSD function for the tramway, the PSD based on the measured data of Meishin expressway in Japan is used because of no useful data for monorail structures. Those profiles of steering and stabilizing tracks are assumed by authors.

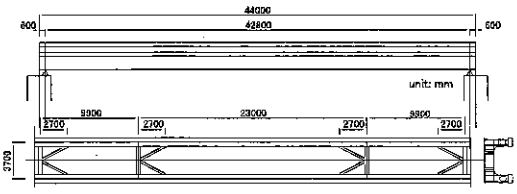

(1) Rationalized type

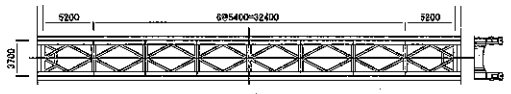

(2) Conventional type

Fig. 2 Typical ground plan of monorail bridges

$$S_{z0}(\Omega) = \frac{\alpha}{\Omega^n + \beta^n} \qquad (13)$$

where, $S_{z0}(\Omega)$ is the PSD of the roughness power spectrum density, Ω is roughness frequency. PSD function factor of surface roughness are as follows;

Running track : $\alpha = 0.001$, $\beta = 0.05$, $n = 2.00$
Steering track : $\alpha = 0.002$, $\beta = 0.05$, $n = 1.00$
Stabilizing track : $\alpha = 0.0015$, $\beta = 0.05$, $n = 1.00$

3.3 Numerical model of bridge

(1) FE bridge model

Rationalized (R. b.) and conventional (C. b.) type bridges are shown in **Fig.2**, and those FE models are appeared in **Fig.3**. The span length of the bridges is 42.8m. Trains are assumed to run on the G1 girder in analysis.

(2) Eigen value analysis

Table 2 shows the mode shape and the natural frequencies of rationalized and conventional bridges by analysis. In **Table 2**, C indicates couple mode; T1, both of the tramways have similar phase; T2, both of the tramways have reverse phase.

3.4 Dynamic characteristic of train

The properties of the train used in this study (**Fig.1**) are summarized in **Table 3**. The analytical frequencies of the train model are shown **Table 4**. The fundamental frequencies related to the trains' body motion are 1.207 for bouncing and 0.912 for lateral motion. It means there exists few possibility occurring resonance with vertical and lateral motion of bridges in comparing with the dynamic characteristic summarized in **Table 2**.

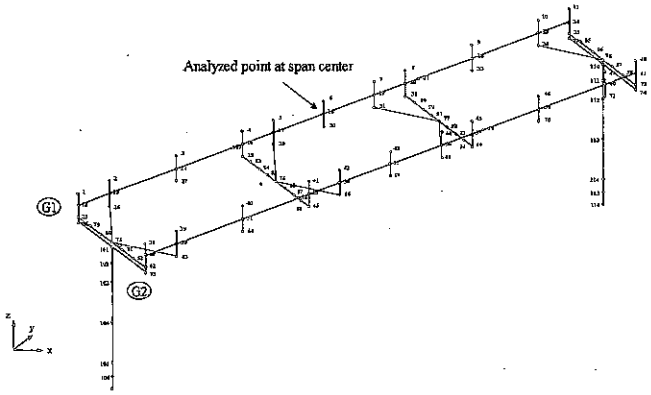

(1) FE Model for rationalized bridge type

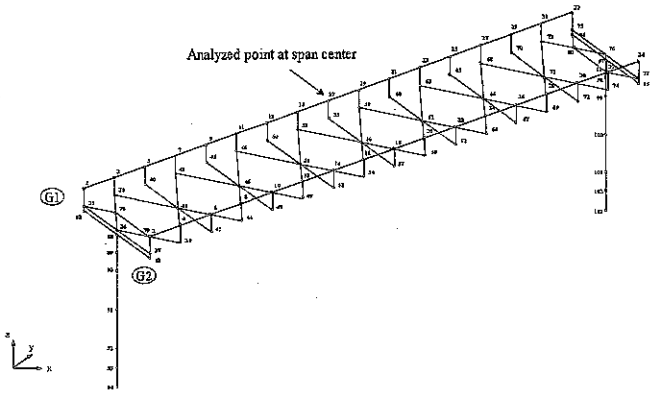

(2) FE Model for conventional bridge type

Fig. 3 FE Model for bridges

4. Analysis Results

4.1 Dynamic response of rationalized and conventional bridges

The displacement response at the center of the span in vertical and horizontal directions and their Fourier spectra (vehicle speed 20m/s, no passengers) are shown in **Fig. 4** and **Fig. 5**, respectively. When the vertical response of the rationalized bridge is compared with that of the conventional bridge, the static response and the dynamic component of the response of the rationalized bridge are slightly smaller than those of the conventional bridge. The static response at the horizontal direction shown in **Fig. 5** is caused by the torsional behavior of the monorail-bridge.

Table 2 Mode shapes and natural frequencies of R.b. and C.b. by analysis

Mode No.	Rationlized bridge	Conventional bridge
1	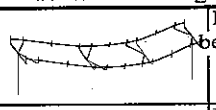 Horizontal bending 1st/T1 1.797 Hz	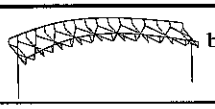 Horizontal bending 1st/T1 2.574 Hz
2	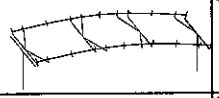 Vertical bending 1st 2.993 Hz	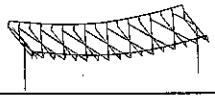 Vertical bending 1st 3.059 Hz
3	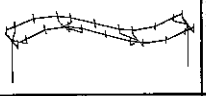 Horizontal bending 2nd/T1 4.883 Hz	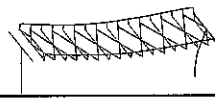 Pier 1st (C vertical bending 4.252 Hz
4	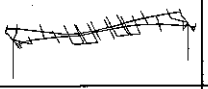 Tortion 1st/T1 5.361 Hz	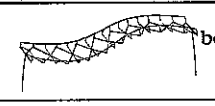 Horizontal bending 2nd/T1 6.322 Hz
5	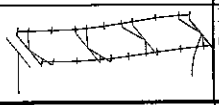 Pier 1st (C vertical bending) 6.129 Hz	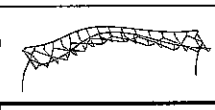 Tortion 1st/T1(C Pier) 8.956 Hz
6	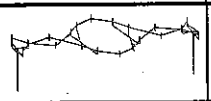 Horizontal bending 1st/T2 7.455 Hz	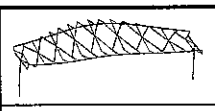 Tortion 1st/T2 9.618 Hz
7	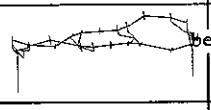 Horizontal bending 2nd/T2 8.730 Hz	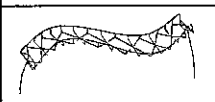 Horizontal bending /T1 (C Pier) 10.966 Hz
8	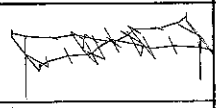 Tortion 1st/T2 9.252 Hz	Vertical bending 2nd (C horizontal bendi 12.466 Hz
9	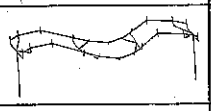 Horizontal bending 3rd/T1 9.444 Hz	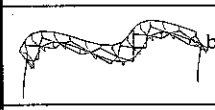 Horizontal bending 3nd/T1 (C horizontal bendi 15.462 Hz
10	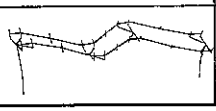 Horizontal bending 2nd/T1 (C Pier) 10.259 Hz	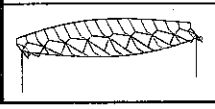 Tortion 2nd/T2 18.752 Hz

Table 3 Properties of monorail train

m_{11}	14.22×10^3 (kg)	m_{21}, m_{22}	6.20×10^3 (kg)	L_{x1}	4.800 (m)
$I_{\theta x11}$	1.997×10^4 (kg·m^2)	$I_{\theta x21}$, $I_{\theta x22}$	2.461×10^3 (kg·m^2)	L_{x2}	4.800 (m)
$I_{\theta y11}$	1.717×10^5 (kg·m^2)	$I_{\theta y21}$, $I_{\theta y22}$	3.488×10^3 (kg·m^2)	L_{x3}	0.7500 (m)
$I_{\theta z11}$	1.717×10^5 (kg·m^2)	$I_{\theta z21}$, $I_{\theta z22}$	9.688×10^3 (kg·m^2)	L_{x4}	1.250 (m)
k_{z11}	9.0×10^5 (N/m)	k_{z21}, k_{z22}	5.170×10^6 (N/m)	L_{y1}	1.490 (m)
k_{y11}	9.80×10^5 (N/m)	k_{y21}, k_{y22}	6.370×10^6 (N/m)	L_{y2}	1.025 (m)
c_{z11}	2.28×10^4 (N·s/m)	c_{z21}, c_{z22}	2.610×10^4 (N·s/m)	L_{y3}	0.7823 (m)
c_{y11}	3.336×10^5 (N·s/m)	c_{y21}, c_{y22}	1.855×10^5 (N·s/m)	L_{y4}	0.200 (m)
$k_{\theta x11}$	1.029×10^6 (N·m)	$k_{\theta x21}$, $k_{\theta x22}$	3.385×10^5 (N·m)	L_{z1}	0.457 (m)
$k_{\theta y11}$	2.074×10^7 (N·m)	$k_{\theta y21}$, $k_{\theta y22}$	2.655×10^6 (N·m)	L_{z2}	0.6300 (m)
$k_{\theta z11}$	2.258×10^7 (N·m)	$k_{\theta z21}$, $k_{\theta z22}$	6.125×10^6 (N·m)	L_{z3}	1.085 (m)

Table 4 Frequency of train

Bouncing:f_{z11}	1.207	Hz
Axle hope(Front):f_{z21}	4.921	Hz
Axle hope(Rear):f_{z22}	4.921	Hz
Lateral translation:f_{y11}	0.9119	Hz
Bogie sway(Front):f_{y21}	4.090	Hz
Bogie sway(Rear):f_{y22}	4.090	Hz
Rolling:$f_{\theta x11}$	1.660	Hz
Axle tramp(Front):$f_{\theta x21}$	4.616	Hz
Axle tramp(Rear):$f_{\theta x22}$	4.616	Hz
Pitching:$f_{\theta y11}$	1.790	Hz
Bogie Windup(Front):$f_{\theta y21}$	4.394	Hz
Bogie Windup(Rear):$f_{\theta y22}$	4.394	Hz
Yawing:$f_{\theta z11}$	2.286	Hz
Bogie tramp(Front):$f_{\theta z21}$	4.003	Hz
Bogie tramp(Rear):$f_{\theta z22}$	4.003	Hz

The dynamic horizontal component of the rationalized bridge is larger than that of the conventional bridge, even though the static horizontal response of the rationalized bridge is smaller than that of the conventional bridge.

The dominant frequency near 1.4Hz in the **Fig. 4** may be the effect of vehicle's bouncing motion of 1.207Hz. The dominant frequency, near 1.71 Hz shown in **Fig. 5**, of the rationalized bridge in horizontal direction can be due to the 1st horizontal bending mode (1.797 Hz) of the rationalized bridge.

4.2 Effect of vehicle speed

The dynamic response of the rationalized bridge is simulated as shown in **Fig. 6** with respect to the vehicle speed of 36km/h(10m/s), 54km/h(15m/s) and 72km/h(20m/s) under the condition of no passengers to investigate the effect of vehicle speed to bridge response. It shows that the response of the bridge tends to increase according to speeds.

4.3 Effect of passenger loading

In **Fig. 7**, the response of the rationalized bridge is shown with respect to the numbers of passengers under the condition of speed 72km/h. It shows that the dynamic response of the bridge tends to decrease according to the passengers numbers.

5. Summary

In this study, the dynamic response of monorail bridges due to moving trains is theoretically analyzed taking account of surface roughness of the track way and coupling vibration between bridges and trains. The following remarks can be concluded from the analytical results.

(1) The dynamic response of the rationalized bridge at the horizontal direction becomes larger than that of the conventional bridge, even though the static response of the rationalized bridge is smaller than that of the conventional bridge.

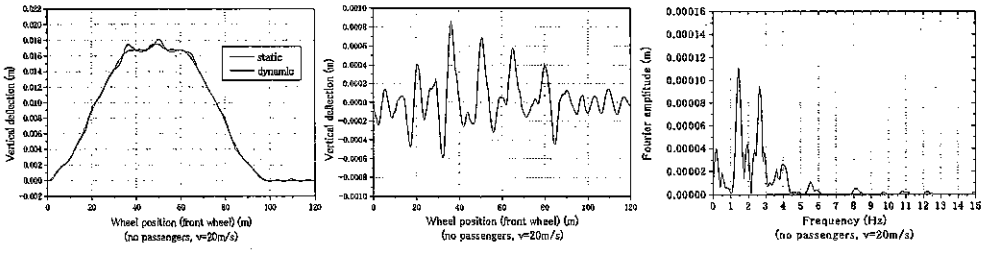

(1) Rationalized bridge

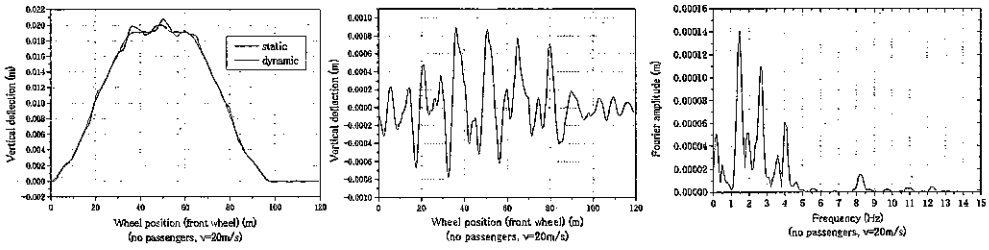

(2) Conventional bridge

Fig. 4 Vertical response at the center of span (Vacancy, v =20m/s)

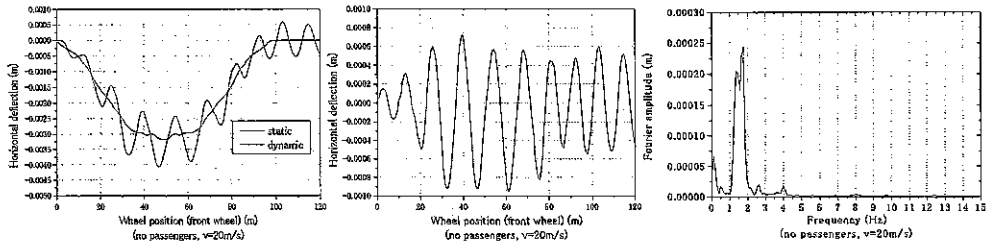

(1) Rationalized bridge

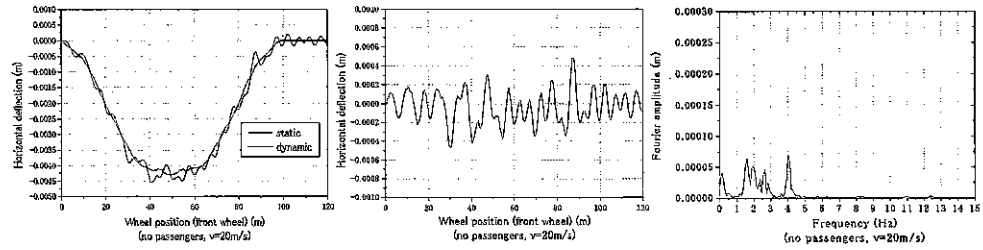

(2) Conventional bridge

Fig. 5 Horizontal response at the center of span (Vacancy, v =20m/s)

(2) The dynamic response of the rationalized bridge tends to increase according to the train speed.

(3) The dynamic response of the rationalized bridge tends to decrease according to the passengers occupant

As a next step for this study, investigations will be focused on the validity of the analytical result by comparing with the field-test data that is in processing.

References

(1) The Osaka monorail rationalization orbital girders examination meeting : The proposal of the rationalization structure of the Osaka monorail steel orbital girders, The research report of a composite orbital girders, 2001.1. (in Japanese)

(2) J. P. Song, K. B. Kim and C. W. Kim : Dynamic responses of automated guideway transit (AGT) vehicle considering pathway and guiderail roughness, Proc. of 8th East Asia-pacific Conference on Structural Engineering and Construction, Paper No.1449, 2001

(3) M. Kawatani and C. W. Kim : Computer simulation for dynamic wheel loads of heavy vehicles, Int. Journal of Structural Engineering and Mechanics. Vol.12, pp.409-428, 2001

(4) The study group of bridge vibration : Measurement and analysis of bridge vibration, Analysis section, Gihodo, 1993 (in Japanese)

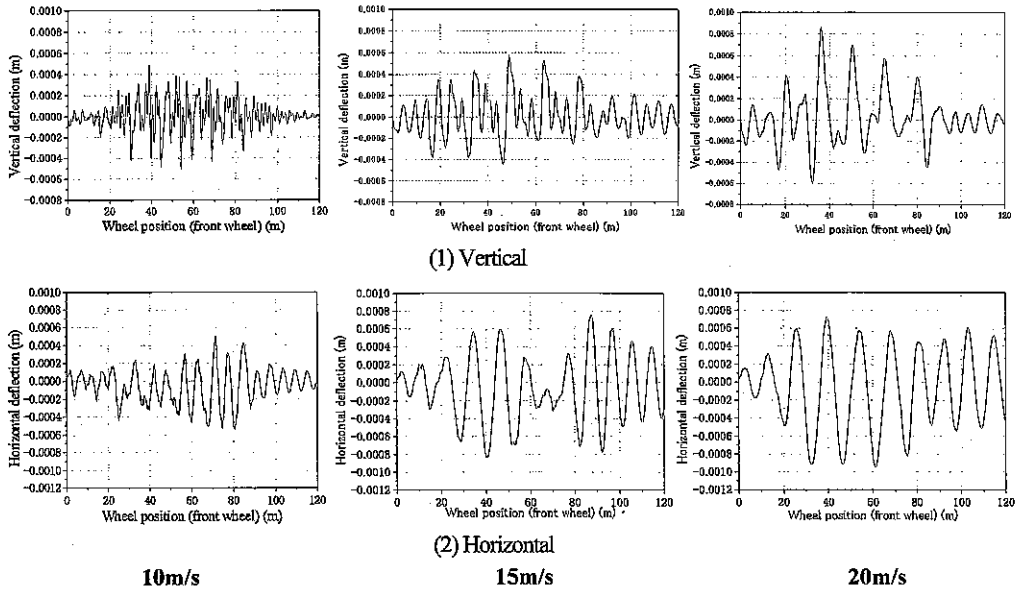

(1) Vertical

(2) Horizontal

10m/s **15m/s** **20m/s**

Fig. 6 Response at the center of span (Vacancy)

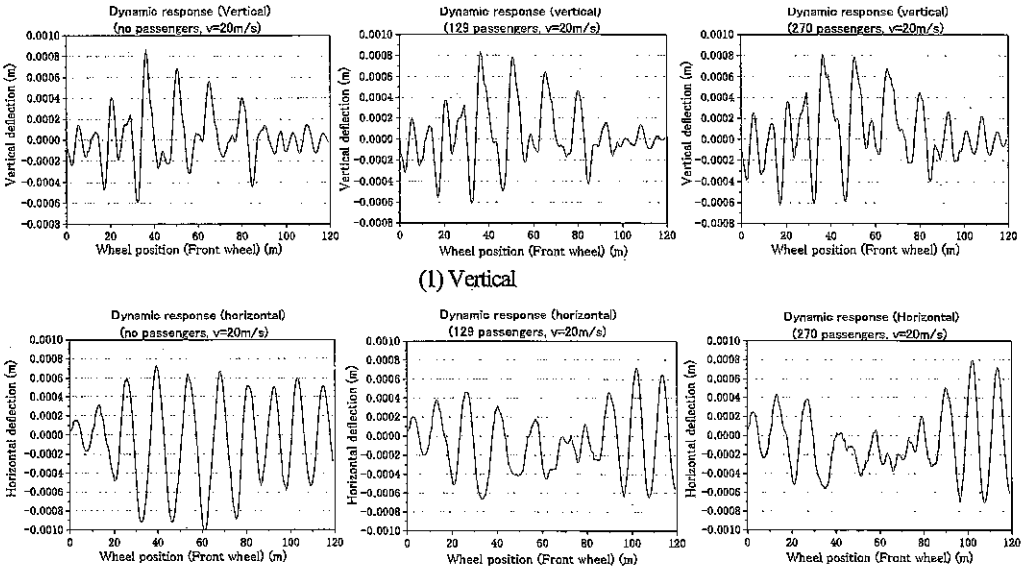

(1) Vertical

(2) Horizontal

Vacancy (26.76tf) **Loaded its half capacity(34.5tf)** **Loaded its full capacity(42.96tf)**

Fig. 7 Response at the center of span (v =20m/s)

Dynamic Response Analysis of Elevated Railway Bridges due to Shinkansen Trains and Influence of Train models

Mitsuo KAWATANI *, Xingwen HE **, Ryo SOBUKAWA** and Seiji NISHIYAMA***

* Dr. of Eng., Prof., Dept. of Civil Eng., Kobe University, 1-1, Rokkodai, Nada, Kobe 657-8501, Japan
** Graduate School of Science and Technology, Kobe University, 1-1, Rokkodai, Nada, Kobe 657-8501, Japan
*** Dr. of Eng., Nikken Sekkei Civil Engineering, Ltd., 2-18-3, Iidabashi, Chiyoda, Tokyo 102-8117, Japan

Railway bridges are usually subject to severe vibrations due to high-speed bullet trains. The needs arise to carry out regular investigations and generate reliable expectations of undesirable vibrations. The reliable expectation of bridge vibrations offers a key to effective countermeasures. Dynamic response analysis is considered effective to meet those needs. This paper seeks to clarify the phenomena of the structural vibrations of elevated bridges due to bullet trains by means of three-dimensional dynamic analysis. Analytical results are compared with experimental ones to demonstrate the validity of the analytical procedure. The further investigation is performed to examine the influence of different train models on analytical results.

Key Words: Dynamic Response Analysis, Train-Induced Vibration of bridges, Shinkansen Train, Nine-Degree-of-Freedom Train Model

1. Introduction

High-speed railway system serving as a momentous role in the transportation between the main cities in Japan has been contributing a great deal to the development of Japanese society, since 1964. Elevated bridges of high-speed railway are usually subject to severe vibrations, which can lead to the deteriorations of bridge structures, due to high-speed bullet trains. Furthermore, there occur environmental vibration problems while the vibrations propagate to the neighboring buildings through the ground. The needs arise to carry out regular investigations and generate reliable expectations of undesirable vibrations[1]. The reliable expectation of bridge vibrations offers a key to effective countermeasures.

First of all it is necessary to clarify the vibration characteristics of elevated bridges, in order to investigate the vibration problems under high-speed bullet trains. Responding to that kind of needs the field bridge tests have been performed in some actual high-speed railway bridges to grasp the features of vibrations due to bullet trains. Moreover, theoretical researches on the vibrations of elevated railway bridges due to traveling trains were being carried out since the middle of 1960's. Considering the train-bridge interaction, Matsumura[2] developed a dynamic response analysis of simple girder bridge due to bogie car. The deflection curve of the simple girder is expressed by orthogonal function while the bogie car is considered as a rigid body with concentrated mass, and the fundamental vibration characteristics of simple girder are summarized. Tanabe, et al[3] carried out an analysis employing three-dimensional finite element method to simulate the interaction of track structures and trains.

At the same time, the researches on dynamic characteristics of highway bridges due to traveling vehicles were also prosperously being carried out. Investigations of the impact coefficient of highway bridges are summarized by Honda, et al[4] and Kawatani[5], et al. In Kawatanis' researches, the dynamic response analysis for a bridge-vehicle interaction system of simple girder and two-degree-of-freedom sprung-mass vehicle model with one front and two rear axles was carried out taking account of the vibration of bending and torsion. And recently, a three-dimensional vehicle model with eight-degree-of-freedom, considering bouncing, pitching and rolling of the vehicle body, parallel hop and axle tramp of the front axle, parallel hop, axle windup motion and axle tramp of the rear axle of vehicle, is developed for dynamic response analyses on various highway bridge-vehicle interaction systems[6].

Dynamic response analyses are considered to be also effective for the investigations of dynamic characteristics of the high-speed railway bridge-train interaction systems. Hereupon in this study, the eight-degree-of-freedom vehicle model mentioned above is developed into a nine-degree-of-freedom train model for the three-dimensional dynamic response analysis program to investigate the vibrations of elevated bridges due to bullet trains.

Considering the structural features of elevated bridges and the high speed of trains, the high-frequency component is predicted to be relatively important in the dynamic response, and the influence of train models is expected. In this study, effects of degree-of-freedom of modeling a train are examined to find the rational train model that can express high frequency vibration appropriately, therefore trains modeled as two- or six-degree-of-freedom of plane model without or with mass of axles, respectively, and nine-degree-of-freedom systems are used as analytical vehicle models.

2. Three-Dimensional Dynamic Response Analysis

2.1 Analytical procedure[7]

Dynamic response of high-speed railway elevated bridges due to bullet trains is calculated taking account of the rail surface roughness. The elevated bridges are modeled as three-dimensional beam elements and the simultaneous dynamic differential equations of the bridge and moving trains are derived by means of modal analysis. The direct numerical integration of Newmark's β method is effectively applied to solving dynamic differential equations, and the dynamic responses of bridge are calculated. Adopting 1/4 as the value of β, the response can be accurately obtained with the error less than 1/1000 for acceleration at each time step.

The dynamic differential equations of elevated bridges and bullet trains are represented as follows. Since the equations of two- and six-degree-of-freedom train models can be obtained by simplifying the equations of nine-degree-of-freedom train model, herein only the equation of nine-degree-of-freedom train models is described.

2.2 Dynamic differential equation of elevated bridge

The dynamic differential equation of elevated bridge is derived as follows, based on D'Alembert's theory.

$$\boldsymbol{M_b}\ddot{\boldsymbol{w}}_b + \boldsymbol{C_b}\dot{\boldsymbol{w}}_b + \boldsymbol{K_b}\boldsymbol{w}_b = \boldsymbol{f_b} \tag{2.1}$$

Where, $\boldsymbol{M_b}$, $\boldsymbol{C_b}$ and $\boldsymbol{K_b}$ denote mass, damping and stiffness matrices of the bridge system, respectively.

Herein, the damping matrix of bridge $\boldsymbol{C_b}$ is assumed to be calculated by the linear relation between mass and stiffness matrices[8] as follows:

$$\boldsymbol{C_b} = p_1\boldsymbol{M_b} + p_2\boldsymbol{K_b} \tag{2.2}$$

Where, p_1 and p_2 are the ratio coefficients.

The external force vector f_b can be represented as follows:

$$f_b = \sum_{j=1}^{h}\sum_{l=1}^{2}\sum_{k=1}^{2}\sum_{m=1}^{2} \Psi_{jlkm}(t)P_{jlkm}(t) \tag{2.3}$$

Where, $P_{jlkm}(t)$ is the wheel load of the train and $\Psi_{jlkm}(t)$ is called distribution vector distributing the wheel load to the nodes of beam elements. The subscripts j, l, k and m indicate the train number, the bogie, the axle, and the wheel, respectively. All these variables and subscripts will be described in detail in the next section.

The vector of nodal displacement of the bridge, w_b, is derived from modal analysis method and represented by Eq. (2.4)

$$w_b = \sum_i \phi_i q_i = \Phi \cdot q \tag{2.4}$$

Where, q is the generalized coordinate vector of bridge and Φ is the matrix composed by ϕ_i the natural modal vector of bridge. Substituting w_b into Eq. (2.1), the following equation can be derived

$$\boldsymbol{M_b}\Phi\ddot{\boldsymbol{q}} + \boldsymbol{C_b}\Phi\dot{\boldsymbol{q}} + \boldsymbol{K_b}\Phi\boldsymbol{q} = \boldsymbol{f_b}$$

Multiplying both sides by Φ^T, we can get

$$\Phi^T\boldsymbol{M_b}\Phi\ddot{\boldsymbol{q}} + \Phi^T\boldsymbol{C_b}\Phi\dot{\boldsymbol{q}} + \Phi^T\boldsymbol{K_b}\Phi\boldsymbol{q} = \Phi^T\boldsymbol{f_b}$$

According to the orthogonality of normal vectors

While $i \neq j$ $\quad \phi_i^T\boldsymbol{M_b}\phi_j = 0$

$\quad \phi_i^T\boldsymbol{K_b}\phi_j = 0$

Since $\boldsymbol{C_b}$ is linearly composed by $\boldsymbol{M_b}$ and $\boldsymbol{K_b}$,

$\quad \phi_i^T\boldsymbol{C_b}\phi_j = 0$

While $i = j$ $\quad \phi_i^T\boldsymbol{M_b}\phi_j = M_i$

$\quad \phi_i^T\boldsymbol{K_b}\phi_j = K_i$

$\quad \phi_i^T\boldsymbol{C_b}\phi_j = C_i$

Assuming $\phi_i^T f_b = f_i$, the dynamic differential equation of elevated bridge, with respect to generalized coordinate, can be developed as follows:

$$M_i\ddot{q}_i + C_i\dot{q}_i + K_i q_i = f_i \tag{2.5}$$

2.3 Dynamic differential equations of bullet train

The nine-degree-of-freedom train model is shown in **Fig.1** taking account of the mass of axles. The dynamic differential equations of the train are presented as follows:

(1) Dynamic differential equations of train body

$$m_{11}\ddot{z}_{11} + \sum_{l=1}^{2}\sum_{m=1}^{2} v_{lm}(t) = 0 \tag{2.6}$$

$$m_{11}\lambda_{x1}\lambda_{x2}\ddot{\theta}_{y11} - \sum_{l=1}^{2}\sum_{m=1}^{2}(-1)^l\lambda_{xl}v_{lm}(t) = 0 \tag{2.7}$$

$$m_{11}\lambda^2{}_{y1}\ddot{\theta}_{x11} + \sum_{l=1}^{2}\sum_{m=1}^{2}(-1)^m\lambda_{yl}v_{lm}(t) = 0 \tag{2.8}$$

Where,

$$v_{lm}(t) = k_{lm}\{z_{11} - (-1)^l \lambda_{xl}\theta_{y11} + (-1)^m \lambda_{yl}\theta_{x11} - z_{2l} - (-1)^m \lambda_{yl}\theta_{x2l}\} + c_{lm}\{\dot{z}_{11} - (-1)^l \lambda_{xl}\dot{\theta}_{y11} + (-1)^m \lambda_{yl}\dot{\theta}_{x11} - \dot{z}_{2l} - (-1)^m \lambda_{yl}\dot{\theta}_{x2l}\}$$

..... (2.9)

Herein, the subscripts relative to the vibration of train body are described as: l=1, 2 indicates the front and rear bogies, m=1, 2 indicates the left and right of the train, respectively.

(2) Dynamic differential equations of front axle

$$m_{21}\ddot{z}_{21} - \sum_{m=1}^{2} v_{11m}(t) + \sum_{k=1}^{2}\sum_{m=1}^{2} v_{1km}(t) = 0 \quad (2.10)$$

$$m_{21}\lambda_{x3}^2\ddot{\theta}_{y21} - \sum_{k=1}^{2}\sum_{m=1}^{2}(-1)^k \lambda_{x3} v_{1km}(t) = 0 \quad (2.11)$$

$$m_{21}\lambda_{y1}^2\ddot{\theta}_{x21} - \sum_{m=1}^{2}(-1)^m \lambda_{y1} v_{1m}(t) + \sum_{k=1}^{2}\sum_{m=1}^{2}(-1)^m \lambda_{y1} v_{1km}(t) = 0 \quad (2.12)$$

Where,

$$v_{1km}(t) = k_{1km}\{z_{21} - (-1)^k \lambda_{x3}\theta_{y21} + (-1)^m \lambda_{y1}\theta_{x21} - w_k\} + c_{1km}\{\dot{z}_{21} - (-1)^k \lambda_{x3}\dot{\theta}_{y21} + (-1)^m \lambda_{y1}\dot{\theta}_{x21} - \dot{w}_k\}$$

.....(2.13)

Herein, the subscripts relative to the vibration of front axle are described as: k=1, 2 indicates the front and rear wheels of front axle, m=1, 2 indicates the left and right wheels of the train, respectively.

(3) Dynamic differential equations of rear axle

$$m_{22}\ddot{z}_{22} - \sum_{m=1}^{2} v_{12m}(t) + \sum_{k=1}^{2}\sum_{m=1}^{2} v_{2km}(t) = 0 \quad (2.14)$$

$$m_{22}\lambda_{x4}^2\ddot{\theta}_{y22} - \sum_{k=1}^{2}\sum_{m=1}^{2}(-1)^k \lambda_{x4} v_{2km}(t) = 0 \quad (2.15)$$

$$m_{22}\lambda_{y2}^2\ddot{\theta}_{x22} - \sum_{m=1}^{2}(-1)^m \lambda_{y2} v_{1lm}(t) + \sum_{k=1}^{2}\sum_{m=1}^{2}(-1)^m \lambda_{y2} v_{2km}(t) = 0 \quad (2.16)$$

Where,

$$v_{2km}(t) = k_{2km}\{z_{22} - (-1)^k \lambda_{x4}\theta_{y22} + (-1)^m \lambda_{y2}\theta_{x22} - w_k\} + c_{2km}\{\dot{z}_{22} - (-1)^k \lambda_{x4}\dot{\theta}_{y22} + (-1)^m \lambda_{y2}\dot{\theta}_{x22} - \dot{w}_k\}$$

..... (2.17)

Herein, the subscripts relative to the vibration of rear axle are described as: k=1, 2 indicates the front and rear wheels of rear axle, m=1, 2 indicates the left and right wheels of the train, respectively.

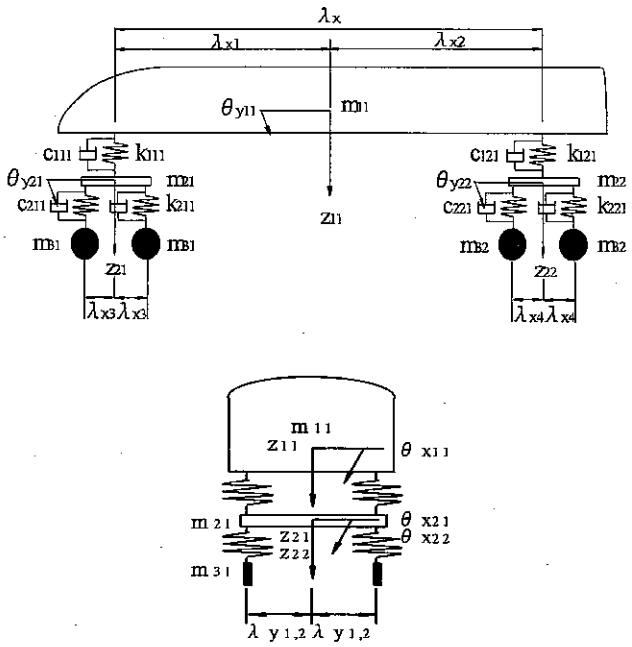

Fig.1 Dimension of train

The distribution vector mentioned in previous section is described in Eq. (2.18).

$$\Psi_{jlkm}(t) = \{0;\bullet\bullet\bullet;0;\psi_{n,jlkm};\psi_{n+1,jlkm};0;\bullet\bullet\bullet;0\}$$

..... (2.18)

The variable $w_k = w_{jlkm}$ denotes the displacement of the wheel taking into account the displacement and surface roughness of the rail

$$w_{jlkm} = w(t, x_{jlkm}) - z_0(x_{jlkm})$$

(l=1, 2, k=1, 2, m=1, 2) ..... (2.19)

Where, $w(t, x_{jlkm})$ is the displacement of rail at the point where the wheel and rail are contacting with each other, and $z_0(x_{jlkm})$ indicates the rail surface roughness.

$$w(t, x_{jlkm}) = \Psi_{jlkm}^T(t) w_b$$

(l=1, 2, k=1, 2, m=1, 2) ..... (2.20)

The wheel loads are represented as follows:

$$P_{lkm}(t) = \frac{1}{4}(1 - \frac{\lambda_{xl}}{\lambda_x})m_{11}g + \frac{1}{4}m_{21}g + m_{3l}g + v_{lkm}(t)$$

(l=1, 2, k=1, 2, m=1, 2) ..... (2.21)

Combining Eqs. (2.6) to (2.8), Eqs.(2.10) to (2.12) and Eqs. (2.14) to (2.16) with Eq. (2.5), the dynamic differential equations of train-bridge interaction system can be obtained.

3. Analytical Model

3.1 Elevated bridge model

A typical high-speed railway elevated bridge of reinforced

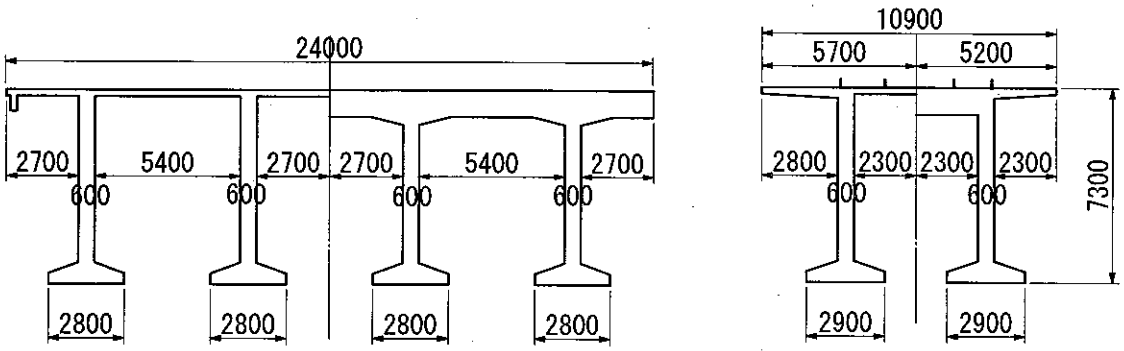

Fig.2 Elevated railway bridge

concrete with the form of portal frame shown in **Fig.2** is adopted for dynamic response analysis in this study. Three blocks (72m) of elevated bridge with 24m length of each block are modeled as three-dimensional beam elements with six-degree-of-freedom at each node, shown in **Fig.3**. The lumped mass system and Rayleigh damping are adopted for the beam elements of bridge. Mass of the ballast and the rail is also taken into account. Double nodes defined as two nodes of independence sharing the same coordinate are adopted at the bottom of the piers of bridges to simulate the effect of the ground spring[9], including the footings and the piles, and the ground spring constants are shown in **Table 1**. Damping constant of 0.03 is assumed for the first and second natural modes of vibration of bridge system. Damping constants for the natural modes of higher order from the third calculated by means described in previous section will be larger than the ones of first and second modes.

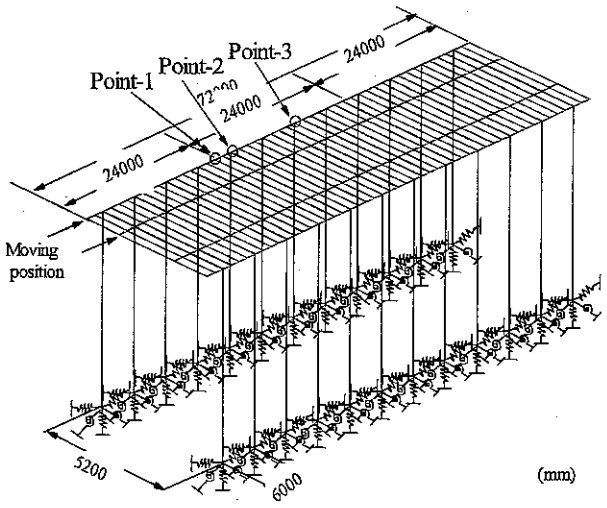

Fig.3 Analytical model of bridge

3.2 Rail model

The rail is also modeled as three-dimensional beam elements with six-degree-of-freedom at each node. Double nodes are also defined here to simulate the elastic effect of sleepers and ballast at the positions of sleepers. The property of the rail and the spring constant of the track are shown in **Table 2**. The vertical spring constant of the track is derived from the ratio of the wheel load to the displacement in the vertical direction of rail. The horizontal spring constant of the track is assumed to be 1/3 of the value in vertical direction. Only the roughness in vertical direction of the rail is considered and the surveyed value of the rail roughness is shown in **Fig.4**.

Table 1 Ground spring constant

	Longitudinal	Transverse
Vertical spring of pile top (kN/m)	3.86×10^6	
Rotating spring of pile top (kN·m/rad)	3.64×10^6	2.42×10^6
Horizontal spring of footing (kN/m)	4.84×10^3	4.72×10^3
Horizontal spring of pile top (kN/m)	8.22×10^4	8.08×10^4

Table 2 Property of railway

Area (m^2)	7.75×10^{-3}
Mass (t/m)	0.0608
Moment of inertia (m^4)	3.09×10^{-5}
Spring constant of track (MN/m)	70

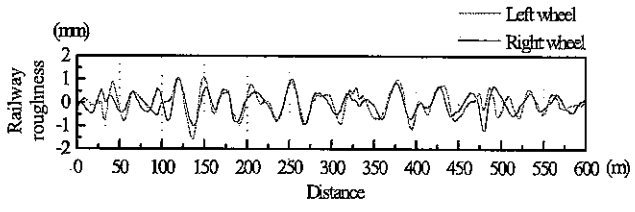

Fig.4 Railway roughness

3.3 Train model

Bullet trains composed of sixteen cars are modeled as two-, six-, and nine-degree-of-freedom systems, in order to investigate the influence of train models on the dynamic responses of elevated bridges. The two-degree-of-freedom plane train model and the nine-degree-of-freedom three-dimensional train model taking into account the mass of axles are shown in **Fig.5**. The six-degree-of-freedom train model that also takes account of the

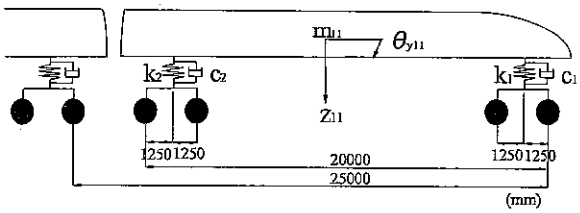

(1) 2-degree-of-freedom system

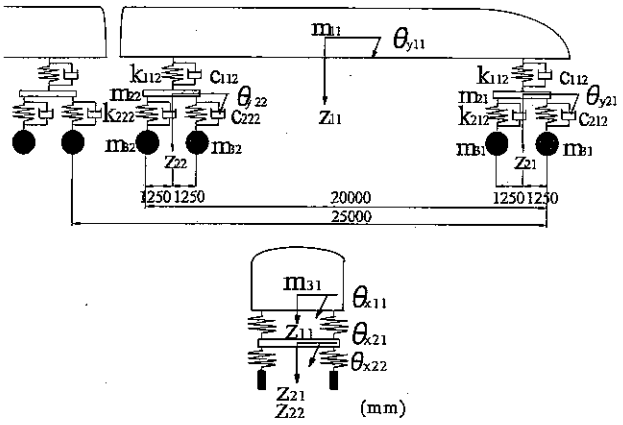

(2) 9-degree-of-freedom system

Fig.5 Train models

Table 3 Dynamic properties of moving trains

(1) 2-degree-of-freedom system

Total mass (t)	m	45.32
Spring constant k (N/m)	k_1,k_2	1.28×10^6
Damping coefficient c (N·s/m)	c_1,c_2	6.96×10^6
Natural frquency (Hz)	f	1.17

(2) 9-degree-of-freedom system

Mass (t)	m_{11}	32.818
	m_{21},m_{22}	2.639
	m_{31},m_{32}	0.9025
Spring constant k (N/m)	k_{11},k_{12}	8.86×10^5
	k_{21},k_{22}	2.42×10^6
Damping coefficient c (N·s/m)	c_{11},c_{12}	4.32×10^4
	c_{21},c_{22}	3.92×10^4
Natural freqency upper (Hz)	f_u	1.07
Natural freqency lower (Hz)	f_l	7.41

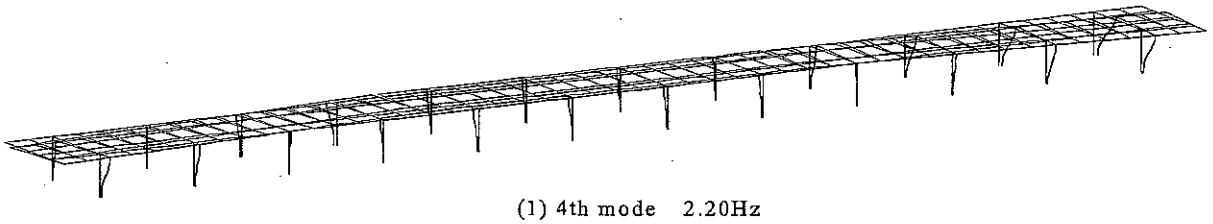

(1) 4th mode 2.20Hz

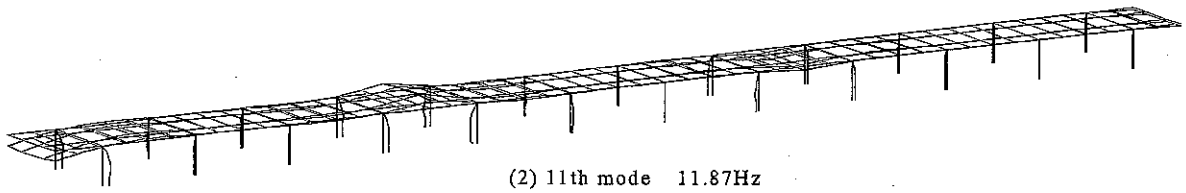

(2) 11th mode 11.87Hz

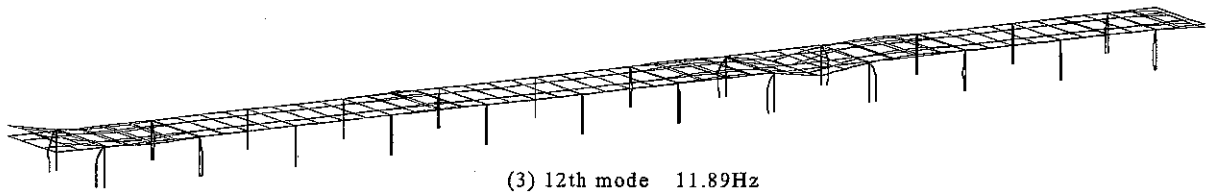

(3) 12th mode 11.89Hz

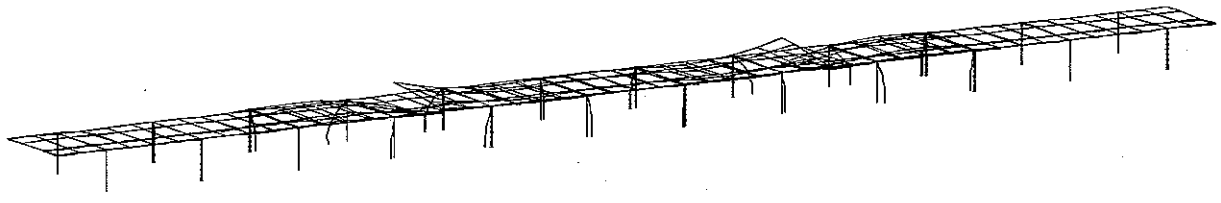

(4) 14th mode 13.90Hz

Fig.6 Natural mode shapes and Natural frequencies of bridge

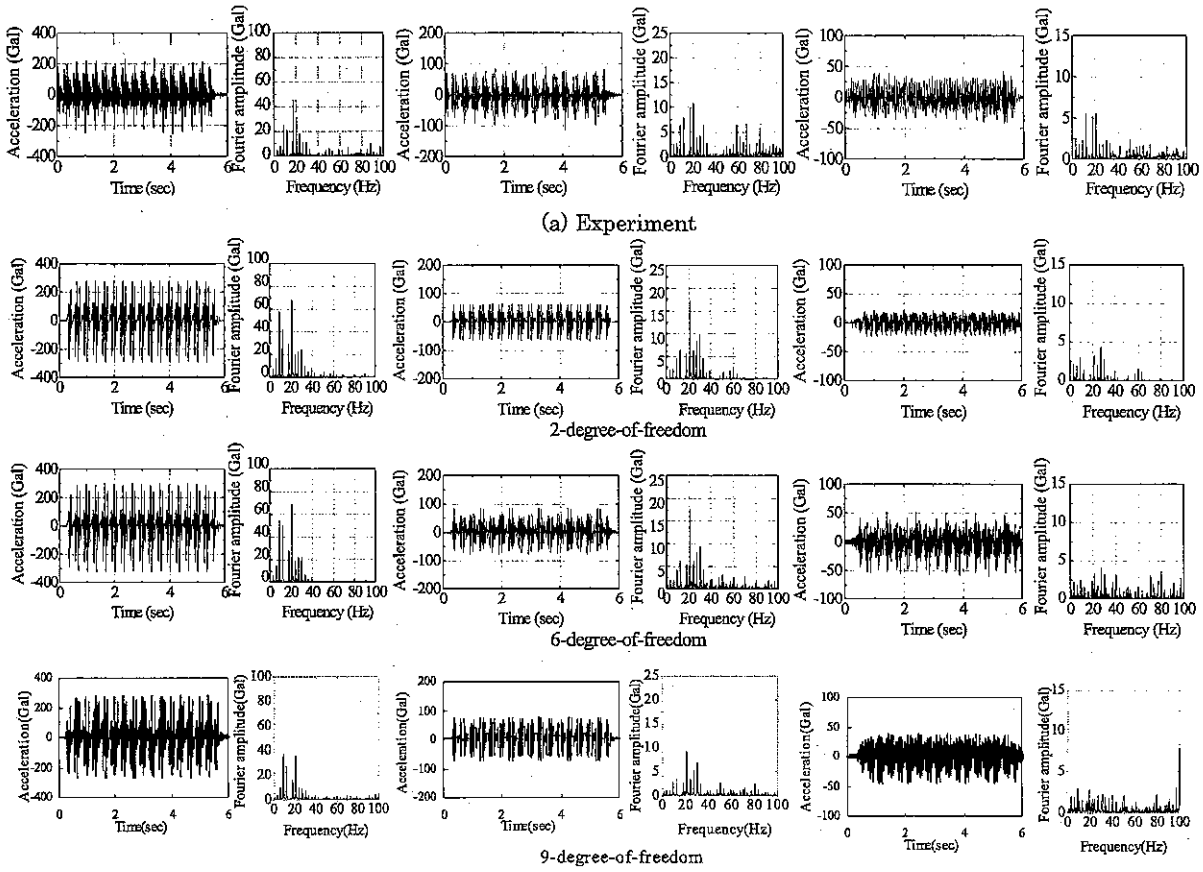

Fig.7 Acceleration of Bridge

Table 4 Maximum acceleration and R.M.S. value of bridge

(9-degree-of-freedom, speed v=270km/h)

	Maximum acceleration (Gal)		R.M.S. value (Gal)	
	Experiment	Analysis	Experiment	Analysis
Point1	239.4	279.4	79.8	106.5
Point2	91.4	78.3	29.0	26.8
Point3	43.1	36.9	14.9	14.8

mass of axles can be obtained by simplifying the three-dimensional model into plane model. The effect of the mass inertia of wheels is not considered in this analysis. The dynamic properties of moving trains are shown in **Table 3**. The velocity of the trains is assumed to be 270km/h.

4. Analytical results

4.1 Natural modes and Natural frequencies of bridge

The eigenvalue analysis of bridge model is performed and the mode shapes are shown in **Fig.6**. The first through the ninth modes indicate the vibration in the horizontal direction of the bridge. The predominant frequency of the horizontal natural mode is observed to be 2.20Hz, showing good agreement with the value of filed test which is 2.19Hz. Therefore, the validation of bridge model can be confirmed. Predominant frequencies of vertical bending natural mode and torsional mode are about 11.9Hz and 13.9Hz, respectively. The highest frequency taken into account in this analysis is assumed to be about 102Hz corresponding to the 277th natural mode. The predominant frequency of the rail mode is lager than 200Hz, but it is considered that the influence of rail can be neglected in the analysis.

4.2 Influence of train models on acceleration response of elevated bridge

The experimental values and analytical ones at the point-1 through point-3 of the elevated bridge indicated in Fig.3, referring to the velocity of 270km/h of the train, are investigated to examine the influence of vehicle models. Herein, point-1, point-2 and point-3 respectively indicate the point of hanging part, the top of the first pier and the top of the third pier of elevated bridge, with respect to the direction that the train runs towards. The experimental values and analytical acceleration responses simultaneously with the Fourier spectra at point-1 through point-3, referring to two-, six-, nine-degree-of-freedom train models, are shown in Fig.7, respectively. The responses at point-1, of which the high-frequency components are observed relatively small, indicate no notable differences according to the train models. Contrastively, the responses at point-2 and point-3, of which the high-frequency components are relatively important, indicate remarkable differences according to the train models. The analytical results of six- and nine-degree-of-freedom train models are relatively coinciding with the experimental values, compared with the results of two-degree-of-freedom train models. Furthermore, the analytical results of nine-degree-of-freedom train model are considered indicating better agreement with experimental values, compared with the results of six-degree-of-freedom train model.

4.3 Estimation of acceleration responses and predominant frequencies of elevated bridge

The acceleration responses and predominant frequencies of elevated bridge are estimated with the analytical results of nine-degree-of-freedom train model, showing good agreement with the experimental values in **Fig.7**, thus the validation of this analytical procedure can be confirmed. The analytical acceleration responses displayed larger amplitudes, and the vibrations are predominant at the lower parts of frequencies, compared with experimental values at point-1 in **Fig.7**. The reasons are considered as that the hanging parts of elevated bridge are connected with neighboring ones by rail and ballast in the actual structures, but only the effects of the rail are taken account of in the analysis. The maximum acceleration responses and R.M.S values corresponding to experiment and analysis are shown in **Table 4**, respectively. Both acceleration and R.M.S values indicate the largest values at point-1 of bridge, the maximum acceleration response at point-2 that is close to the hanging part showed larger value, compared with the values of point-3. The high-frequency components, in the range of about 60Hz to 100Hz, are relatively important in responses of the tops of piers, compared with the response of hanging part.

5. Conclusions

In this study, dynamic response analysis of elevated railway bridges due to bullet trains is carried out and the analytical results are estimated compared with the experimental values. The conclusions are summarized as follows:

(1) The dynamical characteristics of high-speed railway elevated bridge are clarified by carrying out dynamic response analysis with three-dimensional elevated bridge model and nine-degree-of-freedom bullet train model.

(2) In the case that the high-frequency components of vibration are predicted relatively important in a dynamic response analysis of elevated railway bridges due to bullet Trains, the train models will considerably influence the analytical results, and a three-dimensional train model taking account of axle mass will lead to better analytical accuracy compared with plane model.

(3) The predominant vibrations occur at the hanging parts of elevated bridge, and even the point on the top of the pier, which is close to the hanging part, will show larger response compared with the point that is far from the hanging part.

References

1) Seki, M., Inoue, Y. and Naganuma, Y.: Reduction of subgrade vibration and track maintenance for Tokaido Shinkannsen, *WCRR'97*, Vol.E, 1997.
2) Matsuura, A.: A Study of Dynamic Behavior of Bridge Girder for High Speed Railway, Proceedings of the Japan Society of Civil Engineers, No.256, pp.35-47, 1976.12. (In Japanese)
3) Tanabe, M., Wakui, H. and Matsumoto, N.: The finite element analysis of dynamic interactions of high-speed Shinkansen, rail, and bridge, ASME Computers in Engineering, Book No. G0813A, 17/22 (1993)
4) Honda, H., Kobori, T. and Yamada, Y.: Some Considerations on Dynamic Effect of Highway Steel Girder Bridges under Moving Vehicles, Proceedings of JSCE/Japan Society of Civil Engineers, No.350/I-2, pp.359-362, 1984.10. (In Japanese)
5) Kawatani, M. and Nishiyama, S.: Dynamic Response Characteristics of Highway Bridges with Roadway Roughness under Moving Vehicles, Journal of Structural Engineering, Vol.39A, pp.733-740, 1993.3. (In Japanese)
6) Kawatani, M., Yamada, Y. and Dakeshita, Y.: Dynamic Response Analysis of Plate Girder Bridge due to 3-dimensional Vehicle Model, Proceedings of JSCE/Japan Society of Civil Engineers, No.584/I-42, pp.79-86, 1998.1. (In Japanese)
7) Kawatani, M., Kobayashi, Y. and Kawaki, H.: Influence of Elastomeric Bearings on Traffic-Induced Vibration of Highway Bridges, Transportation Research Record, No.1696,

Vol.2, pp.76-82, 2000 (5th International Bridge Engineering Conference, Tampa, USA, April 3-5, 2000).
8) Agabein, M.E.: The Effect of Various Damping Assumptions on the Dynamic Response of Structure, Bulletin of International Institute of Seismology and Earthquake Eng., Vol.8, pp.217-236, 1971.
9) Kobori, T. and Kubo, M.: A Practical Dynamic Analysis Method of Continuous Girder Bridge with Spring Connections on Spring Supports, Proceedings of JSCE/Japan Society of Civil Engineers, No.356/I-3, pp.395-403, 1985.4. (In Japanese)

(Received July 31, 2003)

FE Model Update of Seohae Bridge

Jah-Geol Yoon *, Sung-Pil Chang**, Young-In Baek***

* Ph.D., Technology Research Institute, Daelim Industrial Co. Ltd., 146-12, Susong-dong, Jongno-gu, Seoul, 110-732, Korea
**Professor, School of Civil, Urban & Geo-systems Eng., #38-320, Seoul National University, San56-1, Sillim-dong, Gwanak-gu, Seoul, 151-742, Korea
*** M. of Eng., Technology Research Institute, Daelim Industrial Co. Ltd., 146-12, Susong-dong, Jongno-gu, Seoul, 110-732, Korea

Seohae Bridge, completed in December 2000, is located at the west cost of Korea. The main structure of Seohae Bridge is a three-span cable stayed bridge with a 470m-long main span and two 200m-long side spans. A long-term monitoring system for Seohae Bridge was employed to investigate the structural response of the bridge in order to identify the deterioration rate over a long-term period. To update the finite-element (FE) model built for the bridge maintenance and to identify initial behavior of the bridge, static and dynamic loading tests were performed before opening the bridge to the public. In this paper, procedures and results of the initial loading test and baseline model evaluation of the Seohae Bridge are described.

Key Words: Seohae bridge, cable-stayed bridge, baseline model, model update, Initial loading test

1. Introduction

Seohae Bridge with 7310m total length, is a sea part of Seohaean Highway in Korea.[1)] The main part of Seohae Bridge, completed in December 2000, is a three-span cable-stayed bridge with a main span length of 470m, and side spans of 200m each. It has two concrete pylons and steel composite deck, and its cables are arranged in semi-harp type. Figure 1 shows the cable-stayed bridge.

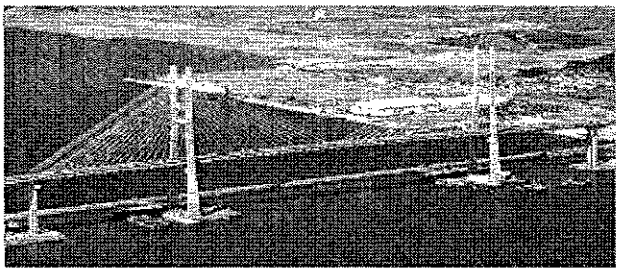

Fig. 1 Aerial photograph of Seohae Bridge

Measured structural responses, such as natural frequencies, mode shapes and displacement, are frequently used to evaluate the current status of bridge structures. Long-term monitoring system of Seohae Bridge was employed to monitor the structural response of the bridge and identify the deterioration rate over a long-term period.[2)] All real time data is transmitted via fiber-optic cables to the operation center located at Hangdam Island. An operation computer accepts data streams, processes the data using the specialized software for the Seohae Bridge and displays the on-line data.

Static and dynamic loading tests were performed before opening the bridge to the public to identify initial behavior of the bridge. The finite-element (FE) model was updated with the measured data, to increase the accuracy of structural analysis. The updated model built for the bridge maintenance will be used for further state evaluation of Seohae Bridge, as a baseline model.

2. Initial FE Model

To evaluate the baseline model for further maintenance, first of all, we developed initial FE model from design documents and updated with the measured data of the initial loading test. An initial FE Model was constructed with 850 nodes and 1421 elements. Figure 2 shows the modeling in which the steel composite deck of

Seohae Bridge was modeled in 3 parallel beam lanes and stringers.

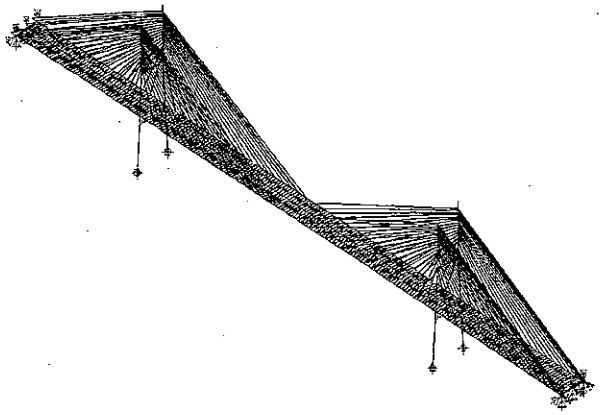

Fig. 2 FE Model of Seohae Bridge

3. Static Loading Test

Six loading trucks with 33.0-ton weight were used for static loading tests, and three different loading cases were applied. Displacements of girders and pylons were measured for each loading case using survey instruments as well as sensors of monitoring system. Table 1 explains the static loading. Geometry survey without loading was performed two times to reduce survey error and evaluate the error level. To avoid radiation heat effecting on structural deformation, all measurements were performed at dawn. Maximum displacement of the girder was around 135mm downward by level survey and 128.1mm by laser sensor, for 1/2 section loading of mid span.

Table 1 Static loading schedule

Load case	Load location	Weight	Date
LC0-a		Without load	2000.10.17
LC1	L/2 section of center span	32.99 ton truck 6 ea.	2000.10.18
LC2	L/4 section of center span	32.99 ton truck 6 ea.	2000.10.20
LC3	L/2 section of side span	32.99 ton truck 6 ea.	2000.10.19
LC0-b		Without load	2000.10.21

The deflections of the bridge under the test truck loading were computed using the initial model before update. Table 2 and Figure 3 show the measured deformations and the calculated respectively. While the correlation is not ideal in LC3, it is very satisfactory on the whole.

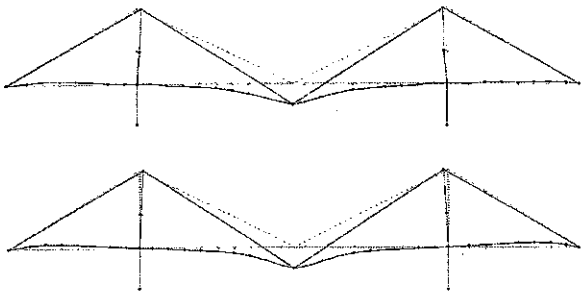

Fig. 3 Comparison between measured (up) and calculated (down) deformation shape of static load case LC1

Table 2 Static deformation of major location

Load case	Loading location on deck	
	Measured	Calculated
LC1	135 mm	131.1 mm
LC2	54 mm	59.6 mm
LC3	46 mm	62.2 mm

4. Dynamic Loading Test

For the measurement of dynamic response of the bridge, Seohae Bridge monitoring system was used, and no additional instruments were installed. Two kinds of dynamic loading, a test truck passing on 2000.10.18 and public traffic on 2000.12.1, were applied for the test and there was no significant difference between the data. Firstly, natural frequencies were evaluated from the acceleration data under the test truck passing. Secondly, polynomial curve fitting technique was applied to the averaged magnitude spectrum, and exact natural frequencies were obtained as the result. Figure 4 shows the averaged magnitude spectrum of vertical direction.

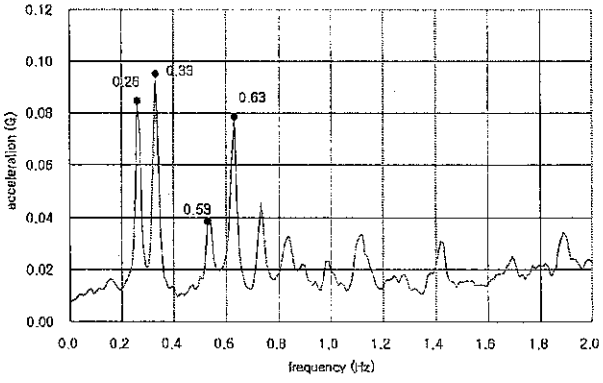

Fig. 4 Averaged magnitude spectrum of vertical direction

Finally, natural frequencies and mode shapes of first 4 vertical bending modes and 1 lateral bending mode were identified. Table 3 shows the results of measured natural frequencies. Measured fundamental frequency, 0.262Hz, was found to be the symmetric vertical bending mode's. Considerable differences between measured and calculated frequencies were found and had to be minimized during the next step in updating the model, which will be described in the next section.

Table 3 Natural frequencies of the bridge

Calculated	Measured	Error %	Description
0.244 Hz	0.262 Hz	6.9 %	1st vertical bending
0.307 Hz	0.331 Hz	7.3 %	2nd vertical bending
0.345 Hz	0.362 Hz	4.7 %	1st lateral bending
0.525 Hz	0.534 Hz	1.7 %	3rd vertical bending
0.597 Hz	0.629 Hz	5.1 %	5th vertical bending

5. Formulation for BC evaluation

Figure 5 shows the modeling method of simple cable stayed bridge with rotational boundary condition (BC). Because rotational masses are neglected, the model is a single degree of freedom (SDOF) system rather than a three degrees of freedom (DOF) system. Therefore, it calculates single modal frequency.

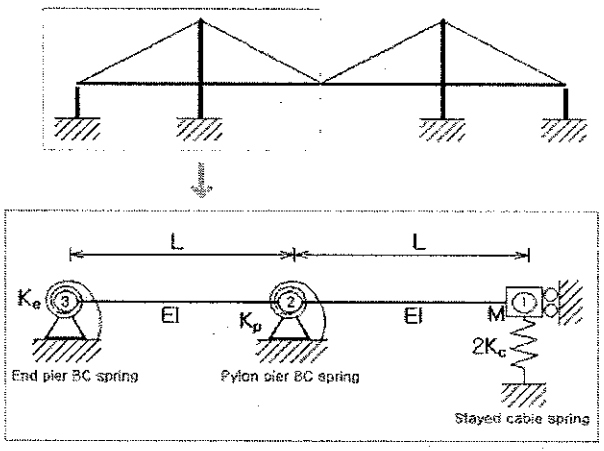

Fig. 5 Modeling of simple cable stayed bridge

If one of BC springs of the model has been neglected, the solution is simple. Eq. (1a) and (1b) show the theoretical solution of Eigen values, which neglects pylon BC spring and end BC spring, respectively.

$$\lambda_e = \frac{1}{M}\frac{192\frac{E^3I^3}{L^3}+56\frac{E^2I^2}{L^2}K_cL^2+60\frac{E^2I^2}{L^2}K_e+16\frac{EI}{L}K_cK_eL^2}{28\frac{E^3I^3}{L^3}L^2+8\frac{E^2I^2}{L^2}L^2K_e} \quad \text{(1a)}$$

$$\lambda_e = \frac{1}{M}\frac{192\frac{E^3I^3}{L^3}+56\frac{E^2I^2}{L^2}K_cL^2+48\frac{E^2I^2}{L^2}K_p+8\frac{EI}{L}K_cK_pL^2}{28\frac{E^3I^3}{L^3}L^2+8\frac{E^2I^2}{L^2}L^2K_p} \quad \text{(1b)}$$

Eq. (1a) and (1b) can be rewritten as Eq. (2a) and (2b) respectively.

$$\lambda_e = \frac{2K_c}{M\frac{EI}{L}}+\frac{1}{ML^2}\left(6.8571-0.6429\frac{8K_e}{28\frac{EI}{L}+8K_e}\right) \quad \text{(2a)}$$

$$\lambda_p = \frac{2K_c}{M\frac{EI}{L}}+\frac{1}{ML^2}\left(6.8571-0.6429\frac{8\times 4K_p}{28\frac{EI}{L}+4K_p}\right) \quad \text{(2b)}$$

Eq. (2a) and (2b) can be simplified to Eq. (3a) or (3b), which represent the natural frequency as a function of BC spring stiffness. It is a kind of sigmoid function, as shown in Figure 6. Using curve fitting technique, coefficient *A*, *B* and *C* of Equation (3a) or (3b), can be determined with theoretical modal analysis result set of Seohae Bridge, and this new method for BC estimation of cable stayed bridge is named as 'SDOF method'.

$$\lambda(K) = A + B\frac{K}{C^* + K} \quad \text{(3a)}$$

$$\lambda(K) = A + B\frac{K}{10^C + K} \quad \text{(3b)}$$

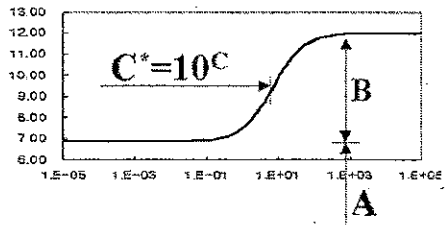

Fig. 6 Explanation of sigmoid function coefficients

6. Update Result of Seohae Bridge

Applying curve-fitting technique to Eq. (3b), Eq. (4) was evaluated from full model of Seohae Bridge. Eq. (4) shows the fundamental frequency as a function of BC spring stiffness of Seohae Bridge. Eq. (5) means measured fundamental frequency of the bridge.

$$\lambda(K_p, K_e) = 0.05991 + 0.0105\frac{K_e}{10^{5.8141}+K_e} + 0.0020\frac{K_p}{10^{56.2294}+K_p} \quad \text{(4)}$$

$$\lambda(K_p, K_e) = 0.262^2 \quad \text{(5)}$$

Eq. (6) can be derived from Eq. (4) and Eq. (5), and represents the relation between the end pier BC spring stiffness and the pylon pier BC spring stiffness. Figure 7 plots Eq. (6) and explains that the end pier BC spring stiffness is dominant over that of pylon pier.

$$K_e = \frac{1.42193\times10^{13} + 6.46454\times10^{6}\cdot K_p}{4.41118\times10^{6} + 5.54683\cdot K_p} \quad (6)$$

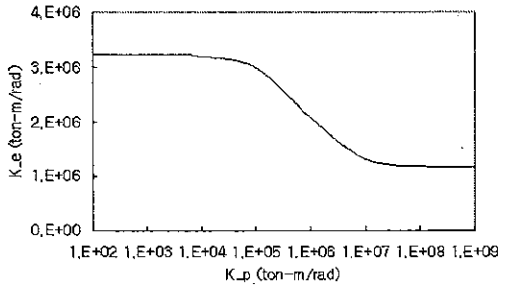

Fig. 7 Relation between end pier BC spring constant and it of pylon of Seohae Bridge

If there is an assumption that the values of end pier BC spring stiffness and pylon pier BC spring stiffness are the same, Eq. (4) can be more simplified as Eq. (7). BC spring constant can be evaluated between Eq. (7) and Eq. (5).

$$\lambda(K) = 0.05991 + 0.0105\frac{K}{10^{5.8141}+K} + 0.0020\frac{K}{10^{56.2294}+K} \quad (7)$$

Table 4 shows the result of comparison between the SDOF method, which is newly developed in this research and traditional sensitivity method, a kind of inverse analysis for system identification. Some differences were found between two methods, but they are considerably satisfactory.

Table 4 Result comparison between SDOF method and Sensitivity method

	SDOF method	Sensitivity method
Rotational spring constant of support	4.32E6 ton-m/rad	4.76E6 ton-m/rad
Vertical bending stiffness coefficient of deck	110.2 %	108.9 %
Lateral bending stiffness coefficient of deck	130.9 %	130.9 %

Table 5 compares the modal analysis result of baseline model and the measured frequencies. The updated result was satisfactory and average error of first 5 natural frequencies was reduced to 0.6 % while that of the initial model was calculated as 5.1 % as seen in Table 3.

Table 5 Update results of Seohae Bridge

	ID	Baseline model	Initial loading 2000.Oct	Long-term monitoring 2001.Dec
Natural freq.	V1	0.263 Hz	0.262 Hz	0.26 Hz
	V2	0.329 Hz	0.331 Hz	0.33 Hz
	L1	0.362 Hz	0.362 Hz	0.37 Hz
	V3	0.542 Hz	0.534 Hz	0.53 Hz
	V5	0.625 Hz	0.629 Hz	0.62 Hz
Static disp.	LC1	123.5 mm	128.1 mm	-

7. Long-Term Monitoring

Table 5 also shows another natural frequency data measured 14 months later by the long-term monitoring system as mentioned above. The natural frequencies can represents the any changes of the dynamic system of the bridge and it is one of major measuring item having been monitored up to now. It can be concluded that there is no significant frequency change during the period from October 2000 to December 2001.

8. Conclusion

Baseline model of Seohae Bridge has been developed using measured responses of initial loading test. During the model update procedure, rotational spring elements were adopted to replicate support boundary conditions, and the SDOF method was introduced to estimate support rotational spring constant of cable stayed bridge. The updated result using the new method was satisfactory and it can be said that the SDOF method is better than the traditional method, because it is based on the analytical solution and does not require iteration.

References

1) Chan-Min PARK and Woo-Jong KIM, Design of the Cable-Stayed Bridge in SeoHae Bridge, *IABSE Conference Seoul 2001: Cable Supported Bridges-Challenging Technical Limits*, IABSE Report Vol.84, pp. 28-29, Seoul, 2001

2) Sung Kon KIM, Intelligent Bridge Maintenance System Development for Seo-Hae Grand Bridge, *IABSE Conference Seoul 2001: Cable Supported Bridges-Challenging Technical Limits*, IABSE Report Vol.84, pp. 34-35, Seoul, 2001

(Received July 31, 2003)

End-Cross Beam Reinforcement as a Countermeasure against Traffic-Induced Vibration of Six-Span Continuous Steel Two-Girder Bridge

Chul-Woo Kim*, Mitsuo Kawatani** and Naoki Kawada***

* Ph.D., Dept. of Civil Eng., Kobe University, Rokkodai, Nada, Kobe 657-8501, Japan
** Dr. of Eng., Professor, Dept. of Civil Eng., Kobe University, Rokkodai, Nada, Kobe 657-8501, Japan
*** Asia Civil Eng., Co. LTD., Kyoto 600-8133, Japan

Dynamic response analyses of a six-span continuous steel two-girder bridge with reinforced end-cross beam under moving vehicles are carried out to investigate reduction effects on traffic-induced vibration of the bridge according to the reinforcement, since the simplified structural system and the wide girder spacing can make the bridge more sensitive to the vibration. Analytical results demonstrate that bumps near an expansion joint cause high-frequency vibrations at end-cross beams and deck slabs near the expansion joint. It is observed that the end-cross beam reinforcement functions as restraining the powers of vibrations at frequency range over 10Hz. It is evident that reinforcing of the end-cross beam up to brackets of cantilevered parts will guarantee reduction of undesirable high-frequency vibrations at the members of the cantilevered parts of twin-girder bridges due to heavy vehicles.

Key Words: End-cross beam reinforcement; six-span continuous two-girder bridge; traffic-induced vibration; 3-D dynamic analysis

1. Introduction

Bridges equipped twin-girder system have been adopted as one of the most common structural types for bridges with span length around 50m because of advantages they offer with regards to fabrication, erection, etc. On the other hand, the wider girder spacing and more simplified structural system of two-girder bridges than conventional multi-girder bridges can give rise to changing the dynamic characteristics of the bridge, and can make the bridge to be easily vibrated by external dynamic loads like wind, moving vehicles, etc.

The bump near an expansion joint is another important factor that causes excessive impulsive dynamic wheel loads with the high-frequency characteristics. The impulsive dynamic wheel load will give severe effects on members especially located near bumps, since the impulsive energy of a vehicle can be dissipated within a short period because of large damping of the vehicle [1]. The impulsive wheel load at the expansion joint can also be a source to cause undesirable noises and vibrations, and, what is worse, the impulsive wheel load tends to travel farther from the expansion joint according to the vehicle speed [1]. The undesirable vibrations occurred at the members near expansion joints of steel bridges will influence to nearby grounds and buildings through supports and piers [2], and also give rise to complaints related to the infra-sound [3]. The undesirable vibration, so called an environmental vibration, has been one of major technical problems because of its high possession rates of viaducts in land scarce major cities. It has also been reported that the frequency range of the undesirable vibration on human reception is located over 50Hz [4].

A number of studies on reinforcing end parts of steel bridges have been performed to prevent the undesirable vibration and enhance the resistance of expansion joints and decks near expansion joints. Chubb and Kennedy [5] observed reduction effects on dynamic responses after stiffening end-sway bracings of an existing steel bridge from field-test. Yamada and Kawatani [6] investigated the effect of girder-end reinforcement on reducing traffic-induced vibrations of a conventional multi-girder steel bridge by the dynamic response analysis, and mainly focused on the reduction effect on dynamic responses of

main girders and end-sway bracings. It also have been reported that the end-cross beam reinforcement can extend life cycle of decks and expansion joints of steel girder bridges [7]. Nanjo et al. [7] also suggested the possibility that suppress the traffic-induced vibration. However, few investigations focused on the vibration reduction of steel two-girder bridges with continuous span due to the end-cross beam reinforcement have been reported.

In order to enhance our understanding in effects of the end-cross beam reinforcement on traffic-induced vibration of continuous span steel two-girder bridges, analytical investigations for a six-continuous steel two-girder bridge equipped reinforced end-cross beam in designing stage are carried out in this study.

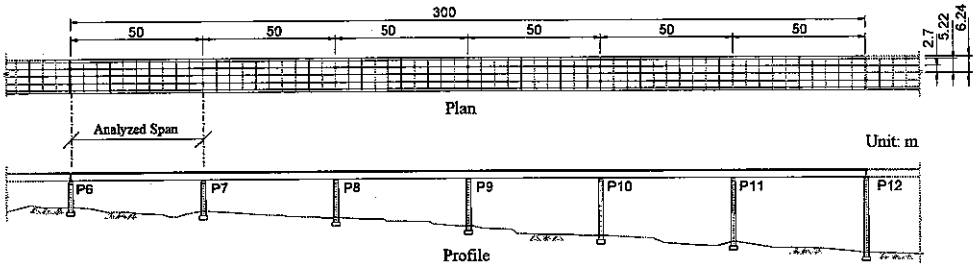

(a) General view of bridge

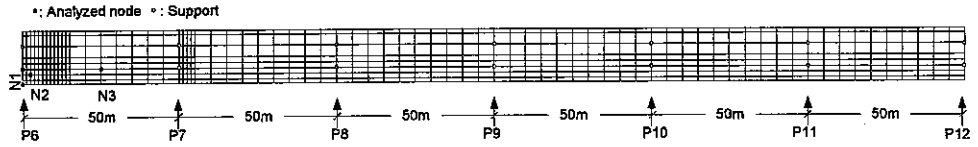

(b) FE model

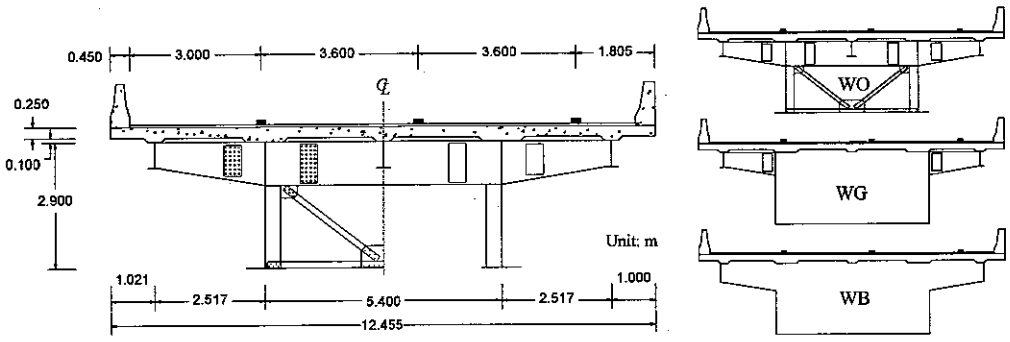

(c) Typical cross section (d) Reinforcing patterns

Fig. 1 Bridge and reinforcing patterns

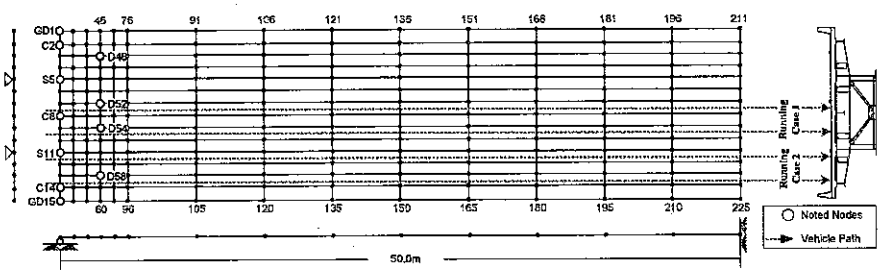

Fig. 2 Simplified FE model of two-girder bridge with single span

2. Analytical Model

2.1 Bridge model

The bridge model has total span of 300m (50m@6=300m) with 5.4m girder-spacing, and the width of the bridge is 12.5m wide. It adopts wide cantilevered decks (about 3.5m) supported by brackets. The bridge has the stringer to restrain the large deflection of the RC deck.

The general layout, FE model of the bridge, typical cross section and devised end-cross beam reinforcing patterns are shown in **Fig. 1**. The nodes N1 to N3 are the points of comparing the acceleration response with that of the bridge model simplified as a single span model.

The end-cross beam as well as the cross beam at each support are assumed to be reinforced by a RC block with thickness of 50cm. The symbols WO, WG and WB in **Fig. 1d)** indicate the reinforcing patterns; 1) WO indicates the section without any reinforcement; 2) WG is the section with reinforcing between two girders; 3) WB is the section with reinforcing up to the brackets. The RC block at the cross beam is assumed to completely link with decks.

Finite element (FE) method and modal analysis are taken as tools for analyzing the bridge. A lumped mass system and Rayleigh damping are adopted to form mass and damping matrices of the bridge model, respectively. The damping constant of the bridge is assumed as 2 % for the first mode and the second one.

One of six continuous spans idealized as a bridge model with one end roller supported and other end fixed is shown in **Fig. 2**. The simplified FE model for the bridge appeared in **Fig. 2** consists of 225 nodes, 196 plate elements and 158 beam elements. The symbols GD1, C2, C8, C14, GD15, D48, D52, D54 and D58 in **Fig. 2** indicate the noted nodes for dynamic response analysis. The GD, C and D in **Fig. 2** denote the guard-rail, the cross beam and the deck slab, respectively. The numbers following the symbols coincide with the node number of the FE model. Running case 1 and running case 2 indicate, respectively, the vehicle paths on the central lane and the low speed lane considered in the analysis.

2.2 Vehicle model

A three-axle dump truck with gross weight of 191kN idealized as experimentally calibrated 8DOF model [8] is adopted as a heavy vehicle running on the bridge. Detailed properties of the vehicle are shown in **Table 1**. Fundamental frequencies of the vehicle for the bouncing and the axle-hop are 3.0 Hz and 17.9 Hz, respectively.

Table 1 Properties of vehicle model

Geometry (*m*)	Tread	1.80
	Distance between front and rear axle	3.99
	Distance of tandem axle	1.20
	Distance between front axle and C.G.*	2.99
Weight (*kN*)	Sprung mass including payload	171.20
	Steer axle unsprung mass	4.90
	Drive axle unsprung mass	14.70
Spring constant (*kN/m*)	Front leaf spring	1,577.00
	Rear leaf spring	4,724.00
	Front tire	3,146.00
	Rear tire	4,724.00
Damping coefficient (*kN·s/m*)	Front left suspension	4.60
	Front right suspension	4.60
	Rear left suspension	13.72
	Rear right suspension	13.72
	Front tire	9.11
	Rear tire	27.34

*C.G.: Centre of Gravity

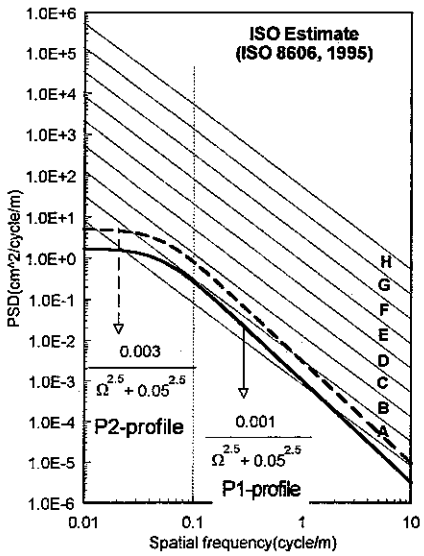

Fig. 3 PSD Curves of roadway roughness

2.3 Roadway roughness

Roadway surface profiles used in the dynamic response analysis are generated by Monte-Carlo simulation (MCS) method based on power spectral density (PSD) functions [9], and the PSD curve and the ISO estimate [10] are shown in **Fig. 3**. In generating roadway profiles by using MCS method, the parameters in the PSD function are assumed as $\alpha=0.001$, $\beta=0.05$ and $n=2.5$ for the P1 profile based on the measured data at viaducts of Hanshin expressway in Japan, and $\alpha=0.003$,

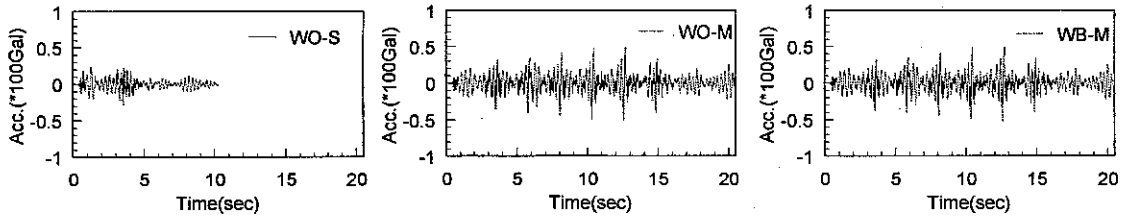

(a) acceleration at the span center of the 2nd span

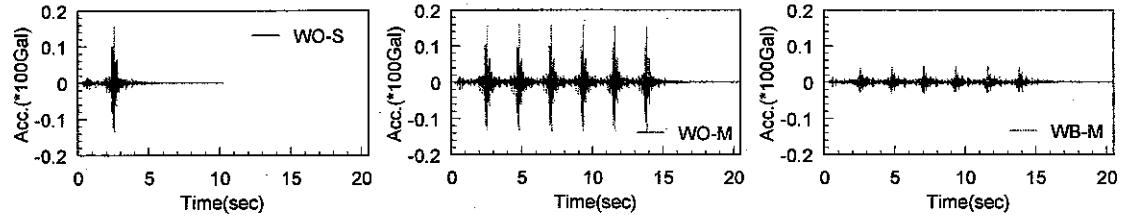

(b) acceleration at the deck near pier P7

Fig. 4 Acceleration responses of two-girder bridge

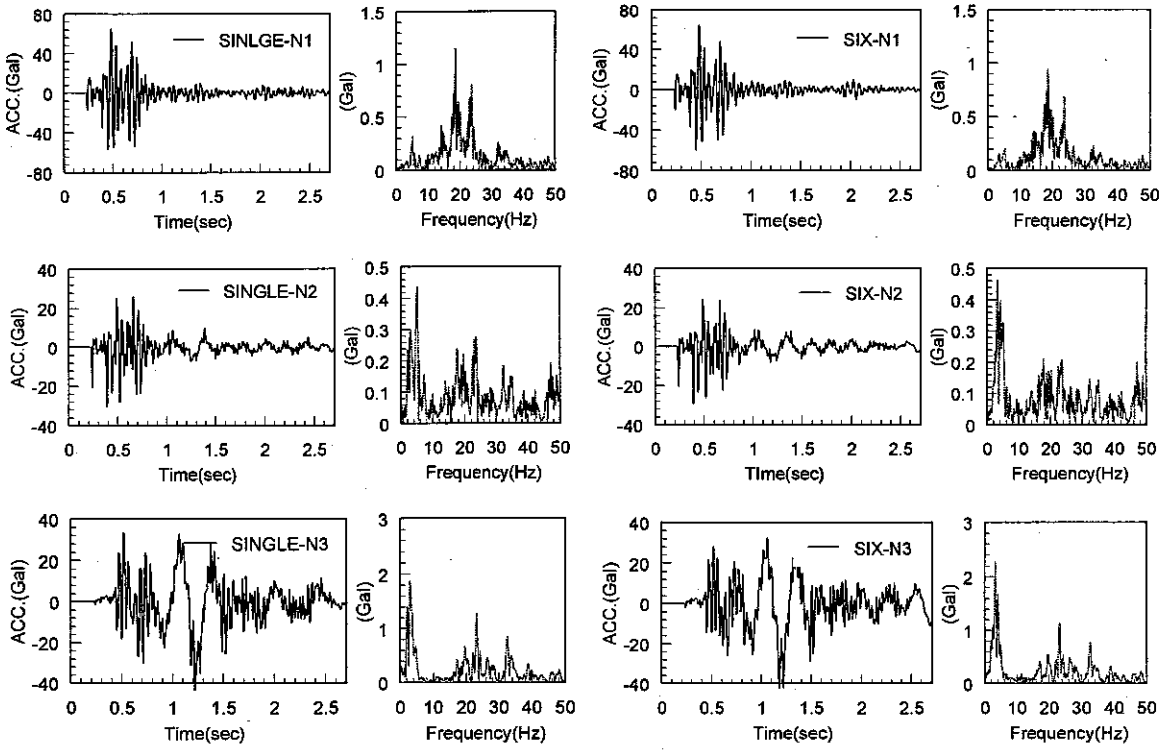

(a) Single span bridge model (b) Six-continuous span bridge model

Fig. 5 Acceleration responses and Fourier spectra of two-girder bridge: v=80km/hr

β=0.05 and n=2.5 for the P2 profile are used to represent rough roadway compared with the P1-profile. The bump at the expansion joint is idealized as a half sine curve with 20mm height and 600mm width. In analysis, one sample profile of MCS of a given roadway condition is used just to compare the relative vibration reduction effect according to the reinforcement, although a statistical analysis is necessary.

3. Preliminary Analysis

A preliminary investigation is carried out using the FE model shown in **Fig. 1**, under conditions of vehicle speed of 80km/hr, running case 2, a single vehicle running and a series of vehicles running with a critical headway of 50.22m estimated based on the fundamental torsional mode of the bridge (1.77Hz) using the relation as shown in Eq. (1).

$$L_{cr} = n \cdot T_i \cdot v \qquad (1)$$

where, L_{cr} indicates critical headway(m); T_i, i_{th} natural period of bridge(sec); v, vehicle speed(m/sec); n, an integer number.

Typical acceleration responses at the span center of the second span (the span between Pier P7 and Pier P8) and at the deck near the reinforced cross beam on P7 pier are shown in **Fig. 4**. The symbols -S and -M indicate the results under the condition of the single vehicle running and multi vehicles running, respectively. It shows that it is difficult to reduce the acceleration response of the girder by the end-cross beam reinforcement, and the dynamic responses of the girder are more easily affected by a series of vehicles running with the critical headway. On the other hand, the acceleration response at the deck near the reinforced cross-beam is dramatically reduced due to reinforcing cross-beam. The acceleration amplitude of the deck remains constant regardless of the vehicle numbers. It means the end-cross beam reinforcement is effective on reducing dynamic responses of the local member. Moreover it encourages the use of single vehicle running model in investigating the dynamics of local members, even in the case of the continuous span bridge.

Acceleration responses and Fourier spectra of the simplified single span model are compared with those responses of the six-continuous model, to verify the validity of the single span model. The vehicle speed is assumed to be 80km/hr, and the vehicle path follows the running case 2.

The acceleration responses and their Fourier spectra between the two models show good agreement as shown in **Fig. 5**. Thus, the effect of the end-cross beam reinforcement can be determined by using the single span model.

Therefore, in this study, the effect of the end-cross beam reinforcement on traffic-induced vibration of the six-span continuous steel two-girder bridge is investigated using the simplified model under the condition of single vehicle running.

4. Analytical Results

In the traffic-induced dynamic response analysis of the single span bridge model, vertical accelerations are estimated by superposing up to the 100th mode (165.03 Hz for the model WO, 173 Hz for the model WG and 174 Hz for the model WB), since the dynamic responses at the deck slab and the end-cross beam are sufficiently converged within the 100th mode from the preliminary analysis. In the analysis, vehicle speeds are adopted as 40km/hr and 60km/hr and assumed to be constant.

4.1 Vertical acceleration responses

Vertical accelerations at D58 node located on the bracket of the bridge according to the running case are shown in **Fig. 6**. It is

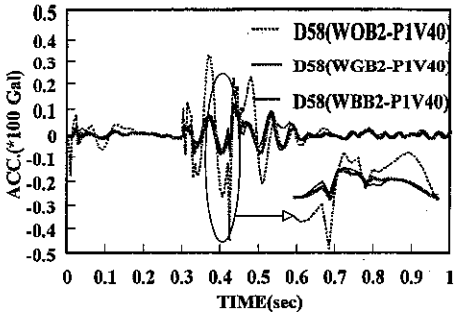

(a) Running case 1

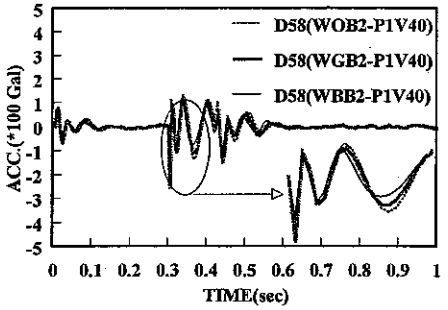

(b) Running case 2

Fig. 6 Acceleration responses at D58 node; *v=40 km/hr*, very good roadway and bump=2cm

noteworthy that the vertical scale of the **Fig. 6(b)** is 10 times larger than that of **Fig. 6(a)**. The symbol B2 means that the bump height of 2 cm at the expansion joint is considered in the analysis. The letter P1 indicates the roadway surface profile P1 (see **Fig. 3**), and V40 denotes the vehicle speed 40km/hr.

Figure 6(a) demonstrates that both reinforcing patterns WG and WB act on reducing the peak acceleration at the end-cross beam and decks near a bump due to the vehicle running on the central lane (Running case 1). When the vehicle is running on the slow speed lane (Running case 2, see **Fig. 6(b)**), however, it is observed that it is difficult to reduce the peak acceleration response of the nodes located on the bracket of the bridge by the reinforcing pattern WG. On the other hand, the reinforcing pattern WB acts on reducing peak vertical accelerations of the nodes on the bracket, although the reducing effect is weaker than the case of vehicle running on the central lane.

How the bump affects the dynamic characteristics of members located near the bump of an expansion joint is shown in **Fig. 7**. B0 in **Fig. 7** indicates that no bump at the expansion joint is considered in the analysis.

Natural modes of the bridge corresponding to the dominant frequencies appeared in **Fig. 7** are shown in **Fig. 8** with natural frequencies. It is observed that the power spectrum above 9Hz tends to increase due to the impulsive dynamic wheel load of vehicles generated during running on bumps, from the **Fig. 7**.

The dominant frequencies near 3.7Hz (**Fig. 7(b)**) and 18Hz (**Fig. 7(a)**), which cannot be found in natural frequencies of the bridge, are considered to depend on the effect of vehicle's

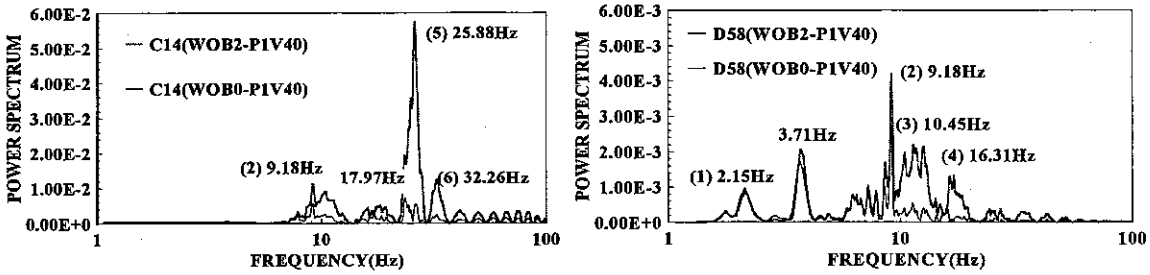

a) End-cross beam b) Deck slab

Fig. 7 PSD Curves of acceleration at C14 and D58 nodes; Running case 2, *v=40 km/hr* and Very good roadway

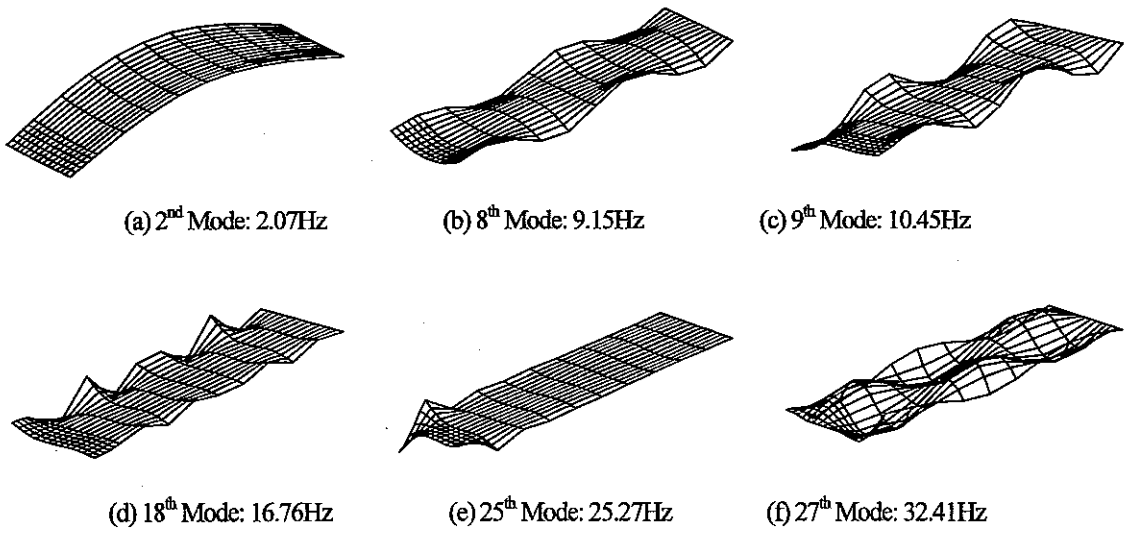

(a) 2nd Mode: 2.07Hz (b) 8th Mode: 9.15Hz (c) 9th Mode: 10.45Hz

(d) 18th Mode: 16.76Hz (e) 25th Mode: 25.27Hz (f) 27th Mode: 32.41Hz

Fig. 8 Mode shapes corresponding to dominant frequencies in **Fig. 7**

bouncing (3.0Hz) and axle-hop motion (17.9Hz), respectively. It demonstrates that the 8th(9.15Hz), 9th(10.45Hz), 18th(16.76Hz), 25th (25.27Hz) and 27th (32.41Hz) modes shown in **Fig. 8**, which are in relation with modes of cross beams and decks near the end-cross beam, are the modes corresponding to the dominant frequencies appeared in **Fig. 7**.

It is thus possible to conclude that dominant frequencies of the end-cross beam and the deck near bumps have tendency to transfer to higher frequency regions due to the impulsive dynamic wheel load generated by a vehicle running over bumps.

The vibration acceleration level (VAL) taken from the 1/3 octave band spectral analysis at the noted nodes with respect to the reinforcing patterns are shown in **Fig. 9**. The vertical and horizontal scales in the figures indicate VAL (dB) and central frequency (Hz), respectively. It represents that both reinforcing patterns WG and WB give similar reduction effect under the condition of running case1. The reducing effect can be expected covering most of the frequency range; 4Hz ~ 100Hz for the deck slab. On the other hand, when vehicle is running on the low speed lane (running case 2), the vibration reduction cannot be observed by the reinforcing pattern WG but by the pattern WB.

From the 1/3 octave spectral analysis, it is observed that the reinforcing the end-cross beam can suppress high-frequency vibrations.

4.2 Assessment of reduction effects

To investigate the vibration reduction effect with respect to the end-cross beam reinforcing patterns quantitatively, a vibration reduction level (Eq. (2)) of the acceleration responses is defined.

$$VRL(dB) = -20\log_{10}(A_{WR} / A_{WO}) \qquad (2)$$

where, A_{WR} is the root mean square (RMS) values of dynamic responses due to reinforcing end-cross beam; A_{WO}, the RMS values of dynamic responses due to without any reinforcement; *VRL*, the vibration reduction level in deci-Bel (*dB*).

Figure 10 shows the summarized results of the VRL under the condition of running case1 according to reinforcing patterns. For C8 node located under the vehicle path, the VRL reaches to about 12dB and 13dB according to reinforcing pattern WG and

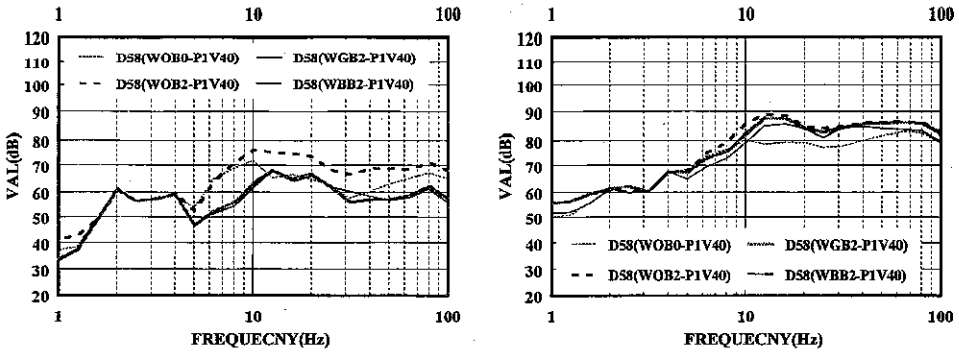

(a) Running case 1 (b) Running case 2

Fig. 9 1/3 octave spectra of node58 at bracket

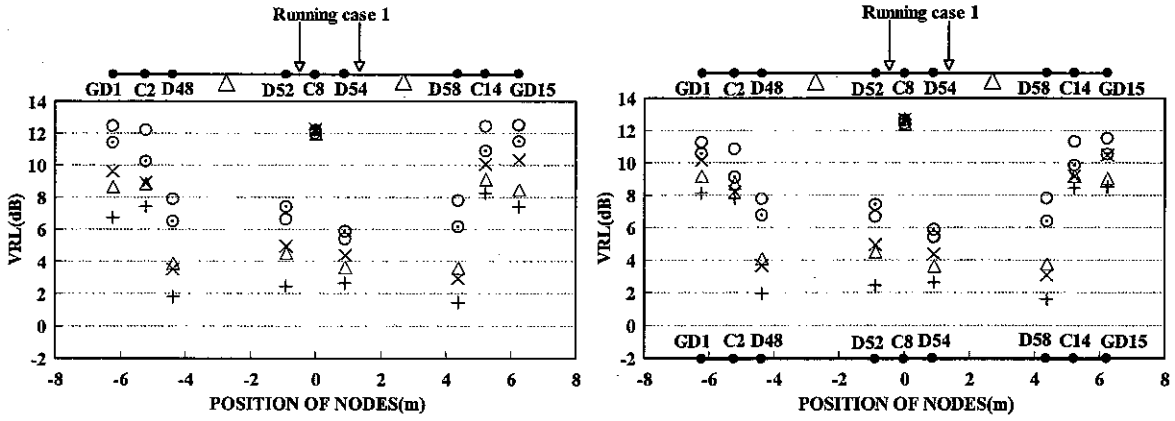

(a) Reinforcing pattern WG (b) Reinforcing pattern WB

Fig. 10 Vibration reduction level at noted nodes; Running case 1

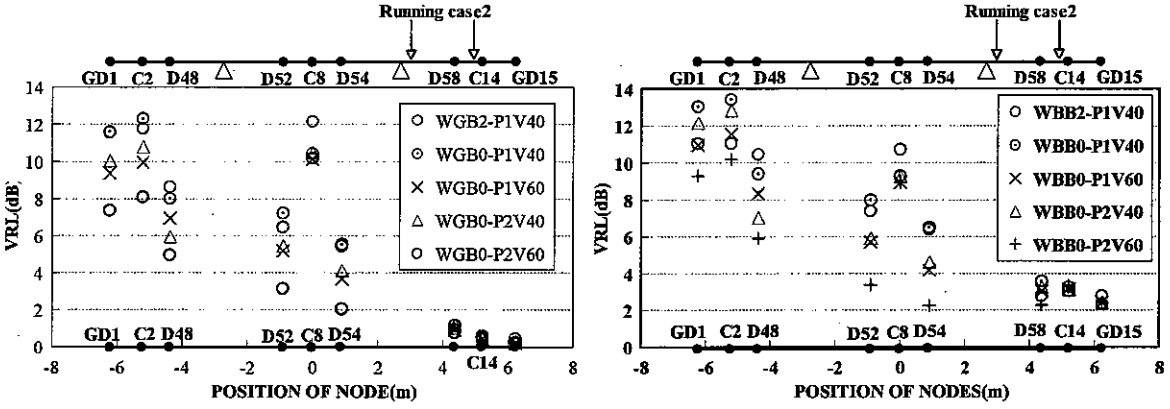

(a) Reinforcing pattern WG (b) Reinforcing pattern WB

Fig. 11 Vibration reduction level at noted nodes; Running case 2

WB, respectively.

The summarized result for running case 2 is shown in **Fig. 11**, and it shows the VRL of nodes under the vehicle path reach to 3dB according to the reinforcing pattern WB, on the other hand, those vibration reduction effects are located near 1.5dB by the reinforcing pattern WG.

For nodes under the vehicle path, the vibration reduction effect at each running case keeps constant level regardless of the vehicle speed and the roadway roughness condition. The results thus represent, when a vehicle is running on the central lane (Running case 1), both reinforcing patterns WG and WB give similar reduction effect for the nodes under the vehicle path. On

the other hand, more reliable reduction effect can be expected by reinforcing pattern WB than by reinforcing pattern WG, when vehicle is running on the low speed lane. For the members experiencing peak vibration under vehicle paths, constant vibration reduction effects can be expected regardless of the parameters by the end-cross beam reinforcement.

5. Conclusions

The end-cross beam reinforcement is adopted as a countermeasure against the traffic-induced high-frequency vibration in this study. This study shows that the simplified single span model under the condition of a single vehicle running can give good results in determining the end-cross beam reinforcing effect of the local members, even though the bridge consist of six continuous spans. This study also shows that bumps near expansion joints play an important role to magnify the power spectrum at the high-frequency region. The 1/3 octave spectral analysis demonstrates that the reinforcing end-cross beam can suppress high frequencies that has been reported as a major vibration source of complaints, thus the reinforcing method will guarantee reduction of undesirable high-frequency vibration. For steel twin-girder bridges with wide decks and brackets, the reinforcing up to the bracket gives effective vibration reduction.

References

1) Kawatani, M. and Kim, C.W., Effects of gap at expansion joint on traffic-induced vibration of highway bridge, Proc. Int. Conference on Developments in Short and Medium Span Bridge Engineering '98, Calgary, Canada, CD-ROM, 1998.
2) Fukada, S., Kajikawa, Y., Hayashi, H., Yoshikawa, M. and Sanuki, Y., Vibration characteristics of highway bridge with isolators and jointless system under moving vehicles, Proc. Int. Conference on Developments in Short and Medium Span Bridge Engineering '98, Calgary, Canada, CD-ROM, 1998.
3) Fukasawa, Y., Sugiyama, K., Nakahara, K. and Mizukami, H., Fundamental characteristics of low frequency sound radiated from highway bridges under the passage of heavy vehicles, J. of Structural Eng., JSCE, 37A, pp.945-956, 1991. *(in Japanese)*
4) Sanuki, Y., Kajikawa,Y., Shinkai, M. and Iwatsu, M., Estimation of the validity of jointless method as vibration proof construction, Proc. of 2nd Colloquium on Vibration Control of Structures, JSCE, Part B, pp.151-158, 1993. (*in Japanese*)
5) Chubb, M. S. and Kennedy Reid, I. L., Crossbeam replacement, Bridge Modification, Thomas Telford, London, pp.241-254, 1995.
6) Yamada, Y. and Kawatani, M., Analytical study on reduction of traffic-induced vibration due to reinforcement procedure at girder end, J. of Structural Eng., JSCE, 43A, pp.737-746, 1997. *(in Japanese)*
7) Nanjo, A., Mori, Y., Sasaki, K., Sonoda, K. and Kiso, S., Experimental study on RC end cross beams for the seismic resistance of a steel plate girder bridge, J. of Construction Steel, JSSC, 8, pp.179-186, 2000. (*in Japanese*)
8) Kawatani, M. and Kim, C.W., Computer simulation for dynamic wheel loads of heavy vehicles, Int. J. of Structural Engineering and Mechanics, 12(4), pp.409-428, 2001.
9) Honda, H., Kajikawa, Y. and Kobori, T., Spectra of road surface roughness on bridges, J. of Structural Division, ASCE, 108(9), pp.1956-1966, 1982.
10) ISO 8608. Mechanical Vibration – Road Surface Profiles – Reporting of Measured Data, 1995; British Standard, BS 7853, 1996.

(Received July 31, 2003)

Bridge Weigh-in-Motion System using Reaction Force Method

Kentaro Yamada*, Tatsuya Ojio**

*Ph.D., Professor
**M. of Eng., Research Associate
Department of Environmental Engineering and Architecture (Civil Engineering)
Graduate School of Environmental Studies, Nagoya University, Cikusa-ku, Nagoya 464-8603, Japan

A BWIM (Bridge Weigh-in-Motion) system using strain response corresponding to reaction force was developed. Edges associated with the axles passing over the supports corresponded to their axle weight, and thus axle load could be detected. The method was axle detector-free BWIM system and was successfully used at three bridge locations to measure weight distribution of trucks in service. It gave not only total weight of trucks, but also their axle loads and spacing between axles, which in turn was used to identify type of trucks. The measured axle load distribution can be used to evaluate damage associated with the trucks in service, which is one of the most important factors for bridge monitoring.

Key Words: Bridge Weigh-in-Motion, reaction force, bridge monitoring, fatigue

1. Introduction

In March 2002, a new design specification for Highway Bridges was published, where fatigue design for highway bridges was specifically introduced. It specified design life of the highway bridge as 100 years. The detailed fatigue design should follow the Fatigue Design Manual of Highway Bridges, which was published at the same time. It basically follows the same concepts as the JSSC Fatigue Design Recommendation (FDR) for Welded Structures, which was published in 1993. For highway bridges some welded details described in the JSSC FDR were not recommended due to their low fatigue strength associated with high stress concentration.

In Japan about 140,000 highway bridges longer than 15 m exist, and about 40 percent of them are steel bridges. Those bridges were designed with live load corresponding to the full loading of trucks on the bridges, as well as a single design truck of 200 kN. When weight of the design truck was increased by 25 percent in 1994, from 200 kN to 250 kN, as well as design load for deck system from 80 kN to 100 kN, the Ministry of Land, Infrastructure and Transport (MLIT) carried out investigation on evaluating sustainability of existing highway bridges by re-assessing the design in the office. When the design shows stresses larger than the allowable stresses, service stress measurements were carried out in the main members of the highway bridges using stress histogram recorders.

During this process, there existed small number of trucks which causes rather high stress ranges, i.e. four to six times larger than that due to the design truck of 250 kN. Since overload permissions are given to individual trucks according to their configuration, i.e. number of axles and length of the truck, up to about 500 kN, the large stress ranges observed in service were often due to illegally overloaded trucks.

Measurement of weight of trucks in service is important not only for determination of design load of highway bridges, but also for evaluation of durability of existing bridges. A few roadside weigh stations were installed and weight measurements were periodically carried out nationwide for this purpose.

When the weight of truck was measured without stopping traffics, it is often called Weigh-in-Motion (WIM) system. The first of this kind was installed in Japan in 1968 in the Meishin Expressway. Since then numerous WIM systems have been used in Japan. Scales were often installed at tollgates of expressways to give warning to truck drivers in case of overloading. Due to the existence of extremely heavy overloaded trucks, the MLIT started installing more accurate WIM systems, such as a newly developed multiple-sensor WIM (MS-WIM). The system can provide the weight of trucks within five percent, as well as the information of license plates. With such accuracy of measurement, it can be used for the law enforcement, if the MLIT desires.

Alternative approach is to use Bridge Weigh-in Motion (BWIM), i.e. using bridge members as a scale. The BWIM system has been developed in Japan in 1980's, by Miki et al. [1] using the same concept as Moses [2]. Matsui et al. used crack opening of reinforced concrete deck to measure wheel loads [3]. The authors also developed a BWIM system using longitudinal ribs of orthotropic steel deck of a steel box girder bridge [4].

Since then the authors developed several BWIM systems without axle detectors. Development of inexpensive digital data recorders and memory enable us to establish several measuring stations with limited fund available. In 1998, a BWIM was developed by using vertical members and stringers of Warren truss bridge, both of which had relatively short influence line of less than 10 m [5]. A concept of so-called "Influence Area

Method" was developed. This concept was later used to develop BWIM using stringers of plate girder bridges [6], [7], [8]. The plate girder bridges are commonly used for highway bridges in Japan, and therefore it seemed that it opened a way to establish BWIM at any place in Japan.

In 2001, a new approach was developed for BWIM system, namely "Reaction Force Method". It used strain and time history at vertical stiffener or web over the supports, which corresponded to reaction forces. As described later, the Reaction Force Method enabled us to measure axle loads, as well as the spacing between axles. From a database of type of trucks and their axle spacing, we could also categorize type of trucks run on the bridge in service.

2. Reaction Force Method

2.1 BWIM using Reaction Force Method

The influence line of simply supported girder is shown in Fig. 1. When a truck with three axles runs over the girder, the response wave of the reaction force is the linear summation of the influence lines multiplied by the weight of each axle. It is noted that a sharp edge occurs, when each axle passes over the support. The amount of edge corresponds to the weight of axle. Therefore, the weight of each axle can be estimated by detecting the edge and by calculating the amount of the edge. In this case test trucks with known axle loads are needed for calibration. The time differences of the edges correspond to the distance between the axles, and can be estimated when velocity of the truck is known. The velocity of the truck is also estimated by comparing the response waves measured at both sides of the supports.

2.2 Examples of Measurements

The Reaction Force Method was used successfully to measure weight of trucks in service at three bridge locations, Yokkaichi Viaduct on heavily loaded National Route (NR) 23, Kojima Viaduct on Higashi-Meihan Expressway. The method was also used at Minato Bridge in Chiba, but is not referred in this paper.

Yokkaichi Viaduct was constructed in 1964. It located on NR 23, which carries over 80,000 vehicles per day with four lanes, in the southwest of Nagoya. The instrumented bridge is shown in Fig. 2. The bridge is 29m long with six girders supporting northbound and southbound traffics. The measurement was carried out for one week in December 2001 using Reaction Force Method. Strain gages were attached at both sides of the girder supports to obtain velocity of trucks.

The second measurement was carried out at Kojima Viaduct in the Higashi-Meihan Expressway in the west of Nagoya. The average velocity of traffic on this highway was about 80 to 110 km/h, 30 to 40 km/h faster than the national highways. The Kojima Viaduct is a simple girder of 35 m long, as shown in Fig. 3.

Strain gages were attached at the end vertical stiffeners over the support, as shown in Fig. 4. Examples of strain waves measured at end vertical stiffeners over two supports are shown in Fig. 5. The one with edges was measured at the support under the traffic lane. It showed almost the same strain response as expected from the influence line of the reaction force, while the other showed the strain response of vertical stiffener outside of the traffic lane. Note that no sharp edge appeared when the measurement was taken outside of traffic lane.

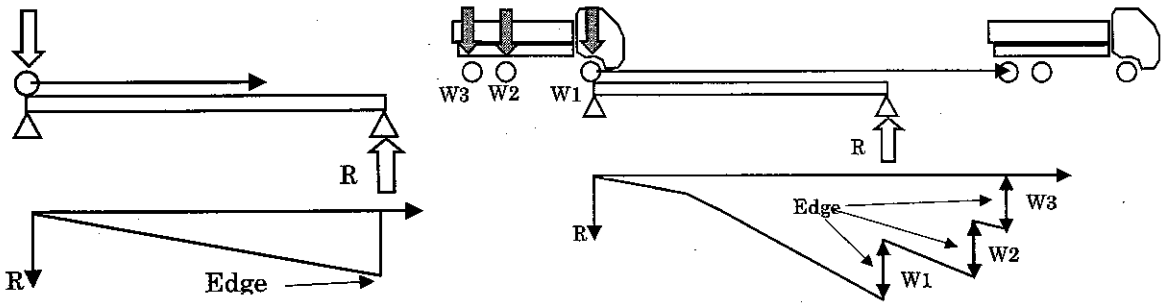

Fig. 1 Influence line of reaction force and response wave due to a three-axle truck.

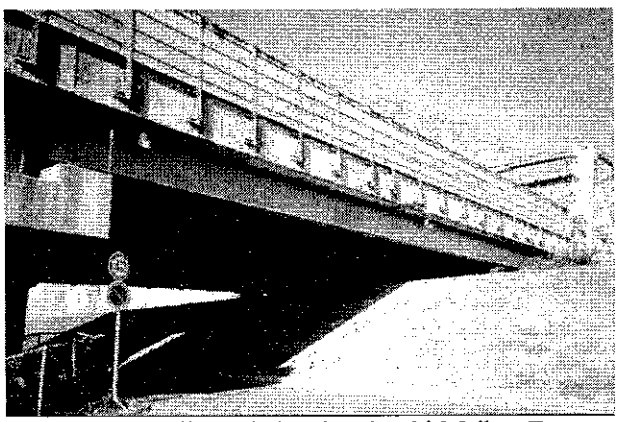

Photo. 1 Kojima Viaduct in Higashi-Meihan Expressway.

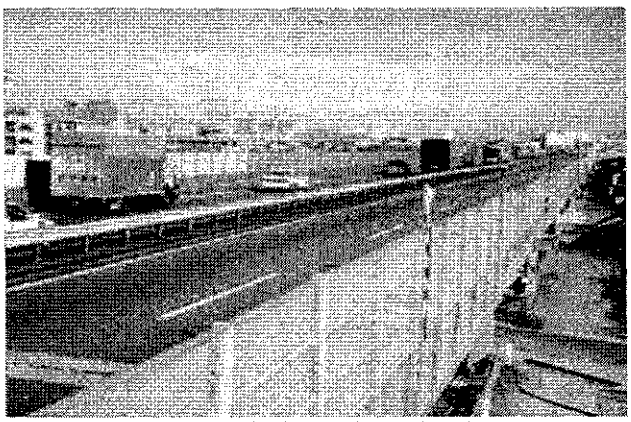

Photo. 2 Yokkaichi Viaduct in National Route 23.

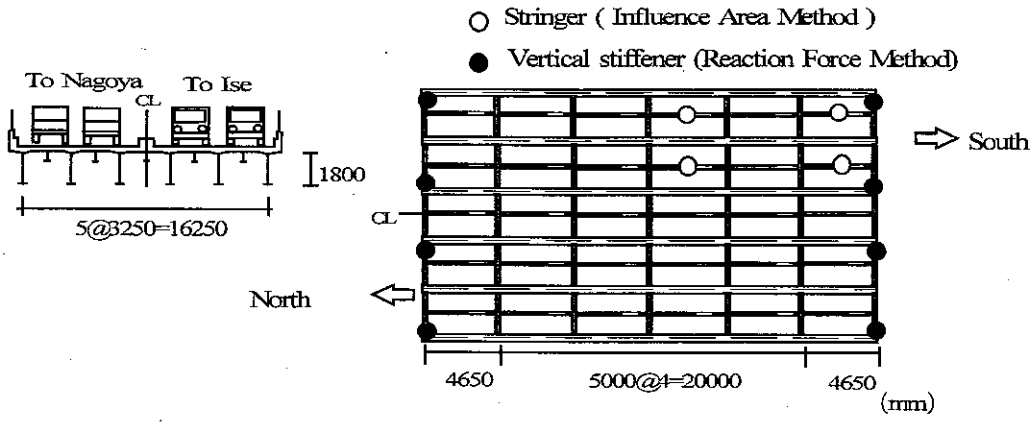

Fig. 2 - Yokkaichi Viaduct

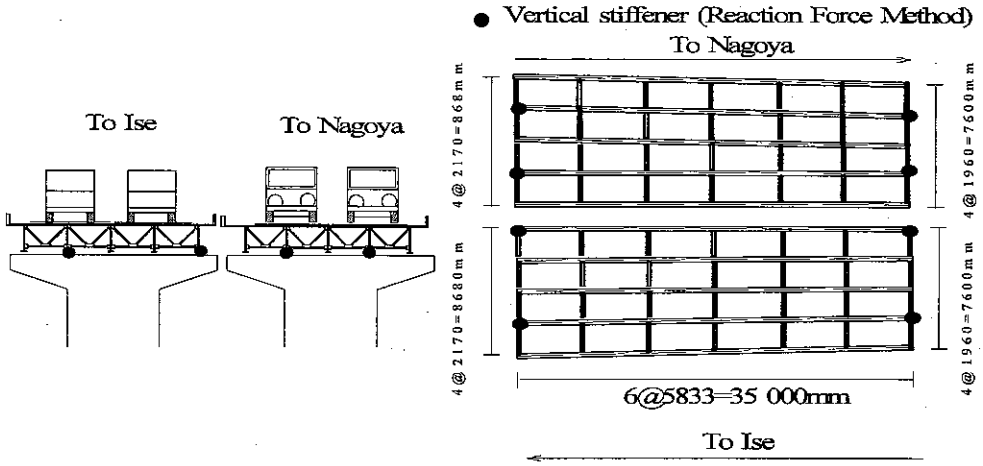

Fig. 3 Kojima Viaduct

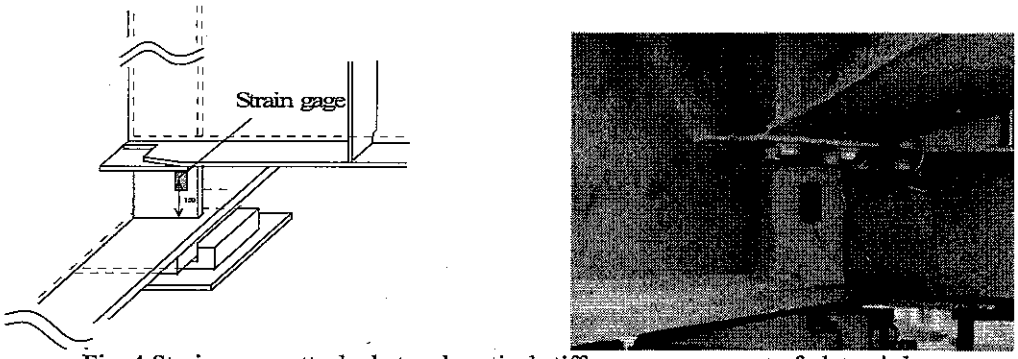

Fig. 4 Strain gages attached at end vertical stiffener over support of plate girder.

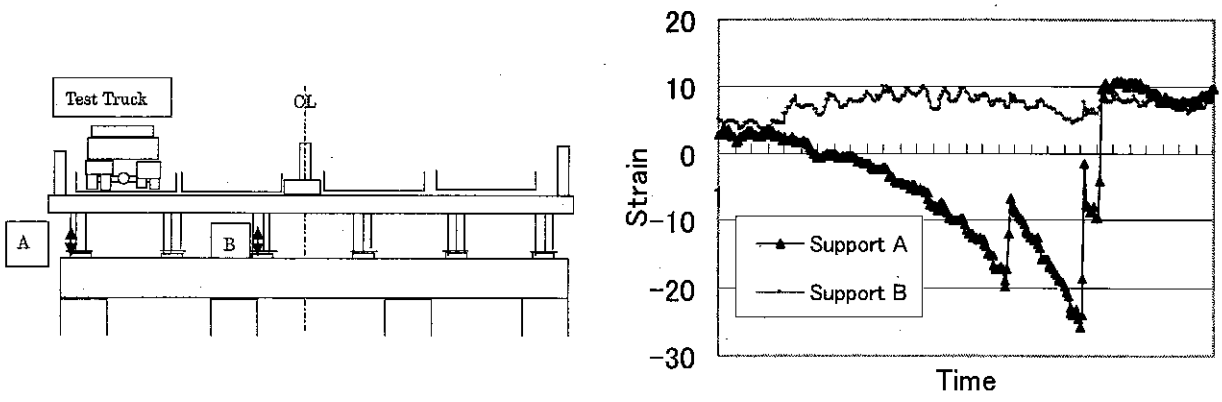

Fig. 5 Strain responses at two end vertical stiffeners.

2.3 Calibration and Accuracy

The estimated GVW and axle loads of the test trucks are compared with statically measured values, as shown in Fig. 6. In this measurement GVW is the summation of each axle. It was found that estimation of each axle showed rather large error, possibly due to the dynamic effect of each axle. However, the GVW showed less scatter of the data, and it was concluded that we could obtain the GVW with the same level of accuracy as the Influence Area Method [8].

3. Weight Distribution of Trucks in Service

3.1 Frequency of Trucks and Their Weight

Fig. 7 shows the relationship between the GVW and its relative frequency measured at Yokkaichi Viaduct. The relative frequency is calculated by dividing frequency of a certain weight of the trucks by daily truck traffic DTT, or the number of trucks measured. The relative frequencies show the same trend in every day, even on Saturday and Sunday when the number of trucks is much less. Note that there are two peaks, at 100 kN and 200 kN. The first peak corresponds to be the average weight of empty or lightweight trucks, and the second peak corresponds to the average of loaded trucks. Many trucks were above 200kN, the former weight limit of a rigid-body truck.

It was found that about 17 percent of trucks weigh more than 200 kN, which is heavier than the design trucks [9]. Some of them were illegally overloaded trucks. However, we were unable to distinguish them from trucks with special permission. The MLIT issues special permission to heavier trucks up to around 500kN according to the length of trucks, the number of axles or wheels. The trucks with special permission can be operated with some special conditions.

3.2 Comparison of Different Test Sites

One of the purposes of BWIM is to measure characteristics of truck traffics in different route. Once the difference in traffic volume and their weight is known, we may be able to correlate it with deterioration of pavement and bridge members associated with loading, and eventually the information can be reflected in maintenance plan.

1) Type of Trucks and Their Frequency

The Reaction Force Method enables us to measure axle loads and accurate axle spacing of trucks. The information of number of axles and their spacing can be compared with a database of configurations of typical trucks being used in Japan, and type of trucks can be identified, as shown in Fig. 8. The data was from Yokkaichi Viaduct and Kojima Viaduct. Unlike Europe or North America we can observe a large number of light trucks with two-axle or three-axle trucks with rigid body on our highways. It is also noticed that the trailer trucks with five or six axles run in the national route, and only a few was observed in the expressway.

2) Frequency Distribution of Axle Load

Fig. 9 shows frequency distribution of axle loads measured at Yokkaichi Viaduct and Kojima Viaduct. Although at this stage some difference between estimated and statically measured axle loads exists. It is mainly due to dynamic effect of the moving axles. The long-term measurement of the axle loads showed some trend. Note that single tires and double tires are also distinguished from type of trucks and their axle spacing.

The axle loads of single tires exhibit two peaks, i.e. at 25 kN and 50 kN. They correspond to front tires, i.e. steering wheel, or rear wheel of light truck. The double tires show a peak at 50 kN for empty trucks, and then wide variation of axle loads for loaded trucks. The data shows about the same peaks, but Yokkaichi Viaduct carries heavier axle loads than Kojima Viaduct.

3) Relative Frequency of GVW for Truck Type

Unlike Europe and the U.S., three axle trucks are commonly used in Japan. The three axle trucks with rigid frame weigh about 100 kN without cargo and about 200 kN with cargo. They carry various cargos of different weight, and therefore measured GVW varies. On the other hand, dump trucks and tank lorries show relatively clear peak of GVW, at 100 kN and 200 kN, which show loaded and unloaded condition of such trucks. The dump trucks weighing over 200 kN is illegally overloaded trucks. Such trend is observed both Kojima Viaduct and Yokkaichi Viaducts.

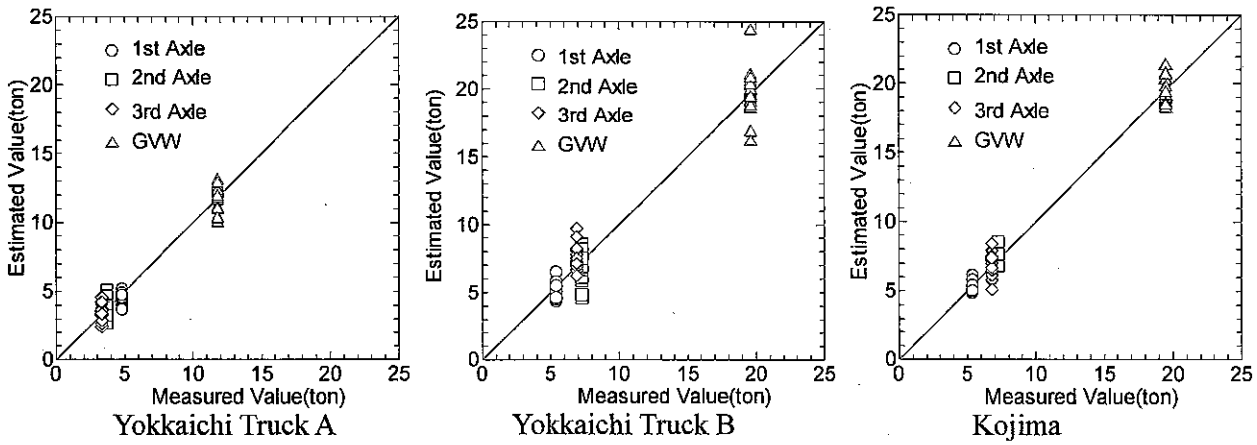

Yokkaichi Truck A　　Yokkaichi Truck B　　Kojima

Fig. 6 Estimated GVW and axle weight of test trucks by Reaction Force Method.

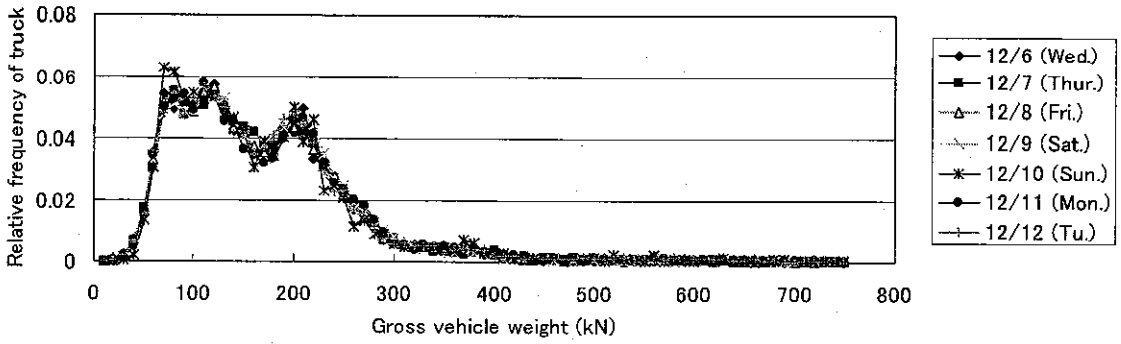

Fig. 7 Relative frequency of GVW measured at Yokkaichi Viaduct.

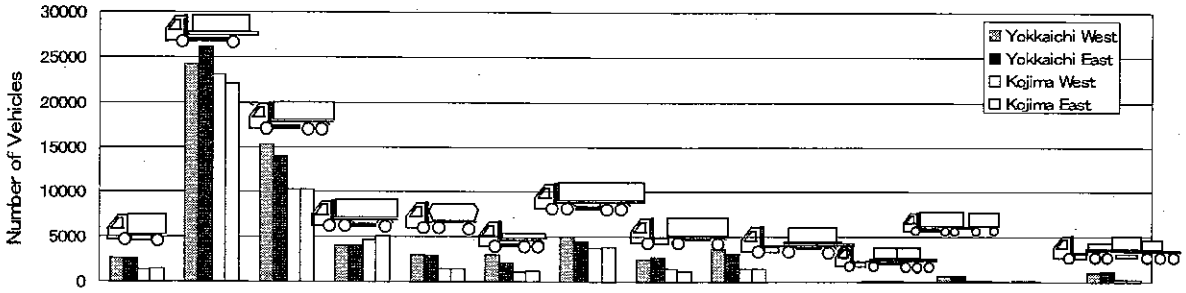

Fig. 8 Traffic volume for truck class (168 hours)

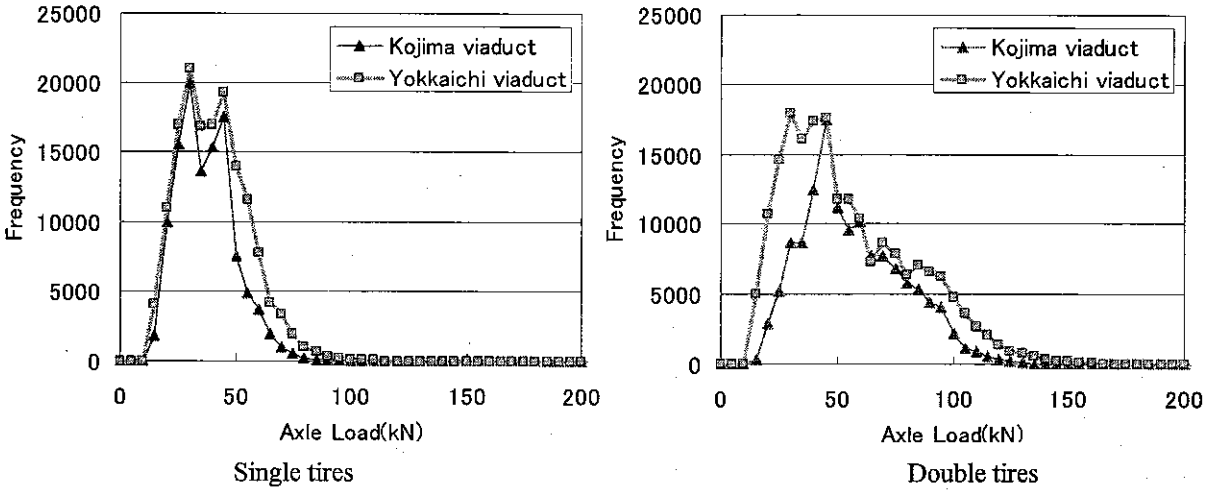

Fig. 9 Frequency distribution of axle loads

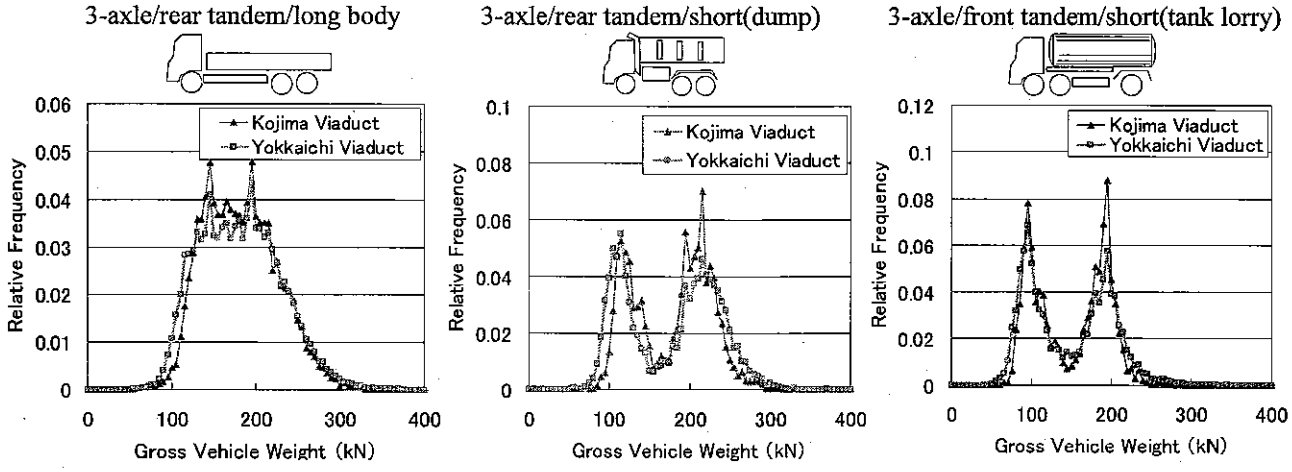

Fig.10 Example of relative frequency of three-axle trucks.

The relative frequencies of each type of the trucks are in good agreement between Kojima Viaduct and Yokkaichi Viaduct. The relatively uniform pattern of the GVW for each truck type exists, and the weight distribution of each highway depends on the rate of each truck type in the total truck traffics. It suggests that weight distribution of truck traffic of the highway of interest can be estimated by knowing the amount of each type of trucks in a day.

4. Fatigue Damage Calculation by WIM Data

One of the main purposes of measurement of weight distribution of trucks in service is to identify the effect of these trucks on accumulated damage of bridge members. A typical example is fatigue problems, which can be estimated by computing fatigue damage index based on Miner's cumulative damage rule.

4.1 Fatigue Damage Index

Fatigue damage index DI can be defined as Eq. 1, where W is range of reaction force or stress range induced by moving load on bridge surface and n is its number of cycles. The values W and n are counted by Rain Flow Counting method. The power of m is the slope of strength curve, such as S-N diagram of the structural element of interest.

$$DI = \sum W^m n \qquad (1)$$

The slope m can be given, for example, as 3 for welded joints, 4 for asphalt pavement, and 12 for concrete deck. In order to compute DI for a member of interest, one can assume influence line of the member. Then, the measured axle loads are loaded to the influence line, and resulted response waves are counted by Rain Flow counting method. Thus, the numerical evaluation of the damage index DI of any length of influence line can be computed.

In the following discussion, an influence line of a simply supported beam is assumed, as shown in Fig. 11. It can be continuous beam, if one desires. Several values of the length of the influence line, L, are assumed, for example, as 30 m for main girders, 2 m for concrete deck, and 5 m for stringers.

4.2 Fatigue Damage Index by WIM Data

For main girders the computed DI is plotted in Fig. 12 for both Yokkaichi and Kojima Viaducts. It can be seen that both viaducts show peak of DI at around 200 kN. Total DI of Yokkaichi Viaduct is about 1.3 times larger than that of Kojima Viaduct. It implies that Yokkaichi Viaduct in the NR23 carries heavier trucks than the Kojima Viaduct in the tall road.

Numbers of trucks over median value of DI are about 14 percent for Kojima Viaduct and 11 percent for Yokkaichi Viaduct for the total number of measured trucks. It implies that one half of damage is due to heavier trucks of less than 20 percent of total number of trucks.

Although the power of m for concrete still needs to be clarified, we can use the power of m=12 for concrete decks to compute DI. Concrete decks have relatively short influence line, for example L=2 m, and are mainly subjected to axle loads. We assume that the concrete decks follow the same damage concepts as is used for fatigue of welded members, and the DI is computed. The results are shown in Fig. 13, where the computed DI is plotted for the truck weight. The result shows that small number of heavy trucks, such as over 200 kN, causes majority of damage to the concrete decks, or members with short influence line. It is specifically demonstrated that only one truck of 800 kN caused a large damage to Yokkaichi Viaduct.

4.3 Extremely Heavy Vehicles

In the mid 1980s the Public Works Research Institute of Ministry of Construction (presently MLIT) developed so-called Histogram Recorder. The system records stress ranges and number of cycles for relatively long time. It was one kind of long term monitoring system of existing highway bridges. The data can be used directly to evaluate fatigue damage of members of interest.

When the system was used to measure stress ranges of medium span plate girder bridges in major highways, a few number of extremely large stress ranges were often observed. They were five to six times larger than the stress ranges due to 200 kN design truck. Therefore, existence of extremely heavy trucks on our highway has been known. However, it was not known what kind of trucks causes such large stress ranges in the main girders.

When we started research on measurement of weight distribution of trucks in service, video recording was used at the same time as measurement was carried out. Time stamps for video recording and the data recorder enable us to trace pictures of trucks corresponding to the extremely large stress ranges.

Examples of the picture of the extremely heavy trucks are shown in Photo 3. The pictures were taken during stress measurement of a simple box girder bridge in NR23 in Nagoya. What are shown in the pictures are three truck cranes with six axles, which weigh over 1500 kN according to their catalogues, and a overloaded five axle trucks. In order to transport such heavy-duty truck cranes on highways, they were to be dismantled into three parts, i.e. carrier, boom and machine part. They also need special permission to transport. Therefore, they were illegally operated trucks.

Since such extremely heavy trucks cause large damage to bridge members, it seems that strict enforcement of the laws on such trucks can effectively reduce damage to members such as concrete decks.

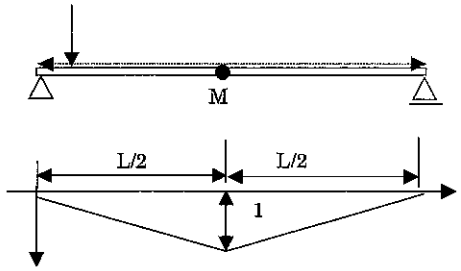

Fig.11 Influence line for calculation of DI

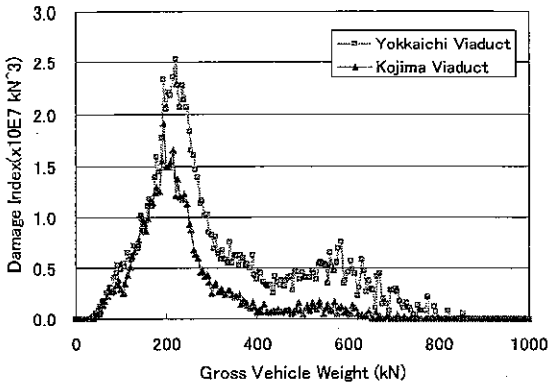

Fig. 12 Computed DI for main girders (m=3, L=30 m)

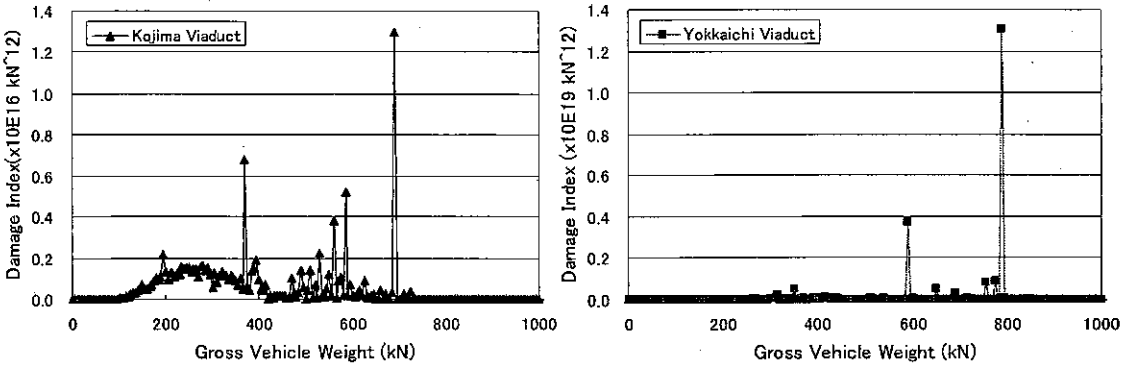

Fig.13 Computed damage index DI for concrete decks. (m=12, L=2 m)

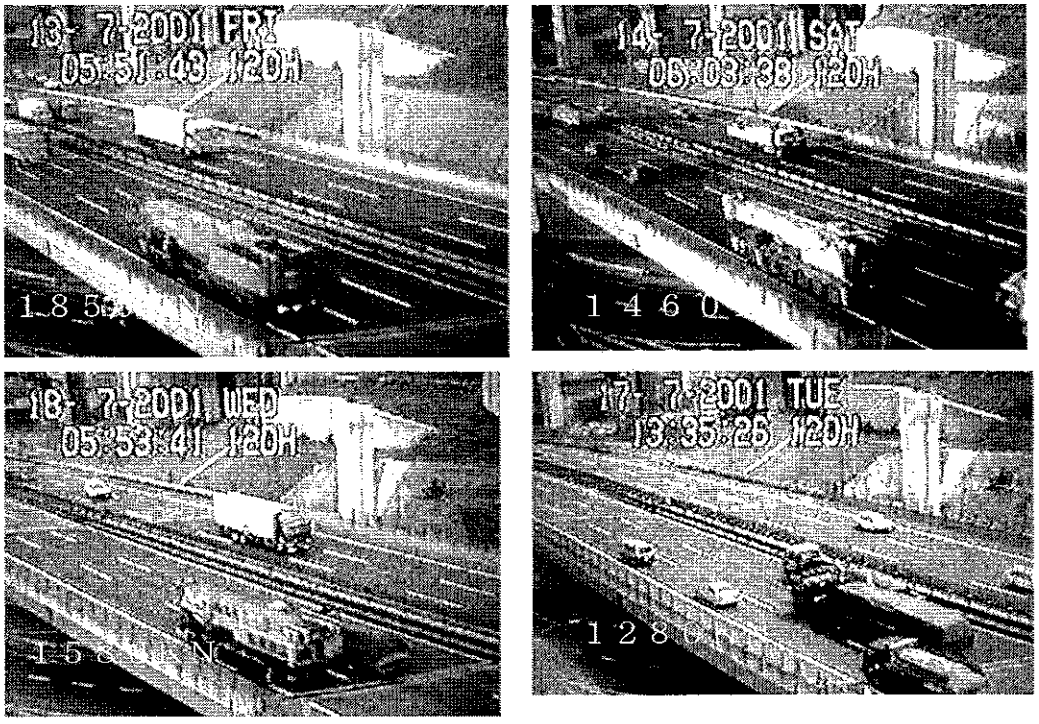

Photo 3 Examples of extremely heavy trucks, i.e. truck cranes and an overloaded truck.

5. Conclusions

The authors developed two BWIM (Bridge Weigh-in-Motion) systems, namely "Influence Area Method", which used strain response waves of members with short influence line, and "Reaction Force Method", which used the response waves corresponding to the reaction force. The latter seems simple, where sudden changes of response wave, or edges, correspond to axle loads of trucks. The edges can be detected and compared with the calibrated value for test trucks. The method enabled us to measure each axle load and spacing between the axles of trucks in service. From such information we can identify type of trucks in service as well.

The measured weight of trucks in service revealed some interesting characteristics, such as difference in traffic patterns of the heavily loaded national route and the expressways. The pattern of truck weight directly affects the damage caused by the truck traffics in service. The fatigue damage index DI, which is based on the Miner's cumulative damage rules, is introduced to compare the traffic-induced damage to the bridge members.

Some examples of computed DI revealed that for main girders about 50 percent of damage seems to come from heavier trucks, which count less than 20 percent of measured number of trucks. When one consider short influence line of 5m with power of m=12, such as for the concrete decks, a small number of heavy truck seems to cause the most of the damage. It reveals that strict enforcement of the law on such illegally overloaded trucks can effectively reduce damage of the bridge members.

The BWIM systems can be used in conjunction with other parameters, for example such as traffic-induced vibration and traffic-induced noise, which seem to be closely related to the type and weight of trucks in service.

Acknowledgements

A part of the paper was published in 2002 in the report ICOM 457, which was dedicated to the 60th anniversary of Professor Manfred Hirt, ICOM, EPFL. We also thank to Chubu Branch of Ministry of Land, Infrastructure and Transport, Japan Highway Public Corporation and Nagoya Expressway, who cooperate with us in carrying out the measurements under service conditions. Messrs. M. Wakao and T. Inden contributed to develop BWIM systems in various stages, and are also highly acknowledged. This research was partially supported by the Ministry of Education, Science, Sports and Culture, Grant-in-Aid for Scientific Research (B), No.14350241, 2002-2003.

References

[1] Miki, C., Meta, M., Murakoshi, J., Yoshimura, S. (1987) "Estimation of Weight of Moving Truck", Bridge and Foundation Engineering, 1987-4, pp.41-45. (In Japanese)

[2] Moses, F. (1979) "Weigh-in-Motion System using Instrumented Bridges", Transportation Engineering Journal, Proceedings of ASCE, Vol.105, No.TE3

[3] Matui, S., El-Hakim, A. (1989) "Estimation of Axle Loads of Vehicle by Crack Opening of RC Slab", Journal of Structural Engineering, JSCE, pp.407-418. (In Japanese)

[4] Ojio, T., Yamada, K., Kainuma, S., Obata, T., Furuichi, T. (1998) "Estimation of Traffic Loads using Strain Recording in Orthotropic Steel Deck", Journal of Structural Engineering, JSCE, Vol.44A, pp. 1141-1151. (In Japanese)

[5] Ojio, T., Yamada, K., Shinkai, H. (2000) "BWIM Systems using Truss Bridges", Proceedings of Bridge Management 4, pp.378-385.

[6] Ojio, T., Yamada, K., Fukatsu, S., Kobayashi, N. (2001) "Bridge Weigh-in-Motion System using Stringers of Plate Girder Bridge, Proc. of 8th EASEC, Singapore, Paper No. 1284.

[7] Ojio, T., Yamada, K., Kobayashi, N., Mizuno, Y. (2001) "Development of Bridge Weigh-in-Motion System using Stringer of Steel Plate Girder Bridge", Journal of Structural Engineering, JSCE, pp.1083-1091. (In Japanese)

[8] Ojio, T., Yamada, K. (2002) "Bridge weigh-in-Motion System using Stringers of Plate Girder Bridge", Pre-Proceedings of the Third International Conference on Weigh-in-Motion (ICWIM3), pp.209-218.

[9] Ojio, T., Yamada, K., Fukatsu, S. (2002) "Evaluation of Fatigue Damage of Highway Bridges Based on Bridge Weigh-in-Motion", Journal of Structural Engineering, JSCE, pp.1055-1062. (In Japanese)

[10] COST-323 (1999) "European WIM Specification", Weigh-in-Motion of Road Vehicles, Final Report, Appendix 1.

[11] Ojio, T., Yamada, K., Wakao, M., Inden, T. (2003) "Bridge Weigh-in-Motion using Reaction Force and Analysis of Traffic Load Characteristics", Journal of Structural Engineering, JSCE, pp.743 -753. (In Japanese)

[12] Yamada, K., Ojio, T. (2002) "Bridge Weigh-in-Motion System to Measure Service Loading", Les 60 ans du Professeur Manfred A. Hirt, ICOM457, pp.93-103.

On ISO Draft DIS 18649 for Bridge Vibration Measurement and Its Evaluation

Toshiyuki Oshima* • Akinori Nakajima** • Jun Tsunabuchi***

*Dr. of Eng., Professor, Dept. of Civil Engineering, Kitami Institute of Technology (〒 090-8507, 165, Koen-cho, Kitami, Japan)
**Dr. of Eng., Professor, Information and Control Systems Science, Graduate School of Engineering, Utsunomiya University (〒 321-8585, 7-1-2, Yoto, Utsunomiya, Japan)
***Chief Engineer, Mitsubishi International Corporation, (50 California Street, Suite 3300, San Francisco, Ca 94111, USA)

In this article, the drafts of ISO standard about the bridge vibration test and its evaluation are introduced briefly, that is, "Guidelines for dynamic tests and investigations on bridges and viaducts"(ISO14963) and "Evaluation of results from dynamic tests and investigations on bridges"(ISO18649). The work of drafting these standard documents is carried out by one of the working groups of ISO/TC108/SC2 and the drafts will be published in the near future through the voting as an FDIS.

The construction of the technical committee ISO/TC108 and its subcommittee are also introduced here.

Key Words : *ISO standard, dynamic test, evaluation, bridge vibration, monitoring*

1. Introduction

The formal name of the technical committee ISO/TC108 is "Mechanical vibration and shock", and The Japan Society of Mechanical Engineers is a host institution in Japan. However, the scope of the work under ISO/TC108 and its subcommittees covers the board area of mechanical vibration and shock, and their effects on humans, machines, vehicles and structures. Moreover the scope of ISO/TC108 includes the general actuators, sensors and associated measurement instrumentation, analytical method and data processing. Therefore, ISO/TC108 deals with the standardization of bridges and structures of highway and railway systems associated with the civil engineering field.

The technical committee ISO/TC108 consists of six subcommittees that execute the technical working as indicated below. However, there are a couple of working groups which belong directly to the technical committee and treat the work items such as terminology, nomenclature, signal processing, condition assessment and monitoring etc.

SC1 Machine balancing

SC2 Measurement and evaluation of mechanical shock and vibration of machines, vehicles and structures

SC3 Use and calibration of vibration and shock instruments

SC4 Human exposure to shock and vibration

SC5 Condition monitoring and diagnostics of machines

SC6 Vibration and shock generating systems

TC108 Working groups Terminology, Nomenclature, Signal processing, Measurement, Evaluation and Control, Methods, etc

The subcommittee, that executes the work item associated with the document introduced here, belongs to SC2 and consists of a couple of working groups as indicated below.

WG1 Vibration of machines

WG2 Vibration of ships

WG3 Vibration of stationary structures

WG7 Vibration of machines with active magnetic bearings

WG8 Prediction of groundborne vibration arising from rail systems in tunnels

WG16 Vibration and shock resistance of sensitive

equipment

Now the draft for international standards, that is, "Guidelines for dynamic tests and investigations on bridges and viaducts" (which is referred as ISO14963)[1] and "Evaluation of results from dynamic tests and investigations on bridges" (which is referred as ISO18649)[2] are considered in WG3.

The convenor of this working group and its secretariat asked the Japanese positive contribution to WG3 activity in 1997. Then, T. Oshima, who was the chairman of the past relevant task committee under Japan Society of Civil Engineers (JSCE) at that time, was to become the expert of WG3 and to cooperate for drafting document ISO14963. In process of drafting ISO14963, T. Oshima proposed the new work item (ISO18649) associated with the evaluation of the results from dynamic tests which is not included in ISO14963. WG3 started on drafting of the document associated with ISO18649 under the project leader of T. Oshima.

Now, Task Committee of JSCE on "Monitoring of bridge vibration and its standardization (A.Nakajima is the chairman of the committee)" supports the work of drafting documents ISO14963 and ISO18649 by sending the experts (T.Oshima, A.Nakajima and J.Tsunabuchi).

This article introduces mainly the content of the drafts of ISO18649 and ISO14963.

2. Content of Drafts of ISO14963 and ISO18649

As mentioned above, ISO/TC108/SC2/WG3 is working on drafting documents of ISO14963 "Guidelines for dynamic tests and investigations on bridges and viaducts" and ISO 18649 "Evaluation of results from dynamic tests and investigations on bridges". Then, the content of these drafts is introduced according to the draft frame in the following.

2.1 ISO14963 "Guidelines for dynamic tests and investigations on bridges and viaducts"

(1) Scope

The purpose of this international standard is to provide general criteria of dynamic tests of bridges. These can supply information on the dynamic behavior of bridges as a basis for condition monitoring or system identification. The scope of this international standard is as follows:

1. Classification of dynamic test for construction and service condition.
2. Indication of investigation and control of whole structures and their parts.
3. List of the equipment for excitation and measurement.
4. Classification of techniques of investigation with reference to suitable methods for signal processing, data presentation and reporting.

(2) Classification of bridges, construction method and substructure

In this chapter, the classifications of bridges, their function, construction method, superstructures and substructures are given, since the dynamic behavior of the bridges is highly influenced by these factors.

(3) General criteria for testing

As criteria for the testing, the choice of the test technique, the excitation methods, the response measuring system and the importance of the preceded numerical analysis before the test are given in this chapter.

(4) Testing equipment

In this chapter, the general comments of the excitation equipment and measurement equipment are shown and the general comments of the control, acquisition and analysis system are also shown. More detailed information is given in Annex.

(5) Techniques of investigation

The general consideration of the excitation methods, that is, the application technique of the artificial excitation and ambient natural actions are given in this chapter.

(6) Testing and inspection

The matter to be paid special attention for the application of each test and the principle to be adopted in regard to the specific circumstances of testing such as the testing during construction, the testing of the completed construction, the investigation and controls during operation, and the monitoring system are given in this chapter. Furthermore, the general comments of the monitoring for the data acquisition are explained and the matter to be paid attention for the traffic monitoring, the seismic monitoring, the wind

monitoring and the multi-functional monitoring are shown.

(7) Final report

In this chapter, the content to be given in the final report such as the test procedure, test design, test report and the analysis of test results and conclusion are explained.

(8) Annex A & B

Two informative annex, that is, "Excitation systems and their specification" and "Measurement equipment and its specification" are given.

2.2 ISO18649 "Evaluation of results from dynamic tests and investigations on bridges"

(1) Scope

The purpose of this international standard is to provide methodlogy for evaluation of results from dynamic tests and investigations on bridges and viaducts. It complements the procedure for conducting the tests as given in ISO14963 and describes the techniques for data analysis and system identification, the modeling of the bridge and the surrounding environment, and the evaluation of the measured data.

This international standard gives guidance of the assessment of measurements carried out over the life cycle of the bridge. The stages of the life cycle are during construction and prior to commissioning, during commissioning trials, during specified periods throughout the life of the bridge and immediately prior to decommissioning the bridge.

The stage of the life cycles and the overview of the bridge vibration monitoring are quoted from those in "Guidelines for Bridge Vibration Monitoring"[3] published by a subcommittee in JSCE. The overview of the bridge vibration monitoring shows the relationship between the life cycle of the bridge, the objectives of the vibration monitoring, the required monitoring and the evaluation, and the measuring technique/testing, the analysis/theory, the evaluation method.

(2) Vibration measurement

Measurement accompanied with vibration monitoring may be carried out on bridges under construction, in commissioning and in service. In this chapter, the general consideration on the vibration monitoring during each stage is described.

1. Monitoring of a bridge during construction and for commissioning

   The objectives of vibration monitoring during construction and for commissioning are the evaluation of structural performance, the assessment of safety and serviceability of the bridges during construction and upon completion etc.

   The vibration monitoring is required for the evaluation of construction management such as the measurement of the cable tension for the control of the profile of the cable-stayed bridge and the confirmation of the safety and the quality control of construction work. In general, the natural frequency, damping and the dynamic response of the structure and its surrounding area are used for the evaluation of structural performance.

   In order to confirm the safety of the structures against earthquake, wind and fatigue during construction and upon completion, the vibration monitoring is required and the measured data is compared with the assumed values in design process. Vibration monitoring is also used to evaluate the serviceability and the environmental compatibility on a completed bridge. Furthermore, it is important to get the initial vibration characteristics on a completed bridge for the purpose of the diagnosis of structural performance and the future design of the similar structures.

2. Monitoring of a bridge in service

   The objectives of vibration monitoring of the bridge in service are the evaluation of the traveling load, structural performance and safety etc. for the maintenance management of bridges.

(3) Data analysis and method of structural identification

Structural identification is conducted to investigate the modal parameters such as the natural frequency of the bridge and to produce the correlated numerical model to the experimental measurements. The identification methods may adopt either the time domain or the frequency domain procedures depending on the problem. In this chapter, the structural identification procedures in the time domain and the frequency domain are briefly explained and the consideration in conducting the structural identification such as digi-

tizing the data are described.

The identification method of the dynamic characteristics of the system with closely spaced modes and the random decrement method for the identification of the system under the ambient vibration are introduced as the time domain identification method. The identification method in the frequency domain is useful for getting not only a single transfer function but also the multiple transfer functions and conducting the statistical analysis of the modal characteristics. For higher-frequency modes, the application of the structural identification and inverse analysis can be used to identify the vibration characteristics of the data from a limited number of measurement points.

(4) Modelling bridge and their surrounding environment

1. Modelling bridge structures
   A bridge structure is a three-dimensional structure which has beam, plate, pillar, foundation and other elements. The bridge type is classified into several types such as the girder bridge, the truss bridge, the arch bridge, the suspension bridge and the cable-stayed bridge etc. To model those geometrical structures, structural and material characteristics of members should take into account. Depending on the problem to be solved, the simplified model or the sophisticated model should be used.
2. Modelling traffic loads In the analysis of coupling vibration between bridge and vehicle, the vehicle must be modelled adequately depending on the problem. Vehicle modelling with surface roughness of the track is important to fit numerical simulation results with the measured results.
   For modelling of a railway vehicle, a multi-body vibration model composed of carbody, truck and wheelset connected with springs and dampers should be used and the number of vehicles in a train, length of train and wheelbase are factors to be considered in calculation of the dynamic amplitude of the bridge response.
3. Modelling of human walking and its dynamic effect
   Modelling of human walking and its dynamic effect on the bridge including the lateral load model of human walking are used to evaluate the vibration serviceability of pedestrian bridge.
4. Wind load
   Static wind load or dynamic one for bridge design is taken into account depending on the problem to be solved.
5. Modelling of ground for viaduct vibration
   In the analysis of coupling vibration between the viaduct and its surrounding ground, the surrounding ground including the stratification, embedded structures and other systems should be modelled adequately.

(5) Evaluation of monitored data and its application

1. Method of evaluation and evaluation criteria
   Measured data are analysed in order to yield information on bridge performance, and quantitative or qualitative decisions made based on this information. Monitoring data is evaluated for safety, integrity diagnosis, serviceability and environmental effect of structures, and in the evaluation process, reasonable or standardized values or limit state values of evaluation parameters should be used as an evaluation standard.
   In the evaluation process, one of the following four categories or their combination are used depending on the problem.

   Category 1 When values of limit states exist. The basis of the evaluation is to check whether the monitored values exceed the limit state.

   Category 2 When defined values or defined ranges of condition exist. The basis of the evaluation is to compare the monitored data with those defined values or ranges.

   Category 3 When estimated values for healthy condition or similar condition of structure exist. If the evaluation values for limit states or defined states are not clear, the values which are estimated numerically for the case of healthy condition or similar condition are useful. In this case the basis of the evaluation is to check whether the monitored data exceed those estimated values or they are within the range of estimated values with acceptable error.

   Category 4 When monitored data for previous

condition or numerical values for similar conditions exist. If previously monitored data or data for an assumed condition are available, the measured data can be compared with those data to evaluate how much the structure improved or deteriorated.

In evaluation, the factors such as measurement uncertainty in monitoring data, variability of structural characteristics and the difference between actual and standard condition should be considered.

2. Evaluation during construction
   For the evaluation of bridge vibration during construction, limit values of vibration are given by authorities. The manager of construction should utilize the monitoring data such as amplitude, velocity, damping and frequency of vibration to decide how to manage the construction considering the usage of the damping device.
3. Evaluation of structural safety in service
   In evaluating the damage in structures, the modification or rehabilitation of structures and the safety of damaged bridges, the vibration monitoring is used and compared with the former data. Furthermore, the statistical distribution of stress for the bridge element is mainly used to evaluate the fatigue condition of bridges and the derailment of a moving train is used to evaluate the train running safety.
4. Evaluation of serviceability
   Serviceability on a highway bridge, a railway bridge and a pedestrian bridge is evaluated mainly by comparing the measured acceleration or velocity with the criterion.

(6) Evaluation of environmental vibration

Ground vibration and infrasound due to viaduct should be evaluated through measured data. Frequency and magnitude of the measured data should be compared with the criteria for the comfort and performance of the human body subject to vibration

(7) Annex A, B & C

Three informative annex "Data analysis in time and frequency domains", "Identification of vibration characteristics" and "Modelling of walking load" are given in detail.

3. Stage of Proposed Drafts

3.1 ISO14963 "Guidelines for dynamic tests and investigations on bridges and viaducts"

ISO14963 was circulated as a DIS (Draft International Standard) in 2001 and got agreement from almost national standard bodies and the comments from the national standard bodies were reviewed. Then, the revised document was submitted to ISO/CS for circulation as an FDIS (Final Draft International Standard) recently.

3.2 ISO18649 "Evaluation of results from dynamic tests and investigations on bridges"

ISO18649 was circulated as a DIS from 2002/12 to 2003/5 for voting and got the agreement from almost national standard bodies. After reviewing the comments from the national standard bodies adequately, the revised document will be submitted as an FDIS.

4. Summary

In this article, we introduce the contents of the drafts of ISO14963 "Guidelines for dynamic tests and investigations on bridges and viaducts" and ISO18649 "Evaluation of results from dynamic tests and investigations on bridges" which are discussed in ISO/TC108/SC2/WG3. In particular, the draft of ISO18649 was proposed by Japanese expert T. Oshima and was supported much by one of the task committees of JSCE. Both standards will be published as an international standard in the near future.

Acknowledgement

The authors are grateful to members of the task Committee of JSCE on "Monitoring of bridge vibration and its standardization" for their comments and discussion during drafting the both documents.

REFERENCES

1) ISO/DIS14963, Guidelines for dynamic tests and investigations on bridges and viaducts, ISO/TC108/SC2/WG3, 2002.
2) ISO/DIS18649, Evaluation of results from dynamic tests and investigations on bridges, ISO/TC108/SC2/WG3, 2002.
3) Subcommittee on Bridge Vibration Monitoring, Committee of Structural Eengineering, Japan Society of Civil Engineers : Guidelines for Bridge Vibration Monitoring, Japan Society of Civil Engineers, 2000.10.

(Received July,31,2003)

SUBMITTED PAPERS
(Japanese)

ＧＦＲＰ引き抜き成形材を用いた歩行者用床版橋と振動使用性

Vibration serviceability of pedestrian slab bridges developed using GFRP pultrusion members

前田研一*，北山暢彦**，中村一史***，林耕四郎****，梶川康男*****
Ken-ichi Maeda, Nobuhiko Kitayama, Hitoshi Nakamura, Koshiro Hayashi, Yasuo Kajikawa

* 工博，東京都立大学大学院教授，工学研究科（〒192-0397 東京都八王子市南大沢 1-1）
** 石川島播磨重工㈱，橋梁事業部基本計画部（〒135-8731 東京都江東区豊洲 2-1-1）
*** 工修，東京都立大学大学院助手，工学研究科（〒192-0397 東京都八王子市南大沢 1-1）
**** 旭硝子マテックス㈱，Ｃ＆Ａ推進部主席技師（〒229-1112 神奈川県相模原市宮下 1-2-27）
*****工博，金沢大学大学院教授，自然科学研究科（〒920-8667 石川県金沢市小立野 2-40-20）

This study examined the vibration serviceability of single span pedestrian slab bridges with different span length and effective width, developed using pultrusion members of GFRP (Glass Fiber Reinforced Plastic) as new structural materials. Application of fixed end support condition that it can largely reduce the deflection in comparison with the simple support condition was proposed, and the difference of both support condition was also compared and was examined. Because the material bending rigidity was low, and the cross section was decided in the deflection restriction.

Key Words : GFRP, Pultrusion member, Pedestrian bridge, Vibration serviceability
キーワード：炭素繊維強化プラスチック，引き抜き成形材，歩道橋，振動使用性

1. 緒　論

近年，繊維強化プラスチック（FRP）が土木構造物の新素材として注目されるようになり，これを一次構造材料に適用した FRP 製の歩道橋，道路橋の研究開発が，国内外で精力的に進められている[1)-5)]．

なかでも，ガラス繊維強化プラスチック（Glass Fiber Reinforced Plastic ; GFRP）製の歩道橋は，世界各国で着実に実績を積みつつある．軽量で作業性に優れ，架設時には従来の機材に比べ小規模なもので十分対応でき，急速施工も可能である．さらに，塩害など環境面で極めて不利な地域への適応性に優れ，維持管理性も高い．

2000 年３月，我が国においても，最初の GFRP 製の実橋として，伊計平良川線ロードパーク連絡歩道橋（２径間連続鈑桁橋形式；支間割 19.7＋17.2m，有効幅員 3.5m）が沖縄県に竣工した[6),7)]．しかしながら，塩害対策として採用されたものではあるものの，主桁にハンドレイアップ材を用いたこともあり，ライフサイクルコストで評価してもなお，コスト面で課題が残された．したがって，特に材料コストを大幅に削減できる設計法の確立と，主桁連結部のより合理的な接合方法の検討が急務とされた．

また，同時に，歩道橋のレベルであれば，ハンドレイアップ材のみならず，引き抜き成形材も十分に適用できるとされ，主桁部材の製作コストの大幅な削減の可能性が指摘された．これは，引き抜き成形材の生産技術が飛躍的に向上して，大型断面材を製造できるようになっており，歩道橋の主桁に GFRP 引き抜き成形材を用いることも可能になってきたからである．

本研究[8)]は，このような観点から，GFRP 引き抜き成形材を用いて，床版橋形式の単径間歩道橋を開発し，試設計結果に基づいて実現性を検証するとともに，歩道橋特有の振動使用性について，支間長および有効幅員を変えて検討したものである．

GFRP 引き抜き成形材の曲げ弾性率は，ハンドレイアップ材よりは高いものの，鋼材に比べてかなり低く，たわみ制限で断面が決定される可能性が予測されたことから，単純支持条件に比べ，たわみを大きく低減できる両端固定支持条件の適用も提案し，両支持条件の差異についても比較，検討することとした．また，振動使用性の検討にあたっては，材料の比重が小さく，質量も小さくなることを考慮して，固有振動数のみならず，簡易計算法による動的応答によっても評価するものとした．

2. 設計条件と材料特性

一次構造材料として，市販されている GFRP 引き抜き成形材の既製品から，梁背が最も高い I 形材（300×150×14.0×10.0mm）と，最大断面のシート材（1000×4.0mm）を選び，等間隔に並べられた I 形材の上面，下面に Deck Plate，Bottom Plate として数層のシート材を配置した断面

表-1 GFRP 引き抜き成形材の材料特性

	曲げ弾性率 (GPa)	曲げ強度 (MPa)	せん断強度 (MPa)	比重	線膨張係数 (/℃)
主桁・床版	30	260	100	1.9	1.0×10^{-5}
地覆，高欄	—	—	—	1.6	0.7×10^{-5}

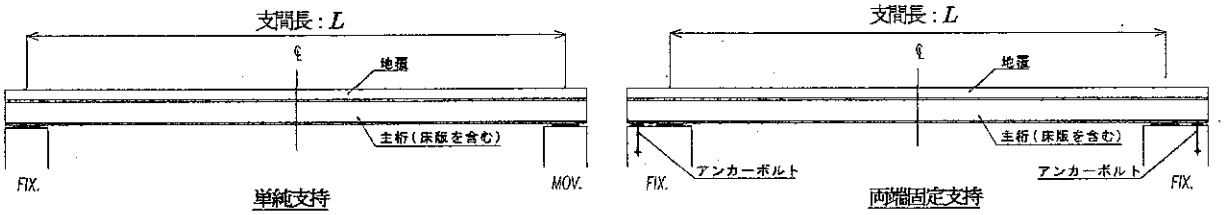

図-1 両端支持条件と支間長

構成の床版橋形式歩道橋を考え，試設計を行って適用可能な最大支間長を求めるとともに，橋軸方向の連結部の接合方法，および，振動使用性についても検討することとした．

設計条件は，単径間で，有効幅員を 1.5m，3.6m，4.5m の3種とし，モルタル舗装を除く全ての部材に GFRP 引き抜き成形材を用いて，それらの主要な材料特性を表-1 に示す値とした．I 形材とシート材，および，各層のシート材は工場建屋内においてプレス下で接着剤により接合することとし，それらが一体化された断面を抵抗断面とした．

地覆，高欄，および，舗装の死荷重（Bridge）はそれぞれ，0.126kN/m，0.560kN/m，および，1.202kN/m とした．また，設計基準には「立体横断施設技術基準・同解説（昭和 54 年版[9]）」」を適用して，活荷重は 3.5kN/m^2，温度変化は±30℃とし，使用性を確保するための静的なたわみの制限値，および，回避すべきたわみ振動数の帯域はそれぞれ，*L/600*（*L*：支間長），および，1.5～2.3Hz とした．

主桁両端の支持条件としては，図-1 に示すように，単純支持条件のみならず，両端固定支持条件も対象とすることとした．これは，表-1 に示した梁試験結果に基づく曲げ弾性率の値が鋼材に比べてかなり小さく，許容応力度によってではなく，たわみ制限によって主桁断面が決定される可能性が高かったことから，活荷重に対するたわみを低減することを図ったものである．なお，静的な断面力や，たわみ量，および，たわみ振動数の算出は，概略設計でもあり，梁公式によるものとした．

3. 試設計結果とその考察

試設計にあたっては，図-2 に示す両支持条件に共通な一般部の断面図のように，3種の有効幅員に応じて等間隔に並べられた I 形材の本数を，有効幅員 1.5m の場合，3 本，5 本，7 本，3.6m の場合，5 本，9 本，14 本，4.5m の場合，6 本，11 本，17 本とそれぞれ変化させるものとした．すなわち，図-2 は，各有効幅員について，I 形材の本数がそれぞれ最多の場合の断面図を示したものである．

試設計結果として，3種の有効幅員に対する単純支持条件，および，両端固定支持条件の適用可能支間長を，I 形材の本数を上述のように変化させるとともに，Deck Plate，Bottom Plate となる上，下面のシート材の層数を変えて板厚（4mm×層数）を変化させた場合について，表-2 に示す．これらは，たわみ制限から決定されたもので，詳細は省略するが，曲げ強度に対する最大応力度の安全率は，両端固定支持条件の場合でも 7～8 程度と大きかった．

表-3 には，表-2 に対応し，I 形材の本数とシート材の板厚の組み合わせによる I 形材，シート材の単位長さあたりの合計重量を示すが，この合計重量が支持条件に無関係であることは明らかである．さらに，図-3 には，表-2 に対応して，支持条件別，有効幅員別に，I 形材の本数が最多の場合のたわみ振動数と適用可能支間長との関係を示す．

まず，表-2 から，単純支持条件の場合，適用可能支間長が 15m を超えるには，シート材を 7 層にしても不十分なのに対して，両端固定支持条件の場合には，2 層で十分であり，7 層にすれば，25m に迫ることが解る．適用可能支間長が，有効幅員の増幅にしたがって，若干短くなる傾向についても確かめられる．また，表-3 からは，I 形材を必要最小限の本数とし，シート材の層数を増やす方が，適用可能支間長を伸ばすうえで経済的であることが解る．

さらに，図-3 からは，たわみ振動数が，長支間化に伴って回避すべきたわみ振動数の帯域に近付くこと，および，有効幅員にはほとんど依存しないことが解る．

4. 橋軸方向の連結部の接合方法

試設計の結果，かなりの支間まで適用可能なことが解ったが，架設現場への輸送の問題からは，橋軸方向連結部の接合が不可欠となる．そこで，ここでは，図-4 に示すブラインドリベットを用いた接合案を考えることとした．せん断接合用リベットの一種であり，自動車をはじめとする機械部品の接合に主に用いられてきたものであるが，簡単な工具（リベッター）によって，外面または内面からのどちらか1面からの作業のみで接合できる特色がある．

鋼，ステンレス，アルミ合金などの製品があり，現在の最大呼径は 6.4mm，最大長さは 40mm で，接合可能な最大板厚（かしめ板厚）は 35.5mm であるが，特注品であれ

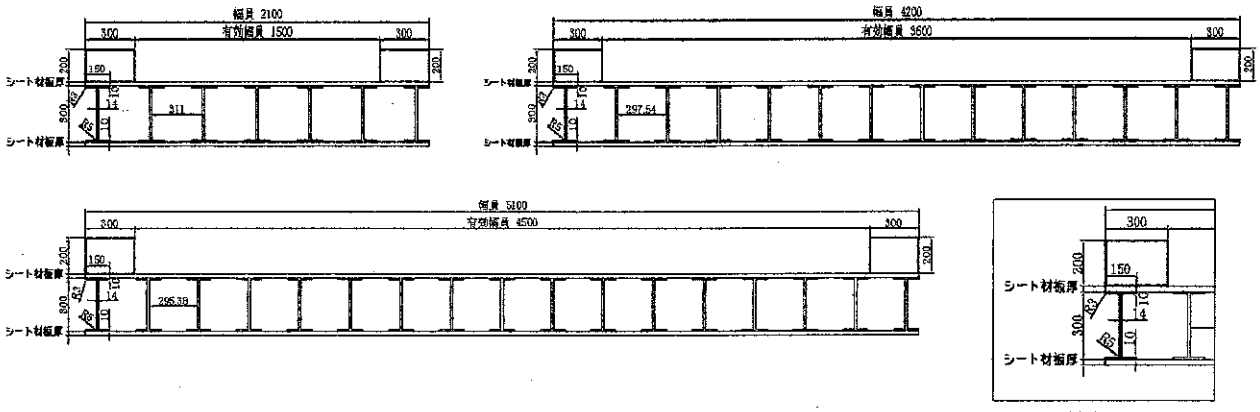

図-2 一般部の断面構成

表-2 I形材の本数，シート材の層数と適用可能支間長

有効幅員 (m)	支持条件	I形材数 (本)	適用可能支間長 (m)					
			4mm×2層 ×2面	4mm×3層 ×2面	4mm×4層 ×2面	4mm×5層 ×2面	4mm×6層 ×2面	4mm×7層 ×2面
1.5	単純支持	3	9.2	10.3	11.2	12.1	12.9	13.6
		5	9.7	10.7	11.6	12.4	13.1	13.8
		7	10.1	11.1	11.9	12.7	13.4	14.0
	両端固定支持	3	15.7	17.6	19.2	20.7	22.0	23.3
		5	16.6	18.3	19.8	21.2	22.5	23.6
		7	17.3	18.9	20.3	21.6	22.9	24.0
3.6	単純支持	5	8.5	9.6	10.5	11.3	12.1	12.7
		9	9.0	10.0	10.8	11.6	12.3	13.0
		14	9.5	10.4	11.2	11.9	12.6	13.2
	両端固定支持	5	14.6	16.4	18.0	19.3	20.6	21.8
		9	15.4	17.1	18.5	19.8	21.0	22.2
		14	16.3	17.8	19.1	20.4	21.5	22.6
4.5	単純支持	6	8.4	9.5	10.4	11.2	11.9	12.6
		11	8.9	9.9	10.7	11.5	12.2	12.8
		17	9.4	10.3	11.1	11.8	12.5	13.1
	両端固定支持	6	14.4	16.2	17.8	19.2	20.4	21.6
		11	15.3	16.9	18.3	19.6	20.8	22.0
		17	16.1	17.6	19.0	20.2	21.3	22.4

表-3 I形材とシート材の合計重量

有効幅員 (m)	支持条件	I形材数 (本)	I形材とシート材の合計重量 (kN/m/Bridge)					
			4mm×2層 ×2面	4mm×3層 ×2面	4mm×4層 ×2面	4mm×5層 ×2面	4mm×6層 ×2面	4mm×7層 ×2面
1.5	単純支持および両端固定支持	3	1.03	1.35	1.67	1.99	2.31	2.63
		5	1.30	1.62	1.94	2.25	2.57	2.89
		7	1.56	1.88	2.20	2.52	2.84	3.16
3.6		5	1.94	2.57	3.21	3.85	4.49	5.13
		9	2.46	3.10	3.74	4.38	5.02	5.65
		14	3.12	3.76	4.40	5.04	5.67	6.31
4.5		6	2.34	3.12	3.89	4.67	5.44	6.22
		11	3.00	3.77	4.55	5.33	6.10	6.88
		17	3.79	4.57	5.34	6.12	6.89	7.67

ば，より大きな呼径，長さのものの製造も可能とされている．呼径が小さく，所要本数が多くなることが短所であるが，GFRPの場合は，孔空けは容易で，架設現場であっても十分に接合が可能であり，実施例もみられる．なお，応力的には十分余裕があることから，孔引きによる影響を無視できるとともに，全強で設計する必要はない．

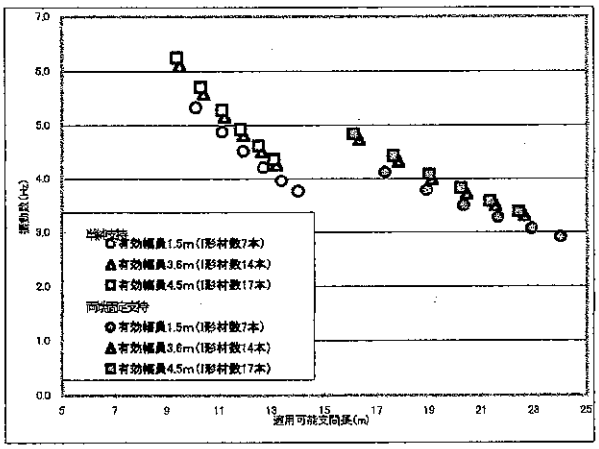

図-3 たわみ振動数と適用可能支間長

ブラインドリベットによる連結部の接合

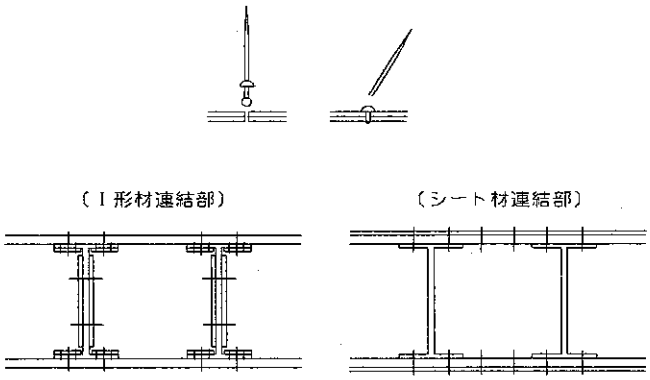

図-4 橋軸方向の連結部の接合

5. 動的応答による振動使用性の評価

試設計の結果，図-3 に示したように，たわみ振動数が，長支間化に伴って回避すべきたわみ振動数の帯域に近付くことが解った．そこで，最長支間で最小振動数となった両端固定支持条件で，有効幅員 1.5m，I 形材の本数 7 本，Deck Plate，Bottom Plate となる上，下面のシート材の板厚 28mm（7 層）の場合について，簡易計算法による動的応答値によっても振動使用性を検討することとした．

検討にあたっては，回避すべきたわみ振動数の帯域 1.5～2.3Hz に達することを予測し，たわみ制限として，図-3 に示した $L/600$（L：支間長）のみならず，$L/500$，$L/400$ の場合についても検討することとした．前出の文献 9)におけるたわみ制限は，あくまでも鋼歩道橋に対する規定であり，応力的に十分に余裕があることなどを考えれば，$L/350$ 程度までは緩和してもよいと考えられるからである．

動的応答値を求める簡易計算式としては，BS5400 などで適用され，桁橋の最大応答加速度 a (m/sec^2) を簡便に算定できる次式によるものとした[10),11)]．

$$a = 4\pi^2 f_i^2 w K \phi \qquad (1)$$

ここに，f_i は最低次のたわみ振動数 (/sec)，w は 700N の鉛直集中荷重による静的最大たわみ (m) である．K は，単純桁橋の場合を K=1.00 とした桁構造形式に関する形状関数であり，両端固定支持条件を側径間が極端に短い 3 径間連続桁橋と考え，ここでは K=0.92 とした．ϕ は，最大支間長と減衰定数 h をパラメータとして与えられる動的応答係数である．

すなわち，上式は，体重 700N の人ひとりの共振歩調による桁橋の最大応答加速度を算定するものである．表-4 に，減衰定数 h を変えて，各たわみ制限の適用可能支間長に対応する最大応答加速度 a を算定した結果を示す．

表-6 から，たわみ制限を $L/400$ まで緩和すると，回避すべきたわみ振動数の帯域に達するが，減衰定数 h を 0.8% 程度まで確保できれば，最大応答加速度 a は，文献 9)の解説に記載された我が国における代表的な恕限度の一つである 0.1g（g；重力加速度）近くにまで抑えられることが解る．

表-4 減衰定数と最大応答加速度

適用可能支間長 (m) [たわみ制限]	たわみ振動数 (Hz)	最大応答加速度 (m/sec^2) 減衰定数 0.5%	減衰定数 0.6%	減衰定数 0.8%
24.03 [$L/600$]	2.91	1.312	1.196	1.094
25.53 [$L/500$]	2.58	1.289	1.175	1.083
27.50 [$L/400$]	2.22	1.265	1.146	1.038

しかしながら，BS5400 では，最大応答加速度 a (m/sec^2) の恕限度として，

$$a \leqq 0.5 \cdot f_i^{0.5} \qquad (2)$$

を規定しており，これを満たすためには，1.0%を大きく超える減衰定数 h を確保することが必要であるといえる．

なお，前述の我が国最初の実橋である伊計平良川線ロードパーク連絡歩道橋（2 径間連続桁橋；支間割 19.7＋17.2m）では，振動試験が実施されており，減衰定数 h の実測値として約 1.5%という値が得られている[12)]．しかし，本橋は鈑桁橋形式で，対傾構や床組などにボルト継手があり，それらが減衰性を高めたものと考えられており，さらなる検討が必要である．

6. 結　言

GFRP 引き抜き成形材を用いて開発した，床版橋形式の単径間歩道橋の試設計結果とその考察，橋軸方向連結部の

接合方法，および，振動使用性の検討結果からは，つぎのようなことなどがいえた．

(1)単純支持条件，および，提案した両端固定支持条件ともに，たわみ制限により断面が決定され，有効幅員の増幅に伴って適用可能支間長が若干短くなる傾向にあるものの，両端固定支持条件の場合には，Deck Plate，Bottom Plateとしての上，下面のシート材の板厚を8mm（2層）とすることで，適用可能支間長15mを超えることができる．

(2)シート材の板厚を28mm（7層）までさらに厚くすることによって，両端固定支持条件の場合，適用可能支間長25mに迫ることができるが，単純支持条件の場合には，適用可能支間長15mでさえ超えることができない．

(3)シート材の層数を増やし，上，下面のシート材の間隔を保持するためのＩ形材を必要最小限の本数としたほうが，適用可能支間長を伸ばすうえで経済的である．

(4)ブラインドリベットを用いた橋軸方向連結部の接合案は，合理的で，架設現場における作業性にも優れており，架設条件の制約をかなり緩和できる．

(5)たわみ振動数は，有効幅員にはほとんど依存せず，長支間化に伴って回避すべきたわみ振動数の帯域に近付くが，たわみ制限が*L/600*，*L/500*（*L*：支間長）の場合には，その帯域に達することはない．

(6)たわみ制限を*L/400*まで緩和すると，回避すべきたわみ振動数の帯域に達するが，減衰定数を0.8%程度まで確保できれば，体重700Nの人ひとりの共振歩調による最大応答加速度は，我が国における代表的な怒限度の一つである0.1ｇ（ｇ；重力加速度）近くに抑えられる．

(7)たわみ制限*L/400*の場合に，同様の共振歩調による最大応答加速度がBS5400の怒限度$0.5\cdot f_i^{0.5}$（f_i：最低次たわみ振動数）を満たすためには，1.0%を大きく超える減衰定数を確保する必要がある．

したがって，実現性は高いといえるが，接着剤接合断面の平面保持性と耐久性，および，ブラインドリベットを用いた橋軸方向連結部の安全性と耐久性の検証，減衰特性の把握など，実現に至るには種々の課題が残されている．

謝　辞

本研究のデータ整理・CAD製図等にあたっては，東京都立大学大学院生の神原由紀君の協力を得た．多大な貢献に対して，ここに，心より謝意を表したい．

参考文献

1) T. Keller, et al. : Advanced Materials, Structural Engineering International, IABSE, Vol.9, No.4, pp.250-301, 1999.
2) T. Keller, et al. : Advanced Materials, Structural Engineering International, IABSE, Vol.12, No.2, pp.66-116, 2002
3) 建設省土木研究所：繊維強化プラスチックの土木構造材料への適用に関する共同研究報告書（Ｉ）――次構造材料としてのＦＲＰの適用事例調査―，共同研究報告書第210号，1998.
4) 建設省土木研究所：繊維強化プラスチックの土木構造材料への適用に関する共同研究報告書（II），共同研究報告書第252号，2000.
5) 明嵐政司，西崎到，木嶋健，佐々木巖：繊維強化プラスチックの橋梁への適用事例に関する研究，土木学会ＦＲＰ橋梁に関するシンポジウム論文集，pp.13-18，2001.
6) 北山暢彦，佐伯彰一，山城和雄：沖縄ロードパーク歩道橋の設計，土木学会ＦＲＰ橋梁に関するシンポジウム論文集，pp.103-106，2001.
7) 北山暢彦，宇野名右衛門：「伊計平良川線ロードパーク連絡歩道橋」の設計・製作・架設，石川島播磨技報，橋梁特集号，pp.82-86，2001
8) 神原由紀，前田研一，中村一史，北山暢彦，林耕四郎：GFRP引き抜き成形材を用いた歩行者用床版橋に関する基礎的研究，土木学会第58回年次学術講演会講演概要集，2003.
9) 日本道路協会：立体横断施設技術基準・同解説（昭和54年版），1979.
10) 日本鋼構造協会：これからの歩道橋ー付・人にやさしい歩道橋計画設計指針ー，技報堂出版，pp.120-123，pp.186-190，1998.
11) 土木学会：橋梁振動モニタリングのガイドライン，構造工学シリーズ10，pp.165-168，2001.
12) 張惟敦，鎌田敬治，佐伯彰一，山城和雄：ＦＲＰ製歩道橋の主桁剛性および固有振動数に関する実験的評価，石川島播磨技報，橋梁特集号，pp.77-81，2001.

(2003.7.31受付)

長周期の路面凹凸を有したニールセンローゼ橋の振動使用性

The vibration serviceability of Nielsen System Lohse Girder Bridge with long period of road surface roughness

深田宰史*，梶川康男**，北村洋太郎***，原田政彦****，清水英樹*****
Saiji Fukada, Yasuo Kajikawa, Yotaro Kitamura, Masahiko Harada and Hideki Shimizu

*博(工)，金沢大学大学院助手，自然科学研究科（〒920-8667 金沢市小立野 2-40-20）
**工博，金沢大学大学院教授，自然科学研究科（　　同上　　）
***金沢大学大学院，自然科学研究科（　　同上　　）
****博(工)，大日本コンサルタント㈱，北陸支社構造技術室（〒930-0175 富山市願海寺 633 番地）
*****大日本コンサルタント㈱，北陸支社構造技術室（　　同上　　）

The vibration problem had been occurred in the Aimoto Bridge, which is Nielsen System Lohse Girder Bridge, due to running Vehicle. In this study, we performed loading tests in this bridge in order to grasp vibration characteristics and serviceability of this bridge subjected to vehicle's movement. We also measured the road surface roughness of this bridge to find the cause of the vibration. As the result of examination, it has been shown that Aimoto Bridge has vibration characteristics in low frequency range and low damping. Moreover the pavement on this bridge had road surface roughness with long period. After this measure, the road surface roughness was improved. We performed again the same loading tests as before improving road roughness. Finally, we checked the improvement of the vibration serviceability due to running vehicle.
Key Words : road surface roughness, vibration characteristics, vibration serviceability
キーワード：路面凹凸，振動特性，振動使用性

1. まえがき

車両が橋梁上を走行した場合，凹凸を有した路面上を車両が走行することで車両振動が生じ，さらに，その車両と橋梁の連成振動により橋梁の振動が増幅される．

車両振動では，車両の前後輪ばね上振動数（1～3Hz 前後）とばね下振動数（10～20Hz）が卓越し，橋梁の卓越振動数と近接した場合，共振により大きな振動が生じる．

これらの車両が路面上を走行した場合，一種の強制加振状態となっており，路面凹凸周波数，車両の走行速度と凹凸波長から決まる加振振動数，および車両のばね振動数が車両振動の増減を握る重要なパラメータとなる．

伸縮継手部近傍の段差[1]により車両のばね下振動が誘起されることは知られているが，伸縮継手部を含む前後 10m の路面性状により，車両のばね上振動が誘起されることも近年の研究[2)3)]によりわかってきた．

さらに，周期性を有した路面凹凸上をある走行速度で大型車両が走行すると，その加振振動数と車両のばね振動数との共振により，大きな加振力が橋梁に加えられ，その振動数領域と橋梁の卓越振動数が近接していた場合，さらに大きな振動が生じることになる．

過去の事例として，路面凹凸が 6～8c/m の周期性を帯びた高架橋上を大型車両が 80km/h で走行した場合，3.2Hz の後輪ばね上振動数が大きく誘起され，高架橋のたわみ振動が 3.28Hz に存在していたために，その高架橋周辺の家屋において振動問題が生じた例がある[4)]．

このように，橋梁の振動が大きくなる要因として，周期性を有した長周期の路面凹凸と車両の走行速度やばね振動数との関係が挙げられる．

本研究で対象としたニールセンローゼ桁橋，愛本橋においては，車両がこの橋梁上を走行した際に，幅員両脇にある歩道上において比較的大きな振動が生じ，使用性が問題となっていた．本研究では，その要因を分析するために，路面，車両および橋梁，各々に着目して路面凹凸，車両振動および橋梁振動を計測した．結果的に，路面の周期性が見られ，同時に橋梁側においても車両ばね上振動数領域に多くの卓越振動数が存在し，それらの減衰定数が小さいことが大きく揺れている原因と判断した．そこで，路面性状を改善するという対策を講じることにした．路面改善後においても対策前と同様な計測を行い，歩道部における振動使用性がどれだけ改善されたのか実験的に検討した．本文では，それら一連の結果を述べる．

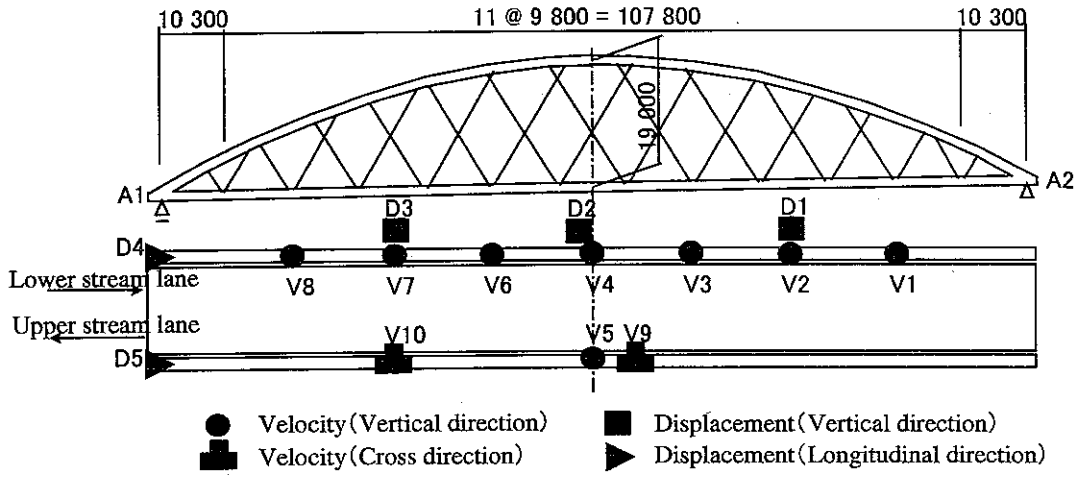

Fig.-1 General elevation and the measured points of the objective Bridge

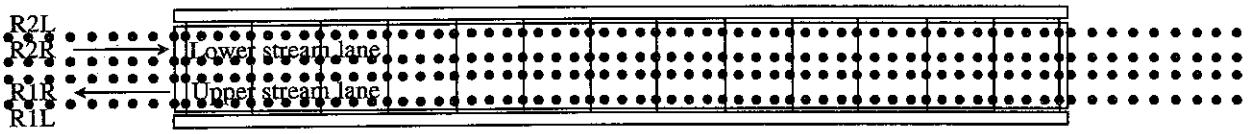

Fig.-2 The Measured points (●) of the road surface roughness by level measurement

2. 橋梁概要

本研究で対象とした愛本橋は，富山県下新川郡宇奈月町に架設された道路橋（一等橋）である．本橋は，橋長130m（支間長 128.4m）のバスケットハンドル型ニールセンローゼ桁橋である．有効幅員は，8.5m（車道 7.0m+歩道 0.75m×2）であり，両側に歩道が設置されている．一般図を Fig-1 に示す．初代の愛本橋は，刎橋であったが，明治 20 年頃の大洪水により流失した．現在の愛本橋は，それよりも 300m 程下流の地点に昭和 47 年架設された．

3. 実験概要

対象橋梁の振動特性を把握するために，車両を用いた静的載荷実験，衝撃加振実験および車両走行実験を行った．また，車両と橋梁との連成振動を調べるために車両走行実験時の車両振動を計測した．さらに，対象橋梁上の路面凹凸性状を把握するために，3m プロフィルメータと水準測量による路面凹凸の計測を行った．

橋梁における変位および振動速度の計測については，変位計を 5 個，サーボ型速度計（東京測器㈱製・VSE－15，計測周波数 0.1～70Hz）を 10 個用いて計測した．橋梁の鉛直変位は，橋面上からワイヤーを垂らし，地面にアンカーすることで地面との鉛直方向の変位を変位計により計測した．速度計の配置は，鉛直振動モードと水平およびねじれ振動モードを計測できるように配置した．変位および振動速度に関する測点配置図を Fig.-1 に付記する．

3. 1 路面凹凸の計測

対象橋梁の路面凹凸性状を把握するために，各車線の左右車輪位置（R1L,R1R,R2R,R2L,Fig.-2 参照）における路面凹凸を 3m プロフィルメータにより計測した．計測距離は，取付け 20m の土工部（A1 側と A2 側）と橋梁部 130m の計 170m である．計測した凹凸データは，0.1m 間隔でサンプリングした．また，3m 以上の周期を有する路面凹凸については水準測量により計測した．水準測量の計測間隔は，3m 以内になるように，土工部では 2.5m 間隔，橋梁部ではそれぞれの横桁間隔を 4 等分した距離とした．水準測量における計測箇所を Fig.-2 に示す．

3. 2 静的載荷実験

対象橋梁が有する剛性の確認および実験結果と解析結果との比較から，解析モデルの剛性の妥当性を確認するために静的載荷実験を行った．この実験では，Fig.-3 に示す総重量が約 196kN の試験車両を用いて，後輪 2 軸中心を 1/8 点ずつ載荷して，そのときの鉛直変位および支承の橋軸変位を計測した．なお，試験車の重量は，路面の補修工事前後において多少重量が異なり，Table-1 のようになっていた．

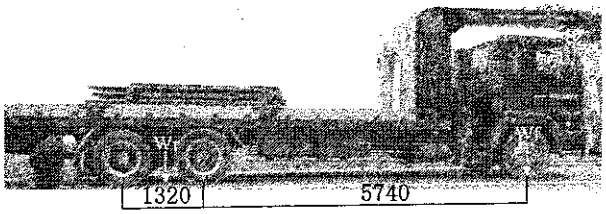

Fig.-3 Test Vehicle

Table-1 Weight of the Test Vehicle (unit:kN)

	Wf	Wr	Total
Before improvement	67.60	128.00	195.60
After improvement	65.62	153.12	218.74

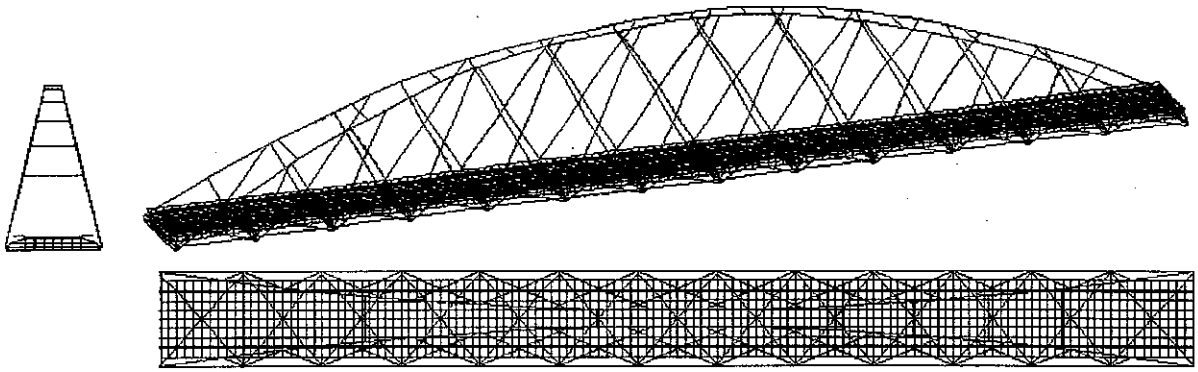

Fig.-4　Analytical model

3. 3　衝撃加振実験

対象橋梁の振動特性（卓越振動数，モード減衰定数）を調べるために，上述した大型車両を用いて，前輪を踏み台より落下させる衝撃加振実験を行った．加振点は，1/8 点から 1/2 点まで 1/8 点ずつ変化させた．また，曲げ振動モードおよびねじれや水平振動モードを卓越させるために，幅員中央（センターラインを跨ぐ）および偏心（下流側に寄せる）の 2 通りで行った．

3. 4　車両走行実験・車両振動計測

車両走行時の動的応答特性を把握し，対象橋梁の振動使用性について検討するために車両走行実験を行った．車両走行実験では，40，50，60km/h の走行速度で実施した．走行方向は，各走行速度に対して，上流側走行と下流側走行（Fig.-1）の往復走行を 2 回ずつ行った．

車両走行実験時の車両と橋梁の連成振動を調べるために，車両側の振動を計測した．車両側には，前輪および後輪のばね上とばね下に加速度計を計 4 個設置した．

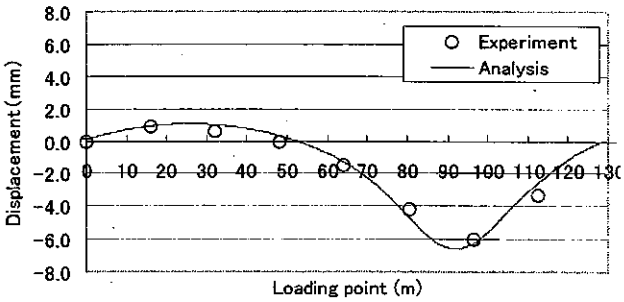

(a) Span 1/4 point

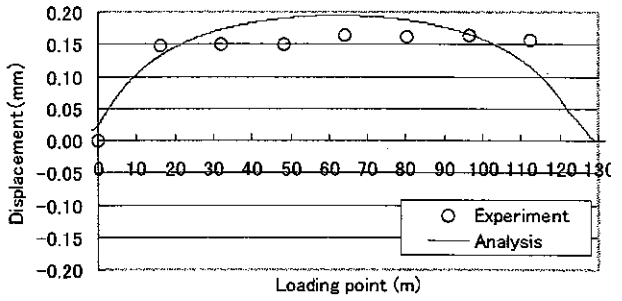

(b) Movable shoe point

Fig.-5　Results of the static experiment and analysis

4. 解析概要

実測では把握できない振動モード形状を解析上で把握するために，3 次元の解析モデルを作成した．解析モデル図を Fig.-4 に示す．解析モデルは，床版および縦桁のウェブをシェル要素にモデル化し，それ以外の部材は，梁部材としてモデル化した．地覆は重量のみ考慮した．支承部の橋軸方向は，微小振幅時では摩擦力による拘束が大きいので，ここではばね部材としてモデル化した．

本研究では，この解析モデルを用いて静的解析を行い静的載荷実験の結果と比較することにより，解析モデルで用いた剛性の確認を行った．また，サブスペース法を用いて固有値解析を行い，実験によって得られた卓越振動数や振動モードとの比較を行った．

5. 実験・解析結果

5. 1　静的特性

試験車両の後輪 2 軸中心を橋梁支間の 1/8 点ずつ移動載荷したときの実験と解析の結果を Fig.-5 に示す．

Fig.-5(a)および Fig.-5(b)は，それぞれ支間 1/4 点の鉛直変位および A1 可動支承の橋軸方向変位を示している．設計上可動となっている支承の拘束条件として，解析では微小振幅時であること考慮して，摩擦によるばね支持として，橋軸方向のばね部材（ばね定数 5.0E5kN/m）でモデル化した．

Fig.-5(a)より，支間 1/4 点は，測定点に車両が載荷された時にその最大値を示しており，大型車両 1 台の載荷により鉛直変位は，実験，解析上ではともに約 6～6.5mm 程度下方向に変位している．また，支間 1/4 点載荷では，逆対称変形しており，車両が 3/4 点に載荷すると上方向に変位している．

Fig.-5(b)に示した A1 可動支承の橋軸方向変位は，約 0.2mm 程度変位しており，解析では概ねばね部材でモデル化できている．

以上より，実験値と解析値は概ね一致した値を示しており，解析モデルの剛性評価の妥当性を確認できた．

5. 2 振動特性

(1) 卓越振動数

補修前後に行った実験より得られた卓越振動数とモード減衰定数を Table-2 に示す．また，解析より得られた固有振動数を同表に付記するとともに，解析により得られた固有振動モード図を Fig.-6 に示す．

対象橋梁においては，車両の前後輪のばね上振動数領域（1～3Hz 前後）に数多くの卓越振動数が存在していることがわかる．特に，鉛直方向振動において，3 次のたわみ逆対称 1 次振動と 5 次のたわみ対称 1 次振動および 8 次のたわみ逆対称 2 次振動と 10 次のねじれ振動が近接して卓越し，うなり現象が生じていた．

また，面外方向の振動モード（1, 2, 4, 7, 9, 10 次）は，鉛直方向の振動モードと近接して存在している．8 次のたわみ逆対称 2 次振動は，車両の後輪ばね上振動数領域（3Hz 付近）に卓越しており，10 次のねじれ振動と共に，車両走行時の卓越が顕著であった．

解析では，可動支承部の拘束条件を可動とした場合と微小振幅時の摩擦による拘束を考慮して固定とした場合，およびばね部材とした場合（実験値の支承部の橋軸方向変位に一致するようにばね定数を決めた）の 3 つの結果を示した．

これより，支承の拘束条件を可動から固定とした場合，面内最低次振動が対称 1 次振動から逆対称 1 次振動へと変化している [5]．実際の卓越においても面内最低次振動は，逆対称 1 次振動であることから設計どおりの拘束条件になっていないことがわかる．

(2) モード減衰

補修前後に行った実験より得られたモード減衰定数を Table-2 に付記した．減衰定数を範囲で記述している部分は，加振ケース（加振振幅）による振幅依存性の影響がでていたものと考えられる．減衰定数の算出には，ERA[6] を用いた．100Hz サンプリングのデータから 3000 個用いてハンケル行列を作成し，その行と列のサイズを 3：1 とした．特異値分解後の採用次数は 32 とした．

大型車両が退去した後の振動が長く続いていたことからも，対象橋梁では全体的に減衰定数が小さい．また，その減衰特性を Fig.-7 に示した全振動エネルギーに対する各部材のひずみエネルギー比 [5] から考察する．

3 次のたわみ逆対称 1 次振動においては，ストランドのひずみエネルギー比が 76%占めており，減衰が小さいことと関係している [5] と考えられる．また，5 次のたわみ対称 1 次振動では，低次の面内振動で唯一支承による寄与が大きく，摩擦力に起因した構造減衰の寄与が大きい [7]．対称振動では，摩擦力に起因した構造減衰の寄与が大きいことから，本橋の場合でも 5 次，6 次振動において振幅依存性が見られる．

面外振動においては，上弦材やストラット部材などの鋼材の寄与が大きいが，4 次の上弦材面外 2 次振動や 7 次の上弦材面外 3 次振動では，減衰が小さい．

Table-2 Vibration Characteristics

Mode	Frequency(Hz)					Damping ratio(%)	
	Analysis			Experiment		Experiment	
	Move	Spring	Fix	Before	After	Before	After
1	1.12	1.27	1.41	1.17	1.18	0.7～1.3	0.7～1.3
2	1.37	1.37	1.37	1.56	1.56	0.5～0.7	0.5～0.7
3	1.62	1.62	1.62	1.59	1.59	0.2	0.2～0.3
4	1.74	1.75	1.77	1.92	1.91	0.1	0.1
5	1.50	1.76	1.85	1.69	1.70	0.2～0.4	0.2～0.4
6	2.27	2.30	2.32	2.39	2.38	0.4～0.7	0.4～0.7
7	2.53	2.53	2.53	2.67	2.67	0.1	0.1
8	3.06	3.07	3.07	3.05	3.04	0.2～0.3	0.2
9	3.29	3.37	3.47	3.63	3.64	0.3	0.1～0.2
10	3.49	3.49	3.51	3.40	3.40	0.2～0.3	0.2

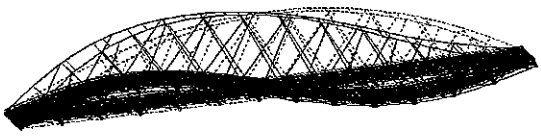

(a) 3 mode : Asymmetry 1st mode

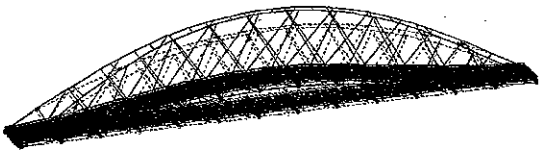

(b) 5 mode : Symmetry 1st mode

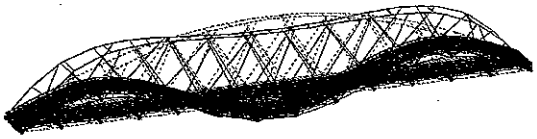

(c) 6 mode : Symmetry 2nd mode

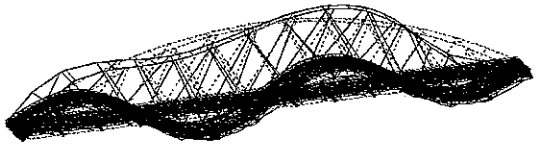

(d) 8 mode : Asymmetry 2nd mode

Fig.-6 The mode shapes of the Aimoto Bridge

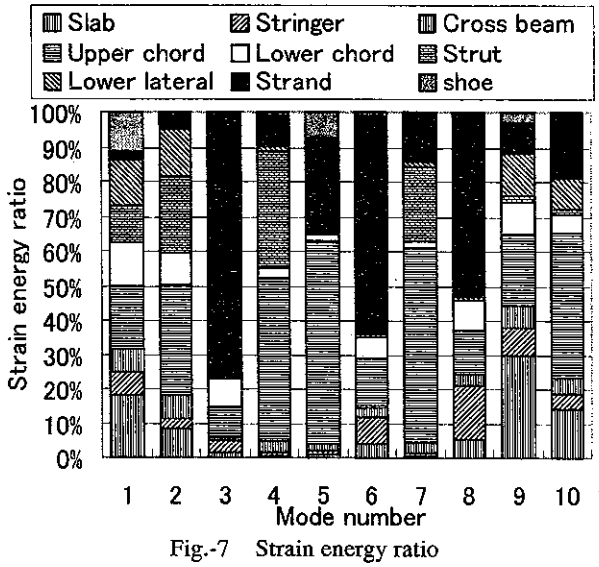

Fig.-7 Strain energy ratio

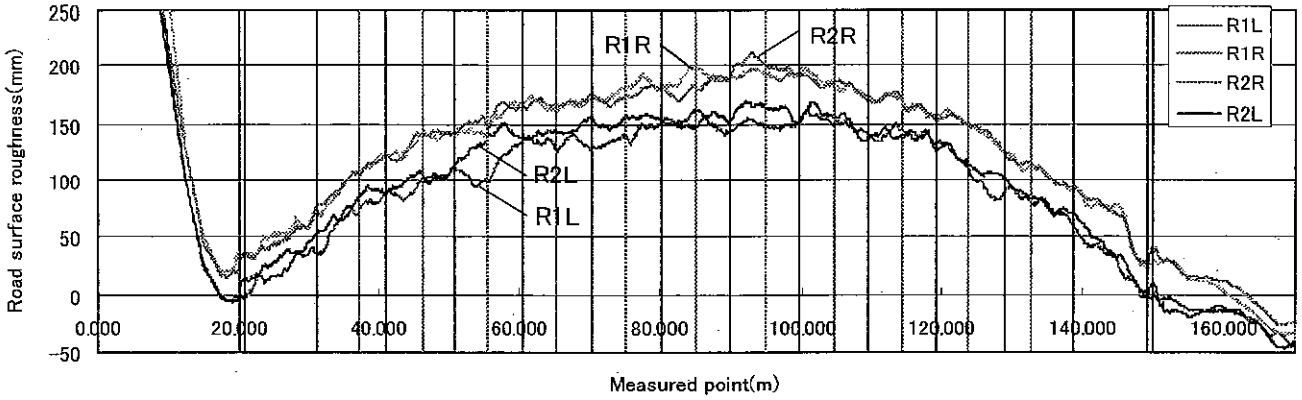

(a) Before improvement

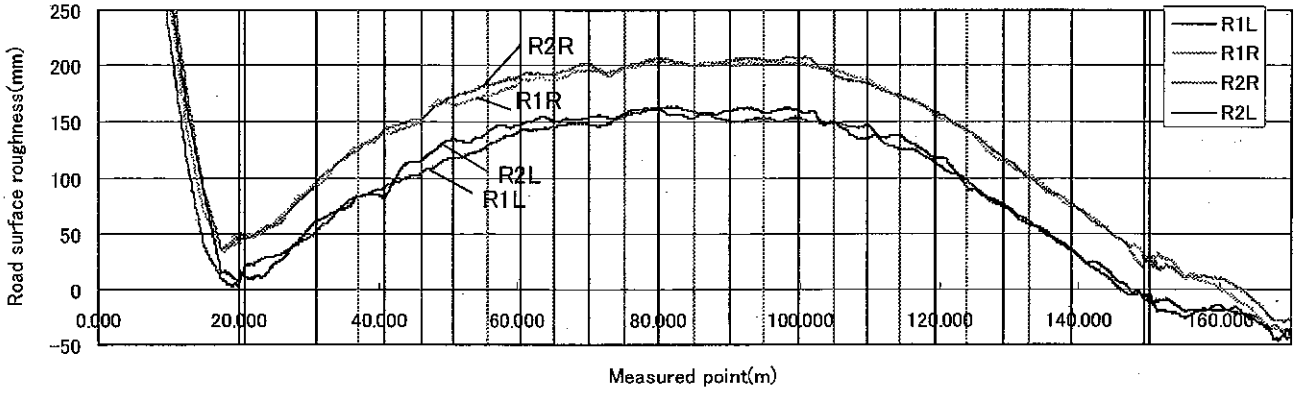

(b) After improvement

Fig.-8 Road surface roughness

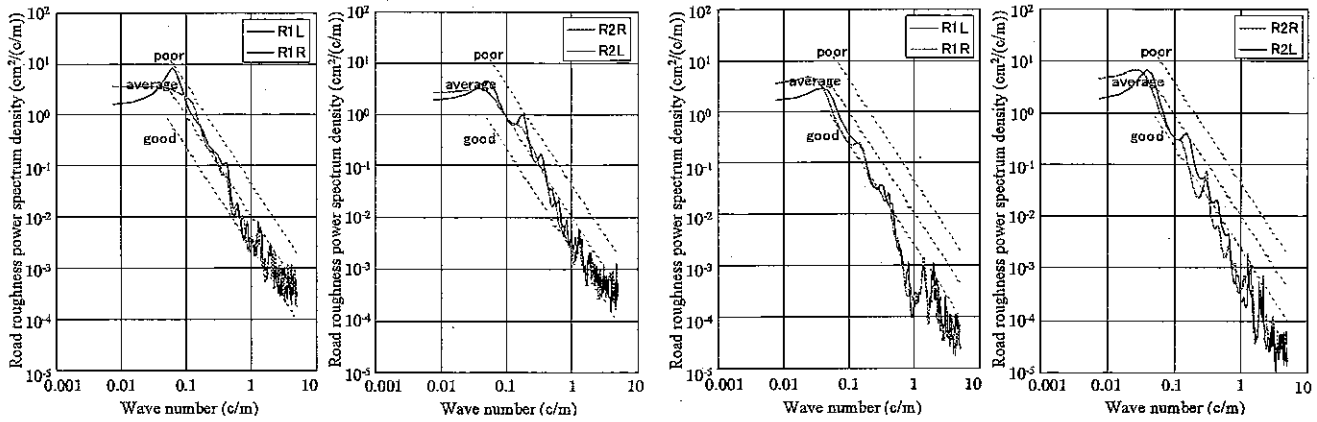

(a-1)Before improvement (R1) (a-2)Before improvement (R2) (b-1)After improvement (R1) (b-2)After improvement (R2)

Fig.-9 Road roughness power spectrum density by MEM

5. 3 路面凹凸性状

対象橋梁の路面凹凸性状を把握するために，3m プロフィルメータを用いて各車線の左右車輪位置（Fig.-2 参照）における路面凹凸を計測した．計測した凹凸データは，0.1m 間隔でサンプリングした．3m 以上の周期を有する路面凹凸については水準測量により計測した．水準測量の計測間隔は，3m 以内になるように，土工部では 2.5m 間隔，橋梁部ではそれぞれの横桁間隔を 4 等分した距離とした．計測距離は，取付け 20m の土工部（A1 側と A2 側）と橋梁部 130m の計 170m である．

水準測量による凹凸データと 3m プロフィルメータにより計測した凹凸データを合成したものを Fig.-8 に示す．同図では，路面改良前後における各車線の左右車輪位置での路面凹凸を示している．左側が A1 側となっており，橋梁部は 20m～150m である．さらに，Fig.-8 の凹凸波形に対して MEM による路面凹凸パワースペクトル密度を算出して Fig.-9 に示す．また，同図には，ISO による評価基準（悪：poor，普通：average，良：good）を付記した．

(1) 補修前

対象橋梁は，厚さ 5cm のコンクリート舗装であるが，架設以来，補修は一度も行われていない．Fig.-8(a)より，補修前では，片振幅の最大で 10mm の路面凹凸がある上に，

Table-3　Loading Frequency

Wave number(c/m)	Wavelength (m)	Frequency(Hz)		
		40km/h	50km/h	60km/h
0.35～0.42	2.4～2.9	3.8～4.6	4.8～5.8	5.7～6.9
0.19	5.3	2.11	2.64	3.17
0.13	7.7	1.44	1.81	2.17
0.0615	16.3	0.68	0.85	1.02

Table-4　σ and IRI

		Lower side		Upper side	
		Left	Right	Right	Left
σ (mm)	Before	2.98	2.62	2.47	2.62
	After	0.94	1.11	1.08	1.38
IRI (m/km)	Before	5.04	4.11	3.98	4.36
	After	1.61	1.67	1.49	2.29

凹凸の起伏が大きい．これらをMEMによるスペクトルから考察すると，上流側車線(R1)，下流側車線(R2)ともに0.35～0.42c/m（2.4～2.9m）に卓越が見られ，ISO基準の“普通”と“悪”の間にある．下流側車線(R2)の左車輪位置では，0.19c/m（5.3m）に“悪”に達する卓越が見られる．また，上流側車線(R1)の右車輪位置では，0.13c/m（7.7m）付近の凹凸が，左車輪位置では，0.0615c/m（16.3m）付近の凹凸が“悪”付近に卓越し，長周期成分が悪い評価となった．これに対して，走行速度をパラメータとして加振振動数を算出し，Table-3にまとめた．これは，あくまでも車両長を考慮しない車両が移動した場合の結果であり，厳密な加振振動数とはいえないが，凹凸波長5.3～16.3mを有する凹凸では，車両が40～60km/hで走行すると，約1Hz～3Hzで加振されることになる．

路面凹凸のパワースペクトル密度とISO基準との比較以外に標準偏差σ[8]と国際ラフネス指数IRI[9)10)]による評価を行い，Table-4にまとめた．

標準偏差については，道路維持修繕要綱に維持修繕要否判断の目標値が記されており，交通量の多い一般道路においては3mプロフィルメーターで得られた測定値を1.5m間隔で読み取った値の標準偏差で4.0～5.0を目標値としている．それに対して，対象橋梁の値は目標値以内となっており，修繕の必要性がないと判断される．

また，国際ラフネス指数では，約4～5の範囲であり，“古い舗装，表面の損傷”と評価された．

(2) 補修内容

橋梁振動の分析から明らかとなった車両振動数領域に存在している卓越振動数や減衰特性を変化させる構造的な補修は費用の面から見ても容易ではない．加振源となっている車両振動に寄与している路面は，少なくとも車両振動および橋梁振動を増幅させていることは明らかである．そのため，補修内容として，厚さ5cmのコンクリート舗装を切削し，厚さ5cmのアスファルト舗装へと打ち換えることになった．

(3) 補修後

補修後の路面凹凸波形をFig.-8(b)に示す．また，その波形に対するパワースペクトル密度をFig.-9(b)に示す．これより，補修前と同様に，下流側車線(R2)の左車輪位置では，0.16c/m(6.25m)，右車輪位置では0.3c/m(3.3m)に“普通”に達する卓越が見られる．また，上流側車線(R1)では左右車輪位置ともに0.15c/m(6.7m)付近と0.3～0.4c/m（2.5m～3.3m）付近の凹凸が，“普通”と“良”の間に卓越している．これらの卓越は，補修前より卓越エネルギーは小さくなっているため影響は小さいものと考えられる．

また，Table-4より，補修前と同様にIRIとσを比較すると，補修後は，どちらも半分以下に低減している．IRI値は，“新しい舗装”と評価された．

5．4　車両走行による動的応答

対象橋梁では，車両がこの橋梁上を走行した際に，幅員両脇にある歩道上において比較的大きな振動が生じていた．ここでは，路面補修前後における車両と橋梁の振動に着目する．

橋梁の振動として，試験車両が下流側車線（A1側からA2側方向へ走行）を走行速度60km/hで走行した時の測点V1(Fig.-1参照)の速度波形とそのスペクトルをFig.-10とFig.-11に示す．

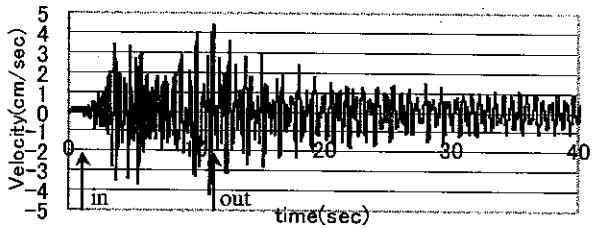

(a) Before improvement

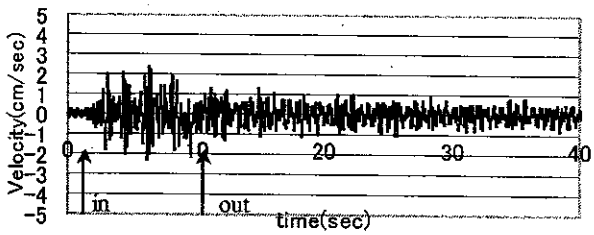

(b) After improvement

Fig.-10　The velocity response of the bridge

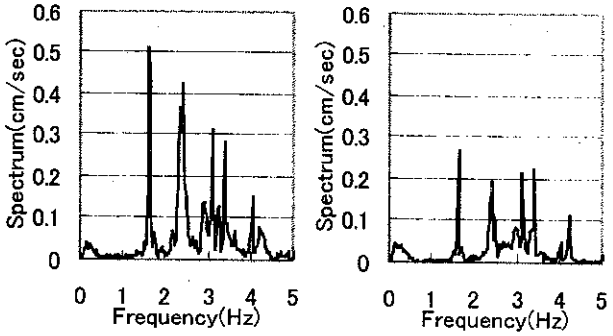

(a) Before improvement　(b) After improvement

Fig.-11　The velocity spectrum of the bridge

また，上述した走行ケースにおける車両側の応答として，後輪ばね上の加速度波形とそのスペクトルを Fig.-12 と Fig.-13 に示す．スペクトルは，車両が橋梁上を走行している 1024 データとした．

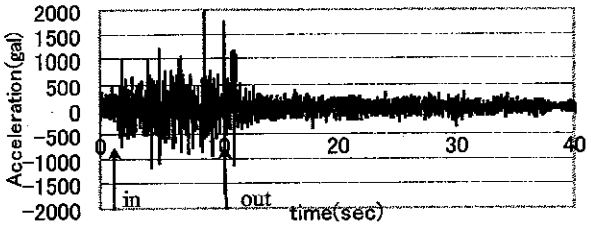

(a) Before improvement

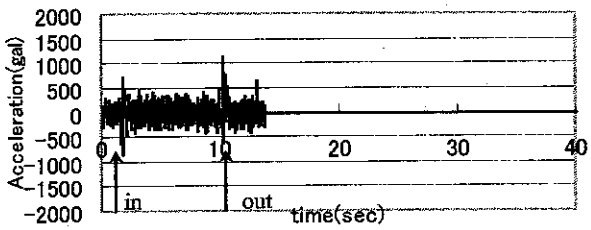

(b) After improvement

Fig.-12 The acceleration response of the test vehicle

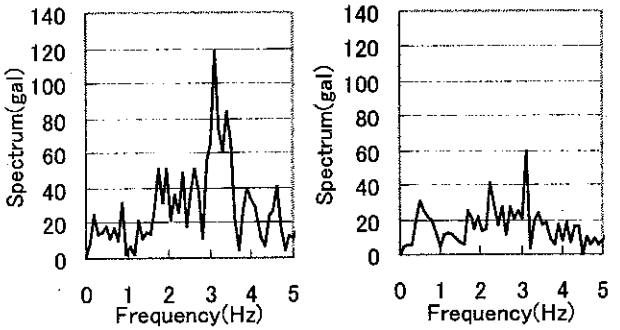

(a) Before improvement (b) After improvement

Fig.-13 The acceleration spectrum of the test vehicle

Fig.-10 および Fig.-11 より，補修前に大きく卓越していた逆対称 1 次振動（1.6Hz）と対称 2 次振動（2.4Hz）は，補修後には約半分に低減している．これは，補修によって，この振動数領域の車両による加振力が減少したためと考えられる．

車両の応答は，橋梁との連成振動も含まれた波形であるため，路面-車両による車両振動の影響だけを述べるのは困難であるが，Fig.-12 に示した後輪ばね上の加速度波形からは，明らかに低減していることがわかる．また，Fig.-13 より，それらの低減した振動数領域は，ばね上振動数 3.1Hz を含め，2Hz 付近の卓越も小さくなっている．補修後では，依然として伸縮継手部の段差は解消されていないため，車両が橋梁に進入および退去する時に大きな応答を示しており，この段差を適切に処理することによりさらに小さな応答を得ることができると考えられる．

5. 5 振動使用性

大型車両が対象橋梁上を走行した際に，幅員両脇にある歩道上において比較的大きな振動が生じ，使用性が問題となっていた．そこで，試験車両が対象橋梁上を走行した時の振動速度波形から，振動速度の実効値を算出した．実効値の算出は，時定数 0.63 秒ごとの 2 乗平均値の平方根より求めた．その実効値の最大値を用いて振動使用性の検討を行う．各走行ケースにおける実効値の最大値を Table-5 に示す．各走行ケースは 2 回ずつ行っており，同表ではその平均値を示している．

既往の研究[11)-13)]より，196kN 車両 1 台の走行に伴う振動において，応答速度の実効値は，1.7cm/sec 以下が望ましいとされている．本研究においても，怨限度を 1.7cm/sec として振動使用性について検討する．

Table-5 Root Mean Square of the responses velocity

(a) Before improvement

Vehicle velocity	running direction	Max value of the Root mean square (cm/sec)									
		V1	V2	V3	V4	V5	V6	V7	V8	V9	V10
Slow	upper side	1.30	1.63	1.52	0.66	1.52	1.41	1.55	1.30	1.24	1.30
	lower side	1.27	1.45	1.27	0.81	1.18	1.05	1.30	1.14	1.12	1.29
40km/h	upper side	1.74	1.86	1.78	1.71	1.65	1.58	1.51	1.76	0.87	0.80
	lower side	1.70	1.47	1.61	1.97	1.79	1.63	1.55	1.65	1.08	1.01
50km/h	upper side	2.20	2.04	2.26	1.79	2.00	2.09	2.05	3.08	1.00	1.13
	lower side	2.34	2.06	2.29	2.48	1.93	2.12	1.85	2.50	0.96	1.21
60km/h	upper side	2.04	1.68	2.02	2.14	1.66	2.03	2.08	2.18	0.84	1.18
	lower side	2.30	2.31	2.55	2.69	1.75	2.39	1.82	2.15	1.05	1.27

(b) After improvement

Vehicle velocity	running direction	Max value of the Root mean square (cm/sec)									
		V1	V2	V3	V4	V5	V6	V7	V8	V9	V10
Slow	upper side	0.48	0.68	0.65	0.62	0.94	0.64	0.60	0.56	0.13	0.17
	lower side	0.30	0.25	0.31	0.32	0.69	0.28	0.29	0.26	0.18	0.16
40km/h	upper side	1.23	1.26	1.17	1.19	1.48	1.25	1.18	1.52	0.21	0.19
	lower side	1.26	1.16	1.20	0.94	1.04	0.96	0.95	1.46	0.21	0.27
50km/h	upper side	1.27	1.33	1.38	1.32	1.25	1.63	1.58	1.54	0.27	0.26
	lower side	1.65	1.12	1.35	1.13	1.01	1.42	0.97	1.36	0.22	0.28
60km/h	upper side	1.14	1.12	1.05	1.20	0.94	1.32	1.15	1.72	0.19	0.20
	lower side	1.41	0.94	0.94	1.06	1.25	1.08	1.05	1.21	0.22	0.27

これより，走行速度 40km/h 以上では，1.7cm/sec を超える測点が多数あり，大きな振動が生じていることがわかる．特に，7/8 点（V8）では，50km/h 走行時に実効値で約 3cm/sec，最大値で 5cm/sec 弱もの大きな振動が生じていた．大型車両が走行した際の卓越振動モードは Fig.-6 に挙げたものが主に卓越したが，支間 7/8 点および 1/8 点では，いずれが卓越しても節にならない上に，ジョイントからの衝撃力も受けやすい．さらには，たわみ逆対称 2 次振動数は大型車両のばね上振動数と近いこともからも大きな振動が生じたものと考えられる．

これに対して，補修後の値を見ると，60km/h 走行の V8 測点で 1.7cm/sec を超えただけであった．40～60km/h 走行時の面内方向の測点では，1～6 割減少しており，路面の改善だけで使用性がかなり改善された．

6. まとめ

本研究では，ニールセンローゼ桁橋である愛本橋において，大型車両がこの橋梁上を走行した際に，幅員両脇にある歩道上において比較的大きな振動が生じ，使用性が問題となっていた．そこで，その要因を分析するために，路面，車両および橋梁，各々に着目して路面凹凸の計測，車両振動および橋梁振動実験を行った．結果的に，路面性状を改善するという対策を講じた．路面改善後においても対策前と同様な実験を行い，歩道部における振動使用性がどれだけ改善されたのか検討した．

本研究により得られた知見を以下に示す．

(1)静的荷重に対する対象橋梁の鉛直変位は，実験値と解析値を比較すると概ね一致した値を示していた．これより，本研究で用いた解析モデルの妥当性が示された．

(2)卓越振動数は，車両の前後輪ばね上振動領域(1～3Hz)に数多く存在していた．また，解析上で支承の拘束条件を可動から固定とした場合，面内最低次振動が対称 1 次振動から逆対称 1 次振動へと変化しており，実際の卓越においても面内最低次振動は，逆対称 1 次振動であることから設計どおりの拘束条件になっていなかった．

(3)3 次のたわみ逆対称 1 次振動においては，ストランドのひずみエネルギー比が 76%占めており，減衰が小さいことと関係していると考えられる．対称振動では，摩擦力に起因した構造減衰の寄与が大きいことから，本橋の場合でも 5 次，6 次振動において振幅依存性が見られた．

(4)補修前の路面凹凸計測から，凹凸波長 5.3m，7.7m および 16.3m が，ISO 基準の“悪”付近に卓越おり，この長周期成分が車両振動や橋梁振動を増幅させていた．補修後には，依然として長周期成分の卓越が見られたが，それらの卓越は小さく，車両振動や橋梁振動に与える影響は小さかった．

(5)補修前に車両が走行した際の速度応答は，提案されている恕限度 1.7cm/sec を超える測点が多かった．しかし，路面補修により，その値を超える測点がほとんどなくなり，振動使用性はかなり改善された．

参考文献

1) 本田秀行，梶川康男，小堀為雄：道路橋の伸縮装置部の凹凸性状，土木学会論文報告集，第 324 号，pp. 173～176，1982. 8.
2) 徳永法夫，西村昴，薄井王尚：伸縮継手近傍の路面段差が地盤振動に与える影響とその改善対策の検討，環境技術，Vol. 27，No. 7，pp. 501-509，1998. 7.
3) 米田昌弘，徳永法夫：路面上の緩やかな段差によって誘起される橋梁交通振動に対する解析的考察，鋼構造論文集，Vol. 7，No. 25，pp. 79-87，2000. 3.
4) 讃岐康博，梶川康男，深田宰史，枚本正信：プロフィルメータでの測定路面から実路面への近似法の提案，構造工学論文集，Vol. 47A，pp. 399-410，2001. 3.
5) 米田昌弘：ニールセン型ローゼ桁橋の構造減衰特性に及ぼす吊材の影響，土木学会論文集，No. 651/IV-47，pp. 157～162，2000. 6.
6) Juang,J.N. and Pappa,R.S.: An Eigensystem Realization Algorithm for Modal Parameter Identification and Model Reduction, Journal of Guidance, Vol.8, No.5, pp.620-627, Sept.- Oct., 1985.
7) 米田昌弘：橋梁の可動支承部における摩擦力に起因した構造減衰特性に関する 2，3 の考察，土木学会論文集，No. 492/IV-23，pp. 137～145，1994. 6.
8) 日本道路協会：道路維持修繕要綱，1978. 7.
9) （著）Sayers, M. W.，（訳）笠原篤，関口幹夫，加藤昌太郎：道路縦断プロファイルからの IRI の算出（上），舗装，Vol. 31，No. 7，pp. 21-27，1996. 7.
10) （著）Sayers, M. W.，（訳）笠原篤，関口幹夫，加藤昌太郎：道路縦断プロファイルからの IRI の算出（下），舗装，Vol. 31，No. 8，pp. 12-17，1996. 8.
11) 小堀為雄，梶川康男：橋梁振動の人間工学的評価法，土木学会論文報告集，第 230 号，pp. 23～31，1974. 10.
12) 川谷充郎，下村和也，野寄一郎，山口史夫，矢幡武人，小林義和：広幅員単弦ローゼ桁橋の走行荷重下の振動使用性実験，橋梁振動コロキウム’97 論文集，pp. 285-292，1997. 10.
13) 松本信之：橋梁の使用性評価，橋梁振動コロキウム’97 論文集，pp. 19-34，1997. 10.

(2003. 7. 31 受付)

遺伝的アルゴリズムを適用した橋梁交通荷重の推定法

A Fundamental Study on Traffic Load Monitoring System using Genetic Algorithm on Highway Bridges

米田昌弘*，枝元勝哉**
Masahiro YONEDA*，Katsuya EDAMOTO**

＊ 工博　近畿大学教授　理工学部社会環境工学科　（〒577-8502 東大阪市小若江 3-4-1）
＊＊ 博士（工学）　川田工業株式会社技術開発室 室長　（〒321-3325 栃木県芳賀郡芳賀町芳賀台 122-1）

Heavy traffics cause fatigue damages in members of bridge. For rational maintenance of bridge structures, it is necessary to know the frequency of trucks and their weight. This paper describes a new monitoring system using genetic algorithm (GA) to estimate gross weight of truck passing on bridges in service. The simulation analyses based on the genetic algorithm are performed for various types of truck model passing on highway bridges. Based on these results, it was found that the new method based on genetic algorithm could be acceptable for identification of gross weight of truck passing on highway bridges in service.

Key Words : maintenance, genetic algorithm, monitoring system, identification
キーワード：維持管理，遺伝的アルゴリズム，モニタリングシステム，同定

1．まえがき

建設事業をとりまく社会経済情勢が大きく変化する中で，建設市場もかつてないほどの大きな構造変化に直面している．公共工事に対するコスト縮減は社会的に大きな要請となっており，新規事業に対してはこれまでのような右肩上がりの増加を見込むことはできない．しかしながら一方で，コスト縮減の状況下にあっても，これまでに蓄積された膨大な社会資本を正しく機能させるためには，今までにもまして適正な維持管理が必要である．

ところで，交通量の増加と車両の大型化は，環境振動問題のみならず，活荷重応力も大幅に増大させることから，平成 5 年 11 月には活荷重応力の低減を目的として設計荷重が B 活荷重（TL-25）に変更された．しかしながら，総重量 245kN（=25tonf）以上の過積載車が橋梁上を通行する場合も多く，橋梁交通荷重を正しく把握することは，橋梁構造物を維持管理する上できわめて重要な作業であると強く認識されている．橋梁交通荷重を推定する技術として，橋梁上を走行する車両によって生じる橋梁部材の応答値から車両荷重を推定するシステム“Bridge Weigh-in-Motion（BWIM）”が知られている．BWIM は米国で道路橋の疲労損傷が問題になり始めたのを契機に Moses[1] によって提案されたものであり，わが国でも Moses の手法を基本とした西川ら[2] の研究や三木ら[3] の研究，コンクリート床版のひび割れを用いる松井らの研究[4]，小塩・山田らの研究[5]～[7] など，数多くの研究者によってそれぞれ有用な手法が提示されている．

これらの手法の中でも，橋梁の縦リブに貼付したひずみゲージの応答波形から，橋梁交通荷重を推定する小塩・山田らの計測システムはすでに実在橋梁にも適用されており，一連の研究成果は高く評価されている．しかしながら，小塩・山田らの手法は縦リブにひずみゲージを貼付することから，その適用は縦リブを有する橋梁に限定される．一方，鋼 I 桁橋は施工の省力化や工費の節減をはかるため，従来の多主桁形式から少数主桁形式へと移り変わりつつあるが，少数主桁橋（合理化橋）では縦リブが存在しないことから，小塩・山田らの手法では橋梁交通荷重を推定できない．

このような状況のもと，縦リブが存在しない少数主桁橋にも適用できる，簡便で実用性の高い橋梁交通荷重を計測できるシステムの開発が実務技術者から強く望まれていた．そこで，著者らは，GA（遺伝的アルゴリズム）を適用して，少数主桁橋にも適用できる，従来よりも簡易で経済的な橋梁交通荷重の推定法を提案し，実用化に向けた基礎的な研究をすでに実施している[8]．ところで，たとえどのような手法であっても

橋梁交通荷重を推定する際にはキャリブレーション値（実測値と解析値の比を表す補正係数）が必要であり，従来は対象橋梁に対して交通止めを実施し，諸元の明確な試験車両を橋梁上に停車させて静的変位や静的ひずみを計測する必要があった．また，実際，著者らの先の論文でも，事前に静的載荷試験を行うものとし，キャリブレーション値は既知であるとしていた．しかしながら，交通止めを実施するためには特別な許可が必要であり，変位計の設置やひずみゲージの貼付は一般に煩雑な作業をともなう．これに対し，GA（遺伝的アルゴリズム）を適用する手法では，一般車両の通行が途絶えた時に，試験車両を一定速度で走行させればキャリブレーション値を算出できる可能性があると予想される．そこで，本研究では，車両諸元が既知の大型車両を走行させた場合の動的応答量を計測し，GA を適用してキャリブレーション値を算出する手法について検討することとした．その結果，交通止めをともなう静的載荷試験を実施しなくても，GA を適用すれば，キャリブレーション値を容易に算出できるとの知見が得られた．

文献 8)にも報告したように，GA を適用すれば，特別な装置を利用しなくとも車両速度を算出でき，車両の総重量や等価軸距も十分な精度で推定できる可能性がある．それゆえ，キャリブレーション値の算出方法も含め，GA を適用する有用性と簡便性を十分に提示できたと考えられることから，本論文で GA を用いた橋梁交通荷重の推定方法を総括することとする．なお，実際の橋梁では過積載車が併走する走行状態もあり得るが，一般的には単独走行する場合が最も多いことが知られている．それゆえ，本研究では，単純桁橋梁上を 1 台の車両が走行する場合を対象として GA の適用性を検討することとした．

2．遺伝的アルゴリズムを適用した推定法

(1) 提案した手法の概要

遺伝的アルゴリズムとは，生物の進化の過程で起こる自然淘汰，交叉，突然変異などの遺伝的仕組みを模擬した手順のことで，具体的には，仮想生物（個体）を想定し，コンピュータ内でその遺伝子（染色体）を 0 と 1 の 2 進数列で表示する．そして，遺伝的仕組みを模擬したプログラムで仮想生物（個体）を何世代にもわたって進化させ，環境に最も適合する個体を探索し，その遺伝子（染色体）から最適解を求めようとするものである．

遺伝的アルゴリズムを適用して橋梁交通荷重を推定する場合，軸重と軸間距離（たとえば，2 軸車であれば，前輪と後輪の軸重 P_1，P_2 および軸間距離 a_{12}）から構成された一つの個体が環境に適合する程度（a_{12}

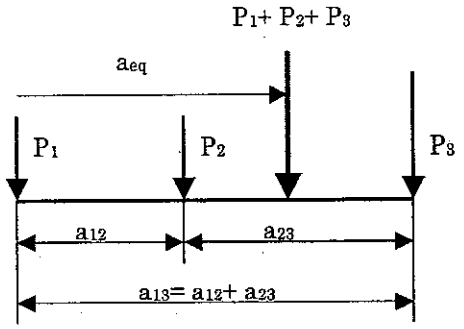

Fig.1 Equivalent axle distance

だけ離れた軸重 P_1，P_2 によって生じる応答の解析値と実測値が一致する程度）は，次式で定義した目的関数 J_{GA} の逆数（適応度関数）で評価される．

$$J_{GA} = \sum_{i=1}^{n} \left| CAL \times R_{c,i} / R_{m,i} - 1.0 \right| \tag{1}$$

ここに，CAL はキャリブレーション値，$R_{c,i}$ は解析値，$R_{m,i}$ は計測された応答，n は GA で利用する計測データの個数である．なお，解析値はマトリックス構造解析を実施しなくても，コンピュータ内で影響線解析を実施すれば容易に算出することができる．

(2) 推定する車両諸元

橋梁上にはトラック類のみならずセミトレーラーなど様々な軸数を有する重交通車両が走行する．GA を適用してそれぞれの軸重と軸間距離を推定した場合，総重量は非常に高い精度で推定できるものの，個々の軸重を正しく推定するのは困難である[8]．これは，計測値を満足する軸重と軸間距離の組み合わせが幾つも存在するためである．それゆえ，GA を適用して橋梁交通荷重を推定する場合には，個々の軸重と軸距から算定した等価軸距を評価指標として採用する必要がある．ここに，等価軸距とは，Fig.1 に示すように，荷重列を一つの集中荷重に置換した場合の作用位置（前輪から測った軸距）である．したがって，Fig.1 中に記した記号を用いれば，3 軸車の等価軸距 a_{eq} は次式で算定される．

$$a_{eq} = \frac{P_2 \times a_{12} + P_3 \times a_{13}}{P_1 + P_2 + P_3} \tag{2}$$

参考までに，本研究で対象とした TYPE-1～TYPE-6 車両を Fig.2 に示す．また，TYPE-1～TYPE-6 の軸重，軸距，総重量および等価軸距を Table 1 にまとめる．なお，等価軸距と総重量が正しく算出されれば，大型車両のカタログ値などと照合することによって車種の特定は可能であると考えられる．

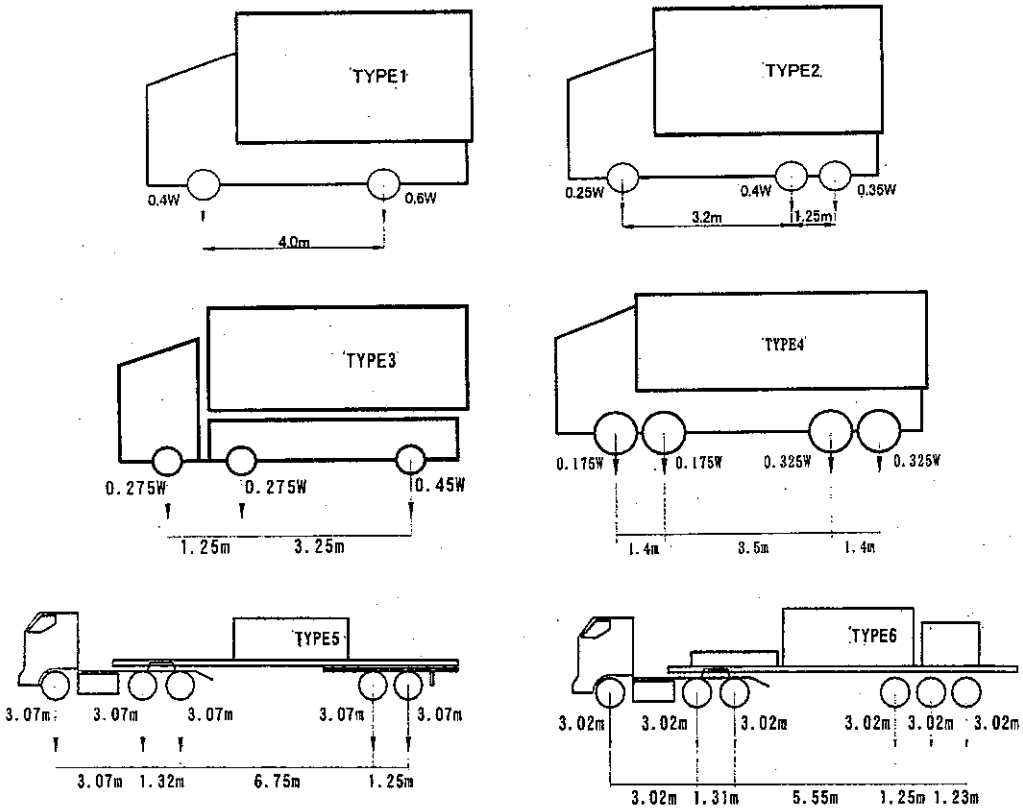

Fig2. Various types of truck

Table 1 Dimensions of various types of truck

(a) Axle weight and gross weight

Truck model	Axle weight (kN)						Gross weight (kN)
	P_1	P_2	P_3	P_4	P_5	P_6	
TYPE-1	98.000	147.000	–	–	–	–	245.000
TYPE-2	61.250	98.000	85.750	–	–	–	245.000
TYPE-3	67.375	67.375	110.250	–	–	–	245.000
TYPE-4	42.875	42.875	79.625	79.625	–	–	245.000
TYPE-5	69.874	90.542	91.708	119.952	117.915	–	490.000
TYPE-6	60.368	83.378	82.467	92.257	94.306	77.224	490.000

(b) Axle distance and equivalent axle distance a_{eq}

Truck model	Axle distance (m)					a_{eq} (m)
	a_{12}	a_{13}	a_{14}	a_{15}	a_{16}	
TYPE-1	4.000	–	–	–	–	2.400
TYPE-2	3.200	4.450	–	–	–	2.837
TYPE-3	1.250	4.500	–	–	–	2.369
TYPE-4	1.400	4.900	6.300	–	–	3.885
TYPE-5	3.070	4.390	11.140	12.390	–	7.098
TYPE-6	3.020	4.330	9.880	11.130	12.360	7.193

(3) キャリブレーション値の算出

一般に，実橋における実際の剛性は解析で用いる剛性よりも大きく，計測値は解析値よりも幾分小さな値を呈する場合が多いことが知られている．それゆえ，どのような手法を適用する場合にも，事前にキャリブレーション値（補正係数）CAL を算定する必要がある．

従来の手法では，対象橋梁に対して交通止めを実施し，諸元の明確な試験車両を橋梁上に停車させて静的変位や静的ひずみを計測する必要があった．しかしながら，交通止めを実施するためには特別な許可が必要であり，変位計の設置やひずみゲージの貼付は一般に煩雑な作業をともなう．

これに対し，具体的には 3 章で述べるように，GA を適用する手法では，一般車両の通行が途絶えた時に，諸元の明確な試験車両を一定速度で走行させれば容易にキャリブレーション値を算出でき，従来の手法と比べて事前の準備作業の観点からもきわめて有用な手法である．

(4) 走行位置と走行速度

説明を容易にするため，ここでは主桁間隔が 5.70m の 2 主桁橋があり，中央点の上流側と下流側に加速度計を設置したものとする．加速度計では加速度を計測することになるが，電気的に 2 回積分してフィルター処理すれば，車両走行にともなう静的変位を算定することができる．

もし仮に，車両が橋の幅員中央部を走行したとすれば，鉛直たわみ変形のみが生じ，ねじれ変形は生じることはない．これに対し，車両の走行位置が幅員中央部から離れるにしたがって，当然のことながら，鉛直たわみ成分に加え，ねじれ成分も生じることになる．参考までに，Fig.3 には橋の中央部および左右の主桁上（±2.85m の位置）を車両が走行した場合の桁中央点における静的最大変位を示す．この図から，車両の走行位置は上・下流側のピックアップから算出したねじれ角から容易に算定できることがわかる．したがって，キャリブレーション値を算出するための車両走行試験時に，車両走行位置とねじれ角の関係を把握しておけば，一般車両の走行位置を把握できると言える．また，Fig.3 において，左右の主桁上を車両が走行した場合にも，上・下流側のピックアップで計測した静的変位の平均値は橋の中央部を車両が走行した場合の値に等しくなっていることがわかる．このことは，式(1)中の $R_{c,i}$（解析値）は平面骨組構造モデルの影響線解析を実施すれば算定できることを意味している．

従来の手法で橋梁交通荷重を推定する場合，車両の走行速度が必要となる．GA を適用する手法でも車両の走行速度が必要となるが，車両の走行速度をパラメータとして GA を適用すれば，3 章で述べるように，

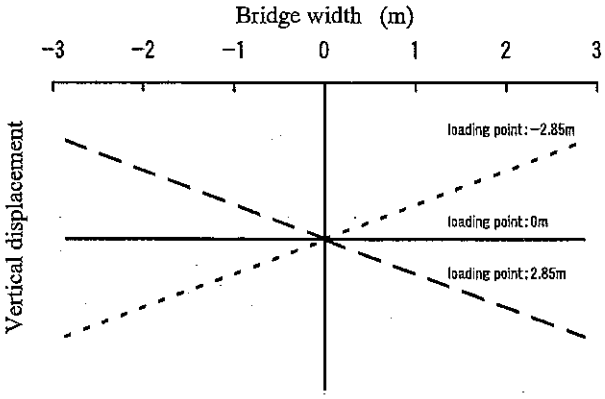

Fig.3 Relationship between loading point and vertical displacement

車両の走行速度を算出することができる．このことも，GA を適用する手法の大きな利点であり，橋梁交通荷重を推定する有用な手法であると考えている．

3．単純桁橋に対する数値計算例

(1) 2 軸車を用いたキャリブレーション値の算出

対象とした橋梁は，橋長が 50m で断面 2 次モーメントが I=1.388m⁴ の単純梁である．試験車として用いた車両は Fig.2 に示した TYPE-1 の 2 軸車両であり，前輪荷重 P_1，後輪荷重 P_2 および軸間距離 a_{12} はそれぞれ $P_1 = 49.000kN$，$P_2 = 196.000kN$，$a_{12} = 4.0m$ と正確に計測されたものと仮定する．この TYPE-1 車両（試験車両）を 60km/h の速度で走行させ，橋梁に進入してから退出するまでの鉛直変位を橋の中央点で計測する．応答波形には静的成分と動的成分が存在するが，フィルター処理や波形の平均化処理を施せば，Fig.4 に示すように静的成分のみを抽出することが可能である．

前輪荷重 P_1 が橋梁に進入してから t_1，t_2，t_3 秒後における静的変位成分の計測値を y_{1m}，y_{2m}，y_{3m}，解析値を y_{1c}，y_{2c}，y_{3c} とする．一般に，実橋の剛性は解析で用いる値よりも大きいことから，計測値は解析値よりも幾分小さな値を呈する場合が多い．したがって，キャリブレーション値（補正係数）を CAL と表示すれば，

$$\left.\begin{aligned} y_{1m} &= CAL \times y_{1c} \\ y_{2m} &= CAL \times y_{2c} \\ y_{3m} &= CAL \times y_{3c} \end{aligned}\right\} \qquad (3)$$

と表される．ここに，キャリブレーション値は以下の検討を実施して決定されるが，本章の解析ではキャリブレーション値の正解値を $CAL = 0.90$ と仮定する．

試験車両の走行速度を 60km/h に設定しても実際には幾分変化する．そこで，走行速度を 58km/h，59km/h，60km/h，61km/h，62km/h と仮定し，未知量であるキャリブレーション値を 0.8 から 1.2 まで変

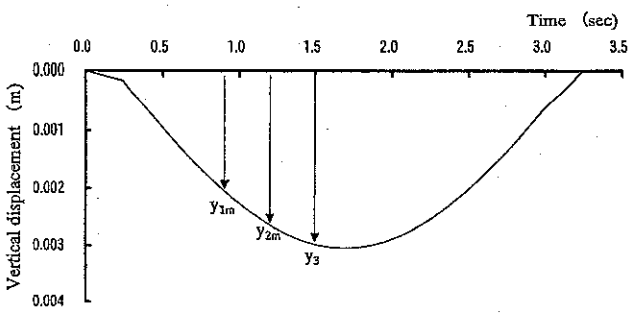

Fig.4 Static displacement during the passage of 2-axle truck

Table 2 Conditions for calibration for TYPE-1

Estimated values of a truck		P_1, P_2, a_{12}
Number of individual		2
Number of generation		1
Probability of crossover		0.50
Probability of mutation		0.03
Selection		Roulette rule
Variable range of estimated values	P_1	98.0kN
	P_2	147.0kN
	a_{12}	4.00 m

化させて，それぞれのキャリブレーション値に対応する適応度関数を求めることとした．なお，本ケースでは前輪荷重 $P_1(=49.000kN)$，後輪荷重 $P_2(=196.000kN)$，軸間距離 $a_{12}(=4.0m)$ が正確に計測されたものと仮定していることから，GA の適用にあたっては 2 軸車両を使用し，適用条件は Table 2 に示すように個体数を 2，世代数を 1 に設定している．走行速度が 58km/h，60km/h，62km/h の場合に得られたキャリブレーション値と適応度関数の関係を Fig.5～Fig.7 に示す．また，それぞれの走行速度に対応する適応度関数とキャリブレーション値を Table 3 にまとめる．これらの結果から，目標値である 60km/h で走行した場合には $CAL = 0.90$ と正しいキャリブレーション値が算出されていることがわかる．また，目標速度の 60km/h に対して実際の走行速度が 58km/h と 62km/h であってもそれぞれ $CAL = 0.92$，$CAL = 0.88$ のキャリブレーション値が算出されていることがわかる．

上の適用例では，試験車（TYPE-1 の 2 軸車両）の前輪荷重 P_1，後輪荷重 P_2 および軸間距離 a_{12} が正確に計測されたものと仮定していた．しかしながら，いくら厳密に計測しても，軸重や軸間距離には若干の計測誤差が含まれる可能性がある．そこで，前輪荷重 $P_1(=49.000kN)$，後輪荷重 $P_2(=196.000kN)$，軸間距離 $a_{12}(=4.0m)$ に±2.5％の誤差があるものとし，Table 4

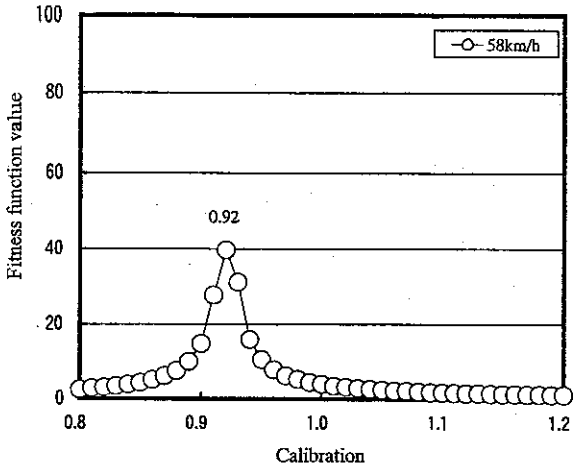

Fig.5 Relationship between calibration and fitness function value (58km/h)

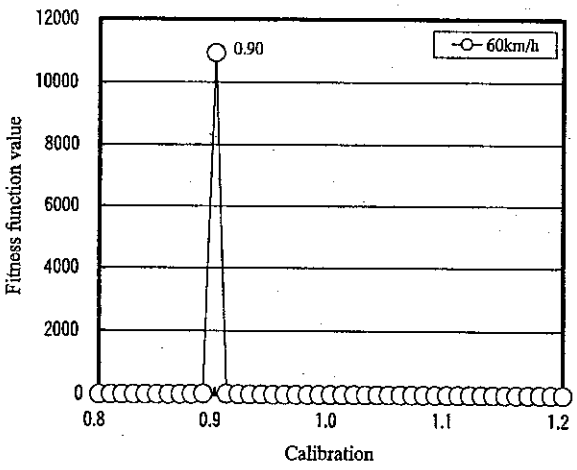

Fig.6 Relationship between calibration and fitness function value (60km/h)

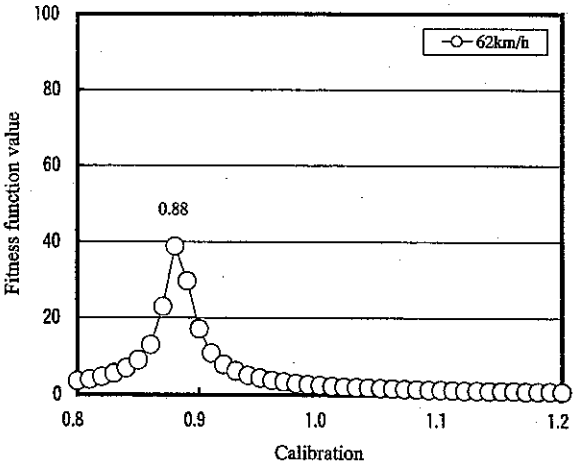

Fig.7 Relationship between calibration and fitness function value (62km/h)

に示す条件のもとで GA を適用することとした．一例として，車両速度が 60km/h に対するキャリブレーション値と適応度関数の関係を Fig.8 に示す．また，適

Table 3 Summary of calibration for TYPE-1 truck

Truck velocity	Fitness function value	Calibration
58 km/h	39.7	0.92
59 km/h	81.2	0.91
60 km/h	10939	0.90
61 km/h	77.2	0.89
62 km/h	38.8	0.88

Table 4 Conditions for calibration for TYPE-1 (with ±2.5% variation)

Estimated values of a truck		P_1, P_2, a_{12}
Number of individual		200
Number of generation		300
Probability of crossover		0.50
Probability of mutation		0.03
Selection		Roulette rule
Variable range of estimated values	P_1	95.55kN～100.45kN
	P_2	143.325kN～150.675kN
	a_{12}	3.90m～4.10m

Table 6 GA conditions for 6-axle truck

Number of individual		200
Number of generation		300
Probability of crossover		0.50
Probability of mutation		0.03
Selection		Roulette rule
Variable range of estimated values	P_1	29.4kN～196.0kN
	P_2～P_5	0.0 kN～196.0kN
	P_6	49.0kN～196.0kN
	a_{12}	1.0 m～13.0 m
	a_{13}～a_{16}	3.0 m～13.0 m

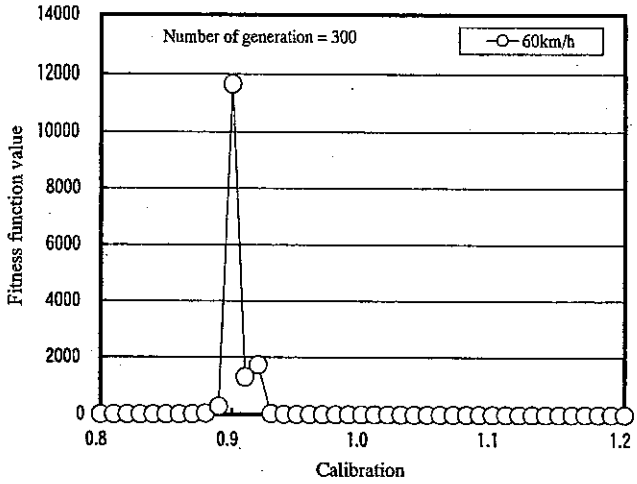

Fig.8 Relationship between calibration and fitness function value (with ±2.5% variation)

Table 5 Summary of calibration for TYPE1 truck (with ±2.5% variation)

Truck velocity	Fitness function value	Calibration
58 km/h	50.7	0.93
59 km/h	121.8	0.93
60 km/h	11670	0.90
61 km/h	107.5	0.90
62 km/h	49.3	0.88

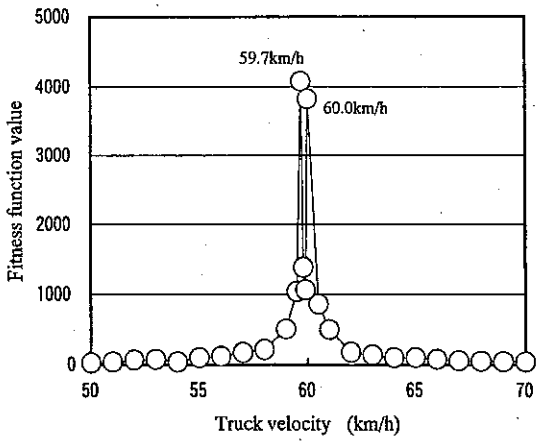

Fig.9 Relationship between truck velocity and fitness function value (TYPE-1, CAL=0.9)

応度関数が最大となるキャリブレーション値を Table 5 にまとめる．Table 5 から，適応度関数の最大値は 60km/h の場合に生じ，キャリブレーション値は *CAL* = 0.90 と正確に算出されていることがわかる．また，この時の等価軸距と総重量の推定値はそれぞれ 2.401m，245.24kN であり，真値である 2.400m，245.00kN と非常に良く一致する結果となっている．なお，その他の走行速度に対応するキャリブレーション値は 0.88～0.93 であり，適応度関数の値はさほど大きくないものの，実務上は十分な精度でキャリブレーション値を推定できるものと言える．

(2) 車両走行荷重の算出

キャリブレーション値 *CAL* を設定できたことから，任意車両が走行した場合の等価軸距と総重量を推定することとした．対象とした車両は TYPE-1～TYPE-6

Table 7 Comparison with estimated and exact values (TYPE-1)

	Estimated values		Exact values
	59.7 km/h	60.0 km/h	
a_{eq}	2.375m	2.406m	2.400m
Gross weight	247.59kN	245.68kN	245.00kN

Table 8 Comparison with estimated and exact values (TYPE-2～TYPE-6)

		Estimated values	Exact values
TYPE-2	a_{eq}	2.845 m	2.837 m
	Gross weight	248.11 kN	245.00 kN
TYPE-3	a_{eq}	2.379 m	2.369 m
	Gross weight	246.76 kN	245.00 kN
TYPE-4	a_{eq}	3.884 m	3.885 m
	Gross weight	246.60 kN	245.00 kN
TYPE-5	a_{eq}	7.049 m	7.098 m
	Gross weight	482.11 kN	490.00 kN
TYPE-6	a_{eq}	7.127 m	7.193 m
	Gross weight	489.78 kN	490.00 kN

であり，60km/h で橋長 50m の単純桁橋を走行するものとする．ただし，紙面の都合上，本節では，キャリブレーション値の算出に用いた TYPE-1 車両が走行した場合の検討結果について詳述する．

GA を適用するにあたっては，6 軸以下のすべての車両に対応できるように Table 6 に示す条件を設定するものとした．したがって，TYPE-1 車両を対象とした場合にも，キャリブレーション時に使用した 2 軸車両と推定するパラメータ（本節でのパラメータは 6 つの軸重と 5 つの軸距）が異なっていることに留意が必要である．キャリブレーション値を正確な $CAL = 0.9$ に設定した場合の車両速度と適応度関数の関係（300 世代目の最適結果）を Fig.9 に示す．Fig.9 から，59.7km/h と 60.0km/h にそれぞれ明確なピークが認められるものの，車両速度をほぼ正しく推定していることがわかる．また，Table 7 からわかるように，等価軸距と総重量は，59.7km/h で 2.375m と 247.59kN，60.0km/h で 2.406m と 245.68kN のように推定されており，いずれも TYPE-1 車両の真値である 2.400m，245.00kN と非常によく一致している．

次に，キャリブレーション値 CAL の厳密な値は $CAL = 0.9$ であるが，キャリブレーション値の算出過程で誤差が含まれ，$CAL = 0.93$ と評価した場合についても GA の適用性を検討することとした．Table 6 に

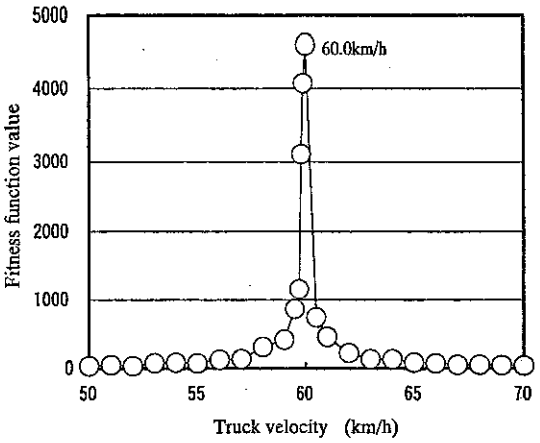

Fig.10 Relationship between truck velocity and fitness function value (TYPE-1, CAL=0.93)

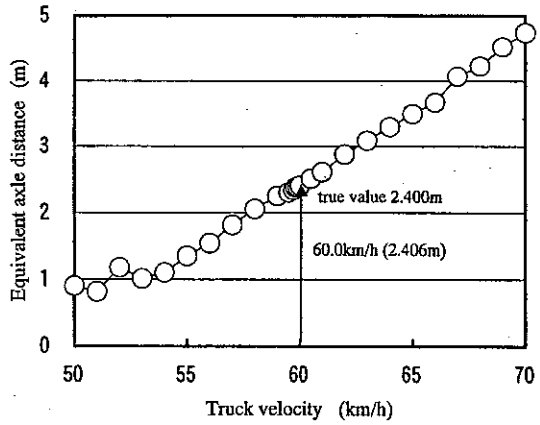

Fig.11 Relationship between truck velocity and equivalent axle distance (TYPE-1, CAL=0.93)

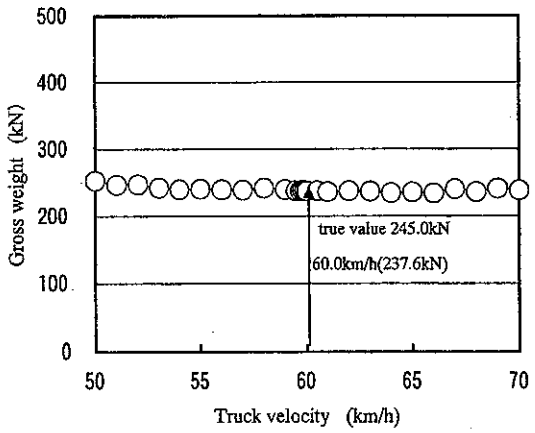

Fig.12 Relationship between truck velocity and gross weight (TYPE-1, CAL=0.93)

示す条件を採用して得られた，車両速度と適応度関数の関係（300 世代目の最適結果）を Fig.10 に示す．Fig.10 から，この場合には 60.0km/h のみに明確なピークが認められ，車両速度をほぼ正しく推定していることがわかる．また，Fig.11 と Fig.12 からわかるように，等価軸距と総重量の推定値は 2.406m，

237.63kN となっており，いずれも TYPE-1 車両の真値である 2.400m，245.00kN と比較的によく一致している．なお，結果は省略するが，補足的に実施したその他の計算結果を考慮すれば，キャリブレーション値 CAL の誤差は，たとえば上の例で言えば，245.00kN×0.90/0.93=237.10kN のように，総重量の推定値に影響することを付記しておく．

以上は，TYPE-1 車両に対する検討結果であったことから，TYPE-2～TYPE-6 車両についても同様の検討を実施することとした．GA による推定値（300 世代目の最適結果）と真値の対比結果を Table 8 に示す．この表から，たとえどのような車両であっても GA を適用すれば，非常に高い精度で橋梁交通荷重を推定できると言える．

4．まとめ

本論文は，GA（遺伝的アルゴリズム）を適用して少数主桁橋にも適用できる，従来よりも簡易で経済的な橋梁交通荷重の推定法を検討したものである．得られた主要な結果を以下にまとめる．

(1) 橋長 50m の単純梁上を 2 軸車（前輪荷重 $P_1 = 49.000kN$，後輪荷重 $P_2 = 196.000kN$，軸間距離 $a_{12} = 4.0m$）が速度 60km/h で通行する場合を想定し，車両諸元が既知の大型車両を走行させた場合の動的応答変位を用いてキャリブレーション値を算出する手法を検討した．その結果，交通止めをともなう静的載荷試験を実施しなくても，GA を適用すれば，非常に高い精度でキャリブレーション値を容易に算出できるとの知見が得られた．

(2) 2 軸車のみならず 3 軸車や 4 軸車さらにはセミトレーラーなどの 6 軸車を想定して，GA による橋梁交通荷重の推定法について検討した．その結果，いずれの車両タイプに対しても，走行速度のみならず，総重量と等価軸距をきわめて精度良く推定できることがわかった．

(3) キャリブレーション値 CAL の厳密な値は $CAL = 0.9$ であるが，キャリブレーション値の算出過程で誤差が含まれ，$CAL = 0.93$ と評価した場合についても GA の適用性を検討することとした．その結果，キャリブレーション値 CAL の誤差は総重量の推定値に影響するが，総重量の推定誤差は-3％（0.90/0.93×100=97％）程度であり，GA を適用した橋梁交通荷重の推定法は実務において十分に適用できることがわかった．

本論文で提案した GA による橋梁交通荷重の推定法は，使用するピックアップ数が 2 個程度でも適用できる可能性が高く，従来手法と比べてきわめて安価な方法と考えられる．本研究で，GA を適用する有用性と簡便性を十分に提示できたと考えられることから，今後は早急に計測システムの構築を図り，実際の橋梁交通荷重に適用する実用化研究を実施していく所存である．本論文が，橋梁の維持管理に携わる実務技術者にとって示唆に富んだ有益な技術資料になることを心から願う次第である．

参考文献

1) Moses, F. ：Weigh-in-Motion System Using Instrumented Bridges, Proc. Of ASCE, Vol.105, No.TE3, pp.233 ～ 249 , January, 1979.
2) 西川和廣，村越　潤，宮崎和彦：橋梁を用いた車両重量の計測（WIM）システムの開発，土木技術資料 38-1，1996.
3) 三木千壽，水ノ上俊雄，小林裕介：光通信網を使用した鋼橋梁の健全度評価モニタリングシステムの開発，土木学会論文集，No.686/VI-52，pp.31～40，2001 年 9 月．
4) 松井繁之，Ahmed El-Hakim：RC 床版のひびわれの開閉量による輪荷重の測定に関する研究，構造工学論文集，Vol.35A，pp.407～418，1989 年 3 月．
5) 小塩達也，山田健太郎，貝沼重信，小幡敏幸，古市　亨：鋼床版部材を用いた走行車両の輪重推定，構造工学論文集，Vol.44A，pp.1141～1151，1998 年 3 月．
6) 小塩達也，山田健太郎，小林直人，水野良浩：鋼 I 桁橋の縦桁を用いた Bridge Weigh-in-Motion システムの開発，構造工学論文集，Vol.47A，pp.1083～1091，2001 年 3 月．
7) 小塩達也，山田健太郎，深津　伸：BWIN による大型車両の実体調査と橋梁の疲労損傷度評価，構造工学論文集，Vol.48A，pp.1055～1062，2002 年 3 月．
8) 米田昌弘，枝元勝哉：GA を適用した橋梁交通荷重の推定法に関する研究，構造工学論文集，Vol.49A，pp.755～765，2003 年 3 月．

（2003 年 7 月 31 日受付）

主桁下フランジ応力を用いた車両重量計測について

Bridge weigh-in-motion using lower flange strain of main deck

勝浦　啓*，荒川　卓哉*，天野　信雄*，野田　整一**
Hiroshi Katsuura, Takuya Arakawa, Nobuo Amano, Seiichi Noda

*三菱重工業株式会社　横浜研究所（〒231-8715 神奈川県横浜市中区錦町 12 番地）
**三菱重工業株式会社　横浜製作所（〒231-8715 神奈川県横浜市中区錦町 12 番地）

A Bridge Weigh-in-Motion method, that presumes vehicles weight from the response strain of a bridge main girder even if many vehicles run between paths and speed changes, developed. For the purpose of the presumed accuracy evaluation, the field examination carried out on the condition that an test vehicles run and a common vehicles pass for continuation bridge of two-box girders of a motorcycle line and the 1 direction run lane. The test results were that gross total weight could presume in −1%−+2% of accuracy.

Key Words : BWIM, monitoring weight of vehicles, bridge
キーワード : BWIM, 車両重量計測, 橋梁

1. はじめに

道路構造物の老朽化の進行により，今後は維持補修費の急増が予測されている一方，公共工事に対するコスト縮減要請により，維持補修費の削減が求められている現状にある．

維持補修費の削減には，従来の事後保全ではなく，予防保全が有効であると言われており，その為には，構造物の劣化を予測し，補修する時期を推定すると共に，どの程度のコストが発生するかを計画する技術開発が望まれている．

構造物の多種類存在する劣化の中で，疲労劣化については，構造物の疲労強度，発生応力，繰返し回数が，耐用期間を決める主要因であり，これらを把握できれば，余寿命推定が可能になると考える．

上記主要因の中で，発生応力に関連する車両重量を計測する手法として，直接的に軸重を計測する為に，路面に埋め込み式計測機器を設置する方法があるが，施工に時間がかかる，設置コストが高いなどの課題があることから，多数の橋梁に設置できない状況にあると推定される．それに対して，橋梁上を走行している車両の重量を橋梁の部材の応答から推定する，施工が比較的簡単である手法として，BWIM（Bridge Weigh-in-Motion）が広く知られている．

本手法は，Moses[1]が提案したものであり，わが国では，本手法を改良した三木らの研究[2]や，ＲＣ床版のひび割れの開閉量を利用した松井らの研究[3]や，橋梁部材や支点反力を用いた小塩らの研究[4)~8)]など，多くの研究がなされている．

これらの研究は，橋梁を通過する車両が単独の場合や，通過速度が変わらない場合についての研究であり，疲労劣化の一要因である繰返し回数が多く，複数車両の同時走行や速度変化が想定される都市部の高架橋では，改良が必要と考えられる．

そこで，筆者らは，複数車両が径間内を走行しても，速度が変化しても，橋梁部材の応答から，車両重量を推定することができる方法を検討し，本報告では，その手法の推定精度評価を目的として実施した，単車線，一方向走行車線の２箱桁２径間連続橋での試験車両走行時，並びに一般車両走行時のフィールド試験結果について報告する．

2. 車両重量推定ロジック

2. 1 推定基本ロジック

前章で述べた，「複数車両が径間内を走行しても，速度が変化しても，橋梁部材の応答から，車両重量を推定することができる」手法として考えたのは，橋面上に存在する車軸数と位置，並びに橋梁部材の歪値を用いて，梁の曲げモーメントによる発生歪の計算式から，逆解析を行う方法である．

以下に，本報告でのフィールド試験で使用した 2 径間連続橋梁上を 4 軸車両が通行する場合の推定ロジックを示す．解析モデルを Fig. 1 に示す．

推定ロジックでの考え方は，橋梁を 3 点支持の一様断面梁と仮定して，橋面上のある位置に車両が存

在する時刻に，主桁で発生する曲げモーメントによる歪は，各軸重$W_1 \sim W_4$により発生する歪値の線形な重ね合わせであることに着目したものである．歪計測位置を車軸が通り過ぎていない時刻，すなわち，(1) 式の条件の時に発生する歪は，(2) 式せ表現され，歪計測位置を車軸が通り過ぎた時間，すなわち，(3) 式の条件の時に発生する歪は，(4) 式で表現されることを考慮する必要がある．式の中のε (t) は計測点における発生歪を表し，tは，1 軸目の位置がxのときの時刻である．

W の添え字は，車軸番号を表し，bの添え字は，車軸番号−1 を表しており，$b_0 = 0$である．

$$x \geq b_3 \quad a \geq x \quad a \leq L \cdots\cdots\cdots\cdots (1)$$

$$\varepsilon(t) = \sum_{i=1}^{4} B_i(x) \cdot W_i \cdots\cdots\cdots\cdots (2)$$

$$x \geq a + b_3 \quad x \leq L \cdots\cdots\cdots\cdots\cdots (3)$$

$$\varepsilon(t) = \sum_{i=1}^{4} A_i(x) \cdot W_i \cdots\cdots\cdots\cdots (4)$$

ここで，

$$A_i(x) = \frac{a}{4L^3EZ}\left\{4L^3 - 5L^2(x - b_{i-1}) + (x - b_{i-1})^3\right\} \cdots (5)$$

$$B_i(x) = \frac{1}{4L^3EZ}\left\{a(x - b_{i-1})^3 + (4L^3 - 5aL^2)(x - b_{i-1})\right\} \cdots (6)$$

E：ヤング率，Z：断面係数

次に，計測された歪εと軸数 N，並びに軸の位置 x，$b_1 \sim b_8$から軸重を逆解析する方法を述べる．

例えば，(1) 式の条件の場合，第 1 軸の位置がx_1, x_2, x_3, x_4となる時刻t_1, t_2, t_3, t_4で計測された歪$\varepsilon(t_1), \varepsilon(t_2), \varepsilon(t_3), \varepsilon(t_4)$から，$W_1 \sim W_4$は (7) 式で与えられる．(7) 式の Bi マトリクスは橋諸元データ（断面係数，ヤング率，スパン長），歪計測位置，車軸位置と車軸間距離で構成されるものであることから，４つの時刻でのこれらの数値と発生歪の計測ができれば，軸重が推定でき，それらを加算して，車重が推定できることになる．

$$\begin{bmatrix} W_1 \\ W_2 \\ W_3 \\ W_4 \end{bmatrix} = \begin{bmatrix} B_1(x_1) & B_2(x_1) & B_3(x_1) & B_4(x_1) \\ B_1(x_2) & B_2(x_2) & B_3(x_2) & B_4(x_2) \\ B_1(x_3) & B_2(x_3) & B_3(x_3) & B_4(x_3) \\ B_1(x_4) & B_2(x_4) & B_3(x_4) & B_4(x_4) \end{bmatrix}^{-1} \begin{bmatrix} \varepsilon(t_1) \\ \varepsilon(t_2) \\ \varepsilon(t_3) \\ \varepsilon(t_4) \end{bmatrix} \cdot (7)$$

本推定ロジックは，各車軸の橋軸方向の位置とそのときの歪により，車軸重量が算出されるものであることから，車両の速度変化があっても，また，複数の車両が径間上を走行していても，影響を受けないと言える．

2．2 推定フロー

Fig．2 に軸重推定フローを示す．軸重算出に必要な軸数，第 1 軸位置，軸間距離，軸通過時の発生歪は，本報告における試験では，以下の手法で計測した．

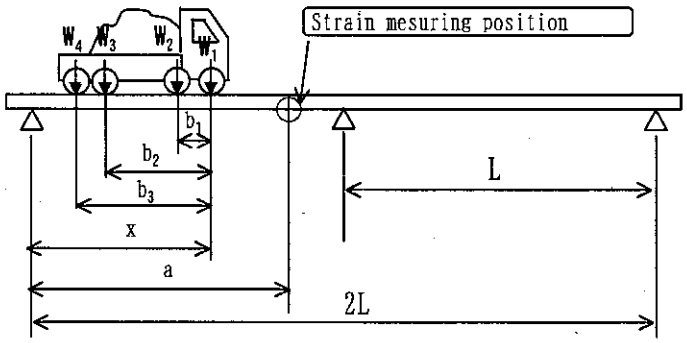

Fig．1 Analysis model

まず，橋軸方向にある距離をおいて設置した，複数の車両通過検知用光電センサ SV_i で，走行速度を検出する．次に，橋軸方向の 1 点に設置した，車軸検出用光電センサ SJ で，車軸数とその通過時間を検出し，事前に計測してある走行速度を用いて，軸間距離を算出する．主桁歪の計測には，歪ゲージを用いた．

図中の実線は計測する項目を，点線は事前に把握しておく項目を，1 点鎖線は計算する項目を示す．

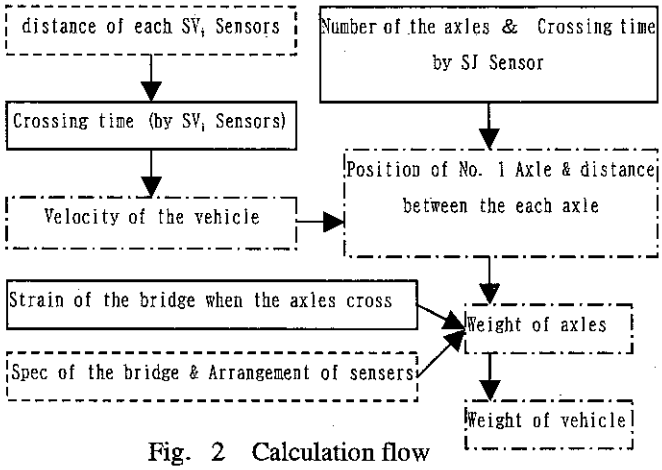

Fig．2 Calculation flow

3． フィールド試験

3．1 対象橋梁

前章で述べた，車重推定ロジックの検証と推定精度を評価する目的で，フィールド試験を行った．使用した橋梁は，photo．1, 2 に示す様に，2 径間連続 2 箱桁 RC 床版橋で，陸橋へのアプローチ部，単車線，1 走行方向の個所である．

3．2 計測機器

今回の試験で使用した各センサの設置位置を Fig．3 に示す．Photo．3 は，複数の車両通過検知用光電センサ SV_2 の設置状況である．

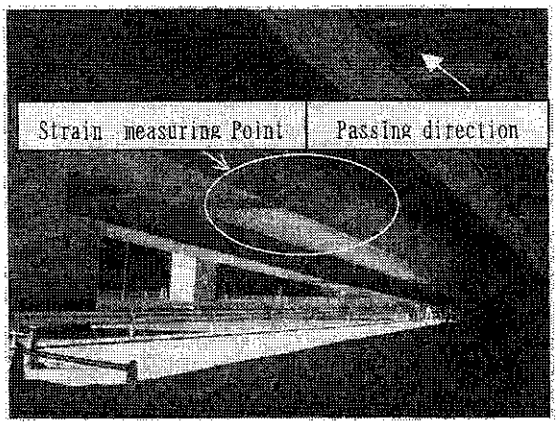

Photo. 1 Object Bridge view from lower angle

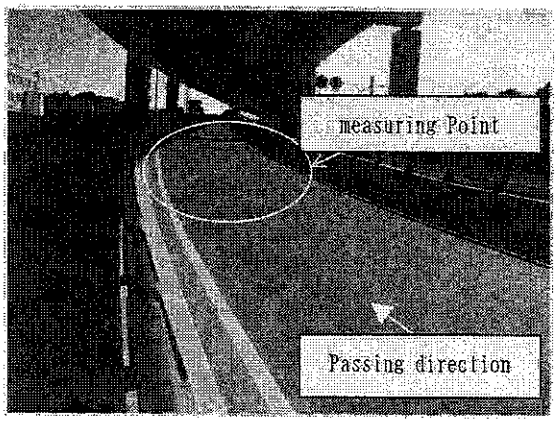

Photo. 2 Object Bridge view from upper angle

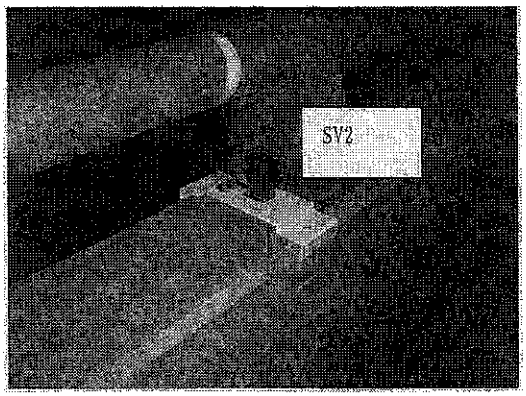

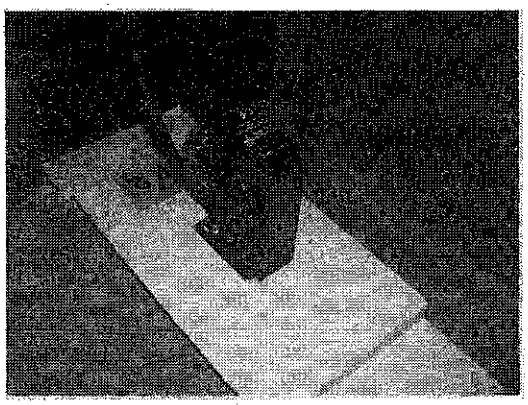

Photo. 3 location of SV2 sensor

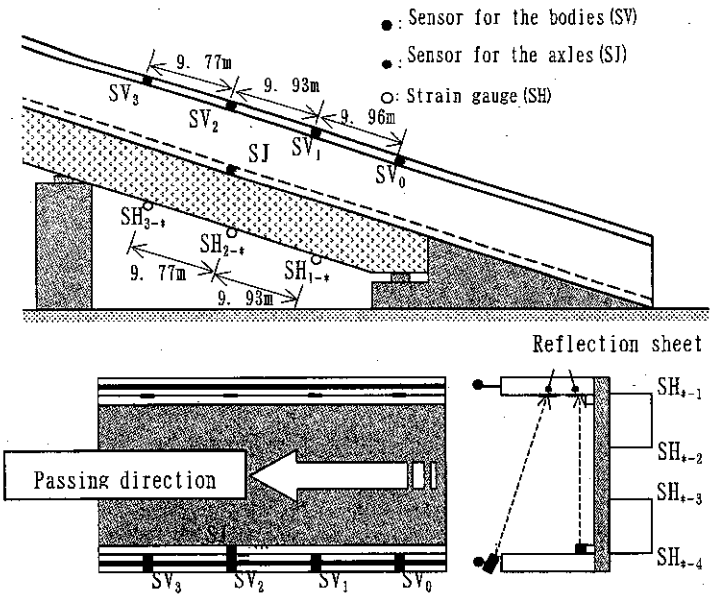

Fig. 3 Arrangement of sensors

歪ゲージは，径間の長手方向に，１径間長の 1/4L, 1/2L, 3/4L 位置に，橋軸直角方向にある４つのウエブの下フランジ面に，橋軸方向の歪が計測できる様に貼付けた．貼り付け状況を Photo. 4 に示す．

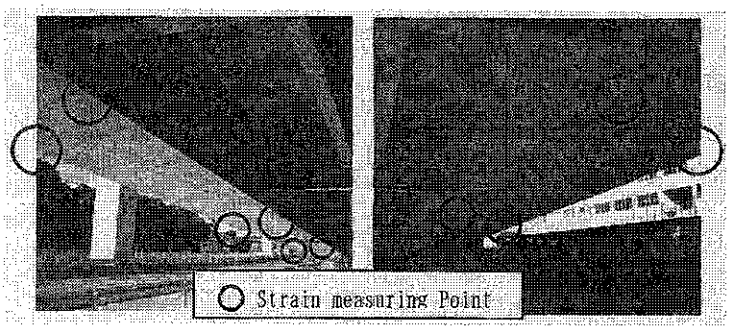

Photo. 4 Location of strain gauges

3．3 試験条件

試験車両走行試験では，走行速度をパラメータとして，20, 40, 60km/h の場合について，実施した．その後，一般車両走行時の計測を行った．

3．4 試験車両

本試験で使用した試験車両の外形図を Fig. 4 と Photo. 5 に，計測した各軸重を Table. 1 に示す．

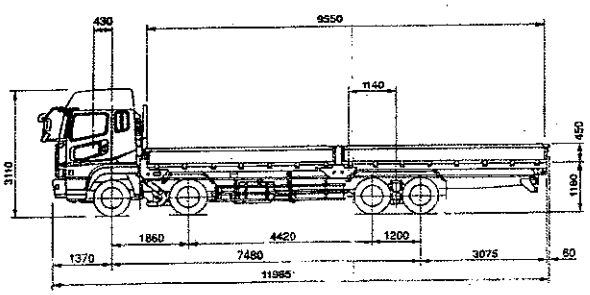

Fig. 4 Outline of the used vehicles

試験車両の荷台にコンクリートブロックを搭載し，総重量が約 20tonf になる様に調整したものである．

Photo. 5 the used vehicles

Table. 1 Specification of the used vehicles

weight of axles [ton]	1st	2nd	3rd	4th	Total
	4.47	4.58	6.87	7.49	23.42

distance of axles [m]	1st～2nd	2nd～3rd	3rd～4th
	1.86	4.42	1.20

4. 試験結果

まず，試験車両を走行させた場合の試験結果について述べ，その後，一般車両走行時の試験結果について述べる．

4. 1 軸数検知結果

車両走行速度が 60km/h での軸通過検知用光電センサ出力を Fig. 5 に示す．今回の試験で使用した軸数は４であり，使用した計測機器で，軸数検知が可能であることを確認した．４軸通過後に計測されている信号は，後輪に設置されている泥除けであることは分かっており，実際の運用においては，短い時間検出信号は，軸として検出しないロジックにしておく必要があることが分かった．

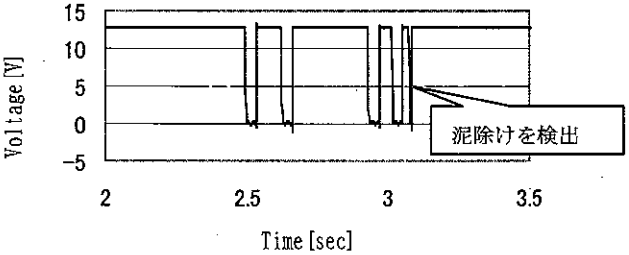

Fig. 5 Output of the sensor for axles

4. 2 軸間距離算出結果

車両走行速度が 60km/h での車両通過検知用光電センサ出力を Fig. 6 に示し，３回実施した試験結果で得られた軸間距離の推定精度を Table. 2 に示す．

軸間距離の算出は，SV_1 と SV_2 が遮断されて電圧が落ちる時間差（t_{1_2}）と２つのセンサ設置距離の関係から算出した通過速度と，軸通過検知センサ出力とから算出した．その結果，推定軸間距離の精度は，今回の試験条件では，0－6%の誤差で算出可能であることを確認した．

Table. 2 Comparison of the distance of axles

Velocity [km/h]	axle position	true value [m]	once		twice		three times	
			estimated value [m]	ratio	estimated value [m]	ratio	estimated value [m]	ratio
20	1st～2nd	1.86	1.97	1.06	1.92	1.03	1.97	1.06
	2nd～3rd	4.42	4.55	1.03	4.48	1.01	4.56	1.03
	3rd～4th	1.20	1.21	1.01	1.21	1.01	1.22	1.02
40	1st～2nd	1.86	1.87	1.01	1.87	1.01	1.88	1.01
	2nd～3rd	4.42	4.44	1.00	4.41	1.00	4.44	1.00
	3rd～4th	1.20	1.21	1.01	1.20	1.00	1.21	1.01
60	1st～2nd	1.86	1.88	1.01	1.85	0.99	1.96	1.05
	2nd～3rd	4.42	4.46	1.01	4.38	0.99	4.58	1.04
	3rd～4th	1.20	1.20	1.00	1.20	1.00	1.22	1.02

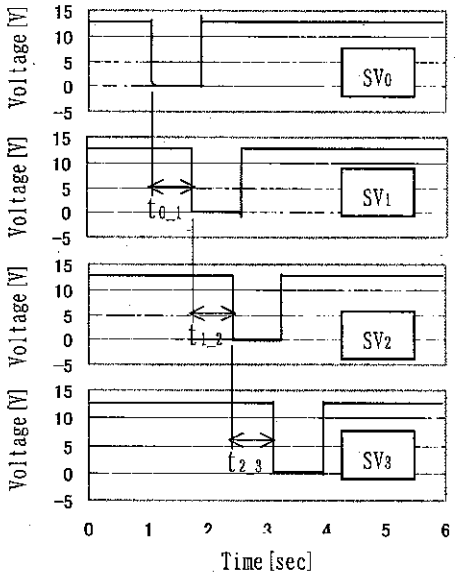

Fig. 6 Output of the sensor for velocity

4. 3 車両重量算出結果

4. 3. 1 試験車両走行時

車両走行速度が 60km/h 時の試験における 1/2L 点に貼り付けた４枚の歪ゲージの時刻歴波形を Fig. 7 に示す．

Fig. 7 からわかるように，今回使用した橋梁では，橋軸直角方向では，歪の分布はほとんど発生していないことから，重量を算出するにあたっては，1/2L 点の SH_{2-1}, SH_{2-2}, SH_{2-3}, SH_{2-4} の平均歪を用いた．

また，車両通過により発生する，主桁の曲げひずみには，静的な成分に，動的な曲げ振動が重畳していることが確認できた．

２章で述べた様に，本重量推定ロジックは静的な荷重で発生する歪を線形に重ね合わせたものが観測されることが前提条件であることから，この様に動的な成分が含まれると，推定精度の劣化が懸念された．そこで，時刻歴波形について，フィ

ルター処理を行い，振動成分を極力取り除く工夫を施してある．

車重推定に必要となる橋の断面係数については，振動成分の少なかった，試験車両が 20km/h で走行した場合の 3 回の計測結果の平均値からキャリブレーションをした値を用いている．ただし，この数値は，事前に図面から算出した断面係数に対し，約-3%の誤差であった．

Fig. 8 に横軸に速度，縦軸に測定重量一推定重量のグラフを示すが，総重量に関しては-1～+2%の精度で推定可能であることが分かった．

一方，総重量の算出に用いている各軸重については，Table. 3 と Fig. 9 に示すように，最大 40%程度の誤差が発生することが分かっている．

車両走行速度が 20,40km/h の場合は各軸共に似た傾向の推定精度になっているが，60km/h では，1 軸目の推定値が低く，2 軸目の推定値が高くなっている．なぜ，この様な傾向になるかの詳細な分析には至っていないが，要因の 一つとして考えられるのは，車両走行速度が 60km/h では橋の振動成分の影響を大きく受けていることが考えられる．

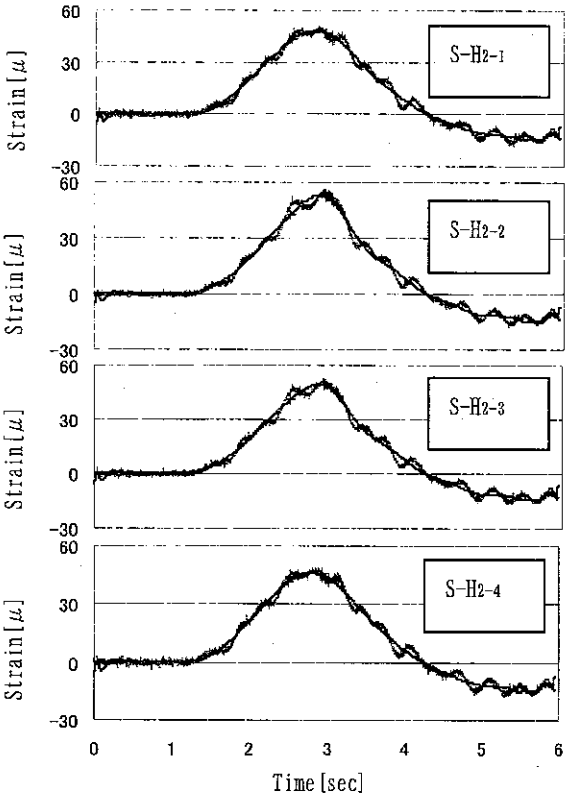

Fig. 7 Output of the strain gauge

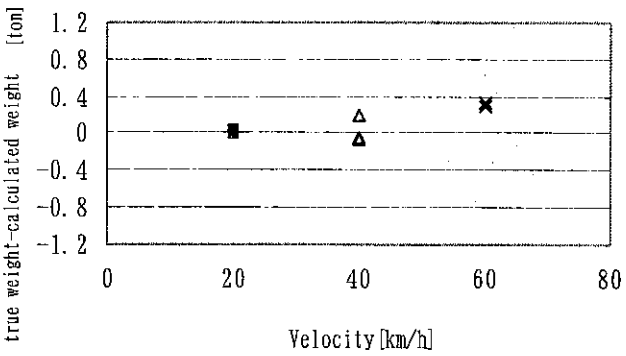

Fig. 8 Result of calculation of the weight of vehicle

Table. 3 Comparison of the weight of axles

Velocity [km/h]	axle position	true weight [ton]	once		twice		three times		average	
			estimated weight [ton]	ratio	estimated weight [ton]	ratio	estimated weight [ton]	ratio	estimated weight [ton]	ratio
20	1st	4.47	4.64	1.04	4.87	1.09	5.33	1.19	4.94	1.11
	2nd	4.58	3.81	0.83	3.90	0.85	3.17	0.69	3.63	0.79
	3rd	6.87	8.29	1.21	7.83	1.14	8.73	1.27	8.28	1.21
	4th	7.49	6.70	0.89	6.84	0.91	6.16	0.82	6.57	0.88
40	1st	4.47	5.62	1.26	4.61	1.03	5.56	1.24	5.26	1.18
	2nd	4.58	3.00	0.65	4.35	0.95	3.41	0.74	3.59	0.78
	3rd	6.87	6.85	1.00	7.31	1.06	6.87	1.00	7.01	1.02
	4th	7.49	8.00	1.07	6.97	0.93	7.64	1.02	7.54	1.01
60	1st	4.47	2.77	0.62	3.56	0.80	3.06	0.68	3.13	0.70
	2nd	4.58	6.38	1.39	5.66	1.23	6.50	1.42	6.18	1.35
	3rd	6.87	7.69	1.12	8.33	1.21	8.26	1.20	8.10	1.18
	4th	7.49	6.25	0.83	5.53	0.74	5.30	0.71	5.69	0.76

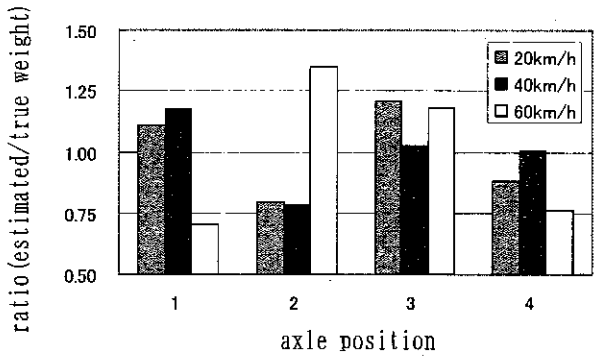

Fig. 9 Result of the ratio of each axles

4．3．2 一般車両走行時

次に，本手法を用いて，一般車両が走行している状態に対して，行った車重推定結果について，述べる．

(1)単独走行時

一般車両が単独で走行している状態の 3 ケースについて，分析を行った．分析の対象とした時刻は，前後に他車両が走行していないものを選定した．車両の軸数は 3 軸，4 軸，4 軸である．このときの走行速度と軸重算出結果を Table. 4 に示す．

(2)車両連行時

車両が連行している場合の 1 ケースについて分析を行った．車両は Photo. 6 に示すように左側に 2 台が先行し，右側を 2 台が後から走行する形である．車両の軸数は先頭から 3 軸，3 軸，4 軸，4 軸の計 14 軸である．このときの推定アルゴリズム

は，各車両の各軸が車軸通過検知センサ SJ を通過したときの歪値と，車両速度と軸間距離から推定した，この時刻での他軸の存在位置を用いて行っている．

各車両の軸間距離の算出には試験車両と同じ方法で，SV_1～SV_2の通過速度を用いた．各軸の位置の算出は，SJ 通過後の軸位置の算出には SV_1～SV_2,SV_2～SV_3の通過速度を，SJ 通過前の軸位置の算出には SV_0～SV_1の通過速度を用いた．このときの軸重算出結果を Table. 5 に示す．各車両共に，総重量は 13ton 以下であり，重い荷物を搭載していない状態であったことが推定できる．

Table. 4 Result of the weight of single passage

Case	Number of axles	Velocity [km/h]			Tolal Weight [ton]
		SV0～SV1	SV1～SV2	SV2～SV3	
1	3	49.43	47.68	47.11	26.0
2	4	56.75	54.36	51.66	7.7
3	4	50.13	49.39	48.58	13.1

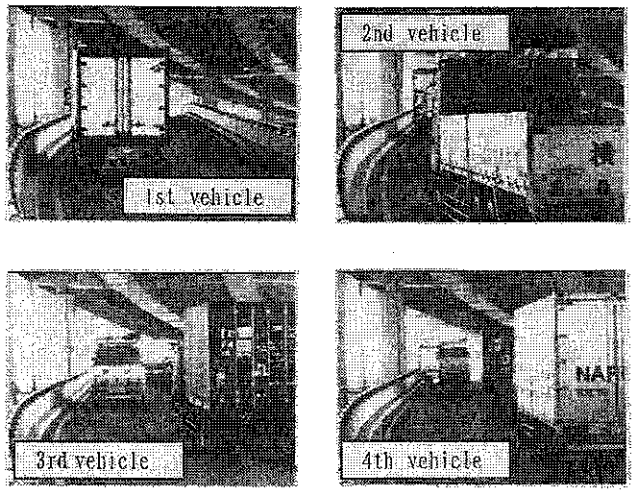

Photo. 6 the vehicles of passage in a row

Table. 5 Result of the weight of passage in a row

Passing sequence	Number of axles	Velocity [km/h]			Tolal Weight [ton]
		SV0～SV1	SV1～SV2	SV2～SV3	
1st	3	43.6	42.8	42.6	12.8
2nd	3	48.0	43.7	41.3	5.6
3rd	4	46.9	44.0	41.1	8.4
4th	4	46.8	44.6	41.8	6.5

5. おわりに

本報告では，複数車両が径間内を走行しても，速度が変化しても，部材の応答から，車両重量を推定することができる方法を検討し，その手法の推定精度評価を目的として，単車線，一方向走行車線の２箱桁２径間連続橋での試験車両走行時，並びに，一般車両走行時のフィールド試験を実施した．その結果，以下のことを明らかにした．

(1) 総重量に関しては-1～+2%の精度で推定可能であった．

(2) 軸重については，最大 40%程度の誤差が発生することが分かった．この要因の一つとして橋の振動成分の影響を大きく受けていることが考えられ，今後は各軸重を高精度で推定する手法の検討が課題である．

(3) 車両が連行して走行している場合でも各車両の車重を推定することが可能であることを確認した．

(4) 今後は，本報告で使用した橋梁以外に種類の橋梁や，複数車線，渋滞発生時などの車両速度に変化がある場合についての推定精度評価を行っていきたい．

謝辞

本報告で，借用させて頂いた試験実施橋梁を所有する横浜市殿には，多大なるご協力を頂いた．ここに記して感謝の意を表します．

参考文献

1) Moses，F．：Weigh-in-Motion System Using Instrumented Bridges, Proc, Of ASCE, Vol.105, No.105, No.TE3, pp.233～249,
2) 三木千寿，村越潤，米田利博，吉村洋司：走行車両の重量測定，橋梁と基礎，1987-4，P41-44
3) 松井繁之，Ahmed EL-HAKIM：RC 床版のひび割れの開閉量による輪荷重の測定に関する研究，構造工学論文集,Vol.35A,1989-3
4) 小塩達也，山田健太郎：鋼床版部材を用いた走行車両の輪重推定，構造工学論文集,Vol.44A,1998-3，P.1141-1151
5) 小塩達也，新海英昌，山田健太郎：橋梁部材の影響面積を用いた走行車輌の重量推定に関する研究，土木学会第 54 回年次学術講演会，pp.456-457，1998.
6) 小塩達也，山田健太郎：鋼 I 桁橋の縦桁を用いた Bridge Weigh-in-Motion システムの開発，構造工学論文集,Vol.47A,2001-3
7) 小塩達也，山田健太郎，小林直人，深津伸：鋼 I 桁橋を用いた Bridge Weight-in-Motion による自動車荷重のモニタリング，橋梁振動コロキウム 01 論文集
8) 小塩達也，山田健太郎，若尾政克，因田智博：支点反力による BWIM を用いた自動車軸重調査と荷重特性の分析，構造工学論文集,Vol.97A,2003-3

（2003．7．31 受付）

道路橋の交通振動により放射される低周波音の理論解析

Theoretical Analysis of Low Frequency Noise Radiated by Traffic-induced Vibration of Bridge

川谷充郎*，河田直樹**，十名正和***，金 哲佑****
Mitsuo Kawatani, Naoki Kawada, Masakazu Tona and Chul-Woo Kim

*工博 神戸大学教授 工学部建設学科（〒657-5801 神戸市灘区六甲台町 1-1）
** （株）エース 基盤整備本部 技術第二部（〒600-8133 京都市下京区七条通加茂川筋西入稲荷町 458）
*** 神戸大学大学院 自然科学研究科博士前期課程建設学専攻 学生（〒657-5801 神戸市灘区六甲台町 1-1）
**** 神戸大学招聘外国人研究者 （〒657-5801 神戸市灘区六甲台町 1-1）

The purpose of this study is better evaluation of low frequency noise with reflection radiated by traffic-induced vibration of bridge. The sound pressure level at noted point is calculated from the velocity of slab which is computed from the analysis of dynamic response of bridge due to moving vehicles. The influence of sound reflection at ground is considered by using the image method. The analytical results of dynamic response of bridge coincide with experimental ones. It is also able to evaluate low frequency noise by analyses more precisely considering reflection effect on ground.

Key Words : low frequency noise, traffic-induced vibration of bridge, dynamic response analysis, sound radiation
キーワード：低周波音，橋梁交通振動，動的応答解析，音響放射

1. まえがき

昭和 50 年代より，環境問題の一つとして日常生活に多くの悪影響をもたらす低周波音が社会的に注目を浴びており，橋梁の交通振動によって放射される低周波音についても例外ではない．近年の我が国の道路橋は，交通車両の大型化とそのような大型車交通量の増加により振動が大きくなり，周辺地域住民からの苦情件数は年々増加している [1),2)]．道路橋における低周波音は，一般的なタイヤ転動時騒音や車両エンジン音等の“騒音”とは異なり，車両が道路橋上を走行する際に床版から発生するスパン音や，車両がジョイントを通過する際に発生するジョイント音など，構造物から放射される空気振動のことをいう [1),2)]．また，人間が聞きとることが非常に困難な騒音であり，それを感知できる音圧レベルには個人差がある [3)]ことから，現在も道路管理者はその対策に苦慮している．

橋梁から放射される低周波音に関する研究については，今市らが橋桁を平板にみなし，これが曲げおよびねじり振動する場合についての音響放射を求め [4)]，大島ら [5),6)]が梁理論および帯板要素法によって，床版から放射される空気振動の解析を行い，低周波数領域で実験結果とよく一致することを確認している．また，杉山ら [7),8)]によって床版を理想化した版より放射される低周波音について解析し，上部構造の違いによる放射音の特性変化を明らかとしており，近年では五郎丸ら [9)]が 2 主桁橋における点加振による低周波音の放射特性を境界要素法により評価し，また山口ら [10)]によって地形を考慮した 1 次モードの橋梁振動による波動伝播特性を明らかとしている．

本研究では，すでに供用されている実道路橋を対象に，走行荷重により放射される低周波音を理論的手法によりシミュレーションすることを目的とする．対象とする橋梁の音源は床版のみとし，走行荷重に伴う床版振動は車両-橋梁の連成振動解析を実施することにより再現する．また，それによりに得られる橋梁の加速度応答，および橋梁周辺の音圧レベルについて，実測値と比較することによりその妥当性を検証する．さらに橋梁周辺の音場特性や，地盤反射の影響，また車両速度や床版厚の影響についても評価する．

2. 解析手法

2.1 橋梁交通振動解析

放射音の理論解析にあたり，まず橋梁と走行車両の連成振動解析を実施する．床版を Flat 要素，主桁・横桁・壁高欄を梁要素とする有限要素モデル化橋梁と，8 自由度振動系車両の連成振動方程式をたて，これを Newmark-β 法を用いて逐次積分することで橋梁各部の動的応答を計算する [11~15)]．本手法による解析結果は，これまでの研究により主桁および床版の動的応答が現地実測結果とよく一致していることを確認している [11~14)]．

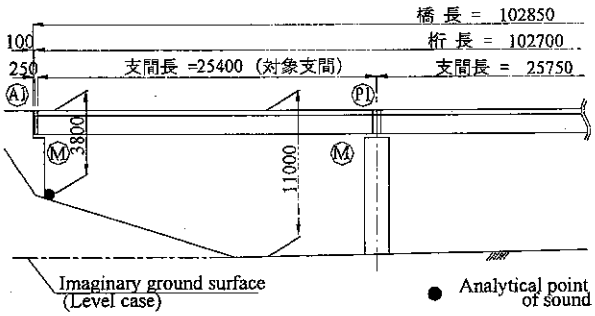

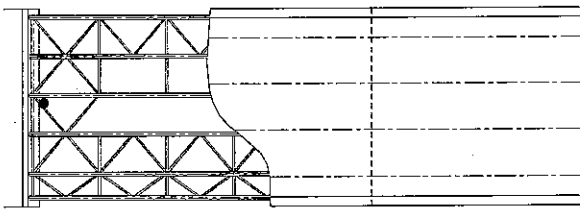

Fig.1 General view of bridge

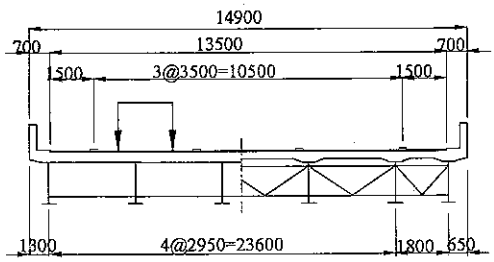

Fig.2 Sectional view of bridge

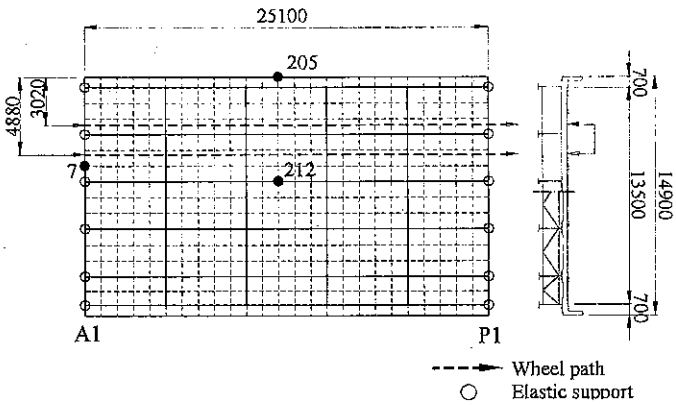

Fig.3 Analytical model of bridge

Table 1 Spring constants of elastomeric support

direction		Steel bearing (Entrance)	Rubber bearing (Exit)
Z	kN/m	2.814E+06	3.805E+05
X	kN/m	0 (free)	1.642E+03
Y	kN/m	∞ (fix)	1.642E+03
θ_Z	kN·m/rad	∞ (fix)	1.537E+03
θ_X	kN·m/rad	0 (free)	1.537E+03
θ_Y	kN·m/rad	0 (free)	1.537E+03

X:Longitudinal direction Y:Transverse direction Z:Vertical direction

2.2 放射音解析

橋梁周辺への放射音は，床版上に配置された仮想の半球状の呼吸球音源により発生するものとする．その際，床版を無限平面バッフルと考えると，床版上の点音源による音圧 $dp(r,t)$ は，速度ポテンシャル($\phi=\phi(r,t)$)より次式により求まる[7]．

$$dp(r,t) = -\rho_0 \frac{\partial d\phi}{\partial t} = i\rho_0 \omega \frac{v dA}{2\pi r} e^{i(\omega t - kr)} \qquad (1)$$

ここで，r は点音源から受音点までの距離，ρ_0 は空気密度(11.9N/m^3)，ω は固有円振動数，k は音波の波数，dA は床版の微少要素面積であり，また v は橋梁交通振動解析により求まる速度振幅スペクトルである．

音の放射による音圧 $p(r,t)$ は，式(1)を橋面積全体で積分することで求まる．

$$p(r,t) = \int_s dp(r,t) = \int_s i\rho_0 \omega \frac{v dA}{2\pi r} e^{i(\omega t - kr)} \qquad (2)$$

また，音圧の実効値 $p_{rms}(r,t)$ は以下のように表される．

$$p_{rms}(r,t) = \sqrt{\left(\frac{1}{t}\int_0^t p(r,t)^2 dt\right)} \qquad (3)$$

さらに，この音圧の実効値 $p_{rms}(r,t)$ を音圧レベル SPL に換算する．

$$SPL(r,t) = 20\log_{10}\frac{P_{rms}(r,t)}{P_0} \qquad (4)$$

ここで P_0 は最小可聴値 (2.0×10^{-5}N/m^2)である．

本研究では，この音圧レベル SPL を用いて低周波音の評価を行う．

3. 解析モデル

3.1 橋梁モデル

本研究において対象とする橋梁の一般図を Fig.1, Fig.2 に示す．支間長 25.40+2@25.70+25.40m＝102.2m，総幅員 14.90m の 4 径間連続 6 主鈑桁橋である．この橋梁は元来連続する単純桁橋であったが，環境対策のため現在はノージョイント連続化されており，また床版上面増し厚補強，桁端部の RC 巻き立て補強も実施されている．さらに，支承は A1 部で鋼製支承，P1 部でゴム支承に取り替えられている．

解析に用いる橋梁モデルを Fig.3 に示す．連続桁橋であることから 4 径間とするべきであるが，計算容量を抑えるため着目する起点側 1 径間部のみを単純桁として考える．床版を Flat 要素，主桁・横桁・壁高欄を梁要素としてモデル化し，床版増し厚および桁端部 RC 巻き立て補強を考慮する．また各要素の断面諸元算定においては，本橋は非合成桁であるが，実際には合成桁橋に近い挙動を示すことを考慮して合成桁として扱う．床版は厚さ 25cm の等方性床版として求める．床版コンクリートと鋼との弾性係数比は，n=8.75(Ec=2.35×10^{6}N/cm^2)，Es=2.06×10^{7}N/cm^2)とする．

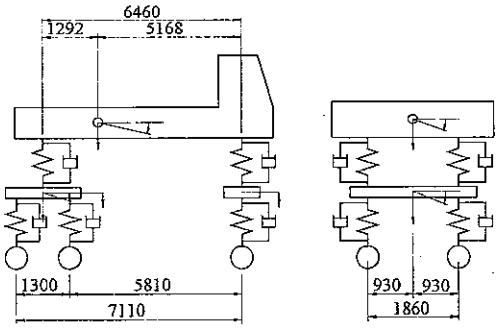

Fig.4 Vehicle model with 8-degree-of freedom

Table 2 Dynamic property of moving vehicle

Total Weight		196 kN
Axle Weight	Front	49 kN
	Rear	147 kN
Natural Frequency	Front	2.83 Hz
	Rear	2.83 Hz
Wheel Distance	Front	5.168 m
	Rear	1.292 m
Axle Distance	Front	5.810 m
	Rear	7.110 m

支承条件として，A1 部において鋼製支承が採用されているが，実際には桁の鉛直変形の影響を受けると考え，A1 では主桁の鉛直弾性変形，P1 部ではそれにゴムの弾性変形を加えて考慮することとする．そのため支承位置で2重節点を定義し，その節点間にばね要素を設ける．解析に用いる支承部のばね定数を Table 1 に示す．質量は Lumped Mass として与え，各節点に振り分ける．

3.2 走行車両モデル

本解析の用いる走行車両は，実際の試験走行に用いられた 20tf(196kN)トラックを想定し，Fig.4 に示す 8 自由度の三次元車両にモデル化する．車両諸元を Table 2 に示す．走行条件についても試験走行の状況に合わせ，第一走行車線を 3 台連行（車頭間隔=30m），速度はともに 75km/hr とする．

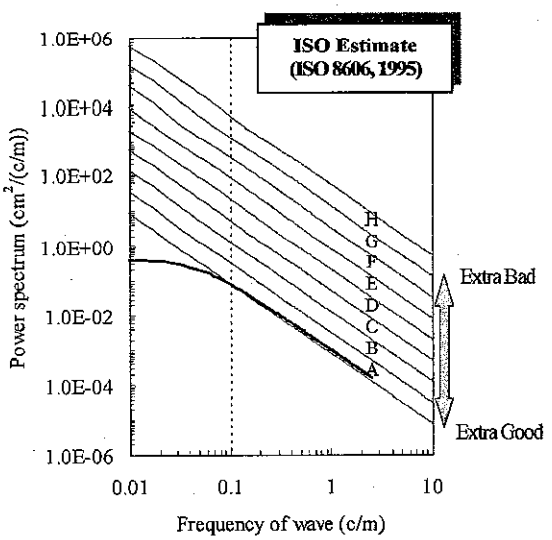

Fig.5 Power spectra of roadway roughness

3.3 路面凹凸

対象橋梁上で実測された路面凹凸値がないため，式(5)に示される路面凹凸パワースペクトル密度 S_{z0}（Ω）を用いて，モンテカルロシミュレーションにより路面凹凸波形を発生させる．

$$S_{z0} = \alpha \ /(\Omega^n + \beta^n) \qquad (5)$$

α，β，n は路面凹凸特性を決定するパラメータであり，名神高速道路完成直後の実測結果に基づくパラメータ(α =0.001(cm²/(m/c)), β=0.05(c/m), n=2.00)[16]を用いる．Fig.5 に路面凹凸スペクトルを示す．供用中である実橋を勘案し，橋梁端部においては 1.0cm の路面段差を設ける．

4. 橋梁動的応答解析結果

4.1 固有値解析

固有値解析結果のうち，4 次までの振動モードおよび固有振動数を Fig.6 に示す．1 次モードがたわみ，2 次モードがねじり振動となっている．3 次，4 次モードは橋軸を中

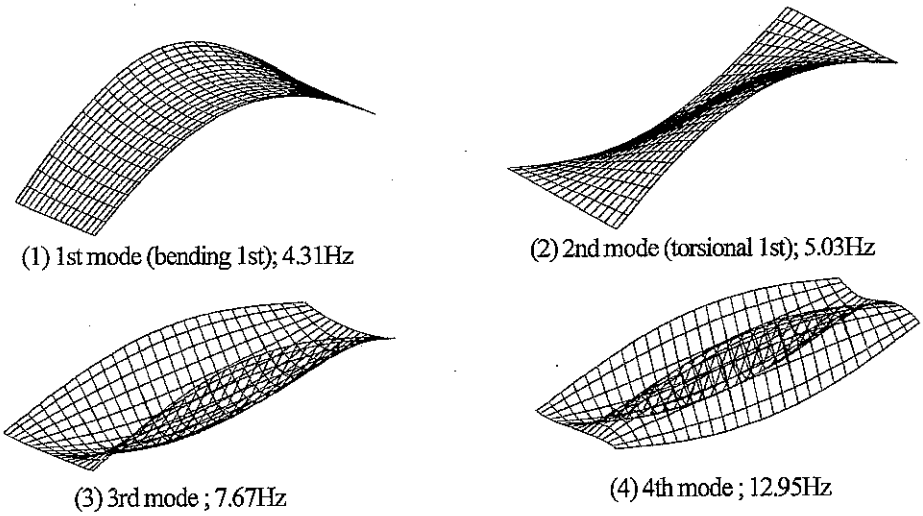

(1) 1st mode (bending 1st); 4.31Hz

(2) 2nd mode (torsional 1st); 5.03Hz

(3) 3rd mode ; 7.67Hz

(4) 4th mode ; 12.95Hz

Fig.6 Natural mode shapes and frequencies

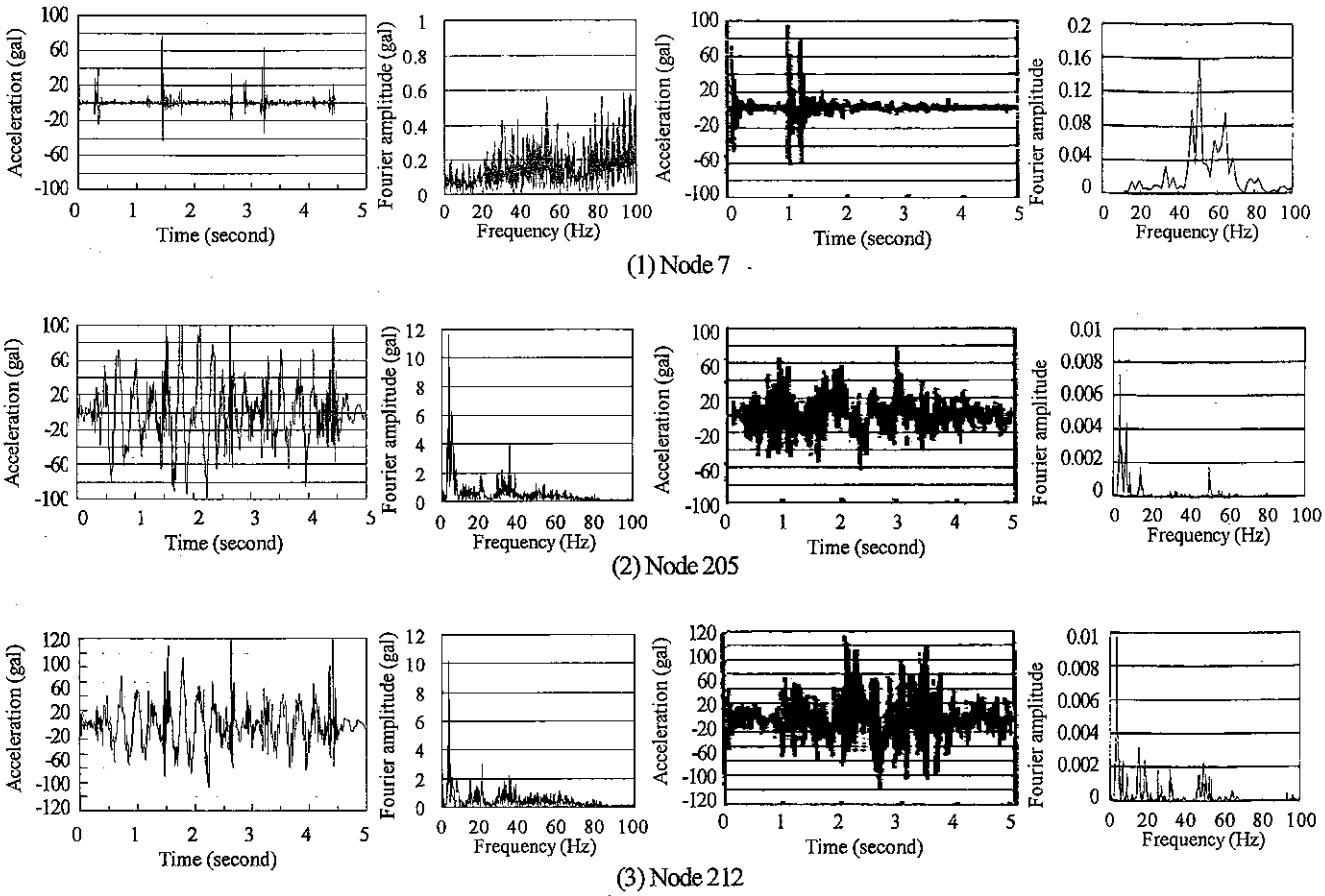

Fig.7 Acceleration of bridge ; V=75km/hr, 3-vehicles, Headway=30m

心に曲げが生じる，低い次数では現れにくいモード形状であるが，対象橋梁が3車線を有しており，一般的な橋梁に比較し，橋長に対する幅員が大きいことが影響していると考えられる．三次元動的応答解析で考慮するモード次数は，音圧解析において対象とする低周波音の周波数が，人間の日常生活に悪影響を及ぼすとされる 100Hz 程度までであること[1),2)]を考慮して，50次（f_{50}=101.6Hz）までとする．

4.2 橋梁加速度応答

解析によって得られる加速度応答と，試験走行による実測値をフーリエスペクトルとともに Fig.7 に示す．着目位置は，Fig.3 に示す車両進入側の端横桁上(Node 7)，支間中央の高欄上(Node 205)，支間中央の主桁上(Node 212)である．Node 7 においては，解析値，実測値ともに車両進入時における衝撃的，瞬間的な応答が現れているのがわかり，その最大加速度はほぼ一致している．解析結果におけるフーリエスペクトルは，実測結果に比較し 70Hz 以上の成分を多く含んでいるが，他の部材に比較し応答値が小さいため，低周波音の評価には差し支えないと考えられる．

Node 205 および Node 212 における加速度応答を実測値と比較すると，両者とも若干解析結果の方が大きくなっており，特にピーク値には 30Gal 程度の差がある．これは，実測精度の問題，また連続桁を単純桁としてモデル化したことによる差であると考えられる．ただし，両者のフーリエ振幅はともに卓越振動数がほぼ一致しており，低周波音を評価するための橋梁動的解析モデルとしては妥当であるといえる．もっとも卓越している振動数 4Hz 近傍は橋梁の1次たわみモードに対応し，また幅広の幅員で左走行車線を走る条件より，Node205 からは 5～10Hz のねじれの固有振動数が現れていることがわかる．

ここで得られた橋梁の応答のうち，低周波音解析には床版の速度応答をフーリエ変換したものを利用する．

5. 低周波音解析結果

音速を 340m/sec，100Hz の音を対象とすれば 1 波長は 3.40m である．音の干渉や広がりをできるだけ正確に評価するためには，点音源をその波長の 1/5～1/6（約 60cm）おきに配置させる必要がある．そこで本研究では，橋梁応答解析における床版 Flat 要素は 1 辺約 1.0m を 4 分割（1 辺約 50cm）し，新たな節点は近接する既知の応答結果を平均することで，約 50cm おきに点音源を配置させることとする．これにより，橋面に相当するバッフル上には 1683 個の点音源が配置されることになる．

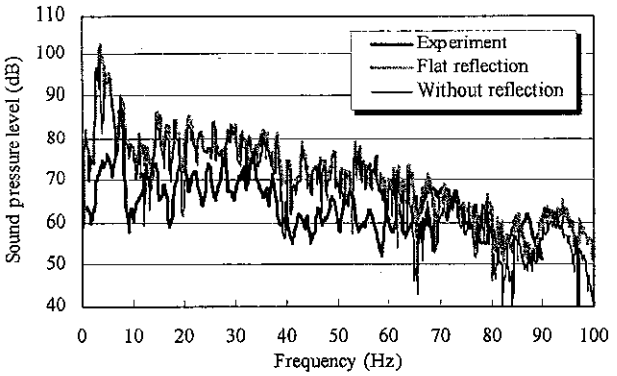

Fig.8 Sound pressure level

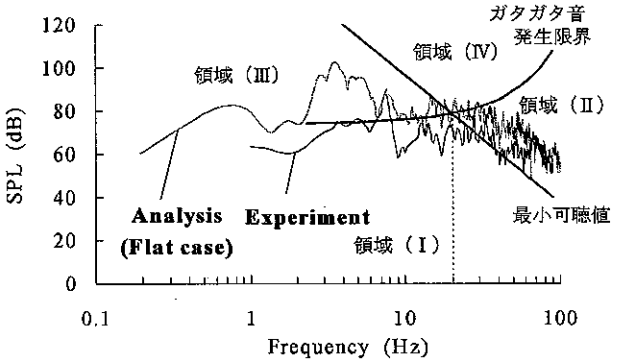

Fig.9 Classification of sound pressure level

5.1 音圧レベル

解析により音圧レベルを算出する位置は，実測結果の得られている基点部地表面（Fig.1 参照）とする．Fig.8 に音圧レベルの実測結果，および地盤の反射を考慮するケースと考慮しないケースのそれぞれの解析結果を比較して示す．なお，地盤の反射に関しては鏡像法を用い，音は地盤面で全反射すると考える[4]．橋梁動的応答解析において実測値より解析結果の方が加速度が大きく現れていたことから，低周波音の解析結果も実測結果より大きくなっている．また，解析結果では橋梁の 1 次モードに対応する 4Hz 付近でピークを示すのに対し，実測結果は橋軸に対するたわみモードに対応する 8Hz 近傍でピークを示す．橋梁の実測加速度応答によれば，4Hz 近傍が卓越していることから，実橋においても解析値に近い 4Hz 近傍の音圧はさらに大きいのではないかと考えられる．実測結果に比べ解析結果は，60Hz 以上でそれ以下の振動数域の音圧レベルに比較し小さくなる傾向となる．この理由として実橋梁では桁からの低周波音も観測されているものと考えられるのに対し，本解析が床版のみを対象としているためと考えられる．

解析値における地盤反射を考慮した結果では，考慮しない場合よりも全体的に若干大きくなっており，直接音と反射音の合成が生じていることが分かる．

次に，実測および解析によって得られた音圧レベルの評価を行う．Fig.9 に示すように，最小可聴値およびガタガタ音発生のそれぞれの限界値曲線により，音圧レベルのスペクトル図は 4 つの領域に分割することができる[17]．そ

Table 3 Natural frequencies of bridge

(Hz)

Mode Number	Natural frequencies	
	t=25cm	t=19cm
1	4.31	4.71
2	5.03	5.44
3	7.67	8.37
4	12.95	14.20

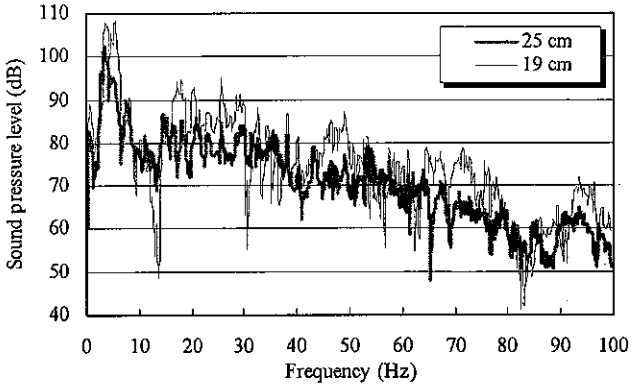

Fig.10 Effect of slab thickness (3-vehicles, Headway=30m)

れぞれの領域の状態を以下に示す．

領域（Ⅰ）：戸障子，窓ガラス等がガタガタ鳴ることもなく，どんな低周波音も感知されない．

領域（Ⅱ）：戸障子・窓ガラス等がガタガタ鳴ることはないが，低周波音が何らかの形で感知され，生理的な苦痛を感じることが多い．

領域（Ⅲ）：低周波音自体直接的には感知されないことが多いが，戸障子・窓ガラスなどがガタガタ鳴るという物理的な現象によって間接的に感知される．

領域（Ⅳ）：戸障子・窓ガラス・雨戸などの建具類がガタガタ鳴る一方で,低周波であっても音圧レベルが高いため音として感知される場合が多く,低周波音公害としてかなり厳しい状況にさらされる．

実測された音圧レベルは 8Hz 付近で領域(Ⅲ)，30～40Hz および 50Hz 以降で領域(Ⅱ)に属していることがわかる．

5.2 床版厚による影響

対象橋梁の元来の床版厚は 19cm であったが，床版補強のため 6cm の上面増し厚が行われ，現在は 25cm の厚さとなっている．ここでは，床版厚の違いにより橋梁から放射される低周波音にどのような違いが現れるのか解析的に評価する．これまでに検討してきた床版厚 25cm に対し，建設当初の床版厚 19cm の橋梁モデルを作成し，周辺の音圧レベルを比較する．まず，Table 3 にそれぞれの床版厚の場合の橋梁固有振動数を示す．振動モードは Fig.6 と同様である．床版厚を薄くし，質量が小さくなる影響で固有振動数は大きくなっている．

次に，それぞれの床版厚のケースにおける，Fig.1 に示す受音点位置での音圧レベルを Fig.10 に示す．車両台数は 3 台，車頭間隔 30m であり，水平な地盤面の反射波を考慮している．13～15Hz 付近では床版厚 25cm の方が大きい音

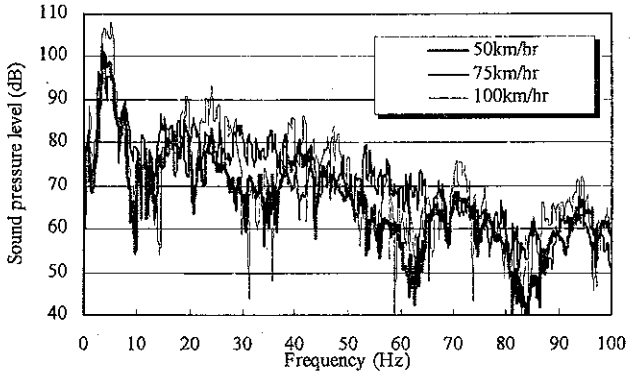

(1) Sound pressure level

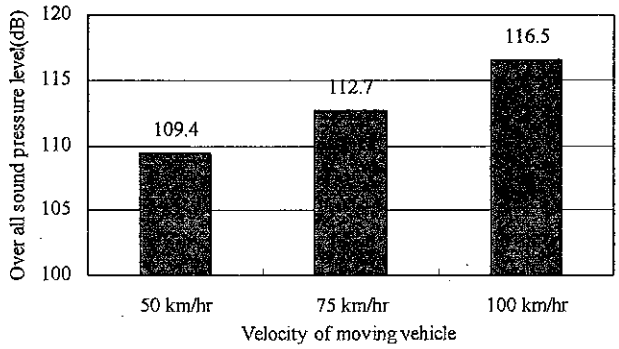

(2) Over all sound pressure level

Fig.11 Effect of moving velocity (3-vehicles, Headway=30m)

圧レベルを示すが，それ以外の振動数域においては 19cm の方が音圧は大きくなっている．Over all 音圧レベル[18]は，床版厚 25cm の 112.7dB に対し，19cm の場合は 117.3dB となった．これより，補強を目的とした床版上面増し厚を行った結果，周辺の音環境についても改善されていることが推測できる．

5.3 車両速度による影響

一般的に車両の速度が上がれば橋梁の動的応答が大きくなる．ここでは，車両速度によって周辺の音圧レベルがどの程度変化するのか解析によって明らかとする．Fig.11(1)に速度 50km/hr, 75km/hr, 100km/hr の場合の，Fig.1 に示す受音点位置での音圧レベルを示す．これまでと同様，車両台数は 3 台，車頭間隔は 30m，水平地盤の反射波を考慮した結果である．橋梁の 1 次，2 次モードに起因する 4～5Hz においては，車両速度が大きくなれば音圧も上昇する傾向となる．しかし，それ以外の振動数領域においては車両速度による相関はみられない．これは，車両が橋梁上に位置している時間がその速度により異なり，低次モード以外の振動数領域では路面凹凸による影響が大きくなるためではないかと考えられる．

ここで，速度による影響を総合的に評価するため，それぞれの速度のケースにおける Over all 音圧レベルを比較する．Fig.11(2)に示すとおり，車両速度が増加するとそれに応じて音圧が上昇することが分かり，これまでの研究における，車両速度により橋梁動的増幅率が増加するという結果にも一致する．

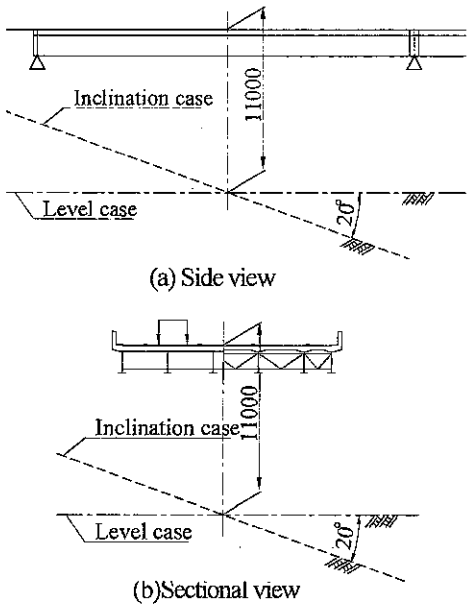

Fig.12 Imaginary ground surface

5.4 音の放射特性

音の合成に関しては本研究対象の音の波長が長いため，その干渉の影響は橋梁から離れた箇所で顕著になると考えられる．ここでは，橋梁周辺の音の放射特性について検討を行い，また実架設地点の条件を考慮して地盤の傾斜による影響も考察する．地盤の傾斜に関して Fig.12 に図示する．傾斜角度は架設地点の状況に合わせ，橋軸・直角ともに 20° とする．Fig.13 に橋軸方向への音圧レベル放射特性を，Fig.12 の 2 ケースと地盤反射を考慮しないケースと併せて示す．着目断面は幅員中央とする．ここで，図示している音圧レベルは，G 特性などの補正は行っていない Over All レベルである．どのケースもスパン中央付近を最大として音圧が広がっており，橋梁がたわむモードの影響が大きく現れている．各地盤条件を比較すると，地盤を考慮しない場合は橋梁から遠ざかるに従い床版中心を点音源とした音響放射に近くなり，ほぼ円状に広がる．一方水平な地盤を考慮した場合は地盤からの反射波との干渉により音は円状に広がらず，また全体的に音圧レベルも大きくなる．特に地表付近での音圧レベルが大きくなる傾向となる．さらに地盤の傾斜を考慮した場合は，傾斜した地盤からの波の干渉により，高さ 6～8m においてスパン中央ではなく，A1 から 10m 付近の音圧が大きくなり，水平地盤のケースとは異なる傾向を示す．

また同様に，Fig.14 には地盤の傾斜を考慮した際の，橋軸直角方向への音圧レベル分布状況を示す．着目断面はスパン中央である．最大の音圧レベルを示す位置はほぼ車両が走行する位置に相当しており，3 次モードおよび 4 次モードの寄与がうかがえる．また，Fig.13 と同様，地盤面付近では音圧レベルが上昇する傾向となることがわかる．

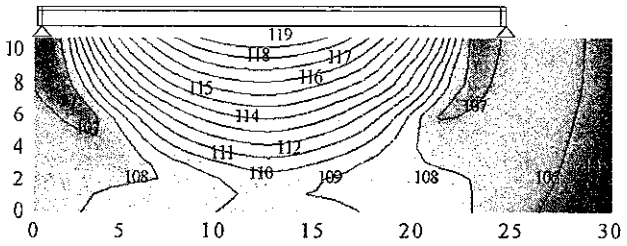

(1) Without reflection case

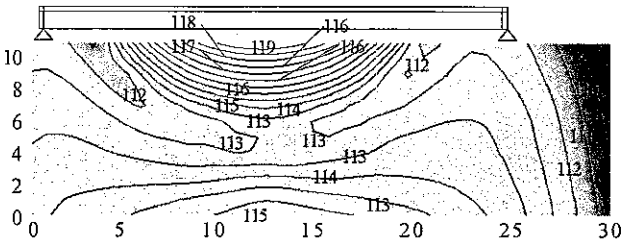

(2) Level case

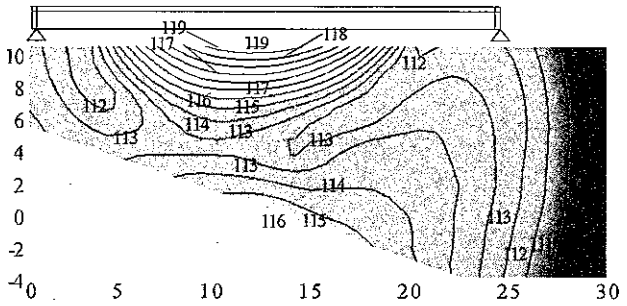

(3) Inclination case

Fig.13 Distribution of over all sound pressure level (Side view)

6 まとめ

本研究で行った橋梁の動的応答解析および低周波音解析により得られた結果を以下に示す.

(1) 床版を Flat 要素，その他の主桁，横桁などは梁要素でモデル化した橋梁と，8 自由度系の走行車両モデルとの連成振動解析を実施することにより，走行試験による実測値をほぼ再現することができた.

(2) 橋長に対し幅員の広い橋梁では，橋軸まわりの曲げが生じるモードが低い次数で発生することを確認した.

(3) 床版のみを対象とした橋梁からの音響放射解析においては，ほぼ実測された音圧レベルを再現することができた.

(4) 地盤面での反射波による影響で，周辺の音圧が上昇することが明らかとなった.

(5) 地盤面の傾斜の影響で音響放射特性が変化し，場所によっては音圧が上昇する傾向になることが分かった.

(6) 車両速度が速くなると，それに応じて周辺の音圧レベルも大きくなることを確認した.

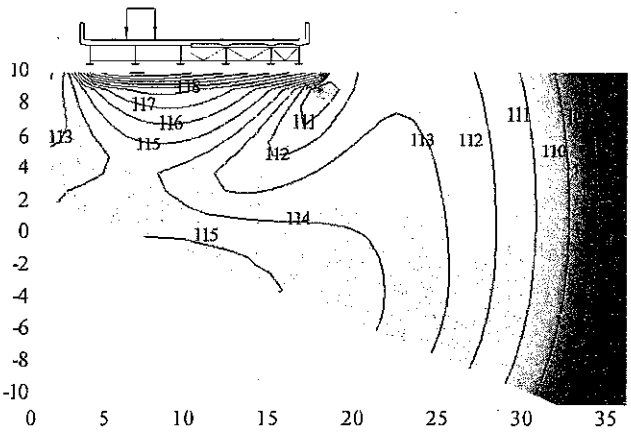

Fig.14 Distribution of over all sound pressure level (Sectional view)

(7) 床版厚 19cm の場合よりも，25cm の方が周辺の音圧レベルが低くなることが明らかとなった.

謝辞

低周波音に関する貴重なご意見を頂いた，神戸大学建設学科建築系助教授 阪上公博博士に深くお礼申し上げます.

参考文献

(1) 環境庁大気保全局：低周波音の測定方法に関するマニュアル, 2000.

(2) 環境省環境管理局大気生活環境室：低周波音防止対策事例集, 2002.3.

(3) 時田保夫：低周波音の評価について，日本音響学会誌, Vol.41, No.11, pp.806-812, 1985.

(4) 今市憲作，辻本良信，高畠伸，北川晃一：道路橋の振動に伴う音響放射の理論，日本機械学会論文集 C 編 巻 408 号, pp.904-912, 1980.

(5) 大島俊之，能町純雄：走行車両により橋梁から放射される低周波空気振動の解析，日本音響学会誌, Vol.39, No.1, pp.11-18, 1983.

(6) 大島俊之，能町純雄，月田良博，三上修一：はり理論による低周波空気振動の放射音圧レベルの解析，土木学会論文集, No.356/I-3, pp.527-536, 1985.4.

(7) 深沢泰晴，杉山俊幸，中原和彦，水上浩之：車両走行時に道路橋から放射される低周波騒音の基本特性，構造工学論文集, Vol.37A, pp.945-956, 1991.3.

(8) 杉山俊幸，小林俊哉，清水顕誠：鋼橋およびコンクリート橋から放射される低周波音の特性の比較と鋼橋の防音対策に関する一考察，構造工学論文集, Vol.45A, pp.671-681, 1999.3.

(9) 五郎丸英博，近藤正伸，小森 武，箱崎雄治：2主桁橋の振動に伴う低周波騒音の放射特性，土木学会第 57 回年次学術講演会講演概要集，I-561, 2002.9.

(10) 山口宏樹，松本泰尚，加藤誠之：地形を考慮した道路橋の低周波音伝播解析に関する基礎研究，土木学会第 57 回年次学術講演会講演概要集，I-565,

2002.9.
(11) 川谷充郎，山田靖則，嶽下裕一：三次元車両モデルによる桁橋の動的応答解析，土木学会論文集，No.584/I-42, pp.79-86, 1998.1.
(12) 川谷充郎，山田靖則，金 哲佑，川木秀昭：道路橋交通振動の三次元解析による床版応答の評価，構造工学論文集, Vol.44A, pp.827-834, 1998.3.
(13) 川谷充郎，安松敏雄，川木秀昭，織田敏章，下村公一朗：２主桁橋の走行荷重による三次元動的応答解析，鋼構造年次論文報告集，Vol.7, pp.533-540, 1999.11.
(14) 川谷充郎，下村公一朗，西村宣男，安松敏雄，金 哲佑，河田直樹：弾性支承を有する鋼２主桁橋の走行荷重下の三次元動的応答解析，土木学会第56回年次学術講演会講演概要集，Ⅰ-A143, 2001.10.
(15) Chul-Woo Kim, Mitsuo Kawatani, Naoki Kawada: Improving dynamic serviceability of steel twin-girder bridge due to moving vehicle, Third International Conference on Current and Future trends in bridg design, Construction and Maintenance Shanghai, China, September 2003.
(16) 川谷充郎・小林義和・高森和恵：曲げとねじりを考慮した単純桁橋の走行荷重による非定常連成不規則振動解析，土木学会論文集，No.570/I-40, pp.231-238, 1997.7.
(17) 山田伸志：超低周波音と低周波音，環境技術研究会，1984.7.
(18) 前川純一，森本政之，阪上公博：建築・環境音響学 第２版, pp.28, 共立出版, 1990.

(2003.7.31 受付)

サスペンション構造の違いによる高架橋振動への影響

The influence of the traffic vibration upon Highway Bridge due to running vehicles with the difference suspension

梶川康男*，深田宰史**，林下貴彦***，山田健太郎****，小塩達也*****
Takahiko Hayashishita, Yasuo Kajikawa, Saiji Fukada, Kentaro Yamada and Tatsuya Ojio

*工博，金沢大学大学院教授，自然科学研究科（〒920-8667　金沢市小立野 2-40-20）
**博士（工学），金沢大学大学院助手，自然科学研究科（　　同上　　）
***　金沢大学大学院，自然科学研究科（　　同上　　）
****Ph.D.，名古屋大学大学院教授，環境学研究科（〒464-8603　名古屋市千種区不老町）
*****工修，名古屋大学大学院助手，環境学研究科（　　同上　　）

The problem of the traffic vibration is complicated because of many vehicles parameters as velocity, weight and suspension and so on. Recently it is clearly shown that the traffic vibration of the bridge is reduced due to running vehicle with air suspensions. However it is not clear whether the traffic vibration upon the Highway Bridge and that of the surrounding environment is reduced. Therefore, in this study using the vehicle with leaf suspensions and with air suspensions we investigated the influence of the traffic vibration upon Highway Bridge and that of the surrounding environment.

Key Words: air suspension, traffic vibration
キーワード：エアサスペンション，交通振動

1. はじめに

車両の大型化，交通流の増大により，道路交通振動が橋梁の周辺環境に与える影響が大きくなっている．また，道路交通振動により苦情が発生しても，振動規制法における要請限度値とその振動苦情の実態が必ずしも一致していないのが現状である[1]．

橋梁における交通振動では，加振源となる車両のパラメータ[2)3)]（車種，走行速度，走行車線，車両総重量，卓越振動数，減衰特性等）が，橋梁－橋脚－地盤という伝播経路と受振側の家屋に与える影響が大きく，各測点での応答は大きく異なる．この車両パラメータが数多くあるために，振動問題を複雑化しているといえる．

特に，最近の車両は，エアサスペンションが搭載され積荷の高品質輸送と走行安定性を向上させている．これは，車両パラメータの中でも減衰機構を向上させたものである．この車両減衰機構の向上が橋梁の振動を低減する効果があるといわれ[4)]，試験橋梁における走行実験の結果[5)]についても述べられている．しかし，実際の高架橋やその周辺環境において計測した事例がない．

そこで本研究では，従来の板ばね構造によるリーフサスペンション（リーフサス）車両とエアサスペンション（エアサス）車両を用いて，車両が走行した際の交通振動による高架橋とその周辺環境への影響について調べた．

2. 実験概要

2.1　対象橋梁の概要

本研究における対象橋梁は，東名阪道上り線の小島高架橋の一部である支間長 35m，5 主桁を有する単純鋼 I 桁橋（A2－P10 間）である．Fig.1 に一般図を示す．また，Fig.2 に対象橋梁における測点配置図を示す．

本実験では，T 型の P10 橋脚に着目して橋脚まわりを重点的に測点を配置した．そのため，対象橋梁は A2－P10 間であるが，隣接する 3 径間連続桁橋の側径間（P10－P9 間）も計測対象とした．主桁においては，P10 橋脚を中心として A2－P10 径間と P10－P9 径間の支間中央にそれぞれ鉛直方向に加速度計を設置した．P10 橋脚においては，橋脚天端に 3 箇所（両張り出し部と脚柱上）それぞれ 3 軸方向の加速度計を設置するとともに，地盤上では，橋脚基部と官民境界に加速度計を設置した．なお，ここで設置した加速度計はすべて振動レベル計（RION，VM－52）を用いて加速度出力している．また，可動支承の可動状況を観測するため，耳桁の支承の橋軸方向変位を計測した．P10 橋脚においては，T 型橋脚となっているため，両張り出し部の橋軸および鉛直方向の変位を計測した．また，A2－P10 径間の支間中央の鉛直変位も計測した．さらに，A2－P10 径間の G1 桁と G4 桁における端垂直補剛材に生じる鉛直方向ひずみを測定し，支点反力に比例するひずみ量を測定した[6)]．

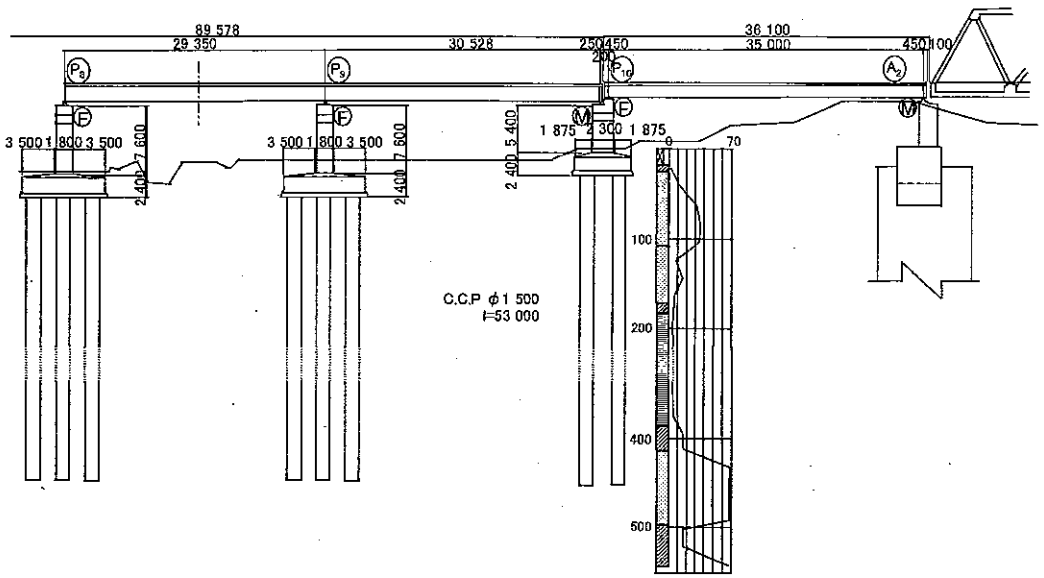

Fig.1 General view of the objective bridge

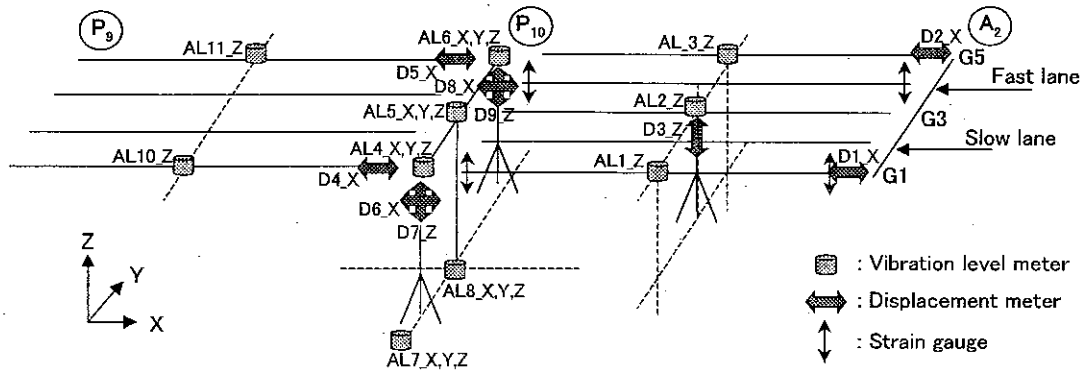

Fig.2 Measurement points

2.2 試験車両の概要

本実験で用いた試験車両は，リーフサスを有した車両（三菱，FU50JUZ）とエアサスを有した車両（いすゞ，CYJ51W3）の2台を用いた．各試験車両の諸元をTable 1に，一般図をFig.3に示す．試験車両はどちらも，車両の大型化に伴い近年急速に普及している245kN車両を用いた．リーフサス車両は3軸，エアサス車両は前輪2軸，後輪2軸の4軸車両で後輪2軸部がエアサスペンションを搭載している．試験車両の測点配置としては，前輪，後輪のばね上およびばね下の4箇所に圧電型加速度計を設置した．試験車両の測点配置図をFig.3に付記した．

Table 1 Properties of the vehicles

			Leaf suspension	Air suspension
Total mass		kN	239.904	241.276
Front mass		kN	79.135	100.303
Rear mass		kN	160.769	140.973
Full length		mm	11975	11990
Wheel base	L2+L3+L4	mm	7190	7335
Front overhang	L1	mm	1370	1400
	L2	mm	—	1850
	L3	mm	5870	4275
	L4	mm	1320	1210
Rear overhang	L5	mm	3355	3195
Front tred	L6	mm	2050	2080
Rear tred	L7	mm	1845	1870

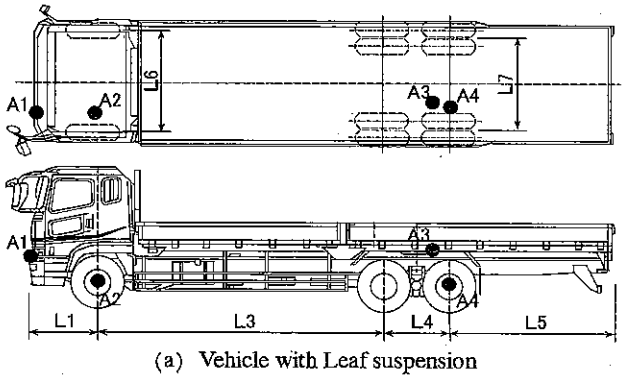

(a) Vehicle with Leaf suspension

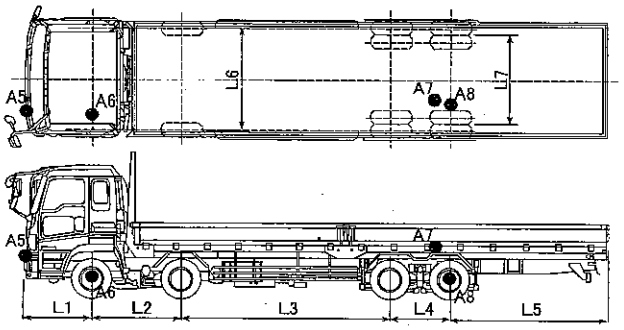

(b) Vehicle with Air suspension

Fig.3 General view of vehicles and Measurement points

● : Acceleration meter

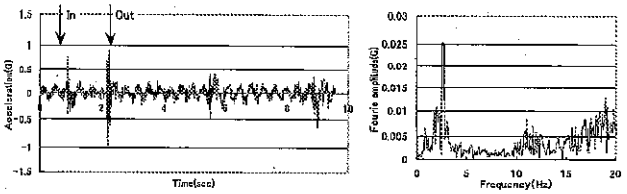

(a) Acceleration of A3　(b) Spectrum of (a)

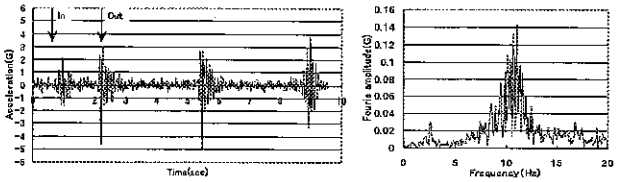

(c) Acceleration of A4　(d) Spectrum of (c)

Fig.4 Response of the vehicle with Leaf suspension

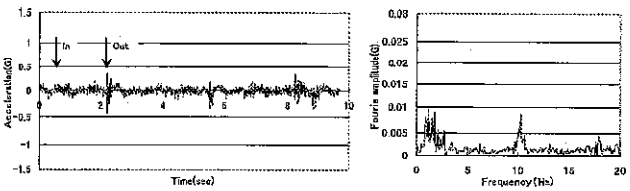

(a) Acceleration of A7　(b) Spectrum of (a)

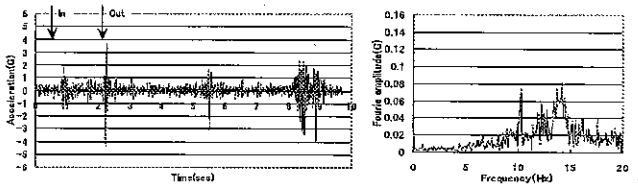

(c) Acceleration of A8　(d) Spectrum of (c)

Fig.5 Response of the vehicle with Air suspension

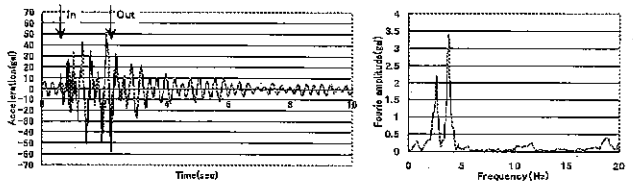

(a) Acceleration of AL_Z　(b) Spectrum of (a)

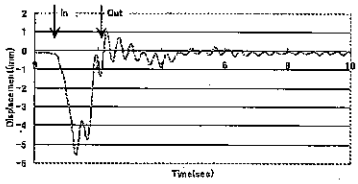

(c) Displacement of D3_Z

Fig.6 Response of the vehicle with Leaf suspension

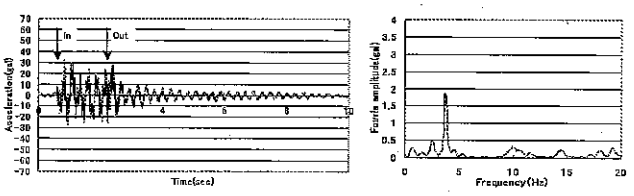

(a) Acceleration of AL_Z　(b) Spectrum of (a)

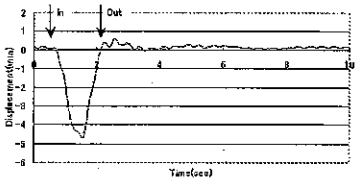

(c) Displacement of D3_Z

Fig.7 Response of the vehicle with Air suspension

2.3 実験内容

本実験では，リーフサス車両とエアサス車両を用いて試験車走行実験を行った．

実験内容として，走行速度（80，100km/h），走行車線（追越車線，走行車線）をパラメータとして，単独走行および連行走行させた．なお，交通規制は行わず，一般車の交通量が少ない時間帯に実験を行った．

3. 実験結果

本実験における結果として，リーフサス車両およびエアサス車両が走行車線を 100km/h で走行した場合を例にとり，各測点における応答波形を示す．

3. 1 車両の振動特性

Fig.4 にリーフサス車両,Fig.5 にエアサス車両の後輪ばね上とばね下の加速度波形とスペクトルを示す．

これにより，Fig.4 (a) と Fig.5 (a) のばね上加速度波形においては，リーフサス車両において，進入および退去のジョイント通過時に約 1G の加速度を記録している．一方，エアサス車両においては，エアサスペンション機能の効果が表われ 0.4G 程度となっており，ばね上の橋梁に対する加振力が小さくなっている．また，Fig.4 (b) と Fig.5 (b) に示したスペクトルでは，リーフサス車両が 2.7Hz に大きな卓越が見られるのに対して，エアサス車両は，1.1Hz～1.7Hz に広く分布している．

Fig.4 (c) と Fig.5 (c) のリーフサス車両とエアサス車両のばね下の加速度波形において，進入および退去のジョイント通過時の最大加速度で比較すると優位な差は見られないが，エアサス車両では，若干減衰が大きくなっていることがわかる．また，Fig.4 (d) と Fig.5 (d) に示したスペクトルでは,エアサス車両の振動数が高く，3 つの大きな卓越が見られる．一方，リーフサス車両は，板ばね特有の 10Hz を中心とした山型の分布となっている．どちらの車両も一般的に言われているばね下の分布領域 10Hz～20Hz の範囲といえる．

3. 2 桁上の応答

リーフサス車両およびエアサス車両が走行した時の G1 桁支間中央における加速度波形 (Fig.2 : AL1_Z) と G3 桁支間中央における変位波形 (Fig.2 : D3_Z) をそれぞれ Fig.6 および Fig.7 に示す．

これより，加速度と変位の動的振幅は，エアサス車両が走行した場合の方が小さくなっていることがわかる．

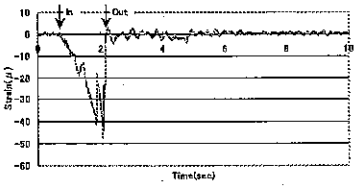

(a) Strain of G1 girder

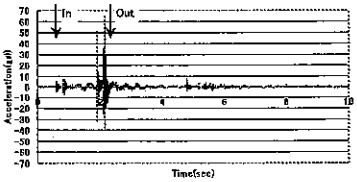

(b) Acceleration of AL_4X

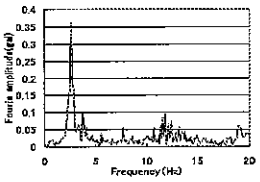

(c) Spectrum of (b)

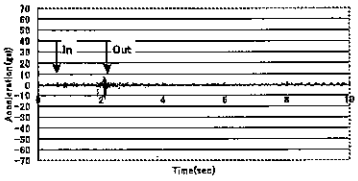

(d) Acceleration of AL_4Y

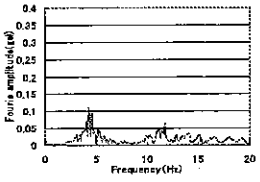

(e) Spectrum of (d)

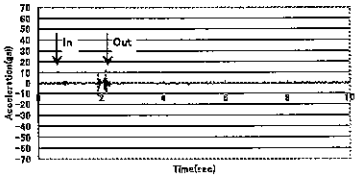

(f) Acceleration of AL_4Z

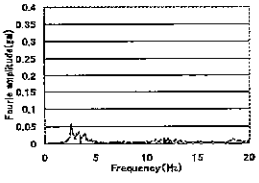

(g) Spectrum of (f)

Fig.8 Response of the vehicle with Leaf suspension

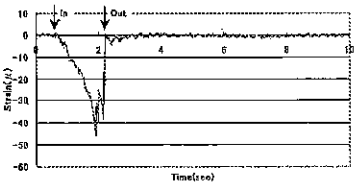

(a) Strain of G1 girder

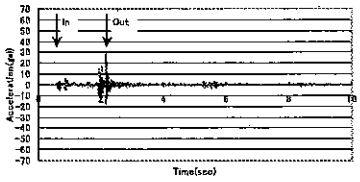

(b) Acceleration of AL_4X

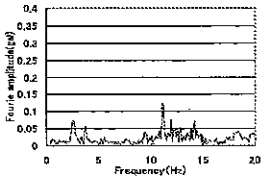

(c) Spectrum of (b)

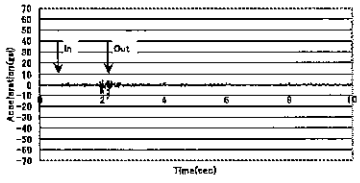

(d) Acceleration of AL_4Y

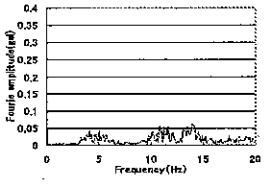

(e) Spectrum of (d)

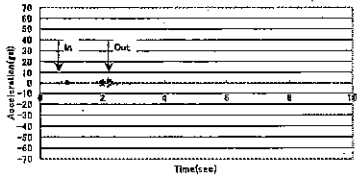

(f) Acceleration of AL_4Z

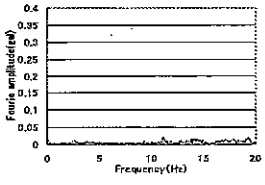

(g) Spectrum of (f)

Fig.9 Response of the vehicle with Air suspension

G1 桁の加速度波形のスペクトルから卓越振動数としては，2.6Hz のたわみ 1 次振動と 3.7Hz のねじれ 1 次振動がどちらも卓越しているが，エアサス車両走行時の方がたわみ 1 次振動の卓越がかなり小さくなっている．

リーフサス車両とエアサス車両がそれぞれ走行した場合の鉛直変位における動的振幅量の違いについて Table 2 では，リーフサス車両とエアサス車両が走行速度と車線を変化させて単独走行した場合の G3 桁支間中央における鉛直変位（Fig.2：D3_Z）の動的増幅率[7]を示した．これより，リーフサス車両は，動的増幅率が 1.1～1.2 程度であるが，エアサス車両は，1.0～1.1 程度となっており，その違いが顕著に表われている．

Table 2 Dynamic Increment Factor of D3_Z

Vehicle speed	Lane	Leaf suspension	Air suspension
80km/h	Slow lane	1.226	1.047
	Fast lane	1.124	1.040
100km/h	Slow lane	1.234	1.066
	Fast lane	1.219	1.036

3．3　橋脚天端の加速度応答

Fig.8（a）および Fig.9（a）にリーフサス車両およびエアサス車両が走行した場合の G1 桁（P10 橋脚側）端垂直補剛材（Fig.2：ST-5）の鉛直方向ひずみを示す．このひずみ量からは，車両の各軸が通過したピークが波形から読み取れるため，橋脚に与える車両外力の入力時刻が把握できる．

Fig.8（b）～（g）および Fig.9（b）～（g）にリーフサス車両およびエアサス車両が走行した場合の橋脚天端 G1 桁における 3 軸方向の加速度波形（Fig.2：AL4）とそのスペクトルを示す．これより，車両が走行した場合，P10 橋脚は橋軸方向に大きく振動していることがわかる．これらの各波形をリーフサス車両およびエアサス車両で比較すると，橋軸方向と鉛直方向において加速度振幅が低減している．しかし，橋脚天端では，すべての走行ケース，橋脚天端すべての測点で低減していない（3.6 節参照）．

また，橋脚天端上の 3 軸方向の各スペクトルをリーフサス車両およびエアサス車両で比較すると，どちらの車両が走行した場合もばね下振動数領域 10Hz～20Hz の卓越振動数のスペクトルエネルギーはそれほど差異がないが，たわみ 1 次（2.6Hz）およびねじれ 1 次（3.7Hz）の卓越振動数においてエアサス車両の方が小さくなっている．これは，エアサス車両は，ばね下振動に対しては，リーフサスと同程度の加速度振幅となっているのに対して，ばね上振動に対する加速度振幅は小さくなっているためと考えられる．

また，端垂直補剛材に貼付したひずみ波形と対応させてみると，各加速度波形の 2 つのピークはそれぞれ，前

軸によるものと，後輪2軸分によるものであることがわかる．後輪2軸分の重量の方が大きいために加速度のピーク値も後輪通過時が大きくなっている．

3．4　橋脚の変位応答

リーフサス車両およびエアサス車両が走行した場合のP10橋脚の橋軸方向変位挙動に着目する．なお，P10橋脚における支承はすべて鋼製支承（黄銅支承板支承）であり，A2−P10間の単純径間側は固定支承となっている．

Fig.10では，リーフサス車両およびエアサス車両が走行した場合の測点D1（A2側G1可動支承）とD6（P10橋脚G1側）における橋軸方向変位を示している．D1では，ほとんど移動量がないが，D6では，たわみに伴う橋軸方向の変位が可動支承より大きいことがわかる．これをリーフサス車両およびエアサス車両の走行で比較すると，上部構造の振動を受けて，動的成分がリーフサス車両の走行では大きいことがわかる．

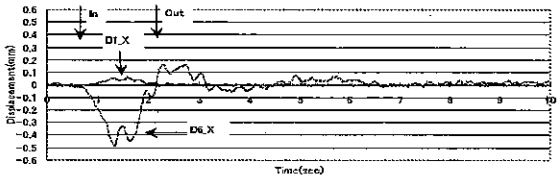

(a) Response of the vehicle with Leaf suspension

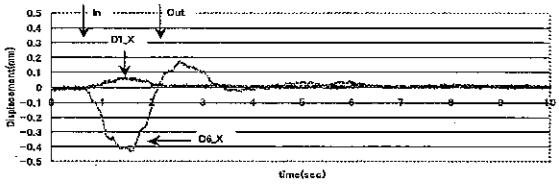

(b) Response of the vehicle with Air suspension

Fig.10 Displacement of D1_X and D6_X

3．5　官民境界の地盤応答

リーフサス車両およびエアサス車両が走行した場合の官民境界における地盤上の3軸方向の加速度波形（Fig.2：AL7）をFig.11およびFig.12に示す．

地盤上の加速度波形からは，退去時に2つのピークが見られ，Fig.8（a）およびFig.9（a）から，前軸と後軸2軸分の通過に伴うものであることがわかる．地盤上においても橋脚天端と同様に橋軸方向が大きな振幅となっている．地盤に伝播している主な卓越振動数としては，たわみ1次振動，ねじれ1次振動が大きく卓越し，高周波領域では，ばね下振動数領域10Hz～20Hzが卓越している．また，地盤上の3軸方向の各スペクトルをリーフサス車両およびエアサス車両で比較すると，どちらもばね下振動数領域10Hz～20Hzの卓越振動数のスペクトルエネルギーはそれほど差異がないが，たわみ1次（2.6Hz）およびねじれ1次（3.7Hz）の卓越においてエアサス車両の方が小さくなっている．

3．6　各測点の最大振動加速度レベル

リーフサス車両とエアサス車両がそれぞれ80km/h，100km/hで走行，追越車線を走行した際の各測点における最大振動加速度レベルの最大値をTable 3にまとめ，各測点での影響について考察する．なお，Fig.13に測点概要図を示す．

一般的に，道路交通振動の計測では，ある時間区分のL_{10}の振動レベル値を求めて要請限度値との比較をする．しかし，ここでは桁や橋脚の振動を扱っているため人体の振動感覚補正を行わない振動加速度レベルを比較対照とし，単独走行の比較であるため最大値の比較とした．

まず主桁上に着目する．測点としては，AL1_Z～AL3_Z

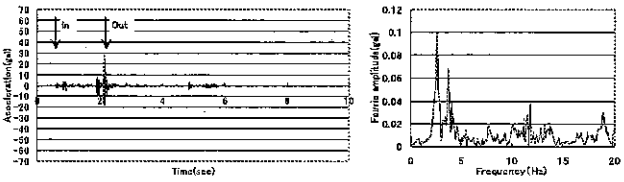

(a) Acceleration of AL_7X　(b) Spectrum of (b)

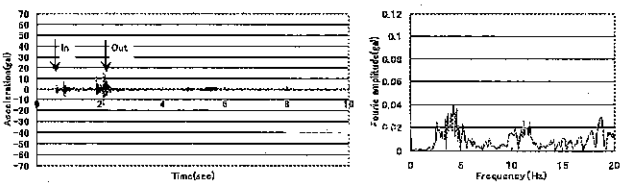

(c) Acceleration of AL_7Y　(d) Spectrum of (c)

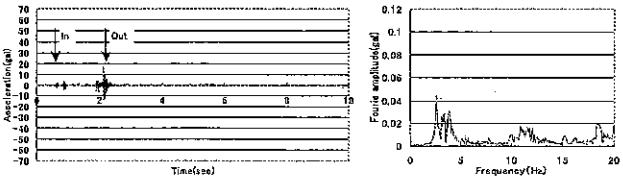

(e) Acceleration of AL_7Z　(f) Spectrum of (e)

Fig.11 Response of the vehicle with Leaf suspension

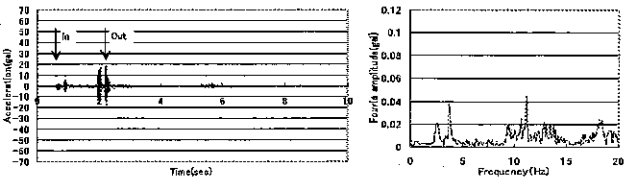

(a) Acceleration of AL_7X　(b) Spectrum of (b)

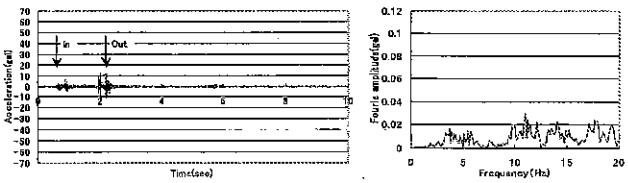

(c) Acceleration of AL_7Y　(d) Spectrum of (c)

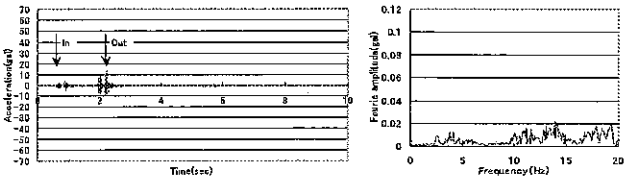

(e) Acceleration of AL_7Z　(f) Spectrum of (e)

Fig.12 Response of the vehicle with Air suspension

Table 3 Max vibration acceleration level (unit : dB)

	Leaf suspension				Air suspension			
	80km/h		100km/h		80km/h		100km/h	
Points	Slow	Fast	Slow	Fast	Slow	Fast	Slow	Fast
AL1_Z	85.6	82.7	88.1	85.8	78.9	80.7	81.8	79.8
AL2_Z	88.3	82.6	88.3	86.8	77.9	80.5	80.2	84.1
AL3_Z	92.1	84.8	90.7	89.3	81.7	81.7	80.7	80.8
AL4_X	78.6	76.7	81.3	78.6	79.2	76.4	78.8	79.7
AL4_Y	72.7	74.0	74.3	75.9	73.0	74.4	72.1	78.1
AL4_Z	75.4	75.0	78.2	78.0	77.4	76.5	76.8	79.3
AL5_X	79.5	79.3	81.4	80.0	77.3	78.2	75.7	80.8
AL5_Y	65.7	66.4	67.8	68.3	64.9	67.9	68.3	68.2
AL5_Z	66.3	66.2	68.7	68.4	64.3	66.8	64.0	68.2
AL6_X	78.7	79.9	80.8	83.1	80.3	81.0	79.9	83.8
AL6_Y	75.3	74.2	76.9	74.4	73.7	73.0	71.7	76.1
AL6_Z	77.3	77.9	78.8	84.9	76.7	82.0	79.9	85.5
AL7_X	71.9	74.5	75.9	79.2	76.3	77.1	76.0	79.2
AL7_Y	69.3	72.8	70.9	76.3	69.5	74.1	70.6	77.1
AL7_Z	68.7	72.3	71.1	74.6	71.1	72.8	71.2	74.4
AL8_X	80.0	80.3	82.8	82.7	80.3	82.2	82.1	83.3
AL8_Y	74.9	74.8	77.3	78.8	75.8	76.9	76.8	79.4
AL8_Z	77.2	76.1	79.5	80.5	79.3	78.3	78.1	81.5
AL10_Z	62.2	61.3	64.3	63.2	62.5	62.3	63.9	63.2
AL11_Z	55.7	59.9	58.8	61.5	55.2	61.1	58.4	61.0

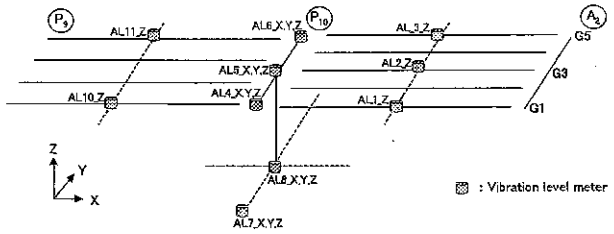

Fig.13 Measurement points

およびAL10_ZとAL11_Zである．主桁上では，ほとんどの測点で低減しており，A2－P10径間では，2dB（約2割）～10dB（約7割）もの低減が見られた．車両ばね上振動数に近い卓越振動数を有する上部構造では，エアサス車両による低減が顕著に見られる．

次に，橋脚上に着目する．測点としては，AL4_XYZ～AL6_XYZである．橋脚上では，エアサス車両走行による主桁のような大きな低減は見られず，逆に増加している測点も見られる．

次に地盤上に着目する．測点としては，AL7_XYZ～AL8_XYZである．地盤上では，ほとんどの測点において，リーフサス車両とエアサス車両の走行による変化が小さいまたはエアサス車両走行の方が増加している．

これより，橋脚上や地盤上では振動加速度レベルの最大値がリーフサス車両とエアサス車両では変化が小さいまたはエアサス車両の方が大きくなっている場合がある．これは，橋脚，地盤に伝播する振動はジョイントの段差によるばね下振動の衝撃力である．Fig.4（c）とFig.5（c）から，ばね下振動の加速度振幅は，リーフサス車両とエアサス車両で大差ないことからエアサス車両による振動低減が見られないと考えられる．

4. まとめ

本研究では，リーフサス車両とエアサス車両が走行した際の交通振動による高架橋とその周辺環境への影響について実験的に調べた．

本研究により得られた知見を以下にまとめる．

(1) 車両側の計測からエアサス車両は，ばね上振動における加速度振幅がリーフサス車両に比べて低減されているため，ばね上の橋梁に対する加振力は小さい．

(2)車両ばね上振動数に近い卓越振動数を有する上部構造では，エアサス車両の走行による加速度や変位などの動的振幅の低減が見られた．

(3)車両側の後輪ばね下測点から加速度振幅に差が見られなかった．また，橋脚天端や地盤上における加速度スペクトルからも，エアサス車両とリーフサス車両のばね下振動数領域 10Hz～20Hz におけるスペクトルエネルギーには差が見られなかった．

(4) エアサス車両では，ジョイント通過に伴うばね下振動の加速度振幅がリーフサス車両と大差がなかったことから，エアサス車両の走行による橋脚上および地盤上の最大振動加速度レベルの低減が見られなかった．

本実験は，4軸のエアサス車両，3軸のリーフサス車両を試験車として用いた結果を述べたが，車両構造の違いによる各測点の応答は異なる結果となった．したがって，今後は，一般車の走行状態を長期にわたり計測して数多くサンプルすることにより，車両と各測点の応答の関係を統計的に処理する必要性があると考えられる．

参考文献

1) 環境省編：平成 14 年版 環境白書，ぎょうせい，pp.119-120，2002.5.

2) 讃岐康博，梶川康男，深田宰史，杁本正信：プロフィルメータでの測定路面から実路面への近似法の提案，構造工学論文集，Vol.47A，pp.399-410，2001.3.

3) 深田宰史，梶川康男：短スパンPC橋の環境振動特性，橋梁振動コロキウム '01 論文集，pp.167-174，2001.10.

4) 辻靖三，足立義雄，大西博文，桐越信：新版 道路環境，山海堂，pp.197-201，2002.6.

5) 佐藤弘史，間渕利明，大石哲也，西川和廣，玉越隆史，笘之内博行：道路交通振動に与える車両サスペンションの影響，橋梁振動コロキウム '01 論文集，pp.181-185，2001.10.

6) 因田智博，若尾政克，山田健太郎，小塩達也：支点反力を用いたBridge Weigh-in-Motionの開発と交通荷重測定，土木学会第 57 回年次学術講演会講演概要集，I-725，pp.1449-1450，2002.9.

7) 橋梁振動研究会編：橋梁振動の計測と解析，技報堂出版，pp.39-42，1993.10.

(2003.7.31 受付)

鋼トラス橋通行管理のためのシミュレーション

Numerical Simulation for the Traffic control at the Corroded Truss Bridge

佐藤　恒明*，伊倉　直樹**，宮本　裕***，鬼塚　信弘****
Tsuneaki SATO, Naoki IKURA ,Yutaka MIYAMOTO and Nobuhiro ONIZUKA

* 博士(工) 木更津高専助教授，環境都市工学科（〒292-0041 木更津市清見台東 2-11-1)
**学士(工) 前木更津高専専攻科環境建設工学専攻（〒292-0041 木更津市清見台東 2-11-1)
*** 工博 岩手大学教授，工学部建設環境工学科（〒020-8551 盛岡市上田 4-3-5)
**** 博士(工) 木更津高専講師，環境都市工学科（〒292-0041 木更津市清見台東 2-11-1)

The Choshi Bridge has been exposed to sea breeze over 40 years. At present, this bridge is suffering corrosion at the several truss panel points apparently. First of this paper, the traffic control of this corroded truss bridge is examined by numerical simulation. And secondly, for the earthquake occurrence, the important points to be inspected are suggested by time-history response analysis. Simulation results show the usefulness of the inspection of floor beams at the panel points.

Key Words : Corroded Truss Bridge, Traffic Control, Numerical Simulation

1. まえがき

利根川の河口部に昭和 37 年に架橋された銚子大橋は，千葉県の東総地域と茨城県の鹿島地域を結ぶ重要な橋に位置付けられ，供用開始後，約 40 年が経過している．銚子大橋の全長は約 1.2ｋｍであり，橋の中央部は，全長 407.4mの鋼トラス橋になっている．架橋地点が河口部という潮風の厳しい環境下にあるため，鋼トラス橋の各部材の腐食が著しく，最近 10 年間に床組下フランジをＬ形プレートで補強しフッ素樹脂系の超厚膜塗装をしてきた．

また，橋の管理者である千葉県は，銚子大橋の現状を把握するために，トラス格点部近傍を中心に腐食の進行状況を調査しており，超厚膜塗装をはがして調べた結果，腐食が進行していることがわかった．

本研究は，まず耐荷力の面から第１径間に旧道路橋示方書規定の活荷重を載荷して，通行車両の重量制限について検討した．また，第１径間の下弦材にはゲルバー・ヒンジがあり，その真上の上弦材は，スライド構造の冗材となっている．このゲルバー・ヒンジ部を連続化し，５径間連続トラス橋とした場合についても検討した．

次に，地震時の緊急点検の面から近傍で観測された地震加速度波形を震度５強相当に増幅して橋脚から橋軸直角方向に入力し，時刻歴応答解析を行って緊急点検時の着目部位を検討した．下路トラス橋では，橋床部の慣性力が主構部に比べて大きく，下弦材側の格点部で応答加速度も大きくなると予想される．そこで，下弦材格点部を対象にシェル要素を用いた詳細モデルを作成して，最大加速度応答時の応力状態を調べた．千葉県は，震度５以上の地震が発生した場合，車両の通行を一時的に止めて，地震力を直接受ける支承部や橋門構などを中心に緊急点検する．本橋の点検通路は，**Fig.1** に示すように横桁中央部に添架されているため，下弦材格点部を直接点検することは極めて困難である．そこで，多数の下弦材格点部の中で比較的大きな応力状態になる格点部を数値解析で検討した．

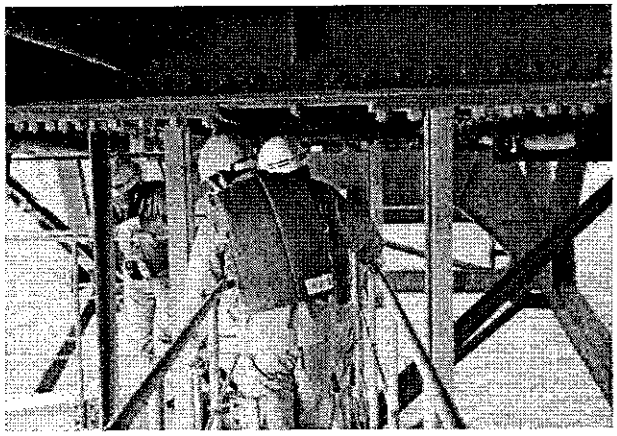

Fig.1　A state of the inspection

2．解析モデルと腐食量の設定

2.1 解析モデル

解析モデルを Fig.2 に示す．主構や床組および上下横構を３次元はり要素でモデル化し，コンクリート床版をシェル要素でモデル化している．第１径間と第５径間にあるゲルバー・ヒンジ部とその真上にある上弦材のスライド構造を再現するために，ヒンジ部に関連する下弦材および縦桁と上弦材の境界条件を指定した．また，床版の重心と床組の図心までを部材長とする鉛直の剛部材を，シェル要素と３次元はり要素の間に挿入した．なお，床版と床組の間にあるスラブアンカーの地震時非線形性は考慮しない．

モデルの検証については，第２径間の横桁スパン中央の上下フランジで測定された曲げ応力の測定値と解析値の比較から，解析モデルは妥当と判断した．

2.2 腐食量

最近の調査結果からトラスの格点部近傍で 1.0 ～2.0 mm の腐食が測定されたため，上弦材・下弦材の 15 断面および斜材の 18 断面については，断面を構成する各鋼板の当初設計時の板厚に対して一律 2.0 mm を減じた．その値を Table 1 に示す．

板厚は，各部材の断面積や強軸回りの断面二次モーメント，弱軸回りの断面二次モーメント，ねじりモーメントを計算する際に必要となるが，入力データ上では，鋼板が均一に減厚していることになり，実際の腐食状況よりも厳しい入力値と考えられる．上・下横構と横桁および縦桁についても同様に Table 1 に示す腐食量を減じた．

なお，床組の下フランジに添接された補強用の L 形プレートについては，腐食の進行はないものとして減厚していない．

Table 1　Data on corroded plates

上弦材・下弦材・斜材	断面構成板	2.0mm
上横構・下横構	鉛直板 水平板	2.0mm 6.0mm
横桁	上フランジ ウェブ 下フランジ	2.0mm 1.0mm 6.0mm
縦桁	上フランジ ウェブ 下フランジ	2.0mm 1.0mm 4.0mm

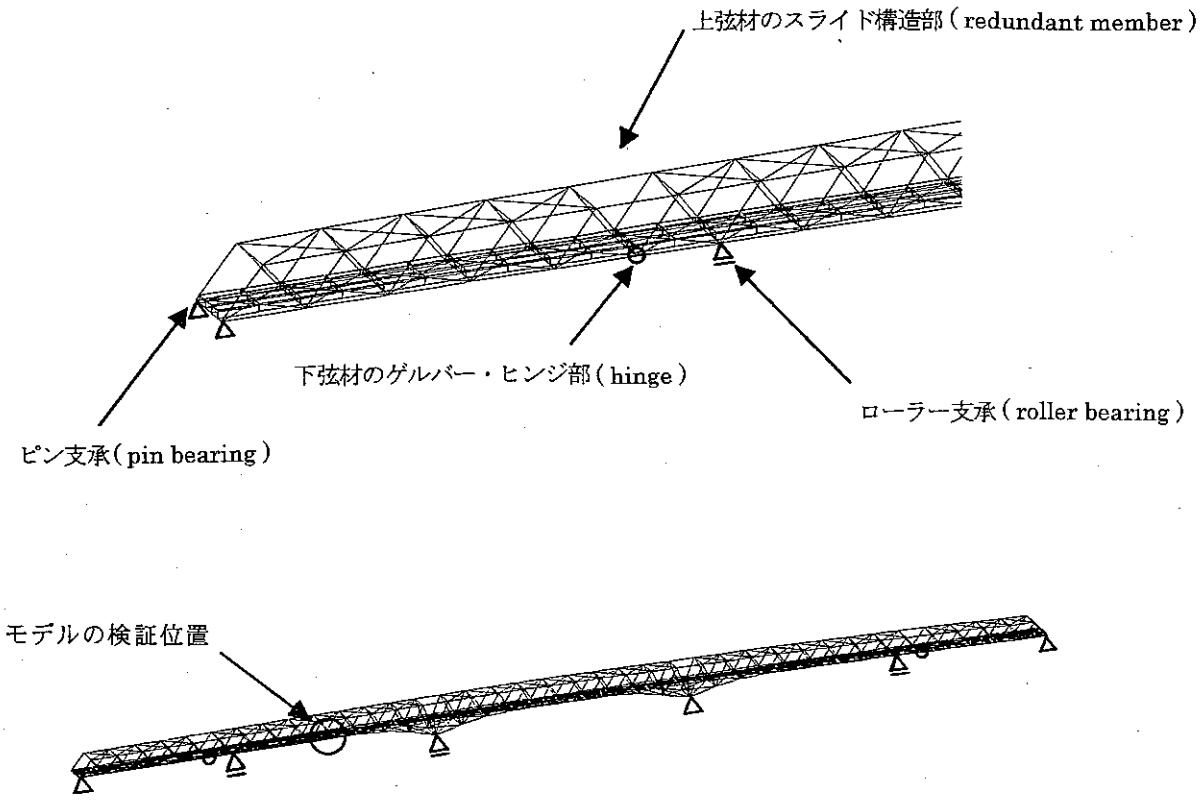

Fig. 2　Model of analysis

3．通行車両の重量制限について

既設の橋梁を維持管理する上で，健全度診断[1]は重要であり，維持管理システムの構築[2]と運用は，道路管理者の責務である．そこで耐荷力の面から，設計活荷重を載荷して腐食の進行が主構の応力増加に及ぼす影響を調べる．

活荷重は，旧道路橋示方書から等分布荷重と一つの線荷重のL-14荷重およびL-20荷重とし，各部材の影響線をそれぞれ作成し，各部材に対して最も不利になるように活荷重を載荷した．床版を含む全自重 21,200KN の死荷重は，下弦材の各格点に 320KN を均等に載荷した．

3.1 解析結果および考察

(1) たわみ性状について

Fig. 3 a),b) に第１径間の斜材(D1,D2)用および上弦材U3用の活荷重載荷による変形図を示す．両グラフとも縦軸はたわみ量，横軸は橋軸方向を示している．腐食ありからヒンジ部を連続化すると，全体的にわずかにたわみが減少し，特にヒンジ部の周辺では，腐食なしとほぼ同じ程度までたわみが減少している．下弦材のゲルバー・ヒンジ部を連続化して，５径間連続トラス橋とした場合では，第１径間と第２径間の上・下弦材が一体となって外力に抵抗するためと考えられる．

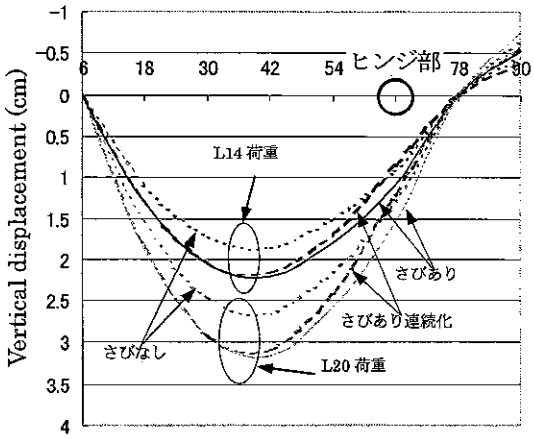

a) Live-load for D1,D2

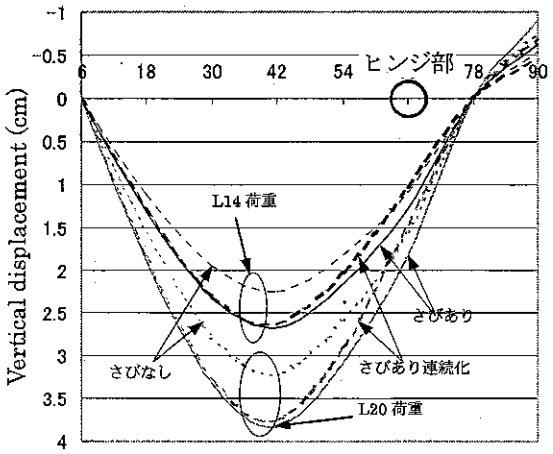

b) Live-load for U3

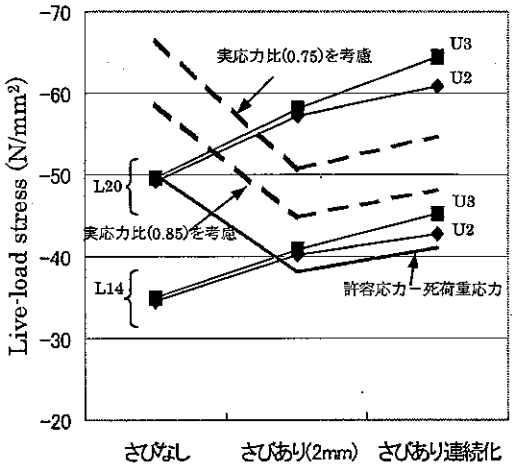

c) Upper chord member

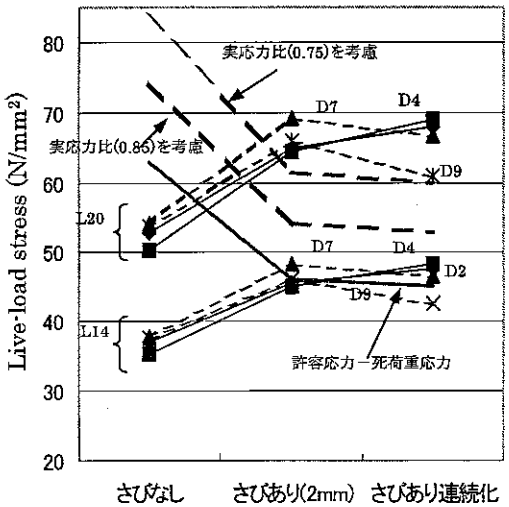

d) Diagonal member

Fig. 3 Vertical displacement and live-load stress of mail truss in the first span

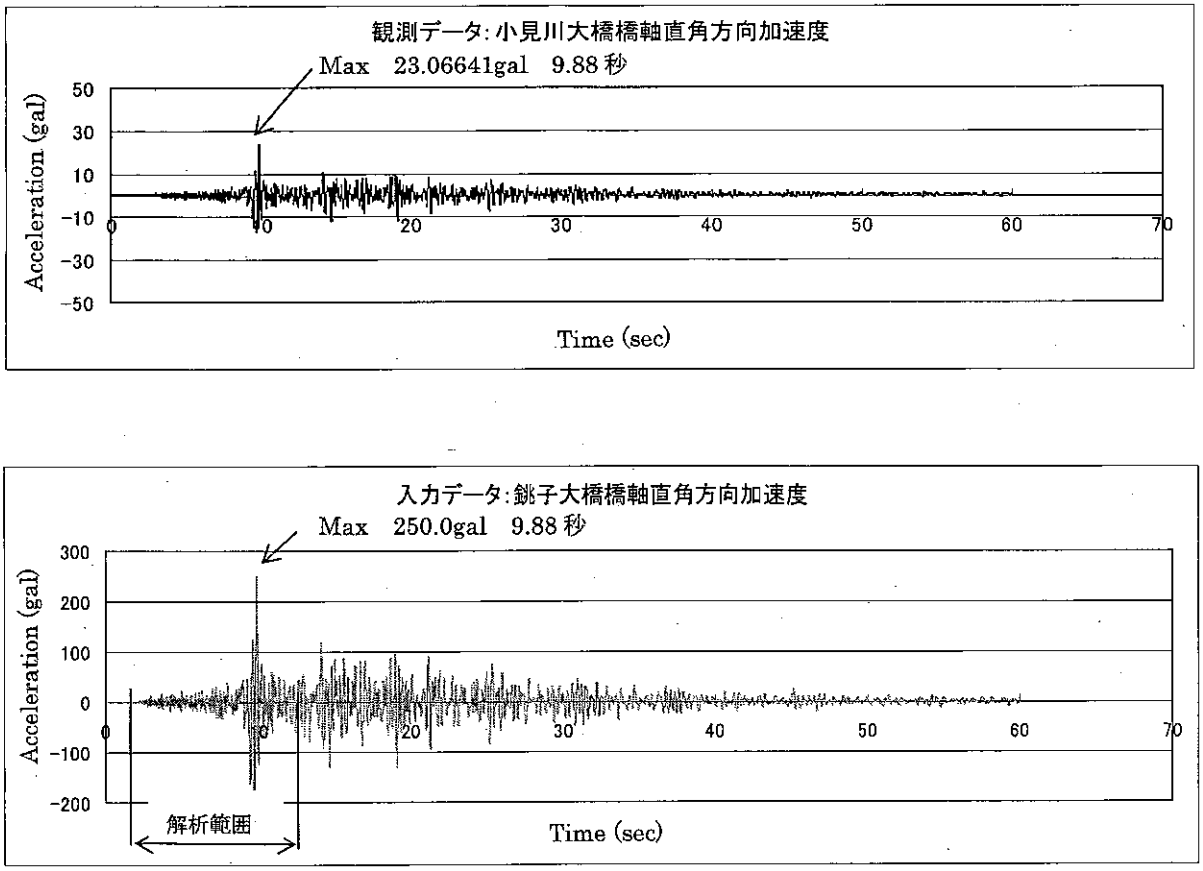

Fig. 5 Seismic wave data for time-history response analysis

(2) 活荷重による部材応力について

Fig. 3 c),d) に腐食の進行に伴う第1径間の上弦材(U2, U3) および斜材(D2,D4,D7,D9)の活荷重応力の変化を示し，Fig. 4 に第1径間の主構の部材番号を示す．Fig. 3 c),d) は，腐食の有無およびヒンジ部を連続化した場合の3ケースを示している．ここで，実応力比[3]とは,計算応力に対する実測応力の割合であり，一般に実橋は，計算応力に対して15%～25%の余裕を有している．L-20荷重による第1径間の上弦材(U2,U3) および斜材(D2,D4,D7, D9)の活荷重応力は，腐食ありと連続化の場合では，実応力比(0.75～0.85)を考慮した許容範囲を上回った．また，ヒンジ部を連続化し5径間連続トラス橋とした場合，第2径間と第1径間の上弦材の一体化によって,上弦材の外力に対する働きが増すため，上弦材(U2,U3) の応力は減少しないことがわかった．連続化の注意点である．

L-14 荷重の場合では，許容応力をわずかに越えるが，実応力比(0.75～0.85)を考慮した許容範囲に入らない．

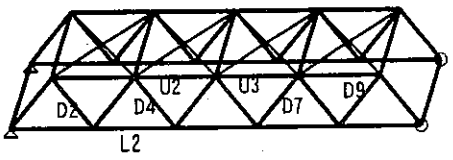

Fig. 4 Main truss in the first span

(3) 通行制限について

主構断面を構成する鋼板の腐食が，現在のところ均一に2mm減厚している状態には至っていないと考えられるため，現状では20トンを超える車両の通行を制限することとし，主構の腐食が，近い将来，一律に2mmの腐食ありと同等の状態に至った場合には，20トン車両の通行制限を実施する必要がある．

4．地震時の点検部位について

銚子地方に震度5強相当の地震が発生し，本橋が橋軸直角方向に揺れる場合の時刻歴応答解析[4),5)]を行った．

4.1 入力波形

本橋では地震波の加速度データがなかったため，Fig. 5 に示すように，上流の小見川大橋で2001年5月25日に観測された地震波を震度5強相当[6)]の最大250galまで増幅し，橋脚から橋軸直角方向に地震加速度を100分の1秒刻みで入力して，地震発生後2.00秒から12.00秒までの10秒間時刻歴応答解析を行った．ここで最初の2.00秒間は,入力加速度がきわめて小さいため解析には使用していない．したがって，入力加速度の最大値250galは9.88秒時であるが，解析ではこれを7.88秒時としている．また，道路橋示方書の規定に従って死荷重のみを考慮した．

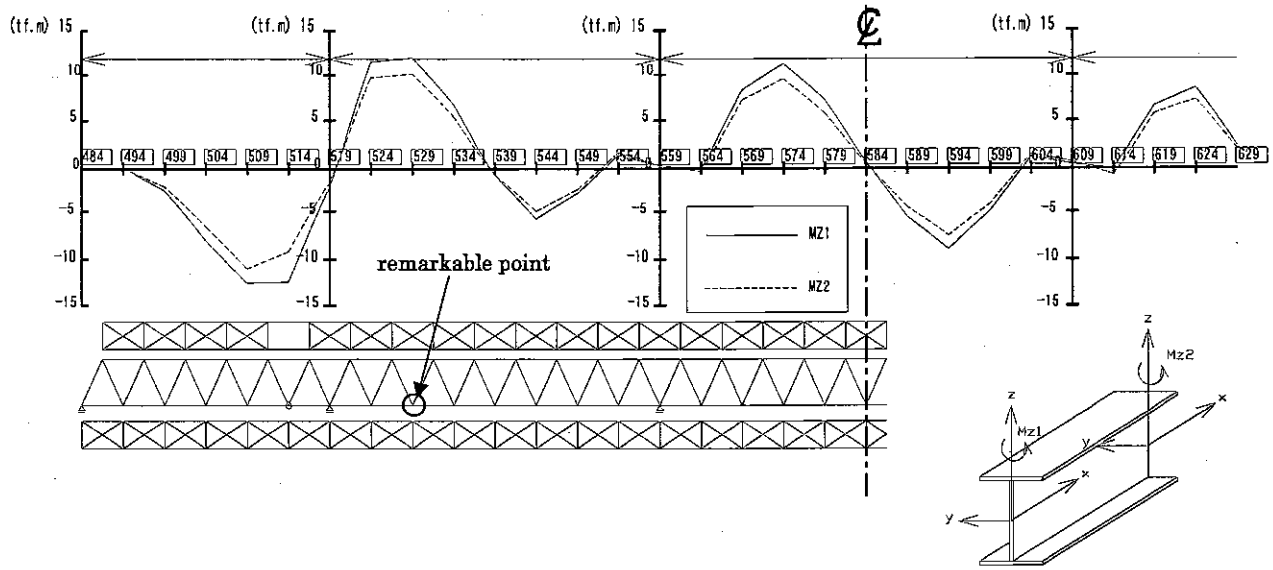

Fig.6　Out of plane bending moment Mz (8.09 sec)

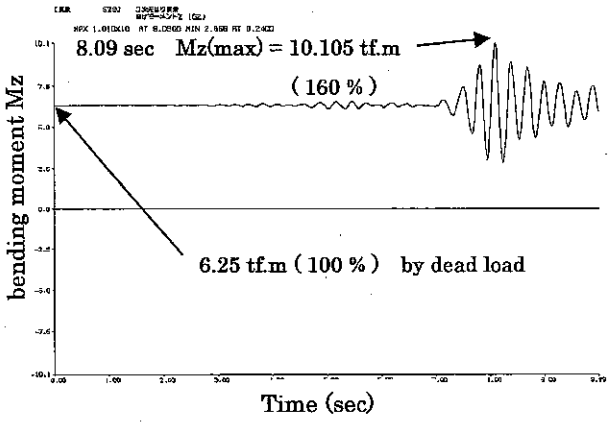

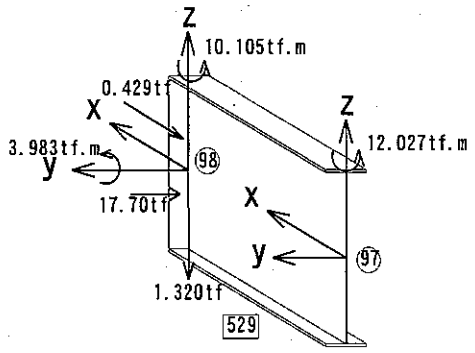

Fig.7　Section force of floor beam in the second span

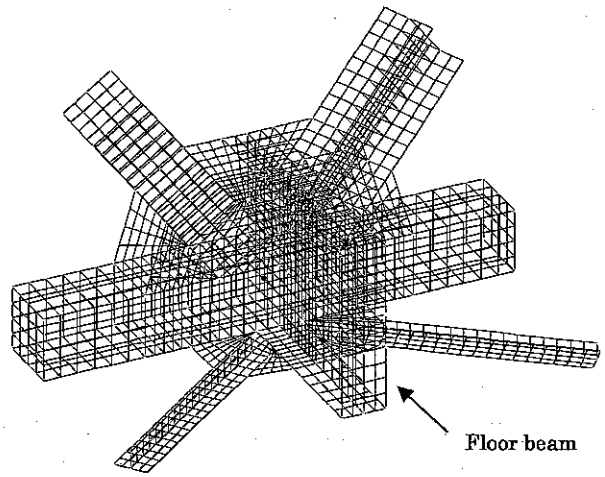

Fig.8　FEM model of panel point in the second span

4.2　解析結果および考察

Fig.6 に示す着目部位は，第２径間の比較的橋脚に近い位置にある横桁であり，この横桁の面外曲げモーメント Mz の時間変化を Fig.7 に示す．死荷重のみが作用している初期状態に比べて，8.09 秒後には約 1.6 倍の最大応答値となった．Fig.6 は，第１径間から中央径間までの横桁について，同時刻の面外曲げモーメント Mz の値を示している．この時刻の前後を詳細に調べた結果，8.09 秒時の時刻の値が，ほとんどの横桁における最大値であった．

8.09 秒時の第２径間や中央径間のほぼ中央では，橋軸直角方向に最大の応答水平変位を示す．しかしながら，各径間のほぼ中央にある横桁の両端部では橋軸方向の変位差はほとんど生じない．このため，第２径間や中央径間のスパン中央付近の横桁では，Fig.6 に示すように面外曲げ Mz は小さくなると考えられる．

これに対して橋脚に比較的近い横桁では，隣接する径間の変形の影響を受けるため，横桁の両端部に橋軸方向の変位差を生じて，Fig.6 に示すように面外曲げ Mz が大きくなると考えられる．

そこで，Fig.6 に示す着目部位の格点部について Fig.8

に示すように腐食による減厚を考慮したFEMモデルを作成し，時刻歴応答解析から得られた8.09秒時の断面力を，各部材の端部に作用させて応力状態を検討した．境界条件は，文献7），8）を参考にして，下弦材の下フランジ外側端部の部材軸方向節点について上下方向変位のみを拘束し，斜材と下弦材の部材軸線が集まる原点において3方向の変位を拘束して，各部材端部に面外曲げを含む断面力を作用させた．なお，数値解析には有限要素法汎用構造解析プログラムMSC/Visual Nastran for Windows[9]を使用した．

Fig.9に着目する格点部近傍の横桁上フランジ応力状態を示す．白色で表示しているところが約210 N/mm^{2}の値であり，使用鋼材SS400材の降伏点に比較的近い値であった．本橋が橋軸直角方向に地震を受ける場合に，橋脚に比較的近い位置にある横桁端部の上フランジに応力集中が生じると考えられる．また，この部位は，**Fig.10**に示すように第2径間では路面側から目視可能な格点の上面である．震度5以上の地震発生時における緊急点検の際に，支承部や橋門構と同様に，この部位を点検することにより下弦材格点部のダメージを概略推定できると考える．

5．まとめ

常時の通行管理および地震時の通行管理の面から，腐食による鋼板の減厚を考慮したモデルを作成して数値解析を行った．検討した結果を以下に示す．

(1) 主構の各構成鋼板の減厚状態が，均一に2 mmと同等の状態に至った場合には，20トン車両の通行制限を実施し，現状では20トンを超える車両の通行を制限する必要がある．

(2) 震度5以上の地震発生時における緊急点検の際に，支承部や橋門構と同様に，橋脚に比較的近い下弦材格点部の横桁端部上フランジ近傍を点検することにより，格点部のダメージを概略推定できると考える．

6．謝辞

鋼トラス橋の腐食測定データおよび貴重な資料を提供していただいた千葉県土木部道路維持課の積田宣明主幹に厚くお礼を申し上げます．

参考文献

1) 土木学会鋼構造委員会鋼橋の余寿命評価小委員会：鋼橋における劣化現象と損傷の評価，鋼構造シリーズ7，土木学会，1996.
2) 土木学会構造工学委員会橋梁振動モニタリング研究小委員会：橋梁振動モニタリングのガイドライン，構造工学シリーズ10，土木学会，2000.
3) 鉄道総合技術研究所：鉄道構造物等設計標準・同解説 鋼・合成構造物，pp.163-164, 1992.
4) 渡辺昇・宮本裕：時刻歴地震応答解析法，技報堂出版株式会社，1996.
5) アーク情報システム：TDAPⅢ(Windows版)，2000.
6) 千葉県土木部:震災時における行動マニュアル, 2000.
7) 佐藤恒明・倉西茂・中沢正利：鋼トラス橋の床桁ウエブに生じる面外二次応力の数値的原因分析，土木学会論文集No.492/VI-23，pp.87-95, 1994.
8) 保坂鐵矢・堀地紀行・礒江暁：トラス格点部合理化構造の検討，土木学会構造工学論文集 Vol.46A，pp.1353-1364, 2000.
9) 日本エムエスシー：MSC/Visual Nastran for Windows, 2002.

(2003年7月31日受付)

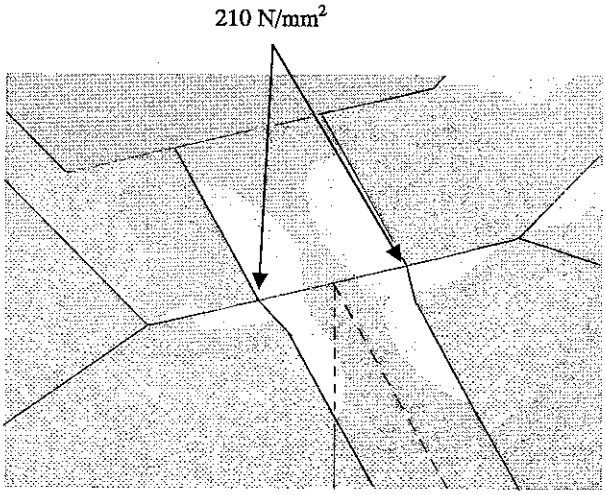

Fig.9 Stress of upper flange at the floor beam

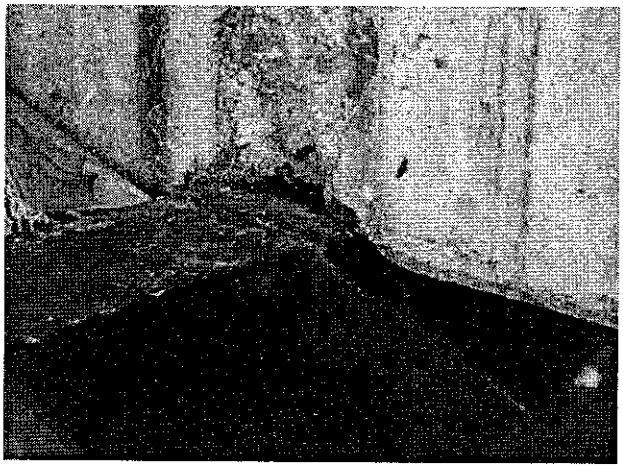

Fig.10 View of upper flange at the floor beam

老朽化した石橋基礎の沈下と破壊挙動に関する不連続体変形法解析

Discontinuous Deformation Analysis on base subsidence and failure behavior of old stone bridge

相川 明*
Akira AIKAWA

*正会員　工博　国立大分高専助教授（〒 870-0152 大分市牧 1666 番地）　E-mail: aikawa@oita-ct.ac.jp

The Shirate Bridge, located in Oita, is an old rock arch bridge on a national public road. It was constructed over 90 years ago, and thus has become weathered over the years and is slightly damaged at its base of abutment. As old rock bridges in nature are discontinuous, their stability will be governed by the distribution of discontinuities and their mechanical properties. This paper describes 2-dimensional numerical discontinuous model studies of a rock bridge using discontinuous deformation analysis (DDA) based on the site investigation of the bridge. The discontinuous numerical model of a bridge consists of an assemblage of polygonal stone blocks, abutment, roadbed and rockmass. The logistical function-shaped subsidence curves were inputted as an external forced displacement into the base of the discontinuous numerical model. The relationship of base subsidence on the failure mode and the development process are discussed in detail. The results indicate that the larger the base subsidence, the more discontinuous motions become dominant. The threshold concerning continuous and discontinuous behaviors may exist at about 20 cm of the base subsidence.

Key Words : *discontinuous deformation analysis (DDA), failure behavior, stability of old stone bridge, subsidence of abutment, assemblage of polygonal blocks*

1. はじめに

九州内には大小数百に及ぶ石橋が現存しており，それらの多くは，生活に不可欠な橋梁として，いまでも利用されている．しかしながら，施工後長い年月を経て，風化や劣化が進行しているものが多く，老朽化した石橋の安定性評価法の確立と，補強や維持管理のあり方が課題となっている．

そのような一例として，大分県日田市内で国道の道路橋として供用されている「白手橋」(**Fig.1**) が，施工後 80 年もの長い年月を経て，橋脚の基礎部分に洗掘を受け，その安定性が危惧されるようになってきた．本論文は，この石橋をケーススタディとして，石橋の安定性について数値解析的に検討するものである．

Fig.1 The Shirate Bridge in Hita, Oita.

2. 不連続体解析による安定性評価

橋梁の安定性評価にはこれまでは連続体力学が主に用いられてきた．一方，石橋は本質的に様々な形状を有する岩石ブロックからなる不連続体構造物であり，岩石ブロックの境界で変位と応力が不連続であり，引張り応力は伝達されない．また，岩石ブロックの境界の接触面が，面で接触するのか，点で接触するのか，あるいは，接触点がどの位置なのかにより，その後の変形挙動や崩壊モード大きくが異なってくる．これら不連続性に起因する変形挙動や破壊挙動に関しては，石橋のみに限定した問題ではなく，地震や劣化により不連続面が発生したコンクリート橋にも共通の問題といえる．これらの不連続性を考慮して橋梁の安定性評価を行うには不連続体力学による必要がある．

連続体力学では，圧縮，引張りやせん断応力による変形挙動や破壊現象を主に考えてきたが，石橋を，岩石ブロックの集合体からなる不連続体構造で表現すると，個々の岩石ブロックにせん断力が作用すると，すべりだけではなく，せん断応力に起因する偶力により，岩石ブロックには回転力が発生する．不規則な岩石形状に回転が生じると，岩石の配位の変化による局所的

な体積膨張が生じ，岩石ブロック間に微少な不連続面や応力集中が発生し，橋梁の安定性や振動特性に影響するものと考えられる．すなわち，老朽化した石橋の安定性や地震時の挙動に関しては，石橋を構成する岩石ブロックの配位の変化によるダイレタンシー特性が，石橋全体の挙動特性に影響するが，この点に関しては殆ど未解明のままである．

したがって，石橋の変形挙動や崩壊挙動の解明には，個々の岩石ブロックの挙動を再現して，石橋内の局所的なダイレタンシー特性を明らかにする必要がある．局所的なダイレタンシー特性は，石橋全体の破壊の進行に関与する要因であるが，従来の連続体モデルや，円形や球形近似による不連続体モデルでは，岩石ブロックの配位の変化や回転による体積膨張を再現できず，基本的なメカニズムの解明につながっていない面があった．

本研究は，岩石ブロックの配位の変化や回転による局所的な体積膨張現象を再現するために，まず，現況調査に基づいて，石橋を2次元の多角形ブロックの集合体からなる不連続体構造でモデル化した．つぎに，不連続変形法解析により，作成したモデルの橋脚部分に，洗掘による沈下挙動として，鉛直方向の強制変位を加えて，橋脚の沈下挙動を数値解析的に再現し，橋梁の安定性に関する検討を行ったものである．

解析には，大変形を伴う動的再現性および回転挙動の再現性に優れる不連続変形法解析 (DDA) を用いた．DDA は多角形で構成される弾性体ブロック集合体の動的な数値解析手法である [1)-3)]．各ブロックの剛体変位，剛体回転，要素ひずみを未知数として，Hamilton の原理に基づく運動方程式について，ポテンシャルエネルギーを変分原理により最小化して平衡方程式を導出する．変位型の FEM による弾性体の大変形解析の一種であり，その定式化も FEM と同様の手順を踏む．接触バネを用いる点は個別要素法に類似するが，ブロックには互いに貫入がなく，かつ，引張力も作用しないという付帯条件を停留値問題に付加し，具体的には貫入によるポテンシャルエネルギーを最小2乗法で評価する Penalty 法を用いる．また，ブロックの接触部では Mohr-Coulomb 則により，摩擦によるエネルギー損失が考慮される [4)]．別の見方をすると，1ブロック=1Finite Cover となる Manifold 法の特殊な場合とみなせる [5)]．

3. 石橋の現況調査結果

3.1 橋梁本体の状態

「白手橋」は，全長 20.700 m，橋梁上面長 13.300 m，幅員 7.500 m の石造りのアーチ橋である．橋梁の中心をなす輪石，要石，壁石ともに施工当時のものである．アーチは，左右の橋脚間隔 9.100 m 上に，スパンライズ比 0.30 で 28 個の輪石を円弧状に配置し，壁石は全て水平積み構造であり，石材の不連続面は千鳥に配置されている．川の上流から下流に至る形状をみると，川幅は狭いにもかかわらず，川面は深くえぐれた形状で急涯をなしており，両岸を構成する岩が非常に硬く安定した岩盤からなるものと想定される．

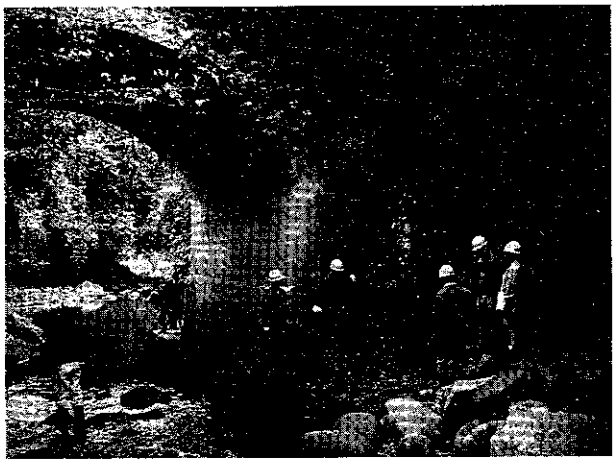

Fig.2 Bridge abutment, embankment (approach block) and concrete layer for reinforcement.

輪石，要石，壁石には，花崗岩や阿蘇溶結凝灰岩の硬質な石材（一軸圧縮強度 500 kgf/cm^2 以上）が用いられており，挟みの部分の成分は不明であるが，いずれも加工精度は高く，隙間は密着した状態であり，施工後非常に長い時間が経過したにも拘わらず，ブロック間には殆ど緩みはない．

Fig.2 に石橋の橋脚と基礎部分を示す．石橋施工後に作られたものと思われるが，石橋のアーチ部分および両橋脚の内側に補強用コンクリート（厚さ 50cm）が施されている．さらに，両岸の橋脚部側方には橋台が補強のため施工されている．

Fig.3 はアーチのコーナー部の補強コンクリートの拡大図であるが，岩石のブロック間はモルタルが充填されており，コンクリート補強部分についても丁寧に養生されており，ハンマーによる打音検査結果では強度はかなり高いものと推定される．

3.2 洗掘箇所付近の状態

Fig.4 は，橋脚基礎の洗掘箇所である．橋脚の側面に，補強のために石積みによる橋台が施工されているが，基礎部分のコンクリートが奥行き 1〜2m にわたり，深く洗掘されており，基礎が浮いた状態である．

橋脚部の洗掘箇所付近については，コンクリートの材質がアーチの本体の補強部に比べて劣るようである．また，洗掘箇所上の石積みについても風化変質が進んでいる．橋台部分の石材は，材質，加工精度ともに橋梁本体に比べると劣っており，一軸圧縮強度が 100〜200 kgf/cm^2 の軟岩を用いている．橋台部分は，岩石の表面加工精度が低いために，ブロック間に隙間を生じ，隙間に粘土やグージがつまり，排水も十分に行われていないために，強度面ではかなり劣化している．

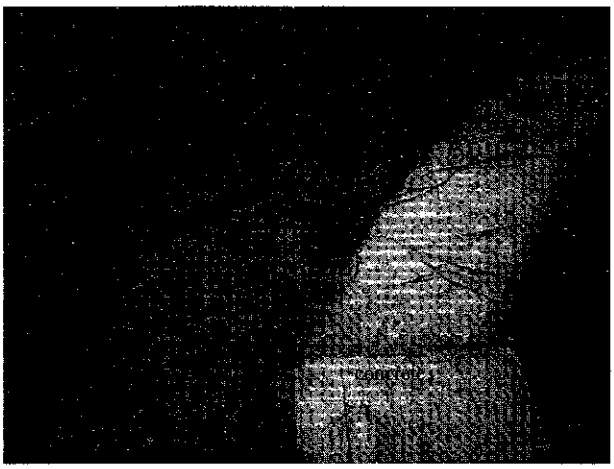

Fig.3 Corner of bridge arch; arch blocks of rock bound with cement and inner 500 mm-thick concrete layer for reinforcement.

Fig.4 Abutment base. The foundation of abutment base was washed out deeply by the water torrent.

3.3 橋梁の不安定性に寄与する要因

石橋の安定性は，岩自体の挙動と，岩石間の不連続面の挙動からなる．本石橋のような，硬岩からなる加工精度が高い石橋では，岩自体の変形は小さく，変形挙動の殆どは，相対的な弱面である岩石の隙間の挙動，すなわち，不連続面の挙動が支配的である．

不連続面の間隔，不連続面の開口の程度，風化や劣化，挟み込みの状態，間隙水の状態等が不安定性に寄与する大きな要因である．また，不連続面に開口を誘発する上載荷重の不均一性，左右の橋脚部分の不同沈下や，橋梁左右の取り付け部分の岩の破砕や変形，地震や上載荷重による上流側や下流側向きの面外方向の動きなどが不安定性に寄与する外的な要因となる．

本石橋の場合，橋梁を構成する岩の強度が，外力に比べて非常に硬く，橋梁の変形挙動の大部分は不連続面のせん断変形や開口現象によるものと考えられる．

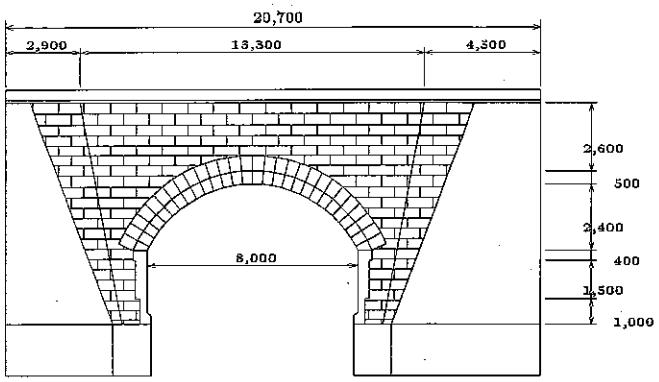

Fig.5 Discontinuous numerical model of stone bridge made with the picture analysing system and CAD. (unit mm)

4. 不連続変形法解析モデル作成と解析条件

4.1 モデルの作成方法

工事事務所に保存されていた原図と現場写真をもとに，**Fig.5** の不連続体モデルを作成した．岩石ブロックの形状に関しては，現場写真をもとに，個々の岩石の形状を CAD を用いてパソコンに取り込み，さらに，テキストデータに変換して数値化したものである [6)-7)]．

現場調査結果より，橋梁の施工されている地山は非常に堅牢な溶結凝灰岩からなることから，左右両岸の急峻な斜面を一体のブロックで表し，その間に石橋の石積み構造を多角形ブロックの集合体で表現した．多角形ブロック間は互いに応力や変位が不連続となる．

アーチおよび橋脚内側のコンクリート補強部も多角形ブロックで表現した．また，左右の橋脚の基礎部分のコンクリートは矩形ブロックとし，左右の岩盤および基礎部分は固定とし，左側の橋脚のみ洗掘による沈下を強制変位にて与えることにした．

4.2 解析に用いた物性値

解析に用いた物性値を **Table 1** に示す．岩石の物性値は，密度 2.770 g/cm^2，ヤング率 20 GPa，ポアソン比 0.15，内部摩擦角 55° とし [8)]，アーチ内側の補強部と両橋脚の基礎部分のコンクリート関しては，密度 2.400 g/cm^2，ヤング率 2 GPa，ポアソン比 0.25，内部摩擦角 30° とした．岩石およびコンクリートの圧縮強度は 20 MPa とし，モルタル充填面の引張強度 1 MPa，粘着力 0.1 MPa を仮定した．物性値に関しては，今後パラメトリックな検討が必要と考える．

解析で用いた諸定数を **Table 2** に示す．諸定数の詳細については参考文献に譲るが [3)]，接触バネ剛性はプログラムによる自動設定値であり，ヤング率×ブロックの平均直径の大きさが用いられる．計算は，各条件について，0.001 秒ごとで 5000 回の計算とした．

Table1 Material constants

members	stone rockmass	concrete deck
density ρ (g/cm^3)	2.770	2.400
modulus of elasticity E (GPa)	20.0	2.0
Poisson's ratio ν	0.15	0.25
friction angle ϕ (°)	55	30
cohesion C (N/m^2)	0	0

Table2 Numerical parameters for DDA

	Item	Value
1	minimum edge length parameter e_0	1×10^{-3}
2	assumed maximum displacement ratio g_2	1×10^{-3}
3	upper limit of time interval used in each time step g_1 (sec)	1×10^{-3}
4	stiffness of contact spring g_0 (automatically selects)	defaults
5	factor of over-relaxation used by SOR iteration method q_q	1.4

4.3 荷重条件

石橋自重に加えて，大型トレーラー等の上載荷重として，路面に 50 tonf/m^2 を載荷し，洗掘が危惧される左側の橋脚底部に，鉛直下向きの強制沈下量を与えた．沈下量は全く沈下がない健全な状態から，最大 100cm までとし，その間を 5 cm ずつ最終沈下量の大きさを変えた．脚部の沈下量は，1 秒後に最終沈下量となるようなロジスティック関数で表し，強制変位入力後にさらに 1 秒間そのまで放置し，その後の挙動を調べた．

4.4 解析結果の評価法

解析結果に関しては，モデルを構成する各ブロックの重心に計測点を設け，計測点の水平変位，鉛直変位，回転角，応力，ひずみ，体積増加量を出力した．また，橋梁の変形挙動については，路面の沈下量，橋厚の変化に加えて，アーチ天端の沈下量，アーチ部分の水平方向内空変位，アーチ部分の天端と左右との斜め方向の変位の 4 測線について相対変位量を求め，その変位量を測線長で除した無次元量（ひずみ）にて比較する．

5. 解析結果

5.1 橋梁の全体的な変位挙動

解析結果の数例を **Fig.6**〜**Fig.10** に示す．図は左側の橋脚部分の基礎の沈下量 (強制変位) が 10 cm，20 cm，30 cm，40 cm および 80 cm の時のものである．

Fig.6 より，橋脚部分の沈下量が 10 cm のときは，強制変位を与えた左側の橋脚付近にのみ変形が集中し，アーチの左上方付近にわずかに緩みが見られる程度であり，橋梁は全体としての安定性を保っている．

Fig.7 より，橋脚部分の沈下量が 20 cm のときは，左側の橋脚付近の不連続面がわずかに開口し，橋脚下部のブロックの一部にも押し出しが生じている．また，アーチの左上方付近に緩みが増加し，千鳥に配列したブロックの不連続面に沿って斜め方向に開口亀裂が進展している．局所的な体積膨張が生じているものの，橋梁は全体としての一体性を維持している．

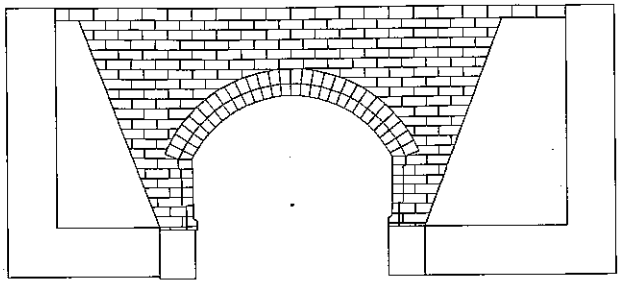

Fig.6 Behavior in case of abutment subsidence 10cm.

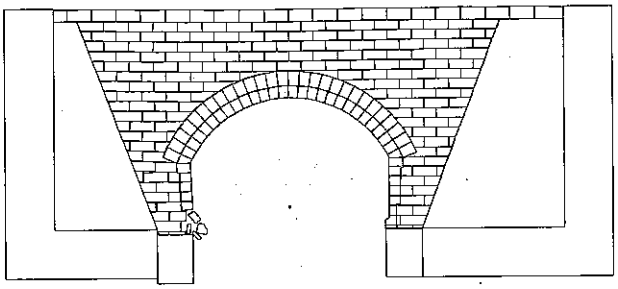

Fig.7 Behavior in case of abutment subsidence 20cm.

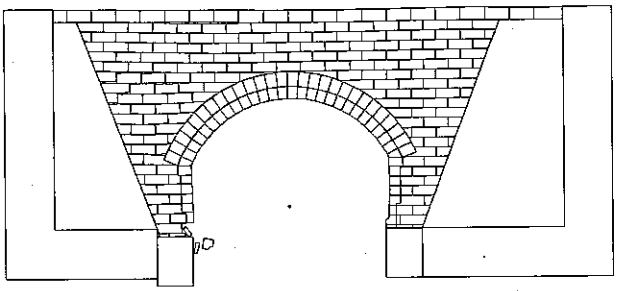

Fig.8 Behavior in case of abutment subsidence 30cm.

Fig.8 より，橋脚部分の沈下量が 20 cm を越えると，大きく挙動が異なり，不連続面が開口部分が広がり，それらが水平方向および斜め方向に進展し，橋梁全体に緩みが大きくなる状況がよくわかる．橋梁の脚部については崩れてきており，脚部沈下により，アーチ部分が全体的に左回転し，左右の対称性がなくなってきている．すなわち，橋脚部分の沈下量が 20 cm を越えると，橋梁の構造としての一体性を維持していないものといえる．

Fig.9 および **Fig.10** より，橋脚部分の沈下量がさらに大きくなると，局所的な破壊から，橋梁全体の破壊に至る状況が視覚的に把握できる．

5.2 道路面（石橋頂部）の鉛直沈下量

Fig.11 は道路面 (石橋頂部) の橋梁左端からの位置に関する沈下曲線である．橋脚の沈下量が大きくなる

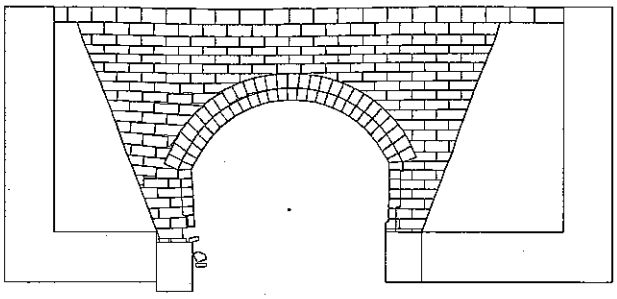

Fig.9 Behavior in case of abutment subsidence 40cm.

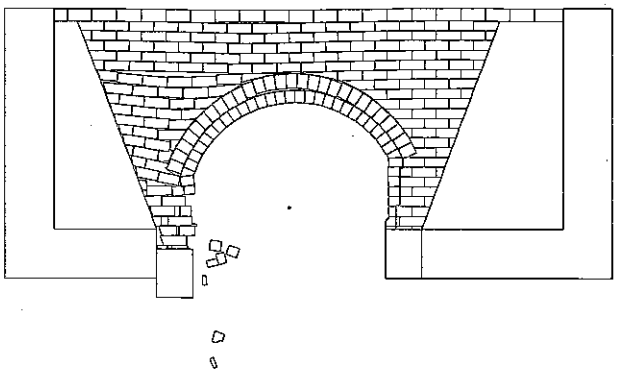

Fig.10 Behavior in case of abutment subsidence 80cm.

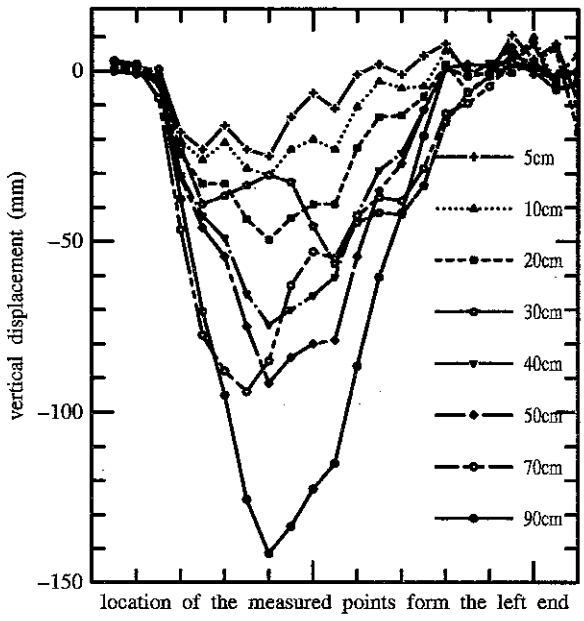

Fig.11 Vertical displacement of bridge deck.

につれて，路面の沈下量も増加する．強制変位が小さいときは，強制変位を与えた左側付近に集中して沈下が多く発生するが，強制変位量が大きくなると広い範囲にわたって沈下が生じる傾向がある．

5.3 道路面とアーチ頂部の平均沈下量

Fig.12 は，路面の平均沈下量とアーチ天端の沈下量を示したものである．アーチの天端部分の沈下量は，脚部の強制変位量が 0 ～ 20 cm の範囲ではほぼ比例の関係にあるが，強制変位量が 25 ～ 30 cm にかけて急激に

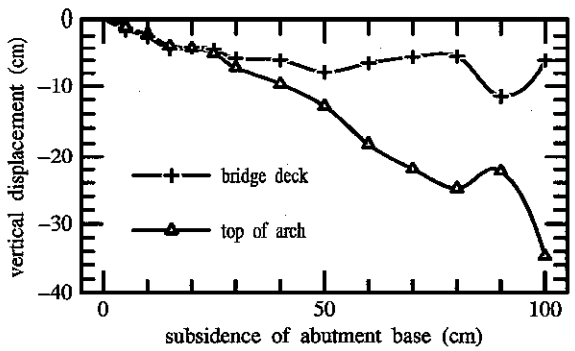

Fig.12 Vertical average displacement of bridge deck and arch top.

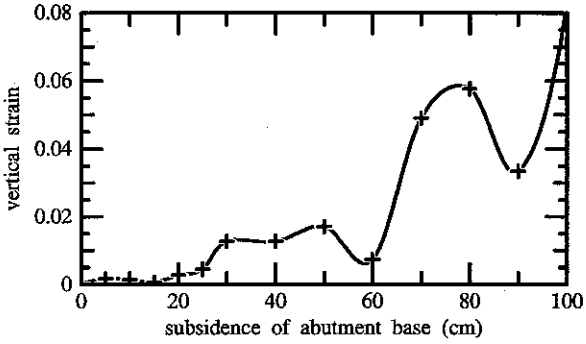

Fig.13 Vertical strain between bridge deck and arch top.

アーチの天端部分が 5 cm 程沈下している．

強制変位量が 20 cm を越えたところから，路面の沈下量よりは，アーチ部分の沈下量が増加しており，このことから，アーチ上部の不連続面が鉛直方向に開口し，石橋内部に体積膨張が生じていることがわかる．

5.4 橋厚のひずみ分布

Fig.13 は橋厚の鉛直方向のひずみ変化を示したものである．橋厚のひずみ分布は，脚部の強制変位量 20 cm 付近まではあまり変化が見られないが，脚部の強制変位量 20 cm を越えたあたりから大きな変化が見られる．脚部の強制変位量が 15 ～ 20 cm を越えたあたりでひずみが比例関係ではなくなり，その後増加している．また，脚部の強制変位量が 60 cm 近傍で大きな変動があり，その後勾配が急になりはじめた点が危険性の目安になると思われる．

5.5 石橋アーチ部分の変形

Fig.14 および **Fig.15** は，石橋のアーチ部分の変形について，鉛直方向，水平方向，天端と左端，天端と右端の 4 測線に関する内空変位量を測線長でわった相対変位 (ひずみ) の分布傾向を示したものである．いずれの測線についても，脚部の強制変位量の増加に伴いひずみが増加する傾向が見られ，左側の斜め方向ひずみについては顕著な増加傾向である．

鉛直方向と水平方向のひずみは，ほぼ同じ大きさで増加するが，斜め方向のひずみについては，右側のひ

ずみの増加はわずかであるが，左側は増加が顕著であり，左脚部の沈下によりアーチ全体が左方向に回転し，左右の対象性が失われていることがわかる．

5.6 脚部の強制変位量と石橋の安定性

上述の結果より，脚部の強制変位量が 15 ～ 20 cm を越えたあたりで，橋梁の変形挙動に非線形性が増加し，また，前掲の **Fig.7** のように，強制変位量 20 cm を越えると，左橋脚部のブロックが崩落しはじめており，この時点で石橋は機能的に道路しての供用は困難と考えられる．すなわち，本石橋に限ってではあるが，脚部の強制変位量が 15 ～ 20 cm 付近に，橋梁の構造的な安定性を考える際の，挙動の閾値があるもいえる．

Fig.14 および **Fig.15** の相対変位に関して，強制変位量が 60 cm に達した付近から大きく増加しており，この 2 度目の変化が現れた時点で，石橋のアーチ構造全体が崩壊目前の危険な状態にあるものと判断できる．

6. まとめ

本研究は，施工後長い年月を経て，老朽化した石橋について現況調査を実施するとともに，不連続変形法解析により，橋脚部分に洗掘が発生した場合の破壊の状況を再現し，橋脚の洗掘による影響を数値解析的に調べたものである．

従来の連続体モデルでは，応力状態や変位については十分な再現性を有するものの，破壊現象の進展挙動，とくに局所的な変位挙動や体積増加挙動については十分には再現できなかった．本研究では，DDA による不連続体モデルを用いることにより，局所的な破壊の進展挙動を考えることが可能であることが確認できた．

本解析では，岩石ブロックの形状特性と表面摩擦のみをパラメータとしており，従来のモデルのような仮想的な構成式を用いていない．解析結果によると，構成式を仮定しなくても，形状特性と摩擦特性のみで破壊挙動の再現が可能であることが示された．

本論文では解析結果をもとに破壊状況の分析を行ったが，他の既存構造物の破壊の定義と付合させることにより，安全性評価に資することが可能であると考える．

解析結果に関しては，主に沈下に関する変形挙動に着目して整理したが，モデル内の全ブロックについての変形量，回転角，応力とひずみ，および，体積増加について定量的な結果が得られている．今後，局所的な体積増加量を破壊進展の定量的な指標としてとらえることにより，石橋の劣化の影響解析が可能である．

今回は，橋梁に緩みがない健全な状態を初期状態として解析したが，緩みが生じた状況を初期状態として，地震等の動的荷重を加えることにより，劣化状況と構造上の不安定性の関係についても応用できる．解析と現象との整合性を確保する必要があり，これらは今後の課題である．

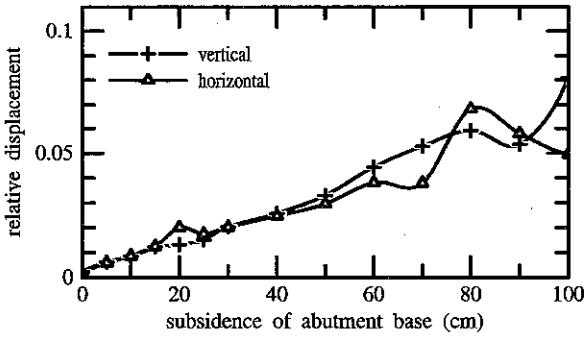

Fig.14 Relative displacements (strains) of internal air of bridge arch with respect to vertical and horizontal direction.

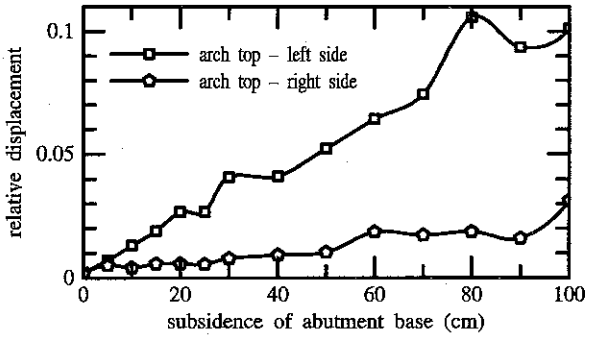

Fig.15 Relative displacements (strains) of internal air of bridge arch, with respect to the distances between crown top to right and left sides.

参考文献

1) Shi,G.H. and Goodman,R.E.: Discontinuous Deformation Analysis - A New Method for Computing Stress, Strain and Sliding of Block System, *Key Questions in Rock Mechanics: Proc. 29th U. S, Symposium*, pp. 381-393, 1988.
2) Shi,G.H. and Goodman,R.E.: Generalization of Two-dimensional Discontinuous Deformation Analysis for Forward Modeling, *Int J. Numer. Ani. Methods Geomech*, 13, pp. 359-380, 1989.
3) Shi,G.H. and Yeung,M.R.: Discontinuous Deformation Analysis Program Version 96 User's Manual, 1996.
4) 大西有三, 佐々木猛: FEM,DDA から Manifold Method へ, 第 3 回 Manifold Method 実用化研究会, pp.1-14, システム総合研究所, 1995.
5) Shi,G.H.: Manifold Method, 第 7 回 Manifold Method 実用化研究会, pp.13-52, システム総合研究所, 1996.
6) jw_software club: CAD JW_CAD 徹底解説, 建築知識, 1994.
7) 山浦聡: J1T,JWC → TXT,TXT → JWC 変換ソフトウェア, ベクター, 1997.
8) 日本材料学会編: 岩の力学, 丸善, 1993.

(2003.7.31 受付)

屋根付き木造トラス道路橋の振動測定による構造特性の検討

Study on structural property of covered timber highway bridge by vibration measurement

加藤雅史*，山下昇一**
Masafumi Kato, Syoichi Yamashita

*工博，九州東海大学教授，工学部都市工学科（〒862-8652 熊本市渡鹿９－１－１）
**工修，日本クリエイティブシステム(株)　（〒270-1151 千葉県我孫子市本町２－２－１６）

Aso-bou Bridge constructed in Kumamoto Prefecture is a timber highway bridge which used glued laminated timber, and is a first covered highway bridge in Japan. The structural type of this bridge which has the span length of 39.9 m is simple lattice truss.
In this study, field vibration test of Aso-bou Bridge was carried out. The purpose of the test is 1) to obtain the initial information for the maintenance, 2) to accumulate the feedback data to design of the same type bridges. The measured natural frequencies and vibration modes are compared with the past measured data of timber bridges and steel/concrete highway bridges. Moreover, the reason why this bridge has high fundamental frequency compared with another bridges is examined.

Key Words : covered timber bridge, vibration test, structural characteristics,
キーワード：屋根付き木橋，振動試験，構造特性

1. はじめに

近年，土木構造物は量の時代から質の時代へと変わりつつある．橋梁の分野においても，安全で経済的であるだけの橋から，高品質で周囲の環境との調和を保ち美しい景観を提供するとともに環境負荷の少ない橋梁が要求されるようになってきている．

このように社会的ニーズが変化する中で，木材特有の景観や感触の良さ，環境に対する負荷の少なさ等が見直されて，1980 年代後半から木橋が次々と建設されるようになってきた．これら木橋は，我が国では近代木橋と呼ばれ，主要部材には木材を貼り合わせた集成材や西アフリカ産の硬いエッキ材等が，部材の接合には鋼製の結合具が用いられる．このように木橋建設の技術が進歩する中で，1999 年に我が国初の屋根付き木造道路橋である阿蘇望橋が熊本県内に建設された．

そこで，①阿蘇望橋の今後の維持管理のための初期値として健全時（完成時）の振動特性を把握すること，②木橋の振動特性データの蓄積，特に唯一の屋根付き道路橋の振動特性データとして今後の設計へのフィードバック資料とすること，の２点を目的として，現地振動試験を実施した．

本論文では，健全状態にある阿蘇望橋の現地振動試験に基づく固有振動特性について述べるとともに，実測値を支間長ならびに構造特性の視点から他の木橋や鋼橋・コンクリート橋の固有振動特性と比較することにより，屋根付き道路橋である本橋特有の構造特性について考察を加えている．

2. 阿蘇望橋の概要

阿蘇望橋は熊本県阿蘇郡波野村内の広域基幹林道阿蘇東部線に架かる橋梁として 1999 年秋に架設された．本橋は橋長が 41.6m，支間長が 39.9m で，我が国で初めての屋根付き道路橋である．また，木造のトラス橋として我が国最大級の支間長を有する橋梁である．阿蘇望橋の全景を Photo 1 に示す．

構造形式は屋根付きラチストラス橋で，構造部材には集成材が使用されているが，特に強度を要する下弦材や床版

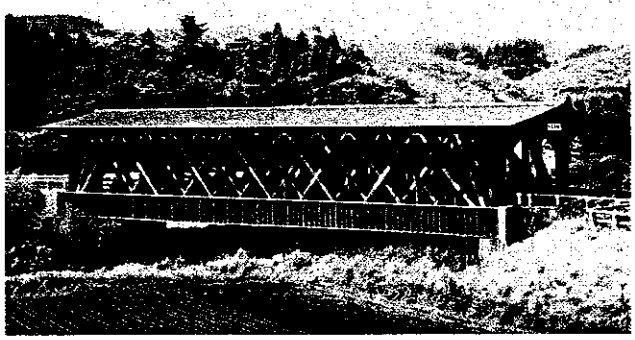

Photo 1　Aso-bou Bridge

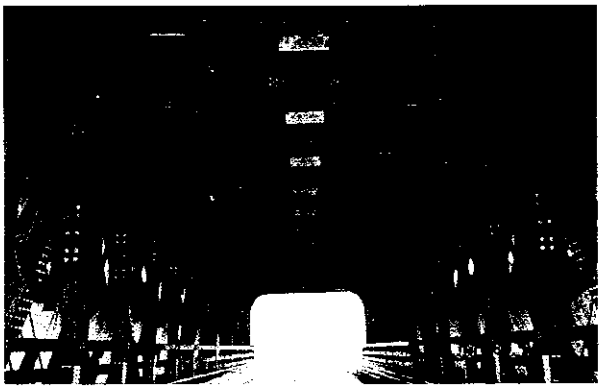

Photo 2　Inside of Aso-bou Bridge

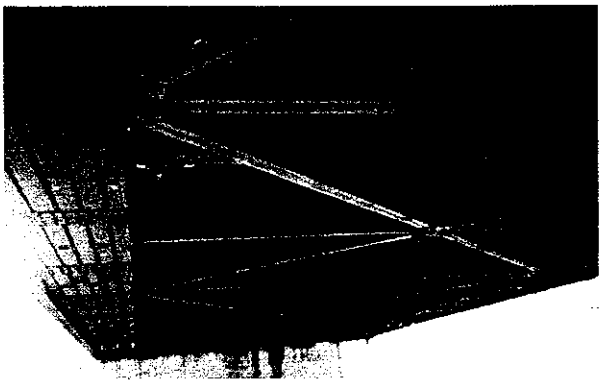

Photo 3　Lower chord and cross beam of Aso-bou Bridge

Table 1　Design conditions and materials of Aso-bou Bridge

Design conditions	
Structural Type	Covered Timber Lattice Truss
Live Load	25 tonf (A Live Load)
Bridge Length	41.6 m
Span Length	39.9 m
Effective Width	0.75 + 5.5 + 0.75 m
Substructure	Abutment : Inverted T-type Concrete Abutment
	Foundation : Caisson Type Pile
Material	
Truss	Glued Laminated Timber (Japanese Cedar, Japanese Cypress)
	Atmospheric Corrosion Resisting Steel
Slab	Glued Laminated Timber (Japanese Cedar, Japanese Cypress)
Roof	Sawn Wood (Japanese cedar)

を支える横桁にはＩ型の耐候性鋼材が使用されており，木と鋼との複合構造となっている．上弦材，柱材，床版には地元のスギやヒノキを使用した大断面集成材を使用し，屋根部にはスギの製材が使用されている．なお，木材防腐処理には，防腐剤(AAC)加圧注入と防腐塗装が行われている．

阿蘇望橋の内部構造の様子を Photo 2 に，下弦材等の様子を Photo 3 に示す．また，設計諸元および使用部材を Table 1 に示す．

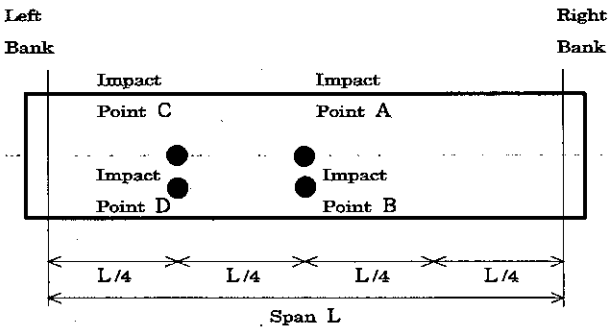

Fig. 1　Impact point by vehicle stepping over method

Photo 4　Impact by vehicle stepping over method

3. 振動試験

振動試験は，同時に実施した静的載荷試験で使用した総重量約 200kN のダンプトラック２台を利用し，車輪踏台落下法と車両走行法[1) 2)]により加振して行った．車輪踏台落下法では Fig. 1 に示す路面上の４ヶ所で Photo 4 のように衝撃加振を行った．また，車両走行法では幅員方向の中央走行と上流側車線走行の２パターンで車両走行による加振を行った．なお，ダンプトラックの走行速度は約 40km/h とした．

本来，振動測定は屋根部分も含め橋梁各部に振動計を設置して行うのが望ましいことであるが，静的載荷試験の日程の関係で振動計を数多く揃えることができなかった．このため，振動測定点は路面部付近のみとし，支間 1/4 点，1/2 点，3/4 点のそれぞれ幅員方向両側の６点とした．各振動測定点では，Photo 5 のようにサーボ型加速度計をトラス下弦材の上に乗っている横桁上に置き，鉛直方向および橋軸直角水平方向に設置した．そして，各加振方法での加振による橋梁の振動波形を計測し，データレコーダに記録した．

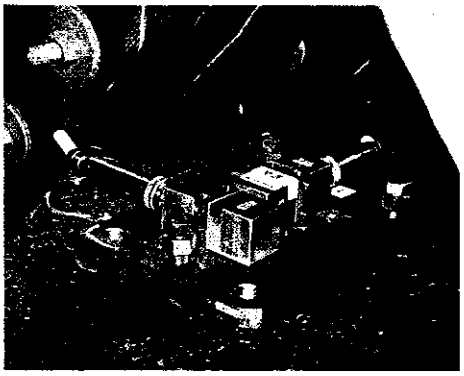

Photo 5　Setting of accelerometer

Table 2　Results of vibration test

Mode Order	Natural Frequency	Mode Shapes	
1	4.79 Hz	Vertical Symmetric 1st	
2	6.10 Hz	Lateral Symmetric 1st	
3	6.30 Hz	Torsional Symmetric 1st	
4	11.52 Hz	Vertical Asymmetric 1st	
5	13.80 Hz	Lateral Asymmetric 1st	
6	14.01 Hz	Vertical Symmetric 2nd	
7	14.50 Hz	Torsional Asymmetric 1st	

4. 振動試験結果

振動測定データはスペクトル解析（パワースペクトル，コヒーレンス，フェイズ分析）を行い，固有振動数および振動モードを推定した．この際に，振動測定データの分析対象範囲は事前に予備的に実施した調査結果および測定精度を考慮して16Hz 以下とした．

振動試験より得られた振動特性をまとめてTable 2に示すが，橋梁の全体振動としての面内対称１次，面内逆対称１次，面内対称２次，面外対称１次，面外逆対称１次，ねじれ対称１次，ねじれ逆対称１次の合計７つの振動モードの固有振動特性が得られた．

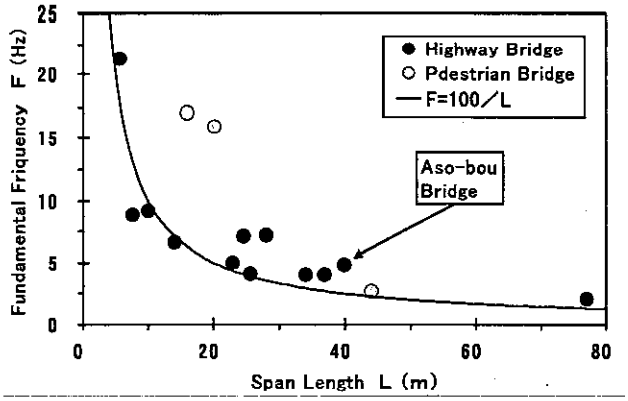

Fig. 2　Relationship between fundamental frequency and span length of timber Bridge

5. 固有振動特性の他橋梁との比較

ここでは，振動試験より得られた阿蘇望橋の固有振動特性を，過去に他の近代木橋において得られている実測値および一般的道路橋における実測値と比較する．

5.1　他の木橋との比較

一般に，橋梁の支間長が長くなるに従って鉛直方向の基本固有振動数は小さくなる傾向があり，その減少傾向は基本固有振動数を f_1（Hz），最大支間長をL（m）とするとき，概算的には次式で評価されることが多い．

$$f_1 = 100 / L \qquad \cdots\cdots\cdots\cdots\cdots\cdots (1)$$

Fig. 2 は過去に近代木橋において振動測定が行われた14 橋の測定結果[3] に阿蘇望橋の実測値を加え，式(1)の曲線とともに基本固有振動数と最大支間長の関係を示したものである．

阿蘇望橋は支間長が 39.9m であることから，式(1)によれば f_1 の値は約 2.5Hz となる．しかし，実測値から得た鉛直方向の基本固有振動数（面内対称１次）は 4.79Hz であり，支間長で比べたときに阿蘇望橋は基本固有振動数が高いことになる．Fig. 2 において，近代木橋における実測値は $f_1 = 100/L$ のライン付近にあるが，その中でも阿蘇望橋の基本振動数は高めの値であると言える．

また，本田ら[3] が述べているように，近代木道路橋の基本固有振動数は一般道路橋とほぼ同等であるであると考えられることから，阿蘇望橋の基本固有振動数はその構造特性に起因して高い値になっているものと考えることができる。

5.2　一般的道路橋との比較

次に，構造形式も考慮に入れて阿蘇望橋の振動特性を他の一般道路橋と比較する．加藤・島田[4] は，過去に計測された道路橋など 192 橋の振動測定データを重回帰分析

することによって，構造形式と最大支間長から橋梁の鉛直方向の基本固有振動数を推定する次式を得ている．

$$fv = 10^{\alpha} \cdot L^{-0.828} \quad \cdots\cdots\cdots\cdots (2)$$

α ＝1.793＋b

fv：鉛直方向の基本固有振動数（Hz）

L　：最大支間長（m）

bの値は下の該当する項の値の和

トラス橋	0.082
ランガー・ローゼ橋	0.060
アーチ橋	0.127
吊橋	−0.088
鋼床版のとき	−0.108
床版なしのとき	0.250

そこで，構造形式も考慮に入れて阿蘇望橋の振動特性を他の一般的橋梁と比較することとし，阿蘇望橋と同じ支間長 39.9m のトラス橋の基本固有振動数を式(2)から推定し，阿蘇望橋の実測値と比較した．その結果，実測値が 4.79Hz であるのに対し，式(2)による推定値は 3.54Hz となり，実測値の方が約 35％高い値である．このことから，阿蘇望橋の振動特性は一般のトラス道路橋とも異なっていると考えられる．

6. 阿蘇望橋の構造特性の検討

以上のことを踏まえて，阿蘇望橋の鉛直方向の基本固有振動数が一般のトラス橋と比較して高い振動数となった理由について構造特性の面から検討する．

6.1 曲げ剛性と重量

橋梁振動の基礎となる梁の曲げ振動の固有振動数は，梁の長さ，重量，曲げ剛性，支持条件によって決まる．この中で，梁の長さについては支間長別に比較しており，支持条件に関しては一般のトラス橋と変りがない．そこで，ここでは阿蘇望橋の面内曲げ剛性と重量から阿蘇望橋の振動特性について考察を行う．

面内曲げ剛性は，静的載荷試験の結果を用いて計算することができる．ここでは，振動試験と同時にダンプトラック（総重量約 200kN）を用いて実施した静的載荷試験の結果を使用する．支間中央幅員中央１台載荷時と支間中央の上流側と下流側に１台ずつ計２台載荷時の支間中央下弦材のたわみ測定値と車両重量から両者の関係を近似直線で求めると，次式のようになった．ここに，Pは荷重（kN），Yはたわみ（m）である．

$$Y = 8.04P \times 10^{-6} \quad \cdots\cdots\cdots\cdots (3)$$

単純梁の支間中央に集中荷重が作用したときの支間中央のたわみは次式で表される．ここに，Eは弾性係数，Iは断面２次モーメント，Pは荷重，Lは支間長，Yは支間中央のたわみである．

$$Y = PL^3/(48EI) \quad \cdots\cdots\cdots\cdots (4)$$

式(4)のYに式(3)、Lに阿蘇望橋の支間長 39.9m を代入すると曲げ剛性EIが計算でき、$EI = 1.646 \times 10^8$ kN·m^{2}となる．

一方，重量については、設計計算書によれば阿蘇望橋の総重量は 4131.68kN である．

次に，以上により求めた曲げ剛性と重量から阿蘇望橋の固有振動数を求める．橋梁振動の基礎となる単純梁の固有振動数は式(5)で求められるので，式(5)に阿蘇望橋の値を代入して固有振動数を計算した．ただし，橋軸方向の単位長さあたりの重量γAには阿蘇望橋の総重量を橋長で割った値を使用した．

$$f_n = \frac{1}{2\pi}\left(\frac{n\pi}{L}\right)^2 \sqrt{\frac{EIg}{\gamma A}} \quad \cdots\cdots\cdots\cdots (5)$$

f_n：単純支持梁のn次固有振動数

L　：支間長

γ　：単位体積重量

A　：断面積

E　：弾性係数

I　：断面２次モーメント

g　：重力加速度

n　：振動次数

計算の結果、基本固有振動数は 3.974Hz となった．しかし，式(5)は単純梁の固有振動数を求める理論式であることから，計算された固有振動数は阿蘇望橋と同等の支間長，重量，曲げ剛性を持った単純桁橋の固有振動数であり，トラス橋の固有振動数とはならない．トラス橋の固有振動数の推定値を得るためには式(5)から得た結果を補正しなければならない．

固有振動数の補正には式(2)を利用する．式(2)から阿蘇望橋と同一支間長 39.9m の桁橋とトラス橋の基本固有振動数を求めると，桁橋は 2.934Hz，トラス橋は 3.543Hz となる．これより，トラスの固有振動数は桁橋の固有振動数の 1.208 倍であることがわかる．そこで，ここではトラス橋の基本固有振動数を同一支間長の桁橋の 1.2 倍と考えることとする．

式(5)に阿蘇望橋の支間長，曲げ剛性と重量を代入して求めた単純桁の基本固有振動数 3.974Hz を 1.2 倍して，トラス橋の基本固有振動数を求めると，4.801Hz となり，実測値 4.79Hz とほぼ一致する．このことは，阿蘇望橋の鉛直方向基本固有振動数（面内対称１次）の実測値が信頼性の高いものであることを示してもいる．

以上より，阿蘇望橋の支間長，重量，曲げ剛性を使用してトラス橋の基本固有振動数を計算すると，阿蘇望橋の実

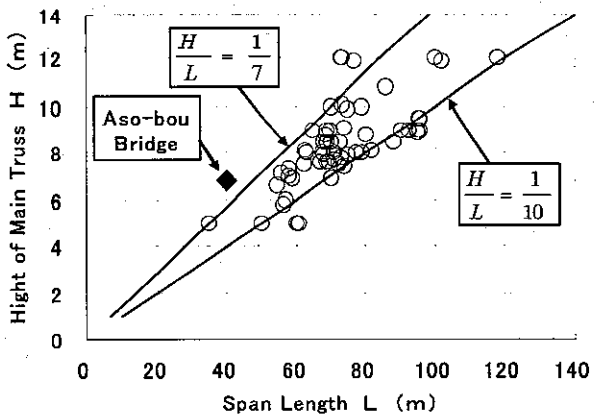

Fig. 3 Relationship between height of main truss and span length

測値に非常に近い値となり，阿蘇望橋の支間長のみを使用してトラス橋の基本固有振動数を式(5)から計算すると実測値よりもかなり低い値となる．このことから，阿蘇望橋の基本固有振動数が同支間長の一般のトラス橋に比べて高い値になるのは重量と曲げ剛性の関係によるものであると考えられる．

6.2 トラス主構高の検討

阿蘇望橋の特徴的な構造特性としては，屋根付き橋梁であることが挙げられる．そして，この屋根を車両の通行に必要な高さに持ち上げるために，他のトラス橋よりトラスの高さ（主構高）が高くなっていることが考えられる．

そこで，一般的なトラス道路橋の主構高を最近の道路橋年報（日本道路協会発行）より調査し，支間長と主構高の関係を求めると Fig. 3 に示すようである．

Fig. 3 に示すように，トラス道路橋は支間長を L，主構高を H とすると，その関係は一般に H/L＝1/7 の線と H/L＝1/10 の線の間にある．阿蘇望橋の支間長は 39.9m であるから，その主構高は一般的には 4.0～5.5m ということになるが，実際には 6.8m と大きな値となっており，一般的な主構高より 24～70％高いことになる．仮に，支間長 39.9m のトラス橋の一般的な主構高を 5.0m とすると，阿蘇望橋の主構高は 36％高いことになる．

Fig. 4 のような上弦材と下弦材による断面２次モーメント I は次式で表される．ここで，I_1 および I_2 は上弦材および下弦材の図心軸回りの断面２次モーメント，A および B は上弦材および下弦材の断面積である．

$$I = y_1^2 A + I_1 + y_2^2 B + I_2 \quad \cdots\cdots\cdots\cdots (6)$$

通常，トラス橋においては，式(6)における I_1，I_2 の値は $y_1{}^2A$，$y_2{}^2B$ に比べて非常に小さくなるので，断面２次モーメント I は次の式(7)よって表されると考えてもよい．

$$I \fallingdotseq y_1^2 A + y_2^2 B \quad \cdots\cdots\cdots\cdots\cdots\cdots (7)$$

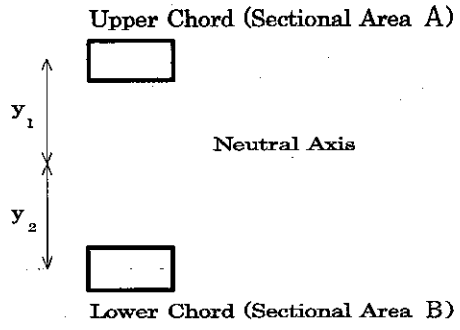

Fig. 3 Simplified model of truss section for calculating geometrical moment inertia

仮に，トラス中立軸が上弦材と下弦材の中央にあるとすると，式(5)と式(7)からトラス主構高と固有振動数は比例関係にあることになる．実際には，床版やトラスの斜材などの影響があるため必ずしも比例するとはいえないが，トラスの高さが高くなることによって固有振動数が高くなることは明らかである．

前述したように，阿蘇望橋の鉛直方向基本固有振動数の実測値は一般的なトラス橋の基本固有振動数より約 35％高く，阿蘇望橋の主構高はトラス橋の一般的な主構高より 36％高い．したがって，阿蘇望橋の主構高の高いことが基本固有振動数が高くなっている大きな理由であると考えられる．

7. おわりに

本研究では，①阿蘇望橋の今後の維持管理のための初期値として健全時（完成時）の振動特性を把握すること，②木橋の振動特性データの蓄積，特に唯一の屋根付き道路橋の振動特性データとして今後の設計へのフィードバック資料とすること，の２点を目的として，現地振動試験を実施した．そして，健全状態にある阿蘇望橋の現地振動試験に基づく固有振動特性について述べるとともに，実測値を支間長ならびに構造特性の視点から他の木橋や鋼橋・コンクリート橋の固有振動特性と比較し，屋根付き道路橋である本橋特有の構造特性について考察を加えた．その主な結果を列挙すると，以下のようである．

1）橋梁の全体振動としての面内対称１次，面内逆対称１次，面内対称２次，面外対称１次，面外逆対称１次，ねじれ対称１次，ねじれ逆対称１次の合計７つの振動モードの固有振動特性が得られた．
2）阿蘇望橋の鉛直方向基本固有振動数の実測値は一般的なトラス橋の基本固有振動数より約 35％高い．
3）阿蘇望橋は屋根付き橋梁であることから屋根を車両の通行に必要な高さに持ち上げるために，トラス主構高がトラス橋の一般的な主構高より 35％程度高くなっている．
4）単純化した理論式で考えると，はりの固有振動数は断

面２次モーメントと比例関係にある．したがって，上記３）に述べたように他のトラス橋より構造的にトラス主構高が高く，それにより断面２次モーメントが大きくなり，これが阿蘇望橋の基本固有振動数が高くなっている大きな理由と考えられる．

なお，現地振動試験では，スケジュールの関係で振動計を数多く揃えることができず，振動測定点は路面部付近のみであった．このため，屋根部の振動性状については調査することができなかった．そこで，屋根部の振動性状を推定し橋梁全体の振動性状との関係を把握するために数値解析モデルによる固有振動解析などを行っているが，これについては別の機会に報告したい．

現地振動試験の実施に際して，熊本県および波野村の関係各位ならびに（財）林業コンサルタンツの皆様にご配慮・ご協力を頂いた．ここに記して感謝の意を表します．

参考文献

1) 橋梁振動研究会編：橋梁振動の計測と解析，技報堂出版，1993.
2) 加藤雅史：新設橋の実橋載荷試験，プレストレストコンクリート，Vol.39，No.1，pp.109-115，1997.
3) 北城章・小川史彦・草薙貴信・本田秀行：集成材等を用いた木橋の現状と実験に基づく振動特性，構造工学論文集，Vol.48A，pp.369-376，2002.
4) 加藤雅史・島田静雄：橋梁実測振動特性の統計解析，土木学会論文報告集，No.311，pp.49-58，1981.

（2003.7.31 受付）

端部分離型上路式ＰＣ吊床版橋の振動特性の検討

A study of vibration characteristics of hybrid stress ribbon deck bridge

大木太*，吉川卓**，角本周***，梶川康男****
Futoshi Ooki, Taku Yoshikawa, Meguru Tsunomoto, Yasuo Kajikawa

*工修，オリエンタル建設(株)，第二技術部（〒102-0093 東京都千代田区平河町2-1-1）
**工修，オリエンタル建設(株)，第二技術部（〒102-0093 東京都千代田区平河町2-1-1）
***工修，オリエンタル建設(株)，福岡支店技術部（〒810-0001 福岡市中央区天神4-2-31）
****工博，金沢大学大学院教授，自然科学研究科（〒920-8667 金沢市小立野2-40-20）

On stress ribbon deck bridge, since suspended slab deck and abutment were connected rigidly, dead load and live load were acting on the foundation as horizontal load. For this reason, horizontal load will become large as span becomes long. Since hybrid stress ribbon deck bridge separates suspended slab deck and abutment, it can reduce horizontal load. Moreover, since diagonal member is used for a strut, rigidity becomes strong and aeroelastic stability improves. In this study, eigenvalue and dynamic response analysis were simulated about former type stress ribbon deck bridge and hybrid stress ribbon deck bridge. Using the result, we examined the aeroelastic stability and vibration serviceability of the bridge.

Key Words : hybrid stress ribbon deck bridge, aeroelastic stability, vehicle's movement, vibration serviceability
キーワード：端部分離型上路式吊床版橋，耐風安定性，車両走行，振動使用性

１．はじめに

上路式吊床版橋は，懸垂架設工法によることで，桁下空間の条件に左右されず，かつ，大型架設機材を用いないで短期間に施工できることから，特に急峻な地形条件における道路橋に適した構造形式である[1)]．一方，上路式吊床版橋は常時に下部構造に大きな水平力が作用することから，その水平力の低減を図ることが工費を縮減する上で重要となる．そこで，国土交通省発注の新丸山ダム資材運搬線小和沢仮橋（設計・施工一括型，総合評価落札方式）において，橋台に作用する水平力が従来型の上路式吊床板橋に比べて大幅に低減できる端部分離型の上路式吊床版橋を提案した[2)]．

道路橋の設計においては，動的外力に対する検討としては，通常，耐震性および耐風安定性の照査が行われている．一方，車両走行時の振動使用性については，活荷重によるたわみを制限することで照査したものとみなしているのが一般的であり[3)]，設計段階で詳細に検討した事例は少ない．しかしながら，躯体重量が軽くフレキシブルな構造では，たわみ制限を満足していても車両走行時の振動使用性が問題となる可能性がある[4)]．そこで，提案した端部分離型上路式吊床版橋では，耐震性および耐風安定性の照査に加えて，大型車両の走行シミュレーションにより動的応答を予測し，振動使用性を満足するように部材寸法や配置を設定した．本報告は，この端部分離型上路式吊床板橋の振動特性，耐風安定性および車両走行時の振動使用性にの検討結果を，従来型の上路式吊床板橋と比較して示すものである[5)～7)]．

２．構造概要

検討対象の橋は，岐阜県内の新丸山ダム建設におけるトンネル掘削土砂の運搬等に用いる仮橋であり，上路式吊床版橋としては国内最大支間となる道路橋である[1)]．また，本橋の設計活荷重はＡ活荷重ではあるが[8)]，総重量440kNのトンネル掘削用ドリルジャンボの通行も想定して設計されている．なお，本橋は，新丸山ダムの完成後に，建設地点からの撤去および移設を想定しているため，解体しやすさに配慮した構造としている．小和沢仮橋の一般図および断面図をFig. 1およびFig. 2に，設計条件および使用材料をTable 1およびTable 2に示す．また，比較対象とした従来型の上路式吊床版橋の一般図をFig. 3に，両形式の主な相違点である上部構造と橋台との接合部をFig. 4に示す．

提案した端部分離型上路式吊床版橋は，従来型に比べて以下のような特徴がある．

（１）従来型では橋台に剛結していた吊床版端部を，橋台から分離して上床版と接合することにより，躯体自重は主に吊ケーブルで支持し，活荷重は吊床版，上床板および鉛直材からなるトラス桁としての曲げ剛性で支持する

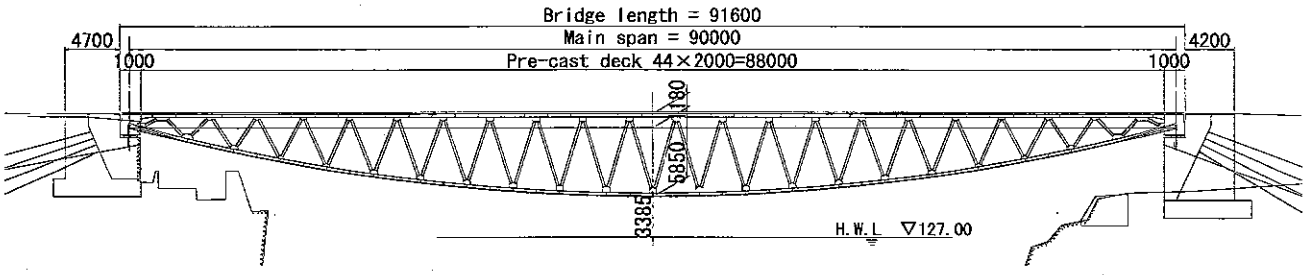

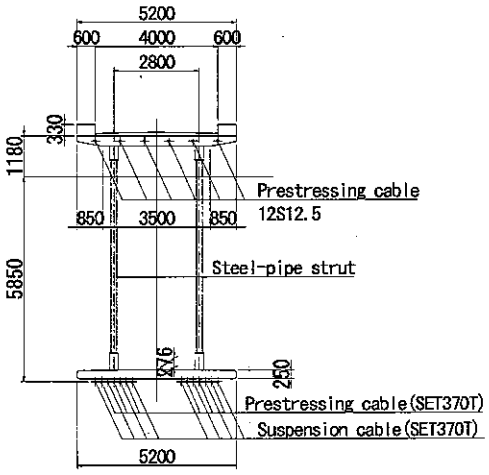

Fig. 2 Cross-section of the Bridge

Table 1 The Design Condition

Bridge Type	Highway Bridge
Bridge Length	91.630 m
Suspended Span	90.000 m
Effective Width	4.000 m
Live Load	A Type Live Load Heavy Load (Total 440 kN)
Basic Designed Sag	5.850 m

Table 2 Used Material

Concrete	Superstructure : f'_{ck}=40N/mm^2 Abutment : f'_{ck}=30N/mm^2
PC Tendons	Suspension Cable : SET370T Prestressing Cable (Suspended Slab) : SET370T Prestressing Cable (Upper Slab) : 12S15.2B
Ground Anchor	F360TA
Steel Pipe	STK490, ϕ 190.7, t=8.2mm

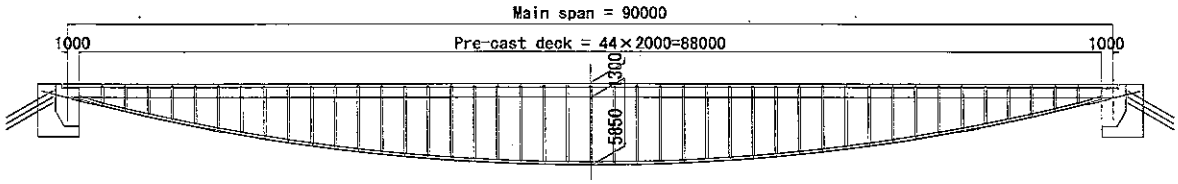

Fig. 3 General Side View of Former Type Stress Ribbon Deck Bridge

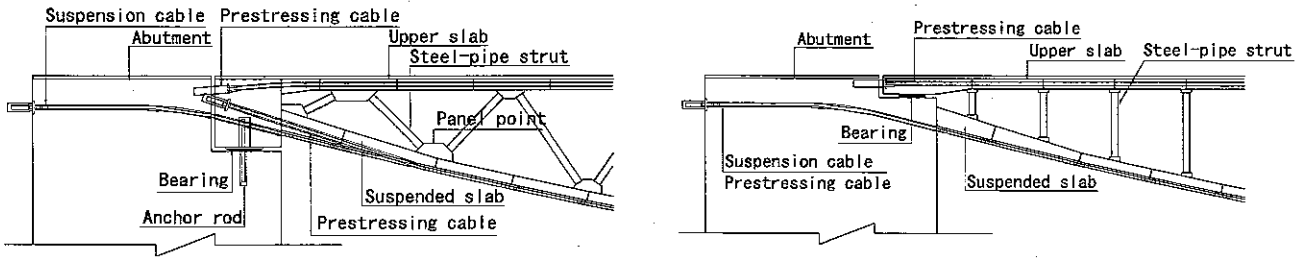

(a) Hybrid Stress Ribbon Deck Bridge (b) Former Type Stress Ribbon Deck Bridge

Fig. 4 Detail of Joint between Superstructure and Abutment

構造とした．その結果，橋台に作用する水平力は，従来型に比べて約40%低減されている．

(2)吊ケーブルおよび吊床版にプレストレスを導入するＰＣケーブルとも，解体性に配慮して全てプレファブタイプの外ケーブルとし，吊床版にはサドルを介して接合している．なお，吊床版にプレストレスを導入するＰＣケーブルは，従来型では橋台に定着しているが，端部分離型では上部構造端部に定着している．

(3)吊床版と上床版とを繋ぐ鉛直材は，一般炭素鋼鋼管をトラス状に配置する方式とし，全体剛性や耐風安定性の向上を図っている[7]．

端部分離型および従来型の上路式吊床版橋の設計結果を，Table 3 に示す．ここで，A 活荷重に対するたわみは従来型で支間長の 1／2000 程度，端部分離型で支間長の 1／4000 程度であり，いずれも道路橋のたわみ制限を十分満足する結果となっている[3]．

Table 3 Comparison in Hybrid Stress Ribbon Deck Bridge with Former Type Stress Ribbon Deck Bridge[2)]

			Former Type	Hybrid Type
Horizontal Force for Abutment (kN)	At Permanent Load (P)		20687	13152 (0.64)
	(P)+Live Load		23816	13451 (0.56)
	(P)+Live Load+Lowering Temp.		25183	14364 (0.57)
Displacement Caused by the A Type Live Load (mm)	Maximum	L/4 Point	50 (L/1800)	16 (L/5625)
		L/2 point	39 (L/2308)	23 (L/3913)
	Minimum	L/4 Point	-31 (L/2903)	0 (L/ −)
		L/2 point	-14 (L/6429)	0 (L/ −)
Change of Stress Caused by the A Type Live Load (N/mm^2)	Suspension Cable		11.2	17.3
	Prestressing Cable (Suspended Slab)		11.2	10.8

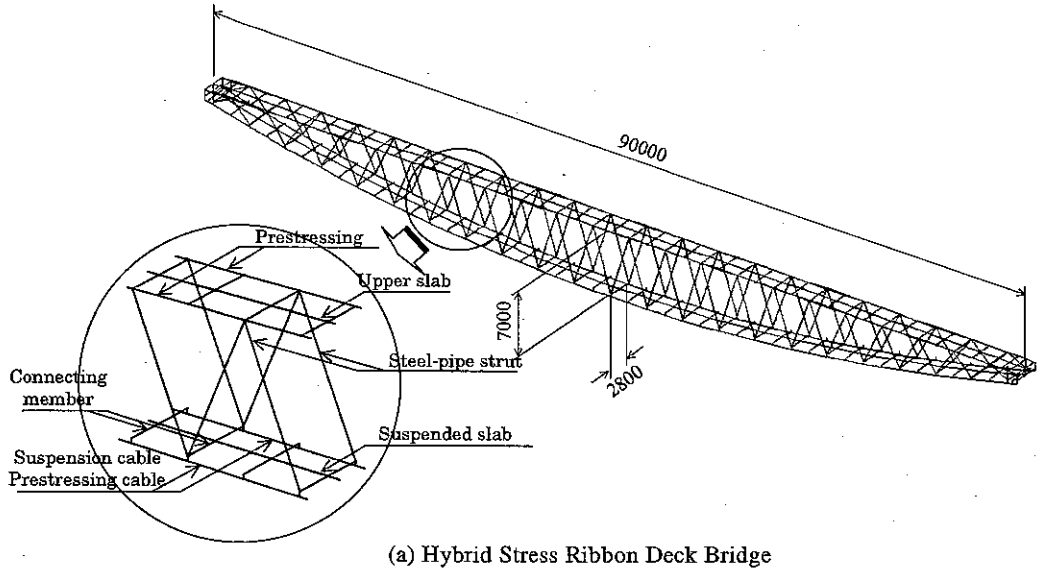

(a) Hybrid Stress Ribbon Deck Bridge

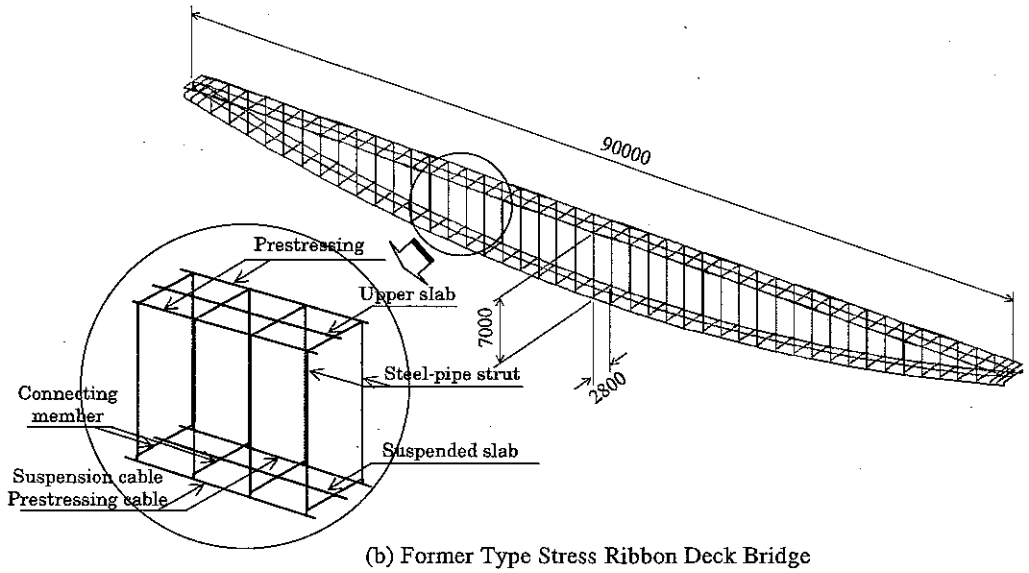

(b) Former Type Stress Ribbon Deck Bridge

Fig. 5 Analysis Model

3．解析モデル

端部分離型上路式吊床版橋および従来型の上路式吊床版橋の固有振動特性および動的応答特性を検討するために，それぞれ Fig. 5(a)および Fig. 5(b)に示す３次元骨組構造にモデル化した[9)]．解析モデルでは，上床版，吊床版および鉛直材ははり要素，吊ケーブルは幾何剛性を考慮したケーブル要素，吊床版および上床版へのプレストレス導入用のＰＣケーブルはトラス要素でモデル化した．また，吊ケーブルおよび吊床版へのプレストレス導入用のＰＣケーブルを外ケーブルとし，上床版へのプレストレス導入用のＰＣケーブルをアンボンドケーブルとしていることから，ケーブル端部の定着点を除いて，仮想横繋材と各ケーブルの間にはサドル部材に相当する剛なトラス要素を設けて橋軸方向にはスライドするものとした．なお，各部材の剛性は，本検討では両形式とも同一であ

るとしている．また，吊ケーブルの幾何剛性は，各形式の永久荷重作用時のケーブル張力に応じて設定している．

解析モデルの境界条件は，端部分離型上路式吊床版橋は吊ケーブル端部を完全固定，吊床版端部を単純支持とした．一方，従来型の上路式吊床版橋は吊床版端部，吊ケーブルおよび吊床版へのプレストレス導入用のＰＣケーブル端部を完全固定，上床版端部を単純支持とした．

4．固有振動特性

4．1　固有振動モード

Fig. 5 に示す解析モデルを用いて，サブスペース法により固有振動解析を行った．固有振動解析結果として，各形式の固有振動モードを Fig. 7 および Fig. 8 に，固有値を Table 4 に示す．

従来型の上路式吊床版橋では，鉛直たわみの最低次モードは逆対称モードであり，次いで対称モードになっており，両モードの固有振動数は近接している．また，低次のねじれモードは，水平モードと連成したモード形状を示している．これらの特性は，サグ比の大きい吊構造の特性といえる[10]．

一方，端部分離型上路式吊床版橋では，鉛直たわみの最低次モードは対称モードであり，次いで逆対称モードになっており，両モードの固有振動数は従来型に比べて近接していない．また，ねじれモードは，水平モードと分離されている．これらの特性は，従来型の上路式吊床版橋の特性とは異なり[5)～7)]，桁構造により近い特性であるといえる．これは，端部分離型上路式吊床版橋の完成系の剛性は，吊床版，上床板および鉛直材からなる単純トラス桁としての曲げ剛性が卓越することが主な要因であると考えられる．

なお，従来型は端部分離型に比べて，耐風安定性や車両走行時の振動使用性において問題となる振動数領域により多くの固有振動モードが存在する結果となっている．

4．2　各振動モードのひずみエネルギー比

固有値解析より得られた各振動モードに対して，全振動エネルギーに対する各構成部材のひずみエネルギー比を算出した結果を Fig. 8 に示す[10]．ここで，表中の Cable の区分には，吊ケーブル，吊床版および上床版へのプレストレス導入用のＰＣケーブルを含めて示している．

従来型の上路式吊床版橋では，鉛直たわみ振動モード（1 次，2 次，5 次，6 次，7 次，8 次，10 次）においては，全振動エネルギーに占めるケーブルのひずみエネルギーの比率が高い．また，ねじれと水平の連成モード（3 次，4 次）においては，上床版および吊床版のひずみエネルギーの比率が高くなっている．

一方，端部分離型上路式吊床版橋では，鉛直たわみ振動モード（2 次，4 次，6 次，9 次）においては，ケーブルのひずみエネルギーに比べて上床版，吊床版および鉛直材の占めるひずみエネルギーの比率が高く，高次振動モードになるほど鉛直材のひずみエネルギーが大半を占めるようになる．この結果は，端部分離型上路式吊床版橋の剛性は，吊床版，上床板および鉛直材からなる単純トラス桁としての曲げ剛性が卓越することを裏付けるものである．また，ねじれ振動モードにおいては，鉛直材のひずみエネルギーの比率が高く，鉛直材がねじり振動数の増加に寄与していることが示されている．

なお，端部分離型は従来型に比べて，全振動モードを通じてケーブルのひずみエネルギーの比率が低い．このことは，端部分離型と従来型とのモード減衰の相違の要因になるものと考えられる[10]．

5．耐風安定性

吊床版橋は，設計耐用期間内に想定される風による作用に応じて，安全性および供用性の観点から定められる耐風性能を確保するように設計しなければならない[1)]．ここで，橋への風による作用は多様であるが，上部構造の断面形状や固有振動特性から，本検討ではねじれフラッターに対する照査を行った[1),11)]．

ねじれフラッターの照査風速 U_{rf} は，道路橋耐風設計便覧に準拠して，建設地点における再現期間 100 年の風速の期待値から，地表粗度や耐用年数等に応じて式(1)～(3)により算出した[11)]．

$$U_{rf} = 1.2 \times E_{rl} \times U_d \tag{1}$$

$$U_d = E_l \times U_{10E} \tag{2}$$

$$U_{10E} = U_{10} \times (0.57 - 0.093 ln(ln(R/(R-1)))) \tag{3}$$

ここで，U_{10} は建設地点における再現期間 100 年の風速の期待値（＝30m/s），U_{10E} は再現期間 R 年の風速の期待値であり，E_l は地表粗度や平水位からの橋の高さに関する補正係数（＝0.82），E_{rl} は気流の乱れに関する補正係数（＝1.25）である．また，再現期間 R 年は，検討対象の橋が仮橋であることから耐用年数 N を 5～20 年とし，再現期間の風速の期待値が耐用年数内に超えない確率 P が 60%となるように，式(4)に基づいて設定した[11)]．

$$P = (1 - 1/R)^N \tag{4}$$

耐用年数とねじりフラッター照査風速の関係を，Table 5 に示す．

一方，ねじりフラッターの発現風速は，式(5)により算出した．

$$U_{cf} = 3.4 \times f_t \times B \tag{5}$$

ここで，f_t は最低次のねじれ振動数であり，B は橋の総幅である．また，係数 3.4 はトラス断面の一様気流中での部分模型風洞実験結果から得られたフラッター発現の無次元風速より設定している[11)]．式(5)により算出した端部分離型上路式吊床版橋および従来型の上路式吊床版

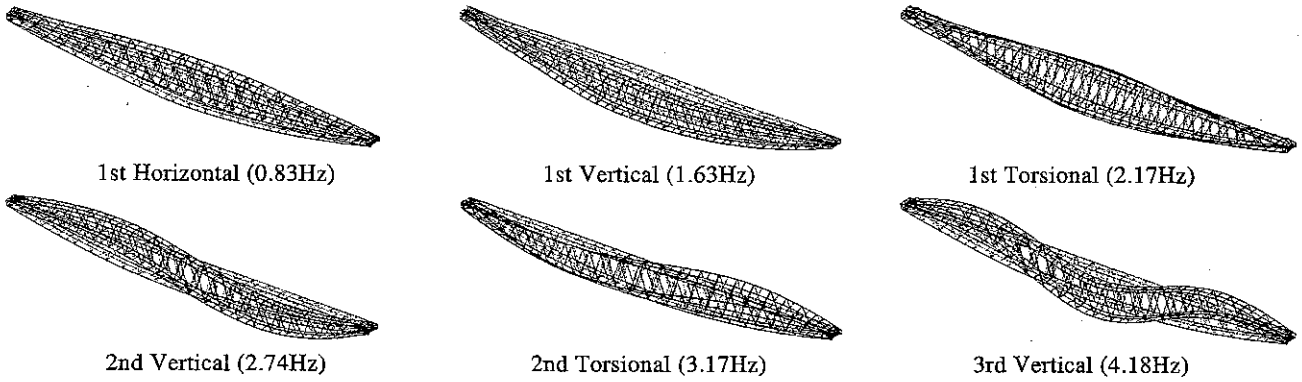

Fig. 6 Mode Shapes of Hybrid Stress Ribbon Deck Bridge

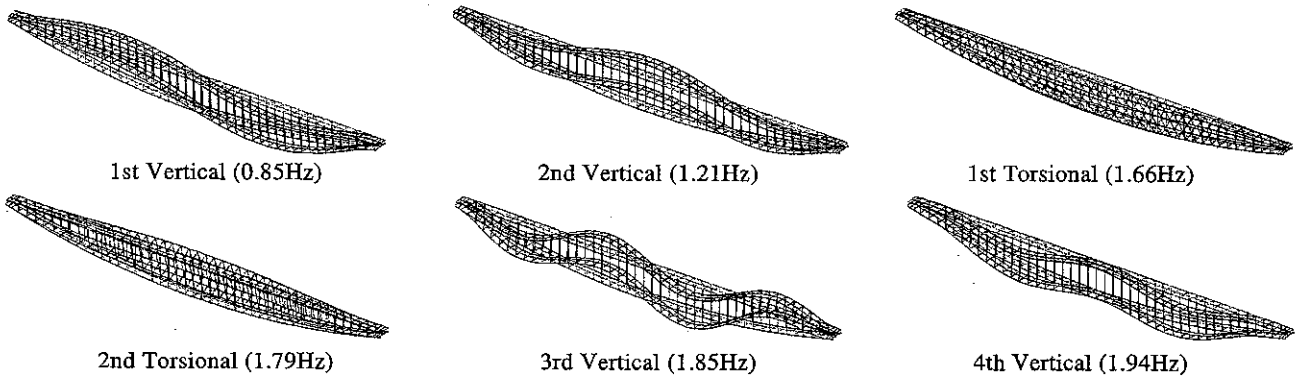

Fig. 7 Mode Shapes of Former Type Stress Ribbon Deck Bridge

Table 4 Natural Frequencies

(a) Hybrid Stress Ribbon Deck Bridge

	Modal shapes	Frequency (Hz)
1	1st horizontal	0.831
2	1st vertical (symmetrical)	1.633
3	1st torsional mode	2.172
4	2nd vertical (anti-symmetrical)	2.739
5	2nd torsional mode	3.171
6	3rd vertical (symmetrical)	4.182
7	3rd torsional mode	4.433
8	4th torsional mode	4.805
9	4th vertical (anti-symmetrical)	5.635
10	5th torsional mode	6.003

(b) Former Type Stress Ribbon Deck Bridge

	Modal shapes	Frequency (Hz)
1	1st vertical (anti-symmetrical)	0.851
2	2nd vertical (symmetrical)	1.212
3	1st torsional mode	1.659
4	2nd torsional mode	1.786
5	3rd vertical (anti-symmetrical)	1.852
6	4th vertical (symmetrical)	1.935
7	5th vertical (symmetrical)	2.538
8	6th vertical (anti-symmetrical)	3.087
9	3rd torsional mode	3.600
10	7th vertical (symmetrical)	3.835

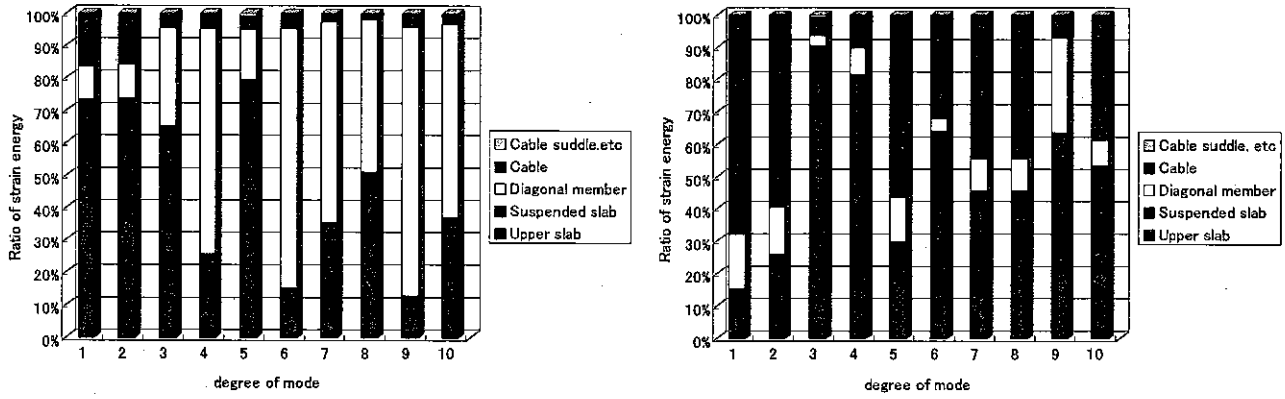

(a) Hybrid Stress Ribbon Deck Bridge (b) Former Type Stress Ribbon Deck Bridge

Fig. 8 Ratio of Strain Energy of Constitutive Member on Each Natural Vibration Mode

Table 5　Verify of Flutter

Life Time (year)	Wind Velocity for Verify U_{rf} (m/s)	Hybrid Stress Ribbon Deck Bridge			Former Type Stress Ribbon Deck Bridge		
		Torsional Freq. (Hz)	Wind Velocity U_{cf} (m/s)	Verify $U_{cf} \geqq U_{rf}$	Torsional Freq. (Hz)	Wind Velocity U_{cf} (m/s)	Verify $U_{cf} \geqq U_{rf}$
50	36.9	2.172	38.4	OK	1.694	29.9	NG
20	33.6			OK			NG
15	32.8			OK			NG
10	31.4			OK			NG
5	28.8			OK			OK

橋に対するフラッター発現風速を，Table 5 に示す．

フラッターに対する耐風安定性は，従来型の上路式吊床版橋では耐用年数 10 年以上においては満足できない結果となったが，端部分離型上路式吊床版橋では耐用年数 50 年においても十分に満足できる結果となっている．

6．車両走行時の振動使用性

検討対象の橋は，新丸山ダム建設におけるトンネル掘削土砂の運搬等に使用されるため，土砂を満載したダンプトラック等が頻繁に走行することとなる．しかしながら，現在までに国内で架設された上路橋吊床版橋には，大型車両が橋梁上を頻繁に走行する状況の橋が無いことから[1)]，大型車両走行時の振動使用性について設計段階で検討する必要がある．そこで，Fig. 5 に示す解析モデルを用いて，大型車両を走行させた場合のシミュレーション解析により橋の各部の動的応答を算出し，振動使用性について検討した．なお，検討対象の橋は主に土砂や建設資材を積載した大型車両の通行のみを想定しているが，本検討では歩行者が同時に利用するものとして，歩行者の振動に対する恕限度を指標として検討した．

動的応答解析では，路面凹凸を考慮した車両－橋梁系の運動方程式を，Newmark β 法（時間間隔 0.01sec，β ＝1／4)により直接積分して応答値を算出した．ここで，減衰マトリックスとしては，Rayleigh 減衰を仮定した．なお，Rayleigh 減衰の基準振動数は，端部分離型上路式吊床版橋では鉛直たわみ１次モードと４次モードの，従来型の上路式吊床版橋では鉛直たわみ１次モードと７次モードの固有振動数とし，モード減衰定数は，車両走行時の振動レベルを考慮して 1.0%とした．

動的応答解析における車両モデルとしては，道路橋示方書の設計自動車荷重を参考にして総重量245kNおよび196kN の３軸大型車両を想定し[8)]，Fig. 9 に示すように，部材の面外方向の曲げやねじれ振動などの立体的な挙動に対応できる 11 自由度系のモデルを用いた[12)]．車両モデルのパラメータを，Table 6 に示す．

車両走行のシミュレーションは，走行位置を幅員中心とし，走行速度は検討対象の橋の設計速度である 20km/h とした．また走行レーンの路面凹凸は，ISO 基準の「普通」程度の路面凹凸に適合する波形を用いた[12)]．

端部分離型上路式吊床版橋および従来型の上路式吊床

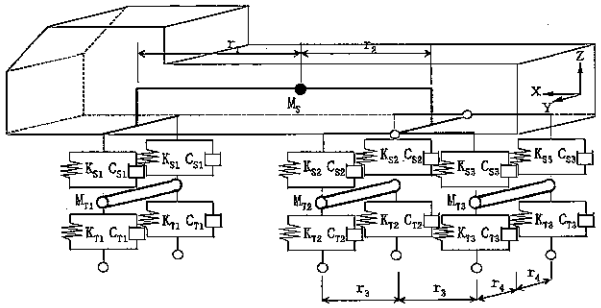

Fig. 9　Vehicle's Model

Table 6　Parameters of Vehicle's Model

Total Weight (kN)	245.0	196.0
M_s (kN・s²/m)	217.6	176.4
M_{t1} (kN・s²/m)	7.8	3.92
M_{t2} (kN・s²/m)	9.8	7.84
M_{t3} (kN・s²/m)	9.8	7.84
r_1 (m)	4.970	2.500
r_2 (m)	1.480	1.350
r_3 (m)	0.675	0.650
r_4 (m)	0.950	1.000
K_{s1} (kN/m)	913	639
K_{s2} (kN/m)	2282	2556
C_{s1} (kN・s/m)	4.26	2.45
C_{s2} (kN・s/m)	10.78	9.80
K_{t1} (kN/m)	3553	1775
K_{t2}, K_{t3} (kN/m)	4441	3549
C_{t1} (kN・s/m)	5.88	2.94
C_{t2}, C_{t3} (kN・s/m)	7.60	5.88

版橋の鉛直方向速度応答を Fig.10 および Fig.11 に，鉛直方向変位応答を Fig.12 および Fig.13 に示す．速度応答は，245kN 車走行時および 196kN 車走行時ともに端部分離型の方が従来型に比べて小さい応答となっている．特に，支間中央においては，両者の差が顕著に表れており，従来型に比べて端部分離型の速度応答は半分程度の値となっている．なお，196kN 車走行時の最大速度応答は，端部分離型で約 3.0cm/sec，従来型で約 4.5cm/sec であり，いずれも BS5400 に規定された制限値 5.7cm/sec 以下となっている[13)]．変位応答は，従来型に比べて端部分離型の鉛直変位は 1／3～1／4 程度になっている．

245kN 車および 196kN 車走行時の鉛直速度応答から，各着目点の実効値を算出した結果を Table 7 に示す．ここで，速度応答の実効値は，車両が橋上を通過している時間全体で自乗平均して算出している[14)]．端部分離型

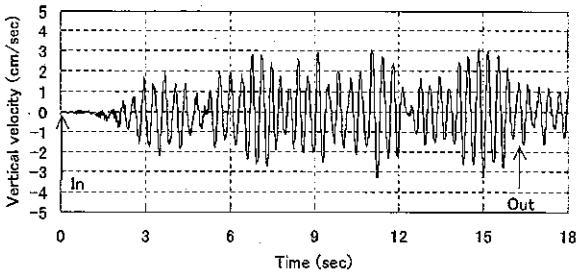

(a) 245kN Vehicle's Model (L／4 Point)

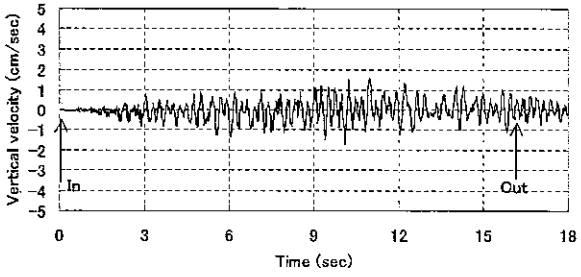

(b) 245kN Vehicle's Model (L／2 Point)

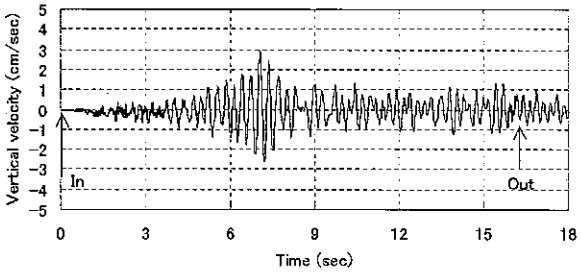

(c) 196kN Vehicle's Model (L／4 Point)

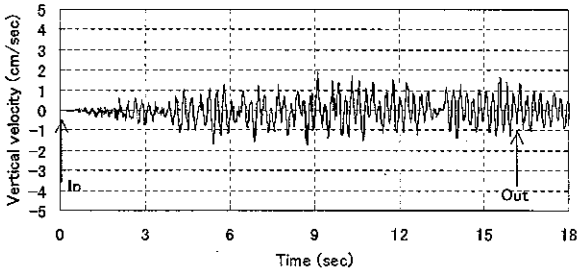

(d) 196kN Vehicle's Model (L／2 Point)

Fig.10 Vertical Velocity under Vehicle's Movement (Hybrid Stress Ribbon Deck Bridge)

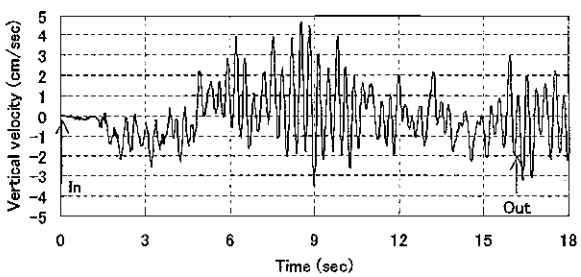

(a) 245kN Vehicle's Model (L／4 Point)

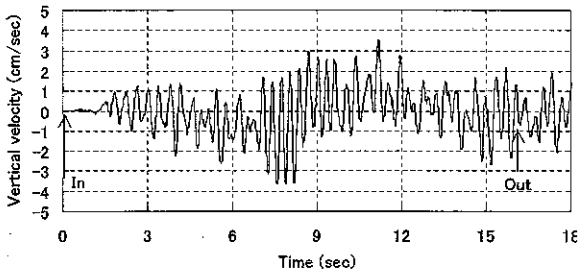

(b) 245kN Vehicle's Model (L／2 Point)

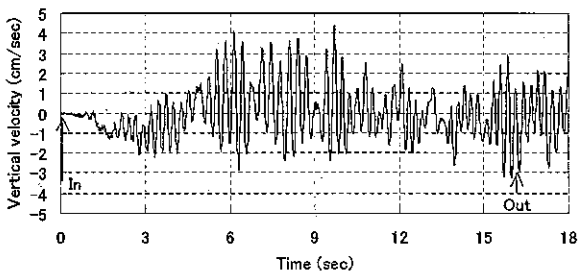

(c) 196kN Vehicle's Model (L／4 Point)

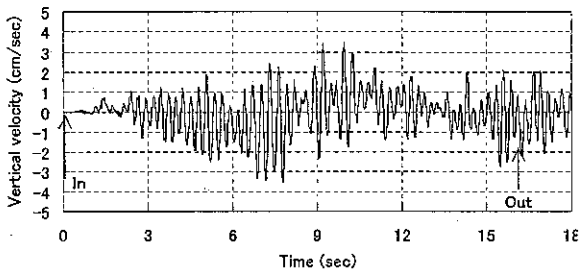

(d) 196kN Vehicle's Model (L／2 Point)

Fig.11 Vertical Velocity under Vehicle's Movement (Former Type Stress Ribbon Deck Bridge)

Table 7 Root Mean Square of Vertical Velocity (cm/sec)

Bridge Type	Vehicle's Weight	Point of Bridge						
		L／8	L／4	3L／8	L／2	5L／8	3L／4	7L／8
Hybrid Stress Ribbon Deck Bridge	245kN	0.91	1.29	0.97	0.49	1.04	1.22	0.82
	196kN	0.58	0.68	0.50	0.60	0.43	0.59	0.51
Former Type Stress Ribbon Deck Bridge	245kN	1.53	1.34	0.99	1.18	1.37	1.54	1.45
	196kN	1.52	1.34	1.08	1.09	1.29	1.33	1.18

では，196kN 車走行時の実効値は 245kN 走行時の 1／2 程度となる．一方，従来型では，車両重量によらず同程度の実効値となっている．なお，端部分離型の方が従来型に比べて着目点によっては半分程度の実効値となっているが，いずれの速度応答の実効値とも車両走行時に歩行者が「少し歩きにくい」と感じる閾値 1.70cm/sec を下回っており，振動使用性は問題ないと考えられる．しかしながら，Table 3 の活荷重たわみはたわみ制限値に対して十分余裕があることから，振動使用性をたわみ制限のみで評価して橋の部材剛性を設定した場合には，速度応答が歩行者の振動に対する忍限度を超える可能性が高いものと考えられる．

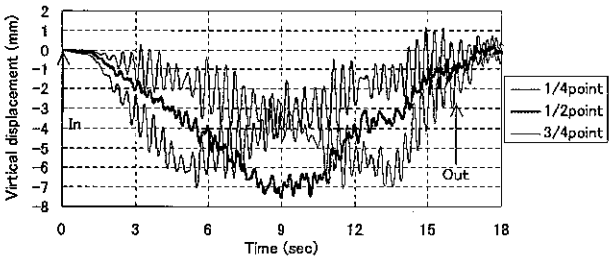

(a) 245kN Vehicle's Model

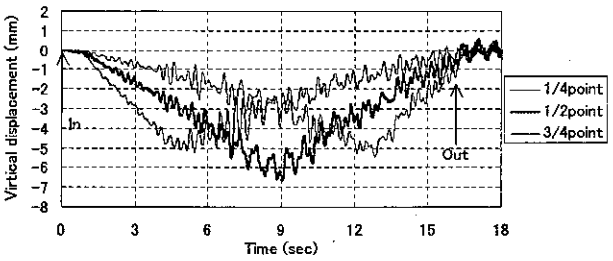

(b) 196kN Vehicle's Model

Fig.12 Vertical Displacement under Vehicle's Movement (Hybrid Stress Ribbon Deck Bridge)

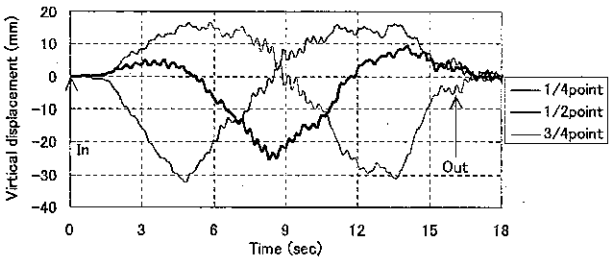

(a) 245kN Vehicle's Model

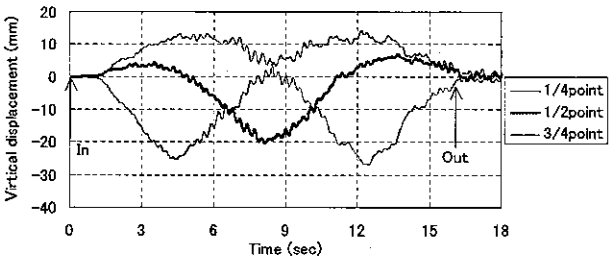

(b) 196kN Vehicle's Model

Fig.13 Vertical Displacement under Vehicle's Movement (Former Type Stress Ribbon Deck Bridge)

7．まとめ

本検討では，端部分離型上路式吊床版橋の固有振動特性，耐風安定性，車両走行時の振動使用性について，従来型の上路式吊床版橋と比較して解析的に検討した．本検討により得られた知見を以下に示す．

（1）提案した端部分離型上路式吊床版橋は，完成系においては単純トラス桁として剛性が卓越することから，従来型の上路式吊床版橋に比べて，全体剛性が向上し，固有振動数も全体的に高くなっている．

（2）提案した端部分離型上路式吊床版橋は，ねじれ振動数が従来型に比べて高くなり，ねじりフラッターに対する耐風安定性が向上している．

（3）提案した端部分離型吊床版橋は，車両走行時の速度応答および変位応答が従来型に比べて小さく，歩行者が同時に利用する場合でも，大型車両走行時における振動使用性も問題ないものと考えられる．

今後，実橋において振動実験を行って，解析結果と実験結果の比較により，本解析モデルと今回得られた知見の妥当性を検証する必要がある．

参考文献

1) (社)プレストレストコンクリート技術協会：PC吊床版橋設計施工基準(案)，2000.11.
2) 吉川卓，三浦弘禎，神谷裕司，角本周：再利用を考慮した上路式吊床版橋の設計（新丸山ダム小和沢仮橋），第12回プレストレストコンクリートの発展に関するシンポジウム論文集，2003.10.（投稿中）
3) 梶川康男：たわみと振動感覚，橋梁交通振動に関するコロキウム論文集，PART A，pp.47-54，1995.11.
4) 深田宰史，梶川康男，原田政彦：車両走行によるニールセンローゼ橋の振動特性，土木学会第57回年次学術講演会講演概要集，第Ⅰ部，pp.1177-1178，2002.9.
5) 鳥野清，成富勝，日笠山徹巳，小坪清真：上路式ＰＣ吊橋の動特性とその改善，構造工学論文集，Vol.32A，pp.691-698，1986.3.
6) 梶川康男，唐下義文，深田宰史，松元香保里：４径間連続上路式吊床版橋の振動実験と解析，構造工学論文集，Vol.44A，pp.835-842，1998.3.
7) 梶川康男，深田宰史，久保修平，近藤真一：斜材を有する上路式PC吊床版歩道橋の振動特性，構造工学論文集，Vol.48A，pp.389-397，2002.3.
8) (社)日本道路協会：道路橋示方書・同解説，Ⅰ共通編，2002.3.
9) 梶川康男，深田宰史，大木太，角本周，町勉，熊谷高：外ケーブル併用吊床板橋の構造と振動特性，構造工学論文集，Vol.48A，pp.377-388，2002.3.
10) 角本周，梶川康男：PC吊床版橋の減衰定数の評価と振動使用性照査における影響，土木学会論文集，No.612／Ⅰ－46，pp.337-348，1999.1.
11) (社)日本道路協会：道路橋耐風設計便覧，1991.7.
12) 橋梁振動研究会編：橋梁振動の計測と解析，技報堂出版，1993.10
13) BSI：Steel, Concrete and Composite Bridges, Part 2. Specification for loads, *BS5400*, 1978.
14) 梶川康男：振動感覚を考慮した道路橋の使用性解析に関する考察，土木学会論文報告集，第304号，pp.4758，1980.12.

(2003.7.31 受付)

ヒンジ部を連続化した8径間PCラーメン橋の振動特性

Vibration characteristics of 8 spans prestressed concrete rigid frame bridge with joint less

梶川　康男*，深田　宰史**，宇田川　敏 ***
Yasuo KAJIKAWA, Saiji FUKADA and Satoshi UDAGAWA
*　工博　　金沢大学大学院教授，自然科学研究科（〒920－8667 金沢市小立野2丁目40番20号）
**　博（工）　金沢大学大学院助手，自然科学研究科（　　同上　　）
***　　金沢大学大学院学生，自然科学研究科（　　同上　　）

Tedori River Bridge is the bridge, which consists from eight spans rigid frame with hinge shoes. This bridge is located on the national highway No.8 over Tedori River (This bridge was constructed by cantilever election method in 1977). In this bridge, serious damage on the hinge shoes was observed. The hang down of the main girder is mainly considered the cause. A possibility of causing trouble to the running performance and the safety of pedestrians were expected, therefore, repair of burying and continuation-zing joints with concrete immediately were performed to cancel the level difference of a road surface. In this study, we performed vibration tests and showed the changes of vibration characteristics of this bridge with joints (before repair) and with joint less (after repair).

Key words: prestressed concrete rigid frame bridge, vibration characteristics
キーワード：PCラーメン橋，振動特性

1. はじめに

本研究で対象とする手取川大橋（Fig.-1）は，石川県能美郡川北町の一般国道8号線上に架設されている橋長464.6m，支間長463.6m（50.0m＋6@60.6m+50.0m）の8径間有ヒンジPCラーメン橋である．手取川大橋の一般図および断面図をFig.-2およびFig.-3に，橋梁諸元をTable-1に示す．

本橋の構造的特徴は，橋脚を中心として張り出し架設した主桁からなるT型の単体構造が，せん断力を伝えるヒンジ沓（Fig.-4）によってジョイントされている．

本橋は，昭和52年1月に架設されてから長期間が経過している．また，国道8号上に架設されていることから，交通量が昼夜を問わず非常に多く，車両荷重の増加などの様々な条件から，主原因と考えられるヒンジの垂れ下がりによって支間中央部に大きな段差が生じていた．この段差によって通行車両からの衝撃的な振動が，大きな打撃音を伴って橋梁に加えられる．この悪循環により，中央ヒンジ沓の摺動部の磨耗とともに，車両走行性の低下や一般歩行者が通行した際の安全性が懸念されるなど，橋梁の使用性に関わる問題が生じていた．

一般的に，このような問題[1)2)]が生じる原因[3)-5)]としては，コンクリートのクリープ，乾燥収縮による桁の垂れ下がり以外に次のような原因が考えられる．

① プレストレスの低下

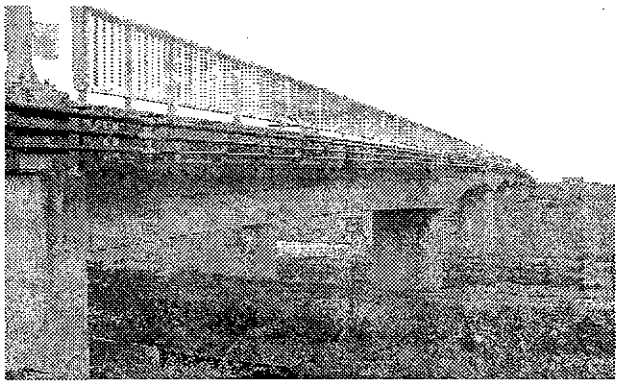

Fig.-1 Tedori River bridge

② 橋脚の傾き

③ 中央ヒンジ沓の磨耗による構造系の変化

しかしながら，いずれも明確な結論には至っておらず，早急な補修が必要とされていた．

そこで本研究では，補修前段階において本橋のヒンジ沓の損傷がどの程度進行し，どの程度の振動が生じているのかを把握するために，ヒンジ沓の目視点検および大型車両1台を用いた準静的および動的載荷試験を行った．

その結果，本来のヒンジ沓は，上下で接してせん断力のみを伝達する仕組みになっているが，J5（Fig.-5）のようにヒンジ本来の機能を果たしている沓もあれば，J6（Fig.-6）のようにヒンジ下部が接触し，上部に空隙が生じている状態の沓もあった．このヒンジ沓の損傷により

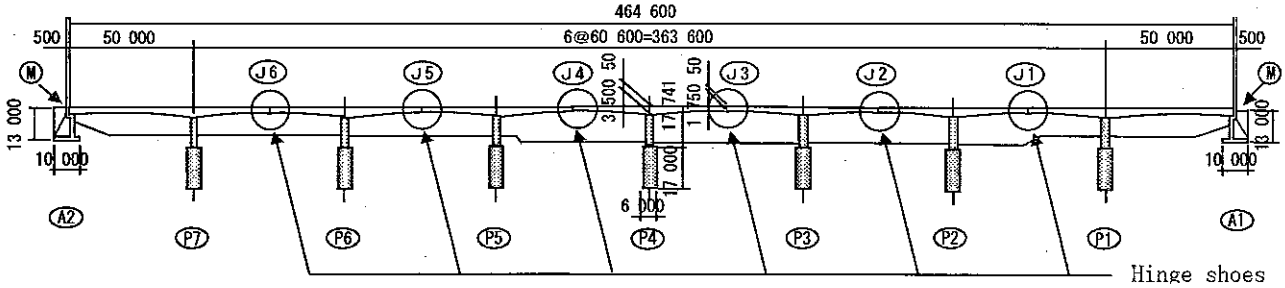

Fig.-2 General view of Tedori River Bridge

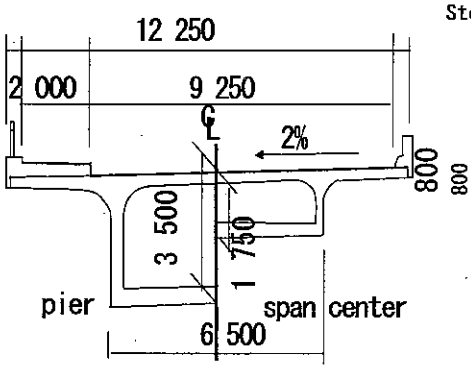

Fig.- 3 Cross section

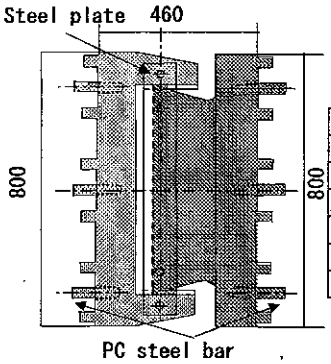

Fig.-4 Hinge shoe

Table-1 Structural property

Bridge length	464.6m
Span length	50.0 + 6 @ 60.6 + 50.0 = 463.6m
Effective width	9.25 + 2.0 (sidewalk)m
Girder height	max : 3.5m min : 1.7m
Lower slab width	6.5m
Completion	January, 1977
Client	Hokuriku Chiken

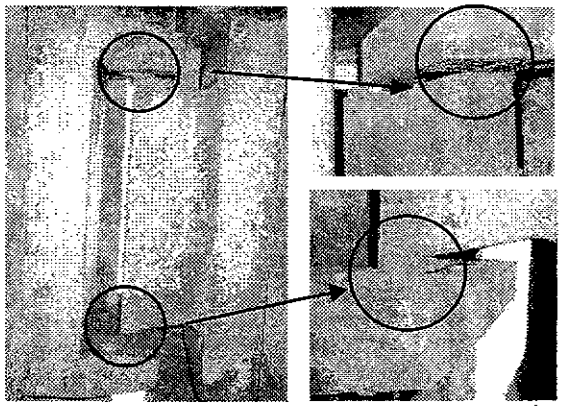

Fig.-5 Normal hinge shoe (J5)

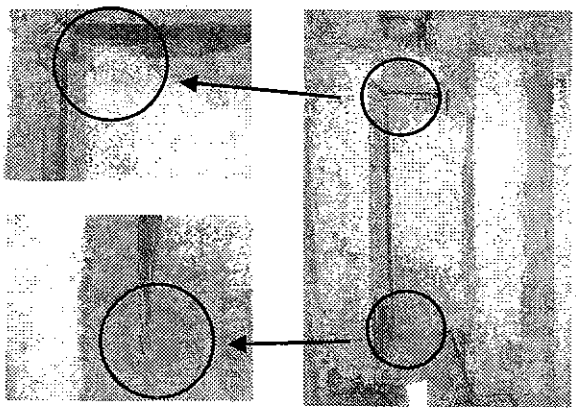

Fig.-6 Damaged hinge shoe (J6)

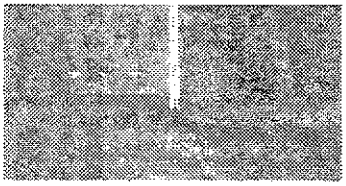

Fig.- 7 Expansion joint (sidewalk)

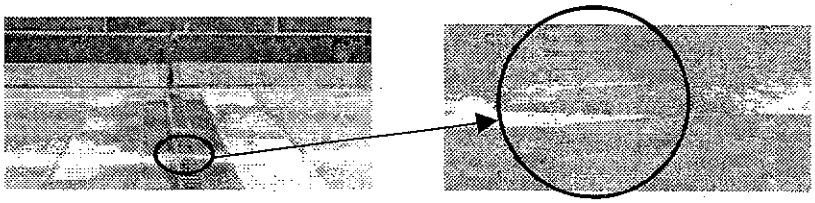

Fig.-8 Finger joint (J6)

歩道部の重ね合わせ型の伸縮継手（Fig.-7）やフィンガージョイント（Fig.-8）に2～3cmの隙間が，車両の通行の度に開いたり閉じたりしていた．

この結果をもとに補修案が様々提案され，最終的にはジョイント部をコンクリートで埋め，さらに外ケーブルで補強する連続化が採用された．これにより，本橋の構造系が変化したことから，補修効果や振動特性の変化を調べるために補修前と同様な実験を補修後においても行った．本文では，それら一連の結果を述べる．

2. 実験概要

本橋の変位挙動ならびに振動挙動を把握するために大型車両（総重量 196kN）を用いた載荷実験を行った．調査時間帯は，交通量の比較的少ない深夜に通行規制をして実施した．調査は，各径間中央の6箇所のヒンジ沓を対象とした．相対変位を計測するために，3方向（橋軸，橋軸直角，鉛直）の上流，下流両側5箇所に変位計を設置して行った．次に，地盤を不動点とした絶対変位をJ5，J6の2箇所において計測した．測点配置図をFig.-9(a),(b)に示す．走行ケースは，通常の走行レーンを走行

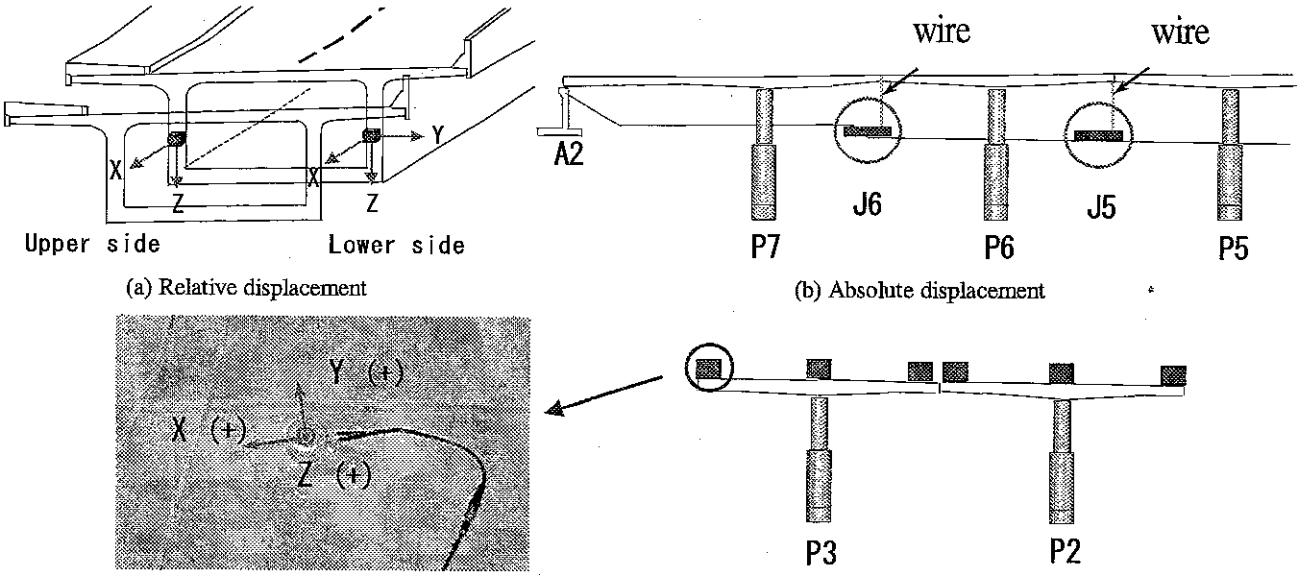

(a) Relative displacement

(b) Absolute displacement

(c) Vibratory level meter

Fig.-9 Position of measurement

Table-2 Cross section property

	A (m^2)	Iy (m^4)	Iz (m^4)	J (m^4)	M (tf/m)
main girder (side span)	2.416E+01 ～ 6.017E+00	2.651E+01 ～ 2.940E+00	1.091E+02 ～ 5.236E+01	3.077E+01 ～ 6.794E+00	6.465E+01 ～ 1.930E+01
main girder (center span)	2.410E+01 ～ 5.230E+00	2.632E+01 ～ 2.250E+00	1.089E+02 ～ 4.286E+01	3.067E+01 ～ 5.410E+00	6.451E+01 ～ 1.733E+01
pier	1.607E+01	4.011E+01	1.072E+01	1.139E+01	4.016E+01

A: Cross section area (m^2)

Iy: Moment of inertia of area around the Y axis (m^4)

Iz: Moment of inertia of area around the Z axis (m^4)

J: Torsional constant (m^4)

M: Mass per length (tf/m)

方向（A1 側⇔A2 側）を変えて走行する 2 ケース，道路の右側走行および構造中心位置走行の 4 ケースで行った．

2. 1 （準）静的載荷試験

本橋梁は，夜間でも交通量が非常に多い国道 8 号上に位置するため，長時間通行規制を行うのは困難であった．この制約条件から，各測点に静的に載荷していくのは不可能であったため，試験車を 5km/h 程度の徐行をさせて準静的に影響線を把握することにした．

2. 2 動的載荷試験

動的な走行外力が加えられた時の挙動を把握することにより，振動を含めた動的な変位挙動および加速度応答を把握する．本試験では，試験車の走行速度を 30, 50, 60km/h の 3 パターンに変化させて単独走行を行った．

次に，本橋梁では，車両走行による動的な外力が作用していることから，振動挙動についても把握する必要がある．そこで，振動レベル計（RION, VM－52）を用いて，T 型単体構造としての動的な加速度応答を計測した．測点は，事前の目視点検においてヒンジ沓部分の損傷が特に進行していた P2,P3 橋脚回りを中心として 6 箇所に設定して計測を行った．振動レベル計の配置図を Fig.-9 (c) に示す．

3. 解析概要

車両走行実験で把握しきれない部分の本橋の挙動を調べるために，本橋のモデル化を行った．本橋の解析モデルを Fig.-10 に示す．解析モデルは，総節点数 1142，総要素数 1141 の 3 次元骨組み構造とし，箱桁断面の図心軸に沿って一本の梁部材に置き換え，橋軸方向の桁高の変化については，線形に変化させた．また，各橋脚も梁部材にモデル化した．主桁と橋脚の接合部は，ラーメン橋の構造形式を考慮して剛部材とした．さらに，T 型単

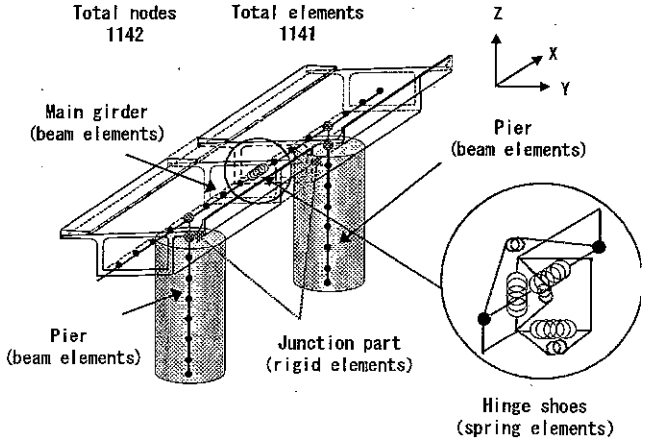

Fig.-10 Analytical model

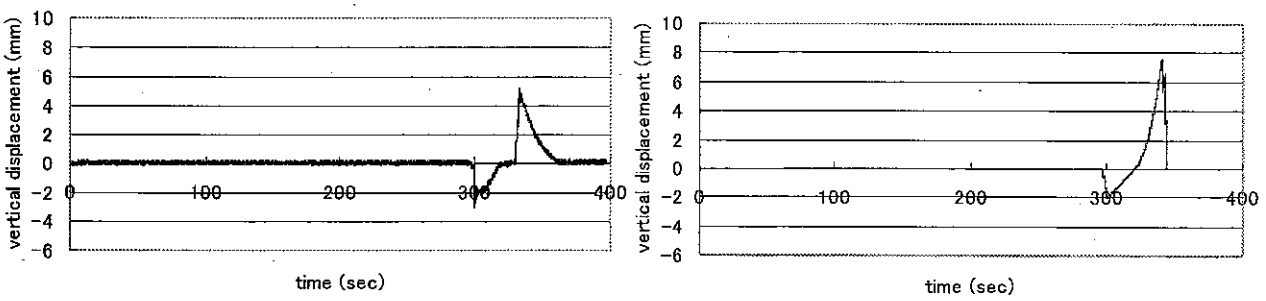

(a) Experiment (J6, absolute displacement)　(b) Analysis (J6,absolute displacement)

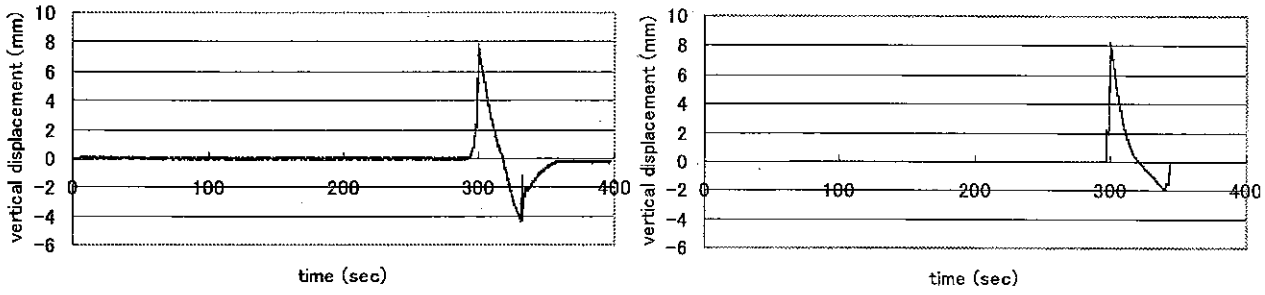

(c) Experiment (J5, absolute displacement)　(d) Analysis (J5, absolute displacement)

Fig.-11 Response of displacement

体構造をジョイントしているヒンジ沓をばね部材に置き換えて，そのばね定数を変化させて，様々な条件下でのヒンジ沓の挙動を把握した．

4. 実験結果と解析結果の比較

4. 1 準静的特性

試験車両がA1からA2方向へ左車線を徐行した時の実験値と解析により得られたJ5,J6の鉛直方向の絶対変位をFig.-11に示す．解析では，各径間のヒンジ沓部分のばね定数を0にしてヒンジ沓の凸型と凹型が接触しない状態を仮定した．

実験値より，車両が測点上を通過した時にJ6では約6mm，J5では約8mmの最大変位が生じていることがわかる．解析値のグラフを見ると，J5,J6とも最大変位が生じる部分までは，実験値とほぼ同じ挙動を示しており，解析モデルの剛性評価が妥当であったことを確認することができた．しかしながら，車両が着目点から退去する部分に関しては，解析値が急激に0に戻っているのに対し，実験値はヒンジ沓の接触により，緩やかな変化を示している．

4. 2 ヒンジ沓の変位挙動

準静的載荷試験において得られた変位の波形を見ると，ヒンジ沓の凸型と凹型が接触しない場合の変位挙動は，解析においてもよく再現できているといえるが，それらのヒンジが接触している場合は,再現できていない．

左右のヒンジが接触しているJ2を対象として,以下に試験車両がジョイントから橋脚を経て次のジョイントへ移った時のヒンジ沓の挙動をFig.-12より考察する．

① ヒンジの磨耗によって下側に空隙が生じているため，ジョイント J3-P3 間の片持ち先端，ジョイント J3 上に車両が移った時に，一気に5mm程度の相対変位が生じる．この際，ヒンジ沓では下側が接触する．また，P3に近づくに従い，相対変位が減少していき，P3上で0に戻る．

② P3-J2 間を車両が走行すると下方向に変位する．ジョイント J2 の手前においてヒンジ沓の上側において接触する．ここで，左右のヒンジが同時に動くことにより，相対変位に減少が生じている．（グラフの○印）

③ J2-P2間の片持ち先端,J2上に車両が移った時に，一気に10mm程度の相対変位が生じる．この際，ヒンジ沓では下側が接触する．

④ P2-J1 間を車両が走行すると，上側において J2 部分のヒンジの接触によって同時に変位するために，J3-P3 間通過時よりも相対変位が大幅に減少している．P1側の片持ちに移ったときに，変位はほぼ0になる．

5. 補修方法の検討

供用後長期間が経過した本橋の，桁の垂れ下がりによって，車両通行時に中央ヒンジ沓の左右のヒンジに空隙ができ，打撃音を伴って伸縮装置の摺動部に上下動が発生しているという問題を受けて，ヒンジ沓の補修が実施されることになった．その補修対策として大きく分類すると，緊急補修と根本的補修の2つに分類することができる．

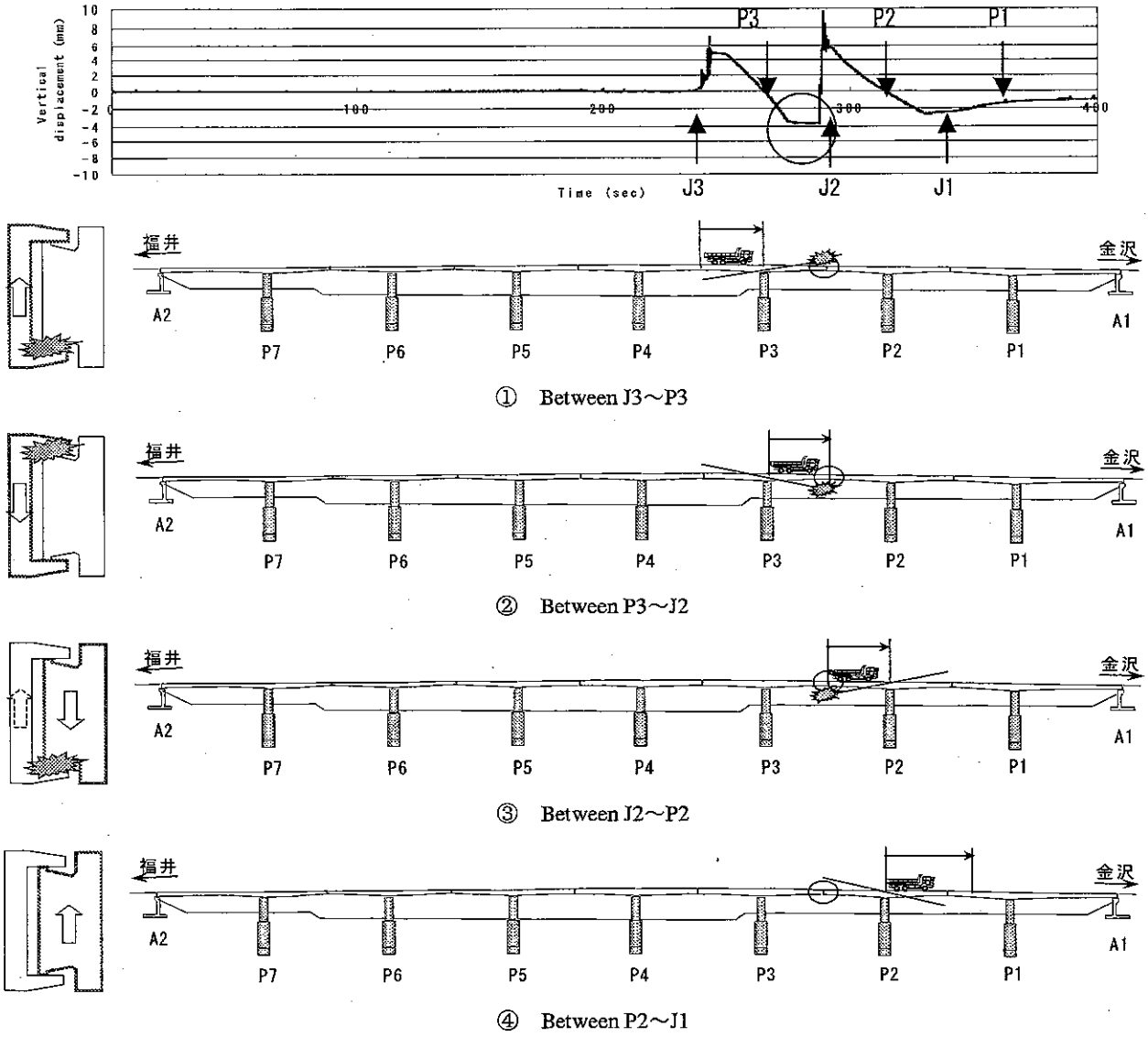

Fig.-12 Response of displacement at the damaged hinge shoe

＜緊急補修＞
① 隙間への鋼板挿入
＜根本的補修＞
① 中央ヒンジ沓の補強
② 改良した中央ヒンジ沓への取り替え
③ PC 構造での連続化

以上が挙げられるが，採用された方法は，PC 構造での連続化であった．つまり，ジャッキアップによって各径間の段差量を均一にした後，ヒンジ沓を鉄筋コンクリートで埋めて連続化し，箱桁内部において外ケーブルによって補強を行うという方法が用いられた．

この補修を受けて，補修前と同様に測点を配置し，大型車両を用いて再び静的および動的載荷試験を行った．

6. 振動挙動

試験車両が A2 から A1 方向へ幅員中央を走行速度 50km/h で走行した時の補修前後の振動挙動として，J2 位置における鉛直方向の加速度波形とそのスペクトルを Fig.-13 に示す．加速度波形を見ると，補修によって振動振幅が大幅に軽減されていることがわかる．また，車両が橋面上を退去した後の加速度スペクトルより，補修前において 3.07Hz に，補修後において 2.44Hz と 3.42Hz に卓越が見られた．これは，連続化により複数の振動モードが励起したためと考えられる．

次に，試験車両が A2 から A1 方向へ左車線を走行速度 30km/h で走行した時の P2 橋脚上水平面での振動挙動を加速度のオービット線図を用いて，補修前後で比較した．Fig.-14 にオービット線図と橋軸直角方向の加速度スペクトルを示す．これより補修前において，桁が橋軸直角方向への大きく振動しており，面内だけでなく面外方向への振動も生じていたことがわかる．これらの振動が補修によって大幅に軽減されている．またスペクトルより，補修によって卓越振動数が高くなっている．

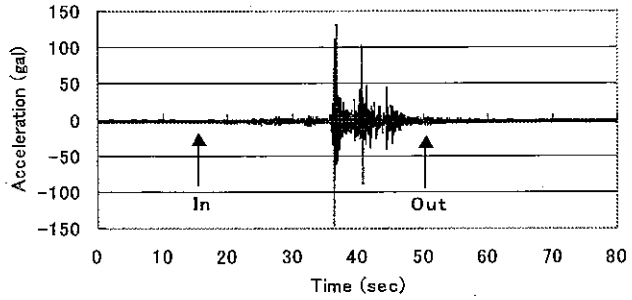

(a) Acceleration (before repair)

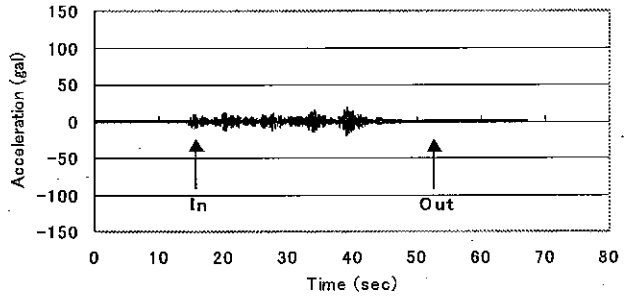

(b) Acceleration (after repair)

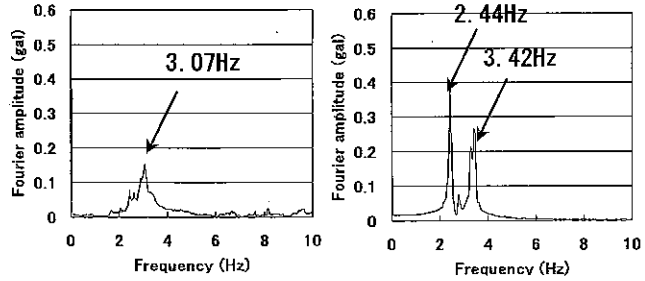

(c) Spectrum (before) (d) Spectrum (after)

Fig.-13 Comparison of before and after repair (50km/h, A2→A1, Center line, J2, Vertical direction)

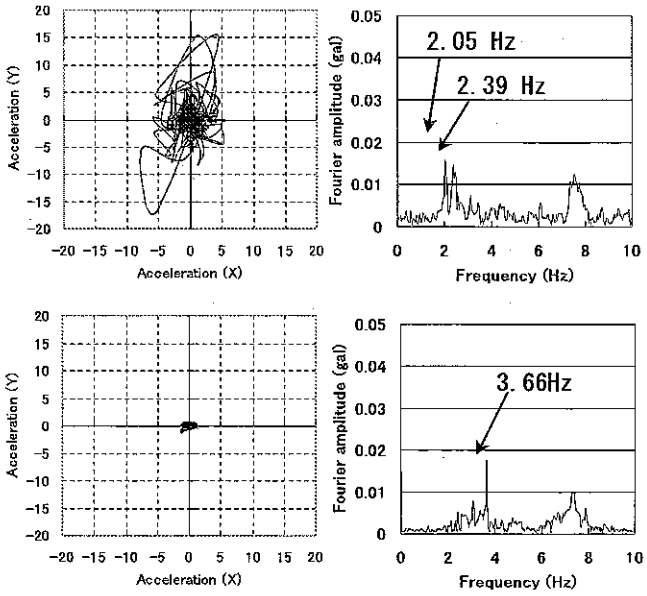

Fig.-14 Comparison of before and after repair (30km/h, A2→A1, P2 X-Y)

7. まとめ

本研究では，交通荷重によってヒンジ沓の損傷が進行していた手取川大橋（8径間有ヒンジPCラーメン橋）を対象として，ジョイント部を埋めて連続化する補修が行われた補修前後の2度にわたって準静的載荷試験および動的載荷試験を行った．

本研究により得られた知見を以下に示す．

(1) 準静的載荷試験より，各径間のジョイント部分の変位挙動を把握した．特に，損傷が進行しているヒンジ沓において，車両の移動とともにヒンジ沓の凸型と凹型が接触する様子を把握することができた．

(2) 実験で把握しきれない部分の挙動に関しては，有限要素法を用いた解析によって検討を行った．車両載荷によりヒンジ沓が最大変位を生じる部分の変位挙動を良く再現できたことから，解析モデルの剛性評価が妥当であったことを確認することができた．

(3)橋脚を中心としたT型単体構造の振動挙動に関して補修前と補修後を比較することで，補修によってどの程度振動が軽減したのか把握した．補修によって鉛直方向だけでなく，面外方向においても振動が大きく軽減されており，十分な補修効果があった．

参考文献

1) 酒井和廣：美陵高架橋の補修，橋梁と基礎，Vol.17，No8，pp.86-89，1983.8.

2) ディビダーク橋支点沈下に関する研究会：ディビダーク橋支点沈下に関する報告書，（財）阪神高速道路管理技術センター，1988.3.

3) 国広哲男，今井勤，佐藤浩一：PC長大橋のクリープたわみ，橋梁と基礎，Vol.2，No5，pp.1-16，1968.5.

4) 高藤傳，関慎吾：長大PC道路橋のたわみ特性と補修方法について，日本大学理工研究所所報，pp.245-274，1981.3.

5) 百島祐信：カンチレバー架設したプレストレストコンクリート橋における断面力および挙動の研究，土木学会論文報告集，第240号，pp.113-128，1975.8.

(2003.7.31受付)

鋼少数主桁橋の耐風安定性と振動特性に関する実験的検討

The evaluation of the vibration characteristics and aerodynamic stabilities of a bridge with fewer girders

村越　潤*、麓　興一郎**、芦塚　憲一郎***、清田　錬次****、宮崎　正男*****
Jun MURAKOSHI, Koichiro FUMOTO, Kenichiro ASHIZUKA, Renji KIYOTA and Masao MIYAZAKI

*(独)土木研究所、構造物研究グループ橋梁構造チーム上席研究員（〒305-8516　茨城県つくば市南原１番地６）
**同上、橋梁構造チーム主任研究員（同上）
***日本道路公団、構造技術課(〒100-8979 東京都千代田区霞ヶ関３－３－２)
****日本橋梁建設協会、振動部会長（〒104-0061　東京都中央区銀座２丁目２番18号）
*****同上

Bridges with fewer girders become popular as one of the new bridge form and are applied to the bridge span that is longer than 50m. However, it is reported that these bridges have the low structure dumping which affects aerodynamic stability as compared with the conventional many girders etc and it is necessary for aerodynamic design to examine the structure dumping etc. There are very few cases of the vibration experiments by the vibration machine. We conducted vibration experiments of a bridge that has about 60m center span by the vibration machine, and investigated the structure dumping etc., Moreover, the difference in the aerodynamic characteristic by the difference in structure dumping was checked by wind tunnel experiment (spring support examination).

キーワード：鋼少数主桁、耐風安定性、振動試験、風洞試験

1．はじめに

鋼少数主桁橋は既に多くの機関で採用され、合理化橋梁の一つとして定着しつつある。当初この形式は比較的短い支間長に適用されていたが、最近では適用支間を大幅に伸ばした事例も見受けられるようになった。しかしながら、従来の桁橋と比較してその耐風性に留意する必要のあることも報告されており、今後の普及を踏まえると風洞試験を行い、耐風安定性を推定するための手法について検討していく必要がある。一方、耐風安定性の推定に当たっては固有振動数や構造減衰等の振動特性を把握することが重要であるが、これまで、鋼少数主桁橋において起振機を用いて、振動特性を計測した実施例は極めて少ない。

そこで、本文では高欄種類の異なる鋼少数主桁橋を対象とし、構造減衰が異なることによる耐風特性の違いを風洞試験（バネ支持試験）結果で報告するとともに、鋼少数主桁橋の振動特性を把握するため、実橋において起振機を用いて実施した振動実験の結果について報告する。なお、本研究は日本橋梁建設協会との共同研究「少数主桁橋における耐風安定性推定手法の開発」の一環として実施した。

2．鋼少数主桁橋模型の風洞試験

2．1　検討内容

実際の設計事例を参考に、高欄の種類の異なる２種類の断面を図－１および表－１のように設定し、それぞれ1/40スケールの２次元剛体模型を製作した。各モデルとも共通の壁高欄もしくは鋼製高欄を持ち、いずれも高さを1.1mとしている。ばね支持試験は、表－２に示す試験条件をパラメータとして実施したが、ここでは特徴的な結果を抜粋して示す。なお、ばね支持試験は２自由度系にて行ったが、振動数比と対数減衰率の条件によっては、たわみ振動とねじれ振動の相互干渉が確認される場合もあり、この場合には１自由度系による確認計測を実施した。対数減衰率については、実際に実橋を起振機で振動させたデータが少ないことを踏まえて、安全性及び耐風特性を確認するために、0.02～0.06の間で考慮することとした。

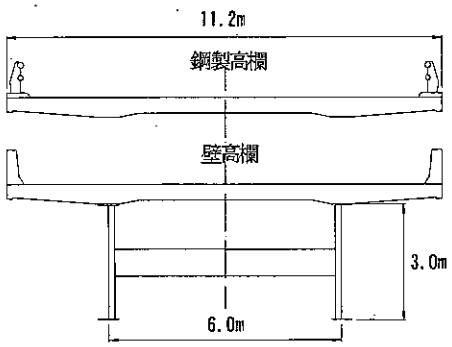

図－１　検討対象とした鋼少数主桁断面

表－１　鋼少数主桁模型の諸元

諸　元	模型値
幅員	280mm (11.2m)
桁高	75mm (3.0m)
桁間隔	150mm (6.0m)
振動数比（ねじれ/たわみ）	1.20 (1.22)
重量	15.7kgf/m(15.8tf/m)

（　）は実橋値

表－２　試験条件

条　件	パラメータ
高欄形状	壁高欄、鋼製高欄
対数減衰率	δ= 0.02, 0.03, 0.04, 0.05, 0.06
仰角	α＝＋３°，±０°，－３°

２．２　検討結果

一様流中で風の迎角０°において、壁高欄、鋼製高欄それぞれ、対数減衰率δを0.02、0.04、0.05に変化させた際のたわみの風速－振幅応答図を図－２に、ねじれの風速－振幅応答図を図－３に示す。

（１）高欄の影響

壁高欄と鋼製高欄の違いによる応答振幅の比較に着目する。まず、図－２の渦励振に着目すると、いずれの場合でも鋼製高欄タイプの方が壁高欄タイプより振幅が小さくなっている。また、その発現風速も高くなっていることがわかる。次に、発散振動に着目しても、鋼製高欄の場合にはいずれのケースにおいても壁高欄より発現風速がいくらか高くなっている。この傾向は+3°と−3°に迎角を変えた場合も同様であった。このことから、構造減衰に関わらず、壁高欄と鋼製高欄の耐風安定性の傾向は同様であると推定れる。

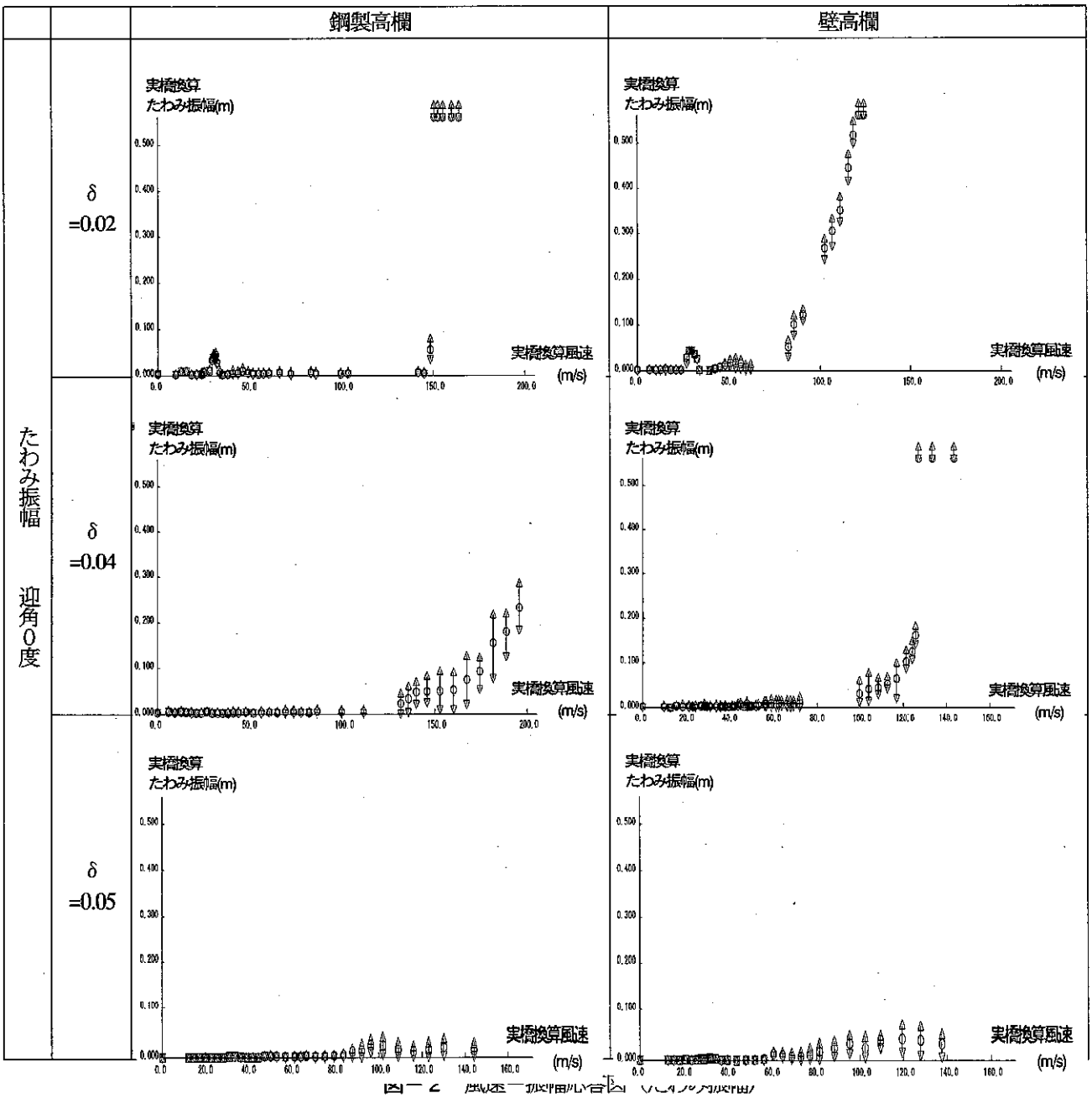

図－２　風速－振幅応答図（たわみ方向振幅）

（2）構造減衰による違い

対数減衰率δを0.02、0.04、0.05に変化させた際のたわみとねじれの風速－振幅応答図に着目する。

図－2のたわみについては、鋼製高欄、壁高欄双方ともδ＝0.02の際に確認される渦励振はδ=0.04では消滅している。発散振動についてもδ＝0.04で鋼製高欄、壁高欄双方とも発現風速が高風速域に移動しており、たわみ振動については、δ=0.04以上であれば、耐風安定性が確保（道路橋耐風設計便覧[1]（以下：耐風便覧）が規定している設計基本風速より求めた照査風速（通常70m/s前後）では有害な振動現象が発現しない。）されていることがわかる。ちなみにδ＝0.05の場合、発散振動も消滅している。この傾向は、ここでは示していないが、迎角が変わっても同様であり、たわみ振動においては、δ=0.04以上の場合、壁高欄、鋼製高欄の違いはなく耐風安定性が確保されていることがわかる。

図－3のねじれについては、鋼製高欄、壁高欄双方とも、δ＝0.02の際には、渦励振と高風速域ではあるが発散振動が確認できる。δ=0.04の場合、たわみ振動では、渦励振が消滅したが、ねじれの場合は鋼製高欄、壁高欄双方とも渦励振の振幅は小さくはなっているが、消滅には至っていない。発散振動についてはδ＝0.02の際より、さらに高風速域に発現域が移動している。δ=0.05の場合、鋼製高欄では渦励振はほぼ消滅し、発散振動の発現域はδ=0.04の場合よりさらに高風速域に移動する。壁高欄では、δ=0.04の風速域にあった渦励振は消滅し、発散振動は、高風速域の渦励振にかわっている。この傾向は、迎角が変わっても同様であった。

よって、照査する際、安全側である一様流中でも、構造減衰δが0.05以上の場合、壁高欄、鋼製高欄双方とも耐風安定性が確保されていることがわかる。以上のことからも、鋼少数主桁の耐風安定性を特定する上でその構造減衰の設定が重要となることが理解される。

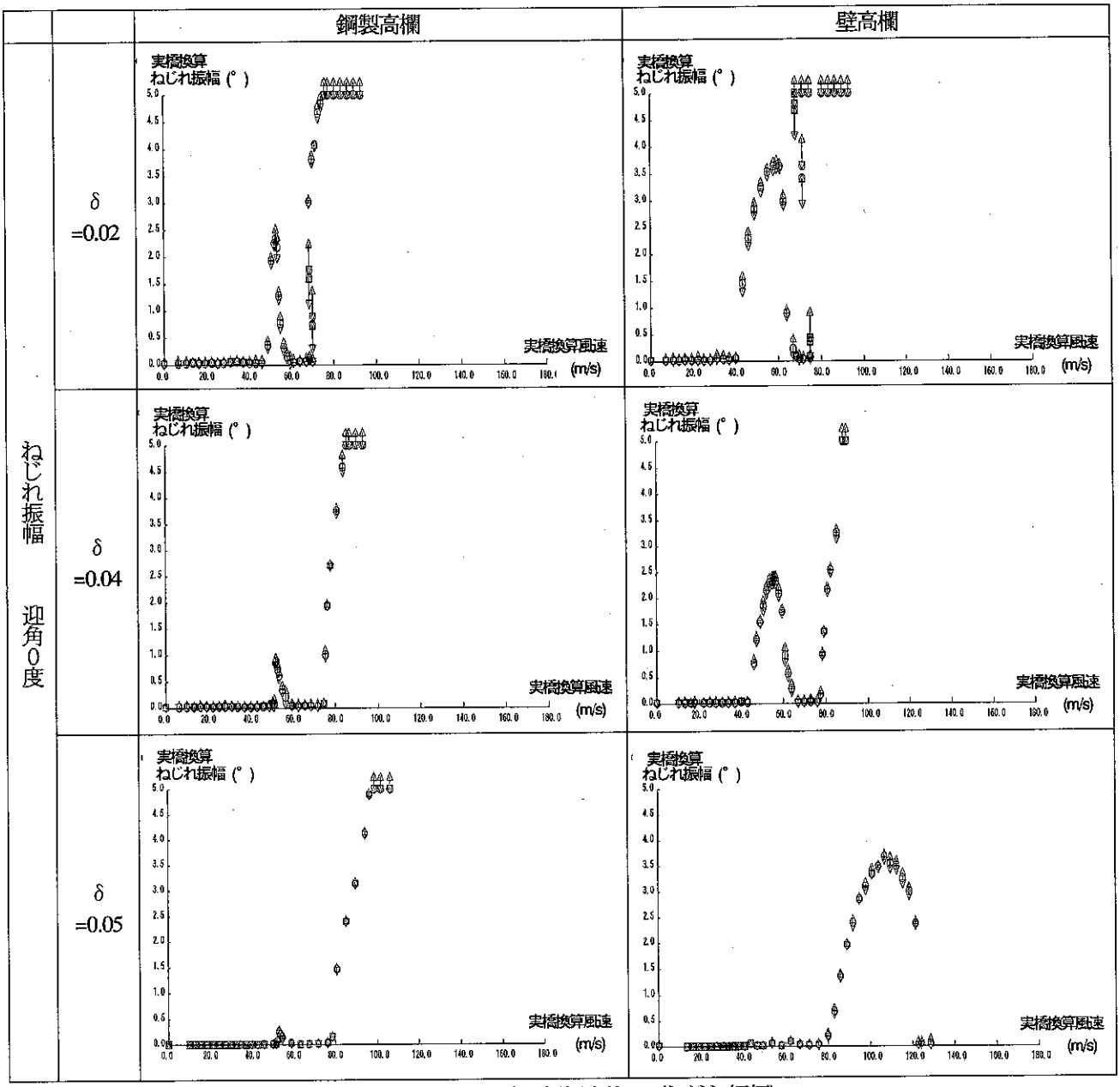

図－3　風速－振幅応答図（ねじれ振幅）

3. 実橋における振動試験

3．1 実験内容

耐風安定性を推定する手法について検討していくに当たり、固有振動数や構造減衰がどの程度あるのかということは重要なことである。しかし、鋼少数主桁橋において、これまで起振機を用いて振動特性を実験的に検討した事例は極めて少ない。そこで、支間が60m程度の実橋について実際に起振機を用いた振動試験を行い、構造減衰等の振動特性を確認した。

対象とした橋梁は、日本道路公団の鋼少数主桁橋(橋長225m、幅員11m、最大支間長60mの4径間連続橋,反力分散支承)である（図－4参照)。起振機は土木研究所所有（水平方向最大加振力 12t/台、0.2Hz-20Hz）のものを使用した(写真－1)。

試験としては、常時微動観測、定常加振試験（スイープ加振)、及び自由減衰振動試験を実施した。常時微動観測は起振機の加振振動数の範囲を特定するためのもので、床版上に設置したサーボ型加速度計により、常時微動を観測した。定常加振試験は桁の固有振動数を調査するためのもので、各振動モードについて、常時微動観測で推定した固有振動数の前後20％程度の範囲で、起振機により加振振動数を変化（スイープ）させ、共振曲線を求めた。自由減衰振動実験は桁の固有振動数における構造減衰率を調査する目的のもので、起振機により、加振が定常状態となった時点で起振装置を急停止させ、減衰波形データから固有振動数、構造減衰率を求めるものである。対象モードは鉛直たわみ1次、ねじれ1次であり、事前に骨組みモデルを使用した数値解析により得られたモードは表—3のとおりである。図－4に起振機と使用したサーボ型加速時計の設置位置を示す。

なお、自由減衰振動実験では、鉛直たわみ1次及びねじれ1次振動モードともそれぞれ11回計測した。また、計測時の気象状況は、気温10℃、無風状態であった。

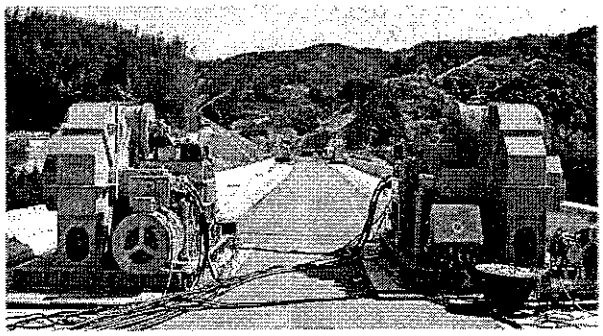

写真－1　起振機設置状況

表—3　モード解析結果

振動モード	固有振動数(Hz)
鉛直たわみ1次	1.51
ねじれ1次	2.18
振動数比(ねじれ/たわみ)	1.44

3．2 振動実験結果

（1）常時微動観測

常時微動観測を実施し、パワースペクトル解析の結果から、本橋の曲げ1次振動モードは1.9Hz、ねじれ1次振動モードは2.2Hz前後にあることが推定できた。

（2）定常加振試験

常時微動観測の結果より、定常加振試験を実施した、図－5に結果を示す。これによると各振動数は鉛直たわみ1次振動モードは1.88Hz、ねじれ1次振動モードは2.15Hz、振動数比（ねじれ1次/鉛直たわみ1次）は1.14と推定された。なお、鉛直たわみ1次振動モードについては表－3に示す解析値と若干差がみられる結果となった。

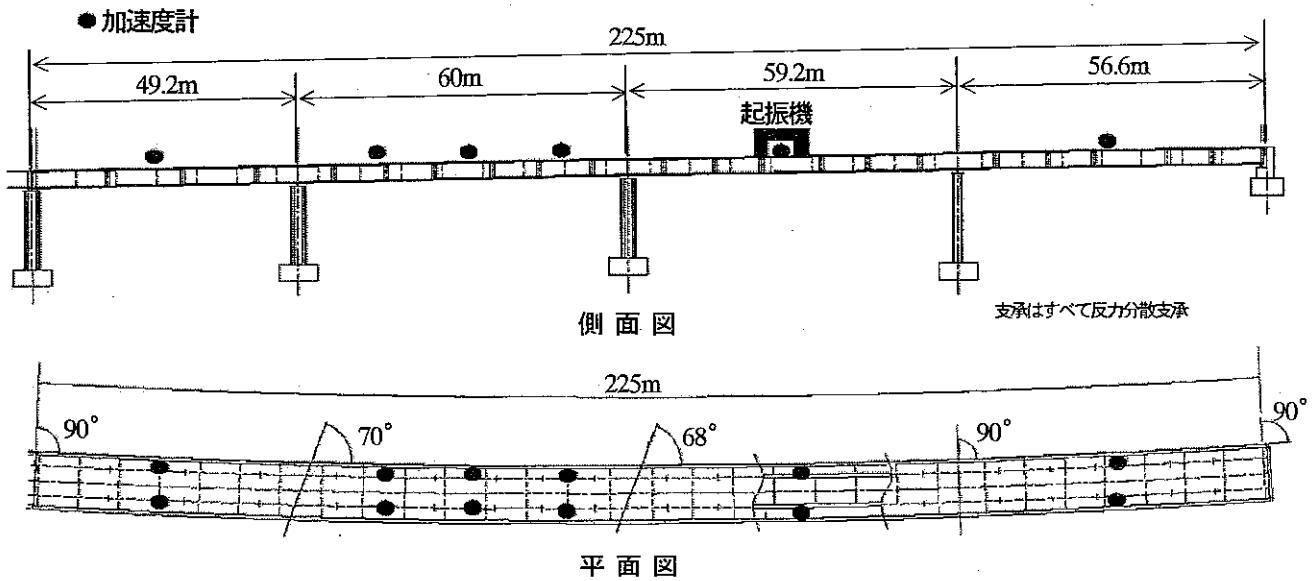

図－4　振動実験を行った鋼少数主桁橋の一般図

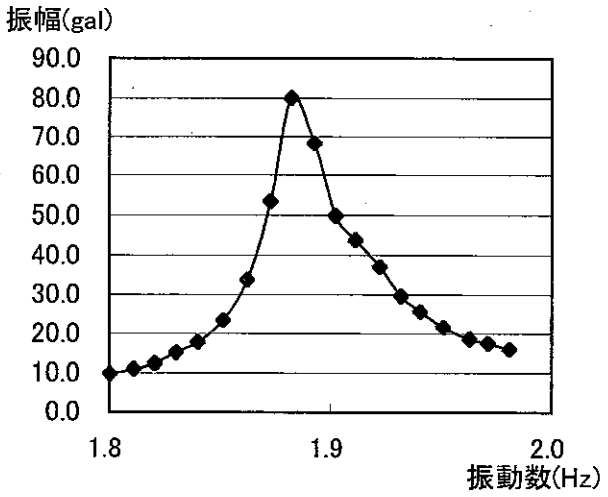

(a) 鉛直たわみ１次振動モード共振曲線

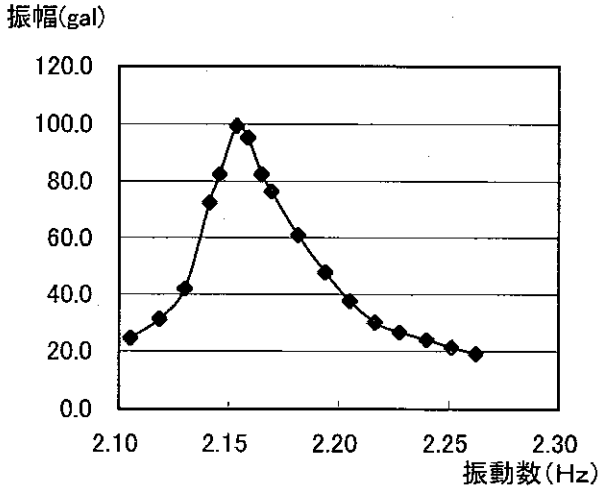

(b) ねじれ１次振動モード共振曲線

図－５ 定常加振試験結果

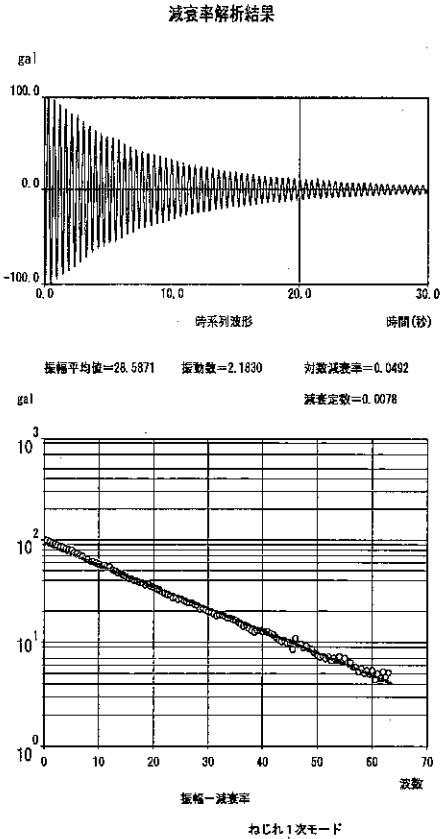

図―６ 対数減衰率の推定

表－４ 対数減衰率の推定結果

振動モード	対数減衰率推定値	
	推定値の範囲	平均
鉛直たわみ１次	0.043－0.048	0.044
ねじれ１次	0.048－0.052	0.050

(3) 自由減衰試験

定常加振試験の結果により、起振機を桁の共振振動数に合わせて桁を加振させ、桁の振動が所定の加速度となった時点で急停止させる自由減衰試験を行い、桁の対数減衰率を計測した（図―６参照）。

図―６をみると値のバラツキが少なく精度の高い値がとれたことがわかる。

対数減衰率については、ねじれ１次、鉛直たわみ１次ともにそれぞれ11回計測した。表―４に対数減衰率の推定結果をまとめた。

表―４をみても、推定値の範囲のばらつきが少ない。このことからも精度の高い値が計測できたことを示している。

4. 考察

1) 固有振動数

過去において、鋼少数主桁橋において起振機以外の手段（クレーンを使用した振動試験等）での振動試験が報告されている。それによると、振動数比は1.05から1.27である[2][3][4][5](表－５参照)。今回の結果は、それらの事例と近い値となった。

これは、今回、常時微動で計測した固有振動数の値と起振機で計測した値がほぼ等しいことから、常時微動計測でも、十分な値が推定できると思われる。

2) 対数減衰率

対数減衰率は耐風便覧[1]によると、吊橋と斜張橋以外の桁橋でねじれ,たわみ双方とも$\delta=0.75/\sqrt{L}$ ただし$\delta>0.04$（L:支間長）と規定されている。この規定を適用すれば、支間長100m以下のものは、$\delta>0.075$となる。しかし、起振機以外の手段で行われた過去の鋼少数主桁橋の振動試験の報告によると鉛直たわみでは$\delta=0.013-0.064$、ねじれでは$\delta=0.043-0.083$

と対数減衰率が耐風便覧[1]の推定式に比べ低い範囲となっている[2][4][5](表—5参照)。

これは、そもそも耐風便覧[1]発刊時には、今回のような鋼少数主桁はなく、それに関するデータが反映されてないことが考えられる。また、それ以外の要因として、他起振機以外の振動試験では構造物の固有周期に合わせることができないため、大振幅（共振状態）で振動させられず、振幅が小さいことによる誤差を含み易くなることや、対数減衰率は振幅依存性があるといわれ、振幅が小さい場合と大きい場合では同じ橋でも対数減衰率が異なり、振幅が小さい場合、対数減衰率が小さめに出やすいことなども考えられる。

今回は起振機を使用した実験であり、比較的大きな振幅で対数減衰率を推定していることもあり、精度は高いと思われる（図—6参照）。本結果を従来のものと比較すると、対数減衰率は$\delta \geqq 0.04$であり、耐風便覧[1]の推定値は下まわるが、過去の報告されている対数減衰率との比較では、鉛直たわみの場合は中間あたりに、ねじれの場合は、低い方に近い値であることがわかった。

今回計測した実橋の対数減衰率の値と風洞試験の結果より、本実橋と同程度の支間長を有する鋼少数主桁橋であれば、耐風安定性に問題ないことが推定される。しかし、鋼少数主桁橋の対数減衰率が耐風便覧[1]で考えられたものより低いという報告を裏づけるものであった。

5. まとめ

鋼少数主桁橋の2次元剛体模型風洞試験及び実橋振動試験により以下のことがわかった。

1）風洞試験より、対数減衰率$\delta > 0.05$の場合であれば、耐風安定性を確保していること。

2）鋼少数主桁橋の振動試験により、支間50mを超えても鉛直たわみ1次は0.04以上、ねじれ1次振動では0.05以上の対数減衰率を見込めること、鉛直たわみ1次振動数の解析による予測は改良の余地があること。

今後は、鋼少数主桁橋の振動数の推定手法を検討するとともに、対数減衰率と支間長の関係を整理し、支間長を反映した耐風安定性の推定手法を検討する予定である。

表—5　鋼少数主桁橋の過去における実橋振動試験による振動数比（ねじれ/鉛直たわみ）と対数減衰率

ケース	振動数比 (ねじれ/たわみ)	対数減衰率	
		鉛直たわみ1次	ねじれ1次
利別川第一橋 (最大支間長86.5mの6径間連続橋)	1.05	0.040～0.046	0.081～0.083
日計平高架橋 (最大支間長48.5mの4径間連続橋)	1.08	0.062～0.068	0.062～0.098
千鳥の沢川橋 (最大支間長53mの4径間連続橋)	1.11	0.064	0.064
最大支間長64.7mの12径間連続鋼少数主桁橋	1.27	0.013	0.043

参考文献

1)(社)日本道路協会：道路橋耐風設計便覧、平成3年7月

2)水口　和之、西星　匡博：ＰＣ床版連続合成２主桁橋（日計平高架橋）の実橋振動実験、土木学会第55回年次学術講演会講演概要集、Ⅰ-B103、1999.9

3)中村　元、宮越　信、藤浪　紀雄、橘　吉宏、皇中　真一、枝元　勝哉：利別川第一橋（ＰＣ床版連続合成２主桁橋）の実橋振動試験、土木学会第55回年次学術講演会講演概要集、Ⅰ-B108、1999.9

4)大垣賀　津雄、西尾　研二、山本　晃久、石毛　立也、中村　元、川尻　克利、長井　正嗣：千鳥の沢川橋－ＰＣ床版連続合成２主桁橋－の実橋振動試験、土木学会第54回年次学術講演会講演概要集、Ⅰ-B253、1999.9

5)渡辺　二夫、播金　昭浩、黒田　健二、成田　直矢：長支間鋼少数主桁橋の耐風特性、土木学会第57回年次学術講演会講演概要集、Ⅰ-478、2002.9

(2003.7.31受付)

振動による変位とその頻度を計測する簡易な計測器の開発と適用試験

Development of handy system to measure vibration-induced displacement

山田　聡*，山田　健太郎**，小塩　達也***
Satoshi YAMADA, Kentaro YAMADA, Tatsuya Ojio

*工博，トピー工業株式会社（〒441-8510　愛知県豊橋市明海町1）
**Ph.D.，名古屋大学大学院教授　環境学研究科（〒464-8603　名古屋市千種区不老町）
***工修，名古屋大学大学院助手　環境学研究科（〒464-8603　名古屋市千種区不老町）

A simple and handy system to measure vibration-induced displacement is developed. It consists of three accelerometers, a processor and dry battery and stored in a small watertight box. Measured acceleration is transformed into displacement. If relationship between displacement and stress at point of interest is known, one can also obtain stress range histogram to be used for fatigue assessment of the structures. The system works for four weeks with dry battery and is suitable to measure long term displacement and stress range histograms. Calibration and laboratory tests of the system are carried out, and trial measurement, which the system is attached to actual lighting pole, is carried out.

Key Words: acceleration, displacement, histogram measurement, fatigue
キーワード：加速度，変位，頻度計測，疲労

1. はじめに

標識柱や照明柱など柱部に鋼管を用いた構造物では，鋼管の基部を補強するためにリブを取り付けた構造となっている．過去には，このリブの溶接止端部に疲労き裂が発生した事例[1]がいくつか報告されており，最悪の場合は標識柱が倒壊することがある．特に，高架橋に設置される標識柱や照明柱の場合，路下に落下すると重大な2次災害に繋がるため，維持管理の上で重要な問題である．

これまで，標識柱や照明柱の疲労損傷は問題視されておらず，一般的には耐風上の設計を行うのみで，疲労安全度に関する検討は行われていない．基部の疲労強度に関しては，名古屋大学などで検討が進められている[2)-8)]．最近では，耐震性を向上させるため，鋼製の支承をゴム支承に交換することで，橋梁が振動しやすくなる場合がある．また，門型標識柱の上部に重量が2～3tにおよぶ電光掲示板が設置されることにより，標識柱の振動変位が大きくなり，基部への繰り返し応力の作用が顕著になると推定される．したがって，今後こうした疲労損傷は増加すると考えられる．

標識柱や照明柱の基部の疲労照査を行うためには，損傷が推定される基部のリブ端部にひずみゲージを貼り付け，一定期間の応力頻度分布を計測し，疲労寿命を推定する方法が用いられている．この方法は，問題となる箇所の応力頻度を直接計測して疲労寿命を求めるため，有効な方法である．しかし，計測にあたって機器が大掛かりになり，作業空間上の制限などからも，計測箇所が限られていた．標識柱や照明柱のように数量の多い構造物では，疲労損傷を予測するには，簡易な応力頻度計測が必要である．

標識柱や照明柱は交通荷重により振動し，変形を繰り返している．標識柱のように比較的簡単な構造であれば，柱の変位量と基部に作用する応力は一意に対応する．本研究では，標識柱や照明柱が振動するときの加速度に着目した．加速度計を用いて，加速度の変化を変位に直し，変位の頻度分布を簡易に推測する計測器を開発する．疲労損傷の評価は，理論計算あるいはFEMによる解析を用いて，変位を着目点の応力に置き換えることで可能になる．この計測器の精度の検証および構造物への適用性を確認した．

2. 従来の応力頻度計測の問題点と計測器開発の目的

標識柱や照明柱の基部のリブ端部の疲労寿命を推定するためには，Fig.1に示すような方法を用いることが多い．まず，リブの溶接止端部付近にひずみゲージを貼付し，ヒストグラムレコーダーによって数時間から数日程度にわたって連続計測する．次に，パソコン等にそのデータを収録して，レインフロー法などの分析手法を用いて頻度分布を得る．その結果から，疲労設計指針の継手分類[9)]に従って，同様の継手の強度等級を参照し，マイナー則を用いて，疲労寿命の計算を行うことができる．

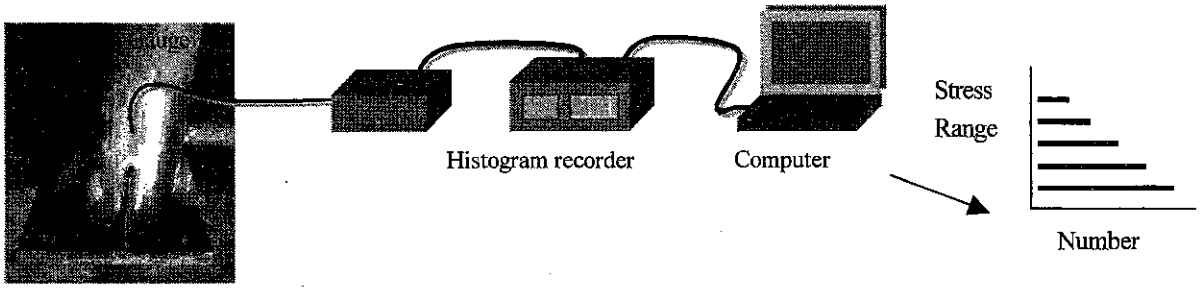

Fig.1 Sample of histogram measurement

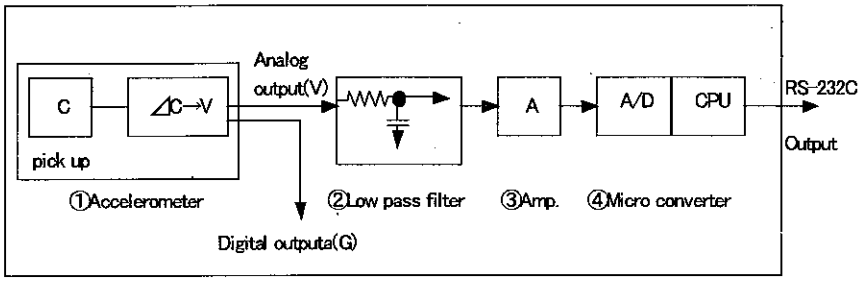

Fig.2 The method of internal processing of a measuring instrument

しかし，これらの機器を用いた頻度計測は，計測にあたって機器設置時の作業のために交通規制を要し，また，電源・足場の確保などコストがかかり，必然的に計測箇所が限られる．

簡易に各標識柱の振動の程度を計測でき，かつ，概略の疲労寿命が推定できれば，今後，膨大な数量に及ぶ標識柱や照明柱の維持管理を行う上で有効である．

本研究では，振動のように動的な現象から得られる加速度を検出するセンサー部，それらを逐次，頻度分布へ変換するする処理部，および電源を一体化して，ひとつの装置で頻度計測ができる計測器を開発し，実構造物への適用試験を行うことを目的とした．

3. 計測器の原理と特徴

3.1 基本的な考え方

標識柱のように比較的単純な構造物の場合，振動によりその基部に作用する応力は，通常の供用下では，構造物の変位量と線形関係にあるとみてよい．したがって，柱のある高さの変位量がわかれば，基部に作用する応力は，柱の断面諸元をもとに構造解析を行って求めることができる．一定の期間に，柱のある高さでの変位量とそれが作用した繰返し数を計測すれば，基部の応力頻度に換算することができ，応力頻度計測と同等の結果を得ることができる．本装置では，振動によって発生する振動加速度を測定し，振動周期と加速度の振幅から変位を推定して，変位の頻度分布を求めることとした．

3.2 検知部に用いた加速度計

計測器は安価で大量生産を指向するため，低コストな静電容量型の加速度計を用いた．近年のマイクロマシン技術により，静電容量型の加速度計は小型化しており，用いた加速度計は大きさ 5×5×2mm で，0.6mA 以下の低消費電力型である [10]．2方向について，最大±19.6m/s^2(=2G)までの計測が可能で，0.0196m/s^2 の分解能を持つ．適用温度は-10℃～60℃で，頻度計測に十分な耐久性を有する．

3.3 内部処理の方法

標識柱が振動していない静止位置を基準に円振動数 ω で正弦振動しているとすれば，振動変位 d は以下の式で表せる．

$$d = k \cdot \sin(\omega \cdot t) \tag{1}$$

ここで，k は定数，t は時間である．これを2回微分すると，加速度が得られ，以下の式のようになる．

$$a = -k \cdot \omega^2 \cdot \sin(\omega \cdot t) \tag{2}$$

つまり，加速度 a は変位 d と位相が逆で同周期の関数になる．

実際の標識柱や照明柱の計測結果によれば，これらの構造物は橋梁と大型車両の振動数に近いモードが車両走行時に励振され，大きな振動となることが報告されている [2), 6)]．短い時間に着目すれば，上述のように正弦関数を仮定して，最大加速度と振動数から変位量を推定できると考えられる．そこで加速度波形から極大値，極小値，ゼロクロス点を検出し，極大・極小値から加速度の両振幅を，ゼロクロス点の時刻から振動数を求め，変位の両振幅を求めることとした．

計測器の内部処理の流れを Fig.2 に示す．以下にその詳細を示す．

① 標識柱の振動による加速度の変化を，内蔵する加速度計がサンプリング速度 10ms で計測し，逐次，電圧を出力する．
② この電圧からローパスフィルタによりノイズ成分を除去する．
③ 得られた電圧をアンプによって増幅する．
④ マイクロコンバータ内で電圧をデジタル変換し，計数処理を行う．

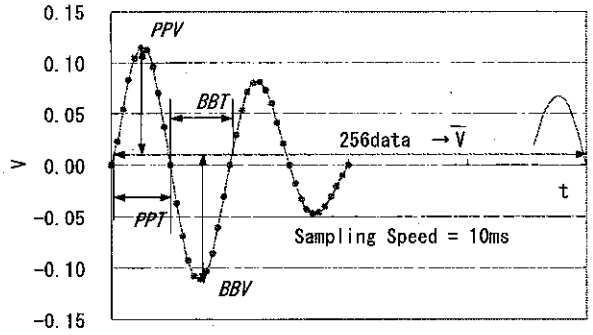

Fig.3 The output of voltage, and the calculation method of displacement

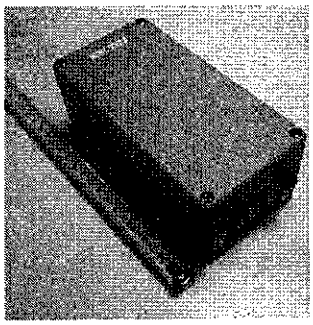

Photo.1 Appearance of a handy system

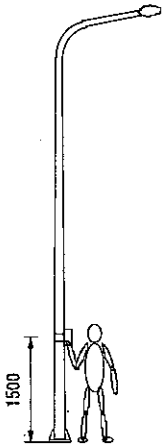

Fig.4 Attachment of a handy system

Fig.3 に示すように，計数処理では 256 データごとに電圧の平均値を取り，それに続く電圧値が平均値を越えてから極大値となり，再び平均値を下回る時点までの経過時間を *PPT* とする．また，その間の極大値を *PPV* とする．同様に，平均値を下回った時点から極小値となり，再び平均値を上回る時点までの経過時間を *BBT* とし，その間の極小値を *BBV* とする．これより，加速度が *PPV* から *BBV* へ時間 1/2(*PPT*+*BBT*)で変化するとして変位量に換算する．

本装置では，マイクロコンバータ内に時間に対応した係数表を用意し，電圧の変化量にこの係数をかける簡易な方法で変位を求めた．なお，この係数表は，後述する検証試験の定振幅振動試験において，変位計を用いて校正を行って求めたものを用いた．

以後，同様に *BBV* から次の極大値 *PPV* への変化を変位量に換算し，頻度分布を逐次計測する．この方法では，頻度データのみを記録するため，データを保存する記憶空間を節約でき，省電力化に貢献している．

3.4 計測器の仕様と適用の範囲

過去の標識柱や照明柱の計測結果[2), 6)]によれば，

① 単柱のみの照明柱，あるいは片持ち式(F 型)の標識柱では振動モードは 1 次～2 次

② 門型標識柱の振動モードは 1 次～6 次

という結果が得られている．

①における柱の振動の支配的なモードでは，基部を支点とした半波長の振動形状となっている．②では，門型形式のはり部の振動性状の違いでいくつかのモードに分かれるが，標識柱が橋軸直角方向に振動する面内せん断モードが卓越する．柱の部分に着目すると①と同じく基部を支点とした半波長の振動形状となる．標準的な照明柱・標識柱の高さが 6m 以上あることを考えると，基部から高さ 2m 程度までの範囲であれば，変位と基部の応力はほぼ 1 対 1 の関係にあると考えてよい．これらの標識柱・照明柱の振動周波数は 2Hz～10Hz 程度で，特に 3Hz 前後が支配的である．そこで，計測器は，周波数でおよそ 2Hz～8Hz 程度の領域を，変位量で 0.5～2.5mm の範囲を計測できるものとした．

開発した計測器は，Photo.1 に示すように，16×8×6cm の防水型の密閉容器に加速度計，マイクロコンバータ，および電源を組み込んだものである．市販の乾電池で計測ができる低消費電力型であり，外部電源が不必要で 4 週間程度連続使用が可能である．

Fig.4 に示すように，標識柱の基部から 1.5m 程度（人の手で設置可能）の位置に計測器をバンド等で固定して一定期間設置し，その間の変位の頻度計測を行う．計測終了後は，計測器を回収し，入出力端子(RS-232C)からパソコンへ計測結果を転送して頻度計測結果を得ることができるため，従来のひずみゲージによる方法に比べて非常に簡易で安価な計測器となる．

4. 検証試験

製作した計測器の測定精度を検証するため，定振幅振動試験と変動振幅試験を行った[11)]．

4.1 定振幅振動試験

計測器の精度を確認するため，疲労試験機を変位制御で振幅を一定として，数種類の周波数ごとに一定回数動作させ，試験機に取り付けた計測器がその数を検出するかを検証した．変位量は 0.1～2.1mm，周波数は 1～4Hz，繰返し数は 1000 回とした．変位量はひずみゲージ式変位計を用いて実際の変位量を測定し，比較の対象とした．

試験結果を Fig.5 に示す．横軸は変位量，縦軸は計測率を表している．計測率とは（計測器で計測した回数）/（実際の載荷回数）である．この図より，周波数 1Hz では精度はやや劣り，変位 1.5mm 以下で 8 割以下の検出率となるが，周波数が 2Hz 以上なら 0.4mm 以上の変位を 95%程度は検出することができる．したがって，3Hz 程度で振動するものであれば，0.4mm 以上はほぼ正確に計数できる．

さらに，周波数が 2Hz～4Hz の範囲について，変位量を 0.3mm～2.4mm まで 0.1mm ごとに試験機に与えて同様の計測を行い，計測器内部の変位への変換係数表の校正を行った．計測器のカウントレベルは 0～2.5mm までを 5 等分し，レベル 1(L1)は 0.5mm 以下，レベル 2(L2)は 0.5～1.0mm，レベル 3(L3)は 1.0～1.5mm，レベル 4(L4)は 1.5～2.0mm，レベル 5(L5)は 2.0mm 以上とした．Fig.6 に例として 3Hz のときの各レベルの計測結果を示

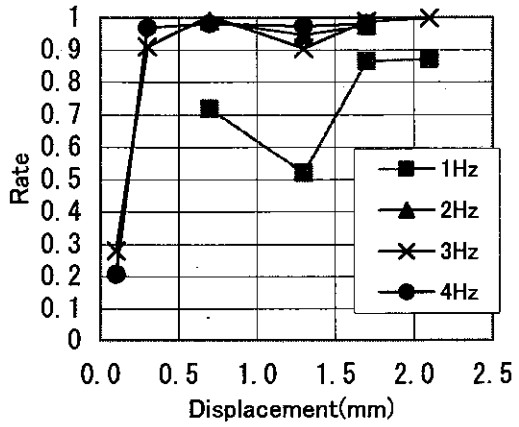

Fig.5 The result of a constant amplitude examination

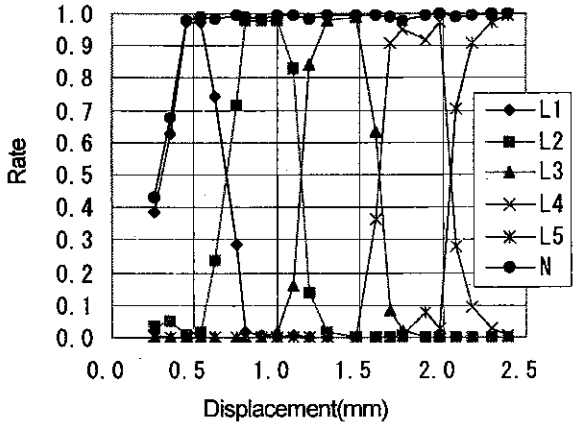

Fig.6 Evaluation of the error for every level

す．Fig.6 の L1～L5 は計測器の各レベルの計数値であり，N は L1～L5 の合計を示す．試験結果から，計測器の変位の計測誤差は変位量が周波数によって若干異なるが，0.1mm～0.2mm 程度である．

4.2 変動振幅振動試験

疲労試験機で 0～2.5mm の変位をランダムに発生させて変動振幅を与え，計測器がレベルごとに区分けした回数を検出するかを確認した．比較のため，従来の頻度計測と同じ計測方法として，変位計を用いて計測器内部の加速度計と同じサンプリング速度(10ms)で動的に計測を行い，変位の頻度分布を求めた．計測結果を Fig.7 に示す．図中の棒グラフは変位計から得られたデータをレインフロー法により計数し，①0.1mm と②0.5mm ごとの頻度分布にしたものであり，シンボルは計測器の計測結果③である．各レベルのカウント数にやや差はあるものの，各周波数ともに作用させたランダム波の合計は10%以内の誤差で検出している．また，このときの計測器内部の加速度計の電圧出力と実変位量の履歴の一部を Fig.8 に示す．これより，変位と加速度は逆位相で同一周期であることが確認できた．

Fig.7 の結果から，疲労寿命の試算を行った結果を Table 1 に

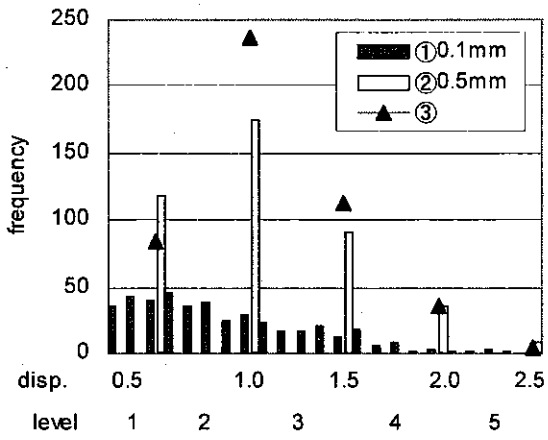

Fig.7 Comparison of the frequency distribution by displacement transducer and handy system

Table 1 Trial calculation of the ratio of a fatigue life

	σ_{eq} (Ratio)	N	life (Raito)
①	100	427	100
②	104	427	90
③	101	457	90

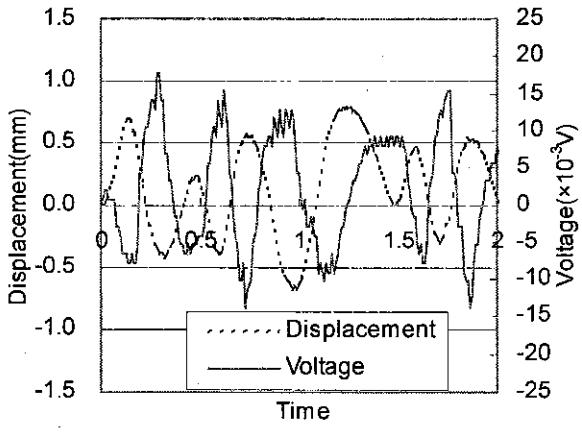

Fig.8 Correspondence between output of the accelerometer inside a handy system and displacement

示す．変位計の計測結果①から等価応力範囲を計算したものを 100 としたとき，②から同様に求めると 104 となる．計測器の計測結果から等価応力範囲の比を求めると 101 となった．これらより，作用した繰返し数から疲労寿命の比を試算すると，従来の方法である頻度計測の結果から得られる疲労寿命に対し，10%程度の誤差となった．

5 実照明柱による適用試験

5.1 試験の概要

実構造物に対する計測器の適用性を確認するため，橋梁上に設置された照明柱にこの計測器を取り付け，計測を行った．

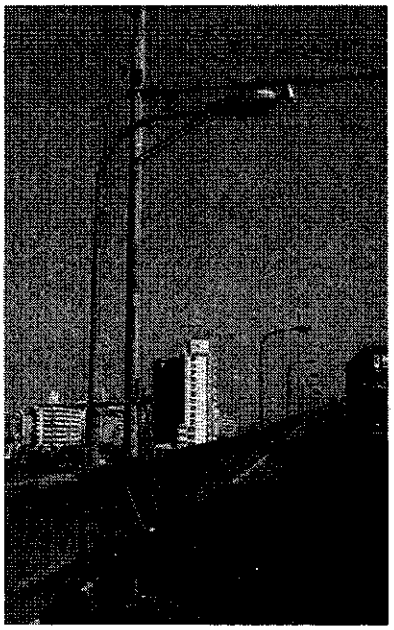

Photo.2 The lighting pole which measured

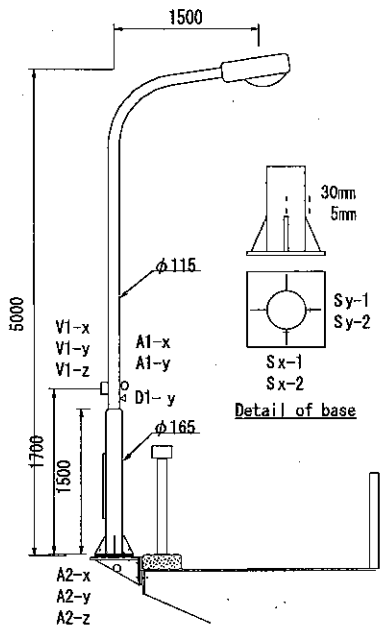

Fig.9 The outline lighting pole and measurement location

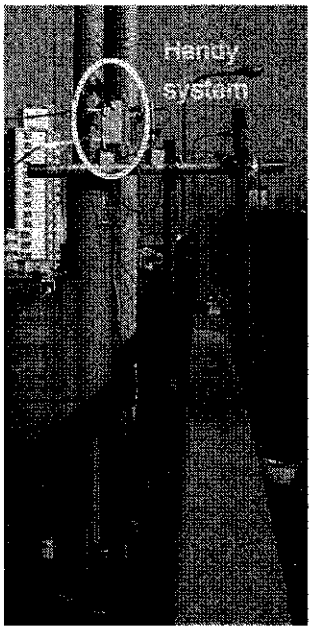

Photo.3 The situation of measurement

対象とした照明柱は，片側3車線の一般国道の橋梁上にあり，耳桁に取り付けられたブラケットにボルトを用いて取り付けられている．現場状況を Photo.2 に示す．また，照明柱の概要と計測個所を Fig.9 に，計測状況を Photo.3 に示す．この照明柱の基部から 1700mm の位置に製作した計測器，市販の加速度計，変位計を設置した．計測器はx，y，zの3方向を同時計測した(V1-x，y，z)．ここで，xは橋軸方向，yは橋軸直角方向，zは鉛直方向である．加速度は橋軸方向，橋軸直角方向を計測した(A1-x，y)．変位は橋軸直角方向のみである(D1-y)．また，基部のリブ付近にはひずみゲージを貼付し(Sx-1，2，Sy-1，2)，併せて基部にも加速度計を設置した(A2-x，y，z)．一般車両通行下で20分間の振動計測を行い，加速度計，変位計，ひずみゲージはサンプリング速度200Hzで応答波形を計測した．変位計とひずみゲージについては，得られたデータよりレインフロー法を用いて，頻度分布を計算した．計測器は，内部加速度計の応答波形を取得すると共に，装置から出力される頻度計測結果を得た．

5.2 計測結果

(1)供用下における加速度，変位，応力の対応

本計測では，照明柱は橋軸直角方向が最も大きな振動方向となった．計測によるこの方向の加速度と変位の応答波形を比較したものを Fig.10 に示す．これらは20分間の計測を通じて概ね類似の波形となっており，実橋に設置された照明柱の一般車両交通下での振動状態では，加速度の変化から変位量を推定することは十分可能であると考えられる．同様に，変位と基部の応力の応答波形を比較したものを Fig.11 に示す．これらの応答波形もよく一致し，変位から応力を推定することも可能である．

計測された変位の振動波形からパワースペクトルを算出すると，標識柱は橋軸直角方向に 3.04Hz と 8.25Hz の振動モードが卓越しており，応力もほぼ同一の振動モードが確認された．しかし，加速度波形からは，前述のモード以外に 25Hz 付近にも卓越領域が存在した．

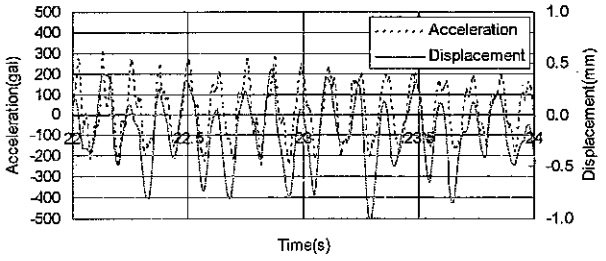

Fig.10 Correspondence between acceleration and displacement

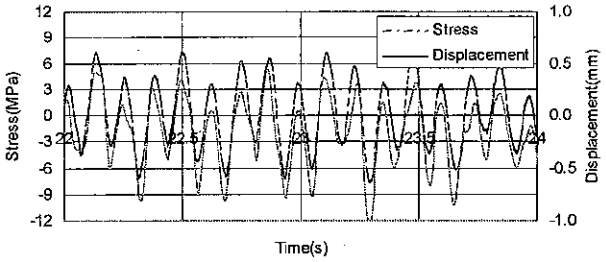

Fig.11 Correspondence between Stress and displacement

(2)頻度計測結果

照明柱に取り付けた変位計，ひずみゲージの計測結果から得られた頻度分布および，計測器から得られた頻度分布の結果を Fig.12 に示す．この図では，Fig.11 の変位計と応力の計測結果から応力値をひずみに対応させ，相当するレベルとしてカウントした．これらより，各頻度分布の傾向は概ね一致するものの，変位計の頻度分布の結果に対し，応力頻度分布はやや小さくな

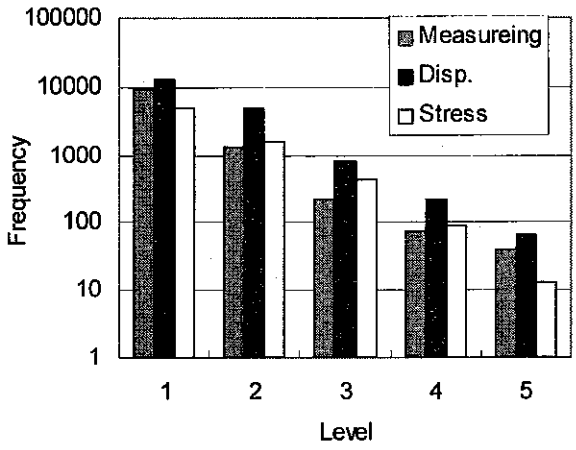

Fig.12 Correspondence between Stress and displacement

る傾向を示し，簡易計測器の結果は応力頻度分布と近い傾向となった．

今回の計測では，作業空間の制約から，変位計は橋梁の歩道上に工事用の鋼製パイプを組み合わせた架台によって設置した．この架台の剛性が十分ではなかったことから，変位の計測結果に架台の振動も含まれると考えられ，これが変位と応力の頻度分布の誤差の原因の一つになっていると推察される．

本計測器は加速度から変位を推定しており，実験室で行った振動試験ではよく一致した．実際に橋梁上で計測された加速度の波形では，複数の振動モードが存在し，25Hz にも卓越周波数帯がある．本計測装置の今回の仕様では 2～8Hz 程度を対象としており，これを用いた推定方法では，標識柱の振動モードによっては，厳密には一致しなかった．しかしながら，計測現場での取り扱いは容易であり，概略の応力頻度分布の推定には十分適用が可能であると考えられる．

6. 結論

構造物の疲労損傷を簡易に評価するために，変位の頻度分布を得る計測器を開発し，適用試験を行った．それにより得られた結果を以下に示す．

1) 標識柱が振動するときには振動による加速度が生じる．この振動加速度に着目し，加速度の時間変化から変位を推定して頻度を蓄積する計測器を開発した．
2) 計測器は小型で，外部電源が必要なく，4 週間程度の連続計測が可能である．従来の応力頻度計測に比べ，安価で簡易な計測器である．
3) 開発した計測器について，定振幅振動試験と変動振幅試験を行った．適用できる振動周波数は 2Hz 以上で，0.4mm 以上の変位を計測できる．振動試験の結果より，計測誤差は 10%程度であることを確認した．
4) 着目点の応力と計測点の変形が一意に定まれば，ひずみゲージによる応力頻度計測から求める疲労寿命に対して，10%程度の誤差で寿命推定が可能である．
5) 現場での取り扱いも容易であり，概略の変位の頻度分布の計測に適用が可能である．

本計測器については，簡易な変位頻度計測装置として特許を出願中である．

謝辞

本研究の一部は文部省科学研究費補助金（基盤研究(B) (1) 14350241 研究代表者 山田健太郎）の補助の下に行われた．計測器の製作に関して，(有)ローム理研の関係各位に協力をいただいた．ここに記して感謝の意を表する．

参考文献

1) 宮脇潔，時譲太，奥西史伸：門型標識柱基部構造の改良について，阪神高速道路公団技報，第 19 号，pp.38-44，2001.2.
2) 名古屋高速道路公社，名古屋大学大学院土木工学専攻：橋梁付属構造物の疲労に関する調査研究報告書，2000.
3) 小塩達也，李相勲，山田健太郎，森成顕，森下宣明：交通荷重による標識柱の振動と疲労耐久性，構造工学論文集 Vol.47A，pp.1009-1017，2001.
4) 名古屋高速道路公社，名古屋大学大学院土木工学専攻：高架橋付属物の耐久性評価技術に関する研究報告書，2001.
5) 小塩達也，山田健太郎，森田俊樹，李相勲，仙田勉，前野裕文：都市内高架橋に設置された付属構造物の振動と疲労に関する研究，土木学会年次学術講演会講演概要集，Vol.56，pp.262-263，2001.
6) 山田健太郎，小塩達也，李相勲，森田俊樹：交通振動下における橋梁付属物の疲労に関する調査研究 報告書，2001.1.
7) Gilani, A., and Whittaker, A.: Fatigue-life evaluation of steel post structures. I:Background and Analysis, *J. Struct. Engrg.*, ASCE, 126(3), pp.322-330. 2000.
8) Gilani, A., and Whittaker, A.: Fatigue-life evaluation of steel post structures. II:Experimentation, *J. Struct. Engrg.*, ASCE, 126(3), pp.331-340. 2000.
9) 日本鋼構造協会：鋼構造物の疲労設計指針・同解説，1996.
10) Analog Devices, Inc. : ADXL202E* Low-Cost ±2g Dual-Axis Accelerometer with Duty Cycle Output, *Technical Materials of Analog Devices*, Inc., 2000.
11) 山田聡，小塩達也，山田健太郎：振動による変位とその頻度を計測する簡易な計測器の開発，鋼構造論文集，vol.10，NO.38，pp.81-89，2003.6.

(2003 年 7 月 31 日受付)

一般電話回線を用いた遠隔データ収集システムの実施事例

Examples of remote measurement system by general telephone network

稲葉尚文*，陸門英男**
Naofumi Inaba, Hideo Mutsukado

* 日本道路公団 関西支社 構造技術課（〒530-0003 大阪市北区堂島 1-6-20）
** 日本道路公団 関西支社 大阪技術事務所（〒565-0805 大阪府吹田市清水 15-1）

This paper report example of remort measurement system by general telephone network. We have measure transition of strains on continuous composite two gardersbridge for 1000 days. The strains is equivalent to pre-stress to direction of bridge axis. It is added by the Jack up and down method for canceling tension stress by negative bending moment on middle supports in the continuous girder. We control data transmition and measurement system software from our office far away about 100km by general telephone network. We are using two types network. One is wired network "ISDN", it is stable but suitable urban area or neighbor. the other is portable telephone network "Docomo", it is influenced radio condition but adaptable local area. This system is recognized usefully at long-team and long distance area measurement.

Key Words : *remort measurement,* *general telephone network,* *portable telephone network*
キーワード： *遠隔計測,* *一般電話回線,* *携帯電話回線*

1．はじめに

長期間にわたる現地計測・観測の場合，従来のシステムでは現地の計測器や記録器に蓄積したデータを定期的にあるいは必要に応じて作業員が現地に出向いて回収していた．そのため，回収作業に要する人件費が必要であり，次回の回収作業までの期間はシステムの異常などのトラブルを察知する事ができず，当然それに対処することもできなかったためデータの欠損が生じることもあった．この問題に対する解決策としては，想定されるあらゆるトラブルに対する防護装置を設置する必要があり，多大な費用を要するものであった．

しかしながら，近年では，電話回線を利用したデータ通信が簡易にできるソフトウェアなどが市販されるようになったり，携帯電話回線の拡充や太陽電池セルの低価格化，またそれらに対応した計測機器の登場により，遠隔地の計測におけるデータの回収および計測機器や計測システムソフトウェアのコントロールが比較的簡易に実現できるようになってきた．

本報告では，実際の計測現場に遠隔コントロールシステムを適用した２事例を紹介し，各々の利点，また改善すべき点を明確にすることにより今後の現場計測の参考資料となることを望むものである．

2．電気・電話ともに固定回線が利用できた事例

まず１例めは，比較的好条件での適用例として，舞鶴若狭自動車道 舞鶴東IC～小浜西IC間に位置する大津呂川橋における事例を紹介する．対象橋梁の全景をFig. 1に，計測用ハウスの設置状況をFig. 2に示す．

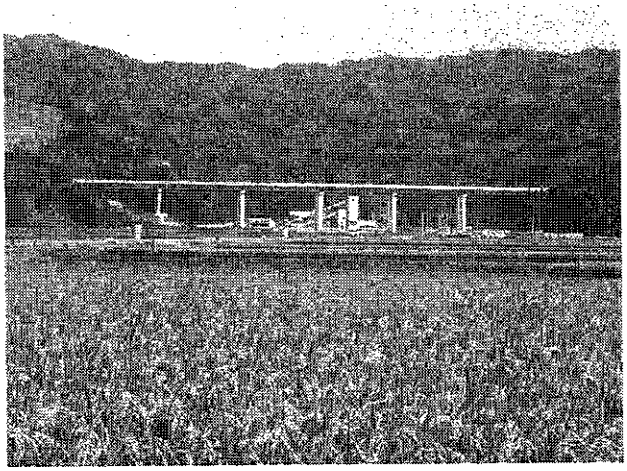

Fig. 1 Panoramic view of the Ohtsuro-gawa bridge

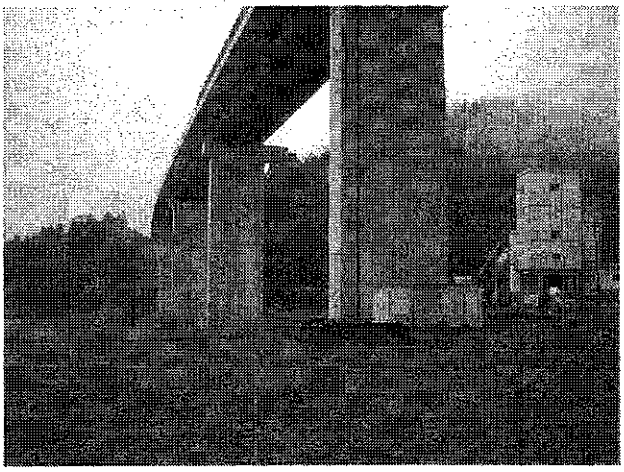

Fig. 2 Container house for measurement (Ohtsuro-gawa bridge)

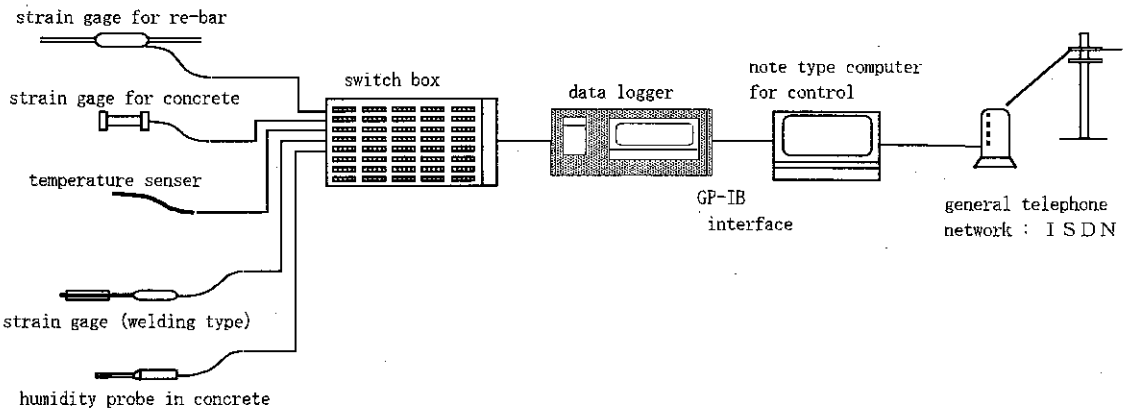

Fig. 3 Components diagram of measurement system (Ohtsuro-gawa bridge)

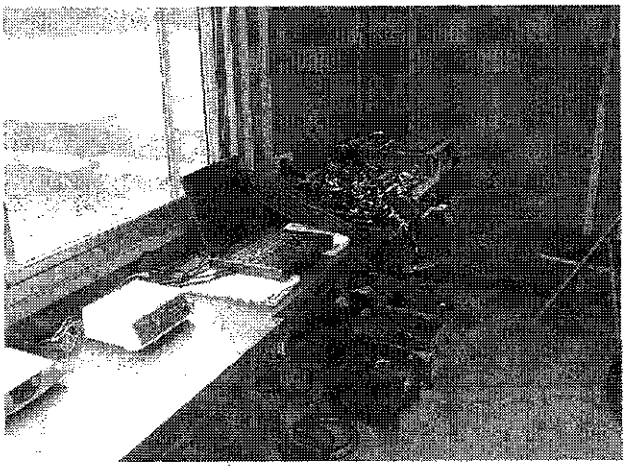

Fig. 4 Equipments for measurement (Ohtsuro-gawa bridge)

大津呂川橋は，近年脚光を浴びている合理化に優れたPC床版鋼連続合成２主桁橋であり，中間支点の負曲げモーメントによる引張力をキャンセルするためにジャッキアップダウン工法を採用して橋軸方向プレストレスを導入している．この軸方向プレストレスの経時変化をひずみの変化として３年間にわたり計測している[1]．現在３年目の計測を継続中であるが，当初の１年間は１時間間隔でひずみデータを計測しており，２年目以降は３時間間隔の計測としている．

データロガーおよびパソコンのハードディスクに記憶したデータを，電話回線を使用して計測現場から約100km離れた事務所からアクセスして回収している．計測システムの構成をFig. 3に，設置状況をFig. 4に示す．

この事例では，対象橋梁の下に比較的広い用地があり計測用ユニットハウスを設置する余裕があった．また，橋梁の下を町道が交差しており，町道に沿って商用電力および電話線が既存であったため，新規の電柱設置などの工事が不要であり，枝線の引き込みのみで利用できた．

したがって，電源は関西電力の一般商用電力（100V）を使用しており，安定した電力供給を確保している．しかし，計測中に落雷などによる停電が発生したためと考えられるシステムの不調が生じたこともあった．基本的に，データロガーは停電回復後もスケジュール通りのインターバル計測を再開する（停電中の計測は当然停止している）システムとなっており，パソコンはノート型であるので短時間の停電では問題ないはずであったが，データ収録が停止するなどの症状が出た．この原因については詳細に検討中である．現在ではシステム全体の電源が停止しないようにバッテリーを使用した無停電システムを追加して暫定的に対応している．

また，電話回線についてはNTTの一般回線（有線）を引き込み，ISDN回線としてデータ通信を行っている．こちらについても，初期に一度トラブルが発生したが，原因は単純な設定ミスであることが判明し，その後はトラブルは発生していない．

システム全体の構成としては，Fig. 5に示すように，データロガー（静ひずみ計）が持っているインターバル計測機能により１時間または３時間間隔に測定したデータをデータロガー内部のメモリーに蓄える．それをGP-IBでパソコンから吸い取り演算処理した後，パソコン画面にグラフ表示するとともにファイルに保存する．ここまでを現場のパソコン内部のソフトウェアで自動的に処理させている．このグラフ表示は，ISDN回線を接続することにより，ブラウザーでモニタリングすることができ，データはFTPによる転送が可能であったが，OSとFTPソフ

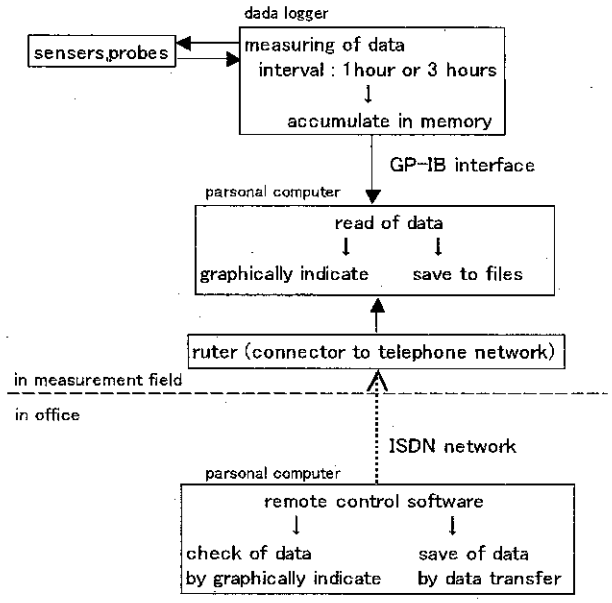

Fig. 5 Flow chart on data acquisition (Ohtsuro-gawa bridge)

トのマッチングの問題等が生じ動作が不安定であったため，現在では市販のリモートコントロールソフトを使用している．

計測システム動作のチェックは毎日行い，データの転送は蓄積したデータ量に応じて数日毎に行っている．

3．電気・電話とも固定回線が利用できなかった事例

次に２例めは，悪条件での適用例として，播磨自動車道　播磨JCT～播磨新宮IC間に位置する中谷川橋（Fig.6）における事例を紹介する．

中谷川橋も前事例の大津呂川橋と同様，PC床版鋼連続合成２主桁橋であり，ジャッキアップダウン工法により導入した軸方向プレストレスの経時変化をひずみの変化として３年間にわたり計測している[2]．データロガーによりひずみを計測しているのは大津呂川橋と同様であるが，中谷川橋ではパソコンを使用せず，データロガーから直接データを電話回線で転送している．当該橋梁における計測システムの構成をFig.7に，計測機器の設置状況をFig.8に，ソーラーパネルの設置状況をFig.9にそれぞれ示す．

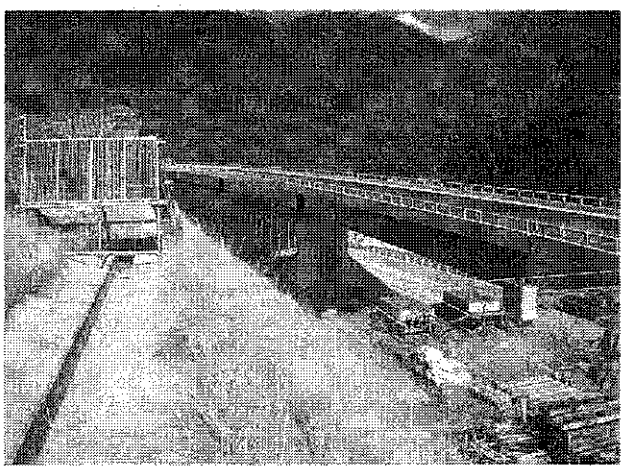

Fig.6　Panoramic view of the Nakatani-gawa bridge

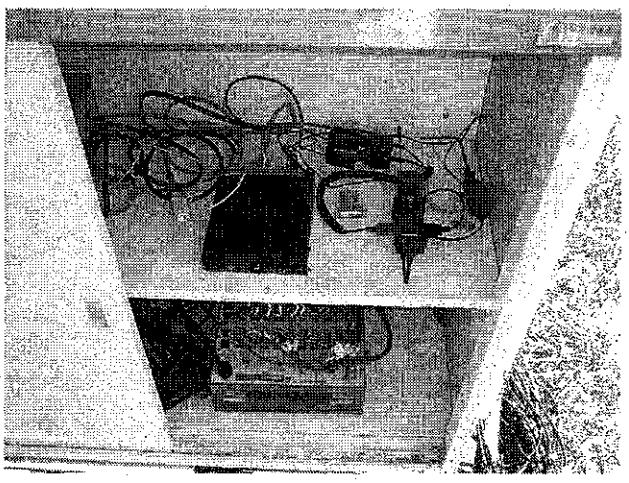

Fig.8　Equipments for measurement (Nakatani-gawa bridge)

本事例では，対象橋梁の下は谷になっており計測用ユニットハウスを設置する余裕がなく，本線横のわずかなスペースに計測機器を設置している．そのため，本線通行車両からできる限り目立たないように高さの低い（h=1000）スチールBOXに計測機器を収納している．さらに，山間部であることと計測開始が供用前であり商用電源が確保できなかったことから，太陽電池パネルを設置し太陽光発電した直流電力を自動車用高性能バッテリーに充電するシステムにより電源を確保している．計測機器のコントロールにパソコンを使用した場合，消費電力が大きくなり太陽電池パネルも多く必要となることから，コストパフォーマンスを考慮してパソコンの使用を控えた．計測開始から現在まで，電力不足によるトラブルは無い．

電話回線についても，山間部であり一般回線（有線）が設置されていないことから，携帯電話を使用することとした．当然PHSは圏外で使用不可であり，データロガーのコントロールユ

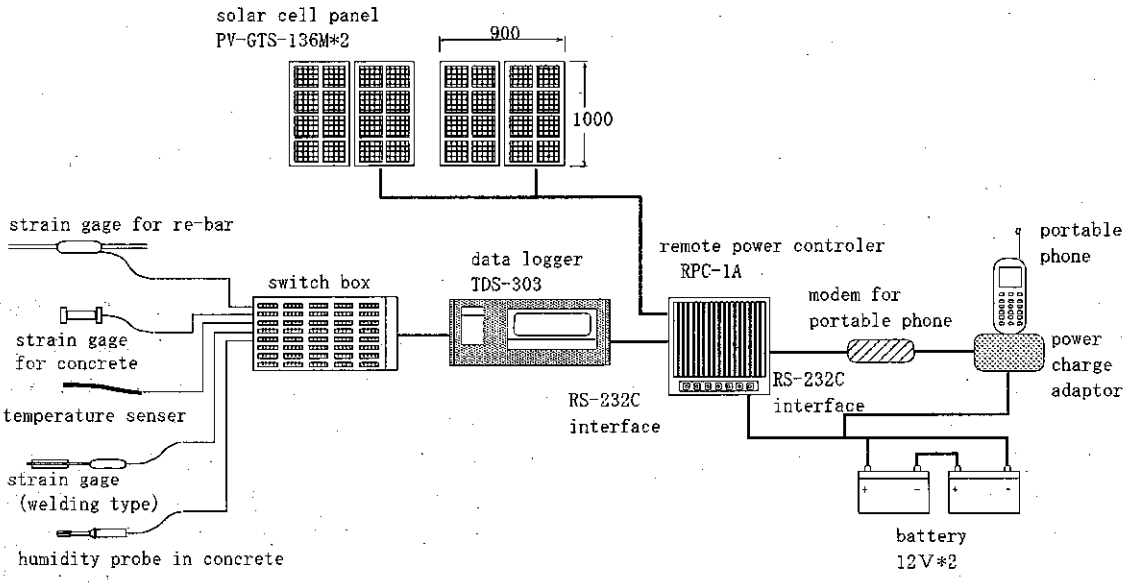

Fig.7　Components diagram of measurement system (Nakatani-gawa bridge)

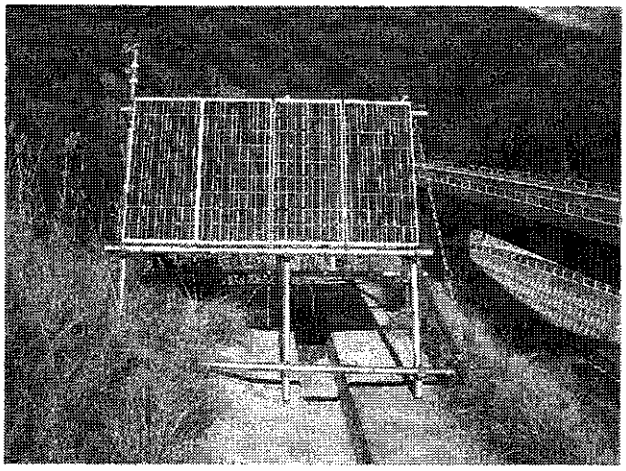

Fig. 9　Solar cell panel (Nakatani-gawa bridge)

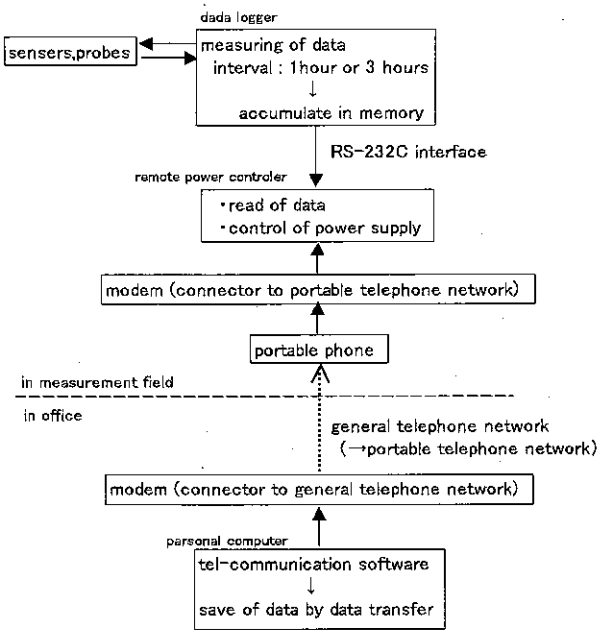

Fig. 10　Flow chart on data acquisition (Nakatani-gawa bridge)

ニットとの相性が確認されていたという制約条件から携帯電話と携帯電話用モデムを採用した.

システム構成としては, Fig. 10に示すように, データロガー(静ひずみ計)が自己のインターバル計測機能により1時間または3時間間隔に測定しデータをデータロガー内部のメモリーに蓄えることは大津呂川橋と同様であるが, データロガーのコントロールは, リモートパワーコントローラというRS-232Cインターフェイスによりデータの回収, 計測器電源の制御を行う機器によっている. この機器自身もRS-232Cインターフェイスにより制御するため, 携帯電話用モデムと接続している.

データの回収手順は, 遠隔地である事務所のパソコンおよびモデムから現地の携帯電話にデータ通信モードで接続し, ハイパーターミナルなどの通信ソフトでコマンドを送信して通常時は測定時以外はスリープモードとなっているデータロガーを覚醒させ, データの回収を行う.

本システムの最大の利点は, 消費電力が小さいためバッテリーベースの電源システムで稼働できることである. 数カ月間であれば, 自動車用バッテリーなどの使用により計測が可能である. 本事例では3年間の計測期間であったため, バッテリーに充電するために太陽電池パネルを設置した.

現状における欠点としては, モデムの転送速度が遅いためデータ回収に時間がかかること, そのため転送途中に電波状態が悪くなって通信が途絶えると最初からやり直さなければならないこと, また, 一度システム不調が生じた場合, どの機器がどんな状態であるかが解らないことなどが挙げられる. 電波状態が悪いのは本システム固有の問題ではないが, 本システムを適用せざるを得ないような電源および電話回線が確保しにくい環境条件の現場は, 山間部や僻地であることが想定されることから電波状態もあまり良くないものと考えられる. また, 何が原因でシステム不調となっているのか解らないことに関しては結局現地に行ってメンテナンスする必要があるため, 状態が解るか解らないかは心理的に納得する要素とも言える.

4. おわりに

以上, 2橋における適用事例を紹介したが, これら電話回線を利用した遠隔データ収集システムは, 従来の一定期間ごとにデータを回収する方式と比較すると, 日々の計測状況や正確な動作を確認することが可能であり, 落雷や停電その他のアクシデントによるシステム不調やデータの欠落に対して, 過度の防護設備によるコスト増加なしに確実な計測が可能となる. そのことから, 長期および遠隔地の計測においては非常に有効なシステムであることが確認できた.

本事例における各々の機器およびシステムはどれも最先端と言えるものではないが, それゆえ使用実績から評価されるそれなりの信頼性はあるため十分実用に耐えうるものである. ただし, 唯一パソコンの耐環境性能がシステムの他の機器に比べて低い点について改善の余地が残されていると考える. しかし, 最近では, 耐環境型パソコンも機種は僅少であるが市販されているようであり, 致命的な問題では無くなっていくものと思われる.

最後に, 現地計測を実施するに当たってご協力いただいている株式会社フジエンジニアリング西星匡博氏に謝意を表する次第である.

参考文献

1) 大山理, 坂本純男, 大久保宣人, 安川義行, 稲葉尚文：大津呂川橋のクリープおよび乾燥収縮挙動に関する実験的研究, 土木学会第57回年次学術講演会講演概要集 I-386, pp. 771-772, 2002.

2) 稲葉尚文, 安部健, 中野幹一郎, 入部孝夫：連続合成2主桁橋のクリープ, 乾燥収縮に関する一考察, 土木学会第57回年次学術講演会講演概要集 I-734, pp. 1467-1468, 2002.

(2003. 7. 31 受付)

制振ダンパによる伸縮装置の振動、騒音低減

Vibration and noise reduction of expansion joint by the response control damper

小山博*，三瓶太一**，稲田大輝***，中町華都雄****，新井哲治*****
Hiroshi Koyama, Taichi Sanpei, Hiroki Inada, Katuo Nakamachi, Tetsuji Arai

*,**,***日本鋳造㈱ エンジニアリング開発部（〒210-9567 川崎市川崎区白石町 2-1）
****工博 鋼管計測㈱ 計測診断部（〒210-0855 川崎市川崎区南渡田町１番１号）
*****㈱フコク(〒370-0723 群馬県邑楽郡千代田町千代田工業団地)

Expansion joint used for bridges, the modular expansion joints which can respond to the big amount of movements and contraction is used these days. Partly, expansion joints vibration and noise reduction are also needed. As one measure for vibration and noise reduction, the newly developed vibration suppression damper was tried on the beam of expansion joint. Laboratory experiment on actual size experiment model was conducted. It investigated the applicability of this vibration suppression damper, the vibration suppression characteristic, and applied to the expansion joint on actual steel bridge. Consequently, at specific frequency, oscillating reduction of 10dB or more was able to be realized, and reduction of about 4dB (A) was able to be realized in the noise level.

Key Words : expansion joint, vibration, response control damper, noise
キーワード：伸縮装置，振動，制振ダンパ，騒音

1. はじめに

昨今、橋梁の伸縮装置では、大きな伸縮量に対応できるモジュラージョイントが多く用いられてきている。車両走行に伴う橋梁振動、騒音は、伸縮装置段差や路面凸凹により振動が励起された車両が橋梁を加振することで発生すると考えられており、一部の橋梁では伸縮装置自体の振動、騒音低減が必要とされている。従来の対策としては、伸縮装置前後のすりつけの改良、伸縮装置の下面に詰め物を挿入したり、下面をカバーで覆う等の方法である。

その低減対策の一つとして、発生源の一つとして考えられる走行車両の通過によるモジュラージョイントのビーム振動を低減すれば、効果があると考え、伸縮装置のビームに新開発の制振ダンパを設置する事を試みた。実際の伸縮装置を用いた実物大実験モデルによる室内実験により本制振ダンパの適用性、制振特性について調査した。この結果に基づいて装置諸元の最適化を図り、本制振ダンパを実際の鋼製橋梁の伸縮装置に取り付け、効果を測定した。

2. モジュラージョイント、制振ダンパの構造

2.1 モジュラージョイントの構造

モジュラージョイントの構造を図－１に示す。特殊な断面の鋼材とシールゴムを組み合わせることにより、小さな伸縮量から大きな伸縮量まで対応可能であり、止水は橋面排水、荷重は単純梁で支持する。

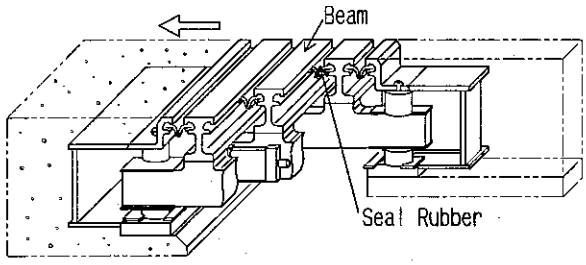

Fig. 1 Modular expansion joint

2.2 制振ダンパの構造

制振ダンパの構造及び取り付け方を図―２に示す。制振ダンパは、密閉された容器に封入されたシリコンオイルと防振ゴムによって減衰させ、弾性支持されている。制振ダンパは、実験では伸縮装置のビームの下面に万力で取り付けた。

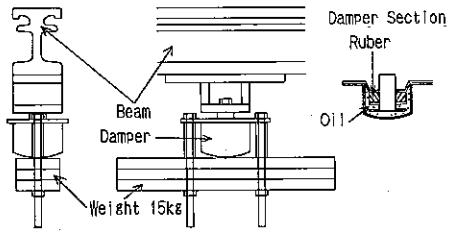

Fig. 2 **response control damper**

3. 実物大実験モデルによる室内実験

ビームの固有周期は、ビーム断面性能、支持支間等により決定されるが、事前に固有周期を測定し、200Hz 前後であることを確認した。その結果より、ダンパを調整した。実物大実験モデルにてモジュラージョイントのビームにダンパを取り付けた時の制振効果、減音効果を測定した。ダンパは、ビームの支間の中央に取り付けた。ビームをインパクトハンマーで加振した。図－3に実物大実験モデル、表－1に実験条件を示す。

Photograph.1

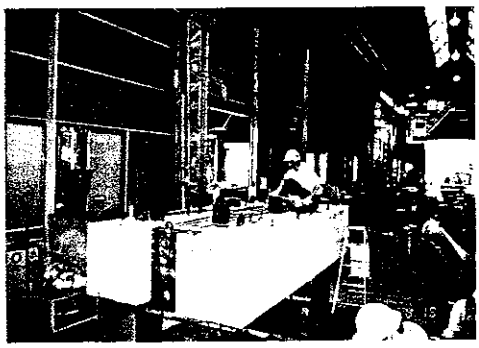

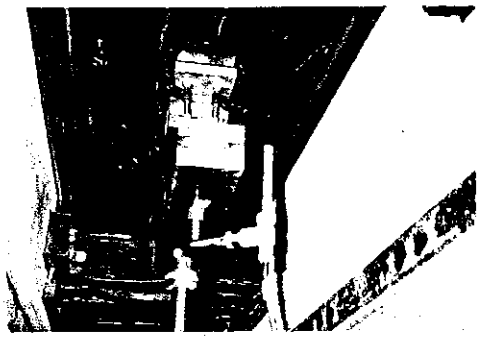

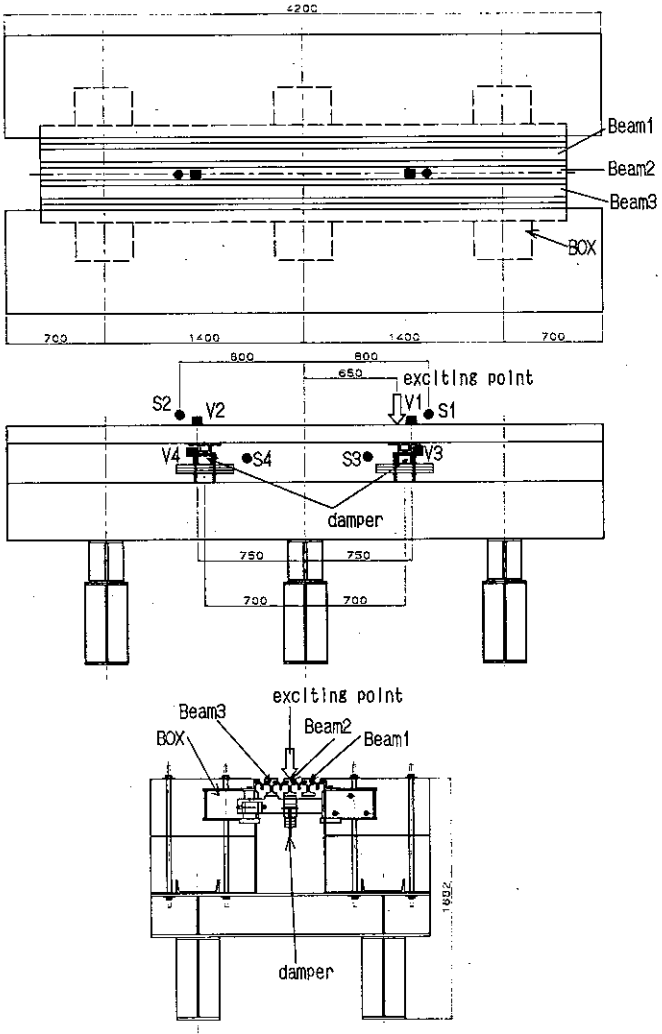

Fig. 3 Actual size experiment model

Table. 1 Experiment conditions

Experiment conditions		Note
Name	Weight(kg)	
no damper	-	
Type H	15	National period of damper 195Hz
Type H	20	National period of damper 180Hz
Type M	15	National period of damper 180Hz
Type S	15	National period of damper 150Hz

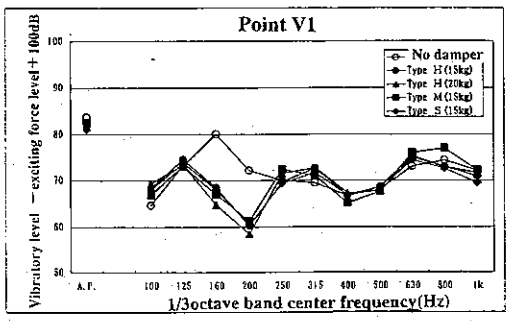

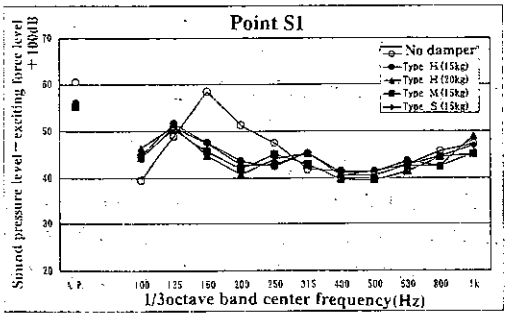

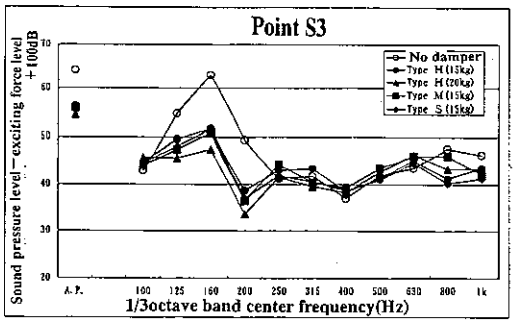

Fig. 4 1/3octave band analysis result

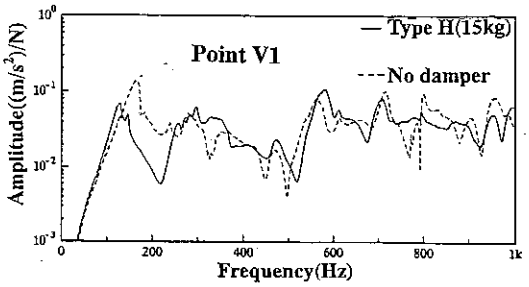

Fig. 5 Comparison of damper Type H(15kg) and no damper

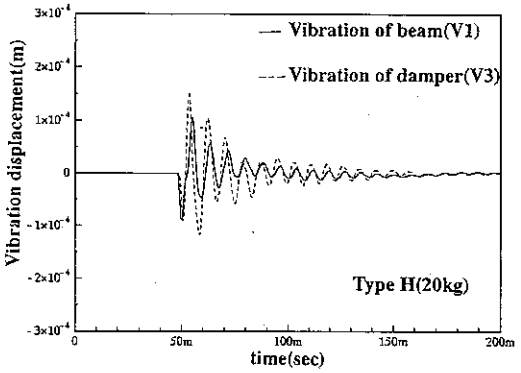

Fig. 6 damper Type H(20kg)
Comparison of damper Point V1 and V3

ダンパを付加することにより、ビームの振動については、1～3dBの低減効果があった。特定の周波数では、11～15dBの低減であった。騒音については、上面では5～6dBの低減、下面では10～13dBの低減効果で、特定の周波数では10～15dBの低減となった。また図－6に示すようにビームの振幅も小さくなっていた。

この結果を実橋に使用するダンパの参考とした。

4. 実橋梁での伸縮装置測定

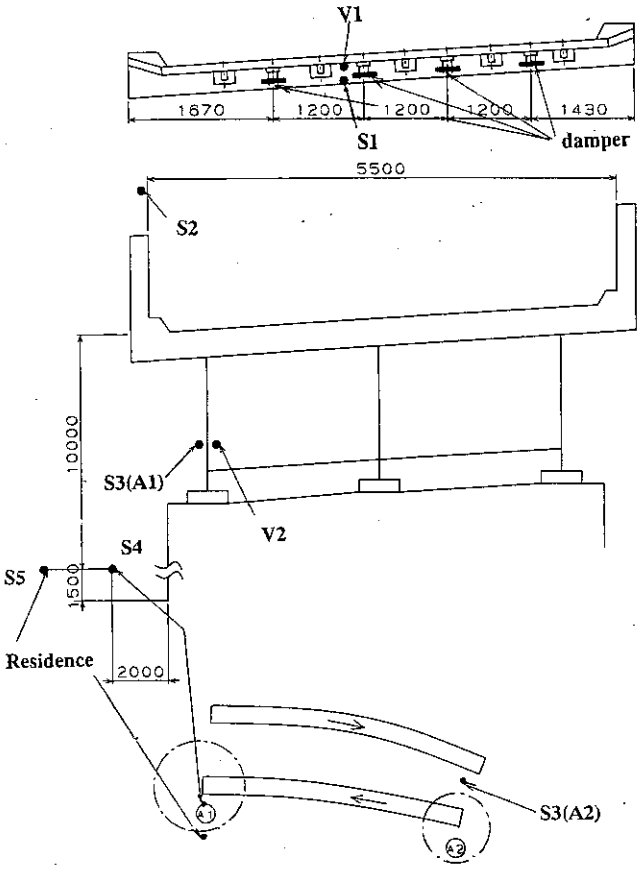

Fig. 7 Outline figure

実際の鋼製橋梁のモジュラージョイントにダンパを取り付け振動、騒音の低減の効果があるか確認をおこなった。

この橋梁には、ビームが一本のモジュラージョイントが使用されている。図－7に示すように、Ａ1、Ａ2　2ヶ所測定を行った。

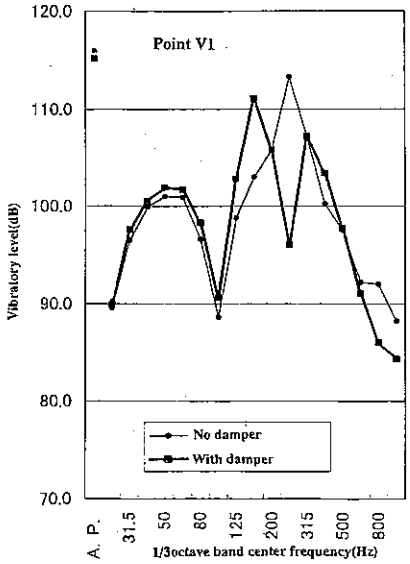

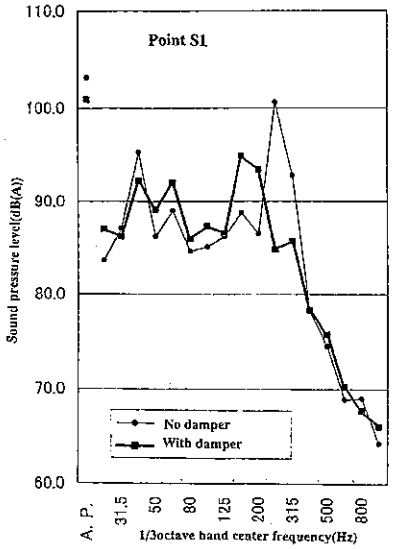

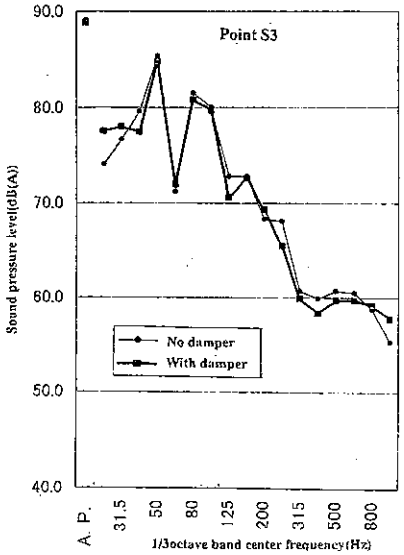

Fig. 8 A2 The analysis result at the time of track passage

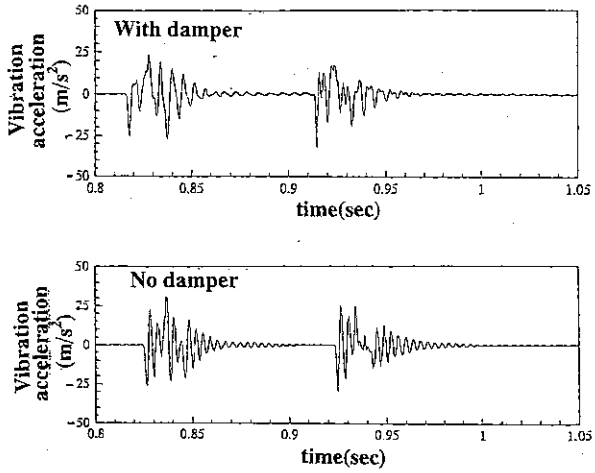

Fig. 9 A2 Vibration of the beam at the time of track rear wheel passage

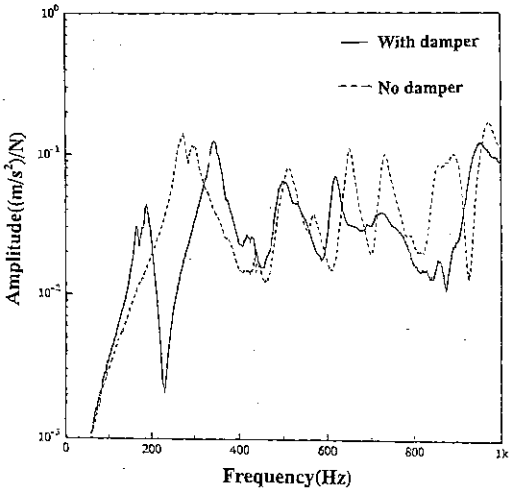

Fig. 10 A2 Comparison of damper and no damper

Ａ２については、自重と荷合計１８トンのトラックを約速度５０km/h で走行させた。その結果を図－８～１０に示す。ダンパを付ける事により、ビームの振動は2dB、直下の騒音は3dBの効果があったが、約10m離れた場所では、効果は無かった。

Ａ１については、Ａ２と同様にダンパを取り付けた。乗用車を約 80km/h で走行させた。その結果を図－１１～１３に示す。また参考に図－１２のトラックの場合（速度、重理容、種類雑多、1/1 オクターブバンド）を測定したものを示す。

Ａ２と同様に、ダンパを取り付けることによりビームの振動は4dB、直下の騒音は4dB 低減するが、民家前のＳ５では、1dB の低減にすぎない。

トラックについては、図－１２に示すようにＳ４で約3dB の低減効果があった。ちなみに乗用車の場合Ｓ４では、1dB 未満の低減効果しかなかった。この橋梁では、トラックの場合、各周波数における最大の騒音は250Hz、乗用車では、630 Hz であった。ダンパは、250 Hz の当たりで効果があるように調整していた(重り12.5kg)。そのためトラックの場合に効果があらわれた。

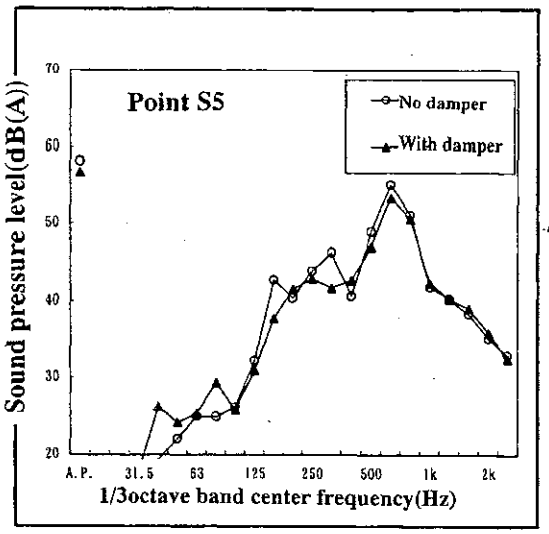

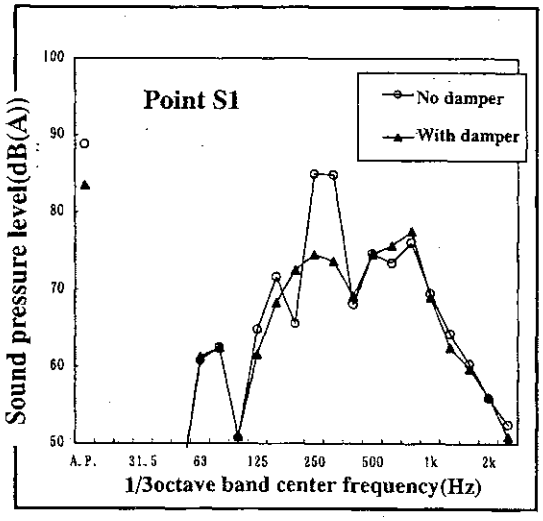

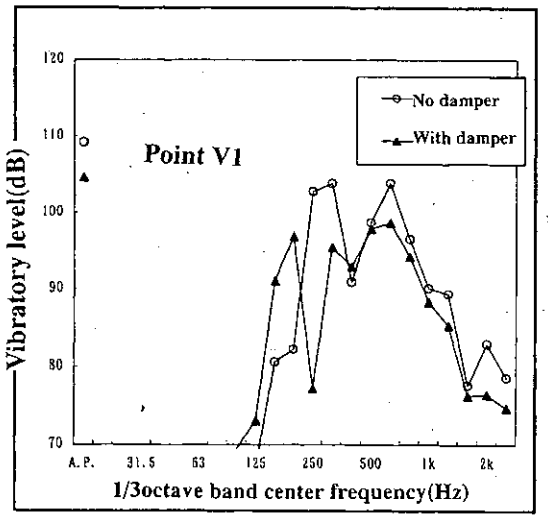

Fig. 11 A1 The analysis result Comparison of damper and no damper

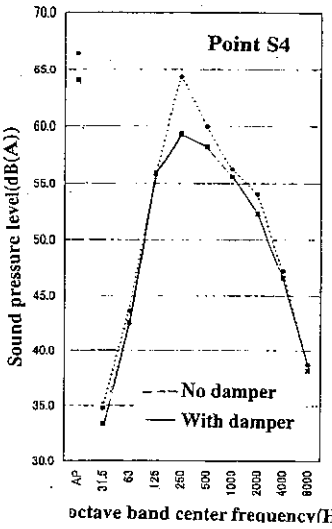

Fig. 12 A1 The analysis result at the time of track

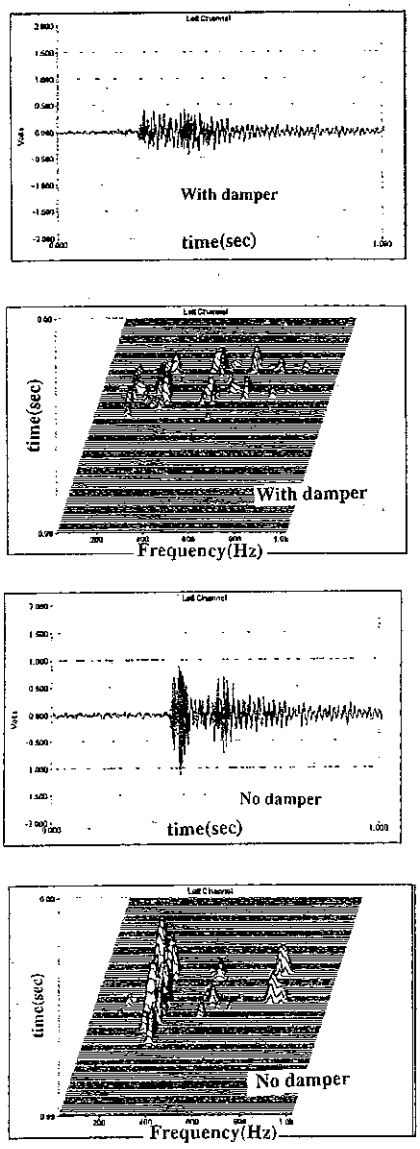

Fig. 13 A1 Comparison of damper and no damper.

5. まとめ

実物大実験モデルによる室内実験及び実橋梁での測定より、以下のことが結論づけられる。

1) ダンパ自体の効果、ビームの振動の減衰による減音はあるが、ダンパの性質上特定の周波数のみに効果がある。
2) 個々の物件の最大騒音の周波数を把握して、ダンパをその最大の周波数に調整できれば、ビームにダンパを取り付けることにより騒音、振動を今回以上に低減できる。
3) 伸縮装置直下近傍では、ダンパの効果があるが、民家等近辺では効果は少ない。それは、ビームから放射される騒音よりも、ビーム以外、例えば、自動車のタイヤ、ボディから出る騒音の方が大きいと考えられる。今回ある程度ビームから発生すると思われる騒音を低減させたにもかかわらず、民家等近辺では効果が少なかった事からも、推測される。

参考文献

1) 騒音制御工学ハンドブック（社団法人日本騒音制御工学会編）：技報堂, 2001.
2) 鈴木信二、中尾健太郎、佐藤弘史、橘義規、林家洋：車両走行に伴う橋梁振動の発生メカニズムに関する研究, 振動制御コロキウム'01 論文集 pp.133-140, 2001.10
3) 村井逸郎、佐野千裕、佐藤弘史、葛西俊二、橘義規：TMD による橋梁振動及び低周波音抑制効果に関する実橋実験, 振動制御コロキウム'01 論文集 pp.141-146, 2001.10

(2003.7.31 受付)

高架橋上に設置された照明柱の振動計測および制振装置の同構造物への適用

Vibration Characteristic of a Lightening Pole on an Elevated Highway Bridge and Effect of TMD for Mitigating Vibration

石橋知彦*，北田俊行**
Tomohiko Ishibashi, Toshiyuki Kitada

*那須電機鉄工株式会社，技術開発本部（〒555-0041 大阪市西淀川区中島2丁目12-5）
**工博　大阪市立大学教授，大学院工学研究科（〒558-8585 大阪市住吉区杉本3丁目3-38）

Recently, damage of pole type structures on elevated bridges due to the vibration of the pole type structures through the bridge vibration caused by automobiles runnning on the bridges become one of the important issues to be solved. The damage consequently result in the degradation of the function and shortening of the fatigue life of the damaged pole type structures. Dealt with in this paper is the vibration characteristic of a lighting pole on an elevated highway bridge and the mitigation of the vibration by using a TMD(Tuned Mass Damper). From the field observation of the vibration of the lighting pole, it is verified that the pole has no problem from the point of view of the fatigue strength even if without TMD, but by using the TMD, the pole's fatigue life can be extended to about 10 times the fatigue life in case of the pole without the TMD.

Key Words: bridge vibration, fatigue life, TMD, pole type structure
キーワード: 橋梁振動，疲労寿命，TMD，柱状構造物

1. はじめに

近年，高速道路などの高架橋上に設置された柱状構造物において，橋桁上を通過する車両が橋梁を揺らし，その振動が柱状構造物を揺らす，『橋梁交通振動』が問題となる場合がある。この振動がみられる箇所においては，見た目の恐怖感の他に，搭載機器の劣化や構造物自体の疲労寿命の低下が懸念される。

本論文では，高架橋上に設置された道路照明柱各部の加速度およびひずみを計測することによって，照明柱の振動特性把握や疲労寿命検討を行った結果について述べている。また，その振動対策の一案として同調質量型制振装置（Tuned Mass Damper：以下「TMD」と略称）を試験的に適用したので，その効果の確認実測結果についても述べている。

2. 対象とした橋梁と照明柱

今回対象とした照明柱が設置されている橋梁はスパン13.5mの桁橋で，照明柱はその中心付近に設置されていた。

対象とした照明柱（灯具高さ12m，アーム長さ0.8m）の概略図をFig.1に示す。

この照明柱の固有振動数および一般化質量を調べるために固有値解析を行った。照明柱の2次の振動モード（橋軸直角方向1次モード）をFig.2に，固有値解析結果をTable 1に示す。解析は『STAN/3D』および『STAN/3D-E』を用いて行った。

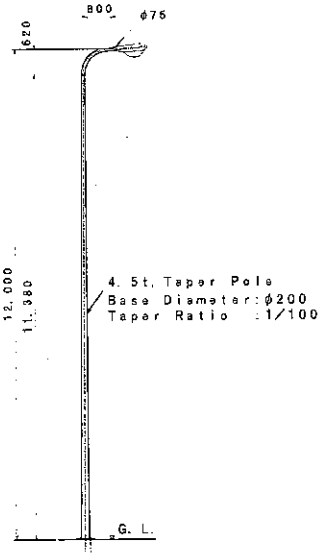

Fig.1 Outline of the Lighting Pole (unit:mm)

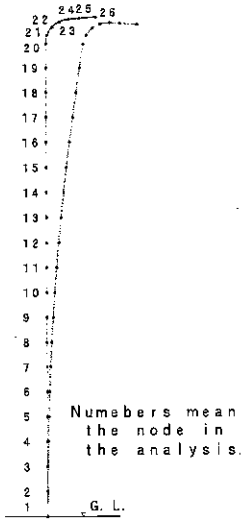

Fig.2 2nd Mode of the Lighting Pole

Table 1 Result of Eigenvalue Analysis

Order	Eigenvalue(Hz)
1st	1.06
2nd	1.06
3rd	4.66
4th	4.69
5th	9.58
6th	10.06
7th	17.85
8th	18.34

3. 制振装置

今回，振動対策の一案として減衰付加効果が得られる制振装置を試験的に取り付けた。制振装置には様々な種類のものが提案されているが，電源を必要としないパッシブ型の制振装置の中で大きな減衰が得られるTMDを採用した。TMDはその名の示すとおり装置内部のおもりを構造物の振動に同調させることにより，効率よく減衰を得るものであり，ばね，質量，およびダンパーの3要素によって構成される。

今回採用したのは著者らが既に開発したTMD[1]で，減衰機構に磁気ダンパーを用いたものである。開発したTMDの概要をFig.3に示す。装置は水平方向にスライドする重錘を側面4方向からコイルばねにて支持し，重錘の振動数を調整する構造となっている。磁気ダンパーとしては磁力が強く安価なネオジム磁石を採用した。永久磁石を用いた磁気ダンパーは古くから知られており[2]，通常は対向するNS極の磁力線間に電気伝導率の優れた導体（今回は銅を使用）を挿入し，その導体が磁力線を横切るときに生じる誘導電流により減衰を得るのが一般的である。

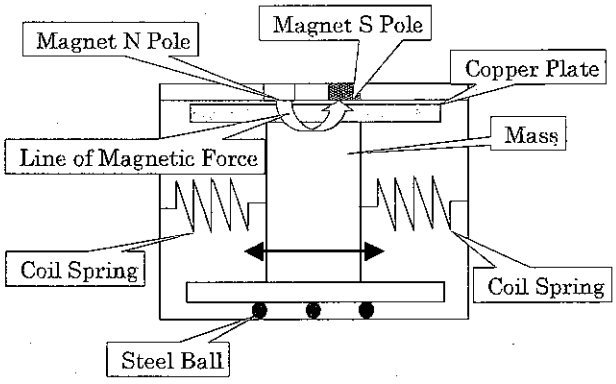

Fig.3 Outline of TMD Used

しかし，装置の小型化・コストダウンを図るためにFig.4に示すように，同一平面上に磁石のNS極の磁極の向きを変えて放射線状に配置した磁気ダンパーを考えた。磁石をこのような配置にしてもFig.3に示すような磁力線が形成され，これを導体が横切ることにより減衰力が生じるものと考えられる。減衰力の調整は磁石の個数や磁束密度を変えること以外に磁石と導体間の距離を変化させることで実現することができる。

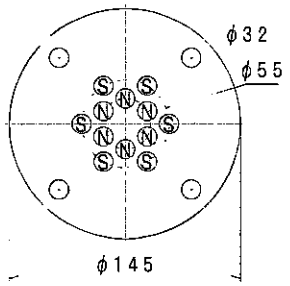

Fig.4 Location of Magnets

固有値解析結果および現地での目視による状況確認より，1次モード（橋軸方向1次）および2次モード（橋軸直角方向1次）が卓越していたので，これを制振対象モードとした。この場合，制振装置の取付位置としては，制振対象モードにおいて最も大きく揺れる照明灯具位置とするのが望ましいが，照明柱の機能や装置の構造からFig.1の直線部最上部とした。制振装置の設置状況をFig.5に示す。照明柱全体の一般化質量に対する重錘(Mass)の質量比は7.0%とした。装置は外径φ165.2，高さ約230mmの鋼管に内蔵し，総質量は約20kgであった。

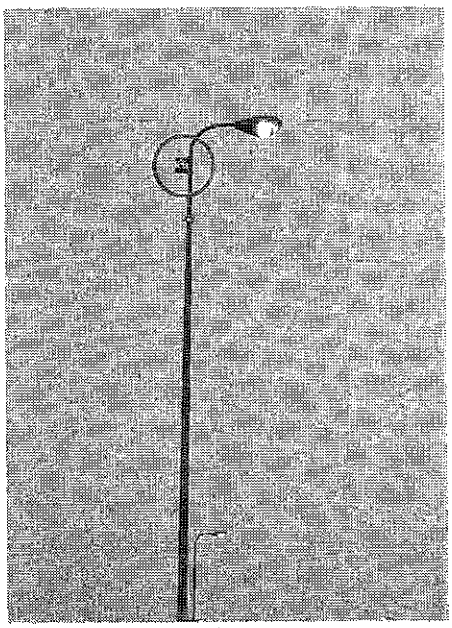

Fig.5 Installation of the TMD

4. 計測方法

計測は照明柱の各部にひずみ式の加速度計センサおよびひずみゲージを取り付けることにより行った。計測セ

ンサの取付位置をFig.6に示す。照明柱に入力する加速度を調べるためにベースプレートに加速度計を3方向，それに対する応答を調べるために制振装置取付部（直線部最上部）に加速度計を2方向，応答により照明柱基部に発生するひずみ（応力度）を調べるためにベースプレートリブの上部にひずみゲージを2方向設置した。

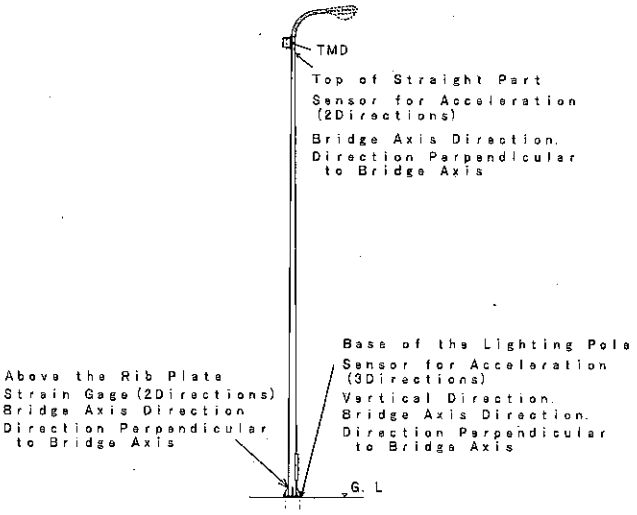

Fig.6 Location of Sensors

照明柱脚部の計測センサ設置状況をFig.7に示す。また，計測システムの概要をFig.8に示す。ひずみゲージはテーパー柱造管部およびリブプレートの溶接ビード線にかからない場所に設置した。サンプリングの周波数は100Hzとし，制振装置の取付前後でそれぞれ24時間計測を行った。

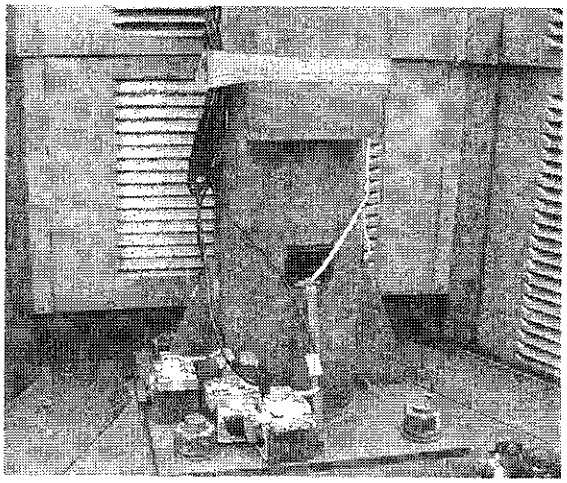

Fig.7 Installation of Sensors
at Base of the Pole

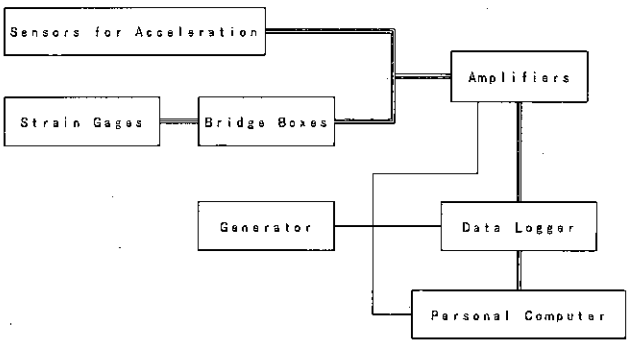

Fig.8 System of Observation

5. 計測結果

5.1 疲労寿命の算定

ひずみゲージによるリブ付近での応力度測定結果を用いて，リブ部分の疲労に対する寿命予測の検討を行った。疲労寿命の算定は，以下のように行った。すなわちまず，レインフロー法により計測した24時間における作用応力度の度数分布を作成した。さらに，そのデータが連続して続くと仮定し，リブ部分の強度等級をG等級として累積損傷度を用いたMinerの方法[3]により寿命予測を行った。疲労寿命の算定結果をTable 2に，各応力範囲における24時間の度数分布をFig.9に示す。

Table 2 Prediction of Pole's Fatigue Life

Direction	①without TMD (years)	②with TMD (years)	②／①
X	79.9	905.0	11.3
Y	185.7	2141.7	11.5

X:Direction Perpendicular to Bridge Axis
Y:Bridge Axis Direction

Table 2より，照明柱は橋軸方向よりも橋軸直角方向の揺れが卓越していること，制振装置の取付により推定疲労寿命は取り付けない場合に比べて両方向とも約11倍に改善されることがわかる。

制振装置取付前後では計測日時が異なり，照明柱への入力外力は同一ではないが，Fig.9を見ると，制振装置を取り付けることによって，大きな作用応力の発生頻度が少なくなっていることがわかる。たとえば，橋軸直角方向の作用応力は，20Mpaの応力レベルでは，制振装置を取り付けることにより，度数が30程度から0程度に減少していることがわかる。

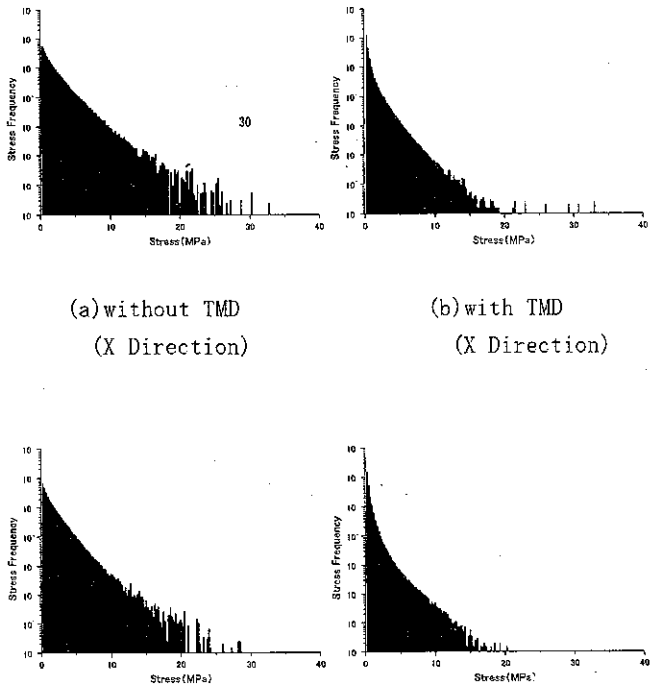

(a)without TMD (X Direction)　(b)with TMD (X Direction)

(c)without TMD (Y Direction)　(d)with TMD (Y Direction)

Fig.9 Stress Frequency Distribution(in 24 hours)
(X:Direction Perpendicular to Bridge Axis)
(Y:Bridge Axis Direction)

5.2 加速度

制振装置取付前の照明柱各部の加速度の時系列データ例をFig.10に,制振装置取付後の加速度の時系列データ例をFig.11に示す。

Fig.10およびFig.11より，脚部の加速度は3方向で概ね同様の変化を示しており，1つの方向で大きな加速度を記録している部分では他の2方向も大きな加速度を記録している。加速度の大きさは鉛直方向，橋軸直角方向，および橋軸方向の順になっている。照明柱上部の応答は概ね脚部の加速度に対応して大きくなっているため，振動要因は風よりも交通振動が支配的であると考えられる。また，照明柱の応答は橋軸直角方向が大きくなっているが，これは脚部の橋軸直角方向の加速度が大きいことと，照明柱が鉛直方向の加速度に対して橋軸直角方向に揺れる形状をしていることによるものと考えられる。

Fig.10（取付前）に示した照明柱上部の応答の振幅スペクトルをFig.12に，Fig.11（取付後）に示した照明柱上部の応答の振幅スペクトルをFig.13に示す。

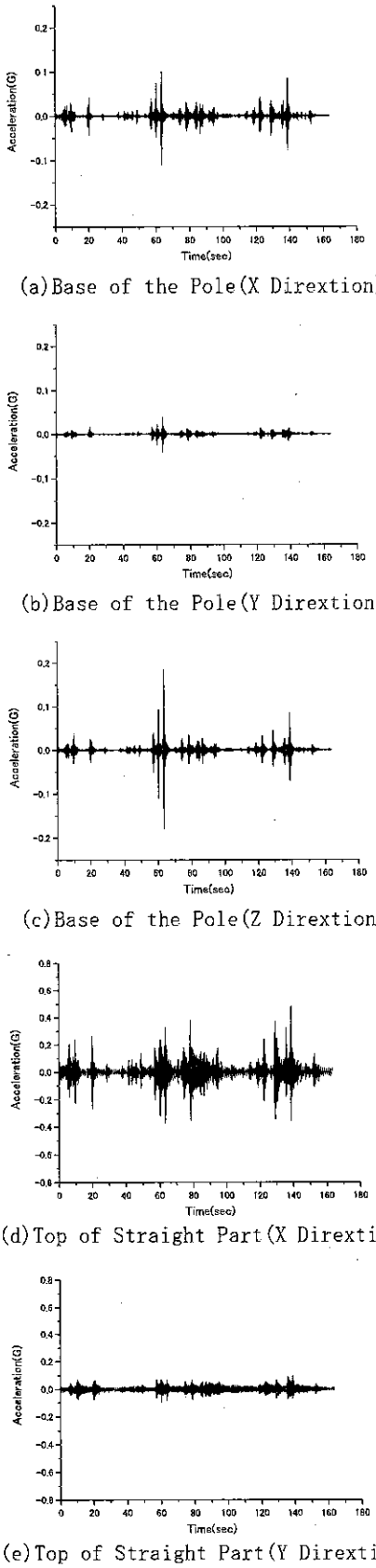

(a)Base of the Pole(X Direxion)

(b)Base of the Pole(Y Direxion)

(c)Base of the Pole(Z Direxion)

(d)Top of Straight Part(X Direxion)

(e)Top of Straight Part(Y Direxion)

Fig.10 Time History of Acceleration (without TMD)
(X:Direction Perpendicular to Bridge Axis)
(Y:Bridge Axis Direction)
(Z:Vertical Direction)

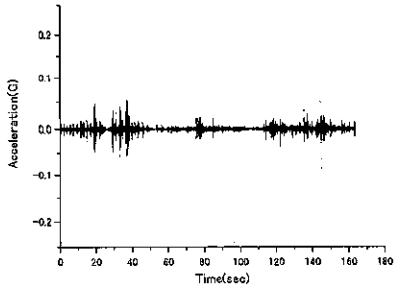

(a)Base of the Pole(X Direxion)

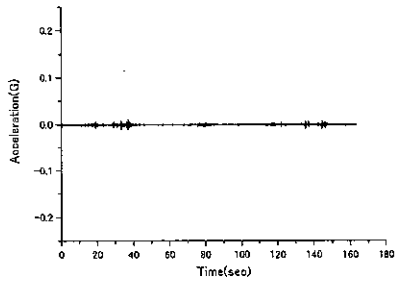

(b)Base of the Pole(Y Direxion)

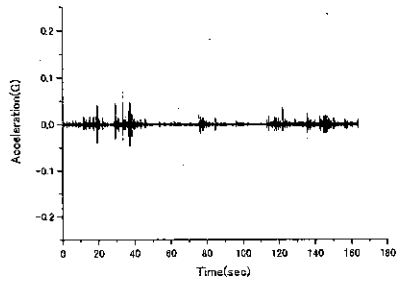

(c)Base of the Pole(Z Direxion)

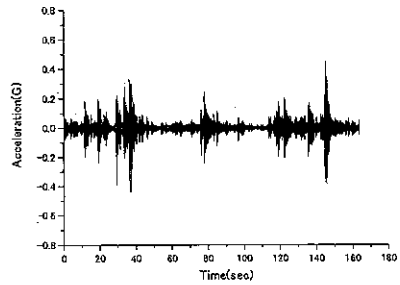

(d)Top of Straight Part(X Direxion)

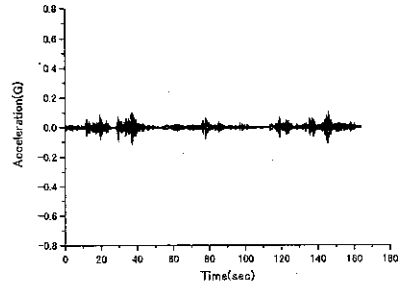

(e)Top of Straight Part(Y Direxion)

Fig. 11 Time History of Acceleration (with TMD)
(X:Direction Perpendicular to Bridge Axis)
(Y:Bridge Axis Direction)
(Z:Vertical Direction)

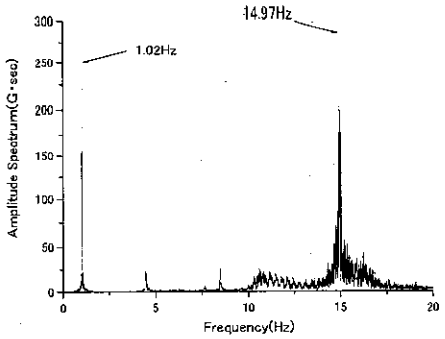

(a) Direction Perpendicular to Bridge Axis

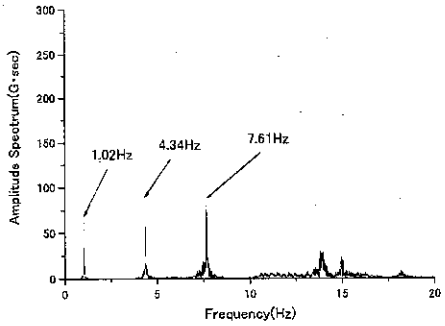

(b) Bridge Axis Direction

Fig. 12 Amplitude Spectrum
at Top of Straight Part(without TMD)

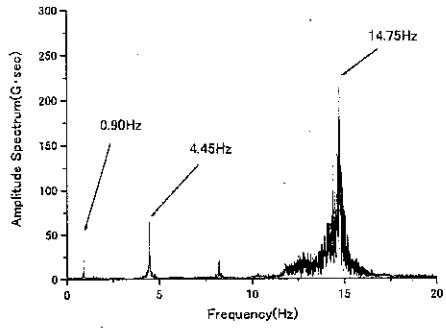

(a) Direction Perpendicular to Bridge Axis

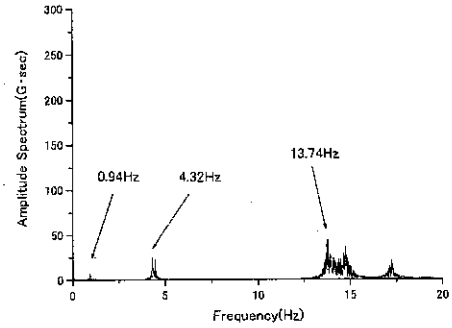

(b) Bridge Axis Direction

Fig. 13 Amplitude Spectrum
at Top of Straight Part(with TMD)

Fig.12 および Fig.13 より，制振装置取付により，対象モードである1次および2次モードのスペクトルが大幅に低減されていることが確認できる。装置取付後のピーク振動数が取付前に比べて落ちているのは，装置重量の影響によるものと考えられる。また，15Hz 付近にも大きなピークが認められるが，これは照明柱の7次および8次モードに対応していると考えられる。

Fig.11（取付後）に示した照明柱脚部の振幅スペクトルを Fig.14 に示す。12Hz～15Hz にスペクトルのピークが認められる。これが橋梁の鉛直方向の1次固有振動数であると考えられる。この数値は既往の研究成果[1]によく一致している。Fig.12 および Fig.13 に見る照明柱の応答スペクトルの 15Hz 付近のピークはこの振動との共振によるものと考えられる。

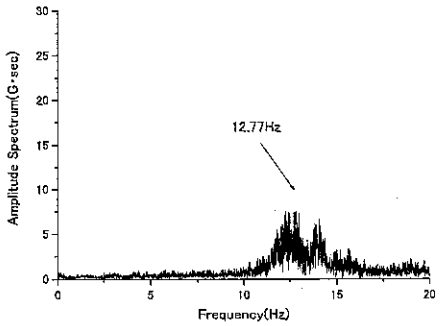

(a) Direction Perpendicular to Bridge Axis

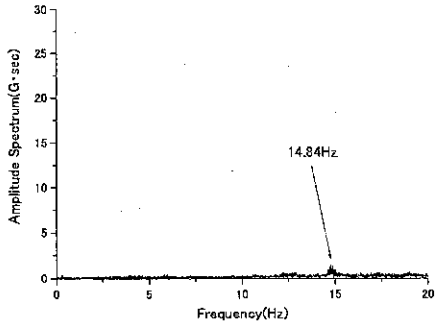

(b) Bridge Axis Direction

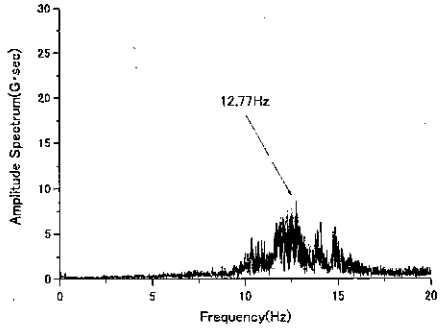

(c) Vertical Direction

Fig.14 Amplitude Spectrum at Base of the Pole(with TMD)

6. まとめ

本研究では，高架橋に設置された照明柱における交通振動による振動状況を調べるために計測を実施し，さらにその振動対策の一案として制振装置（TMD）を試験的に取り付け，その効果を確認した。今回確認した事項について以下にまとめる。

(1) 今回計測した照明柱の推定疲労寿命は制振装置取付前で約 80 年であり，照明柱の供用期間中に疲労が問題になることはないと考えられる。

(2) 制振装置の取り付けにより，推定疲労寿命は約 11 倍へと改善された。照明柱に入力された外力は同じではないが，照明柱の応答により発生した応力の度数分布を見ると，制振装置を取り付けることによって，大きな作用応力の発生頻度がかなり少なくなっていることがわかった。また，同程度の外力の応答結果の振幅スペクトルが対象モードにおいて大きく低減されていることが確認できた。これらのことから本研究で用いた制振装置の効果が認められた。

(3) 照明柱に入力された外力の振動数は 12Hz～15Hz が卓越しており，これが計測した照明柱が設置されている橋梁の鉛直方向の1次固有振動数であると考えられる。これが照明柱の7次および8次の固有振動数と共振していた。しかし，この成分は振動数が高いため変位が非常に小さく，対象とした照明柱の柱の疲労強度および搭載機器の損傷に与える影響は問題にならないことがわかった。

(4) 以上より，今回効果を調べるために試験的に用いた制振装置は対象とした照明柱について必ずしも取り付けなければならないという必要性はない。しかし，振動が問題となっている高架橋上の照明柱や標識柱の振動対策の一つとして，制振装置の設置は充分に有効な手段であることがわかった。

(5) 灯具の球切れ頻度など，搭載機器に対する効果については引き続き経過を見守る必要がある。

参考文献

1) 石橋知彦・畑中章秀：柱状構造物を対象とした小型制振装置の開発，土木学会第 57 回年次学術講演会概要集Ⅰ-601，2002
2) 背戸一登：磁気減衰を活用した振動制御法，日本機械学会論文集C編，第56巻525号，pp. 1079～1086，1990.
3) 日本鋼構造協会編：鋼構造物の疲労設計指針・同解説，技報堂出版，1993.
4) 加藤雅史・島田静雄：橋梁実測振動特性の統計解析，土木学会論文報告集，No311，pp. 49～58，1981.

(2003. 7. 31 受付)

道路橋付属構造物の損傷可能性管理マップに関する基礎的研究

Fundamental Study on Development of Management Map for Potential Damage to Portal Marker Columns and Lighting Poles on Highway Bridges

○井舎英生*，北田俊行**，山口良弘***，徳増　健****
Hideo Isha, Toshiyuki Kitada,
Yoshihiro Yamaguchi and Ken Tokumasu

*後期博士課程，大阪市立大学大学院，工学研究科，都市系専攻（〒558-8585 大阪市住吉区杉本 3-3-138）
**工博，大阪市立大学大学院教授，工学研究科，都市系専攻（〒558-8585 大阪市住吉区杉本 3-3-138）
*** 阪神高速道路公団，計画部，交通環境室（〒541-0056 大阪市中央区久太郎町 4-1-3）
**** 阪神高速道路公団，保全施設部，保全技術課（〒541-0056 大阪市中央区久太郎町 4-1-3）

Vibration due to traffic and wind causes almost all fatigue damage to portal marker columns and lighting poles on highway bridges. Early detection and quick repair of the damage is important for the safety of traffic. Development of a practical system, which can evaluate and manage the possibility of the existence and occurrence of the damage efficiently, is necessary. It's, therefore, useful to make a vibration level map that can classify the vibration into some levels corresponding to the extent of the fatigue damage of these columns and poles. Fundamental research on making the vibration level map is carried out in this study. The vibration characteristics decided by the position and types of portal marker columns and lighting poles is investigated through Modal frequency response analysis. This vibration level map can be used to develop a fatigue damage level map of these columns and poles. The vibration level map is effective in deciding the priority of inspection works to detect the damage.

Key Words:　Measuring Vibrations, Detecting Damage, Portal Marker Column, Lighting Pole

1. はじめに

交通荷重を起因とする橋桁の振動は，橋梁付属構造物である照明柱や標識柱などに常時振動や共振振動を生じさせる．これらの構造物には，振動疲労による損傷が発生することがあり，その損傷の早期発見および補修は，道路安全管理上から重要である．しかし，都市高速道路の大部分は橋梁部であるので，損傷発見のための点検対象となる付属構造物の数量も多いという課題がある．

効率的で適切な点検が可能となるように，付属構造物に点検の優先順位を付ける健全度評価システムを構築することが有益である．このシステムには，効率的で適切な点検作業を行うために損傷の発生や存在の可能性を評価できる管理マップ（以下，損傷可能性管理マップという）を作成することが必要と考えられる．この管理マップは，振動変位の程度を評価し，その後に疲労強度評価を行うことにより作成されるものである．

本研究では，付属構造物の振動変位の程度を表す「振動度マップ」作成法の技術的検討を行っている．具体的には，理想化した交通荷重により橋梁と付属構造物とからなる全体構造物に対してモーダル法による周波数応答解析を行い，その解析結果に基づいて振動の程度の比較評価および振動度マップ試作に関して考察している．

2. 振動度マップ

振動度マップとは，付属構造物の振動変位の程度を表す振動度フラッグにより分類し管理するものであり，Fig.1 に概念図を示す．具体的には，橋梁と付属構造物との共振性により振動変位振幅の程度が異なる．変位振幅量に例えば 5 段階のレベルを設定して振動度フラッグとして分類し評価するものである．Fig.1 図中の f_s/f_b は，付属構造物と橋梁の固有振動数の比率を，L_s/L_b は橋梁支間長に対する構造物の設置位置を表している．

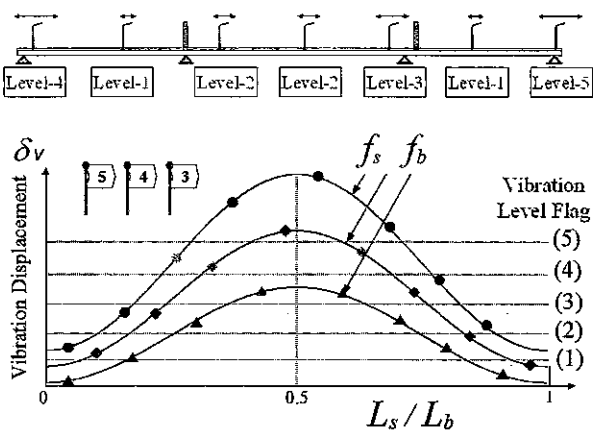

Fig.1 Example of Vibration Level Map and Flag

3. 付属構造物の振動特性

3.1 振動の状況

橋梁路面および照明柱と門型標識柱との振動状況の測定を2001年に阪神高速道路16号大阪港線にて行った．Fig.2に示す単箱桁4径間連続桁橋に9本の照明柱と1基の門型標識柱が設置されている．Fig.3には橋梁の断面および付属構造物の設置状態を示す．

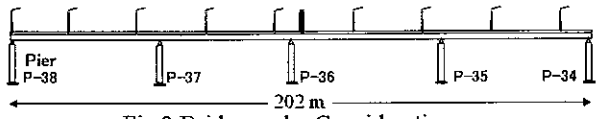

Fig.2 Bridge under Consideration

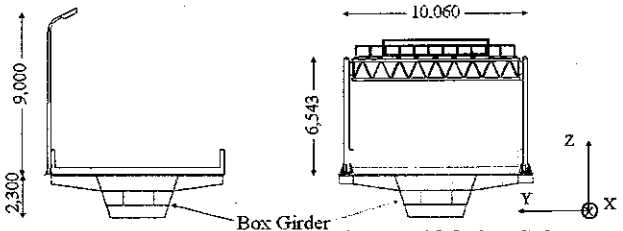

(a) Lighting Pole (b) Portal Marker Column

Fig.3 Structures under Consideration

3.2 照明柱と橋梁路面との振動測定結果

Fig.4には，中央橋脚付近の照明柱が設置されている断面の路面中央，側道および照明柱の柱基部における鉛直方向の振動変位をサーボ型変位センサーにより測定し，スペクトル解析した結果を示している．図中のスペクトル値は3箇所の測定結果を表している．測定結果の解析により路面（橋桁）の振動は1.5Hz～6.5Hzの範囲に比較的卓越したスペクトルが観測された．

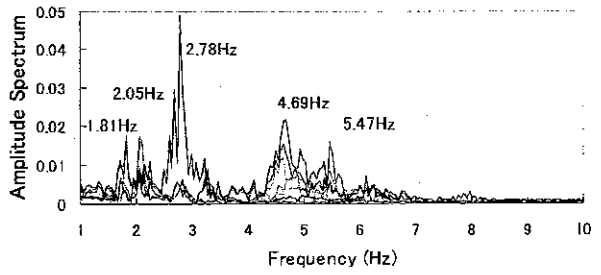

Fig.4 Vertical Vibration of Road Surface with Lighting Pole

3.3 照明柱の振動測定結果

照明柱の柱部および頭頂部の数箇所に変位センサーを取付けて面内,面外の振動変位を測定した[1),2)]．Fig.5(a)は，面外（橋軸）X方向の振動変位のスペクトルを示したものであり，1次振動は1.42Hz，2次振動は4.69Hzである．Fig.5 (b)は，面内水平（橋軸直角）Y方向の振動変位のスペクトルを示したものであり，1次振動は1.32Hz，2次振動は4.93Hzである．Fig.5 (c)は，頭頂部における鉛直Z方向の振動変位のスペクトルを示したものであり，1次振動は1.32Hz，2次振動は4.93Hzである．水平振動と鉛直振動は両方共に面内振動であるので振動数は一致している．路面（橋桁）の振動数は，1.5Hz～6.5Hzの範囲で卓越しているが，照明柱の応答は面内,面外ともに1次および2次振動モードの卓越振動である．

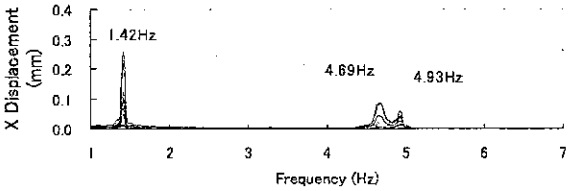

(a) Amplitude Spectrum in X Direction (Out of plane)

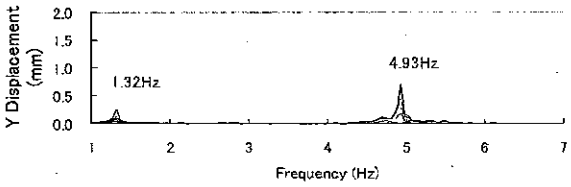

(b) Amplitude Spectrum in Y Direction (In plane)

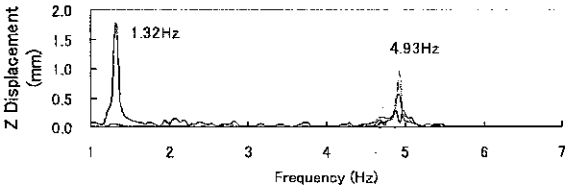

(c) Amplitude Spectrum in Z Direction (In plane)

Fig.5 Results of Spectrum Analysis for Measured Vibration Data of Lighting Pole

3.4 照明柱の固有振動解析

骨組構造モデルによる固有振動解析結果（振動数，振動モード）をFig.6に示す．ただし，柱基部は完全固定条件としている．

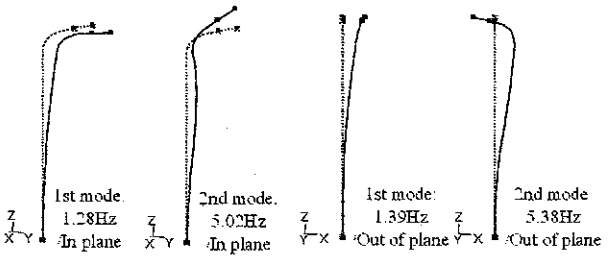

Fig.6 Natural Frequency and Vibration Modes of Lighting Pole

照明柱の固有振動数について，測定値と解析値とを比較してTable.1に示す．面内,面外ともに1次振動数は良好に一致している．

Table.1 Result of Measurement and Analysis

Natural Frequency / Methods	In Plane (Hz)		Out of Plane (Hz)	
	1st mode	2nd mode	1st mode	2nd mode
Measured Result	1.32	4.93	1.42	4.69
Analytical Result	1.28	5.02	1.39	5.38

3.5 門型標識柱と橋梁路面との振動測定結果

Fig.7は，中間橋脚付近の門型標識柱が設置されている路面中央，側道および門型標識柱の柱基部における鉛直方向の振動変位をサーボ型変位センサーにより測定し，スペクトル解析した結果を示している．図中のスペクトル値は3箇所の測定結果であり，橋梁の振動は，1.5Hz～6.5Hzの範囲に卓越したスペクトルが観測された．

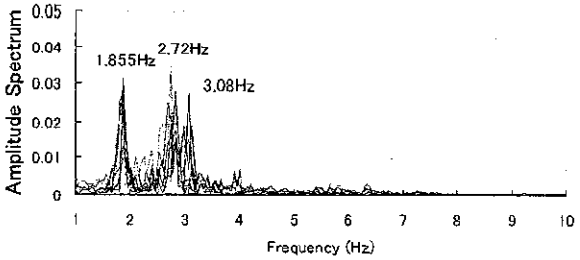

Fig.7 Vertical Vibration of Road Surface with Portal Marker Column

3.6 門型標識柱の振動測定結果

門型標識柱の柱部および上部梁トラス部の数箇所にサーボ型変位センサーを取付けて面内,面外の振動変位を測定した[1),2)]．路面（橋桁）の測定された鉛直 Z 方向の振動数は，Fig.7 に示すように，1.5Hz～6.5Hz の範囲である．門型標識柱の応答振動は面内および面外ともに 1 次振動モードのみが観測された．2 次モードでの振動は橋桁の振動範囲外のために現れなかったものと考えられる．

Fig.8 (a)は，面外 X 方向（橋軸方向）振動変位のスペクトルを示したものであり，面外 1 次振動は 3.66Hz である．Fig.8(b)は，面内水平（橋軸直角）Y 方向の振動変位のスペクトルであり，面外 1 次振動は 3.13Hz である．

Fig.8(c)は，上部梁中央部の鉛直 Z 方向の振動変位のスペクトルであり，面内 1 次振動は 3.13Hz である．

面内水平と鉛直は共に同一面であるので振動数は一致している．

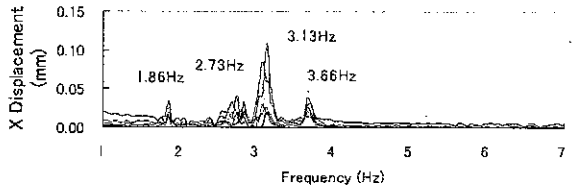

(a) Amplitude Spectrum in X Direction (Out of plane)

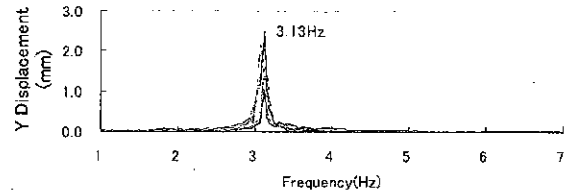

(b) Amplitude Spectrum in Y Direction (In plane)

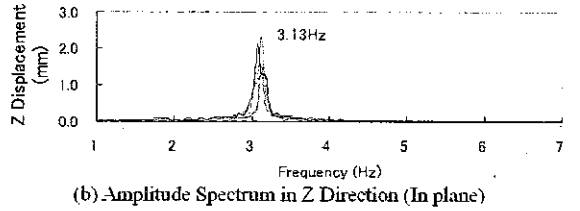

(b) Amplitude Spectrum in Z Direction (In plane)

Fig.8 Results of Spectrum Analysis for Measured Vibration Data of Portal Marker Column

3.7 門型標識柱の固有振動解析

骨組構造モデルによる固有振動解析結果（振動数，振動モード）を Fig.9 に示す．電光表示盤の重量は 1.2tonf である．解析における 4 本の柱基部の拘束条件は完全固定としている．しかし，実構造物の柱基部は橋桁ブラケットと連結されており，ブラケットの剛性により標識柱の固有振動数に差異が生じることがある．また，電光表示盤構造の剛性も固有振動数に影響する．

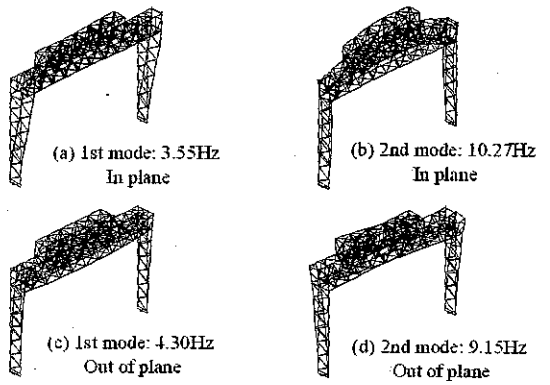

Fig.9 Natural Frequency and Vibration Modes of Portal Marker Column (Type: M1200)

門型標識柱の振動数の測定値と解析値とを比較して Table.2 に示す．解析値の振動数が少し高いのは，柱基部の完全固定条件によるものと考えられる．実物の門型標識柱基部の橋桁取付けブラケットの剛性を考慮すると良好に一致することが確認されている[1),2)]．

Table.2 Result of Measurement and Analysis

Natural Frequency / Methods	In Plane (Hz)	Out of Plane (Hz)
	1st mode	1st mode
Measured Result	3.13	3.66
Analytical Result	3.55	4.3

4. 理論解析による振動度マップの試作

4.1 振動度マップ試作の対象とした橋梁区間

2001 年に実施した振動測定データを活用する観点より，振動度マップ試作の対象区間として Fig.2 で示した橋梁（橋脚 P-34～P-38）を選定した．Photo.1 はその橋梁および 2001 年に実施した路下の歩道上でのビデオカメラ，および光学式変位測定器による振動測定の状況を示す．

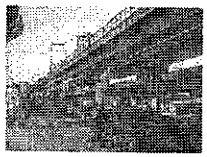

Photo.1: View of Bridge

Fig.10 は，対象の橋梁と付属構造物を示す．

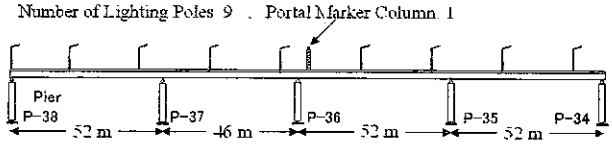

Fig.10 Model Bridge for Investigation of Vibration Level Map

4.2 理論解析による振動応答特性

橋脚,橋梁,照明柱および門型標識柱からなる Fig.10 に示す全体構造モデルを有限要素法（骨組構造）でモデル化して，固有振動解析および交通荷重を理想化してモーダル法による周波数応答解析を行った．

この理論解析を行うことにより，照明柱および門型標識

柱の設置位置の違いや門型標識柱の電光標示盤重量の違いなどによる振動応答特性を求めることができる．

これにより振動応答変位のレベルの違いを分析評価して振動度フラッグを付けることが可能と考えられる．振動応答変位から応力振幅を計算して疲労寿命を評価し，疲労損傷の発生時期を評価することになるが，本研究では振動度マップの試作までの技術開発を研究対象とした．

4.3 付属構造物の種類

1) 照明柱の数量と設置位置

Fig.11(a),(b)に実照明柱および全体構造モデルにおける照明柱モデルを示す．照明柱は，対象橋梁に約 20m毎に 9 本設置されている．しかし，設置位置と振動度との関係を解析し評価するために，Fig.11(c),(d)に示す 2 種類の設置位置 (L1～L9, La1～La9) の 2 モデルを解析した．

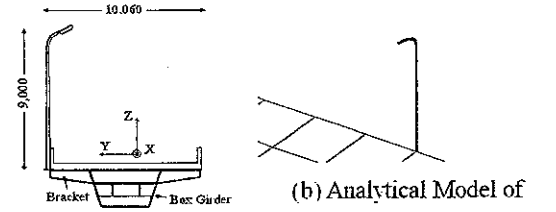

(a) Lighting Pole for Analysis　(b) Analytical Model of Lighting Pole on Model

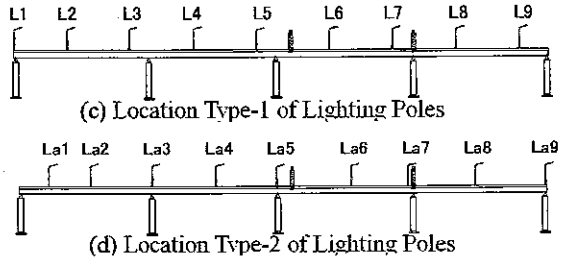

(c) Location Type-1 of Lighting Poles

(d) Location Type-2 of Lighting Poles

Fig.11 Locations of Lighting Poles on Model Bridge

2) 門型標識柱の種類

対象橋梁区間における実門型標識柱は，中央橋脚 P-36 から約 4m 離れた位置にある 1 基 (Model-M1) のみである．しかし，設置場所による比較評価の観点から中間橋脚 P-35 の真上にも 1 基 (Model-M2) 設置した．また，電光標示盤の重量は，ゼロ tonf，1.2tonf，および 2.8tonf の 3 種類とした．Fig.12 には，2 基の設置モデルを示す．

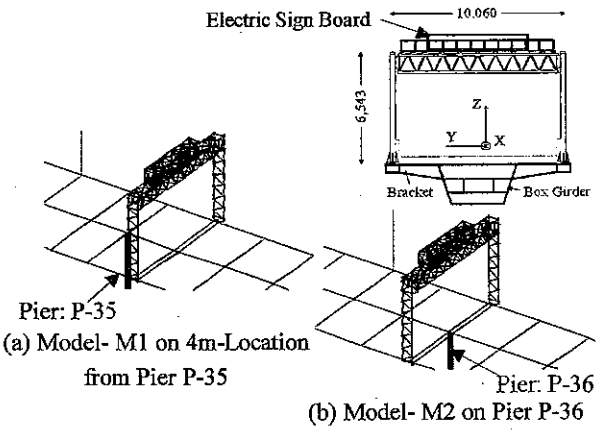

(a) Model- M1 on 4m-Location from Pier P-35

(b) Model- M2 on Pier P-36

Fig.12 Portal Marker Columns on Model Bridge

4.4 全体構造の固有振動解析

1) 橋脚・橋梁・付属構造物の全体構造モデル

昭和 61 年の構造物製作当時の図面を基にして構造解析モデル化に必要な諸元（寸法，板厚など）の調査整理を行い，解析に必要となる諸データ（部材の断面積，断面 2 次モーメント，ねじり定数や重量など）を決定した．

Fig.13 に示す単箱桁断面は，等価な剛性を持つ格子骨組構造にモデル化した．● 印は格子節点である．

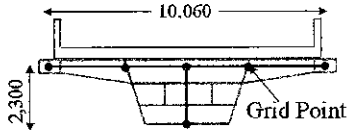

Fig.13 Grid Framed Structure for Box Girder Section under Consideration

設計製作時に実施された構造解析のデータが存在していれば，今回の解析用データとの比較が容易であったが今回は行うことができなかった．構造解析のモデル化の妥当性は，固有振動解析結果と橋梁路面の振動測定結果とが比較的に良好に一致していることにより確認した．特に 1 次の固有振動数は両者とも近い結果となっている．Fig.14 には全体振動解析モデルを示す．なお，橋梁上部構造の重量は，約 1723tonf である．

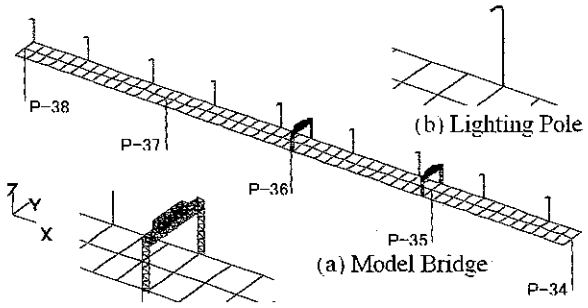

(b) Lighting Pole

(a) Model Bridge

(c) Portal Marker Column

Fig.14 Analytical Model of Model Bridge for Modal Frequency Response Analysis

2) 固有振動解析結果

橋梁本体,照明柱 9 本および門型標識柱 2 基からなる全体構造モデルの 1 次振動数 1.28Hz～64 次振動数 10.51Hz までを求めた．なお，1.28Hz は照明柱の固有振動数である．Fig.15 は橋梁本体の 1 次～4 次の振動モードと振動数を示している．橋梁本体の振動に連成して付属構造物の振動が現れていることが分かる．

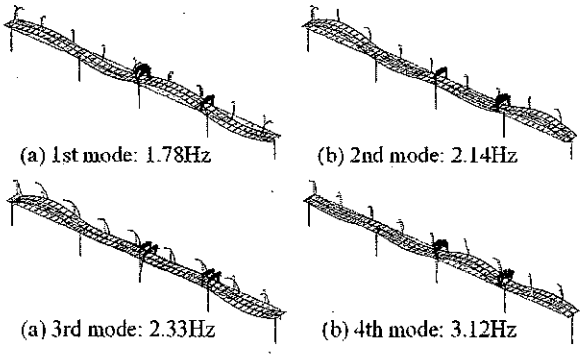

(a) 1st mode: 1.78Hz　(b) 2nd mode: 2.14Hz

(a) 3rd mode: 2.33Hz　(b) 4th mode: 3.12Hz

Fig.15 Vibration Mode and Frequency of Model Bridge

4.5 モーダル法による周波数応答解析

式(1)で表せる全体構造モデルの運動方程式において，交通荷重を調和外力として理想化し，実測された橋梁の主な振動範囲である 1～7Hz に対してモーダル法による周波数応答解析を行った．

$$[M]\left\{\frac{d^2x}{dt^2}\right\}+[C]\left\{\frac{dx}{dt}\right\}+[K]\{x\}=\{F\}\exp(i\omega t) \quad (1)$$
$$\omega=2\pi f \quad (f:1\sim 7Hz)$$

理想化した荷重 $F=W_0$ は，橋梁上部構造重量の約 1/10 の分布荷重とした．また，各モードの減衰率は 0.0253 とした．調和外力の種類は，Fig.16(a).(b)に示すように同位相荷重および逆位相荷重とした．

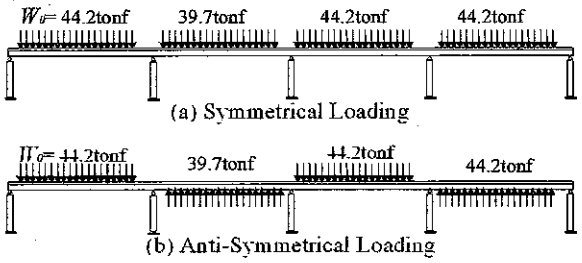

Fig.16 Loading Condition for Modal Frequency Response Analysis

5. 照明柱の周波数応答解析結果

Fig.17 には応答変位を計算した照明柱頭頂部の着目点 A の位置を示す．また，Fig.18～Fig.20 における応答変位は，相対変位（点 A－点 B）を示している．

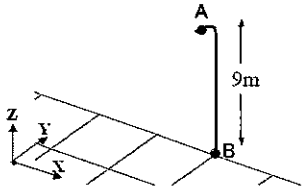

Fig.17 Point-A of Lighting Pole for Modal Frequency Response Analysis

Fig.18 には，面外（橋軸）X 方向の応答変位のスペクトルを示している．なお，表示は支点上と支間中央部付近の L1,La2,La3,La4,La5,La6,La7,La8 および La9 とした．

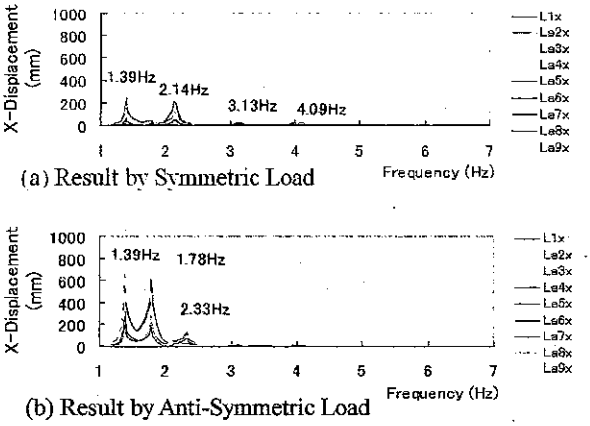

Fig.18 Spectrum of Response X-Displacement of Point-A (Lighting Pole)

Fig.19 は，面内（橋軸直角）Y 方向の応答変位のスペクトルを示している．また，Fig.20 は，鉛直（橋軸直角）Z 方向の応答変位のスペクトルを示している．

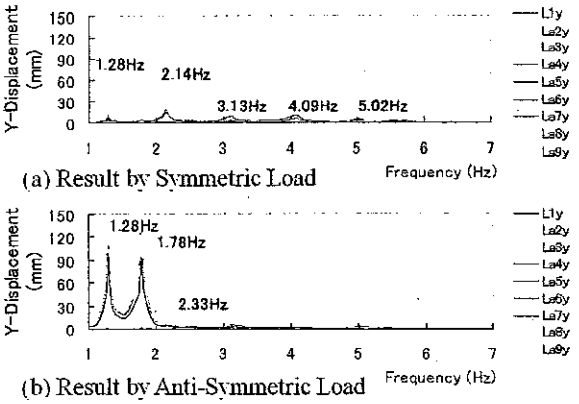

Fig.19 Spectrum of Response Y-Displacement of Point-A (Lighting Pole)

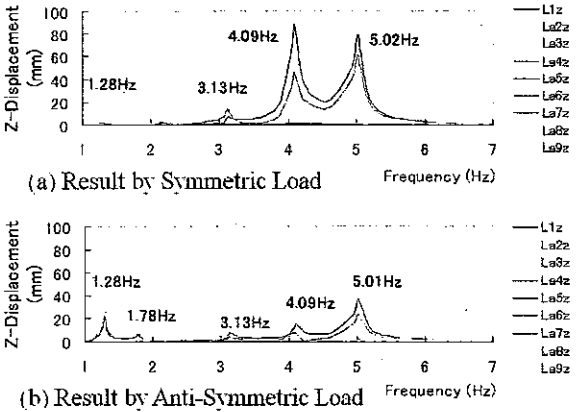

Fig.20 Spectrum of Response Z-Displacement of Point-A (Lighting Pole)

Fig.18～Fig.20 に示すように，周波数 1Hz～7Hz 領域における照明柱の応答変位は，1 次および 2 次の固有振動数付近で大きくなっていることが分かる．

6. 照明柱の設置位置と振動度

6.1 設置位置と応答変位

Fig.18～Fig.20 に示した応答変位の中で，それが大きい周波数を取り出して，18 本の照明柱の設置位置とその応答変位について分類整理した．Fig.21～Fig.23 は，X 方向，Y 方向，Z 方向の応答変位を示している．

Fig.21 の示すように，面外（橋軸）X 方向の応答変位は，設置位置が両端および中央橋脚付近の方が，支間中央付近より大きいことが分かる．この理由は，支点上の橋桁たわみ回転角が，支間中央部よりも大きいことによるものである．Fig.22,23 に示すように，面内（橋軸直角）Y 方向および鉛直 Z 方向の応答変位は，各支間中央付近の方が各橋脚支点付近よりも大きい結果となっている．この理由は，支間中央部のたわみが，橋脚支点付近よりも大きいことによるものである．

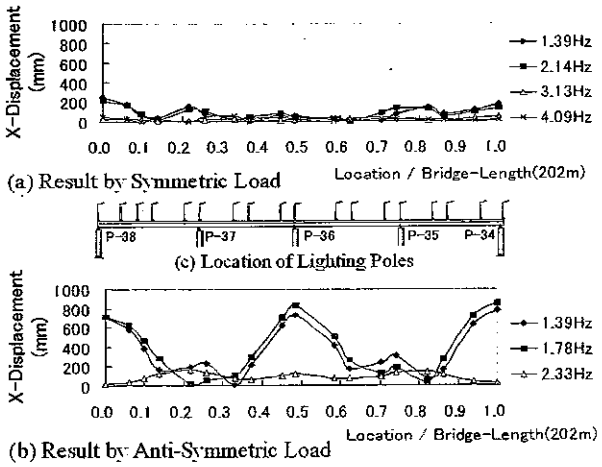

Fig.21 Vibration Level Map of X-Displacement (Lighting Pole)

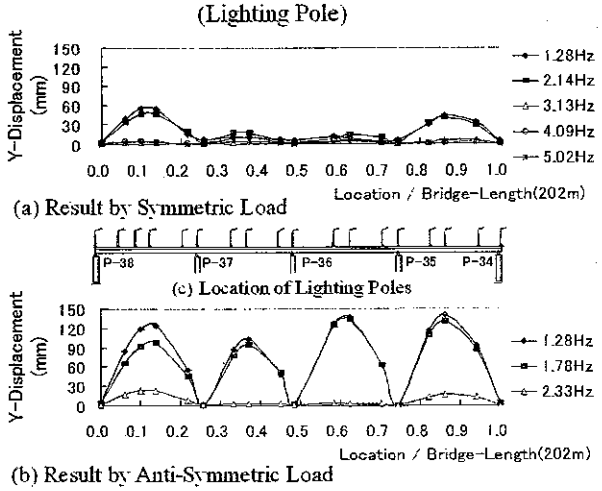

Fig.22 Vibration Level Map of Y-Displacement (Lighting Pole)

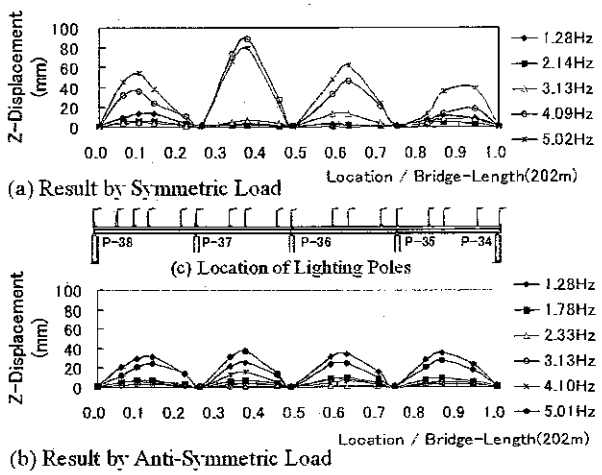

Fig.23 Vibration Level Map of Z-Displacement (Lighting Pole)

7. 門型標識柱の電光標示盤重量と固有振動数

門型標識柱の電光表示盤重量は，異なる 3 種類について検討した．その重量は，1.2 tonf（以下，M1200 型という），2.8 tonf（以下，M2800 型という）および 0.0 tonf（以下，M0000 型という）である．Fig.24 および Fig.25 は，M2800 型および M0000 型の門型標識柱における固有振動解析の結果を示している．なお，M1200 型は Fig.9 に示す．

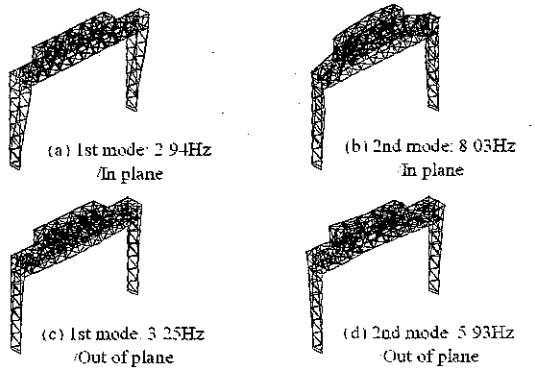

Fig.24 Natural Frequency and Vibration Modes of Portal Marker Column (Type: M2800)

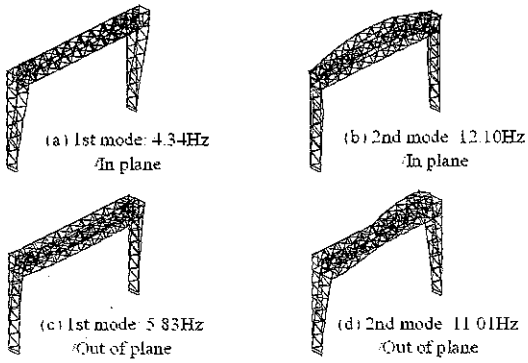

Fig.25 Natural Frequency and Vibration Modes of Portal Marker Column (Type: M0000)

Table.3 および Fig.26 に，電光表示盤重量と振動数との関係を表す．これらの図表より，電光標示盤の重量変化は固有振動数に影響を及ぼすことが分かる．

Table.3 Natural Frequency for 3-Types Portal Marker Columns

（Unit: Hz）

Weight of Portal Marker	Weight of Electric Sign Board	1st mode In plane	2nd mode In plane	1st mode Out of plane	2nd mode Out of plane
3.3 Tonf	0 Tonf	4.34	12.18	5.83	11.01
	1.2 Tonf	3.55	10.27	4.30	9.15
	2.8 Tonf	2.94	8.03	3.26	6.93

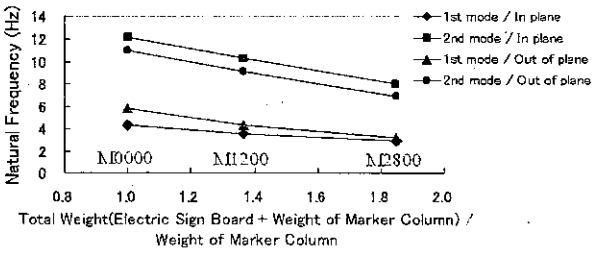

Fig.26 Natural Frequency of 3-Types Portal Marker Columns

8. 門型標識柱の周波数応答解析

Fig.27 に示す橋梁上の 2 箇所に門型標識柱（M1 および M2）を設置し，電光表示盤重量 3 タイプについて周波数応答解析を行った．図中の着目点 A，B および C は，応答変位の出力位置である．

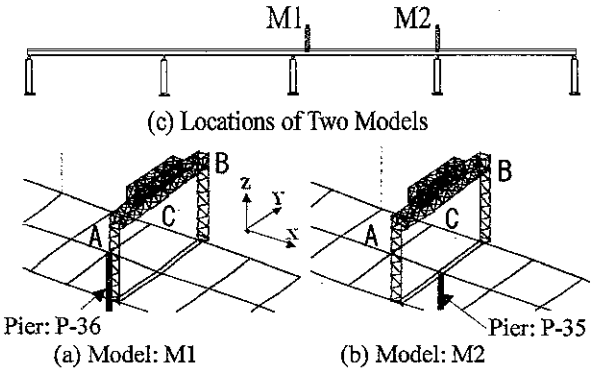

Fig.27 Two Models for Portal Marker Columns

8.1 M1200 型標識柱の応答変位

面外（橋軸）X 方向の応答変位のスペクトルを Fig.28 に，面内（橋軸直角）Y 方向の応答変位のスペクトルを Fig.29 に，鉛直 Z 方向の応答変位のスペクトルを Fig.30 に示す．

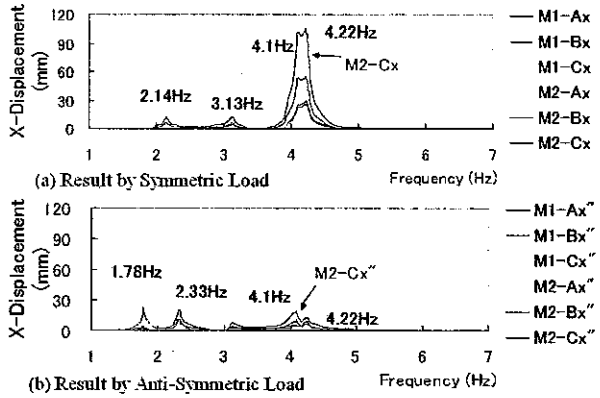

Fig.28 Spectrum of Response X-Displacement of Point-A, B, C (Type: M1200)

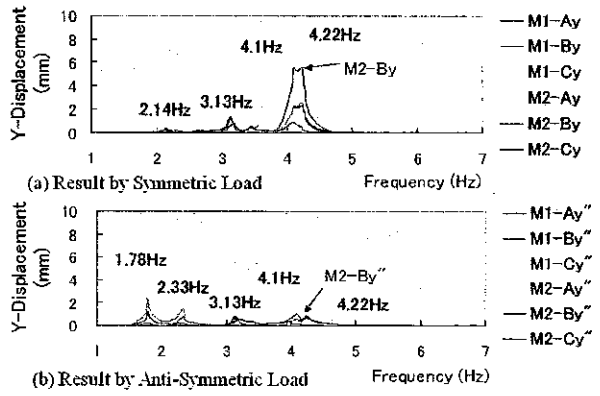

Fig.29 Spectrum of Response Y-Displacement of Point-A,B,C (Type: M1200)

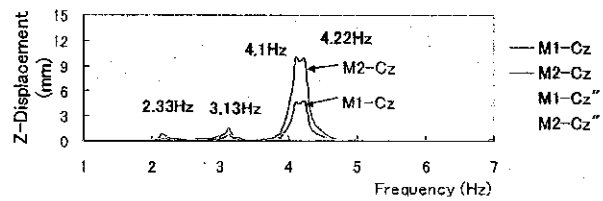

Fig.30 Spectrum of Response Z-Displacement of Point-C (Type: M1200)

1Hz～7Hz 領域の調和外力に対して，M1200 型標識柱の応答変位は，Table.3 に示す 1 次の固有振動数付近および橋桁との連成固有振動数付近での振動数において，その応答変位のピークが現れている．なお，1 次振動数 3.55Hz 以下の領域における応答変位は橋桁の変形と連成した剛体モード的な変形である．2 次振動数は 7Hz 以上であるので応答変位への影響は少ない．

8.2 M2800 型標識柱の応答変位

面外（橋軸）X 方向の応答変位のスペクトルを Fig.31 に，面内（橋軸直角）Y 方向の応答変位のスペクトルを Fig.32 に，鉛直 Z 方向の応答変位のスペクトルを Fig.33 に示す．

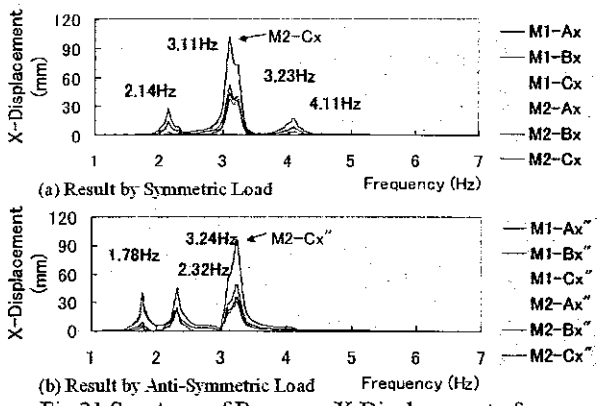

Fig.31 Spectrum of Response X-Displacement of Point-A,B,C (Type: M2800)

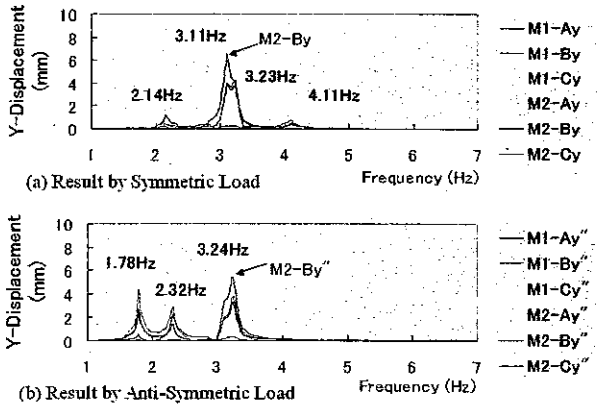

Fig.32 Spectrum of Response Y-Displacement of Point-A,B,C (Type: M2800)

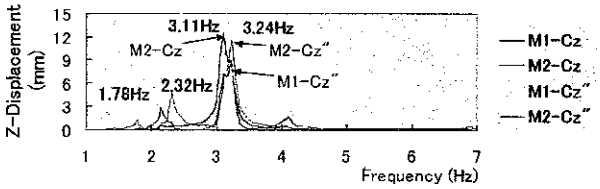

Fig.33 Spectrum of Response Z-Displacement of Point-C (Type: M2800)

M2800 型標識柱の応答変位も M1200 型と同様に 1 次固有周期付近および橋桁との連成固有周期付近での振動数においてその応答ピークが現れている．なお，2.94Hz 以下の領域における応答変位は橋桁の変形と連成した剛体モード的な変形である．

8.3 M0000 型標識柱の応答変位

面外（橋軸）X 方向の応答変位のスペクトルを Fig.34 に，面内（橋軸直角）Y 方向の応答変位のスペクトルを Fig.35 に，鉛直 Z 方向の応答変位のスペクトルを Fig.36 に示す．

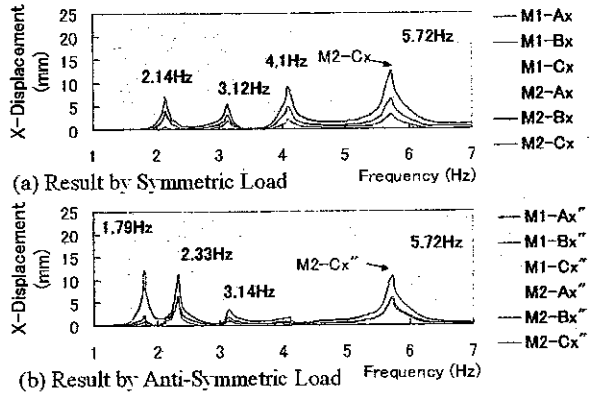

(a) Result by Symmetric Load

(b) Result by Anti-Symmetric Load

Fig.34 Spectrum of Response X-Displacement of Point-A,B,C (Type: M2800)

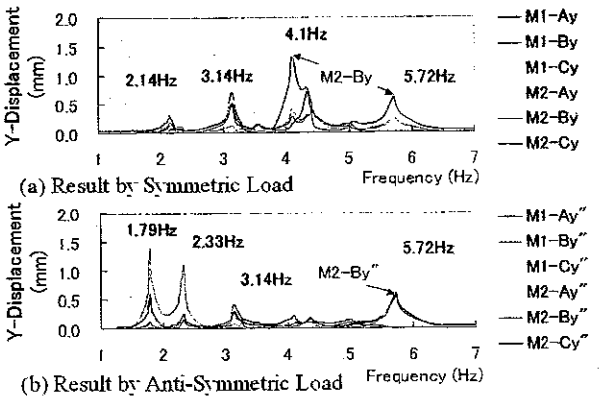

(a) Result by Symmetric Load

(b) Result by Anti-Symmetric Load

Fig.35 Spectrum of Response Y-Displacement of Point-A,B,C (Type: M0000)

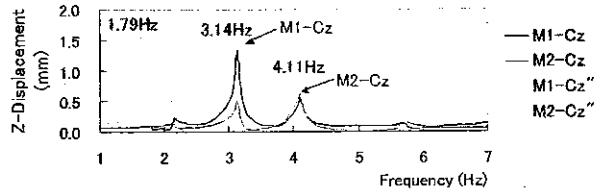

Fig.36 Spectrum of Response Z-Displacement of Point-C (Type: M0000)

M0000 型標識柱の応答変位についても同様に 1 次固有周期付近および橋桁との連成固有周期付近での振動数においてその応答ピークが現れている．なお，4.34Hz 以下の領域における応答変位は橋桁の変形と連成した剛体モード的な変形である．

8.4 門型標識柱の設置位置と振動度

面内 X 方向，面外 Y 方向および鉛直 Z 方向の応答変位は，橋脚支点上に設置されているモデル M2 の方がモデル M1 よりも大きいことが分かる．これは，支点上の方がたわみ角が大きいことによるものと考えられ，3 種類の M1200 型，M2800 型および M0000 型について共通の結果である．

8.5 門型標識柱の電光標示盤重量と振動度

電光表示盤重量の違いは，応答変位量に影響しており，M2800 型が M1200 型よりも応答変位量が大きい結果となっている．M0000 型の 1 次固有振動数は，他の 2 種類に比べて高いので応答変位は小さい結果となっている．

9. まとめ

本研究において，照明柱および門型標識柱の振動度マップ試作法として行った振動解析結果の評価により得られた知見を以下にまとめる．

(1) モーダル法による周波数応答解析の結果は，概ね予測された妥当な傾向を示しており，振動度マップ作成を可能とする有効な方法であることが確認された．

(2) 振動度マップ作成には，付属構造物の固有振動数 f_s，橋梁の固有振動数 f_b，設置位置 L_s および橋梁支間長 L_b などがパラメータになることが分かった．

(3) 橋桁のたわみ角およびねじれ角が，付属構造物の振動変位の程度（振動度）に大きく影響することが分かった．

今後の課題として以下のことが考えられる．

・振動度マップの作成には，実際の交通荷重による振動応答変位の定量的評価が必要である．

・損傷可能性管理マップの作成には，振動変位の定量的評価に基づいて疲労強度を評価し，損傷の存在と発生の可能性をランク分けする技術の確立が必要である．

謝辞

本研究において実施した付属構造物の振動測定および振動解析において，サーボ型変位センサーによる測定で(株)日本工業試験所に，ビデオカメラによる測定で(株)ニチゾウテックに，光学式変位測定器による測定でツィンマージャパン(株)に，FEM による振動解析では(有)テクノアートクルーズおよび(有)計算工房に，多大の協力をいただいた．ここに記して感謝の意を表します．

なお，本研究の一部は，平成 14 年度科学研究費補助金：基盤研究(B)(1)「社会環境の変化に伴う交通荷重実態調査と橋梁の劣化予測モニタリング手法の開発（研究代表者：山田健太郎）」の一環として行ったものである．

参考文献

1) 井舎英生,北田俊行,山口隆司,宮脇　潔,乙黒幸年,時譲太;道路橋の標識柱・照明柱における損傷の早期発見に関する基礎的研究,土木学会 橋梁振動コロキウム'01 論文集,pp.239-244,2001

2) Hideo ISHA, Toshiyuki KITADA, Takashi YAMAGUCHI, Kiyoshi MIYAWAKI, Yukitoshi OTOGURO and Jota TOKI: Development of A Practical System for Detecting Portal Marker Columns and Lighting Poles with Damage on Highway Bridges, Proceedings of the 6th Japan-Korea Joint Seminar on Steel Bridges, pp.31-42, August 2001

(2003.7.31 受付)

道路橋付属構造物の損傷と振動特性に関する実験的研究

Experimental Study about Vibration Characteristics of Portal Marker Columns with Damage on Highway Bridges

○井舎英生*，北田俊行**，谷　憲一***
Hideo Isha, Toshiyuki Kitada, Kenichi Tani

*後期博士課程，大阪市立大学大学院，工学研究科，都市系専攻（〒558-8585 大阪市住吉区杉本 3-3-138）
**工博，大阪市立大学大学院教授，工学研究科，都市系専攻（〒558-8585 大阪市住吉区杉本 3-3-138）
***前期博士課程，大阪市立大学大学院，工学研究科，都市系専攻（〒558-8585 大阪市住吉区杉本 3-3-138）

Early detection of damage to portal marker columns on highway bridges is important for safe road management. It is useful that the existence of the damage can be specified by vibration measurements in a place located far from portal marker columns. Vibration characteristics, such as natural vibration periods and modes of a structure with damage change compared with those with the damage in accordance with the extent of the damage. It can be considered that the location and the extent of the damage can be judged through analyzing the vibration data measured by a digital video from locations underneath the highway bridge under consideration. Various types of damage are generated to experimental models of portal marker columns, and a vibration experiment is carried out in this study. Furthermore, the experimental results are compared with the result by the vibration analysis of an analytical model. The relations between the extent of damage and vibration characteristics can investigated through the vibration measurement and the analysis of the portal marker column.

Key Words:　*Measuring Vibrations, Detecting Damage, Portal Marker Column*

1. はじめに

都市高速道路橋の附属構造物である標識柱や照明柱の損傷は，これまでの研究により交通や風による振動疲労が主な原因であることが明らかにされている．

損傷の存在は，振動数や振動モードなどの振動特性の変化に現れるので，その振動特性を適宜に測定することによって損傷の早期発見ができれば道路安全管理上からも有益である．これらの疲労損傷の有無を把握するためには，付属構造物の点検を行う必要がある．しかし，従来行なわれている点検方法では，交通規制が必要であること，点検が困難な場所にあること，点検対象となる付属構造物の数量が多いことなど幾つかの課題がある．

これらの課題解決策の一つとして Photo.1 に示す様に，離れた場所からビデオカメラや光学式変位測定器などにより振動特性を測定することを提案したが [1]，これらの振動測定法によりどの程度の損傷の有無が発見できるのかを明らかにする必要がある．

本研究では，損傷の存在が振動特性に及ぼす影響を実験的および解析的に研究を行っている．標準的な門型標識柱の模型を製作し損傷を与えた振動実験および構造解析モデルによる固有振動解析を実施している．その結果を解析評価することにより，損傷の箇所とその程度との関係について，すなわち損傷と振動特性との関係について明らかにしている．Fig.1 は，振動実験の対象とした実門型標識柱の概略を示している．

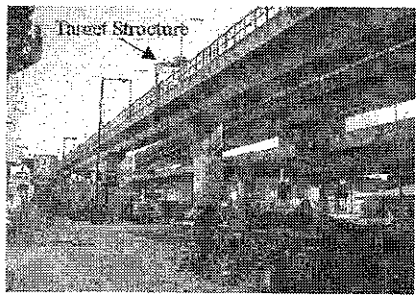

Photo.1 Situation of Vibration Measurement from a distance

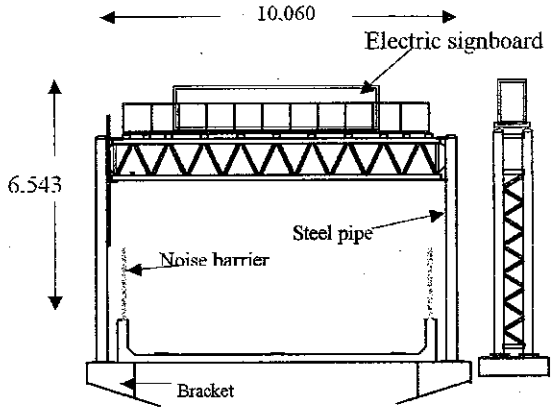

Fig.1 Gate-Type Portal Marker Column

2. 橋梁上の門型標識柱の振動特性と損傷の事例

橋梁路面および門型標識柱の振動状況の測定を 2001 年に阪神高速道路 16 号大阪港線にて行った [1]. Fig.2 にサーボ型変位センサーで測定した路面の鉛直方向の振動変位のスペクトル解析結果を示す. 門型標識柱の振動数は, ビデオカメラによる画像を画像データ解析して得られたものであり, Fig.3(a)に面内水平（橋軸直角）方向の振幅スペクトルを, Fig.3(b)に面外（橋軸）方向の振幅スペクトルを示す. Photo.2 には, 画像データ解析を行った部分を示す. なお, 門型標識柱の上部には約 1.2 トンの電光表示盤が設置されている.

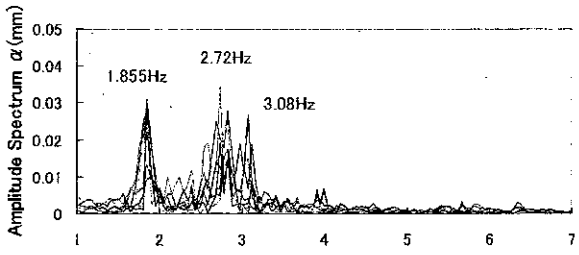

Fig.2 Vertical Vibration of Road Surface with Portal Marker Column

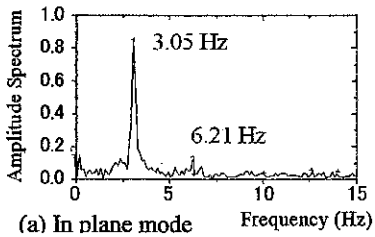

(a) In plane mode

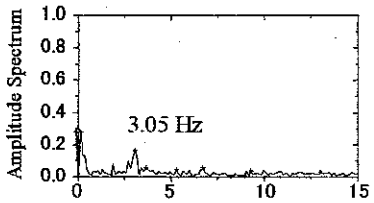

(b) Out of plane mode

Fig.3 Results of Measurement and Spectrum analysis in case of Gate-Type Marker Column (Digital video camera)

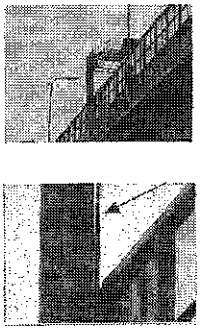

Photo.2 Image Data Analysis Part

損傷に関しては, これまでにも幾つかの事例が報告されているが, 本研究では Photo.3 に示すような柱基部の溶接部損傷および梁部トラス斜材と下弦材の溶接部損傷を対象として取り扱った. これらの損傷によって標識柱の面外（橋軸）方向および面内（橋軸直角）方向の振動特性に変化が現れる事例に着目する.

(a) Column base part with damage

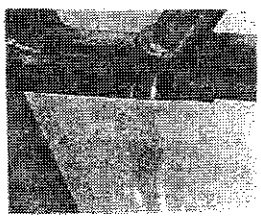

(b) Fracture of weld part

Photo.3 Damage Example of Gate-type Portal Marker Column

3. 実験の概要

3.1 実験供試体

Fig.4 は, 門型標識柱の実験供試体の概略を示している. 実験場の設備環境により, 実構造モデルではなく縮尺スケールが実物の約 1/10 の供試体を 3 体製作した. 材料にはステンレス鋼を用いた. 実際の門型標識柱は, 橋桁と取付けブラケットにより結合されている. 固有振動数は, ブラケットの剛性によって変化することが確認されているので [1], 実験供試体の下部に横桁を取付けて同様の剛性効果を表現できるようにした. Photo.4 には, 製作した実験供試体を示している.

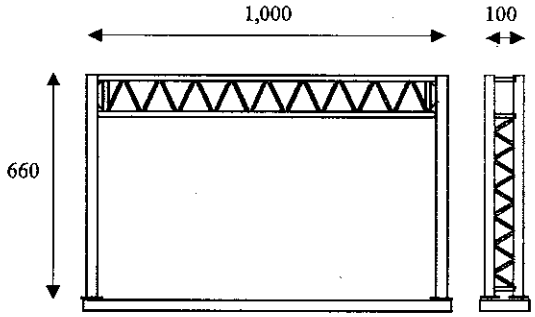

Fig.4 Outline of Portal Marker Frame for Experiment (Unit: mm)

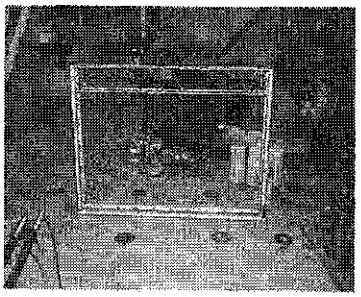

Photo.4 Experimental Model

Table.1 は, 実験供試体の製作に使用した部材を表している.

Table.1 Cross-Sectional Dimensions

Items	Outside Diameter (mm)	Thickness (mm)	Weight (gf)	
			No.1	No.2
Column base part	25.0	1.0	3815.2	3803.6
Column horizontal member	10.0	0.5		
Beam top & lower cord	4.0	0.5		
Column vertical bent	3.0	0.5		
Beam horizontal bent	4.0	0.5		
Column horizontal bent	10.0	0.5		
Beam1 (Support part)	25.0	0.5		
Beam2 (Support part)	10.0	0.5		

3.2 損傷の種類

Photo.3 で示した損傷事例に従って，実験供試体と解析モデルとに損傷を導入した．Fig.5 に示す位置に損傷タイプとして A,B,C,D,E および F の損傷を与えた．柱基部の損傷タイプ A,B,E,F は，損傷レベルを 4 段階として設定した．Fig.6 に，柱円管に設定した損傷レベル A1,A2,A3 および A4 を示す．また，梁部トラス斜材の C,D の損傷は，パイプ直径が小さいため全断面損傷とした．

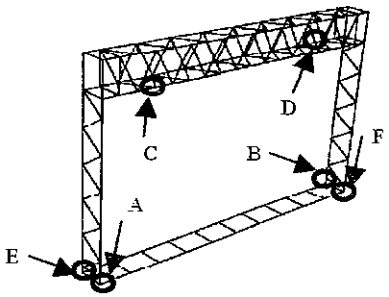

Fig.5 Locations of Damage

Fig.6 Damage Levels of Column Base

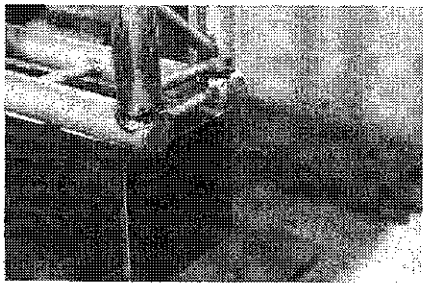

Photo.5 Damage Situation in Experiment

Table.2 は，導入された損傷タイプの組合せパターンを示している．損傷の導入の順序は，数字の順番である．

Table.2 Damage Patterns

Measurment order	No.1	No.2
	Damage patterns	Damage patterns
1	No damage	No damage
2	A1	C
3	A2	CD
4	A3	CDA1F1
5	A4	CDA2F2
6	A4C	CDA4F4
7	A4CD	CDA4F4E1
8	A4CDB2	CDA4F4E1B1
9	A4CDB4	
10	A4CDB4E1	
11	A4CDB4E1F1	

3.3 実験供試体の設置

Photo.6 に示すように 100ton アクチュエーター試験機に治具と供試体とを設置した．治具とアクチュエーターはボルトで 締結し，供試体と治具とは鉄板 2 枚を支持部にはさみ，ボルトで締め付けることにより拘束している．供試体の下部横桁と供試体支持フレームとの拘束において，左右対称の拘束にすると面内（水平）の揺れが起こりにくい．よって，少し非対称拘束にすることにより面内の揺れを実現している．供試体の錘は，上部トラスの上弦材に 1 個約 8kg のおもりを 3 列 3 段ずつ合計約 72kg 載荷して．実際の標識柱の固有振動数に近づけた．

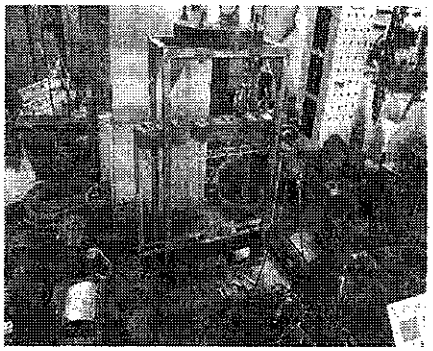

Photo.6 Scenery of Experiment

測定器具は，Fig.7 に示すように供試体の柱上部に面内および面外方向，梁部トラス斜材中央部に鉛直方向の揺れを測定するために加速度計を設置した．またアクチュエーターの揺れが正常に機能していることを確認するために，面内・面外・上下方向に変位計 cdp10 を設置した．

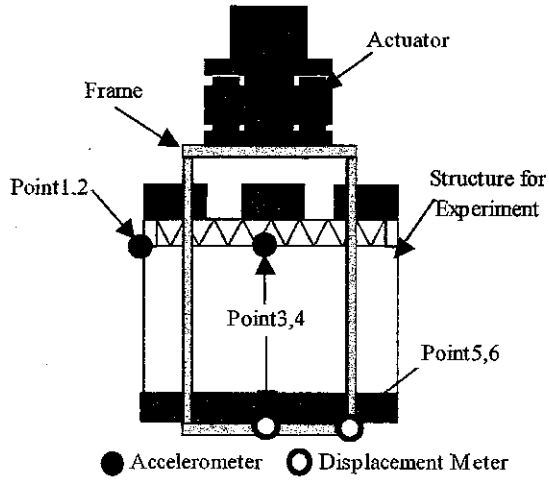

Fig.7 Installation position of measuring instrument

測定方法は，供試体に設置した加速度計・変位計のデータを動ひずみ計で増幅し，A/D 変換ボードを介してパソコンに直接データを入力することにより加速度応答値を得た．動ひずみ計の設定は，加速度計サンプリング周波数は，0～50Hz 程度までの振動数領域を対象とすることから 100Hz を用い，アクチュエーターの内部電圧も含め，各測点におけるデータ個数 7 個として測定を行った．動ひずみ計の設定は，加速度計は range と較正値を 500

$\mu\varepsilon$，変位計は range と較正値を 5000$\mu\varepsilon$ とした．

Table.3 Performance of accelerometer

No	Frequency (hz)	Rated power (μV/V)	Calibration factor (G/1μV/V)
1	0～130	622	0.008038
2	0～125	614	0.00815
3	0～110	649	0.007704

3.4 自由振動実験

損傷の無い健全時と損傷時に対して，面内・面外モードの自由振動が生じるように手動で供試体を加振させ，面内および面外の振動モードでの固有振動数を測定した．次にアクチュエーターで供試体に強制振動を与え，自由振動の場合の振動数と振動モードとの一致を確認した．門型標識柱の柱基部と上部梁に損傷を与えた振動実験の結果を以下の Fig.8，Fig.9 および Table.4，5 に示す．

実験では，実験 1 回目，2 回目と同じ供試体を用いて 2 度繰り返し，実験の再現性を確認した．また，実験と解析結果の整合性を確認すべく，様々な損傷パターンによる振動数を求めた．Fig.8 は健全な供試体と損傷状態（損傷タイプA4）の振動波形を示している．この振動波形を見ても損傷の有無は判然としないが，波形の減衰率に着目すると，Fig.8(b)の方が大きいことから，損傷による影響を受けていることが分かる．Fig.9 に示すフーリエスペクトル解析の結果により，卓越振動数は，健全な標識柱 5.006Hz から損傷タイプ A4 において 4.839Hz に減少している．これは，損傷の存在により標識柱の面内水平剛性が低下することによるものである．

このように，Fig.8 の振動波形から Fig.9 のスペクトル解析を行うことにより，振動数の変化を評価して損傷の有無を判定することが可能となると考えられる．

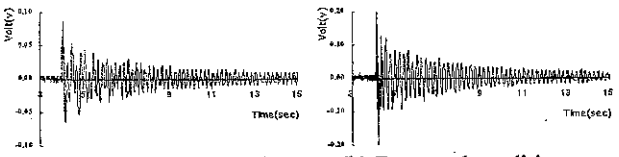

(a) Non-damage condition　(b) Damaged condition (Damage Type: A4)

Fig.8 Vibration Wave (1st mode /in plane)

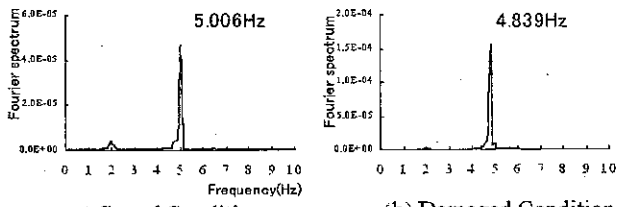

(a) Sound Condition　(b) Damaged Condition (Damage Type: A4)

Fig.9 Natural Frequency (1st mode /in plan)

Table,4,5 から損傷状態の結果に着目すると，Fig.3 の実測値では，1 次の面内・面外振動数がともに約 3Hz であるのに対し，実験では面内 1 次が約 5Hz，面外 1 次が約 2Hz となり，差異が生じた．その要因としては，供試体の面外よりも面内の剛性が高い供試体の構造的特性や測定時と実験時との変位拘束状態が異なるためと考えられる．実験 1 回目と 2 回目との結果において，TYPE-1 と TYPE-2 との結果に差が生じた．これは，変形拘束のボルトの締め具合による微妙な差がスペクトルに差を生じさせたと考えられる．

Table.4 Experimental Results (TYPE-1)

TYPE	1	1st Experiment		2nd Experiment	
Measurment order	Damage patterns	1st In-plane(Hz)	1st Out-of-plane(Hz)	1st In-plane(Hz)	1st Out-of-plane(Hz)
1	No damage	4.791	2.003	5.006	2.002
2	A1	4.760	2.002	5.006	1.952
3	A2	4.736	2.002	4.955	1.949
4	A3	4.735	1.920	4.894	1.947
5	A4	4.721	1.901	4.839	1.752
6	A4C	4.661	1.810	4.777	1.739
7	A4CD	4.554	1.798	4.616	1.760
8	A4CDB2	4.427	1.794	4.594	1.708
9	A4CDB4	4.339	1.519	4.506	1.521
10	A4CDB4E1	4.222	1.326	—	—
11	A4CDB4E1F1	4.127	1.321	—	—

Table.5 Experimental Results (TYPE-2)

TYPE	2	1st Experiment		2nd Experiment	
Measurment order	Damage patterns	1st In-plane(Hz)	1st Out-of-plane(Hz)	1st In-plane(Hz)	1st Out-of-plane(Hz)
1	No damage	4.700	1.920	4.827	1.669
2	C	4.591	1.898	4.709	1.669
3	CD	4.463	1.899	4.616	1.669
4	CDA1F1	4.406	1.920	4.606	1.686
5	CDA2F2	4.363	1.904	4.594	1.629
6	CDA4F4	4.309	1.457	4.454	1.377
7	CDA4F4E1	4.237	1.448	4.454	1.366
8	CDA4F4E1B1	4.292	1.253	4.343	1.336

実験結果を評価すると，損傷箇所が増加するにつれて，供試体の固有振動数は低下している．しかし，少しの損傷では振動数の低下が僅かであることは，これまでの研究でも明らかになっている．A1，A2 および A3 程度の小さな損傷レベルでは，振動数の変化は微小であることが確認された．A4，C，D 程度の全断面損傷の規模になると振動数に明確な変化が現れている．なお，柱基部の損傷では，面外モードの振動数に顕著な変化が現れている．また，梁部トラス斜材の損傷では，面内モードの振動数に顕著な変化が現れている．これは，構造特性から考えて妥当な結果である．

4. 固有振動解析用の骨組構造モデル化と解析結果

4.1 骨組構造へのモデル化

損傷のある標識柱の振動特性の変化を解析して，損傷のある箇所とその程度を予測できる方法を開発する場合

に，実験や実測した振動特性結果と整合性のある振動解析用の骨組構造モデルを作成することが重要である．一般的には，構造物の設計図面や材料表により作成した構造モデルの剛性や質量分布また構造基部の拘束度などが，実構造と乖離している場合がある．

本研究の振動解析用の構造モデル作成においても考慮すべき点がある．Fig.10 に示す門型標識柱では，柱基部と取付けブラケットとの連結部の剛性，柱ー横梁結合部の剛性，および情報電光表示盤の剛性と質量配分などが振動特性に大きく影響することが明らかとなっている[1]．解析モデルは，Fig.11 に示すような 3 次元の梁要素を用いてモデル化した．ステンレス鋼の材料定数は，ヤング係数が 21,000kgf/mm^2，密度 8.01x10^{-10}kg/mm^3，およびポアソン比を 0.3 とした．拘束条件は実験と同じ位置に X，Y，Z 方向の変位を拘束した．実験で供試体に載せた錘は，解析モデルにおいては集中質量として梁上部と柱上部との節点に合計 72kgf を載せている．損傷の設定は，損傷タイプ，断面の損傷レベル（A,B,C,D,E,F），設置箇所を実験におけるケースと同様にして梁要素断面の変化として表現した．

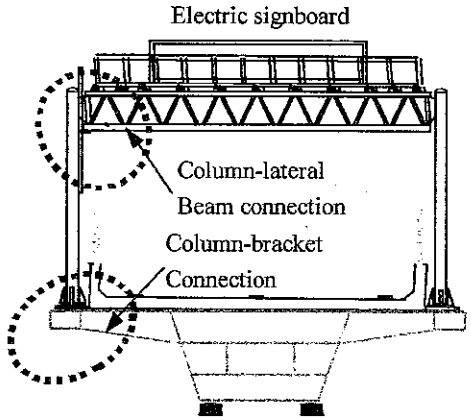

Fig.10 Framed Structure Modeling for Gate-Type Portal Marker Column

4.2 固有振動解析と実験結果との比較

4.1 で述べた骨組構造モデルを用いて固有振動解析を行い，損傷による振動特性の変化を調べた．Table.6,7 には，それぞれ実験供試体 TYPE-1 と TYPE-2 との両モデルの解析結果を示す．TYPE-1, 2 ともに実験結果と同様，実測値に比べ面外・面内 1 次の振動数に差が生じた．また，損傷箇所が増えるほど振動数の低下率が大きいことも確認できた．損傷タイプから，柱基部の損傷は面外 1 次の振動数に，梁部トラス斜材は変化が面内 1 次の振動数に変化が顕著に現れ，これは実験結果と同じ傾向を示した．

実験と構造モデルとによる固有振動解析の振動数に違いがある要因は，下部横桁ブラケットの拘束の違いや剛性の違い，柱と上部梁結合部の剛性および拘束条件などに起因しているものと考えられるが，損傷と振動数の低減率の傾向は概ね一致している．損傷レベルの結果に着目すると実験結果と同様に，円管断面の損傷 A1，A2 A3 では振動数の変化は微小であった．しかし，全断面破損の

Table.6 Analytical Results (TYPE-1)

TYPE	1	Analysis result		Rate of reduction	
Measurment order	Damage patterns	1st In-plane(Hz)	1st Out-of-plane(Hz)	1st In-plane(%)	1st Out-of-plane(%)
1	No damage	4.642	2.851	0.000	0.000
2	A1	4.639	2.846	0.062	0.196
3	A2	4.635	2.842	0.155	0.330
4	A3	4.569	2.814	1.566	1.298
5	A4	4.480	2.375	3.475	16.716
6	A4C	4.326	2.372	6.801	16.801
7	A4CD	4.184	2.371	9.865	16.846
8	A4CDB2	4.182	2.367	9.904	16.997
9	A4CDB4	4.131	2.100	10.998	26.351
10	A4CDB4E1	4.129	2.099	11.052	26.386
11	A4CDB4E1F1	4.014	2.055	13.534	27.926

Table.7 Analytical Results (TYPE-2)

TYPE	2	Analysis result		Rate of reduction	
Measurment order	Damage patterns	1st In-plane(Hz)	1st Out-of-plane(Hz)	1st In-plane(%)	1st Out-of-plane(%)
1	No damage	4.642	2.851	0.000	0.000
2	C	4.460	2.847	3.912	0.144
3	CD	4.318	2.842	6.972	0.323
4	CDA1F1	4.316	2.838	7.017	0.470
5	CDA2F2	4.311	2.832	7.118	0.677
6	CDA4F4	4.131	2.100	10.998	26.351
7	CDA4F4E1	4.129	2.099	11.052	26.386
8	CDA4F4E1B1	4.014	2.055	13.534	27.926

A4 タイプの損傷になると振動数の低減は顕著となり，面外 1 次の振動数が 3~4%程度低減する．このことは 4 本柱を持つ門型標識柱の面外方向の剛性が大きく低下することに起因しているものと考えられる．Fig.11 には，健全な場合と損傷を与えた場合との振動モードを示している．面内 1 次と面外 1 次の低次においては，振動モードには変化が認められなかった．これは，2 次と 1 次の低

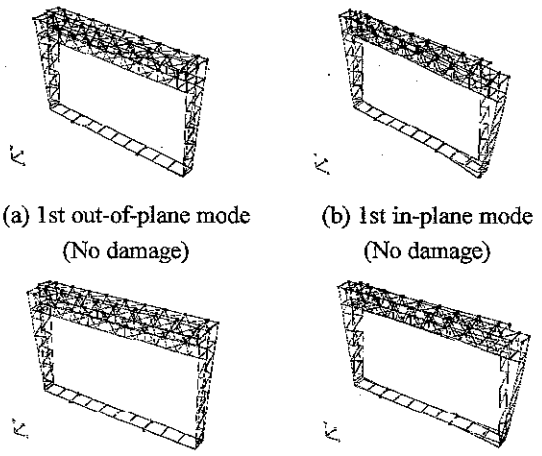

(a) 1st out-of-plane mode (No damage)　(b) 1st in-plane mode (No damage)

(a) 1st out-of-plane mode (Damage pattern:A4CDB4)　(b) 1st in-plane mode (Damage pattern A4CDB4)

Fig.11 Natural Modes of the Gate-Type Portal Marker column

次モードの領域では各モードの振動数に開きがあるので，少しの振動数の低下で2次から1次振動モードへの変化を誘起することには至らなかったものと考えられる．

5. 損傷と振動特性の変化

Fig.12(a),(b),(c),(d)には，本研究で対象とした門型標識柱の実験供試体における損傷パターンと振動数の低減との関係を示す．Fig12(a)には，供試体 TYPE-1 の面内振動数の変化を示す．グラフ横軸は，Table.4,5,6,7 に示す損傷パターン番号を表している．

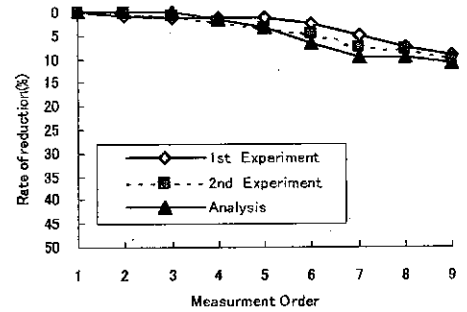

(a) 1st in-plane mode (TYPE-1)

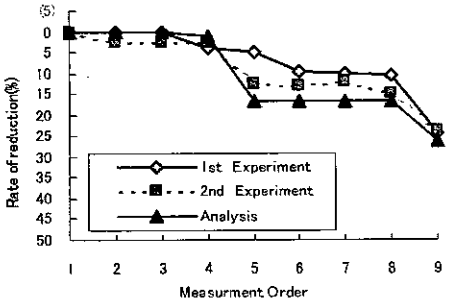

(b) 1st out-of-plane mode (TYPE-1)

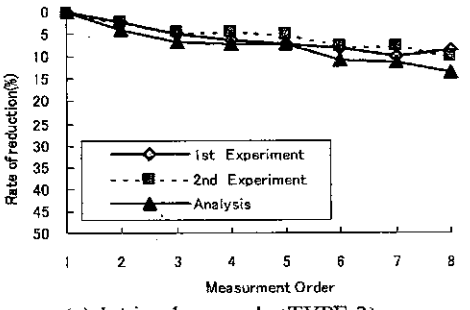

(c) 1st in-plane mode (TYPE-2)

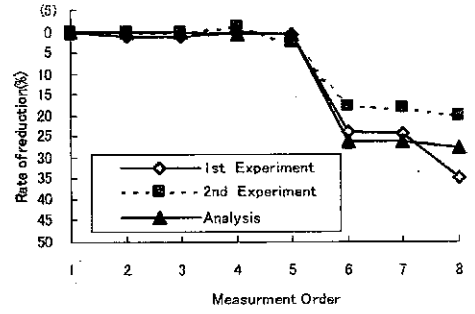

(d) 1st out-of-plane mode (TYPE-2)

Fig.12 Relationship of Rate of Reduction of Damage Patterns

横軸の番号が大きくなるに従って損傷規模が大きくなる．損傷の個所は Fig.9 図中の記号 A,B,C,D,E,F である．

実験結果と解析結果とは，定性的には良好に一致している．以下に，損傷がある場合の健全な状態からの振動数の低減について考察している．

(1) 損傷パターンが A1,A2,A3,A4 の場合，面内 1 次振動数は，0.1～4% 程度の低減，面外 1 次振動数は，0.2～17% 程度の低減である．
(2) 損傷パターンが A4C,A4CD,A4CDB2,A4CDB4 の場合，面内 1 次振動数は，7～11% 程度の低減，面外 1 次振動数は，17～27% 程度の低減である．
(3) 損傷パターンが C,CD,CDA1F1,CDA2F2 の場合，面内 1 次振動数は，4～7% 程度の低減，面外 1 次振動数は，0.1～0.7% 程度の低減である．
(4) 損傷パターンが CDA4F4,CDA4F4E1,CDA4F4E1B1 の場合，面内 1 次振動数は，7～14% 程度の低減，面外 1 次振動数は，26～28% 程度の低減である．
(5) 柱基部の損傷パターン A1～A3 までは，振動数の低減は微小であるが，全断面損傷 A4 や上部梁部トラス斜材の損傷 C, D が存在する損傷パターンになると振動数の低減が顕著になる．柱基部の損傷パターンでは面外振動モードに，梁部トラス斜材の損傷パターンでは面内振動モードに変化が顕著になっている．

6. まとめ

(1) 門型標識柱の基部や上部梁の損傷と振動特性との関係が明らかとなった．
(2) 円管断面の 1/4～3/4 程度の損傷では振動数の低減は僅かであり，振動数の測定で損傷の有無を判断するのは難しいことが明らかとなった．
(3) 円管の全断面損傷や梁部トラス斜材の全断面損傷が存在する損傷パターンになると，振動数の低減は顕著に現れる．このような場合は，離れた場所からのビデオカメラによる振動数の変化を測定することによって損傷の有無の判断は可能になると考えられる．

謝辞

本研究において実施したビデオカメラによる門型標識柱の振動測定においては，(株)ニチゾウテックに多大の協力をいただいた．ここに記して感謝の意を表します．

なお，本研究は，科学研究補助金：基盤研究(A)(1)「既設鋼道路橋の疲労抵抗度診断とレトロフィッティング技術の開発に関する研究（代表者：三木千壽)」の一環として行ったものである．

参考文献

1) 井舎英生，北田俊行，山口隆司，宮脇潔，乙黒幸年，時譲太：道路橋の標識柱・照明柱における損傷の早期発見に関する基礎的研究，土木学会橋梁振動コロキウム'01（2001 年 10 月）

(2003.7.31 受付)

ご注意　当該出版物の内容を複写したり他の出版物へ転載するような場合は，
必ず土木学会の許可を得て下さい。

平成15年8月29日発行
編　集　者：〒160-0004　東京都新宿区四谷一丁目無番地
土木学会　構造工学委員会
橋梁振動モニタリングとその標準化研究小委員会
委員長　中島章典
発　行　者：東京都新宿区四谷一丁目無番地　社団法人　土木学会　古木守靖
発　行　所：社団法人　土木学会
〒160-0004　東京都新宿区四谷一丁目無番地
電話 03-3355-3441(代表)　FAX03-5379-0125

印刷：㈱トキワコーポレーション